Vol. 20, No. 2, June, 2021
ISSN (Print): 0972-6268; ISSN (Online) : 2395-3454

Nature Environment & Pollution Technology

A Multidisciplinary, International Journal on Diverse Aspects of Environment

Technoscience Publications
website: www.neptjournal.com

Technoscience Publications
A-504, Bliss Avenue, Balewadi,
Opp. SKP Campus, Pune-411 045
Maharashtra, India

www.neptjournal.com

Nature Environment and Pollution Technology

(An International Quarterly Scientific Research Journal)

Published by : Mrs. T. P. Goel, B-34, Dev Nagar, Tonk Road, Jaipur-302 018 Rajasthan, India

Managing Office : Technoscience Publications, A-504, Bliss Avenue, Balewadi, Pune-411 045, Maharashtra, India

E-mail : contact@neptjournal.com; journalnept@gmail.com

INSTRUCTIONS TO AUTHORS

Scope of the Journal

The Journal publishes original research/review papers covering almost all aspects of environment like monitoring, control and management of air, water, soil and noise pollution; solid waste management; industrial hygiene and occupational health hazards; biomedical aspects of pollution; conservation and management of resources; environmental laws and legal aspects of pollution; toxicology; radiation and recycling etc. Reports of important events, environmental news, environmental highlights and book reviews are also published in the journal.

Format of Manuscript

- The manuscript (*mss*) should be typed in double space leaving wide margins on both the sides.
- First page of mss should contain only the title of the paper, name(s) of author(s) and name and address of Organization(s) where the work has been carried out along with the affiliation of the authors.

Continued on back inner cover...

Nature Environment and Pollution Technology

Vol. 20, No. (2), June 2021

CONTENTS

The Journal is Currently Abstracted and Indexed in:

International Scientific Indexing (UAE) with Impact Factor 2.236 (2018)

NAAS Rating of the Journal (2019) = 3.85

Scopus®, SJR (0.127) 2019

Index Copernicus (2018) = 135.97

EI Compendex of Elsevier

Indian Science Abstracts, New Delhi, India

Chemical Abstracts, U.S.A.

Pollution Abstracts, U.S.A.

Elsevier Bibliographic Databases

Paryavaran Abstract, New Delhi, India

Zoological Records

Indian Citation Index (ICI)

Scopus CiteScore (2019) = 0.5

Electronic Social and Science Citation Index (ESSCI)

EBSCO: Environment Index™

Ulrich's (Refereed) database

CrossRef (DOI)

DOAJ

Zetoc

Google Scholar

ProQuest, U.K.

J-Gate

Environment Abstract, U.S.A.

British Library

Centre for Research Libraries

WorldCat (OCLC)

JournalSeek

Connect Journals (India)

CSA: Environmental Sciences and Pollution Management

Research Bible (Japan)

Indian Science

Geobase

Elektronische Zeitschriftenbibliothek (EZB)

SHERPA/RoMEO

Directory of Science

CNKI Scholar (China National Knowledge Infrastructure)

Access to Global Online Research in Agriculture (AGORA)

AGRIS (UN-FAO)

Present in UGC-CARE List (Group II)

UDL-EDGE (Malaysia) Products like *i*-Journals, *i*-Focus and *i*-Future

www.neptjournal.com

Nature Environment and Pollution Technology

Nature Environment and Pollution Technology
An International Quarterly Scientific Journal

p-ISSN: 0972-6268
(Print copies up to 2016)
e-ISSN: 2395-3454

Vol. 20 | No. 2 | pp. 447-458 | 2021

Original Research Paper

https://doi.org/10.46488/NEPT.2021.v20i02.001

Open Access Journal

Simulation and Prediction of Zhuzhou Urban Wetland Landscape Pattern Based on LCM Model

Wen Zhan*, Huifeng Cheng† and Shouyun Shen***
*Central South University of Forestry and Technology, Changsha 410004, China
**Changsha Environmental Protection College, Changsha 410018, China
†Corresponding author: Huifeng Cheng; t20050233@csuft.edu.cn

Nat. Env. & Poll. Tech.
Website: www.neptjournal.com

Received: 18-03-2020
Revised: 08-06-2020
Accepted: 15-06-2020

Key Words:
Urban Wetland
LCM
Landscape pattern
Land use change

ABSTRACT

The urban wetland is a precious wealth of the city, which has a very important role and value for the development of human and society. Zhuzhou is a traditional industrial city in China, which is located in the lower reaches of the Xiangjiang River and rich in urban wetland resources. In order to protect, utilize and manage urban wetland resources scientifically, based on LCM model platform, using Landsat series remote sensing images and other data, this paper systematically analyses the land use change process of Zhuzhou urban wetland from 2006 to 2016 and simulates and forecasts the urban wetland landscape pattern in 2021. The prediction results show that the urban wetland in Zhuzhou city will change continuously in 2021, but the overall change is relatively small, which is basically consistent with the change trend and regain of urban wetland in 2006~2016. Among them, the change of paddy fields area is the largest, with a total decrease of 1364.8ha; the increase of reservoirs area is 82.4ha; the decrease of pond area is 34.6ha, while riverine wetland is basically unchanged. In addition, Zhuzhou urban wetland landscape pattern change is affected by both natural and human factors, while human activities have a more significant impact on the wetland, with both positive and negative effects.

INTRODUCTION

Throughout the ages, human beings live by the water, and cities are built by the water. Wetland provides water for urban production and life and creates a harmonious and comfortable living environment for people. Zhuzhou city is located in the lower reaches of Xiangjiang River system in Hunan Province, China. As one of the first eight key industrial cities, Zhuzhou urban wetland has been seriously affected, especially the area and quantity of wetland has been shrinking, because of the huge consumption of natural resources due to the traditional industrial characteristics dominated by the heavy chemical industry for a long time. In the 21st century, Zhuzhou has stepped into a new process of rapid urbanization, becoming an important part of China's "two type construction demonstration area" - Changsha Zhuzhou Xiangtan City Group. Urban development and construction are also actively undergoing transformation and upgrading. The land use presents a new development trend and spatial layout, and the urban wetland landscape pattern changes accordingly. Therefore, it is of great significance for the scientific protection, utilization and management of Zhuzhou urban wetland resources and the revelation of the law of urban land use change to analyze the temporal and spatial change characteristics of urban wetland landscape pattern and carry out future scenario simulation.

At present, there is no scientific definition of the concept of urban wetland in a strict sense. The academic community generally believes that urban wetland refers to the ecological system with transitional nature of land and water in the urban area, such as coast and estuary, river bank, shallow water marsh, water source protection area, natural and artificial pond, and wastewater treatment plant (Wang & Lv 2007), which is the complex of artificial wetland, semi-artificial wetland and natural wetland. Relevant researches on urban wetland at home and abroad are mainly focused on wetland dynamic pattern research (He et al. 2020, Qin et al. 2020, Liu 2011, Gong et al. 2011, Kong et al. 2012, Gong 2013), wetland ecosystem service function and value evaluation research (Bernard et al. 2020, Chen & Yang 2012, Vileisis 1997, Xie et al. 2006, Wang et al. 2010, Pang 2014, Gao et al. 2017, Yang et al. 2017), wetland ecological restoration and technology research (Eric et al. 2020, James & Greg 2007, Cui & Yang 2001, Xu & Huang 2010, Tuo 2002, Shen 2003), wetland protection and management research (HAO et al. 2019, Wang et al. 2019, Zhan et al. 2012), etc.

Generally speaking, the evolution of urban landscape pattern is mainly reflected in land use/land cover change (LUCC) (Turner et al. 1995). The urban wetland is not only a type of urban landscape but also a way of urban land use. Wetland use characteristics directly reflect the

nature and process of human activities' interference on urban wetland ecosystem and can be used as the main sign of wetland ecosystem landscape pattern characteristics (Fu 2001). Therefore, it is of great practical value to analyze the characteristics of urban wetland use change and make scenario analysis and simulation prediction of its future development trend (Wu et al. 2013). At present, many kinds of LUCC simulation and prediction models have been applied in landscape pattern research and practice. According to different research objects, theoretical basis and technical methods, there are mainly the following types: Optimization model (Rounservell 2000), System Dynamics model (Muller & Zeller 2002), Cellular Automata model (Jantz et al. 2010, Guan et al. 2011, He et al. 2011, Zheng et al. 2010, Li & Yeh 2002, Torrens & O'Sullivan 2001), Multi-Agent model (Mase 1995), Integrated model, etc. Among them, the Integrated model combines different model technologies, integrates different model methods, and seeks the most appropriate simulation solutions for different problems. This kind of model is relatively more scientific, easy to operate, easy to dynamic control, more in line with reality. The main models widely used include Clue (Veldkamp & Fresco 1996), Clue – s (Luo et al. 2010, Zheng et al. 2012, Li et al. 2011, Zhou et al. 2012), LCM (Amir & Mohammad.2019, Chen et al. 2019, Liu et al. 2017, Mishra et al. 2014, Su et al. 2018, Wei 2015, Yang 2012), etc.

Based on the above background, this study relies on LCM model platform, using Landsat series remote sensing image data, socio-economic multi-source data, analyses the spatial and temporal changes and influencing factors of Zhuzhou urban wetland from 2006 to 2016, and simulates and forecasts the urban wetland landscape pattern in 2021. It is hoped to provide scientific reference for Zhuzhou city planning, macro policy making and sustainable development of urban wetland.

MATERIALS AND METHODS

Research Area Overview

Zhuzhou city is located in the lower reaches of the Xiangjiang River, in the east of Hunan Province, China. As of 2016, Zhuzhou has a total area of 11247.55 km^2. The urban area is about 853.4 km^2, and the built-up area is 142 km^2. The urban area has a permanent population of about 780,000, which governs four administrative areas (Fig. 1): Tianyuan District, Lushong District, Hetang District and Shifeng District. This paper takes Zhuzhou urban wetland as the research object, selects Zhuzhou urban area in 2016 as the specific research scope, covering the existing central urban area and built-up area.

Data Source and Preprocessing

Research data source

The research data in this paper mainly includes image data, basic data and statistical data. Among them, the Landsat series remote sensing image data (30M) and DEM data in 2006, 2011 and 2016 are from the geospatial data cloud platform of the computer network information centre of the Chinese Academy of Sciences (http://www.gscloud.cn); Zhuzhou city administrative boundary (2016) and Zhuzhou

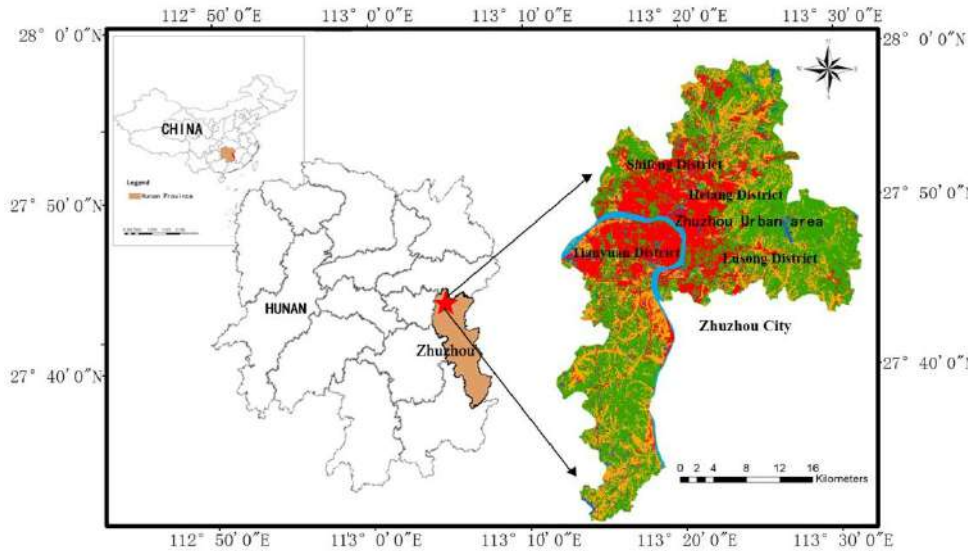

Fig. 1: Location of the study area.

wetland census patch data (2010) are provided by Zhuzhou Forestry Bureau; the statistical data (2006~2016) are from Zhuzhou Statistical Years; the data of water resources (2006~2016) are from Zhuzhou Water Resources Bulletin. In addition, Zhuzhou City Master Plan (2006~2020) and Zhuzhou City land use status map are provided by Zhuzhou City Planning and Design Institute; Google HD satellite map of Zhuzhou City (2006~2016) is downloaded from the internet with 91 satellite map assistant software.

Classification of Urban Wetland Landscape

Based on the Ramsar Convention and the current urban land classification standard of the wetland classification system in China, Zhuzhou urban wetland landscape is divided into two categories and five sub categories, and the construction land and woodland are included in the classification system as non-wetland landscape (Zhan et al. 2020). The specific classification and description is shown in Table 1.

Data Interpretation

In this paper, Envi5.3, ArcGis10.4 and other spatial analysis and processing platforms are used to preprocess all remote sensing images. Ecognition software is used to segment the processed remote sensing images in multi-scale and spectral difference, to realize the preliminary classification of Zhuzhou wetland landscape, and human-computer interactive interpretation combined with artificial visual interpretation. Finally, the accuracy of all remote sensing images is above 80%, which meets the accuracy of medium resolution remote sensing images and the requirements of this study (Fig. 2).

Research Methods

Land Change Modeler for Ecological Sustainability (LCM) is a software platform integrating remote sensing image processing and geographic information system software Terr Set. It is a software model developed by Clark lab and Conservation International for many years. It integrates MLP-ANN, Logistic Regression, Markov Chain/External Matrix model, Soft and Hard prediction and a series of models, which are suitable for the context analysis of various land changes.

Main process of LCM model prediction: Firstly, based on the multi-source wetland information data of Zhuzhou city and the remote sensing image interpretation map of urban wetland in 2006, 2011 and 2016, the LCM model platform is used to analyze the structure and spatial change of wetland land, and the influencing factors of wetland land change are preliminarily selected. Then with the help of 2006 and 2011 wetland remote sensing image interpretation map, taking Zhuzhou City Master Plan (2006~2020) as the potential impact of intervention changes, the LCM platform is used to build the transformation potential model, determine the land change impact factors, and simulate the urban wetland land use change in 2016. Next, the simulation results are compared with the actual distribution map of Zhuzhou urban wetland in 2016 to verify and improve the accuracy of LCM model construction. Finally, based on the remote sensing images of 2011 and 2016, the tested and improved LCM model is applied to simulate and predict the land use change of Zhuzhou urban wetland in 2021, and the final research results are obtained after analysis and calculation (Fig. 3).

Table 1: Classification of urban wetland in Zhuzhou city.

Category	Primary type	Secondary type	Description
Urban wetland	Natural wetland	Riverine wetland	Permanent river, including rivers and their tributaries, stream, waterfall seasonal (with seasonal attributes) or intermittent (no obvious seasonal dependence)rivers, streams, floodplains(refers to the flood of floodwaters on both sides of the river）
	Artificial wetland	Reservoirs	Reservoir, lake, barrage, water storage area formed by dam, park wetland
		Pond	Agricultural pond, water storage pond，Aquatic ponds such as fish and shrimp culture and small landscape water bodies
		Paddy fields	Rice fields, lotus, water bamboo fields, etc.
		Wastewater treatment plant	Sewage plant, treatment pool, oxidation pool, etc.
Non Urban wetland	Construction land		The land for the construction of buildings and structures is for urban and rural housing, public facilities, industrial and mining land, energy, transportation, water conservancy, communications and other infrastructure.
	Woodland		All the land for trees, bamboos, shrubs and ground covers.

Note:
(1) In this study, a riverine wetland refers to a natural river with an average width of more than 30m and a length of more than 5km.
(2) In this study, reservoirs wetland is more than 8ha artificial water body, while the pond wetland is less than 8ha artificial water body.
(3) Hunan Province is one of the main rice producing areas in China. In this paper, there are large areas of paddy fields, which play an important role in the Zhuzhou urban ecosystem. Therefore, paddy fields are one of the main types of urban wetland research in this paper.

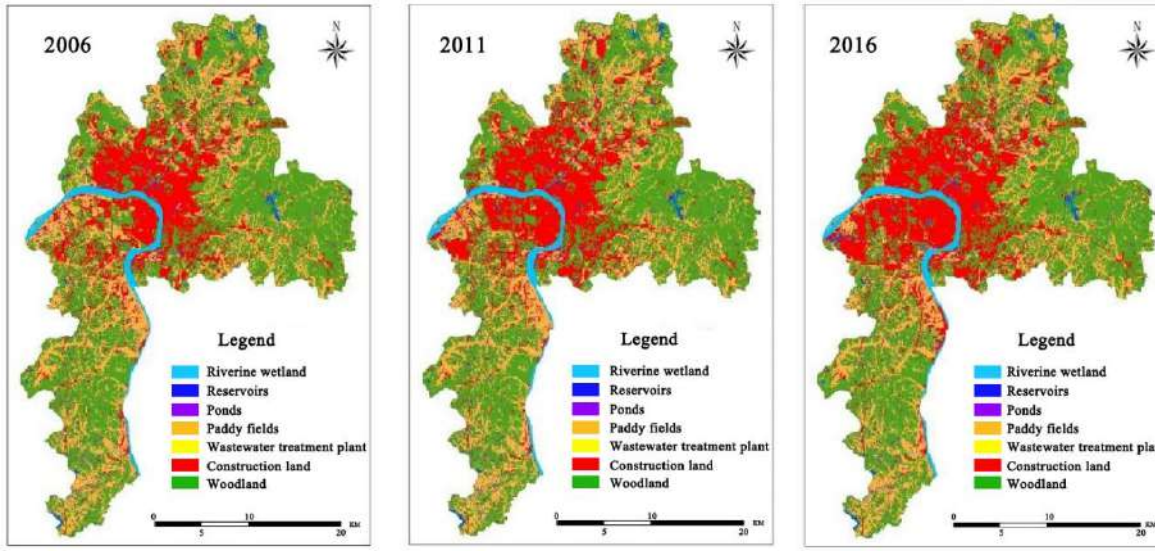

Fig. 2: Classification map of an urban wetland landscape in Zhuzhou city in 2006, 2011 and 2016.

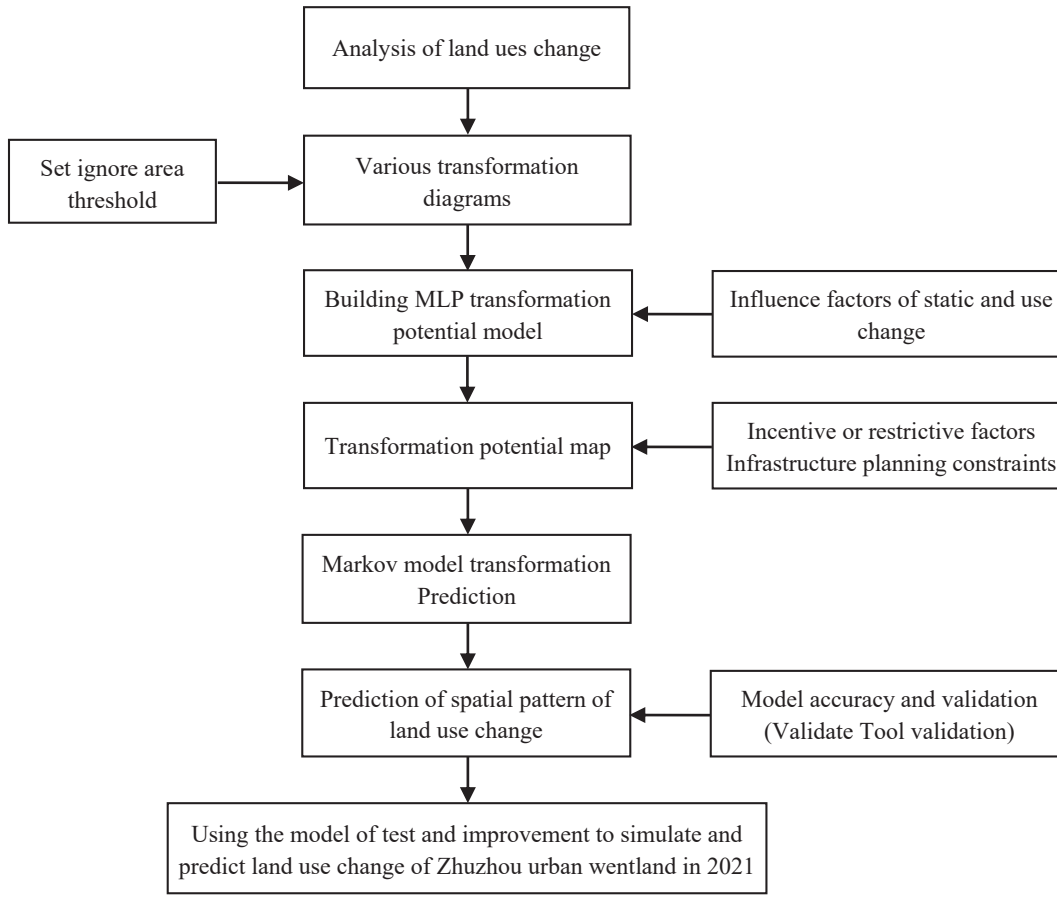

Fig. 3: Schematic diagram of LCM model construction process.

Key to LCM Model Construction

Determine the influencing factors of urban wetland land use change. Index analysis method is used to verify the relevance, and Cramer'v index value is selected for index quantitative evaluation. The calculation formula is as follows:

$$\text{Cramer's V} = \sqrt{\frac{x^2}{nxmin[(r-1),(s-1)]}} \quad \ldots(1)$$

In the formula, X^2 represents chi-square test results, R and S represent the number of rows and columns respectively, and N represents the number of samples. Cramer's V is 0.15 or a little higher, indicating that the influencing factor has a good correlation with the land use change; Cramer's V is 0.4 or a little higher, indicating that the influencing factor has a good correlation with the land use change.

Build MLP model of urban wetland transformation potential. MLP-ANN and Logistic Regression were used to construct and transform the model, and the potential index of model variables was calculated.

Markov Chain model was used to predict the variation of land use transformation in urban wetland potential transformation map, and the transformation probability matrix of urban wetland land was obtained.

Validate tool is used to test the modified Soft and Hard prediction model and obtain the prediction map of the spatial pattern change of urban wetland. Among them, the Hard prediction model results in the prediction map of urban wetland land use change. The results of the Soft prediction model are the distribution map of the vulnerability of urban wetland land use change. However, the distribution map does not show the specific result of land change, but indicates the degree of change of extremely changing areas, which is a change trend set of all selected transitions.

RESULTS AND ANALYSIS

Analysis of Wetland Land use in Zhuzhou City from 2006 to 2011 and 2011 to 2016

The land use of urban wetland reflects not only the basic relationship between wetland and urban land use change, but also the succession relationship of urban wetland landscape pattern and its interaction with urban development. In this study, the basic data and spatial changes of Zhuzhou urban wetland in 2006, 2011 and 2016 are obtained by using multi-source data and LCM platform, as shown in Table 2, Fig. 4 and Fig. 5.

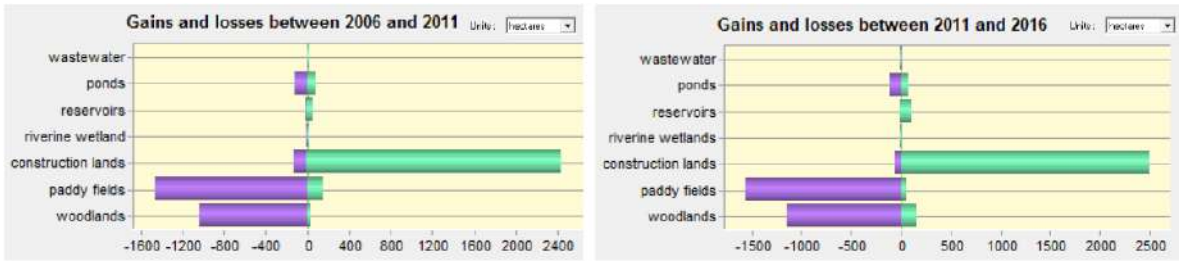

Fig. 4: Gain and loss of Wetland Land in Zhuzhou city during 2006~2011 and 2011~2016.

Table 2: Changes of Wetland Land in Zhuzhou city from 2006 to 2016.

Category	Land type	Area（ha）			Variation and range	
		2006	2011	2016	Variation in 2006-2016 (ha)	The rate of five-year dynamic change in 2006-2016 (%)
Wetland type	Riverine wetland	2216.7	2215.0	2208.9	-7.8	-0.18
	Reservoirs	474.8	527.0	619.6	144.8	15.25
	Pond	2346.5	2302.2	2262.5	-84.0	-1.80
	Paddy fields	22648.0	21332.9	19819.9	-2828.1	-6.25
	Wastewater treatment plant	4.1	4.4	12.2	8.1	98.78
	subtotal	27690.1	26381.4	24923.1	-2767	-5.00
Non Wetland type	Construction land	14952.7	17277.1	19724.2	4771.5	15.96
	Woodlands	43456.0	42440.3	41445.5	-2010.5	-2.31
	subtotal	58408.7	59717.4	61169.7	2761	2.36
Wetland rate		32.16%	30.64%	28.95%	3.21%	-

The results show that:

1. From the perspective of land use area changes, from 2006 to 2016, Zhuzhou urban wetland mainly changed from artificial wetland land to construction lands, while there was a small amount of mutual transformation between various types of artificial wetlands, and a small amount of non wetland land to artificial wetland. Among them, the change of paddy fields area is the largest, with a total decrease of about 2828.1 ha, with a five-year dynamic rate of 6.25%; the cumulative increase of reservoirs wetland area is about 144.8 ha with a five-year dynamic rate of 15.25%; the mutual increase and decrease of pond wetland area, with a total decrease of about 84 ha, with a five-year dynamic rate of 1.80%; the increase and decrease of riverine wetland and wastewater treatment area are relatively small. However, the dynamic degree of five-year change of wastewater treatment plant area is the highest among all wetland types, reaching 98.78%. In addition, the change of construction land area is the largest among all land types, with a cumulative increase of about 4771.5 ha, and its five-year dynamic rate of change is 15.96%; the same change of woodland area is more, with a cumulative decrease of about 2010.5 ha, and its five-year dynamic rate of change is 2.31%.
2. From the perspective of various land use spatial changes (Fig. 5), during 2006~2016, Zhuzhou urban wetland land use changes were mainly concentrated in the outskirts of the urban built-up area, and extended to the north and south with the main urban area as the centre, with Tianyuan District as the key change area, and there were some changes in Shifeng District, Lusong District and Hetang district. Among them, the change of land use in reservoirs wetland area is concentrated in Tianyuan District and Hetang District, which is mainly transferred from paddy fields and pond wetland, in the form of urban wetland park; the change of paddy fields is mainly concentrated in Tianyuan District, Shifeng District and Lusong District, which is mainly converted into construction land; the change of pond wetland is mainly concentrated in Tianyuan District and Shifeng District, which is mainly converted into construction land. In addition, the spatial change of riverine wetland and wastewater treatment plant is very small, which can be ignored.

Influencing Factors of Urban Wetland Change in Zhuzhou City

Using ArcGIS 10.4 software and Cramer's V index value calculation, combined with multi-source data, this study has determined five types of urban wetland impact factors: elevation, slope, distance from the public and commercial centre, distance from the centre of human disturbance and distance from the main road. The correlation verification results are as follows (Fig. 6): the Cramer's V of elevation is 0.1663; the Cramer's V of the slope is 0.1703; the Cramer's V of distance from the public and commercial centre is 0.0951; the Cramer's V of distance from the centre of human disturbance is 0.0851; the Cramer's V of distance from the main road is 0.0965.

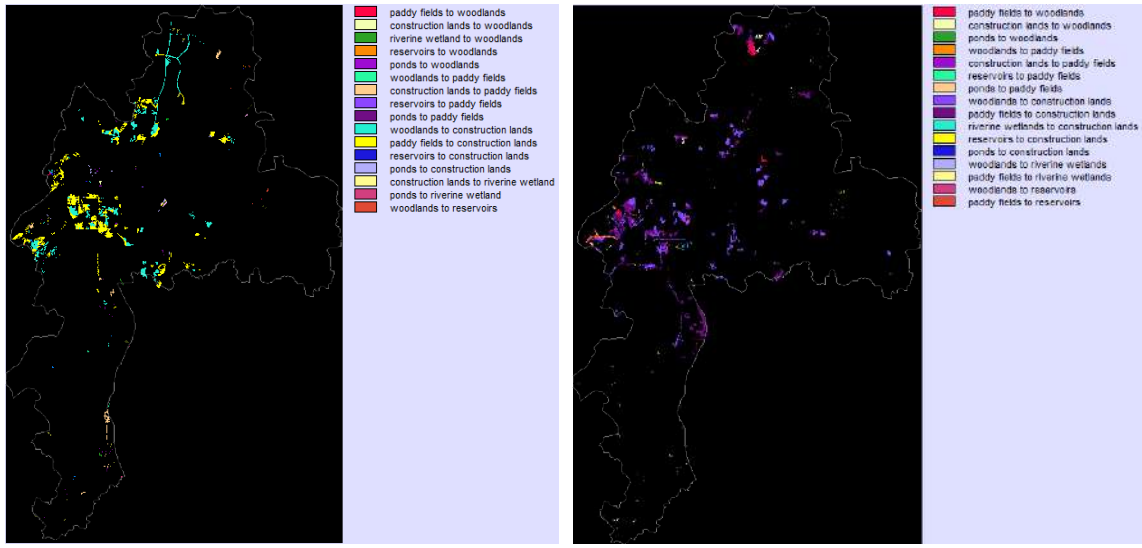

Fig. 5: Land use spatial change map of Zhuzhou city in 2006-2011 and 2011-2016.

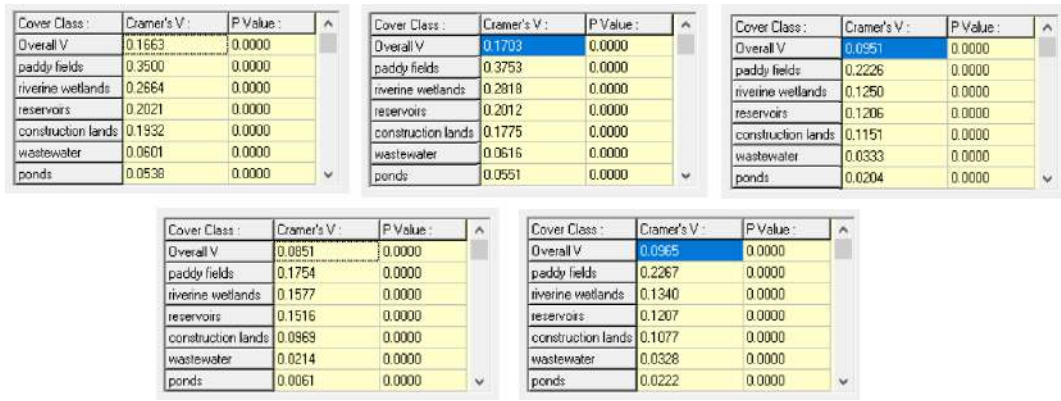

Cover Class :	Cramer's V :	P Value :
Overall V	0.1663	0.0000
paddy fields	0.3500	0.0000
riverine wetlands	0.2664	0.0000
reservoirs	0.2021	0.0000
construction lands	0.1932	0.0000
wastewater	0.0601	0.0000
ponds	0.0538	0.0000

Cover Class :	Cramer's V :	P Value :
Overall V	0.1703	0.0000
paddy fields	0.3753	0.0000
riverine wetlands	0.2818	0.0000
reservoirs	0.2012	0.0000
construction lands	0.1775	0.0000
wastewater	0.0616	0.0000
ponds	0.0551	0.0000

Cover Class :	Cramer's V :	P Value :
Overall V	0.0951	0.0000
paddy fields	0.2226	0.0000
riverine wetlands	0.1250	0.0000
reservoirs	0.1206	0.0000
construction lands	0.1151	0.0000
wastewater	0.0333	0.0000
ponds	0.0204	0.0000

Cover Class :	Cramer's V :	P Value :
Overall V	0.0851	0.0000
paddy fields	0.1754	0.0000
riverine wetlands	0.1577	0.0000
reservoirs	0.1516	0.0000
construction lands	0.0969	0.0000
wastewater	0.0214	0.0000
ponds	0.0061	0.0000

Cover Class :	Cramer's V :	P Value :
Overall V	0.0965	0.0000
paddy fields	0.2267	0.0000
riverine wetlands	0.1340	0.0000
reservoirs	0.1207	0.0000
construction lands	0.1077	0.0000
wastewater	0.0328	0.0000
ponds	0.0222	0.0000

Fig. 6: Test explanatory power of elevation, slope, distance from public and commercial service centres, distance from main disturbance centres and distance from main roads.

The results of the above five kinds of factors showed that elevation, slope, distance from the public and commercial centre, distance from the centre of human disturbance, distance from the main road were all related to the land uses change of Zhuzhou urban wetland. Among them, the natural factors (elevation, slope) have a strong correlation, while the human factors (distance from the administrative and commercial centre, distance from the human disturbance centre, distance from the main road) have a relatively weak correlation.

Construction of Transition Potentials Model

Using LCM model platform, the sub-models of riverine wetland use change, reservoirs land use change, ponds land use change, paddy fields land use change, woodland land use change and construction land use change are combined to model transformation potential. After analysis and calculation, 21 maps of transformation potential of various classes are obtained, some of which are shown in Fig. 7 and Fig. 8. In these maps, the value of colour increases with the change from cold colour to warm colour, which indicates that the potential of one type of land to another is greater. After a comprehensive analysis of all the transformation potential maps, the results show that: the closer to the central urban area, the higher the transformation potential of all kinds of urban wetlands in Zhuzhou city, especially in the flat area, the greater the transformation potential of pond and paddy fields to construction land; the lower the transformation

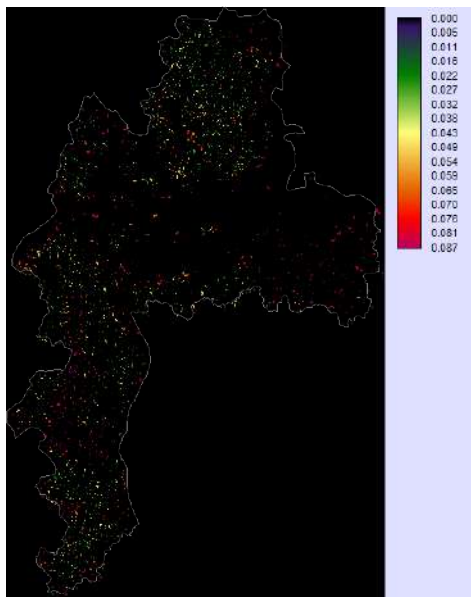

Fig. 7: Transition of pond into construction land potential.

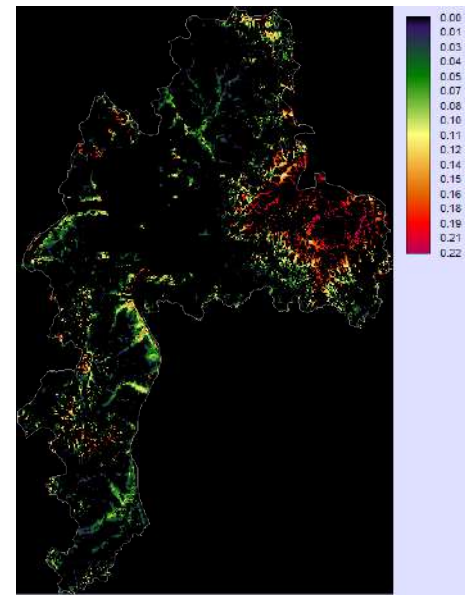

Fig. 8: Transition of paddy fields into construction land potential.

potential of wetlands in the peripheral area of the city, especially in the mountainous area with a large slope, the lower the transformation potential of all kinds of wetlands; the potential of intertype transformation is generally low, but the potential of transformation from a small number of regional ponds and paddy fields to reservoirs areas is large.

Simulation Prediction and Result Test of Urban Wetland Land Use Change in 2016

In the LCM platform, Markov Chain method is applied to calculate the transformation probability matrix of the urban wetland land transfer changes in 2016, and the probability matrix results (Table 3) are obtained, which reflect the transformation probability matrix between various types of land. Using the result and the Hard prediction model, we can finally generate the prediction map of urban wetland land use in Zhuzhou city in 2016.

In order to verify and provide the accuracy of LCM construction, this study uses validate tool to compare the prediction map of wetland land use in Zhuzhou city in 2016 with the current map of wetland land use in Zhuzhou city. The validate tool classifies the capacity of maintaining land use type area (maintaining quantity consistency) in LCM modelling into three categories: none (no [n]), complete (perfect [P], medium [M]). Based on the traditional kappa coefficient formula, four kinds of kappa expansion indexes are generated by adding spatial information parameters: random Kappa index (kno), location Kappa index (klocation), hierarchical location Kappa index (klocation strata), and standard Kappa index (kstandard). The test results (Fig. 9) show that: the comprehensive index of kapps coefficient of all the tested is higher than 0.8, the consistency of the two comparison drawings is high, the difference is small, and the simulation and prediction effect is good. It is predicted

Table 3: Probability matrix of land class transformation.

Given:	Probability of changing to:						
	Riverine wetlands	Reservoirs	Ponds	Paddy fields	Wastewater treatment plant	Woodlands	Construction land
Riverine wetlands	0.9965	0.0000	0.0000	0.0000	0.0000	0.0135	0.0000
Reservoirs	0.0000	0.9700	0.0117	0.0134	0.0000	0.0030	0.0419
Ponds	0.0015	0.0865	0.9501	0.3123	0.0005	0.0235	0.2260
Paddy fields	0.0000	0.0518	0.0420	0.9354	0.0000	0.0201	0.2606
Wastewater treatment plant	0.0000	0.0000	0.0000	0.0000	1.0000	0.0000	0.0000
Woodlands	0.0000	0.1532	0.2244	0.0131	0.0000	0.9760	0.3233
Construction land	0.0002	0.0325	0.0264	0.0076	0.0000	0.0508	0.9913

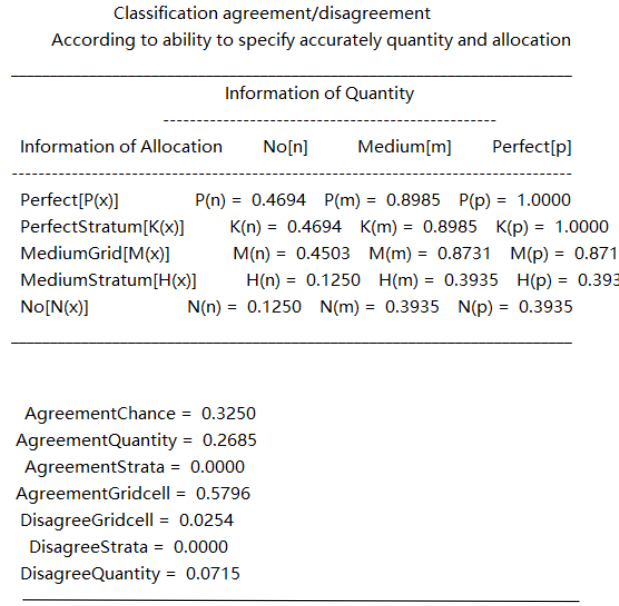

Fig. 9: Validation of urban wetland land use change prediction in 2016.

that the LCM model of Zhuzhou Urban Wetland in 2016 is effective and up to standard.

Simulation and Prediction of Land Use Change of Urban Wetland in 2021

Based on the remote sensing image interpretation map of Zhuzhou city in 2011 and 2016, this paper uses the LCM to simulate and predict the urban wetland land use change in 2021, and finally obtains the land use change prediction map (hard prediction map) and vulnerability distribution map (soft prediction map) of Zhuzhou city in 2021 and relevant data (Table 4, Fig.10, Fig.11), among which the hard prediction map is a wetland land use map with the same classification as the input data; the soft prediction map is a continuous map showing the vulnerability of urban wetland land use in 2021, which does not indicate what will change but indicates the extent of urban wetland land use in areas with rapid changes.

The prediction results in 2021 show that the overall change of Zhuzhou urban wetland is relatively small compared with 2016. Among them, the area of riverine wetland remained unchanged basically; the area of reservoir area increased by 82.4 ha in total, with a five-year dynamic rate of 9.75%, mainly distributed in Shifeng District in the north of urban area; the area of pond wetland increased or decreased with a total of 34.6 ha, with a five-year dynamic rate of 1.53%; the area of paddy fields still decreased the most, with a total of 1364.8 ha and a five-year dynamic rate of change of 6.89%, mostly concentrated in the outskirts of the central city, mainly converted into construction land, but the analysis found that the basic farmland is still well protected and controlled. In addition, urban construction land is further expanded from the central urban area to the surrounding areas, especially in the north and east of the urban area, with a cumulative increase of 2289.3 ha and a five-year dynamic rate of 11.61%.

CONCLUSION AND DISCUSSION

(a) At present, "Urban Wetland" does not have a completely scientific and recognized concept, but the research on urban wetland has been one of the hot spots in the academic circle. In this paper, referring to domestic and foreign practices and current standards, combined with the current situation of Zhuzhou wetland, the urban wetland is divided into riverine wetland, reservoirs, pond, paddy fields, wastewater treatment plant and other

Table 4: Table of predicted changes of Urban wetland land in Zhuzhou city from 2016 to 2021.

Category	Land type	Variation and range			
		2016	2021	Variation in 2016~2021(ha)	The rate of five-year dynamic change in 2016-2021(%)
Wetland type	Riverine wetland	2208.9	2219.1	10.2	0.46
	Reservoirs	619.6	680.0	60.4	9.75
	Pond	2262.5	2227.9	-34.6	-1.530
	Paddy fields	19819.9	18455.1	-1364.8	-6.89
	Wastewater treatment plant	12.2	13.8	1.6	13.11
	subtotal	24923.1	23595.9	-1327.2	-5.33
Non Wetland type	Construction land	19724.2	22013.5	2289.3	11.61
	Woodlands	41445.5	40535.3	-910.2	-2.20
	subtotal	61169.7	62548.8	1379.1	2.26
Wetland rate		28.95%	2671%	2.24%	-

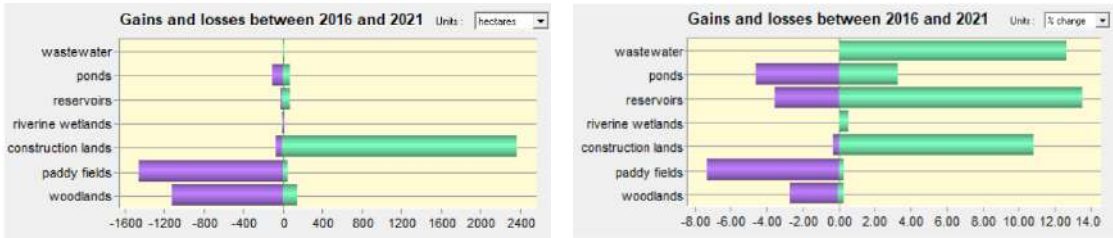

Fig.10: Gain and loss and proportion change of Zhuzhou urban wetland in 2016~2021.

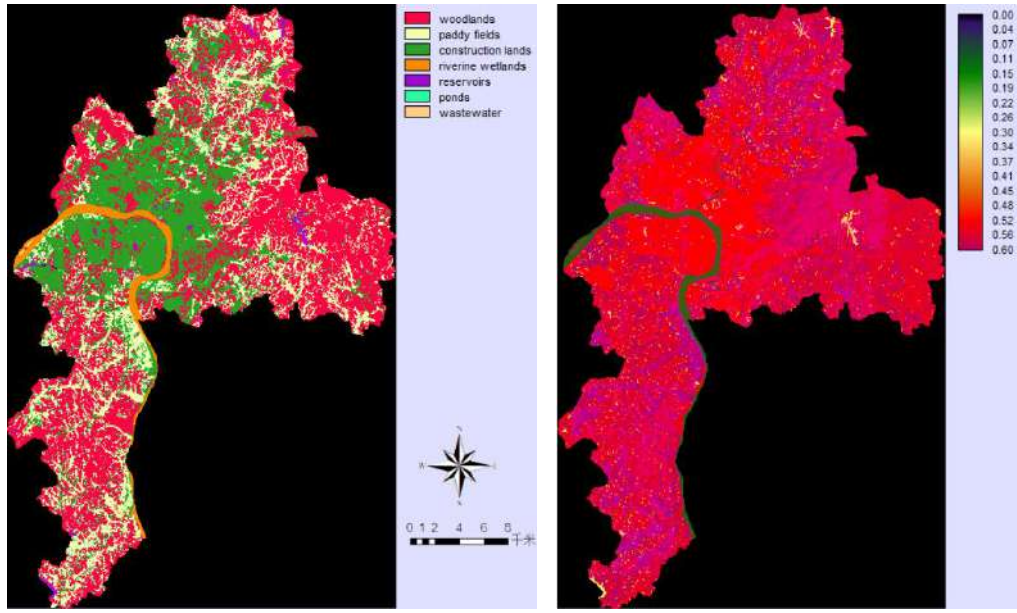

Fig. 11: Change hard and soft prediction of urban wetland land use in Zhuzhou City in 2021.

types to carry out relevant research, which has certain theoretical and practical reference value.

(b) Through the analysis and research on the land use change of urban wetland in Zhuzhou city from 2006 to 2016, the results show that: on the one hand, the overall spatial layout and area of Zhuzhou urban wetland have remained relatively stable in the past decade, most of the change areas are concentrated in the periphery of the central urban area, mainly from the artificial wetland to the construction land; on the other hand, during the period of 2006~2016, Zhuzhou's urbanization process has been intensified, and a large number of ponds and paddy fields in suburban areas have changed into various types of urban construction land. In addition, the research results also reflect that Zhuzhou city is actively transforming and upgrading its urban development, and the construction of ecological civilization has achieved preliminary results: Xiangjiang River water resources have been gradually effectively protected, and the number of reservoirs and ponds represented by wetland parks has increased, and most of them are concentrated around the river, irrigation land and pool concentration areas. These analyses are basically consistent with the current situation of Zhuzhou's urban development.

(c) The simulation and prediction results of Zhuzhou urban wetland in 2021 are consistent with the overall change trend of the wetland from 2006 to 2016, and basically, conform to the Master Planning of Zhuzhou City (2006-2020) and the actual development direction. This shows that the research methods and achievements based on LCM can be used as auxiliary technical tools for urban master planning and urban wetland system planning, and provide scientific support for the overall protection and sustainable utilization of urban wetland resources.

(d) To some extent, the research results of Zhuzhou wetland land use change reflect the basic characteristics of urban wetland landscape pattern: the degree of landscape fragmentation and separation is large, and the diversity and evenness of landscape are poor. In addition, the evolution of wetland landscape pattern is driven by many natural and human factors, among which natural geographical conditions are one of the key factors affecting wetland land use, and human activities also have a huge impact on wetland land use, with both positive and negative effects. Therefore, it is necessary to monitor the wetland resources of Zhuzhou city (including wetland area, wetland spatial change, wetland environmental quality, wetland biodiversity, etc.) in a long-term and dynamic way, and master the driving force of urban wetland landscape evolution in an all-round way. At the same time, we can use the methods and results of this study, combined with the Zhuzhou city master plan, to determine the key areas of urban wetland construction in the future, and speed up the construction of wetland park and waterfront space.

(e) It is suggested to strengthen the protection and utilization of wetland in Zhuzhou from the urban planning stage. On the one hand, expand the control scope of the

existing urban blue line, bring important artificial wetlands into the blue line protection scope, and strengthen the social service function of urban wetland. On the other hand, the primary protection status of the Xiangjiang River is further emphasized. A buffer zone is set around the blue line to build protective green space and strictly control other construction. Furthermore, it is suggested to carry out the special planning of the Zhuzhou wetland system and incorporate it into the urban master plan, so as to realize the strategic goal of Zhuzhou's ecological civilization city construction.

(f) Due to the limitation of the original spatial resolution (30 × 30m) of the Landsat series remote sensing image, which is the basic data source used in this study, there are some limitations in the extraction of urban wetland information data, especially for some riverine wetlands whose average width of the water surface is less than 30m, which cannot be effectively identified. Therefore, it has a certain impact on the accuracy and effectiveness of the simulation prediction and result analysis of LCM. In the follow-up research, we can try to choose a higher resolution HD remote sensing image to solve such problems. In addition, as a kind of comprehensive model, the intelligent architecture of LCM needs to be improved, and the involvement of multi-source data information is also an important direction of model improvement.

FUNDING

This research is funded by the Research Foundation of Education Bureau of Hunan Province, China (Grant No. 14B196, 18C1802, XJT2015(291)-186); Key Project of Science and Technology plan of Hunan Province, China (Grant No. 2018NK2052).

ACKNOWLEDGMENTS

This study is supported by Hunan Education Department's "12th five-year plan" Key Discipline Funding Project (2011-76); The state forestry administration's 13th five-year key discipline.

REFERENCES

Amir Ansari and Mohammad, H. Golabi. 2019. Prediction of spatial land use changes based on LCM in a GIS environment for Desert Wetlands-A case study: Meighan Wetland, Iran. International Soil and Water Conservation Research, 7(1).

Bernard Ekumah, Frederick Ato Armah, Ernest K.A. Afrifa, Denis Worlanyo Aheto, Justice Odoiquaye Odoi and Abdul-Rahaman Afitiri 2020. Geospatial assessment of ecosystem health of coastal urban wetlands in Ghana. Ocean and Coastal Management, 193.

Chen, C. and Yang, Z. F. 2012. What are ecosystem services? Research review on the advances in evaluating urban wetland ecosystem profitabilities. Journal of Safety and Environment, 12(04): 147-154.

Chen, K. X., Cong, P. F., Lu, W. Z. and Qu, L. M. 2019. Comparison of the CA-Markov and LCM models in simulating wetland change in the Yellow River Delta. Journal of Geo-information Science, 21(12):1903-1910.

Cui, B.S. and Yang, Z. F. 2001. Research review on wetland ecosystem health. Chinese Journal of Ecology, (03): 31-36.

Eric, D., Stein, Cheryl, L., Doughty, Jeremy Lowe, Megan Cooper, Evyan Borgnis Sloane and Danielle Liza Bram 2020. Establishing targets for regional coastal wetland restoration planning using historical ecology and future scenario analysis: the past, present, future approach. Estuaries and Coasts, 42(2): 207-222.

Fu, B. J. 2001. Landscape Ecology and Application. Beijing: Science Press.

Gao, Y., Cui, L.J. and Wang, F. L. 2017. Evaluation of wetland ecosystem services based on big data. Water Resources and Hydropower Engineering, 48(09): 1-9+23.

Gong, Y. B. 2013. The spatial-temporal pattern evolution of wetland landscape an its driving mechanism in Changsha. Central South University of Foresty and Technology.

Gong, Z. N., Zhang, Y. R. and Gong, H. L. 2011. Evolution of wetland landscape pattern and its driving factors in Beijing.Journal of Geographical, 66(01): 77-88.

Guan, D. J., Li, H. F., Inohae, T., Su, W., Nagaie, T. and Hokao, K. 2011. Modeling urban land use change by the integration of cellular automaton and Markov model. Ecological Modelling, 222(20/21/22): 3761-3772.

HAO, S., Wang, C. L. and Lin, H.W. 2019. Design and assessment of biodiversity in urban wetland parks: Take Liupanshui Minghu National Wetland Park as an example. Acta Ecologica Sinica, 39(16): 5967-5977

He, D., Jin, F. J. and Zhou, J. 2011. The changes of land use and landscape pattern based on Logistic-CA-Markov Model -A Case Study of Beijing-Tianjin-Hebei Metropolitan Region. Scientia Geographica Sinica, 31(8): 903-910.

He, J. H., Pan, Y. and Liu, D. F. 2020. Analysis of the wetland ecological pattern in Wuhan City from the perspective of ecological network. Acta Ecologica Sinica, 40(11): 1-12.

James, S. B. and Greg, A. O. 2007. Modeling the hydrologic response of groundwater dominated wetlands to transient boundary conditions: Implications for wetland restoration. Journal of Hydrology, 332: 467-476.

Jantz, C. A., Goetz, S. J., Donato, D. and Claggett, P. 2010. Designing and implementing a regional urban modeling system using the SLEUTH cellular urban model. Computers, Environment and Urban Systems, 34(1): 1-16.

Kong, C. F., Wang, J. and Zhang, Y. 2012. Evolution of Wuhan urban wetlands landscape pattern and its driving mechanism. Acta Scientiarum Naturalium Universitatis Sunyatseni, 51(04):119-128.

Li, Y. Q., Deng, O. and Zhang, D. Y. 2011. Land use and ecosystem service value scenarios simulation in Dangjiangkou reservoir area. Transactions of the Chinese Society of Agricultural Engineering (Transactions of the CSAE), 27(5): 329-335.

Li, X. and Yeh, A. G. O. 2002. Neural-network-based cellular automata for simulating multiple land use changes using GIS. Int. J. Geograph. Inform. Sci., 16(4): 323-343.

Liu, G. 2011. The Research on the Landscape Successions and the Carbon Storage of Hong-Hu Wetland in China. Central South University of Foresty and Technology.

Liu, S. L., An, N. N., Yin, Y. J., Cheng, F. Y. and Dong, S. K. 2017. Landscape pattern analysis and prediction of land-use change in the Guangxi coastal area. Acta Ecologica Sinica, 37(18): 5915-5923.

Luo, G. P., Yin, C. Y. and Chen, X. 2010. Combining system dynamic model and CLUE-S model to improve land use scenario analyses at regional scale: A case study of Sangong watershed in Xinjiang, China. Ecological Complexity, 7(2): 198-207.

Maes, P. 1995. Modeling adaptive autonomous agents. In: C.G. Langton (Ed.), Artificial Life: An overview, The MIT Press, Cambridge, MA,135-162.

Mishra, V.N., Rai, P.K. and Mohan, K. 2014. Prediction of land use changes based on land change modeler (LCM) using remote sensing: a case study of Muzaffarpur (Bihar), India. Journal of the Geographical Institute" Jovan Cvijic", SASA, 64(1): 111-127.

Muller, D. and Zeller, M. 2002. Land use dynamics in the central highlands of Vietnam: a spatial model combining village survey data with satellite imagery interpretation. Agricul. Econom., 27(3): 333-354.

Pang, B. L. 2014. Study on reducing double counting in wetland ecosystem services valuation. Chinese Academy of Forestry.

Qin, P., Zhang, Z. H. and Liu, Q. 2020. Influences of anthropogenic disturbance on coastal urban wetland: taking Qingdao City for example. Urban Problems, 03: 4-12.

Rounservell M.D. 2000. Geographic Human Regionale. http://www.geo.ucl.ac.be/unites/geog/etudes/notes/web2134/geog2134.htm, 2000.01.20.

Shen, X. L. 2003. Ecological environment of East Lake: vicissitude and recovery. Environmental Science & Technology, (04): 24-26+65.

Su, Y. Q., Lai, R. W. and Luo, W.W. 2018. Dynamic change and prediction of land use in Jinjiang city based on LCM model. Forest Resources Management, (01): 96-102.

Torrens, P. M. and O'Sullivan, D. 2001. Cellular automata and urban simulation: where do we go from here. Environ Planning B: Plan Design, 28: 163-168.

Tuo, Y.M. 2002. Eutrophication of Dianchi and its trend and treatment. Environmental Science Survey, 21(1): 35-38.

Turner, H. B. L., Skole, D. and Sanderson, S. 1995. Land-use and land-cover change science/research plan. IGBP Report No.35 and HDP Report No.7. Stochkholm: IGBP.

Veldkamp, A. and Fresco, L. O. 1996. CLUE-CR: an intergrated multi-scale model to simulate land use change scenarios in Costa Rica. Ecological Modelling, 91(1/2/3): 231-248.

Vileisis, A. 1997. Discovering the unknown landscape: a history of America□s wetlands. Washington, D C. and Covelo, USA: Island Press.

Wang, F. Z., Zhou, Z. X. and Zheng, Z. M. 2010. Evaluation on non-use values of typical lake wetlands in Wuhan. Acta Ecologica Sinica, 30(12): 3261-3269.

Wang, L. H., Xu, S. W., Lin, H. W. and Wu, S. S. 2019. Comprehensive performance evaluation after completion of the urban wetland park: Case study of the Daguan wetland park in Guangzhou City. Acta Ecologica Sinica. 39(16): 6001-6016.

Wang, J. H. and Lv, X. G. 2007. Urban wetland: Its concept, ecological services and protection. Chinese Journal of Ecology, (04): 555-560.

Wei, L.S. 2015. Land use change prediction based on IDRISI-LCM model-case study of the Zhuanghe City. LiaoNing Normal University.

Wu, L., Hou, X. Y. and Xu, X. L. 2013. Land use and landscape pattern changes in coastal areas of Shandong province, China. Transactions of the Chinese Society of Agricultural Engineering, 29(05): 207-216+293.

Xie, G.D., Xiao, Y. and Lu, C. X. 2006. Study on ecosystem services: progress, limitation and basic paradigm. Chinese Journal of Plant Ecology, 30(2):191-199.

Xu, M. Q. and Huang, Y. Y. 2010. Restoration and reestablishment of the damaged ecosystem of inland waters. Acta Ecologica Sinica, 1185: 79-101.

Yang, L. T. 2012. Building and simulation of Fuzhou city land use change LCM model. Fujian Agriculture and Forestry University.

Yang, L., Kong, F. L. and Xi, M. 2017. Ecosystem services assessment of wetlands in Qingdao based on meta-analysis. Chinese Journal of Ecology, 36(04): 1038-1046.

Zhan, W., Shen, S. Y. and Liu, G. 2012. Studies of development modes of Honghu lake wetland tourism based on protecting its landscape characters. Journal of Central South University of Forestry & Technology. 32(02):131-135.

Zhan, W., Cheng, H. F. and Shen, S. Y. 2010. Evaluation of urban wetland ecosystem service value in Zhuzhou City. Nature Environment and Pollution Technology, 19(02): 453-467.

Zheng, Q. H., Luo, G. P. and Zhu, L. 2010. Prediction of landscape patterns in Ili River Delta based on CA Markov model. Chinese Journal of Applied Ecology, 21(4): 873-882.

Zhou, R., Su, H. L. and Wang, X. J. 2012. Simulation and accuracy assessment of village land use change based on CLUE-S model. Resources and Environment in the Yangtze Basin, 21(2): 174-180.

Zheng, X. Q., Zhao, L. and Xiang, W. N. A. 2012. Coupled model for simulating spatio-temporal dynamics of land-use change: A case study in Changqing, Jinan, China. Landscape and Urban Planning, 106(1): 51-61.

Nature Environment and Pollution Technology
An International Quarterly Scientific Journal

p-ISSN: 0972-6268
(Print copies up to 2016)
e-ISSN: 2395-3454

Vol. 20 | No. 2 | pp. 459-466 | 2021

Original Research Paper

https://doi.org/10.46488/NEPT.2021.v20i02.002

Open Access Journal

Model of Solid Waste Management (SWM) in Coastal Slum Settlement: Evidence for Makassar City

Nani Anggraini*†, Ramdiana Muis, Fitri Ariani***, Sattar Yunus**** and Syafri*****

* Department of Environmental Engineering, Universitas Bosowa, Makassar, 90231, Indonesia
**Department of Urban and Regional Planning, Universitas Muhammadiyah, Pare-Pare, 91131, Indonesia
***Department of Chemical Engineering, Universitas Bosowa, Makassar, 90231, Indonesia
****Department of Mechanical Engineering, Universitas Muslim Indonesia, Makassar, 90231, Indonesia
*****Department of Urban and Regional Planning, Universitas Bosowa, Makassar, 90231, Indonesia
†Corresponding author: Nani Anggraini; nani.anggraini@universitasbosowa.ac.id

Nat. Env. & Poll. Tech.
Website: www.neptjournal.com

Received: 21-04-2020
Revised: 27-05-2020
Accepted: 25-06-2020

Key Words:
Solid waste management
Slum area
Coastal settlement
Waste generation

ABSTRACT

Makassar City slum settlement has a complex solid waste management problem located in a coastal area, divided by canals, inhabited by middle-class people who live with limited environmental facilities, and some build semi-permanent houses on the sea. This study aims to investigate the solid waste management in coastal slum settlement including waste generation, storage, collection system also community lifestyle, and coastal settlement characteristics. The method used in this study was quantitative and qualitative. The result of the analysis shows that the volume of waste generation category was about 49.47% compost potential, 25.57% inorganic recycling potential, and 24.96% residue material. Solid waste management is not going well in this area where most of the households did not get access to the communal trash bin and collection route. Recommendations for the solid waste management model are given to overcome existing problems by onsite composting and selling waste online and offline, and small amounts of residual waste discharged to the final disposal.

INTRODUCTION

Indonesia is one of the developing countries in the world, which is an archipelago and Makassar City is a metropolitan city located on Sulawesi Island. Makassar has a strategic position as it is located between the south and north in the provinces of South Sulawesi. Thus, the rapid growth of urbanization and industrialization within the area is unavoidable, resulting in Makassar being an area of mixed commercial-residential industrial along with the problem of water, air and soil pollution, which in turn can disturb human health (Sattar et al. 2012, Sattar et al. 2019). This, of course, requires efforts to overcome (Rashid et al. 2014).

In general, Solid Waste Management (SWM) is one of the most popular urban environmental problems in many developing countries because of the increase in urban, economic and industrial activities, especially in fast population exploding countries like India and Indonesia (Nyakaana 1996, Ramesh et al. 2009, Sattar et al. 2014). Poor Municipal SWM practices can result in land, water, and air pollution, improper disposal leads to the spreading of diseases and unhygienic conditions besides spoiling the aesthetics (Kirpalani et al. 2005, Raharjo et al. 2018). Furthermore, a gradual increase in waste generation coupled with inadequate services for solid waste management (SWM) intensifies the problems related to SW. This escalating problem has crucial effects on the environment, threatening the health of humans as well as incurring economic, biological and environmental losses (Moftah et al. 2016). The cities in a developing country using 20-55% of their budget in solid waste management, only 40-80% of the waste is collected (Yavini & Musa 2013). The waste is transported to the final disposal site is just 63.9%, the remaining small portion is managed at the source and the majority of the remainder is not transported so that it ends in an empty land, waterways, water bodies, and around the streets, and settlements. For the city of Makassar, 1,000 tons of garbage per day is transported to the final disposal with an open dumping system, the remaining 450 tons per day is not managed or not transported. Households are the biggest waste producer, reaching 62.99% compared to other sectors such as trade and services, offices and others (Indonesian Ministry of Environment 2012).

Recorded that 75% of households in Indonesia are not accustomed to sort out waste. Currently, there are widespread environmental movements initiated by the private sector, academics, and the government but their value has not shown significant changes (Indonesian Ministry of En-

vironment 2012). When in fact, the separation of recyclable waste material would lead to a reduction in the quantity of solid waste (Sharma 2008). The fact, residents in villages or even sub-urban areas around 66.8% choose to burn waste and only 1.2% are recycled (Indonesian Ministry of Environment 2017). Another report suggested that this condition is exacerbated by the weak political power of those who realize the importance of environmental management. The struggle to preserve the environment is only supported by a small group of the middle class who lack political power in decision making, also stated that there were a few people who had knowledge but were still being environmentally unfriendly (Kutanegara 2014). So, what must be done is to build awareness, understanding, and community participation to behave in an environmentally friendly manner.

This study takes the area of research in the coastal settlements of Makassar city because it is one of the Waterfront Cities in Indonesia having many coastal settlements with a population of about 1,46 million people (Makassar Statistical Center 2019). Most of the coastal settlement in Makassar City was originally formed from the fisherman who utilizing marine resources as the source of life. However, dramatic city development transforms this settlement into slums with limited facilities of life, and one of their big problems is waste management.

Cambaya village is one of the slum settlements in the coastal area where some people build informal wooden houses over the sea with poor social services and amenities. This study was focused on waste management that takes place in this area. Solid Waste Management (SWM) defined as scientific disciplines related to generation control waste, storage, collection, transfer and transportation, and processing waste (Tchobanoglous 1993). The generation of solid waste depends on several factors such as lifestyle, habits of food, living standard, season, and commercial activities degree (Upadhyay et al. 2012). However, managing waste is a complex activity that required appropriate technical solutions, cooperation between all stakeholders, and adequate organization capacity (Marshal & Farahbakash 2013).

Slum area identical to low-class people where the highest fraction of waste from this area is organic waste (Thakuria 2009, Miezah et al. 2015). In addition, the composition of urban waste is changing with the increasing use of packing materials and plastics (Asnani 2006). Furthermore, parameters of solid waste management will be an efficient support tool for the comparison and selection of effective alternative management of solid waste management programs (Qdais et al. 1997, Chang & Davila 2008, Hancs et al. 2011). For this reason, it is necessary to collect and manage statistical data on waste management, which is usually inadequate, especially in developing countries (Buenrostro et al. 2001). Thus, a study on solid waste and its proper management to minimize its effect on the environment becomes of utmost importance. Therefore, this study tries to calculate the composition of waste, and divide it into potential components of compost, recycle, and residual waste. After that, community characteristics assessment survey was also conducted because participation from the community has a direct bearing on efficient SWM. The next stage was conducting an ongoing SWM assessment. In the absence of a basic facility of storage and collection of waste from source, communities are prone to dumping waste on the streets, open space, drains, and water bodies in the vicinity creating unsanitary situations (Asnani 2006). Finally, this study tries to give recommendations for the SWM model that can be applied.

MATERIALS AND METHODS

Study Area Description

Makassar city has many slum areas, but this study picked Cambaya Settlement because of its location on the coast, and it is divided by canals that drain water from large rivers in the upstream area. So, this area is a complex area for SWM research. Fig. 1 shows a map of Indonesia and the arrow is pointing to the location of Cambaya Village (5.110958 E,119.4248602 S). The village is situated close to the old city of Makassar. Fig. 2 displays the blow-up location of the slum area Cambaya that were divided into permanent and semi-permanent houses where some houses are built over the sea.

Survey of Waste Generation

This activity was conducted to calculate the volume, weight, and composition of waste generation from every household per day. This survey used the Indonesian National Standards (SNI) 19-3964-1994 concerning Methods for Taking and

Fig. 1: Location of the case study

Fig. 2: Blow up location of Cambaya slum area.

Measuring Samples of the Generation and Composition of Urban Waste. The digital scale and volume measurement tools were used. For the determination of samples, the calculation used are as below.

$$(K) = \frac{S}{n} \quad \ldots(1)$$

(S) = Number of People

(n) = Number of people per household

(S1) = proportion of the number of permanent housing/ high income households = 25%

(S2) = proportion of the number of semi-permanent housing/ moderate-income households = 30%

(S3) = proportion of the number of non-permanent housing/ low income households = 45%

The garbage from housing:

1. permanent = S1 x K
2. semi-permanent = S2 x K
3. non-permanent = S3 x K

An effective solid waste management model is needed through the evaluation of the characteristics and rate of the solid waste generation which is one of the important first steps towards effective solid waste management (Qu et al. 2009, Tiruneh et al. 2015. Truong et al. 2017).

Survey of Community Characteristics

Survey questionnaires were carried out to find out the community lifestyle who lived in Cambaya village, where education level, household size, and income are significant factors that influence household generation rate (Truong et al. 2017). Questionnaires were distributed to respondents who live in two types of houses (permanent and semi-permanent). The questionnaire asked about solid waste management activities (sorting, storage, collecting, and transportation) and their current behaviour.

Direct interviews also were conducted with housewives who become the women leader of the community to explore the waste generation daily from the households. The village chief was also asked about the activities of the people. The data analysis technique used is a qualitative descriptive analysis technique by tabulating primary data.

Mapping of Solid Waste Management

The overlay map was used in the mapping of spatial coverage for the garbage collection vehicle route and trash bin user area using the ArcGIS application.

RESULTS AND DISCUSSION

Settlement Characteristics

Some of the buildings were built over the land boundary. The street in this settlement is a narrow alley about 50 cm in width. This situation makes it difficult to do several activities including waste management. Visualization of house characteristics is shown in Fig. 3.

Table 1 illustrates the general characteristics of the community. Most of the respondents were female, as solid waste management encourages the participation of females. Most of the respondents have a low level of education and have below the regional minimum wage. This situation influences their attitude towards waste management. It can be seen from the amount of garbage around residential areas and water bodies. A study found that the reasons for the waste management cases were lack of information relating to health, low knowledge level, tradition, culture, and economic situation as well as low level of living standard (Shahmoradi & Rad 2009).

Waste Generation Result

Fig. 4 below describes the result of the waste generation survey of waste weight. From this survey, the average waste generation per household was 1.8 kg Organic Waste

Fig. 3: Settlement characteristics.

per day per household, and inorganic waste 1.31 kg per day per household.

The volume of waste generated in the Cambaya Coastal Area was dominated by 58% organic waste and 42% inorganic waste. Furthermore, from Table 2 it can be concluded that if the onsite waste processing is done (onsite composting and recycle), only 24.96% will be transported to the final disposal as residue. This waste was potentially thrown into the water bodies if there is no proper waste management. A study reported that Municipal Solid Waste (MSW) generally includes degradable (paper, textiles, food waste, straw, and yard waste), partially degradable (wood, disposable napkins, sludges) and nonbiodegradable (leather, plastics, rubbers, metals, glass, ash from fuel-burning like coal, briquettes, wood, electronic waste). Generally, Municipal Solid Waste is managed as a collection from the street and disposed of at landfills (Jha et al. 2008).

Table 1: Characteristics of communities.

Characteristics	Value (%)
Number of people per house	
6 people	15
5 people	39
4 people	20
Others	26
Livelihood	
Fishermen	35
Labourer	41
Others	24
Income per month	
IDR 1,000,000-2,000,000*	50
IDR 2,000,000-3,000,000	20
Others	30
Education	
Elementary School	53
Junior High School	26
Others	21

*below the regional minimum wage

Storage System

The existing storage system was used as an individual, communal, and some of them throw trash directly into the water bodies (canal and sea) especially for those who live over the sea or in front of the canal. The communal trash bin is only in front of the main road as secondary solid waste storage, but most people use an individual

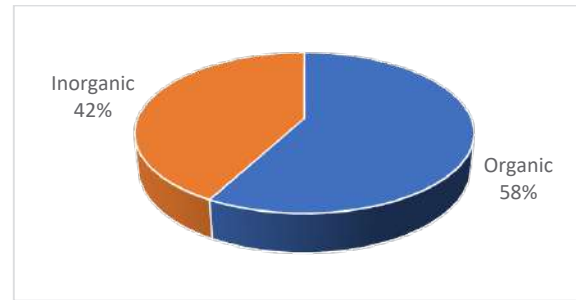

Fig. 4: Average percentage of the weight of organic and inorganic waste generation.

Table 2: Waste component calculation.

Type of Garbage	Value (%)	Explanation
Organic (Compost Potential)	49.47	Leftover, leaves, and twigs.
Inorganic (Recycling Potential)	25.57	*Paper, plastic, metal, and bottles
Residue	24.96	Textiles, cloth, rubber, leather, and other materials.

*Potential Recycling is adjusted to the data of items sold in the collectors (Waste Bank and Trash Mall)

Fig. 6: Individual trash bin.

Fig. 5: Communal trash bin.

Fig. 7: No trash bin (Trash over water bodies).

trash bin for primary solid waste storage. Some of the families collect rubbish from an individual bin and brought it to the communal bin located on the main road. The visualization of the type of trash bin used is shown in Figs. 5, 6, and 7.

Data from a previous study showed that about 80% of the community not yet separate their waste because of a lack of materials, knowledge, and motivation as well as they cared less about environmental conditions (Anggraini 2018).

Collecting and Transport System

The collection is carried out by janitors on the main road with the frequency of transportation as every day or 7 times a week. After collecting the garbage from households, they bring it to a temporary waste container. A cleaning fee is charged to the people. Type of the garbage collection vehicle is a three-wheeled motor (Viar). Most areas are not passed by Viar due to road conditions that cannot be passed by collection vehicles. This condition makes it difficult for the community, so some of them have to transport garbage independently to the communal trash bin, and some choose to dispose of their garbage around the settlement. Visualization of the collection service and route is shown in Fig 8. The mushrooming settlement colonies are developed in an unplanned way, thus, posing several constraints on the city's municipal services (Sharma et al. 2007).

Existing Solid Waste Management Model

The solid waste management model goes on as seen in Fig. 9. All garbage produced by households depends on transport personnel who have limited services so that not all garbage can be transported (about 20-30% uncollected). People with low income also have limitations in paying waste fees.

Recommendation of Solid Waste Management Model

The design and operation of appropriate solid waste management systems are necessary for ensuring good sanitation and a clean environment (Gawaikar & Deshpande 2006). The model in Fig. 10 shows the Solid Waste Management Recommendation Model for reducing the waste chain that leads to Final Disposal. This model is chosen to overcome the main problem faced in SWM, which is the limitations in terms of waste collection. This model wants to change the old paradigm of waste management that takes place in the research area to a new paradigm that is more sustainable by utilizing existing waste recycling agents.

The characteristics of settlements with narrow streets make it difficult to waste carts to enter, making it difficult for people to get services in terms of garbage collection. The limited facilities and knowledge about the environment give

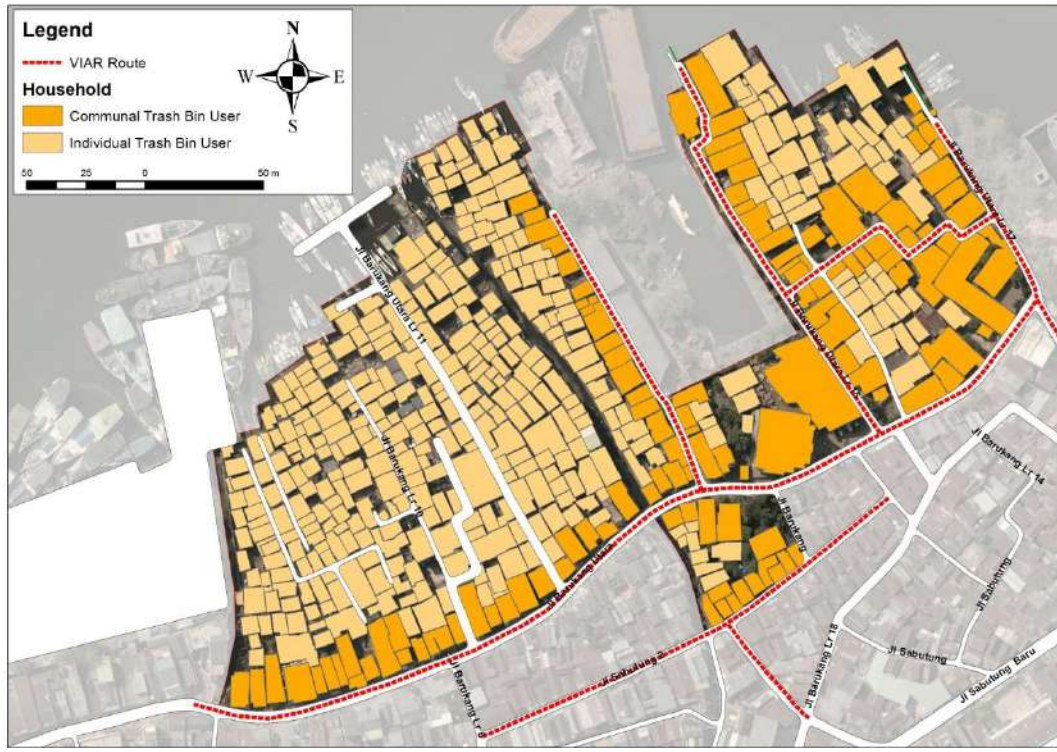

Fig. 8: Collecting vehicle route and trash bin user area.

the potential to dispose of waste into water bodies such as canals and the sea.

The solution of waste management is not limited to the end-of-pipe system, but management system such as waste reduction from its source, waste-sorting, until recycling process (Wijayanti et al. 2015). Recycling and compost concepts are considered pillars of sustainable solid waste management (Cheru 2011). Furthermore, recycling is one of the best methods of solid waste reduction. Similarly, the method can be applied in certain other aspects to decide on the most appropriate option to achieve the best expected results (Purohit et al. 2015). The existence of the Trash Mall and Waste Bank provides an opportunity for the community to sell recycled waste, the difference is that the Trash Mall uses an online system while the Waste Bank uses the offline system. Waste bank or "Bank Sampah" is the concept of waste management in Indonesia and developing countries in Southeast Asia in the management of recycled waste to get money in the form of savings that are established in an environment that is usually around 1000 inhabitants (Khair et al. 2019). The online system support by Trash Mall is something new, up to date by utilizing the technological sophistication of allowing the community to order via smartphone and recycled waste will be picked up by officers, this makes it easier than the offline system. In terms of sales prices, the offline system provides a slightly higher price, but the community needs to bring its

Fig. 9: Flow Diagram for existing solid waste management model.

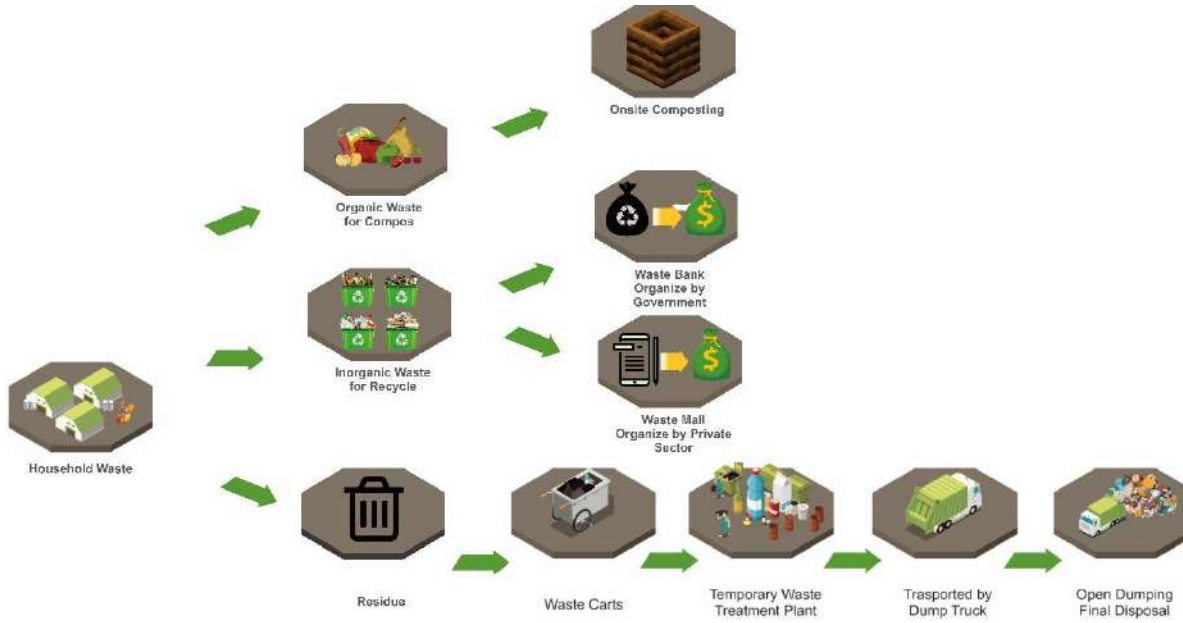

Fig. 10: Solid waste management recommendation model.

recycling waste to the nearest Waste Bank office. This model can be used for other residential areas especially those that have the same characteristics as the study area.

There is a need for onsite composting using both communal and individual systems because the organic waste potential for compost (leftover food, leaves, and twigs) is about 49.47%. This system can be run by women who are mostly housewives. The remaining small amount is 24.96% residual waste will end up at the final disposal and become the responsibility of the government in its transportation and processing.

CONCLUSION

The study regarding solid waste management was carried out. The different factors and strategies of solid waste management were determined. Solid Waste Management in Cambaya coastal slum settlement is not going well yet because of several reasons such as characteristics of settlement, characteristics of citizens who live there, and lack of MSW facilities. The waste generation in Cambaya Village is dominated by organic waste 58% and inorganic waste 42%. Most of the citizens did not get access to communal storage and collection, so potentially waste from households is thrown directly to water bodies. It needs serious waste management to minimize pollution of the coastal area. If properly managed according to the recommendations of the SWM model, only 24.96% of the residue will be transported to the final disposal.

REFERENCES

Anggraini, N. 2018. Study on the measurement of garbage dumps in the Cambaya coastal area. Multek Journal, 13(3): 550-558.

Asnani, P.U. 2006. India Infrastructure Report, Urban Infrastructure. Oxford University Press. New Delhi, India.

Buenrostro, O., Bocco, G. and Vence, J. 2001. Forecasting generation of urban solid waste in developing countries - A case study in Mexico. J. Air Waste Manage. Assoc., 51: 86-93.

Chang, N.B. and Davila, E. 2008. Municipal solid waste characterizations and management strategy for the Lower Rio Grandle Valley: Texas. Waste Manag., 28(5): 776-94.

Cheru, S. 2011. Assessment of Municipal Solid Waste Management Services in Dessie Town. Master Thesis, Addis Ababa University.

Gawaikar, V. and Deshpande, P. 2006. Source specific quantification and characterization of municipal solid waste. IE(I). Journal Env., l86: 33-38.

Hancs, A., Novak, P., Dvorak, M., Habart, J. and Svehla, P. 2011. Composition and parameters of household bio-waste in four seasons. Waste Manage., 31: 1450-1460.

Indonesian Ministry of Environment. 2012. Environmental Care Behavior Indicators (Results of a Survey of Environmental Care Behavior in 33 Provincial Capitals). Jakarta, Indonesia.

Indonesian Ministry of Environment. 2017. Indonesian Waste Management Information System. Jakarta, Indonesia.

Indonesian National Standards (SNI) 1994. SNI No.19-3964-1994 concerning Methods for Taking and Measuring Samples of the Generation and Composition of Urban Waste. Jakarta, Indonesia.

Jha, Arvind K., Sharma, C., Nahar Singh, Ramesh, R., Purvaja, R. and Gupta, Prabhat K. 2008. Greenhouse gas emissions from municipal solid waste management in Indian megacities: A case study of Chennai landfill sites. Chemosphere, 71: 750-758.

Kirpalani, C., Jain, N. and Bassin, J.K. 2005. Municipal solid waste management in Jaipur city: An overview. Nature Environment and Pollution Technology, 4(1): 143-148.

Khair H., Siregar I. Y., Rachman I. and Matsumoto, T. 2019. Material for analysis of waste bank activities in Indonesia: Case study of Medan city. J. Indonesian Journal of Urban and Environmental Technology, 3(1): 28-46.

Kutanegara, P.M. 2014. Building an Indonesian Society that Cares About the Environment, Ministry of Environment of the Republic of Indonesia. Gadjah Mada University Press.

Makassar Statistical Center 2019. Makassar City Profile. Makassar, Indonesia.

Marshal, R.E. and Farahbakash, K. 2013. Systems approach integrated solid waste management in developing countries. J. Elsevier, 33: 988-1003.

Miezah, K., Danso, K.O., Kadar, Z., Fei-Baffoe, B. and Mensah, M.Y. 2015. Municipal solid waste characterization and quantification as a measure towards effective waste management in Ghana. J. Elsevier, 46: 15-27.

Moftah, S.A.W., Markovic, D., Moftah, S.A.O. and Nesseef, L. 2016. Characterization of household solid waste and management in Tripoli City-Libya. Open Journal of Ecology, 6: 435-44.

Nyakaana, J.B. 1996. Solid waste management in urban centers: The case of Kampala City-Uganda. J. East African Geographical Review, 19:1.

Purohit, Pulkit and Ramachandran, M. 2015. Selection of flywheel material using multicriteria decision making fuzzy topsis. Indian Journal of Science and Technology, 8(33). doi: 10.17485/ijst/2015/v8i33/80028.

Qdais, H.A., Hamonda, M.F. and Newham, J. 1997. Analysis of residential solid waste at generation sites. Waste Manage. Res., 15: 395-406.

Qu, X., Li, Z., Xie, X., Sui, Y., Yang, L. and Chen, Y. 2009. Survey of composition and generation rate of household wastes in Beijing, China. Waste Management, 29: 2618-2624.

Raharjo, S., Ruslinda, Y., Bachtiar, V.S, Regia, R.A, Fadhil, M., Rachman, I. and Matsumoto, T.S. 2018. Investigation on municipal solid waste characteristics from commercial sources and their recycling potential in Padang City, Indonesia. IOP Conf. Series: Material Science and Engineering, 288: 012134.

Ramesh, N., Meenambal, T. and Murugan, K. 2009. Municipal solid waste from Erode municipality, Tamilnadu, India. Nature Environment and Pollution Technology, 8(1): 21-28.

Rashid, M., Sattar, Y., Ramli, M., Sabariah and Puji, L. 2014. PM_{10} black carbon and ionic species concentration of urban atmospheric in Makassar of South Sulawesi Province, Indonesia. J. Atmospheric Pollution Research, 5: 610-615: doi: 10.5094/APR.2014.070.

Sattar, Y., Rashid, M., Ramli, M. and Sabariah, B. 2014. Black carbon and elemental concentration of ambient particulate matter in Makassar Indonesia. IOP Conf. Series: Earth and Environmental Science. 18. 012099: doi: 10.1088/1755-1315/18/1/012099.

Sattar Yunus., Mohd. Rashid., Ramli Mat., Sabariah Baharun and Hasfalina C. Man 2019. Characteristics of the PM_{10} in the urban environment of Makassar, Indonesia. J. Urban and Environmental Engineering, 13(1): 198-207: doi: 10.4090/juee. 2009. v13n1.198207.

Sattar, M. Rashid., R. Mat and L. Puji 2012. A preliminary survey of air quality in Makassar City South Sulawesi Indonesia. J. Teknologi (Sciences & Engineering), 57: 123-136.

Shahmoradi, B. and Rad, S.M.M. 2009. Investigation on people's knowledge, attitude, and operation of municipal solid waste management in Sanandaj City, Iran. Nature Environment and Pollution Technology, 8(3): 539-544.

Sharma, A., Sharma, C. and Sharma, A.K. 2007. Characteristics and management of municipal solid waste in national capital territory of Delhi. Indian Journal Environmental Protection, 27(10): 897-904.

Sharma, R. 2008. Municipal solid waste management in Ajmer City, Rajasthan: An overview. Nature Environment and Pollution Technology, 8(4): 741-744.

Tchobanoglous, G., Hilary, T. and Samuel, V. 1993. Integrated Solid Waste Management. McGraw-Hill, Inc: New York.

Thakuria, M.N. 2009. A study on municipal solid waste management in Bongaigaon, Assam. Nature Environment and Pollution Technology, 8(4): 741-744.

Tiruneh, B.M., Venkateswarlu, M. and Gopala Krishna, B.V. 2015. Solid waste generation and solid waste disposal site management in urban areas: The case of Dessie Town, Amhara National Regional State, Ethiopia. International Journal of Advanced Scientific and Technical Research, 5(3): 293-307.

Truong, L.M., Trang T. T. and Dieu, T. T. M. 2017. Preliminary development a mathematical model for estimating household solid waste generation rate: the case of Ho Chi Minh City, Vietnam. Nature Environment and Pollution Technology, 16(2): 351-362.

Upadhyay, V., Jethoo, A. S. and Poonia M.P. 2012. Solid waste collection and segregation: A case study of MNIT Campus, Jaipur. J. IJEIT, 1(3).

Wijayanti, D.R. and Suryani, S. 2015. Waste bank as community-based environmental governance: A lesson learned from Surabaya. Procedia Social and Behavioral Sciences, 184: 171-179.

Yavini, T.D. and Musa, A.A. 2013. Municipal solid waste and pollution management in Jalingo Metropolis: Problems, challenges and strategies. J. Environment, 2(05): 125-133.

Nature Environment and Pollution Technology
An International Quarterly Scientific Journal

p-ISSN: 0972-6268
(Print copies up to 2016)
e-ISSN: 2395-3454

Vol. 20 | No. 2 | pp. 467-479 | 2021

Original Research Paper

https://doi.org/10.46488/NEPT.2021.v20i02.003

Open Access Journal

Adsorption of Dyes by Chitosan-Selenium Nanoparticles: Recent Developments and Adsorption Mechanisms

John Britto, P. Barani, M. Vanaja, E. Pushpalaksmi, J. Jenson Samraj and G. Annadurai†
Division of Nanoscience, Sri Paramakalyani Centre for Excellence in Environmental Sciences, Manonmaniam Sundaranar University, Alwarkurichi-627 412, India
†Corresponding author: G. Annadurai; gannadurai@msuniv.ac.in

Nat. Env. & Poll. Tech.
Website: www.neptjournal.com

Received: 27-05-2020
Revised: 08-07-2020
Accepted: 25-07-2020

Key Words:
Rhodamine
Chitosan-selenium nanoparticles
Langmuir isotherm
Justicia adhatoda

ABSTRACT

Most of the dyes are a dangerous class of water contaminants that have affected the environment drastically. Nano-sized compositeis the best decision cutting edge adsorbent for the evacuation of water poisons as such materials are related to the attributes of straightforwardness, adaptability, adequacy, and high surface reactivity. In this investigation, we have synthesized a nanostructured Chitosan-Selenium nanoparticle by green synthesis method using *Justicia adhatoda* plant leaves extract. Synthesis and characterization of Chitosan-Selenium nanoparticle were described by UV-visible spectroscopy, FTIR spectrum examinations, Particle Size Analysis, and XRD Spectrum analysis. From the outcomes, it was inferred that the Chitosan-Selenium nanoparticle was additionally utilized as an adsorbent for the expulsion of Rhodamine dye from the aqueous solution. Langmuir isotherm model was effectively usedfor the adsorption study of Chitosan-Selenium nanoparticle adsorbent. For the adsorption studies, parameters such asdosages, pH, and temperature were studied. The adsorption process was remarkably fast and reached equilibrium within 24hrs. The isotherm information was steady with the Langmuir model, and the most extreme adsorption limits of the Chitosan-Selenium nanoparticle adsorbent was 34.5mg.g^{-1} for Rhodamine dye. Accordingly, nanoparticleswill be the only wayfor the future planned water treatment process.

INTRODUCTION

Industrial, agricultural and domestic wastes, due to the rapid development in technology, are discharged in several environments. Generally, this discharge is directed to the nearest water sources such as rivers, lakes, and seas. The textile dyeing process is an important source of contamination responsible for the continuous pollution of the environment. Textile, paper, painting, and coating industries are majorsources of dye pollutants. A large amount of dye wastewateris emptied into freshwater bodies which have negativeconsequences on the environment and human health (Oliveiraet al. 2008). Wastewater from dye-stuff and textile industries have dye concentrations below 1 g/dm^3, high alkalinity, Biochemical Oxygen Demand (BOD), Chemical Oxygen Demand (COD), and total dissolved solids (Kaushik & Malik 2009). The reactive, directive, and acid dye widely used in silk, cotton, and wool processing as dyes (El-Sharkawy et al. 2007). Dye wastewater that ends up in freshwater bodies causes havoc to aquatic species by increasing toxicity in COD. It also affects the photosynthetic activities of aquatic plants through the reduction of light penetration (Oliveira et al. 2008). It has been reported that high COD,BOD values, particulate matter (PM) and sediments, grease, and oil in effluents lead to the depletion of dissolved oxygen creating serious consequences on aquatic species (Wang et al. 2011, Hamza & Hamoda 1980, Shaul et al. 1982, Shelley et al. 1980). The methods of colour removal from industrial effluents include biological treatment, coagulation, flotation, adsorption, oxidation, and hyperfiltration. Among the treatment options, adsorption has become one of the most effective and comparable low-cost methods for the decolourization of textile wastewater. Different adsorbents have been used for the removal from aqueous solutions of various materials, such as dyes, metal ions, and other organic materials include perlite (Dogan et al. 2000, Demirbas & Dogan 2002, Dogan & Alkan 2003) bentonite (Bereket et al. 1997), silica gels (Mohamed et al. 1996), fly ash (Mohan et al. 2002, Gupta et al. 2000), lignite (Allen et al. 1989), peat (Ho& Mckay 1998), silica (Mckay et al. 1981). However, all these processes are costly and cannot be used by small industries to treat a wide range of dye wastewater (Dogan et al. 2000). The adsorption process provides an attractive alternative for the treatment of contaminated waters, especially if the sorbent is inexpensive and does not require an additional pretreatment step before its application (Mckay et al. 1981, Ho & Mckay

1998,Ashraf 2016, Nurchi et al. 2014, Chang et al. 2014, Arica et al. 2017, 2019, Bayramoglu et al. 2012,Bayramoglu & Yilmaz 2018). A wide range of nanomaterials such as metals, metal oxide, polymer composites, and nanoparticles incorporating activated carbon, biomass, and clay minerals, etc. have been included. Adsorption requires less land area, least effect to toxic chemicals, greater flexibility in the design, and operation and superior removal of organic contaminants. Therefore, significant attention has been directed to adsorption as a process for colour removal from wastewaters since it offers the most economical and effective treatment methods. Therefore, adsorption became one of the most effective methods to remove the colour from textile wastewater. The objective of this paper was to explore the removal of Rhodamine dye in an aqueous solution by adsorption on the Chitosan-Selenium nanoparticle. The influence of several parameters on adsorption such as dosages, pH, and temperature on the adsorption process was also studied.

MATERIALS AND METHODS

Chemicals and Collection of Plant Material

All the chemicals were purchased from Himedia Private Ltd, Mumbai. The plant *Justicia adhatoda* leaves were collected from Sri Paramakalyani Centre of Excellence in Environmental Sciences, Manonmaniam Sundaranar University, Alwarkurichi.

Preparation of Adathoda Leaf Extract

Fresh and young leaves (5g) of the Adathoda plant were washed thoroughly with distilled water and cut into fine pieces. Leaves were subsequently macerated in 20 mL of Tris-HCl (pH7.5) with the help of mortar and pestle. A thick slurry of leaf thus recovered was subjected to centrifugation at 10,000 rpm for 5 min at 4°C. The supernatant was transferred into fresh sterile centrifuge tubes followed by its preservation in refrigerated conditions. The aqueous extract of leaf obtained in this manner was used as a precursor for the synthesis of selenium nanoparticles.

Synthesis of Selenium Nanoparticle

In a typical synthesis of selenium nanoparticles, the leaf extract (2 mL) which contains dissolved phytochemicals was added dropwise into 20 mL of sodium selenite solution (10mM). The addition of the leaf extract was carried out under magnetic stirring. The content was later on placed on to a rotator orbital shaker operating at 200rpm for 24 h. The incubation of the mixture was performed at 30°C in dark conditions. The reduction of selenium ions was monitored by sampling an aliquot (3 mL) of the mixture at intervals of 12 h, followed by measurement of the UV-Vis spectrophotometer. To find out the absorption maximum, a spectral scanning analysis was carried out by measuring the optical density of the content from wavelength 250 to 750 nm.

Synthesis of Chitosan-Selenium Nanoparticle (CS-Se NPs)

Stock solutions of sodium selenite (20mmol/L) and ascorbic acid solution (80mmol/L) were prepared with double-distilled water at room temperature. 1 gm of chitosan (CS, 1% w/w) was dispersed in 4% (w/w) acetic acid at room temperature and stirred for complete dissolution. For the preparation of the CS-Se NPs solution, 1mL (10 mM) of sodium selenite solution, ascorbic acid, and chitosan solution were mixed and the solution was subjected to vigorous mixing. Then, the reaction mixture was diluted to 10 mL with distilled water. The sample was filtered and dried in the hot air oven at 150°C for using adsorption studies.

Batch Equilibrium Studies

Batch adsorption experiments were carried out by agitating 1g of the Chitosan-Selenium nanoparticle with the effect of initial Rhodamine dye concentrations was carried out by shaking 100 mLRhodamine dye solutions of desired concentrations (20 to 100 mg/L) with 1g of the adsorbent at different dosages (1.0, 2.0 and 3.0g/L) pH (5.8, 6.8 and 9.4) and temperature (30°C, 45°C, and 60°C) using an orbital shaker operating at 200 rpm. Before the measurement of colour, the dye solutions were filtered through Whatman No. 1 filter paper to exclude the adsorbent particles. Dye concentrations were measured at the wavelengths corresponding to their maximum absorbance using a spectrophotometer. The effect of pH was studied by adjusting the pH of dye solutions using 1 N H_2SO_4 or 1 N NaOH solution pH was measured using a pH meter. The samples were withdrawn from the shaker at a pre-determined time of 24hrs. The residual concentrations of Rhodamine dye were measured using UV spectrophotometer equipment (Shimadzu UV/Vis 1601 Spectrophotometer, Japan). The maximum wavelength of this dye is λ_{max}555 nm.

Mass Balance Equation

Throughout the experiment the mass balance equation was used, to find the amount of protein adsorbed in each flask which was determined by the equation,

$$Q = V (C_o - C_e)/W \quad \text{... (1)}$$

Where,

Q - Adsorption capacity (mg/g)

C_o - Initial concentration of Rhodamine dye (mg/L)

C_e - Final concentration of Rhodamine dye(mg/L)

V - Solution volume of Rhodamine dye (L)

W - Mass of adsorbent (g)

So using this equation the amount of dye being adsorbed by the adsorbent was determined.

RESULTS AND DISCUSSION

The synthesis of selenium nanoparticles was preliminarily analysed by the colour change of the reaction mixture. The reaction mixture contains sodium selenite solution, ascorbic acid, and plant extract. The plant extract was used as a reducing agent forthe synthesis of nanoparticles. Ascorbic acid was used as an initiator of the reduction reaction. All the solutions were mixed and colour change was occurring from colourless sodium selenite solution to ruby red colour. A similar result was observed by Kirupagaran et al.(2016), synthesized selenium nanoparticles using an extract of *Leucas lavandulifolia* and Fenugreek seed extract (Ramamurthy et al. 2013). Visual observation of the chitosan stabilized selenium nanoparticles solution showed a colour change from light yellow to brick red indicating the formation of red-coloured elemental Se resulting in the selenium nanoparticle formation (Bajaj et al. 2012). This red colour due to the excitation of surface plasmon vibrations of selenium nanoparticles provides a convenient spectroscopic signature of their production whereas no colour change could be demonstrated in a solution of selenium selenite as a negative control. Many related studies revealed that metal reduction and precipitation might involve a complex of either reductase, capping proteins, quinones or cytochromes, electron shuttles, or phytochelatins that are known to reduce and stabilize various metal, metal oxides and metal sulphide nanoparticles (Bajaj et al. 2012).

UV-Vis Spectrophotometer

Reduction of selenium ions into selenium nanoparticles during exposure to plant extracts and ascorbic acid was observed using UV-Vis spectra. The metal nanoparticles have free electrons, which give the SPR absorption band, due to the combined vibration of electrons of metal nanoparticles. Chitosan stabilized selenium nanoparticles shown the SPR band at 450 and 310 nm indicates the formation of selenium nanoparticles. Some of the minor peaks were also observed due to the presence of biomolecules from chitosan Fig.1. Previous studies have shown that the spherical Se-NPs contribute to the absorption bands at around 250-400nm in the UV-Visible spectra (Fesharaki et al. 2010) reported λ_{max} at 280 nm (Lin et al. 2005) at 355 nm (Shen et al. 2000) at 380 nm. The UV data may support further characterization of *Adhatoda* leaf extract and chitosan mediated selenium

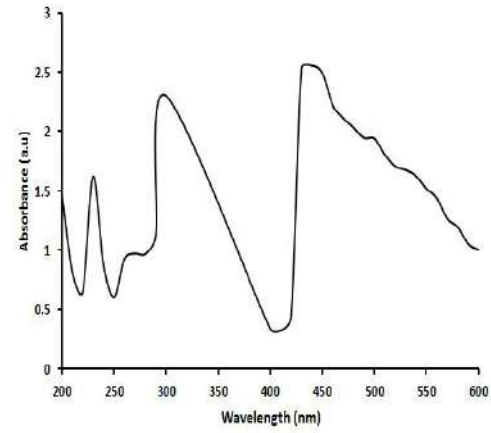

Fig. 1: UV-Vis spectra of chitosan mediated synthesized selenium nanoparticles.

nanoparticles. Chitosan stabilized selenium nanoparticles were purified by membrane dialysis process. Dialysed nanoparticles were dried in a hot air oven at 60°C for 4 h. The powder form of the selenium nanoparticles was used for further analysis.

FT-IR Analysis

The functional groups present in green synthesized chitosan-selenium nanoparticles were identified by FTIR spectra. FTIR analysed at different wavenumber range from 4000 to 500cm^{-1}. The functional groups involved in the synthesis of selenium nanoparticles using chitosan were detected with the help of FT-IR analysis (Fig. 2). Broadband at 3226cm^{-1} was observed due to the presence of O-H stretching carboxylic acids. A very small band at 2878 cm^{-1} was formed corresponds to C-H stretch alkanes. A strong narrowband was positioned at N-H bend primary amines. A small band at 1297 cm^{-1} indicates the presence of N-O symmetric stretching Nitro compounds and C-N stretching aromatic amines. A narrow band was formed at 1023 due to C-N

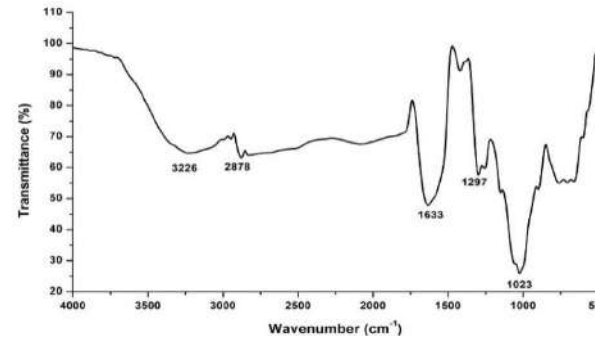

Fig. 2: FTIR spectrum of chitosan-selenium nanoparticles.

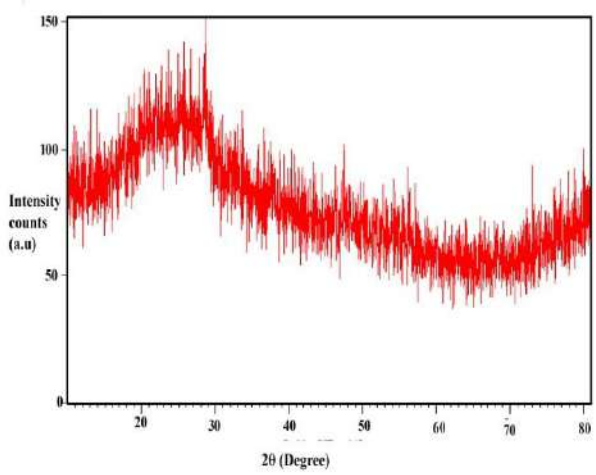

Fig. 3: XRD Spectrum of the chitosan-selenium nanoparticle.

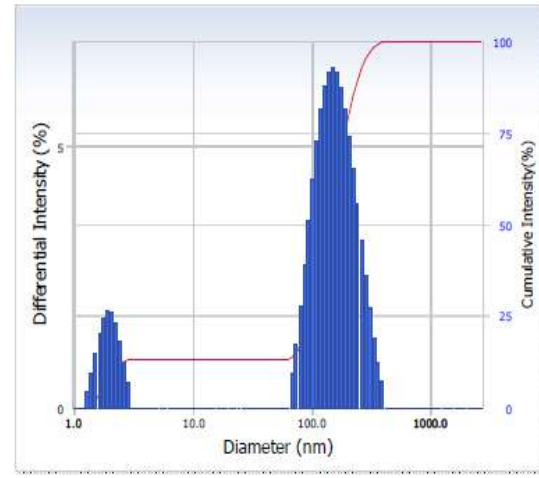

Fig. 4: Particle size analysis of chitosan-selenium nanoparticles.

stretch aliphatic amines. Therefore, the FT-IR results imply that the chitosan-selenium nanoparticles were successfully synthesized and capped with bio-compounds present in the leaf aqueous extract and chitosan by using a green method.

X-ray Diffraction

The crystal structure and the phase composition of chitosan-selenium nanoparticles were determined, using XRD techniques shown in Fig. 3. The XRD pattern suggests that the sample is nanocrystalline and matches very well with that of the standard selenium powder confirming the formation of selenium particles using leaf extract. The calculated lattice constants are a = 4.363 A° and c = 4.952 A° which are in agreement with the literature value (JCPDS File No.06-0362). The clear peaks of cubic phases at 23.68, 29.12, 40.71, 45.24, 48.05, and 51.28° were assigned to (100), (101), (110), (111), (200) and (201) crystalline planes which may be due to the presence of additional bioactive compounds present in the *Adathoda* leaf extract (Shen et al. 2000). Chitosan coupled selenium nanoparticles not shown specific crystalline planes and definite shapes indicate that synthesized nanocomposite is a polydispersed amorphous structure.

Particle Size Analysis

Fig. 4. shows the number of frequency histograms of particle size data on a linear scale. The smooth curve drawn through the histogram is a valid size-frequency curve insufficient particle-sare counted and the size interval is at least ten (Kirupagaran et al. 2016). As it is observed in Fig. 4 the average size distribution of the chitosan-selenium nanoparticle is 87-152 nm.

Adsorption Isotherm of Rhodamine Dye

The equilibrium adsorption isotherm is of fundamental importance in the design of adsorption systems. The isotherm expresses the relation between the mass of dye adsorbed at a particular temperature and dosages and the liquid phase of dye concentration. For any adsorption investigation one of the most important parameters required to understand the behaviour of the adsorption process in the adsorption isotherm (Jain et al. 2003, Jumasiah et al. 2005, Kadirvelu et al. 2005, Kamel et al. 2009). The shape of an isotherm not only provides information about the affinity of the dye molecule for adsorption but also reflects the possible mode of adsorbing dye molecule. The most common way of obtaining an adsorption isotherm is to determine the concentration of dye solution before and after the adsorption experiments, although several attempts have been made to find the adsorbed amount.

Effect of Dosages

The effect of adsorbent dosages on Rhodamine dye uptakes for three different dosages (Chitosan-Selenium Nanoparticle) (1.0, 2.0, and 3.0 g/L) is shown in Fig. 5. It can be observed that as the dosages were increased, the adsorption of dye increases. The results show that there is a gradual increase in adsorption with increasing dosages. Such an effect of probably due to the inability of the large dye molecule to penetrate all the internal pore structure Chitosan-Selenium nanocomposite and a similar phenomenon was reported previously for the adsorption of certain dyes on various adsorbents (Mckay 1984. Feng et al. 2001. Ferrero 2000). The results revealed that the dye uptake increased with increasing dosages at1.0 g/L 16.14 mg/g. 2.0g/L, 24.36.0 mg/g and 3.0g/L, 33.90 mg/g). This is due to the larger surface area made available for adsorption. It was also observed that the increase in dosages, increases the dye

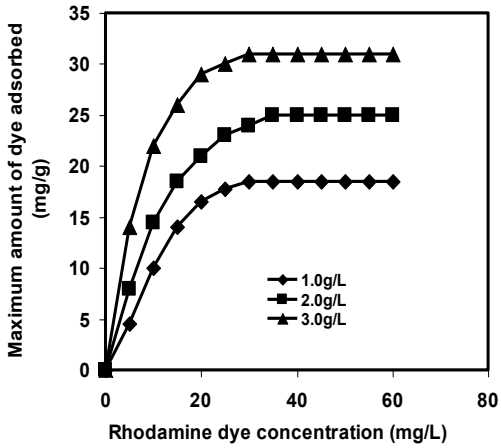

Fig. 5: Effect of specific dye uptake at different dosages (Chitosan-Selenium nanoparticle) with Rhodamine dye concentration.

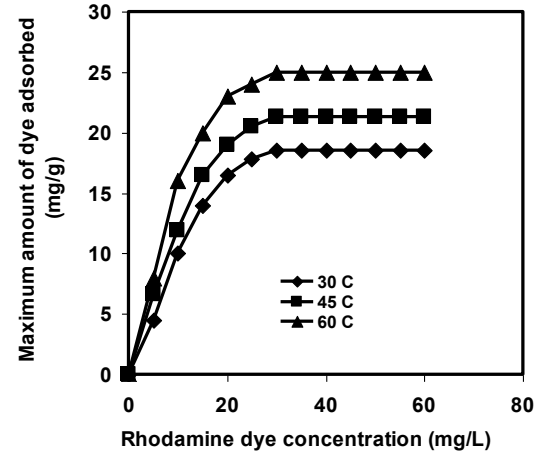

Fig. 6: Effect of specific dye uptake at different temperatures (Chitosan-Selenium nanoparticle) with Rhodamine dye concentration.

uptake. It is obvious that the smaller particles, which have higher solid-liquid interfacial areas, will have higher adsorption rates.Thus dye uptake was maximum at a higher adsorbent dosage. This could be attributed to the fact that as the adsorbent dosage is increased, more adsorption sites are available for dye, thus enhancing the uptake. Also, with increasing adsorbent load, the quantity of dye adsorbed onto the unit weight of the adsorbent gets reduced, thus causing a decrease in q_e value with increasing Chitosan-Selenium nanoparticle loading (Rathinam et al. 2007).

Effect of Temperature

Temperature is an important parameter for the adsorption process. A plot of the Rhodamine dye uptake as a function of temperature (30, 45, and 600°C) is shown in Fig. 6. The results revealed that the dye uptake increased with increasing temperature at 30°C, 16.14 mg/g, 45°C, 24.36.0 mg/g, and 60°C, 25.60 mg/g). The adsorption of dye at higher temperatures was found to be greater compared to that at a lower temperature. The curves indicate the strong tendency of the process for monolayer formation (Sivaraj et al. 2001, Annadurai et al. 2002, Yu et al. 2002, Ravi Kumar 2000,Muzzarelli 1973). The increase in temperature would increase the mobility of the large dye ion and also produces a swelling effect within the internal structure of the Chitosan-Selenium nanoparticle, thus enabling the large dye molecule to penetrate further (Muzzarelli 1973, Faria et al. 2004). Therefore, the adsorption capacity should largely depend on the chemical interaction between the functional groups on the adsorbent surface and the adsorbate and should increase with temperature rising (Rinaudo 2006,Knorr et al.1985, Kawamura et al.1997). This effect is characteristic of a chemical reaction or bond being involved in the adsorption process. The increase in adsorption with temperature could be due to changes in pore size, an increase in kinetic energy of dye molecule, and enhanced rate of diffusion of sorbate (Aksu 2002, Rathinam et al. 2007).

Effect of pH

Fig. 7.showsthe effect of pH on adsorption of the Rhodamine dye onto Chitosan-Selenium nanoparticle. In general, uptakes were much higher in acidic solutions than those in neutral and alkaline conditions. The maximum values of the adsorption capacity ratio between acidic and alkaline conditions reached 12.14 to 19.49 mg/g, respectively. At lower pH more protons will be available to protonate amino groups of chitosan molecules to form groups $–NH^{3+}$, thereby increasing the electrostatic attractions between negatively charged dye anions and positively charged adsorption sites and causing an increase in dye adsorption (Gardiner & Brune 1978, Ganesh et al. 1994, Fu & Viraraghavan 2001, Forgacs et al. 2004). This explanation agrees with our data on the pH effect. It can be seen that the pH of aqueous solution plays an important role in the adsorption of Rhodamine dye onto Chitosan-Selenium nanoparticle. The results showed a direct influence of the pH of the solution on the heterogeneous adsorption process. In alkaline solutions, adsorption efficiency was more than that in acidic solutions. It is because the decomposition of Chitosan- Selenium nanoparticle takes place in acidic and neutral solutions (Daneshvar et al. 2007).

Langmuir Isotherm

The Langmuir isotherm (1916, 1918) has found successful application to many other real sorption processes and it can be used to explain the sorption of Rhodamine dye into

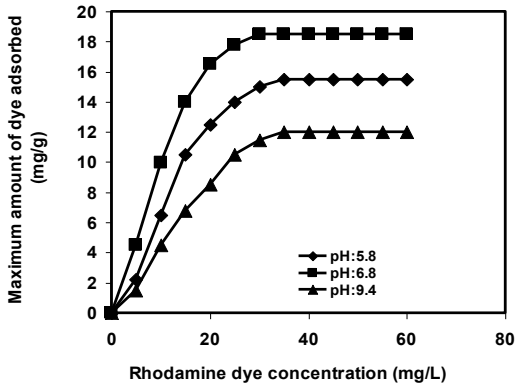

Fig. 7: Effect of specific dye uptake at different pH (Chitosan-Selenium nanoparticle) with Rhodamine dye concentration.

Chitosan-Selenium nanoparticle. A basic assumption of the Langmuir theory is that sorption takes place at specific sites within the adsorbent (Kawamura et al. 1993, Lee& Low 1987, Wei et al.1992). The data obtained from the adsorption experiment conducted in the present investigation were fitted in different Rhodamine dye concentrations, dosages, pH, and temperature in the isotherm equation. The saturation monolayer can be represented by the expression (2).

$$q_e = \frac{KbC_e}{(1+bC_e)} \quad \ldots (2)$$

Linear Regression of Langmuir Isotherm -Chitosan-Selenium Nanocomposite-Rhodamine Dye

A plot of Langmuir isotherm Type – I - IV (C_e/q_e Vs C_e- Type-I. 1/qe vs $1/C_e$ – Type – II. q_e Vs qe/C_e - Type- III. q_e/C_e Vs q_e –Type- IV) (Table1)resulted in a linear graphical relation indicating the applicability of the above model (Different dosage 1.0, 2.0, and 3.0g/L, pH: 5.8, 6.8, and 9.4. Temperature: 30°C, 45°C, and 60°C) as shown in Figs.8-19. The values are calculated from the slope and intercept of different straight lines representing the different dosages, pH, and temperature (q_m) adsorption capacity. The Langmuir isotherm constant (K_L) in Eqn (3 - 7) is a measure of the amount of dye adsorbed when the monolayer is completed. Monolayer capacity (q_m) of the adsorbent for the dye is comparably obtained from adsorption isotherm. The observed statistically significant (at the 95% confidence level) linear relationship as evidence of these by the R^2 values (close to unity) indicate the applicability of the isotherm (Langmuir isotherm) and surface.

The Langmuir isotherm constants along with correction coefficients are reported in Tables2-5.It is also clear from the shape of the adsorption isotherm, that it belongs to the L_2 category of isotherm, which indicates the normal (or) Langmuir type of adsorption (Chiou et al. 2003, Yui et al.1994, Rinaudo 2006, Kurita 2001). Such isotherms are often encountered when the adsorbate has a strong intermolecular attraction for the surface of the adsorbent. The L_2 shape of the isotherm observed in the present care implies that Rhodamine dye molecules must have been strongly attached to the Chitosan-Selenium nanoparticle. Langmuir equation can be written in four linearized types, the Langmuir constants q_m and K_L values can be calculated by plotting between type 1- C_e/q_e versus C_e, type 2 - $1/q_e$ versus $1/C_e$, type 3 - q_e versus q_e/C_e, and type 4q_e/C_e versus q_e, Langmuir isotherms, respectively.

The linear method does not test whether the experimental data are linear. It assumes the experimental data were linear and predicts the slope and intercepts that make a straight line that predicts the best-fit of experimental equilibrium data (Yoshida & Takemori 1997, Gupta et al. 1989, Giunchedi et al. 1998, Ghosh & Bhattacharyya 2002, Gupta et al. 2003). The linear method assumes that the scatter of points around the line follows a Gaussian distribution and the error distribution is the same at every value of *X*. The linear method just predicts the *Y* for the corresponding *X*. It considers only the error distribution

Table 1: The different linearized forms of Langmuir and Freundlich equations.

Isotherm	Linear Regression	Plot
Langmuir Isotherm Type 1- (Eqn-3)	$C_e/q_e = (1/K_L q_m)+(C_e/q_m)$	$C_e \ / \ q_e.vs.C_e$
Langmuir Isotherm Type 2- (Eqn-4)	$1/q_e = (1 \ / \ q_m)+(1 \ / \ K_L q_m C_e)$	$1 \ / \ q_e.vs.1 \ / \ C_e$
Langmuir Isotherm Type 3- (Eqn-5)	$q_e = q_m - (q_e \ / \ K_L C_e)$	$q_e.vs.q_e \ / \ C_e$
Langmuir Isotherm Type 4- (Eqn-6)	$q_e \ / \ C_e = K_L q_m - K_L q_e$	$q_e \ / \ C_e.vs.q_e$
Freundlich Isotherm (Eqn-7)	$Log(C_e) = Log(K_F)+1 \ / \ nLog(C_e)$	$Log(q_e)vs.Log(C_e)$

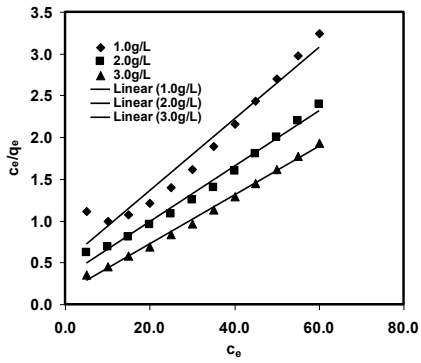

Fig. 8: Langmuir isotherm (Type – I) for the adsorption of Rhodamine dye using Chitosan-Selenium nanocomposite at different Dosages with dye concentration.

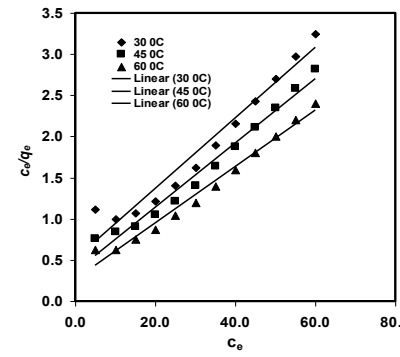

Fig. 9: Langmuir isotherm (Type – I) for the adsorption of Rhodamine dye using Chitosan-Selenium nanocomposite at different Temperatures with dye concentration.

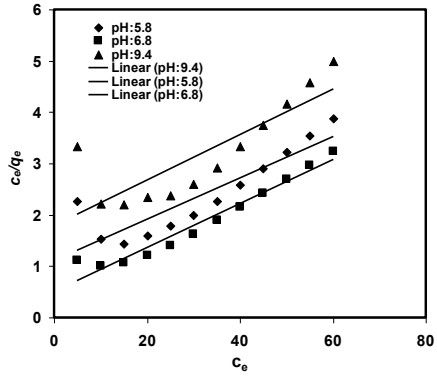

Fig. 10: Langmuir isotherm (Type – I) for the adsorption of Rhodamine dye using Chitosan-Seleniumnanocomposite at different pH with dye concentration.

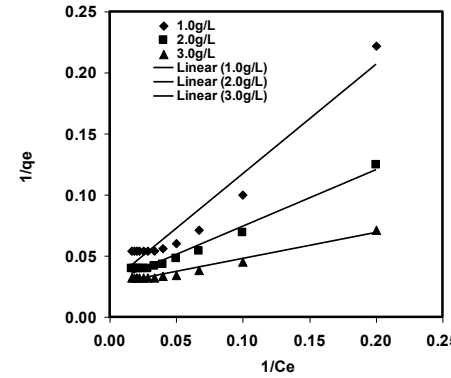

Fig. 11: Langmuir isotherm (Type – II) for the adsorption of Rhodamine dye using Chitosan-Selenium nanocomposite at different Dosages with dye concentration.

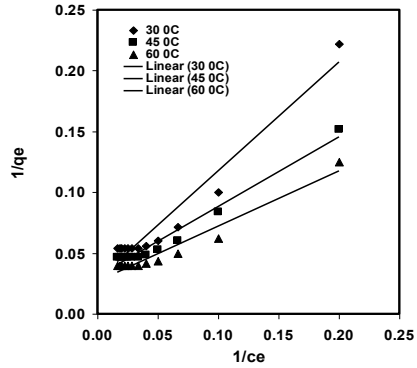

Fig. 12: Langmuir isotherm (Type – II) for the adsorption of Rhodamine dye using Chitosan-Seleniumnanocomposite at different Temperatures with dye concentration.

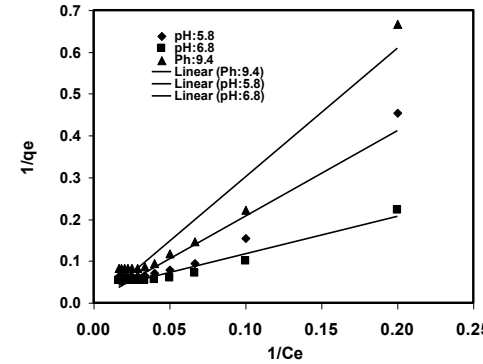

Fig. 13**:** Langmuir isotherm (Type – II) for the adsorption of Rhodamine dye using Chitosan-Selenium nanocomposite at different pH with dye concentration.

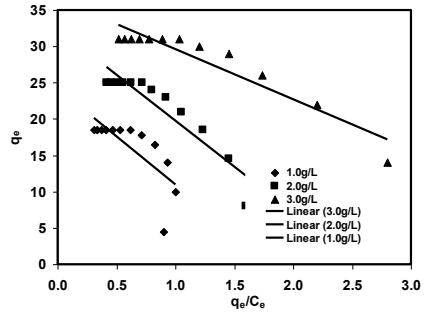

Fig. 14: Langmuir isotherm (Type – III) for the adsorption of Rhodamine dye using Chitosan-Selenium nanocomposite at different Dosages with dye concentration.

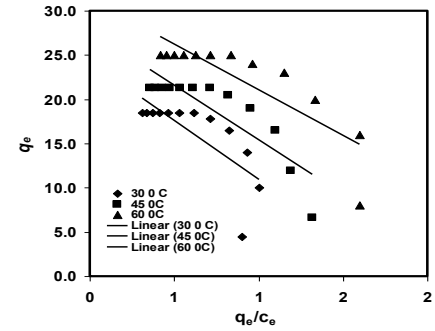

Fig. 15: Langmuir isotherm (Type – III) for the adsorption of Rhodamine dye using Chitosan-Selenium nanocomposite at different Temperatures with dye concentration.

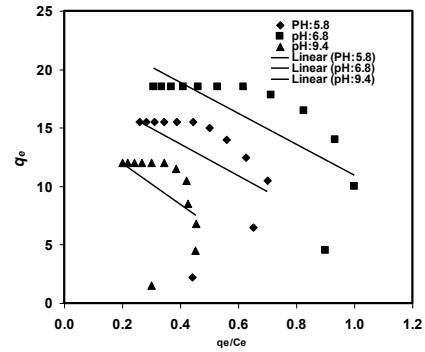

Fig. 16: Langmuir isotherm (Type – III) for the adsorption of Rhodamine dye using Chitosan-Seleniumnanocomposite at different pH with dye concentration.

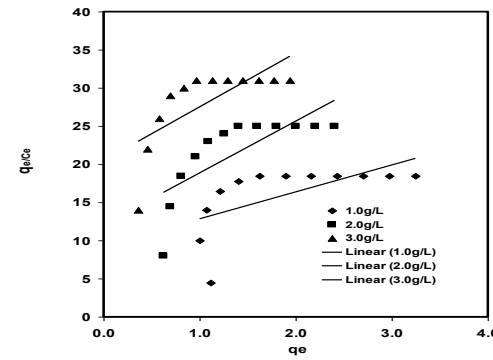

Fig. 17: Langmuir isotherm (Type – IV) for the adsorption of Rhodamine dye using Chitosan-Selenium nanocomposite at different Dosages with dye concentration.

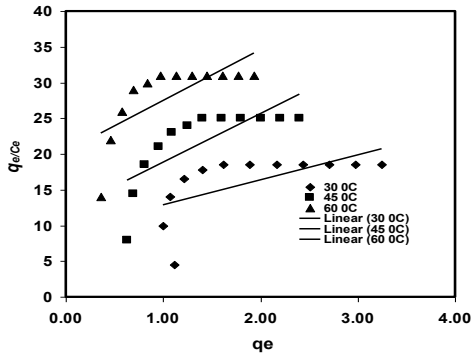

Fig. 18: Langmuir isotherm (Type – IV) for the adsorption of Rhodamine dye using Chitosan-Seleniumnanocomposite at different Temperatures with dye concentration.

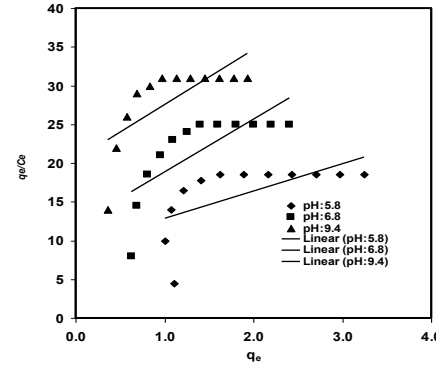

Fig. 19:Langmuir isotherm (Type – IV) for the adsorption of Rhodamine dye using Chitosan-Seleniumnanocomposite at different pH with dye concentration.

along the *Y*-axis irrespective of the corresponding *X*-axis resulting in the different determined parameters.

Freundlich Isotherm- Rhodamine Dye-Chitosan-Selenium Nanoparticle

Freundlich (1906) isotherm is used for the heterogeneous surface energies system. The sorption isotherm is the most convenient form of representing the experimental data at different dosages like Chitosan- Selenium nanoparticle withdosages, pH, and temperature as shown in Fig.20-22.

$$q_e = K_F C_e^{1/n} \quad ...(8)$$

$$\ln q_e = \ln K_F /(1/n) \ln C_e \quad ...(9)$$

The various constants, associated with the isotherm are the intercept, which is roughly on the indicator of sorption capacity (kf), and the slope (1/n) sorption intensity values recorded in Table 2 from Equations 8 and 9. Freundlich isotherm has been illustrated to be a special case of heterogeneous surface energies and it can be easily extended to this case. It has been stated by Krajewska (2005)& Kawamura et al.(1997), that magnitude of the exponent 1/n indicates the favourability and capacity of the adsorbent/adsorbate system. The values n>1 represent favourable adsorption

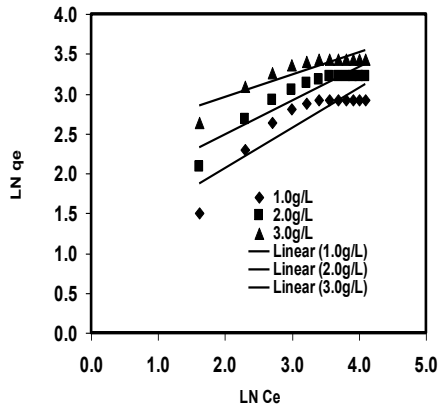

Fig. 20: Freundlich isotherm for the adsorption of Rhodamine dye using Chitosan-Seleniumnanocomposite at different Dosages with dye concentration.

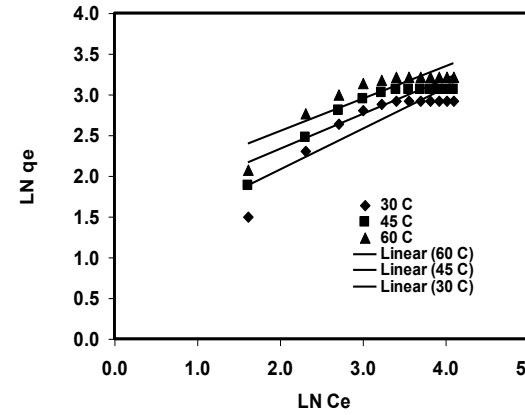

Fig. 21:Freundlich isotherm for the adsorption of Rhodamine dye using Chitosan-Seleniumnanocomposite at different Temperatures with dye concentration.

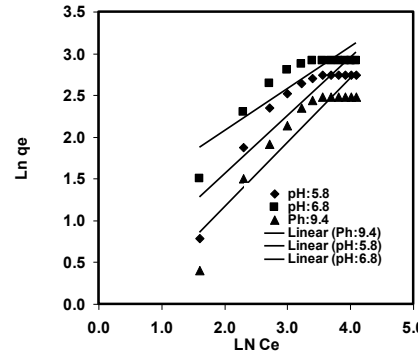

Fig. 22: Freundlich isotherm for the adsorption of Rhodamine dye using Chitosan-Selenium nanocomposite at different pH with dye concentration.

conditions. In most cases, the exponent between 1<n<10 shows beneficial adsorption.

Mechanism of adsorption according to the process of adsorption occurs either in a single step or in the combination of the steps such as film or external diffusion, pore diffusion, surface diffusion, and adsorption on the pore surface. It was also reported that adsorption on the adsorbent surface proceeds in three steps: (1) migration to the surface, (2) dissociation (or deprotonation) of complexes in an aqueous solution. Once equilibrium is attained, the migration of the solute species from the solution stops. Under this situation, it is possible to measure the magnitude of the distribution of the solute species between the liquid and solid phases. The magnitude of this kind of distribution is a measure of the efficiency of the chosen adsorbent in the adsorbate species. When a powdered solid adsorbent material is made in contact with a solution containing dyes, the dyes first migrate from the bulk solution to the surface of the liquid film. This surface exerts a diffusion barrier.

This barrier may be very significant or less significant (Gupta et al. 2005, Karthikeyan et al. 2010). The involvement of a significant quantum of diffusion barrier indicates the dominant role taken up by the film diffusion in the adsorption process. Furthermore, the rate of an adsorption process is controlled either by external diffusion, internal diffusion, or by both types of diffusions. The external diffusion controls

Table 2: Langmuir and Freundlich isotherm constants at different dosages, pH, and temperature(Chitosan- Selenium nanocomposite-Rhodamine dye).

Dosages(g/L)	Langmuir IsothermType - I	Freundlich Isotherm model parameters
1.0 g/L	q_m =2.34. K_L = 0.84. R^2 = 0.9558	K_F = 0. 8011. 1/n = 0.9314. R^2 = 0.8011
2.0 g/L	q_m = 30.21. K_L = 0.10. R^2= 0.9873	K_F = 0.4211. 1/n = 0.6063. R^2 = 0.8640
3.0 g/L	q_m = 34.13. K_L = 0.21. R^2= 0.9952	K_F = 0.2829. 1/n = 0.4185. R^2 = 0.8117
Temperature (°C)	Langmuir Isotherm Type - I	Freundlich Isotherm model parameters
30	q_m = 23.36. K_L = 0.84. R^2= 0.9558	K_F = 0.3953. 1/n = 0.5671. R^2 = 0.7889
40	q_m = 25.58. K_L = 1.00. R^2= 0.9793	K_F = 0.4291. 1/n = 0.6787. R^2 = 0.8253
60	q_m = 29.24. K_L = 1.30. R^2= 0.9829	K_F = 0.5005. 1/n = 0.9314. R^2 = 0.8011
pH	Langmuir Isotherm Type - I	Freundlich Isotherm model parameters
5.8	q_m =22.73. K_L = 0.0245. R^2= 0.6922	K_F = 0.5005. 1/n =6.1843. R^2 = 0.8205
6.8	q_m =25.00. K_L = 0.0359. R^2= 0.7843	K_F = 0.4211. 1/n =0.9314. R^2 = 0.8011
9.4	q_m =23.36. K_L =0.0840. R^2= 0.9558	K_F = 0.2829. 1/n = 2.6247. R^2 = 0.8636

Table 3: Langmuir isotherm constants at different dosages, pH,and temperature (Chitosan-Seleniumnanocomposite-Rhodamine dye).

Dosages (g/L)	Langmuir Isotherm – Type – II
1.0 g/L	q_m = 36.23 . K_L = 0.031 . R^2= 0.9476
2.0 g/L	q_m = 35.97 . K_L = .060 . R^2= 0.9793
3.0 g/L	q_m = 37.88 . K_L = 0.123 . R^2= 0.9724
Temperature (°C)	Langmuir Isotherm – Type – II
30	q_m = 36.23 . K_L = 0.031 . R^2= 0.9476
40	q_m = 32.63 . K_L = 0.054 . R^2= 0.9693
60	q_m = 37.31 . K_L = 0.059 . R^2= 0.9491
pH	Langmuir Isotherm – Type – II
5.8	q_m = 161.29. K_L = 0.0022 . R^2 = 0.9422
6.8	q_m = 312.50. K_L = 0.0024 . R^2= 0.9301
9.4	q_m = 36.23 . K_L = 0.031 . R^2= 0.9476

Table 4: Langmuir constants at different dosages, pH, and temperature (Chitosan-Selenium nanocomposite- Rhodamine dye).

Dosages (g/L)	Langmuir Isotherm – Type – III
1.0 g/L	q_m = 36.48 . K_L = 0.15 . R^2= 0.8894
2.0 g/L	q_m = 32.48 . K_L = 0.087 . R^2= 0.8656
3.0 g/L	q_m = 24.20 . K_L = 0.082 . R^2= 0.5551
Temperature (°C)	Langmuir Isotherm – Type – III
30	q_m = 24.20. K_L = 0.08 . R^2= 0.5511
40	q_m = 27.73. K_L = .08 . R^2= 0.7468
60	q_m = 31.33. K_L = 0.10 . R^2= 0.7114
pH	Langmuir Isotherm – Type – III
5.8	q_m = 19.05 . K_L = 0.07 . R^2= 0.2210
6.8	q_m = 13.25 . K_L = 0.08 . R^2= 0.5511
9.4	q_m = 17.50 . K_L = 0.06 . R^2= 0.2039

the migration of the solute species from the solution to the boundary layer of the liquid phase. However, the internal diffusion controls the transfer of the solute species from the external surface of the adsorbent to the internal surface of the pores of the adsorbent material (Karthikeyan et al. 2010 and Gupta et al. 2003b). It is now well established, that during the adsorption of dye over a porous adsorbent, the following three consecutive steps were taken place (Crank 1975 and Karthikeyan et al. 2010) (i) Transport of the ingoing adsorbate ions to the external surface of the adsorbent (film diffusion), (ii) Transport of the adsorbate ions within the pores of the adsorbent except for a small amount of adsorption, which occurs on the external surface (particle diffusion) and (iii) Adsorption of the ingoing adsorbate ions on the interior surface of the adsorbent (Weber & Morris 1963 and Karthikeyan et al. 2010).

CONCLUSION

In this study, the ever-increasing problem of dye pollutants and ways of dye remediation has been discussed. The environment-friendly technique of adsorption is brought

Table 5: Langmuir constants at different dosages, pH, and temperature (Chitosan-Selenium nanocomposite-Rhodamine dye).

Dosages (g/L)	Langmuir Isotherm – Type – IV
1.0 g/L	q_m = -2.64 . K_L = -3.5255. R^2= 0.3889
2.0 g/L	q_m = -1.77 . K_L = -6.8158 . R^2= 0.5725
3.0 g/L	q_m = -2.89 . K_L = -7.0853 . R^2= 0.5082
Temperature (°C)	Langmuir Isotherm – Type – IV
30	q_m = -2.64 . K_L = -3.525 . R^2= 0.3889
40	q_m = -2.46 . K_L = -4.545 . R^2= 0.4655
60	q_m = -2.56 . K_L = -5.625 . R^2= 0.4445
pH	Langmuir Isotherm – Type – IV
5.8	q_m = -2.64 . K_L = -3.5255 . R^2= 0.3889
6.8	q_m = -1.77 . K_L = -6.8185 . R^2= 0.5725
9.4	q_m = -2.89 . K_L = -7.0852 . R^2= 0.5082

into the light. The enhanced properties of the nanomaterials because of their small size and ways of synthesizing them have been summed up. The plant *Justicia adhatoda* leaf extract is used to produce Chitosan-Selenium nanocomposite which acts as good reducing agents for the preparation of Chitosan-Selenium nanocomposite. Likewise, chitosan–selenium nanocomposite was prepared by a simple step. UV-. Vis spectra show characteristics peak for Chitosan-Selenium nanocomposite. XRD shows the crystalline structure of Chitosan-Selenium nanocomposite, whereas the amorphous structure of chitosan-selenium nanocomposite indicates chitosan strongly coated with selenium nanoparticles. FTIR shows that functional groups responsible for the synthesis of the process are phenols, carboxylic acid, primary amine and nitro compounds, etc. for both nanoparticles. The average particle size range was noted for Chitosan-Selenium nanocomposite as 87-152 nm, respectively. Adsorption depends upon the chemical nature of the material, various physicochemical experimental conditions such as solution pH, adsorbent dosage, temperature. Adsorption technology provides an attractive pathway for further research and improvement in more efficient nanoparticles, with higher adsorption capacity, for numerous dyes to eliminate the dyes discharged from various industries and thus reduce the contamination of water.

REFERENCES

Aksu, Z. 2002.Determination of the equilibrium, kinetic and thermodynamic parameters of the batch biosorption of nickel(II) ions onto *Chlorella vulgaris.* Process Biochemistry, 38(1): 89-99.

Alkan, M. and Dogan, M. 2001. Adsorption of copper (II) onto perlite. J. Colloid Interf. Sci., 243(2): 280-291.

Allen, S. J., Mckay, G. and Khader, K. Y. H. 1989. Equilibrium adsorption isotherms for basic dyes onto lignite. J. Chem. Technol. Biotechnol., 45: 291-302.

Annadurai, G., Juang, R.S. and Lee, D.J. 2002. Use of cellulose-based wastes for adsorption of dyes from aqueous solutions. J. Hazard. Mater., **B92,** 263-74.

Arica, T.A., Ayas, E. and Arica, M.Y. 2017. Magnetic MCM-41 Silica particles grafted with poly (glycidyl methacrylate) brush: modification and application for removal of direct dyes. Microporous and Mesoporous Materials, 243(1): 164-175.

Arica, T.A., Kuman, M., Gercel, O. and Ayas, E. 2019. Poly (dopamine) grafted bio-silica composite with tetraethylenepentamine ligands for enhanced adsorption of pollutants. Chemical Engineering Research and Design, 141: 317-327.

Ashraf, M.W. 2016. Removal of methylene blue dye from wastewater by using supported liquid membrane technology. Polish Journal of Chemical Technology, 18(2): 26-30.

Baba, I.M., Lai, P. and Yifeng, X. 2020. Adsorption of methylene blue using chemically enhanced *Platanus orientalis*leaf powder: kinetics and mechanisms. Nature Environment and Pollution Technology, 9(1): 29-40.

Bajaj, M., Schmidt, S. and Winter, J. 2012. Formation of Se (0) Nanoparticles by *Duganellasp* and *Agrobacterium sp*. isolated from Se-laden soil of North-East Punja India. Microbial Cell Factories,11(1).

Bayramoglu, G. and Yilmaz, M. 2018. Azo dye removal using free and immobilized fungal biomasses: Isotherms, kinetics, and thermodynamic studies. Fibers and Polymers, 19(4): 877-886.

Bayramoglu, G., Altintas, B. and Arica, M.Y. 2012. Synthesis and characterization of magnetic beads containing aminated fibrous surfaces for removal of Reactive Green 19 dye: Kinetics and thermodynamic parameters. Journal of Chemical Technology & Biotechnology, 87(5): 705-713.

Bereket, G., Arogus, A.Z. and Ozel, M. Z. 1997. Removal of Pb (II), Cd (II), Cu (II) and Zn (II) from aqueous solutions by adsorption on bentonite. J. Colloid Interf. Sci., 187(2): 338-343.

Chang, K.L., Chen, C. C., Lin, J., Hsien, J.F., Wang, Y., Zhao, F., Shih, Y.H., Xing, Z.J. and Chen, S.T. 2014. Rice straw-derived activated carbons for the removal of carbofuran from an aqueous solution. New Carbon Materials, 29(1): 47-54.

Chiou, M.S. and Li, H.Y. 2003. Adsorption behaviour of reactive dye in aqueous solution on chemical cross-linked chitosan beads. Chemosphere, 50: 1095.

Crank, J. 1975. The Mathematics of Diffusion, 2nd Ed. Clarendon, Oxford.

Daneshvar, N., Rasoulifard, M.H., Khataee, A.R. and Hosseinzadeh, F. 2007. Removal of C.I. Acid Orange 7 from aqueous solution by UV irradiation in the presence of ZnOnanopowder. Journal of Hazardous Materials, 143: 95-10.1

Demirbas, O. and Dogan, M. 2002. The removal of Victoria blue from aqueous solution by adsorption on a low-cost material. Adsorption, 8: 341-349.

Dogan, M. and Alkan, M. 2003. Adsorption kinetics of methyl violet onto perlite. Chemosphere, 50: 517-528.

Dogan, M. and Alkan, M. 2003. Adsorption kinetics of Victoria blue onto perlite. Fresenius Environ. Bull., 12(5): 418-425.

Dogan, M. and Alkan, M. 2003. Removal of methyl violet from aqueous solution by perlite. J. Colloid Interf. Sci., 267: 32-41.

Dogan, M., Alkan, M. and Onganer, Y. 2000. Adsorption of methylene blue from aqueous solution onto perlite. Water Air Soil Pollut., 120: 229-248.

El-Sharkawy, E.A., Soliman, A.Y. and Al-Amer, K.M. 2007. Comparative study for the removal of methylene blue via adsorption and photocatalytic degradation. J. Colloid Interface Sci., 310: 498-508.

Eren, E. and Afsin, B. 2007. Investigation of a basic dye adsorption from aqueous solution onto raw and pre-treated sepiolite surfaces. Dyes and Pigments, 73(2): 162-167.

Faria, P.C.C., Orfao, J.J.M. and Pereira, M.F.R. 2004. Adsorption of anionic and cationic dyes on activated carbons with different surface chemistries. Water Res., 38: 2043-2052.

Feng, C.W., Ru, L.T. and Juang, R.S. 2001. Kinetic modeling of liquid-phase adsorption of reactive dyes and metal ions on chitosan. Water Research, 35: 613-18.

Ferrero, F. 2000. Oxidative degradation of dyes and surfactant in the Fenton and Photo-Fenton treatment of dye house effluentscolor. Technol., 116: 148-153.

Fesharaki, P.J., Nazari, P., Shakibaie, M., Rezaie, S.M., Banoee, S., Abdollahi, M. and Shahverdi, A.R. 2010. Biosynthesis of selenium nanoparticles using *Klebsiella pneumoniae* and their recovery by a simple sterilization process. Brazilian Journal of Microbiology, 41: 1517-8382.

Forgacs, E., Cserhati, T. and Oros, G. 2004. Removal of synthetic dyes from wastewater: A review. Environ. Int., 30: 953-971.

Freundlich, H.M.F. 1906. Uber die adsorption in losungen. ZeitschriftPhysikalischeChemie, 57: 385-470.

Fu, Y. and Viraraghavan, T. 2001. Fungal decolorization of wastewaters: A review. Bioresource Technol., 79: 251-262.

Ganesh, R., Boardman, G.D. and Michelsen, D. 1994. Fate of azo dye in sludges. Water Res., 28(13): 67-76.

Gardiner, D.K. and Brune, B.J. 1978. Textile wastewater treatment and environmental effects. J.Soc. Dyers and Colorists, 94: 339-348.

Ghosh, D. and Bhattacharyya, K.G. 2002. Adsorption of methylene blue on Kaolinite. Appl. Clay Sci., 20: 295-300.

Giunchedi, P., Genta, I., Conti, B., Muzzarelli, R.A.A. and Conte, U. 1998. Preparation and characterization of ampicillin loaded methylpyrrolidinone chitosan and chitosan microspheres. Biomaterials, 19: 157-161.

Gupta, G.S., Prasad, G., Panday, K.K. and Singh, V.N. 1989. Removal of chrome dye from aqueous solution by fly ash. Water Soil. Pollut., 37: 13-24.

Gupta, V. K., Ali, I. Suhas and Mohan, D. 2003. Equilibrium uptake and sorption dynamics for the removal of a basic dye (basic red) using low-cost adsorbents. J. Colloid Interface Sci., 265: 257-264.

Gupta, V. K., Mittal, A. and Gajbe, V. 2005. Adsorption and desorption studies of a water-soluble dye, Quinoline Yellow, using waste materials. J. Colloid Interface Sci., 284: 89-98.

Gupta, V. K., Mohan, D., Sharma, S. and Sharma, M. 2000. Removal of basic dye (rhodamine-B and methylene blue) from aqueous solution using bagasse fly ash. Sep. Sci. Technol., 35(13): 2097.

Hamza, A. and Hamoda, M.F. 1980. Multiprocess treatment of textile wastewater. In: Proceedings of the 35th Industrial Waste Conference, Purdue University, Lafayette, Indiana, p.151.

Ho, Y. S. and Mckay, G. 1998. Sorption of dye from aqueous solution by peat. Chem. Eng. J., 70(2): 115-124.

Jain, A.K., Gupta, V.K., Bhatnagar, A. and Suhas 2003. Utilization of industrial waste products as adsorbents for the removal of dyes. Journal of Hazardous Material B, 101: 31-42.

Janos, P., Buchtova, H. and Rýznarova, 2003. Sorption of dyes from aqueous solutions onto fly ash. Water Research, 37(20): 4938-4944.

Jumasiah, A., Chuah, T.G., Gimbon, J., Choong, T.S.Y. and Azni, I. 2005. Adsorption of basic dye onto palm kernel shell activated carbon: sorption equilibrium and kinetics studies. Desalination, 186: 57-64.

Kadirvelu, K., Karthika, C., Vennilamani, N. and Pattabhi, S. 2005. Activated carbon from industrial solid waste as an adsorbent for the removal of Rhodamine-B from aqueous solution: Kinetic and equilibrium studies. Chemosphere, 60: 1009-1017.

Kamel, D., Sihem, A., Halima, C. and Tahar, S. 2009. Decolourization process of an azoique dye (Congo red) by photochemical methods in homogeneous medium. Desalination, 247: 412-422.

Karthikeyan, S., Sivakumar, B. and Sivakumar, N. 2010. Film and pore diffusion modeling for adsorption of Reactive Red 2 from aqueous solution on to activated carbon prepared from bio-diesel industrial waste. E-Journal of Chemistry, 7(1): 175-184.

Kaushik, P. and Malik, A. 2009. Fungal dye decolorization: Recent advances and future potential. Environ. Int., 35: 127-141.

Kawamura, Y., Mitsuhashi, M., Tanibe, H. and Yoshida, H. 1993. Adsorption of metal ions on polyaminated highly porous chitosan chelating resin. Ind. Eng. Chem. Res., 32: 386-391.

Kawamura, Y., Yoshida, H. and Asai, S. 1997. Effects of chitosan concentration and precipitation bath concentration on the material properties of porous crosslinked chitosan beads. Sep. Sci. Technol., 32: 1959-1974.

Kirupagaran, R., Saritha, A. and Bhuvaneswari, S. 2016. Green synthesis of selenium nanoparticles from leaf and stem extract of Leucaslavandulifolia Sm. and their application. J.Nanosci. Tech., 2(5): 224–226.

Knorr, D. 1985. Food technology. In: R.R. Colwell, E.R. Pariser and A.J. Sinskey (Ed.), Biotechnology of Marine Polysaccharides, Vol. 85, Hemisphere, New York. p. 313.

Krajewska, B. 2005. Membrane-based processes performed with use of chitin/chitosan materials Sep. Purif. Technol., 41: 305-312.

Kurita, K. 2001. Controlled functionalization of polysaccharide chitin. Progress in Polymer Science, 26(9): 1921-1971.

Langmuir, I. 1916. The constitution and fundamental properties of solids and liquid. J. Am. Chem. Soc., 38(11): 2221-2295.

Langmuir, I.J. 1918. The adsorption of gases on plane surface of glass, mica, and platinum. J. Chem.Soc., 40: 1361-1366.

Lee, C.K. and Low, K.S. 1987. The removal of cationic dyes by a natural moss 1-adsorption studies. Pertanika, 10: 327-334.

Lin, Z.H. and Wang, C.R.C. 2005. Evidence on the size-dependent absorption spectral evolution of selenium nanoparticles. Mater. Chem. Phys., 92: 591-594.

Mall, I. D., Srivastava, V. C., Agarwal, N. K. and Mishra, I. M. 2005. Adsorptive removal of malachite green dye from aqueous solution by bagasse fly ash and activated carbon-kinetic study and equilibrium isotherm analyses. Colloids and Surfaces A, 264(1-3): 17-28.

Mallikarjuna, K., Narasimha, G., Dillip, G.R., Praveen, B. and Shreedhar, B. 2011. Green synthesis of silver nanoparticles using *Ocimum* leaf extract and their characterization. Dig. J. Nanomat. Biostruc,. 6: 181-186.

McKay, G. 1980. Color Removal by Adsorption. American Dye-stuff Reports, p. 38.

Mckay, G. 1984. Analytical solution using a pore diffusion model for a pseudo-irreversible isotherm for the adsorption of basic dye on silica. AICHE J., 30: 692.

Mckay, G. M.S. and Otterburn, A.G. 1981. Sweeney, Surface mass transfer processes during colour removal from effluent using silica. Water Res., 15: 327-331.

Mohamed, M.M. 1996. Adsorption properties of ionic surfactants on molybdenum-modified silica gels. Colloid Surf. A: Physicochem. Eng. Aspects, 108: 39-48.

Mohan, D., Singh, K.P. and Kumar, K. 2002. Removal of dyes from wastewater using fly ash, a low-cost adsorbent. Ind. Eng. Chem. Res., 42: 1965-1976.

Muzzarelli, R.A.A. 1973. Natural Chelating Polymers, Pergamon Press, Oxford.

Nurchi, V. M. M. Crespo-Alonso, and Biesuz, R. 2014. Sorption of chrysoidine by row cork and cork entrapped in calcium alginate beads. Arabian Journal of Chemistry, 138-133 :(1)7.

Oliveira, L.S., Franca, A.S., Alves, T.M. and Rocha, S.D.F. 2008. Evaluation of untreated coffee husks as potential biosorbents for treatment of dye contaminated waters. J. Hazard. Mater., 155: 507-512.

Ramamurthy, C.H., Sampath, K.S., Arunkumar, P., Suresh Kumar, M., Sujatha, V. and Premkumar, K. Thirunavukkarasu, C. 2013. Green synthesis and characterization of selenium nanoparticles and its augmented cytotoxicity with doxorubicin on cancer cells. Bioprocess Biosyst. Eng., 36: 1131-1139.

Rathinam, A., Nishtar, N. F., Jonnalagadda, R. and Balachandran, U. 2007. Equilibrium and thermodynamic studies on the removal of basic black dye using calcium alginate beads. Colloids and Surfaces A: Physicochem. Eng. Aspects, 299: 232-238.

Ravi Kumar, M.N.V. 2000. A review of chitin and chitosan applications. React. Funct. Polym., 46: 1-27.

Rinaudo, M. 2006. Characterization and properties of some polysaccharides used as biomaterials. Macromol. Sympl., 245-246: 549-557.

Senthilkumar, S.R. and Sivakumar, T. 2014. Green tea (Camellia sentences) mediated synthesis of zinc oxide (ZnO) nanoparticles and studies on their antimicrobial activities. Inter. J. Pharm. Pharm. Sci., 6: 461-465.

Shaul, G.M., Barnett, M.W. and Dostal, K.A. 1982. Treatment of dye and pigment processing wastewater by activated sludge process. In Proceedings of the 37th Industrial Waste Conference, Purdue University, Lafayette, Indiana, p. 677.

Shelley, M.L., Randall, C.W. and King, P.H. 1976. Evaluation of chemical-biological and chemical physical treatment for textile dyeing and finishing waste. J. WPCF, 4: 753.

Shen, Y., Xiufang, W., Xie, A., Huang, L. and Zhu, J. 2000. Synthesis of dextran/Se nanocomposites for nanomedicine application. Mater. Chem. Phys., 109: 534-540.

Sivaraj, R., Namasivayam, C. and Kadirvelu, K. 2001. Orange peel as an adsorbent in the removal of Acid Violet 17 (Acid Dye) from aqueous solutions. Waste Manag., 21: 105.

Wang, Z., Xue, M., Huang, K. and Liu, Z. 2011. Textile dyeing wastewater treatment. Advances in Treating Textile Effluent, 5: 91-116.

Weber, W. J. and Morris, C. J. 1963. Kinetics of adsorption on carbon from solution. J. Sanit. Eng. Div., 89: 31-60.

Wei, Y.C., Hudson, S.M., Mayer, J.M. and Kaplan, D.L. 1992. The crosslinking of chitosan fibers. J. Polym. Sci. Polym. Chem., 30: 2187.

Yoshida, H. and Takemori, T. 1997. Adsorption of direct dye on cross-linked chitosan fibre: Breakthrough curve. Water Sci. Technol., 35: 29-37.

Yu, M.C., Skipper, P.L., Tannenbaum, S.R., Chan, K.K. and Ross, R.K. 2002. Arylamine exposures and bladder cancer risk. Nutat. Res. Fund. Mol. M., 21: 506-507.

Yui, T., Imada, K., Okuyama, K., Obata, Y., Suzuki, K. and Ogawa, K. 1994. Molecular and crystal structure of the anhydrous form of chitosan. Macromolecules, 27: 7601-7605.

Nature Environment and Pollution Technology
An International Quarterly Scientific Journal

p-ISSN: 0972-6268
(Print copies up to 2016)
e-ISSN: 2395-3454

Vol. 20 | No. 2 | pp. 481-490 | 2021

Original Research Paper

https://doi.org/10.46488/NEPT.2021.v20i02.004

Open Access Journal

Greener Approach to Metallic Nanoparticles: A Review

S. Arora†*, M. Latwal*, K. D. Bahukhandi, D. Kumar***, T. Vemulapalli**, S. Egutoori** and N. A. Siddiqui****

*Department of Chemistry, University of Petroleum and Energy Studies, Dehradun (UK), India
**Department of Health Safety & Environment, University of Petroleum and Energy Studies, Dehradun (UK), India
***Dolphin (PG) Institute of Biomedical and Natural Sciences, Dehradun (UK), India
†Corresponding author: S. Arora; shefali.arora@ddn.upes.ac.in

Nat. Env. & Poll. Tech.
Website: www.neptjournal.com

Received: 05-05-2020
Revised: 21-06-2020
Accepted: 26-06-2020

Key Words:
Biosynthesis
Metal nanoparticles (MNPs)
Plant extract
Plant metabolites

ABSTRACT

Nanoscale based materials are gaining more attention due to their unique physical, chemical and thermodynamic properties. Nowadays the "Green" nanoparticle synthesis has attracted more attention as it is using environmentally acceptable solvent systems which act as eco-friendly reducing and capping agents. This review focuses on a detailed analysis of the bio-production of metal nano-particles by a biological agent, the various factors affecting the morphology, size, and yield of metal nanoparticles, the role of plant metabolites, and the experimental procedure in the synthesis of nanoparticles. This review also gives a platform for the role of natural plant biomolecules involved in the bio-reduction of metal salts during the nanoparticle synthesis, interaction of nanoparticles with various biomolecules, biological application and future directions are discussed as a step towards making a pollution-free environment.

INTRODUCTION

The "green" synthesis of metallic nanoparticles has received increasing attention due to the development of eco-friendly technology in material science. Preparation of nanoparticles via chemical procedure also produces a very high amount of hazardous by-products so the investigation of new chemical and physical methods has to be developed. Thus, there is a need for 'green chemistry' that includes a clean, cheap, nontoxic and environment-friendly method of nanoparticle synthesis (Mukherjee et al. 2001). The plants that can be used for the production of nanoparticles could be a better option in comparison to other environmentally benign biological processes as they eliminate the elaborate and conventional process of maintaining cell cultures (Gour et al. 2019). Biosynthetic methods for the production of nanoparticles would be more useful if nanoparticles were synthesized extracellular using plants or their extracts and in a controlled way in terms of their size, dispersity and shape. Biogenic synthesis of nanoparticles with controlled morphology needs more attention, as the biogenic synthesis of nanoparticles is carried out by using biological means like bacteria (Husseiny et al. 2007), fungi (Kumar et al. 2007), actinomycetes (Ahmad et al. 2003a), lichens (Shahi et al. 2003), algae (Chakraborty et al. 2009), etc. The biogenic entities are found to secrete a large amount of proteins which are found to be responsible for the metal-ion reduction and morphology control (Thakkar et al. 2010). Progress in the field of nanotechnology has been rapid and with the development of innovative synthesis protocols and characterization techniques (Sharma et al. 2009). But most of the synthesis methods are limited to the synthesis of nanoparticles in small quantities and poor morphology. Using plant extract is cheaper than microorganisms as it does not require culture preparation or maintenance of aseptic conditions. The synthesis of nanoparticles using microbes (Kathiresan et al. 2010) and plant extracts cost mainly depends on the many aspects like the metal particles and isolate the chemicals added as the precursor for the nanoparticle synthesis.

Metal nanoparticles have marvellous applications in the area of catalysis, optoelectronics, diagnostic biological probes and display devices, medicine, agriculture and industry. They have been used in the drug delivery system, biomedical devices, biosensors, optics, solar batteries, semiconductors etc. Synthesis of nanoparticles using biological entities has great interest due to their unusual optical (Lin et al. 2000), chemical (Krolikowska et al. 2003), photoelectrochemical (Ahmad et al. 2003b) and electronic properties (Chandrasekharan et al. 2000). The most effectively studied nanoparticles today are those made from noble metals, in particular Ag, Pt, Au, Zn, Cu, Fe, Ni, U, Zr, Se, Te, Ni and

Pd. Nanoscale biosynthesis of two noble metal Ag and Au is of particular interest and importance. It has been reported that silver nanoparticles (SNPs) are non-toxic to humans and most efficient against bacteria, virus and other eukaryotic microorganisms at low concentrations without any side effects (Jonge et al. 2005) and gold nanoparticles produced by using phytochemicals or other extract components remain stable for a certain time (Singh et al. 2010). Moreover, plants and species mediated, stabilized or capped gold nanoparticle (AuNPs) may cross the cytotoxicity barrier which is a basic requirement in the field of biomedical application of AuNPs (Das et al. 2011). In continuation of this, we summarize the various aspects of "metal nanoparticle using plants" in this review. Here we discuss the biogenesis of nanoparticle, interaction of nanoparticles with various biomolecule, role of plant metabolites in the binding and reduction of metal ion, experimental procedure and characterization of nanoparticles and finally application and future prospects.

BIOPRODUCTION OF NANOPARTICLES

Various types of physical and chemical methods are used for the synthesis of nanoparticles. The use of these methods requires both strong and weak chemical reducing and protective agents like sodium borohydride, sodium citrate and alcohols. These agents are mostly toxic, flammable, cannot be easily disposed of due to environmental issues and also show a low production rate (Bar et al. 2009). It leads to in search of alternatives that could be eco-friendly and does not cause any harm to human and domestic animals health. One of the primary processes in biosynthesis involves bioreduction. The cell wall of the microorganisms plays a major role in the intracellular synthesis of nanoparticles. The cell wall being negatively charged interacts electrostatically with the positively charged metal ions. The enzymes present within the cell wall bioreduce the metal ions to nanoparticles, and finally the smaller sized nanoparticles get diffused of through the cell wall. Bacterial was the first species to synthesize nanoparticles and later on the use of various fungi, actinomycetes and more recently plants was also succeeded. The rate of reduction of metal ions using biological agents is found to be much faster and also at ambient temperature and pressure conditions.

NANOPARTICLE SYNTHESIS IN BACTERIA

Many microorganisms can synthesize inorganic nanoparticles like silver, gold, magnesium, cadmium sulphide and silicon oxide nanoparticles. The resistance caused by the bacterial cell for silver ions in the environment is responsible for its nanoparticles synthesis. Previously the synthesis of nanoparticles via bacteria has enlarged comprehensively due to its immense application. *Bacillus species* has been investigated to synthesize metal nanoparticles and proved bacteria as a potent source to decrease silver and fabrication of extracellularly, consistently circulated nanoparticles, ranging from 10-20 nm size (Sunkar et al. 2012). *Lactobacillus*, a common bacterial strain present in the buttermilk, synthesizes both Au and Ag NPs of well-defined morphology under standard conditions. Nair et al. (2002) and Shahverdi et al. (2007) reported the synthesis of metallic nanoparticles of Ag using the cultural supernatants of *Klebsiella pneumonia*, *Escherichia coli* and *Enterobacter cloacae*. Shirley and co-workers reported the antibacterial activity of silver nanoparticles synthesized from a novel strain of *Streptomyces* sp. (Shirley et al. 2010). A tremendous potential antibacterial activity is shown by novel silver nanoparticles against the multi-drug resistant gram-positive and gram-negative bacterial strains were greatly established. The most widely acknowledged mechanism for the biosynthesis of silver nanoparticles is the presence of the enzyme nitrate reductase which converts nitrate into nitrite. This has been observed in *Bacillus licheniformis* which is known to secrete NADPH and NADPH-dependent enzymes like nitrate reductase that effectively converts Ag^{+} to Ag^{0}.

Bacteria are also used to synthesize gold nanoparticles. Sharma et al. (2012) reported that complete cells of a novel strain of *Marinobacter pelagius are* responsible for the production of stable, monodisperse gold nanoparticle. Prasad et al. (2007) have reported the use of *Lactobacillus* strains to synthesize the titanium nanoparticles. Several bacterial strains have been reported for the synthesis of silver, gold, magnetite, palladium, platinum, selenium, zinc oxide, cadmium sulphide, titanium, titanium dioxide and copper nanoparticles (Ramanathan et al. 2013, Arshad et al. 2017).

NANOPARTICLE SYNTHESIS IN FUNGI

Fungi may be used to grow nanoparticles of different chemical composition and sizes. Fungi acts as a "Nanofactory" for the production of metal nanoparticles especially silver nanoparticles. Fungi produce well-defined structured nanoparticles with good monodispersity. Fungi can produce larger amounts of nanoparticles as compared to bacteria because they secrets large amounts of proteins which directly affects the higher productivity of nanoparticles (Mohanpuria et al. 2008). Fungi have a high binding capacity with the metal ions in the intracellular region, they are easy to culture on solid substrate fermentation, they can grow on the surface of an inorganic substrate during culture leading to an efficient distribution of metals as a catalyst. The main advantage of nanoparticles extracellularly from fungi is that a large quantity of enzyme which is in a pure state and free

from cellular protein can be easy to apply for the simple downstream process. *Phoma glomerata* has been identified to produce silver nanoparticles, and its activity against *E.coli, S. aureus* and *P. aeruginosa* has been reported (Birla et al. 2009). Bioreduction of aqueous $AuCl^{4+}$ was done by using the fungus *Verticillium* sp. that produces gold nanoparticles with well-defined dimensions and good monodispersity. Investigations carried out on 20 different fungi reveals that fungi are extremely good candidates in the synthesis of metal and metal sulphides nanoparticles. The genus *Penicillium* seems to have a promising candidate for the silver nanoparticle synthesis, where production proceeds *via* extracellular mechanism (Sadowski et al. 2008). *Humicola sp.* has been reported to synthesize highly stable, protein capped silver nanoparticles which were non-toxic to cancer cells as well (Syed et al. 2013).

NANOPARTICLE SYNTHESIS IN ACTINOMYCETES, YEAST AND ALGAE

Actinomycetes are the class of microorganisms that has some of the properties of fungi and bacteria. Actinomycetes are now getting important for the synthesis of metallic nanoparticles because of their characteristic to produce secondary metabolites such as antibiotics. Synthesis of Au nanoparticles by using the extremophilic actinomycete, *Thermomonospora* sp which yielded polydisperse Au nanoparticles has been investigated by Sastry et al. (2003). The intracellular synthesis of Au nanoparticles by using alkalotolerant *Rhodococcus* sp. have been reported. It was observed that the concentration of nanoparticles was more on the cytoplasmic membrane than on the cell wall. This may be due to the reduction of the metal ions by enzymes present in the cell wall and on the cytoplasmic membrane but not in the cytosol (Ahmad et al. 2011).

The synthesis of cadmium nanoparticles by using *Candida glabrata* and *Schizosaccharomyce pombe* has been reported by Dameron et al. (1989). Kowshik et al. (2003) have identified yeast *Torulopsis* sp. being capable of intracellular synthesis of PbS crystallite when exposed to aqueous Pb^{2+} ions and CdS nanoparticles synthesized intracellularly by using *Schizosaccharomyces pombe* (yeast cells). The silver and gold nanoparticles biosynthesis was also investigated (Mourato et al. 2011) by taking an extremophilic yeast strain that was isolated from acid mine drainage. Algae are a diverse group in the plant kingdom that are also being explored. Hosea et al. (1986) investigated the gold nanoparticles on the algae *Chlorella vulgaris*. The rapid formation of Au nanoparticles through extracellular biosynthesis in marine alga *Sargassum wightii* was investigated. Scarano et al. (2003) reported the fabrication of phytochelatin coated CdS nanocrystals by using the phytoplanktonic alga *Phaeodactulum tricornatum*.

NANOPARTICLE SYNTHESIS IN PLANT EXTRACT

Biosynthesis reaction of nanoparticles is an important branch of bio-production of nanoparticles with the use of plant extract. As the size, dispersity and shape of nanoparticles can be controlled by the biosynthetic processes for nanoparticles when nanoparticles were produced extracellular using plants. Plants use can also be suitably scaled up for large-scale synthesis of nanoparticles. Gardea-Torresdey et al. (2002) firstly reported the preparation of gold and silver nanoparticles by living alfalfa plants. Some specific plant parts or the whole plant, specially angiospermic plants, are used for the great synthesis of nanoparticle (Kumar et al. 2014). Fabrication of inorganic nanoparticles by plants is rapid, cost-effective and eco-friendly process (Kavitha et al. 2013). The synthesis can be done by both intra and extracellular methods, such as leaf broth (Shivshankar et al. 2004, Lalitha et al. 2013, Ahmed et al. 2015, Ahmed et al. 2016), sun-dried leaves (Senthilkumar et al. 2014), fruits (Dubey et. al. 2010), seeds, bark, root etc. Metal nanoparticles prepared by chemical and biological methods use reducing agents for the reduction of metal ions and protective agents or phase transfer agents to stabilize the nanoparticle. Biosynthesis of metal nanoparticles, using plant leaf material as reductants as well as capping agent, is currently under exploitation. It is an eco-friendly, cost-effective and more efficient alternative method for large scale synthesis of metal nanoparticles.

During the process of production of nano-particles, the plant extract is simply mixed with a solution of metal salt at room temperature. It is a quick reaction and usually takes minutes to complete. Nanoparticle properties and production time depend on various characteristics of plant extract, namely its concentration, the concentration of the metal salt, pH, temperature and contact time. Another good advantage for taking the plant extract is that the plants supplement both the reducing as well as stabilizing agents for the nanoparticles which otherwise have to be externally added in other methods. Present studies have depicted that the therapeutic effects of plants, from which the nanoparticles are being prepared, provide the perfect vehicles to act upon the site of action and eliminate the need to artificially develop a drug for that specific ailment.

FACTOR AFFECTING THE NANOPARTICLE SYNTHESIS

Several factors influence the reduction process of metal

ions into NPs. Various optimum bio-reduction conditions are substrate and biocatalyst concentration, electron donor capacity, pH, exposure time, temperature, buffer strength, mixing speed, light that can be controlled. The (nano) environmental conditions determine the average size and size distribution of NPs, which is a very important feature for the technological use of such materials. However, very little has so far been elucidated for living plants.

The pH value of the medium influences the size of nanoparticles under formation in both extracts and living plants. For example, the size of gold nanoparticles was controlled by altering the pH of the medium in *Avena sativa* (Shankar et al. 2007). However, pH has a major impact on the size rather than on the shape of the nanoparticle formed. The reaction mechanism for the formation of magnetite nanoparticles has been found to be influenced by pH when co-precipitation method was followed (Armendariz et al. 2004). One of the most interesting aspects of NPs biosynthesis is the fact that this process occurs at ambient temperature. However, the temperature of the reaction medium is a critical factor that determines the nature of nanoparticles formed. For the production of anisotropic nanoparticles with the fine-tuning of the shape, size and optical properties temperature variations in reaction conditions are also an important factor. When *Cymbopogon flexuosus* was evaluated to produce gold nanoparticles at higher temperatures, the percentage of gold nano triangles relative to spherical particles were significantly reduced at high temperature, whereas low temperature mostly promoted nano triangle formation (Faiyas et al. 2010, Rai et al. 2006). The size of gold nanoparticles was shown to increase at higher reaction temperatures as explained by an increase in fusion efficiency of micelles which dissipates supersaturation (Muralidharan et al. 2011). Some other factors also play a remarkable role in nanoparticle synthesis. According to the Schikorr reaction, the size and crystallinity of magnetite nanoparticles were found to increase with increasing molar ratios of ferric/ferrous ions during synthesis by the hydrothermal synthesis method (Mizutani et al. 2008). The polyol and water-soluble heterocyclic components were mainly responsible for the reduction of silver ions or chloroaurate ions (Huang et al. 2007). An incubation of sun-dried biomass of *Cinnamomum camphora* leaf with aqueous silver or gold precursors at ambient temperature produces both silver nanoparticles (55-80 nm) and triangular or spherical gold nanoparticles. The major difference in the shape of silver and gold nanoparticles could be ascribed to the comparative potential of protective and reductive biomolecules from leaf extracts. The concentration of the substrate also affects the size of the nanoparticle. The sizes of gold nanoparticles decrease with increasing NaCl concentrations (size ranges, 5-16 nm) than those synthesized without the addition of NaCl (size ranges 11-32 nm) (Mohamad et al. 2011). Several other factors have also been reported that affect the geometry and size of metal nanoparticles (Soni et al. 2001, Vijayaraghavana et al. 2017).

PLANT METABOLITES IN THE BINDING AND REDUCTION OF METAL ION

Various plant metabolites for e.g. alkaloids, sugars, terpenoids, phenolic compounds, polyphenols and proteins having an important role in the synthesis of nanoparticles via the bioreduction of metal ions.

Flavonoids contain various nanoparticle groups capable of nanoparticle formation (Singh et al. 2018). It has been suggested that the tautomeric transformation of flavonoids from the enol-form to the keto-form may release a reactive hydrogen atom that can reduce metal ions to form nanoparticles. Ahmed et al. (2010) reported that the formation of silver nanoparticles in *Ocimum basilicum* (sweet basil) extracts transform flavonoids, luteolin and rosmarinic acid from the enol- to the keto-form. Some flavonoids are capable to chelate metal ions with their carbonyl groups or π-electrons. For example, quercetin is a flavonoid with very strong chelating activity, because it can chelate at three positions involving the carbonyl and hydroxyls at the C3 and C5 positions and the catechol group at the C3' and C4' site. These groups chelate various metal ions such as Fe^{2+}, Fe^{3+}, Cu^{2+}, Zn^{2+}, Al^{3+}, Cr^{3+}, Pb^{2+}, and Co^{2+}. The presence of such mechanisms may help the flavonoids to be adsorbed onto the surface of a nascent nanoparticle. It has been postulated the terpenoids are often associated with nanoparticles. Terpenoids are a class of organic polymers synthesized in plants from five-carbon isoprene units, which show strong antioxidant activity (Shankar et al. 2003). Initially, it was suggested that terpenoids play a key role in the transformation of silver ions into nanoparticles in reactions using extracts from geranium leaves. The main terpenoid i.e. Eugenol, in *Cinnamomum zeylanisum* (cinnamon) extracts, was investigated to play the main role in the bioreduction of $HAuCl_4$ and $AgNO_3$ to nanoparticles (Singh et al. 2010). It was suggested that dissociation of a proton of the eugenol OH-group results in the formation of resonance structures capable of further oxidation. This process is accompanied by the active reduction of metal ions, followed by nanoparticle formation.

The sugars present in plant extracts can also act as a catalyst in the formation of metal nanoparticles. It is known that monosaccharides such as glucose-containing an aldehyde group can act as reducing agents. Monosaccharides containing a keto-group, e.g. fructose, can act as antioxidants only when they have undergone a series of tautomeric

transformations from a ketone to an aldehyde. The reducing ability of disaccharides and polysaccharides depends on the ability of individual monosaccharide components to form an open-chain form within an oligomer and hence, to provide access (of a metal ion) to an aldehyde group. Glucose is able to participate in the synthesis of metal nanoparticles of different morphologies, whereas fructose facilitates the synthesis of monodispersed nanoparticles of gold and silver. It was shown (Panigrahi et al. 2004) that sucrose is not too capable to reduce silver nitrate or palladium chloride into nanoparticles. An open chain-form structured produced by the acid hydrolysis of sucrose into free glucose are responsible for the synthesis of nanoparticles with the replacement of metal by tetrachloroauric and tetrachloroplatinic acids (Makarov et al. 2014). Nowadays it is believed that the sugar aldehyde group is oxidized into a carboxyl group via the nucleophilic addition of OH-, which in turn gives to the reduction of metal ions and capable of the formation of nanoparticles.

Peptides, proteins and amino acids present in plant extracts probably play a very important role in determining the shape of nanoparticles and affect the overall yield of nanoparticles. It was investigated that protein molecules that help in the formation of nanoparticles from metal ions show high reducing activity and a high potential for attracting metal ions to the regions of a molecule that are responsible for reduction, but that their chelating activity is not excessive. Amino acid sequence of a protein can greatly affect the size, amount and morphology of nanoparticles. They can bind to the metal ions through the amino and carbonyl groups of the main chain or through side chains, such as the carboxyl groups of aspartic and glutamic acid or a nitrogen atom of the imidazole ring of histidine. Other side chains binding metal ions include the thiol, thioether, hydroxyl and carbonyl groups (Glusker et al. 1999). Side thiol groups and amino groups are also responsible for the reduction of metal ions. Few phenolics, lipids, terpenoids, biopolymers, ascorbic acid, hydroxypropyl starch and lignin have also been reported for the binding and reduction of several metal ions (El-Rafie et al. 2011, Kumari et al. 2016, Iravani et al. 2020).

EXPERIMENTAL PROCEDURE INVOLVED IN THE SYNTHESIS OF NANOPARTICLES USING PLANT EXTRACT

The use of plant extract for biosynthesis reaction for the production of nanoparticles was fairly investigated and described. The leaf reductants present in leaf extracts are mainly used in the preparation of metal nanoparticles. Plants act as a suitable vehicle for the synthesis of metal nano-particle and they are formed directly in living plants by reduction of the metal ions absorbed as a soluble salt. The main mechanism considered for the synthesis of nanoparticles mediated by the plants is due to the presence of phytochemicals. The major phytochemicals responsible for the spontaneous reduction of ions are flavonoids,

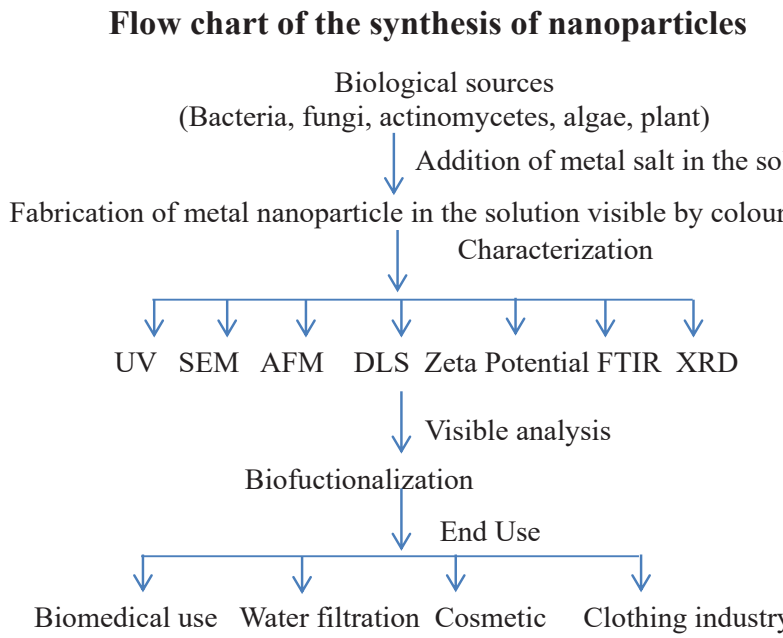

Fig 1: General procedure for synthesis of nanoparticles.

terpenoids, carboxylic acids, quinones, aldehydes, ketones and amides. The aqueous solution of metal nitrate (mM) is treated with plant extract at ambient temperature and filtered. The supernatant is heated between 50-85°C leading to the formation of nanoparticles. The change in the colour is monitored through a UV-VIS spectrophotometer. SEM, EDAX measurements are performed to estimate the size, shape and quantity of the nanoparticles

BIOLOGICAL PERSPECTIVE OF VARIOUS METALLIC NANO-PARTICLES

The green synthesis of silver nanoparticles and its application for mosquito control has been investigated by Mondal et al. (2014). For the generation of maximum stable nanoparticles in an aqueous medium, it was found that aqueous silver ions can be reduced by aqueous root extract of *P. hysterophorus.* Larvae were exposed to varying concentration of plant extract, aqueous silver nitrate solution and synthesized silver nanoparticles for 0, 24 and 48 hours separately. Aqueous root extract depicted moderate larvicidal effects; however, the maximum efficacy (60.18%) was seen with the prepared silver nanoparticles against the larvae of *Culex quinquefasciatus*.

Zinc oxide nanoparticles have been reported to be incorporated in polymeric matrices in order to provide an antimicrobial activity to packaging material and improve packaging properties (Espitia et al. 2012). Colloidal nanoparticles give good responses to incident light, making them useful as sensors. The potential uses of nanoparticle biosensors in research and diagnosis. Recently the nanoparticles have been employed for ultrasensitive detection of cancer in human serum. Not only diagnosis but silver, gold and zinc oxide nanoparticles have been reported to show anticancer activity (Mirzaei et al. 2017). D'Britto et al. (2012) investigated the medicinal plant extracts used for blood sugar and obesity therapy and exhibit excellent inhibition of invertase activity. Extract of *Azardirecta indica, Cephalandra indica, Calotropis procera and Syzygium jambolanum,* prepared together, is an elixir for the treatment of blood sugar and obesity by homoeopathic medicine. It is established that inhibitors of -glucosidases such as invertase, amylase etc, can suppress the digestion and adsorption of carbohydrates and also inhibit postprandial hyperglycemia and thus helps in Diabetes therapy. In this study, the invertase inhibitor action of the elixir was tested in order to put more light on the therapeutic mechanism of this elixir. Moreover, rapid bio-reduction of Au^{3+} and Ag^{+} ions to their respective nanoparticles was achieved using the same extract of these medicinal plants. Cytotoxicity (MTT assay) and genotoxicity (COMET assay) experiments have been performed on these nanomaterials. Invertase inhibition activity was excellent. MTT results proved the bio-compatible nature of these biochemically synthesized gold and silver nanoparticles

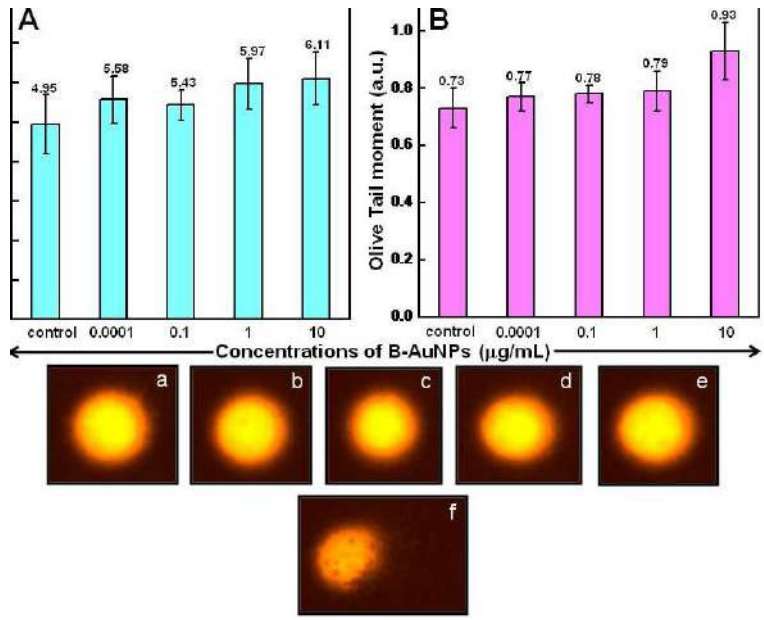

Fig. 2: COMET results obtained from 3 h exposure of HepG2 cells with different concentrations of BAuNPs. Two comet parameters, % tail DNA (A) and Olive tail moment (B) were considered as a measure of DNA damage. Figure a, b, c, d and e are images of comet showing the pattern of DNA after the exposure of HepG2 cells to 0 <g/mL, 0.0001 <g/mL, 0.1 <g/mL, 1 <g/mL and 10 <g/mL concentration of B-AuNPs respectively. Figure 'f' represents the comet pattern obtained after treatment with100 <g/mL of B-AuNPs.

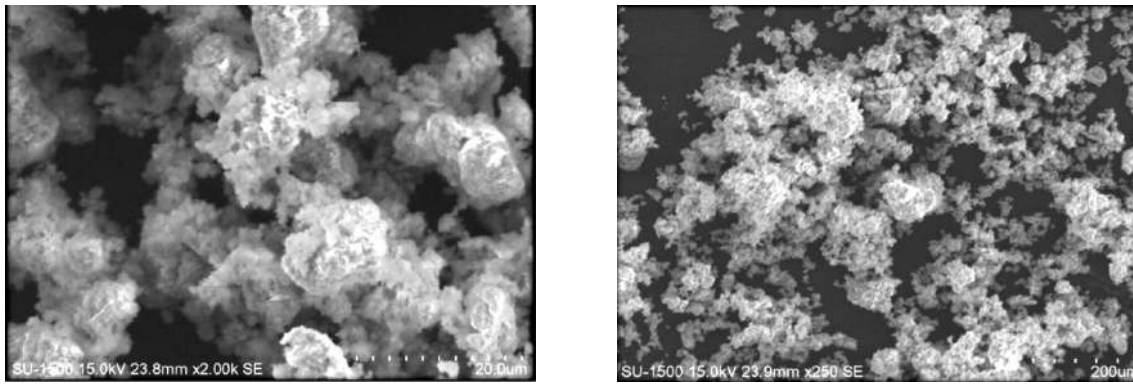

Fig. 3: SEM images of zinc oxide nanoparticles.

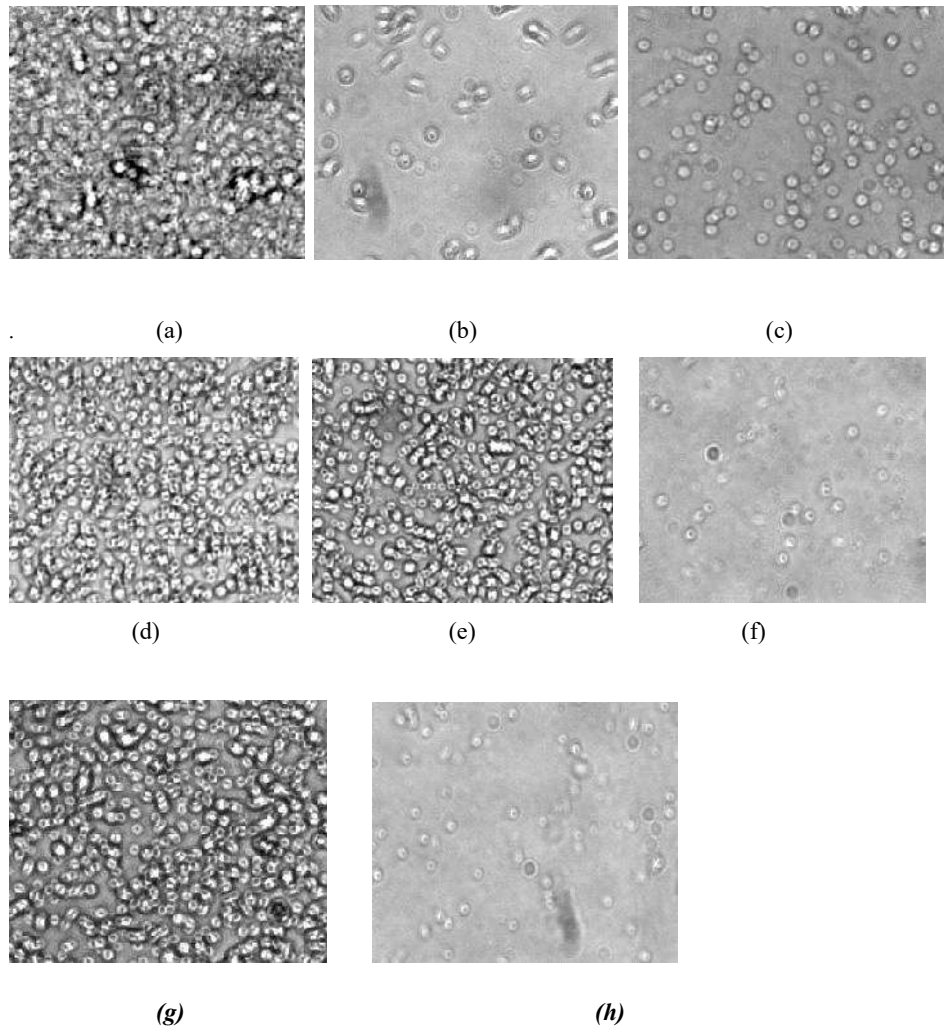

Fig. 4: Effect of silver nanoparticles on in biofilm quenching and prevention of S.aureus biofilm formation under inverted microscope (40X) (a): Negative control (intact biofilm); (b): Positive control (Biofilm Quenched using 20% SDS); (c): Silver nanoparticles; (d): Gentamicin (10>g/mL); (e): Chloramphenicol (20>g/mL); (f): SilverNanoparticles + Gentamicin (10>g/mL); (g): 1mMsilver nitrate; (h): Silver nanoparticles in prevention of biofilm formation.

upto 10-4M concentration towards HepG2 cells. The overall study suggested that these biogenic metal nanoparticles are non-cytotoxic and non-genotoxic upto 10-4M.

Green synthesis of ZnO nanoparticles by *Calotropis gigantea* was reported by Ca et al. (2013). The finding focused on the green synthesis of ZnO nanoparticles by utilizing the bio components of leaves extract of *Calotropis gigantean* and Zinc nitrate. The ZnO nanocrystallites of an average size range of 30-35 nm have been synthesized by a rapid, simple and eco-friendly method. Zinc nanoparticles were characterized using scanning electron microscopy (SEM) and X-ray diffraction (XRD). The particles obtained are spherical in nature and are agglomerates of nanocrystallite. The X-ray patterns show a hexagonal crystal type for ZnO. The results coincide with the literature XRD pattern for hexagonal wurtzite ZnO. The size of nanocrystallites is calculated by considering XRD data by Debye-Scherrer's Formula.

Alumina nanoparticles (AlNP) were synthesized from aluminium nitrate using extracts of tea, coffee and triphala a well known herbal plant as well as a nontoxic and eco-friendly green material (Sutradhar et al. 2013). In addition, excellent reproducibility of these nanoparticles, without the use of any additional capping agent or stabilizer will have great advantages in comparison with microbial synthesis, avoiding all the tedious and hygienic complications.

Chaudhari et al. (2012) investigated the prevention of biofilm formation, quenching and effect of biosynthesized silver nanoparticles on *Staphylococcus aureus* The synthesis of silver nanoparticles was done by using *B. megaterium* supernatant and 1 mM silver nitrate. These silver nanoparticles showed enhanced quorum quenching activity against *Staphylococcus aureus* biofilm and prevention of biofilm formation which can be seen under an inverted microscope (40 X). The synergistic effect of silver nanoparticles along with antibiotics in biofilm quenching was found to be effective.

FUTURE DIRECTIONS AND CONCLUSION

Increasing awareness towards green chemistry and biological processes has led to a desired and influenced process that is environment-friendly for the synthesis of non-toxic nanoparticles. The biological agents in the form of algae, plants and microbes have emerged as an efficient candidate for the synthesis of nanoparticles. On account of the rich biodiversity of plants, mediated nanoparticle synthesis has become a subject of interest around the globe with different plant species being rapidly explored and evaluated for synthesizing nanoparticles. Plants or their extracts can be efficiently used in the synthesis of nanoparticles as a greener route. Control over the shape and size of nanoparticles seems to be very easy with the use of plants. The synthesis of metal nanoparticles in plant extracts (plant biomasses), despite obvious limitations, has significant potential and a number of substantial advantages relative to traditional methods of nanoparticle synthesis. However, to go in for cost-effectively with nanoparticles prepared via physical and chemical methods, it is necessary to scale these methods of nanoparticle production using plant material and to develop schemes for keeping expenses in check during their synthesis. Promoting the biosynthesis of nanoparticles can influence the commercial applications of these nanoparticles in the field of pharmaceuticals and other medical sciences Nanoparticles synthesized via plants have been used for human benefit. The mechanism of plants in synthesizing nanoparticles is yet to be completely elucidated. Auxiliary research in this field can further increase the potential and scope in the biosynthesis of nanoparticles. Future research on plant-mediated biological synthesis of nanoparticles with unique optoelectronics, physicochemical and electronic properties are of great importance for applications in the areas of chemistry, electronics, electrochemical sensor, biosensors, medicine, healthcare and agriculture. Further progress is desirable in order to revolve the impression of nanoparticle technology into a rational practical approach.

REFERENCES

Ahmad, A., Mukherjee, P., Senapati, S., Mandal, D., Khan, M.I., Kumar, R. and Sastry, M. 2003a. Extracellular biosynthesis of silver nanoparticles using the fungus *Fusarium oxysporum.* Colloids. Surf. B 28: 313-318.

Ahmad, A., Senapati, S., Khan, M.I., Kumar, R. and Sastry, M. 2003b. Extracellular biosynthesis of monodisperse gold nanoparticles by a novel extremophilic actinomycete, *Thermomonospora sp*. Langmuir, 19: 3350-3553.

Ahmad, N., Sharma, S., Alam, M.K., Singh, V.N., Shamsi, S.F., Mehta, B.R. and Fatma, A. 2010. Rapid synthesis of silver nanoparticles using dried medicinal plant of basil. Colloids Surf. B. Biointerfaces., 81: 81-86.

Ahmad, N., Sharma, S., Singh, V.N., Shamsi, S.F., Fatma, A. and Mehta, B.R. 2011. Biosynthesis of silver nanoparticles from *Desmodium triflorum:* a novel approach towards weed utilization. Biotechnol. Res. Int. 2011, Article ID 454090 1-8.

Ahmed, M.J., Murtaza, G., Mehmood. A. and Bhatti, T.M. 2015. Green synthesis of silver nanoparticles using leaves extract of *Skimmia laureola*: Characterization and Antibacterial Activity. Mater. Lett., 153: 10-13.

Ahmed, S., Ahmad, M., LalSwami, B. and Ikram, S. 2016. A review on plants extract mediated synthesis of silver nanoparticles for antimicrobial applications: A green expertise. J. Adv. Res., 28-17 :7.

Armendariz, V., Herrera, I., Peralta-Videa, J.R., Yacaman, M.J., Troiani, H., Santiago, P. and Gardea-Torresdey, J.L. 2004. Size controlled gold nanoparticle formation by *Avena sativa* biomass: use of plants in nanobiotechnology. J. Nanopart. Res., 6: 377-82.

Arshad, A. 2017. Bacterial synthesis and applications of nanoparticles. Nano. Sci. Nano. Technol., 11: 119.

Bar, H., Bhui, D.K., Sahoo, G.P. Sarkar, P. Pyne, S. and Misra, A. 2009. Green synthesis of silver nanoparticles using seed extract of *Jatropha curcas*. Colloids Surf. A: Physicochem. Eng. Asp., 348: 212-216.

Birla, S.S., Tiwari, V.V., Gade, A.K., Ingle, A.P., Yadav, A.P. and Rai, M.K. 2009. Fabrication of silver nanoparticles by Phoma glomerata and its combined effect against *Escherichia coli, Pseudomonas aeruginosa* and *Staphylococcus aureus*. Lett. Appl. Microbiol., 48: 173-179.

Ca, V., Hiremath, S., Chandraprabha, M.N., Antonyraj, M.A.L., Gopal, I.V., Jain, A.A. and Bansal, A. K. 2013. Green synthesis of ZnO nanoparticles by Calotropis Gigantea. Proceedings of National Conference on "Women in Science & Engineering" (NCWSE 2013), SDMCET Dharwad, pp. 112-116.

Chakraborty, N., Banerjee, A., Lahiri, S., Panda, A., Ghosh, A.N. and Pal, R. 2009. Biorecovery of gold using cyanobacteria and eukaryotic alga with special reference to nanogold formation – a novel phenomenon. J. Appl. Phycol., 21: 145-152.

Chandrasekharan, N. and Kamat, P.V. 2000. Improving the photoelectrochemical performance of nanostructured TiO2 films by adsorption of gold nanoparticles. J. Phys. Chem. B., 104: 10851-10857.

Chaudhari, P.R., Masurkar, S.A., Shidore, V.B., Suresh, P. and Kamble, S.P. 2012. Effect of biosynthesized silver nanoparticles on *staphylococcus aureus* biofilm quenching and prevention of biofilm formation. International Journal of Pharma and Bio Sciences, 3: 222-229.

D'Britto, V., Devi, P.P., Prasad, B.V., Dhawan, A., Mantri, V.G. and Prabhune, A. 2012. Medicinal plant extracts used for blood sugar and obesity therapy shows excellent inhibition of invertase activity: synthesis of nanoparticles using this extract and its cytotoxic and genotoxic effects. Int. J. life sci. Pharma Res., 2: 61-74.

Dameron, C.T., Reese, R.N., Mehra, R.K., Kortan, A.R., Carroll, P.J. Steigerwald, M.L. Brus, L.E. and Winge, D.R. 1989. Biosynthesis of cadmium sulphide quantum semiconductor crystallites. Nature, 338: 596-597.

Das, R.K., Gogoi, N. and Bora, U. 2011. Green synthesis of gold nanoparticles using *Nyctanthes arbortristis* flower extract. Bioprocess Biosyst. Engg., 34: 615-619.

Dubey, S.P., Lahtinen, M. and Sillanp, M. 2010. Tansy fruit mediated greener synthesis of silver and gold nanoparticles. Proc. Biochem., 45: 1065-1071.

El-Rafie, M.H., El-Naggar, M.E., Ramadan, M.A. Fouda, M.M.G. and Al-Deyab, S.S. 2011. Environmental synthesis of silver nanoparticles using hydroxypropyl starch and their characterization. Carbohydrate Polymers, 86: 630-635.

Espitia, P.J.P., Soares, N.F.F., Coimbra, J.S.R., Andrade, N.J., Cruz, R.S. and Medeiros, E.A.A. 2012. Zinc oxide nanoparticles: synthesis, antimicrobial activity and food packaging applications. Food Bioprocess. Technol., 5: 1447-1464.

Faiyas, A.P.A., Vinod, E.M., Joseph, J., Ganesan, R. and Pandey, R.K. 2010. Dependence of pH and surfactant effect in the synthesis of magnetite (Fe_3O_4) nanoparticles and its properties. J. Magn. Magne. Mater., 322: 400-404.

Gardea-Torresdey, J.L., Parsons, J.G., Gomez, E., Peralta-Videa, J., Troiani, H.E., Santiago, P. and Jose-Yacaman, M. 2002. Formation and growth of Au nanoparticles inside live alfalfa plants. Nano. Lett., 2: 397-401.

Glusker, J., Katz, A. and Bock, C.W. 1999. Metal ions in biological systems. Rigaku J., 16 : 8–16.

Gour, A. and Jain, N.A. 2019. Advances in green synthesis of nanoparticles. Artificial Cells, Nanomedicine, and Biotechnology, 47(1): 844-851.

Hosea, M., Greene, B., McPherson, R., Henzl, M., Alexander, M.D. and Darnall, D.W. 1986. Accumulation of elemental gold on the alga *Chlorella vulgari.* Inorganica Chimica Acta, 123: 161-165.

Huang, J., Li, Q., Sun, D., Lu, Y., Su, Y., Yang, X., Wang, H., Wang, Y., Shao, W., He, N., Hong, J. and Chen, C. 2007. Biosynthesis of silver and gold nanoparticles by novel sun dried *Cinnamomum camphora* leaf. Nanotechnol., 18: 105104-105114.

Husseiny, M.I., El-Aziz, M.A., Badr, Y. and Mahmoud, M.A. 2007. Biosynthesis of gold nanoparticles using *Pseudomonas aeruginosa*. Spectrochim. Acta A: Mol. Biomol. Spectrosc., 67: 1003-1006.

Iravani, S. and Varma R.S. 2020. Greener synthesis of lignin nanoparticles and their applications. Green Chemistry, *22*(3): 612-636.

Jonge, S.H., Yeo, S.Y. and Yi, S.C. 2005. The effect of filler particle size on the antibacterial properties of compounded polymer silver fibers. J. Mat. Sci., 40: 5407-5411.

Kathiresan, K., Alikunhi, N.M., Pathmanaban, S., Nabikhan, A. and Kandasamy, S. 2010. Analysis of antimicrobial silver nanoparticles synthesized by coastal strains of *Escherichia coli* and *Aspergillus niger*. Can. J. Microbiol., 56: 1050-1059.

Kavitha, K.S., Syed, B., Rakshith, D., Kavitha, H.U., Rao, H.C.Y., Harini, B.P. and Satish, S. 2013. Plants as green source towards synthesis of nanoparticles. Int. Res. J. Bio. Sci., 2: 66-76.

Kowshik, M., Ashtaputre, S., Kharrazi, S., Vogel, W., Urban, J., Kulkarni, S.K. and Paknikar, K.M. 2003. Extracellular synthesis of silver nanoparticles by a silver- tolerant yeast strain MKY3. Nanotechnol., 14: 95-100.

Krolikowska, A., Kudelski, A., Michota, A. and Bukowska, J. 2003. SERS studies on the structure of thioglycolic acid monolayers on silver and gold. Surf. Sci., 532: 227-232.

Kumar, A.S., Ansary, A.A., Ahmad, A. and Khan, M.I. 2007. Extracellular biosynthesis of CdSe quantum dots by the fungus, *Fusarium Oxysporum.* J. Biomed. Nanotechnol., 3: 190-194.

Kumar, V., Pammi, P.P., Kollu, S.V., Satyanarayana, P. and Shameem, K.V. 2014. Green synthesis and characterization of silver nanoparticles using Boerhaavia diffusa plant extract and their antibacterial activity. Ind. Crops Prod., 52: 562-566.

Kumari, R., Singh, J.S. and Singh, D.P. 2016. Biogenic synthesis and spatial distribution of silver nanoparticles in the legume mungbean plant (*Vigna radiata* L.). Plant Physiology and Biochemistry, 110: 158-166.

Lalitha, A., Subbaiya, R. and Ponmurugan, P. 2013. Green synthesis of silver nanoparticles from leaf extract Azhadirachta indica and to study its anti-bacterial and antioxidant property. Int. J. Curr. Microbiol. App. Sci., 2: 228-235.

Lin, S.M., Lin, F.Q., Guo, H.Q., Zhang, Z.H. and Wang, Z.G. 2000. Surface states induced photoluminescence from Mn^{2+} doped CdS nanoparticles. Solid State Common, 115: 615-618.

Makarov, V.V., Love, A.J., Sinitsyna, O.V. et al. 2014. "Green" nanotechnologies: synthesis of metal nanoparticles using plants. Acta Naturae, 6(1): 35-44.

Mirzaei, H. and Darroudi, M. 2017. Zinc oxide nanoparticles: Biological synthesis and biomedical applications. Ceramics International, 43: 907-914.

Mizutani, N., Iwasaki, T., Watano, S., Yanagida, T., Tanaka, H. and Kawai, T. 2008. Effect of ferrous/ferric ions molar ratio on reaction mechanism for hydrothermal synthesis of magnetite nanoparticles. Bull. Mater. Sci., 31: 713-717.

Mohamad, M.F., Kamarudin, K.S.N., Fathilah, N.N.F.N.M. and Salleh, M.M. 2011. The effects of sodium chloride in the formation of size and shape of gold (Au) nanoparticles by microwave-polyol method for mercury adsorption. World Acad. Sci. Eng. Technol., 74: 691-695.

Mohanpuria, P., Rana, K.N. and Yadav, S.K. 2008. Biosynthesis of nanoparticles: Technological concepts and future applications. J. Nanopart. Res., 10: 507-517.

Mondal, N.K., Chowdhury, A., Dey, U., Mukhopadhya, P., Chatterjee, S., Das, K. and Datta, J.K. 2014. Green synthesis of silver nanoparticles and its application for mosquito control. Asian Pac. J. Trop. Dis., 4: 204-210.

Mourato, A., Gadanho, M. Lino, A.R. and Tenreiro, R. 2011. Biosynthesis of crystalline silver and gold nanoparticles by extremophilic yeasts. Bioinorg. Chem. Appl., Article ID 546074, 8.

Mukherjee, P., Ahmad, A., Mandal, D., Senapati, S., Sainkar, S.R. Khan, M.I., Parishcha, R. Ajaykumar, P.V., Alam, M., Kumar, R. and Sastry, M. 2001. Fungus-mediated synthesis of silver nanoparticles and their immobilization in the mycelial matrix: a novel biological approach to nanoparticle synthesis. Nano. Lett., 1: 515.

Muralidharan, G., Subramanian, L., Nallamuthu, S.K., Santhanam, V. and Kumar, S. 2011. Effect of reagent addition rate and temperature on synthesis of gold nanoparticles in microemulsion route. Ind. Eng. Chem. Res., 50: 8786-8791.

Nair, B. and Pradeep, T. 2002. Coalescence of nanoclusters and formation of submicron crystallites assisted by *Lactobacillus* strains. Crystal Growth and Design, 2: 293-298.

Panigrahi, S., Kundu, S., Ghosh, S., Nath, S. and Pal, T. 2004. General method of synthesis for metal nanoparticles. J. Nanoparticle Res., 6: 411-414.

Prasad, K., Jha, A.K. and Kulkarni, A.R. 2007. *Lactobacillus* assisted synthesis of titanium nanoparticles. Nanoscale Res. Lett., 2: 248-250.

Rai, A., Singh, A., Ahmad, A. and Sastry, M. 2006. Role of halide ions and temperature on the morphology of biologically synthesized gold nanotriangles. Langmuir, 22: 736-741.

Ramanathan, R., Field, M.R., O'Mullane, A.P., Smooker, P.M., Bhargava, S.K. and Bansal, V. 2013. Aqueous phase synthesis of copper nanoparticles: a link between heavy metal resistance and nanoparticle synthesis ability in bacterial systems. Nanoscale, 5(6): 2300-2306.

Sadowski, Z., Maliszewska, I.H., Grochowalska, B., Polowczyk, I. and Kozlecki, T. 2008. Synthesis of silver nanoparticles using microorganisms. Materials Science-Poland, 26: 419-424.

Sastry, M., Ahmad, A., Khan, M.I. and Kumar, R. 2003. Biosynthesis of metal nanoparticles using fungi and actinomycete. Curr. Sci., 85: 162-170.

Scarano, G. and Morelli, E. 2003. Properties of phytochelatin-coated CdS nanocrystallites formed in a marine phytoplanktonic alga (*Phaeodactylum tricornutum, Bohlin*) in response to Cd. Plant Science, 165: 803-810.

Senthilkumar, S.R. and Sivakumar, T. 2014. Green tea (Camellia Sinensis) mediated synthesis of zinc oxide (ZnO) nanoparticles and studies on their antimicrobial activities. Int. J. Pharm. Pharm. Sci., 6: 461-465.

Shahi, S.K. and Patra, M. 2003. Microbially synthesized bioactive nanoparticles and their formulation active against human pathogenic fungi. Rev. Adv. Mater. Sci., 5: 501-509.

Shahverdi, A.R., Minaeian, S., Shahverdi, H.R., Jamalifar, H. and Nohi, A.A. 2007. Rapid synthesis of silver nanoparticles using culture supernatants of Enterobacteriaceae: A novel biological approach. Process Biochem., 42: 919-923.

Shankar, S.S., Ahmad, A., Pasricha, R. and Sastry, M.J. 2003. Bioreduction of chloroaurate ions by geranium leaves and its endophytic fungus yields gold nanoparticles of different shapes. Mater. Chem., 13: 1822-1846.

Sharma, N., Pinnaka, A.K., Raje, M., Fnu, A., Bhattacharyya, M.S. and Choudhary, A.R. 2012. Exploitation of marine bacteria for production of gold nanoparticles. Microb. Cell. Fact., 11: 86.

Sharma,V.K., Yngard, R.A. and Lin, Y. 2009. Silver nanoparticles: green synthesis and their antimicrobial activities. Adv. Colloid Interface Sci., 145: 83-96.

Shirley, A., Dayananda, B., Sreedhar, B., Syed, G. and Dastager, C.C. 2010. Antimicrobial activity of silver nanoparticles synthesized from novel *Streptomyces* species. Dig. J. Nanomater. Biostruct., 5: 447-451.

Shivshankar, S., Ahmed, A., Ankamwar, B., Sastry, M., Rai, A. and Singh, A. 2004. Biological synthesis of triangular gold nanoprisms. Nature, 3: 482-488.

Singh, A.K., Talat, M., Singh, D.P. and Srivastava, O.N. 2010. Biosynthesis of gold and silver nanoparticles by natural precursor clove and their functionalization with amine group. J. Nanopart. Research, 12: 1667-1675.

Singh, J., Dutta, T., Kim. K.H., Rawat, M., Samddar, P. and Pawan Kumar. 2018. 'Green' synthesis of metals and their oxide nanoparticles: applications for environmental remediation. Journal of Nanobiotechnology, 16: 84.

Soni, N. and Prakash, S. 2011. Factors affecting the geometry of silver nanoparticles synthesis in *Chrysosporium Tropicum* and *Fusarium Oxysporum*, Amer. J. Nanotechnol., 2: 112-121.

Sunkar, S. and Nachiyar, C.V. 2012. Microbial synthesis and characterization of silver nanoparticles using the endophytic bacterium *Bacillus cereus*: a novel source in the benign synthesis. Global Journal of Medical Research, 12: 43-49.

Sutradhar, P., Debnath, N. and Saha, M. 2013. Microwave-assisted rapid synthesis of alumina nanoparticles using tea, coffee and triphala extracts. Adv. Manuf., 1: 357-361.

Syed, A., Saraswati, S., Kundu, G.C. and Ahmad, A. 2013. Biological synthesis of silver nanoparticles using the fungus *Humicola sp.* and evolution of their cytotoxicity using normal and cancer cell lines. Spectrochim. Acta. A Mol. Biomol. Spectrosc., 114: 144-147.

Thakkar, K.N., Mhatre, S.S. and Parikh, R.Y. 2010. Biological synthesis of metallic nanoparticles. Nanomed., 6: 257-262.

Vijayaraghavana, K. and Ashokkumar, T. 2017. Plant-mediated biosynthesis of metallic nanoparticles: A review of literature, factors affecting synthesis, characterization techniques and applications. Journal of Environmental Chemical Engineering, 5: 4866-4883.

Nature Environment and Pollution Technology
An International Quarterly Scientific Journal

p-ISSN: 0972-6268
(Print copies up to 2016)
e-ISSN: 2395-3454

Vol. 20 | No. 2 | pp. 491-498 | 2021

Original Research Paper

https://doi.org/10.46488/NEPT.2021.v20i02.005

Open Access Journal

An Empirical Research on Pig Farmers' Adoption Behaviours of Waste Disposal

Wenjie Yao*(**)† and Liguo Zhang*
*School of Economics, Jiangxi University of Finance and Economics, Nanchang, 330013, China
**Zhejiang University of Water Resources and Electric Power, Hangzhou, 310018, China
†Corresponding author: Wenjie Yao; rantom_821024@163.com

Nat. Env. & Poll. Tech.
Website: www.neptjournal.com

Received: 04-05-2020
Revised: 29-05-2020
Accepted: 16-07-2020

Key Words:
Pig farmers
Waste disposal
Adoption behaviour
Environmental subsidy

ABSTRACT

Based on the field survey data of 608 pig farmers in Zhejiang Province, this paper carries out empirical analysis on pig farmers' current adoption behaviours of waste disposal and its influencing factors and the change of pig farmers' waste disposal behaviour intention caused by the implementation of environmental subsidy and its influencing factors. The research shows that the implementation of environmental subsidy has a great impact on the willingness of pig farmers to change their waste disposal behaviours, and they will be more inclined to adopt the behaviours that can fully realize the utilization of resources to dispose of their waste. The implementation of environmental subsidy is effective and can encourage pig farmers to change the existing relatively unreasonable and inefficient waste disposal behaviours on the premise that the pig breeding scale, the expected net income from waste disposal, the knowledge of waste reduction methods, the willingness of waste disposal training, the awareness of policies to ban and limit pig breeding, the distance between the pig farm and the nearest river and many other factors can be controlled. Therefore, the government should focus on implementing environmental subsidy for waste disposal with high utilization of resources such as biogas technology and composting technology.

INTRODUCTION

Waste disposal in pig breeding production has direct environmental effects. Although there are many treatment methods at present, due to the shortage of funds, lack of experience and shallow understanding of the utilization value of waste, pig farmers tend not to adopt the treatment behaviour with a high degree of resource utilization. In many places, waste is applied excessively to cultivated land for a long time without any treatment, resulting in high nutrient concentration, soil structure destruction, crop yield reduction, diseases and insect pests (Jipeng et al. 2012). Especially, when the serious disconnection between agriculture and animal husbandry leads to insufficient supporting farmland (Kaijun et al. 2004), direct discharge of waste cannot produce economic benefits but aggravate environmental degradation.

In recent years, waste treatment technology has not been paid much attention. Most pig farmers have already bought some equipment but focus only on energy recycling or fertilizer processing, through which waste can be sold or given away. However, most of the organic fertilizer production enterprises lack economies of scale, it is difficult to make profits, product quality is uneven, and the industry is actually in a state of vicious competition with low price and low quality (Cuimian et al. 2004, Hongtao et al. 2010). In *The Energy and Environment Project Construction Plan for Large and Medium-Sized Livestock and Poultry Farms* compiled by China's Ministry of Agriculture in 2000, the economic benefits of large and medium-sized methane projects such as Shanghai Spark Farm, Shenyang Masan Farm and Hangzhou Xizi Farm were calculated. The results show that large and medium-sized farms could produce good economic benefits by using biogas project to treat waste, but the promotion and construction of biogas were slow due to technical obstacles and scale constraints. Yubo et al. (2009) found that the biogas promotion and construction ratio of scale pig breeding enterprises around Wuhan was only 60%. To effectively realize harmless, reduction and resource utilization, waste disposal should meet the requirements of environmental tolerance and technical applicability (Hongkun 2002). Therefore, people begin to introduce advanced composting technology and equipment from abroad. However, the current problem is that some pig farmers blindly invest to cope up with the environmental protection inspection without carrying out comprehensive technical and economic evaluation and environmental effect evaluation, resulting in high cost, low efficiency and equipment idle and other consequences.

In many parts of China, the government has enacted various forms of policies to control non-point source pollution by reducing the number of pig farms. However, the positioning of such policies deviates and the implementation effect is not high, especially the farmers' behaviour is not given the necessary attention. To ensure the sustainable development of the pig breeding industry with unified economic and environmental benefits, the government should guide pig farmers to carry out more spontaneous environmental protection behaviours and share environmental protection input in the form of subsidies. Based on the field survey data of 608 pig farmers in Zhejiang Province, we have empirically studied the subsidy expectation and its influencing factors of pig farmers to dispose of waste by themselves under the established breeding mode. The results show that most pig farmers were willing to accept subsidies to deal with waste under the established breeding mode, and the environmental subsidy was indeed feasible, which is consistent with the research conclusion of Liange et al. (2016). However, whether environmental subsidy can motivate pig farmers to change the current relatively unreasonable and inefficient waste disposal behaviour is directly related to the effectiveness of the policy itself (Zilberman et al. 1997, Khanna et al. 2002). Some scholars have investigated the willingness of pig farmers to adopt safe veterinary drugs (Xiumin 2007), the adoption of biogas technology by livestock farmers (Xinyu 2007), the adoption of biogas technology for waste disposal by large-scale pig farmers (Hao et al. 2008), the development degree of biogas project in large-scale pig farms (Bin 2009), and the environmental protection investment level of livestock farmers (Yi et al. 2012). They not only talk about some problems related to waste disposal adoption behaviours, but also provide some useful methods and conclusions. However, most of these studies do not take environmental subsidy as exogenous variables to investigate livestock farmers' specific waste disposal behaviours. Systematic studies on livestock farmers' selection of multiple waste disposal methods under different conditions, especially as a way to evaluate the effectiveness of environmental subsidy, are still rare.

Based on the previous conclusions, we continue to carry out empirical analysis on pig farmers' current adoption behaviours of waste disposal and its influencing factors and the change of pig farmers' waste disposal behaviour intention caused by the implementation of environmental subsidy and its influencing factors. It is expected to provide a realistic basis for formulating the environmental subsidy for collective action motivation in the treatment of non-point agricultural pollution and lay a foundation for exploring effective forms of public participation in environmental protection action.

THEORY AND MODEL

Theoretical Framework

Based on the field investigation, we determined the four main adoption behaviours of pig farmers' waste disposal, namely "direct discharge", "sale or gift", "biogas fermentation" and "Compost, returning to the field, or aquaculture". The willingness to change the behaviour of waste disposal reflects the extent to which policy incentives can enable pig farmers to correct the practice of direct discharge and consciously adopt other recycling behaviours. Based on related literature (Khanna et al. 2002, Xiumin 2007, Xinyu 2007, Hao et al. 2008, Bin 2009, Yi et al. 2012, Ning 2014, Chao 2019, Jianhua et al. 2019, Limei & Yaqing 2019, Ruishi et al. 2019, Limei & Xiuling 2020) and combining the field survey, we first examine the current pig farmers' waste disposal adoption behaviours. Then, it is assumed that if the environmental subsidy is implemented based on the subsidy expectation (Liange et al. 2016) of the established breeding mode, pig farmers will inevitably have some behavioural change intention to dispose of wastes by themselves. The influencing factors of the above two situations are analysed from the perspectives of individual, economic, psychological and social characteristics.

Individual characteristics reflect the subjective possibility of pig farmers to adopt waste disposal behaviour. Generally speaking, the longer raising pigs, the richer the experience, but not necessarily a strong sense of environmental protection, which depends on the degree of education and cadre identity or not. People with low education level may choose "direct discharge" because they cannot master the environmental protection technology of waste recycling, and they are not willing to change the existing waste disposal behaviours. And for the current policies to ban and limit pig breeding, cadres can recognize the purpose of environmental protection, so it is possible to adopt the waste disposal behaviours that can effectively realize the utilization of resources, and is willing to change the existing waste disposal behaviours.

Economic characteristics reflect the objective ability of pig farmers to adopt waste disposal behaviour. The source of investment in environmental protection is not determined by the annual income of raising pigs alone, but by the average annual household income. The scale of environmental investment is directly controlled by the pig breeding scale. The economics of waste disposal behaviours can be expressed by the expected net income from waste disposal. The low average annual household income, the large pig breeding scale or the low expected net income from waste disposal means that the external environmental cost will be relatively high, and it is possible to choose "direct discharge"

at present. If the environmental subsidy is implemented, existing waste disposal behaviours may be changed.

Psychological characteristics reflect the conscious tendency of pig farmers to adopt waste disposal behaviours. It includes pollution level evaluation, waste management evaluation, knowledge of waste reduction methods, the willingness of waste disposal training, awareness of policies to ban and limit pig breeding. In general, the more active the tendency of environmental protection consciousness, the more likely to adopt the waste disposal behaviours that can effectively realize the utilization of resources, and the more willing to change the existing waste disposal behaviours.

The social characteristics reflect the constraints of pig farmers to adopt waste disposal behaviours. The large distance between pig houses and the nearest river means that it is not easy to discharge waste directly into the river. Therefore, pig farmers may be inclined to adopt economic and cost-effective treatment methods and are willing to change existing waste disposal behaviours. Technical support for waste disposal is more important than technical convenience. If the number of waste treatment technical service stations is small, rather than far away, pig farmers may choose to "direct discharge" due to lack of technical support and may not be willing to change existing waste disposal behaviours. The more annual number of pollutant discharge standard inspection, the less likely pig farmers are to choose "direct discharge", but the more likely they are to change existing waste disposal behaviours.

Model Building

Pig farmers' current adoption behaviours of waste disposal are disordered and multi-classification dependent variables. So we used the disordered multi-classification Logit model, and assigned values of 0, 1, 2 and 3 to waste disposal behaviours of "direct discharge", "sale or gift", "biogas fermentation", "Compost, returning to the field, or aquaculture". For "sale or gift", "biogas fermentation" and "Compost, returning to the field, or aquaculture", the degree and cost of waste resources utilization increase successively. Only "direct discharge" cannot effectively realize the utilization of waste resources. Therefore, in Logit regression, the group with an assigned value of 0 was used as the reference group to analyze the influencing factors of the other three kinds of adoption behaviours of waste disposal that can effectively realize resource utilization. The specific form of disordered multi-classification Logit model is as follows:

$$\log\left(\frac{B_{1i}}{B_{0i}}\right) = \alpha_0^1 + \sum_{k=1}^{n} \alpha_k^1 X_{ki} \quad \ldots(1)$$

$$\log\left(\frac{B_{2i}}{B_{0i}}\right) = \alpha_0^2 + \sum_{k=1}^{n} \alpha_k^2 X_{ki} \quad \ldots(2)$$

$$\log\left(\frac{B_{3i}}{B_{0i}}\right) = \alpha_0^3 + \sum_{k=1}^{n} \alpha_k^3 X_{ki} \quad \ldots(3)$$

Here, B_{0i}, B_{1i}, B_{2i} and B_{3i} are the probabilities of waste disposal behaviours mainly adopted by the i-th pig farmer, including "direct discharge", "sale or gift", "biogas fermentation", and "Compost, returning to the field, or aquaculture", and $B_{0i} + B_{1i} + B_{2i} + B_{3i} = 1$; X_{ki} is the k-th influencing factor of a waste disposal behaviour mainly adopted by the i-th pig farmer; α_0^1, α_0^2, α_0^3 and α_k^1, α_k^2, α_k^3 are the corresponding regression coefficients.

If the environmental subsidy is implemented, whether a pig farmer is willing to change the existing main waste disposal behaviour is a type 0-1 dichotomizing dependent variable. So we used the binary Logit model to estimate the influencing factors of waste disposal behaviour change intention. For the dependent variable "waste disposal behaviour change intention", a pig farmer who had been willing to change the existing main waste disposal behaviour was assigned a value of 1, while a pig farmer who had been unwilling to change the existing main waste disposal behaviour was assigned a value of 0. The specific form of the binary Logit model is as follows:

$$\log it(T_i) = \alpha_0 + \sum_{k=1}^{n} \alpha_k X_{ki} + \eta \quad \ldots(4)$$

Here, T_i is the probability that the i-th pig farmer is willing to change the existing main waste disposal behaviour; X_{ki} is the k-th influencing factor of the waste disposal behaviour change intention of the i-th pig farmer; α_0 and α_k are the corresponding regression coefficients; η is the random error. We set 13 independent variables (Table 1). Especially for subjective variables, due to the difference of qualitative dimension, the assignment is also different.

EMPIRICAL ANALYSIS

We conducted a random sampling questionnaire survey on pig farmers in 10 administrative villages in Jiaxing, 42 administrative villages in Ningbo and 17 administrative villages in Quzhou. Before the official survey began, we randomly visited 10 pig farmers in each area, conducted a preliminary survey in the form of face-to-face interview, and then modified and improved the questionnaire according to the actual situation. The official investigation was carried out from March 2018 to June 2019. Before that, the governments had planned prohibited and restricted breeding zones in some jurisdictions, and most pig farms in these zones

Table 1: Independent variables and their instructions.

Independent Variables		Symbol	Instructions
Individual characteristics	Degree of education	X1	Years of academic education: Primary school = 6, Middle school = 9, High school = 12, Junior college = 15, Undergraduate = 16
	Cadre identity or not	X2	No = 0, Yes = 1
Economic characteristics	Average annual household income	X3	Ten thousand Yuan
	Pig breeding scale	X4	The amount of pig raised at the end of every year
	Expected net income from waste disposal	X5	Not very good = -1, Almost flat = 0, Very good = 1
Psychological characteristics	Pollution level evaluation	X6	No =1, Slight = 2, General = 3, Serious = 4
	Waste management evaluation	X7	Very dissatisfied =1, Relatively dissatisfied = 2, Reserved opinions = 3, Relatively satisfied = 4, Very satisfied = 5
	Knowledge of waste reduction methods	X8	Very unclear =1, Relatively unclear = 2, Basically clear = 3, Relatively clear = 4, Very clear = 5
	Willingness of waste disposal training	X9	No = 0, Yes = 1
	Awareness of policies to ban and limit pig breeding	X10	No = 0, Yes = 1
Social characteristics	Distance between pig farm and the nearest river	X11	km
	Number of waste treatment technical service stations	X12	Number
	Annual number of pollutant discharge standard inspection	X13	Number

had been shut down. Therefore, to ensure the accuracy and reliability of survey information as far as possible, part of the data obtained from the official survey (especially "pig breeding scale") comes from the actual situation at the time of the implementation of the policy. After a brief training on the purpose, content, scientific way of asking questions, questionnaire filling method and matters needing attention of the survey, 210 questionnaires (including 10 copies of pre-survey, 630 copies in total) were distributed in each village, and 625 copies were collected. Through information screening and reliability assessment, 608 valid questionnaires were confirmed, accounting for 97.28%.

Data Statistics

Considering that a pig farmer may adopt multiple waste disposal behaviours, we took the main adoption behaviour as the only adoption behaviour. The statistical results show that the waste disposal behaviours currently adopted by most pig farmers are inclined to fully realize the utilization of resources; if the environmental subsidy is implemented, 83.22% (506 households) pig farmers are willing to change the existing waste disposal behaviour, while 16.78% (102 households) pig farmers are not. As can be seen from Table 2, the implementation of environmental subsidy has a great

Table 2: Statistical results of pig farmers' waste disposal behaviour changes.

Existing status \ Environmental subsidy assumption		Direct discharge		Sale or gift		Biogas fermentation		Compost, returning to field, or aquaculture		Total	
		Sample	Ratio, %	Sample	Ratio, %	Sample	Ratio, %	Sample	Ratio, %	Sample	Ratio, %
Direct discharge	Sample	21	100.00	17	18.28	38	15.97	77	30.08	153	25.16
	Ratio, %	13.73	-	11.11	-	24.84	-	50.33	-	100.00	-
Sale or gift	Sample	0	0.00	10	10.75	20	8.40	43	16.80	73	12.01
	Ratio, %	0.00	-	13.70	-	27.40	-	58.90	-	100.00	-
Biogas fermentation	Sample	0	0.00	16	17.20	29	12.18	93	36.33	138	22.70
	Ratio, %	0.00	-	11.59	-	21.01	-	67.39	-	100.00	-
Compost, returning to field, or aquaculture	Sample	0	0.00	50	53.76	151	63.45	43	16.80	244	40.13
	Ratio, %	0.00	-	20.49	-	61.89	-	17.62	-	100.00	-
Total	Sample	21	100.00	93	100.00	238	100.00	256	100.00	608	100.00
	Ratio, %	3.45	-	15.30	-	39.14	-	42.11	-	100.00	-

Note: - is the default.

impact on pig farmers' willingness to change their waste disposal behaviours, and pig farmers will be more inclined to adopt the behaviours that can fully realize the utilization of resources to deal with waste.

Regression Results

We used STATA 11 statistical software to estimate the parameters of the two models respectively with the maximum likelihood estimation method, and further screened the independent variables of the binary Logit model by the stepwise forward regression method (the standard of P-value of all variables selected was set at 0.100). The results show that the regression equations are well fitted (Table 3 and Table 4).

DISCUSSION

It can be seen from Table 3 that both "degree of education" and "cadre identity or not" in individual characteristics have a significant positive impact on the current two waste disposal behaviours of "biogas fermentation" and "compost, returning to field, or aquaculture", and have no significant impact on the current waste disposal behaviour of "sale or gift". Compared with "direct discharge", the higher the education level, the stronger the awareness of environmental protection, and the easier to master the corresponding advanced technology. In addition, cadres are more politically progressive and have a greater sense of responsibility to dispose of waste by themselves, so they are more inclined to adopt the two

Table 3: Regression results of disordered multi-classification Logit model for pig farmers' adoption behaviours of waste disposal.

Independent Variables	Sale or gift		Biogas fermentation		Compost, returning to field, or aquaculture	
	Coefficient	Standard Error	Coefficient	Standard Error	Coefficient	Standard Error
X1	0.035 2	0.045 9	0.085 3**	0.039 0	0.075 0**	0.034 4
X2	1.385 4	0.937 2	1.815 3**	0.791 4	1.835 6**	0.763 0
X3	0.015 8	0.036 7	0.018 4	0.037 1	-0.065 3	0.041 4
X4	0.000 8*	0.000 4	0.000 1	0.000 4	0.000 7*	0.000 4
X5	0.899 2***	0.334 0	0.752 4**	0.298 9	0.763 4***	0.270 8
X6	0.157 8	0.206 9	0.274 0	0.172 8	0.282 0*	0.153 8
X7	0.312 5	0.190 0	-0.085 7	0.156 4	0.238 8*	0.140 7
X8	0.240 0	0.204 3	0.306 3*	0.173 5	0.418 9***	0.155 8
X9	-0.327 2	0.333 4	-0.012 9	0.284 8	0.040 5	0.249 7
X10	0.152 6	0.314 8	0.218 8	0.262 2	0.051 9	0.229 1
X11	-0.166 7	0.588 2	0.588 0	0.468 9	0.896 2**	0.421 3
X12	-0.007 6	0.196 4	-0.003 5	0.163 4	-0.190 4	0.147 6
X13	0.102 5**	0.056 3	0.094 7**	0.047 8	0.016 0	0.044 0
Constant	-2.660 9**	1.070 8	-2.376 3***	0.905 8	-1.996 8**	0.811 1
Sample Size	608		Log likelihood		-750.165 1	
LR chi2	86.18***		Pseudo R^2		0.054 3	

Note: ***, ** and * respectively indicate that the estimated results are significant at the levels of 1%, 5% and 10%.

Table 4: Gradually (forward) regressive results of binary Logit model for pig farmers' willingness to change waste disposal behaviour.

Independent Variables	Coefficient	Standard Error
X4	0.001 1**	0.000 5
X5	-0.494 9**	0.227 9
X8	-0.240 9*	0.143 6
X9	0.675 1***	0.240 2
X10	0.917 7***	0.230 8
X11	1.083 3**	0.456 7

Sample Size	608	Log likelihood	-253.757 7
LR chi2	42.51***	Pseudo R^2	0.077 3

Note: ***, ** and * respectively indicate that the estimated results are significant at the levels of 1%, 5% and 10%. Pearson's test value of model regression is 520.04 (P value is 0.839 2), which doesn't reach the significance level of 5%.

waste disposal behaviours of "biogas fermentation" and "compost, returning to the field, or aquaculture". This is similar to the research results of Yi et al. (2012). However, if the environmental subsidy is implemented, individual characteristics have no significant impact on pig farmers' willingness to change their waste disposal behaviours. The possible reason is that the established education level and political status make pig farmers have a limited understanding of the adopted waste disposal behaviours, believing that the current is the most effective.

In terms of economic characteristics, "pig breeding scale" has a significant positive impact on the current two waste disposal behaviours of "sale or gift" and "compost, returning to the field, or aquaculture", and has no significant impact on the current waste disposal behaviour of "biogas fermentation". It may be because, in the pig breeding industry, the promotion and construction of biogas lags far behind the development of production scale. Besides, "expected net income from waste disposal" has a significant positive impact on the current three waste disposal behaviours of "sale or gift", "biogas fermentation" and "compost, returning to the field, or aquaculture". As can be seen from Table 4, if the environmental subsidy is implemented, "pig breeding scale" and "expected net income from waste disposal" have respectively significant positive and negative impacts on pig farmers' willingness to change their waste disposal behaviours, while "average annual household income" has no significant influence. At the same time, "average annual household income" has no significant impact on the three current waste disposal behaviours of "sale or gift", "biogas fermentation" and "compost, returning to the field, or aquaculture". So the average annual household income may not necessarily go into waste disposal.

In terms of psychological characteristics, both "pollution level evaluation" and "waste management evaluation" have a significant positive impact on the current waste disposal behaviour of "compost, returning to the field, or aquaculture", and have no significant impact on the current two waste disposal behaviours of "sale or gift" and "biogas fermentation". Obviously, "compost, returning to field or aquaculture" is more environmentally friendly than "sale or gift" and "biogas fermentation" without "direct discharge". In addition, "knowledge of waste reduction methods" has a significant positive impact on the current two waste disposal behaviours of "biogas fermentation" and "compost, returning to the field, or aquaculture", and has no significant impact on the current waste disposal behaviour of "sale or gift". The main reason is that the higher the awareness level of pig farmers, the easier it is to adopt these two kinds of waste disposal behaviours with higher utilization of resources. Meanwhile, if the environmental subsidy is implemented, "knowledge of waste reduction methods" has a significant negative impact on pig farmers' willingness to change their waste disposal behaviours. Because the efficient operation of the reduction link can greatly reduce the workload of the treatment link, there is no need to change the existing waste disposal behaviours. If the environmental subsidy is implemented, both "willingness of waste disposal training" and "awareness of policies to ban and limit pig breeding" have a significant positive impact on pig farmers' willingness to change their waste disposal behaviours, but have no significant impact on the current three waste disposal behaviours of "sale or gift", "biogas fermentation" and "compost, returning to the field, or aquaculture". It can be seen that these two factors are merely the pure environmental protection consciousness tendencies towards "direct discharge", and fail to produce an effect on the selection of waste disposal behaviours of resource utilization. Besides, if the environmental subsidy is implemented, both "pollution level evaluation" and "waste management evaluation" have no significant impact on pig farmers' willingness to change their waste disposal behaviours. The possible reason is that the waste disposal behaviour change intention depends to some extent on the pig farmers' own environmental benefit rather than environmental awareness, which is confirmed by the significant negative impact of "expected net income from waste disposal" in economic characteristics.

In terms of social characteristics, "distance between the pig farm and the nearest river" has a significant positive impact on the current waste disposal behaviour of "compost, returning to the field, or aquaculture", and has no significant impact on the current two waste disposal behaviours of "sale or gift" and "biogas fermentation". If the environmental subsidy is implemented, "distance between the pig farm and the nearest river" has a significant positive impact on pig farmers' willingness to change their waste disposal behaviours. This is because, compared with direct discharge, the closer the pig farm is to the nearest river, the less likely it is to discharge directly into the river. However, the higher the cost of waste self-treatment, the more likely the pig farmers is to adopt the waste disposal behaviours with higher economic benefits. Also, the annual number of pollutant discharge standard inspection has a significant positive impact on the current two waste disposal behaviours of "sale or gift" and "biogas fermentation", and has no significant impact on the current waste disposal behaviour of "compost, returning to the field, or aquaculture". This is because, compared with direct discharge, if only to cope with environmental protection inspection, adopt the waste disposal behaviour of "compost, returning to the field, or aquaculture" will inevitably lead to high cost, low efficiency, equipment idle and other consequences. If it is not to cope

with the environmental protection inspection, that is to say, waste disposal is a conscious environmental protection behaviour, when the environmental subsidy is implemented, annual number of pollutant discharge standard inspection will naturally have no significant impact on pig farmers' willingness to change their waste disposal behaviours. Besides, if the environmental subsidy is implemented, the number of waste treatment technical service stations has no significant impact on pig farmers' willingness to change their waste disposal behaviours, and has no significant impact on the current three waste disposal behaviours of "sale or gift", "biogas fermentation" and "compost, returning to the field, or aquaculture" The former may be because objective environmental protection technology conditions still play a role through the subjective emphasis on environmental protection technology, which is confirmed by the significant positive influence of "willingness of waste disposal training" in psychological characteristics. The latter may be caused by the low technical requirements and environmental standards used by most waste treatment technical service stations for a long time, which are out of line with the current laws and regulations and existing some misleading results.

CONCLUSIONS

The implementation of environmental subsidy has a great impact on the willingness of pig farmers to change their waste disposal behaviours, and pig farmers will be more inclined to adopt the behaviours that can fully realize the utilization of resources to dispose of their waste. If the environmental subsidy is implemented, the bigger the pig breeding scale, the lower the expected net income from waste disposal, the less the knowledge of waste reduction methods, the more the willingness of waste disposal training, the higher the awareness of policies to ban and limit pig breeding, the greater the distance between the pig farm and the nearest river, the greater the incentive for pig farmers to change their existing waste disposal behaviours. Therefore, the implementation of environmental subsidy is effective and can encourage pig farmers to change the existing relatively unreasonable and inefficient waste disposal behaviours.

In terms of policies, the government should focus on implementing environmental subsidy for waste disposal with high utilization of resources, encourage pig farmers with higher education and cadre identity to adopt biogas technology and composting technology, and guide pig farmers with larger scale to adopt composting technology. In addition, the government should establish main roads and water source areas as prohibited and restricted breeding areas. In particular, pig farmers who discharge waste directly into rivers shall be severely punished and forced to adopt waste disposal behaviours that can effectively realize resource utilization. Finally, the government should encourage pig farmers to participate in training on various waste treatment technologies, strengthen professional training on waste reduction methods for pig farmers, and increase the publicity of the environmental protection orientation of the policies to ban and limit pig breeding.

REFERENCES

Bin, L. 2009. Study on determinants of biogas engineering development in large-scale pig farms: the case from Fujian. Fujian Agriculture and Forestry University, Fuzhou, China.

Chao, Y. 2019. Study on cleaner production behaviour of large-scale pig farms. Shandong Agricultural University, Taian, China.

Cuimian, Z., Zhanwu, W. and Hongtao, L. 2004. Current situation and future approaches of solid animal waste utilization. Journal of Hebei Agricultural Sciences, 8(2): 100-103.

Hao, H., Hui, Z. and Danping, Y. 2008. An analysis of the determinants in option of biogas technology for swine farmers in Jiangsu Province. China Biogas, 26(5): 21-25.

Hongkun, H. 2002. Studies on waste treatment and utilization in large scale animal farm. Chinese Academy of Agricultural Sciences, Beijing, China.

Hongtao, L., Chen, T.B., Zheng, G.D., Gao, D. and Lei, M. 2010. Comparative analysis of organic and chemical fertilizer production energy consumption, input cost and environmental benefit: sewage sludge composting as example. Ecology and Environmental Sciences, 19(4): 1000-1003.

Jianhua, W., Junying, T. and Lu, C. 2019. Resource utilization method and influencing factors of farmers' behaviours towards livestock and poultry waste. China Population, Resources and Environment, 29(5): 127-137.

Jipeng, Z., Jinzhi, Z. and Juanmin, Z. et al. 2012. Investigation on current situation and mode of pig waste management in Jiaxing city. Zhejiang Journal Animal Science and Veterinary Medicine, 5: 19-21.

Kaijun, W., Dongxia, J., Shuxia, Z. et al. 2004. Technology and policy of pollution control in livestock and poultry breeding. Chemical Industry Press Co., Lid. , Beijing, China.

Khanna, M., Isik, M. and Zilberman D. 2002. Cost-effectiveness of alternative green payment policies for conservation technology adoption with heterogeneous land quality. Agr Econ, 27(2): 157-174.

Liange, Z., Wenjie, Y. and Xueyuan, W. 2016. Study on pig farmers' subsidy expectations for waste disposal in Zhejiang Province. Chinese Journal of Animal Science, 52(6): 62-67.

Limei, L. and Xiuling, H. 2020. Pollution control status and policy implications of large-scale pig breeding: based on the survey data of farmers. Journal of Fujian Agriculture and Forestry University (Philosophy and Social Sciences), 23(2): 78-86.

Limei, L. and Yaqing, H. 2019. Influencing factors and regulatory strategies on large-scale pig farmers' environmentally friendly behaviors: An exploratory research based on grounded theory. Journal of Ecology and Rural Environment, 35(10): 1259-1267.

Ning, Z. 2014. The empirical research of livestock farms' livestock waste treatment and its influence on livestock breeding effect: A case study of layers' manure treatment behaviour. China Agriculture University, Beijing, China.

Ruishi, S., Pan, S.T., Yuan, Y.X. and Lu, Q. 2019. Effect of environmental regulation on the behaviour of farmers to recycling the dispose wastes. Journal of Arid Land Resources and Environment, 33(9): 17-22.

Xinyu, P. 2007. Study on biogas technology adoption behaviour and green subsidy policy of livestock farming pollution prevention: evidence from specialized pig breeding households. Chinese Academy of Agricultural Sciences, Beijing, China.

Xiumin, W. 2007. The willingness of pig farmers to adopt safe veterinary drugs and its influencing factors: based on the empirical analysis of pig farmers in Sichuan Province. Chinese Rural Economy, 9: 17-24, 38.

Yi, Y., Hui, Z. and Hao, H. 2012. Study on the factors affecting breeding farmers' environmental investment in the perspective of pollution subsidies: based on the survey of farmers from Shanghai, Jiangsu and Zhejiang. China Population, Resources and Environment, 22(2): 159-163.

Yubo, W., Meng, X.H., Zhou, H.C. and Zhou, R. 2009. Path designed for the sustained development of intensive livestock and poultry breeding industry based on circular economy: based on the example of Wuhan. Hubei Agricultural Sciences, 48(6): 1492-1496.

Zilberman, D., Khanna, M. and Lipper, L. 1997. Economics of new technologies for sustainable agriculture. Aust. J. Agr. Resour. Ec., 41(1): 63-80.

Nature Environment and Pollution Technology
An International Quarterly Scientific Journal

p-ISSN: 0972-6268
(Print copies up to 2016)
e-ISSN: 2395-3454

Vol. 20 | No. 2 | pp. 499-507 | 2021

Original Research Paper

https://doi.org/10.46488/NEPT.2021.v20i02.006

Open Access Journal

Metal Contamination in *Macrobrachium rosenbergii* from Sarawak River, Malaysia and its Health Risk to Human

F. A. Idrus†, M. M. Basri, K. A. A. Rahim and A. C. Lee

Faculty of Resource Science and Technology, Universiti Malaysia Sarawak, 94300 Kota Samarahan, Sarawak, Malaysia

†Corresponding author: F. A. Idrus; aifarah@unimas.my

Nat. Env. & Poll. Tech.
Website: www.neptjournal.com

Received: 02-06-2020
Revised: 03-09-2020
Accepted: 16-09-2020

Key Words:
Heavy metals
Macrobrachium rosenbergii
Human health risk
Sarawak river

ABSTRACT

An assessment of heavy metal concentration in wild-captured *Macrobrachium rosenbergii* (giant freshwater prawns) from their natural habitat is important since it is susceptible to environmental pollution due to the rapid development and human activities along the Sarawak River. This study aimed to estimate the heavy metal contamination in muscles, exoskeletons and gills of the *M. rosenbergii* and to estimate the health risk assessment to human consumption. The concentration of heavy metals was analyzed by the flame atomic absorption spectrophotometer and the flow injection mercury system. The metal concentrations in prawns were detected in the following order: Hg < Cd < Co < Cu < Zn; in all body parts ($P < 0.05$), where a high concentration of metals was recorded in gills due to its function as the excretion site of contaminants from the body. A positive correlation of Co, Cu, and Zn in muscles and gills was observed with the increasing size of prawns. The human health risk assessment indicated a less potential adverse health effect of prawns for consumption from Sarawak River (hazard index values < 1). All samples contained metals below the Joint FAO/WHO Expert Committee on Food Additives (JECFA) permissible limit for human consumption (Cd < 2 mg/kg; Cu < 30 mg/kg; Zn < 150 mg/kg; Hg < 1 mg/kg). Therefore, *M. rosenbergii* from the Sarawak River were not contaminated enough to prevail high risk on human health, but regular monitoring is suggested for seasonal variability of heavy metals in *M. rosenbergii* for safeguarding human health.

INTRODUCTION

Heavy metal contamination has got serious attention worldwide due to the increase in agricultural, industrial and fisheries activities, domestic wastes and technological usage (Aytekin et al. 2019, Mostafiz et al. 2020). The fast-growing population in Kuching (the capital city of Sarawak, Malaysia) has seen the increasing water demand, resulting in poorly treated effluents, the main generator of the 'black and grey waters' flowing into the Sarawak River. The 'black water' refers to wastewater from septic tanks and 'grey water' is the water discharge from kitchens, bathrooms and washing areas (Natural Resources and Environmental Board Sarawak 2017). Both 'black and grey waters' effluents may contribute heavy metals to the environment (Eriksson et al. 2010). Moreover, water quality in the Sarawak River was classified as Class III with a low concentration of heavy metals (Natural Resources and Environmental Board 2001). However, the concentration of heavy metals such as mercury (Hg), cadmium (Cd), lead (Pb) and zinc (Zn) was found considerably high in sediment, which was potentially toxic to sensitive organisms (Natural Resources and Environmental Board 2001).

Heavy metals from the effluents can stay for a long time in aquatic environments, such as rivers, then can contaminate aquatic organisms and enter the food chain, subsequently creating significant health risks and economic costs for residents (Yunus 2020, Aytekin et al. 2019). As heavy metals are non-biodegradable, they can accumulate in water and sediment, and can be transferred to living organisms such as fish and crustaceans (Mostafiz et al. 2020), through bioaccumulation and biomagnification. Fish and crustaceans that stay at the higher trophic levels of the food chains are considered to be one of the important groups for transferring heavy metals to humans. The prolonged consumption of heavy metals may lead to severe effect on living organisms. Hg is known as a deadly and accumulative poison even when consumed in small quantities, and capable of deadening nerve receptor in humans, thus considered as a public health problem. Cd is a highly toxic metal and accumulates primarily in liver and kidney of mammals through the food chain. Exposure of cobalt (Co) to *Macrobrachium rosenbergii* may reduce the female fecundity (Stalin et al. 2019). Although Copper (Cu) involves in the prawns' oxygen-carrying pigment haemocyanin, it may also cause poisoning to humans. Poisoning by Cu and Zn may cause

gastrointestinal disorders, diarrhoea, stomatitis, tremor, depression, vomiting and ataxia (Anani & Olomukoro 2018). The development of the waterfront in Sarawak River may give negative impacts on the aquatic organisms such as *M. rosenbergii* or locally known as giant freshwater prawn. *M. rosenbergii* were commonly served as regional and local fisheries importance, and economic values since they meet the high demand of protein source and have high domestic and export potential (Banu & Christianus 2016). This species is abundant in Sarawak River and can be wild-captured by local fishermen. However, rapid urbanization along the Sarawak River may increase the contamination of heavy metals in the water and sediment. Moreover, there is still no study on the heavy metal contamination in the wild *M. rosenbergii* particularly in Sarawak River. Contamination of this type of prawn with heavy metals may give a potential risk to human health. Therefore, this study sought to (1) quantify the contamination level of heavy metals (Cd, Co, Cu, Zn, Hg) in *M. rosenbergii* from the Sarawak River, and (2) calculate the health risk assessment to humans upon consumption of contaminated prawns.

MATERIALS AND METHODS

M. rosenbergii were captured using the fishing rod from the Sarawak River on 12th October 2016 at the longitude 01°33'40.3" N and latitude 110°20'34.0" E (Fig. 1). Surface sediment samples were collected by the plastic corer. All samples were then stored in the zipper polyethylene bags, labelled properly and placed in the cooler box with ice during the transportation to the Aquatic Chemistry Laboratory. The total wet weight and the total length of the individual prawn were recorded before the dissection (Table 1). In the laboratory, prawn and sediment samples were kept at -20°C in a freezer. The mature male and female *M. rosenbergii* can be identified by observing their second pleopod, as explained in detail in Idrus et al. (2018).

Table 1: Total length and total weight of *M. rosenbergii* samples (n = 21).

Sex	n	Reproductive state	Total length (cm)	Total weight (g)
Female	13	Mature	14.32 ± 1.86	26.11 ± 9.10
Male	8	Mature	17.45 ± 2.81	59.55 ± 3.50

There were significant differences between female and male prawns ($p < 0.05$) total length and total weight.

The dissected muscle, exoskeleton, and gill were weighed and dried in the oven at 60°C until it achieved a constant weight to ensure it was completely dry. About 80% weight differences were recorded between wet and dried samples, due to moisture loss during the drying process. Before the digestion process, dried samples were ground to powder form using the mortar and pestle. The digestion process was done by heating 0.2 g of the sample in 5 mL of concentrated HNO_3 (Tu et al. 2008) on the hot plate until the solution turns clear (Idrus et al. 2018). Sediment samples were air-dried and ground before digestion using the aqua regia method as in Hseu et al. (2002) by heating on a hot plate. All samples, including the standard solutions, were pre-concentrated by using the multielements pre-concentration step by solid phase extraction using iminodiacetate chelating resin (Toyopearl AF Chelate-650M) method as described in Idrus et al. (2018), before analyzing the heavy metal concentrations. Cd, Co, Cu and Zn were analyzed by Flame Atomic Absorption Spectrophotometer (FAAS; Thermo Scientific iCE 3500), and Hg by the Flow Injection Mercury System (FIMS; Perkin Elmer-FIMS 400). All readings were determined in three replicates. The standard calibration of each metal was

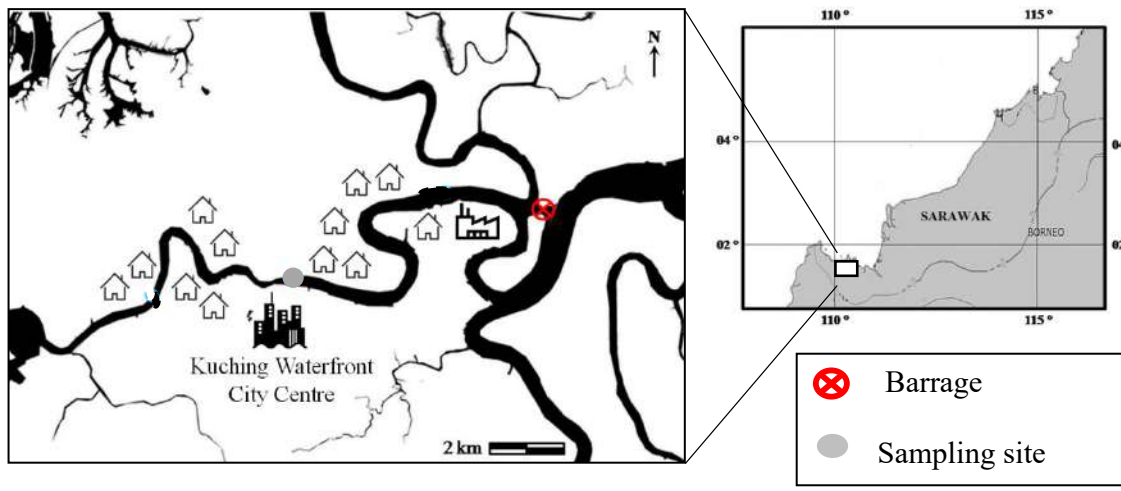

Fig. 1: Sampling site for *M. rosenbergii* in Sarawak River.

Table 2: Feedback from the respondents (n = 100; male: 46 persons, female 54 persons) from the survey of daily consumption of *M. rosenbergii* by the residents nearby the Sarawak River

Parameters	Minimum	Maximum	Average
Age (years old)	21	67	
Body weight (kg)	39	90	60
Estimation of weight of prawns intake daily (g/day)	50	300	150

performed with r^2 between 0.9937 and 0.9996. In this study, the certified reference materials (CRMs) from the National Research Council Canada of LUTS-1 (non-defatted lobster hepatopancreas) were used for *M. rosenbergii* samples and MASS-4 was used for sediment samples. CRMs analyses were followed the same methods as for prawn and sediment samples.

The survey of daily consumption of *M. rosenbergii* was done by questionnaire to the local residents (n = 100) that live close to Sarawak River. The summary of the survey is given in Table 2. All respondents got the prawns from the Sarawak River, either by catching themselves or bought from other fishermen who caught them from the Sarawak River.

The daily intake of metal (DIM) was calculated to estimate the average daily metal accumulation in a consumer for specified bodyweight, without taking into account the possible metabolic excretion of the metal. The DIM was calculated based on Equation (1) given by Islam et al. (2017).

$$DIM = \frac{K_{conversion\ factor} \times C_{metal} \times D_{average\ prawn\ intake}}{B_{average\ body\ weight}} \quad ...(1)$$

where $K_{conversion\ factor}$ = Conversion factor of 0.1455 was used based on the moisture content of the samples (Islam et al. 2017); C_{metal} = Metal concentration in prawns (µg/g); $D_{average\ prawn\ intake}$ = Average daily intake of prawns by the local residents around Sarawak River (150 g/day, $B_{average\ body\ weight}$ = Average body weight (60 kg, (Table 2). This intake figure includes all modes of prawn meals.

The health risk index (HRI) was calculated using the Equation (2) as in Cui et al. (2004).

$$HRI = \frac{DIM}{RfD} \quad ...(2)$$

where DIM = Daily intake of metal (µg/kg/day); RfD = Oral reference dose established by USEPA. If the HRI value is larger than 1 for any metal in food from oral consumption, it means that the consumer population was at a potential health risk. The calculation of HRI was depended on the DIM value and the oral reference dose established by USEPA (1994, 2001), where the RfD values for Cd was 0.83 µg/kg/day, Cu was 500 µg/kg/day, Zn was 1000 µg/kg/day and Hg was 0.10 µg/kg/day. For Co, there was no established reference value given by USEPA, therefore an RfD value of 30 µg/kg/day for Co (Finley et al. 2012) was used in this study.

The hazard index (HI) was used to estimate the potential human health risks upon consuming more than one metal, where the HI is the sum of the HRI derived from the prawns, as shown in Equation (3):

$$HI = \Sigma HRI = HRI_{Cd} + HRI_{Co} + HRI_{Cu} + HRI_{Zn} + HRI_{Hg} \quad ...(3)$$

where HRI_{Cd}, $HRI_{Co,}$ HRI_{Cu}, HRI_{Zn}, HRI_{Hg} are the health risk indexes as calculated in Equation (2) or also known as hazard quotients for Cd, Co, Cu, Zn, and Hg, respectively. It is assumed that the HI value larger than 1 will give adverse effects on human health due to the multiple metal exposures.

All metal concentrations data were expressed in mg/kg of the flesh weight (wet weight) ± standard deviation (mg/kg FW). The variations between metals content in different body parts of the prawns and their size and gender were tested by two-way ANOVA, while variations of total length and total weight were tested by *t*-test. The Pearson's Correlation and linear regressions were used to compare the correlation of metals in muscle, exoskeleton and gill of *M. rosenbergii.* In all cases, the level of significance was set at □ = 0.05. The statistical analyes were performed by using SPSS for Windows Version 22.

RESULTS AND DISCUSSION

The obtained values and metals recovery of Cd, Co, Cu, Zn and Hg are given in Table 3, which suggest the efficiency of the chelation methods used.

The allometric length-weight relationship of the *M. rosenbergi* was done using the Equation 4 as provided by Rocha et al. (2015):

Table 3: The heavy metals recovery of Cd, Co, Cu, Zn and Hg in LUTS-1 and MASS-4.

CRM	Metals	Certified value	Obtained value	Recovery (%)
LUTS-1 (mg/kg)	Cd	14.2 ± 1.0	12.9 ± 0.6	91 ± 4
	Co	0.34 ± 0.04	0.37 ± 0.06	109 ± 4
	Cu	107 ± 8	116 ± 11	108 ± 7
	Zn	82.9 ± 2.2	86.4 ± 3.5	104 ± 5
	Hg (µg/kg)	16.7 ±2.2	14.1 ± 1.5	84 ± 6
MASS-4 (mg/kg)	Cd	0.28 ± 0.04	0.31 ± 0.03	110 ± 2
	Co	13.0 ± 0.8	11.8 ± 1.3	91 ± 6
	Cu	32.9 ± 1.8	35.1 ± 1.2	106 ± 3
	Zn	147 ± 6	155 ± 9	105 ± 5
	Hg	0.09 ± 0.04	0.07 ± 0.02	107 ± 6

$$W = aL^b \quad \ldots(4)$$

where W = weight; L = length; a = regression intercept; b = slope. Therefore, by performing logarithmic transformations, the linear relationships could be represented by the equation $W = 0.00393L^{3.305}$ ($R^2 = 0.939$).

Heavy Metal Concentrations in *M. rosenbergii*

The concentrations of heavy metals in gill, exoskeleton and muscle of *M. rosenbergii* are given in Table 4.

The distribution of heavy metals in the body parts of *M. rosenbergii*, collected from the Sarawak River, followed this trend: Zn > Cu > Co > Cd > Hg. In general, the concentration order of heavy metals in the body parts was found to be gills > exoskeleton > muscle. The results showed that there was no significant difference ($P > 0.05$) between male and female *M. rosenbergii.* Overall, all the samples contained heavy metal concentrations below the permissible limits of Joint FAO/WHO Expert Committee on Food Additives (JECFA 2012) for human consumption (Cd < 2 mg/kg; Cu < 30.00mg/kg; Zn < 150 mg/kg; Hg <1 mg/kg). Our heavy metal concentrations were also lower than the permitted values for Cu (< 30 mg/kg), Zn (< 100 mg/kg), and Hg (< 1 mg/kg) set by the Malaysian Food Regulations (1985), except low difference was recorded for Cd (< 1 µg/g). However, no safe limits were recorded for Co in both JECFA (2012) and Malaysian Food Regulations (1985), hence, no comparisons could be made in this study.

Cd, Co, Cu, and Zn concentrations in gills were positively correlated ($r^2 > 0.500$) to the total length of the prawns (Fig. 2) and were significant ($P < 0.05$). The positive relationship of heavy metal accumulation in organisms was often associated with their long time exposure to contaminants (Idrus et al. 2018, Elahi et al. 2012). Heavy metals can accumulate in prawn body parts which may transfer the chemical composition from one trophic level to another in the food chain, thus, giving human health a negative effect. Heavy metals were usually taken from the environment such as sediment by the prawns, then, distributed by circulation and subsequently accumulated in target organs, for example, gills.

In this study, the highest concentrations of all heavy metals were found in the gills. Gills are metabolically active body parts in the prawn and have a high tendency to accumulate heavy metals. This is due to the position and function of gills in which located as the starting points of heavy metals absorption and their function as the excretion site of contaminants from the body (Stanek et al. 2014). Moreover, gills are the primary target when crustaceans are exposed to waterborne pollutants, as gills are the major route for metal uptake (Seogianto et al. 2013, Fonseca et al. 2016). The concentration of Cd in *M. rosenbergii* in this study (1.51 ± 0.06 mg/kg) was lower than *Penaeus semisulcatus* from Jazan (6.33 ± 2.08 mg/kg) (Gendy et al. 2015), with the main source of Cd at their study sites was from the agricultural activities. However, their concentrations for Zn (24.00 ± 7.80 mg/kg), Cu (3.00 ± 1.00 mg/kg), and Co (0.33 ± 0.10 mg/kg) in the prawns' gills were lower than our study. In comparison with the range concentrations of Cu (140.6-423.1 mg/kg), Cd (18.10-38.07 mg/kg) and Zn (125.5953.4 mg/kg) in *Penaeus semiculatus* gills from

Table 4: Average concentrations of heavy metals (mg/kg wet wt) in different body parts of *M. rosenbergii* collected from the Sarawak River, and the safety limits (mg/kg wet wt)

Heavy metals	Body Parts	Concentrations in average		JECFA (2012) limit	MFR (1985) limit
		Male	Female		
Cd	Muscle	0.46 ± 0.08	0.50 ± 0.05	2.00	1.00
	Exoskeleton	0.79 ± 0.60	0.57 ± 0.23		
	Gill	1.53 ± 0.06	1.51 ± 0.06		
Co	Muscle	n.a.	n.a.	NS	NS
	Exoskeleton	5.67 ± 2.33	3.99 ±1.01		
	Gill	15.17 ± 0.83	13.77 ± 1.23		
Cu	Muscle	10.18 ± 3.82	6.62 ± 2.28	30.00	30.00
	Exoskeleton	10.47 ± 5.30	7.65 ±3.04		
	Gill	21.58 ± 4.58	17.09 ± 1.91		
Zn	Muscle	13.76 ± 2.24	10.87 ± 1.13	150.00	100.00
	Exoskeleton	6.98 ± 3.02	7.36 ± 0.64		
	Gill	59.17 ±12.13	52.56 ± 7.44		
Hg	Muscle	n.a.	n.a.	1.00	1.00
	Exoskeleton	n.a.	n.a.		
	Gill	0.13 ± 0.02	0.11 ± 0.03		

n.a. is not available, due to the concentrations were below the detection limit of the particular metals; NS, not specified; JECFA: Joint FAO/WHO Expert Committee on Food Additives; MFR: Malaysian Food Regulations

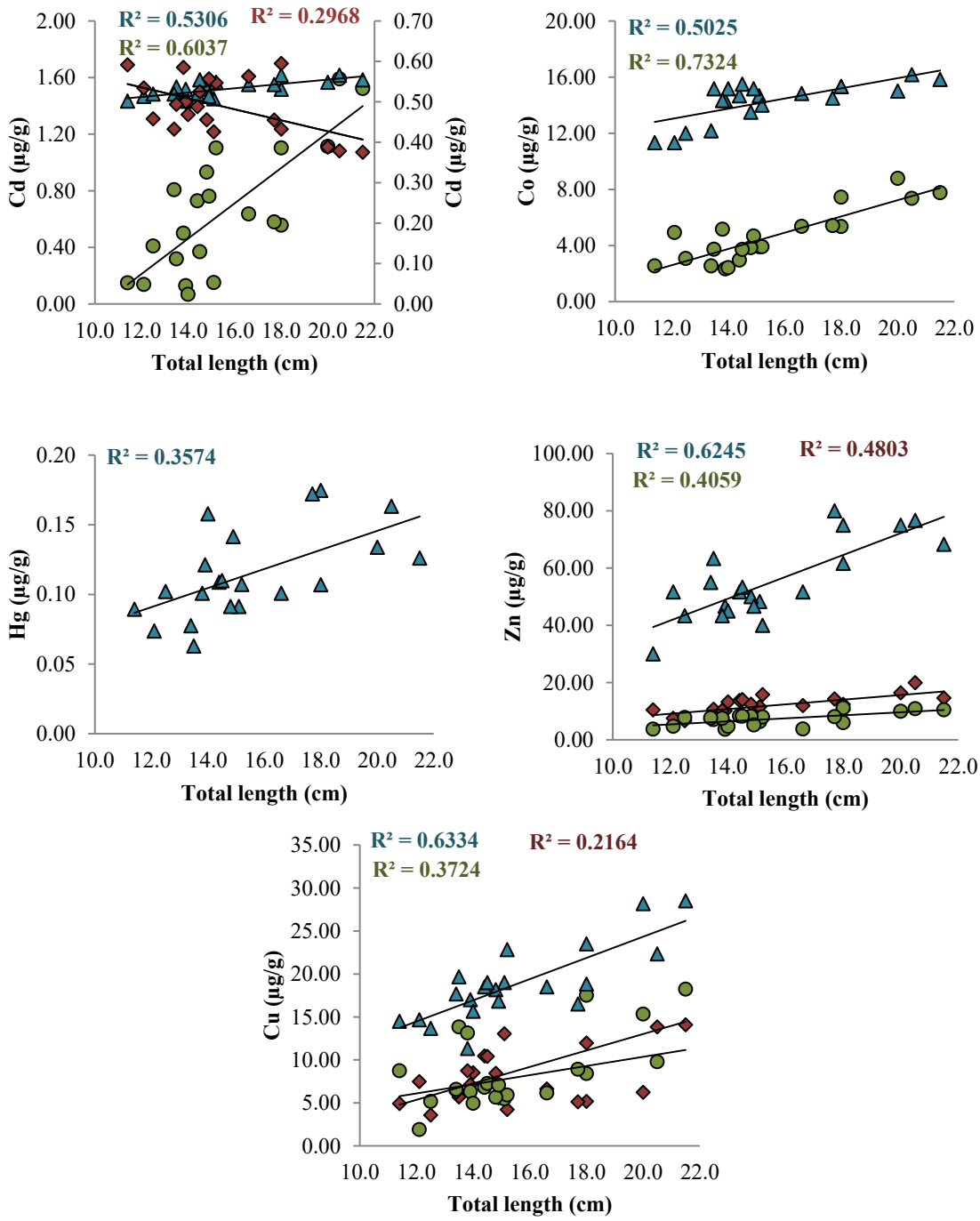

Fig. 2: Relationship between Cd, Co, Cu, Zn, Hg concentrations (mg/kg) and the total length (cm) of *M. rosenbergii* in muscle (red diamond), exoskeleton (green circle) and gills (blue triangle) from Sarawak River.

Yumurtalik, Turkey,our values (Cu: 21.58 ± 4.58 mg/kg; Cd: 1.53 ± 0.06 mg/kg; Zn: 59.17 ± 12.13 mg/kg) were very much lower than them. Meanwhile, Mostafiz et al. (2020) obtained very high concentrations of Cu (83.94 ± 18.32 mg/kg) and Zn (211.57 ± 42.09 mg/kg) in cephalothorax area (including gills) of wild *M. rosenbergii* in selected rivers of Chittagong and Chandpur, Bangladesh, as compared to this study, due to polluted rivers with heavy metals.

Cu and Zn were also recorded higher in exoskeleton and muscle, with slightly positive ($P < 0.05$) relationship (Fig. 2) shown in comparison with their total length. Zn is an essential metal for prawn and important in immune function, reproduction and body growth. Zn can reduce the adverse effect of phytic acid on the growth of prawns (*Litopena vannamei*) and also can increase the availability of macro minerals and micro minerals in the prawns (Bharadwaj et al. 2017). Zn also acts as a co-factor in many enzyme systems and essential component for metalloenzymes. It also involves in the signaling of molecules, DNA replication and repairing of the prawn cells, hence, increasing the survival rate of *M. rosenbergii* (Thirunavukkarasu et al. 2019). The increase of Zn concentration in the muscle occurred simultaneously by low concentration in the exoskeleton, suggesting a dynamical exchange of Zn between these two body parts. However, Cu concentrations were about the same in the exoskeleton and the muscle because Cu is known as one of the important components in the respiratory pigment haemocyanin and Cu is needed to trigger the enzymes and respiratory proteins. Cu and Zn in the prawn diet is a crucial route of accumulation in their body, particularly the muscles. High accumulation of Cu and Zn in muscles and exoskeleton can increase over time. Moreover, *M. rosenbergii* spends much of their time partially buried in the soft sediment and this may be the reason for the high Cu and Zn accumulation in prawns. It was in agreement with relatively high concentrations of Zn (84.54 ± 10.22 mg/kg) and Cu (22.47 ± 3.90 mg/kg) in the sediment samples from the Sarawak River (Table 5). Our Cu concentrations in the *M. rosenbergii* muscles were nearly in the same range (19.35-34.23 mg/kg) for *P. semiculatus* muscles (Aytekan et al. 2019). However, their values (37.43-61.42 mg/kg) for Zn in the prawn muscles were higher than ours (10.87-13.76 mg/kg) (Aytekan et al. 2019). Our Zn and Cu values in the muscles were lower than the values obtained by Mostafiz et al. (2020) in their wild and farmed *M. rosenbergii*. Tu et al. (2008) also found higher concentrations of Cu and Zn in their *M. rosenbergii* muscles and exoskeletons.

Cd was recorded in the exoskeleton and muscle of our prawn samples. Statistically, the Cd concentrations in muscle and exoskeleton did not show a significance difference ($P > 0.05$). However, the relationship between total length and Cd concentration was slightly negative ($r^2 = 0.2968$) in muscles. There was no clear reason that the smaller size of prawns has accumulated more Cd in their muscles, while sediment samples did not contaminate with Cd (1.17 ± 0.02 mg/kg, Table 5). Cd concentrations in muscles and exoskeletons in this study were higher than the values obtained by Tu et al. (2008). On the other hand, our values were lower than Cd values reported by Islam et al. (2017) in both muscles and exoskeletons of their *M. rosenbergii* samples from Bagerhat, Bangladesh. In general, heavy metal content in exoskeletons and muscles may be reduced in the process of moulting where it involves the shedding of the hard chitinous exoskeleton layer, replaced by a new layer during the active grow (Stanek et al. 2014) and increasing new muscles. Therefore, the accumulation pattern of heavy metals in the exoskeleton and muscle of *M. rosenbergii* is hard to understand. Several factors such as diet, changes in metabolic rate, the hormonal and reproductive status may also influence metal accumulations in different sex of crustaceans (Idrus et al. 2018, Elahi et al. 2012).

The Hg concentration was not available for muscle and exoskeleton because it was below the detection limit of the FIMS. The gill was the only body part that contained a detectable concentration of Hg which was 0.125 ± 0.024 mg/kg in male and significantly higher ($P < 0.05$) than in female (0.107 ± 0.033 mg/kg). This lower Hg level may be due to their developed ability to excrete toxic elements from their body (Pourang et al. 2004). As the bioaccumulation process takes place through the absorption of metals via various routes including dietary and ambient environment (Arnot & Gobas 2006), metal contents in the body of *M. rosenbergii* might be higher than in the surrounding environment.

Bioaccumulation Factor

Bioaccumulation factor (BAF) was calculated to assess the evolution of metals in different body parts of prawn samples collected from Sarawak River. BAF is the ratio of the concentration of contaminants in relation to its habitat environment (sediments). In this study, BAF was calculated as the ratio of metal concentrations in prawn and sediment samples using Equation 5 (Santoro et al. 2009).

$$BAF = M_{Body\ part} / M_{sediment} \quad \ldots(5)$$

where $M_{Body\ part}$ is metal concentration in *M. rosenbergii* body parts, $M_{sediment}$ is metal concentrations in sediment.

If the BAF value was below 1, it may indicate that bioaccumulation was low and below the safety limit in our prawn samples, and if the BAF value was more than 1, it is described as an increase of heavy metals level beyond the threshold (Anani & Olomukora 2019). The BAF values for

Table 5: The concentrations (mg/kg) of heavy metals in the sediment of the Sarawak River.

	Cd	Co	Cu	Zn	Hg
Sediment	1.17 ± 0.02	6.89 ± 0.93	22.47 ± 3.90	84.54 ± 10.22	0.05 ± 0.01

all body parts of *M. rosenbergii* are presented in Table 6. Our results reveal that Cd, Co and Hg are bioaccumulative in prawn (female and male) gills, as related to the sediment concentrations. These results indicate that Cd, Co and Hg are more easily available than other metals. The bioavailability could be controlled by metals speciation, food chain, physicochemical factors, particulate matter, organic carbon content and cation exchange capacity (Monikh et al. 2015). In this study, it also showed higher BAF values of heavy metals occurred in the gills and due to this, organ is known as the target organ for detoxification and circulation of heavy metals. Since Cu and Zn are required by prawns for their biological processes, these metals were distributed in their whole body, thus, leaving only residue quantity in the target organ (gill) (Monikh et al. 2015). The present study also showed that BAF values were slightly higher in male prawns, due to their larger size compared to female prawns. In comparison with the previous study in Kerang River (Idrus et al. 2018), the BAF value of Cu in male prawns' muscle was lower than this study, but recorded higher Cu BAF value in the exoskeleton. The BAF of Cd value from the present study was considerably higher than the value in *M. rosenbergii* from the Mekong River Delta (Tu et al. 2008). However, a relatively lower concentration of Cd was recorded in the exoskeleton of their younger prawns compared to adults can be related to the lower frequency of the moulting process (Kouba et al. 2010).

Human Health Risk Assessment

The DIM value was calculated considering the average metal content and daily intake of giant freshwater prawns eaten, either as a whole prawn or as ingredients in their meal. The DIM for the present study is given in Table 7. In this study, the DIM values for Cu (2.29 µg/kg body weight per day), Zn (9 µg/kg body weight per day), Cd (0.32 µg/kg body weight per day), and Hg (0.015 µg/kg body weight per day) were less than the provisional maximum tolerable daily intake (PMTDI) values set by JECFA (2012) for Cu (500 µg/kg body weight per day), Zn (1000 µg/kg body weight per day), Cd (1 µg/kg body weight per day), and Hg (60 µg/kg body weight per day). According to this finding, therefore, it can be concluded that the local population was safe from the health risk from ingestion of these metals.

The food chain is the most important pathway of heavy metals to humans, which could lead to significant human health risk. Considering the health risk of metals through dietary oral intake of the *M. rosenbergii* in Sarawak River, it is, therefore, useful to estimate the exposure level to humans in every element to oral RfD. The HRI associated with the individual elements of Cd, Co, Cu, Zn and Hg due to prawn consumption was calculated as given in Table 7. The highest HRI value was recorded in Cd (0.39), and the lowest value from Cu (0.002) for adults' consumption. Crustaceans and shellfish are natural accumulators of Cd, especially if they

Table 6: The BAF values of Cd, Co, Cu, Zn and Hg in different body parts of *M. rosenbergii* in the Sarawak River, related to the sediment concentrations.

Sex	Body part	Cd	Co	Cu	Zn	Hg
Female	Muscle	0.43 ± 0.04	N.A	0.30 ± 0.10	0.13 ± 0.01	N.A
	Exoskeleton	0.49 ± 0.20	0.58 ± 0.15	0.34 ± 0.14	0.09 ± 0.008	N.A
	Gill	1.29 ± 0.05	2.00 ± 0.18	0.76 ± 0.09	0.62 ± 0.09	2.20 ± 0.60
Male	Muscle	0.39 ± 0.07	N.A	0.45 ± 0.17	0.16 ± 0.03	N.A
	Exoskeleton	0.68 ± 0.51	0.82 ± 0.34	0.47 ± 0.24	0.08 ± 0.04	N.A
	Gill	1.31 ± 0.05	2.20 ± 0.12	0.96 ± 0.20	0.70 ± 0.14	2.60 ± 0.40

N.A is not applicable as no value was obtained in the respective body parts

Table 7: The calculated daily intake metal (DIM, µg/kg/day), health risk index (HRI) and hazard index (HI) values for heavy metals from the Sarawak River, and the provisional maximum tolerable daily intake (PMTDI, µg/kg/day).

$K_{conversion\ factor}$	$D_{average\ prawn\ intake}$ (g/day)	$B_{average\ body\ weight}$ (kg)	Metals	Cmetal (µg/g)	Rf_D	DIM	PMTDI	HRI	HI
0.1455	150	60	Cd	0.89	0.83	0.32	1	0.39	0.69
			Co	11.83	30	4.30	-	0.14	
			Cu	6.31	500	2.29	500	0.002	
			Zn	24.76	1000	9.00	1000	0.009	
			Hg	0.04	0.1	0.015	60	0.15	

$K_{conversion\ factor}$ is followed Islam et al. (2017), $D_{average\ prawn\ intake}$ is average daily intake of *M. rosenbergii* of the local residents near Sarawak River; $B_{average\ body\ weight}$ is average body weight of the local residents near Sarawak River; C_{metal} is average metal concentrations; Rf_D (µg/kg/day) is oral reference dose established by USEPA (1994, 2001), PMTDI (JECFA 2012).

are exposed to the polluted environment with those metals such as sediment. In this study, the concentration of Cd in the sediment was 1.17 ± 0.02 mg/kg. *M. rosenbergii* is an example of some freshwater decapods that are bottom feeders, thus, they are at risk to concentrate more heavy metals than surface feeder prawns (Anani & Olomukoro 2019). Accumulation of Cd in the human body may cause Parkinson's and Wilson's diseases (Hossen et al. 2015). Children also are at risk to have lower IQ and experience interference in the nervous system as Cd tend to accumulate in the choroids plexus in brain tissues, where the blood-brain barrier was absent in the young age (Wang & Du 2013). Besides, it has been observed that Cd can be stored for a long time in the kidney, which can lead to tubular necrosis (Rehman et al. 2018). The accumulated metals in the *M. rosenbergii* was measured as the HI, based on the HRI. If the HI value was more than 1, it is considered hazardous to human health. In this study, the HI value was 0.69, indicating that prawns from Sarawak River are still safe for human consumption and has lower health risk.

CONCLUSION

In conclusion, the concentrations of Cu, Zn and Hg in *M. rosenbergii* from the Sarawak River were within the permissible limits of JECFA and Malaysian Food Regulation, except for Cd, which was slightly higher than the recommended value by the Malaysian Food Regulation. There is a need to establish a safety limit for Co to ensure that a comparison can be made. The concentrations of Cd, Cu, Co, Zn and Hg were significantly correlated to their total body length, therefore, it was expected that bigger prawns could possess a higher concentration of metals in their body parts. Health hazard risks for most of the heavy metals were low; therefore, *M. rosenbergii* from Sarawak River were safe to be consumed in a considerable amount regularly.

ACKNOWLEDGEMENTS

The authors would like to thank the provider of Grant RAGS/STWN01(01)/1178/2014(01) and UNIMAS for their support of this work.

REFERENCES

Anani, O.A. and Olomukoro, J.O. 2018. Health risk from the consumption of freshwater prawn and crab exposed to heavy metals in a tropical river, Southern Nigeria. Journal of Heavy Metal Toxicity and Diseases 3:1-7. https://10.21767/2473-6457.10024.

Anani, O.A. and Olomukoro, J.O. 2019. Assessment of metal accumulation and bioaccumulation factor of some trace and heavy metals in freshwater prawn and crab. In: Genaro Diarte-Plata and Ruth Escamilla-Montes (Eds.), Crustacea, IntechOpen. https://doi.org/10.5772/intechopen.88103.

Aytekin, T., Kargın, D., Çogun, H.K., Temiz, O., Varkal, H.S. and Kargın, F. 2019. Accumulation and health risk assessment of heavy metals in tissues of the shrimp and fish species from the Yumurtalik coast of Iskenderun Gulf, Turkey. Heliyon, 5(8): e02131. https://doi.org/10.1016/j.heliyon.2019.e02131.

Banu, R. and Christianus, A. 2016. Giant freshwater prawn *Macrobrachium rosenbergii* farming: A review on its current status and prospective in Malaysia. J. Aquac. Res. Dev. 7: 2. https://doi:10.4172/2155-9546.1000423.

Bharadwaj, A.S., Patnaik, S., Browdy, C.L. and Lawrence, A.L. 2017. Availability of dietary zinc sources and effects on performance of pacific white shrimp *Litopenaeus vannamei* (Boone). International Journal of Recirculating Aquaculture, 13: 1-10. http://doi.org/10.21061/ijra.v13i0.1514.

Cui, Y.J., Zhu, Y.G., Zhai, R.H., Chen, D.Y., Huang, Y.Z., Qui, Y. and Liang, J.Z. 2004. Transfer of metals from soil to vegetables in an area near a smelter in Nanning, China. Environ. Int., 30: 785-791. https://doi.org/10.1016/j.envint.2004.01.003.

Elahi, M., Esmaili-Sari, A. and Bahramifar, N. 2012. Total mercury levels in selected tissues of some marine crustaceans from Persian Gulf, Iran: Variations related to length, weight and sex. Bull. Environ. Contam. Toxicol., 88: 60-64. https://doi:10.1007/s00128-011-0451-4.

Eriksson, E., Srigirisetty, S. and Eilersen, A.M. 2010. Organic matter and heavy metals in greywater sludge. Water Sa., 36: 139-142. http://dx.doi.org/10.4314/wsa.v36i1.50921.

Finley, B.L., Monnot, A.D., Gaffney, S.H. and Paustenbach, D.J. 2012. Dose response relationships for blood cobalt concentrations and health effects: A review of the literature and application of a biokinetic model. J. Toxicol. Environ. Health, Part B: Critical Reviews, 15: 493-523, https://doi:10.1080/10937404.2012.744287.

Fonseca, A.R., Fernandes, L.F.S., Monteiro, S.M., Fontainhas-Fernandes, A. and Pacheco, F.A.L. 2016. From catchment to fish: Impact of anthropogenic pressures on gill histopathology. Sci. Total Environ., 550: 972-986. https://doi.org/10.1016/j.scitotenv.2016.01.199.

Gendy, A.E., Farraj, S.A. and Hedeny, M.E. 2015. Heavy metal concentrations in tissues of the shrimp *Penaeus semisulcatus* (De Haan, 1844) from Jazan, Southern Red Sea Coast of Saudi Arabia. Pakistan J. Zool., 47(3): 671-677. http://zsp.com.pk/pdf47/671-677%20(10)%20PJZ-2170-15%2010-5-15%20El%20Gendy%20et%20al%20-revised%20final.pdf

Hameed, A.S.S. and Bonami, J.R. 2012. White tail disease of freshwater prawn, *Macrobrachium rosenbergii*. Indian J. Virol., 23: 134-140. https://doi:10.1007/s13337-012-0087-y.

Hossen, M.F., Hamdan, S. and Rahman, M.R. 2015. Review on the risk assessment of heavy metals in Malaysian clams. Sci. World J., 2015: 1-7. http://dx.doi.org/10.1155/2015/905497.

Idrus, F.A., Basri, M.M., Rahim, K.A.A., Rahim, N.S.A. and Chong, M.D. 2018. Concentrations of cadmium, copper, and zinc in *Macrobrachium rosenbergii* (Giant Freshwater Prawn) from natural environment. Bull. Environ. Contam. Toxicol., 100: 350-355. https://doi.org/10.1007/s00128-018-2270-3.

Islam, G.R., Habib, M.R., Waid, J.L., Rahman, M.S., Kabir, J., Akter, S. and Jolly, Y. 2017. Heavy metal contamination of freshwater prawn (*Macrobrachium rosenbergii*) and prawn feed in Bangladesh: A market-based study to highlight probable health risks. Chemosphere, 170: 282-289. https://doi.org/10.1016/j.chemosphere.2016.11.163.

JECFA 2012. Joint FAO/WHO food standards programme Codex committee on contaminants in food. Sixth Session, Maastricht.

Jewel, M.A.S., Haque, M.A., Amin, R., Hasan, J., Lubna Alam, Mondal, S. and Ahmed, S. 2020. Heavy metal contamination and human health risk associated with sediment of Ganges River (Northwestern Bangladesh). Nature Environment and Pollution Technology, 19(2): 783-790. https://doi.org/10.46488/NEPT.2020.v19i02.035.

Kouba, A., Buřič, M. and Kozák, P. 2010. Bioaccumulation and effects of heavy metals in crayfish: A review. Water Air Soil Pollut., 211: 5-16. https://doi.org/10.1007/s11270-009-0273-8.

Mah, D.Y.S., Hii, C.P., Putuhena, F.J. and Lai, S.H. 2011. River modelling to infer flood management framework. Water SA, 37: 121-126.

Malaysian Food Regulation 1985. Malaysian Law on Food and Drugs. Malaysian Law Publishers, Kuala Lumpur.

Monikh, F.A., Maryamabadi, A., Savari, A. and Ghanemi, K. 2015. Heavy metals' concentration in sediment, shrimp and two fish species from the northwest Persian Gulf. Toxicology and Industrial Health, 31(6): 554-565. https://doi.org/10.1177%2F0748233713475498.

Mostafiz, F., Islam, M.M., Saha, B., Hossain, M.K., Moniruzzaman, M. and Habibullah-Al-Mamun, M. 2020. Bioaccumulation of trace metals in freshwater prawn, *Macrobrachium rosenbergii* from farmed and wild sources and human health risk assessment in Bangladesh. Environmental Science and Pollution Research, 27: 16426-16438. https://doi.org/10.1007/s11356-020-08028-4.

Natural Resources and Environmental Board Sarawak 2017. Target of cleaner, 'healthier' Sarawak River by 2021. Available at: http://www.nreb.gov.my/modules/web/pages.php?mod=news&sub=news_view&nid=272.

Pourang, N., Dennis, J.H. and Ghourchian, H. 2004. Tissue distribution and redistribution of trace elements in shrimp species with the emphasis on the roles of metallothionein. Ecotoxicology, 13: 519-533. https://doi.org/10.1023/B:ECTX.0000037189.80775.9c.

Rehman, K., Fatima, F., Waheed, I. and Akash, M.S.H. 2018. Prevalence of exposure of heavy metals and their impact on health consequences. J. Cell Biochem., 119: 157-184. https://doi.org/10.1002/jcb.26234.

Rocha, S.S.D., Silva, R.L.S.D., Santos, J.D.L. and Oliveira, G.D. 2015. Length-weight relationship and condition factor of *Macrobrachium amazonicum* (Heller, 1862) (Decapoda, Palaemonidae) from a reservoir in Bahia, Brazil. Nauplius, 23: 146-158. http://dx.doi.org/10.1590/S0104-64972015002308.

Saher, N.U. and Kanwal, N. 2019. Assessment of some heavy metal accumulation and nutritional quality of shellfish with reference to human health and cancer risk assessment: A seafood safety approach. Environmental Science and Pollution Research, 26: 5189-5201. https://doi.org/10.1007/s11356-018-3764-6.

Santoro, A., Blo, G., Mastrolitti, S. and Fagioli, F. 2009. Bioaccumulation of heavy metals by aquatic macroinvertebrates along the Basento River in the South of Italy. Water Air Soil Pollut., 201: 19-31. https://doi.org/10.1007/s11270-008-9923-5.

Sarkar, T., Alam, M., Parvin, N., Fardous, Z., Chowdhury, A., Hossain, S., Haque, M. and Biswas, N. 2017. Assessment of heavy metals contamination and human health risk in shrimp collected from different farms and rivers at Khulna-Satkhira region, Bangladesh. Toxicology Reports. https://www.scipedia.com/public/Sarkar_et_al_2016a.

Stalin, A., Suganthi, P., Mathivani, S., Broos, K.V., Gokula, V., Sadiq Bukhari, A., Syed Mohamed, H.E., Singal, R.K. and Venu-babu, P. 2019. Effect of cobalt-60 gamma radiation on reproductive disturbance in freshwater prawn *Macrobrachium rosenbergii* (De Man, 1879). Toxicology Report, 6: 1143-1147. https://doi.org/10.1016/j.toxrep.2019.10.021.

Stanek, M., Dabrowski, J., Dlugosz, J. and Janicki, B. 2014. Impact of the anthropogenisation on the metals bioaccumulation and distribution in the Spiny-Cheek Crayfish (*Orconectes limosus* Raf.) from Lake Gaplo, Poland. Int. J. Environ. Res., 8: 1315-1322.

Thirunavukkarasu, M., Periyakali, S.B., Subramanian, R. and Perumal, S. 2019. Influence of two different dietary zinc sources in freshwater prawn *Macrobrachium rosenbergii* post larvae. J. Ocean. Limnol., 37: 290-299. https://doi.org/10.1007/s00343-018-7253-z.

Tu, N.P.C., Ha, N.N., Ikemoto, T., Tuyen, B.C., Tanabe, S. and Takeuchi, I. 2008. Bioaccumulation and distribution of trace elements in tissues of giant river prawn *Macrobrachium rosenbergii* (Decapoda: Palaemonidae) from South Vietnam. Fish Sci., 74: 109-119. https://doi.org/10.1111/j.1444-2906.2007.01474.x.

USEPA 1994. Integrated Risk Information System Toxicological Summary for Cadmium. Available at: https://cfpub.epa.gov/ncea/iris2/chemicalLanding.cfm?substance_nmbr=141.

USEPA 2001. Integrated Risk Information System Methylmercury (MeHg). Available at: https://cfpub.epa.gov/ncea/iris/iris_documents/documents/subst/0073.htm.

Wang, B. and Du, Y. 2013. Cadmium and its Neurotoxic Effects. Oxidative Medicine and Cellular Longevity, 2013: 1-13. http://dx.doi.org/10.1155/2013/898034.

Yunus, K., Zuraidah, M.A. and John, A. 2020. A review on the accumulation of heavy metals in coastal sediment of Peninsular Malaysia. Emerald Publishing Limited.

Nature Environment and Pollution Technology
An International Quarterly Scientific Journal

p-ISSN: 0972-6268
(Print copies up to 2016)
e-ISSN: 2395-3454

Vol. 20 | No. 2 | pp. 509-516 | 2021

Original Research Paper

https://doi.org/10.46488/NEPT.2021.v20i02.007

Open Access Journal

A Statistical Methodology for Impact Study on Irrigation Tank Rehabilitation

B. Anuradha†, L. Iyappan, P. Partheeban, C. Hariharasudan and Y.J. Breetha
Department of Civil Engineering, Chennai Institute of Technology, Chennai, Tamil Nadu, India
†Corresponding author: B. Anuradha; anu_bas2003@yahoo.com

Nat. Env. & Poll. Tech.
Website: www.neptjournal.com

Received: 03-06-2020
Revised: 07-08-2020
Accepted: 27-08-2020

Key Words:
Tank rehabilitation
Irrigation management
Cropping pattern
Irrigation intensity

ABSTRACT

Tank systems are essential for the agricultural growth and the livelihood of rural populations in India. Comprehending the multiple benefits from these traditional systems, tank rehabilitation has been one of the policy significances at the state level. The study was undertaken with the objective of assessing the impact of tank rehabilitation on cropped area, cropping pattern change, cost returns and income of farmers in a selected study village of south Tamil Nadu. The study was conducted on the basis of primary data obtained from 102 sample farmers belonging to "Pelasur" village of Thiruvannamalai district in south Tamil Nadu using a stratified sampling method. There was a significant difference in the cropped area, cropping intensity and irrigation intensity among the farmers before and after tank rehabilitation. It is found that there is an increase of 41.02 ha cultivated area and an increase in the net amount of Rs. 7,99,945. Many farmers shifted from paddy to sugarcane (cash crops) cultivation due to the availability of excess surface water in the tank and improved water table in their wells. Cropping intensity has been increased to 26% in the post-rehabilitation period. Thus, investment in tank rehabilitation shows a positive implication on marginal farmers and landless labours. Using SPSS, a paired-sample t-test is applied for analysing data collected from respondents.

INTRODUCTION

India is experiencing a wide variety of climate in its 329Mha total geographic area. Out of which 143Mha is under cultivation which supports 40% of the population (Vaidyanathan 2006). In order to meet out the above-mentioned support, 108Mha is under rainfed agriculture and the remaining area depend on conserved water in various storage structure like dams, reservoir, tanks etc. (Sengupta 1985, Shah 2009, Jana et al. 2012, Sowbi & Sabarish 2017). Southern states of India like Tamil Nadu, Karnataka, and Andra Pradesh widely depends on tank irrigation for agricultural activities. As per government records, there are 1,43,000 numbers of tanks existing altogether in the above-mentioned states which include 39000 tanks in Tamil Nadu alone (Sakthivadivel 2005). These structures were made by our ancestor some decades ago to meet out the multiple needs of local village people and also maintained by the local body (Vaidyanathan 2006, Narayanamoorthy 2007). The tank receives water in the form of runoff from its own catchment during rainfall with respect to the terrain. This conserved water is released through the sluice for irrigation purpose with the help of shutters provided for flow control. Water reaches the field by gravity since tanks are located in the upper level and field in the lower level (Shah & Raju 2001). Three to four sluice are in the tank bed depending upon the size and capacity of the tank. Each field channel from the sluice is divided into head, middle and tail reach of the command area. The local village landholders distribute water for irrigation among themselves in an equitable manner (Meinzen-Dick 2007, Persha et al. 2011, Fischer et al. 2014, Jagger et al. 2018). The periodical tank management was increasingly neglected in due course might be the strong reason behind the dysfunctional of irrigation tank component structures in terms of silting tank bed, supply channel and weed infestation results in the reduction of the storage capacity of the tank. Tank bunds became weaker in nature which results in leakage and breaches. Considering the degradation rate, few tanks were selected and planned to rehabilitate for regaining their design standard (Meinzen-Dick 2007, Aubriot & Prabhakar 2011, Kiran Kumara 2018). With the context of farmers, participation and management tank were rejuvenated for improving their performance level. Tank rehabilitation should facilitate more augmentation of water, strengthening tank bund in order to protect it from flood damage, improvise water storage capacity, magnifying availability of water for irrigation, promotes conjunctive use of surface and groundwater, reduce tank bed filtration, increase crop cultivation, facilitates groundwater recharge, increase the reliability of fishing in tank dead storage during the summer season, provide additional income through tank bund rehabilitation, or short-duration crops grown in tank bed during the dry season and should provide sustainable benefits to the users (Chiranjeevalu 1988, Govindaiah 1992,

Easter 1997, Chattopadhyaya 2003, Agarwal & Narain 2004, Singh et al. 2004, Sivasubramaniam 2006, Palanisamy & Easter 2010, Balamurugan 2013). These water storage structures saved natural resources which enhance biomass production, manage the problems of drought, increase the ground water table, employment generation and elevate the socio-economic conditions of the tank users (Anuradha & Ambujam 2011, Shah & Sakthivadivel 2018).

MATERIALS AND METHODS

The research has devised a combination of qualitative and quantitative methodology in which primary and secondary sources are very thoughtfully tapped for information and perspectives. The focus of the contemporary study is to examine the impact of tank rehabilitation before and after on landholding and landless people in the rural tank. Hence, tank owning various livelihood options were selected to conduct interviews with landholders and focus group discussions with landless people. Since the study emphasises the improvements in livelihood options for direct and indirect users of the tank, data were collected for pre and post-rehabilitation periods in the study area.

The data collected through the interview schedule was properly coded, master tabulated and analysed using the Statistical Package for Social Science (SPSS). Details collected through focus group discussion were documented in order to describe the developments experienced by users in the post-rehabilitation period. The methodology adopted in the present study that is discussed under the following sub-heads: Operational definition, Field setting, Respondents, Sampling framework, Sources of data, Data collection tools, Data analyses and Limitations. The operational definitions of various terms involved here in this study are presented, which may be trivial but are necessary for clarity of understanding. Irrigation: Irrigation is defined as the totality of means employed by farmers to augment and control the supply of water to soil for the purpose of production of crops (Adams 1989). Tank Rehabilitation: Tank rehabilitation is defined as restoring the tank components to their original design standards and to facilitate efficient water management and improved cropping practices and thereby providing better livelihoods for both direct and indirect tank users (Sakthivadivel et al. 2006, Anuradha 2008, Khandker et al. 2020, Naru & Jana 2017). Livelihood: Livelihood comprises people, their capability and their means of living including food, income and assets (Shah 1998, Dharmasena 2019).

Pelasur tank located in a rural area of Thiruvannamalai district, Tamil Nadu, India was selected for this study and the tank was rehabilitated with huge amounts funded by the European Economic Community. Since this study vastly concentrates on other livelihood options related to the tank water, it was necessary to select the village which possesses more tank-based livelihood options including agriculture. After selecting the tank, the command area was divided into three segments representing head, middle and tail reaches. Later with the help of village Adangal records, farming households were identified and listed, which constitute the population frame for the study. Also, other indirect tank water users and the landless group were identified to conduct a discussion for getting relevant information on multiple tank uses for livelihood improvement. As stated earlier, the aim of the current study is to survey the impact of before and after tank rehabilitation conditions on landholding and landless group. Households of both the gender (women and men farmers) that has possessed a minimum one acre of land under the Pelasur tank command area was taken into consideration. Respondents from the above-mentioned households were selected by a stratified method. The landless population is grouped with respect to their livelihood occupations and the entire group was taken into consideration while selecting the respondents for conducting focus group discussion (Welgama & Wanigasunder 2012).

Probability sampling can significantly enhance the descriptive sample. There are many types of probability samples that are likely to be encountered but this study was proposed to use a stratified sampling because it lends an extra component of accuracy to a simple random or systematic sample. The benefit of stratified sampling is that it incredibly improves the chance of proper representative of strata in the sample. At least two stratifying criteria can be utilized as a pair. The present study is stratified based on four strata. Before going in for stratifying the family households, the list of farming households in the study villages was collected from Adangal register maintained by the respective Village Administrative Officers (VAO). The Adangal is the source for the Government revenue and contains basic statistical information.

The impact of tank rehabilitation being the focus of the study, stratification with sampling unit i.e. households was felt necessary. Hence, while selecting a stratified sampling, the households were divided into different strata i.e. land holding, reach, farmers category and well-owning status. At the primary phase of stratification, the population was stratified by the model of landholding, in which two strata, landholding and landless gatherings were created At the primary phase of stratification, the populace was stratified. Landholding and landless households refer to households with land size greater than or equal to 50 cents and less than 50 cents correspondingly. At the second phase of stratification, the first stage of landholding farmers has been subdivided into head, middle and tail reach depending upon the location of

the land. At the third stage, the respective second stage has been subdivided into marginal, small and other category of farmers reliant on the extent of respondents landholding. The classification of farmers, according to the Tamil Nadu Government, fall under a broad category of marginal, small, semi-medium, medium and large farmers. The statistics of the Tamil Nadu Government (2006) show that there are 72% of marginal farmers followed by the small farmers, medium, semi-medium and large farmers constituting 17%, 7.7%, 2.8% and 0.5% respectively. Since the last three categories are small compared to the first two, the main focus of the study was concentrated on marginal and small farmers. However, the above three categories have been coalesced to form other farmers category. The same pattern of categorisation has been adopted by many irrigation management related projects. One such adaptation was followed in the Base Line Survey of Irrigation Commands, a Tamil Nadu Water Resources Consolidation Projects study undertaken by the Centre for Water Resources, Anna University, during the year 2000 and (Sophia & Anuradha 2005). A similar example of categorisation has been approved by many irrigation management related projects. One such modification was followed in the Base Line Survey of Irrigation Commands, a Tamil Nadu Water Resources Consolidation Projects study incorporated by the Centre for Water Resources, Anna University, during the year 2000 and (Sophia & Anuradha 2005).

According to the methodology, the marginal farmers are the individuals who hold less than 1 ha of land in the tank command area, small farmers hold 1 and 2 ha and the other farmers' category more than 2 ha of the irrigated plot. The sample was then selected from each subdivided classification utilizing probability proportional to size. Sample from head reach, middle reach and tail reach comes to were haphazardly chosen. The reality of random sampling is significant in light of the fact that it reflects assurance to attain findings that can be produced past the limits of the individuals who take an interest in the research. It allows one to demonstrate the probability that the result derived from the sample is likely to be found in the population from which the sample was taken. This is only possible if a random sample has been selected.

Total numbers of marginal, small and other farmers were collected from the Adangal Records in the study village and slightly more than 20% of them in each category were selected as respondents. Both men and women pattadhars were taken as respondents. The latter one was very meagre in number. Category wise, details of the total number of farmers in the selected study village and the selected sample with percentage are provided in Table 1.

Table 1: Reach-wise distribution of sample farmers in the study village.

Sl. No.	Farmer's category	Pelasur Village		
		Total number of farmers	Sample selected	Percentage
1.	Marginal	50	14	28.00
2.	Small	74	22	29.70
3.	Others	287	66	22.30
	Total	411	102	24.81

Since the present study also seeks to identify the impact of irrigation tank rehabilitation for together direct users and indirect users, it was decided that obtaining direct data straightforwardly from the respondents would be the most reliable sources through which the key focus of the study could be analysed. Despite the fact that the examination basically depends upon essential sources it still seeks data for some supportive and supplemental information, which are ancillary in nature (Long & Grafton 2020). The secondary data were gathered from significant records such as land registration records (Adangal Registers), documentation from Government agencies, documents of different levels of Water Users Association and information and figures from Census documents. Village maps were collected from the Survey and Land Records department of the Government of Tamil Nadu.

Tools of Data Collection

So as to accomplish the proposed objectives, combinations of qualitative and quantitative techniques were utilized to assemble data. Impact of tank rehabilitation in some issues such as the number of seasons cultivated, changes in cropping patterns, sources of irrigation were addressed through a schedule. Though many questions were included in the interview schedule, other qualitative methods such as stakeholders' meetings and group discussions with certain categories of non-farm and off-farm involved villagers too added important information. The information drawn were analysed and presented in the respective sections.

The quantitative tool selected for the study was an interview method through which the required primary data were elicited from the respondents. Since the respondents constitute both literates and illiterates categories, the method adopted was found to be most appropriate. Interviews were held with 15 women and 178 men farmers in the study village. Interviews were conducted separately for the respondents and their responses were immediately noted in the schedule. There were some difficulties in the initial stages in getting information about the landholding size and income of the respondents but later when the purpose of the study was

explained in detail the respondents felt free to give answers to all the statements incorporated in the schedule.

MODULES OF QUESTIONNAIRE

The interview began with questions identified with some segment attributes of the families and continued with family background. A detailed list of contents in seven parts of the schedule is given below:

- Bio-data of the respondents: Name, age, education, community, family size, occupation, livestock details and family background.
- Cropping pattern, land inheritance, the extent of land possessed (individual and family), size of operational holding and season wise crop raised in wet, dry and garden land.
- Season wise source of irrigation and reasons for the change in source during the post rehabilitation period, alternative source during the scarcity period.
- Land use and season wise type of crop cultivated, yield in bags or tons, input and output cost per ha of land.
- Groundwater usage: Number of wells, type of wells, energy used, horsepower, depth of well, depth of water table, frequency and duration of pumping groundwater, local water market, well expenses and conjunctive use.
- Type and source of irrigation in different stages of crop growth, number of well and tank irrigation and sufficiency of irrigated water in the field.
- Total expenses for the land possessed by the respondents including, seed, nursery, transplantation, fertilisers, weeding, harvest and transportation cost.

Audio and Video Recording

Interviews were conducted with landholding farmers, landless poor, women and other vulnerable groups. The entire proceedings were recorded in a tape recorder and a hand camera. This helped to retrieve the material and analyse as and when new thoughts generate about the type of analysis. This is an added improvement due to the availability of electronic equipment.

Data Analysis

The information subsequently acquired were the first master tabulated in Microsoft Excel sheet using suitable coding and the variables for incorporation in the analysis were chosen and transferred into raw data files. Further, it was organized into SPSS-23.0 files for analysis which in certainty proved to be a necessary part of the research. Appropriate data analysis was carried and for simplicity and practical usefulness, only limited but more useful tools such as simple frequency and percentage table, and cross tables were used. The key objective of frequency distribution and percentage table was to summarise the comprehensive information. Cross tabulation is a procedure of Bivariate analysis, which is one of the modest and most commonly used ways for investigating the connection between at least two factors. Since this study concentrates on tank users both before and after its rehabilitation period, comparative analysis like Paired-samples t-test (which is a compare means analysis) in SPSS was taken into consideration.

Paired Sample *t*-test

The paired samples t-test compares the means of two variables. It computes the differences between two variables for each case and tests to see if the average difference is significantly different from zero (Pham & Jimenez 2012, Constance & Cribbie 2012). The observed data were from the same subject or a matched subject and were drawn from a population with a normal distribution. Subjects are often tested in a before-after situation (across time, with some intervention occurring such as tank rehabilitation). The paired t-test is actually a test where the differences between the two observations are 0. So, if D represents the difference between observations, the hypotheses are:

H_o: $D = 0$ (the difference between the two observations is 0)

H_a: $D \neq 0$ (the difference is not 0)

The test statistic is t with n-1 degrees of freedom. If the p-value associated with t is low (< 0.05), there is evidence to reject the null hypothesis. Thus, one would have evidence that there is a difference in means across the paired observations.

Hence, this is an ideal test to study the impact of rehabilitation in two different tanks during pre and post-rehabilitation periods.

RESULTS AND DISCUSSION

Season wise Area Cultivated in Wetland before and after Rehabilitation by Pelasur Respondents

Table 2 and Fig.1 clearly explicate the increase in total wetland cultivated area in the post rehabilitation period. There is a reduction in first and second season paddy cultivation, which is compensated by a drastic increase in annual crop cultivation. Availability of assured water supply throughout the year for irrigation either through surface or subsurface sources is the major reason for the change in cropping pattern. This indicates the positive impact of tank

rehabilitation in Pelasur village. Also, there is an increase of 9 ha area of cultivation in the third season paddy crop during the post-rehabilitation period. Paddy is overpriced in the third season while marketing, labour cost is low due to surplus-labour availability and easy availability of fertiliser may be the reasons for increased third season paddy cultivation. Area cultivated during the third season is very low when compared to the total cultivated area and hence the availability of labour and fertiliser is high. Since the climate is hot, pesticide and rat problems are low in the third season when compared to the first and second seasons.

The output presented in Table 3 confirms the outcome that a significant positive relationship exists between the total area cultivated in wetland and the tank rehabilitation ($r = 0.866$, $p < 0.05$). Therefore, the increased total area cultivated in the wetland during the first season is highly related to tank rehabilitation.

Observations in Table 4 related to the total area cultivated in the tank command area before and after the tank rehabilitation were randomly assigned to confirm that responses are due to the tank rehabilitation and not due to other factors. Paired t-test technique was used to test the null hypothesis and contrast the outcomes to demonstrate that there is a distinction between the total area cultivated before and after the tank rehabilitation.

The analysis output reveals that there is no difference between the total area cultivated by the respondents in pre and post-rehabilitation periods. Tank rehabilitation does not significantly improve the area cultivated in the wetland during the first season, $t(101) = 0.520$, $p > 0.05$. Hence, it is

Table 2: Season wise area cultivated in wetland before and after rehabilitation by Pelasur respondents.

Sl. no.	Description	Area cultivated before rehabilitation (ha)	Area cultivated after rehabilitation (ha)	Difference (ha)
1	Total cultivated area	138.28	162.92	24.65
2	First season	46.14	39.95	-6.19
3	Second season	43.79	28.49	-15.30
4	Third season	4.13	12.57	8.45
5	Annual crop	44.21	81.91	37.70

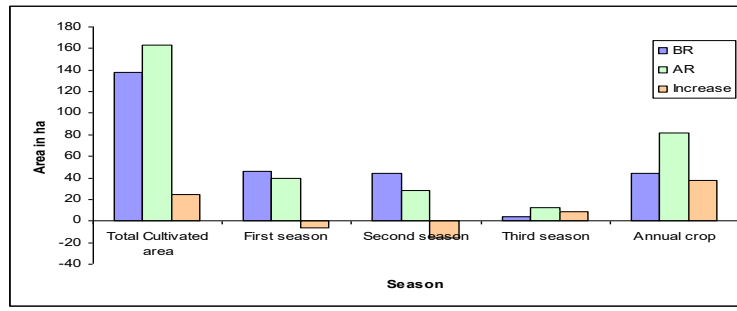

Fig.1: Season wise area cultivated in wetland before and after rehabilitation by Pelasur respondents.

Table 3: Paired samples correlations for first season wetland before and after rehabilitation by Pelasur respondents.

Description		Number of total respondents	Correlation	Sig.
Pair 1	Wetland cultivable area first season before rehabilitation and Wetland cultivable area first season after rehabilitation	102	0.866	0.000

Table 4: Paired samples t-test for first season wetland before and after rehabilitation by Pelasur respondents.

Description		Paired Differences					T	df	Sig. (2-tailed)
		Mean	Std. deviation	Std. error mean	95% confidence interval of the difference				
					Lower	Upper			
Pair 1	Wetland cultivable area first season before rehabilitation and wetland cultivable area first season after rehabilitation	-0.060	1.179	0.116	-0.292	0.171	-0.520	101	0.604

concluded that the area cultivated in the post-rehabilitation period is highly correlated with the tank rehabilitation but does not show significant change during the first season of paddy cultivation.

The output presented in Table 5 confirms the result that a significant positive relationship exists between total area cultivated with annual crop (sugarcane) in wetland and tank rehabilitation ($r = 0.651$, $p < 0.05$). Therefore, an increased total area cultivated with annual crop (sugarcane) in wetland is associated with tank rehabilitation.

To test the null hypothesis of no difference between total area cultivated during pre and post-rehabilitation periods, paired t-test was used to compare the results. As can be seen from the output presented in Table 6, a significant difference exists between the total area cultivated with annual crop (sugarcane) in wetland by the respondents in pre and post-rehabilitation periods. Tank rehabilitation significantly improves the total area cultivated with annual crop (sugarcane) in wetland, $t(101) = 5.379$, $p < 0.05$

Season wise Crops Cultivated in Wetland before and after Rehabilitation by Pelasur Respondents

Table 7 portraits the percentage of respondents cultivating crops in wetland before and after the tank rehabilitation. It is clear that before rehabilitation 52% of the total respondents cultivated paddy as their first season crop (i.e. from June to September), which was reduced to 42% now. Even though the data show that wetland respondents are not cultivating groundnut in the command area, it is not the case in the overall scenario. Cultivating groundnut in wetlands by the well-owing farmers in the third season is in practice and the reason enlightened by them is that it provides good green manure for succeeding paddy crop which increases the yield/ha. Being a legume crop, groundnut can fix the atmospheric nitrogen and thereby improve soil fertility.

Cultivating groundnut with well water is practised both in wetland as well as in garden land. Cultivating groundnut as the first crop in wetland is not in practice both before and after the rehabilitation in Pelasur. Since summer season (third season) is the suitable period for groundnut cultivation, whereas 1% of the total respondents before rehabilitation and 2% after rehabilitation cultivate groundnut as a second crop. Those two respondents have oil extraction machine and doing oil selling business along with agriculture. Around 41.2% of the total respondents were cultivated paddy as the second crop and this is reduced to 35.3% during the post-rehabilitation period. The increased water table in command area wells helps in increased third season cultivation from 4.9% to 13.7% in the post-rehabilitation period. Sugarcane crop scenario shows an incredibly positive impact of tank

Table 5: Paired sample correlations for annual crop cultivated in wetland before and after rehabilitation by Pelasur respondents.

Description		N	Correlation	Sig.
Pair 1	Wetland cultivable area annual before rehabilitation and wetland cultivable area annual after rehabilitation	102	0.651	0.000

Table 6: Paired sample t-test for annual crop cultivated in wetland before and after rehabilitation by Pelasur respondents

Description		Paired Differences					T	df	Sig. (2-tailed)
		Mean	Std. deviation	Std. error mean	95% confidence interval of the difference				
					Lower	Upper			
Pair 1	Wetland cultivable area annual before rehabilitation and wetland cultivable area annual after rehabilitation	-0.912	1.714	0.169	-1.249	-0.576	-5.379	101	0.000

Table 7: Season wise crops cultivated in wetland before and after rehabilitation by Pelasur respondents

Sl. no	Season	Percentage of respondents							
		Before rehabilitation				After rehabilitation			
		Paddy	Groundnut	Sugarcane	None	Paddy	Groundnut	Sugarcane	None
		%	%	%	%	%	%	%	%
1	First season	52	0	0	47.1	42	0	0	55.9
2	Second season	41	1	0	57.8	35	2	0	62.7
3	Third season	4.9	0	0	95.1	14	1	0	85.3
4	Annual	0	0	30.4	69.6	0	0	54.9	45.1

rehabilitation through the increased cultivated area from 30% to 55% after the rehabilitation.

Hence, the overall circumstances show that even though the paddy cultivation area was reduced during the post-rehabilitation period, there is a significant increase in the sugarcane cultivation area in Pelasur. Availability of a farm road facility till the tail reach for loading and unloading sugarcane is the key reason reported by the farmers. Earlier it was very difficult for the tail reach farmers to transfer the produce from the field. Transporting sugarcane bundles from the field to the main road leading to more number of labours and labour charge. Now with the availability of a farm road, farmers can bring bundles easily through small carts to the place where trucks are ready to take sugarcane to the sugar mill. Also, farmers who are engaged in some other occupation had gone for sugarcane cultivation, since it is not necessary to take much care on sugarcane crop during the growth stage as in the case of paddy crop. Consequently, farmers like to develop crops that require less close to individual responsiveness. Paddy being a short duration seasonal crop requires less attention in spite of its varieties (Reddy et al. 2008). Guaranteed water supply during the time is additionally a fundamental purpose behind the cropping change.

Respondents quoted that sugarcane is a cash crop and has a constant market rate. i.e. rate/ton does not vary with respect to market surplus or scarcity. Moreover, the rate/ton keeps on increasing with time and never decreases. For paddy, there are ups and downs in rate/bag even within the season itself and with respect to market surplus and scarcity. Another reason cited by respondents is that problem caused by rats is less in sugarcane when compared to paddy which leads to a reduction in yield/ha. Tail reach soil is more suitable for cultivating sugarcane than paddy due to its slight salinity nature. Sugarcane can withstand mild flood and drought to some extent when compared to paddy. This tempts farmers in Pelasur village to cultivate sugarcane as their major crop. Very few farmers are cultivating sugarcane three times (i.e. 3 years) continuously and paddy for the fourth year. The peculiar reason attributed is the changing cropping pattern at regular intervals of time, which might help to make up the soil nutritious and increase the yield of both the crops. Further, changes in the cropping pattern from paddy to sugarcane in the neighbouring field induce farmers to adopt the same after they are aware of the income incurred by sugarcane cultivators. In future, sugarcane cultivation is relied upon to build more with innovative changes, for example, the spread of high yielding crop varieties, harvesting techniques, utilization of pesticides, insecticides and composts, mechanization of farm work, lack of capable workers for paddy cultivation and so forth. Hence, farmers feel that cultivating sugarcane is more profitable than paddy. Help from sugar mill (by providing crop insurance, loan for initial investment, lending fertiliser at right time at desirable cost, arranging mini contract labours for sugarcane cutting etc.,) tempts farmers in Pelasur to change cropping pattern from paddy to sugarcane.

CONCLUSION

The main objective of tank rehabilitation is to alleviate poverty and raise the standard of living of the small and marginal farmers in the rural areas who have access to a large irrigation system. There is an increase of 9 ha area of cultivation in the third season paddy crop during the post-rehabilitation period. Around 41.2% of the total respondents have cultivated paddy as a second crop and this is reduced to 35.3% during the post-rehabilitation period. But sugarcane crop scenario shows an incredibly positive impact of tank rehabilitation through the increased cultivated area from 30% to 55% after the rehabilitation. Many farmers shifted from paddy cultivation to sugarcane since it is a cash crop. Paired sample t-test result shows that there is an increase in the total area cultivated is highly associated with tank rehabilitation. Hence equal importance should be given to both tank infrastructure and command area development for enhancing agricultural productivity. Hence, a tank as a common property resource can be protected and kept sustainable for long periods.

REFERENCES

Adams, W. M. 1989. Definition and development in African indigenous irrigation. Journal of Azania: Archaeological Research in Africa, 24(1): 21-27.

Agarwal, A. and Narain, S. 2003. Dying Wisdom. Centre for Science and Environment, New Delhi.

Anuradha, B. 2008. Impact of rehabilitation of tanks in peri-urban areas. 20th International Congress in Irrigation and Drainage, Lahore, 112.

Anuradha, B. and Ambujam, N.K. 2011. Impact of irrigation tank rehabilitation on garden land agriculture - a case study in rural village of Tamilnadu. International Journal of Agricultural and Statistical Sciences, 7(2): 493-498.

Aubriot, O. and Prabhakar, P. I. 2011. Water institutions and the 'revival of tanks' in South India: What is at stake locally? Water Alternatives, 4(3): 325-346.

Balamurugan, P. 2013. Rural tanks and their modernisation for sustainable rural development. International Conference Proceedings-I, Annamalai University, Annamalainagar.

Chattopadhyaya, S. 2003. Scarcity admist plenty: A study on tanks of Kerala state. In: Tanks of South India, (Ed). Centre for Science and Environment, NewDelhi.

Chiranjeevalu, P. 1988. Tank Irrigation and Agricultural Development. Kanishka Publishing House, NewDelhi.

Constance, A. Mara and Robert A. Cribbie 2012. Paired-samples tests of equivalence. Communications in Statistics. Simulation and Computation, 41(10): 1928-1943.

Dharmasena P.B. 2019. Agricultural research for sustainable food systems in Sri Lanka: volume 1: a historical perspective. Springer Nature Singapore Pte Ltd Cascaded Tank-Village System: Present Status and Prospects.

Easter, W. 1997. Tank Development: The North Eastern Thailand Experience. Anna University, Chennai.

Fischer, A., Tadesse, D., Weldesemaet, Y. T. and Ashenafi, Z. T. 2014. On the interplay of actors in the co-management of natural resources-A dynamic perspective. World Development, 64: 158-168.

Govindaiah, T. 1992. Tank rehabilitation and integrated rural development. Institute of Research in Social Sciences, Bangalore.

Jagger, P., Sellers, S., Kittner, Das, I. and Bush, G. K. 2018. Looking for medium-term conservation and development impacts of community management agreements in Uganda's Rwenzori Mountains National Park. Ecological Economics, 52: 199-206.

Jana, S. K., Palanisami, K. and Das, A. 2012. Prospect of sustainable tank irrigation option in the dry zones of West Bengal. Indian Journal of Agricultural Economics, 67(2): 225-37.

Khandker, V., Gandhi, V.P. and Johnson, N. 2020. Gender perspective in water management: the involvement of women in participatory water institutions of eastern India. Water, 12(196): 1-20.

Kiran Kumara, T. M., Shiv Kumar, Dharam Raj Singh and Kingsly Immanuelraj 2018. Participation in community based tank irrigation system in a rainfed region of India. Indian Journal of Agricultural Sciences, 88(4): 596-600.

Long C. R. and Grafton, Q. 2020. Water pricing and the value-add of irrigation water in Vietnam: Insights from a crop choice model fitted to a National household survey. Agricultural Water Management, 228: 1-8.

Meinzen-Dick, R. 2007. Beyond panaceas in water institutions. Proceedings of the National Academy of Sciences, 104(39): 15200-15205.

Narayanamoorthy, M. A. 2007. Tank irrigation in India: A time series analysis. Water Policy, 9 (2): 193-216.

Naru, S. and Jana, S.K. 2017. A Study on Tank Irrigation Productivity in Saline Zone of South 24 Parganas. Vidyasagar University, Midnapore Sebak Kumar Jana University.

Palanisamy, K. and Easter, W. 2010. Small scale surface tank irrigation in Asia. Water Resources Research, 33(2).

Persha, L., Agrawal, A. and Chhatre, A. 2011. Social and ecological synergy: Local rulemaking, forest livelihoods, and biodiversity conservation. Science, 331: 1606-1608.

Reddy, V.R., Reddy, M.G., Reddy, Y.V. and Soussan, J. 2008. Sustaining rural livelihoods in fragile environments. Resource endowments and policy interventions-A study in the context of participatory watershed development in Andhra Pradesh. Indian Journal of Agricultural Economics, 63(2): 69-187.

Sakthivadivel, R. 2005. Two decades of tank rehabilitation in India: Investment institutional and policy issues. IWMI, Tata water policy research program, and annual partners meet, Anand.

Sengupta, N. 1985. Irrigation-traditional vs. modern. Economic and Political Weekly, 20 (45): 1919-1938.

Shah, M. 2009. Participatory watershed development: An institutional framework. (In) Making Water everybody's Business. Agarwal A, Khurana I and Narain S (Eds). Centre for Science and Environment, New Delhi.

Shah, Manisha and Sakthivadivel, Ramaswamy 2018. Will Kudimaramathu make communities "think tanks" again? International Journal of Engineering and Technology, 7 (4): 6878-6883.

Shah, T. 1998. Water against poverty: livelihood-oriented water resource management. Water Nepal, 6(1): 117-143.

Shah, T. and Raju, V. 1988. Groundwater markets and small farmer's development. Economic and Political Weekly, 26: 23-28.

Singh, A.K. 2004. Impact of watershed development in traditional tank systems: a caste study. Journal of Rural Development, 33(1).

Sivasubramaniam, K. 2006. Sustainable development of small water bodies in Tamilnadu. Economic and Political, 2: 2854-2863.

Sophia, J.D. and Anuradha, B. 2005. Two decades of tank rehabilitation in India: Investment institutional and policy issues. IWMI, Tata Water Policy Research Program and Annual Partners Meet, Anand.

Sowbi, R.B. and Sabarish, A.K.V. 2017. A review- tank and its role in recharging groundwater. International Journal of Civil Engineering and Technology (IJCIET), 8(10): 207-212,

Thang, V. Pham and Connie, R. Jimenez 2012. An accurate paired sample test for count data. ECCB, 28: 596-602.

Vaidyanathan, A. 2003. Tanks of South India. Centre for Science and Environment, NewDelhi.

Vaidyanathan, A. 2006. India's Water Resources: Contemporary Issues of Irrigation. Oxford University Press, New Delhi.

Welgama, N.K.K. and Wanigasunder, W.A.D.P. 2012. The impact of rehabilitation approaches in the sustainability of the management of small tanks in Sri Lanka. International Journal of Economics and Management Engineering, 6(12): 3745-3753.

Nature Environment and Pollution Technology
An International Quarterly Scientific Journal

p-ISSN: 0972-6268
(Print copies up to 2016)
e-ISSN: 2395-3454

Vol. 20 | No. 2 | pp. 517-531 | 2021

Original Research Paper

https://doi.org/10.46488/NEPT.2021.v20i02.008

Open Access Journal

Causes and Consequences of Reforming in Electricity Production and Consumption Pattern on Promoting Sustainable Development in Iran: An Economic Analysis

Ali Mohammadipour
Economics Consultant, Department of Energy, Iranian Association for Energy Economies, Tehran, Iran
†Corresponding author: Ali Mohammadipour; dr.ali.mohammadipour@gmail.com

Nat. Env. & Poll. Tech.
Website: www.neptjournal.com

Received: 02-04-2020
Revised: 19-06-2020
Accepted: 25-06-2020

Key Words:
Power Industry
CO_2 emissions
Sustainability
Sustainable development

ABSTRACT

In line with the 2015 Paris Agreement, the present study examines the efficiency of Iran's electricity industry compared to world standards. In 2018, Iran is ranked second in the world in terms of direct subsidies to the electricity industry, while subsidies for fossil fuels as the main feedstock for power plants are also higher. The results of the study indicate that despite the privatization of the electric industry since 2005, centralized economic management and the provision of extensive direct and indirect subsidies have led to the expansion of inefficiencies in the production and consumption of electricity. Lack of cost-based pricing is a major factor in the production of inefficient units and the determination of electricity prices at very low levels (as a result of subsidies) is the main reason for the inefficient use of electricity in Iran. The undeniable role of fossil fuels in energy production has stabilized Iran's second-largest power plant sector in CO_2 emissions in the Middle East, and as a consequence of no noticeable changes in the energy production process, the carbon intensity index and carbon intensity for electricity consumption, have fluctuated slightly. However, the energy intensity and energy intensity for electricity consumption, unlike the developed countries, have shown an upward trend, indicating a decline in energy and electrical energy efficiency in the Iranian economy. The index of fundamental reforms in electricity production, exactly the reverse of the successes in Iceland, Switzerland, Norway, Sweden and Luxembourg, is less than 8%, which is against sustainable development goals. It is crucial to take advantage of countries' successful experiences in electricity price reform and to address the four key components proposed.

INTRODUCTION

Energy, and especially electricity, is one of the most important inputs of production which, as a fundamental input, plays an important role in the economic growth and development of any country. The lack of proper energy utilization and even weak access to electricity is the main cause of economic and social backwardness in different societies. As a result of increasing efficiency in energy production and consumption, especially electricity, living standards and welfare of communities will increase and economic growth and development will be achieved. Economic growth, by greater use of all production factors and electricity, will increase the production of final goods. Both the increase in energy consumption and the production process of intermediate and final goods require environmental degradation and environmental pollution. According to Environment Kuznets Curve Hypothesis, there is an inverse U relationship between economic growth and environmental pollution, and economic growth will be valuable if it continues to reduce environmental pollution (Sajadifar et al. 2016). With the industrial development of societies, the role of the electricity industry in the economic development programs of countries has increased. The dramatic growth in demand for this strategic input has led researchers to look for ways to increase efficiency in electricity generation and to focus more on factors affecting production costs and electricity prices (Pourebadollahan et al. 2019) Price changes in energy carriers and their impact on electricity prices are important concerns for the electricity market players and observers. In Iran, electricity prices are set according to the government's tariff, and fuel prices for power plants are also subsidized. Therefore, the supply and demand side of the electricity market is kept away from the effects of fuel price fluctuations and all the risks of price changes are transferred to the government (Moshiri et al. 2018). According to International Energy Agency (2019b) reports in 2018, Iran has the largest amount of subsidies to the energy sector in the world, and in terms of electricity subsidies (after China), it is the second largest in the world. In addition to widespread subsidies, the strong dependence of power plants on fossil fuels has intensified CO_2 emissions.

The present study, considering environmental concerns, examines the production process and electricity consumption pattern and seeks to provide solutions for implementing sustainable development in the Iranian electric industries.

ELECTRICAL INDUSTRIES IN IRAN

Iran, as the first country in the Middle East, began restructuring studies in the electricity industry, and by making the power plants profitable, the private sector has a greater desire to enter the electricity market and speed up the privatization process. In 2014, the fourth Iranian stock exchange, Electricity-Based Energy Stock Exchange, was launched (Kianvand & Farzinvash 2015).

Private sector activity remained modest at less than 14% by 2012, and in 2013 there was a significant jump in the nominal and practical capacity of the private sector. According to the plan, by 2022, 15747 MW (MegaWatts) of power will be built by the non-governmental sector, of which 12,468 MW will be added to thermal power plants and the rest to renewable (mostly solar) power plants. Currently, 44.9 percent of the total nominal capacity of the country's power plants belongs to the Ministry of Energy, 46.3 percent to the private sector, 7.5 percent to large industries, and 1.3 percent to the Iranian Atomic Energy Organization. According to Fig. 1, in 2017 the ratio of practical to nominal capacity of the country's power plants is 86.6% and the same ratio for the private sector is 83.1%.

Iran has electrical connections with countries with a common land border. The regional electricity cooperation plan could cause Iran to transfer electricity to non-neighbouring countries and ultimately a precondition for connecting Iran's electricity to the European electricity grid. One of the major goals of the Energy Ministry is to improve the country's position in the role of Energy Bridge and become the electricity hub in the region. Very small amounts of electricity trade in Iran can be seen in Fig. 2 and exports have increased more than imports since 2007.

RESEARCH BACKGROUND

According to Bose (2010) and Stern (2014), environmental concerns and the increasing depletion of fossil fuel resources have led to the efficient use of heat and power cogeneration systems. According to the U.S. Environmental Protection Agency (2014) report, the emissions of environmental pollutants in the most widely used technologies in heat and power cogeneration systems for solar thermal renewables, non-renewable fuel cells, internal combustion engines and microturbines are 0, 0.02, 0.79 and 0.15 Kg of CO_2 produced per kWh, respectively. According to Foley et al. (2014), as the price of Natural Gas increases, the wholesale price of electricity will also increase. Wang & Wei's (2016) study supports Porter's hypothesis in China and, according to this hypothesis, stricter environmental regulations increase

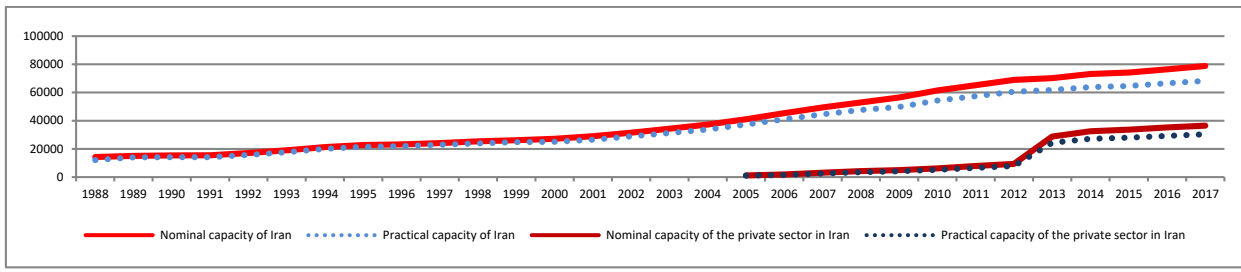

Reference: Ministry of Power. 2020. An Overview of Energy Statistics in Iran (30 year energy statistics).

Fig. 1: Nominal and practical capacity of the power industry in Iran (with private sector capacity) - Data unit: Megawatt

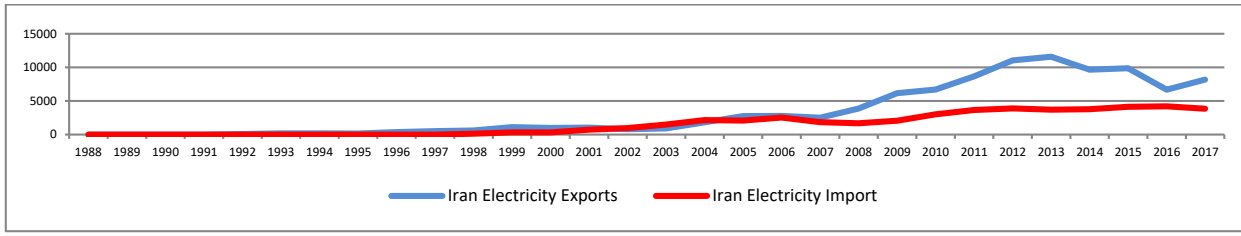

Reference: Ministry of Power. 2020. An Overview of Energy Statistics in Iran (30 year energy statistics).

Fig. 2: Exports and imports of electricity in Iran - Data unit: Million kWh.

efficiency and improve innovation and enhance commercial competitiveness. According to Shih et al. (2016) in Taiwan, with the decline of land capacity and population growth, the environment is becoming increasingly important and more action must be taken to replace renewable energy.

According to Razmi et al. (2010), due to the many shortcomings in creating a competitive environment in the Iranian electricity market, the reduction of concentration and the move to the competitive market should be considered by the planners. Razini et al. (2011) outline three scenarios for the future of Iran's electricity industry, stating that by 2030, fossil-fuel resources can be reduced to 67% by renewable energy planning. According to Sajadifar et al. (2016), operational plans should be implemented in order to conserve available resources and reduce environmental degradation due to adverse efficiency changes for Iran and neighbouring countries during 2007-2012. According to Majdzadeh Tabatabaei et al. (2016), in Iran only electricity generation from renewable wind energy is activated and there is still no growth in solar and biogas production. According to Kachoi & Amidpour (2016), the intensity of CO_2 emission in the scenario of increasing the efficiency of the power generation sector is lower than the continuation scenario of the current trend and can be drastically reduced in the scenarios of renewables. According to Kiani et al. (2017), new energies, despite being unfinished and having no negative external effects, impose significantly higher costs to the government than non-renewable resources. According to Gholipour Khatir et al. (2018), the positive effect of subsidy removal on the technical efficiency of power plants in Iran cannot be verified; however, in private power plants, increasing the input-output ratio increases efficiency.

ANALYZING SUSTAINABLE DEVELOPMENT DIMENSIONS IN IRANIAN ELECTRIC INDUSTRIES

The concept of sustainability emerged in response to the increased understanding that contemporary development practices were leading to a crisis in a social and environmental sense. The term "sustainable development" thus became the buzzword for alternative development strategies that could be "envisioned as continuing far into the future" (Wheeler Stephen 2013). There are several definitions of sustainability, but some are more inclusive than others. The official definition adopted by the United Nations (UN) came from the Brundtland report which defined sustainable as "development that meets the needs of the present generation without compromising the ability of future generations to meet their own needs" (Tladi 2007). Environmental, economic and social aspects are three important dimensions of sustainable development (UN 2011). These dimensions are discussed below for sustainable development in the electricity industry in Iran.

Production Process Analysis in the Electric Industries in Iran

The increasing emissions of greenhouse gases into the atmosphere as a result of the overuse of fossil fuels have become one of the most undesirable effects of economic development and have recently become a global issue. In Iran, the power plant sector, with 30.2% share of the total CO_2 emissions, is the largest emitter of greenhouse gases (Kachoi & Amidpour 2016). According to IEA (2019a) reports, Iran was ranked 24th in the world in terms of CO_2 emissions in 1980, 14th in 2000, 9th in 2010 and 8th in 2016 and 2017, with the increasing volume of pollution, compared to Canada.

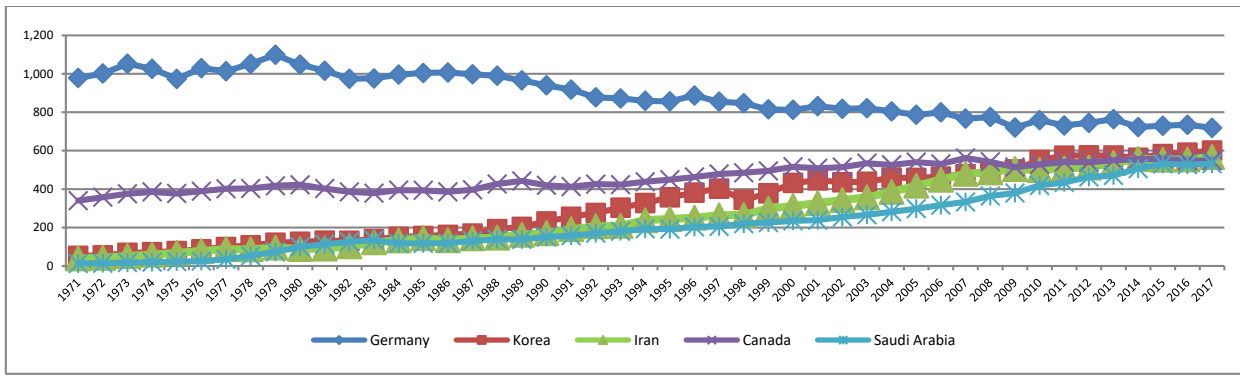

Reference: IEA. 2019a. CO_2 Emissions from Fuel Combustion Highlights.

Fig. 3: CO_2 emissions in selected countries (6th to 10th world CO_2 emissions rates) - Data unit: Million tons of CO_2.

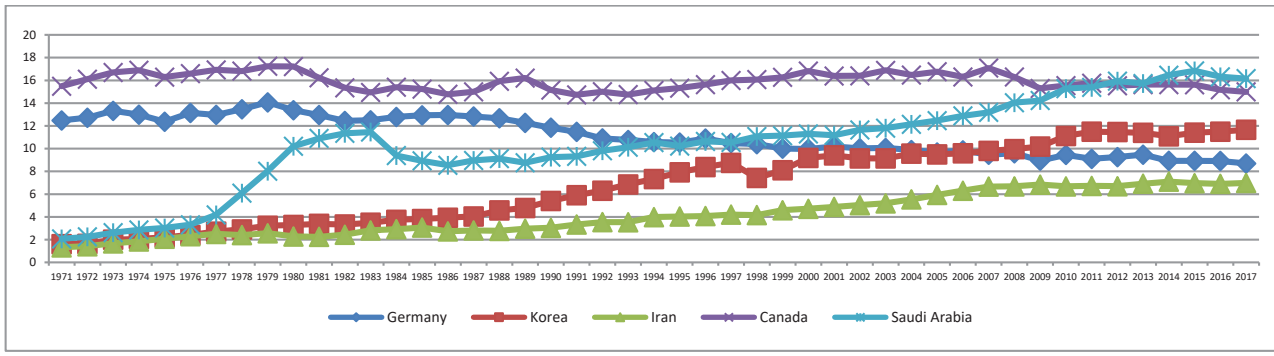

Reference: IEA. 2019a. CO_2 Emissions from Fuel Combustion Highlights.

Fig. 4: CO_2 emissions/population index in selected countries (6^{th} to 10^{th} world CO_2 emissions rates).

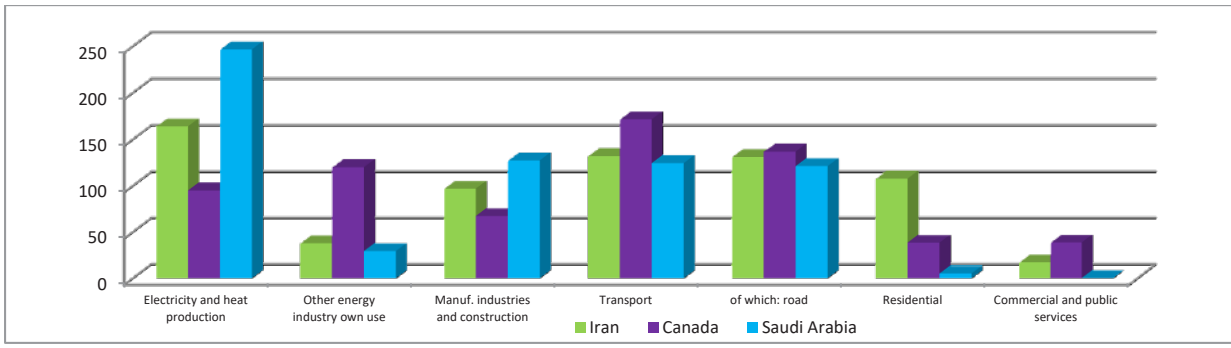

Reference: IEA. 2019a. CO_2 Emissions from Fuel Combustion Highlights.

Fig. 5: CO_2 emissions in different parts of Iran, Canada and Saudi Arabia in 2017 - Data unit: Million tons of CO_2.

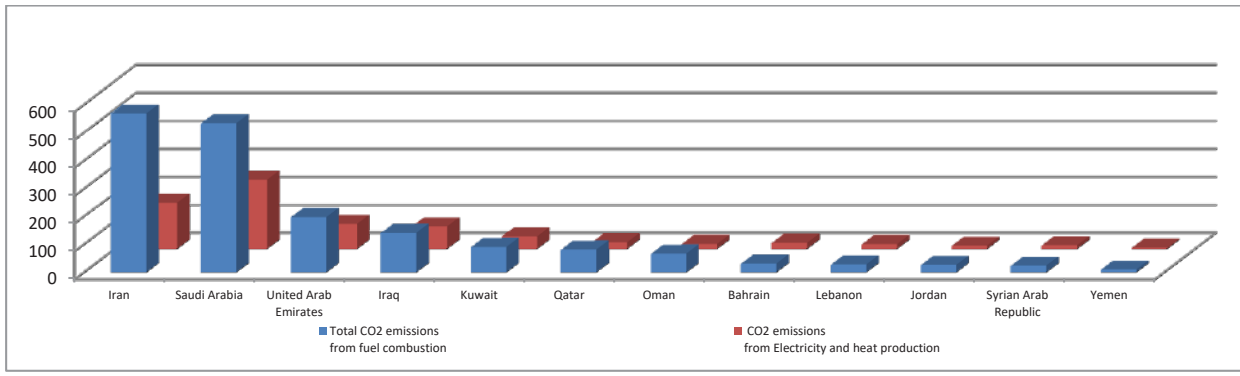

Reference: IEA. 2019a. CO_2 Emissions from Fuel Combustion Highlights.

Fig. 6: Comparison of CO_2 emissions in the Middle East (with emphasis on the electricity sector) in 2017 - Data unit: Million tons of CO_2.

Germany ranks second in the world in terms of CO_2 emissions after the USA in 1971 but has managed to reach 6^{th} in the world in the last 50 years using sustainable development policies. According to Fig. 3, a completely reverse trend is taking place in Iran and Saudi Arabia, and with the intensification of CO_2 emissions, Iran's rank in the world has continued to rise.

Iran is better off in terms of CO_2 emissions/population index than the countries mentioned, but worrying is the upward trend in Fig. 4. Of course, the uptrend of this index is

Table 1: The world's first 14 countries in terms of CO_2 emissions in the power plant sector in 2017 - Data unit: Million tons of CO_2.

S. No.	Country	Total CO_2 emissions from fuel combustion	CO_2 emissions from Electricity and heat production	Share of Electricity and heat production from CO_2 emissions
1	People's Rep. of China	9 257.9	4 591.3	49.59
2	United States	4 761.3	1 822.8	38.28
3	India	2 161.6	1 100.4	50.91
4	Russian Federation	1 536.9	773.5	50.33
5	Japan	1 132.4	554.9	49.00
6	Korea	600.0	322.1	53.68
7	Germany	718.8	303.9	42.28
8	Saudi Arabia	532.2	246.6	46.33
9	South Africa	421.7	225.5	53.47
10	Indonesia	496.4	195.9	39.46
11	Australia	384.6	191.5	49.79
12	Chinese Taipei	268.9	165.3	61.48
13	Iran	567.1	163.9	28.90
14	Mexico	446.0	153.7	34.47

Reference: IEA. 2019a. CO_2 Emissions from Fuel Combustion Highlights.

much more dangerous in Saudi Arabia, however, Germany, with its principled management, has been able to downtrend this index, too.

According to Fig. 5, Iran is better off than Saudi Arabia in terms of CO_2 emissions from electricity and heat production, but less favourable than Canada. Also, the electrical industries and transportation are in the first and second tier of CO_2 emissions in Iran. Therefore, considering the first category of electrical industries in CO_2 emission, this issue should be addressed which is the main topic of the present article.

According to Fig. 6, Iran emits the highest amount of CO_2 in the Middle East and has the highest CO_2 emissions from electricity and heat production in the region after Saudi Arabia.

According to Table 1, Iran is ranked 13th in the world despite lower relative GDP, with 164 million tons of CO_2 released in 2017. The electricity market is vertically linked to other commodities such as fuel (Natural Gas, Diesel Fuel, etc.) or CO_2 emission permits. Electricity on a large scale cannot be stored, so a balance between production and consumption on a continuous and moment-by-moment basis must be carefully ensured (Moshiri et al. 2018).

The government has tried to replace Natural Gas with other fossil fuels due to its ease of use, reduced maintenance costs and reduced environmental impact (relative to other fossil fuels). Therefore, in Fig. 7, Natural Gas consumption in power plants has changed dramatically in the last two

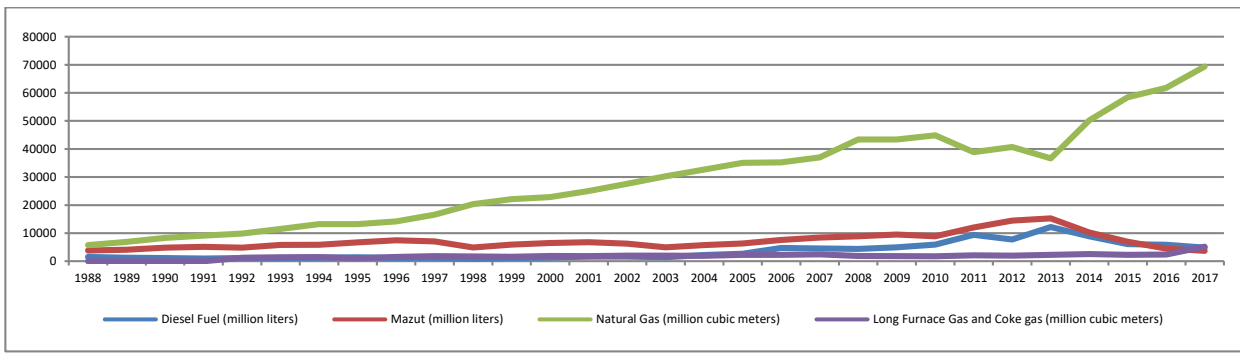

Reference: Ministry of Power. 2020. An Overview of Energy Statistics in Iran (30 year energy statistics).

Fig. 7: Fuel consumption trends in all Iranian power plants, by type of fuel.

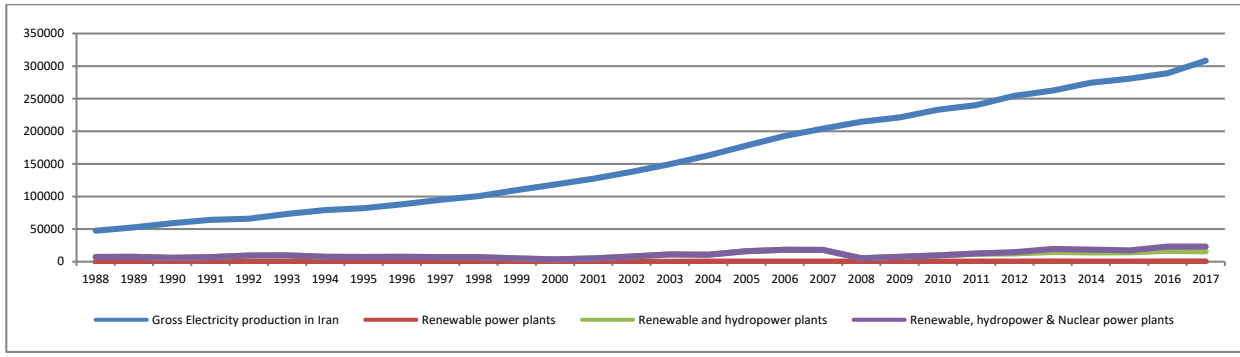

Reference: Ministry of Power. 2020. An Overview of Energy Statistics in Iran (30 year energy statistics).

Fig. 8: Trend of Gross Production of Electricity in Iran, By Specifying the Role of Non-Fossil Sectors - Data unit: Million kWh.

decades, reaching 69.4 billion cubic meters in 2017.

But first, in conditions of shortage of Natural Gas (in the cold months of the year), power plants will inevitably use alternative fuels, namely Diesel Fuel for gas and combined cycle power plants, and Mazut for steam power plants. Therefore, disconnecting the gas fuel, limiting the transportation and storage of liquid fuel, generates restrictions on the operation of the electricity grid. The use of fossil fuels instead of Natural Gas also contributes to the spread of malodour and severe environmental pollution.

Second, according to Fig. 6, even the extensive consumption of Natural Gas by Iranian power plants has not been favourable and has resulted in very high CO_2 emissions.

According to Fig. 8, the share of renewable energy from Gross Production of Electricity in the past three decades has never exceeded 0.15%, so its role in Iran's electricity production is negligible. The share of hydropower plants in electricity production has also fallen from 15% to 5% over the same period. The main reason for the decline in the relative share of hydropower plants is the slow pace of their increase compared to the development of the power plant sector in Iran. Electricity production at hydropower plants has increased from 7 (in 1988) to 15 (in 2017) TWh, and has doubled after thirty years. However, total electricity production in the same period has more than six times increased from 48 (in 1988) to 308 (in 2017) TWh. Finally, the Gross Production of Electricity in nuclear power plants was zero till 2011 and increased to 7.5 TWh in 2017. The index of Fundamental Reforms in Electricity Production (non-use of fossil fuels in the electricity production process), including total share of renewable power, hydropower and nuclear power plants in Iran's gross electricity production in 2017 was 7.56%.

According to Table 2, the index of Fundamental Reforms in Electricity Production in Iran is very poor compared to the 30 sample countries and needs to be revised regularly. Highly successful countries in the world, such as Iceland, Switzerland, Norway, Sweden and Luxembourg, have managed more than 90% of their electricity production from non-fossil fuel sources.

Real Government Support for Iran's Electric Industry

Based on the economic theories of the public sector and in accordance with Twomey et al. (2005) and Guler & Gross (2005), maximum social welfare and public satisfaction are formed in a situation in which the price of each commodity is equal to the final cost of its production and in the electricity industry based on the degree of market concentration and competitiveness, one can understand the nature of pricing and the degree of competition or monopoly in the market. Market competitiveness means reducing the power of market drivers to exploit fluctuations, and in this regard, especially in the electricity market, monopoly power to set disproportionate prices is a major concern of market regulators. According to Shahidepour et al. (2005), the set of intrinsic and non-intrinsic factors such as low elasticity of electricity demand, inability to economically store electricity, transmission line congestion, delayed return on investment in electricity, etc. allow this to happen. According to Tirole (2014), due to the lack of competitiveness of many markets, government intervention using a variety of methods, such as economic regulation, is necessary to bring markets closer to full competition. Despite the ongoing privatization process, the electric industry in Iran still does not have a competitive structure, and the government only protects consumers by paying massive subsidies.

According to Table 3, in 2018 China, Iran and Russia paid the highest subsidies to the electrical industry at 25, 17 and 14 real million dollars, respectively, which is 56, 24 and 38 percent of their total subsidies.

China generally ranked first in the world in subsidies to the electricity sector, only temporarily falling to third and

Table 2: The index of Fundamental Reforms in Electricity Production in Iran compared to 30 countries in 2017 - Data unit: TWh

Country	Electricity from Fossil Fuels	Hydropower	Nuclear power	Electricity from Biofuels and Waste	Geothermal	Solar, Wind and more	Gross production of electricity	Fossil Fuel Share in Electricity Production (%)	The index of Fundamental Reforms in Electricity Production (%)
Iceland	0.0	14.1	-	-	5.2	-	19.2	0.18	**99.82**
Switzerland	0.9	37.0	20.4	2.9	-	1.7	62.9	1.43	**98.57**
Norway	2.7	143.0	-	0.4	-	3.1	149.3	1.81	**98.19**
Sweden	2.9	64.6	63.0	12.0	-	17.7	160.2	1.81	**98.19**
Luxemburg	0.2	1.4	-	0.3	-	0.3	2.2	9.09	**90.91**
France	57.1	54.4	398.4	9.8	-	34.5	554.1	10.30	**89.70**
Slovakia	4.6	4.8	15.1	1.5	-	0.7	26.7	17.23	**82.77**
New Zealand	7.8	25.0	-	0.6	7.5	2.2	43.1	18.10	**81.90**
Finland	13.0	14.8	22.5	12.0	-	5.1	67.4	19.29	**80.71**
Canada	131.6	394.5	99.4	14.0	-	34.9	674.4	19.51	**80.49**
Austria	15.8	42.6	-	5.5	-	7.5	71.3	22.16	**77.84**
Denmark	8.2	-	-	6.6	-	15.6	30.4	26.97	**73.03**
Belgium	25.6	1.4	42.2	6.8	-	10.2	86.2	29.70	**70.30**
Spain	125.3	21.0	58.1	6.8	-	63.7	274.8	45.60	**54.40**
England	158.7	8.8	70.3	36.9	-	61.1	335.9	47.25	**52.75**
Germany	345.2	26.2	76.3	58.7	0.2	148.4	655.0	52.70	**47.30**
Czech Rep.	47.7	3.0	28.3	5.1	-	2.9	87.0	54.83	**45.17**
Chile	43.9	22.0	-	5.5	0.1	7.4	79.0	55.57	**44.43**
Portugal	34.8	7.5	-	3.6	0.2	13.2	59.3	58.68	**41.32**
USA	2660.1	325.1	838.9	78.5	18.1	336.5	4257.2	62.48	**37.52**
Italy	185.7	37.9	-	21.8	6.2	43.5	295.1	62.93	**37.07**
South Korea	390.8	7.0	148.4	8.1	-	11.2	565.5	69.11	**30.89**
Ireland	21.7	0.9	-	0.9	-	7.5	30.9	70.23	**29.77**
Turkey	209.2	58.2	-	2.1	6.1	21.6	297.3	70.37	**29.63**
Greece	44.4	4.1	-	0.8	-	9.5	58.8	75.51	**24.49**
Japan	838.3	88.3	32.9	34.2	2.5	89.0	1085.2	77.25	**22.75**
Netherlands	94.1	0.1	3.4	6.3	-	12.8	116.6	80.70	**19.30**
Mexico	260.2	30.1	10.9	1.6	5.9	10.7	319.5	81.44	**18.56**
Australia	219.4	16.5	-	3.6	-	20.6	260.2	84.32	**15.68**
Poland	145.5	3.0	-	6.7	-	15.1	170.3	85.44	**14.56**
Iran	285.0	15.4	7.5	0.1	-	0.4	308.3	92.44	**7.56**

Reference: Ministry of Power. 2020. An Overview of Energy Statistics in Iran (30 year energy statistics).

fifth in 2013-2015 and then returning to first. Iran and Russia are also ranked second and third in the world, though in the three years since China's decline from first place, Russia has taken first place. According to table 4, the six countries mentioned have always been at the top of the list of subsidies to the electrical industry in the world.

According to Fig. 9, Iran is always among the first countries in the world in terms of subsidies to the electricity industry.

According to Fig. 10, from 2010 to 2013 China and from 2013 onwards Mexico has devoted the largest share of its subsidies to the electricity industry. Despite Iran's second rank in terms of subsidies to the electricity industry, the relative share of electricity industry subsidies in Iran is far less than the six above-mentioned countries, which is illustrated in Figs. 11 and 12.

Due to the abundance of Natural Gas in Iran, and according to Fig. 11, the share of Natural Gas far exceeds the

Table 3: Top 10 Countries Paying Most Subsidies for Electricity in 2018.

N.	Country	2010	2011	2012	2013	2014	2015	2016	2017	2018
The top 10 countries in the world are the largest subsidies for the electricity sector - Unit: Real 2018 million USD										
1	China	31,617	33,600	24,943	14,453	11,151	7,062	28,196	22,624	**24,857**
2	Iran	12,978	12,985	17,917	15,425	15,006	12,791	4,963	14,419	**16,587**
3	Russia	17,228	15,835	16,748	16,737	17,064	16,561	21,641	9,442	**14,334**
4	Mexico	6,924	5,778	5,911	5,769	5,164	6,786	10,093	11,685	**13,502**
5	Saudi Arabia	15,204	14,353	14,827	14,138	13,609	13,536	10,701	10,975	**12,793**
6	Egypt	2,677	3,974	4,353	4,623	3,806	3,682	3,443	8,131	**12,137**
7	Indonesia	6,418	7,681	7,574	8,712	13,516	8,656	11,549	5,387	**7,330**
8	Venezuela	2,147	1,587	2,557	6,808	4,546	2,506	2,087	4,667	**6,512**
9	India	2,992	4,053	3,237	5,471	3,540	2,750	2,614	0	**4,351**
10	South Africa	0	0	0	0	0	2,684	6,014	5,324	**4,158**
The top 10 countries in the world are the largest subsidies for the electricity sector - Unit: Percentage										
1	China	72	73	66	49	43	35	64	56	56
2	Iran	18	23	19	18	19	25	16	30	24
3	Russia	54	48	51	51	51	48	65	44	38
4	Mexico	42	23	24	40	66	100	93	99	99
5	Saudi Arabia	26	21	20	20	20	24	27	25	29
6	Egypt	18	19	21	22	23	35	43	42	46
7	Indonesia	35	28	21	26	36	47	63	29	23
8	Venezuela	16	12	14	24	17	24	28	30	32
9	India	13	10	7	12	10	14	17	0	17
10	South Africa	-	-	-	-	-	100	100	100	100

Reference: IEA. 2019b. Fossil-Fuel Subsidies Report.

Table 4: Top 6 countries in the world in terms of subsidies paid to the electricity industry in the last decade.

Country	2010	2011	2012	2013	2014	2015	2016	2017	2018
China	1	1	1	3	5	5	1	1	**1**
Iran	4	4	2	2	2	3	7	2	**2**
Russia	2	2	3	1	1	1	2	5	**3**
Mexico	5	7	7	7	7	6	5	3	**4**
Saudi Arabia	3	3	4	4	3	2	4	4	**5**
Indonesia	6	5	5	5	4	4	3	7	**7**

Reference: IEA. 2019b. Fossil-Fuel Subsidies Report.

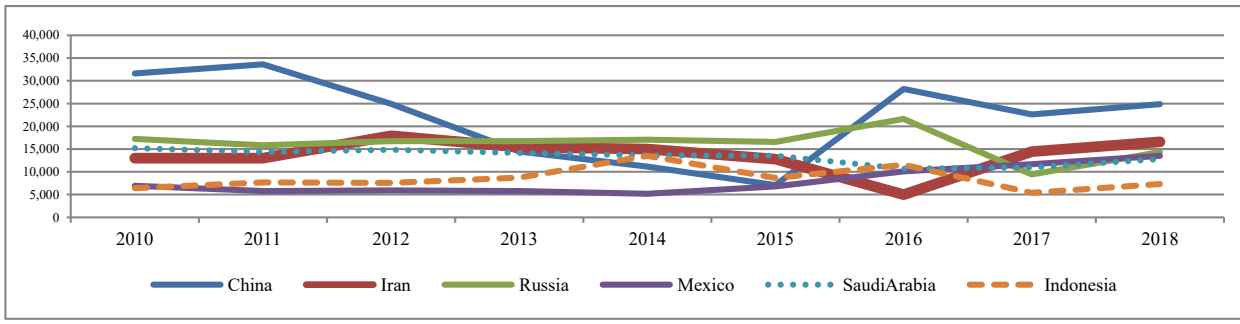

Reference: IEA. 2019b. Fossil-Fuel Subsidies Report.

Fig. 9: The trend of subsidies paid to the electric industry in the first 6 countries - Data unit: Real 2018 million USD.

global average of subsidies paid, and the relative share of the oil and electricity sectors is lower than the global average.

According to Fig. 12, the electricity industry is the lowest in terms of subsidies compared to the gas and oil sectors. Thus, much more support for the two gas (Natural Gas) and oil (Diesel Fuel, Mazut and other fuels) sectors, that supply most of the power plant's fuel, indirectly affects the electricity industry. Obviously, the sum of direct and indirect subsidies constitutes the actual amount of subsidies to the electricity industry, and under such widespread subsidies, the supply and demand mechanisms in this industry will undoubtedly be ineffective and economic theories will lose their effectiveness. A rapid increase in energy consumption, acceleration of environmental pollution, desire to smuggle energy from Iran to neighbouring countries, decreasing industrial and economic efficiency and imposing the burden of energy subsidies on the government budget were among the most significant adverse effects on the Iran economy resulting from the pricing of energy carriers at a much lower level than the world price. Therefore, the first step in reforming the pattern of energy consumption, and especially electricity, is to gradually reduce the amount of direct and indirect subsidies to the industry. In order to realize the supply and demand mechanisms in this industry, efficiency

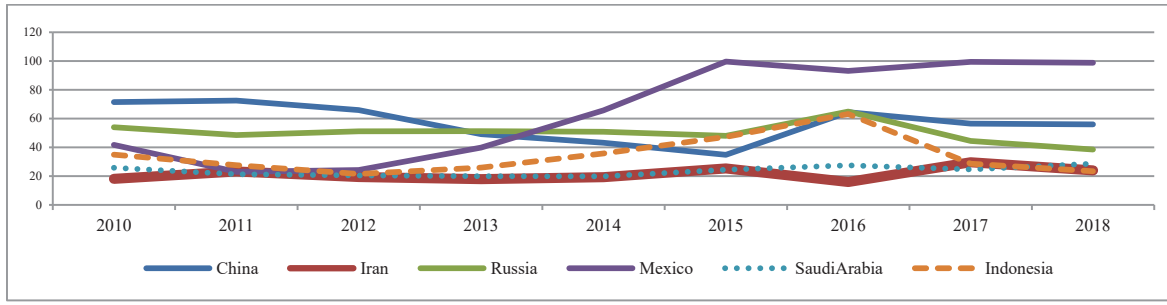

Reference: IEA. 2019b. Fossil-Fuel Subsidies Report.

Fig. 10: Share of subsidies paid to the electricity industry to total subsidies in the first 6 countries - Unit: Percentage.

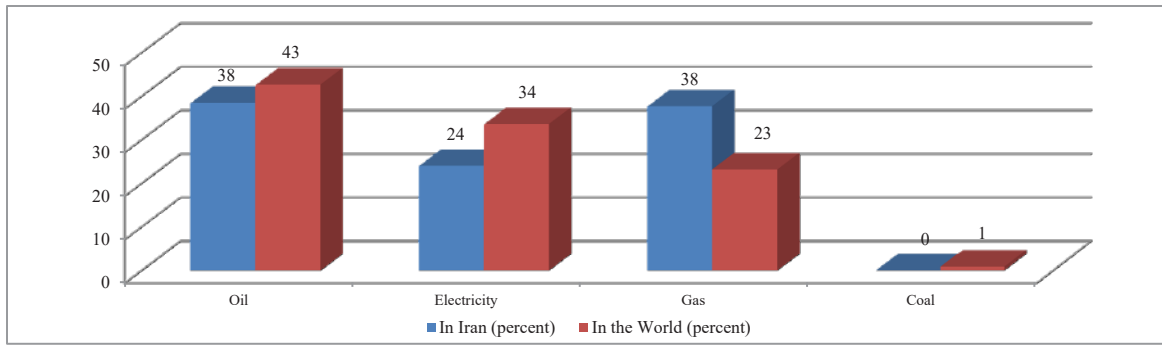

Reference: IEA. 2019b. Fossil-Fuel Subsidies Report.

Fig. 11: Relative share of subsidies paid to the four major sectors in Iran and the world in 2018 - Unit: Percentage.

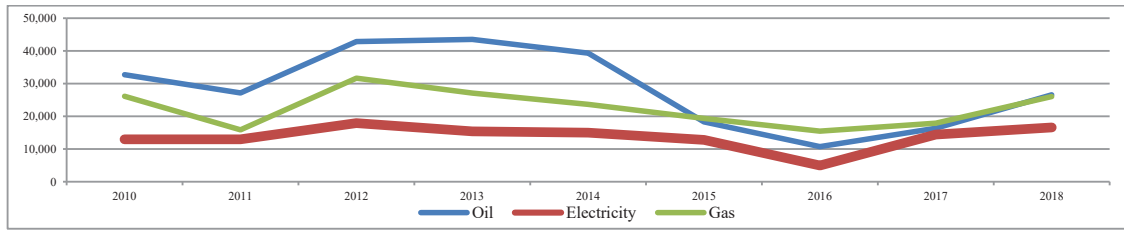

Reference: IEA. 2019b. Fossil-Fuel Subsidies Report.

Fig. 12: Amounts of subsidies paid to various sectors of Iran in 2018 - Data unit: Real 2018 million USD.

and maximum prosperity in the electricity industry will be established according to economic theories.

Social Indicators of Energy Abuse in Iran

The unrealistic prices of electricity produced and the fuels consumed in power plants have an adverse effect on the social indicators that are analysed below. The energy intensity index (or TPES per GDP) is calculated by dividing the total primary energy consumption index by GDP, which is the inverse of energy efficiency. The carbon intensity index is also calculated by dividing CO_2 emissions by total primary energy consumption.

According to Fig. 13, the carbon intensity index over the 50-year period has been relatively low fluctuating. Carbon intensity has changed from 95 (in 1971) to 88 (in 2017), Iran's GDP per population has been on a steady upward trend since 1981, and energy intensity has also increased substantially.

According to Fig. 14, the energy intensity index for Germany, USA and France, as well as for the world average, has been declining, which means a tangible increase in energy efficiency in the world and advanced economies. At the same time, the energy intensity for the Iranian economy over the past 50 years has been quite reversed with global developments and unfortunately has always increased.

According to Fig. 15, the carbon intensity index for electricity consumption, despite relative fluctuations, has changed from 72.1 (in 2005) to 71.7 (in 2017), which is insignificant.

According to Fig. 16, the energy intensity index for electricity consumption, similar to the energy intensity index, has an upward trend, which means the continued decline in electrical energy efficiency in Iran. (While reducing overall energy efficiency) This indicates the need for urgent fundamental reform.

ANALYZING THE SUCCESSFUL EXPERIENCES OF ELECTRICITY PRICE REFORM IN THE WORLD

The strategic role of energy carriers in economic and

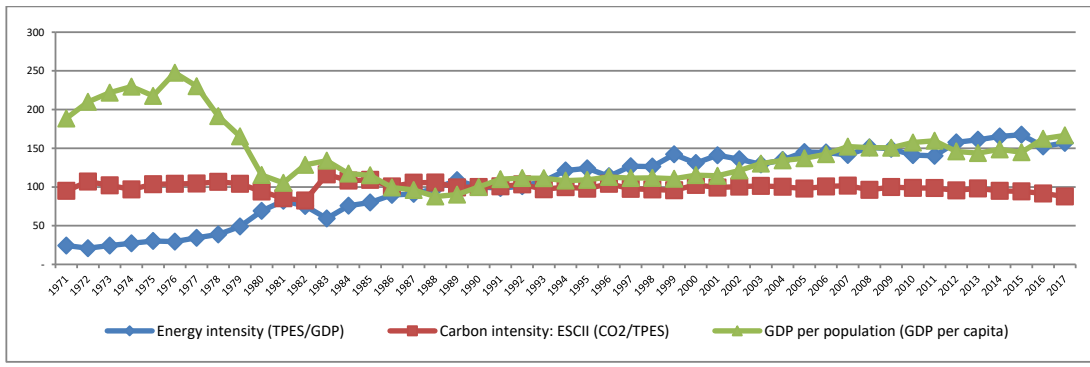

Reference: IEA. 2019a. CO_2 Emissions from Fuel Combustion Highlights.

Fig. 13: Comparison of energy intensity, carbon intensity and GDP per population indexes of Iran in 2017.

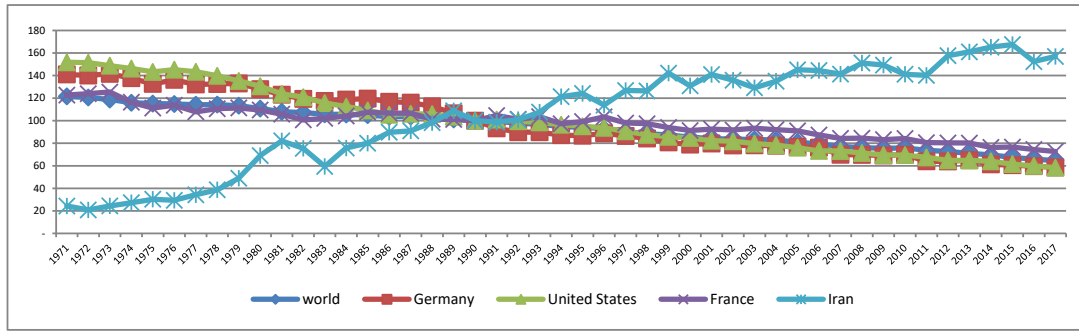

Reference: IEA. 2019a. CO_2 Emissions from Fuel Combustion Highlights.

Fig. 14: Comparison of energy intensity index in Iran, Germany, US, France and the world average in 2017.

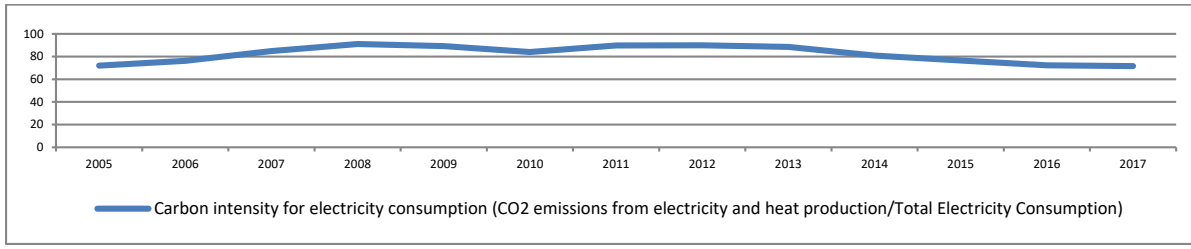

Reference: Ministry of Power. 2019. Energy Balance Sheet – 2017.

Fig. 15: Carbon intensity index trend for electricity consumption in Iran (power plant section).

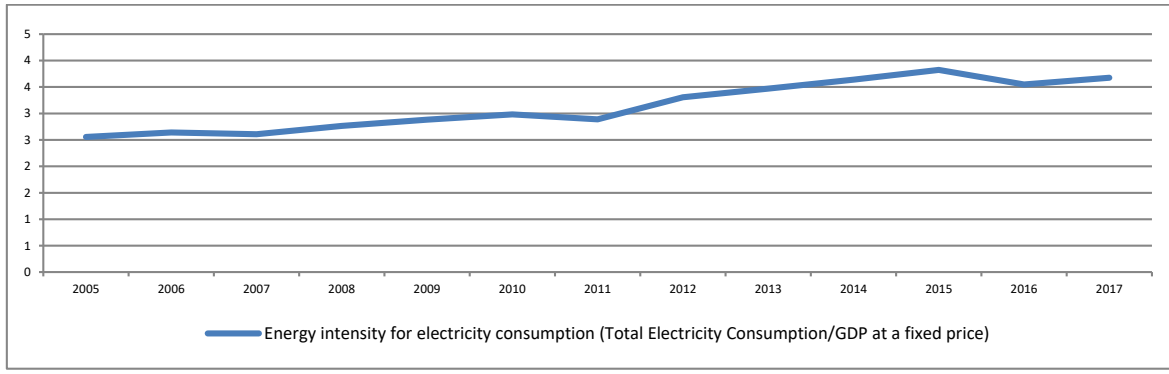

Reference: Ministry of Power. 2019. Energy Balance Sheet – 2017.

Fig. 16: Energy intensity index trend for electricity consumption in Iran (power plant section).

social development has made the energy sector one of the main focal points for subsidies. However, contrary to the original objectives, the granting of subsidies has imposed enormous social, economic and environmental costs on communities, some of which have only been mentioned. Under the 2015 Paris Global Agreement, governments, using funds derived from the reduction of energy subsidies, must lay the groundwork for massive investment in renewable energy and also reduce fossil fuel consumption by setting targeted guidelines and laws (Merrill et al. 2017). A review of the global experience of reforming energy subsidies in 28 countries suggests that obstacles to reform, such as lack of sufficient information on the actual volume of subsidies, lack of government credibility, concerns about the adverse effects of subsidies removal on poor households, contradictions with the interests of groups benefiting from the current situation, as well as the reverse effects of removing subsidies on inflation, international competition and domestic energy price fluctuations and so on, make the implementation of the reform program costly and challenging in many countries (Amirkhanlo 2018). The results of electricity subsidy reform in different countries are summarized in Table 5.

According to reports from the IMF (2013), Coady et al. (2016), Krane (2018) and the IEA (2019b), the strategy of adjusting subsidies for the electricity industry may vary depending on the circumstances of each country, but there are four key components to the success of electricity industry reform as a result of the above mentioned studies:

Design a Comprehensive Strategy for Reform

Successful reform always has a clear, long-term reform strategy that leads to increased efficiency in energy consumption and supply. There is a strong inverse relationship between the volume of subsidies and the quality of services, reflecting the diminishing effect of subsidies on investment in the sector. People are often reluctant to pay higher prices until the quality improves. Reforms in this sector should not only seek to increase access and quality of services but should also eliminate operational inefficiencies (such as high distribution losses and improper collection of bills). Having a comprehensive and long-term plan is the main reason for the success of reducing electricity subsidies in Armenia, Brazil and Kenya.

Keep up with the Gradual Increase in Prices

In the IMF's comparative studies, the average time required for a reform to succeed is 5 years on average, and generally, the gradual increase in prices depends on the political and

Table 5: Summary and results of reforming electricity subsidies in different countries in the world.

Country	Reform episode	Reform outcome	Reform impact	IMF-Supported Program during the reform episode	Conditionality on energy subsidy reform
Armenia	Mid-1990s	Successful	The electricity sector financial deficit declined from 22 percent of GDP in 1994 to zero after 2004	Yes	Yes
Turkey	1980s	Successful	Generated additional revenues for maintenance	Yes	Yes
Philippines	2001	Successful	Subsidies declined from 1.5 percent of GDP in 2004 to zero in 2006	No	-
Brazil	1993-2003	Successful	0.7 percent of GDP	Yes	Yes
Mexico	1999/2001/2002	Unsuccessful	not applicable	Yes	No
Kenya	Mid-1990s	Successful	Subsidies declined from 1.5 percent of GDP in 2001 to zero in 2008	Yes	Yes
Uganda	1999	Successful	2.1 percent of GDP	Yes	Yes

Reference: IMF. 2013. Case studies on energy subsidy reform: lessons and implications.

social conditions, the financial position, the social security and insurance system, and so on. According to the experiences of Mauritania 2008 and Nigeria 2012, the sharp rise in prices can be a serious obstacle to reform. In 7 of the 28 cases under study (such as Brazil and Peru), they used the price step-up approach in the electricity industry and initially for high-end subscribers in residential, commercial and public services.

Adopt Political Measures in Line with Reforms

Targeted measures to mitigate the effect of rising prices on the poor to win public support are crucial in reforming subsidies. Cash payments to offset the costs of subsidy reform can be limited to the consumption of the poorest sections of society and conserve government funds because poor families typically consume less energy than rich families. In Armenia, Brazil, Kenya and Uganda, electricity tariffs were kept constant to the minimum level of consumption, but for high consumption levels, tariffs increased. In the Philippines, very poor families were also subsidized for electricity consumption.

Remove Policy from Price Mechanism

Automated mechanisms are generally used to eliminate non-market energy pricing and reduce the adverse effects of reform. In South Africa, the Philippines and Turkey, the most detailed information about this mechanism and its implementation, through government and media policies, has been reported. However, in some cases, the adoption of such mechanisms has failed due to the significant transfer of international prices to consumers.

In order to prevent a sharp rise in domestic prices, the main point in the failure of reforms sustainability, a price-adjusting rule with an automated pricing mechanism can be used. Adjustment mechanisms, if backed by appropriate macroeconomic policies, can stave off inflationary expectations and gradually offset the effects of sharp increases in international prices and exchange rates to domestic prices to drastically reduce the likelihood of prices returning to the pre-reform period.

DISCUSSION AND CONCLUSION

Current patterns of energy production and use, while contributing to economic growth, are also a threat to environmental sustainability, health, and well-being of present and future generations. Therefore, paying attention to environmental impacts in economic activities is an important necessity (Sajadifar et al. 2016). In the not too distant future, the world will face two major crises of environmental pollution from fossil fuel combustion and increasing acceleration to complete these resources. Two strategies: diversifying the energy supply system and energy consumption management, are the main solutions (Barimani et al. 2018).

Necessity of Reforming Electricity Generation Pattern Through Revision of Production Process and Reduction of Fossil Fuel Consumption

The results of this study indicate that due to the low volatility of carbon intensity index during 47 years and carbon intensity index for electricity consumption during 13 years, no significant changes in the energy production process and especially electricity in Iran have been done. Due to the massive consumption of fossil fuels in power plants, the externality costs of power generation has increased significantly. The use of strategies adopted in developed countries, to account for the externality costs on the price of

electricity, will certainly justify the production of electricity from renewable sources in Iran. On the other hand, the long construction time of electricity projects and their dependence on the economy has necessitated planning for the future of the electricity grid in order to meet timely and economical electricity demand. Under Article 50 of the Sixth Economic Development Plan of Iran, the government is required to raise the share of renewable and clean power plants, with the priority of investing in the non-governmental sector and with maximum internal capacity utilization, to at least 5% of the country's electricity capacity by the end of the program. But there are actually numerous problems in operating it. Analysis of Iran's electricity industry data shows that electricity generation from renewable sources (wind, solar, biogas and thermal recycling) in Iran has always been negligible (and increased to 476.9 MW in 2017, which is only 0.6% of the country's total power capacity), and even after privatization and a number of reforms, the index of fundamental reforms in electricity production in 2017 has grown to only 7.6%, which can be worrying. However, in highly successful countries such as Iceland, Switzerland, Norway, Sweden and Luxembourg, over 90% of electricity production comes from sources other than fossil fuels. Hydropower plants in these countries have the highest electricity production and, after hydropower, each of these countries has invested heavily in one or some renewable resources to suit their needs. Hydropower plants (due to power generation through dam construction, flood control, agricultural and potable water supply, reduced fuel consumption, environmental pollution, ease of use, poor domestic consumption, quick stop and start, grid frequency control, poor maintenance cost and easier power plant construction) are the most favoured and, for these reasons, the dominant part of successful countries. Iran's hydropower capacity has increased by 372 MW in 2017, and it is planned to increase 1313 MW to hydropower plants by 2022. However, the share of hydropower plants in electricity production has actually been declining for the last three decades. Comparison of the index of fundamental reforms in electricity production with 30 sample countries as well as the results of Razini et al. (2011), Sajadifar et al. (2016) and Kachoi & Amidpour (2016) studies, the necessity of revising the process of electricity generation and reduction of fossil fuel consumption can be confirmed and emphasized. The use of alternative (renewable) energy sources, while reducing dependence on an energy carrier and diversifying the energy supply system, has both the advantages of energy saving and the reduction of energy pollution.

Necessity of Reforming the Pattern of Electricity Consumption Through Price Management and Targeted Reduction of Subsidies

Electricity has been one of the strategic inputs of production in any country whose long-term growth depends on the ability of power plants to supply electricity efficiently. Paying large direct and indirect subsidies to Iran's power industry, while reducing tangible efficiency, makes fuel power plants enter the process of production at an unrealistic and lower price as well as makes electricity available to the end consumer at a lower price than the actual level. As such, large industries and power producers have no economic incentive to invest and plan to save on fossil fuel or electricity as feed. The only significant and applicable government policy is the extensive effort to replace Natural Gas with other fossil fuels as shown in Fig. 7. Finally, the end user of electricity in all sectors, given the fact that it receives electricity far below its actual cost, has no incentive to invest and use modern technology to reduce electricity consumption. According to Kiani et al. (2017), the main problem of the government, in general, is the unwillingness of the people to pay the extra costs due to the replacement of renewable energies with other energies and even the lack of optimal participation in the implementation of government programs in this regard. Paying for subsidies makes it even worse that, unfortunately, in 2018, Iran has paid the most subsidies in the world.

The study of the energy intensity and energy intensity for electricity consumption and their undesirable trend in Iran can indicate worrisome in the area of socio-economic effects of abuse and increase inefficiency for both energy and electricity. The energy intensity in Iran, with a continuous upward trend, has risen from about 24 (in 1971) to a very alarming 157 (in 2017). However, the steady decline in this index over the same period for average world economy and developed countries indicates the degree of deterioration and the need for quick corrective action. According to Asadi et al. (2016), lower fuel prices of power plants and lower electricity prices have led to uneconomic and relatively higher electricity consumption, which means the need for higher electricity generation and imposing heavy subsidy costs on the government. And given that the electricity generation process is also based on the wider use of fossil fuels, more use of fossil fuels means imposing a second subsidy pressure on the state (imposing more subsidies on gas and oil sectors as indirect subsidies for the electricity industry) and creating wider pollution due to the greater use of fossil fuels. Therefore, this is contrary to the goals of sustainable development. This issue, along with Iran's unfavourable global rank in providing large subsidies, the increasing trend of energy intensity and CO_2 emissions in Iran and the results of studies by Majdzadeh Tabatabaei et al. (2016) and Gholipour Khatir et al. (2018), emphasizes the need to accelerate the implementation of reforms in the subsidies and the pattern of energy consumption (particularly electricity).

Implementation of electricity consumption management, by promoting energy efficiency, guarantees optimum and economical utilization of it and will lead to the reduction of energy pollution in Iran.

POLICY SUGGESTIONS

The need to create efficiency and increase productivity in the energy consumption pattern and its production process concurrently is of particular importance in order to achieve sustainable development, and the following suggestions should be taken seriously:

1. Reducing subsidies in the electricity sector alone cannot be effective, because power plants get fuel from both gas and oil derivatives sectors, which have much more subsidies. Therefore, the reduction of subsidies in the form of a comprehensive plan will be formulated in all three sections and special attention will be paid to the links between these three sections. The government's policy of late 2019 to begin lowering the subsidy on Gasoline alone may not be optimal, as reforming the price of one energy carrier will cause double disruption of market mechanism and investment to replace other (relatively cheap) energy carriers.
2. Heavy investment in sustainable development by the government is crucial. Worryingly, the inefficient use of the revenue generated by the reduction of subsidies and the use of this revenue to cover current expenditures and the government's budget deficit cannot be effective at all. For example, the production of hybrid cars alone cannot mean less Gasoline and Diesel Fuel consumption, but also according to Merrill et al. (2017), heavy infrastructure investment such as the creation of a major hybrid vehicle manufacturing structure, the creation of car charging stations, the transfer of transportation system from fossil fuel consumption to electricity, and several important incentive investments and policies should be made by the government.
3. Due to the heavy cost of building renewable power plants and the study of Kiani et al. (2017) on the necessity of government action in this regard, while reducing subsidies, resources should be utilized to improve the electricity generation process. In the absence of this improvement, all policies in the area of sustainable development can lead to failure. In the example above: by investing heavily in hybrid cars and transferring their fuel from fossil fuels to electricity, the direct consumption of fossil fuels in cars and transportation system will decrease and electricity consumption will increase sharply. However, if the electricity generation process continues to be associated with greater use of fossil fuels, there will again be an increase in the use of fossil fuels to generate more electricity. This phenomenon means getting caught in a vicious cycle.
4. The second strategic solution for the heavy cost of transferring the electricity generation process from fossil fuels to renewables is to exploit the potential in hydropower. Unfortunately, unlike the successful experiences in developed countries, the share of hydropower plants in electricity production in Iran has been declining, which can be clearly deduced by comparing the index of fundamental reforms in electricity production with the 30 countries in Table 2. Accordingly, the government should formulate an efficient plan to increase the tangible utilization of hydropower plants and build new ones.
5. Given the unsuccessful implementation of the subsidy reform plan in Iran in the last decade and the recent government planning to re-enforce it, it is crucial to take advantage of successful countries' experience in reforming the electricity industry and paying attention to the four key components mentioned. Cross-sectional increasing energy prices (motivated by price gaps between home and abroad) may not be an efficient activity, because, according to some countries' experiences, after a while and for various reasons, subsidies generally return to pre-reform conditions. Therefore the implementation of the price-adjusting rule, along with the automated pricing mechanism and the specific role of the government in the remote control of this mechanism, is of particular importance in ensuring the success of energy price reform. This should definitely be used in Iran.

REFERENCES

Amirkhanlo, M. 2018. Review of current issues of Iranian economy. Center for Research and Economic Studies. Economic deputy. Iran Chamber of Commerce. Industries and Mines and Agriculture (ICCIMA). Tehran, pp. 1-75.

Asadi, F., Karim, M.H. and Feshari, M. 2016. The competitiveness of Geothermal power compared to conventional methods of electricity generation in Iran. Journal of Iranian Energy Economics, 5(18): 1-27.

Barimani, M., Salnasaryan, A., Sadeghi, H. and Kaabi-Nejadian, A. 2018. Modeling of prioritization of policies in the development of the power generation industry of Iran using LEAP. Quarterly Energy Economics Review, 14(58): 139-168.

Bose, B.K. 2010. Global warming: energy, environmental pollution, and the impact of power electronics. Institute of Electrical and Electronics Engineers (IEEE), 4(1): 6-16.

Coady, D., Parry, I., Sears, L. and Shang, B. 2016. How large are global fossil fuel subsidies? World Development, 91: 11-27.

Foley, E., Blomberg, M. and Girard, L. 2014. 2013 wholesale electricity prices in New England rose on higher Natural Gas prices (pipeline constraints and higher demand pushed up prices for both natural gas and power). ISO New England (responsible for the reliable operation of New England's electric power generation…). Press Release, pages 1-3.

Gholipour Khatir, F., Mazyaki, A. and Houri Jafari, H. 2018. Effect of cutting subsidies on technical efficiency of power plants in Iran. Quarterly Energy Economics Review, 14(57): 125-146.

Guler, T. and Gross, G. 2005. A framework for electricity market monitoring. 15th Power Systems Computation Conference (PSCC). Liege. Belgium, pp. 22-26.

IMF. 2013. Case studies on energy subsidy reform: lessons and implications. Prepared by: a staff team led by Clements, B., and comprising Coady, D., Fabrizio, S., Dizioli, A. and et al. International Monetary Fund: Washington, D.C. - Tax expenditure.

International Energy Agency. 2019a. CO_2 Emissions from Fuel Combustion Highlights. Statistics and full analysis of emissions stemming from energy use. IEA Publications. 2019 Edition. France.

International Energy Agency. 2019b. Fossil-Fuel Subsidies Report. IEA fossil fuel subsidies database: contains fossil-fuel subsidies estimates by country from the IEA's World Energy Outlook 2019. For more information on this publication please visit: https://www.iea.org/weo.

Kachoi, M. and Amidpour, M. 2016. The scenario analysis on greenhouse gas emission mitigation potential in the Iranian electricity sector using LEAP model. Iranian Journal of Energy, 19(3): 101-115.

Kiani, S., Shahraki, J., Shahraki, A. and Akbari, A. 2017. Application of double-bounded dichotomous choice contingent valuation to study the possibility of using new energy in Iran's power generation. Journal of Iranian Energy Economics, 6(22): 133-163.

Kianvand, M. and Farzinvash, A. 2015. The effect of electricity forward contracts trading in the energy exchange on the volatility of spot prices in Iran electricity market. Journal of Iranian Energy Economics, 4(16): 181-207.

Krane, J. 2018. Political enablers of energy subsidy reform in Middle Eastern oil exporters. Nat. Energy, 3: 547-552.

Majdzadeh Tabatabaei, Sh., Hadian, E. and Zibaei, M. 2016. Determining proper subsidy to renewable energy in Iran: a Hybrid approach of CGE model. Journal of Iranian Energy Economics, 5(17): 129-167.

Merrill, L., Bridle, R., Klimscheffskij, M. et al. 2017. Making the switch: from fossil fuel subsidies to sustainable energy. Nordic Council of Ministers. Nordic co-operation, TemaNord 2017: 537, Rosendahls, Denmark, pp. 1-81.

Ministry of Power. 2019. Energy Balance Sheet-2017. (Amini, F., Shafizadeh, M. et al.). Office of Planning and Macroeconomics of Electricity and Energy. First Edition. Iran.

Ministry of Power. 2020. An Overview of Energy Statistics in Iran (30 year energy statistics). (Shafizadeh, M., Amini, F. et al.). Office of Planning and Macroeconomics of Electricity and Energy. First Edition. Iran.

Moshiri, S., Morovat, H. and Nasiri, A. 2018. The impact of liberalizing fuel prices on power plants' offered electricity prices using an agent based model. Quarterly Energy Economics Review, 14(56): 1-34.

Pourebadollahan, C. M., Fallahi, F., Heydari, K. and Kiani, P. 2019. Economic regulation design for the electricity distribution companies of Iran. Quarterly Energy Economics Review, 15(60): 191-225.

Razini, S., Moghadastafreshi, S.M. and Bothaei, S.M. 2011. Scenario planning with the aim of future study on Iran power generation industry. Iranian Journal of Energy, 13(35): 1-14.

Razmi, J., Ghaderi, S.F. and Zokaei Ashtiani, A. 2010. Analysis of competitive assessment indexes in electricity market of Iran. Journal of Business Management, University of Tehran, 2(2- Serial Number 5): 41-60.

Sajadifar, S.H., Asali, M., Fathi, B. and Mohamadbagheri, A. 2016. Measuring energy consumption efficiency using Data Envelopment Analysis (DEA) with undesirable factors. The Journal of Planning and Budgeting, 20(4): 55-70.

Shahidepour, M., Yamin, H. and Lee, Z. (as authors). 2005. Market operations in electric power systems forecasting, schedduling, and risk management. Seifi, H., Yousefi, G. & Pedram, M.H. (as translators). Power Networks Studies and Planning Center, Tarbiat Modarres University, Tehran, pp. 1-665.

Shih, Y., Shi, N., Tseng, C., Pan, S. and Chiang, P. 2016. Socioeconomic costs of replacing Nuclear power with fossil and renewable energy in Taiwan. Energy, 114: 369-381.

Stern, J. 2014. International gas pricing in Europe and Asia: a crisis of fundamentals. Energy Policy, 64(C): 43-48.

Tirole, J. 2014. Market power and regulation. The Economic Sciences Prize Committee of the Royal Swedish Academy of Sciences, scientific background on the Sveriges Riksbank Prize in Economic Sciences in Memory of Alfred Nobel, pp. 1-52.

Tladi, D. 2007. Sustainable development in international law: an analysis of key Enviro-Economic instruments. Environmental law. Pretoria University Law Press. Pretoria. South Africca, pp. 274.

Twomey, P., Green, R., Neuhoff, K. and Newbery, D. 2005. A review of the monitoring of market power: the possible roles of transmission system operators in monitoring for market power issues in congested transmission systems. Journal of Energy Literature, 11(2): 3-54.

United Nations. 2011. Sustainable development report on Africa I: managing land-based resources for sustainable development. Economic Commission for Africa, UNCSD.

U.S. Environmental Protection Agency. 2014. Catalogue of CHP technologies. Combined Heat and Power Partnership, page 1.

Wang, K. and Wei, Y. M. 2016. Sources of energy productivity change in China during 1997–2012: a decomposition analysis based on the Luenberger productivity indicator. Energy Economics, 54: 50-59.

Wheeler Stephen, M. 2013. Planning for sustainability: creating livable, equitable and ecological communities. Routledge. London and New York. UK & USA, pp. 288.

Nature Environment and Pollution Technology
An International Quarterly Scientific Journal

p-ISSN: 0972-6268
(Print copies up to 2016)
e-ISSN: 2395-3454

Vol. 20 | No. 2 | pp.533-539 | 2021

Original Research Paper

https://doi.org/10.46488/NEPT.2021.v20i02.009

Open Access Journal

Study of the Insecticidal Potential of Diatomaceous Earth from Sig (Algeria) on the *Dermestes haemorrhoidalis* - A Pest of Stored Food Products

A. Djadi*,†, M. Bouzid* and B. Bezzazi***

* Unité de Recherche Matériaux, Procédés et Environnement/Université M'Hamed Bougarra, Boumerdes, Algérie, Avenue de l'indépendance, 35000, Boumerdès, Algérie

** Unité de Recherche en Analyse et Développement Technologique en Environnement, Centre de Recherche Scientifique et Technique en Analyses Physico-Chimiques, Bousmail, BP 384, Zone Industrielle Bou-Ismail RP 42004, Tipaza, Algérie

†Corresponding author: A. Djadi; a.djadi@univ-boumerdes.dz

Nat. Env. & Poll. Tech.
Website: www.neptjournal.com

Received: 20-04-2020
Revised: 20-05-2020
Accepted: 25-06-2020

Key Words:
Dermestes haemorrhoidalis
Diatomaceous earth
Insecticidal activity
Natural insecticide

ABSTRACT

The insecticidal activity of the Diatomaceous Earth (DE) of Sig was assessed against the *Dermestes haemorrhoidalis*, which is the main pest affecting wheat stored in Blida, a central region of Algeria and one of the four cereal regions managed by the Algerian Inter-branch Cereals Office (AICO). The formulation was tested at two different doses: 500 and 1000 ppm against adults of the species. The bioassays were carried out in 1-litre glass jars containing soft wheat with an average moisture content of 60% mixed with diatomaceous earth and maintained at 27°C and 70% of humidity. The effectiveness of the treatment was assessed by recording adult mortality after 2, 7 and 14 days. Sig's diatomite showed significant insecticidal activity against *Dermestes haemorrhoidalis* after only two days of treatment with both doses 500 and 1000 ppm. After 14 days, average mortality was more than 95% even at 500 ppm. Furthermore, electron microscopy of the diatomite particle from Sig (Algeria) reveals the architecture of the frustule. It shows a porous and brittle siliceous shell made largely of diatomite "skeletons". This research work allowed getting insights into the mechanism of action of diatomite on the *Dermestes haemorrhoidalis*. On the other hand, the identification of diatomite of Sig was performed by X-ray diffraction and infrared.

INTRODUCTION

Chemical pesticides are widely used around the world. Their negative impact on animal and plant health has been widely highlighted in the literature (Testud & Grillet 2007, Hazarika 2011, Ghorab & Khalil 2016, Richardson et al. 2019). Metabolites from carbamates and phosphines, which are toxic substances, persist in nature in large quantities (Meiniel 1977, Steeve 2013, Lotti & Moritto 2005, Martin-Reina et al. 2017). The control of insects that destroy stored food still relies on chemicals, but following the growing concerns regarding the issue, a renewed interest in Diatomaceous Earth (DE) has been shown in recent years in the field of applied sciences (Ebadollahi & Sadeghi 2018, Athanassiou et al. 2016). This is particularly the case for the disinfection of premises and protection of stored food (Banks & Fields 1995, Bridgeman 1998, Desmarchelier et al. 1992, Korunić et al. 2016). Indeed, DE has long been used to protect the stored grain. These fossils give, after extraction, crushing and grinding, a fine powder primarily composed of amorphous silicon dioxide (SiO_2) with a small amount of aluminium, iron, magnesium, CaO and sodium oxide. The highly porous, inert and sharp architecture of the frustules of the DE is used for its abrasive and desiccating properties (Quarles & Winn 1996, Korunić et al. 2016).

The insecticidal activity of DE is essentially attributed to dehydration of the insect provoked by damage to the cuticle layers of the integument. The DE particles are trapped on the insect's body and absorb lipids in the waxy layer of the epicuticle causing degradation of the exoskeleton (Ebeling 1971, Korunić et al. 2016, Mewis & Ulrichs 2001).

However, insecticidal efficiency depends significantly upon the physical, chemical and morphological characteristics of the diatomite species in DE (Korunić et al. 2016, Rojht et al. 2010) and particle size (Korunić 2013, Subramanyam & Roesli 2000). It also depends upon the resistance of the host insects (Aoues et al. 2017).

The use of DE to control food pests offers a number of advantages: it does not leave chemical residues, has low toxicity, is inexpensive and can be easily disposed (Korunić et al. 2016). DE has been used to treat wheat contaminated with C. ferrugineus. It has also been used for the elimination of *Sitophilus oryzae* and red flour beetle *Tribolium castaneum*

Herbst from rice and wheat (Korunic et al. 2016).

The objective of this paper is to describe the physico-chemical analysis of Sig's DE and to carry out a preliminary test regarding pest control potential on food pests under natural storage conditions in the hot and humid region of Blida, Algeria.

MATERIALS AND METHODS

Preparation of the Samples

The diatomite used in this work is a raw Algerian white diatomite from the National Company of Mining Products Non-Ferrous and Useful Substances (ENOF) deposit located at 5 Kms from southeast of the city of Sig in the Wilaya (province) of Mascara, hereafter referred to as diatomite of Sig (DTS). The collected diatomite samples were crushed and dried, ground as finely as possible and sieved to a particle size less than 63 µm. The obtained products were subject to physicochemical, spectroscopic and structural characterization, and used in all the experiments.

White grains used in the experiments were first sieved to remove impurities and then stored hermetically in glass jars at room temperature.

An experimental unit consisted of a glass jar containing 1 kg of soft wheat, to which DTS powder was added and then carefully hand-mixed. Fifty (50) adult insects (*Dermestes haemorrhoidalis*), *Dermestidae* family and **Beetles** order, 2 weeks old on average, was introduced into the jar. The same procedure was followed for each concentration of DTS with an interval of 2, 7 and 14 days of exposure.

An additional jar containing untreated wheat was used (as control sample) for each series of tests. Three treated samples: 500 ppm, 1000 ppm and control (untreated) were used for each time interval. After 2, 7 and 14 days of exposure, the contents of the jars were screened, living and dead insects were collected and counted. Mortality is expressed as a percentage of adult deaths out of the total number of beetles found in each jar. The experiments were carried out from May to July 2019.

The *Dermestes haemorrhoidalis* adults used for the experiments were obtained from a wheat stock in the region of Blida. The insects were kept under the same infestation conditions at a temperature of 25 ± 1 °C and relative humidity (RH) of %60 on average. Identification of the pest was carried out using a key developed by Oleobel and Tran, (1993). The species are stored food beetles: black beetle of the pantry (*Dermestes haemorrhoidalis*) (Fig. 1).

Characterization of DTS

The X-ray diffraction (XRD) analysis of the DTS powder was carried out using a BRUKER D8 ADVANCE Eco,

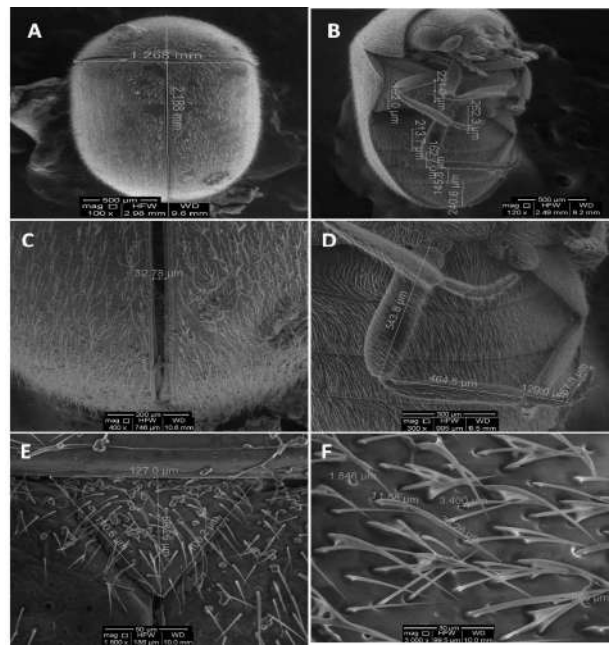

Fig. 1: SEM observation of untreated *Dermestes haemorrhoidalis*, A, C and E: dorsal side, B and D: ventral side, F: Dorsolateral face showing cuticular thoracic depressions surrounding the sensory bristles.

equipped with a Cu anticathode (λ = 1.5418 Å) generating a power of 40 mA, 45 KV and mode 2 THETA, scanning area [3.0001- 89.999482°], a step of 0.020171°, time per step: 0.5 s. Software for the acquisition and processing of data are respectively: Data Collector and High Score Plus of PANalytical.

To study the thermal properties of DTS, samples of (2 mg) were measured using the SeikoSSC5200 thermal analyser (model 220 TG/DTA) at heating and flow rates of 10-50°C/min and 100 mL/min, respectively. Analysis and data processing software are TA Instrument Explorer and TA Universal Analysis, respectively.

DTS grain scanning electron microscopy was performed with a Quanta 250 from FEI and a tungsten filament as an electron source.

The infrared absorption spectra were plotted with a BRUKER Alpha type device; the analysis was done in ATR mode with a resolution of 2 cm^{-1} for 24 scans.

The elementary analysis of DTS was carried out with Rigaku ZSX Primus II X-ray Fluorescence Spectrometer, elementary coverage: ^{4}Be à ^{92}U. Closing window, Rh-anode, 3 kW or 4 kW, 60 kV. Primary X-ray filter: Al25, Al125, Ni40 and Ni400. Heavy Element Detector: Scintillation Counter (SC).

The volumetric distribution of DTS was assessed by laser granulometry using MALVERN MATERSIZER 2000 granulometer equipped with Scirocco as a dry dispersion accessory; sensitivity normal, absorption 0.1 and obscuration 5,68%.

Statistical Analysis

ANOVA was used to evaluate the treatment and exposure time of DTS on mortality of *Dermestes haemorrhoidalis*. The results are presented as mortality percentage of *Dermestes haemorrhoidalis* at 500 ppm and 1000 ppm of DTS, respectively and the exposure time of 2, 7 and 14 days respectively.

RESULTS AND DISCUSSION

Phase quantification of DTS by XRD analysis was conducted using MAUD software as illustrated in Fig. 2. DTS powder consists of amorphous and crystalline phases. The main constituents of crystalline phases are $CaCO_3$, SiO_2, Al_2O_3, Fe_2O_3 on the MAUD database records. The results agree with the result obtained by Pokorný et al. (2017).

The SEM of DTS (Fig. 3) shows the pores and the cylindrical and/or disc form of this powder. The average size of the diatomite particles determined by laser granulometry

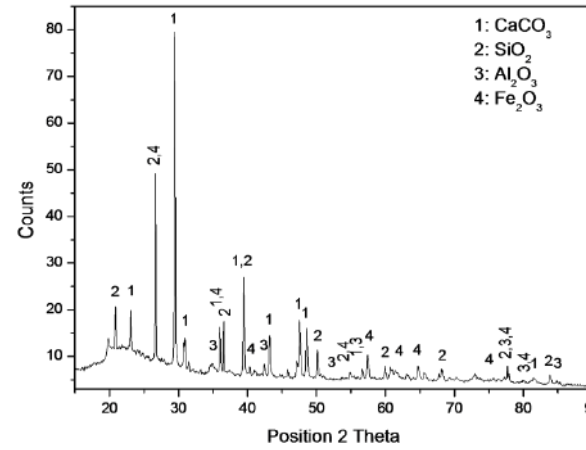

Fig. 2: X- ray diffraction pattern of diatomite of Sig (DTS).

is ~ 12 µm (Fig. 4), with a specific surface area of 1.61 m^2/g. the average particle diameter is in the range 3,802 - 34,674 µm; similar results were obtained by Fragoulis et al. (2005) where they found a diameter < 30 µm.

The elemental composition of DTS was obtained by X-ray Fluorescence (XRF); the fire loss is 7.4% and the moisture content is 2.5%. Results of the chemical analysis of the material (Table 1) show that the diatomite is largely made up of silica, CaO and aluminium oxide. Other elements are present but in much smaller amounts.

Fourier Transform Infrared Spectroscopy (FTIR) analysis of DTS (Fig. 5) shows the main absorption bands of our untreated diatomite are in agreement with the literature (Yuan et al. 2004, Caliskan et al. 2011). Indeed, the wide band in the wave number range 3100 - 3500 cm^{-1} characterizes the vibration of the OH group of water contained in the DTS, as well as the Si-OH group, which are observed at 3690 and 3614 cm^{-1}, OH and Si-OH, respectively. The weak vibration at 3600 cm^{-1} indicates the presence of unbound water, i.e. free OH. On the other hand, water deformation appears at 1640 cm^{-1} (Yuan et al. 2004) while vibrations centred at 1440, 875 and 712 cm^{-1} indicate CO_2 deformation (Yuan et al. 2004, Caliskan et al. 2011). The characteristic peaks of the skeleton (Si - O - Si) are located at 1073 and 997 cm^{-1} (Caliskan et al. 2011). The band centred at 874 cm^{-1} corresponds to the elongation vibration of the silanol group (Si-O). The peaks at 798 and 713 cm^{-1} are due to Si-O-H vibrations. The absorption peak around 570 cm^{-1} can be assigned to the deformation vibration of the entity Si-O-Si. The intense band at 460 cm^{-1} is relative to the angular vibration of (Si - O - Al) and /or (Si - O - Si) (Caliskan et al. 2011).

Results of the simultaneous thermogravimetric analysis (TGA) and differential scanning calorimetry (DSC) analysis of the DTS are shown in Fig. 6. The evolution of diatomite in

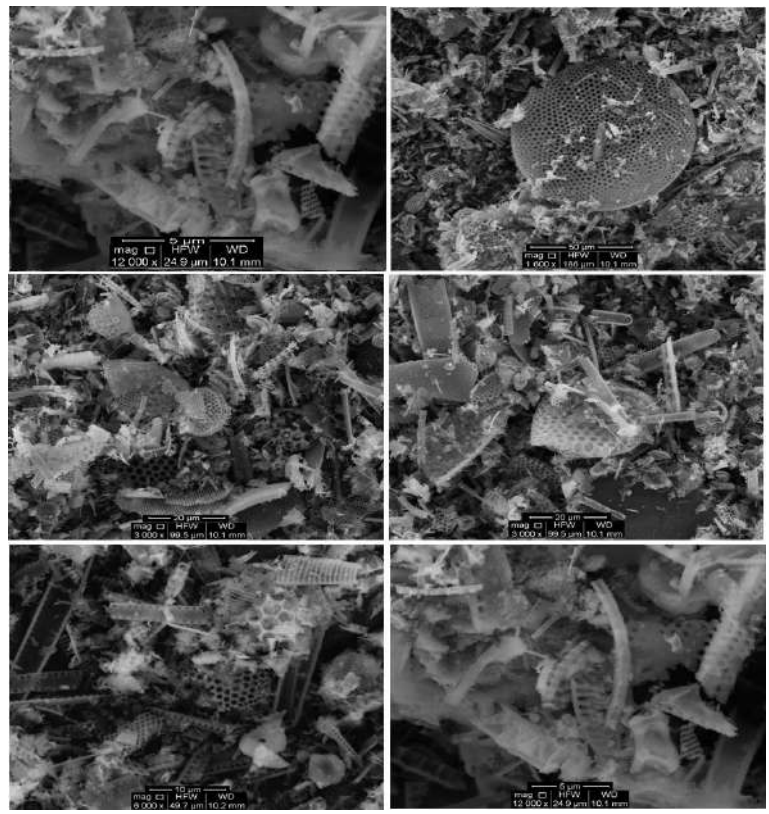

Fig. 3: SEM observation of the diatomite of Sig (DTS) at different magnifications.

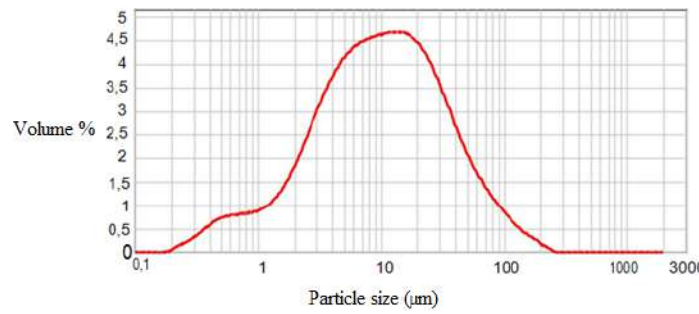

Fig. 4: Particle size distribution of diatomite of Sig (DTS).

Table 1: Chemical composition of diatomite of Sig.

Constituent and weight %									
CO_2	Na_2O	MgO	Al_2O_3	SiO_2	P_2O_5	SO_3	K_2O	CaO	TiO_2
9.40	0.26	1.27	3.87	64.08	0.16	0.08	0.89	17.64	0.26
Constituent and weight %									
MnO	Fe_2O_3	NiO	ZnO	Rb_2O	SrO	ZrO_2	Cl		
0.01	1.77	0.01	0.01	0.01	0.05	0.01	0.15		

the TGA agrees well with the literature (Meradi et al. 2015, Mendioroz et al. 1989). The DTS placed on the balance at 15°C with a step of 10°C/min. The spectrum (Fig. 6 A) shows a mass loss of 3.31% between 100 and 200°C; water

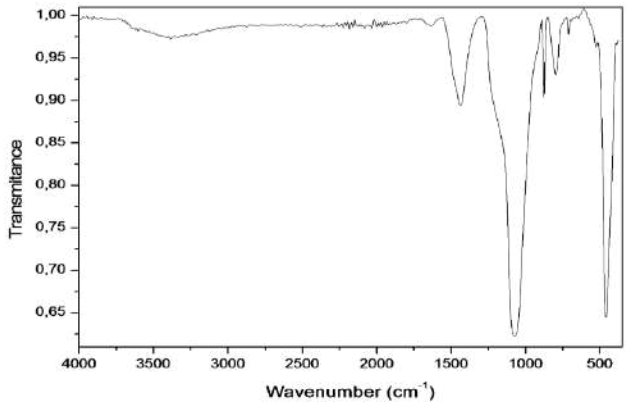

Fig. 5: Fourier Transform Infrared Spectroscopy spectra of diatomite of Sig (DTS).

vapours that escape, represent humidity. The mass loss of 16% between 300 and 700°C corresponds to the decomposition of the organic material and the dehydroxylation of the silanol group. The organic material results primarily from the impurity content of the deposit produced by chemical precipitation, atmospheric contact and environmental conditions, as well as from amorphous silica, the main constituent of diatomite. Metal oxides, clays, carbonates may also be present (Mendioroz et al. 1989). The literature also reports the phenomenon attributed to the dehydroxylation of calcium hydroxide (Benkacem et al. 2016).

As can be seen from the DST results (Fig. 6 B), the first endothermic peak at 106.45°C corresponds to water desorption whereas the second, at 689.07°C, corresponds to the dehydroxylation (Meradi et al. 2015, Mendioroz et al. 1989).

The SEM Examination of the cuticular surfaces of the *Dermestes haemorrhoidalis* treated with DTS reveals that the dorsal cuticle is evenly covered with fragments of the diatomite frustule on the integumentary surface (Fig. 7).

Table 2 shows the percent mortality of *Dermestes haemorrhoidalis* at 500 and 1000 ppm of DTS following exposure for 3different periods of time (2, 7 and 14 days).

The mortality of *Dermestes haemorrhoidalis* is in agreement with results obtained by Ebeling (1971) and Golob (1997). Indeed, a concentration of 1000 ppm generated mortality of 56.0±1.15% after 2 days, 78.7±0.67% after 7 days and 90.7±0.67% within14 days, and is higher than the result obtained with 500 ppm with 50.7±0.67% after 2 days, 56.7±4.37% after 7 days and 80.7±0.67% after 14 days.

Table 3: Shows that treatment and exposure time of *Dermestes haemorrhoidalis* by DTS gives a very significant correlation ($P \leq 0.001$).

Complete pest annihilation was not observed for two reasons:

1. The high RH (60% on average) caused saturation of the DTS and allowed the insect to recover any water loss.
2. In general, diatomite exhibits an activity consistent with its chemical constitution (Athanassiou et al. 2005).

The diatomite of the regions of Sig Algeria, with 90% efficacy against *Dermestes haemorrhoidalis* and many other nuisances, can be considered as an appreciable natural insecticide material. Indeed, this non-metallic material offers the sought-after advantage of being, available, low cost, and -biocompatible. It also possesses excellent physicochemical properties such as non-toxicity, lightness, unique structure of the pores, porosity, excellent absorption capacity, chemical inertness and large available reserves (Sun et al. 2013).

Diatomite is an economical and beneficial solution for human, animal and plant health.

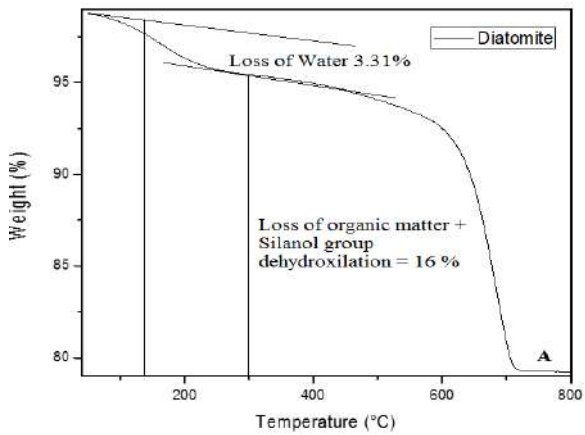

Fig. 6. A: Thermogravimetric Analysis (TGA) of diatomite of Sig (DTS).

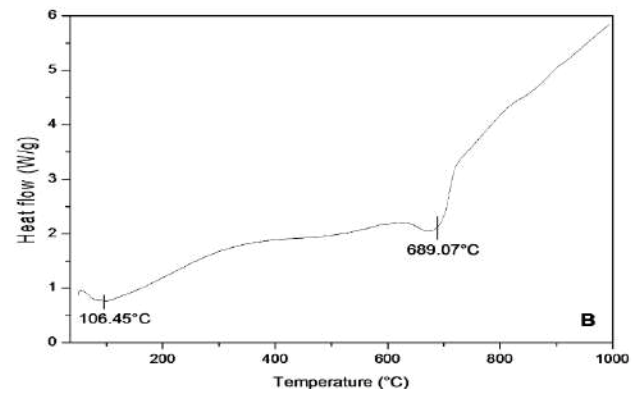

Fig. 6. B: Differential Scanning Calorimetry (DSC) analysis of diatomite of Sig (DTS).

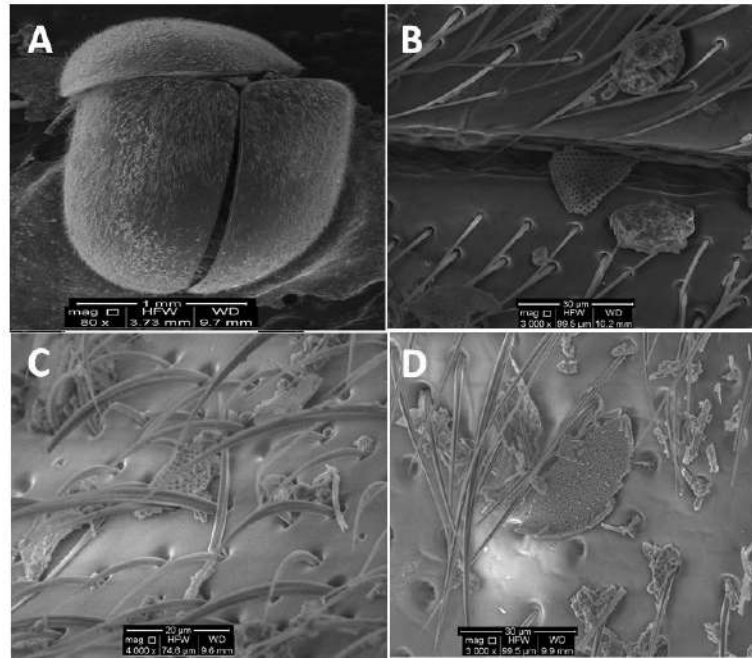

Fig. 7: SEM images of *Dermestes haemorrhoidalis* treated with diatomite of Sig (DTS) particles, A: dorsal side, B: Fragments of siliceous frustule in the dorsal fringe of the insect, C and D: Cuticular sites on the dorsal surface surrounding sensory bristles contaminated with DTS.

Table 2: Mean (±SE) percent mortality of *Dermestes haemorrhoidalis* when exposed to diatomite of Sig (DTS) for 2, 7 and 14 days.

Duration of exposure (days)	Treatment (ppm of DTS)		F_{df}, P
	500	1000	
	Mortality of *Dermestes haemorrhoidalis*		
2	50.7±0.67%	56.0±1.15%	$15.7_{1,4}$, 0.02
7	56.7±4.37%	78.7±0.67%	$31.7_{1,4}$, 0.005
14	80.7±0.67%	90.7±0.67%	$100.1_{1,4}$, <0.001

Table 3: ANOVA table showing the significance of treatment and exposure time on mortality of *Dermestes haemorrhoidalis*.

$Variable_{df}$	F, *P*
$Treatment_{1,12}$	90.12, < 0.0001
$Exposure_{2,12}$	195.19, < 0.0001
$Treatment*Exposure_{2,12}$	12.21, 0.001

CONCLUSION

The study confirms the natural pest control property of the diatomite from Sig (Algeria). The DTS gives satisfactory results with a mortality rate of 90% within 14 days on *Dermestes haemorrhoidalis,* the main pest of wheat in the region of Blida (Algeria). Physicochemical characterisation shows that, by its particular structure, morphology and texture, our diatomite is naturally endowed to control the pest. This siliceous material is an active structure on the cuticle of the *Dermestes haemorrhoidalis*. Scanning Electron Microscopy reveals the dispersion and absorbance properties of the diatomite on the cuticle. It also shows the abrasive and lacerating effects of the diatomaceous earth. This control capacity on *Dermestes haemorrhoidalis* populations highlights the ecological advantage of the diatomite from Sig.

REFERENCES

Aoues, K., Boutoumi, H. and Benrima, A. 2017. Etat phytosanitaire du blé dur locale stocké en Algérie. Rev. Agrobiologia., 7(1): 286-296.

Athanassiou, C. G., Kavallieratos, N. G., Economou, L. P., Dimizas, C. B., Vayias, B. J., Tomanović, S. and Milutinović, M. 2005. Persistence and efficacy of three diatomaceous earth formulations against *Sitophilusoryzae* (Coleoptera: Curculionidae) on Wheat and Barley. J. Econ. Entomol., 98(4): 1404-1412.

Athanassiou, C. G., Kavallieratos, N. G., Chiriloaie, A., Vassilakos, T. N., Fătu, V., Drosu, S., Ciobanu, M. and Dudoiu, R. 2016. Efficacy of natural diatomaceous earth deposits from Greece and Romania against four stored grain beetles: the effect of temperature and relative humidity. Bull. Insectology., 69(1): 25-34.

Banks, H.J. and Fields, P. 1995. Physical methods for insect control in stored-grain ecosystems. In. Jayas D, White NDG, MuirWE (Eds.), Stored-grain ecosystems. New York, USA: Marcel Dekker. pp. 353-407.

Benkacem, T., Hamdi, B., Chamayou, A., Balard, H. and Calvet, R. 2016. Physicochemical characterization of a diatomaceous upon an acid treatment: a focus on surface properties by inverse gas chromatography. Powder Technol., 294: 498-507.

Bridgeman, B. 1998. Application technology and usage pattern of diatomaceous earthin stored product protection. In: Proc. 7th Int. Working Conf. on Stored-product Protection, Beijing. Sichuan Publishing House of Science & Technology, Chengdu, China. pp. 785-789.

Caliskan, N., Kul, A. R., Alkan, S., Sogut, E. G. and Alacabey, I. 2011. Adsorption of Zinc (II) on diatomite and manganese-oxide-modified diatomite: A kinetic and equilibrium study. J. Hazard. Mater., 193: 27-36.

Desmarchelier, J. M., Wright, E. J. and Allen, S. E. 1992. Dryacide (R): a structural treatment for stored-product insects. In: Corey SA, Dall DJ, Milne WM (Eds.), Proceedings of the Australian Applied Entomological Research Conference. Canberra, ACT. pp. 483-485.

Ebadollahi, A. and Sadeghi, R. 2018. Diatomaceous earth and kaolin as promising alternatives to the detrimental chemicals in the management of Spodopteraexigua. J. Entomol., 15(2): 101-105.

Ebeling, W. 1971. Sorptive dusts for pest control. Annu. Rev. Entomol., 16(1): 123-158.

Fragoulis, D., Stamatakis, M. G., Papageorgiou, D. and Chaniotakis, E. 2005. The physical and mechanical properties of composite cements manufactured with calcareous and clayey greek diatomite mixtures. Cem. Concr. Compos., 27(2): 205-209.

Ghorab, M.A. and Khalil, MS. 2016. The effect of pesticides pollution on our life and environment. J. Pollut. Eff. Cont., 4: 159.

Golob, P. 1997. Current status and future perspectives for inert dusts for control of stored product insects. J. Stored. Prod. Res., 33(1): 69-79.

Hazarika, R. 2011. Effect of occupational exposure of pesticides on health of farmers of the agricultural fields of Sorbhug Area of Lower Assam. Nat. Environ. Pollut. Technol., 10(2): 237-241.

Korunić, Z., Rozman, V., Liška, A. and Lucić, P. 2016. A review of natural insecticides based on diatomaceous earths. Poljoprivreda, 22(1): 10-18.

Korunić, Z. 2013. Diatomaceous earths: natural insecticides. Pestic. Phytomed. (Belgrade)., 28(2): 77-95.

Lotti, M. and Moretto, A. 2005. Organophosphate-Induced Delayed Polyneuropathy. Toxicol. Rev., 24(1): 37-49.

Martin-Reina, J., Duarte, J. A., Cerrillos, L., Bautista, J.D. and Moreno, I.G. 2017. Insecticides reproductive toxicity profile: organophosphate, carbamate and pyrethroids. J. Odtoxins., 4(1): 7.

Meiniel, R. 1977. Tératogénie des anomalies axiales induites par un insecticide organophosphoré (le parathion) chez l'embryon d'oiseau. Roux's. Arch. Dev. Biol., 181(1): 41-63.

Mendioroz, S., Belzunce, M. J. and Pajares, J. A. 1989. Thermogravimetric study of diatomites. J. Therm. Anal., 35: 2097-2104.

Meradi, H., Atoui, L., Bahloul, L., Boubendira, K., Ouazdia, A. and Ismail, F. 2015. Characterization by thermal analysis of natural kieselguhr and sand for industrial application. Energy Procedia., 74: 1282-1288.

Mewis, I. and Ulrichs, C. 2001. Action of morphous diatomaceous earth against different stages of the stored product pests Tribolium confusum, Tenebrio molitor, Sitphilusgranarius and Plodiainterpunctella. J. Stored. Prod. Res., 37: 153-164.

Oleobel, A. and Tran, M. 1993. Les Coléoptères des denrées alimentaires entreposées dans les régions chaudes. Orstom/CTA, 425 p.

Pokorný, J., Pavlíková, M., Záleská, M. and Pavlík, Z. 2017. Properties of cement-based composites modified using diatomaceous earth. AIP Conference Proceedings 1866, 040031.

Quarles, W. and Winn, P. S. 1996. Diatomaceous earth and stored product pests. IMP Practitioner, 18(5/6): 1-10.

Richardson, J.R., Fitsanakis, V., Westerink, R.S.H. and Kanthasamy, A.G. 2019. Neurotoxicity pf pesticides. Acta Neuropathologica, 138: 343-362.

Rojht, H., Athanassiou, C. G., Vayias, B. J., Kavallieratos, N., Tomanović, Ž., Vidrih, M., Kos, K. and Trdan, S. 2010. The effect of diatomaceous earth of different origin, temperature and relative humidity against adults of rice weevil (*Sitophilus oryzae* [L.], Coleoptera, Curculionidae) in stored wheat. Acta. Agric. Slov., 95(1): 13-20.

Steeve, H., Thany, P.R. and Guy, L. 2013. Neurotoxicity of pesticides: its relationship with neurodegenerative diseases. Med. Sci., 29(3): 273-278.

Subramanyam, B. and Roesli, R. 2000. Inert dusts alternatives to pesticides in stored-product IPM. In: Subramanyam B, Hagstrum DW (Eds.), Springer, Boston, MA.

Sun, Z., Yang, X., Zhang, G., Zheng, S. and Frost, R.L. 2013. A novel method for purification of low-grade diatomite powders in centrifugal fields. Int. J. Miner. Process., 125: 18-26.

Testud, F. and Grillet, J.P. 2007. Insecticides organophosphorés, carbamates, pyréthrinoïdes de synthèse et divers. EMC-Pathologie Professionnelle, pp.1-24.

Yuan, P., Wu, D. Q., He, H. P. and Lin, Z. Y. 2004. The hydroxyl species and acid sites on diatomite surface: a combined IR and Raman study. Appl. Surf. Sci., 227: 30-39.

Nature Environment and Pollution Technology
An International Quarterly Scientific Journal

p-ISSN: 0972-6268
(Print copies up to 2016)
e-ISSN: 2395-3454

Vol. 20 | No. 2 | pp. 541-550 | 2021

Original Research Paper

https://doi.org/10.46488/NEPT.2021.v20i02.010

Open Access Journal

Performance of Vertical Flow Constructed Wetlands Planted with Indigenous Species for Decentralized Wastewater Treatment and Biomass Production in Kerala, India

Jaya S. Pillai and A. N. Brijesh Nair†
*School of Civil Engineering, Vellore Institute of Technology, Vellore-632 014, Tamil Nadu, India
†Corresponding author: A. N. Brijesh Nair; brijeshnair.an@vit.ac.in

Nat. Env. & Poll. Tech.
Website: www.neptjournal.com

Received: 08-06-2020
Revised: 21-07-2020
Accepted: 27-08-2020

Key Words:
Ecological sanitation
Indigenous species
Biomass production
Vertical flow constructed wetlands

ABSTRACT

This study evaluates the performance of tropical subsurface vertical flow constructed wetlands (VFCW) having indigenous plants as decentralized ecological treatment systems for municipal wastewater treatment combined with biomass production. The VFCW mesocosms were planted with lignocellulosic grass species suitable to climatic conditions of Kerala such as Cumbu Napier Hybrid grass (*Pennisetum purpureum)*, Gamba grass (*Andropogon gayanus*) and Palisade grass (*Urochloa brizantha*). The VFCWs were operated at a hydraulic loading rate (HLR) of 0.1md^{-1} and hydraulic retention time (HRT) of 1 day. During the study period, the planted VFCWs attained significant pollutant removal efficiency than the control system with an unplanted filter bed. The VFCW planted with Cumbu Napier Hybrid grass obtained average removal efficiencies of TSS (89.80%), BOD (89.90%), COD (78.10%), Nitrates (69.07%), TN (44.33%), and Phosphates (51.20%). In the VFCW system planted with Palisade grass, the average removal efficiencies observed were Turbidity (98.70%), TSS (89.50%), BOD (87.90%), COD (72.70%), Nitrates (62.07%), TN (43%), and Phosphates (47%). The treated effluent concentration from both the units conformed to the USEPA guidelines for non-potable water reuse standards. The average biomass yield of Cumbu Napier Hybrid grass during the study period was found to be significantly higher when compared to Gamba grass and Palisade grass.

INTRODUCTION

Inadequate access to drinking water and sanitation is one of the most ubiquitous challenges faced by humanity in developing countries. Constructed wetlands (CWs) are decentralized small-scale systems for wastewater treatment having low energy and minimal operational requirements (Brix 1994b, Gross et al. 2009, Hoffmann et al. 2011, Vasudevan et al. 2011). CWs are the artificial replica of natural wetlands, designed and developed to optimize the functions of plants, soil, and the rhizosphere microorganisms that occur in the natural wetlands for pollutant removal (Vymazal 2010). As it is an eco-friendly treatment process with low energy and maintenance requirements and evades the use of chemicals, CWs are largely recognized in many countries (Lee et al. 2009, Vymazal 2011, Avila et al. 2019). Subsurface vertical flow CWs are gaining significance as an eco-technological wastewater treatment technology and can play a vital role in realizing the concepts of ecological sanitation (Langergraber & Muellegger 2005, UN-HABITAT 2008, Masi 2009, Hoffmann et al. 2011, Pillai &Vijayan 2013). They can also be used as onsite flexible treatment systems that can be applied at an individual household level or on a community basis (Hoffmann et al. 2011).

The choice of plants is a significant aspect in determining the pollutant removal efficiency and performance of subsurface flow CWs. The plants influence the level of oxygen in the wetland bed, enable physical filtration, prevent VFCW systems from getting clogged and offer a large surface area for microbial colonization (Brix 1994a, 1994b, 1997). The most frequently used macrophyte in subsurface flow constructed wetlands is *Phragmites australis* most commonly used in Europe, Canada, Australia and parts of Asia and Africa. The second most commonly used plant for subsurface flow CWs is *Typha* (e.g. *latifolia, domingensis, orientalis* and *glauca*) spp. and they are used in North America, Australia, Africa, and East Asia. Yet another plant species is *Scirpus* (e.g. *lacustris, validus, californicus* and *acutus*) spp. largely used in North America, Australia, and New Zealand. *Juncus effusus* and *Eleocharis* sp. are mostly used in Asia, Europe and North America (Vymazal 2011). Moreover, some ornamental species such as *Iris pseudacorus* and *Canna* have been experimented in CWs in the tropical and subtropical countries (Ling et al. 2009, Abou-Elela & Hellal 2012). The efficiency of *Cyperus papyrus* for the treatment of municipal wastewater in subsurface flow CWs has been researched by many authors (Perbangkhem & Polprasert 2010, Abou-Elela

& Hellal 2012, Avila et al. 2019). The use of Napier grass (*Pennisetum purpureum*) in VFCWs has been reported for the treatment of greywater in India (Pillai &Vijayan 2013) as well as for swine wastewater treatment in Thailand (Klomjek 2016).

The CWs provide an efficient mechanism for the removal of nutrients while facilitating a suitable environment for the cultivation of grasses, a potential feedstock for ethanol production. An integrated approach for combining wastewater treatment with biomass productivity in subsurface flow CWs can realize environmental pollution control as well as biofuel production (Yi Chung et al. 2011). The biomass produced by plants provides supplementary values as cattle fodder, biofuel, medicines, pulp and paper, soil conditioner and compost. In addition, CWs offer environmental benefits such as green space, sequestration of carbon dioxide, creation of habitats for wildlife and preservation of biodiversity (Kadlec & Wallace 2009, Vymazal 2010, 2011, Perbangkhem & Polprasert 2010, Hoffmann et al. 2011). Thus, it becomes essential to identify local, resilient, and valuable perennial grasses with high biomass yield and potential for contaminant removal (Pillai & Vijayan 2013).

Subsurface flow CWs are often significant for developing countries in tropical regions with warm and humid weather throughout the year (Kivaisi 2001, Chelliapan et al. 2011, Caselles-Osorio et al. 2011, Almuktar et al. 2018). The possibility of applying CWs as decentralized ecological sanitation systems is substantial in India, but the rate of adoption and replication of the technology has been extremely slow (Pillai & Nair 2015). This study aims to assess the performance of tropical subsurface vertical flow constructed wetland (VFCW) mesocosms using native grass species for the treatment and reuse of wastewater. The VFCW units using different grass species appropriate to the tropical conditions of Kerala such as Cumbu Napier Hybrid grass (*Pennisetum purpureum*), Gamba grass (*Andropogon gayanus*) and Palisade grass (*Urochloa brizantha*) were evaluated and compared for their overall performance and effectiveness in the treatment and utilization of municipal wastewater. The biomass yield from the different planted VFCWs was also studied and compared.

MATERIALS AND METHODS

Description of the Study Site

This research was conducted in Thiruvananthapuram, the capital city of the state of Kerala, which is located on the southwestern tropical Malabar coast of India. Though the city has a separate sewerage and drainage system, the coverage is only about 37% and 50% respectively. In the uncovered areas of the city, sewage from households is disposed to septic tanks, borehole latrines and community toilets. The remaining untreated wastewater gets directly discharged into open drains, canals, streams, rivers and other surface water bodies. Even though the city has a centralized sewage treatment plant (STP) of capacity 107 MLD constructed at Muttathara to treat the sewage load of the entire corporation area, the inflow to the STP is only 44 MLD. The existing gap in the sewerage network of the city is about 63% (TMC & KWA 2016).

Characterization of Influent Wastewater

Municipal wastewater used as an influent to the VFCWs was obtained from the outlet of the grit chamber of the STP located at Muttathara in the district of Thiruvananthapuram. The grab samples were collected manually and analysed for the following parameters: pH, Temperature, Turbidity, Biochemical Oxygen Demand (BOD), Chemical Oxygen Demand (COD), Total Suspended Solids (TSS), nitrates, Total Nitrogen (TN), phosphates and heavy metals. The physico-chemical analysis of the influent and treated samples was carried out as per the standard methods. (APHA 2005). The influent BOD concentration ranged from 175 $mg.L^{-1}$ to 192 $mg.L^{-1}$, while COD values varied between 390 $mg.L^{-1}$ and 430 $mg.L^{-1}$. The concentration of suspended solids ranged from 259 $mg.L^{-1}$ to 302 $mg.L^{-1}$. The average concentration of nitrates, TN and phosphates were 3.37 $mg.L^{-1}$, 52.6 $mg.L^{-1}$ and 13.58 $mg.L^{-1}$ respectively. The presence of heavy metals such as copper, lead, chromium, mercury and cadmium were found to be less than 0.01 $mg.L^{-1}$. The detailed characterization of the influent municipal wastewater is presented in Table 1.

The influent organic loading rate (OLR) used in this study varied between 17.5 and 19.2 g BOD_5 $m^{-2}d^{-1}$ at a constant hydraulic loading rate (HLR) of 0.1 md^{-1}. The

Table 1: Characteristics of influent municipal wastewater.

Parameters	Unit	Average ± SD
pH	-	6.73 ± 0.21
Temperature	◦	28 ± 0.79
Turbidity	NTU	130 ± 4.03
TSS	$mg.L^{-1}$	279 ± 15.25
BOD	$mg.L^{-1}$	180 ± 5.06
COD	$mg.L^{-1}$	412 ± 13.63
Nitrates	$mg.L^{-1}$	3.37 ± 0.39
Total Nitrogen	$mg.L^{-1}$	52.6 ± 4.54
Phosphates	$mg.L^{-1}$	13.58 ± 0.79
Heavy metals (Cu, Cd, Cr, Hg, Pb)	$mg.L^{-1}$	< 0.01

OLR and HLR recommended by Brix and Arias (2005) for VFCWs in Denmark were 10-40 g BOD_5 $m^{-2}d^{-1}$ and 0.05-0.06 md^{-1}. Prochaska et al. (2007) experimented with OLR of 20-40 g BOD_5 $m^{-2}d^{-1}$ and HLR 0.08-0.17 md^{-1} in N. Greece. In warm climates, an OLR of 30-35 g BOD_5 $m^{-2}d^{-1}$ and HLR of 0.2 md^{-1} has been successfully experimented (Hoffmann et al. 2011). Stefanakis & Tsihrintzis (2012) used three high OLR of 89.9, 105.7 and 180.9 g BOD_5 $m^{-2}d^{-1}$ at HLR of 0.19, 0.26 and 0.44 md^{-1} to treat synthetic wastewater for long term in VFCWs.

VFCW System Configuration

The VFCW systems were constructed in the campus of an educational institution in the district of Thiruvananthapuram in Kerala. The design criteria of the subsurface VFCWs were taken from the constructed wetlands manual (USEPA 2000, Kadlec et al. 2000, Brix & Arias 2005, UN-HABITAT 2008). The experimental VFCW mesocosms (labelled VFCW1-VFCW3) were made of rectangular plastic containers each of length 0.65 m, width 0.45 m and depth 0.45 m. To study the effect of macrophytes in the removal of contaminants, a control VFCW without plants was used. The characteristics and design parameters of the VFCW units are presented in Table 2.

The depth of filter bed in a subsurface flow CW is normally limited to almost the rooting depth of plants so that the plants are in constant contact with the influent wastewater and can contribute to the treatment process (UN-HABITAT 2008). In this study, the substrate materials used as filter media consisted of gravel, coarse sand, and coco-peat (coir fibre pith). The lowest layer of the filter bed was filled with a 10 cm thick layer of gravel (porosity= 0.42) of size varying from 10 to 20 mm. Above that, a 20 cm thick layer of coarse river sand (d_{10} = 0.3 mm, uniformity coefficient =4, porosity =0.39) was laid followed by an 8 cm thick layer of coco-peat. The coco-peat used in the study had a pH of 6.2, bulk density 0.09 g cm^{-3}, electrical conductivity 0.16 $mScm^{-1}$ and porosity 0.65. In order to prevent any accumulation of water, a 2 cm thick gravel layer was placed on the top surface of the wetland bed. The VFCW systems were provided with an inlet and outlet arrangement. The slope of the bottom bed was oriented 1% towards the outlet. The schematic representation of the filter bed is illustrated in Fig. 1.

Table 2: Design Parameters of experimental VFCW units

Parameters	Unit	Value
Length	m	0.65
Width	m	0.45
Depth	m	0.45
Design flow	m^3d^{-1}	0.03
Hydraulic Loading Rate	m d^{-1}	0.1
Hydraulic Retention Time	day	1
Slope	%	1

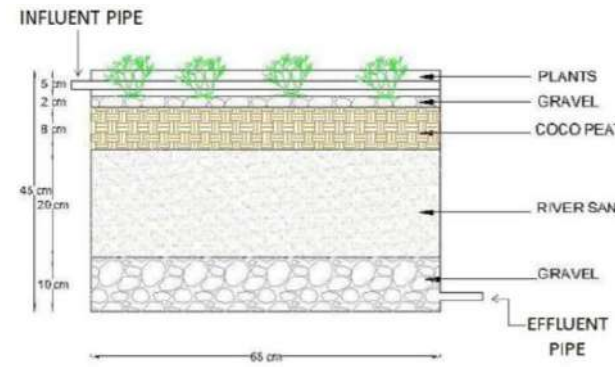

Fig. 1: Schematic representation of the filter bed profile in the VFCW mesocosms.

Plant Species

The fodder grass species used in this study were collected from the forage farm of Kerala Agricultural University (KAU). The grass species planted in the first (VFCW1) unit was Cumbu Napier Hybrid grass (*Pennisetum purpureum)* which is an interspecific hybrid between fodder Cumbu (*Pennisetum glaucum)* and *Napier grass* (*P. purpureum* Schumach). This hybrid variety termed "CO5" was developed by KAU and is regarded as a valuable fodder grass with high biomass productivity. It can be grown perennially in tropical regions and is adapted to the climate of Kerala. The grass is reported to have profuse tillering capacity, high yield potential, quick regeneration, high leaf to stem ratio, high dry matter and crude protein content and is also recognized as a potential biofuel crop. The second experimental (VFCW2) system was planted with Gamba Grass (*Andropogon gayanus*) which is a common perennial forage grass of the tropical regions with short rhizomes. The third experimental (VFCW3) system was planted with Palisade grass (*Urochloa brizantha*) which is a rhizomatous perennial grass and often used as a forage for livestock. The grass is best adapted to humid and sub-humid tropics and survives drought better than many other tropical species of grasses (KAU 2011).

Construction and Operation of VFCW Systems

The stem cuttings of Cumbu Napier hybrid grass and the slips of Gamba and Palisade grass were planted in the wetland bed of VFCW1, VFCW2, and VFCW3 respectively. The plant density provided was 14 plant stems/m^2. Initially, for the establishment of the grasses, they were daily watered

with freshwater for 30 days. Thereafter, an acclimatization period of 30 days was provided by feeding the VFCW systems with municipal wastewater. The treatment of wastewater in the control and planted VFCW systems was further continued for ten months from March 2019 to December 2019. The influent municipal wastewater was initially collected in a feeding tank, which was then fed intermittently to the VFCWs through the inlet. During the entire treatment period, wastewater was fed into the VFCW systems at a HLR of 0.1 m/day. A distribution pipe with perforations at the bottom was used to uniformly distribute the wastewater onto the surface of the wetland bed. The wastewater fed on to the surface of the bed percolated vertically down through the different layers of the filter media and the treated effluent was collected from the outlet. Hydraulic retention time (HRT) of 1 day was provided in the experimental and control VFCW systems. Between successive feeds, a dosing interval of 2 days was given.

Influent and treated wastewater were sampled monthly from the inlet and outlet of the VFCW units and analysed for various physical and chemical parameters. During the entire operational period, the biomass from the planted VFCW systems was harvested four times. The initial harvesting was done after 4 months of planting and the subsequent harvests at an interval of 2 months. The grasses were cut approximately 5 cm above the bed surface. The above-ground biomass yield of the grasses from the planted VFCW systems was estimated and assessed for their nitrogen and phosphorus constituents.

RESULTS AND DISCUSSION

Performance and Treatment Efficiency of VFCW Systems

The efficiency of subsurface constructed wetlands can be expressed in terms of percent concentration reduction and percent mass removal of the pollutants (Kadlec & Wallace 2009, Stefanakis &Tsihrintzis 2012). In this study, the overall performance and treatment efficiency of the different VFCW units were analysed on the basis of average influent and effluent concentrations and percent removal of the pollutants. Fig. 2 presents the removal of pollutants (percent removal efficiency) in the control and planted VFCWs during the entire operational period. The concentrations of the treated effluent from the various systems are given in Table 3.

Turbidity: Turbidity was significantly reduced in the effluent obtained from the control as well as the planted VFCW mesocosms. In all the experimental VFCWs planted with Cumbu Napier grass, Gamba grass and Palisade grass, the mean turbidity removal efficiency observed was greater than 97%. The control system without plants obtained a mean turbidity removal of 87.84%. The removal of turbidity in the various VFCWs during the study period is shown in Fig. 2a.

Suspended solids: The TSS removal efficiency in the various VFCW mesocosms with time is shown in Fig.2b. The VFCW1 system planted with Cumbu Napier grass had a mean TSS removal of 89.80%, whereas for planted systems with Gamba grass (VFCW2) and Palisade grass (VFCW3) it was observed as 78.45% and 89.50% respectively. In the control system, the removal efficiency observed was 65.39%. The mean values of concentrations of TSS in the final effluent treated using control and planted systems are shown in Table 3.

Removal of TSS in CWs can be attributed to sedimentation, filtration, interception, adsorption and root zone treatment. The voids and media grain structure have a significant influence on the trapping of the suspended solids during the flow path (Abdelhakeem et al. 2016, Tsihrintzis 2017, Avila et al. 2019). The substrate materials such as sand, coco-peat,

Table 3: Statistical data of concentration of various physico-chemical parameters in the effluent obtained after treatment from the VFCW systems (mean value ± standard deviation)

Parameters	Unit	Treated effluent from the control system	Treated effluent from VFCWs planted with			Treated effluent quality standards (MoEFCC, India)	
			Cumbu Napier Hybrid grass (VFCW1)	Gamba grass (VFCW2)	Palisade grass (VFCW3)	Into inland surface water	On land for irrigation
pH	---	6.9 ± 0.02	7.1 ± 0.32	7 ± 0.12	7.1 ± 0.32	6-9	6-9
Turbidity	NTU	15.80 ± 1.02	1.55 ± 0.73	3.03 ±1.54	1.70 ± 1.40	---	---
TSS	$mg.L^{-1}$	96.67 ± 11.70	28.37±12.15	60.16 ± 13.85	29.18 ±13.10	100	100
BOD	$mg.L^{-1}$	112.67 ± 5.86	18.20 ±13.94	42.56 ± 27.31	21.83 ± 12.19	30	100
COD	$mg.L^{-1}$	267.02± 12.52	90.23 ± 24.19	119.25 ± 45.07	112.54 ± 39.46	250	250
Nitrates	$mg.L^{-1}$	3.17 ± 0.37	1.05 ± 0.66	1.44 ± 0.67	1.29 ± 0.62	10	Not specified
TN	$mg.L^{-1}$	45.42 ± 3.32	29.06 ± 5.05	30.90 ± 5.98	29.75 ± 6.21	---	---
Phosphates	$mg.L^{-1}$	12.80 ± 0.73	6.61 ± 1.53	7.01 ± 1.63	7.19 ± 1.46	5	Not specified

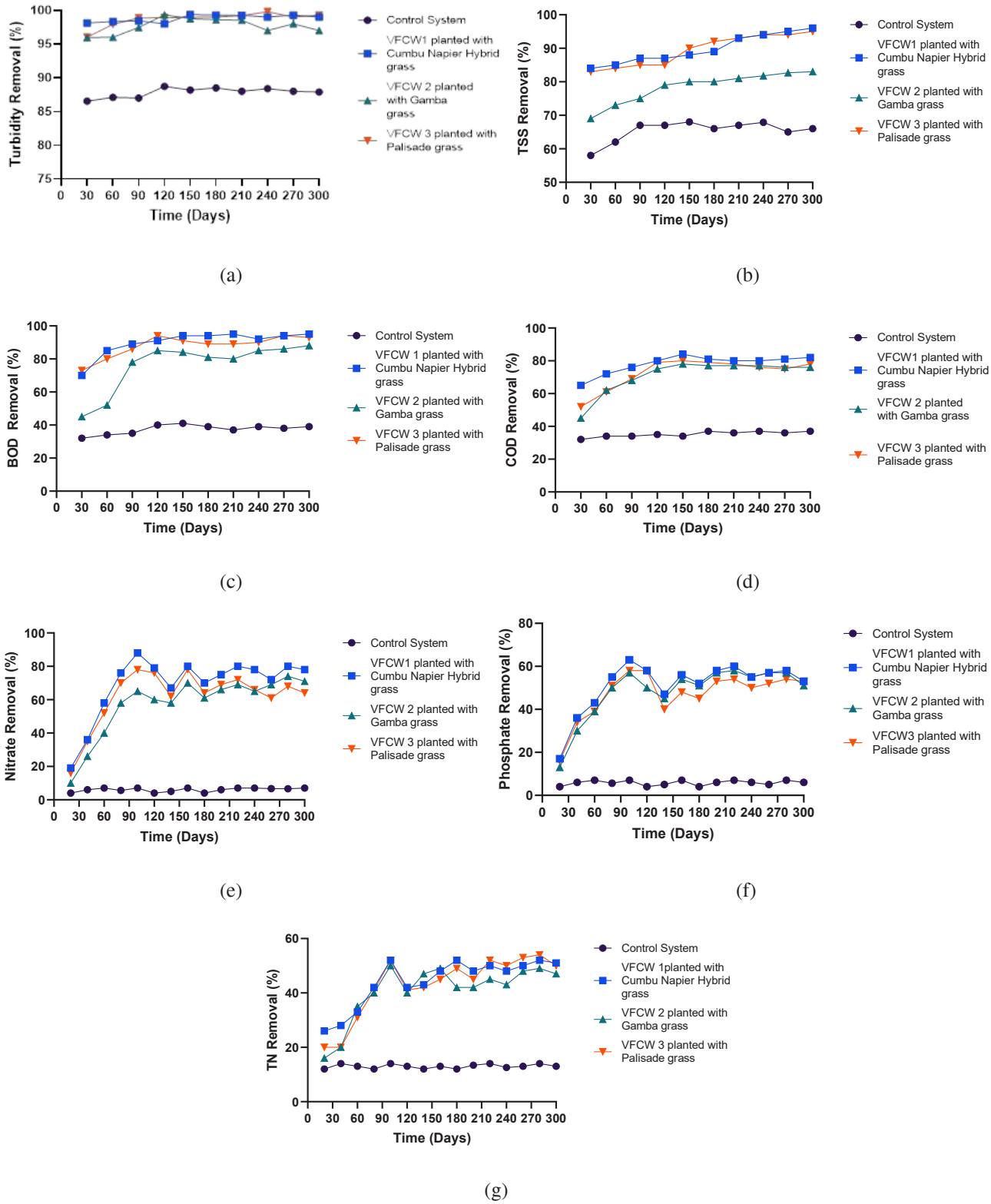

Fig. 2: Removal of various pollutants in the control and planted VFCW systems during the entire operational period (a) Turbidity; (b) TSS; (c) BOD; (d) COD; (e) Nitrates; (f) Phosphates; (g) TN.

and gravel, as well as the roots of the plants, acted as the filters to trap the suspended particles (Brix 1994a, USEPA 2000). Vertical flow systems are highly efficient in removing suspended solids, provided the bed clogging problems are managed through a load and rest operation regime (Kadlec & Wallace 2009). The removal efficiency obtained from the control and planted systems indicated the positive influence of plants in the removal of suspended solids. This signifies the role of root zone treatment and filtration by impaction of suspended particles in the roots and stems of the plants in subsurface flow systems.

Organic matter: In the control unit, the mean BOD removal efficiency observed was only 37.4%. For planted VFCWs, the mean removal efficiency of BOD observed was 89.9%, 76.4%, and 87.9% for systems vegetated with Cumbu Napier Hybrid grass, Gamba grass, and Palisade grass respectively (Fig. 2c). In the VFCW1 using Cumbu Napier hybrid grass, the mean COD removal efficiency was observed as 78.1% while the removal efficiency of other systems planted with Gamba grass and Palisade grass was 71.1% and 72.7%. The control unit attained a mean COD removal of 35.2% (Fig. 2d). In the planted VFCWs, it was observed that the performance improvement in the removal of organic matter occurred after about 90 days of treatment. This trend continued with the growth of the plants and stabilized thereafter, attaining an almost steady removal rate during the study period.

Attached and suspended bacterial growth is mainly responsible for the removal of soluble organic compounds which are degraded aerobically and anaerobically. The removal of BOD in the planted VFCW systems occurs due to the biodegradation of organic matter that takes place in the biofilm together with the roots of plants and stems and the surface of the substrate (UN -HABITAT 2008, Avila et al. 2019). The intermittent flow regime in the VFCWs enables the formation of a vadose zone allowing for diffusion of atmospheric oxygen into the CW media (Kadlec & Wallace 2009).

Nutrient removal: The concentration of nitrates, total nitrogen, and phosphates in the influent and treated effluent were analysed to determine nutrient removal in the planted and control VFCWs. The results showed that the nutrient removals in the planted VFCWs were significantly higher than that in the control system. This indicated the importance of the presence of plants and the uptake of nutrients by them. The VFCW1 using Cumbu Napier Hybrid grass attained high removal of nitrate, phosphate, and TN in comparison to other planted systems. The mean removal efficiencies obtained for the VFCW1 system planted with Cumbu Napier hybrid grass were: Nitrates (69.07%), Phosphates (51.2%) and TN (44.33%). In VFCW2 planted with Gamba grass, the removal efficiencies observed were as follows: Nitrates (57.47%), Phosphates (48.27%), Total Nitrogen (40.87%). For the VFCW3 system planted with Palisade grass, the mean removal efficiencies observed were: Nitrates (62.07%), Phosphates (47%) and TN (43 %). Removal of nitrates, phosphates and TN in the different VFCWs during the treatment period is shown in Figs. 2e, 2f and 2g, respectively.

The processes for nitrogen removal in CWs are varied including volatilization of ammonia, nitrification, denitrification, plant and microbial uptake, ammonification, nitrate reduction to ammonium, anaerobic ammonia oxidation, sorption, desorption, burial, and leaching (UN-HABITAT 2008). But only very few processes eventually remove TN from wastewater while most processes just convert nitrogen into its various other forms. The pH values of the effluent from the planted systems were just above 7, which indicated that conditions were suitable for nitrification within the wetland bed. Ammonia gets oxidized to nitrate with the help of nitrifying bacteria in the aerobic zones of the VFCWs. The oxygen essential for nitrification is supplied by atmospheric transmission and leakage from the roots of the plants. In vertical flow constructed wetlands, very high nitrification proceeds but, due to the absence of entirely anaerobic conditions in the wetland bed, denitrification is very limited in these systems (Vymazal 2007, 2010).

The processes for the removal of phosphorus in constructed wetlands include adsorption, complexation and precipitation, storage, plant uptake (with subsequent harvest) and biotic assimilation (UN-HABITAT 2008, Vymazal 2010). Removal of phosphorus is generally reported to be low in subsurface constructed wetlands unless special media with high sorption capacity are used (Vymazal 2007). The results obtained show that the removal of phosphates is effective in the planted VFCWs when compared to the control system (Fig. 2f).

The grasses were harvested four times during the treatment period and it was observed that during each cutting cycle, the removal of nutrients increased with the growth of the plant and then slightly declined as the plants reached a maturing stage. In order to study the direct contribution of plants in nutrient removal, the harvested above-ground biomass was analysed for nitrogen and phosphorus. The average nitrogen uptake for Cumbu Napier, Gamba and Palisade grass was obtained as 37 $g.m^{-2}$, 11.12 $g.m^{-2}$ and 20.5 $g.m^{-2}$ whereas, the average phosphorus uptake was 2.7 $g.m^{-2}$, 0.81 $g.m^{-2}$ and 1.2 $g.m^{-2}$ respectively. This is supported by the values reported in the literature for above-ground nitrogen ranging from 2-64 g Nm^{-2} and for phosphorus in the range 0.01-19 g P m^{-2} (Vymazal 2007). According to Langergraber

(2005), for a subsurface CW treating municipal water, potential nutrient uptake of about 1.9% of the influent nitrogen and phosphorus loading can be expected.

Comparison of Treatment Efficiency

For all the physical and chemical parameters analysed, the planted VFCW mesocosms obtained high removal efficiency than the control system without plants. The results indicated the significance of plants, their rooting systems and associated microorganisms.

In the case of planted vertical flow wetlands, high pollutant removal efficiency was observed in VFCW1 using Cumbu Napier Hybrid grass when compared to the systems planted with Gamba grass and Palisade grass. The mean pollutant removal efficiency of the VFCWs during the entire study period is shown in Fig. 3.

The phytoremediation potential of the different grasses can be attributed to their root morphology, tillering rate, adaptation to the polluted environment, regeneration capacity, nutrient uptake and biomass productivity. The best removal efficiencies were observed in the system planted with Cumbu Napier hybrid grass with high nutrient uptake and biomass yield. Both Cumbu Napier Hybrid grass and Palisade grass has tolerated very well the treatment conditions showing high vegetative growth and biomass productivity when compared to Gamba grass. Cumbu Napier and Palisade grass have a profuse root system, penetrating deep into the soil and an abundance of fibrous roots spreading into the topsoil horizons. This deep, dense and fibrous rooting system can enhance the root zone treatment by facilitating more microbial fixation sites, sufficient residence time of wastewater, entrapment of suspended particles, large surface area for adsorption of contaminants, assimilation in plant tissues and oxygen for the oxidation of organic and inorganic matter in the rhizosphere. Whereas, Gamba grass has a shallow root system with fibrous roots close to the surface and short rhizomes which can be one of the reasons for its comparatively low removal of organic matter and suspended solids. The biomass yield of Gamba grass was found to be much less when compared to Cumbu Napier and Palisade grass (Fig. 5).

Statistical Analysis

Tukey's multiple comparison test was used for statistical analysis in order to determine significant statistical differences in the performance and efficiency of wastewater treatment between the different groups of treatments (control system, VFCW1, VFCW2, and VFCW3). All statistical analyses were performed at 0.05 significant levels. The statistical analysis was carried out using the software package Graph Pad Prism 8.2.1.

The statistical data of effluent concentration obtained after treatment from the control and planted VFCW systems is given in Table 3. The box-whisker plots for the effluent concentrations of each parameter during the study period are shown in Fig. 4 (a,b,c,d,e,f). The final effluent values were compared with the Indian standards of treated effluent quality for disposal into inland surface water as well as onto land for irrigation (MoEFCC India 2016). Results proved that the final effluent concentration from the control and all the planted VFCWs reached the Indian standards required for disposal onto land for irrigation. The effluent concentration values were also compared with the USEPA guidelines for water reuse (USEPA 2004). The effluent concentration from VFCW1 and VFCW3 conformed to the standards required for non-potable reuse of water according to the guidelines given by USEPA.

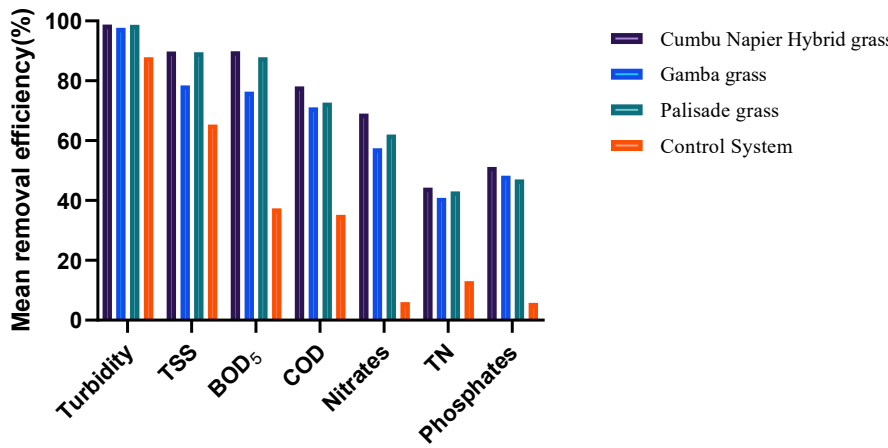

Fig. 3: Mean removal efficiency of pollutants in the different VFCW systems.

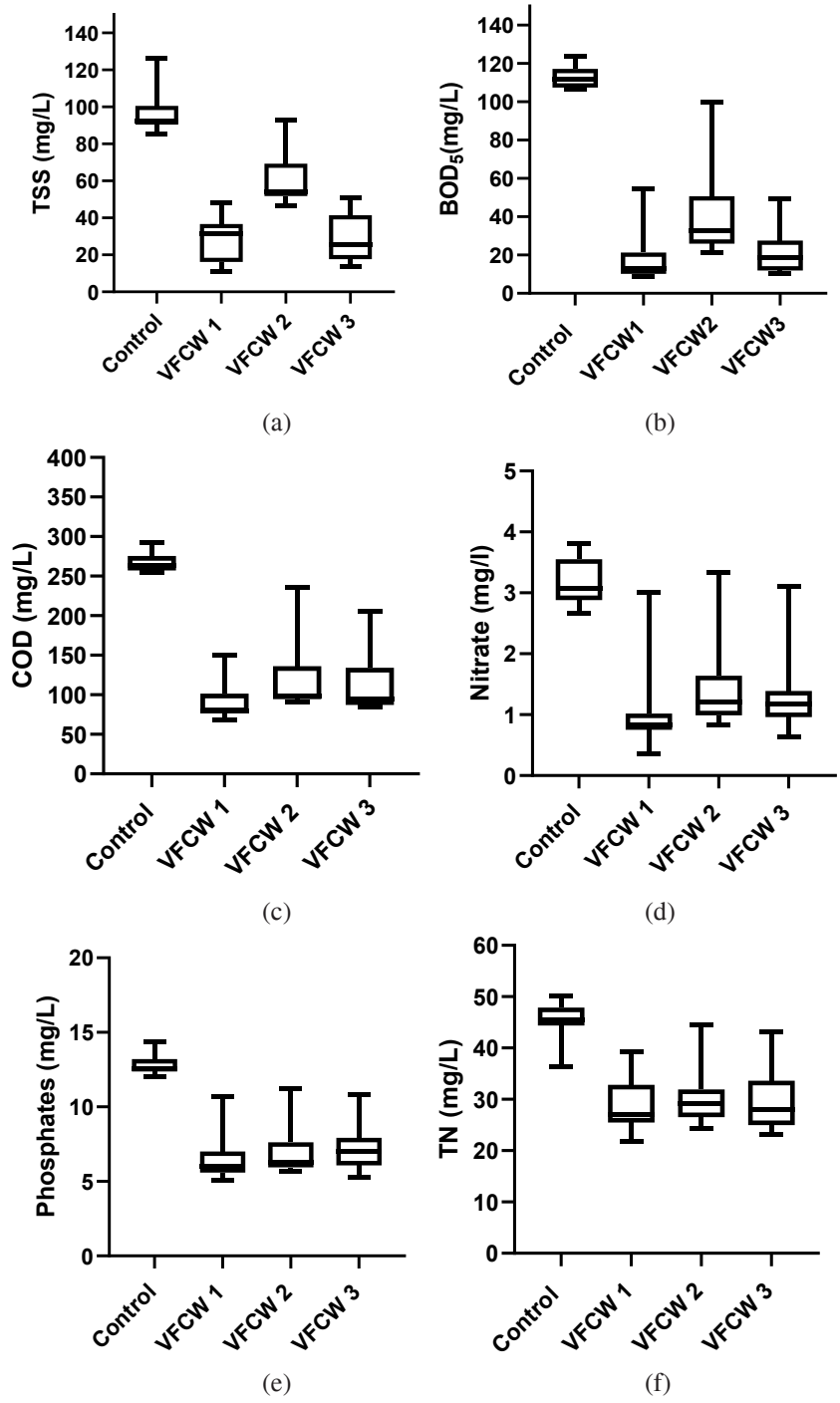

Fig. 4: Box-Whisker graphs for effluent concentrations during the study period for (a) TSS; (b) BOD; (c) COD; (d) Nitrates; (e) Phosphates; (f) TN.

According to statistical analysis for the removal of suspended solids, organic matter and nutrients, there was a significant difference ($p<0.05$) in the treatment between the control system and all the experimental planted VFCW systems (VFCW1, VFCW2, and VFCW3). Among the planted VFCWs, in the removal of TSS, Tukey's multiple comparison results proved that there was a significant difference ($p<0.05$) between VFCW1 and VFCW2 as well as between VFCW2 and VFCW3. But there was no significant difference ($p= 0.999$) between VFCW1 and VFCW3 in the removal of TSS.

Similar results were obtained for the removal of BOD among the planted systems. The VFCW1 and VFCW3 removed BOD efficiently, but there was no significant difference between the two. Whereas significant difference ($p<0.05$) was observed in the treatment between VFCW1 and VFCW2 as well as between VFCW2 and VFCW3.

There was no significant difference amongst the VFCWs planted with different species for the removal of COD, nitrates, TN, and phosphates.

Biomass Yield

During the study period of ten months, the grasses planted in the different experimental VFCW systems were harvested four times. The first cutting was done after 120 days of planting and the subsequent cuttings at an interval of 60 days. The average green biomass yield of Cumbu Napier hybrid grass from the four harvests was 4.5 $kg.m^{-2}$, whereas the average green yield of Gamba grass and Palisade grass were 1.36 $kg.m^{-2}$ and 1.91 $kg.m^{-2}$ respectively. The average dry biomass yield of Cumbu Napier hybrid grass, Gamba grass, and Palisade grass were obtained as 1.5 $kg.m^{-2}$, 0.45 $kg.m^{-2}$, and 0.64 $kg.m^{-2}$ respectively. The biomass yield of Cumbu Napier Hybrid grass was found to be significantly ($p<0.05$) higher than that of Gamba grass and Palisade grass. The average biomass yield of the different grasses obtained from four harvests is presented in Fig. 5.

From the study, it was also observed that the biomass yield of all the grasses declined after each cutting cycle. This can be due to the restrictions in the space and availability of nutrients in the VFCW mesocosms as the plant grows. In this study, the grasses were grown in the VFCW systems without applying any external fertilizer, but the plants extracted the required nutrients and water from the influent wastewater. This is supported by Klomjek (2016) who reported on the feasibility of using Giant Napier grass (*Pennisetum purpureum* cv. King grass) and Dwarf Napier grass (*Pennisetum purpureum* cv. Mott) in vertical flow wetlands for the treatment of swine wastewater in Thailand. The potential of Napier Bajra Hybrid grass (*Pennisetum purpureum X Pennisetum typhoides)* for greywater treatment and its high biomass yield in VFCWs has also been reported by Pillai & Vijayan (2013).

CONCLUSIONS

The study indicated the significance of plant presence and the role of root zone treatment in removing the pollutants in VFCWs. The planted systems using Cumbu Napier Hybrid grass and Palisade grass attained high pollutant removal efficiency, though there was no significant statistical difference between the two. The final effluent from the control and planted systems complied with the Indian standards of treated effluent quality required for irrigation. The green and dry biomass yield of Cumbu Napier Hybrid grass were found to be significantly higher when compared to Gamba grass and Palisade grass.

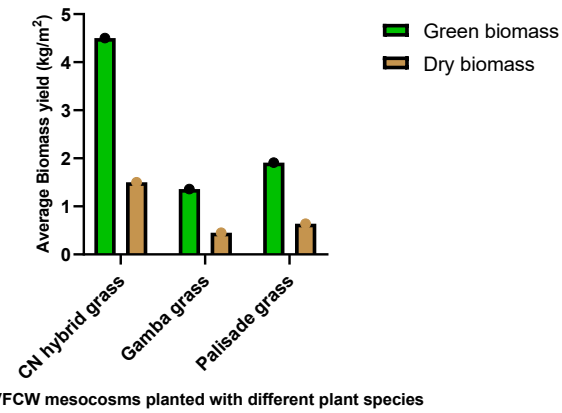

Fig. 5: Average above ground biomass yield from the planted VFCWs.

The VFCWs planted with Cumbu Napier hybrid grass and Palisade grass indicated their suitability to be used as ecological sanitation systems for the decentralized treatment of municipal wastewater and its reuse with regards to subsequent valuable biomass production. In addition to improvement in water quality, the plant harvest provides value-added materials, which can considerably reduce the expenses of treatment. Further investigations are required to investigate the bioethanol production potential of these lignocellulosic grass species.

ACKNOWLEDGEMENT

The authors gratefully acknowledge the Mar Baselios College of Engineering and Technology, Thiruvananthapuram, Kerala, India for providing financial support and facilities required for the study.

REFERENCES

Abdelhakeem, S. G., Aboulroos, S. A. and Kamel, M. M. 2016. Performance of a vertical subsurface flow constructed wetland under different operational conditions. Journal of Advanced Research, 7: 803-814.

Abou-Elela, S. I. and Hellal, M. S. 2012. Municipal wastewater treatment using vertical flow constructed wetlands planted with Canna, Phragmites and Cyprus. Ecological Engineering, 47: 209-213.

Almuktar, S.A., Abed, S.N. and Scholz, M. 2018. Wetlands for wastewater treatment and subsequent recycling of treated effluent: a review. Environmental Science and Pollution Research, 25: 23595-23623.

APHA, 2005. Standard Methods for the examination of water and wastewater, 21st Edn. American Public Health Association, Washington DC.

Avila, F. G., Chavez, J. P., Chimbo, F. Z., Moscoso, S. D., Pino, L. F. and Anazco, A. A. 2019. Performance of Phragmites Australis and Cyperus papyrus in the treatment of municipal wastewater by vertical flow subsurface constructed wetlands. International Soil and Water Conservation Research, 7: 286-296.

Brix, H. 1994 a. Functions of macrophyte in constructed wetlands. Water Science and Technology, 29(4): 71-78.

Brix, H. 1994 b. Use of constructed wetlands in water pollution control: Historical development, present status and future perspectives. Water Science and Technology, 30(8): 209-223.

Brix, H.1997. Do Macrophytes play a role in constructed treatment wetlands? Water Science and Technology, 35(5): 11-17.

Brix, H. and Arias, C.A. 2005. The use of vertical flow constructed wetlands for onsite treatment of domestic wastewater: New Danish Guidelines. Ecological Engineering, 25(5): 491-500.

Caselles-Osorio, A., Villafañe, P., Caballero, V. and Manzano, Y. 2011. Efficiency of mesocosm-scale constructed wetland systems for treatment of sanitary wastewater under tropical conditions. Water, Air and Soil Pollution, 220(1-4): 161-171.

Chelliapan, S., Rani, S. H., Din, M. F. and Yusof, M. B. 2011. Overview of subsurface constructed wetlands application in topical Climates. Universal Journal of Environmental Research and Technology, 1(2): 103-114.

Gross, A., Sklarz, M., Yakirevich, A. and Soares, M. 2009. A recirculating vertical flow constructed wetland for the treatment of domestic wastewater. Desalination, 246(1-3): 617-624.

Hoffmann, H., Platzer, C., Winker, M. and Muench, E. V. 2011. Technology Review of Constructed Wetlands: Subsurface Flow Constructed Wetlands for Greywater and Domestic wastewater treatment. Sustainable Sanitation-Ecosan Program. Retrieved from www.gtz.de/ecosan.

Kadlec, R. H. and Wallace, S. D. 2009. Treatment Wetlands (2nd ed.). CRC Press, USA.

Kadlec, R., Knight, R., Vymazal, J., Cooper, P. and Haberl, R. 2000. Constructed Wetlands for Water Pollution Control: Processes, Performance, Design and Operation, Scientific and Technical Report No.8. IWA, London.

KAU, 2011. Package of Practices and Recommendations: Fodder Crops. Kerala Agricultural University, Thrissur.

Kivaisi, A. K. 2001.The potential for constructed wetlands for wastewater treatment and reuse in developing countries: a review. Ecological Engineering, 16(4): 545-560

Klomjek, P. 2016. Swine wastewater treatment using vertical subsurface flow constructed wetland planted with Napier grass. Sustainable Environment Research, 26: 1-7.

Langergraber, G. 2005. The role of plant uptake on the removal of organic matter and nutrients in subsurface flow constructed wetlands: a simulation study. Water Science and Technology, 15(9): 213-223.

Langergraber, G. and Muellegger, E .2005. Ecological Sanitation-a way to solve global sanitation problems? Environment International, 31: 433-444.

Lee, C.G., Fletcher, T. D. and Sun, G. 2009. Nitrogen removal in constructed wetland systems. Eng. Life Science, 9(1): 11-22.

Ling, T.Y., Apun, K. and Zainuddin, S.R .2009. Performance of pilot-scale biofilters and constructed wetland with ornamental plants in greywater treatment. World Applied Sciences Journal, 6(11): 1555-1562.

Masi, F. 2009. Water reuse and resource recovery: the role of constructed wetlands in the Ecosan approach. Desalination, 246: 27-34.

MoEFCC, 2016. CETP-Gazette. Ministry of Environment, Forests and Climate Change, Government of India. Retrieved 2019, from www.moef.gov.in

Perbangkhem, T. and Polprasert, C. 2010. Biomass production of papyrus (*Cyperus papyrus*) in constructed wetland treating low-strength domestic wastewater. BioResource Technology, 101: 833-835.

Pillai, J. S. and BrijeshNair, A. N. 2015. Subsurface flow constructed wetlands: review of applications and recent developments. Pollution Research, 34(4): 745-755.

Pillai, J. S. and Vijayan, N. 2013. Wastewater Treatment: an ecological sanitation approach in a constructed wetland. International Journal of Innovative Research in Science, Engineering and Technology, 2(10): 5193-5204.

Prochaska, C. A., Zouboulis, A. I. and Eskridge, K. M. 2007. Performance of pilot scale vertical flow constructed wetlands, as affected by season, substrate , hydraulic load and frequency of application of simulated urban sewage. Ecological Engineering, 31: 57-66.

Stefanakis, A. I. and Tsihrintzis, V. A. 2012. Effects of loading, resting period, temperature, porous media, vegetation and aeration on performance of pilot-scale vertical flow constructed wetlands. Chemical Engineering Journal, 181: 416-430.

TMC and KWA, 2016. Service Level Improvement Plan Final, AMRUT, Sewerage System, Thiruvananthapuram Municipal Corporation and Kerala Water Authority. Retrieved 2019, from http://www.corporationoftrivandrum.in/ amruth

Tsihrintzis, V.A. 2017. The use of vertical flow constructed wetlands in wastewater treatment. Water Resources Management, 31(10): 3245-3270.

UN-HABITAT, 2008. Constructed Wetlands Manual. UN-HABITAT Water for Asian Cities Programme Nepal, Kathmandu. Retrieved from www.unhabitat.org.

USEPA, 2000. Manual: Constructed Wetlands Treatment of Municipal Wastewaters. EPA/625/R-99/010, US Environmental Protection Agency, Office of Research and Development, Cincinnati, Ohio.

USEPA, 2004. Guidelines for Water Reuse. EPA/625/R-04/108, US Environmental Protection Agency, Office of Wastewater Management, Washington DC .

Vasudevan, P., Griffin, P., Warrin, A., Thapilayil, A. and Tandon, M. 2011. Localized domestic wastewater treatment: Part I - Constructed wetlands (An overview). Journal of Scientific and Industrial Research, 70(8): 583-594.

Vymazal, J. 2007. Removal of nutrients in various types of constructed wetlands. Science of the Total Environment, 380(1-3): 48-65.

Vymazal, J. 2010. Constructed wetlands for wastewater treatment. Water, 2: 530-549.

Vymazal, J. 2011. Constructed wetlands for wastewater treatment: five decades of experience. Environmental Science and Technology, 45(1): 61-69.

YiChung, W., ChunHan, K., FangChih, C., PenYuan, C., TzuFen, L., YiongShing S. et al. 2011. Bioenergy production potential for aboveground biomass from a subtropical constructed wetland. Biomass and Bioenergy, 35(1): 50-58.

Nature Environment and Pollution Technology
An International Quarterly Scientific Journal

p-ISSN: 0972-6268
(Print copies up to 2016)
e-ISSN: 2395-3454

Vol. 20 | No. 2 | pp. 551-559 | 2021

Original Research Paper

https://doi.org/10.46488/NEPT.2021.v20i02.011

Open Access Journal

Assessment of Water Quality Status of Water Bodies Using Water Quality Index and Correlation Analysis in and Around Industrial Areas of West District, Tripura, India

Bishu Karmakar† and Mahesh Kr. Singh
Department of Chemistry, Tripura University, Suryamaninagar, Tripura, India
†Corresponding author: Bishu Karmakar; bishuk5@gmail.com

Nat. Env. & Poll. Tech.
Website: www.neptjournal.com

Received: 25-04-2020
Revised: 29-06-2020
Accepted: 13-07-2020

Key Words:
Industrialisation
Water quality index
Seasonal variations
Surface water

ABSTRACT

Industrialization, urbanisation and agricultural development cause pollution in water bodies due to the discharge of wastewater directly or indirectly. The present study aims to assess the water quality of water bodies in and around A D Nagar, Badharghat, Dukli and Budhjungnagar Industrial Estates, West Tripura during pre-monsoon and post-monsoon in the year 2016 to 2018. Biological parameters namely DO, BOD, Total Coliform, Faecal Coliform and COD, Physico-chemical parameters namely pH, EC, TDS, Bicarbonates, Chlorides, Sulphates, Total Hardness, Calcium, Magnesium etc. and heavy metals were analysed using standard methods as prescribed by APHA. The analysed parameters were compared with the standards prescribed by BIS. The BOD values for all the water bodies were beyond the prescribed standard limit except the pond located at the southern side of Jutemill, Hapania (S-3) during pre-monsoon season. The Total Coliform values for water bodies located at the eastern and northern side of Badharghat Industrial Estate were beyond the prescribed standard limit. The seasonal variations of water quality have also been observed. Water Quality Index values reflected that the 75% of surface water samples were of poor quality and 25% were of good quality in both the season. Correlation study revealed that positive and significant correlations between the pairs of selected parameters in surface water samples were observed. This study reveals that the surface water of these water bodies needs proper treatment before consumption and it also needs to be protected from the domestic as well as industrial contamination.

INTRODUCTION

Freshwater is essential to support the living creature as it helps in the growth of the entire living organism. The main source of freshwater comprises the lotic (rivers and streams) and lentic (ponds and lakes) water bodies. The rising population, industrialisation and urbanisation change the quality of freshwater. Generally, these resources are degrading gradually due to anthropogenic impacts, lack of awareness among people and lack of legal and institutional framework (Gulia et al. 2017, Pavan & Banerjee 2015). The water bodies, especially ponds are generally small in size but these are valuable sources of water in rural areas for the purpose of domestic, irrigation, fisheries etc. The rainwater is one of the main sources of such village ponds. The water of ponds is being polluted mainly due to discharge of wastes from the residential area, sewage outlets, detergents, automobiles oil waste and industrial wastewater (Ancy & Shaji 2016). In India, approximately 70% of water becomes contaminated due to the release of domestic sewage and industrial effluents into freshwater bodies (Sheetal & Sudan 2017). It is very much important to know the quality of water before its consumption since the consumption of water containing impurities will cause various water-borne diseases. From the literature survey, it has been found that there is no water quality report of freshwater bodies in and around the A. D. Nagar, Badharghat, Dukli and Budhjungnagar industrial estates. Therefore, the present study was designed to assess the status and quality of selected pond water.

STUDY AREA

The West Tripura district is the largest among the eight Districts of Tripura and lies approximately between latitude 23°16' to 2414°' north and longitude 9109°' to 9147°' east having an area of approximately 983.63 sq. km. and population of 9.17 lakhs as per Census India, 2011. The major four industrial estates such as A.D. Nagar (8.41 acres), Badharghat (20.525 acres), Dukli (45.77 acres) and Bodhjungnagar Industrial Estate (535.73 acres) are located in the West Tripura District. The three industrial estates such as A.D. Nagar, Badharghat, Dukli Industrial Estate are located in the urban area nearer to Agartala, State capital and the

distance between these estates are very less. The Bodhjungnagar Industrial Estate is located in a rural area that is far away from the Agartala [TIDC]. The industries such as distillery, rubber-based unit, waste recycling units, thermal power plants, steel rolling plant, food processing, stone crusher, brick kilns, dairy, automobile, pharmaceuticals, rubberwood treatment, spices, tyre & tube, hot mix plant, latex processing, cattle feed etc. are found in the study areas and have high water pollution potential (Singh & Karmakar 2017). The details of sampling locations and study maps are illustrated in Table 1 and Fig. 1 respectively.

MATERIALS AND METHODS

In the present study, the sampling was done during morning hour (8 am to 9 am) in the month April-May (pre-monsoon) and October-November (post-monsoon) in the year 2016 to 2018. The water samples were collected in hard polyethene bottles of 1.5 litre capacity with stopper. Each bottle was washed with 2% nitric acid and then rinsed three times with distilled water (Khwaja & Aggarwal 2016). The samples were collected from three different points and were mixed to prepare an integrated sample. After sample collection, some physical, as well as chemical reactions, would change the quality of the water sample; therefore to minimize this change the samples were preserved as early after the collection. The water samples were preserved by adding chemical preservatives and by lowering the temperature (Kumar et al. 2014). The temperature was measured by thermometer immersed directly in the water body. The parameters like pH, Electrical Conductivity (EC), Total Dissolved Solids (TDS) were measured *in situ* using the potable HI 98130 Combo pH/ EC/ TDS meter (Hanna Instruments). The Dissolved Oxygen was fixed instantly on the spot and analysed immediately

Table 1: Details of sampling locations in and around A D Nagar, Badharghat and Dukli and Budhjungnagar Industrial Estates.

Sample No	Locations	Latitude	Longitude
A D Nagar, Badharghat and Dukli Industrial Estates			
S-1	Pond located at eastern side of Badharghat Industrial Estate	N 23°47′′44′N	E 91°16′′10′ E
S-2	Pond located at northern side of Badharghat Industrial Estate	N 23°47′′51′ N	E 91°16′′12′ E
S-3	Pond located southern side of Jutemill, Hapania	N 23°47′′1′ N	E 91°16′′5′ E
S-4	Pond, Chowhan Para, Dukli	N 23°47′′3′ N	E 91°17′′32′ E
Budhjungnagar Industrial Estate			
S-5	Community Pond, ADC Birbal Para	N 23°53521 N	E 91°22741 E
S-6	Pond, Rajchantai	N 23°53567 N	E 91.22730 E
S-7	Pond, Laxmipur, Dulal Debnath	N 23°51724 N	E 91°20588 E
S-8	Lake, Rajarband	N 23°52550 N	E 91°20348 E

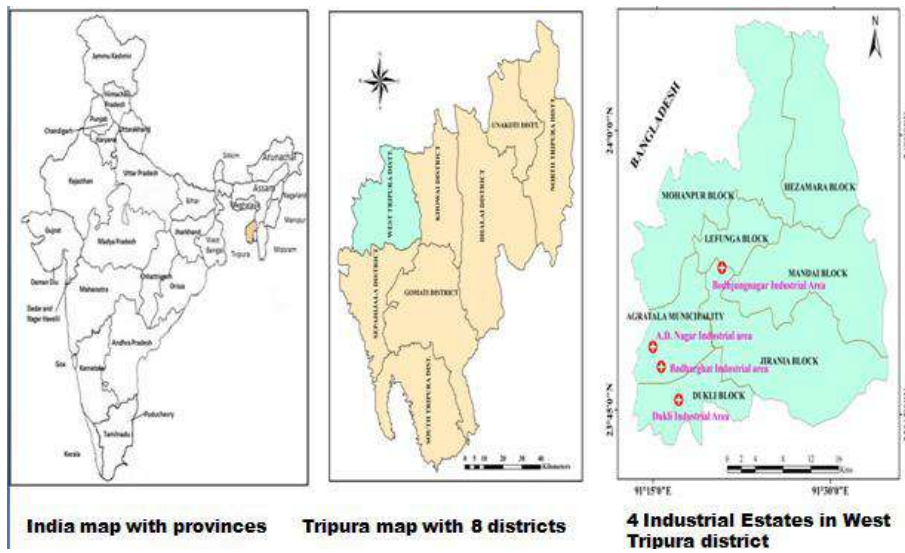

Fig. 1: Map showing the A D Nagar, Badharghat, Dukli and Budhjungnagar Industrial Estates in West Tripura district, India.

as per Wrinkler's method with Azide modification. BOD was measured followed by incubation of BOD bottle at 21°C for 5 days. COD was determined by the potassium dichromate open reflex method. Total Coliform and Faecal Coliform were determined by the Multiple Test Tube method. Turbidity was measured by a Nepthalo turbidity meter. Total Hardness, calcium (Ca) and magnesium (Mg) were measured complex-metrically, chloride (Cl^-) was measured following argento-metric analysis and sulphate (SO_4^{2-}) and phosphate was measured by spectrophotometer (Thermo fisher: Evolution 201), fluoride (F^-) was measured colourimetrically. Heavy metals were analysed using atomic absorption spectrophotometer (Perkin Elmer AAS 700). The other parameters were analysed by using the standard methods Prescribed by APHA (APHA 2005). The quantitative analytical data are presented in Table 2. Water quality indices have been calculated for every selected location of the study areas to assess the drinking water quality. Correlation analysis was also carried out for the water quality data to predict the inter-relationship between the parameters.

Water Quality Index: Water Quality Index (WQI) represents a large number of water quality data to a single numerical value. It signifies the composite influence of various water quality parameters on the overall quality of water (Ramakrishnaiah et al. 2009). In this study, the water quality index has been calculated considering selected important parameters. The WQI has been calculated by using the standards of drinking water quality recommended by the BIS (BIS 1991). Three steps have been followed to calculate WQI. In the first step, selected parameters have been assigned a weight (wi) according to its relative importance in the assessment of drinking water quality. The weightage has been given to the parameters according to their importance in water quality assessment.

In the second step, the relative weight (Wi) is calculated with the help of the following equation:

$$Wi = wi / \sum_{i=1}^{n} wi$$

Where, Wi is the relative weight, wi is the weight of each parameter and n is the number of parameters.

In the third step, a quality rating scale (qi) for each parameter is calculated by the following equation:

$$qi = (Ci / Si) \times 100$$

Where, Ci is the concentration of each chemical parameter in each water sample in mg/L, and Si is the Indian drinking water standard for each chemical parameter in mg/L.

Using the relative weight and quality rating scale values SI for each parameter is calculated. WQI is thus calculated using the equation mentioned below:

$$SI_i = Wi \cdot qi \quad \ldots(1)$$

$$WQI = \Sigma SI_i \quad \ldots(2)$$

Correlation coefficient: Correlation represents the degree of mutual relationship among two variables. The correlation coefficient (r) is the percentage of difference in the dependent variable explained by the independent variables. The positive sign or values signify the positive correlation correspondingly negative values signify the negative correlation between two variables (Magroliya et al. 2018).

The relationship between two parameters was established by calculating Karl Pearson's correlation coefficient, r, by using the formula as given

$$r = \frac{n \Sigma xy - \Sigma x \Sigma y}{\sqrt{n \Sigma x^2 - (\Sigma x)^2} \sqrt{n \Sigma y^2 - (\Sigma y)^2}} \quad \ldots(3)$$

Where r = Karl Pearson's correlation coefficient, y = Dependent variable, x = Independent variable and n = Number of Observations. If the correlation coefficient is closed to +1 or –1 predicts a good relationship between two variables x and y, and the correlation coefficient r = 0 predicts no relationship between two variables. The correlation between the parameters is considered as strong, when it is in the range of +0.8 to 1.0 and - 0.8 to -1.0, moderate when it is having a value in the range of +0.5 to 0.8 and -0.5 to -0.8, weak when it is in the range of +0.0 to 0.5 and -0.0 to -0.5 (Saxena et al. 2016 and Heydari et al. 2013).

RESULTS AND DISCUSSION

The season-wise minimum, maximum, mean and standard deviation values of the water quality parameters are given in Table 2. The results were compared with drinking water standards [BIS].

The pH values varied between 6.27 to 7.36 with a mean of 6.83 during pre-monsoon and 6.01 to 6.86 with a mean of 6.39 during post monsoon seasons. The pH value was in decreasing trend from pre-monsoon to post-monsoon which may be due to the dilution of rainwater (Rashmi 2016). Electrical conductivity is the ability of an aqueous solution to pass electric current which depends on ions and their total concentration, mobility and temperature. The EC values recorded were in the range of 84.67to 224 μScm^{-1} with a mean of 154.17 μScm^{-1} during pre-monsoon and 104 to 190.7 μScm^{-1} with a mean of 153 μScm^{-1} during post-monsoon seasons. The high EC value indicates the presence of salts and ions in higher concentration (Bajpai et al. 2012). Turbidity is the measure of the light scattered

Table 2: Physico-Chemical Characteristics of Pond water in and around A D Nagar, Badharghat, Dukli and Budhjungnagar Industrial Estate *Units of all the parameter are in mg/L except pH, EC (μScm^{-1}) and Turbidity (NTU).

Parameters	Pre monsoon				Post monsoon			
	Min	Max	Mean	SD	Min	Max	Mean	SD
Temperature	26	27	26.46	±0.33	25.17	25.38	25.42	±0.23
pH	6.27	7.36	6.83	±0.49	6.01	6.86	6.39	±0.35
EC	84.67	224	154.17	±50.44	104.7	190.7	153	±32.64
TSS	16	40	26.67	±9.27	19.33	42	30.25	±7.47
TDS	48	134	96.92	±31.35	66.67	130	97.54	±22.30
Turbidity	33.05	197.67	84.46	±53.08	36.34	197.7	88.88	±51.74
TH	38.86	51.31	44.83	±4.48	44.85	59.78	51.87	±4.98
Total N	17.77	41.35	25.86	±8.05	18.73	43.93	27.45	±8.19
DO	5.18	6.45	5.75	±0.38	5.29	6.23	5.66	±0.29
BOD	3.51	4.7	4.08	±0.45	3.77	4.98	4.46	±0.41
COD	24.67	36.67	29.67	±3.89	28	34.67	31.25	±2.51
TC	376.7	520	447.92	±56.96	426.7	540	484.17	±38.70
FC	220	283.3	255.83	±24.48	253.3	353.3	298.33	±38.38
HCO_3	25.84	105.1	54.43	±30.71	29.25	89.26	52.51	±24.28
Cl	13.7	22	19.44	±2.72	15.37	25.14	21.35	±2.96
SO_4	10.89	28.77	19.03	±5.75	13.23	31.19	20.88	±6.15
PO_4	0.14	0.73	0.34	±0.24	0.2	1.1	0.44	±0.33
NO_3	0.25	2.12	0.99	±0.74	0.26	2.66	1.21	±0.98
Na	1.63	25.82	7.18	±8.85	1.79	29.86	8.11	±10.13
K	0.55	15.36	3.39	±5.14	0.62	17.06	3.78	±0.96
Ca	7.12	9.1	8.24	±0.75	7.96	10.64	9.39	±0.98
Mg	4.42	7.23	5.84	±1.08	5.23	7.97	6.82	±1.08
F	0.19	0.4	0.30	±1.08	0.21	0.39	0.32	±0.07
Fe	0.71	3.41	1.68	±0.93	0.76	3.39	1.76	±0.98
Mn	0.1	0.81	0.27	±0.26	0.12	0.79	0.28	±0.24
Pb	0.01	0.026	0.02	±0.01	0.01	0.024	0.02	±0.01
Cd	0.002	0.007	0.004	±0.002	0.001	0.01	.0005	±0.003
As	0.0002	0.019	0.01	±0.01	0.0004	0.027	0.01	±0.01
Cu	0.02	0.05	0.03	±0.01	0.017	0.05	0.03	±0.01
Zn	0.04	0.45	0.19	±0.16	0.04	0.4	0.18	±0.14
Cr	0.02	0.04	0.03	±0.01	0.017	0.037	0.03	±0.01

by suspended particles. The clay, silt, organic matter, phytoplankton and other microscopic organisms cause turbidity in pond water. Turbidity ranged from 33.05 to 197.67 NTU and 36.34 to 197.7 during pre-monsoon and post-monsoon seasons respectively. The maximum turbidity in water was recorded during post monsoon season which may be due to accumulation of sand, clay, silt, dung and various other pollutants along with rainwater from the surrounding area (Kumar et al. 2014). The oxygen can be dissolved in water from air or is formed by the photosynthetic organism like algae and aquatic plants. The oxygen is poorly soluble gas in water and its solubility depend on the temperature of the water and its partial pressure. The minimum and maximum dissolved oxygen were recorded as 5.18 mg/L and 6.45 mg/L respectively during pre-monsoon season. BOD refers to the oxygen used by the microorganism in the aerobic oxidation of organic matter. Therefore with the increase in the amount of organic matter in the water the BOD increases. The BOD value ranged between 3.51 to 4.7 and 3.77 to 4.98 during pre-monsoon and post-monsoon seasons respectively. The BOD values of all the water samples were beyond the standard limit (BIS: 3 mg/L) in both seasons. The BOD value of

post monsoon season was more than pre monsoon season because of the presence of several microbes in water bodies, which accelerate their metabolic activities with the increase in concentration (Kumar et al. 2014). The Total Coliform numbers per 100 mL of water ranged from 376.7 to 520 and 426.7 to 540 during pre-monsoon and post monsoon respectively. Total Coliform count was increased from pre-monsoon to post-monsoon. The high concentration of organic matter of Faecal origin possibly arises from the industrial activities as well as residential inhabitants. Total hardness values ranged from 38.86 to 51.31 mg/L during pre-monsoon and to 44.85 to 59.78 mg/L during post-monsoon. TH is used to describe the effect of dissolved minerals (mostly calcium and magnesium) determining suitability of water for domestic, industrial and drinking purpose attributed to the presence of ferrous iron, bicarbonates, sulphates, chloride and nitrate of calcium and magnesium. High values of hardness are probably due to regular addition of large quantities of detergents used by the nearby residential localities which drain into the water bodies. The hard water can cause indigestion problem and possibilities of forming calcium oxalate crystals in urinary tracts (Deepa et al. 2016). Calcium and magnesium levels were found increased during post monsoon than pre monsoon seasons. The concentration of iron in the water samples varies from 0.71 to 3.41 mg/L and 0.76 to 3.39 mg/L during pre-monsoon and post-monsoon respectively. The recorded iron levels in water bodies were much higher than BIS standard. The high iron content may be due to the influence of rainfall infiltrating and dissolution of iron-bearing mineral rocks and soils which are leached into these water bodies (Sekar & Suriyakala 2016 and Idoko 2010). The considerable content of manganese was recorded in both seasons. The concentration of other heavy metals such as lead, cadmium, arsenic, copper, zinc and chromium were within the prescribed BIS standard limits during both seasons. The remaining parameters were within the BIS standard limit but seasonal variations were observed.

Water Quality Index: The weights assigned and relative weights for each parameter was given in Table 3. The Water Quality Index classification and its values have been presented in Table 4 and Table 5 respectively. The seasonal variation of WQI and Pie diagram of overall WQI in the study areas are shown in Fig. 2 and Fig. 3 respectively.

The WQI values revealed that the surface water quality was found as a poor category in almost all sampling sites in both seasons. It may be due to the ionic leaching, overexploitation and anthropogenic activities such as discharge of effluents from industrial, agricultural and domestic uses (Jena et al. 2013). It is observed that 75% of surface water of the sampling locations are of poor quality and 25 % of surface water are of good quality. This indicates that water samples of the study areas are highly polluted. They are not suitable for drinking purposes and other useful human activities. The water quality index (WQI) indicates that sampling site S-5 is highly polluted compared to others. This site is nearer to the Budhjungnagar Industrial estate and receives more industrial effluents, wastes and sewage water.

Table 3: Relative weight of selected parameters.

Parameters	Standard (BIS)	Weight (wi)	Relative Weight (Wi)
TDS	500	5	0.052083333
HCO_3^{-1}	200	1	0.010416667
Cl^-	250	5	0.052083333
SO_4^{-2}	200	5	0.052083333
NO_3^{-1}	45	5	0.052083333
Ca	75	3	0.03125
Mg	30	3	0.03125
Na	-	4	0.041666667
K	-	2	0.020833333
Fe	0.3	5	0.052083333
Cr	0.05	5	0.052083333
Pb	0.05	5	0.052083333
Cu	0.05	2	0.020833333
Mn	0.1	5	0.052083333
Cd	0.003	5	0.052083333
Zn	5	1	0.010416667
pH	6.5-8.5	4	0.041666667
As	0.05	5	0.052083333
TH	300	3	0.03125
EC	300	1	0.010416667
F	1.0	5	0.052083333
Temp.	40	1	0.010416667
Turbidity	1	1	0.010416667
BOD	3.0	3	0.03125
DO	5.0	4	0.041666667
PO_4	-	1	0.010416667
FC	-	5	0.052083333
COD	-	2	0.020833333
		$\Sigma wi = 96$	$\Sigma Wi = 1$

Table 4: WQI classification and results (Paul et al. 2016).

WQI Value	Water Quality
<50	Excellent
50-100	Good
100-200	Poor
200-300	Very Poor
>300	Unsuitable

Table 5: Water quality status based on WQI.

Location No.	WQI			
	Pre Monsoon	Water Quality status	Post Monsoon	Water Quality status
S-1	124.18	Poor	122.03	Poor
S-2	135.33	Poor	139.46	Poor
S-3	92.41	Good	90.30	Good
S-4	74.79	Good	80.21	Good
S-5	178.59	Poor	182.93	Poor
S-6	119.60	Poor	123.79	Poor
S-7	116.85	Poor	143.48	Poor
S-8	122.17	Poor	139.37	Poor

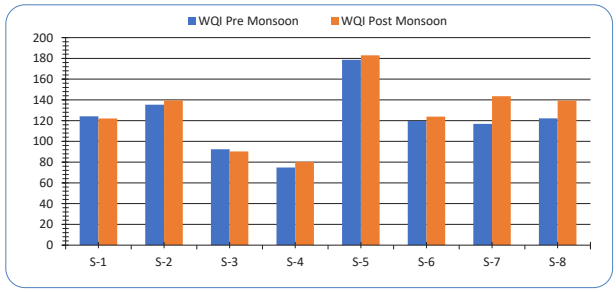

Fig. 2: Seasonal variation of WQI.

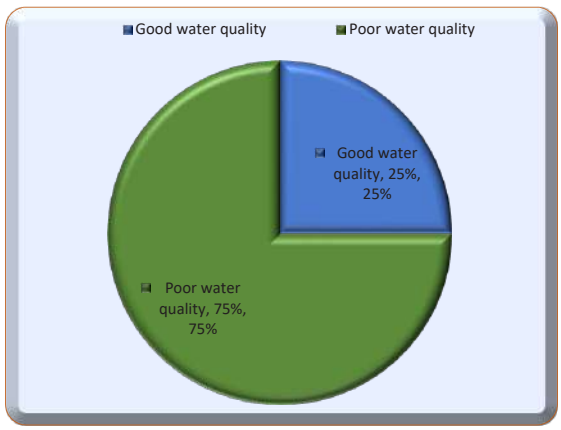

Fig. 3: Pie diagram of overall WQI.

Correlation analysis: The season-wise correlation coefficient (r)values are shown in Table 6 and Table 7 respectively. During pre-monsoon, Electrical conductivity was strongly correlated with TDS (+0.8142). Total Nitrogen was strongly correlated with PO_4(+0.8865) and NO_3(0.9360). HCO_3 was strongly correlated with Na (+0.8372) and K (+0.8073). Sodium was strongly correlated with K (+0.9750). During post monsoon, Electrical conductivity was moderately correlated with TDS (+0.6179), HCO_3 (+0.6573), Na (+0.5997), K (+0.5638) and BOD was strongly correlated with COD (+0.8742) and Total Coliform (+0.8742) and HCO_3 was strongly correlated with Na (+0.8313)). During post monsoon DO was moderately negatively correlated with BOD (-0.5227) which signifies that BOD increases then DO will also decrease (Indu et al. 2015). TDS and EC are positively correlated because electrical conductivity is dependent on the dissolved ions. EC increases with the high value of TDS (Dhamodharan & Shanthakumar 2016). The hardness of water samples is positively correlated with the ions namely bicarbonate, chloride, sulphate, nitrate, sodium, potassium, calcium, and magnesium which determine that the surface water of the study areas are hard water (Sen et al. 2011).

CONCLUSION

The analytical data of water samples reveal that all the parameters show slight seasonal variations. It has been observed that the values of surface quality parameters of the study area are higher during the post-monsoon period reflecting the effect of monsoon and clearly indicated seasonal variation. The water quality indices (WQI) were in the range 74.79 to 182.93 and it is observed that 75% of surface water of the sampling location are of poor quality and 25% of surface water is of good quality. The bacteriological load in the water bodies was the main reason for its poor water quality. The application of the Water Quality Index (WQI) in this study has been found very useful in assessing the overall quality of water. The correlation study on water quality parameters showed that some of the parameters are correlated with each other. It is observed that some of the parameters have a positive or negative correlation between them. This study reveals that the surface water of these waterbody areas needs proper treatment before consumption. These water bodies need to be protected from domestic as well as industrial contamination. The promotion of an awareness campaign among industry owners as well as local people is required to maintain good water quality. The protection, conservation and rejuvenation of water bodies must be treated as an important national as well as international issue. This study may be used by the government policymakers as well as industrial entrepreneurs as baseline information regarding surface water quality in the industrial areas of the West Tripura district to take pollution control measures.

ACKNOWLEDGEMENT

The authors are thankful to the Head, Department of Chemistry, Tripura University for providing infrastructural facilities for carrying out the research work. The authors also acknowledge the help received from the Chairman, Tripura State Pollution Control Board for extending laboratory facilities for analytical works.

Table 6: Correlation coefficients among various surface water parameters during Pre Monsoon Season.

	Temp	pH	EC	TSS	TDS	Turbidity	Hardness	Total N	DO	BOD	COD	TC	FC	HCO_3	Cl	SO_4	PO_4	NO_3	Na	K	Ca	Mg
Temp	1																					
pH	0.2734	1																				
EC	-0.3911	0.4661	1																			
TSS	-0.3273	0.5588	0.9673	1																		
TDS	-0.3608	0.2889	0.8142	0.7132	1																	
Turbidity	-0.5449	-0.7924	-0.2445	-0.2371	-0.1581	1																
Hardness	0.0826	0.1741	0.4473	0.5370	0.3198	0.1687	1															
Total N	-0.4222	-0.8442	-0.3471	-0.3373	-0.3903	0.9006	0.0924	1														
DO	-0.3066	0.6469	0.5483	0.7096	0.2634	-0.1644	0.2366	-0.2712	1													
BOD	-0.4675	-0.1266	0.2611	0.3407	0.1875	0.3178	0.0702	0.3689	0.5148	1												
COD	0.2878	0.1102	0.2725	0.4107	-0.0079	-0.0402	0.4489	0.0460	0.3685	0.4653	1											
TC	-0.5566	0.1494	0.4341	0.5034	0.3431	0.1073	-0.0002	0.1125	0.6970	0.4653	0.300144	1										
FC	-0.0228	0.4939	0.5986	0.7167	0.4689	-0.2527	0.4118	-0.2645	0.7247	0.7048	0.680582	0.750016	1									
HCO3	0.0355	0.8521	0.7175	0.7836	0.5460	-0.6109	0.4223	-0.6138	0.6706	0.2143	0.22875	0.442048	0.738913	1								
Cl	-0.3123	-0.6415	0.2655	0.1587	0.3921	0.5968	0.4548	0.5407	-0.3730	0.1967	0.200678	-0.01085	-0.00198	-0.26989	1							
SO_4	0.1884	-0.3063	-0.7923	-0.8299	-0.7269	0.0448	-0.5227	0.2504	-0.5586	-0.4147	-0.61841	-0.4478	-0.74629	-0.49745	-0.37192	1						
PO_4	-0.3502	-0.6742	-0.3317	-0.2591	-0.4331	0.7364	-0.0325	0.8865	-0.0029	0.6745	0.29997	0.42831	0.066124	-0.45139	0.319356	0.132973	1					
NO_3	-0.3889	-0.9719	-0.3995	-0.4518	-0.3114	0.8922	-0.0733	0.9360	-0.4745	0.2447	-0.03303	-0.0277	-0.4066	-0.79601	0.635848	0.238753	0.784782	1				
Na	-0.3799	0.5685	0.7001	0.6749	0.6013	-0.3919	0.1717	-0.3592	0.5146	0.3227	-0.13898	0.576317	0.522547	0.837223	-0.13354	-0.278	-0.27664	-0.51949	1			
K	-0.3020	0.4693	0.6515	0.6141	0.5978	-0.3569	0.2440	-0.2831	0.3792	0.3411	-0.10147	0.540811	0.527491	0.807374	-0.00908	-0.2486	-0.21841	-0.44068	0.975009	1		
Ca	-0.1444	0.0197	0.3840	0.4156	0.0667	0.2530	0.7696	0.2701	0.0800	-0.1941	0.147782	-0.22352	-0.04722	0.185141	0.398642	-0.17773	-0.00708	0.098703	0.127917	0.147934	1	
Mg	0.1120	0.1120	0.5451	0.5975	0.5668	0.1439	0.8877	0.0503	0.2442	0.3547	0.525888	0.271936	0.64471	0.478925	0.581048	-0.70376	0.034376	-0.04984	0.287492	0.390831	0.46613	1

Table 7: Correlation coefficients among various surface water parameters during Post Monsoon Season.

	Temp	pH	EC	TSS	TDS	Turbidity	Hardness	Total N	DO	BOD	COD	TC	FC	HCO_3	Cl	SO_4	PO_4	NO_3	Na	K	Ca	Mg
Temp	1																					
pH	0.8776	1																				
EC	-0.0016	0.1823	1																			
TSS	0.0240	0.2027	0.8541	1																		
TDS	-0.2637	-0.0613	0.6179	0.6071	1																	
Turbidity	-0.6247	-0.7302	-0.2316	-0.0419	-0.1176	1																
Hardness	0.2839	0.0502	0.3326	0.5605	0.0674	0.3368	1															
Total N	-0.4756	-0.6996	-0.3198	-0.1056	-0.4054	0.8837	0.4070	1														
DO	0.7164	0.5628	-0.4892	-0.5322	-0.7755	-0.4672	-0.1544	-0.1871	1													
BOD	-0.7313	-0.6798	0.2090	0.2735	-0.0681	0.7000	0.1716	0.7325	-0.5227	1												
COD	-0.6913	-0.8016	-0.1559	-0.1822	-0.3809	0.7691	0.0581	0.8518	-0.2582	0.8742	1											
TC	-0.8132	-0.8000	-0.0426	-0.0777	0.0100	0.8757	0.0379	0.6837	-0.5706	0.8742	0.815951	1										
FC	-0.2797	-0.1459	0.1943	0.3683	0.1569	0.5229	0.2543	0.3107	-0.5140	0.5054	0.292303	0.410434	1									
HCO3	0.5186	0.7405	0.6573	0.7145	0.2988	-0.5857	0.2139	-0.5606	0.0328	-0.1880	-0.56905	-0.6172	0.225472	1								
Cl	-0.6605	-0.7298	0.3258	0.4702	0.3630	0.7213	0.5148	0.6723	-0.7734	0.7508	0.599126	0.672245	0.34838	-0.2471	1							
SO_4	0.3392	-0.0343	-0.6527	-0.6358	-0.8007	-0.0334	0.0213	0.3280	0.7088	-0.1423	0.211462	-0.25153	-0.31136	-0.33709	-0.3055	1						
PO_4	-0.4865	-0.5017	-0.3868	-0.2273	-0.5813	0.5633	-0.0794	0.7558	0.0840	0.6970	0.777496	0.513313	0.050141	-0.44091	0.330289	0.291179	1					
NO_3	-0.7001	-0.8580	-0.4047	-0.3152	-0.3376	0.8481	0.0675	0.9014	-0.2357	0.7012	0.891484	0.81313	0.097135	-0.79637	0.62229	0.226597	0.800533	1				
Na	0.1617	0.3132	0.5997	0.7003	0.3587	-0.3686	0.1919	-0.2771	-0.2362	0.1349	-0.2543	-0.43802	0.383879	0.831373	0.07063	-0.20813	-0.26251	-0.52009	1			
K	0.1256	0.2537	0.5638	0.7323	0.4035	-0.3240	0.2524	-0.2119	-0.2767	0.1428	-0.25808	-0.43912	0.320953	0.781625	0.165017	-0.20702	-0.21474	-0.45372	0.98022	1		
Ca	0.2262	0.3295	0.2766	0.6346	0.0215	0.2049	0.5677	0.1953	-0.1398	0.2708	-0.04855	-0.0865	0.71711	0.614497	0.190501	-0.18119	0.059163	-0.1758	0.592967	0.589277	1	
Mg	-0.2208	-0.2208	0.2205	0.3251	0.2009	0.3221	0.8306	0.3770	-0.2242	0.0515	0.076127	0.135315	-0.14548	-0.16435	0.593092	0.036769	-0.12529	0.230456	-0.14194	-0.03543	0.046599	1

REFERENCES

APHA 2005. Standard Method of Examination of Water and Wastewater, 21st Edition, 2005.

Ancy, Mol. P. and Shaji, E. 2016. Physico-Chemical Characteristics of Surface Water Quality of Urban Ponds in Thiruvananthapuram District, Kerala, International Journal of Emerging Trends in Science and Technology, Vol.03, Issue 01, Pages 3431-3437, ISSN 2348-9480.

Bajpai, N., Sikka J. and Sharma, R. 2012. Effect of the Khan river water on chlorophyll content, carotenoids and enzyme activities of Ipomoea fistulosa and Polygonum barbatum. Nature Environ. and Pollution Tech., 11(2): 319-323.

BIS, 1991. Drinking Water Specification: Bureau of Indian Standards; IS: 10500.

Deepa, P., Raveen, R., Venkatesan, P., Arivoli, S. and Samuel, T. 2016. Seasonal variations of physicochemical parameters of Korattur lake, Chennai, Tamil Nadu, India. International Journal of Chemical Studies, 4(3): 116-123.

Dhamodharan, A. and Shanthakumar, S. 2016. Assessment of seasonal variations in surface water quality of Cooum river in Chennai, India - a statistical approach. Global NEST Journal, 18(X).

Gulia, S. K., Ganie, S. A. and Yadav S. S. 2017. Studies on seasonal variations in some physiochemical parameters of the village ponds of Jhajjar District (Haryana), India. Plant Archives, 17(1): 271-281.

Heydari, M. M., Ali, A., Seyed, M.R. and Seyed, Mohammad, A.H. 2013. Correlation study and regression analysis of drinking water quality in Kashan City, Iran, Middle-East. Journal of Scientific Research, 13(9): 1238-1244.

Idoko, O.M. 2010. Seasonal variation in iron in rural ground water of Benue State, Middle belt, Nigeria. Pakistan Journal of Nutrition, 9(9): 1680-5194.

Indu, Abhimanyu Singh & Raveesh Chandra 2015. Study on physico-chemical parameters and correlation analysis of surface water of Nawabganj Lake. International Journal of Current Research, 7(08).

Jena, V., Dixit, S. and Gupta, S. 2013. Assessment of water quality index of industrial area surface water samples. International Journal of Chem. Tech. Research, 5(1): 278-283.

Khwaja, M. Anwar and Aggarwal, V. 2016. Studies on seasonal variation in ground water quality: a statistical approach. Journal of Environmental Research and Development. 11(01).

Kumar, S., Roshni Adiyecha and Tarun Patel 2014. Seasonal variation in the water quality of Lahru pond located in Himachal Pradesh. Int. Journal of Engineering Research and Applications, 4(3): 507-513.

Magroliya, Vasundhara and Trivedi, M. 2018. Statistical correlation and seasonal comparative study of groundwater samples of Jaipur. Environ. Risk Assess. Remediate, 2(3).

Paul, R., Das, S., Nag, S.K. and Singh, M.K. 2016. Deciphering groundwater quality for drinking and irrigation purposes -a study in Lefunga block of West Tripura district, Tripura, India. Journal of Earth Science & Climatic Change, 7(12).

Pavan, M. and Benarjee, G. 2015. Studies on physico-chemical parameters and occurrence of heavy metals in an Urban lake of Warangal district during different seasons. International Journal of Plant, Animal and Environmental Sciences, 5(3).

Ramakrishnaiah, C. R., Sadashivaiah, C. and Ranganna, G. 2009. Assessment of water quality index for the groundwater in Tumkur Taluk, Karnataka State, India. E-Journal of Chemistry, 6(2): 523-530.

Rashmi, S. 2016. Seasonal variation in physico-chemical and biological analysis of Moti Lake, Motihari, East Chamapran, Bihar. Research Journal of Chemical and Environmental Sciences, 4(5).

Saxena, S. and Saxena, U. 2016. Correlation and regression analysis of ground water of Bassi Tehsil, district Jaipur, Rajasthan, India. International Journal of Plant, Animal and Environmental Sciences, 6(1).

Sekar, K. G. and Suriyakala, K. 2016. Seasonal variation of heavy metal contamination of groundwater in and around Udaiyarpalyam taluk, Ariyalur district, Tamil Nadu. World Scientific News, 47-60.

Sen, S., Mrinal, K. P. and Borah, M. 2011. Study of some physico-chemical parameters of pond and river water with reference to correlation study. International Journal of ChemTech Research CODEN(USA): IJCRGG., *3*(4): 1802-1807.

Sheetal, N. and Sudan, S. M. 2017. Water quality assessment of Rajsamand Lake, Rajasthan, India. International Research Journal of Environmental Sciences, 6(6): 22-28.

Singh, M.K. and Karmakar, B. 2017. Assessment of groundwater quality of Budhjungnagar industrial estate and A D Nagar, Dukli & Badharghat industrial cluster of Tripura West District, Tripura State, India by water quality index method. International Journal of Scientific Research in Science and Technology, 3(8).

Nature Environment and Pollution Technology
An International Quarterly Scientific Journal

p-ISSN: 0972-6268
(Print copies up to 2016)
e-ISSN: 2395-3454

Vol. 20 | No. 2 | pp. 561-568 | 2021

Original Research Paper

https://doi.org/10.46488/NEPT.2021.v20i02.012

Open Access Journal

Characterization Studies on Adsorption of Lead and Cadmium Using Activated Carbon Prepared from Waste Tyres

H. Joga Rao†
Department of Chemical Engineering, GMR Institute of Technology, Rajam-532127, Andhra Pradesh, India
†Corresponding author: H. Joga Rao; hjrgmrit@gmail.com

Nat. Env. & Poll. Tech.
Website: www.neptjournal.com

Received: 08-04-2020
Revised: 30-05-2020
Accepted: 04-06-2020

Key Words:
Activated carbon
FTIR
SEM
XRD
Crystalline index

ABSTRACT

The aim of this work was to investigate the utilization of waste tire carbons as a low cost adsorbent for the removal of cadmium and lead ions from an aqueous solution. Surface functional groups would help in getting thorough knowledge about the adsorption capacity of the adsorbent. Thus, activated carbons were prepared from waste rubber tyres and characterized by means of field emission scanning electron microscopy, energy-dispersive X-ray and Fourier transform infrared spectroscopies. The FTIR spectra show that the adsorption peaks are shifted or disappeared and new peaks are formed which was due to the adsorption of lead and cadmium onto the adsorbent surface. It is evident that the characteristic adsorption peak of O-H stretching vibration was shifted from 3900 and 3075 cm^{-1} for lead and the asymmetrical stretching vibration at 3900 cm^{-1} was shifted to 3675 cm^{-1} for cadmium. This shift in peak indicates the interaction between metal ions and –OH groups of adsorbent due to the presence of alcohols, phenols, and carboxylic acid and which shows the decrease of free hydroxyl group content due to the interaction between lead cadmium with –OH groups of the adsorbent. SEM micrograph of adsorbent before adsorption is highly heterogeneous and the surface morphology of the adsorbent is rough. The pores were completely filled with the metal ions after the adsorption of lead and cadmium metals and the pores appear to be smooth. This observation indicates that the metal is adsorbed to the functional groups present inside the pores. From the XRD analysis, the CI index for raw, lead and cadmium loaded activated carbon of waste tyres were found to be 48.91%, 81%, and 54.9% respectively. These values clearly showed the increase in crystalline material present in the adsorbent after the adsorption of metal ions, which was due to the adsorption of metal ions onto the surface of the adsorbent.

INTRODUCTION

Prosperity may serve victory, but at the same time may also serve misfortune. Brisk Industrialization in the early ’70s in India has led to prosperity as per economy and in turn, has also led to hindrance in waste disposal. Deterioration in the environment has created havoc in India. The Industrial Revolution marks a major turning point in history; almost every aspect of daily life was influenced in some way. In particular, average income and population began to exhibit unprecedented sustained growth. The future seemed to be a catastrophe resulting in many unknown diseases created by this Industrial revolution (Akunwa et al. 2014, Nagajyoti et al. 2010). Researchers then focus on this to prevent water pollution and air pollution for improving the quality of water and air. There are several chemical methods for the pre-treatment which may also leave toxic chemicals at the end (Fu et al. 2011, Debasree et al. 2014). The chemical pollutant not only causes safety hazards and medical threats but also disturbs the stability of the environment (Bohli et al. 2013, Amuda et al. 2007). Due to their hazardous effects, persistency and accumulation tendency, heavy metals can pose a risk to human and environmental health (Ku & Peters 1987, Krishnan & Anirudhan 2002). Due to rapid industrialization, toxic metal pollution is increasing causing destabilization in the ecosystem. The trace metals present are divided as heavy metals and light metals based on their densities (Foo & Hameed 2010, Kobya et al. 2005). Toxic heavy metals include chromium, cadmium, mercury, silver, lead and tin, although several nutrient metals, notably zinc, copper and nickel, can also be toxic at elevated concentrations (Momcilovic et al. 2011). If not properly managed, industrial wastewater is responsible for severe damage to the environment and adversely affecting the health of the people. Some of the heavy metal effluents discharged by different industries are shown in Table 1 (Venkatesan & Senthilnathan 2013, Chowdhury et al. 2012). It is of prime importance to prevent the accumulation of heavy metals all above their threshold concentrations. Heavy metals that affect the human organs are shown in Table 2 (Mona et al. 2014, Umar et al. 2015).

Table 1: Heavy metals present in effluents discharged by different industries.

Industry	Heavy metals present in the effluent
Chloro-alkali	Cr, Cd, Cu, Pb, Zn, Hg, Se
Paints and dyes	Cr, Cd, Cu, Pb, Zn, Se
Petroleum refinery	Cr, Cd, Cu, Pb, Zn
Fertilizers	Cr, Cd, Cu, Pb, Zn, Hg, Mn, As
Motor vehicles	Cr, Cd, Pb, Zn, Hg, Se
Mining and metallurgy	Cr, Cd, Cu, Zn, Hg, Se, As

Table 2: Effect of pollutants on human organs.

Heavy metal pollutants	Target organ
Chromium	Stomach, lower respiratory system, skin and lungs
Cobalt	Liver, kidneys and bones
Cadmium	Blood, kidneys, bones and teeth
Nickel	Intestines
Lead	Blood, brain, bones, kidneys and teeth
Mercury	Blood and kidneys
Arsenic	Blood and kidneys

Among all the heavy metals, Pb (II) and Cd (II) are the predominant ones as they are generated from a majority of industrial operations such as metal plating industries, electroplating industries, steel making and alloy industries, petrochemical industries, refining of ores, and battery production (Fu & Wang 2011). In the current years, the need for safe and economical methods for the elimination of heavy metals from contaminated waters has necessitated research interest towards the production of low cost alternatives (Gupta et al. 2011a). The search for new technologies involving the removal of toxic metals from wastewaters has directed attention to adsorption, based on the binding capacities of various materials. In recent years, research interest in the production of low cost activated carbon produced from unused materials has grown. Low cost activated carbons prepared from waste materials containing acidic groups such as hydroxyls and carboxyls were effective in binding metal cations (Girods et al. 2011, Gupta et al. 2011b). With this brief introduction about heavy metal pollution and importance of the lead and cadmium removal in particular from wastewater streams, an attempt has been made to study the use of low cost activated carbon from waste tyres as an adsorbent to treat the simulated metal solutions. In that context, The first aspect is related to the characteristics of the adsorbent such as surface area, porosity and the number of functional groups (Abdulaziz et al. 2013, Umar et al. 2015). The second factor is related to the characteristics of metals that are being sorbed; these include metal speciation in solution. The objective of the present study is to investigate the feasibility of an alternative, low cost and novel adsorbent for efficient removal of cadmium and lead from an aqueous solution. The functional groups on the surface of the adsorbents that contribute to the adsorption are characterized using Fourier transform infrared spectroscopy (FTIR), Scanning Electron Microscope (SEM) and X-Ray Diffraction (XRD) analyses.

MATERIALS AND METHODS

Chemicals and Reagents

The chemicals of AR/LR grades supplied by different standard manufacturing industries are shown in Table 3.

Instrumentation

Orbital shaker, pH Meter with a glass electrode, Filter, Analytical Balance, Atomic Absorption Spectrometer (AAS) (Perkin Elmer model 400A), FTIR, SEM and XRD.

Preparation of Adsorbents

The adsorbents prepared from waste tyres used in the present study were collected in Rajam and Srikakulam, Andhra Pradesh, INDIA. The adsorbents were prepared by carbonization and activation of carbonaceous materials by chemical activation methods (Juan et al. 2013, Nadeem et al. 2006). The dried products of adsorbents were sieved to the desired

Table 3: Chemicals and reagents.

Reagent	Company	Purity	Grade
$Pb(NO_3)_2$	Loba Chemie Pvt. Ltd. Mumbai	99%	AR
$Cd(NO_3)_2$	S. D. Fine Chem. Pvt. Ltd.	99.5%	AR
NaOH	Loba Chemie Pvt. Ltd. Mumbai	98%	AR
HCl	Sarabai Company, India	35%	AR
$ZnCl_2$	Fischer Inorganics Ltd.	70%	LR
H_2O_2	S. D. Fine Chem. Pvt. Ltd.	30%	AR

Fig. 1: Activated carbons prepared from waste tires with an average particle size of 149 µm.

particle size range of 74-177 µm (Fig. 1). SEM micrographs showed the binding of metal ions on the surface of the adsorbents. FTIR analysis indicated the presence of various functional groups such as hydroxyl, carboxyl, amino, etc., on the surface of the adsorbent which was responsible for the adsorption of metals. XRD studies confirmed the crystalline and amorphous nature of the adsorbents.

RESULTS AND DISCUSSION

SEM analysis of Activated Carbon of Waste tyres Adsorbent

SEM is an electron microscope, which provides images of the sample surface by scanning it with a high-energy beam of electrons. The electron interactions with the atoms of the sample produce signals that contain information about the topography, morphology, and composition of the sample surface. The SEM analysis of activated carbon of waste tyres was carried out to study the porosity and surface structure of adsorbent. Fig. 2 shows the SEM micrograph of activated carbon of waste tyres before adsorption. It is evident from the figure that the adsorbent is highly heterogeneous and the surface morphology of the adsorbent is rough. It is clear that the adsorbent has a considerable number of heterogeneous layer pores where there is a good possibility of heavy metal being adsorbed. Figs. 3 and 4 show the SEM micrographs of activated carbon of waste tyres after adsorption of lead and cadmium respectively. It is evident from these figures that the surface texture of activated carbon of waste tyres was completely changed before and after the adsorption of heavy metals. The surface of the metal-loaded adsorbent clearly shows that the surface of the adsorbent dosage was covered with metal ions. The pores were completely filled with the metal ions after the adsorption of lead and cadmium metals and the pores appear to be smooth. This observation indicates that the metal is adsorbed to the functional groups present inside the pores. The surface of the adsorbent became smooth after the adsorption of lead and cadmium metals. Smoothening of the surface is due to the adsorption of metal ions onto the pores of the adsorbent. It may also occur due to the decrease in surface heterogeneity of the adsorbent.

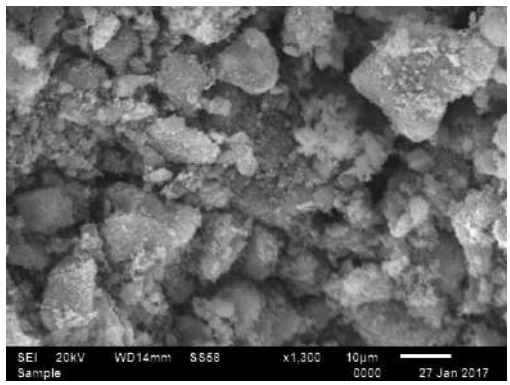

Fig. 2: SEM micrographs of activated carbon of waste tires adsorbent before adsorption.

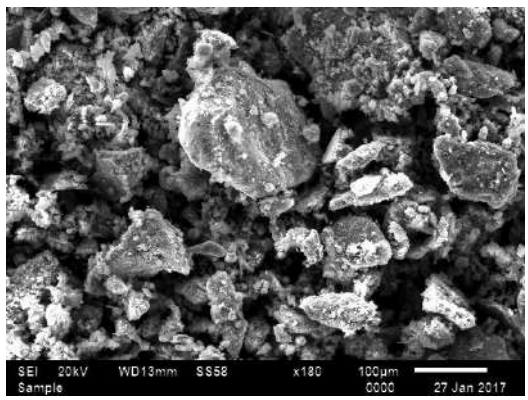

Fig. 3: SEM micrographs of activated carbon of waste tires adsorbent after adsorption with lead.

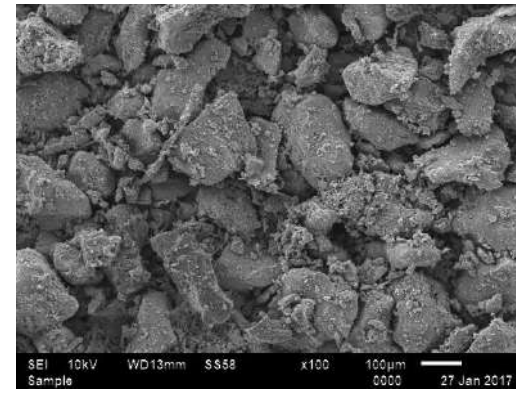

Fig. 4: SEM micrographs of activated carbon of waste tires adsorbent after adsorption with cadmium.

FTIR Analysis of Activated Carbon of Waste tyres Adsorbent

The FTIR is an important tool to identify characteristic functional groups of the adsorbent, which are capable of adsorbing metal ions. The FTIR spectroscopy provides structural and compositional information on the functional groups presented in the sample. The functional groups present in the activated carbon of waste tyres were investigated by FTIR spectra within the range of 400-4000 cm^{-1} wave number. Figs. 5, 6 and 7 show the band positions in the FTIR spectra of the activated carbon of waste tyres before and after lead and cadmium adsorption presented in Table 4. The adsorption spectra (Fig. 6) displayed a number of adsorption peaks indicating the complex nature of activated carbon of waste tyres

and it was composed of various functional groups which are responsible for the binding of lead and cadmium metals. The broad peak at 3000 cm^{-1} corresponds to the C-H, O-H and =C-H stretching vibrations of alkanes, aromatic and carbonyl acids, thus showing the presence of free hydroxyl groups on the adsorbent surface. The peaks at range from 3900 to 3750 cm^{-1} are due to the stretching vibration of O-H. The peak at 2400 cm^{-1} represents the symmetric C-C stretching of the functional group of alkenes present on the adsorbent surface. The sharp peak at 1680 cm^{-1} could be due to the C=C, C=O stretching of alkene, carbonyl and amide stretch. The carboxylic acid groups take part in the adsorption of metal ions from the aqueous solution in addition to the other active sites on the carbon surface. The peak at 1680 cm^{-1} is attributed to the graphite's characteristic sp^2 hybridized C=C aromatic skeletal stretching. The peak present at 1575 cm^{-1} represents the NH (bending) and NO (stretch) stretching vibration of amide and nitro functional groups on the adsorbent surface. While the band at 1350 cm^{-1} corresponds to the C-F, C-N, and N-O, was stretching vibrations of alkyl halide, amine and nitro functional groups on the adsorbent surface. The peaks in the region 1050 and 750 cm^{-1} were associated with adsorption by C-Cl, C-F and C-O groups on the adsorbent surface. It is concluded that the prepared activated carbon material includes oxygen-containing functional groups that provide additional active sites in the adsorption process. The FTIR spectra of activated carbon of waste tyres before and after adsorption of lead (Fig. 5) shows, some of the adsorption peaks are shifted or disappeared and new peaks are formed which was due to the adsorption of lead onto the adsorbent surface. It is evident from this figure that the characteristic adsorption peak of O-H stretching vibration was shifted from 3900 and 3075 cm^{-1} which shows the decrease of free hydroxyl group content due to the interaction between lead and –OH groups of the adsorbent. The peak C-H stretching of alkane at 2860 cm^{-1} was shifted to 2380 cm^{-1}. The peaks at 2400, 1575, 750 cm^{-1} were shifted to 1740, 1500, 860 cm^{-1} due to the presence of carboxyl groups. These changes indicate the interaction between the metal ions and the adsorbent surface. A new peak was formed at 2100 cm^{-1} and 1740 cm^{-1} which indicates the possible involvement of alkyne and ester groups in the adsorption process during the adsorption of metal ions onto the surface of the adsorbent surface. It is apparent from Fig. 7 that different functional groups could be responsible for the adsorption of cadmium. After adsorption of cadmium, the asymmetrical stretching vibration at 3900 cm^{-1} was shifted to 3675 cm^{-1}. This shift in peak indicates the interaction between cadmium and –OH groups of adsorbent due to the presence of alcohols, phenols and carboxylic acid. A new peak at 2830 cm^{-1} was observed due to the chemical reaction involved in the adsorption process. The peak C=O stretch at 1680 cm^{-1} and 1575 cm^{-1} were shifted to 1650 cm^{-1}, and 1500 cm^{-1} due to the presence of carboxyl groups. The peak at 1050 cm^{-1} was shifted to $^{-1}$ and a new peak was observed at 2830 cm^{-1}, which indicates the involvement of alkyne and ester groups in the adsorption process. The shift in

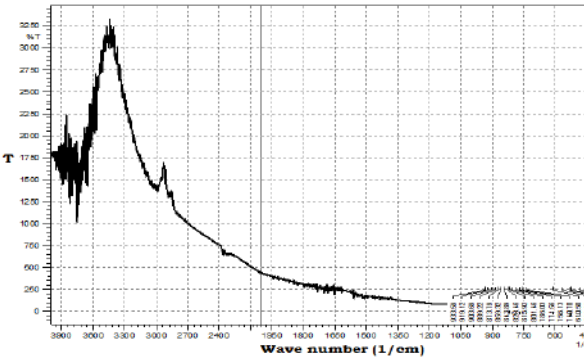

Fig. 5: FTIR spectra of waste tires activated carbon adsorbent before adsorption.

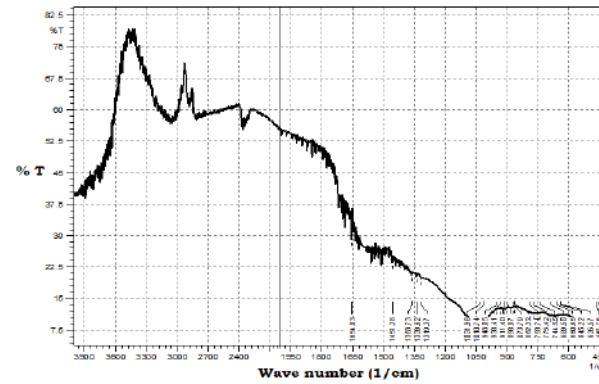

Fig. 6: FTIR spectra of activated carbon of waste tires adsorbent after adsorption of lead.

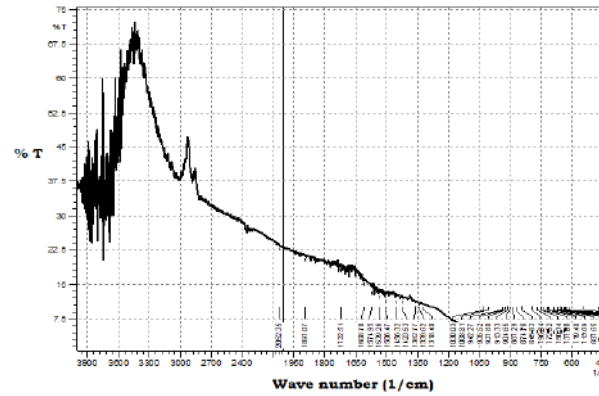

Fig. 7: FTIR spectra of activated carbon of waste tires adsorbent after adsorption of cadmium.

Table 4: FTIR spectra of activated carbon of waste tires adsorbent.

IR frequency range, (cm^{-1})					Type of vibration	Functional groups
WTAC	Lead loaded	Diff.	Cadmium loaded	Diff.		
3900	3900	0	3890	10	OH, Stretch, free	Alcohols
3880			3825	55	OH, Stretch, free	Alcohols
3870			3750	120	OH, Stretch, free	Alcohols
			3675		OH, Stretch, free	Alcohols
3825					OH, Stretch, free	Alcohols
3750					OH, Stretch, free	Alcohols
3000	3075	75	3000	0	C-H, Stretch O-H, Stretch (C=O) =C-H, Stretch	Alkane/Aromatic/Carbonylacid/ Alkene
2850	2860	10	2850	0	C-H, Stretch O-H, Stretch =C-H, Stretch	Alkane/ Carbonyl acid/Aldehydes
	2850		2830		C-H, Stretch O-H, Stretch =C-H, Stretch	Alkane/ Carbonyl acid/ Aldehydes
2400	2380	-20	2390	10	C=C, stretch	Alkene
	2100				Stretch	Alkyne
	1740				C=O, Stretch	Carbonyl/Aldehyde/Ester
1680			1650	30	C=C, stretch C=O, stretch C=O, stretch	Alkene/Carbonyl/Amide
1575	1500	-75	1500	-75	NH, Bending NO, Stretch	Amide/ Nitro
1350					C-F, Stretch C-N, Stretch N-O, Stretch	Alkyl Halide/Amine/Nitro
1050	1050		1040	0	C –Cl, Stretch, =C-H, Bending	Alkyl halide/Alkene
750	860	110	750	0	C –F, Stretch, C-O, Stretch	Alkyl halide/Alcohol

peak values could be due to the formation of a chemical bond between the functional groups present on activated carbon of waste tyres and cadmium. FTIR spectrum of raw activated carbon of waste tyres reveals that there was a large number of hydroxyl and carboxyl groups present on the surface of the adsorbent, which possibly reacted with metal ions in an aqueous solution. These groups may largely contribute to the active adsorption sites required for the adsorption of lead and cadmium metal ions. All these observations indicated the possible involvement of functional groups on the surface of the activated carbon of waste tyres in the adsorption process. These results also indicate that chemisorption could also be involved in the adsorption of lead and cadmium metal ions onto the activated carbon of waste tyres. The FTIR is an important tool to identify characteristic functional groups of the adsorbent, which are capable of adsorbing metal ions.

XRD Analysis of Activated Carbon of Waste tyres Adsorbent

The adsorbent can be crystallographically characterized by means of X-ray diffraction (XRD). Figs. 8, 9 and 10 show the XRD diagram of activated carbon of waste tyres before and after adsorption of lead and cadmium ions. The XRD pattern of raw adsorbent showed a typical spectrum of cellulosic material, with main and secondary peaks at 2θ of 26.42° and 20.6° respectively. The height of the peak and the corresponding position angles are shown in Table 5. The main peak at 26.42° corresponds to the 002 crystallographic planes and it is taken as indicative of the presence of highly organized crystalline cellulose. The secondary peak at 20.6° corresponding to the (101) crystal plane and it is a measure of a less organized polysaccharide structure. The planes at

(002) and (101) indicate the presence of a negative form of cellulose found in the natural source that is cellulose-I polymorphic form. The presence of cellulose indicates the irreversible adsorption of metals through columbic attraction since the negative surface change is acquired by cellulose on contact with water. The cellulose present in the natural materials contains some crystalline oriented zones, which give a certain degree of crystallinity in fibre materials. The crystallinity of the adsorbent strongly depends on the composition of lignin, hemicelluloses and cellulose present in the adsorbent. The crystallinity of the material gives the relative amount of total crystalline material present in cellulose is measured with the help of crystalline index (CI) (Abdulaziz et al. 2013). The CI of the adsorbent was determined using the following equation,

$$\%CI = \frac{I_{002} - I_{am}}{I_{002}} \quad \ldots(1)$$

Where, I_{002} and I_{am} are the intensity of the crystalline peak at (I_{002}, 2θ = 24.1°) and amorphous peak (I_{am}, 2θ = 18.33°) of samples respectively. The CI index for raw, lead and cadmium loaded activated carbon of waste tyres were found to be 48.91%, 81% and 54.9% respectively. These values clearly showed the increase in crystalline material present in the adsorbent after the adsorption of metal ions, which was due to the adsorption of metal ions onto the surface of the adsorbent. These results confirm the SEM micrographs of raw, lead and cadmium-loaded adsorbent. It is evident from the XRD results that significant differences were occurred in the peak intensities for the adsorbent before and after the adsorption of lead and cadmium metals. The peaks obtained from the samples appeared to be largely amorphous. However, some peaks are characteristic of cellulose crystallinity. The results also indicate that the intensity of the peaks was also decreased considerably after the adsorption of lead and cadmium metals. This is due to the destruction of the crystalline structure of activated carbon of waste tyres with the adsorption of metals. The XRD pattern of raw activated carbon of waste tyres showed a characteristic peak at a 2θ value of 26.42°. After the adsorption, this peak was slightly moved to a lower angle at 26.38° for lead, which indicates the adsorption of metal ions onto the surface of activated carbon of waste tyres. The secondary peak at 20.6° for raw adsorbent was slightly moved to a lower angle of 20.75° after the adsorption of lead and cadmium loaded adsorbent dosage. The peaks at 25.1, 29.1, 36.3, 42.1, 47.3, 49.8 and 49.9° corresponding to the peaks height (count/sec) at 105.4, 102.98, 81.83, 139.2,104.8, 159.88 and 147.51 were

Table 5: XRD details of activated carbon of waste tires adsorbent before, and after adsorption of lead and cadmium.

Count/ sec	Activated carbon of waste tires (ACWT)		
	Peak position (2θ) before adsorption	Peak position (2θ) by lead loaded	Peak position (2θ) by cadmium loaded
76.49	6.1541	18.7319	6.3167
41.53	11.4603	19.6817	19.7253
52.31	19.5149	20.7562	20.6987
239.36	20.6081	25.1464	25.1608
105.44	25.1321	26.3881	26.4291
857.57	26.4276	29.3639	29.3962
102.98	29.1980	31.0904	30.9201
67.44	30.8530	36.2937	36.3522
34.22	33.1397	39.2956	39.3081
81.83	36.3922	42.2949	42.2426
77.67	39.2136	45.5652	45.6479
139.26	42.1841	49.8820	47.4495
38.37	43.0645	54.7764	49.9305
38.55	45.5594	59.7418	54.6937
104.88	47.3470	65.3000	59.7431
159.88	49.8569	68.0305	67.9831
147.51	49.9959	73.3603	75.5485
25.42	54.7354	81.1832	79.7290

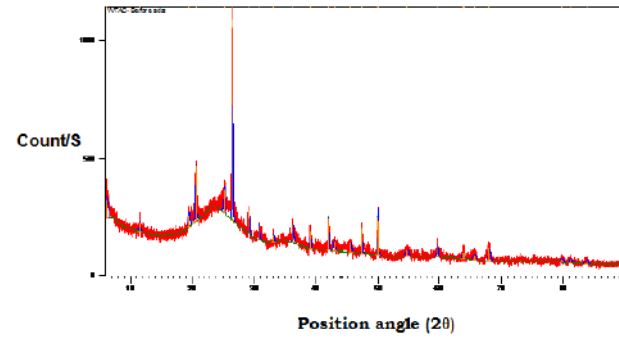

Fig. 8: XRD of activated carbon of waste tires adsorbent before adsorption.

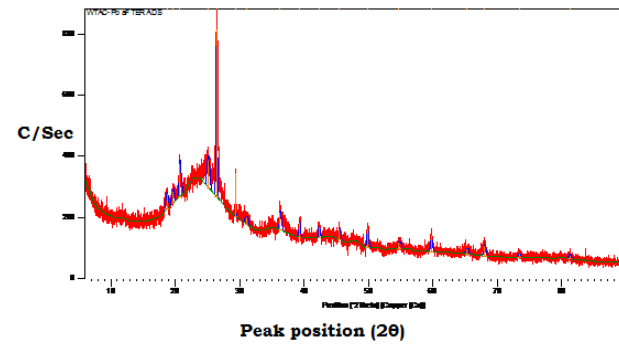

Fig. 9: XRD of activated carbon of waste tires adsorbent after adsorption of lead.

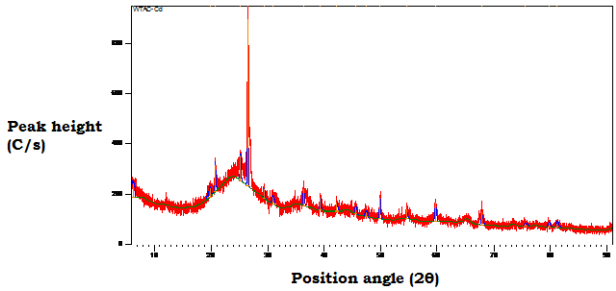

Fig. 10: XRD of activated carbon of waste tires adsorbent after adsorption of cadmium.

slightly changed to 25.1, 29.3, 36.2, 49.8 and 59.7° for lead adsorption and 25.16, 36.35, 39.3, 49.9, 59.74 and 67.98° for cadmium adsorption. New peaks were also observed for lead and cadmium-loaded adsorbent. The shift in peaks, disappearance of peaks and formation of new peaks after adsorption of lead and cadmium samples was due to the chemical reaction involved during the process. Thus, XRD results confirmed that significant interactions were occurring between metal ions and adsorbent surface.

CONCLUSIONS

Activated carbon was prepared from waste rubber tyres and characterized by means of field emission scanning electron microscopy, energy-dispersive X-ray and Fourier transform infrared spectroscopies.

The functional groups present on the adsorbent the corresponding infrared absorption frequencies are before adsorption at optimum conditions show the broad peak at 3000 cm^{-1} corresponds to the C-H, O-H and =C-H stretching vibrations of alkanes, aromatic and carbonyl acids, thus showing the presence of free hydroxyl groups on the adsorbent surface.

It is evident that the characteristic adsorption peak of O-H stretching vibration was shifted from 3900 and 3075 cm^{-1} for lead and the asymmetrical stretching vibration at 3900 cm^{-1} was shifted to 3675 cm^{-1} for cadmium. This shift in peak indicates the interaction between metal ions and –OH groups of adsorbent due to the presence of alcohols, phenols and carboxylic acid and which shows the decrease of free hydroxyl group content due to the interaction between lead cadmium with –OH groups of the adsorbent.

The shift in peak values could be due to the formation of a chemical bond between the functional groups present on activated carbon of waste tyres with metal ions.

FTIR spectrum of raw activated carbon of waste tyres reveals that there was a large number of hydroxyl and carboxyl groups present on the surface of the adsorbent, which possibly reacted with metal ions in an aqueous solution. These results also indicate that chemisorption could also be involved in the adsorption of lead and cadmium metal ion onto the activated carbon of waste tyres.

It is clear that the adsorbent has a considerable number of heterogeneous layer pores where there is a good possibility of heavy metal being adsorbed. The surface of the adsorbent became smooth after the adsorption of lead and cadmium metals. Smoothening of the surface is due to the adsorption of metal ions onto the pores of the adsorbent. It may also occur due to the decrease in surface heterogeneity of the adsorbent.

It is evident from the XRD results that significant differences were occurred in the peak intensities for the adsorbent before and after the adsorption of lead and cadmium metals. The peaks obtained from the samples appeared to be largely amorphous. However, some peaks are characteristic of cellulose crystallinity. The results also indicate that the intensity of the peaks was also decreased considerably after the adsorption of lead and cadmium metals. This is due to the destruction of the crystalline structure of activated carbon of waste tyres with the adsorption of metals.

REFERENCES

Abdulaziz, A., Saadi, A., Saleh, T.A. and Vinod Kumar, G. 2013. Spectroscopic and computational evaluation of cadmium adsorption using activated carbon from Rubber tires. Journal of Molecular Liquids, 188: 136-142.

Akunwa, N.K., Muhammad, M.N. and Akunna, J.C. 2014. Treatment of metal-contaminated wastewater: A comparison of low-cost biosorbents, J. Environ. Manage., 146: 517-523.

Amuda, O. S., Giwa, A. A. and Bello, I. A. 2007. Removal of heavy metal from industrial wastewater using modified activated coconut shell carbon. *Biochem. Eng.* J., 36: 174-181.

Bohli, T., Ouederni, A., Fiol, N. and Villaescusa, I. 2013. Single and binary adsorption of some heavy metal ions from aqueous solutions by activated carbon derived from olive stones. Desalination Water Treat., 70: 1082-1088.

Chowdhury, Z.Z., Zain, S.M., Khan, R.A., Rafique, R.F. and Khalid, K. 2012. Batch and fixed bed adsorption studies of lead (II) cations from aqueous solutions onto granular activated carbon derived from Mangostana garcinia shell. Bioresources, 7: 2895-2915.

Debasree, P., Umesh, M. and Swarup, B. 2014. A comprehensive review on Cd (II) removal from aqueous solution. Journal of Water Process Engineering, 2:105-128.

Foo, K.Y. and Hameed, B.H. 2010. Insights into the modeling of adsorption isotherm systems. Rev. Chem. Eng., 156: 2-10.

Fu, F. and Wang, Q. 2011. Removal of heavy metal ions from wastewaters: a review. J. Environ. Manage., 92: 407-418.

Girods, P., Dufour, A., Fierro, V., Regime, Y., Rogaumea, C. and Zoulaliana, A. 2011. Activated carbons prepared from wood particleboard wastes: Characterization and phenol adsorption capacities. J. Hazard. Mater., 188: 917-921.

Gupta, V.K., Bina, G., Arshi, R., Shilpi, A. and Arunima, N. 2011a. A comparative investigation on adsorption performances of mesoporous activated carbon prepared from waste rubber tire and activated carbon for a hazardous azo dye-Acid Blue 113. J. Hazard. Mater., 186: 891-901.

Gupta, V.K., Bina, G., Arshi, R., Shilpi, A. and Arunima, N. 2011b. Pesticides removal from wastewater by activated carbon prepared from waste rubber tire. Wat. Res., 45: 4047-4055.

Juan, D.M., Neus, P., Ramon, M., Tomas, G., Maria Victoria, N., and Ana, M.M. 2013. Waste tyre pyrolysis-a review. Renewable and Sustainable Energy Reviews, 23: 179-213.

Kobya, M., Demirbas, E., Senturk, E. and Ince, M. 2005. Adsorption of heavy metal ions from aqueous solutions by activated carbon prepared from apricot stone. Bioresour. Technol., 96: 1518-1521.

Krishnan, K. A. and Anirudhan, T.S. 2002. Uptake of heavy metals in batch systems by sulfurized steam activated carbon prepared from sugarcane bagasse pith. Ind. Eng. Chem. Res., 41: 5085-5093.

Ku, Y. and Peters, R.W. 1987. Innovative uses from carbon adsorption of heavy metals from plating wastewaters: Activated carbon polishing treatment. Environ. Prog., 6(2): 119-124.

Momcilovic, M., Purenovic, M., Bojic, A. and Zarubica, A., Randelovid, M. 2011. Removal of lead (II) ions from aqueous solutions by adsorption onto pinecone activated carbon. Desalination Water Treat., 276: 53-59.

Mona, K., Ahmad, K. and Hanafy, H. 2014. Heavy metals removal using activated carbon, silica and silica activated carbon composite. Energy Procedia, 50: 113-120.

Nadeem, M., Mahmood, A., Shahid, S. A., Shah, S. S., Khalid, A. M. and McKay, G. 2006. Sorption of lead from aqueous solution by chemically modified carbon adsorbents. J. Hazard. Mater., 138: 604-613.

Nagajyoti, P.C., Lee, K.D. and Sreekanth, T.V.M. 2010. Heavy metals, occurrence and toxicity for plants: a review. Environ. Chem. Lett., 8(3): 199-216.

Umar, I.G., Emmanuel, O. and Abdul, H.A. 2015. Adsorption of aqueous Cd (II) and Pb (II) on activated carbon nanopores prepared by chemical activation of doum palm shell. Springer Plus, 4: 458.

Venkatesan, G. and Senthilnathan, U. 2013. Adsorption batch studies on the removal of cadmium using wood of derris indica based activated carbon. Research Journal of Chemistry and Environment, 17(5).

Nature Environment and Pollution Technology
An International Quarterly Scientific Journal

p-ISSN: 0972-6268
(Print copies up to 2016)
e-ISSN: 2395-3454

Vol. 20 | No. 2 | pp. 569-578 | 2021

Original Research Paper

https://doi.org/10.46488/NEPT.2021.v20i02.013

Open Access Journal

Isolation and Characterization of Multiple Drug Resistant Human Enteric Pathogens from Sewage Water of Delhi

Rudrangshu Chatterjee*, Dushyant Singh, Swati Tripathi*, Abhishek Chauhan***†, M.L Aggarwal** and Ajit Varma***

*Amity Institute of Microbial Technology, Amity University, Sector-125, Noida, India
**Shriram Institute for Industrial Research, 19, University Road, Delhi-110007, India
***Amity Institute of Environmental Toxicology, Safety and Management, Amity University, Sector-125, Noida, India
†Corresponding author: Abhishek Chauhan; akchauhan@amity.edu

Nat. Env. & Poll. Tech.
Website: www.neptjournal.com

Received: 19-06-2020
Revised: 10-09-2020
Accepted: 16-09-2020

Key Words:
Sewage water
Antibiotics
Multidrug resistant bacteria
Human enteric pathogens

ABSTRACT

Antibiotic resistance is one of the major problems in the medical world, and the sewage waters are the primary habitats to harbour antibiotic resistance bacteria (ARB) especially multi-drug resistance (MDR) human enteric pathogens. The present study dealt with isolation, identification and characterization of human enteric pathogens showing resistance against ten different commonly prescribed antibiotics. These bacterial strains were isolated from different sewage treatment plants located in the suburb of Delhi. Initially, samples were analysed for the presence of pathogenic human enteric bacteria through morphological, biochemical and molecular analysis. Further susceptibility patterns of these isolates were studied towards clinically significant antibiotics. Doxycycline and Metronidazole were found to be most inert antibiotic as it was ineffective against all isolated enteric pathogens, whereas Meropenem was found to be most promising antibiotic. As the resistance of these microorganisms is evolving day by day, proper steps should be taken to prevent it.

INTRODUCTION

Pollution in source water is a problem in developing as well as in all developed countries. In the past few decades, uncontrolled urbanization has caused a serious pollution problem due to the disposal of sewage and industrial effluents to water bodies. Effluent wastewater treatment is the process of removing contaminants from wastewater and household sewage, both runoff (effluents) and domestic. It includes physical, chemical, and biological processes to remove physical, chemical and biological contaminants. Sewage water can be polluted by a wide variety of substances, including pathogenic microorganisms, plant nutrients, toxic chemicals, sediments, heat oil, and radioactive substances (Sharpe 2003, Ishak et al. 2011). Sewage water is one of the major sources of human enteric pathogenic bacteria. Sewage contains human faeces and therefore contains human enteric pathogens i.e. *Salmonella enterica, Salmonella enteritidis, Salmonella typhimurium, Shigella dysenteriae, Enterobacter* spp., *Vibrio* spp. These pathogens are responsible for serious gastrointestinal illness which is a significant cause of waterborne health epidemics. Gastrointestinal disease is considered the third most common cause of death in the world (Hellier & Williams 2007). For combating against these pathogens, antibiotics are generally used which has led to the evolution of multidrug-resistant strains of these pathogens. There is a great need to discover novel antibiotics due to the wide-spread emergence of resistance among pathogenic bacteria against available antibiotics (Goyal et al. 2010, Chauhan et al. 2015).

Although the discovery of antimicrobials leads to various expectations, it has been influenced by the emergence of resistant bacterial strains against antibiotics. It has been reported that the irrigation water system also has been contaminated by these multidrug-resistant bacteria which have a chance to enter in our food chain directly. The presence of multidrug-resistant enterobacter and enteric pathogens has been regarded as a serious problem for a community (Cabrera et al. 2004, Chitnis et al. 2004, Danchaivijitr et al. 2005). A significant increase of Multiple Antibiotic Resistant (MAR) bacteria is observed in various aquatic systems. Human infections caused by such bacteria could be difficult to treat with drugs (Chandrasekaran et al. 1998, Dicuonzo et al. 2001, Lopes et al. 2005).

The aim of this study was to evaluate the antibiotic resistance patterns of human enteric pathogenic bacteria which were isolated from different sewage waters from

the suburb of Delhi. The study involves; (a) Collection of water samples from different sewage treatment plants (b) Isolation and identification of human enteric pathogens from sewage water samples (c) Determination of susceptibility and resistance pattern against ten different antibiotics by agar well diffusion assay (d) Interpretation of the data generated to determine the antibiotic resistance patterns of the isolated bacteria for the benefit of human welfare by increasing general awareness among the people.

MATERIALS AND METHODS

(a) Collection of Water Samples

1lt capacity of bottles was used to collect samples from 10 sewage treatment plants from different locations of Delhi (Table 1). Bottles used were sterilized using gamma radiations. Samples after collection were marked with SW01 to SW10. Sample collection and transportation to the laboratory were performed aseptically. Samples analysis was done within 6 hrs of collection.

(b) Isolation and Identification of Human Enteric Pathogens

Detection of *Escherichia* sp: Membrane filter of 0.45µ was passed with 250mL water sample and placed in MacConkey broth. Eosin methylene blue agar and Mac Conkey agar were streaked for confirmatory identification. Characteristic pink colonies on the former and green metallic colonies on the latter are observed. Further confirmation was done by Gram's staining and HiMedia IMViC biochemical kit for *E. coli* as per IS: 5887(part-1)1976, Reaffirmed 2018.

Detection of *Salmonella* sp: Membrane filter of 0.45µ was passed with 250mL water sample and placed in Buffer peptone water incubating at 37°C for 24 hours. 10mL of Rappaport Vassiliadis medium is inoculated with 0.1mL above grown sample and incubated at 42°C for 24 hours. Further streaking is done on Brilliant green agar and Bismuth sulphide agar where the former is observed for characteristic pink colonies and the latter for black metallic sheen colonies with H_2S. Further confirmation was done by Gram's staining and HiMedia IMViC biochemical kit for *Salmonella* as per IS: 5887(Part-3) 1999, Reaffirmed 2018.

Detection of *Pseudomonas* sp: Membrane filter of 0.45µ was passed with 250mL water sample and placed in Cetrimide broth and then incubated at 37°C for 48 hours. Cetrimide agar Plates were streaked and observed for characteristic green colonies and further confirmation was done by Gram's staining and Biochemical test as per IS: 13428:2005 (Annexure-D).

Detection of *Vibrio* sp: Membrane filter of 0.45µ was passed with 250mL water sample and placed in alkaline peptone water and incubated at 37°C for 24 hours. TCBS Agar is streaked and further confirmed by HiMedia IMViC biochemical kit and Gram's staining as per IS: 5887(Part-5) 1976, Reaffirmed 2018.

Detection of *Shigella* sp: Membrane filter of 0.45µ was passed with 250mL water sample and placed in Nutrient broth. Deoxycholate citrate agar is streaked for further confirmation and observed for characteristic colonies such as small opaque colonies. Further confirmation was done by HiMedia IMViC biochemical kit and Gram's staining for *Shigella* sp as per IS: 5887(part-7)1976, Reaffirmed 2018.

(c) Molecular Identification

Further identification of bacterial isolates using 16srRNA sequencing is done. The sequence reaction using the Sanger dideoxy sequencing kit was performed following the manufacturer's instructions. Basic Local Alignment Search Tool (BLAST) algorithm is used for alignment of trimmed nucleotide sequences of different bacterial iso-

Table 1: Microbiological profiling of sewage water.

S.No.	Sampling Location	Sample Code	Pathogen identified with accession number
1.	Noida Industrial Effluents	SW01	*Salmonella enterica*, AE006468.2 *Escherichia albertii*, NR_025569
2.	Badarpur Power out	SW02	*Pseudomonas stutzeri*, NR_113652.1
3.	Badarpur Power in	SW03	*Salmonella typhimurium*, AE006468.2
4.	Okhla Head	SW04	*Shigella dysenteriae*, NR_026332.1
5.	DND Highway	SW05	*Pseudomonas aeruginosa*, NR_117678.1
6.	Nizamuddin	SW06	*Escherichia coli* JCM1649, NR_112558.1
7.	IP Powerhouse	SW07	*Escherichia marmotae* HT073016, NR_136472.1
8.	Rajghat Power House	SW08	*Pseudomonas fluorescence*, NR_113647.1
9.	Wazirabad Highway	SW09	*Vibrio cholerae*, NR_119302.1
10.	Nijafarbad Industrial Effluents	SW10	*Pseudomonas baetica*, NR_116899.1

lates provided by the National Centre for Biotechnology Information (NCBI).

(d) Antibiotics and their Solutions

Ten antibiotics like – STREPTOMYCIN (Streptomycin IP, Mfd by: Nicolas Piramal India LTD), TETRACYCLINE (Tetracycline hydrochloride capsules IP 250mg, Mfd by- Cipla limited), AMPICILLIN (Ampicillin hydrochloride capsules IP 250mg, Mfd by- Cipla limited), AMOXICILLIN (Amoxicillin Trihydrate capsules IP 250mg, Mfd by- Cipla limited), GENTAMYCIN (Gentamycin IP, Mfd by: Nicolas Piramal India LTD), DOXYCYCLINE (Doxycycline hydrochloride IP 100mg, Mfd by-Cipla limited), CLOXACILLIN (Cloxacillin sodium IP 500mg, Mfd by: Nicolas Piramal India LTD), METRONIDAZOLE (400mg, Mfd by- Eurolife Health Care), VANCOMYCIN (Vancomycin IP, Mfd by-Cipla limited) and MEROPENEM (Meropenem buffer sterile USP, Mfd by- Shenzhen Haibin pharmaceuticals) were used to check susceptibility and resistance pattern of above four bacterial isolates. All these antibiotics were obtained from a local pharmacy store and a working solution having 10µg/mL concentration of each antibiotic was used for the study.

(e) Inoculums Preparation

24hr old bacterial culture was taken for adjustment of 0.5 McFarland density in densitometer to get a bacterial population of 1.0×10^8cfu/mL using saline (0.85% NaCl)

(f) Agar Well Diffusion Assay (Zone of Inhibition Evaluation)

The antibiotic assay was evaluated by agar well diffusion methods. Plates of sterile Muller Hinton Agar (MHA) with 100µL of each adjusted cultures was punched to 6mm diameter well. 100µL of each antibiotic solution were added in wells (Chauhan et al. 2010, Kaushik & Chauhan 2008). Plates were incubated at 37°C overnight. Zone of inhibition was observed in plates where the diameter of zones was calculated using Vernier callipers.

RESULTS AND DISCUSSION

In the present study, ten water samples were collected from ten different sewage water treatment plants located in Delhi. These samples were analysed for the presence of *Escherichia sp, Salmonella sp, Pseudomonas sp, Shigella sp* and *Vibrio* sp.

During the study, three different strains of *Escherichia* i.e. *Escherichia albertii, Escherichia coli* JCM1649 and *Escherichia marmotae* four different strains of *Pseudomonas*, i.e. *Pseudomonas stutzeri, Pseudomonas aeruginosa,*

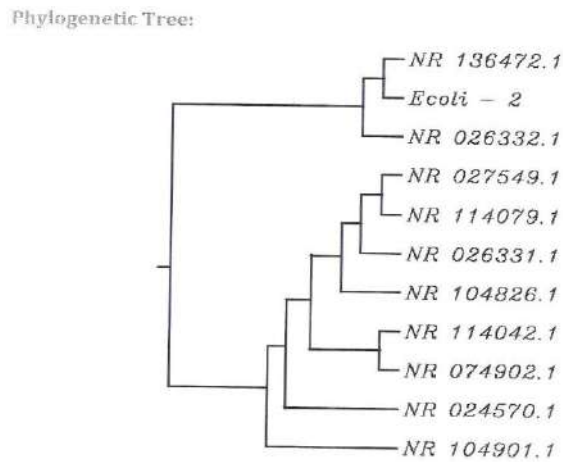

Primer Information

PCR Primer name, Primer Sequences	Sequencing Primer name, Primer Sequences
27F 5′ (AGAGTTTGATCMTGGCTCAS) 3′	785F 5′ (GGATTAGATACCCTGGTA) 3′
1492R 5′ (TACGGYTACCTTGTTACGACTT) 3′	907R 5′ (CCGTCAATTCMTTTRAGTTT) 3′

Fig. 1: Molecular identification of *Escherichia marmotae.*

Phylogenetic Tree:

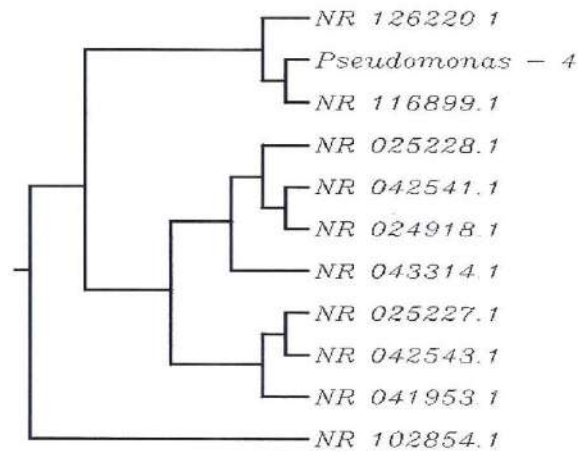

Primer Information

PCR Primer name, Primer Sequences	Sequencing Primer name, Primer Sequences
27F 5′ (AGAGTTTGATCMTGGCTCAS) 3′	785F 5′ (GGATTAGATACCCTGGTA) 3′
1492R 5′ (TACGGYTACCTTGTTACGACTT) 3′	907R 5′ (CCGTCAATTCMTTTRAGTTT) 3′

Fig. 2: Molecular identification of *Pseudomonas baetica.*

Phylogenetic Tree:

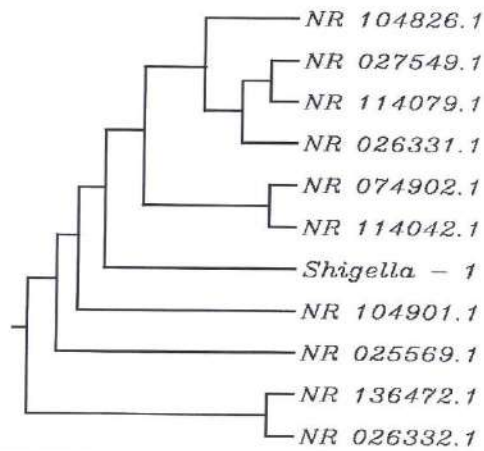

Primer Information

PCR Primer name, Primer Sequences	Sequencing Primer name, Primer Sequences
27F 5′ (AGAGTTTGATCMTGGCTCAS) 3′	785F 5′ (GGATTAGATACCCTGGTA) 3′
1492R 5′ (TACGGYTACCTTGTTACGACTT) 3′	907R 5′ (CCGTCAATTCMTTTRAGTTT) 3′

Fig. 3: Molecular identification of *Shigella dysenteriae.*

Phylogenetic Tree:

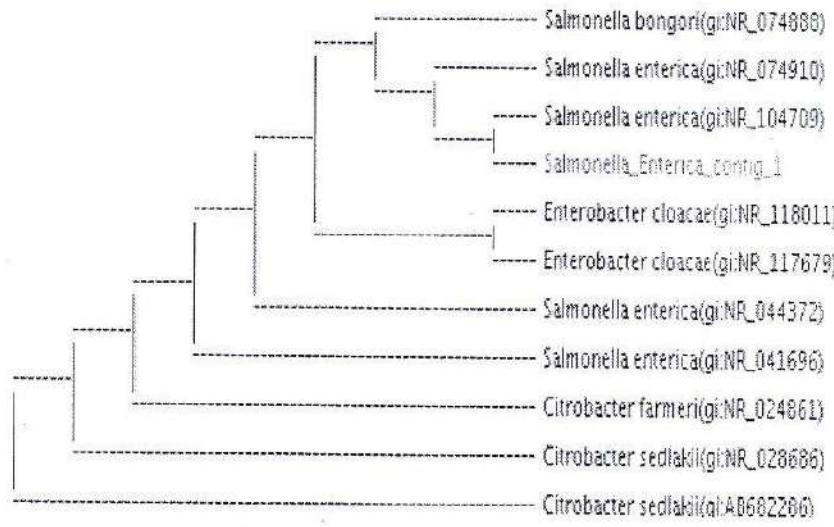

Primer Information

Sequencing Primer Name Primer Sequences	PCR Primer Name Primer Sequences
785F 5' (GGA TTA GAT ACC CTG GTA) 3'	27F 5' (AGA GTT TGA TCM TGG CTC AG) 3
907R 5' (CCG TCA ATT CMT TTR AGT TT) 3'	1492R 5' (TAC GGY TAC CTT GTT ACG ACT T) 3'

Fig. 4: Molecular identification of *Salmonella enterica.*

Phylogenetic Tree:

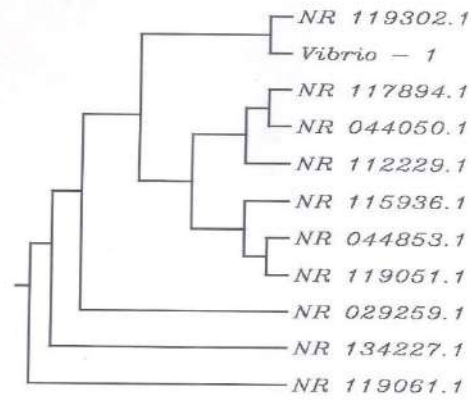

Primer Information

PCR Primer name, Primer Sequences	Sequencing Primer name, Primer Sequences
27F 5' (AGAGTTTGATCMTGGCTCAS) 3'	785F 5' (GGATTAGATACCCTGGTA) 3'
1492R 5' (TACGGYTACCTTGTTACGACTT) 3'	907R 5' (CCGTCAATTCMTTTRAGTTT) 3'

Fig. 5: Molecular identification of *Vibrio cholerae.*

Pseudomonas fluorescence and *Pseudomonas baetica,* two different strains of *Salmonella,* i.e. *Salmonella enterica* and *Salmonella typhimurium,* one *Shigella dysenteriae* and one *Vibrio cholerae* was identified Table 1. All the isolated strains were identified in this study exhibited 96 to 99% sequence similarity to the pathogenic enterobacteriaceae sequence available in NCBI database with lowest E-value and maximum query coverage and maximum identity. The multiple alignment file was then used to create phylogram (Fig. 1 to 5). Phylogenetic tree is a diagram that r epresents evolutionary relationships among organisms. The pattern of branching in a phylogenetic tree shows how species or other groups evolved from a series of common ancestors.

Phylogenetic analysis explores the evolutionary relationships between organisms and is a key element for microbial studies. The development of phylogenetic trees is an important stage in characterizing new pathogens and develops new methods of treating various infections. Molecular sequencing technologies and phylogenetic approaches can be used to learn more about a new pathogen outbreak. This includes finding out about which species the pathogen is related to and subsequently the likely source of transmission. 16S and 23S rRNA gene sequence data reveal a closer relationship between *Salmonella* and *Escherichia coli* than between *Salmonella* and *Citrobacter freundii* (Christensen & Olsen 1998). *Escherichia fergusonii* and *Escherichia albertii* are independent and established species (Seong et al. 2012, Farmer et al. 1985). However, these species were difficult to distinguish from *E. coli* by 16S rRNA gene based phylogenetic analysis.

The susceptibility patterns of all isolated human enteric pathogenic strains were evaluated against ten commonly prescribed antibiotics by using an agar well diffusion assay. In this study, it is clearly seen that the bacterial isolates show non-vulnerability to different antibiotics. The antibiotic

Table 2: Antibiotic resistance patterns of different pathogens.

Antibiotics Used	Zone of inhibition* (in mm)										
	Escherichia albertii	*Escherichia marmotae*	*Escherichia coli JCM1649*	*Pseudomonas stutzeri*	*Pseudomonas aeruginosa*	*Pseudomonas fluorescence*	*Pseudomonas baetica*	*Salmonella enterica*	*Salmonella typhimurium*	*Shigella dysenteriae*	*Vibrio cholerae*
Streptomycin	21	23	17	17	19	18	21	22	21	14	11
Gentamycin	13	15	14	15	17	15	16	0	20	0	13
Tetracycline	20	18	19	0	0	11	23	17	0	16	0
Amoxicillin	0	0	24	11	19	14	0	20	21	18	17
Ampicillin	0	0	24	12	14	13	15	19	21	20	16
Doxycycline	0	0	0	0	0	0	0	0	0	0	0
Meropenem	22	26	27	25	22	26	29	21	24	28	29
Vancomycin	0	0	18	0	15	17	26	17	19	0	12
Metronidazole	0	0	0	0	0	0	0	0	0	0	0
Cloxacillin	0	26	19	14	12	15	22	20	18	14	0

*Zone of inhibition in mm. Diameter including well diameter of 6.0 mm

Table 3: Percentage of pathogens susceptible to antibiotics.

Antibiotic used	% Susceptible pathogens				
	Escherichia sp	*Pseudomonas* sp	*Salmonella* sp	*Shigella* sp	*Vibrio* sp
Streptomycin	100	100	100	100	100
Gentamycin	100	100	50	NZI	100
Tetracycline	100	50	50	100	NZI
Amoxicillin	33	75	100	100	100
Ampicillin	33	100	100	100	100
Doxycycline	NZI	NZI	NZI	NZI	NZI
Meropenem	100	100	100	100	100
Vancomycin	33	75	100	NZI	100
Metronidazole	NZI	NZI	NZI	NZI	NZI
Cloxacillin	66	100	100	100	NZI

NZI: No Zone of Inhibition

resistance patterns in terms of average zones of diameter considering 4 plates for bacterial isolates against each of ten antibiotics of 10µg/mL concentration were calculated and shown in Table 2. The most vulnerable antibiotic was found to be Doxycycline and Metronidazole against which all eleven isolated human enteric pathogens shows 100% resistance (Fig. 6). The percentage of susceptibility against antibiotics was demonstrated in Table 3. All three *Escherichia* isolates were shown 100% susceptible against Streptomycin, Gentamycin, Tetracycline and Meropenem. Intermediate susceptibility was shown by *Escherichia* i.e. 66% towards Cloxacillin. In the case of four *Pseudomonas* isolates 100% susceptible against Streptomycin, Gentamycin, Ampicillin and Meropenem. Intermediate susceptibility ranges from 50% to 75% towards the rest of antibiotics except Doxycycline and Metronidazole. However, two *Salmonella* isolates have shown more susceptibility against six antibiotics used in this study. Both *Salmonella enteric* and *Salmonella typhimurium* have shown 50% susceptibility against Gentamycin and Tetracycline. In the case of *Shigella dysenteriae* and *Vibrio cholera* both have shown 100% resistance against four antibiotics. Susceptibility in terms of zone of inhibition against antibiotics used in the study was shown in Fig. 7a to 7e. Multiple antibiotic resistances have shown by eleven human enteric pathogens isolated. Meropenem was found to be the most promising antibiotic as all eleven human enteric pathogens have shown a high level of susceptibility followed by Streptomycin, Ampicillin, Cloxaxillin, Gentamycin, Amoxicillin, Tetracycline, Vancomycin and Metronidazole. The cumulative effectiveness of the antibiotics as obtained in this study is Meropenem > Streptomycin > Ampicillin > Cloxaxillin > Gentamycin > Amoxicillin > Tetracycline > Vancomycin > Metronidazole.

Antibiotics are an essential part of combating harmful bacterial infections *in vivo*. During the last few decades, infectious diseases have played a significant role in the death of millions in developing countries like India. Because of the mutagenic nature of bacterial DNA, the rapid multiplication of bacterial cells, and the constant transformation of bacterial cells due to plasmid exchange and uptake, pathogenic bacteria continue to develop antimicrobial resistance, thus rendering certain antibiotics useless (Kaushik et al. 2008). It is thus become important to determine the antibiotic resistance pattern of isolated microbes as it is the part of microbial monitoring process of the water (Chatterjee et al. 2012).

The presence of multidrug resistance in human enteric pathogens is not uncommon recently, and its severity has been expanded from town to village and village to everywhere very rapidly. The rapid development of the antibiotic

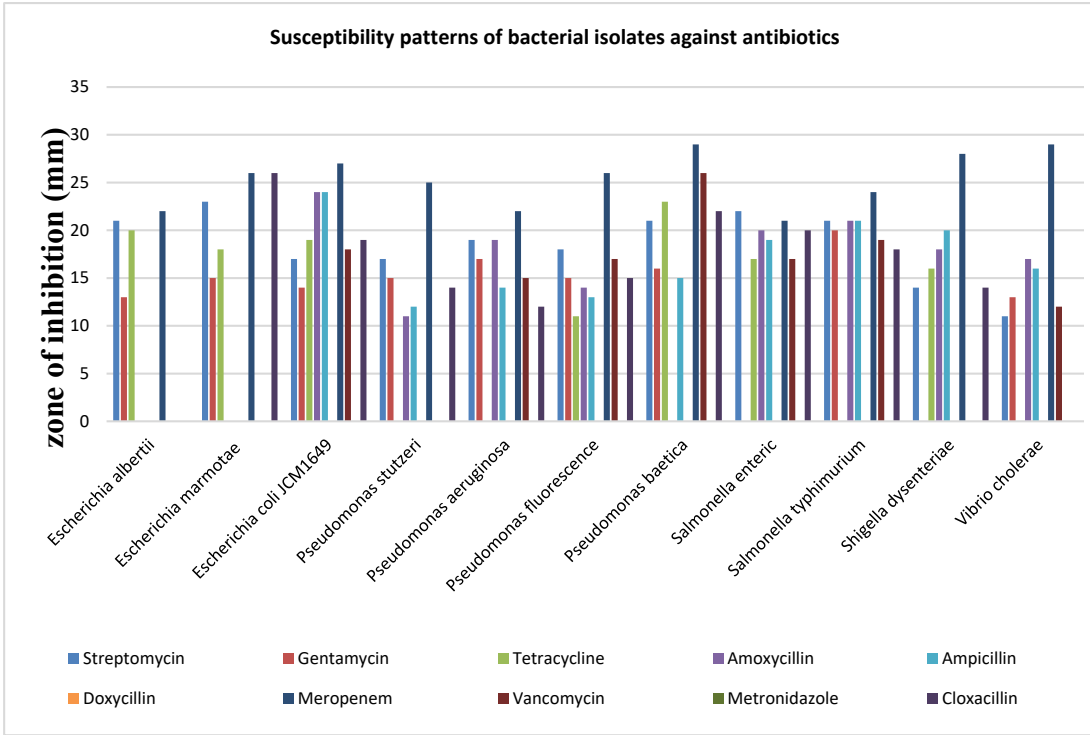

Fig. 6: Susceptibility patterns of bacterial isolates against antibiotics.

(a) **(b)**

a) ***Escherichia marmotae*** **against Meropenem and Tetracycline**

b) ***Pseudomonas baetica*** **against Streptomycin and Gentamycin**

(c) **(d)**

c) ***Salmonella enteric*** **against Amoxicillin and Ampicillin**

d) ***Shigella dysenteriae*** **against Meropenem and Cloxacillin**

(e)

e) ***Vibrio cholerae*** **against Meropenem and Vancomycin**

Mer: Meropenem, **Van:** Vancomycin, **T:** Tetracycline, **Str:** Streptomycin, **Gen:** Gentamycin, **Amox:** Amoxicillin, **Amp:** Ampicillin, **Clox:** Cloxacillin

Fig. 7: Zone of inhibition of bacterial isolates against antibiotics.

resistant pattern of *E. coli*, as well as other microorganisms, might create a devastating health problem (Chauhan & Goyal 2013, Overdevest et al. 2011). Based open these study it was found that most of the isolates in the present study showed multiple tolerances to antibiotics. Since heavy metals are all similar in their toxic mechanism, multiple tolerances are common phenomena among heavy metal resistant bacteria (Chauhan et al. 2015). In sewage water, some substances have the potential to select for antibiotic resistance even though they are not antibiotics themselves. Heavy metals and biocides are two of them. Exposure to heavy metals or biocides results in the selection of bacterial strain also able to resist antibiotics. This shows that there is a close association between metal resistance and antibiotic resistance.

CONCLUSION

An alarming consequence has been occurred due to the widespread emergence of resistance among microorganisms against clinically significant antibiotics. It is clearly indicated that domestic waste and industrial waste are responsible for the development of bacterial resistance along with the risk of human health and the environment. Regular surveillance of the effluent in industrial sites is a must if the risk of disease due to such antibiotic-resistant organisms is to be avoided. Antibiotic resistance development among bacteria is a challenging issue that requires the improvement of next-generation treatment processes in sewage water treatment plants. The emergence of antibiotic resistance among pathogens increases the demand for novel treatment strategies. In this study, results were indicative of very high antimicrobial resistance to Doxycycline and Metronidazole among all bacterial isolates involved in our study. The uncontrolled use of this antibiotic led to the generation of multi-drug resistant strains. The fourth-generation antibiotic i.e. Meropenem is found to have significant efficacy and can be considered appropriate for the empirical treatment of the above four bacterial infections. Alternatives to antibiotics such as herbal medicines, probiotics and lytic bacteriophages can help to decrease the burden of antimicrobial resistance globally. Although the present study can lead to beneficially assist in the identification of alternate drug to control these multidrug-resistant bacterial strains.

ACKNOWLEDGMENTS

The authors are thankful to Dr. K.M. Chacko, Director, Shriram Institute for Industrial Research, Delhi; for facilitating and encouraging the research work.

REFERENCES

Cabrera, R., Ruiz, J., Marco, F., Oliveira, I. and Arroyo, M. 2004. Mechanism of resistance to several antimicrobial agents in Salmonella clinical isolates causing traveller's diarrhoea. Antimicrobial Agents Chemotherapy, 48(10): 3934-3939.

Chandrasekaran, S., Venkatesh, B. and Lalithakumari, D. 1998. Transfers and expressions of a multiple antibiotic resistance plasmid in marine bacteria. Current. Microbiol., 37: 347-351.

Chatterjee, R., Sinha, S., Aggarwal, S., Dimri, A., Singh, D., Goyal, P., Chauhan, A., Aggarwal, M.L. and Chacko, K.M. 2012. Studies on susceptibility and resistance patterns of various *E. coli* isolated from different water samples against clinically significant antibiotics. International journal of Bioassay, 01(11): 156-161.

Chauhan, A. and Goyal, P. 2013. Isolation and Identification of *Escherichia coli* from various foodstuffs and their resistance against clinically significant antibiotics. J. Advance in Biology, 2: 45-53.

Chauhan, A., Garg, S. and Ranjan, A. 2018. Prevalence of microbial contamination of mobile cell phones in general population of Delhi, India. J. Exp. Clin. Microbiol., 1(1): 12-15.

Chauhan, A., Garima, G., Goyal, P. and Kaushik, P. 2010. In vitro antibacterial evaluation of *Anabaena* sp. against several clinically significant microflora and HPTLC analysis of its active crude extracts. Indian Journal of Pharmacology, 42(2): 105-107.

Chauhan, A., Goyal, P., Verma, A. and Jindal, T. 2015. In -vitro antibiotic resistance and heavy metal tolerance patterns of gram-positive and gram-negative bacteria isolated from effluent treated water of Delhi, India. Journal of Current Pharma Research, 5(2): 1449-1458.

Chauhan, A., Goyal, P., Verma, A. and Jindal, T. 2015. Microbiological evaluation of drinking water sold by roadside vendors of Delhi, India. Appl. Water Sci., DOI 10.1007/s13201-015-0315-x.

Chitnis, V., Chitnis, S., Vaidya, K., Ravikant, S. and Patil, S. 2004. Bacterial population changes in hospital effluent treatment plant in central India. Water Research, 38(2): 441-447.

Christensen, H. and Olsen, J. E. 1998. Phylogenetic relationships of Salmonella based on DNA sequence comparison of atpD encoding the beta subunit of ATP synthase. FEMS Microbiol. Lett., 161: 89-96.

Danchaivijitr, S., Wongchanapai, W., Assanasen, S. and Jintanothaitavorn, D. 2005. Microbial and heavy metal contamination of treated hospital wastewater in Thailand. J. Med. Assoc. Thai., 88(10): S59-S64.

Dicuonzo, G., Gherardi, G., Lorino, G., Angeletti, S., Battistoni, F. and Bertuccini, L. 2001. Antibiotic resistance and genotypic characterization by PFGE of Clinical and environmental isolates of Enterococci. FEMS Microbial Letters, 201:205-211.

Farmer III J.J., Fanning G.R., Davis, B.R., O'Hara, C.M., Riddle, C., Hickman-Brenner, F.W., Asbury, M.A., Lowery III, V.A. and Brenner, D.J. 1985. *Escherichia fergusonii* and *Enterobacter taylorae*, two new species of Enterobacteriaceae isolated from clinical specimens. J. Clin. Microbiol., 21: 77-81.

Goyal, P., Chauhan, A. and Kaushik, P. 2010. Assessment of *Commiphora wightii* (Arn.) Bhandari (Guggul) as potential source for antibacterial agent. Journal of Medicine and Medical Sciences, 1(3): 071-075.

Hellier, M.D. and Williams, J.G. 2007. The burden of gastrointestinal disease: Implications for the provision of care in the UK. Gut,. 56: 165-166.

IS 13428: 2005. Detection and Enumeration of *Pseudomonas aeruginosa* (Annexure-D).

IS 5887 (Pt-1) 1976. Reaff: 2018. Isolation, Identification and Enumeration of *Escherichia coli*.

IS 5887 (Pt-3) 1999. Reaff: 2018. General Guidance on methods for the detection of *Salmonella.*

IS 5887 (Pt-5) 1976, Reaff: 2018 Isolation, Identification and Enumeration of *Vibrio cholerae* and *Vibrio parahaemolyticus.*

IS 5887 (Pt-7) 1976, Reaff: 2018. Isolation, Identification and Enumeration of *Shigella.*

Ishak, W.M.F.W., Jamek, S., Jalanni, N.A. and Jamaludin, N.F.M. 2011. Isolation and identification of bacteria from activated sludge and compost for municipal solid waste treatment system. International Conference on Biology, Environment and Chemistry. 24: 450-454.

Kaushik, P. and Chauhan, A. 2008. In vitro antibacterial activity of laboratory grown culture of Spirulina platensis. Indian Journal of Microbiology, 48(3): 348-352.

Kaushik, P. and Goyal, P. 2008. *In vitro* evaluation of *Datura innoxia* (thorn-apple) for potential antibacterial activity. Indian Journal of Microbiology, 48(3): 353-357.

Lopes, M. F. S., Riberio, T., Abrantes, M., Marques, J.J. F., Tenreirom, R. and Crespo, M.T.B. 2005. Antimicrobial resistance profiles of dairy and clinical isolate and type strains of entercocci. Int. J. Food Microbial., 103: 191-198.

Overdevest, I., Willemsen, I., Rijnsburger, M., Eustace, A. and Xu, L. 2011. Extended-spectrum β-lactamase genes of *Escherichia coli* in chicken meat and humans. The Netherlands. Emerg. Infect. Dis., 17(7): 1216-1222.

Seong, W.J., Kwon, H.J., Kim, T.E., Lee, D.Y., Park, M.S. and Kim, J.H. 2012. Molecular serotyping of *Salmonella* enteric by complete rpoB gene sequencing. J. Microbiol., 50: 962-9.

Sharpe, M. 2003. High on pollution: drugs as environmental contaminants. Journal of Environmental Monitoring, 5(3): 43-46.

Wise, R., Hart, T., Cars, O., Streulens, M. and Helmuth, R. 1998. Antimicrobial resistance is a major threat to public health. BMJ, 317(7159): 609-610.

Nature Environment and Pollution Technology
An International Quarterly Scientific Journal

p-ISSN: 0972-6268
(Print copies up to 2016)
e-ISSN: 2395-3454

Vol. 20 | No. 2 | pp. 579-585 | 2021

Original Research Paper

https://doi.org/10.46488/NEPT.2021.v20i02.014

Open Access Journal

Biosorption of Cu(II) from Aqueous Solutions by a Macrofungus (*Ganoderma lobatum*) Biomass and its Biochar

Silin Yang, Yan Wang and Yungen Liu†
Faculty of Ecology and Environment, Southwest Forestry University, Kunming 650224, China
†Corresponding author: Yungen Liu; 84458250@qq.com

Nat. Env. & Poll. Tech.
Website: www.neptjournal.com

Received: 18-03-2020
Revised: 25-04-2020
Accepted: 15-06-2020

Key Words:
Macrofungus
Biochar
Sorption
Copper ion

ABSTRACT

The sorption capacities of the macrofungus viz. *Ganoderma lobatum* (C0) and its biochar (C400) were evaluated for the biosorption of Cu(II) from aqueous solution under different conditions, including adsorbent doses, pH of the solution, contact time and initial Cu(II) concentration. The results showed that *Ganoderma lobatum* could be used as an efficient biosorbent for the removal of Cu(II) ions from an aqueous solution. The desired biosorbent dose in the case of C0 and C400 for Cu(II) adsorption was 4 g/L, and the optimal pH value for biosorption was 8 for Cu(II). The Freundlich isotherm model fitted the absorption data of Cu(II) for both C0 and C400 better than the Langmuir isotherm model, and the adsorption capacity of C0 was better than C400. Our results indicate that C0 has a higher removal efficiency than C400 in adsorbing Cu(II) ions from aqueous solution. Biosorption kinetics were also studied using pseudo-first-order and pseudo-second-order models, which showed that the biosorption processes of Cu(II) ions based on C0 and C400 were in accordance with the pseudo-second-order kinetics.

INTRODUCTION

Water pollution by heavy metals at low concentrations is a worldwide environmental problem. Many methods have been widely used to remove these toxic substances (Fomina & Gadd 2014). However, these methods have become less effective because of low metal concentrations (Wang & Chen 2009). Therefore, as an excellent alternative to conventional techniques, biosorption has emerged as the most promising process for treating pollutants in the aquatic environment, especially the removal of low concentrations of heavy metals in the aqueous environment, because of its high efficiency, low cost, and non-hazardous nature (Javaid et al. 2011, Kapoor & Viraraghavan 1995). In recent years, macrofungi have attracted attention as biosorbents. Many studies have confirmed that copper ions in aqueous solutions are effectively adsorbed by the fruit bodies of macrofungi such as *Pycnoporus sanguineus* (Zulfadhly et al. 2001), *Agaricus macrosporus* (Melgar et al. 2007), *Pleurotus ostreatus* (Javaid et al. 2011), *Auricularia polytricha* (Xinyu et al. 2010), and *Auricularia polytricha* (Yu et al. 2010). Moreover, macrofungi grow prolifically and are found in many parts of the world (Vimala et al. 2011). They are visible in size, tough in texture, and have other physical characteristics that are conducive to their development as biosorbents without the need for immobilization or deployment of a sophisticated reactor configuration, as in the case of microorganisms (Muraleedharan et al. 1994). The adsorption capacity of macrofungi clearly depends on the species (Nagy et al. 2014). To our knowledge, no reports in the literature have examined the biosorption of heavy metal using the macrofungus *Ganoderma lobatum*. It is a species of wood-decaying fungi in the family Ganodermataceae (order Polyporales), widely distributed in China, America and Mexico, growing alone or gregariously on decaying logs and stumps of various hardwoods. The cap is flat and up to 20 cm wide, and the flesh of the cap is dark brown to cinnamon-brown, woody.

The aim of the present work was to investigate the biosorption potential of the fruit body of *Ganoderma lobatum* and its biochar for the removal of Cu(II) from an aqueous solution. Optimum biosorption conditions were determined as a function of the biomass dose, pH, contact time, and initial metal concentration. The Langmuir and Freundlich models were employed to describe equilibrium isotherms. Biosorption mechanisms of Cu(II) onto *Ganoderma lobatum* and its biochar were also evaluated in terms of kinetics.

MATERIALS AND METHODS

Biosorbent Preparation

The macrofungus *Ganoderma lobatum* was collected from Mojiang County, Yunnan Province, China. Fruit bodies were

washed 3 times using distilled water, sun-dried for 3 days, and then dried in an oven at 80°C for 48 h. The dried fruit bodies were ground and then filtered through a 2-mm nylon sieve. The dried samples were placed in clean polyethene sample bags, labelled C0 for future use, and a portion of the dried samples was pyrolyzed in an electrical muffle furnace at 400 °C for 4 h under oxygen-limited conditions. After cooling to room temperature, they were filtered through a 2-mm nylon sieve and stored in clean polyethene sample bags labelled C400 for future experiments.

Reagents and Equipment

All chemicals used in this study were of analytical grade, and deionized water was used for all dilutions. A pH meter (Leici, ZD-2) was used to measure pH values in the aqueous phase. Cu(II) concentrations in the aqueous phase were determined by ICP-OES (VISFA-MPX). Fourier Transform Infrared (FT-IR) spectra of C0 and C400 prepared as KBr pellets were recorded in the 400-4000 cm^{-1} region using a Varian FT-IR 640 spectrometer.

A stock Cu(II) solution of 1000 mg/L was prepared by dissolving 3.8019 g $Cu(NO_3)_2 \cdot 3H_2O$ in 1000 mL of deionized water. The $Cu(NO_3)_2 \cdot 3H_2O$ used in this work was analytical grade and was supplied by Sinopharm Chemical Reagent Co., Ltd. (China). Stock solutions were used to prepare diluted solutions of different working concentrations. HCl (0.1 M) and NaOH (0.1 M) volumetric solutions were used to adjust the solution pH.

Batch Biosorption Experiments

The batch biosorption experiments for C0 and C400 were carried out in 150-mL stoppered conical flasks containing 0.2 g of the biosorbent in 50 mL of the Cu(II) solutions (10 mg/L) separately at room temperature on a rotary shaker at 100 rpm. For optimization of the experimental conditions, batch studies were performed for different metal concentrations (10-200 mg/L), pH (3-10), biosorbent doses (0.4-8 g/L), and contact times (10-1440 min). The contents of the flask were filtered, and the residual metal concentration in the filtrates was determined by ICP-OES (VISFA-MPX). Each sample was evaluated three times, and the results are presented as average values.

To evaluate the adsorption capacity of Cu(II) onto C0 and C400, the amount of Cu(II) adsorbed per unit mass of C0 and C400 was calculated using the following equation:

$$Q_e = \frac{V(C_0 - C_e)}{M} \quad , \quad Q_t = \frac{V(C_0 - C_t)}{M} \qquad \ldots(1)$$

Where Q_e (mg/g) is the amount of Cu(II) biosorbed onto the biosorbent at equilibrium, C_0 and C_e respectively are the initial and equilibrium concentration (mg/L) of Cu(II), V(L) is the volume of the solution and M (g) is the biosorbent dose, Q_t (mg/g) is the amount of Cu(II) biosorbed onto biosorbent at time t (min), and Ct_t (mg/L) is the concentration of Cu(II) at time t (min).

$$R_e = \frac{(C_0 - C_e)}{C_0} \times 100\% \qquad \ldots(2)$$

Where R_e is the ratio between Cu(II) biosorbed at equilibrium and the initial Cu(II) concentration (mg/L).

RESULTS AND DISCUSSION

FT-IR Analysis

Functional groups, such as carbonyl, carboxyl, and hydroxyl groups, have been identified as potential adsorption sites responsible for binding metallic ions to the adsorbent. The FT-IR spectra of C0 and C400 in the range from 400-4000 cm^{-1} were determined and are presented in Fig. 1. For the biomass material C0, the broad and strong absorption

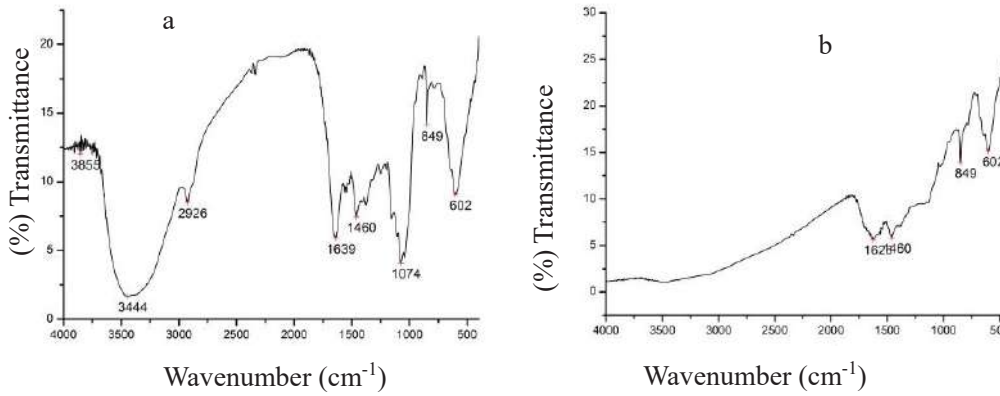

Fig. 1: FT-IR spectrum of the macrofungus (*Ganoderma lobatum*) (a) and its biochar (b).

band at approximately 3200-3600 cm^{-1} could be attributed to stretching vibrations of hydroxyl groups (–OH). The peak observed at 2925 cm^{-1} was due to C–H stretching of CH_2 groups. The band at 1639 cm^{-1} indicated a fingerprint region of C=O, C–O, and O–H groups that exist as functional groups (Wang & Chen 2009). The bands observed at 1074 cm^{-1} were assigned to C–O stretching of alcohols and carboxylic acids (Fig.1a) (Fomina & Gadd 2014). For the calcined C400, the absorption bands of various functional groups disappeared, indicating that the organic structure of the fungal biomass had been decomposed at a high temperature (Fig. 1b). As shown in Fig. 1b, the weak bands at approximately 1620 and 849 cm^{-1} were attributed to the vibrations of C=C and C–C, respectively. FT-IR studies revealed that several functional groups, which can bind transition metal ions including Cu(II), were present in C0. These functional groups were mainly derived from the cellulose, hemicellulose, and lignin of the fungal cell wall, as well as some other kinds of organic components (Dashtban et al. 2009, Pérez et al. 2002).

Effect of the Adsorbent Dose

The effect of the adsorbent dose on the Cu(II) ion removal efficiency is presented in Fig. 2. The removal efficiencies (%) were found to increase steeply with increasing concentrations of C0 and C400 up to a dose of 4 g/L. The maximum removal efficiencies of C0 and C400 respectively were 97.80% and 96.89% at the adsorbent dose of 4 g/L. However, beyond this dose, the increase in removal efficiencies of C0 and C400 were marginal and became nearly constant. Similar results have been reported for metal ion biosorption in an aqueous solution by oyster mushroom (*Pleurotus platypus*) (Vimala & Das 2009). Therefore, the optimum adsorbent dose was considered to be 4 g/L for further experiments. The above

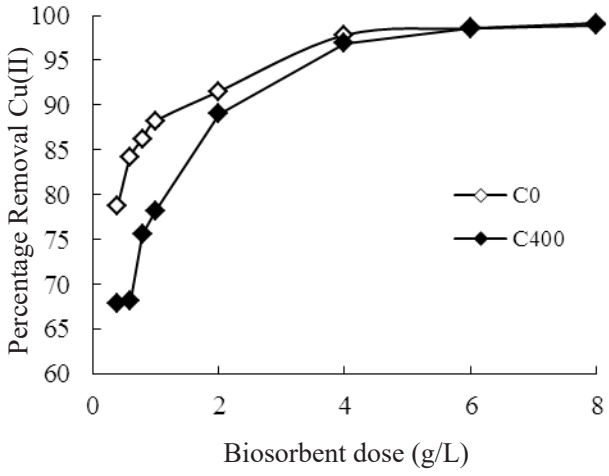

Fig. 2: Effect of the biosorbent dose on Cu(II) removal efficiencies by the macrofungus (*Ganoderma lobatum*) and its biochar.

results can be explained by the finding that the biosorption sites remain unsaturated during the biosorption reaction, whereas the number of sites available for biosorption site increases by increasing the biosorbent dose (Sar & Tuzen 2009b). However, a high adsorbent dose results in aggregates of adsorbent due to interference between binding sites at a higher adsorbent dose or insufficient metal ions in the solution with respect to available binding sites (Rome & Gadd 1987). Moreover, protons might combine with metal ions for ligands and thereby decrease the interaction of metal ions with cell components (Ghorbani et al. 2008, Sağ & Kutsal 1996).

Effect of pH

The effect of initial pH on the removal efficiencies of Cu(II) ions onto adsorbent were investigated from pH 3-10 for the initial metal concentration of 10 mg/L Cu(II) solution. The results for the pH effect on the removal efficiencies of Cu(II) are shown in Fig. 3. The removal efficiencies of C0 and C400 for Cu(II) ions increased from 90% to 97% and from 93% to 97%, respectively, as the pH was increased from 3 to 8. The maximum removal efficiencies of 97 % were found at pH 8 for the two adsorbents. Therefore, all the biosorption experiments were carried out at pH 8. Previous researchers have indicated that pH is one of the most important factors affecting the adsorption of heavy metal ions from aqueous solution. This parameter is directly related to the competition ability of hydrogen ions with metal ions for active sites on the biosorbent surface (Senthilkumar et al. 2011, Tsai et al. 2007). Generally, metal biosorption involves complex mechanisms of ion-exchange, chelation, adsorption by physical forces, and ion entrapment in inter and intrafibrillar capillaries and spaces of the cell structural network of a biosorbent (Chojnacka et al. 2005). At low pH values, protons occupy most of the biosorption sites on the biosorbent surface, and fewer copper ions can be absorbed because of the electric repulsion with protons on the biosorbent. When the pH values increase, biosorbent surfaces are more negatively charged, and the biosorption of metal ions (positive charge) increases and reaches equilibrium at pH 8. Decreases in biosorption at higher pH values (> 8) are due to the formation of soluble hydroxylated complexes of the metal ions and their competition with the active sites, resulting in a repeated decrease in retention (Anayurt et al. 2009, Sar & Tuzen 2009a).

The FT-IR spectroscopic analysis showed that the macrofungus (C0) had various functional groups, and these groups were involved in almost all potential binding mechanisms. Moreover, depending on the pH value of the aqueous solution, these functional groups participate in metal ion binding (Sar & Tuzen 2009a).

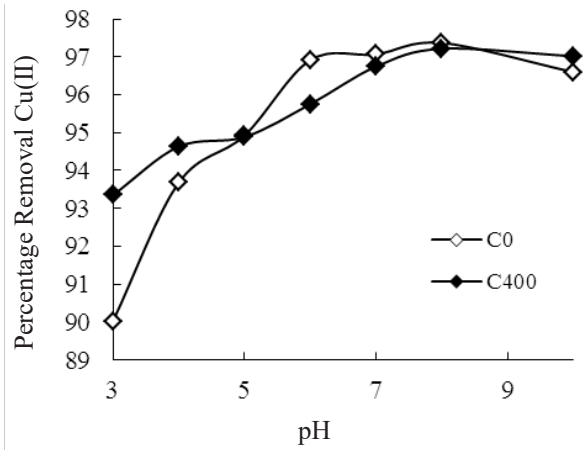

Fig. 3: Effect of the initial pH on the Cu(II) biosorption capacity of the macrofungus (*Ganoderma lobatum*) and its biochar.

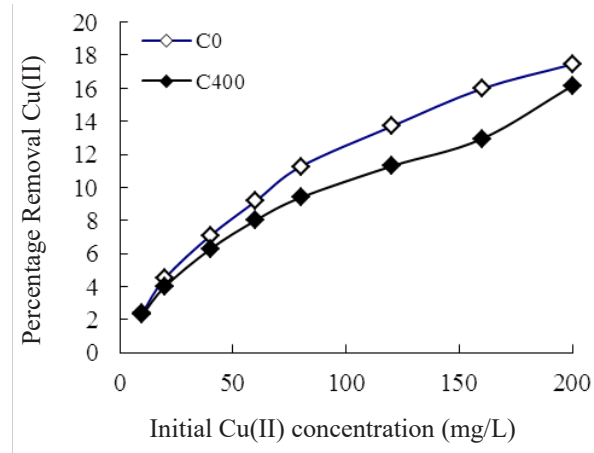

Fig. 5: Effect of the initial Cu(II) concentration on the (II) biosorption capacity of the macrofungus (*Ganoderma lobatum*) and its biochar.

Effect of Contact Time

The effect of contact time on the removal efficiencies of Cu(II) was investigated. The removal efficiencies of Cu(II) by the two biosorbents as a function of time are depicted in Fig. 4. In the case of Cu(II) removal efficiencies by C0 and C400, the removal efficiency reached equilibrium at 480 min, which was chosen as contact time for further experiments. In the initial stages, the removal efficiencies of Cu(II) by C0 and C400 increased rapidly due to the abundant availability of active binding sites on the biosorbents, and with gradual occupancy of these sites, the sorption became less efficient at later stages (Costa & Leite 1991).

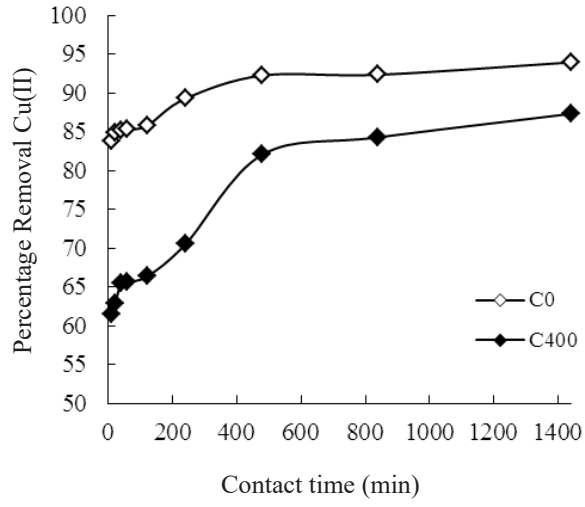

Fig. 4: Effect of contact time on the Cu(II) biosorption capacity of the macrofungus (*Ganoderma lobatum*) and its biochar

The initial concentration of the metal in the solution dramatically influenced the equilibrium uptake of Cu(II). It was noted that the initial concentration increased the sorption of Cu(II), which was generally expected due to the equilibrium process (Fig. 5). This increase in uptake capacity of the biosorbents (C0 and C400) with the increase in initial metal concentrations was due to the higher availability of metal ions (copper) for sorption. Moreover, the higher initial concentration provided increased driving force to overcome all the mass transfer resistance of metal ions between the aqueous and solid phase, resulting in a higher probability of collision between metal ions and sorbents. This phenomenon also results in higher metal uptake (Tewari et al. 2005, Vimala & Das 2009).

Biosorption Isotherm Models

Sorption models are often used to predict the maximum adsorption capacity of the adsorbent. The Langmuir and Freundlich models are the most widely used models for the adsorption of metal ions with biomaterials (Febrianto et al. 2009, Langmuir 1918). The equilibrium adsorption data were analysed according to the Langmuir and Freundlich adsorption isotherm models. The Langmuir model suggests that monolayer sorption on a homogeneous surface occurs without interactions between absorbed molecules. In addition, the model assumes uniform energies of sorption onto the surface and no transmigration of the sorbate (Vimala & Das 2009). The Langmuir model can be written in linear form.

$$\frac{C_e}{Q_e} = \frac{C_e}{q_m} + \frac{1}{K_L q_m} \quad \ldots(3)$$

Where q_m (mg/g) is the monolayer biosorption capacity of the adsorbent, and K_L (L/mg) is the Langmuir sorption

constant related to the free energy of biosorption.

The Freundlich model assumes a heterogeneous sorption surface. The Freundlich model is

$$\ln Q_e = \frac{1}{n}\ln C_e + \ln K_F \quad \ldots(4)$$

Where, K_F (mg/g) is a constant relating the biosorption capacity, and n is an empirical parameter relating to the biosorption intensity, which varies with the heterogeneity of the material.

The linear plots of the Langmuir and Freundlich isotherm models for the sorption of Cu(II) on C0 and C400 are presented in Fig. 6. The linear regression coefficient values (R^2) were presented in Table 1, which indicated that the Langmuir model was not able to adequately describe the relationship between the amounts of Cu(II) adsorbed by the adsorbent and its equilibrium concentration in solution. However, the Freundlich isotherm model exhibited a better fit to the sorption data of Cu(II) for both C0 and C400 than the Langmuir isotherm model, since it provided higher R^2 values. Moreover, the n and K_F of C0 for Cu(II) biosorption were higher than for C400. This result indicated that C0 had greater removal efficiencies for Cu(II) than C400. It is likely that the functional groups of C400 were destroyed during the carbonization process. A comparison of the adsorption capacity of this biosorbent with those of different biosorbents reported by other researchers is provided in Table 2, and it can be concluded that the macrofungus as an effective biosorbent may play an important role in the removal of heavy metals from an aqueous environment.

Biosorption Kinetics

To clarify the biosorption kinetics of Cu(II) ions onto C0 and C400, two kinetic models, the pseudo-first-order and pseudo-second-order model were applied to the experimental data. The linear form of the pseudo-first-order rate equation is given as follows (Senthilkumar et al. 2011):

$$\ln(Q_e - Q_t) = \ln Q_e - K_1 t\,,\ \frac{t}{Q_t} = \frac{1}{K_2 Q_e^{\,2}} + \frac{t}{Q_e} \quad \ldots(5)$$

Table 1: Isotherm equations and parameters for Cu(II) biosorption by the macrofungus (*Ganoderma lobatum*) and its biochar.

Biosorbent	Langmuir				Freundlich			
	Equation	q_m	K_L	R^2	Equation	n	K_F	R^2
C0	y = 0.0544x + 0.7947	18.38	0.0684	0.9697	y = 0.3345x + 1.2132	2.989	3.364	0.9956
C400	y = 0.0609x + 1.2912	16.42	0.0471	0.9408	y = 0.3822x + 0.8368	2.616	2.308	0.993

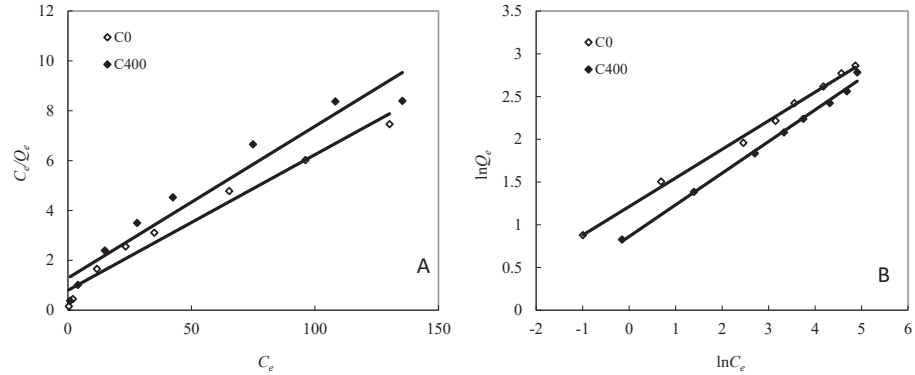

Fig. 6: Linear fitting of the Langmuir (A) and Freundlich (B) isotherms for Cu(II) biosorption of the macrofungus (*Ganoderma lobatum*) and its biochar.

Table 2: Sorption capacity of Cu(II) on different macrofungi.

Biosorbent	Adsorption capacity (mg/g)	pH	Metal concentration (mg/L)	References
Ganoderma lobatum	18.38	8	10-160	Present study
Auricularia polytricha	8.36	5	0-250	(Xinyu et al. 2010)
Auricularia polytricha	18.69	6.03-6.56	10-100	(Yu et al. 2010)
Tremella fuciformis	20.15	6.03-6.56	10-100	(Yu et al. 2010)
Pleurotus ostreatus	8.06	4.5	20-100	(Javaid et al. 2011)

Table 3: The equations and parameters of pseudo-first and second-order kinetics for Cu(II) biosorption by the macrofungus (*Ganoderma lobatum*) and its biochar.

Biosorbent	First-order kinetics				Second-order kinetics			
	Equation	K_1	Q_e	R^2	Equation	K_2	Q_e	R^2
C0	y = -0.0017x - 0.6457	0.0017	0.5242	0.9398	y = 0.2124x + 1.9287	0.0233	4.7080	0.9996
C400	y = -0.0025x + 0.2494	0.0025	1.2832	0.9641	y = 0.2272x + 5.7181	0.0090	4.4014	0.9985

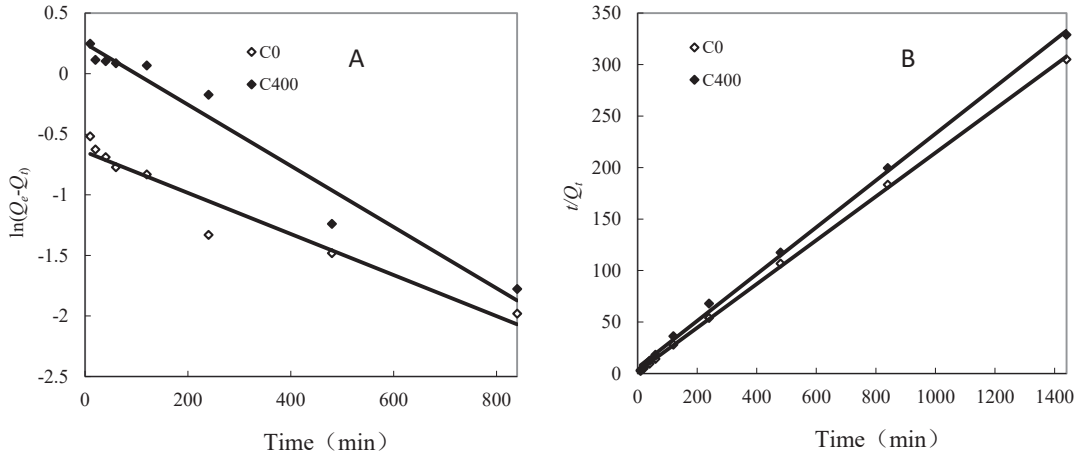

Fig. 7: Linear fitting of the pseudo-first-order (A) and pseudo-second-order (B) kinetics for Cu(II) biosorption by the macrofungus (*Ganoderma lobatum*) and its biochar.

Where K_1 and K_2 are the rate constant of the first-order equation (min^{-1}) and second-order equation (g/mg min), respectively (Cheung et al. 2001).

The values of the rate constants and correlation coefficients for the two models are shown in Table 3. The biosorption mechanisms of Cu(II) ions onto the C0 and C400 biomass does follow the pseudo-second-order kinetic model (Fig. 7). The K_2 value of C0 was significantly higher than C400. This result indicated that the sorption rate of C0 for Cu(II) was greater than C400.

CONCLUSION

The macrofungus as an effective biosorbent of Cu(II) was confirmed. The effects of the biosorbent dose, pH, contact time, and initial copper ion concentration on the removal efficiencies were evaluated. The present results showed that the desired biosorbent dose in the case of *Ganoderma lobatum* and its biochar for Cu(II) adsorption was 4 g/L, and the pH value for biosorption was found to be 8 for Cu(II). The Freundlich isotherm model exhibited a better fit to the sorption data of Cu(II) for both C0 and C400 than the Langmuir isotherm model. The results indicated that C0 had greater removal efficiencies for Cu(II) than C400. This finding can be interpreted as due to the decomposition of the functional groups of C400 during the carbonization process. Equilibrium data showed that the biosorption of Cu(II) ions onto C0 and C400 effectively followed the pseudo-second-order kinetic model. Further research is in progress to explore the mechanism underlying the biosorption process.

ACKNOWLEDGEMENTS

This work was supported by the National Natural Science Foundation of China (21767027).

REFERENCES

Anayurt, R.A., Sari, A. and Tuzen, M. 2009. Equilibrium, thermodynamic and kinetic studies on biosorption of Pb(II) and Cd(II) from aqueous solution by macrofungus (Lactarius scrobiculatus) biomass. Chemical Engineering Journal, 151: 255-261.

Cheung, C.W., Porter, J.F. and Mckay, G. 2001. Sorption kinetic analysis for the removal of cadmium ions from effluents using bone char. Water Research, 35: 0-612.

Chojnacka, K., Chojnacki, A. and Górecka, H. 2005. Biosorption of Cr^{3+}, Cd^{2+} and Cu^{2+} ions by blue-green algae Spirulina sp.: kinetics, equilibrium and the mechanism of the process. Chemosphere, 59: 75-84.

Costa, A.C.A.D. and Leite, S.G.F. 1991. Metals biosorption by sodium alginate immobilized Chlorella homosphaeracells. Biotechnology Letters, 13: 559-562.

Dashtban, M., Schraft, H. and Qin, W. 2009. Fungal bioconversion of lignocellulosic residues; opportunities & perspectives. Int. J. Biol. Sci., 5: 578-595.

Febrianto, J., Kosasih, A., Sunarso, J., Ju, Y.H., Indraswati, N. and Ismadji, S. 2009. Equilibrium and kinetic studies in adsorption of heavy metals using biosorbent: A summary of recent studies. Journal of Hazardous Materials, 162: 616-645.

Fomina, M. and Gadd, G.M. 2014. Biosorption: current perspectives on concept, definition and application. Bioresource Technology, 160: 3-14.

Ghorbani, F., Younesi, H., Ghasempouri, S.M., Zinatizadeh, A.A., Amini, M. and Daneshi, A. 2008. Application of response surface methodology for optimization of cadmium biosorption in an aqueous solution by Saccharomyces cerevisiae. Chemical Engineering Journal, 145: 267-275.

Javaid, A., Bajwa, R., Shafique, U. and Anwar, J. 2011. Removal of heavy metals by adsorption on Pleurotus ostreatus. Biomass & Bioenergy, 35: 1675-1682.

Kapoor, A. and Viraraghavan, T. 1995. Fungal biosorption - an alternative treatment option for heavy metal bearing wastewaters: a review. Bioresource Technology, 53: 195-206.

Langmuir, I. 1918. The adsorption of gases on plane surfaces of glass, mica and platinum. Journal of the American Chemical Society, 40: 1361-1403.

Melgar, M.J., Alonso, J. and García, M.A. 2007. Removal of toxic metals from aqueous solutions by fungal biomass of Agaricus macrosporus. Science of the Total Environment, 385: 12-19.

Muraleedharan, T.R., Venkobachar, C. and Leela, I. 1994. Investigations of fungal fruiting bodies as biosorbents for the removal of heavy metals from industrial processing streams. Separation Science, 29: 1893-1903.

Nagy, B., Măicăneanu, A., Indolean, C., Mânzatu, C., Silaghi-Dumitrescu, L. and Majdik, C. 2014. Comparative study of Cd(II) biosorption on cultivated Agaricus bisporus and wild Lactarius piperatus based biocomposites. Linear and nonlinear equilibrium modelling and kinetics. Journal of the Taiwan Institute of Chemical Engineers, 45: 921-929.

Pérez, J., Muñoz-Dorado, J., de la Rubia, T. and Martínez, J. 2002. Biodegradation and biological treatments of cellulose, hemicellulose and lignin: an overview. International Microbiology, 5: 53-63.

Rome, L.D. and Gadd, G.M. 1987. Copper adsorption by Rhizopus arrhizus, Cladosporium resinae and Penicillium italicum. Applied Microbiology & Biotechnology, 26: 84-90.

Sağ, Y. and Kutsal, T. 1996. The Selective Biosorption of Chromium(VI) and Copper(II) Ions from Binary Metal Mixtures by R. arrhizus. Process Biochemistry, 31: 561-572.

Sar, A. and Tuzen, M. 2009a. Biosorption of As(III) and As(V) from aqueous solution by macrofungus (Inonotus hispidus) biomass: Equilibrium and kinetic studies, Journal of Hazardous Materials, 164: 1372-1378.

Sar, A. and Tuzen, M. 2009b. Kinetic and equilibrium studies of biosorption of Pb(II) and Cd(II) from aqueous solution by macrofungus (Amanita rubescens) biomass, Journal of Hazardous Materials, 164: 1004-1011.

Senthilkumar, P., Ramalingam, S., Sathyaselvabala, V., Kirupha, S.D. and Sivanesan, S. 2011. Removal of copper(II) ions from aqueous solution by adsorption using cashew nutshell. Desalination, 266: 63-71.

Tewari, N., Vasudevan, P. and Guha, B.K. 2005. Study on biosorption of Cr(VI) by Mucor hiemalis. Biochemical Engineering Journal, 23: 185-192.

Tsai, W.T., Lee, M.K. and Chang, Y.M. 2007. Fast pyrolysis of rice husk: Product yields and compositions. Bioresource Technology, 98: 22-28.

Vimala, R., Charumathi, D. and Das, N. 2011. Packed bed column studies on Cd(II) removal from industrial wastewater by macrofungus Pleurotus platypus. Desalination, 275: 291-296.

Vimala, R. and Das, N. 2009. Biosorption of cadmium (II) and lead (II) from aqueous solutions using mushrooms: A comparative study. Journal of Hazardous Materials, 168: 376-382.

Wang, J. and Chen, C. 2009. Biosorbents for heavy metals removal and their future. Biotechnology Advances, 27: 195-226.

Xinyu, J., Haiwei, H., Lixiang, C. and Renduo, Z. 2010. Kinetics and equilibrium of biosorption of Cd^{2+}, Cu^{2+}, Pb^{2+}, Zn^{2+} by macrofungus(*Auricularia polytricha*) biomass. Acta Scientiae Circumstantiae, 30(7): 1431-1438.

Yu, M., Rong, P., Hai-wei, H., Li-xiang, C. and Ren-duo, Z. 2010. Biosorption of Cd(II), Cu(II), Pb(II) and Zn(II) in Aqueous Solutions by Fruiting Bodies of Macrofungi (*Auricularia polytricha and Tremella fuciformis*). Environmental Science, 31(7): 161-169.

Zulfadhly, Z., Mashitah, M.D. and Bhatia, S. 2001. Heavy metals removal in fixed-bed column by the macro fungus Pycnoporus sanguineus, Environmental Pollution,a 112: 463-470.

Nature Environment and Pollution Technology
An International Quarterly Scientific Journal

p-ISSN: 0972-6268
(Print copies up to 2016)
e-ISSN: 2395-3454

Vol. 20 | No. 2 | pp. 587-593 | 2021

Original Research Paper

https://doi.org/10.46488/NEPT.2021.v20i02.015

Open Access Journal

Applicability Assessment of Electrocoagulation in Real Dyeing Wastewater Treatment

D.P. Hung*, L.T.K Oanh*, V.T.D. Chi*, L.N.Q. Thinh*, D.T. Nguyen*, N.Q. Tuan* and H.T.N. Han†**

*Department of Technology, Van Lang University, Ho Chi Minh City, 700000, Vietnam

**Department of Environment, Ho Chi Minh City University of Natural Resources and Environment, Ho Chi Minh City, 700000, Vietnam

†Corresponding author: H.T.N. Han; han.htn_mt@hcmunre.edu.vn

Nat. Env. & Poll. Tech.
Website: www.neptjournal.com

Received: 05-03-2020
Revised: 31-05-2020
Accepted: 21-06-2020

Key Words:
Electrocoagulation
Iron electrodes
Real dyeing wastewater
Wastewater treatment

ABSTRACT

In this study, the applicability of electrocoagulation using iron electrodes in real dyeing wastewater treatment was assessed based on pollutants removal efficiency, sludge generation, energy consumption and operation cost in practice. The effects of current density, pH, conductivity, and reaction time on treatment performance were evaluated. The operation cost of electrocoagulation was calculated including the energy cost, the iron plate cost, generated sludge treatment cost, and added substances cost. The results indicated that the colour, CODcr and TSS removal efficiencies were high and quite stable with short reaction time (reached 92.07 ± 1.21%, 65.7 ± 1.47%, and 89.8 ± 1.2%, respectively, with only 15 min). Average sludge generation, specific energy consumption, and operation cost were determined respectively as 0.645±0.0543 kg/m^3, 1.182 kWh/m^3 and 0.517 USD/m^3. Coagulation-flocculation using $FeSO_4$ was performed as a control experiment as well. Compared to coagulation-flocculation, electrocoagulation has the same removal efficiency but has less generated sludge (only 50%) and little to no added chemicals. Therefore, the operating cost was quite less than the others, with only 0.517 USD/m^3 instead of 1.99 USD/m^3 (equal to 1/3.5).

INTRODUCTION

The real dyeing wastewater has usually extremely variable characteristics depending on the kind of dyes used and production capacity according to customer orders. It is highly coloured and viscous caused by residual dye and suspended solids. It also contains a lot of sodium and chloride ions due to high sodium chloride consumption in processing units (Hussain et al. 2004). In general, developing countries and namely, in Vietnam, the conventional and popular treatment method applied in primary treatment to remove colour and TSS (Total suspended solid) in dyeing wastewater is coagulation-flocculation-sedimentation. However, the amount of generated hazardous sludge and high chemical consumption are the biggest problems of this method.

Electrocoagulation (EC) is well known as the method that can remove colour, COD (chemical oxygen demand), TSS in the textile wastewater by electrolysis reaction using iron or aluminium or stainless steel electrodes. The pollutants can be removed by flocculation, adsorption of contaminants on flocs, sedimentation and floatation in the EC process. Iron electrodes out-performed others (Wang et al. 2016). Easy operation, none used chemicals, low sludge settling time, and less sludge formation are the main advantages of electrocoagulation technology (Khorram & Fallah 2018, Chaturvedi & Satish 2013).

In recent years, most results of the previous studies on electrocoagulation using iron or aluminium electrodes to remove various dye types in textile wastewater showed that the dye and colour removal efficiencies were too high, from 83% to 100%. Each dye type in synthetic wastewater had a different optimal operating condition when treated by the electrocoagulation method. The operating factors significantly affected the treatment performance of dyeing wastewater such as current density, pH, conductivity, and reaction time (Aleboyeh et al. 2008, Arslan-Alaton et al. 2009, Charroenlarp & Choyphan 2009, Daneshvar et al. 2003, 2007, Kashefialasl et al. 2006, Khandegar & Saroha 2013, Khorram & Fallah 2018, Ahmed et al. 2018, Wang et al. 2016, Korbahti et al. 2011, Huynh et al. 2016, Parsa et al. 2011, Yang & McGarrahan 2005, Yuksel et al. 2013). Although the previous studies illustrated that electrocoagulation was able to remove dye and colour with high performance, most of these researches were performed with synthetic wastewater containing a specific dye. Therefore, it is difficult to apply these results to the general practical treatment of real wastewater containing various pollutant's concentration with different kinds of dye. In this study, the

electrocoagulation method using iron electrodes to treat the real dyeing wastewater from textile manufactory was investigated. The effect of pH, current density, reaction time, and conductivity was evaluated to find out the optimal operating condition. The treatment efficiency, sludge generation, energy consumption, and operation cost of the EC process were determined. In addition, the coagulation-flocculation method using $FeSO_4$ was performed as a control experiment. A comparison of the electrocoagulation method and conventional method based on generated sludge, specific energy consumption, and operation cost were evaluated to provide a scientific basis for selecting and replacing technology in the primary treatment of dyeing wastewater.

MATERIALS AND METHODS

Materials

The real dyeing wastewater was taken every day from the output of the equalization tank of the wastewater treatment system at Shoelace dyeing manufactory, Ho Chi Minh City, Vietnam, during October 1st, 2018 to November 16th, 2018 (Toan Hung Co., Ltd., Vietnam). The characteristics of real dyeing wastewater are presented in Table 1. $FeSO_4.7H_2O$ was used as the coagulant in the control experiment. pH and conductivity were controlled by $NaOH/H_2SO_4$ and NaCl, respectively. $FeSO_4.7H_2O$, $NaOH/H_2SO_4$ and NaCl were procured from Xilong Chemical Co. Ltd., China.

Experimental Set Up and Analysis Methods

The experimental bench scale was set up as shown in Fig. 1. In this study, the temperature of wastewater was maintained at the same temperature as the coagulation-flocculation tank in the wastewater treatment system, in the range of 37°C - 40°C by the electrical heater before supplying into the reaction tank. 8 litres of the wastewater was supplied into a polyacrylic reaction tank (200mm × 200mm × 250mm) containing a pair of iron plate electrodes. The dimensions of the 5mm thick plate electrodes are 150mm × 200mm. The gap between the electrodes is 2.5cm. The electrical current was directly supplied from a laboratory DC power supply (DC Regulated power supply - QJ3010E, China).

Table 1: Characteristics of the real dyeing wastewater.

No.	Parameters	Unit	Range of value
1	pH	-	6.58 - 7.21
2	Colour	Pt - Co	500 - 2,513
3	Conductivity	mS/cm	0.36 - 0.78
4	CODcr	mg/L	430 - 1,620
5	TSS	mg/L	478

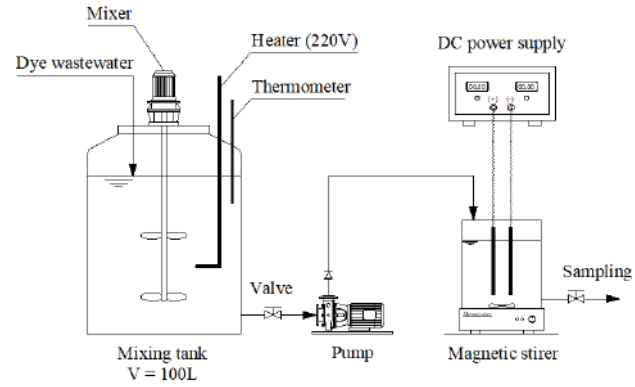

Fig. 1: Schematic diagrams of the electrocoagulation system.

500 mL sample was taken and removed the deposited sludge by settling for 60 min. CODcr, colour, and TSS were determined following the Standard Methods for the Examination of Water and Wastewater (APHA 1995). The mass of generated sludge was evaluated by the determination method of TSS in the treated wastewater. The pH value, temperature, and conductivity were observed by a pH meter (Hana, Germany), thermometer (Okaya Handy Thermo/T200, Japan), conductivity meter (Hana Model 130, Germany), respectively.

Each experiment was repeatedly carried out 3 times and experimental results were analyzed by ANOVA with α = 0.05. Each experiment time was performed with the same homogeneous wastewater sample.

Calculation Methods

Removal efficiency, current density, energy consumption, and quantity of dissolved iron were calculated as previous studies of Huynh et al. (2016) and Chaturvedi & Satish (2013) as follow:

The removal efficiency was calculated as

$$E_{ff} = \frac{C_0 - C_t}{C_0} \times 100 \quad \ldots(1)$$

Where, E_{ff} is the removal efficiency, %. C_0 and C_t are pollutants concentration at initial and t (min) reaction time, respectively.

The current density was calculated through the equation:

$$CD = \frac{I}{S} \quad \ldots(2)$$

Where, CD is the current density, A/m^2.

I is the current (A) and S is total surface area of the electrodes (m^2).

Electrical energy consumption by EC process:

$$E_{EC} = \frac{E_{cell} \times I \times t}{3.6 \times V} \quad \ldots(3)$$

Where, E_{EC} is energy consumption for EC, Wh/m^3. E_{cell} is the cell potential (V). I is the total current (A). t is the electrolysis time (s). And V is the working volume of the reactor (L)

The dissolved iron quantity in the EC process was calculated by equation .

$$W = \frac{i \times t \times M}{n \times F} \quad \ldots(4)$$

Where, W: the amount of dissolution of iron electrode (g); i: current (A); t: reaction time (s); M: Molecular weight of iron; n: number of electrons in oxidation/reduction reaction, $n_{Fe} = 2$; F: Faraday's constant, 96485 C/mol.

RESULTS AND DISCUSSION

The Effect of Current Density

Current density is the most important factor that affects treatment efficiency and energy consumption in the EC process. In this study, the current density was changed in the range of 12.5 A/m^2 - 33.3 A/m^2. pH and electrical conductivity were controlled in the range of 6.7 - 7 and 2.5 mS/cm, respectively. The reaction time was 20 min. The results indicated that current density significantly affected the colour removal (P-value: 0.000749). Colour removal efficiency increased rapidly from 10.78% to 90.8% when current density rose from 12.5 A/m^2 to 20.8 A/m^2 and approximate 94% with a current density of 25 A/m^2. When current density was continuously increased, colour removal performance was slightly increased. It reached nearly 95% when the current density rose to 33.3A/m^2 (Fig. 2a). The higher current density led to consuming more energy. Therefore, the suitable current density value was chosen based on colour treatment efficiency and energy consumption. In this case, the current density of 25 A/m^2 was chosen.

The Effect of pH

pH is the key parameter in the electrocoagulation process (Chafi et al. 2011). It possibly directly affects the removal efficiency and chemical consumption to adjust pH before and after treatment. In this study, the effect of pH on colour removal efficiency was determined with experimental conditions such as pH range from 3 to 9, the current density of 25 A/m^2, the electrical conductivity of 2.5mS/cm, and reaction time of 20 min. The ANOVA analysis results showed that the effect of pH on colour treatment was significant with P-value equal to 2.2×10^{-7}. The observed data is depicted in Fig. 2b. The colour removal efficiency rapidly increased when pH increased from 3 to 7 and reached 94.07% at pH 7. Then, it slightly increased to 95.59% when pH rose from 7 to 9. It was caused by an acidic medium, OH^- ions generated from the cathode reacted with H^+ ions led to lack of OH^- for iron hydroxide formation. When increasing pH, the presence of OH^- ions in solution was risen to enhance the formation and precipitation processes of iron ions. In addition, Fe^{2+} was generated at anode and oxidized to Fe^{3+} by Cl_2, HOCl, and ClO^- in acidic, neutral and alkaline mediums, respectively (Chafi et al. 2011). HOCl is more effective than others. Precipitation of $Fe(OH)_2$ starts at pH = 8 and $Fe(OH)_3$ starts at pH = 3.5 (Magdalena & Aneta 2011).

With this actual dyeing wastewater, pH of influent wastewater nearly equalled to 7, making the optimal pH as 7 for treatment by electrocoagulation process using iron electrodes because no or little chemicals were used to adjust pH value allowing the colour removal efficiency nearly reached the optimal value.

The Effect of Electrical Conductivity

Electrical conductivity was varied at 1.5 mS/cm; 2.0 mS/cm, 2.5 mS/cm and 3.0 mS/cm. Current density, pH and reaction time were fixed at 25 A/m^2, 7 and 20 min, respectively. Although colour removal efficiency in these experiments slightly increased from 92.3% to 93.7% when electrical conductivity rose from 1.5 mS/cm to 2.5 mS, ANOVA analysis results indicated that electrical conductivity didn't affect significantly the colour removal, P-value of 0.119. It was the same with a previous study (Huynh et al. 2016). With the same current density input, the voltage was inversely proportional to electrical conductivity and followed an equation: $y = -2.23x + 16.878$ ($R^2 = 0.9967$). So, the electrical conductivity directly affected energy consumption. Increasing electrical conductivity led to reducing energy consumption in the EC process (Huynh et al. 2016). In this study, electrical conductivity increased from 1.5 mS/cm to 3.0 mS/cm, energy consumption decreased 2.14 times.

The Effect of Reaction Time

Reaction time was surveyed from 5 to 35 min with the current density of 25 A/m^2, pH 7 and EC of 2.5 mS/cm. The obtained results presented in Fig. 2c showed that colour removal performance increased markedly in the first 15 min reaction time and archived at nearly 91%. Extending reaction time, treatment efficiency slowly and trivially increased, reached upto 94.5% within 30 min. It is easy to explain because the amount of dissolved iron ion generated in the first 15 min reaction time was nearly enough for the coagulation and flocculation process. When reaction time rose to 35 min, colour removal slightly reduced to 93% caused by residual iron ions in solution.

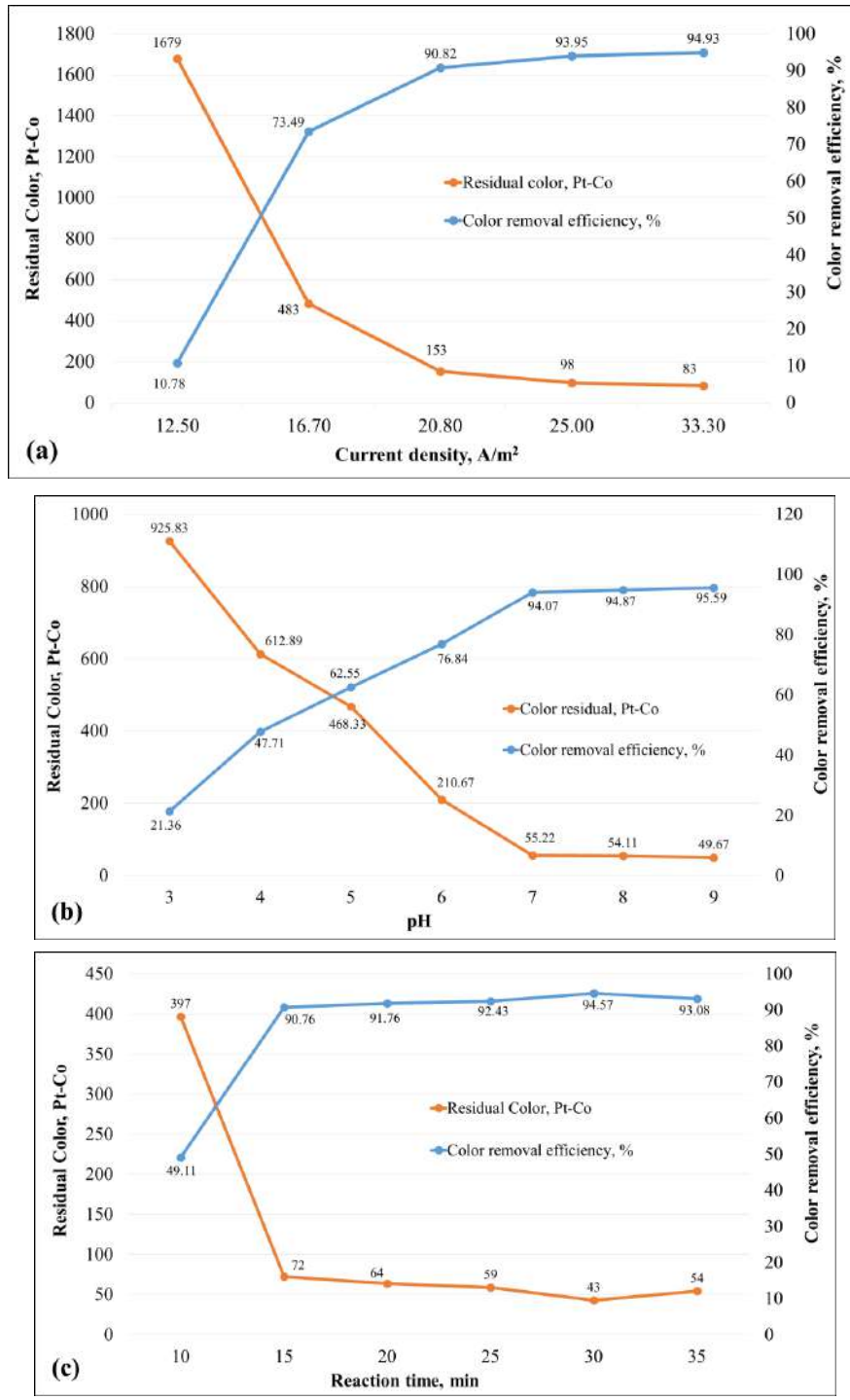

Fig. 2: The average colour removal versus various current density (a), pH value (b) and reaction time (c).

The Treatment Efficiency by Electrocoagulation

In order to determine the applicability of this method into wastewater treatment with the real condition at the factory, the testing was performed with the real wastewater taken in different 25 days. The suitable operating parameters were obtained as current density of 25 A/m^2, non-adjusted pH, electrical conductivity of 2.5 mS/cm and 15 min reaction

time. As depicted in Fig. 3, the results showed that the treatment performance was very high and quite stable even though the characteristics of wastewater in input flow much fluctuated. Namely, during the observed period, the pH, colour, CODcr, TSS, and conductivity were in range of 6.58 - 7.21, 725 Pt-Co - 2,513 Pt-Co, 415 mg/L - 1,692 mg/L, 320 mg/L - 478 mg/L and 0.33 mS/cm - 0.78 mS/cm, respectively. It may be explained as: in the EC process, iron hydroxo complexes formed at the anode has high adsorption properties, forming strong aggregates with pollutants. In addition, the flocculation and adsorption capacity was increased when the pollutant concentration increased due to the higher contacting opportunities between pollutants and coagulants (Kabdasli et al. 2014). It may buffer the fluctuation in inlet flow. The average treatment efficiency was 92.04 ± 1.21%, 65.71 ± 1.47% and 89.8 ± 1.2% corresponding to colour, CODcr, and TSS removal respectively (Table 2). Compared to the discharge standard in Vietnam (QCVN 13:2015/BTNMT, column B), the residual colour and TSS in effluent were lower but residual CODcr was still too much higher than the discharged standard. Therefore, CODcr in the effluent of electrocoagulation reaction was continuously treated by the next stage.

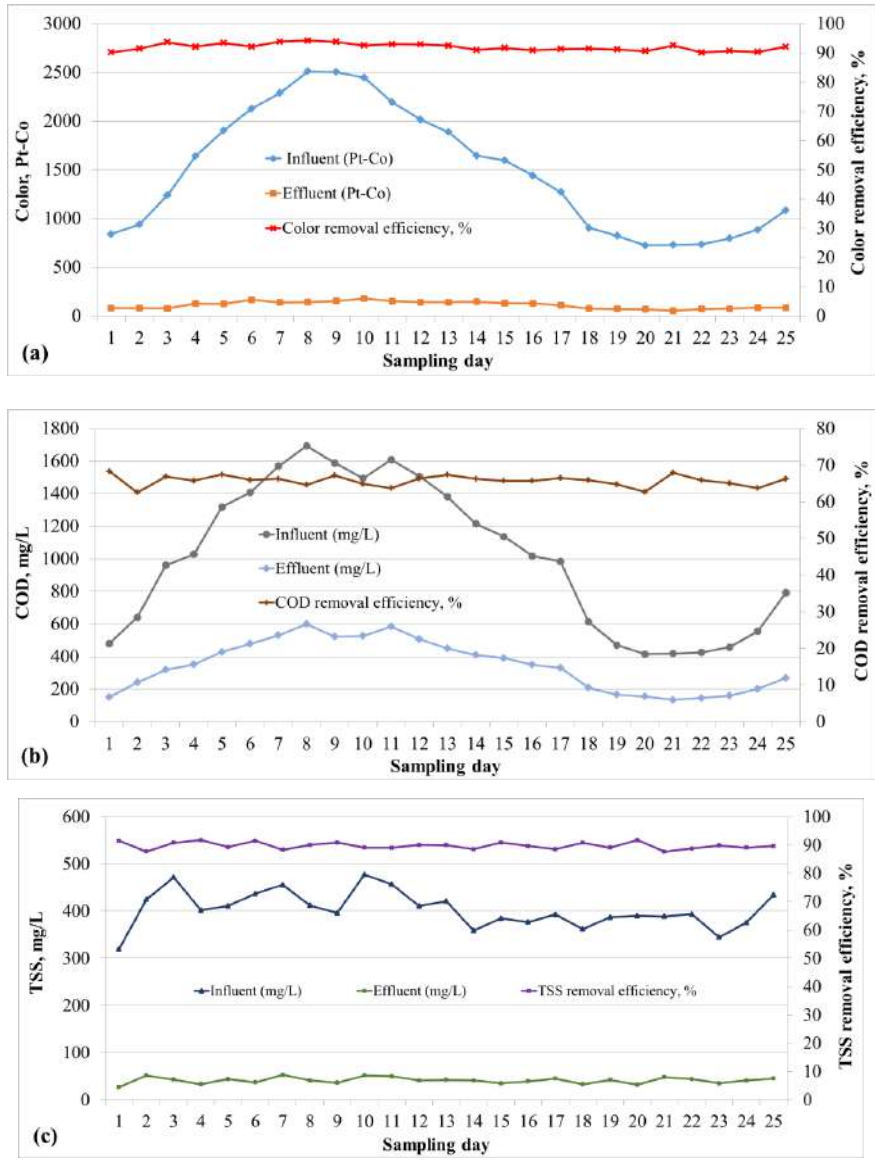

Fig. 3: Variation of concentration and removal efficiencies of Colour, CODcr, TSS.

The average mass of generated sludge including flotation and sedimentation process was 0.645±0.054 g/L (Table 2). Specific energy consumption was evaluated by equation (3), approximately 1.182 kWh/m^3 (Table 2). Iron consumption was determined based on the dissolved iron quantity (Eq. 4) and the total volume of treated wastewater, equal 0.0975 kg/m^3.

Comparisons of Electrocoagulation and Coagulation-Flocculation

The optimal value of pH and coagulant dose of $FeSO_4.7H_2O$ in the coagulation-flocculation process using the same raw wastewater used in the electrocoagulation process were determined by Jar-test experiment. The treatment performance, sludge generation, and chemical use were calculated in coagulation-flocculation as well. With the optimal condition, CODcr, TSS and decolourization efficiency reached 56.8 ± 2.2%, 82.4 ± 2.9%, and 93 ± 0.6%, respectively. Sludge generation was 1.5 ± 0.0419 kg/m^3.

The comparison of the electrocoagulation and coagulation-flocculation based on treatment efficiency, sludge generation, energy consumption, chemical use, and operation cost were summarized and presented in Table 2. Colour removal efficiency was the same in both methods but CODcr and TSS treatment performances in the electrocoagulation were higher. Sludge generation, chemical use in electrocoagulation were quite less than coagulation-flocculation. This is because, in electrocoagulation, TSS was mainly removed by flotation mechanism so the small flocs formed was immediately floated to the surface by many fine bubbles (H_2). It did not need as much ion iron to form big flocs to settle to the bottom as in coagulation-flocculation. Moreover, the coagulant in electrocoagulation was directly generated in situ from the anode, did not contain impurify materials. OH- participated in the flocculation reaction that was formed from H_2O. OH^- generation had been consumed that buffered the pH of the solution during electrocoagulation led to the final pH of effluent changed only slightly. Therefore, there was no need to add chemical to provide OH^- and adjust pH after treating it as the traditional chemical coagulation.

Calculation of the operating cost included the energy cost, iron plate cost, generated sludge treatment cost, and added substances cost. The results showed that the operation cost of electrocoagulation was far much lower than coagulation-flocculation as well, with only 0.517 USD/m^3 instead of 1.99 USD/m^3 as in conventional coagulation, approximately equal to 1/3.5. The main reasons were because of less generated sludge and no added chemical in the electrocoagulation process (with only small amount of NaCl).

Table 2: Comparison of electrocoagulation using iron electrodes and coagulation-flocculation using $FeSO_4$.

Criteria	Electrocoagulation	Coagulation-Flocculation
pH	7.0	11.0
Colour removal efficiency (%)	92 ± 1.21	93 ± 0.61
CODcr removal efficiency (%)	65.7 ± 1.47	56.8 ± 2.2
TSS removal efficiency (%)	89.8 ± 1.2	82.4 ± 2.9
Sludge generation (kg/m^3)	0.645 ± 0.0543	1.5 ± 0.0419
Specific energy consumption (kwh/m^3)	1.182	0.135
NaOH 98% (kg/m^3)	0	0.8 ± 0.02
H_2SO_4 98% (kg/m^3)	0	0.472 ± 0.011
$FeSO_4$ (kg/m^3)	0	0.75
NaCl (kg/m^3)	1.17 ± 0.33	0
Iron plate consumption (kg/m^3)	0.0975	0
Operation cost* (USD/m^3)	0.517	1.99

*The operation cost in both methods was calculated based on the price in Vietnam (Pham Phu Gia Chemical Co. Ltd.).

CONCLUSIONS

This study found the optimal operating parameters for real dyeing wastewater treatment by electrocoagulation using iron electrodes as follows: current density of 25 A/m^2, non-adjusted pH, electrical conductivity of 2.5mS/cm and 15 min reaction time. Electrocoagulation using iron electrodes may be applied in actual dyeing wastewater treatment of shoelace manufactories because it was able to remove colour, CODcr, and TSS in the actual dyeing wastewater with high performance, archived 93±0.6%, 56.8±2.2%, and 82.4±2.9%, respectively. Furthermore, it adapted to the various characteristics of influent very well, released less generated sludge, and consumed low operating cost.

ACKNOWLEDGMENT

We are grateful to Toan Hung Co. Ltd. and Bao Hung Environmental Engineering Corporation for supplying dyeing wastewater and bench-scale reactor.

REFERENCES

Ahmed, S. N., Mohammed, A. A., Peter, A. A. and Shreeshivadasan, C. 2018. Treatment of textile wastewaster using a novel electrocoagulation reactor design. Intech Open, DOI: 10.5772/intechopen.76876

Aleboyeh, A., Daneshvar, N. and Kasiri, M.B. 2008. Optimization of C. I. Acid Red 14 azo dye removal by electrocoagulation batch process with response surface methodology. Chemical Engineering and Processing, 47(5): 827-832.

APHA 1995. Standard Method for Examination of Water and Wastewater, 19th ed., American Public Health Association Inc., New York, Part 2120C, 2540D, 2710C, 5220B.

Arslan-Alaton, I., Kabdaşli, I., Vardar, B. and Tünay, O. 2009. Electrocoagulation of simulated reactive dye bath effluent with aluminum and stainless steel electrodes. Journal of Hazardous Materials, 164(2-3): 1586-1594.

Chafi, M., Gourich, B., Essadki, A.H., Voal, C. and Fabregat, A. 2011. Comparison of electrocoagulation using iron and aluminium electrodes with chemical coagulation for the removal of a highly soluble acid dye. Desalination, 281: 285-292.

Charroenlarp, K. and Choyphan, W. 2009. Reuse of dye wastewater through colour removal with electrocoagulation process. Asian J. Energy Environment, 10(4): 250-260.

Chaturvedi and Satish I. 2013. Electrocoagulation: A novel wastewater treatment method. International Journal of Modern Engineering Research, 3(1): 93-100.

Daneshvar, N., Khataee, A.R., Amani Ghadim, A.R. and Rasoulifard, M.H. 2007. Decolorization of C.I. Acid Yellow 23 solution by electrocoagulation process: Investigation of operational parameters and evaluation of specific electrical energy consumption (SEEC). J. Hazard. Mater., 148(3): 566-572.

Daneshvar, N., Sorkhabi, H.A. and Tizpar, A. 2003. Decolorization of orange II by electrocoagulation method. Sep.Purifi.Technol., 31: 153-162.

Hussain, J., Hussain, I. and Arif, M. 2004. Characterization of textile wastewater. Journal of Industrial Pollution Control, 20(1): 137-144.

Huynh, Ngoc-Han T., Duong, Pham-Hung and Yoon, Y.S. 2016. Removal of C.I. Acid Red 114 dye from wastewater by using ozonation and electrocoagulation. Jacobs Journal of Environmental Sciences, 2(2): 019.

Kabdasli, I., Arslan-Alaton, I., Olmez-Hanci, T. and Tunay, O. 2012. Electrocoagulation applications for industrial wastewaters: a critical review. Environmental Technology Review, 1(1): 2-45.

Kashefialasl, M., Khosravi, M., Marandi, R. and Seyyedi, K. 2006. Treatment of dye solution containing coloured index acid yellow 36 by electrocoagulation using iron electrodes. Int. J. Environ. Sci. Technol., 2(4): 365-371.

Khandegar, V. and Saroha, A.K. 2013. Electrochemical treatment of effluent from small scale dyeing unit. Indian Chem. Eng., 55(2): 1-9.

Khandegar, V. and Saroha, A.K. 2014. Electrochemical treatment textile effluent containing Acid Red 131 dye. J. Hazard. Toxic. Radio. Waste., 18(1): 38-44.

Khorram, A. G. and Fallah, N. 2018. Treatment of textile dyeing factory wastewater by electrocoagulation with low sludge settling time: optimization of operating parameters by RSM. Journal of Environmental Chemical Engineering, 6(1): 635-642.

Korbahti, B.K., Artut, K., Gecgel, C. and Ozer, A. 2011. Electrochemical decolorization of textile dyes and removal of metal ions from textile dye and metal ion binary mixtures. Chem. Eng. J., 173(3): 677-688.

Magdalena, B. and Aneta, P. 2011. Study of pH influence on selective precipitation of heavy metals from acid mine drainage. Chemical Engineering Transaction, 25: 345-350.

Parsa, J.B., Vahidian, H.R, Soleymani, A.R. and Abbasi, M. 2011. Removal of Acid Brown 14 in aqueous media by electrocoagulation: optimization parameters and minimizing of energy consumption. Desalination, 278(1-3): 295-302.

Yang, C.L. and McGarrahan, J. 2005. Electrochemical coagulation for textile effluent decolorization. J. Hazard. Mater., B127(1-3): 40-47.

Yuksel, E., Eyvaz, M. and Gurbulak, E. 2013. Electrochemical treatment of colour index Reactive Orange 84 and textile wastewater by using stainless steel and iron electrodes. Environ. Prog. Sust. Energy, 32(1): 60-68.

Wang, J., Tan H. C., Zhang, Y. L. and Pan Y. Z. 2016. The treatment of high concentration dyeing wastewater with pulse current electrocoagulation. Morden Applied Science,10(5).

Nature Environment and Pollution Technology
An International Quarterly Scientific Journal

p-ISSN: 0972-6268
(Print copies up to 2016)
e-ISSN: 2395-3454

Vol. 20 | No. 2 | pp. 595-600 | 2021

Original Research Paper

https://doi.org/10.46488/NEPT.2021.v20i02.016

Open Access Journal

Soil Fertility Evaluation to Adopt Climate-Smart Agriculture in Mambattu Village, Maduranthakam Block of Kanchipuram District, Tamil Nadu, India

Kalpana Palani†, Selva Preetha Paneer Selvam, Sathya Velusamy and Ramasubramaniyan Ramanathan Melmangalam

National Agro Foundation, Research and Development Centre, Anna University Taramani Campus, Taramani, Chennai-600113, India

†Corresponding author: Kalpana Palani; kalpana.rajesh@nationalagro.org

Nat. Env. & Poll. Tech.
Website: www.neptjournal.com

Received: 22-05-2020
Revised: 20-07-2020
Accepted: 25-07-2020

Key Words:
Soil fertility
Agriculture
Lean farming
Climate change
Sustainable agriculture

ABSTRACT

Assessment of soil fertility is essential to help identify strategies for sustainable agricultural production systems that decrease the negative environmental impact. The objective of this research study is to carry out a preliminary assessment of soil fertility status to adopt climate-smart agriculture to address the climate change challenges that adversely affect crop productivity and livelihoods of the farming community. The research was carried out in Mambattu village, Maduranthakam block of Kanchipuram district, Tamil Nadu. A systematic set of twenty geo-referenced soil samples were collected from the study village using GPS (Global Positioning System) and analysed for pH, EC, available macro, secondary and micronutrients to develop a credible soil fertility index (SFI). The preliminary fertility data of Mambattu village revealed that the pH of soil samples varied from acidic to alkaline with about 40% as neutral while the electrical conductivity showed non-saline and medium status of Organic Carbon (OC). The soil samples were predominantly sufficient in N and some micro nutrients (Fe, Mn), while medium in S and B and deficient in P, K, Ca, Mg, Zn and Cu. Results from initial studies indicate that practices like site specific nutrient management, green manuring, use of organic inputs, use of integrated pest management, seed treatment etc., have a high potential for implementing climate-smart agricultural technologies. Soil fertility evaluation can be an efficient tool to improve soil health which can positively impact crop productivity and be one of the important climate-smart technologies practices adopted by the farmers.

INTRODUCTION

The rural community in India is dependent on agriculture and allied sectors for their livelihoods, either directly as a farmer (own or leased lands) or indirectly as an agricultural labourer (landless). Thus, the agriculture sector provides employment to more than 60% of the Indian population people, which is much more than any other economic sector.

Climate change, which is attributable to the natural climate cycle and anthropogenic activities, has adversely affected agricultural productivity the world over including in India. As large parts of arable land in India are rain-fed, agriculture depends on the rainfall. Thus, rainfed agriculture as largely practised in India will be adversely affected by an increase or decrease in the overall rainfall range but also by the shifts in the timing of the rainfall. Due to increased variation in the rainfall as a combination of many factors including climate change, farm productivity is impacted adversely and this has a serious implication on both food production and the country's food security.

The impact of climate change on water availability will be particularly severe for India because large parts of the country already suffering from water scarcity, to begin with, and are largely dependent on groundwater for irrigation. According to Cruz et al. (2007), India's wetlands and ecosystems are severely degraded due to the decline in precipitation and increased drought conditions. About 54 percent of India faces high to extremely high water stress (Shiao et al. 2015).

The Climate-Smart Agriculture (CSA), a concept initiated by FAO to respond to the combined challenges of climate change and their potential threat to food security; has brought out a rich, resourceful and comprehensive approach to mitigate the risk of climate change. According to the FAO, three main approaches to mitigate climate change include a sustainable increase of agricultural productivity, adaptation and building resilience to climate change and reduction of GHG emissions. Beyond technological solutions, many other practices are both cost-effective and have a positive climatic impact, such as better manure management, integrated crop-livestock management, use of renewable energy, use

of legumes or cover crops, improved animal feeding, and practices that increase soil carbon (Kalpana et al. 2019).

Soil fertility is one of the important factors affecting the yields of the crops. In order to achieve sustainable agriculture production, soil characterization for fertility evaluation of a particular region or area is important. In recent years, due to the imbalanced and inadequate fertilizer use, coupled with low efficiency of other inputs, the response (production) efficiency of chemical fertilizer nutrients has declined tremendously under intensive agriculture. In fact, poor growth, declining yield, pest and disease infestations associated with poor soil fertility are the major threats to marginal farmers of India (Raghunatha Reddy et al. 2019)

Hence, maintaining soil health and sustaining agricultural productivity is a major concern for many farmers. Despite good care and a lot of investments, the farmer is not able to get a reasonable return. Lack of knowledge on periodic soil testing for any nutrient deficiency and seeking the right advice from experts are some of the reasons for declining soil fertility, agricultural productivity and loss to farmers. Though huge information on soil fertility status of soil at the district and state level is available, the village level fertility evaluation is very low in India. Hence, village level soil fertility indexing would be beneficial in understanding the distributions of soil properties at the field scale for refining agricultural management practices and assessing the impact of agriculture on environmental quality (Cambardella et al. 1994). In addition, maintaining or improving the soil quality can provide economic benefits in the form of increased productivity, efficient use of inputs, and improvement in water and air quality. Assessment of soil quality involves measuring physical, chemical and biological soil properties and using these measured values to evaluate changes in the soil as a result of land-use change or management practices (Adolf 2012).

STUDY AREA

Mambattu is a small village/hamlet among the ninety-five villages in Vaiyavoor Panchayath, Maduranthakam block, in the rural region of Kanchipuram district of Tamil Nadu (Fig. 1). It is surrounded by Lathur block towards north, Thirukkazhukunram block towards east, Acharapakkam block towards west, Chithamur block towards the south. It lies between 12°28' N and 79° 83' E and receives an annual rainfall of 1228.5 mm and a mean annual temperature of 38°C. The total geographical area of the taluk is 332.43 ha, while the total area under cultivation is approximately 63.271 ha. According to the Census 2011, the village has 209 families with a total population of 803, with a literacy of 41%, 55.2% employed individual and 44.8% non-working.

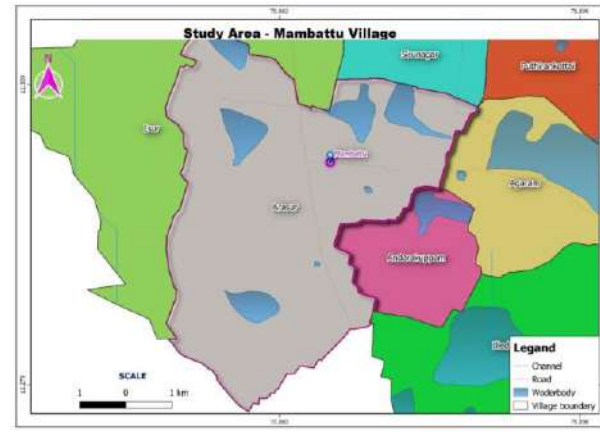

Fig. 1: Study Area - Mambattu village, Maduranthakam block, Kanchipuram district, Tamil Nadu, India.

Of the 55.2% working individual, 6.1% of individuals are cultivators (owner or co-owner) and 52.8% are agricultural labourers. This emphasizes the need to support agriculture through climate agriculture technologies and practices as close to 60% of the population is dependent on agriculture directly or indirectly for their livelihoods. Maduranthakam block is dominated by red soil with sandy loam texture, with major crops cultivated include paddy, sugarcane, maize, ragi, groundnut and coconut. The major sources of irrigation are wells and canal.

The main objective of the study was to explore how Climate Smart Agriculture technological innovations could solve climate-mediated problems in agriculture at the village level. Hence, preliminary work on soil fertility indexing studies was undertaken in the study location to understand the soil fertility status currently. Reassessment of the impact of interventions of the above implemented technology is planned to be carried out in the future.

MATERIALS AND METHODS

Collection of Soil Samples

As an initial step, soil samples were collected for assessing the health status of the soil. In total, 20 geo-referenced surface soil samples from the agricultural fields of the research village were collected using GPS (Global Positioning System) at 0-30 cm depth by adopting the standard procedures of soil sample collection. The collected soil samples were air-dried, gently crushed, sieved using a 2 mm sieve for all analysis except organic matter analysis wherein the sample was sieved using a 0.5 mm sieve. The processed soil samples were preserved in polythene bags for further analysis.

Table 1: Fertility Rating Class and Nutrient Index Value.

S. No.	Nutrient Index	Value
1	Low	<1.67
2	Medium	1.67-2.33
3	High	>2.33

CHEMICAL ANALYSIS OF SOIL SAMPLES

The chemical analysis of the soil samples of all the sites was carried out following standard procedures as per the guide to laboratory establishment for plant nutrient analysis as indicated by FAO (2008) and Tandon (2005).

The Nutrient Index Values were calculated using the following formula:

$$NIV = [(PH \times 3) + (PM \times 2) + (PL \times 1)]/100$$

Where, NIV is Nutrient Index Value, PL, PM and PH are the percentage of soil samples falling in the category of low, medium and high nutrient status and which are given weightage of one, two and three respectively (Ramamoorthy & Bajaj 1969). The fertility ratings and corresponding index values are given in Table 1.

RESULTS AND DISCUSSION

Physico-chemical Properties

The result pertaining to the percent sample category and nutrient index of physico chemical properties of Mambattu village is given in the Table. 2. The pH is an important index of soils that determines the extent of the acidity/ alkalinity and directly influences agriculture productivity. The pH value reflects the integrated effect of the acid-base reactions taking place in the soil system (Mokolobate & Haynes 2002).

The sample soil in the research showed a wide range of pH between 5.53-8.51 with a mean value of 6.92. Moreover, samples showing acidic, neutral and alkaline pH are 35, 40 and 25 per cent respectively with fertility index indicating neutral pH. Most of the soils require the application of organic manures for improvement in the physical condition of the soil as well as for improvement in soil health. EC (mS/cm) of the research field ranged from 0.04 -0.38 mS/cm i.e., less than 0.8 mS/cm, which is within the normal range.

Organic matter has an essential role in agricultural soil, as it supplies plant nutrients, improves the soil structure, improves water infiltration and retention, feeds soil microflora and fauna, and the retention and cycling of applied fertilizer (Johnston 1986). In the study area, organic carbon is low in 40% of soils, medium in 40% soils, and high in 20% of soils. The range of organic carbon in the soil ranges between 0.39-1.09 per cent, with an average mean value of 0.67, which indicates medium fertility index.

Available Macro Nutrients

The results of the percent sample category and nutrient index of macronutrients of Mambattu village are furnished in Table 3. The nitrate content of the soil ranged from 15.0-39.7 mg/kg with a mean value of 25.66 mg/kg, where 90 per cent soil falls under high, 10 percent under medium with no soil sample showing low nitrate category (Fig. 2). Hence, the fertility index of nitrate content of Mambattu soil is high.

The fertility index of phosphorus availability in soils revealed that the phosphorus content is low in acidic soil

Table 2: Percent sample category and nutrient index of the physico-chemical properties of Mambattu village.

S. No.	Parameters	Percent samples			Range	Mean±SD	Nutrient Index Value	Fertility Index
1	pH	Acidic	Neutral	Alkaline	5.53- 8.51	6.92±0.55	1.90	Neutral
		35	40	25				
2	EC (mS/cm)	Harmless	Normal	Harmful	0.04 -0.38	0.15±0.09	1.00	Harmless
		100	0	0				
3	OC (%)	Low	Medium	High	0.39 – 1.09	0.67±0.19	1.80	Medium
		40	40	20				

Table 3: Percent sample category and nutrient index of macronutrients of Mambattu village.

S. No.	Parameters	Percent samples			Range	Mean±SD	Nutrient Index Value	Fertility Index
		Low	Medium	High				
1	Available Nitrogen (mg/kg)	0	10	90	15.0 – 39.7	25.66±5.82	2.90	High
2	Available Phosphorus (Acidic soil) (mg/kg)	100	0	0	8.93 -85.79	28.71±24.70	1.00	Low
3	Available Phosphorus (Alkalin esoil) (mg/kg)	44.4	22.2	33.3	5.81-71.28	24.84±21.32	1.89	Medium
4	Available Potassium (mg/kg)	75	0	25	50.0-257.0	116.10±61.55	1.50	Low

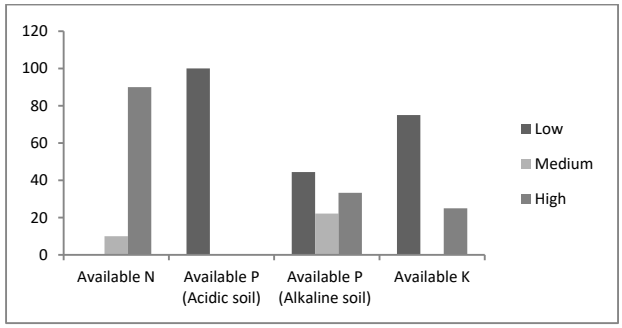

Fig. 2: Fertility rating of macronutrients.

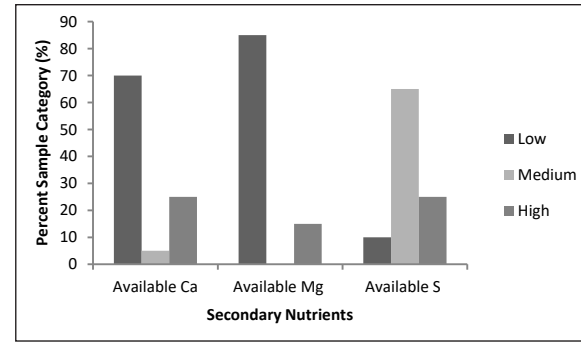

Fig. 3: Fertility rating of secondary nutrients.

and medium in alkaline soil. The percent sample category of acidic soil shows that the 100% samples fall under the low category where phosphorus content ranges from 8.93-85.79 mg/kg with an average of 28.71 mg/kg. The percent sample category of phosphorus content of alkaline soil shows that the 44.4, 22.2 and 33.3 percent falls under low, medium and high respectively with content ranging between 5.81-71.28 mg/kg with a mean value of 24.84 mg/kg. Similarly, the potassium content of the soil ranged from 50.0-257.0 mg/kg, with a mean value of 116.10 mg/kg where the fertility index denotes the soil is low in potassium with 75 percent samples falling under low and the rest under the high category.

The results are significantly influenced by the farming practices of farmers in this region. Most of the farmers are using chemical fertilizers-urea and phosphatic fertilizers only, which contains concentrated amounts of nitrogen and organic carbon, potassium and phosphorus. On the basis of these results of the study, the farmers were advised to use integrated nutrient management practices to maintain optimum levels of all the essential nutrients for plants. Singh & Mishra (2012) reported a similar impact in their study that the low to medium fertility status for nitrogen, phosphorus, potassium and sulphur was due to the imbalanced and insufficient fertilizer use, along with low efficiency of other inputs. The response (production) efficiency of chemical fertilizer has reduced extremely under intensive agriculture (Kalpana et al. 2019).

Available Secondary Nutrients

The results of the percent sample category and fertility index of secondary nutrients of Mambattu village are presented in Table 4. The fertility index of calcium, magnesium and sulphur were low, low and medium respectively. The available calcium content of soil ranged from 458-3869 mg/kg with a mean value of 1492.50 mg/kg, where 70 percent of samples come under the low category (Fig. 3). Similarly, the magnesium content of the soil ranged from 192-893 mg/kg with a mean value of 386.20 mg/kg, where 85 percent of samples were under the low category. The low category of calcium and magnesium in the soil is due to acidic pH. In the study village, the pH of the maximum number of samples was acidic to near neutral. Hence, these soils require high liming material to neutralize the soil acidity and supply Ca and Mg. The choice of suitable liming material based on the content of soil Ca and Mg is a key to provide crops and soils with an adequate quantity of these nutrients. The aim of a liming program is to institute preferred soil pH and to sustain soil fertility levels with an optimum range of Ca and Mg. Other reason for the low levels of Ca might be attributed to the continuous addition of acidifying chemical fertilizers. Similar results were recorded by Amara et al. (2015). Moreover, the sulphur content of the soil ranged between 18.9-60.6 mg/kg with an average value of 28.21 mg/kg, where 65 percent of samples falls under the medium category. From the results, it is confirmed that the soils of all the sites are likely to respond to sulphur fertilization. Similar results were also obtained by Kumar et al. (2011). The medium levels of available sulphur in the soils of the study area might be due to lack of sulphur addition and continuous removal of S by crops (Balanagoudar 1989).

Table 4: Percent sample category and nutrient index of secondary nutrients of Mambattu village.

S. No.	Parameters	Percent samples			Range	Mean ± SD	Nutrient Index Value	Fertility Index
		Low	Medium	High				
1.	Available Calcium (mg/kg)	70	5	25	458 - 3869	1492.50 ± 1074.93	1.55	Low
2.	Available Magnesium (mg/kg)	85	0	15	192 -893	386.20 ± 207.93	1.30	Low
3.	Available Sulfur (mg/kg)	10	65	25	18.9 – 60.6	28.21 ± 9.12	2.15	Medium

Table 5: Percent sample category and nutrient index of micronutrients of Mambattu village.

S. No.	Parameters	Percent samples			Range	Mean±SD	Nutrient Index Value	Fertility Index
		Low	Medium	High				
1	Available Zinc (mg/kg)	100	0	0	0.88 -2.40	1.48±0.38	1.00	Low
2	Available Manganese (mg/kg)	40	15	45	2.26 -49.12	19.62±14.55	2.05	Medium
3	Available Iron (mg/kg)	10	15	75	5.39 – 167.14	45.01±43.73	2.65	High
4	Available Copper (mg/kg)	80	20	0	0.79 – 3.09	1.89±0.66	1.20	Low
5	Available Boron (mg/kg)	15	85	0	0.70 – 1.20	0.92±0.14	1.85	Medium

Available Micronutrients

The results of the percent sample category and nutrient index of micronutrients of Mambattu village are furnished in Table 5. The available zinc content ranged between 0.88-2.40 mg/kg with a mean value of 1.48 mg/kg, whereas the available manganese content of the soil ranged between 2.26-49.12 mg/kg with a mean value of 19.62 mg/kg. Moreover, the available iron content of the soil ranged between 5.39-167.14 mg/kg with a mean value of 45.01 mg/kg. Similarly, the available copper content of soil ranged between 0.79-3.09 mg/kg with a mean value of 1.89 mg/kg, while boron ranged from 0.70-1.20 mg/kg with an average value of 0.92 mg/kg.

From these values, it can be inferred that the maximum percent sample category of zinc, manganese, iron, copper and boron fall under low, high, high, low and medium category respectively (Fig. 4). However, the fertility index of micronutrient content of Mambattu soil showed that zinc and copper were low, whereas the manganese and boron seem to be medium, while the iron was high. Similar results were noticed by Pandiaraj et al. (2017). Soils with an acidic pH range lead to higher solubility and could result in higher availability of Fe content. Thus, acidic soils contain a high range of iron, which is supported by the findings of Khadka et al. (2016) and Methe et al. (2012).

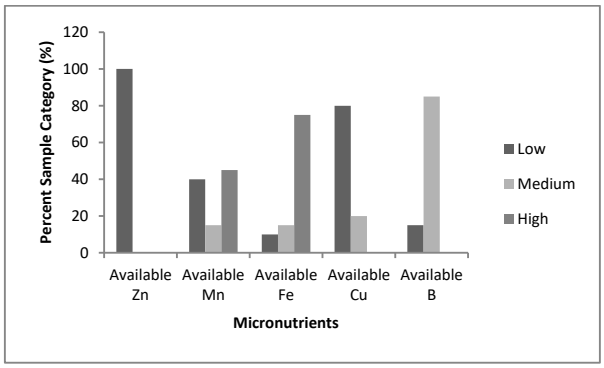

Fig. 4: Fertility rating of micronutrients.

CONCLUSION

The soil fertility index of the Mambattu village revealed that the pH of the soil varied from acidic to alkaline with a major percentage falling under neutral; while the Electrical Conductivity, an indicator of the soluble salt content of the soil is normal. The organic carbon status is medium. The available N, P and K were high, low and low in status, while secondary nutrients like Ca, Mg and S were low, low and medium status respectively. With regard to micronutrients, the soil is sufficient in Fe and Mn, while Zn and Cu are deficient and the boron is intermediate.

Hence, the village is categorized as soil with intermediate fertility status. However, for sustaining agriculture productivity and improving soil fertility status from sufficient to a high level, the most limiting factors controlling the soil fertility that were identified suggested corrective and conservation practices to achieve long-term sustainable production. Thus, the preliminary assessment of the soil fertility status of Mambattu village by using a soil index was used as one of the key information to improve the strategies and effective techniques towards sustainable agriculture. This also strengthens the basic information, the ability to formulate workable solutions towards sustainable crop production and the adoption of best management practices.

Hence, the approach incorporates the evaluation of climate-smart technologies, practices, services, and processes relevant to local climatic risk management. It also identifies opportunities for maximizing adaptation gains associated with local knowledge and further development plans. It also aims to reach out to farmers to adopt knowledge-based practices in order to boost fertility status. These may include practices such as site-specific nutrient management, increased use of organic nutrient sources, sustainable land use and cropping systems, and appropriate strategic agronomic practices. In future, soil fertility evaluation will be undertaken after two or three years in the same village which can be considered as an efficient tool to quantify the impact of climate-smart technologies provided to the farmers along with other crop improvement practices and management strategies to overcome the challenges of climate change.

REFERENCES

Amara, D. M. K., Massaquoi, S. D. A. and Patil, P. L. 2015. Assessment of spatial variability of soil properties in the hot semi-arid northern transition zone of India through remote sensing and geographic information system (GIS). AshEse Journal of Agricultural Sciences, 1: 43-53.

Adolf, V.I., Shabala, S., Andersen, M.N., Razzaghi, F. and Jacobsen, S.E. 2012. Varietal differences of quinoa's tolerance to saline conditions. Plant and Soil, 357(1-2): 117-129.

Balanagoudar, A.B. 1989. Investigation on status and forms of sulphur in soils of North Karnataka. M. Sc. (Agri.) Thesis.

Cambardella, C. A., Moorman, T. B., Parkin, T. B., Karlen, D. L., Novak, J. M., Turco, R. F. and Konopka, A. E. 1994. Field-scale variability of soil properties in central Iowa soils. Soil Science Society of America Journal, 58(5): 1501-1511.

Cruz, R., Harasawa, H., Lal., Murari., Wu, S., Anokhin, Y., Punsalmaa, B., Honda, Y., Jafari, Mostafa, Li, C. and Ninh, N. 2007. Asia. Climate change 2007: Impacts, adaptation and vulnerability. Contribution of Working Group II to the Fourth Assessment Report of the Intergovernmental Panel on Climate Change. 469-506.

FAO, 2008. Climate change and food security: a framework document. Food and Agriculture Organization, Rome.

Johnston, A. E. 1986. Soil organic matter, effects on soils and crops. Soil Use and Management, 2(3): 97-105.

Kalpana, P., Selva Preetha, P., Sathya, V. and Ramasubramaniyan, M.R. 2019. Assessment of soil fertility status for sustainable agricultural production in Chithamur Block, Kanchipuram District, Tamil Nadu, India. Indian Journal of Pure & Applied Biosciences, 7(6): 340-350.

Khadka, D., Lamichhane, S., Khan, S., Joshi, S. and Pant, B.B. 2016. Assessment of soil fertility status of Agriculture Research Station, Belachapi, Dhanusha, Nepal. Journal of Maize Research and Development, 2(1): 43-57.

Kumar, S., Tewari, S.K. and Singh, S.S. 2011. Effect of sources and levels of sulphur and spacing on the growth, yield and quality of spring sunflower (Helianthus annuus). Indian Journal of Agronomy, 56(3): 242-246.

Mokolobate, M. and Haynes, R. 2002. Comparative liming effect of four organic residues applied to an acid soil. Biology and Fertility of Soils, 35(2): 79-85.

Methe, B.A., Nelson, K.E., Pop, M., Creasy, H.H., Giglio, M.G., Huttenhower, C., Gevers, D., Petrosino, J.F., Abubucker, S., Badger, J.H. and Chinwalla, A.T. 2012. A framework for human microbiome research. Nature, 486(7402): p.215.

Pandiaraj, T., Srivastava, P. P. and Susmita Das, S. A. 2017. Evaluation of soil fertility status for soil health card in various tasar growing fields of Bihar and Jharkhand States, India. Int. J Curr. Microbiol. App. Sci., 6(4), 1685-1693.

Raghunatha Reddy, R.L., Shankarappa, T. H., Shankar Reddy Kolle and Satish, M. V. 2019. Review of trends in soil fertility research (2007-2016) using scopus database. Communications in Soil Science and Plant Analysis, 50(8): 1063-1080.

Ramamoorthy, B. and Bajaj, J. C. 1969. Available nitrogen, phosphorus and potassium status of Indian soils. Fertiliser News.

Shiao, T., Maddocks, A., Carson, C. and Loizeaux, E. 2015. Maps explain India's growing water risks. World Resources Institute, 26.

Singh, R. P. and Mishra, S. K. 2012. Available macro nutrients (N, P, K and S) in the soils of Chiraigaon block of district Varanasi (UP) in relation to soil characteristics. Indian Journal of Scientific Research, 97-101.

Tandon, H. L. S. 2005. Methods of Analysis of Soils, Plants, Waters, Fertilisers & Organic Manures. Fertiliser Development and Consultation Organisation.

Nature Environment and Pollution Technology
An International Quarterly Scientific Journal

p-ISSN: 0972-6268
(Print copies up to 2016)
e-ISSN: 2395-3454

Vol. 20 | No. 2 | pp. 601-612 | 2021

Original Research Paper

https://doi.org/10.46488/NEPT.2021.v20i02.017

Open Access Journal

Ecological Safety Evaluation for Water Resources of China Based on Pressure-State-Response Model: A Case from Zhoushan Archipelago

Degang Wang†, Miao Yu, Wei Mo, Dui-an Lv, Jie Cheng and Li Sun
Second Institute of Oceanography, Ministry of Natural Resources, Hangzhou, 310012, China
†Corresponding author: Degang Wang: degang_w@sio.org.cn

Nat. Env. & Poll. Tech.
Website: www.neptjournal.com

Received: 28-08-2020
Revised: 02-12-2020
Accepted: 05-02-2021

Key Words:
Water ecological safety
PSR model
AHP-entropy weight method
Zhoushan archipelago

ABSTRACT

Water resource ecological safety is a key factor in regional economic and social development. The comprehensive evaluation of water resource ecological safety is an important precondition for realizing regional sustainable development with the increasingly serious water ecological crisis. Zhoushan City of China was taken as an example, and the pressure–state–response model (PSR) was used to evaluate the ecological safety status of regional water resources, improve deficiencies in the existing evaluation index system and evaluation method effectively, and put forward three evaluation subsets (18 evaluation indexes). An evaluation index system was established based on these indexes to evaluate the water resource ecological safety. Combined weights of indexes were calculated using the analytic hierarchy process (AHP) and entropy weight method, and water-resource ecological safety indexes were used to evaluate the water-resource ecological safety status in Zhoushan City during 2010–2019. Results show that the water-resource ecological safety level in Zhoushan City during 2010–2019 presents a rising trend and transformed from a serious warning state into a medium warning state as well as a relatively safe state and safe state. This transformation indicates that the ecological safety status in Zhoushan City gradually improves. The comprehensive evaluation value is the minimum (0.15) under the serious warning state in 2013 and the maximum (0.85) under the safe state in 2019. Ammonia nitrogen and chemical oxygen demand (COD) emissions in industrial wastewater, total water supply throughout the year, and governance area of water and soil loss are the main factors that influence the water resource ecological safety in the city. The ecological safety level of regional water resources can be effectively elevated through key measures, such as increasing the water resource supply throughout the year, reducing the application of pesticides and chemical fertilizers, and reducing the discharge of pollutants, including COD and ammonia nitrogen in industrial wastewater. The water resource ecological safety evaluation model based on the PSR model and AHP–entropy weight method that demonstrates a certain application value can provide a novel idea and method to support the ecological safety evaluation of regional water resources.

INTRODUCTION

Water resources constitute an important material basis for human survival and development, and the development and utilization have a direct bearing on people's life, production development, and ecological environment. Water safety has become a key factor in restricting regional social and economic sustainable development with the increasing global population, rapid economic development and urbanization, and increasingly evident water resource security problems, such as water resource shortage, water environment pollution, and sudden water pollution (Uddameri 2019, Chen et al. 2017). Water resource security problems are caused by the mutual influence and restriction of water, nature, economy, and society. Such problems have attracted considerable attention from global and academic communities, making them an important research topic in many internal conferences held by governments and international organizations. Meanwhile, water resource security problems have driven domestic (Chinese) and foreign scholars and experts to investigate water resource security and related problems from various angles, such as water quality evaluation, water-resource ecological safety evaluation, water environmental management, and sustainable development (Shamir 2017, Cao et al. 2018, Zeng et al. 2016, Kourgialas et al. 2018). The quantification and evaluation of water resource ecological safety, namely, effective evaluation of water safety status of a region or drainage basin, constitutes a fundamental and important part of water safety research. The results determine the scientificity of water resource security evaluation and directly guide the follow-up formation of regional water resource utilization and management countermeasures. Therefore, the objective evaluation of regional water-resource safety status is a necessary precondition for facilitating regional

comprehensive, coordinated, and sustainable socioeconomic development as well as maintaining the continuous virtuous cycle of the ecological environment system. Consequently, the regional water-resource safety status has become an important domestic and foreign research topic in the field of water resources.

Water-resource ecological safety evaluation has become a fundamental means for investigating water safety, and scholars have achieved certain progress in the water-resource ecological safety evaluation system and method. Hamilton et al. put forward monitoring approaches with an extensive scope using hazard analysis and critical control point to optimize water-resource safety risk management through a simple mechanism and thus ensure the water resource ecological safety (Hamilton et al. 2006). Dickson et al. established a water security framework for rural, remote, or marginalized communities and evaluated water safety after discussing dimensions and indexes within the framework (Dickson et al. 2016). Norman et al. evaluated the water safety status using the index evaluation method and carried out an empirical demonstration in one community in Canada (Norman et al. 2013). Gain et al. stated that the water resource ecological safety depends not only on the physical availability of freshwater resources relative to water demand but also on social and economic factors, such as sound water resource planning and management method, the ability of institutions to provide water services, and sustainable economic policies (Gain et al. 2016). Jiang et al. used the entropy weight method to establish a complete evaluation system from living water safety, economic water safety, municipal water safety, and ability to prevent water disasters; evaluated the water safety status in the Asia–Pacific region; and demonstrated the optimal water safety status in Australia, New Zealand, Malaysia, and Singapore within the Asia-Pacific Region (Jiang et al. 2015). Zhang et al. formed a water-safety evaluation index system via the analytic hierarchy process (AHP) that can boost the correct evaluation of water safety status in Taizhou City and determine chemical oxygen demand (COD), river pollution percentage, annual precipitation, and municipal water reutilization rate as main factors that influence the water safety status in Taizhou City (Zhang et al. 2017). Shen et al. established a water safety evaluation model through an information entropy-based fuzzy set, determined the water safety evaluation grade by calculating the fuzzy degree of connection and confidence criterion, and evaluated the water safety status in eight administrative regions of Qinghai Province (Shen et al. 2016). Xu et al. used principal component (PCA) and grey relational (GRA) analyses to determine 16 ecological safety evaluation indexes for oasis groundwater in the arid region of Xinjiang and evaluated the groundwater ecological safety status of five irrigation canals through the fuzzy comprehensive evaluation method (Xu et al. 2018). Xu et al. conducted a comprehensive evaluation of water resource sustainability in mainland China using three-layer indexes of water resource quantity, use intensity, and use efficiency and divided China into high, medium, low, and very low regions according to comprehensive evaluation values (Xu et al. 2019). Bui et al. proposed a technical framework for the groundwater-resource ecological safety evaluation based on conventional sustainable development evaluation and AHP methods (Bui et al. 2019). Although foreign studies on the water-resource ecological safety evaluation have achieved considerable progress, the following aspects require further investigation: (1) the evaluation index system fails to reflect correlations among various factors comprehensively and underlying reasons that influence the regional water-resource ecological safety and (2) most scholars have only used single methods to calculate index weights, such as independent application of subjective weighting methods (Olivares et al., 2020; Ren et al., 2019), AHP or objective weighting approaches (Jenifer et al. 2017, Cheng et al. 2019), and entropy weight method. However, errors in index weights determined by single methods will seriously impact the evaluation result.

Therefore, the water-resource ecological safety problem has gradually become an important topic in domestic and foreign academic investigations that have achieved certain research progress. The pressure–state–response model (PSR) is used in this study to solve problems, such as a weak correlation between evaluation indexes and low accuracy of index weights because it can reflect correlations among evaluation indexes and explore the underlying reasons for changes in the ecological safety status of regional water resources. Meanwhile, the AHP–entropy weight method can evade errors caused by the independent use of objective or subjective weight determination methods and accurately evaluate the ecological safety status of regional water resources. The ecological safety evaluation method of water resources based on the PSR model and AHP–entropy weight method in this study will provide a theoretical basis for establishing and optimizing the research system of water resource ecological safety.

The remainder of this study is organized as follows. The study area of the water-resource ecological safety evaluation and data sources are described in Section Two. The PSR model used in the water-resource ecological safety evaluation was analyzed; pressure, state, and influence indexes were established; comprehensive index weights were solved, and comprehensive evaluation indexes were determined in Section Three. The ecological safety evaluation results of water resources in Zhoushan City were obtained and the

water-resource ecological safety status was analyzed and discussed from the four aspects of pressure system, state system, response system, and comprehensive evaluations in Section Four. Finally, the entire study was summarized and conclusions were drawn.

OVERVIEW OF THE STUDY AREA

Zhoushan City is located in the coastal region of Zhejiang Province in southeastern China between east longitude of 121°30′-123°25′ and north latitude of 29°32′-31°04′, with a land area of approximately 1,440.12 km^2 and a sea area of 20,800 km^2. The city is on the western side of the west and low in the north, with a subtropical monsoon climate. Zhoushan is a typical island city and the first to be built on islands. Zhoushan Archipelago is the largest in China consisting of over 4,000 islands. Adjoining large cities, such as Hangzhou and Shanghai, with many geographical advantages, Zhoushan City is an important outward sea portal and channel in the Yangtze River Delta Economic Belt and also a principal port city in China. The geographic location of Zhoushan city is shown in Fig. 1.

Zhoushan Archipelago is an island region and intrinsically deficient in water resources. Its average annual total quantity of water resources is 574,000,000 m^3 and per capita quantity of water resources is 600 m^3, which is only 25.4% that of the entire Zhejiang Province, 23.6% that of China, and one-twelfth that of the world; hence, the archipelago demonstrates the serious shortage of water resources (Qiu et al. 2017). The small average annual precipitation (1,185.85 mm) and evaporation (1,417.59 mm) from the water surface in this region result in a significantly lower runoff volume than that of mainland regions at the same latitude. Moreover, the average annual runoff depth of 550 mm is only equivalent to 58% of the average level of the entire Zhejiang Province. The water transfer and diversion for replenishment are difficult and the freshwater resource shortage worsens due to poor water resource share ability between islands. Meanwhile, the availability of runoffs generated is low and most runoffs are directly discharged into the sea due to special landforms within the archipelago, such as low hills and mountains. Thus, the total impoundage has been insufficient in the archipelago for a long time due to the lack of appropriate reservoir sites for the construction of water storage facilities and the very small catchment area of all reservoirs in this region. Reservoirs may be dried up when a drought occurs. After the national-level Zhoushan Archipelago New District was established by the State Council of China in June 2011, Zhoushan City has been elevated to the national strategic level in the country. Water resources will become an important supporting factor and the water resource ecological safety will suffer extreme challenges in the future all-around development themed by the marine economy, especially under the background of urbanization and high-speed socioeconomic development in the city.

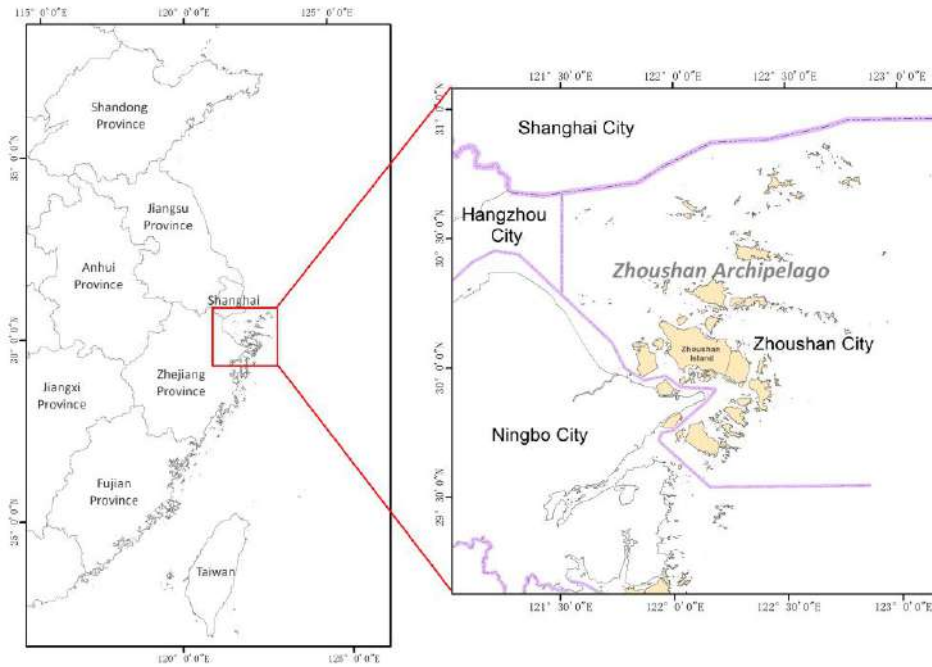

Fig. 1: Geographic location of Zhoushan city.

MATERIALS AND METHODS

Research Data

Original data used in this study were derived from Zhejiang Statistical Yearbook, Zhoushan Statistical Bulletin of National Economy and Social Development, Zhoushan Statistical Yearbook, Zhoushan Environmental Conditions Bulletin, and Zhoushan Water Resources Bulletin from 2010 to 2019 along with other existing water resource-related results in Zhoushan City. Ten years of water resource data of Zhoushan City (2010-2019) were selected to evaluate its water-resource ecological safety status.

PSR Model and Evaluation Indexes

The PSR model was initially proposed by Canadian statisticians, such as Rapport. This model has gradually been applied to studies on various ecological problems and become a framework system for the discipline of environmental quality assessment with the mutual development of United Nations Environment Programs and Organization for Economic Cooperation and Development toward the end of the twentieth century. The PSR model is commonly used in the field of ecological environmental evaluation due to its unique comprehensiveness, flexibility, and strong causal logic relations in the aspect of index selection (Sun et al. 2019, Shi et al. 2018, Bahraminejad et al. 2018, Wang et al. 2018).

The evaluation index system established via the PSR model includes not only the pressure imposed by human beings on the water ecosystem (such as discharge of industrial and domestic wastewater and agricultural irrigation) and human protection of the water ecosystem (such as popularization of water-saving appliances and centralized wastewater treatment) but also the status (such as groundwater resource quantity and water quality and health status) of water resources themselves. Therefore, the PSR model can realize the complete and thorough evaluation of water ecological safety. Water resource characteristics of Zhoushan City were combined according to index selection principles of pertinence, representativeness, dynamics, feasibility, and systematicness to establish the ecological-safety evaluation index system of water resources consisting of the target, criterion, and index layers based on the PSR model, as given in Table 1.

Table 1: Safety evaluation index system of water resources of Zhoushan City.

Target layer	Factor layer	Index layer	Index explanation
Comprehensive water resource safety index	Pressure	P1 Annual total wastewater discharge/10,000 t	Annual total wastewater discharge in the evaluation area
		P2 Annual total industrial wastewater discharge/10,000 t	Annual total industrial wastewater discharge
		P3 Annual COD emission in industrial wastewater/t	Annual total COD emission in industrial wastewater
		P4 Annual ammonia nitrogen emission in industrial wastewater/t	Annual total ammonia nitrogen emission in industrial wastewater
		P5 Application of agrochemical fertilizers/t	Annual total application of chemical fertilizers
		P6 Application of agricultural pesticides/t	Annual total application of agricultural pesticides
		P7 Annual total water consumption/10,000 m^3	Annual total water consumption in the evaluation area
	State	S1 Surface water resource quantity/100 million m^3	Total surface water resource quantity in the evaluation area
		S2 Groundwater resource quantity/100 million m^3	Total groundwater resource quantity in the evaluation area
		S3 Per capita water resource quantity/m^3	Total water resource quantity/total population in the evaluation area
		S4 Water qualification rate in water function zone/%	Water quality in the evaluation area reaches above Class II water quality standard
		S5 Water quantity converted from annual precipitation/100 million m^3	Water resource quantity converted from annual precipitation in the evaluation area
	Response	R1 Governance area of water and soil loss/1,000 ha	Total governance area of water and soil loss
		R2 Water quantity diverted from the mainland/100 million m^3	Annual water quantity diverted from the mainland in the evaluation area
		R3 Reservoir water storage capacity/10,000 m^3	Annual reservoir water storage in the evaluation area
		R4 Annual total water supply/10,000 m^3	Annual total water supply in the evaluation area
		R5 Quota of pollutant discharge fee/10,000 yuan	Pollutant discharge fee annually levied in the evaluation area
		R6 Flood embankment length/km	Flood embankment length in the evaluation area

Determination of Index Weights

Index weight plays a significant role in the ecological safety evaluation result of water resources. AHP, correlation coefficient method, PCA, and entropy weight method are primarily used to determine index weights (Mohammad et al. 2013, Liu et al. 2019). According to the mode of weight assignment, methods can be divided into AHP-represented subjective weight and entropy weight-represented objective assignment methods. If only one of these methods is used in the actual assessment process, the assessment conclusions may be subject to excessively strong subjectivity or objectivity restrictions, leading to a certain deviation from the actual situation. This problem can be effectively solved by calculating comprehensive index weights through the AHP-entropy weight method.

AHP-based weight determination: The AHP method was first proposed by T. L. Saaty, a famous mathematical specialist from the American University of Pittsburgh, in his famous work The Analytic Hierarchy Process in the 1970s. Since then, the AHP method has gradually matured and been widely used by Chinese and foreign scholars.

AHP is a decision-making mode of thinking that decomposes a complicated problem into component factors, which are then combined in a grouped way to form an appropriately ordered hierarchical structure according to memberships. The importance of every two indexes is then compared via expertise to determine the importance ranking (weight value) of each factor to the decision-making objective. This process is generally carried out in five steps, namely, the establishment of hierarchical structure, construction of importance judgment matrix, single hierarchical arrangement of indexes, consistency check, and total index ranking (Canan et al. 2018, Myronidis et al. 2016).

Weight solving through the entropy weight method: The concept of entropy was put forward by the German physicist Rudolf Clausius in 1850. Entropy was then introduced by the American mathematician Shannon into information theory in 1948 to propose the concept of "information entropy," which is the uncertainty measurement of a random variable and used to describe the occurrence probability or uncertainty of a signal in the information source (Reinaldo et al. 2013, Mohamed et al. 2011). High information entropy indicates high uncertainty. Information entropy is expressed as follows:

$$H(p_1, p_2, \quad , p_n) = -\sum_{i=1}^{n} p_i \log_2 p_i \qquad \ldots(1)$$

Where, $H(p_1, p_2, \ldots, p_n)$ is the information entropy and p_i is the occurrence probability of the event i.

The discrete degree of an evaluation index can be assessed using entropy. Small entropy indicates the large information quantity provided by this index, high discrete degree, and strong influence on the overall objective and weight value. Therefore, the entropy weight method, which is an objective weighting tool, can be used to determine the weight of each index and delete indexes with minimal contribution to the evaluation result, while the entropy coefficient is applied to correct the weight of each index and finally obtain objective index weights (Gu et al. 2020, Chen et al. 2019) and provide a basis for the multi-index comprehensive evaluation.

The following initial data factor matrix $B = (b_{ij})_{m\times n}$ is composed of m evaluation objects and n concrete evaluation indexes:

$$B = (b_{ij})_{m\times n} = \begin{pmatrix} b_{11} & & b_{1n} \\ \vdots & \ddots & \vdots \\ b_{m1} & & b_{mn} \end{pmatrix} \qquad \ldots(2)$$

Where b_{ij} is the evaluation value of the object i at the j^{th} index layer. The calculation steps of each index weight are as follows:

1. Calculate p_{ij}, which is the ratio of the j^{th} evaluation index value under the index i, as follows:

$$p_{ij} = \frac{b_{ij}}{\sum_{j=1}^{n} b_{ij}} (i = 1,2,3,\cdots,n; j = 1,2,3,\cdots,m) \qquad \ldots(3)$$

If $p_{ij} = 0$, then we define the following:

$$\lim_{p_{ij}\to 0} p_{ij} \ln p_{ij} = 0 \qquad \ldots(4)$$

2. Calculate entropy E_i of index as follows:

$$E_i = -\frac{\sum_{j=1}^{n} p_{ij} \ln p_{ij}}{\ln(n)} (i = 1,2,3, \quad ,n) \qquad \ldots(5)$$

3. Calculate the entropy v_i (objective weight value) of the index i according to E_i as follows:

$$v_i = \frac{1 - E_i}{\sum_{i=1}^{m} (1 - E_i)} (i = 1,2,3, \quad ,n) \qquad \ldots(6)$$

Comprehensive weight solving method: The comprehensive index weight z_i is generally obtained by integrating proportional, simple multiplication, mean value, and minimum relative information entropy methods with AHP-obtained subjective w_i and entropy weight-determined objective v_i weights. Simple multiplication and mean value methods were selected in this study to solve the comprehensive weight of the water-resource ecological safety index with consideration for scientific rigour and operation convenience as follows:

$$z_i = \frac{w_i v_i}{\sum_{j=1}^{n} w_i v_i} \qquad \ldots(7)$$

Table 2: Water ecological safety status grade in Zhoushan City.

Comprehensive index value	Water ecological safety status
0–0.2	Serious warning
0.2–0.4	Medium warning
0.4–0.6	Prewarning
0.6–0.8	Relatively safe
0.8–1	Safe

Calculation of Comprehensive Water Ecological Safety Evaluation Index

The obtained comprehensive weight z_i was used to solve the following ecological safety evaluation indexes of comprehensive water resources I in Zhoushan City for different years after index standardization:

$$I = \sum_{j=0}^{p} Z_i Y_{ij} \quad \ldots(8)$$

Where Y_{ij} is the index value after the standardization processing and z_i is the comprehensive weight value solved.

Grading of the Water-Resource Ecological Safety Status

The water-resource ecological safety evaluation is graded to reflect the current water ecological safety status. The water ecological safety level should be graded and the evaluation value is then associated with the evaluation grade because the comprehensive value of ecological safety evaluation of water resources fails to incorporate the water ecological safety status directly. Current natural conditions and the social development status in Zhoushan City were combined to grade the level of water ecological safety status (Table 2) according to ecological safety prewarning criteria and existing research results (Sun et al. 2018, Wang et al. 2019).

RESULT ANALYSIS AND DISCUSSION

Research Results

Subjective and objective weights were solved via AHP and entropy weight method, respectively, in the processing and analysis of research data. Equation (5) was then utilized to solve ecological safety evaluation indexes of comprehensive weights of water resources (Table 3).

Equation (6) was used to solve comprehensive evaluation values of water resource ecological safety in Zhoushan City during 2010-2019. Table 4 presents the assessment of ecological safety status grades of water resources according to Table 2.

Table 3: Entropies, subjective weights, objective weights, and comprehensive weights of ecological safety evaluation indexes of water resources in Zhoushan City.

Index layer	Entropy E_i	Subjective weight w_i	Objective weight v_i	Comprehensive weight z_i
P1 Annual total wastewater discharge/10,000 t	0.7449	0.0156	0.0908	0.024
P2 Annual industrial wastewater discharge/10,000 t	0.8102	0.042	0.0676	0.047
P3 Annual COD emission in industrial wastewater/t	0.704	0.109	0.1054	0.191
P4 Annual ammonia nitrogen emission in industrial wastewater/t	0.682	0.1388	0.1132	0.261
P5 Application of agrochemical fertilizer/t	0.8441	0.04	0.0555	0.037
P6 Application of agricultural pesticides/t	0.9225	0.1002	0.0276	0.046
P7 Annual total water consumption/10,000 m^3	0.8467	0.0305	0.0546	0.028
S1 Surface water resource quantity/100 million m^3	0.8916	0.012	0.0386	0.008
S2 Groundwater resource quantity/100 million m^3	0.8902	0.0084	0.0391	0.005
S3 Per capital water resources/m^3	0.8759	0.0389	0.0442	0.029
S4 Water qualification rate in water function zone/%	0.8369	0.004	0.0581	0.004
S5 Water quantity converted from annual precipitation/100 million m^3	0.8902	0.0084	0.0391	0.005
R1 Governance area of water and soil loss/1,000 ha	0.893	0.126	0.0381	0.080
R2 Water quantity diverted from the mainland/100 million m^3	0.8738	0.0495	0.0449	0.037
R3 Reservoir water storage capacity/10,000 m^3	0.8641	0.1034	0.0484	0.083
R4 Annual total water supply/10,000 m^3	0.891	0.1297	0.0388	0.084
R5 Quota of pollutant discharge fee/10,000 yuan	0.9001	0.0264	0.0356	0.016
R6 Flood embankment length/km	0.8294	0.0172	0.0607	0.017

Table 4: Water safety evaluation results of Zhoushan City during 2010-2019.

Year	Evaluation value				Water ecological safety status
	Pressure	State	Response	Comprehensive	
2010	0.27	0.02	0.01	0.30	Medium warning
2011	0.24	0.01	0.06	0.30	Medium warning
2012	0.08	0.04	0.09	0.21	Medium warning
2013	0.07	0.01	0.08	0.15	Serious warning
2014	0.05	0.01	0.17	0.24	Medium warning
2015	0.05	0.03	0.24	0.32	Medium warning
2016	0.07	0.03	0.22	0.32	Medium warning
2017	0.46	0.02	0.25	0.73	Relatively safe
2018	0.54	0.01	0.27	0.83	Safe
2019	0.58	0.05	0.22	0.85	Safe

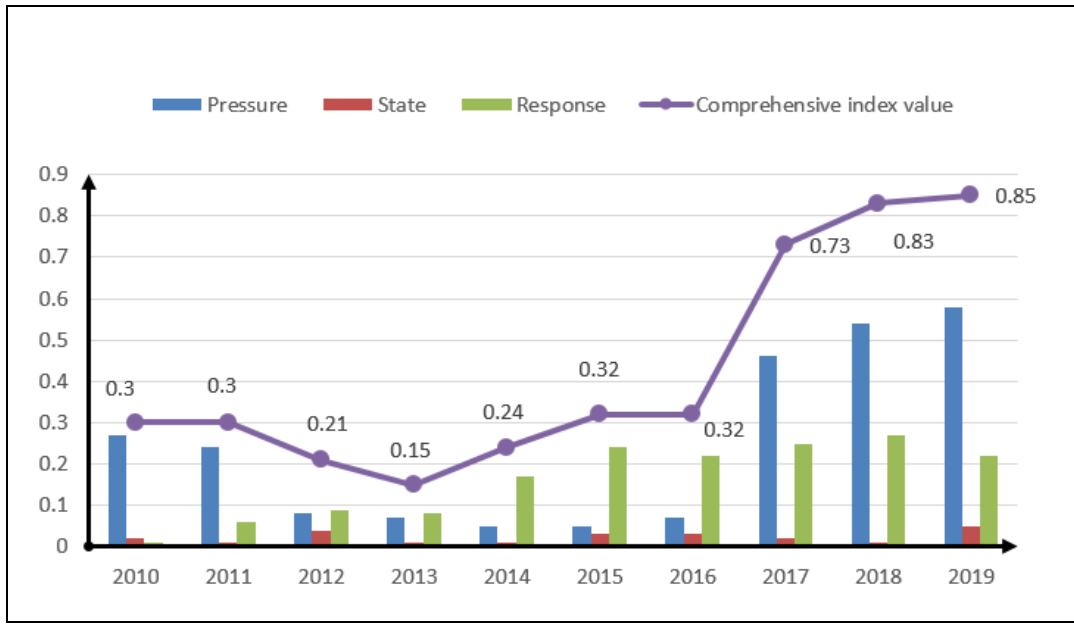

Fig. 2: Variation trend of water resource ecological safety in Zhoushan City (2010-2019).

DISCUSSION

1. Pressure system evaluation: According to the research results (Table 4 and Fig. 2), the evaluated value of water resource safety pressure in Zhoushan City first reduced and then increased during 2010-2019. These values were divided into the following phases: the mean value was (1) approximately 0.255 during 2010-2011, (2) 0.064 during 2012-2016, and (3) 0.527 during 2017-2019. These findings indicated that the pressure faced by the ecological safety system of water resources in Zhoushan City presented a declining–increasing–declining trend. The water-resource ecological safety pressure from 2012 was significantly elevated in Zhoushan City, with the evaluation value declining from 0.24 to 0.08 mainly because the city was accredited as a national-level marine development demonstration area, followed by large-scale social construction and entrance of various industries in a fast development period. Indexes, such as total wastewater discharge, annual industrial wastewater discharge, and COD and ammonia nitrogen emissions in industrial wastewater, continued to increase annually or remained at high levels during this period of rapid development. Although the consumption of agrochemical fertilizers reduced (from 15,697 t to 11,848 t) and the application of agricultural pesticides

reduced to a certain degree, the water ecological safety pressure failed to weaken. Hence, the pressure borne by water ecology in Zhoushan City during this period, mainly came from the indirect water pollution triggered by industrial wastewater discharge and agricultural production in human society.

The evaluation value of water resource ecological pressure in Zhoushan City during 2016-2019 increased from 0.07 to 0.58, and the pressure tolerated by the water ecosystem in this phase gradually remitted mainly because the city experienced a large-scale construction phase with a stable social industrial structure. The annual water consumption gradually increased in Zhoushan (from 155,450,000 m^3 to 162,050,000 m^3). However, the industrial wastewater discharge (from 22,020,000 t to 11,380,000 t), COD (from 6,466 t to 754 t) and ammonia nitrogen (from 238 t to 62 t) emissions in industrial wastewater, and application of agricultural pesticides (from 501 t to 444 t) all declined annually and remitted the pressure faced by the water ecological safety in Zhoushan City to a certain extent with the progress in energy-saving technologies and wastewater treatment means. The variation trend chart of the pressure index is shown in Fig. 3.

2. State system evaluation: The state evaluation value represents the contribution of the current water resource status to water ecological safety. Fig. 4 shows that the variation trend of the state evaluation value is unclear but slightly fluctuating from 2010 to 2019. Values of the water resource ecological state in 2011, 2013, and 2014 were all 0.01, which was relatively small, while those in 2012, 2015, 2016, and 2019 were relatively large at 0.04, 0.03, 0.03, and 0.05, respectively. The ecological safety status value of water resources in Zhoushan City

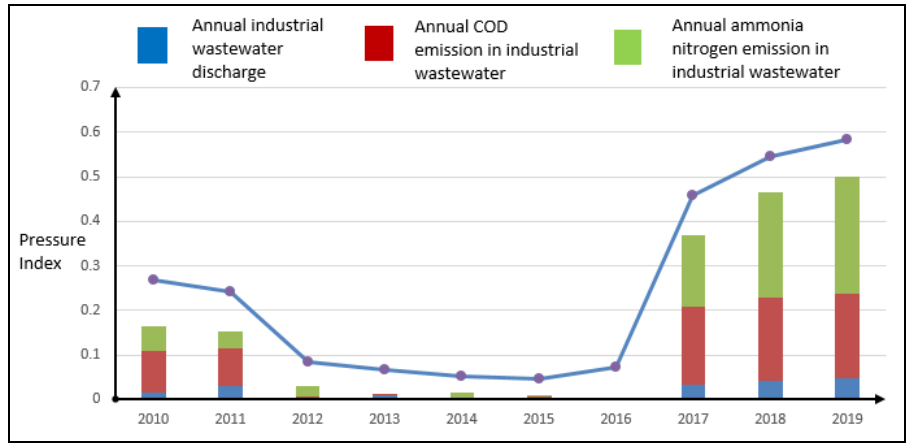

Fig. 3: Variation trend chart of the pressure index.

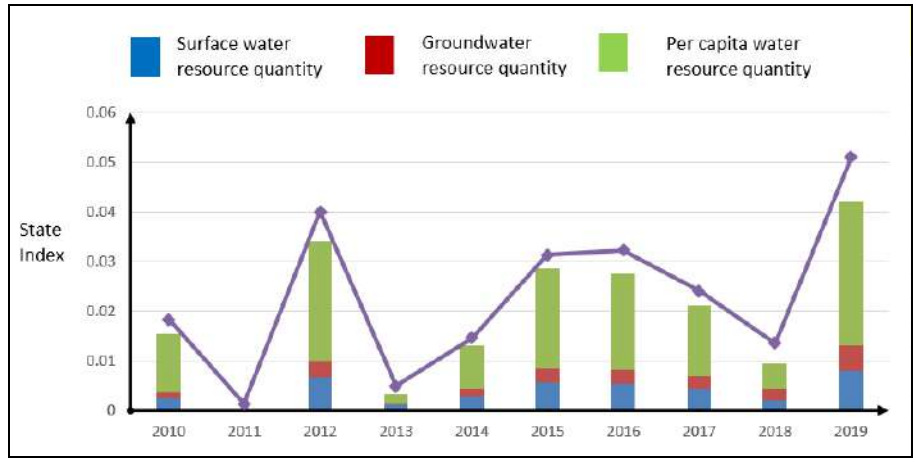

Fig. 4: Variation trend chart of the state index.

was mainly affected by surface water resource quantity, groundwater resource quantity, and water quantity converted from annual precipitation, which exerted the maximum influence. Water resource quantities converted from annual precipitation in the city were 13.7802, 14.7405, and 17.8481 m^3 in 2011, 2013, and 2014, respectively, during which the city experienced three years of minimum precipitation within 2010-2019, with minimum status evaluation values of water resources (0.01). Water resource quantities converted from the annual precipitation in Zhoushan City were 22.6386 and 27.1485 m^3 in 2012 and 2019, respectively, with large evaluation values (0.04 and 0.05). The water qualification rate in the water function zone of the city during 2010-2019 was stable and presented an increasing trend (from 44% in 2014 to 57% in 2019), and water environmental indexes improved to a certain extent. Therefore, water resource quantity converted from precipitation, surface water resource quantity, groundwater resource quantity, and per capita water resources, except for the water qualification rate in the water function zone, exert certain influences on the level of water ecological safety status in Zhoushan City, which is an island region.

3. Response system evaluation: The response evaluation value reflects the effort level made by human society to the protection of the water ecosystem. Fig. 5 shows that the response curve is rapidly rising (from 0.01 in 2010 to 0.22 in 2019) during 2010–2019, thereby indicating that the Zhoushan municipal government made considerable efforts into the improvement of the water ecological safety level after being made aware of the importance of water ecological safety. The municipal government applied effective measures for water resource protection, which reduced not only the water consumption in life and production but also enhanced the development and utilization of unconventional water resources, such as water diversion from the mainland, with the increase in the governance area of water and soil loss, reservoir water storage capacity, annual total water supply, and flood embankment length and the change in pollutant discharge fees. Thus, "increasing water sources and reducing water consumption" was realized. The governance area of water and soil loss increased from 23.46 ha in 2010 to 56.57 ha in 2019, with a growth rate of 141.1%. The annual total water supply elevated from 137,070,000 m^3 in 2010 to 162,050,000 m^3 in 2019, with a growth rate of 18%. The amount of pollutant discharge fees increased from RMB 17,690,000 in 2010 to RMB 30,050,000 in 2019 by 69.9%. The flood embankment length increased from 453 km in 2010 to 939 km in 2019 by 107.3%.

   The response system contributed to achieving the maximum progress in the PSR evaluation system and was an important link to guaranteeing the water resource ecological safety in Zhoushan City during 2010-2019.

4. Comprehensive evaluation: The results in Table 4 showed that the water resource ecological safety is basically under the medium warning status in Zhoushan City during 2010–2016 and comprehensive evaluation indexes are 0.3, 0.3, 0.21, 0.15, 0.24, 0.32, and 0.32. Compared with that in 2012, the annual precipitation

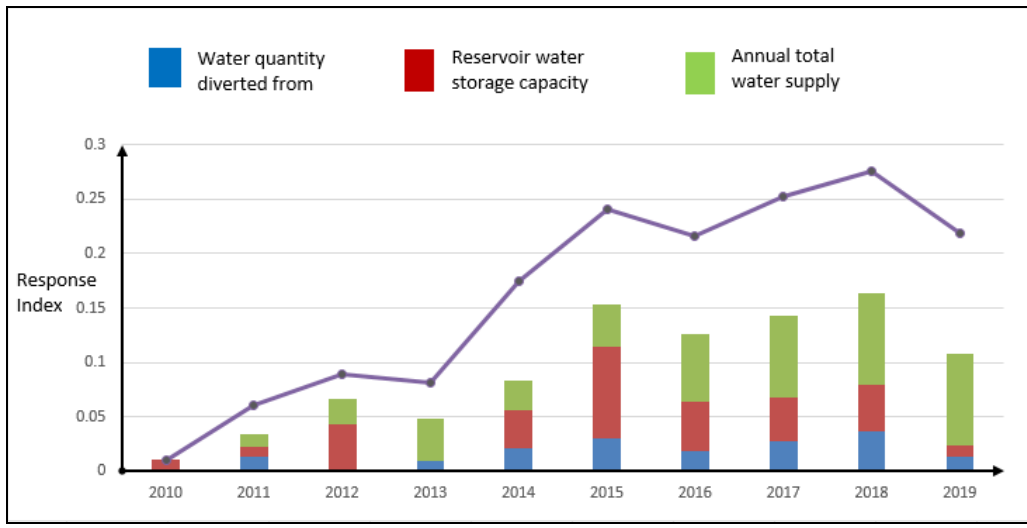

Fig. 5: Variation trend chart of the response index.

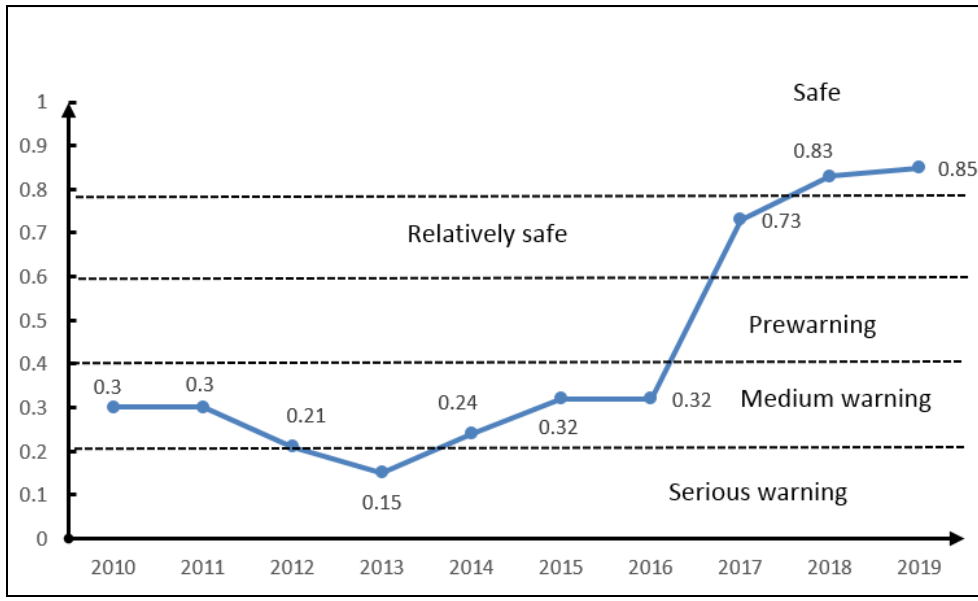

Fig. 6: Comprehensive evaluation results of water resource safety in Zhoushan City during 2010–2019

in the city reduced by 34.1% at only 1,186.4 mm in 2013, which was also the same year that experienced minimum precipitation within the study period. The reduced precipitation seriously impacted the water resource quantity and safety status in the city. Hence, the comprehensive evaluation index of water resource ecological safety reached the minimum value in 2013 at only 0.15 within the 10 years. Comprehensive evaluation indexes of water resource ecological safety presented a rising trend in Zhoushan at 0.73, 0.83, and 0.85 and the overall water ecosystem was under relatively safe and safe statuses during 2017-2019. As shown in Fig. 6, the general curve of comprehensive evaluation indexes first reduced and then increased during 2010-2019. However, the general rising trend of the curve indicated that the water ecological safety status of Zhoushan City was in the process of improvement and optimization.

The water ecological safety status in the city upgraded from a medium warning state to a relatively safe state in 2017 and then realized the transformation from a relatively safe state to a safe state in 2018 after reaching the minimum point in 2013. Relative to 2010, the pressure system somehow deteriorated in 2019. However, the deteriorating trend was curbed already and the pressure borne by the water ecosystem was significantly relieved by the optimization of indexes, such as industrial wastewater discharge, COD and ammonia nitrogen emissions in industrial wastewater, and the application of agricultural pesticides. Notably, wastewater discharge will continue to be a major problem faced by the water ecological safety in Zhoushan. The state system fluctuated to some degree because of the effect of the change in the water resource quantity converted from precipitation. However, indexes, such as water qualification rate, continued to steadily progress and the health status of the water ecosystem gradually improved. The improvement of the response system primarily caused the upgrading of water ecological safety status, governance area of water and soil loss, reservoir water storage capacity, annual total water supply, pollutant discharge fees, and flood embankment length, which were optimized to different degrees. This finding indicated that the capability of Zhoushan City in guaranteeing water ecological safety was comprehensively enhanced.

CONCLUSION

The water resource safety evaluation in the island area of Zhoushan City in China was taken as the research object to clarify influences of factors, such as pressure, state, and response on the water resource safety status and reveal their mutual relationships. Comprehensive weights of different indexes were calculated through the AHP–entropy weight method based on the constructed evaluation index system, influence degrees of different factors on water resource safety status were analyzed via the PSR model, and measures facilitating the sustainable utilization of water resources were proposed. The following conclusions were drawn from this study.

1. The water ecological safety evaluation of Zhoushan City during 2010–2019 demonstrated that the PSR model can evade not only the one-sidedness in the

evaluation of water resource environmental status but also accurately reflect correlations among water ecological safety factors starting from the mutual influence and association between social development and the natural environment. Accordingly, water ecological safety can be evaluated through the PSR-based evaluation system.

2. The weight solving method that integrates the AHP and entropy weight method avoids not only the subjective influence of human preferences but also mitigates the limitation of discrepancy with the real situation caused by variable data deviations in the entropy weight method. Hence, this approach can provide a certain reference for weight determination.
3. The subsystem analysis demonstrated that COD and ammonia nitrogen emissions are the main influencing factors of the pressure subsystem, while water resource quantity converted from precipitation and the water qualification rate in the water function zone are primary influencing factors of the state subsystem. The water-resource ecological safety level can be effectively elevated by increasing the governance area of water and soil loss, reservoir water storage capacity, annual total water supply, and amount of pollutant discharge fees to accelerate reclaimed water engineering construction, such as seawater desalination, and develop and utilize unconventional water resources.

Therefore, the status of regional water resource safety was evaluated using the PSR model; influence degrees of pressure, state, and response on the water resource safety status were determined, and correlations among different influence factors were analyzed to provide a theoretical basis for evaluating the regional water-resource safety status and formulating water-resource sustainable utilization measures. Improving the water resource safety level is important to reduce the industrial wastewater discharge, enhance the reclaimed water engineering construction, and develop and utilize unconventional water resources in the island area. Regional water supply and wastewater recycling can be the focus of future investigations. Meanwhile, the factor of driving force can be further considered in the safety evaluation index system of water resources to realize the comprehensive evaluation of water resource ecological safety.

ACKNOWLEDGMENTS

This study was supported by the Scientific Research Fund of the Second Institute of Oceanography, MNR (Grant no. JT1204).

REFERENCES

Bahraminejad, M., Rayegani, B., Jahani, A. and Nezami, B. 2018. Proposing an early-warning system for optimal management of protected areas (Case study: Darmiyan protected area, Eastern Iran). Journal for Nature Conservation, 46: 79-88.

Bui, N. T., Kawamura A., Bui, D. D., Amaguchi, H., Dan, D.B., Truong, N.T., Do, H.H.T. and Nguyen, C.T. 2019. Groundwater sustainability assessment framework: A demonstration of environmental sustainability index for Hanoi, Vietnam. Journal of Environmental Management, 241(000): 479-487.

Canan, A., Ahmet, B. and Temur Gül Tekin 2018. Sustainability analysis of different hydrogen production options using hesitant fuzzy AHP. International Journal of Hydrogen Energy, 43(39): 18059-18076.

Chen, Y., Lu, H., Li, J. and He, L. 2017. A leader-follower-interactive method for regional water resources management with considering multiple water demands and eco-environmental constraints. Journal of Hydrology, 548: 121-134.

Chen, J., Bian, W., Wan, Z., Zheng, H. and Wang, P. 2019. Identifying factors influencing total-loss marine accidents in the world: Analysis and evaluation based on ship types and sea regions. Ocean Engineering, 191: 106495.1-106495.9.

Cao, X., Ren, J., Wu, M. and Wang, W. 2018. Effective use rate of generalized water resources assessment and to improve agricultural water use efficiency evaluation index system. Ecological Indicators, 86: 58-66.

Cheng, K., Wei, S., Fu, Q., Pei, W. and Li, T. 2019. Adaptive management of water resources based on an advanced entropy method to quantify agent information. Journal of Hydroinformatics, 21(3): 381-396.

Dickson, S. E., Schuster-Wallace, C. J. and Newton, J. J. 2016. Water Security Assessment Indicators: The Rural Context. Water Resources Management, 30(5): 1567-1604.

Gu, Q. and Wang, R. 2020. Evaluation Path Selection of Opening-Up Level of Chinese Coastal Cities Based on Entropy Weight-Topsis-Grey Correlation: From Researches on Ten Coastal Cities. Journal of Coastal Research, 36(115): 636-640.

Gain, A. K., Giupponi, C. and Wada, Y. 2016. Measuring global water security towards sustainable development goals. Environmental Research Letters, 11(12): 124015-124015.

Hamilton, P. D., Gale, P. and Pollard, S. J. T. 2006. A commentary on recent water safety initiatives in the context of water utility risk management. Environmental International, 32(8): 958-966.

Jenifer, M. A. and Jha, M. K. 2017. Comparison of Analytic Hierarchy Process, Catastrophe and Entropy techniques for evaluating groundwater prospect of hard-rock aquifer systems, 5. Journal of Hydrology 48(000): 605-624.

Jiang, H. and Yang, X.L. 2015. Entropy weight-based water security assessment in Asia-Pacific. Progress in Geography, 34(03): 373-380.

Kourgialas, N. N., Karatzas, G. P., Dokou, Z. and Kokorogiannis, A. 2018. Groundwater footprint methodology as policy tool for balancing water needs (agriculture & tourism) in water scarce islands - The case of Crete, Greece. Science of the Total Environment, 615: 381-389.

Liu, Q. and Wu J.B. 2019. Research on effectiveness of internal control based on analytic hierarchy process. Journal of Liaoning Normal University (Natural Science Edition), (1): 31-36.

Myronidis, D., Papageorgiou, C. and Theophanous, S. 2016. Landslide susceptibility mapping based on landslide history and analytic hierarchy process (AHP). Natural Hazards, 81(1): 245-263.

Mohamed, A. E. and Tarek, A. E. H. 2011. New Edge Detection Technique based on the Shannon Entropy in Gray Level Images. International Journal on Computer Science & Engineering, 3(6): 2224-2232.

Mohammad, N.H., Yaser, E.H. and Ahmed, A. K. 2013. Multi-dimensional Framework for Evaluating the Transit Service Performance. Transportation Research, (3): 47-61.

Norman, E.S, Dunn, G., Bakker, K., Allen, D.M. and Albuquerque, R.C.D. 2013. Water Security Assessment: Integrating Governance and Freshwater Indicators. Water Resources Management, 27(2): 535-551.

Olivares, E. A. O, Jimenez, S. I. B., Torres, S.S., Enriquez, J.O.C., Tiefenbacher, J.P. and Takaro, T.K. 2020. A simple method to evaluate of Environmental Management, 261(000): 110164.1-110164.12. groundwater vulnerability in urbanizing agricultural regions. Journal

Qiu, S. S., Yue, W. Z., Zhang, H. and Qi, J. 2017. Island ecosystem services value, land-use change, and the National New Area Policy in Zhoushan Archipelago, China. Island Studies Journal, 12(2): 177-197.

Ren, C.F., Li, Z. H. and Zhang, H. B. 2019. Integrated multi-objective stochastic fuzzy programming and AHP method for agricultural water and land optimization allocation under multiple uncertainties. Journal of Cleaner Production, 210(000): 12-24.

Reinaldo, B., Arellano, V., Javier, E. and Genton, M.G. 2013. Shannon Entropy and Mutual Information for Multivariate Skew-Elliptical Distributions. Scandinavian Journal of Statistics, 40(1): 42-62.

Shen, J.Y., Wu, F.P. and Yu, Q.W. 2016. Strictest comprehensive evaluation of water safety based on fuzzy set pair analysis. Journal of Water Resources and Water Engineering, 27(02): 92-97.

Shamir, E. 2017. The value and skill of seasonal forecasts for water resources management in the Upper Santa Cruz River basin, southern Arizona. Journal of Arid Environments, 137: 35-45.

Sun, L. Y., Miao, C. L. and Yang, L. 2018. Ecological environmental early-warning model for strategic emerging industries in China based on logistic regression. Ecological Indicators, 84: 748-752.

Sun, B., Tang, J., Yu, D. and Wang, P. 2019. Ecosystem health assessment: A PSR analysis combining AHP and FCE methods for Jiaozhou Bay, China. Ocean & Coastal Management, 168: 41-50.

Shi, Y., Li, J. and Xie, M. 2018. Evaluation of the ecological sensitivity and security of tidal flats in Shanghai. Ecological Indicators, 85: 729-741.

Uddameri, V. 2019. JAWRA: Fifty-Five Years of Sustained Contributions for Improved Water Resources Management -The Second Decade (1975-1984). Journal of the American Water Resources Association, 55(2): 285-286.

Wang, G. Z., Li, Z. Y., Zhang, J. Y., Cheng, H., Hao, J. and Gan, R. 2018. Ecological security evaluation of reservoirs in Henan Province by pressure - state - response model. Journal of Water Resources & Water Engineering, 29(4): 12-17.

Wang, S., Zhang, X., Wu, T. and Yang, Y.Y. 2019. The evolution of landscape ecological security in Beijing under the influence of different policies in recent decades. Science of the Total Environment, 646: 49-57.

Xu, K., Bin, L., Xu, X. and Wang, P. 2019. Assessment of Water Resources Sustainability in Mainland China in Terms of Water Intensity and Efficiency. Environmental Management, 63(3): 309-321.

Xu, B. and Zhang, Y. 2018. Assessment of Groundwater Ecosystem Security in Arid Oasis Shihezi Reclamation Area in Xinjiang. Research of Environmental Sciences, 31(5): 919-926.

Zhang, Z.Y., Pan, W.G., Huang, T. and Lin, H. 2017. Comprehensive evaluation and prediction of water security：An empirical analysis based on Taizhou city of Zhejiang Province. Journal of Water Resources and Water Engineering, 28(04): 70-74.

Zeng, X. T., Huang, G. H., Chen, H. L., Li, Y.P., Kong, X.M. and Fan, Y.R. 2016. A simulation-based water-environment management model for regional sustainability in compound wetland ecosystem under multiple uncertainties. Ecological Modelling, 334: 60-77.

Nature Environment and Pollution Technology
An International Quarterly Scientific Journal

p-ISSN: 0972-6268
(Print copies up to 2016)
e-ISSN: 2395-3454

Vol. 20 | No. 2 | pp. 613-618 | 2021

Original Research Paper

https://doi.org/10.46488/NEPT.2021.v20i02.018

Open Access Journal

Tropical Fruit Wastes as an Organic Nutrient Sources for the Cultivation of *Chlorella vulgaris* and *Haematococcus pluvialis*

Y.H. Tan*, Y.J. Khoo, M.K. Chai*† and L.S. Wong****

*College of Engineering, Universiti Tenaga Nasional, Jalan Ikram-Uniten, Kajang, Selangor 43000, Malaysia

**Faculty of Health and Life Science, INTI International University, Persiaran Perdana BBN, Putra Nilai, Nilai, Negeri Sembilan 71800, Malaysia

†Corresponding author: M.K. Chai; mkchai@uniten.edu.my

Nat. Env. & Poll. Tech.
Website: www.neptjournal.com

Received: 30-03-2020
Revised: 02-05-2020
Accepted: 25-06-2020

Key Words:
Chlorella vulgaris
Haematococcus pluvialis
Fruit waste
Organic nutrient source

ABSTRACT

The possibility of replacing the inorganic medium with tropical organic fruit waste medium as a nutrient supplement was evaluated for the cultivation of *Chlorella vulgaris* and *Haematococcus pluvialis* in this study. Various concentrations of tropical fruit waste medium such as papaya, pineapple and mango were prepared to cultivate microalgae of *C. vulgaris* and *H. pluvialis*. The biomass concentration, productivity and specific growth rate were determined and compared with those grown in a fully inorganic medium. For *C. vulgaris,* the use of a 20% tropical fruit waste medium was found to yield higher biomass concentration (4.133-4.533 g/L) compared with cultivation in a fully inorganic medium (3.400 g/L). For *H. pluvialis*, the use of a 10% mango waste medium was found to yield a similar biomass concentration compared with cultivation in a fully inorganic medium (3.400 g/L). These results unveiled the potential of utilizing with tropical organic fruit waste medium as an effective strategy to reduce the cultivation cost of microalgae and treat the tropical fruit waste prior to discharge to the environment.

INTRODUCTION

The economic growth and population growth have rendered fast-growing global energy demand. Currently, energy generation through fossil fuels combustion is still incumbent in most developing countries (International Energy Agency 2019) albeit they have creaked about many environmental problems such as global warming stemming from greenhouse gases emission (BP 2019). Besides, overreliance on non-renewable fossil fuel accelerates resource depletion and increases economic burden due to the fluctuating price of fossil fuel. Given this scenario, alternative energy sources which are sustainable and greener have been proposed. Well-known biofuel such as biodiesel has been recognized as a potential energy source as compared to fossil fuels (Leong et al. 2018).

Biofuels can be derived from renewable sources including plant or microalgae (Raheem et al. 2018, Voloshin et al. 2016). The latter organisms have gain enormous attention recently due to their attractive advantages including high growth rate, high oil productivity, great photosynthetic efficiencies and less requirement of arable land (Bhalamurugan et al. 2018, Thawechai et al. 2016). Apart from the high oil productivity for biodiesel, its untapped potential to produce carbohydrate and protein can be explored for biogas (Ferreira et al. 2017, Tao et al. 2017) and agriculture application (Khatoon et al. 2010). Despite these advantages, the major challenges for scale-up biomass production are high capital and operational cost especially cultivation cost and high requirement for freshwater (Chia et al. 2018). Thus, more studies are needed to evaluate the strategy to remedy this bottleneck. Recently, wastewater (Acién Fernández et al. 2018, Ashokkumar et al. 2019, Wuang et al. 2016) and food waste (Chew et al. 2018, Lau et al. 2014, Zhang et al. 2018) have been formulated as cultivation medium since they are rich in nutrients which can promote microalgae growth while the microalgal growth can purify the waste before discharging into water bodies. This integration strategy renders a win-win situation by reducing environmental pollution and concurrently minimizing the cultivation cost of microalgae.

Tropical fruits are one of the important economic commodities in Malaysia. Despite consumed by Malaysian and exported to other countries, some tropical fruits are used for industrial processing for the production of fruit juice, flavouring and canned fruit. The worldwide popularity and demand for tropical fruits has shown an increasing trend from time to time (Rozhan 2017). Some tropical fruits such as pineapple and durian encompass more than 50% rind and seeds that are not consumable. These fruits wastes are rich in moisture and organic composition therefore the long-term disposal of these fruit wastes to the environment not only results in greenhouse gas emission but also environmental pollution

(Cheok et al. 2018). Hence, treatment of these fruit wastes before disposing of in the environment is necessary. In this context, the integration of tropical fruit waste medium for the cultivation of microalgae can be a potential strategy to solve the aforementioned problems.

The objective of this preliminary study was to investigate the potential of using tropical fruit wastes such as papaya, pineapple and mango as nutrient mediums for the cultivation of *C. vulgaris* and *H. pluvialis*. The optimum concentration for three fruit wastes was identified to evaluate the feasibility of replacing the inorganic medium with tropical fruit waste medium.

MATERIALS AND METHODS

Microalgae Strain Cultivation

Microalgae strain of *C. vulgaris* used in this study was derived from a local lake near Inti International University, while *H. pluvialis* used in this study was obtained from Algaetech Malaysia. Both microalgae were cultivated in a 250 mL conical flask containing 150 mL of Basal's basic medium (BB medium). Microalgae cultures were incubated at room temperature under illumination from cool-white fluorescent tubes for 16:8 hours of the light-dark cycle. During the cultivation, microalgae were manually shaken twice each day to prevent microalgal adherence and congregation.

Growth phases of the cells were investigated by determining cell density using a haemocytometer (Marienfeld-Superior, Neubauer) under a light microscope (Eclipse E-100 LED, Nikon).

Microalgae Cultivation with Fruit Waste Medium

Tropical organic fruits namely papaya, pineapple and mango were purchased from the local market. The fruits were washed and cut. The fruit waste including peel and core was cut, blended and filtered using a kitchen sieve. Then, the Duran bottles containing filtered fruit waste solution were heated in a microwave oven at 400 W for 10 minutes. The bottles were wrapped with aluminium foil and kept in the refrigerator at 4°C to avoid nutrient decomposition. To prepare 250 mL of different concentrations (5%, 10%, 20% and 25%) of papaya, pineapple and mango fruit waste mediums, each fruit waste was diluted with deionized water. Each diluted fruit waste medium was immediately cultivated with 4 mL of 2-days-old *C. vulgaris* and 4-days-old *H. pluvialis*. Microalgae cultivated in BB medium and deionized water was used as positive and negative control respectively. The microalgae were cultivated at the condition as previously described.

Determination of Microalgae Cell Growth

The dry cell weight (DCW) of the microalgae biomass was attained by vacuum filtering 5 mL aliquots of culture using pre-weighted mixed cellulose ester membrane filters with absorbent pads (0.45 μm pore size, 47 mm in diameter). Each loaded filter was dried at 80°C until the weight was constant. To obtain the dry cell weight of microalgae, the dry weight of the blank membrane filter was subtracted from that of the loaded membrane filter.

The DCW was used to calculate the microalgae growth. The biomass concentration, productivity and specific growth rate were calculated using the formulas below (Chew et al. 2018, He et al. 2018):

$$\text{Biomass concentration, } X = (DCW_t/\text{volume of aliquots}) - (DCW_0/\text{volume of aliquots})$$

$$\text{Biomass productivity, } P_b = (X_f - X_0)/(t_f - t_0)$$

$$\text{Specific growth rate, } \mu = (\ln X_f - \ln X_0)/(t_f - t_0)$$

Where X_f and X_0 are the biomass concentration (g/L) on days t_f and t_0 (the end and beginning of the determined growth phase respectively).

Statistical Analysis

All experiments were conducted in triplicates and data were presented as means ± standard error of the mean.

RESULTS AND DISCUSSION

Prior to microalgae cultivation with tropical fruit waste mediums, the growth phase of two microalgae in BBM was determined based on the cell count. The results showed that the *C. vulgaris* entered the log phase during the 2nd day and then entered the stationary phase during the 4th day while *H. pluvialis* initiated log phase during 1st day and entered stationary phase during 8th day. The 2-day-old *C. vulgaris* and 4-day-old *H. pluvialis* had adequate cell density therefore they were inoculated into a 250 mL fruit waste medium. The inoculum of high cell density was imperative to ensure the survival of microalgae in the new environment (Gani et al. 2016).

Effect of Fruit Waste Medium Concentrations on Microalgae Growth

The growth of *C. vulgaris* and *H. pluvialis* in papaya, pineapple and mango fruit wastes at various dilutions and in BB medium are shown in Fig. 1 and Fig. 2. The results demonstrate that these two microalgae could grow in almost all concentrations (10, 15%, 20% and 25%) of papaya, pineapple and mango waste mediums compared to microalgae that grew in negative control which is

deionised water. Microalgae of *C. vulgaris* supplemented with 20% papaya, pineapple and mango yielded biomass concentration of 4.133 g/L, 4.533 g/L and 4.600 g/L respectively at the end of 7 days which is higher than the BB medium at 2.233 g/L (Table 1). *C. vulgaris* in 5% papaya, pineapple and mango waste did not grow well and the biomass concentration was very low, only at 0.667, 1.100 and 0.533 g/L respectively, while *C. vulgaris* in 25% papaya, pineapple and mango wastes yielded 1.500, 1.400 and 1.433 g/L respectively.

As shown in Fig. 2, *H. pluvialis* was able to grow in all concentrations of papaya, pineapple and mango fruit waste mediums. *H. pluvialis* in 10% mango waste yielded biomass concentration of 3.400 g/L at the end of 7 days which is comparable to positive control at 3.500 g/L. Although other concentrations of fruit waste medium yielded biomass concentration that lower than BB medium, a slow and increasing trend was observed.

Papaya, pineapple and mango peels have been discovered to contain organic carbon, protein, vitamins and trace metals (Abdul Aziz et al. 2012, Souza et al. 2016, Siti Roha et al.2013, Suchiritha et al. 2017) which can be supplemented to support microalgae growth. However, the nutrient concentration must be monitored since concentrated nutrient would contrarily reduce microalgae growth. For all the concentration of fruit waste medium up to 25% including the positive control, the *C. vulgaris* grew rapidly during the first 3 days and continued to attenuate slowly until the 7th day, indicating the fruit waste medium did not inflect the growth phase of *C. vulgaris*. The continuous decline or slow increment of biomass concentration after 3rd day probably stemming from the diminishing of nutrients and the cells instigated the stationary phase. In Table 1, the results showed that *C. vulgaris* in 20% fruit waste medium gave the highest biomass concentration and average biomass productivity when compared to BB medium.

For *H. pluvialis*, the cells grew slowly in BB medium and fruit waste mediums within 7th day. As shown in Table 2, *H. pluvialis* in 5% and 10% fruit waste mediums resulted in higher biomass concentration and productivity, indicating that lower fruit waste mediums are more suitable for *H. pluvialis* to grow. Compared to *H. pluvialis*, *C. vulgaris* showed higher biomass concentration and biomass productivity. It is probably because of their varied metabolisms mode. Besides, compared to *C. vulgaris*, *H. pluvialis* preferred growing in a low concentration of fruit waste medium. The high turbidity of the fruit waste medium may force microalgae to grow in heterotrophic or mixotrophic mode. Testaments from previous studies have revealed *C. vulgaris* was capable to grow with higher biomass concentration in various types of mixotrophic or heterotrophic medium (Gao et al. 2019, Lam et al. 2017, Li et al. 2019, Melo et al. 2018), whereas not many studies have unveiled capability of *H. pluvialis* in different types of mixotrophic medium (Sipaúba-Tavares et al. 2015). Further

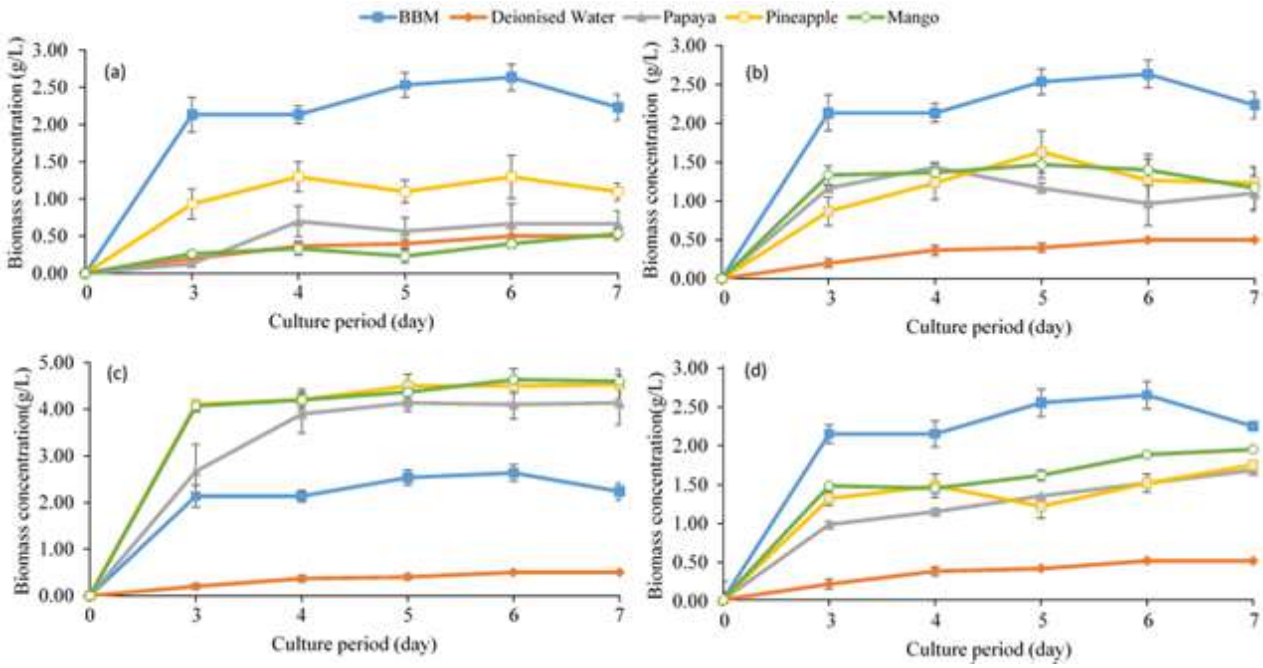

Fig. 1: Biomass concentration of *C. vulgaris* in (a) 5%, (b) 10%, (c) 20% and (d) 25% papaya, pineapple and mango wastes and in BB medium (n = 3).

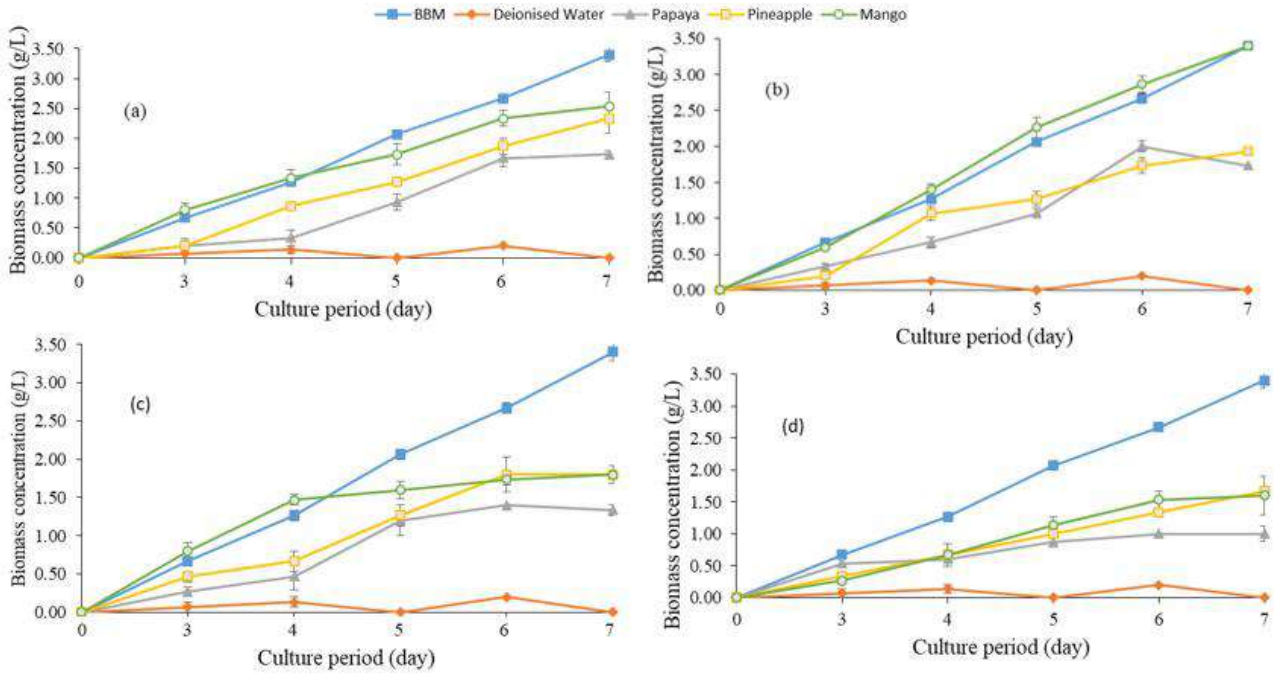

Fig. 2: Biomass concentration of *H. pluviaris* in (a) 5%, (b) 10%, (c) 20% and (d) 25% papaya, pineapple and mango wastes and in BB medium (n = 3).

Table 1: Final dry cell weight (DCW), average biomass productivity (P_b) and average specific growth rates (μ) of *C. vulgaris* in papaya, pineapple and mango waste medium at various concentrations and in BB medium.

Medium		DCW (g/L)	P_b	μ (d^{-1})
BBM		2.233 ± 0.176	0.172 ± 0.015	0.180 ± 0.022
DW		0.500 ± 0.000	0.022 ± 0.008	0.046 ± 0.003
Papaya	5%	0.667 ± 0.176	0.045 ± 0.013	0.040 ± 0.007
	10%	1.100 ± 0.231	0.110 ± 0.013	0.067 ± 0.012
	20%	4.133 ± 0.470	0.244 ± 0.047	0.208 ± 0.021
	25%	1.667 ± 0.333	0.076 ± 0.006	0.145 ± 0.016
Pineapple	5%	1.100 ± 0.115	0.084 ± 0.015	0.105 ± 0.013
	10%	1.233 ± 0.203	0.089 ± 0.009	0.069 ± 0.008
	20%	4.533 ± 0.318	0.319 ± 0.009	0.240 ± 0.034
	25%	1.733 ± 0.120	0.096 ± 0.005	0.164 ± 0.023
Mango	5%	0.533 ± 0.088	0.025 ± 0.004	0.046 ± 0.007
	10%	1.167 ± 0.273	0.113 ± 0.003	0.117 ± 0.004
	20%	4.600 ± 0.153	0.308 ± 0.005	0.365 ± 0.006
	25%	1.933 ± 0.030	0.103 ± 0.007	0.101 ± 0.012

research is required to discover the influence of metabolism mode on the growth of *H. pluvialis.* Moreover, *C. vulgaris* has a shorter log phase than *H. pluvialis*, indicating *C. vulgaris* has faster cell metabolism thereby their cell concentration grow quickly. Greater cultivation time is feasibly required for *H. pluvialis* to achieve higher biomass concentration and average specific growth rate.

The average specific growth rates (μ) during 3-7 days' culture are shown in Table 1. The increasing of papaya and mango waste medium concentration stimulated μ of *C. vulgaris* to increase until the concentration of 20%. μ was dropped in the concentration of 10% pineapple and then increased in the concentration of 20% followed by a decrease in the concentration of 25%. μ attained in papaya, pineapple

Table 2: Final dry cell weight (DCW), average biomass productivity (P_b) and average specific growth rates (μ) of *H. pluviaris* in papaya, pineapple and mango waste medium at various concentrations and in BB medium.

Medium		DCW (g/L)	P_b	μ (d^{-1})
BBM		3.400 ± 0.115	0.314 ± 0.013	0.239 ± 0.009
DW		0.000 ± 0.000	0.015 ± 0.006	0.022 ± 0.007
Papaya	5%	1.733 ± 0.067	0.144 ± 0.022	0.102 ± 0.018
	10%	1.733 ± 0.133	0.179 ± 0.017	0.133 ± 0.014
	20%	1.333 ± 0.115	0.145 ± 0.033	0.090 ± 0.001
	25%	1.000 ± 0.200	0.135 ± 0.023	0.046 ± 0.002
Pineapple	5%	2.333 ± 0.240	0.197 ± 0.021	0.125 ± 0.019
	10%	1.933 ± 0.176	0.192 ± 0.022	0.111 ± 0.017
	20%	1.800 ± 0.200	0.189 ± 0.040	0.077 ± 0.005
	25%	1.667 ± 0.115	0.156 ± 0.017	0.062 ± 0.006
Mango	5%	2.533 ± 0.240	0.283 ± 0.027	0.157 ± 0.004
	10%	3.400 ± 0.200	0.328 ± 0.022	0.161 ± 0.014
	20%	1.733 ± 0.115	0.250 ± 0.026	0.030 ± 0.001
	25%	1.600 ± 0.429	0.161 ± 0.045	0.033 ± 0.010

and mango waste mediums with the concentration of 20% were higher than in BB medium.

For *H. pluvialis*, μ was increased from the concentration of 5% to 10% and then decreased in the concentration of 20% and 25%. These results indicated that fruit waste with a concentration of 10% was ideal for *H. pluvialis* to grow compared with other concentrations while it was not optimised as in BB medium.

This research confirmed that some of the diluted papaya, pineapple and mango waste mediums were capable to grow these two microalgae. Similar results were reported by previous studies (Chew et al. 2018, Heller et al. 2015, Lau et al. 2014, Zhang et al. 2018), using food waste as a nutrient medium for *C. vulgaris.* A high concentration of food waste exhibited an inhibition effect on cell growth while a low concentration of food compost favoured the cell growth. In this study, only 20% of fruit waste medium with *C. vulgaris* have higher biomass concentration, productivity and specific growth rate than those in BB medium. Whereas only *H. pluvialis* in 10% mango waste medium has similar biomass concentration, productivity and specific growth rate compared to those in BB medium. Two reasons can elucidate this phenomenon. First, a high level of turbidity was observed in all fruit waste mediums, and the sediment may be a light barrier for microalgae cultivation. The high turbidity and sediment hinder the light to penetrate the fruit waste medium therefore microalgae were distracted from photosynthesis. This can be confirmed by comparing pigments colour of microalgae that grew in BB medium and fruit waste medium. The cell pigment in the fruit waste medium was paler than those grown in the BB medium. Furthermore, the fruit product usually has a somewhat acidic pH which may not favour most microalgae growth (Difusa et al. 2015, Zhang et al. 2014).

Second, to reduce the cultivation cost, raw and unsterile fruit waste was used in the present study. As it was unsterile, unknown zooplanktons appeared. The presence of zooplanktons competed for nutrient sources thereby reduced the number and biomass concentration of algal cells. Besides, white fungi appeared in all concentration of papaya waste mediums during cultivation. Although combating white fungi was attempted to be removed using spatula, it regrew again and only white fungi in 20% papaya waste medium that growing *C. vulgaris* was successfully eliminated.

CONCLUSIONS

In this study, the recycling of nutrients from tropical fruit waste medium was investigated by the cultivation of *C. vulgaris* and *H. pluvialis* using papaya, pineapple and mango wastes with different concentrations. The highest biomass concentration for *C. vulgaris* and *H. pluvialis* was attained in 20% fruit waste mediums and 10% mango fruit waste respectively. This study demonstrated that papaya, pineapple and mango wastes have feasible to cultivate microalgae. The utilization of tropical fruit waste medium can be an effective strategy to minimize environmental pollution and the microalgae cultivation cost. Determination of nutrient removal rate and metabolites such as lipids, carbohydrates and proteins should be carried out in the future to investigate the economic value of this integrated strategy.

ACKNOWLEDGEMENT

The authors would like to acknowledge UNITEN BOLD2025 Phase 2 Grant No. "10436494/B/2019006" for the financial support.

REFERENCES

Abdul Aziz, N.A., Wong, L.M., Bhat, R. and Cheng, L.H. 2012. Evaluation of processed green and ripe mango peel and pulp flours (*Mangifera indica* var. Chokanan) in terms of chemical composition, antioxidant compounds and functional properties. J. Sci. Food Agric., 92(3): 557-563.

Acién Fernández, F.G., Gómez-Serrano, C. and Fernández-Sevilla, J.M. 2018. Recovery of nutrients from wastewaters using microalgae. Front. Sustain. Food Syst., 2: 1-13.

Ashokkumar, V. Chen, W.H., Kamyab, H., Kumar, G., Al-Muhtaseb, A.H. and Ngamcharussrivichai, C. 2019. Cultivation of microalgae *Chlorella* sp. In municipal sewage for biofuel production and utilization of biochar derived from residue for the conversion of hematite iron ore (Fe_2O_3) to iron (Fe) - Integrated algal biorefinery. Energy, 189: 116128.

Bhalamurugan, G.L., Valerie, O. and Mark, L. 2018. Valuable bioproducts obtained from microalgal biomass and their commercial applications: A review. Environmental Engineering Research, 23(3): 229-241.

BP. 2019. BP Statistical Review of World Energy 2019. In BP. London.

Chia, S.R., Chew, K.W., Show, P.L., Yap, Y.J., Ong, H.C., Ling, T.C. and Chang, J.S. 2018. Analysis of economic and environmental aspects of microalgae biorefinery for biofuels production: A Review. Biotechnol. J., 13(6): 170068.

Cheok, C.Y., Mohd Adzahan, N., Abdul Rahman, R., Zainal Abedin, N.H., Hussain, N., Sulaiman, R. and Chong, G.H. 2018. Current trends of tropical fruit waste utilization. Crit. Rev. Food Sci. Nutr., 58(3): 335-361.

Chew, K.W., Chia, S.R., Show, P.L., Ling, T.C., Arya, S.S. and Chang, J.S. 2018. Food waste compost as an organic nutrient source for the cultivation of *Chlorella vulgaris*. Bioresour. Technol., 267: 356-362.

Difusa, A., Talukdar, J., Kalita, M.C., Mohanty, K. and Goud, V.V. 2015. Effect of light intensity and pH condition on the growth, biomass and lipid content of microalgae *Scenedesmus* species. Biofuels, 6: 37-44.

Ferreira, A., Ribeiro, B., Marques, P.A.S.S., Ferreira, A.F., Dias, A.P., Pinheiro, H.M. et al. 2017. *Scenedesmus obliquus* mediated brewery wastewater remediation and CO_2 biofixation for green energy purposes. J. Clean. Prod., 165: 1316-1327.

Gani, P., Sunar, N.M., Latiff, A.A.A. and Razak, A. 2016. Influence of initial cell concentrations on the growth rate and biomass productivity of microalgae in domestic wastewater. Appl. Ecol. Environ. Res., 14(2): 399-409.

Gao, F., Yang, H.L., Li, C., Peng, Y.Y., Lu, M.M., Jin, W.H., Bao, J.J. and Guo, Y.M. 2019. Effect of organic carbon to nitrogen ratio in wastewater on growth, nutrient uptake and lipid accumulation of a mixotrophic microalgae *Chlorella* sp. Bioresour. Technol., 282: 118-124.

He, Q.N., Yang., H.J. and Hu, C.X. 2018. Effects of temperature and its combination with high light intensity on lipid production of *Monoraphidium dybowskii* Y2 from semi-arid desert areas. Bioresour. Technol., 265: 407- 414.

Heller, W.P., Kissinger, K.R., Matsumoto, T.K. and Keith, L.M. 2015. Utilization of papaya waste and oil production by *Chlorella protothecoides*. Algal Res., 12: 156-160.

International Energy Agency, 2019. World Energy Outlook 2019. International Energy Agency.

Khatoon, N., Sengupta, P., Homechaudhuri, S. and Pal, R. 2010. Evaluation of algae based feed in goldfish (*Carassius auratus*) nutrition. Proc. Zool. Soc., 63(2): 109-114.

Lam, M.K., Yusoff, M.I., Uemura, Y., Lim, J.W., Khoo, C.G., Lee, K.T. and Ong, H.C. 2017. Cultivation of *Chlorella vulgaris* using nutrients source from domestic wastewater for biodiesel production: Growth condition and kinetic studies. Renew. Energy, 103: 197-207.

Lau, K.Y., Pleissner, D. and Lin, C.S.K. 2014. Recycling of food waste as nutrients in *Chlorella vulgaris* cultivation. Bioresour. Technol., 170: 144-151.

Leong, W.H., Lim, J.W., Lam, M.K., Uemura, Y. and Ho, Y.C. 2018. Third generation biofuels: A nutritional perspective in enhancing microbial lipid production. Renew. Sust. Energ. Rev., 91: 950-961.

Li, H., Zhang, Y., Liu, J., Shen, Z., Li, A., Ma, T., Feng, Q. and Sun, Y. 2019. Treatment of high-nitrate wastewater mixtures from MnO_2 industry by *Chlorella vulgaris*. Bioresour. Technol., 291: 121836.

Melo, R.G., Andrade, A.F., Bezerra, R.P., Correia, D.S., Souza, V.C., Brasileiro-Vidal, A.C., Marques, D.A.V. and Porto, A.L.F. 2018. *Chlorella vulgaris* mixotrophic growth enhanced biomass productivity and reduced toxicity from agro-industrial by-products. Chemosphere, 204: 344-350.

Raheem, A., Prinsen, P., Vuppaladadiyam, A.K., Zhao, M. and Luque, R. 2018. A review on sustainable microalgae based biofuel and bioenergy production: Recent developments. J. Clean. Prod., 181: 42-59.

Rozhan, A.D. 2017. Trends in Production, Trade, and Consumption of Tropical Fruit in Malaysia. FFTC Agricultural Policy Platform, 1-8.

Sipaúba-Tavares, L.H., Berchielli-Morais, F.A. and Scardoeli-Truzzi, B. 2015. Growth of *Haematococcus pluvialis* Flotow in alternative media. Braz. J. Biol., 75(4): 796-803.

Siti Roha, A.M., Zainal, S., Noriham, A. and Nadzirah, K. 2013. Determination of sugar content in pineapple waste variety N36. Int. Food Res. J., 20(4): 1941-1943.

Souza, R.A.T., Fonseca, T.A.B., Kirsch, L.S., Silva, L.S.C., Alecrim, M.M., Filho, R.F.C. and Teixeira, M.F.S. 2016. Nutritional composition of bioproducts generated from semi-solid fermentation of pineapple peel by edible mushrooms. Afr. J. Biotechnol., 15(12): 451-457.

Suchiritha, D.S., Suneetha, J.W. and Durga Rani, C.V. 2017. Nutritional properties of papaya peel. Pharma. Innov., 170(67): 170-173.

Tao, R., Kinnunen, V., Praveenkumar, R., Lakaniemi, A.M. and Rintala, J. A. 2017. Comparison of *Scenedesmus acuminatus* and *Chlorella vulgaris* cultivation in liquid digestates from anaerobic digestion of pulp and paper industry and municipal wastewater treatment sludge. J. Appl. Phycol., 29(6): 2845-2856.

Thawechai, T., Cheirsilp, B., Louhasakul, Y., Boonsawang, P. and Prasertsan, P. 2016. Mitigation of carbon dioxide by oleaginous microalgae for lipids and pigments production: Effect of light illumination and carbon dioxide feeding strategies. Bioresour. Technol., 219: 139-149.

Voloshin, R.A., Rodionova, M.V., Zharmukhamedov, S.K., Nejat Veziroglu, T. and Allakhverdiev, S.I. 2016. Review: Biofuel production from plant and algal biomass. Int. J. Hydrogen Energy, 41(39): 17257-17273.

Wuang, S.C., Khin, M.C., Chua, P.Q.D. and Luo, Y.D. 2016. Use of *Spirulina* biomass produced from treatment of aquaculture wastewater as agricultural fertilizers. Algal Res., 15: 59-64.

Zhang, L., Cheng, J., Pei, H., Pan, J., Jiang, L., Hou, Q. and Han, F. 2018. Cultivation of microalgae using anaerobically digested effluent from kitchen waste as a nutrient source for biodiesel production. Renew. Energy, 115: 276-287.

Zhang, Q., Wang, T. and Hong, Y. 2014. Investigation of initial pH effects on growth of an oleaginous microalgae *Chlorella* sp. HQ for lipid production and nutrient uptake. Water Sci. Technol., 70(4): 712-719.

Nature Environment and Pollution Technology
An International Quarterly Scientific Journal

p-ISSN: 0972-6268
(Print copies up to 2016)
e-ISSN: 2395-3454

Vol. 20 | No. 2 | pp. 619-624 | 2021

Original Research Paper

https://doi.org/10.46488/NEPT.2021.v20i02.019

Open Access Journal

Cut-off Percentage of Ethanol in Diesel-Biodiesel Based Fuel Blends and Analysis of Emissions in Four Stroke-Compression Ignition Engines

P. Suresh Kumar*†, N. Prasanthi Kumari and Amit Kumar Sharma*****

*Department of Mechanical Engineering, University of Petroleum and Energy Studies, Dehradun, India

**Department of Electronics and Communications Engineering, University of Petroleum and Energy Studies, Dehradun, India

***Department of Biofuel Research Laboratory, Centre of Alternative Energy Research, University of Petroleum and Energy Studies, Dehradun, India

†Corresponding author: P. Suresh Kumar; psuresh@ddn.upes.ac.in

Nat. Env. & Poll. Tech.
Website: www.neptjournal.com

Received: 04-08-2020
Revised: 08-09-2020
Accepted: 16-09-2020

Key Words:
Ethanol
Biodiesel
Engine performance
Emissions
DI diesel engine

ABSTRACT

One of the major challenging problems faced globally is energy security, and new generation researchers' emphasis is on alternative fuels, which could switch the fossil fuels products entirely or moderately. The current study focuses on the use of ethanol as an alternative fuel for internal combustion engines. The speciality of this fuel is the oxygenated short-chain alcohols. These alcohols may be made through the fermentation of biomass, hence this fuel comes under a renewable source of energy. A four-stroke, single-cylinder, water-cooled and naturally aspirated compression ignition diesel engine was selected for this research. The above engine tested fuels like diesel, blends of diesel and ethanol. Diesel (D 100) (v/v), ethanol 5% with the addition of diesel 95% (E 5) (v/v), ethanol 10% with the addition of diesel 90% (E10) (v/v), ethanol 15% with the addition of diesel 85% (E 15) (v/v) and ethanol 20% with the addition of diesel 80% (E20) (v/v). The influence of the upturn of ethanol in the diesel delivered a decline of nitrogen oxides (NOx), carbon monoxide (CO) and unburnt hydrocarbons (UHC) matched to diesel fuel. It concluded that in these test fuels, E15 has higher brake thermal efficiency; E20 has higher brake specific fuel consumption. For emissions, E20 is the best blend compared to the remaining test fuels.

INTRODUCTION

In the 19th century, the entire world faced fuel crises due to limited petroleum-based fuels and elevation in prices. Shipping, moving, power generation and fields of agriculture mainly use internal combustion engines only. Petroleum and diesel-based fuels increase the emissions like oxides of nitrogen, carbon monoxide, total unburnt hydrocarbons, soot and particulate matter. These emissions percentage increases in the atmosphere and results in several diseases in human, animal and plant life. Since fossil fuel engines give more emissions, the entire world is following inflexible emission regulations. The researchers are focused on finding alternative fuels for internal combustion engines (Ribeiro et al. 2007, Cheung et al. 2008). Biodiesel is a very good alternative to fossil fuels as it easily mix-up with diesel and petroleum products. Generally used biodiesels are sunflower, Karanja, polanga, neem and jatropha, etc. The aforesaid biodiesels can be directly used in internal combustion engines without any major changes in the engines. The advantage of using these biodiesels is reducing the emissions and greenhouse gas discharges, and increase the world farm market with village development (Agarwal 2007). With new technologies ethanol is produced from corn, leftover biomass constituents, barely, molasses and cane (De Caro et al. 2001, Kremer & Fachetti 1965). Additives are added to internal combustion biodiesel engines to improve the mixing properties, reduce the ignition delay and lubricity. The main additives for biodiesel based internal combustion are oxygenates. The advantage of these oxygenate additives is that they improve the cetane number, improves efficiency, reduction of emissions, particulate matter and reduce the knocking. Generally used oxygenates are butanol, ethanol, pentanol and propanol. One of the analysis (Kumar et al. 2013) stated that by using a three-way catalytic converter system almost all the exhaust gases such as nitrogen oxides, unburnt hydrocarbons and carbon monoxide are reduced. Exhaust emission analysis was carried out by different methods such as catalytic converters, exhaust gas recirculation (Kumar et al. 2020, 2013, 2012). Ethanol physicochemical properties are not suitable as a direct fuel. It has low density, viscosity and cetane number. The acceptable diesel and ethanol blend ratio is 20% that means without major changes in the diesel engine, it can operate with all loads.

Another way of reducing emissions in internal combustion engines is using burnt petro-diesel fuels. The main raw materials used for producing ethanol are corn, barley, sugar cane and sugar beets, etc. Ethanol has a high-octane rating and low emission characteristics; its pros and cons clearly explained in the studies by (Schuetzle et al. 2002, Wugao & Zhen 2002). The oxygen percentage in ethanol is 34.73% by mass that enhances the combustion in diesel engines in the test fuel blends. The reduction of emissions of total unburnt hydrocarbons and conversion of carbon monoxide to carbon dioxide due to extra atom of oxygen in ethanol-diesel test fuel blends; even if numerous theories show that NOx emissions are reduced due to increased ethanol percentage in the diesel-ethanol blends (Khan et al. 2018).

Ethanol is directly not used as a primary fuel, but blending with diesel can be used in diesel engines and also used in spark-ignition engines as blended fuel. Sophisticated engine equipment is required to operate with these test fuels (Zhang et al. 2005, Nibin et al. 2005). Kumar et al. 2014 conducted experiments on four-stroke diesel engine with different biodiesel percentages at a constant speed of 1500 rpm. At 15% of biodiesel blends, NOx emissions and smoke are reduced. The fumigation system is a major part of these types of fuels to blend the required percentage. It is observed that internal combustion engine efficiency increases and reduction of emissions taking place in a diesel-ethanol blend. While increasing the ethanol percentage in blends, the brake power, brake specific fuel consumption and brake thermal efficiency are enhanced. The engine with the new blend as test fuel is kept on running for some time until it reaches the constant speed that is 1500 rpm. Then all the readings are noted and observed at peak injection pressures with a comparative analysis between performances and exhaust emissions (Puhan et al. 2009). In a recent research, biodiesel has been used as a supplementary amphiphilic for making micelles that have non-polar end preoccupied with near diesel and glacial bounce on the way to ethanol or butanol (Fernando & Hanna 2004). Another separate study reports the compression ignition engines with diesel and biodiesel as test fuels; the efficiency and pollution discharge depend on the fuel nozzle opening pressure, valve timing for injection and compression ratio (Kumar et al. 2012). In this study, ethanol percentage is increased up to 20% with an increment of 5% and compared with all the ethanol-blended fuels with diesel. Also, this paper establishes a better blending percentage of ethanol with diesel for compression ignition engines.

MATERIALS AND EXPERIMENTAL SET-UP

Preparation of Test Fuel

Initially, the test fuel prepared for running the diesel engine included diesel 95% with ethanol 5% (E 5), diesel 90% with ethanol 10% (E10), diesel 85% with ethanol 15% (E 15) and diesel 80% with ethanol 20% (E20). Ethanol and diesel were purchased from the market and test fuels were prepared as the above-mentioned percentages in the chemistry lab. The test fuel properties of all the fuels are listed in Table 1. Digital bomb calorimeter was used for measuring the calorific value of test fuels and viscometers for measuring kinematic viscosity.

Table 2 comprises the properties of test fuels. For experimental analysis ethanol mixed with diesel in different varying proportions like 5% ethanol and 95% diesel, 10% ethanol and 90% diesel, 15% ethanol and 85% diesel, and 20% ethanol and 80% diesel by volume respectively.

Experimental Test Rig

Fig. 1 shows the diesel engine test rig. It is a water-cooled, natural aspirated, four-stroke single-cylinder computerized engine. Full details and specification of the engine are incorporated in Table 3.

Experimental Procedure

The engine was operated with pure diesel as basic and

Table 1: Properties of diesel and ethanol fuel (Pinzi et al. 2017).

Properties	Diesel $C_{12}H_{23}$ ($C10H_{20} \sim C_{15}H_{28}$)	Ethanol C_2H_5OH
Calorific value kJ/kg	42510	26800
Cetane Number	50	8
Density, kg/m^3 at 20°C	842.4	788
Kinematic viscosity, $\times 10^{-2}$ m^2/s at 20°C	2.8	1.2
Latent heat of evaporation, (kJ/kg)	252	840
Flash point (°C)	79	13.5
Auto ignition temperature (°C)	251	420
Oxygen content (wt %)	0	34.8

Table 2: Properties of test fuel (Kirankumar et al. 2015)

Test Fuel	HHV-Higher Heating Value (MJ/kg)	Density at 15°C, 1bar (kg/m^3)
Diesel	43.4	846
E20	39.01	821
E15	40.35	827
E10	41.22	831
E5	42.08	834

Table 3: Engine specifications.

S. No.	Particulars	Specifications
1	Make	Field marshal Diesel engines
2	Rated Brake Power (BHP/kW)	10/7.35110
3	Rated speed (rpm)	1500
4	Number of cylinders	One
5	Bore x Stroke (mm)	120x139.7
6	Compression ratio	17:1
7	Cooling System	Water Cooled
8	Lubrication System	Forced Feed
9	Cubic Capacity	1580 cc
10	Specific Fuel Consumption	265kW hr OR 195 g/ bhp/hr

Fig. 1: Photograph of diesel engine test rig.

reference fuel for estimating the brake power, brake specific fuel consumption and exhaust gas analysis of other test fuels. For the experimental process with all diesel and ethanol blends, an individual fuel experiment was run for apiece test fuel event, the test rig as shown in Fig. 1. For tests, four different loads 25%, 50%, 75% and 100% were considered. While testing engine speed, 1000 rpm and compression ratio 17:1 was preserved. The cooling water flowing inside the engine jackets and calorimeter was attuned at 63°C. The diesel engine test rig was on the go and endorsed to track for 15-20 minutes to go on steady mode. The diesel machine functional constraints such as brake power or brake thermal efficiency and brake specific fuel consumption were noted for further calculations. By using AVL gas analyser for exhaust gases like unburnt hydrocarbons, oxides of nitrogen, carbon dioxide and carbon monoxide were also noted.

RESULTS AND DISCUSSION

Performance Assessment

In this paper performance analysis was studied by the parameters such as brake thermal efficiency and brake specific fuel consumption. BTE and BSFC against different loads were compared for diesel and ethanol blends of 5%, 10%, 15% and 20%, i.e. E-5, E-10, E-15 and E-20 respectively. BTE is more in diesel compared with other test fuels. BTE is lower at lower loads for all test fuels and increases with increasing the load because the combustion of fuel is more and hence increase in heat energy follows the increasing of brake thermal efficiency. BSFC is low in diesel compared with other blended test fuels. BSFC is higher at lower loads for all test fuels and it decreases with an increase in load for all test fuels. As the load increases, the fuel rate also increases, which means the fuel combustion completed in less time. Hence, as the load increases, the brake specific fuel consumption decreases for all test and blended fuels.

Brake thermal efficiency: Fig. 2 explains that the brake thermal efficiency (BTE) is one of the most significant engine's performance parameters and indicates how efficiently fuel burnt during combustion can be converted into useful work. The variation of brake thermal efficiency with load for diesel, biodiesel and its ethanol blends (D100, E-5, E-10, E-15 and E20) is shown in Fig. 2. It is observed that the brake thermal efficiency of diesel biodiesel and ethanol blends increased with increasing load for all type of fuel blends. The brake thermal efficiency of E-20 was 22.6 %, 28.1%, 30.9% and 32.9% at 25%, 50%, 75% and 100% load respectively. Furthermore, the BTE of CI engine was found to decrease with the increasing share of ethanol. The BTE of diesel engine was analysed as 34%, 33.6%, 33.2% and 32.9% for E-5, E-10, E-15 and E-20 respectively, which is lower than D100 fuel (34.5%). This is due to combined effect of low caloric value blends, which are accountable for spray characteristics leading to inferior air-fuel mixture formation and combustion resulting in lower brake thermal efficiency.

Brake specific fuel consumption: The brake specific fuel consumption indicates the quantity of fuel supplied to the engine per unit of power production. The variation of BSFC of different diesel ethanol and biodiesel blends (E-5, E-10, E15 and E-20) at different load is shown in Fig. 3

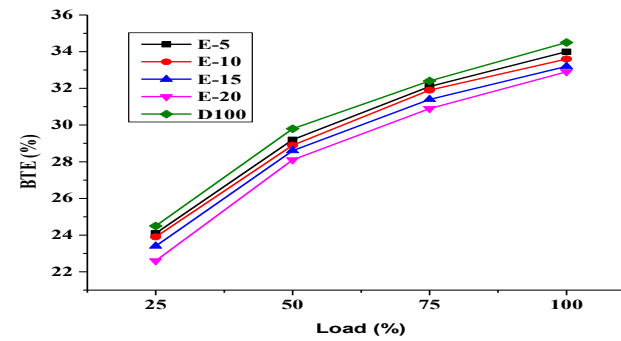

Fig. 2: BTE variation with load for D100, E-5, E-10, E-15 and E-20 at 1500 rpm.

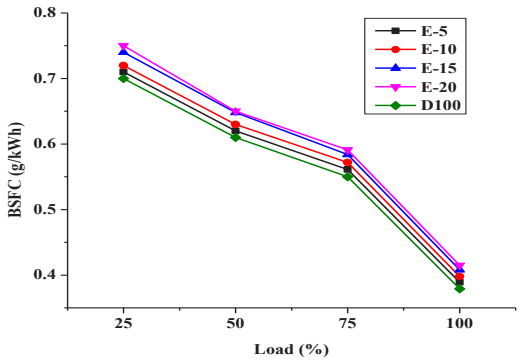

Fig. 3: BSFC variation with load for D100, E-5, E-10, E-15 and E-20 at 1500 rpm.

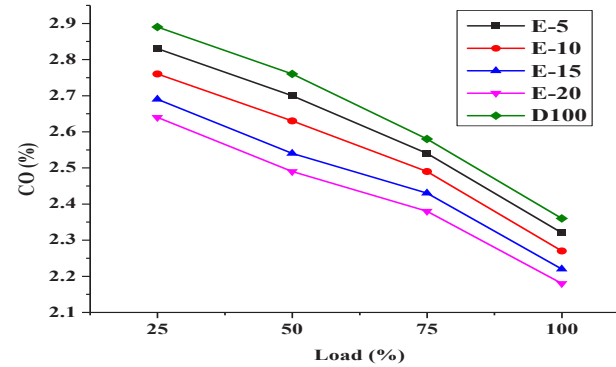

Fig. 4: CO variation with load for D100, E-5, E-10, E-15 and E-20 at 1500 rpm.

compared with base fuel, i.e. diesel. The results revealed that BSFC increased with the increasing amount of ethanol in fuel blends. Maximum BSFC was observed for E-20 (0.415 kW/h) in comparison to E-5 (0.389 kW/h), E-10 (0.398 kW/h), E-15(0.408 kW/h) and D100 (0.379 kW/h) at 100% load. Similarly, the BSFC of the engine was found to be increasing with increasing load. These data attributed in line with reported literature. The reason behind this may be a lower calorific value of fuel blends as calorific value decrease with the increasing share of ethanol.

Exhaust Emission Assessment

Exhaust gas analyser was used for the analysis of exhaust emissions for this study. The main polluted exhaust gas emissions are carbon monoxide (CO), carbon dioxide (CO_2), unburnt hydrocarbons (UHC) and nitrogen oxides (NOx) that are taken into account for exhaust gas emission analysis. These exhaust emissions are compared with diesel fuel to other test fuels. The observations made in this exhaust analysis was that the diesel fuel has a higher value of exhaust emissions compared to the other test fuels. E 20 has lower exhaust gas emission values compared to other test fuels and E 20 has a lower value of adiabatic flame temperature and the most homogenous fuel with respect to other test fuels. The cut off ratio of ethanol and diesel is 20% that means diesel 80% and ethanol 20% gives the best results when compared to other ethanol blended test fuels.

Carbon monoxide: The effect of engine load on CO emissions is shown in Fig. 4. The results revealed that with increasing load, CO emissions decreased because the combustion is more complete as the load increases. Furthermore, CO emissions also decreased with the increasing share of ethanol in fuel blends, e.g. the CO emissions for E5, E10, E15 and E20 was 2.32%, 2.27%, 2.22% and 2.18% respectively at 100% load in comparison to diesel (2.36%). This may be due to the reason that the increasing share of ethanol results in higher oxygen in fuel blends which leads to complete combustion.

Carbon dioxide: The variation of CO_2 with increasing load as shown in Fig. 5. It is observed from the figure that the emission of carbon dioxide increases with increasing load. This is vice versa of CO emissions and indicates that combustion improved with increasing load. Moreover, the emission of carbon dioxide decreased with the increasing share of ethanol in fuel blends. The emission of CO_2 was observed as 3.31%, 3.2 %, 3.1%, 2.99% and 3.4% for E-5, E-10, E-15 and E-20 respectively at 100% load which was lower than diesel (3.4%). This may be due to the reason that the oxygenated fuels result in slightly less CO_2 emission as the biodiesel has less carbon in its molecules and the combustion of ethanol products contain less CO_2 and more H_2O.

Nitrogen oxide: The variation of NOx emissions with diesel-ethanol blends is shown in Fig. 6. The results revealed that with increasing load, NOx emission also increased. NOx emissions increase in all cases as the load increases due to higher combustion temperature. In the case of biodiesel-diesel-ethanol blends, ethanol addition reduces NOx emissions as compared to diesel fuel. The NOx emissions

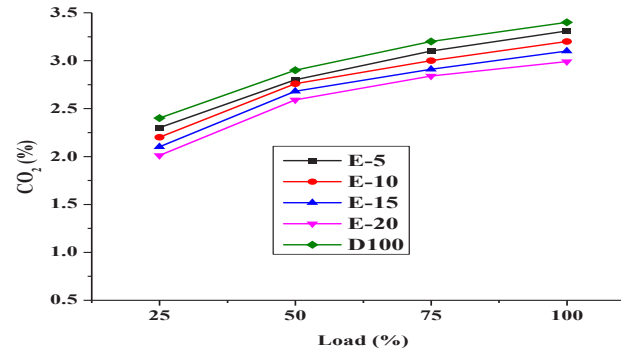

Fig. 5: CO_2 variation with load for D100, E-5, E-10, E-15 and E-20 at 1500 rpm.

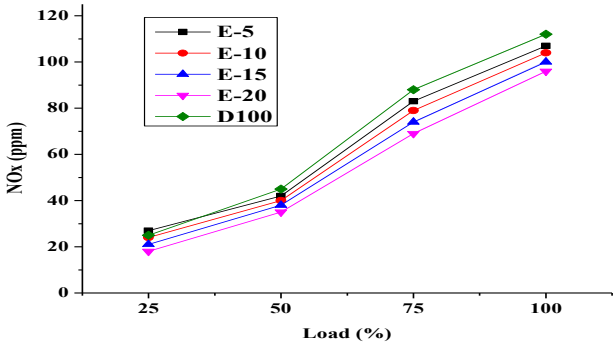

Fig. 6: NO_X variation with load for D100, E-5, E-10, E-15 and E-20 at 1500 rpm.

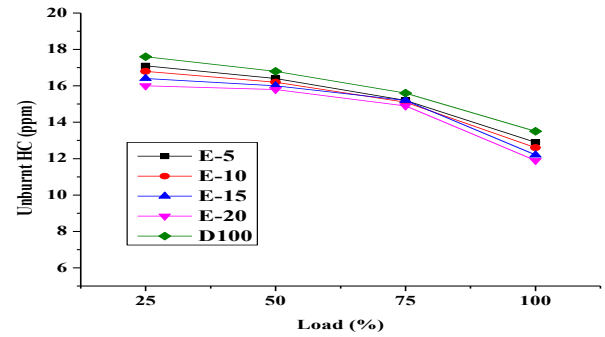

Fig. 7: Unburnt hydrocarbons variation with load for D100, E-5, E-10, E-15 and E-20 at 1500 rpm.

of E-5, E-10, E-15 and E-20 are 107 ppm, 104 ppm, 100 ppm, and 96 ppm in comparison to diesel (112 ppm). This might be because of the cooling effect of ethanol leading to lower cylinder combustion temperatures where NOx is formed, despite the previously noted higher exhaust temperature at low load, but does not contribute to NOx production there because of lower exhaust temperatures than in-cylinder temperatures.

Unburnt hydrocarbons: The effect of diesel-ethanol biodiesel blends on unburn hydrocarbon emissions with the variation of load as shown in Fig. 7. The results showed that unburn hydrocarbons decreased with increasing load. Unburnt hydrocarbons are the results of incomplete combustion. As the load increases, more complete combustion is achieved and less UHC is generated. In addition, UHC emissions decreased with the increasing amount of ethanol in fuel blends. The UHC emissions of E-5, E-10, E-15 and E-20 are 12.9 ppm, 12.6 ppm, 12.2 ppm and 11.9 ppm respectively, which was lower than diesel (13.5 ppm). This may be due to the presence of more oxygenated fuel which leads to complete combustion.

CONCLUSIONS

The present investigation was carried out on a single-cylinder, four strokes, naturally aspirated, water-cooled and compression ignition diesel engine at a constant speed of 1500 rpm.

Brake thermal efficiency was more in diesel fuel compared to ethanol diesel blended fuels. E20 has lower BTE with respect to all other fuel samples.

Brake specific fuel consumption was the least in diesel fuel compared to other test fuels. E20 has higher BSFC with respect to all other blend fuels.

The exhaust emissions such as carbon monoxide, carbon dioxide, unburnt hydrocarbons and nitrogen oxides for E-20 blend was least compared to all other test fuels.

The above test fuels performance and emission characteristics had a noble effect on the output compared to diesel fuel and numerous experimental studies similar to and supported our present findings. Further increasing the ethanol percentage in diesel fuel, i.e. more than 25% is not suggestible because of the following reasons:

1. Increasing the percentage of ethanol in diesel increases the knocking levels.
2. Adding of ethanol content more than 20% in diesel, the negative effects will occur such as less energy content due to which the thermal efficiency decreases because of the reduced burning temperatures.
3. Using of E 20 fuel increases the saving of petro diesel fuel reserves, hence reduces the depletion of petro diesel fuels. The production of E20 fuel increases when the international market demands then their cost may reduce drastically.
4. Confrontational effect of humankind if the higher percentage of ethanol present in diesel blends.

REFERENCES

Agarwal, A.K. 2007. Biofuels (alcohols and biodiesel) applications as fuels for internal combustion engines. Progress in Energy and Combustion Science, 33(3): 233-271.

Cheung, C.S., Cheng, C., Chan, T.L., Lee, S.C., Yao, C. and Tsang, K.S. 2008. Emissions characteristics of a diesel engine fuelled with biodiesel and fumigation methanol. Energy & Fuels, 22(2): 906-914.

De Caro, P.S., Mouloungui, Z., Vaitilingom, G. and Berge, J.C. 2001. Interest of combining an additive with diesel–ethanol blends for use in diesel engines. Fuel, 80(4): 565-574.

Fernando, S. and Hanna, M., 2004. Development of a novel biofuel blend using ethanol- biodiesel- diesel microemulsions: EB-diesel. Energy & Fuels, 18(6): 1695-1703.

Khan, K., Kumar, G., Sharma, A.K., Kumar, P.S., Mandal, C. and Chintala, V. 2018. Performance and emission characteristics of a diesel engine using complementary blending of castor and karanja biodiesel. Biofuels, 9(1): 53-60.

Kirankumar, S., Nagendrababu, D.R. and Apparao, D.K. 2015. Engine performance and emissions with ethanol and diesel-biodiesel blends. International Research Journal of Engineering and Rechnology, 2(5).

Kremer, F.G. and Fachetti, A. 2000. Alcohol as automotive fuel-Brazilian experience (No. 2000-01-1965). SAE Technical Paper.

Kumar, P. Suresh, Bhatnagar, Aditya, Kumari, N. Prasanthi and Sahoo, P. K. 2014. Reduction of NOx emissions with three-way catalytic converter for IDI engine fuelled with diesel, JSVO and their blends. International Journal of Engineering Research & Technology, 2(2): 1-11.

Kumar, P.S., Antony, F. and Sahoo, P.K. 2013. The performance and NOx emissions of a IDI diesel engine at distinct EGR rates fuelled with JB100, JB80, JB60, JB40, JB20 and diesel. International Journal of Engineering Science and Technology, 5(3): 519.

Kumar, P.S., Donga, R.K. and Sahoo, P.K. 2012. Experimental comparative study between performance and emissions of jatropha biodiesel and diesel under varying injection pressures. International Journal of Engineering Sciences & Emerging Technologies, 3(1): 98-112.

Kumar, P.S., Donga, R.K. and Sahoo, P.K. 2012. Experimental comparative study between performance and emissions of jatropha biodiesel and diesel under varying injection pressures. International Journal of Engineering Sciences & Emerging Technologies, 3(1): 98-112.

Kumar, P.S., Joshi, S., Prasanthi Kumari, N., Sharma, A., Nair, S. and Chatterjee, S. 2020. Reduction of emissions in a biodiesel‐fueled compression ignition engine using exhaust gas recirculation and selective catalytic reduction techniques. Heat Transfer, 49(5): 3119-3133.

Nibin, T., Sathiyagnanam, A.P., Sivaprakasam, S. and Saravanan, C.G. 2005. Investigation on emission characteristics of a diesel engine using oxygenated fuel additive. Journal of the Institution of Engineers(India), Part MC, Mechanical Engineering Division, 86: 51-54.

Pinzi, S., Redel-Macías, M.D., Leiva-Candia, D.E., Soriano, J.A. and Dorado, M.P. 2017. Influence of ethanol/diesel fuel and propanol/diesel fuel blends over exhaust and noise emissions. Energy Procedia, 142: 849-854.

Puhan, S., Jegan, R., Balasubbramanian, K. and Nagarajan, G., 2009. Effect of injection pressure on performance, emission and combustion characteristics of high linolenic linseed oil methyl ester in a DI diesel engine. Renewable Energy, 34(5): 1227-1233.

Ribeiro, N.M., Pinto, A.C., Quintella, C.M., da Rocha, G.O., Teixeira, L.S., Guarieiro, L.L., do Carmo Rangel, M., Veloso, M.C., Rezende, M.J., Serpa da Cruz, R. and de Oliveira, A.M. 2007. The role of additives for diesel and diesel blended (ethanol or biodiesel) fuels: A review. Energy & fuels, 21(4): 2433-2445.

Schuetzle, D., Han, W., Srithammavong, P., Akarapanjavit, N., Norbeck, J.M. and Corkwell, K., 2002. The evaluation of diesel/ethanol blends for diesel vehicles in Thailand: Performance and emissions studies. In: Proceedings of the 14th International Symposium on Alcohol (ISAF), pp. 12-15.

Wugao, Z. and Zhen, H. 2002, November. Study of performance and exhaust emission of a compression ignition diesel engine fueled with bio-diesel. In: Proceedings of the 14th International Symposium on Alcohol (ISAF).

Zhang, G.D., Liu, H., Xia, X.X., Zhang, W.G. and Fang, J.H. 2005. Effects of dimethyl carbonate fuel additive on diesel engine performances. Proceedings of the Institution of Mechanical Engineers, Part D: Journal of Automobile Engineering, 219(7): 897-903.

Nature Environment and Pollution Technology
An International Quarterly Scientific Journal

p-ISSN: 0972-6268
(Print copies up to 2016)
e-ISSN: 2395-3454

Vol. 20 | No. 2 | pp. 625-632 | 2021

Original Research Paper

https://doi.org/10.46488/NEPT.2021.v20i02.020

Open Access Journal

Carbon Emission Efficiency Measurement of Construction Industry and Its Treatment Measures-A Case Study of Henan Province, China

Zhang Hui*†, Du Liu Jie, Wang Bai Tian** and Qi Ping***

*Institute of Architecture Engineering, Huanghuai University, Zhumadian 463000, China

**College of Architecture and Civil Engineering, Shangqiu University, Shangqiu 476000, China

†Corresponding author: Zhang Hui: zhhui106@126.com

Nat. Env. & Poll. Tech.
Website: www.neptjournal.com

Received: 13-02-2021
Revised: 15-03-2021
Accepted: 08-04-2021

Key Words:
Construction industry
Carbon emission efficiency
Treatment measures

ABSTRACT

Energy demand and carbon emission in building construction and utilization have presented an increasing trend with urbanization development and improvement of living standard. Improving the carbon emission efficiency of the construction industry is a precondition for allocating carbon emission reduction objectives and interregional experience exchange over carbon emission reduction. An input-output index system was first constructed in this study to obtain the carbon emission efficiency of the construction industry. Carbon dioxide emission of the construction industry was taken as unexpected output, and the super efficiency slack-based measure-data envelopment analysis (SBM–DEA) model was used to estimate the carbon emission efficiency of the construction industry in Henan Province, China during 2008-2019. Finally, treatment measures were proposed to retard the rising trend of carbon emission in the construction industry. Results showed that the mean carbon emission efficiency of the construction industry in Henan Province during 2008-2019 is 1.007 and the carbon emission efficiency of the construction industry reaches the minimum value of only 0.807 in 2012. The carbon emission efficiency of the construction industry in Henan Province demonstrated an overall rising trend with a small amplitude during the investigation period. The results of this study can provide a reference for exploring the efficiency of the construction industry in Henan Province under carbon emission constraint, analyzing and identifying efficiency improvement objectives and methods for the construction industry, and facilitating its sustainable development.

INTRODUCTION

China is in the high-speed development phase of industrialization, urbanization, and modernization at present. Although the country's economy maintains a fast growth trend, serious and realistic problems, such as high energy consumption and emission, still persist. As the pillar industry of national economic development that plays a crucial role in China's economic construction process, the construction industry has progressed considerably in recent years while imposing non-negligible environmental stress on economic development. Moreover, this industry is closely related to national economic development and the improvement of people's livelihood. The construction industry has boosted the national economic development, promoted social progress, and provided job opportunities and material support to relevant national economic sectors with consideration for its industrial characteristics. Meanwhile, building energy conservation demonstrates high potential in solving the future global energy plight and realizing carbon emission reduction. All levels of the Chinese government have aggressively supported the development of a low-carbon economy and promotion of green buildings in the construction industry in recent years. Different regions have achieved an evident decrease in carbon emission intensity and satisfactory progress in energy conservation and emission reduction in the construction industry, with a substantial decrease in the number of heavy pollution days and improved overall air quality.

The construction industry is a typical energy-intensive field characterized by high energy consumption, high emission, and low efficiency. As shown in Fig. 1, the gross domestic product (GDP) of the construction industry in Henan Province, China is steadily increasing from RMB 282,405,000,000 in 2008 to RMB 1,270,168,000,000 in 2019, with an annual average growth rate of up to 16.19%. However, this industry still maintains an extensive development pattern of high input and output that results in inefficient resource utilization, increasing pollutant emissions, and surplus carbon emission. The development pattern of the construction industry in Henan Province must be transformed to enhance its efficiency and maintain pace with the rapid social development and needs of the general public. The production efficiency of this industry must be improved to

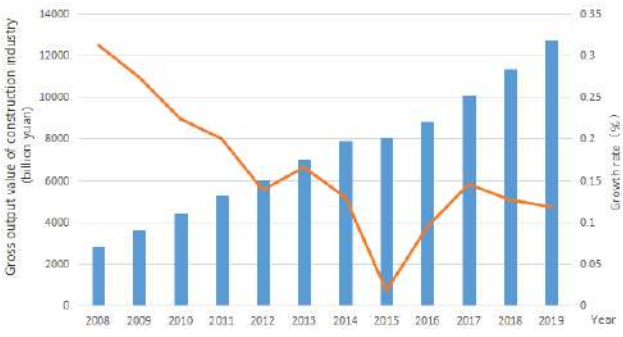

Fig. 1: Gross Output Value and Growth Rate of the Construction Industry in Henan Province During 2008-2019.

acquire high output while reducing the cost; reach the optimal input-output relation; and use the sustainable, efficient, and energy-saving development approach to replace the extensive development pattern.

PAST STUDIES

The current carbon emission of the construction industry is mainly calculated from microscopic and macroscopic angles. The carbon emission of the construction industry is accounted for with a specified area from the macroscopic angle. Domestic (Chinese) and foreign scholars have analyzed environmental influencing factors by focusing on the industrial field as well as technical efficiency, carbon emission efficiency, and economic growth of the industry. Many methods have been proposed to determine the carbon emission efficiency of the construction industry. Cole, R. J. provided a detailed calculation method for analyzing the energy consumption and greenhouse gas emission induced by field construction in the construction industry (Cole 1999). Chau et al. evaluated the building efficiency of construction companies in Hong Kong and revealed that high technical efficiency benefits from cost-effectiveness, large scale, low degree of subcontracting of construction companies, and low proportion of intermediate input consumption (Chau et al. 2001). Ramanathan used data envelopment analysis (DEA) to examine associations among gross national product (GNP), energy consumption, and carbon emission and showed that the carbon emission efficiency varies occasionally (Ramanathan 2006). Colombier et al. expounded on construction energy conservation technology featured by low carbon emission and sustainable development considered the urban construction industry in China as the study object and demonstrated that this technology can reduce the carbon emission and decelerate climatic changes (Colombier et al. 2009). Fan et al. indicated that building construction exerts a very important influence on the environment and a considerable amount of energy will be consumed while substantial greenhouse gases will be emitted in the production, transportation, and installation of construction materials and subsequently conducted a case study on greenhouse gas emission in building construction; the results showed that greenhouse gas emissions of construction materials account for 82%–87% of the total (Fan et al. 2010). Monahan et al. put forward process-based life cycle assessment (LCA) method to estimate carbon emissions of China's construction industry and pointed out that the total energy consumed by the industry is 411 million tce in 2016 and construction activities of city residential, public, and commercial buildings replace rural residences to become the main source of energy consumption and emission (Monahan et al. 2011). Acquaye et al. identified and analyzed emission "hotspots" in the product life cycle using different intervention schemes in the supply chain to reduce greenhouse emissions (Acquaye et al. 2015). Wang et al. proposed a method for calculating emissions in the total life cycle of China's construction industry and introduced multicriteria Gini coefficient as an index of emission permit allocation; the results showed that the overall emission in China's construction industry is increasing, with the maximum emission amount in the building production phase (Wang et al. 2017). Huang et al. stated that the construction industry consumes a large quantity of nonrenewable energy resources and the total CO_2 emission of the global construction industry has reached 5.7 billion tons, which accounts for 23% of the total CO_2 emission from global economic activities in 2009 (Huang et al. 2018). Li et al. calculated direct and indirect carbon emissions during the building foundation and structural construction processes and determined carbon emission sources in the two important construction phases (Li et al. 2017). Cai et al. pointed out that the energy consumption of the construction industry is calculated as a dependent-energy consumption type and should be divided and blended into other industries of China's statistical system and subsequently proposed a concrete method for estimating the carbon emission of the construction industry (Cai et al. 2018). Fang et al. demonstrated that the construction industry can realize clean and sustainable building production and construction and proposed a method for measuring carbon emissions in the construction phase due to the difficulty in calculating carbon emissions from complicated construction processes and numerous participators (Fang et al. 2018). Du et al. investigated club convergence and spatial distribution dynamics of carbon intensity in China's construction industry during 2005-2014; the results showed that carbon intensities of the construction industry in different provinces of China present a "convergence club" characteristic during the study period; extremely low or high level of convergence club indicates strong stability (Du et al. 2018). Zhou et al. showed

that the construction industry is the primary source of carbon emissions in China's economy and used the superslack-based measure-data envelope analysis (super-SBM-DEA) method to estimate the total-factor carbon emission efficiency of the construction industry during 2003-2016; the results showed that the low carbon emission efficiency in China's construction industry presents a declining trend (Zhou et al. 2019). Lu et al. critically reviewed and summarized carbon emissions of green buildings and proposed a comprehensive life-cycle carbon-emission evaluation model (Lu et al. 2020). These studies showed that the production in the construction industry needs a considerable amount of labour, material, and financial inputs, including energy sources and technologies. Studies on the efficiency evaluation of the construction industry have considered labour force, capital, and technology while neglecting environmental factors. Accordingly, the carbon emission of the construction industry was taken as the unexpected output based on the life cycle theory of the construction industry and the slack-based measure-data envelope analysis (SBM-DEA) model was used in this study to estimate the carbon emission efficiency of the construction industry in Henan Province, China during 2008-2019. The SBM-DEA model can scientifically and effectively measure the carbon emission efficiency of the construction industry in Henan Province to realize energy conservation and emission reduction and improve the efficiency of the construction industry. This study can provide a theoretical basis for relevant departments in the construction industry and guidance in the production process of this industry.

MODEL PROFILE AND INDEX SELECTION

SBM-DEA Model

The super-efficiency SBM-DEA model developed from the DEA method is a nonparametric technical efficiency analysis method based on comparisons of evaluation objects. Input minimization and output maximization assumptions of the traditional DEA model have restricted its application in solving problems that consider unexpected outputs. Apart from expected outputs, practical production is usually accompanied by unexpected outputs, such as pollutant discharge and carbon emission. Tone combined the traditional DEA method, introduced the slack variable in the objective function, and proposed the SBM model containing unexpected outputs to solve the efficiency evaluation problem effectively while considering unexpected outputs (Tone 2001).

We assume that n decision-making units (DMU) exist and each DMU is composed of three parts, namely, m input indexes (x), S_1 expected outputs (y_d), and S_2 unexpected outputs (y_u), which can be expressed by the following matrix:

$$X=[x_1,x_2,...,x_n]\in R_{m\times n}>0,$$

$$Y_d=[y_{d1},y_{d2},...,y_{dn}]\in R_{s_1\times n}>0, \quad ...(1)$$
$$Y_u=[y_{u1},y_{u2},...,y_{un}]\in R_{s_2\times n}>0.$$

The production set established when this method is used can be expressed as follows:

$$P=\{(x,y_d,y_u)\mid x>X\lambda,y_d\le Y_d\lambda,y_u\le Y_U\lambda,\lambda\ge 0\}, \quad ...(2)$$

where λ is the non-negative weight vector that expresses returns to scale while ignoring the production.

Slack variables S_-, S_d and S_u are added based on the traditional DEA model to express the input, expected output, and unexpected output slack variables, respectively, and form the following SBM efficiency evaluation model:

$$\rho=\min\frac{1-\frac{1}{m}\sum_{i=1}^{m}\overline{S_i}/x_{i0}}{1-\frac{1}{s_1+s_2}(\sum_{r=1}^{s_1}S_{dr}/y_{dr0}+\sum_{t=1}^{s_2}S_{ut}/y_{ut0})},$$

$$\begin{cases} x_0=X\lambda+S_- \\ y_{d0}=Y_{d0}-S_d \\ y_{u0}=Y_{u0}+S_u \\ S_-\ge 0,S_d\ge 0,S_u\ge 0,\lambda\ge 0 \end{cases}, \quad ...(3)$$

where ρ is the carbon emission efficiency with a value range of 0-1. The efficiency value is equal to 1 when $S_- = S_d = S_u = 0$, and the carbon emission of this DMU is considered efficient. DMUs with an efficiency value of 1 in the last calculation step should be further processed to distinguish multiple DMUs with an efficiency of 1. The super-efficiency SBM model is expressed as follows:

$$\rho^*=\min\frac{1+\frac{1}{m}\sum_{i=1}^{m}\overline{S_i}/x_{ik}}{1-\frac{1}{s_1+s_2}(\sum_{r=1}^{s_1}S_{dr}/y_{drk}+\sum_{k=1}^{s_2}S_{uk}/y_{utk})},$$

$$\begin{cases} x_{ik}\ge\sum_{j=1\ne k}^{n}x_{ij}\lambda_j+S_{-i} \\ y_{drk}\le\sum_{j=1\ne k}^{n}y_{drj}\lambda_j+S_{dr} \\ y_{utk}\ge\sum_{j=1\ne k}^{n}y_{utj}\lambda_j+S_{ut} \\ 1-\frac{1}{s_1+s_2}\ge(\sum_{r=1}^{s_1}S_{dr}/y_{drk}+\sum_{k=1}^{s_2}S_{uk}/y_{utk})>0 \\ S_-\ge 0,S_d\ge 0,S_u\ge 0,\lambda\ge 0 \\ r=1,2,...,s_2,i=1,2,...,m,j=1,2,...,n(j\ne k) \end{cases}, \quad ...(4)$$

where small inputs and unexpected outputs indicate high expected outputs and efficiency value ρ^*.

Index Selection

The construction of the efficiency evaluation index system for the construction industry must incorporate not only the

uniqueness of the construction industry but also combine national environmental protection policies and stipulations for energy conservation and emission reduction. The scientific and reasonableness of input and output indexes are closely related to those of follow-up work, such as efficiency evaluation. First, theory constantly differs from practice. Specifically, subjective factors affect input and output indexes selected and the constructed index system. The efficiency of the constructed index system varies due to the different preferences of people. Second, if the evaluation index system used is unreasonable, then the obtained result will remarkably deviate from the true value. The efficiency evaluation of the construction industry is affected by traditional factors, such as capital, equipment, and labour force. Finally, energy consumption and carbon emission also influence the construction industry because of the international situation and policies regarding energy conservation, emission reduction, and experimental protection. Hence, these factors must be considered in the selection of input and output indexes. The input-output index system shown in Table 1 is established by combining index systems in the existing literature and the data accessibility of the construction industry in Henan Province.

The labour-intensive construction industry highly promotes China's economic development and provides many employment positions to employees of construction enterprises (X1) (Table 1). The quantity of employee inputs can reflect the industry's development status. The efficiency level of the construction industry analyzed through the number of employees can measure the effectiveness of inputs. The labour productivity of construction enterprises (X2) calculated according to the gross output value of this industry measures the output quantity under the given labour input. The ratio of gross output value to quantity of employees in a specific period is generally defined as labour productivity. This index reflects the improvement or degradation of efficiency based on the increase or decrease in the output value of construction products caused by the labour input in different periods. Labour productivity represents technological progress. All kinds of materials, including mechanical production facilities and construction components, must be inputted in the production process of the construction industry to measure the technical equipment rate of construction enterprises (X3). The input of construction materials can reflect the efficiency status of the construction industry. However, the selection of construction materials to reflect the efficiency of the construction industry is not universally applicable because processes and management concepts used as well as the input quantity varies in each region. The index of total profits and taxes of construction enterprises (Y2) is used to investigate profits and taxes. Y2 sums profits and taxes to reflect all actual profits generated in different regions in the corresponding period and the quantized value of social obligations as well as manifests social benefits from the construction industry. Y2 is the index used to measure the output of the construction industry directly and represent construction products produced by the construction industry in one period in the form of total currency. The total output value of the construction industry in different regions can appropriately reflect the market occupancy and economic benefit of the construction industry in a specific region. The house construction area of the construction industry (Y3) reflects the total area output of building construction in the investigation period as an index directly used to measure the output of the construction industry. CO_2 emission (Y4) is an unexpected output index generated by energy use in the construction industry. Y4, which was taken as the unexpected output in the SBM-DEA model in this study, is an important index used to measure the carbon emission efficiency of the construction industry.

All index and other data for the investigation period of 2008-2019 were derived from China statistical database. The CO_2 emission was calculated following Guidelines for National Greenhouse Gas Inventories.

Table 1: Input-Output index system.

Index type	Index (unit)	Index code
Input	Employees of construction enterprises (10,000 people)	X1
Input	Labour productivity of construction enterprises calculated according to the gross output value of the construction industry (yuan/person)	X2
Input	Technical equipment rate of construction enterprises (yuan/person)	X3
Output	Total profits and taxes of construction enterprises (¥ 100 million)	Y1
Output	Gross income of construction enterprises (¥ 100 million)	Y2
Output	House construction area of the construction industry (10,000 m^2)	Y3
Unexpected output	CO_2 emission (10,000 tons)	Y4

RESULT ANALYSIS

Correlation coefficients among seven input and seven output indexes of the construction industry in Henan Province are listed in Table 2.

Table 2 presents that seven variables are highly correlated. The carbon emission efficiency of the construction industry in Henan Province during 2008-2019 was estimated using Formulas (1)–(4). Fig. 2 shows the 2008-2019 values calculated using DEA-SOLVER PRO software.

Fig. 2 shows the declining overall efficiency after the CO_2 emission is taken as an unexpected output and included as an evaluation index for the construction industry in Henan Province. This finding indicated that the efficiency of the construction industry is affected by energy conservation and emission reduction policies. However, with ever-deepened importance attached by the nation and people to the environment, the efficiency evaluation of the construction industry that neglects environmental factors failed to conform with the practical situation. The carbon emission efficiency in Henan Province declined from 1.059 to 1.009 during 2008–2009 likely because the growth rate of the gross output value was small under the influence of the financial crisis in 2008. The increase of carbon emission efficiency from 1.010 to 1.011 during 2009-2010 showed a slow-growth trend likely due to the increase of the gross output value of the construction industry among inputs and outputs. Preparations for the "12th Five-Year Plan" in 2011 were conducted in the previous year. Energy conservation and emission reduction policies were carried out, and Henan Province achieved satisfactory progress in developing the construction industry under the controlled carbon emission. The efficiency value declined again in 2012 and reached the minimum value of 0.807 during the investigation period. This finding indicated that "Central Plains Economic Zone Planning" promoted the urbanization construction in Henan Province and drove the rapid development of the construction industry. However, the province failed to achieve the timely transformation to adapt to such development speed and requirements, and the past production pattern unsuccessfully maintained the effective status of the construction industry. However, the increase of efficiency again in 2013 manifested that the adaptability of the construction industry in Henan Province to the development was slightly enhanced, timely adjustments were performed after the efficiency dropped,

Table 2: Correlation coefficients among seven input and seven output indexes

	X1	*X2*	*X3*	*Y1*	*Y2*	*Y3*	*Y4*
X1	1	0.857	0.257	0.957	0.934	0.916	0.949
X2	0.857	1	0.373	0.93	0.961	0.954	0.888
X3	0.257	0.373	1	0.326	0.422	0.507	0.431
Y1	0.957	0.93	0.326	1	0.986	0.971	0.97
Y2	0.934	0.961	0.422	0.986	1	0.991	0.956
Y3	0.916	0.954	0.507	0.971	0.991	1	0.953
Y4	0.949	0.888	0.431	0.97	0.956	0.953	1

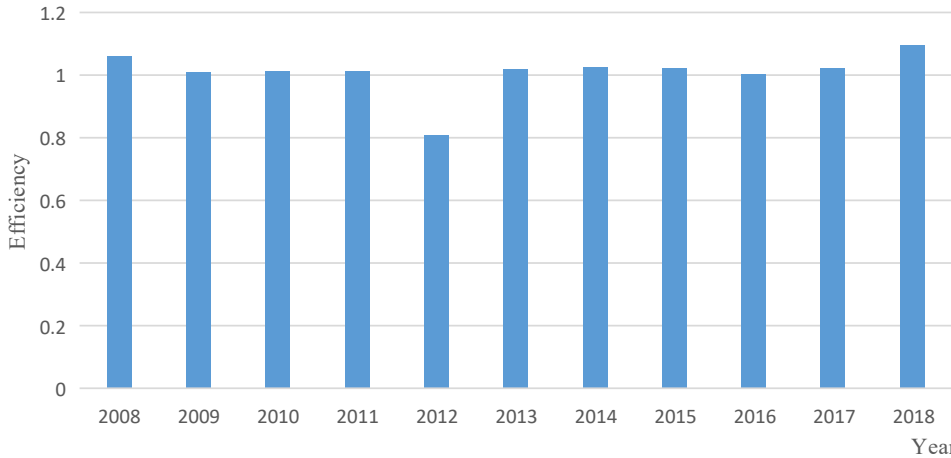

Fig. 2: Carbon emission efficiency of the construction industry in Henan Province During 2008-2019.

and measures were taken to improve the efficiency. The carbon emission efficiency reached its peak at 1.094 in 2018 due to the enhancements applied by the Chinese government in environmental protection while developing the national economy. Multiple plans were formulated for the construction industry to cope with the increasingly enhanced environmental protection effectively. Henan Province actively carried out national policies to determine suitable development patterns. The overall efficiency of the construction industry during this process increased, but the small increase amplitude reflected a large improvement space for the carbon emission efficiency of the construction industry in the province. Moreover, measures related to energy conservation and emission reduction in the construction industry should continue to boost sustainable development.

TREATMENT MEASURES

Improve the Energy Utilization Efficiency and Optimize the Energy Consumption Structure

China's construction industry is typically characterized by the rapid growth of economic aggregate and continuous increase of energy consumption and carbon emission. The energy intensity effect inhibits the growth process of carbon emission intensity in China's construction industry. Hence, the energy utilization efficiency must be improved to reduce the energy intensity effect, enhance the low-carbon consciousness of constructors, reasonably utilize energy sources, reduce the low-efficiency utilization and consumption of energy sources during the construction process, and promote their effective and cyclic utilization. The coal-centred energy consumption in China determines the unreasonable energy consumption structure of the construction industry. The carbon emission coefficient of coal is higher and more carbon is generated during its utilization process compared with those of other energy sources. The energy structure plays an inhibitory role in the growth process of carbon emission intensity. Thus, the energy consumption structure of the construction industry must be further optimized, the consumption of structure of various energy sources should be reasonably planned, and coal utilization should be applied. Moreover, the innovation level of low-carbon technologies should be elevated to accelerate the development and utilization of sustainable and green energy sources.

Optimize the Utilization of Construction Materials and Enhance the Scientific and Technological Strength of Construction Enterprises

The high carbon emission of the construction industry is mainly ascribed to the large usage amount of construction materials. The utilization of green construction materials should be promoted to improve energy utilization efficiency and reduce carbon emissions effectively. The government can encourage construction enterprises to utilize new-type, energy-saving, and renewable construction materials as well as encourage and support construction material manufacturers to produce green construction materials, transform relevant applied technologies, and improve the technological innovation level and competitiveness of construction enterprises in Henan Province further. Furthermore, the recycling of construction solid wastes should be reinforced. Technologies that realize the resource utilization of construction wastes should be aggressively developed, with emphasis on the treatment and recycling of construction wastes. Production technologies and processes of renewable construction materials should be updated. Enterprises must be supported for technological innovation of green construction materials. The design of high-efficiency equipment should be improved to solve the recycling problem of construction solid wastes effectively and promote the green and energy conservation development of the construction industry in Henan Province further. The current energy structure of the construction industry in Henan Province focuses on coal and petroleum utilization, and coal resources play a decisive role in the industrialization development of the construction industry. Hence, the utilization and innovation of coal desulfurization, clean coal, and energy recycling technologies should be strengthened to improve the utilization efficiency and recycling rate of energy sources, such as coal, substantially. The production equipment and processes can be improved through low-carbon technological innovation and the development of new-type materials that can replace energy sources while reducing the utilization rate of fossil fuels.

Strengthen the Pollutant Discharge Management of the Construction Industry and Improve the Resource Utilization Efficiency

The low comprehensive carbon emission efficiency of the construction industry in Henan Province indicated that the resource utilization efficiency of the industry requires urgent improvement and the management level of construction remains unchanged. Therefore, the management level of the construction industry in Henan Province should be improved to enhance resource utilization efficiency. The government can first reinforce the guidance of the construction industry by optimizing the system. Construction enterprises should then improve their management level internally and conduct appropriate adjustments in their organizational structure depending on actual conditions. Although the comprehensive efficiency of the construction industry in Henan Province is generally low, the relatively efficient level can be reached

by altering the management pattern, adjusting inputs and outputs, and introducing relevant technical equipment. The input scale of the construction industry in Henan Province is enlarged, but the scale efficiency demonstrates disproportionate growth. Hence, the scale is independently expanded while the sustainable efficiency improvement of the construction industry is unrealized. This finding indicated that the efficiency improvement of the construction industry in Henan Province can be achieved by expanding not only its industrial-scale but also transforming the extensive input-driven economic growth mode, with emphasis on improving technologies in the construction industry and elevating technological content.

Enhance the Propaganda of Building Emission Reduction Policies and Improve the Autonomous Emission Reduction Awareness of the General Public

The promoting effect of per capita building area is demonstrated by the improvement of building carbon emission efficiency under the enlarged per capita area. However, the energy utilization mode of the general public will make a difference and acceptable energy utilization behaviour can reduce building carbon emissions. The increase of building carbon emissions during the urbanization progress due to the increasing proportion of urban population indicated that the energy utilization mode of the urban population must continue to improve. A low-carbon society should be continuously advocated, and low-carbon economic development should be encouraged. Low-carbon economic development can be combined with a low-carbon lifestyle to improve population quality, drive the recycling efficiency of resources, mitigate the environmental pollution status, improve environmental conditions, and reduce building carbon emissions. The operation phase of building carbon emission during the development process is integrated with the energy utilization of the general public, and the energy utilization mode and habit directly influence the amount of building carbon emissions. Therefore, building emission reduction and environmental awareness of people should be enhanced continuously, the green energy consumption habit must be upheld, and repeated consumption should be avoided. Relevant sectors must reinforce the propaganda of low-carbon lifestyle, popularize low-carbon knowledge, formulate incentive measures for adopting a low-carbon lifestyle, and gradually enhance the awareness of public autonomous emission reduction in the improvement of public autonomous emission reduction awareness.

CONCLUSION

The construction industry is one of three major fields that generate greenhouse gas emissions worldwide. The proportion of energy consumption in industrial production will decline while that of construction energy consumption will continue to grow with the continuous progress of industrial technologies and the elevation of residential living standard. Improving the carbon emission efficiency of the construction industry is the precondition for reducing the total carbon emissions of the construction industry and promoting the reasonable establishment of the building carbon trading mechanism. The CO_2 emission of the construction industry was taken as the unexpected output and then incorporated into the super efficiency SBM-DEA model to measure the carbon emission efficiency of the construction industry in Henan Province, China in the study period of 2008-2019. The results showed that the mean carbon emission efficiency of the construction industry during 2008-2019 is 1.007 and reached the minimum (0.807) in 2012. The carbon emission efficiency of the construction industry in Henan Province realized an overall rising trend during the investigation period, but the amplitude was small. Accordingly, the following treatment measures were proposed: improve the energy utilization efficiency, scientific and technological strength of construction enterprises, resource utilization efficiency, propaganda of building emission reduction policies, and public autonomous emission reduction awareness; optimize the energy consumption structure and utilization of construction materials; and reinforce the pollutant discharge management of the construction industry. An in-depth study can be carried out in the future from the following aspects: accounting scope of building carbon emission, carbon emission database of the construction industry, influencing factors of building carbon emission, and digging of the emission reduction potential of the construction industry.

ACKNOWLEDGEMENT

This work was supported by the practice project of new engineering research in Henan Province (2020JGLX091), the key scientific research project plan of Henan Province Colleges and Universities(21B130001).

REFERENCES

Acquaye, A., Dadhich, P., Genovese, A. and Kumar, N. 2015. Developing sustainable supply chains in the UK construction industry: a case study. International Journal of Production Economics, 164.

Cole, R. J. 1999. Energy and greenhouse gas emissions associated with the construction of alternative structural systems. Building and Environment, 34(3): 335-348.

Cai, W., Feng, W., Huo, T., Ren, H., Wang, X., Zhang, X. and Zhou, N. 2018. China's energy consumption in the building sector: a statistical yearbook-energy balance sheet based splitting method. Journal of Cleaner Production, 185(JUN.1): 665-679.

Colombier, M. and Li, J. 2009. Managing carbon emissions in china through building energy efficiency. Journal of Environmental Management,

90(8): 2436-2447.

Chau, K. W. and Wang, Y. S. 2001. An assessment of the technical efficiency of construction firms in Hong Kong. International Journal of Construction Management, 1(1): 21-29.

Du, Q., Lu, X., Wu, M., Xu, Y. and Yu, M. 2018. Club convergence and spatial distribution dynamics of carbon intensity in china's construction industry. Natural Hazards, 94: 519-536.

Fan, L., Hui, Y., Lei, Z., Shen, Q. and Wang, Y. 2010. Greenhouse gas emissions in building construction: a case study of one Peking in Hong Kong. Building and Environment, 45(4): 949-955.

Fang, Y., Li, H., Ma, Z. and Ng, S. T. 2018. Quota-based carbon tracing model for construction processes in China. Journal of Cleaner Production, 200: 657-666.

Huang, L., Johansen, F., Krigsvoll, G., Liu, Y. and Zhang, X. 2018. Carbon emission of global construction sector. Renewable and Sustainable Energy Reviews, 81(2):1906-1916.

Li, C. Q., Luo, W., Sandanayake, M., Setunge, S. and Zhang, G. 2017. Estimation and comparison of environmental emissions and impacts at foundation and structure construction stages of a building-a case study. Journal of Cleaner Production, 151: 319-329.

Lu, W., Tam, V., Chen, H. and Du, L. 2020. A holistic review of research on carbon emissions of green building construction industry. Engineering, Construction and Architectural Management, 27(5),1065-1092.

Monahan, J. and Powell, J. C. 2011. A comparison of the energy and carbon implications of new systems of energy provision in new build housing in the UK. Energy Policy, 39(1): 290-298.

Ramanathan, R. 2006. A multi-factor efficiency perspective to the relationships among world GDP, energy consumption and carbon dioxide emissions. Technological Forecasting. Social Change, 73(5): 483-494.

Tone, K. 2001. A slacks-based measure of efficiency in data envelopment analysis. European Journal of Operational Research, 130(3): 498-509.

Wang, F. and Zhang, X. 2017. Life-cycle carbon emission assessment and permit allocation methods: a multi-region case study of china's construction sector. Ecological Indicators, 72: 910-920.

Zhou, Y., Liu, W., Lv, X., Chen, X. and Shen, M. 2019. Investigating interior driving factors and cross-industrial linkages of carbon emission efficiency in china's construction industry: based on super-sbm dea and gvar model. Journal of Cleaner Production, 241: 118322.

Nature Environment and Pollution Technology
An International Quarterly Scientific Journal

p-ISSN: 0972-6268
(Print copies up to 2016)
e-ISSN: 2395-3454

Vol. 20 | No. 2 | pp. 633-641 | 2021

Original Research Paper

https://doi.org/10.46488/NEPT.2021.v20i02.021

Open Access Journal

Prediction Model of Agricultural Non-point Source Water Pollution Based on Grey Correlation Method

R. Wang*(**)†, F. X. Yang* and G. M. Qu*****

*Environmental Engineering College, Nanjing Polytechnic Institute, Nanjing-210048, China
**College of Environment, Hohai University, Nanjing-210098, China
***School of Chemical Engineering and Material Science, Nanjing Polytechnic Institute, Nanjing-210048, China
†Corresponding author: R.Wang; wangruijs@163.com

Nat. Env. & Poll. Tech.
Website: www.neptjournal.com

Received: 18-05-2020
Revised: 18-06-2020
Accepted: 16-07-2020

Key Words:
Grey relation method
Agricultural non-point source
Pollution
Prediction model

ABSTRACT

Accurate prediction of non-point source water pollution is conducive to the prevention and control of rural water pollution. To improve the prediction accuracy of agricultural non-point source water pollution and achieve timely prevention and control, a prediction model of agricultural non-point source water pollution based on the grey correlation method is designed. According to the historical data of agricultural non-point source water pollution, the influencing factors of water pollution degree are determined by using the grey correlation method, and standardized pretreatment is carried out. The pretreatment results are transformed into function expression forms, and the original sequences of different influencing factors are generated, which are brought into the function table to achieve the results, and the whitening differential equation is constructed to measure the concentration of agricultural non-point source water pollution. The structure design of the prediction model of agricultural non-point source water pollution can realize the prediction of agricultural non-point source water pollution. The results show that the prediction model of agricultural non-point source water pollution based on the grey correlation method has high prediction accuracy and small prediction error.

INTRODUCTION

When the control level of point source pollution reaches a certain degree, non-point source pollution becomes the main reason for water environment pollution. Around the world, 30-50% of surface water has been affected by non-point source pollution. At present, the effective treatment of point source pollution has been realized, but the non-point source pollution, including nitrate and insecticide, is still in urgent need of treatment (Long et al. 2017, Anooob 2017). Nowadays, non-point source water pollution has become a major threat to human drinking water, which seriously restricts the sustainable development of the economy and society. Compared with point source pollution, it is more difficult to study and control non-point source pollution. In the control of the water environment, it is difficult to fundamentally improve the water quality if only point source pollution control is carried out, and non-point source pollution research is not paid attention to. Water resources are important to support and guarantee economic and social development. It is of great significance to strengthen the research of non-point source pollution for the prevention and control of water pollution. It is because non-point source water pollution has such a bad impact on society and the economy, as well as the important significance of non-point source water pollution control that more and more scholars join in the research of non-point source water pollution, and have made their achievements in related fields.

Non-point source water pollution has attracted the attention of many scholars at home and abroad, who have taken a variety of methods to carry out relevant research on non-point source water pollution. For example, Joy (2018) specifically studied a variety of non-point source models. To analyze these non-point source pollutants, 10 non-point source models were studied, and the advantages and disadvantages of their analysis of SARS source pollutants were tested. According to the results of the study, due to the operational limitations in the test and the difficulty in the calculation, different models are limited in the analysis of non-point source water pollutants. Baiet al.(2018), to analyze the characteristics and laws of non-point source pollution load transfer, selected the Dongjiang River Basin for comprehensive analysis, and the HSPF model was used to simulate the spatiotemporal distribution characteristics of non-point source pollution load such as BOD, TN and TP in the Dongjiang River Basin. The research results show that the HSPF model in the Dongjiang River Basin has a

better simulation application of its SARS source pollution load, which is water for other regions. It provides a way of thinking and reference for the measurement of non-point source pollution load. Zhanget al.(2018) paid close attention to the pollution status of non-point source water. To analyze the pollution load of COD, NH_3-N and TP in Kaijiang River Basin, the three pollution sources in 2015 were estimated by using the emission coefficient method for research, which were rural living source, livestock breeding source and farmland runoff source. According to this method, the total amount of COD, NH_3-N and TP of rural non-point source pollution in Kaijiang River Basin in 2015 is measured, which provides scope guidance for the key treatment of rural non-point source pollution in the Kaijiang River Basin, and provides some guidance for the research in other areas.

The control of non-point source pollution has reached the point of urgency. If the rural areas can effectively predict and control, it will greatly improve the status of non-point source pollution (Dadras et al.2018). It is the most effective way to realize the quantification, impact assessment and pollution control of non-point source pollution to establish a mathematical model to simulate the form and transfer of various non-point source pollution loads in time and space.

This paper focuses on how to improve the prediction accuracy of agricultural non-point source water pollution to achieve timely prevention and control, and designs the prediction model of agricultural non-point source water pollution based on the grey correlation method. Through the structural design of the prediction model of agricultural non-point source water pollution, the accurate prediction of agricultural non-point source water pollution is realized, and the predicted data can be reflected to the relevant departments in time, which can be more effective. The importance of using the model to predict agricultural non-point source water pollution can be seen from the effective formulation of the next development plan.

DESIGN OF AGRICULTURAL NON-POINT SOURCE WATER POLLUTION PREDICTION MODEL

Pretreatment of Agricultural Non-Point Source Water Pollution Historical Data

To determine the influencing factors of water pollution degree, a certain scale of sample size is needed. To obtain a representative and high-quality enough sample set, this paper extensively searches the academic dissertations at home and abroad studying agricultural non-point source water pollution, and obtains the historical sample data (Baranov et al. 2018, Wen et al. 2018) meeting the training requirements of the prediction model through a comprehensive analysis of research methods, research areas, research conclusions, etc. At the same time, the prediction of agricultural non-point source water pollution at home and abroad mostly focuses on the road, so the prediction model is also established for the road runoff. Table 1 gives the historical data sources of this prediction model.

Based on the analysis of the research results on the influencing factors of agricultural non-point source water pollution at home and abroad, the agricultural non-point source water pollution is mainly affected by rainfall characteristics, air pollution, traffic flow and other urban functional areas (Wang 2017). The influencing factors of the model are summarized as shown in Table 2.

The following three points need to be paid attention to in the selection of water pollution indexes: first, cod is an important index to evaluate the pollution degree and control of rainfall-runoff and has a significant correlation with TN, NH_3-N and TP; second, after determining the input

Table 1: Historical data sources of agricultural non-point source water pollution prediction model.

Number	Author	City	Particular year	Forecast times
1	Wang He Yi	Shanghai	2004	6
2	Wang Ye Lei	Nanchang	2007-2008	9
3	Mao Yan Jing	Chongqing	2009	3
4	Chen Ying	Xi'an	2009	36
5	Hao Li Ling	Chongqing	2010-2011	13
6	Han Jing Chao	Fuzhou	2011-2012	17
7	Chen Zi Yu	Guangzhou	2012	4
8	Jiang Yi Zi	Shenzhen	2012	7
9	Song Qian Feng	Chongqing	2011-2012	7
10	Tian Huan	Shenzhen	2014	4
11	Yuan Yan	Suzhou	2014	12
12	Wang Zhao	Xi'an	2014-2015	13
13	Wang Shan	Wuhan	2017	4

Table 2: Influencing factors.

Number	Influence factor	Unit
X1	Pollution types	-
X2	Water pollution intensity	mm/h
X3	Peak pollution intensity	mm/h
X4	Water pollution duration	min
X5	Dry period before water pollution	h
X6	Atmospheric dust fall	t/km^2/ month
X7	PM10	mg/m^3
X8	Vehicle flow	Vehicle/h
X9	Pollution source	-
X10	Functional area	-

Table 3: Sample size of data set.

Water pollution prediction data set	Training sample size	Validation sample size
EMC	45	20
FF30	45	20

(influencing factors) and output (decision variables) of data samples required by the model, it should be directly obtained from the literature, retrieval, research and other methods to supplement the influencing factors of the selected dataset (Liouane et al. 2017). Finally, because the agricultural non-point source water pollution prediction model does not allow the missing value to exist in the prediction of new samples, the missing information cannot be supplemented by the data to be eliminated. Table 3 gives the sample size of the data set after data cleaning.

The influencing factors and decision variables, shown in Table 1, have different dimensions and dimension units, and their numerical values will have different weight effects during model operation, resulting in the reduction of model convergence speed and the distortion of data analysis results. In the support vector machine model, RBF uses the Euclidean distance calculation of sample data, which can avoid the variables with larger values in the influencing factors and control the variables with smaller values. However, the larger numerical difference will still affect the calculation of the water pollution prediction model and reduce the convergence speed of the model (Pierre et al. 2017). Therefore, to eliminate the dimensional influence among variables, it is necessary to standardize the historical data to make the different variables comparable. There are two kinds of commonly used data standardization methods.

The standardization of the maximum-minimum value of the influencing factors, also known as the deviation standardization, is a linear transformation of the historical original data of the influencing factors of water pollution so that the result value is mapped between [0,1]. The conversion function is shown in formula (1):

$$x^* = \frac{x - \min}{\max - \min} \quad \ldots(1)$$

In the formula, max represents the maximum value of water pollution historical raw data sample, min represents the minimum value of water pollution historical raw data sample.

Z-score standardization, also known as normal standardization, uses the mean value and standard deviation of historical raw data of water pollution influencing factors to standardize the historical raw data of water pollution. The processed historical data conform to the standard normal distribution, i.e. the mean value is 0, the standard deviation is 1, and the conversion function is shown in formula (2):

$$x^* = \frac{x - \mu}{\sigma} \quad \ldots(2)$$

In the formula, μ represents the average value of water pollution historical data samples, and σ represents the standard deviation of water pollution historical data samples. The above two methods are used to process the historical data of water pollution, and the grey correlation method is used to standardize the historical data of water pollution influencing factors. The processing results are transformed into function expression forms to generate the original sequence of different influencing factors, which are brought into the function expression results to build the whitening differential equation, and measure the concentration of agricultural non-point source water pollution, to carry out the agricultural treatment design of non-point source water pollution prediction model.

Design Agricultural Non-Point Source Water Pollution Prediction Model

Verhulst put forward the water pollution prediction model for the first time when he studied the law of biological reproduction in 1837 (Wang et al. 2019). The basic idea of the model is that the number of biological individuals growing exponentially is limited by the surrounding environment, and their growth rate gradually slows down, and finally they are fixed at a fixed value. This model is mainly used to describe the process with saturation state, i.e. "S-type process". When Verhulst adds a limited development item into the linear model of agricultural water pollution prediction, it will become a Verhulst nonlinear model as follows:

If the original sequence $X^{(0)} = \left\{X^{(0)}(1), X^{(0)}(2), \cdots, X^{(0)}(r)\right\}$, 1-AGO is $X^{(1)} = \left\{X^{(1)}(1), X^{(1)}(2), \cdots, X^{(1)}(r)\right\}$ and the sequence $Z^{(1)}\left(X^{(1)}(k)\right) = \frac{1}{2}\left(X^{(1)}(k) + X^{(1)}(k-1)\right)$ is generated next to the mean value, the nonlinear model of water pollution can be obtained:

$$X^{(0)}(k) + aZ^{(1)}(k) = b\left(Z^{(1)}(k)\right)^{\alpha} \quad \ldots(3)$$

That is the power model of the point source water pollution prediction model.

$$\frac{dX^{(0)}(k)}{dt} + aX^{(1)}(k) = b\left(X^{(1)}(k)\right)^{a} \quad \ldots(4)$$

It is the whitening differential equation of power model of point source water pollution prediction model.

When $a = 2$, say:

$$X^{(0)}(k) + aZ^{(1)}(k) = b\left(Z^{(1)}(k)\right)^{2} \quad \ldots(5)$$

It is a grey non-point source water pollution prediction model.

$$\frac{X^{(1)}(k)}{dt}+aX^{(1)}(k)=b\left(X^{(1)}(k)\right)^2 \quad \ldots(6)$$

It is the whitening differential equation of grey non-point source water pollution prediction model. Namely:

$$\hat{X}^{(1)}(k)=\left[\frac{b}{a}+\left(\frac{1}{X^{(0)}(1)}-\frac{b}{a}\right)e^{ak}\right]^{-1} \quad \ldots(7)$$

It is the time response formula of grey non-point source water pollution prediction model.

The progressive reduction value is:

$$\hat{X}^{(0)}(k)=\hat{X}^{(1)}(k)-\hat{X}^{(1)}(k-1) \quad \ldots(8)$$

The least square estimation of grey non-point source water pollution prediction model is as follows:

$$\hat{\Phi}=\left(B^TB\right)^{-1}\cdot B^TY=\begin{bmatrix}\hat{a}\\ \hat{b}\end{bmatrix} \quad \ldots(9)$$

Among them,

$$B=\begin{pmatrix}-Z^{(1)}(2) & \left(Z^{(1)}(2)\right)^2\\ \vdots & \vdots\\ -Z^{(1)}(n) & \left(Z^{(1)}(n)\right)^2\end{pmatrix} \quad \ldots(10)$$

From the solution of Verhulst equation, we can see that if $a > 0$, then $X^{(1)}(k)\to 0(k\to\infty);$; if $a< 0$, then $X^{(1)}(k)\to\frac{b}{a}(k\to\infty)$, that is, there is an infinite k, which makes $X^{(1)}(k)$ and $X^{(1)}(k-1)$ fully close, at this time $X^{(0)}(k+1)=X^{(1)}(k+1)+X^{(1)}(k)\approx 0$. If the original prediction data of water pollution history is "s" or part of it is "s", the original prediction data of water pollution history can be directly taken as $X^{(1)}$, and its 1-AGO is $X^{(0)}$. The agricultural non-point source water pollution prediction model is established to directly predict the original data of water pollution

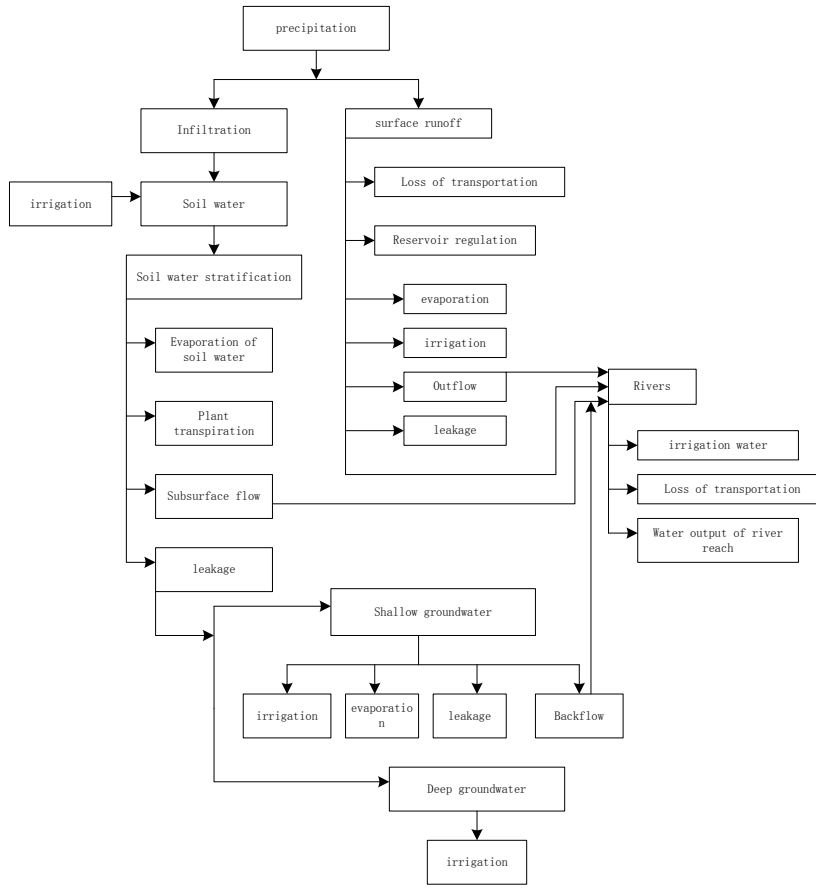

Fig. 1: Structure of agricultural non-point source water pollution prediction model.

history. The structure of agricultural non-point source water pollution prediction model based on grey correlation method is shown in Fig. 1.

To sum up, on the basis of the grey correlation method, the influencing factors of the model are summarized according to the historical data sources of agricultural non-point source water pollution. The data standardization method is used to standardize the historical data of agricultural non-point source water pollution and complete the pretreatment of the historical data of agricultural non-point source water pollution. The power model of the point source water pollution prediction model is used to establish the whitening differential equation, Through the structural design of agricultural non-point source water pollution prediction model, the establishment of agricultural non-point source water pollution prediction model was realized (Alexander et al. 2017).

EXPERIMENTAL ANALYSIS

Experimental Design

In the actual prediction experiment, it is more effective and difficult to determine a specific method than other methods, while the agricultural non-point source water pollution prediction model has the following two advantages over the point source water pollution prediction model.

1. Agricultural non-point source water pollution prediction model has better prediction accuracy and robustness, and can reduce a lot of working time. In the early stage of prediction, generally all the point source water pollution prediction models are applied and then compared, but it is difficult to find the best prediction model through this method.
2. The uncertainty of the point source water pollution prediction model can be dispersed by the combination method, so as to improve the accuracy of the prediction model.

The prediction value $f_i (i = 1, 2, \ldots, k)$ of k models is made for a certain prediction object f, and the error of each water pollution prediction model is as follows:

$$e_i = f_i - f \quad \ldots(11)$$

The variance is:

$$\sigma_{ii} = \left(f_i - \frac{1}{n}\sum_{t=1}^{n} f_{it} \right)_i^2 \quad \ldots(12)$$

Where f_{it} represents the t prediction value of the i prediction model.

If the weight of various water pollution prediction models is $W = (\omega_1, \omega_2, \cdots, \omega_k)^T$, it meets the following requirements:

$$\sum_{i=1}^{k} \omega_i = 1 \quad (\omega_i \geq 0) \quad \ldots(13)$$

Then the basic form of agricultural non-point source water pollution prediction model is:

$$f = \sum_{i=1}^{k} \omega_i f_i \quad \ldots(14)$$

The weighted geometric average prediction model is expressed as follows:

$$f = \prod_{i=1}^{k} f_i^{w_i}, i = 1, 2, \cdots, k \quad \ldots(15)$$

Grey Correlation Method to Determine the Weight

The key to establish the agricultural non-point source water pollution prediction model is how to determine the weight of each point source water pollution prediction model. The weight determination of common non-point source water pollution prediction models includes grey correlation method, arithmetic average method, standard deviation method and simple weighting method. These weighting methods are briefly introduced below.

(1) Traditional Weight Determination Method

Arithmetic average method: This method gives the same weight to each point source water pollution prediction model, and can only be used when the importance of each point source water pollution prediction model is not understood. This method is simple in calculation, but the accuracy of prediction is not high because all prediction models are treated equally.

$$\omega_i = \frac{1}{k}, i = 1, 2, \cdots, k \quad \ldots(16)$$

Reciprocal method of variance: This method is an improvement of arithmetic average method, which requires a certain understanding of the prediction model of source water pollution at each point. The greater the square sum of the prediction errors of the point source water pollution prediction model, the lower the prediction accuracy, so it should be given a greater weight in the non-point source water pollution prediction model.

$$w_i = \frac{D_i^{-1}}{\sum_{i=1}^{k} D_i^{-1}}, i = 1, 2, \cdots, k \quad \ldots(17)$$

Where D_i^{-1} is the sum of the error squares of the$i$ prediction model.

Simple weighting method: The smaller the sum of square error of point source water pollution prediction model is, the greater the weight it should be given to the combined prediction model.

$$w_i = \frac{i}{\sum_{i=1}^{k} i} = \frac{2i}{k(k+1)}, i = 1, 2, \cdots, k \quad \ldots(18)$$

(2) Grey Relation Method to Determine Weight

In information theory, grey relation method is a measure of uncertainty. The larger the amount of information, the smaller the uncertainty, the smaller the grey value, and vice versa. Therefore, we can use the grey correlation method to judge the prediction accuracy of a certain prediction model. The higher the prediction accuracy is, the greater the influence of the prediction model on the combined prediction model is, and the smaller the grey value is. The modeling steps of grey relation method are as follows:

Step 1: Assuming that there are n months and m water pollution prediction models, x_{ij} represents the value (i = 1, 2, …, n; j = 1, 2, …, m) of the j-th prediction model in the i-th month;

Step 2: Calculate the proportion of the value in the i-th month under the j-th prediction model in the prediction model:

$$p_{ij} = \frac{x_{ij}}{\sum_{i=1}^{n} x_{ij}} (i = 1, 2, \cdots, n; j = 1, 2, \cdots, m) \quad \ldots(19)$$

Step 3: Calculate the grey value of the j-th prediction model;

$$e_j = -k \sum_{i=1}^{n} p_{ij} \ln(p_{ij}) \quad \ldots(20)$$

Among them, $k = \frac{1}{\ln(n)} > 0$ meets $e_j > 0$.

Step 4: Grey redundancy of calculation information;

$$d_j = 1 - e_j \quad \ldots(21)$$

Step 5: Calculate the weight of each water pollution prediction model;

$$w_j = \frac{d_j}{\sum_{j=1}^{m} d_j} \quad \ldots(22)$$

Step 6: Calculate the prediction value of non-point source water pollution prediction model in n months;

$$s = \sum_{i=1}^{n} \left(\sum_{j=1}^{m} w_j \cdot p_{ij} \right) \quad \ldots(23)$$

Because the grey correlation method can reflect the utility value of the point source water pollution prediction model more objectively, and the weight obtained has high credibility, this paper uses the grey correlation method to determine the weight value of the non-point source water pollution prediction model.

Model Comparison Results

First, the grey prediction model, the point source water pollution prediction model and the non-point source water pollution prediction model are predicted and tested; secondly, the three prediction models are used to compare the predicted value and the actual value of the three agricultural pollutants, as given in Tables 4 to 9.

According to the comparison of chloride concentration prediction model results in Table 7, the maximum relative error of grey prediction model is 0.103, and the minimum relative error is 0.002; the maximum relative error of point source water pollution prediction model is 0.099, and the minimum relative error is 0.001; the maximum relative error of non-point source water pollution prediction model based on grey correlation method is 0.072, and the minimum relative error, 0.0015, and the total error of the grey prediction model is 0.408, the total error of the point source water pollution prediction model is 0.518, and the total error of the non-point source water pollution prediction model based on the grey correlation method is 0.309. Therefore, the chloride concentration prediction model of this method has the smallest error and the highest precision.

Table 4: Accuracy comparison of prediction models for chloride concentration.

Model	MSE	MAE	MAPE
Grey prediction model	0.1358	0.0399	2.47%
Prediction model of point source water pollution	0.1465	0.0354	5.18%
Prediction model of non-point source water pollution based on grey correlation method	0.1011	0.0269	3.09%

Table 5: Comparison of prediction model accuracy for total calcium concentration.

Model	MSE	MAE	MAPE
Grey prediction model	0.0902	0.0144	5.12%
Prediction model of point source water pollution	0.0617	0.0354	5.18%
Prediction model of non-point source water pollution based on grey correlation method	0.0407	0.0045	4.96%

Table 6: Accuracy comparison of prediction models for TSS concentration.

Model	MSE	MAE	MAPE
Grey prediction model	0.0442	0.0038	3.28%
Prediction model of point source water pollution	0.0425	0.0030	16.54%
Prediction model of non-point source water pollution based on grey correlation method	0.0342	0.0020	1.97%

Table 7: Comparison of prediction model results for chloride concentration.

Sequence	Actual value	Grey prediction model		Prediction model of point source water pollution		Prediction model of non-point source water pollution based on grey correlation method	
		predicted value	relative error	predicted value	relative error	predicted value	relative error
1.	29285	29985	0.103	29367	0.003	29329	0.0015
2.	30490	30293	-0.065	29469	-0.034	30103	-0.0127
3.	32087	30777	-0.041	29595	-0.078	30497	-0.0496
4.	29709	31268	0.052	29752	0.001	30515	0.0271
5.	31830	31767	-0.002	29948	-0.059	30857	-0.0306
6.	32465	32273	-0.006	30193	-0.070	31153	-0.0404
7.	31962	32788	0.025	30502	-0.046	31884	-0.0025
8.	34278	33312	-0.028	30890	-0.099	31893	-0.0696
9.	32234	33843	0.050	31384	-0.026	32331	0.0030
10.	35660	34383	-0.036	32014	-0.102	33093	0.0720

According to the comparison of the results of the total calcium concentration prediction model in Table 8, the maximum relative error of the grey prediction model is 0.188, and the minimum relative error is 0.008; the maximum relative error of the point source water pollution prediction model is 0.254, and the minimum relative error is 0.015; the maximum relative error of the non-point source water pollution prediction model based on the grey correlation method is 0.1318, and the minimum relative error, 0.0032, and the total error of the grey prediction model is 0.705, the total error of the point source water pollution prediction model is 1.279, and the total error of the non-point source water pollution prediction model based on the grey correlation method is 0.4857. Therefore, the error of the total calcium concentration prediction model of this method is the smallest and the accuracy is the highest.

From the comparison of the results of Table 9 TSS concentration prediction model, it can be seen that the maximum relative error of the grey prediction model is 0.243, and the minimum relative error is 0.007; the maximum relative error of the point source water pollution prediction model is 0.256, and the minimum relative error is 0.061; the maximum relative error of the non-point source water pollution prediction model based on the grey correlation method is 0.1454, and the minimum relative error, 0.0001, and the total error of the grey prediction model is 0.652, the total error of the point source water pollution prediction model is 2.444, and the total error of the non-point source water pollution prediction model based on the grey correlation method is 0.5591. It can be seen that the TSS concentration prediction model of this method has the smallest error and the highest precision. It can be seen that the prediction model of agricultural non-point source water pollution based on the grey correlation degree method is better than that based on the point source water pollution prediction model.From the comparison of MAE, MSE and MAPE results, the prediction accuracy of

Table 8: Comparison of results of prediction models for total calcium concentration.

Sequence	Actual value	Grey prediction model		Prediction model of point source water pollution		Prediction model of non-point source water pollution based on grey correlation method	
		predicted value	relative error	predicted value	relative error	predicted value	relative error
1.	2111	2485	0.188	2463	0.167	2218	0.0508
2.	2297	2506	0.090	2829	0.232	2564	0.0063
3.	2587	2751	0.071	3198	0.236	2844	0.0993
4.	2837	3019	0.064	3558	0.254	3211	0.1318
5.	3345	3313	-0.009	3897	0.165	3557	0.0633
6.	3844	3635	-0.054	4208	0.095	3832	-0.0032
7.	4304	3989	-0.073	4486	0.042	4181	-0.0284
8.	4658	4378	-0.060	4728	0.015	4440	-0.0469
9.	4844	4805	-0.008	4934	0.019	4721	-0.0254
10.	4844	5273	0.088	5106	0.054	4991	0.0303

Table 9: Comparison of the results of various prediction models for TSS concentration.

sequence	actual value	Grey prediction model		Prediction model of point source water pollution		Prediction model of non-point source water pollution based on grey correlation method	
		predicted value	relative error	predicted value	relative error	predicted value	relative error
1.	618	786	0.343	721	0.167	649	0.0509
2.	664	710.8	0.070	834	0.256	681	0.0259
3.	776	797.8	0.028	955	0.231	844	0.0879
4.	889	895.4	0.007	1083	0.218	945	0.0632
5.	968	1004.9	0.038	1215	0.255	1108	0.1454
6.	1163	1127.8	-0.030	1349	0.159	1188	0.0215
7.	1324	1265.8	-0.044	1482	0.119	1324	0.0001
8.	1466	1420.6	-0.031	1611	0.098	1532	0.0452
9.	1635	1594.4	-0.025	1734	0.061	1694	0.0359
10.	1698	1789.4	0.036	1848	0.088	1839	0.0831

the agricultural non-point source water pollution prediction model based on the grey correlation method is also higher than the other two prediction models. Therefore, the prediction model of agricultural non-point source water pollution based on the grey correlation method can be used for the prediction of agricultural non-point source water pollution in the near future.

DISCUSSION AND SUGGESTIONS

In view of the shortcomings of the application of the prediction model of agricultural non-point source water pollution based on the grey correlation method, the following suggestions are put forward:

1. Due to the limited level of relevant theories and lack of knowledge about agricultural non-point source water pollution, only common and main influencing factors are listed when selecting the influencing factors of water pollution, and many indexes are not considered fully, so the index system in this paper does not represent all the influencing factors in the process of shale gas development. In addition, the determination of index system weight will be biased, which will affect the final prediction results. Therefore, in the prediction of such problems, we should try to combine the actual situation, preferably with the participation of professionals, so that the prediction model can be more applied to the actual shale gas production project.
2. In the agricultural non-point source water pollution prediction model, neural network method can also be used to determine the weight, and this paper determines the constant weight. To make the agricultural non-point source water pollution prediction model better applied in practice, the combination model with variable weight coefficient needs further study. In this paper, the point source water pollution prediction model, grey model and colony grey prediction model are combined to improve the prediction accuracy, and no more other prediction models are involved. The advantages and disadvantages of more single prediction models need further study, to get a better combination prediction model for practical application.
3. Water environment pollution is the main factor affecting agricultural development. In the detection process of agricultural development wastewater and backwater reuse, special standards should be formulated by the government departments to strictly restrict the treatment process of various types of wastewater. At the same time, the government should encourage the wastewater to be reused as fracturing fluid after it reaches the standard completely, to avoid the waste of water resources. Besides, the developers should strive to develop new environmental protection pressure Crack liquid to reduce water pollution.

CONCLUSION

In this paper, a model of agricultural non-point source water pollution prediction based on the grey correlation method is designed. Firstly, the historical raw data of agricultural non-point source water pollution are preprocessed; secondly, the advantages and disadvantages of three models in small sample data prediction are objectively analysed, and the agricultural non-point source water pollution prediction model is established. In the experiment, the weight is determined by the grey correlation method, and the point source water pollution prediction model, the grey prediction model and the agricultural non-point source water pollution prediction

model based on the grey correlation method are compared. The model is improved, so the prediction ability and accuracy of the model are improved. According to the model, the forecast data can be reported to relevant departments in time, to make the next development plan. Although this paper has completed the design of the agricultural non-point source water pollution prediction model based on the grey correlation degree, the preliminary experimental results are good. But the model has a large amount of calculation and high difficulty of calculation. In the future, we can strengthen the research in this area and design a model with lower difficulty.

ACKNOWLEDGEMENT

The outstanding young backbone teachers of the "Blue Project" in Jiangsu province to develop a target, China (Jiangsu teacher's letter No.42,2018); The Natural Science Foundation of the Jiangsu Higher Education Institutions of China (No.18KJD430005).

REFERENCES

Alexander, K., Pia-Melich, B., Georg, S.K., Thomas, V., Daniel, S., Stuart, M., Julien, M., Joseph, Z., Alessandro, S., Rupert, L. and Siegfried, K. 2017. A new prediction model for evaluating treatment-resistant depression. Journal of Clinical Psychiatry, 78(2): 215.

Anooob, P., Santhoshkumar, A.V. and Roby, C.P. 2017. Impact of particulate pollution on photosynthesis, transpiration and plant water potential of teak (*Tectonagrandis*L.). Current Science, 112(6): 1272-1276.

Bai, X.Y., Wei, S., Shi, X. and Chen X.H. 2018. Using the HSPF model to study the effects of precipitation on nonpoint source pollution in Dongjiang Basin. Journal of Irrigation and Drainage, 37(7): 112-119.

Baranov, A., Salvesen, K.Å., Vikhareva, O. 2018. Validation of prediction model for successful vaginal birth after cesarean delivery based on sonographic assessment of hysterotomy scar. Ultrasound in Obstetrics &Gynecology, 51(2): 189-193.

Dadras, E.Y., Yazdani, A., Nicknam, A. and Eftekhari S.N. 2018. Incorporating source rupture characteristics into the Near-Fault pulse prediction model. Bulletin of the Seismological Society of America, 108(1): 200-209.

Joy, T.A. 2018. Assessing non-point source pollution models: Areview. Polish Journal of Environmental Studies, 27(5): 1913-1922.

Li, Y.P. 2018. Prevention and control of water pollution. China Water-Power Press.

Liouane, Z., Lemlouma, T., Roose, P., Weis, F. and Messaoud, H. 2017. An improved extreme learning machine model for the prediction of human scenarios in smart homes. Applied Intelligence, 48(8): 1-14.

Long, Y.Q., Cui, T.T., Li, W., Wu, C.Y. and Li, Y.G. 2017. Application and sensitivity analysis of geostatistical approach to groundwater pollution source identification. Journal of Hydraulic Engineering, 48(7): 816-824.

Ploton, P., Barbier, N., Couteron, P., Antin, C.M., Ayyappan, N., Balachandran, N., Barathan, N., Bastin, J.F., Chuyong, G., Dauby, G., Droissart, V., Gastellu-Etchegorry, J.P., Kamdem, N.G., Kenfack, D., Libalah, M., Mofack II, G., Momo, S.T., Pargal, S., Petronelli, P., Proisy, C., Rejou-Mechain, M., Sonke, B., Texier, N., Thomas, D., Verley, P., Zebaze Dongmo, D., Berger, U. and Pelissier, R. 2017. Toward a general tropical forest biomass prediction model from very high resolution optical satellite images. Remote Sensing of Environment, 200: 140-153.

Wang, H., Zhang, Feng., Xue Hui-feng. 2019. Construction of Prediction Model and Its Application of Water Pollution Load Intensity Based on Grey Effectiveness. Water Saving Irrigation,(04):72-76.

Wang, L., Chang, Z. and Bao, J. 2017. Prediction model for the thermal conductivity of concrete based on its composite structure. Journal of Hydraulic Engineering, 48(7): 765-772.

Wen, F., Wu, N. and Gong, X. 2020. China's carbon emissions trading and stock returns. Energy Economics, 86: 104627.

Wen, F.H., Zhao, Y.P. and Zhang, M.Z. 2019. Forecasting realized volatility of crude oil futures with equity market uncertainty. Applied Economics, 51(59): 6411-6427.

Wen, S., Xing L.Q. and Zhang H. 2018. Simulation for measurement data pre-processing scheme of 3D target tracking. Computer Simulation, 35(5): 391-396.

Zhang, P.Y., Gou, C.X., Wu, Y., Zhang, D., Li, F. and Mou, Z.S. 2018. Characteristics of rural non-point source pollution in Kaijiang Basin of Sichuan Province. Journal of Agricultural Resources and Environment, 35(5): 398-404.

Nature Environment and Pollution Technology
An International Quarterly Scientific Journal

p-ISSN: 0972-6268
(Print copies up to 2016)
e-ISSN: 2395-3454

Vol. 20 | No. 2 | pp. 643-648 | 2021

Original Research Paper

https://doi.org/10.46488/NEPT.2021.v20i02.022

Open Access Journal

Effect of Municipal Solid Waste Leachate on Soil Enzymes

G.S.J. Shailaja*†, N. Srinivas* and P.V.V. Prasad Rao**

*Department of Environmental Science, GITAM Institute of Science, GITAM University, Visakhapatnam-530045, Andhra Pradesh, India

**Department of Environmental Science, Andhra University, Visakhapatnam-53000, Andhra Pradesh, India

†Corresponding author: G.S.J. Shailaja; sailajaenviron@gmail.com

Nat. Env. & Poll. Tech.
Website: www.neptjournal.com

Received: 09-05-2020
Revised: 03-07-2020
Accepted: 13-07-2020

Key Words:
Municipal solid waste
Leachate
Soil enzymes
Dumpsite

ABSTRACT

The paper aims to investigate the enzyme activity of soils exposed to Municipal Solid Waste (MSW) leachate. Soil enzymes are useful indicators for soil quality management as they respond to changes that occur in soil quality. To determine the effects of MSW leachate, three sites, i.e. Leachate Exposed Site (LES), Partially Leachate Exposed Site (PES) and Control Soil (CS) were considered located in and around Kapuluppada dumpsite which falls under Visakhapatnam city limits. The LES soil receives more leachate washings due to its proximity to waste heaps compared to PES soil. The third site, i.e. CS is located a little away from the MSW heaps and is free from any contamination. The samples were estimated for enzymes like dehydrogenase, invertase, alkaline phosphatase, protease, amylase and cellulase activity using standard assay methods. The following trend was observed: protease>amylase>invertase>alkaline phosphatase>dehydrogenase>cellulase. Our results indicate that the enzymes showed higher activity with MSW leachate washings due to enhanced soil aeration and soil porosity. However, MSW leachate washings had not shown any significant inhibitive effect on organic carbon content, microbial biomass and enzymatic activities.

INTRODUCTION

Enzymes are known to catalyse many biological transformations occurring in soils which may be intracellular or extracellular (Thien & Myers 1992, Deng & Tabatabai 1997, Rao et al. 2000, Fuentes et al. 2006). It is believed that vegetation affects soil enzyme activities as the organic compounds are supplied to soil from plant and animal residues and other dead organisms (Mathur et al. 1980). As enzymes present in soil are of plant, animal and microbial origin, their activities reflect the metabolic status of soils.

Enzymes also participate in the formation and degradation of wastes and contribute to nutrient cycling (Tabatabai 1994, Dick et al. 1994, Taylor et al. 1989, Johansson et al. 2000, Li et al. 2014). The microbes and enzymes present in the soil play an active role in providing fertility to the soil and also involved in the nutrient cycles (biogeochemical cycles) that are essential for the growth of plants. They also act as biological indicators (Chinyere et al. 2013). The enzyme levels in soil vary due to different amounts of organic matter content, composition and activity of living organisms and the biological processes. The role of soil enzymes in the ecosystem will provide an opportunity for biological assessment of soils due to their ease of measurement and response to changes in soil management practices (Dick 1994, Dick 1997, Bandick & Dick 1999, Joachim et al. 2008).

The activity of enzymes involved in the transformation of nutrients is also a measure of soil microbial population (Crecchio et al. 2004). However, any disturbances in the soil system due to wastes/toxic chemicals may lead to a change in the soil system. Therefore, enzyme activities in the soil are indicators of stress management and warn us about soil degradation (Bergstrom et al. 1998, Margesin et al. 2000, Li et al. 2014). Kandeler et al. (1996) reported that a high concentration of heavy metals affects the growth, morphology and metabolism of microorganisms in soils. Baath (1989), Doelman & Haanstra (1989), Aoyama & Nagumo (1996) reported that heavy metals at high concentration reduce soil microbial activities like respiration, ammonification, nitrification and enzyme activities. In addition to the fundamental properties of enzymes in the soil, the data from enzyme assays are used as a guide for soil quality management (Powlson & Jenkinnson 1981, Garcia et al. 2000), an indirect measure of microbial biomass e.g. dehydrogenase activity (Ladd 1978) and a pointer towards the effects caused by wastes (Tyler 1974, Doelman & Haanstra 1979).

In the present study, the impact of MSW leachate exposed soil i.e., LES, PES and CS soil were assayed.

MATERIALS AND METHODS

Study area: The Kapuluppada dumping yard, a 100 acres

of low lying area with good vegetation has a tropical climate with little temperature variations throughout the year with May being the hottest and January the coldest month. It is covered with hills on two sides and a narrow opening connecting to the city on the other side. The total annual rainfall is around 955 mm. Three sites were considered which includes leachate exposed site (LES), partially leachate exposed site (PES) and control soil (CS). These sites are located in and around the Kapuluppada dumpsite which falls under Visakhapatnam metropolitan region.

The soil is red loamy. Various annual and perennial species, the majority being local, can be observed in this area. The Leachate Exposed Site (LES), Partially Exposed Site (PES) and Control Site (CS) are distinctly located in the study area (Fig 1). The LES is located 100 m away from the waste heaps; PES is 500 m away while CS is far away and 500 m away from PES. LES is close to the waste heaps and the leachate generated from the waste heaps continuously flow over the LES soil. During the rainy season and the advent of cyclonic storms the leachate flow increases on the soil surface, hence accumulated is more. The PES receives fewer leachate washings than the LES since it is far away from the waste heaps. The third CS is nearer to the plane grassland and far away from the municipal solid waste heaps and nearly free from contamination.

Sampling Frequency: A 10m × 10m quadrat was selected from each of the sample sites. Each quadrat was divided into 10 sub-plots, each of $1m^2$ area. Soil samples were collected from the subplots with the help of soil corer; tagged and sealed in polythene bags and were brought to the laboratory with necessary precautions. Samples were collected during morning hours on the 10^{th} day of every month from December 2002 to April 2004.

Enzymes in the soil samples were estimated as per the methods specified by Casida et al. (1964), Tabatabai & Bremner (1969), Eivazi & Tabatabai (1977), Speir & Ross (1975) and Cole (1977). All the chemicals and reagents used were of analytical grade and deionized double distilled water (DDW) was used throughout the analysis.

RESULTS AND DISCUSSION

The activities of various enzymes in LES, PES and CS soils are presented in Figs. 2-7. Enzymes are biological

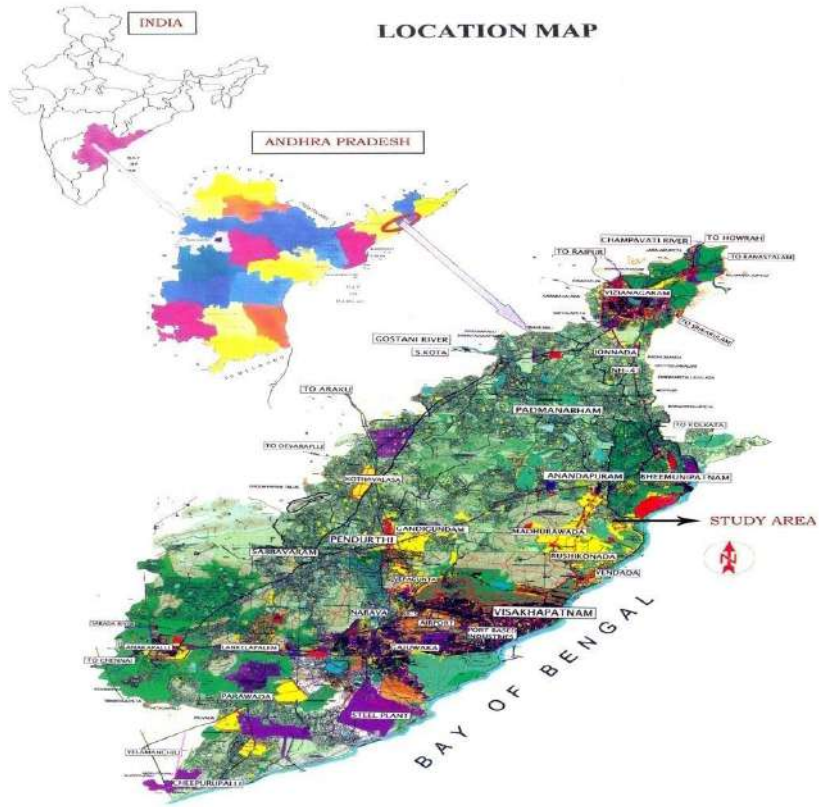

Fig. 1: Visakhapatnam Metropolitan region showing the study area.

catalysts and are of great agronomic and ecological value. Soil enzymes are assayed since many enzymes immediately respond to change in soil fertility. Therefore, enzymes are used as indicators for soil quality management (Powlson & Jenkinson 1981, Garcia et al. 2000, Joachim et al. 2008). Since enzymes react to changes in soil management practice more rapidly they may also be useful as indicators of biological changes (Bandick et al. 1999 and Masciandaro et al. 2004). The activities of various enzymes in LES, PES and CS soils are presented in Figs. 2-7. The dehydrogenase activity of LES soil ranged from 0.004 to 0.066 mg/g/hr, PES 0.005 to 0.045 mg/g/hr and CS 0.002 to 0.043 mg/g/hr. The results indicate that among the three sites dehydrogenase activity was high in LES. The enzyme dehydrogenase is an indicator of biological activity in soils (Burns 1978). It oxidizes soil organic matter (Doelman & Haanstra 1979, Kandeler et al. 1996, Glinski & Stepniewski 1985). In the present study, dehydrogenase activity was reported to be low compared to the other enzymes studied. Among the three study sites, dehydrogenase activity was high in LES soil compared to PES and CS. Rinku et al. (2017) reported that the dehydrogenase activity increased with increasing amounts of uncontaminated sewage sludge in the initial 15 days, but after 30 days it declined. Pitchel & Hayes (1990) also reported low dehydrogenase activity in soil polluted with fly ash. Several authors (Doelman & Haanstra 1979, Rossel & Tarradellas 1991) have reported the inhibition of dehydrogenase by metal pollution. Marzadori et al. (1996) and Chander et al. (1991) have also reported that the activity of dehydrogenase was inhibited particularly by the presence of Pb and Cu in municipal sewage sludge. However, in our study dehydrogenase activity has not shown any significant inhibition in LES and PES soils over CS soil. The result indicates that the dehydrogenase enzyme in the soil indicates the potential of the soil to support biochemical processes essential for maintaining soil fertility (Joachim et al. 2008). Joachim et al. (2008) also suggested that dehydrogenase could be a good indicator of microbial activities in soils in semiarid areas.

Alkaline phosphatase activity of LES and PES site soils ranged from 0.001 to 0.084 and 0.012 to 0.083 mg/g/hr respectively. The enzyme phosphatase plays a vital role in the phosphorus cycle, by allowing orthophosphate to be released from organic and inorganic compounds and thus increasing the bioavailability of phosphorus. Several researchers (Thien & Myers 1992, Deng & Tabatabai 1997, Rao et al. 2000) have also studied the role of phosphatase in the phosphorus cycle and its bioavailability in soil. Phosphatase is commonly used to examine the toxicity of metals (Doelman & Haanstra

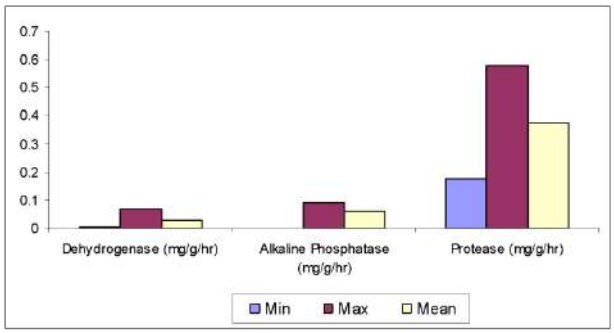

Fig. 2: Min, Max and Mean values of dehydrogenase, alkaline phosphatase and protease activity of LES soil.

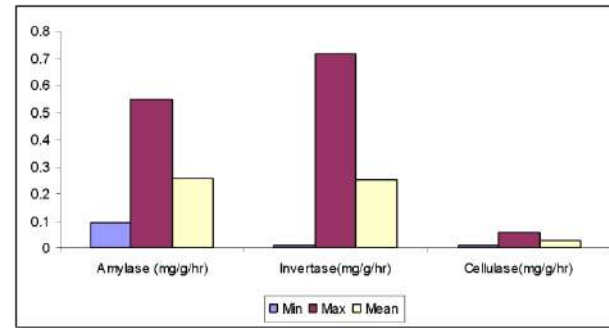

Fig. 3: Min, Max and Mean values of amylase, invertase and cellulase activity of LES soil.

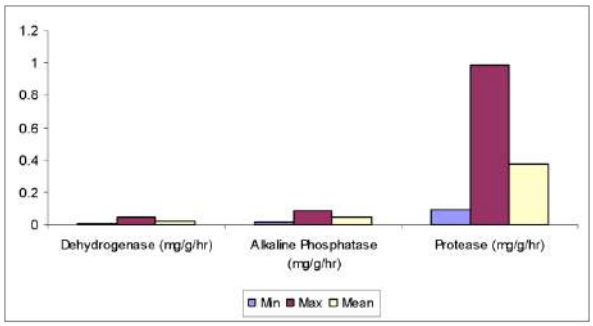

Fig. 4: Min, Max and Mean values of dehydrogenase, alkaline phosphatase and protease of PES soil.

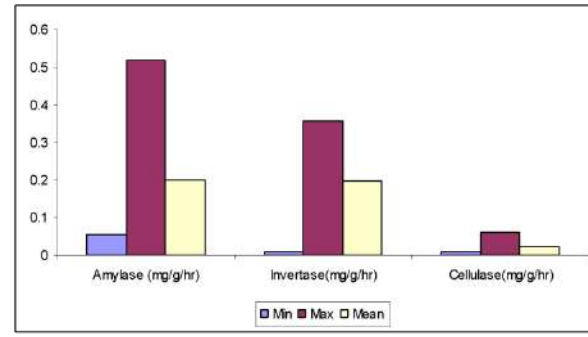

Fig. 5: Min, Max and Mean values of amylase, invertase and cellulase activity of PES soil.

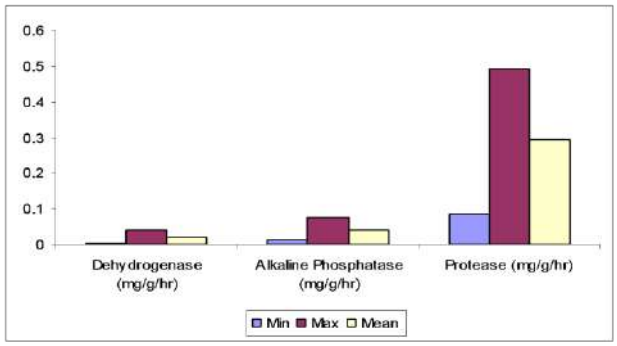

Fig. 6: Min, Max and Mean values of dehydrogenase, alkaline phosphatase and protease activity of CS.

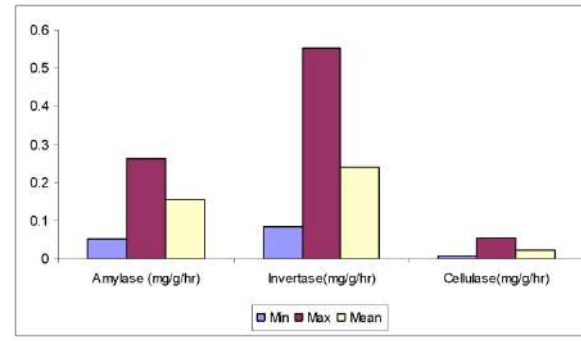

Fig. 7: Min, Max and Mean values of amylase, invertase and cellulase activity of CS.

1989) or organic pollutants such as pesticides. The variations in phosphatase activity may be due to an increase in soil moisture content because phosphatase activity is observed to be higher in saturated soil than in dry soil (Gavrilova & Shimko 1969, Daraseliya et al. 1975). The present study reveals that the alkaline phosphatase activity was not inhibited by leachates despite their heavy metal content (Tam 1998). Chinyere et al. (2013) while studying the soil enzyme activity of Njoku solid waste dump site Owerri municipal, Nigeria, reported that the alkaline phosphatase activity was not affected by waste dumping.

Proteases play an important role in N mineralization (Ladd & Jackson 1982). Urease and protease hydrolyse nitrogen compounds to ammonium using urea and low molecular weight protein substrates respectively (Garcia-Gill et al. 2000). Protease activity occurs partly in the soil as a humocarbohydrate complex (Mayaudon et al. 1975, Bastistic et al. 1980), from arable soil (Ladd 1972, Mayaudon et al. 1975, Hayano et al. 1987), from solid municipal waste compost (Rad et al. 1995) and forest or permanent grassland soils (Nannipieri et al. 1980, 1982, 1985). In the present study protease activity ranged from 0.177 to 0.580 mg/g/hr, 0.091 to 0.563 mg/g/hr at LES and PES soils respectively. Among the three study sites, the LES soil showed increasing protease activity due to more quantity of leachate washings. The present observations along with the earlier observations (Ross 1977, Mishra et al. 1979, 1988, Mohanty & Padhan 1992) suggest that variation in soil protease activity might be due to the changes in soil physicochemical properties and microbial biomass.

The amylase activity at LES and PES sites ranged from 0.091-0.550 mg/g/hr, 0.056 to 0.520 mg/g/hr respectively. Amylase activity was reported to be high at LES soil. Variations in amylase activity were observed among the LES and PES soils due to differential leachate washings. Galstyan (1965), Ross & Roberts (1970), Cortez et al. (1972), Mishra et al. (1984) and Mishra & Pradhan (1987) observed seasonal variations in soil amylase activity.

The invertase activity of LES soil ranged from 0.01 to 0.71 mg/g/hr and PES soil ranged from 0.01 to 0.36 mg/g/hr. The findings indicate that invertase activity varied seasonally (Raguotis 1967, Cortez et al. 1972, Mishra et al. 1984, Mishra & Pradhan 1987). In the present study, invertase activity showed a significant correlation with organic carbon (Vekhrer & Shamshieva 1968, Kiss et al. 1971, Mishra et al. 1979).

Cellulase activity of LES and PES soils ranged from 0.007 to 0.056 mg/g/hr, 0.009 to 0.060 mg/g/hr respectively. The cellulase activity was reported to be high at LES and PES soil over control. However, the LES and PES site soils showed significant variations. Mishra et al. (1984) observed seasonal variations in cellulase activity in some tropical grassland soils and related the variation in cellulase activity to the variation in cellulase secreting microorganisms. Hence, the seasonal variation in cellulase activity may be due to variation in microbial populations, vegetation and physicochemical factors operating in a particular ecosystem.

Correlation among enzymatic activities in the field: The majority of the enzymes were found to be involved in microbial oxidoreductase metabolism. The activity of such enzymes depends on the metabolic state of the soil biota. Dehydrogenase and amylase were found to be significantly correlated with soil microbial biomass in both the LES and PES soils. This indicates that dehydrogenase and amylase activity could be a good indicator of soil microbial activity in MSW exposed soils (Garcia et al. 1994b). A significant increase in dehydrogenase and amylase activity occurred in LES and PES sites than control soil. This is due to the presence of high amounts of humidified organic matter in MSW which is more resistant to microbial mineralization (Garcia-Gill et al. 2000). Tam (1998) reported that dehydrogenase activity in soils receiving wastewater was similar to control throughout the experiment suggesting that the activity was not affected by the addition of wastewater containing heavy metals.

Protease activity was higher in both LES and PES sites. This may be due to the presence of a high concentration of metabolites such as NH_4 (Konig et al. 1966) as a consequence of the mineralization process in soil. Changes in soil phosphatase activity, which play an essential role in the mineralization of organic phosphorus were also observed in both LES and PES sites and exhibited an increase in the enzyme activity. Alkaline phosphatase was significantly correlated with protease ($P< 0.005$). Generally, this enzyme is activated when there is low phosphorus availability in soils.

CONCLUSION

All the enzymes have shown a higher activity with MSW leachate washings. This result may be explained by the improved soil aeration and soil porosity. The strong bonding of enzymes to soil colloids also may protect the enzyme from denaturation. The leachate had not shown any significant effect on the organic carbon content, microbial biomass and enzymatic activities. The reason for the harmfulness of both LES and PES is the leachates that increase in the soil pH which inhibits metal toxicity and converts ammoniacal nitrogen into non-ionized ammonia. Overall, our results have shown that the MSW and the leachate washings have not shown any significant inhibitive effect on soil biological and biochemical properties.

ACKNOWLEDGEMENT

The authors are thankful to University Grants Commission (UGC), New Delhi, India, for providing financial assistance to carry out the work and GITAM University, Visakhapatnam, AP, India, for extending the necessary facilities.

REFERENCES

Aoyama, M. and Nagumo, T. 1996. Factors affecting microbial biomass and dehydrogenase activity in apple orchard soils with heavy metal accumulation. Soil Science and Plant Nutrition, 42: 821-831.

Baath, E. 1989. Effects of heavy metals in soil on microbial processes and population, a review. Water, Air and Soil Pollution, 47: 335-379.

Bandick, A.K. and Dick, R.P. 1999. Field management effects on soil enzyme activities. Soil Biol. Biochem., 31: 1471-1479.

Bastistic, L., Sarkar, J. M. and Mayaudon, J. 1980. Extraction, purification and properties of soil hydrolases. Soil Biol. Biochem., 12: 59-63.

Bergstrom, D.W., Monreal C.M. and King D.J. 1998. Sensitivity of soil enzyme activities to conservation practices. Soil Science Society of America Journal, 62: 1286-1295.

Burns, R.G. 1978. Enzyme activity in soil: Some theoretical and practical considerations. In: Soil Enzymes (Bums R.G., Ed.). Academic Press, London, pp. 295-340.

Casida, L.E., Klein, D.A. and Santro, T. 1964. Soil dehydrogenase activity. Soil. Sci., 98: 371-376.

Chander, K. and Brookes, P.C. 1991. Is the dehydrogenase assay invalid as a method to estimate microbial activity in copper-contaminated soils? Soil Biology & Biochemistry, 23: 909-915.

Chinyere, G.C., Obisike, E.S., Ugbogu, A.E. and Osuocha, K.U. 2013. Studies on municipal solid wastes dumping on soil anions, cations and selected enzymes activities at Njoku sawmill waste dumpsite, Owerri Municipal, Imo State, Nigeria. Ethiopian Journal of Environmental Studies and Management, 6: 774-783.

Cole, M.A. 1977. Lead inhibition of enzyme synthesis in soil. Applied and Environmental Microbiology, 33: 262-268.

Coleman, D.C. 1976. A review of root production processes and their influence on the soil biota of terrestrial ecosystems. In: The Role of Terrestrial and Aquatic Organisms in Decomposition Processes. (Ed.) Anderson J.M. & Macfayden, A. Backwell Scientific Publication. Oxford, pp. 417-434.

Cortez, J., Lossaint, P. and Billes, G. 1972. Soil biological activity in Mediterranean ecosystem III. Enzymatic activity. Rev. Ecol. Biol. Sol., 9: 1-19.

Crecchio, C., Curci, M., Pizzigallo, M., Riccuti, P. and Ruggeiro, P. 2004. Effects of municipal solid waste compost amendments on soil enzyme activities and bacterial genetic diversity. Soil Biol. Biochem., 36: 1595-1605.

Daraseliya, N. A., Kalatozova, G.B. and Dzadzamiya, T.D. 1975. Microbiological and enzymatic activity of podzolic-gley and Kraznozem soils with various moisture contents. Subtrop. Kult, 1: 103-105.

Deng, S.P. and Tabatabai, M. A. 1997. Effect of tillage and residue management on enzyme activities in soils: III. Phosphatases and arylsulfatase. Biol. Fertil. Soils., 24: 141-146.

Dick, R. P. 1994. Soil enzyme activities as indicators of soil quality. In: Doran, J.V., Coleman, D.C., Bezdicek, D.F., Stewart, B.A., (Eds.). Defining Soil Quality for sustainable Environment, Soil Science Society of America, American Society of Agriculture, Madison, pp. 107-124.

Dick, R. P., Sandor, J.A. and Eash, N. S. 1994. Soil enzyme activities after 1500 years of terrace agriculture in the Colca Valley, Peru. Agric. Ecosyst. Environ., 50: 123-131.

Dick, R.P. 1997. Soil Enzyme activities as integrative indicators of soil health. In: Pankhurst, C.E., Doube, B.M., Gupta, V.V.S.R., (Eds.). Biological Indicators of Soil Health, CAB International, Wellingford, pp. 121-156.

Doelman, P. and Haanstra, L. 1979. Effect of lead on soil respiration and dehydrogenase activity. Soil Biol. Biochem., 11: 475-479.

Doelman, P. and Haanstra, L. 1989. Short and long term effects of heavy metals on phosphatase activities in soils: an ecological dose response model approach. Biol. and Fertil. of Soils, 8: 235-241.

Eivazi, F. and Tabatabai, M. A. 1977. Phosphatases in soils. Soil Biol. Biochem., 9: 167-172.

Fuentes, B., Bolan, N., Naidu, R. and Mora, M.D.L.L. 2006. Phosphorus in organic waste-soil systems. J. Soil Sc. Plant Nutr., 6(2): 64-83.

Galstyan, A. Sh. 1965. The dynamics of Ferman processes of soils. DakladyAkad. Army. SSR, 40: 39-42.

Garcia, C., Hernandez, T., Costa, F. and Ceccanti, B. 1994b. Biochemical parameters in soil regenerated by addition of organic wastes. Waste Management and Research, 12: 457-466.

Garcia-Gill, Plaza, J.C., Soler-rovira, C. and Polo, P. 2000. Long-term effects of municipal solid waste compost application on soil enzyme activities and microbial biomass. Soil Biol. Biochem., 32: 1907-1913.

Gavrilova, A. N. and Shimko. 1969. Organophosphate level and phosphatase activity in some soil of the Beloreosslen. SSSR. Vesti. Akad. Navuk. BSSR. Ser. Biyal. Navuk., 6: 35-41, (Chem. Abstr. 72.99560).

Glinski, J. and Stepniewski, W. 1985. Soil Aeration and its Role for Plants. CRC Press, Boca Raton, Florida.

Hayano, K., Takeuchi, M. and Ichishima, M. 1987. Characterization of a metalloproteinase component extracted from soil. Biol. Fert. Soils., 4: 179-183.

Joachim, H.J.R., Makoi, Patrick and A. Ndakidemi 2008. Selected soil enzymes: Examples of their potential roles in the ecosystem. Af. Jr. of Biotech., 7(3): 181-191.

Johansson, E., Krantz-Rülcker, C., Zhang, B.X. and Öberg, G. 2000. Chlorination and biodegradation of lignin. Soil Biology and Biochemistry, 32: 1029-1032.

Kandeler, E. 1996. Nitrate. In: Schinner. F., Ohlinger, R., Kandeler, E., Margesin R (eds). Methods in Soil Biology. Springer, Berlin Heidelberg, New York, pp. 408-410.

Kandeler, E., Kampichler, C. and Horak, O. 1996. Influence of heavy metals on the functional diversity of soil microbial communities. Biol. Fert. Soils, 23: 299-306.

Kiss, S., Dragan-Bilarda, M. and Radulescu, D. 1971. Biological significance of enzymes accumulated in soil. Contrib. Bot. Cluj., 377-397.

Kiss, S., Dragan-Bilarda, M. and Radulescu, D. 1978. Soil polysaccharides: Activity and agricultural importance. Chapter 4. In: Burns, R.G. (ed.) Soil Enzymes. Academic Press, London.

Konig, C., Kaltwasser, H. and Schiegel, H.G. 1966. The formation of urease after use of other nitrogen sources on *Hidrogenumonas*. Archives of Microbiology, 53: 231-241.

Ladd, J.N. 1972. Properties of proteolytic enzymes extracted from soil. Soil Biol. Biochem., 4: 227-237.

Ladd, J.N. 1978. Origin and range of enzymes in soil. In: Burns, R.G. (Ed.). Soil Enzymes, Academic Press, London, pp. 51-56.

Ladd, J.N. and Jackson, R.B. 1982. Nitrogen in agricultural soils. Am. Scc. Agron., Wl. pp. 173-228.

Ladd, J.N. and Paul, E.A. 1973. Changes in enzymatic activity and distribution of acid-soluble amino acid-nitrogen in soil during nitrogen immobilization and mineralization. Soil Biol. Biochem., 5: 825-840.

Li, Q., Liang, J.H., He,Y.Y., Hu, Q.J. and Yu, S. 2014. Effect of land use on soil enzyme activities at karst area in Nanchuan, Chongqing, Southwest China. Plant Soil Environ., 16(1): 15-20.

Margesin, R., Zimmerbauer, A. and Schinner, F. 2000. Monitoring of bioremediation by soil biological activities. Chemosphere, 40: 339-346.

Marzadori, C., Ciavatta, C., Montecchio, D. and Gessa, C. 1996. Effects of lead pollution on different soil enzyme activities. Biology and Fertility of Soils, 22: 53-58.

Masciandaro, G., Ceccanti, B., Benedicto, S., Lee, H.C. and Cook, F. 2004. Enzyme activity and C and N pools in soil following application of mulches. Can. J. Soil Sci., 84: 19-30.

Mathur, S.P., Macdougall, J.I. and McGrath, M. 1980. Levels of activities of some carbohydrases, protease, lipase and phosphatase in organic soils of differing copper content. Soil Sci., 129: 376-385.

Mayaudon, J, Bastistic, L. and Sarkar, J. M. 1975. Proprietes des activites proteolitiquesextraites des sols frais. Soil Biol. Biochem., 7: 281-286.

Mishra, P.C. and Pradhan, S.C. 1987. Seasonal variation in amylase, invertase, cellulase activity and carbon dioxide evolution in tropical protected grassland of Orissa, India, sprayed with carbaryl insecticide. Environment Pollution, 43: 291-300.

Mishra, P.C., Mohanty, R.K. and Dash, M.C. 1979. Enzyme activity in subtropical surface soils under pasture. Ind. J. Agric. Chem., 12(1): 19-24.

Mishra, P.C., Pradhan, S.C., Mishra, P.K. and Sahoo, S. 1988. Protease activity in a grassland soil treated with carboxyl insecticide. Pollution Research, 7(1-2): 13-15.

Mishra, P.C., Satpathy, G.R., Patnaik, H.K. and Dash, M.C. 1984. Effect of Malathion treatment on soil metabolism of a tropical grassland ecosystem of Orissa, India. Proc. Nat. Seminar on Organic Waste Utilization and Vermicomposting. School of Life S. Sambalpur Univ. India, Dec 5-8.

Mohanty, R.K. and Padhan, S. 1992. Comparative studies on soil enzyme activities under two types of crops and adjacent grassland vegetation. Tropical Ecology, 33 (2): 205-213.

Nannipieri, P., Ceccanti, B., Bianchi, D. and Bonmati, M. 1985. Fractionation of hydrolase-humus complexes by gel chromatography. Biol. Fert. Soils, 1: 25-29.

Nannipieri, P., Ceccanti, B., Cervelli, S. and Matarese, E. 1980. Extraction of phosphatase, urease, proteases, organic carbon and nitrogen from soil. SSSAJ, 44: 1011-1016.

Nannipieri, P., Ceccanti, B., Conti, C. and Bianchi, D. 1982. Hydrolases extracted from soil: their properties and activities. Soil Biol. Biochem., 14: 257-263.

Pascual, J.A., Garcia, C. and Hernandez, T. 1999. Lasting microbiological and biochemical effects of the addition of municipal solid waste to an arid soil. Biol. Fertil. Soils, 30: 1-6.

Pitchel, J.R. and Haynes, J. M. 1990. Influence of fly ash on soil microbial activity and populations. J. Environ. Qual., 19: 593-597.

Powlson, D.S. and Jenkison, D.S. 1981. A comparison of the organic matter, biomass, adenosine triphosphate and mineralise nitrogen content of ploughed and direct-drilled soils. J. Agric. Sci. Cambridge., 97: 713-721.

Rad, J.C., Navarro-Gonzalez, M. and Gonzalez-Carcedo, S. 1995. Characterization of proteases extracted from a compost of municipal solid wastes. Geomicrobiol. J., 13: 45-56.

Raguotis, A.D. 1967. Biological activity of sod-podzolic forest soils of the Lithuanian SSR. Pochvovedenie., 6: 51-56.

Rao, M.A., Violante, A. and Gianfreda, L. 2000. Interaction of acid phosphatase with clays, organic molecules and organo-mineral complexes: Kinetic and stability. Soil Biol. Biochem., 32: 1007-1014.

Rinku, D., Suman, C., Tanvi, B. and Sneh, G. 2017. Impact of Long term application of municipal solid waste on physicochemical and microbial parameters and heavy metal distribution in soils in accordance to its agricultural uses. International Journal of Agricultural and Biosystems Engineering, 11(6): 399-407.

Ross, D.J. 1977. Protease activities and its relationship to nitrogen mineralization in some soils under pasture and tussock grassland. N.S.J. Sci., 20: 179-185.

Ross, D.J. and Roberts, H.S. 1970. Enzyme activities and oxygen uptakes of soils under pasture in temperature and rainfall sequences. J. Soil Sci., 21: 368-381.

Ross, D.J. and Speir, T.W. 1979. Biochemical activities of organic soils from sub-antarctictusock grassland on CampbellIsland. Enzyme activities N.Z.J. Sci., 22: 173-182.

Rossel, D. and Tarradellas, J. 1991. Dehydrogenase activity of soil microflora, significance in ecotoxicological tests. Environmental Toxicology and Water Quality, 6: 17-33.

Speir., T.W. and Ross, D.J. 1975. Effects of storage on the activities of Protease, urease, phosphatase and Sulphatase in three soils under pasture. Newzealand Journal of Science, 18: 213-237.

Tabatabai, M. A. 1994. Soil enzymes. In: Weaver R, W., Angle J.S., Bottomley, P.S., (Eds.). Methods of Soil Analysis, Part 2. Microbiological and Biochemical Properties. SSSA Book Series No.5. Soil Sci. Soc. Am. Madison, Wis., pp. 775-833.

Tabatabai, M. A. and Bermner, J.M. 1969. Use of p-nitrophenyl phosphate for assay of soil phosphatase activity. Soil. Biol. Biochem., 1: 301-307.

Tam, N.F.Y. 1998. Effects of wastewater discharge on microbial populations and enzyme activities in mangrove soils. Env. Pollution., 102: 233-242.

Taylor, B.R., Parkinson, D. and Parsons, W.F.J. 1989. Nitrogen and lignin content as predictors of litter decay rates: A microcosm test. Ecology, 70: 97-104.

Thien, S.J. and Myers, R. 1992. Determination of bioavailable phosphorus in soil. Soil. Sci. Soc. Am. J., 56: 814-818.

Tyler, G. 1974. Heavy metal pollution and soil enzymatic activity. Pl. Soil, 41: 303-311.

Vekhrer, E.G.K.T. and Shamshieva, 1968. Activity of some enzymes in soils of central Tein Shan. Pochvovedenie, 3: 94-100.

Nature Environment and Pollution Technology
An International Quarterly Scientific Journal

p-ISSN: 0972-6268
(Print copies up to 2016)
e-ISSN: 2395-3454

Vol. 20 | No. 2 | pp. 649-655 | 2021

Original Research Paper

https://doi.org/10.46488/NEPT.2021.v20i02.023

Open Access Journal

Tyrosinase from *Sepiella inermis* (Van Hasselt [Ferussac & d'Orbigny], 1835) and its Phenol Removal Activity

R. Sivaramakrishnan*, A. Nandhini, P.R. Jaipreethi**, K. Kapilan*, S. Uthra*, S. Kanchana*, D. Yuvaraj** and M. Arumugam*†**

*CAS in Marine Biology, Faculty of Marine Sciences, Annamalai University, Parangipettai, Tamil Nadu, 608502, India
**Vel Tech High Tech Dr. Rangarajan Dr. Sakunthala Engineering College, Avadi, Chennai, 600062, T. N. India
†Corresponding author: M. Arumugam; arumnplab@gmail.com

Nat. Env. & Poll. Tech.
Website: www.neptjournal.com

Received: 05-05-2020
Revised: 22-06-2020
Accepted: 26-06-2020

Key Words:
Chromatography
Enzyme
Marine natural products
Phenol degradation
Tyrosinase

ABSTRACT

Tyrosinase is a ubiquitous enzyme found in most pigmented animals. In the present study, the tyrosinase enzyme was isolated and purified from *Sepiella inermis* ink and its application in phenolic compounds removal from aqueous solution. The presence of the tyrosinase in the *S. inermis* ink was read at 280nm and the crude enzyme was purified by dialysis, ion exchange chromatography, and high-performance liquid chromatography (HPLC). The molecular weight of the purified enzyme was revealed as 30kDa through the SDS-PAGE analysis with 12% polyacrylamide gel. The optimum pH and temperature of the enzyme were found to be 6°C and 55°C respectively. The tyrosinase enzyme was immobilized with sodium alginate for the removal of phenolic contaminants in water. The accelerator with efficiency removed the phenols from the solution at intervals within a few hours. Hence, this study indicated that the isolated tyrosinase enzyme of *S.inermis* ink acts as an accelerator and could be used for the removal of hazardous phenol substances from wastewaters.

INTRODUCTION

Phenol and its derivatives are released as contaminants from different industrial activities. It is no less than two-thirds of phenols formed worldwide are engaged in the chemical synthesis of bisphenol A and phenolic resins (Palma et al. 2010). Apart from colouring and conferring smell to water these phenols and their derivatives are proven toxic substances for aquatic creatures even at mild concentrations (5-25mg/mL). Being toxic to aquatic organisms it is necessary to remove these kinds of pollutants from wastewaters. The available techniques such as recovery and destruction and among the later are being the biological treatments (Palma et al. 2010). These biological methods are considered to be competitive which can able to meet quality standards in a cost-effective manner (Zilli et al. 2010).

Tyrosinase is the enzymes proven polyphenol oxidizer ubiquitously distributed in several living beings that act as a catalyst using O_2 as an oxidant monophenols hydroxylation to o-diphenols and subsequent dehydrogenation of o-diphenols to o-quinones. (Halaouli et al. 2016). Huge innovation exists by means of underutilized waste and its by-products to build new healthy products for consumers (Fatimah & Rabeta 2018). Squid, cuttlefish, and octopus are major seawater catch other than fishes and prawns. These organisms are grouped under the phylum of invertebrate known as Mollusca and the family of Cephalopoda (Fatimah & Rabeta 2018).

In the connection cephalopod, ink is native stuff discharged by cephalopods from their ink sac when they try to get away from predators (Hossain et al. 2018). This ink is produced from the secretion of two glands and at the end process of maturation in a viscous colourless medium (Liu et al. 2011). This by-product can be a possible source of good quality bioactive compounds (Vate & Benjukul 2017). Apart from that squid is an excellent food source for zinc and manganese and high in copper, selenium, vitamin B12, and riboflavin. There is an ever-increasing demand for different enzymes in current industries. Besides, despite the outstanding advancement in chemistry, there is yet no efficient reagent for synthesizing some chemical substances.

One such best example is ortho-hydroxylation of phenolic compounds. This reaction happens in the majority organisms and ends up information for necessary organic chemistry like neurotransmitters of Bendopa family, coumestrol, polyphenolic acids (Haghbeen et al. 2004). Squid ink is used as an additive in food processing. It consists of melanin granules in a viscous colourless medium (Russo et al. 2003). Besides, this squid ink is also applicable for anti-tumour activity, antimicrobial property, phenol removal property, and skin

rejuvenation property. So this study aimed at the isolation of tyrosinase from squid ink and its phenol removal activity from aqueous for the benefit of the environment.

MATERIALS AND METHODS

Sample Collection and Processing

The cephalopod species *S. inermis* was collected from Mudasal Odai landing centre, Tamilnadu coast, India and brought to the laboratory. All the collected species were washed thoroughly twice with distilled water. The squids were dissected and ink glands were removed from the viscera.

Isolation of Cuttlefish Ink

The ink glands were placed in clean plastic containers before placing them into the freezer (-20°C). The ink duct, each weighing 800mg, was cut with sterile scissors, gently squeezed; milked ink was collected and stored at 4°C. The frozen ink was kept in the freeze dryer (-60°C), (Delvac, Chennai, India) for the lyophilization process. The freeze-dried ink kept in an airtight plastic container and then covered with aluminium foil to prevent light penetration (Fatimah & Rabeca 2018). The dried samples were stored in a freezer at -20°C before further analysis.

Extraction of Tyrosinase

The ink sample was lyophilized and obtained as a black powder. The pH was determined with a pH meter (Neifar et al. 2008). This powder was extracted with 40 volumes of 0.1 M tris-HCl buffer. Then it was centrifuged at 18,000 rpm for 30 min at 4°C to remove the melanin using a refrigerated centrifuge (Vate 2017). The pellet was removed and the supernatant was dialyzed against distilled water at 4°C for 48 h and then lyophilized to obtain an off grey powder (270 mg). This powder was re-dissolved in normal saline and used for further studies.

$$Yeild\ of\ tyrosinase\ (\%) = \frac{Weight\ of\ tyrosinase\ obtained}{Weight\ of\ ink\ obtained} \times\ 100 \quad \ldots(1)$$

Dialysis

Activation of the membrane (cellulose membrane) was performed as follows. 100 mL of distilled water was kept boiling for 30 min. Dialysis membrane (HiMedia) was placed in water for 10 min. Finally, the membrane was transferred to freshwater. The sample was dialyzed against distilled water for 42 hours at 4°C. The dialyzed sample was lyophilized to obtain a grey powder (Roy et al. 2014).

Ion Exchange Chromatography Purification of Tyrosinase

5 g of crude extract powder was dissolved in 20mL of 0.5M Tris-HCl buffer (pH 6.8), the solution was applied to a column (1.6 × 38 cm) of DEAE Cellulose (HiMedia) equilibrated with the same buffer, and then the column was eluted with a stepwise gradient of 0.05, 0.1, and 0.5 M in the same buffer at a flow rate of 1mL/min. Fractions of 5 mL were collected and analysed for tyrosinase activity (Naroaka 2000). Each fraction was examined under a UV spectrophotometer.

Effect of pH and Temperature on Enzyme Activity

The effect of temperature on tyrosinase activity was measured in standard assay conditions. Activity assay was performed at different pH and temperatures and the UV absorbance was measured at 475 nm (Neifar et al. 2012). The optimum temperature for enzyme activity was determined by incubating the standard reaction mixture at temperatures ranging from 35°C to 65°C. The activity of tyrosinase was evaluated at different pH values in the range between pH 3 and 10 under assay conditions and the amount of tyrosinase was determined (Zaidi et al. 2015). Buffers used were Tris-glycine (pH 3.0-10.0).

Molecular Weight Determination of Tyrosinase using SDS-PAGE

SDS-PAGE was done with 12% polyacrylamide gel using Tris-glycine buffer (pH 8.3). The crude and purified enzyme was loaded onto a denaturing polyacrylamide gel and compared with standard tyrosinase. The gel preparation method was carried out by referring to Laemlli (1970). The protein patterns of tyrosinase were analysed using sodium dodecyl sulphate-polyacrylamide gel electrophoresis (SDS-PAGE). Tyrosinase samples (0.5 mg/2µL) were dissolved in 0.05M tris-HCl buffer (pH 7.2) and mixed with the sample buffer (0.5 M tris-HCl, pH 6.8 containing 4% (w/v) SDS, 20% (v/v) glycerol) with 10% (v/v) β-mercaptoethanol (β-ME), using the sample to sample buffer ratio of 1:1(30:30µL) (v/v). Samples were loaded onto a polyacrylamide gel made of 12% running gel and 4% stacking gel and subjected to electrophoresis at a constant current of 20mA per gel, using a mini-protein II unit (Bio-Rad Laboratories Inc., Richmond, CA, USA). After electrophoresis, the gel was stained with silver staining.

Preparative-RP-HPLC Purification of Tyrosinase

The culture free supernatant was analysed by high-performance liquid chromatography (Shimadzu, Japan) using C_{18}

column (Luna 5µ, Phenomenex 250mm × 4.6mm). The HPLC gradient program was starting at 8% solvent B and holding for 1 min, then ramping to 75% solvent B in 20 min, holding at 75% solvent B for 10 min, backing to 8% solvent B in 1 min and holding at 8% solvent B for 5min. Solvent A was 98:2 (v/v) water: methanol with 0.1% acetic acid, and solvent B is 10:90 (v/v) water: methanol with 0.1% acetic acid. The HPLC analysis was performed at a flow rate of 1.0mL/min (Roy et al. 2014).

Phenol Removal from Aqueous Environment by Using Immobilized Tyrosinase Enzyme

All phenol enzymatic removal experiments were carried out with constant stirring. The reaction mixture consists of 250mL aqueous phenol solution and crude extract with different tyrosinase concentrations (Kameda et al. 2006) with immobilization of tyrosinase in sodium alginate beads. The partially purified enzyme solution was mixed with a sodium alginate solution in a 2:1 ratio. The mixture was added dropwise into calcium chloride (0.2M) solution with shaking at 4°C. The beads were allowed to wash with distilled water followed by a phosphate buffer of pH 7 (Anwar et al. 2009). The immobilized beads of 20mL of enzymes were prepared and exposed to various concentration of phenol in water. The phenol concentration varied from 1mM to 5mM. The concentration of phenol that remained was estimated by Folin- Ciocalteu reagent after every half an hour. The phenol concentration was determined for each set of concentration to 4h (Roy et al. 2014).

RESULTS AND DISCUSSION

Yield Calculation

The yield calculation was estimated for 20g of ink duct which yields 2g of ink like grey powder. The yield of ink powder was found to be 10% (w/w). The yield of tyrosinase was estimated as 4.18% on the dry weighted basis (w/w). The yield calculation was determined for 2g of lyophilized cuttlefish ink powder extracted by tris-HCL and then tyrosinase was isolated from the ink and the yield was calculated as 80.25mg. In a study conducted by Roy et al. (2014) the net yield of the tyrosinase enzyme was determined as 50.69% from marine actinobacteria. The value of fat content in squid ink powder is slightly higher compared with raw squid which was about 1.0 to 2.0%, where the value considered lowest among all types of seafood (Okuzumi & Fujii 2000).

Anion-Exchange Chromatography Purification of Tyrosinase

The eluted fractions obtained by tris-HCL buffer with different concentrations of 0.05M, 1M, 1.5M through DEAE cellulose column and 0.05M was collected which showed high tyrosinase content. These results are illustrated in Fig. 1. The collected fraction was obtained as a grey colour powder. Purification is usually achieved by filtration, centrifugation, and precipitation and also by chromatographic techniques such as ion exchange, gel permeation, and affinity chromatography. According to Zaidi et al. (2015), the button mushroom of tyrosinase enzyme was purified under Sephadex G-100 column further with the ion exchange chromatography using DEAE-Cellulose column (20 × 1cm).

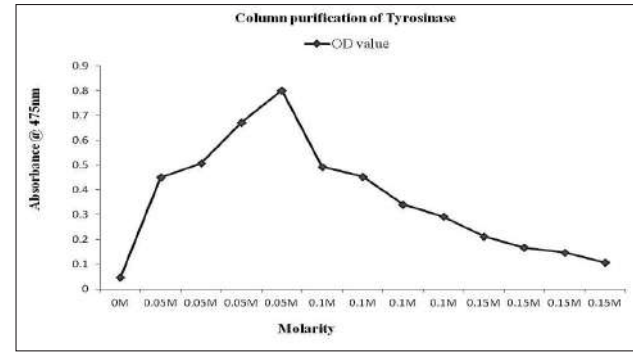

Fig. 1: Purification of tyrosinase using anion-exchange chromatography.

Effect of pH and Temperature on Tyrosinase

Tyrosinases with various physicochemical features have been reported from various organisms. These enzymes generally have a pH optimum in the neutral or slightly acidic range. The results revealed that pH 6.0 was the optimal pH for tyrosinase from *S. inermis* (Fig. 2) using Tris-HCl buffer. Our results also demonstrated that tyrosinase retained about 65 % of its activity after storing at pH 7.0 for 24 h. This means tyrosinase of *S.inermis* had higher pH stability over a wide range of pH values. The influence of pH on tyrosinase activity in crude melanin-free ink was studied in the range of pH 3 to 12 using citric acid/sodium phosphate buffer at 0.1M (Neifar et al. 2012).

The purified tyrosinase was active at a wide range of temperature from 30°C to 65°C with an optimal at 55° C and holding 35% of tyrosinase activity at 55°C, but it lost its activity at 60°C (Fig. 3). Our results were in agreement with the optimum temperature for tyrosinase activity obtained from *S. officinalis* and the enzyme was sustained at 55°C (Neifar et al. 2012). It has been reported that the stability toward the temperature of squid tyrosinase activity of the cephalopod mollusc *Illex argentinus* was stable up to 30°C and complete inactivation was observed at 70°C (Naraoka et al. 2003).

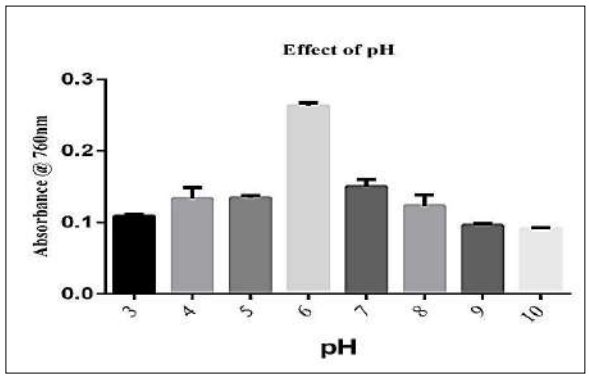

Fig. 2: Optimum pH of Tyrosinase from *S. inermis.*

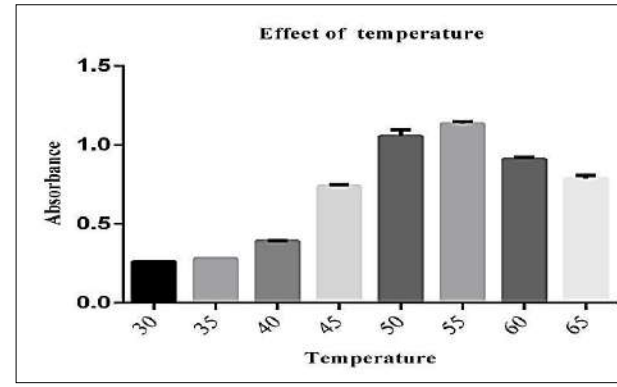

Fig. 3: Optimum temperature of Tyrosinase from *S. inermis.*

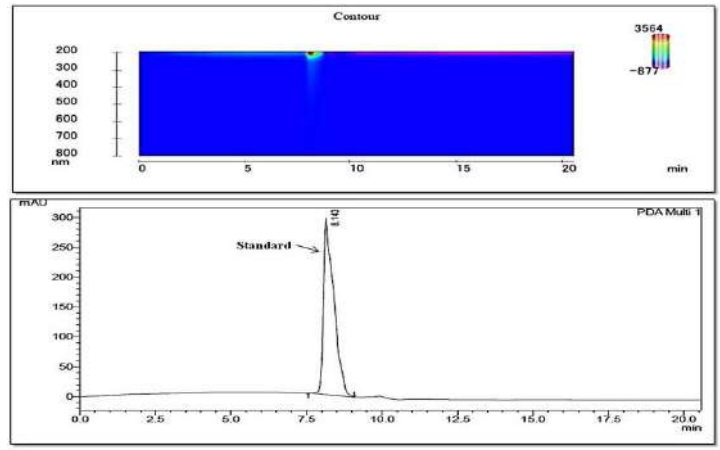

Fig. 4: HPLC chromatogram and contour view for standard Tyrosinase.

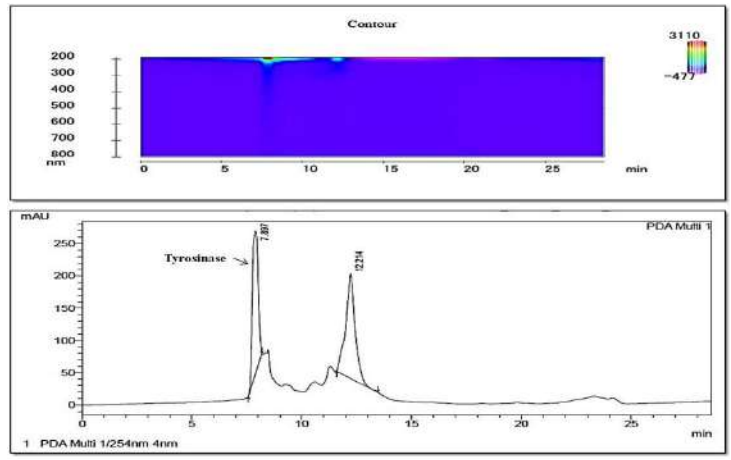

Fig. 5: HPLC chromatogram and contour view for purified Tyrosinase from *S.inermis*.

Fig. 6: SDS-PAGE for the purified and crude sample.

HPLC Analysis of Tyrosinase from *S.inermis*

The HPLC chromatogram of the partially purified enzyme showed a double peak at retention times of 7.897 and 12.214 mins. In which the major peak at R_t 7.897 corresponds to the tyrosinase were confirmed with the standard tyrosinase enzyme. The HPLC analysis of the partially purified tyrosinase enzyme with phosphate buffer as mobile phase revealed a single intense peak which confirmed the purity of the enzyme (Dolashki et al. 2009). Hence the present study revealed that the solvent was also used as a mobile phase in the HPLC purification of the enzyme. Fig.4 & 5 represents the standard, purified tyrosinase chromatogram, and contour view.

SDS PAGE of Tyrosinase

The purity of the enzyme and to determine the molecular weight, electrophoresis is performed using denaturing polyacrylamide gel electrophoresis. The molecular weight of the purified enzyme was determined as 30kDa, analysed by SDS PAGE. Fig. 6 shows the single band, which denotes the presences of tyrosinase when compared with standard tyrosinase from the mushroom. Likewise, Roy et al. (2014) revealed the same range of molecular weight enzyme through SDS-PAGE analysis by the presence of a single protein band that corresponds to approximately 30 kDa.

Phenol Removal Activity of Purified Tyrosinase

The amount of total phenol was determined with the Folin-Ciocalteau reagent. Phenolic compounds are a class of antioxidant agents that acts as free radical terminators. The immobilized enzyme provides improved resistance to alteration in conditions such as temperature or pH. In such a condition, enzymes remain held in position throughout the reaction which leads to easy separation from product, reusability and continuous operation. It is an efficient technique that is being used in industry for enzyme-catalysed reactions. In regards to enzymatic water treatment, immobilized tyrosinase showed better efficiency in terms of reusability, stability and longer viability (Bevilaqua et al. 2002, Molina et al. 2003, Kameda et al. 2006). The immobilization of tyrosinase improved the thermal stability and the gel-entrapped tyrosinase was almost entirely preserved from proteolysis maintaining more than 80% of its activity (Crecchio et al. 1995). The use of cheaper supports for the preparation of immobilized enzyme for such applications is always considered necessary. Hence, sodium alginate was used to immobilize the enzyme to remove phenol from the aqueous solution. Tyrosinase can oxidize a wide range of polyphenolic and phenolics components to their related nontoxic quinones and hence this enzyme has been utilized to remove hazardous and toxic phenolic contaminants from effluent and wastewater (Robb 1995). In the present study, the partially purified enzyme was immo-

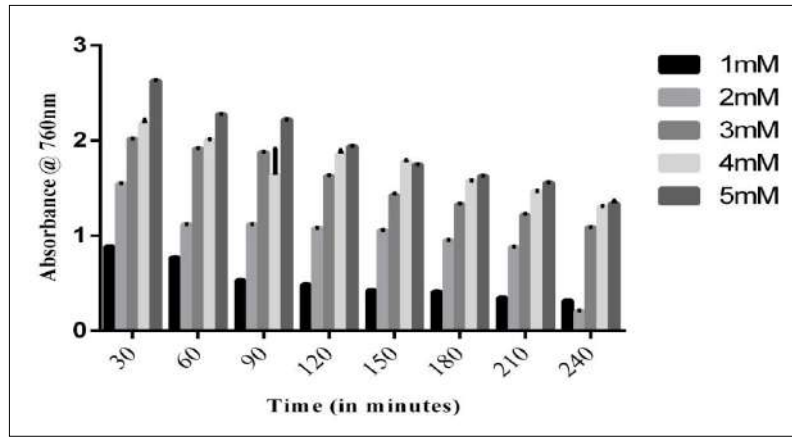

Fig. 7: Phenol removal activity under various concentrations of 1mM to 5mM.

bilized in sodium alginate to remove the phenol from the water. The efficiency came around 48% which showed a better result (Anwar et al. 2009), where the efficiency of the immobilized protease enzyme was found to be 45%. Thus the phenol removal activity was done through several concentrations of phenolic assays by using the immobilized beads. The immobilized enzyme was exposed to various concentration of phenol ranging from 1mM to 5mM for a period of 4 h which resulted in the reduction in the concentration of phenol with an increase in exposure time shown in Fig. 7. The reduction of phenolic components was a function of exposure time. There was a gradual decrease in the percentage of phenol removal from 1mM of phenol to 5mM of phenol. The result of phenol removal showed a slight similarity with the work of Shesterenko et al. (2012). Whereas Maurya & Singh (2010) estimated that the number of total phenolics in extracts was determined with the Folin- Ciocalteu reagent. Gallic acid was used as a standard and the total phenolics were expressed as mg/g gallic acid equivalents (GAE). Concentration of 0.01, 0.02, 0.03, 0.04 and 0.05 mg/ml of gallic acid were prepared in methanol. Thus total phenolic content can be determined.

CONCLUSIONS

The marine cephalopod *Sepialla inermis* was found to be the gifted producer of tyrosinase as well as the potent remover of phenol from aqueous solution. The enzyme was found to be stable even at high temperature, pH and it is also having high enzymatic activity and greater stability than the mushroom tyrosinase enzyme. Immobilized tyrosinase enzyme from *Sepialla inermis* can act as a promising technique for phenol removal from wastewater along with maintaining high stability of the enzyme. Hence, it can be concluded that the tyrosinase enzyme from thiscephalopod can be potentially used in industries to remove phenol from wastewater. Further studies on this particular enzyme can lead to producing a new skin lightening cream and could be used for hyperpigmentation as well in near future.

ACKNOWLEDGMENTS

The authors are indebted to the Ministry of Earth Sciences (MoES), [G4 (2)/14748/2016] under 'Drugs from the sea' program and DST under the program of National Facility for Marine Natural Products and Drug Discovery Research for their financial support. We are especially thankful to Marine Natural Products and Drug Discovery Research Laboratory, CAS in Marine Biology, Annamalai University for providing us HPLC facilities.

REFERENCES

Abida, A., Shah Ali, U.Q., Aliya, R., Samina, I. and Abid Azhar, 2009. Calcium Alginate: A support material for immobilization of proteases from newly isolated strain of *Bacillus Subtilis* KIBGE-HAS. World Applied Sciences Journal, 7: 1281-1286.

Anwar, A., Qader, S. A,, Raiz, A., Iqbal, S., Azhar, A. 2009. Calcium alginate: a support material for immobilization of proteases from newlyisolated strain of Bacillus subtilis KIBGE-HAS. World Appl. Sci. J., 7: 1281-1286

Bevilaqua, J.V., Cammarota, M.C., Freire, D.M.G. and Santi Anna, G.L. 2002. Phenol removal through combined biological and enzymatic treatments. Jr. Brazilian Journal of Chemical Engineering, 19: 151-158.

Crecchio, C., Ruggiero, P. and Pizzigallo, M.D.R. 1995. Polyphenol oxidases immobilized in organic gels: Properties and applications in the detoxification of aromatic compounds. Biotechnol. Bioeng., 48: 585-591.

Dolashki, A., Gushterova, A., Voelter, W., Tchorbanov, B. 2009. Purification and characterization of tyrosinases from Streptomyces albus. Zeitschrift für Naturforschung C, 64(9-10): 724-732.

Fatimah Zaharah, M.Y. and Rabeta, M.S. 2018. Antioxidant and antimicrobial activities of squid ink powder. Journal of Food Research, *2*(1): 82-88.

Haghbeen, K., Jazii, F.R., Karkhane, A.A. and Borojerdi, S.S. 2004. Purification of tyrosinase from edible mushroom. Iranian Journal of Biotechnology, 2: 200.

Halaouli, S., Asther, M., Sigoillot, J.C., Hamdi, M. and Lomascolo, A. 2006. Fungal tyrosinases: new prospects in molecular characteristics, bioengineering, and biotechnological applications. J. Appl. Microbiol., 100: 219-232.

Hossain, M.P., Rabeta, M.S. and Husnul Azan, T. 2019. Medicinal and therapeutic properties of cephalopod ink: a short review. Food Res., 3: 188-198.

Zaidi K.U., Ayesha, S.A. and Sharique, A.A. 2015. Purification and characterization of high potential tyrosinase from macrofungi and its appliance in food engineering. J. Microbiol. Biotech. Food Sci., 5: 203-206.

Kameda, E., Langone, M.A.P. and Coelho, M.A.Z. 2006. Tyrosinase extract From *Agaricus Bisporus* mushroom and its in natural tissue for specific phenol removal. Environmental Technology, 27: 1209-1215.

Laemmli, U.K. 1970. Cleavage of structural proteins during the assembly of the head of bacteriophage T4. Nature, 227: 680-685.

Liu, H., Luo, P., Chen, S. and Shang, J. 2011. Effects of squid ink on growth performance, antioxidant functions and immunity in growing broiler chickens. Asian-Australas. J. Anim. Sci., 24: 1752-1756.

Maurya, S. and Singh, D. 2010. Quantitative analysis of total phenolic content in *Adhatoda vasica* Nees extracts. Int. J. Pharm. Tech. Res., 2: 2403-2406.

Molina, D.L., Hiner, A.N.P., Tudela, J., Canovas, F. and Lopez, J.N.R. 2003. Enzymatic removal of phenols from aqueous solution by artichoke (*Cynara scolymus* L.) extracts. Enzyme Microb. Technol., 33: 738-42.

Naraoka, T., Uchisawa, H., Mori, H., Matsue, H., Chiba, S. and Kimura, A. 2003. Purification, characterization and molecular cloning of tyrosinase from the cephalopod Mollusk, IllexArgentinu. Eur. J. Biochem., 270: 4026-4038.

Naraoka, T., Chung, H.S., Uchisawa, H., Sasaki, J.I. and Matsue, H. 2000. Tyrosinase activity in antitumor compounds of squid ink. Food Science and Technology Research, 6(3): 171-175.

Neifar, F., Ben rebah, Gargouri, A. and Abdelmouleh, A. 2009. Physicochemical characterization of *Sepiella officinalis* ink and the effects of storage conditions on the coagulation process. Journal of the Marine Biological Association of the United Kingdom, 89: 803-807.

Okuzumi, M. and Fujii, T. 2000. Nutritional and functional properties of squid and cuttlefish. Japan: National Cooperative Association of Squid Processors. Tokyo, Japan.

Palma, M.S.A., Shibata, C., Paiva, J.L., Zilli, M. and Converti, A. 2010. Batch liquid–liquid extraction of phenol from aqueous solutions. Chem. Eng. Technol., 33: 39–43.

Robb, D.A. 1995. Exploiting tyrosinase activity in aqueous and nonaqueous media. Acs. Sym. Ser., 600: 159-165.

Roy, S., Ishita, D., Minki, M., Karthik, L., Gaurav, K., Sathish, K. and Bhaskara Rao, K.V. 2014. Isolation and characterization of tyrosinase produced by marine actinobacteria and its application in the removal of phenol from aqueous environment. Front. Biol., 9: 306-316.

Russo, G.L., De Nisco, E., Fiore, G., Di Donato, P., d'Ischia, M. and Palumbo, A. 2003. Toxicity of melanin-free ink of Sepia officinalis to transformed cell lines: identification of the active as tyrosinase. Biochemical and Biophysical Research Communications, 308:293-299

Shesterenko, Y.A., Sevastyanov, O.V. and Romanoyskaya, L.L. 2012. Removal of phenols from aqueous solutions using Tyrosinase immobilized on polymer carriers and inorganic coagulants. J. Water Chem. Technol., 34: 107-111.

Vate, N.K. and Benjakul, S. 2017. Enhancement of gel properties of sardine surimi using squid ink tyrosinase in combination with coconut husk extract. International Journal of Food Engineering, 20: 160-163.

Zilli, M., Kennes, C., Veiga, M.C. and Converti, A. 2010. Biofilters: air purification. In: Flickinger, M.C., Drew, S.W. (Eds.), The Encyclopedia of Bioprocess Technology: Fermentation, Biocatalysis, and Bioseparation, 1: 617- 637.

Nature Environment and Pollution Technology
An International Quarterly Scientific Journal

p-ISSN: 0972-6268
(Print copies up to 2016)
e-ISSN: 2395-3454

Vol. 20 | No. 2 | pp. 657-663 | 2021

Original Research Paper

https://doi.org/10.46488/NEPT.2021.v20i02.024

Open Access Journal

Recent Advances in the Synthesis and Characterization of Nanoparticles: A Green Adeptness for Photocatalytic and Antibacterial Activity

Thambiraj Arthi Feiona, G. Sabeena, Muthiah Sakthi Bagavathy, E. Pushpalaksmi, J. Jenson Samraj and G. Annadurai†

Division of Nanoscience, Sri Paramakalyani Centre for Excellence in Environmental Sciences, Manonmaniam Sundaranar University, Alwarkurichi-627 412, India

†Corresponding author: G. Annadurai; gannadurai@msuniv.ac.in

Nat. Env. & Poll. Tech.
Website: www.neptjournal.com

Received: 26-05-2020
Revised: 18-07-2020
Accepted: 25-07-2020

Key Words:
Green synthesis
Lantana camara Linn.
NiO nanoparticles
Photocatalytic activity
Antibacterial activity

ABSTRACT

The green synthesis of metal oxide nanoparticles is an eco-friendly, rapid, and cost-effective development of novel technologies. The catalyst of nickel oxide (NiO) nanoparticles has been synthesized by the green route's method using *Lantana camara* Linn and nickel chloride. It was found that plant-mediated synthesis of nickel oxide nanoparticles can greatly enhance the antibacterial and photocatalytic activity at very low concentrations. The synthesized plant-mediated NiO nanoparticle was characterized by the structural and optical properties, morphology, and composition of NiO nanoparticles (NPs) with the help of various techniques such as Ultra Violet (UV) spectroscopy, Fourier Transform Infrared Spectroscopy (FTIR), Scanning Electron Microscopy (SEM), X-ray Diffraction (XRD), Particle Size Analyzer (PSA), Fluorescence Spectroscopy (FL) and the photocatalytic activity studies were investigated. The antimicrobial activity was carried out against Gram-positive and Gram-negative bacteria and NiO NPs showed inhibitory activity in both strains of bacteria with excellent selectivity against Gram-positive bacteria.

INTRODUCTION

Nanoparticles (NPs) are a cluster of atoms having at least one dimension in the size range of 1-100 nm. Owing to their unique optical, magnetic, catalytic, and electrical properties, they have potential applications in various fields. The physicochemical properties of NPs are different as compared to those of their bulk counterparts because the surface area to volume ratio increases and quantum effects become dominant as the size decreases. The increase in surface area to volume ratio alters the mechanical, catalytic, and thermal properties of the material (Muhammad et al. 2016). There are several methods for creating nanoparticles, including attrition, pyrolysis, hydrothermal synthesis, and green synthesis. The most common methods are solvothermal, co-precipitation method, bottom-up and top-down synthesis, sol-gel synthesis method, green synthesis, and chemical synthesis method (Joerger et al. 2011). Green synthesis is a cost-effective system and eco-friendly system (Morton et al. 2016). Green synthesis is used in various for different applications and it is used in day-to-day life. Green synthesis of nanoparticles is a cost-effective and eco-friendly system with the added advantage of stabilizing the formed NPs as plant secondary metabolites besides acts as synthetic agents as well as a capping agent. Plant-mediated synthesis of nanoparticles is a green chemistry approach that connects nanotechnology with plants. Plants are nature's chemical factories (Mariam et al. 2014). As the green synthesized nanoparticles are smaller in their small size, they can penetrate small capillaries and are taken up by the cells, which allow efficient drug accumulation at the target (Laokul et al. 2009). Moreover, NPs synthesized by using green chemistry have no or low cytotoxicity as compared to other chemically synthesized NPs which makes them an efficient carrier of drugs for in vivo drug delivery applications. *Lantana camara* Linn (*L. camara*) is a popular ornamental and garden plant that grows up to 2-4 meters in height, with several flower colours such as yellow, red, pink, and white. It also grows naturally at roadsides or riversides up to the elevation of 2,000 meters in tropical and subtropical temperature regions. The leaves of the plant are used in the treatment of tumours, tetanus, rheumatism, malaria, etc., and it is used in the antiseptic and carminative properties have also been reported (Ganjewala et al. 2009, Raju 2000 & Ghisalberti 2000). In the past few decades, metal oxide nanoparticles have been gaining momentum among researchers. One of the most extensively used transition metal oxides is Nickel oxide (NiO) which has a wide bandgap and various applications. They encompass catalysis, lithium-ion batteries, smart windows, antiferromagnetic film, dye-sensitized photocathodes,

photocatalysis, antimicrobial activity, thermal conductivity, and field emission studies. Different kinds of researches were undertaken in NiO NPs prepared by cost-effective and eco-friendly methods that have been used to evaluate their antimicrobial activity and for photocatalytic degradation of rhodamine B. The antibacterial activity of such nanoparticles depends on their stability, size, and concentration added to the bacterial growth medium since this provides greater retention time for interaction of bacterium nanoparticles (Alamelu et al. 2015 & Azam et al. 2012).

In this work, for the first time, we have synthesized nickel oxide nanoparticles using Arabic gum, and nickel chloride as the nickel source, and water as solvent by sol-gel process, without any surfactant and reducing agent, as a cheap and eco-friendly approach to nature. This method has many advantages such as nontoxic, versatile, low cost, and could be used to synthesize other metal oxides. The influence of calcination time on structure, morphology, composition, and photoluminescence property of NiO nanoparticles was investigated in detail and antimicrobial activity of NiO nanoparticles is tested against bacterial species using the disc diffusion method.

MATERIALS AND METHODS

The *Lantana camara* leaves were collected from the Tenkasi area which is near to the Western Ghats region. Nickel chloride ($NiCl_2.6.H_2O$) was purchased from Daijung (Darmstadt, Korea) and used without further purification.

Synthesis of Leaf Extract

The *Lantana camara* leaves were dried for one day under the shadow and are thoroughly washed with distilled water to remove dust particles and sun-dried to remove moisture content and these leaves are cut into small pieces. Then the leaves are boiled in distilled water in a flask for 6 hours and placed in a water bath at a constant temperature for three hours at 400°C. The solution was filtered and finally, 100 mL of leaf extract was obtained and the extract was filtered using Whatman filter paper and finally, the leaf extract was obtained.

Synthesis of Nickel Oxide Nanoparticles

The $NiCl_2$ (0.5M) was prepared individually and mixed with 10 mL of plant extract and kept at room temperature. The colour of the solution was changed from light green to brown colour indicating the formation of NiO nanoparticles and the absorbance of nickel oxide nanoparticles in the solution was monitored at different time intervals using UV-visible spectroscopy.

Photocatalytic Activity

The photocatalytic activity of NiO NPs was evaluated on the degradation of methylene blue (MB) (Merck, India) in an aqueous solution under UV light (125W/m^2, Osram) illumination. A known weight of the catalyst, 0.01g was added to a known volume of 0.2 L dye that resulted in a suspension. The suspension was stirred for uniform exposure of the catalyst to light. The distance between the lamp and the base of the beaker under UV illumination was 13 cm. Each experiment was conducted every 120 min with a 10 mL sample of a liquid drawn every 15 min. The degradation of the dye was monitored after the removal of photocatalyst by centrifugation at 2000 rpm for 30 min. The decreased absorbance was measured at regular intervals of time from 0 to 120 min by using the Shimadzu UV1650 PC spectrometer.

RESULTS AND DISCUSSION

The synthesized NiO nanoparticles are subjected to various characterization studies for their structural, optical, and magnetic properties such as powder XRD, UV-visible spectrometer, FTIR spectrometer, particle size analyser, fluorescence spectroscopy, and SEM analysis. The results obtained are discussed below.

X-ray Diffraction (XRD)

The peaks seem to be appreciably broad that indicates the crystallites of the hydroxide can be in the nanosized range. The structural information and crystallinity of NiO NPs were prepared using *Lantana camara* plant extract by green synthesis method and are further studied by the XRD pattern as shown in Fig. 1. The sharp peaks of NiO NPs are highly crystalline. The observed peaks appreciably broad indicating that the synthesized Nickel hydroxide nanoparticles are crystalline with the hexagonal phase. The diffraction peaks of NiO NPs at $2\theta = 37.21°, 43.29°, 62.88°$ associated with the crystal planes (111), (200), (222) were observed (Mallikarjuna et al. 2017). The obtained result was well-matched with JCPDS No. 1313-99-1. The obtained XRD pattern reveals the formation of NiO NPs and showed no other peaks present in the XRD data. It is observed that peaks are sharp with high intensity for higher calcination time which means that bigger particle size may be generated by increasing the calcination time (Rajesh et al. 2010 & Shanaj et al. 2016). However, it can be observed that, by increasing the calcination temperature up to 400°C, the peaks have been appreciably sharpened which indicates that the growth in the crystallite sizes of NiO has occurred.

It was confirmed that the purity of the NiO phase. The crystalline size of NiO NPs was estimated using the Debye Scherrer formula.

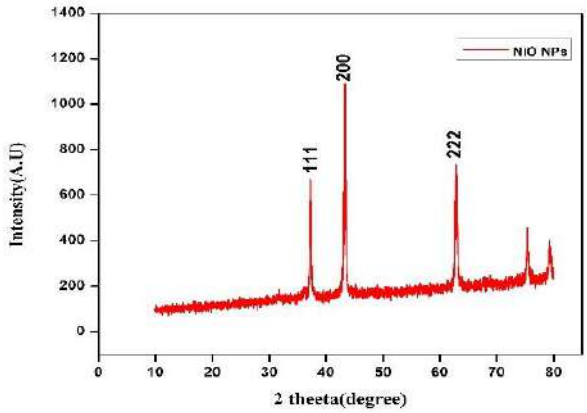

Fig. 1: XRD image of NiO Nanoparticle.

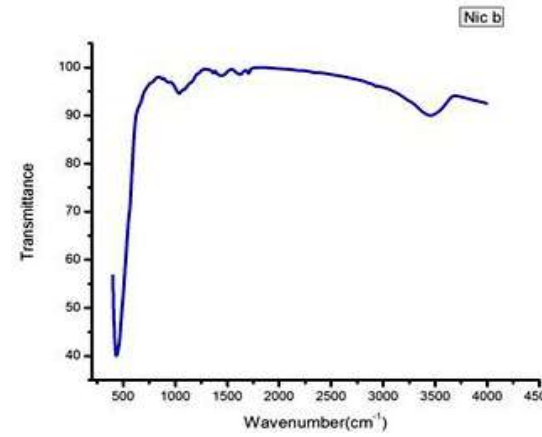

Fig. 2: FT-IR functional group peaks of NiO Nanoparticle.

$$D = 0.89\ \lambda/\beta\cos\theta \qquad ...(1)$$

Where D is the average crystal size λ is a wavelength of the X-ray radiation and β is the full-width half maximum. The calculated average of crystalline size was formed to be 21 nm. The reduced crystalline size may be due to the plant extract that can act as the capping agent and reducing agent with the NiO NPs. Moreover, it will have a remarkable impact on biological activity.

Fourier Transform Infra-Red Spectroscopy (FT-IR)

Fig. 2 shows the FT-IR spectra of the prepared sample of $Ni(OH)_2$ and NiO nanoparticles after calcination at different periods. In Fig. 2, a sharp peak at 3637 cm^{-1} is the characteristic of $Ni(OH)_2$ (Rajesh et al. 2010, Shanaj et al. 2016, Motlagh 2011 & Abolanle 2011). The broad absorption band centred at 3403 cm^{-1} is assigned to O-H stretching vibrations and the weak band at 1633 cm^{-1} is attributed to H-O-H bending vibration because of absorption of water molecules from the air as the sample was synthesized. Fig. 2 shows the FTIR spectra of prepared NiO NPs. The FTIR bands due to metal-oxygen occur in the region of 400-4000 cm^{-1}. The FTIR shows the peaks at 3480 cm^{-1}, 1650 cm^{-1}, 473 cm^{-1}. The intense and wide peak centred at 3480 cm^{-1} assigned to O-H stretching and the peak at 1650 cm^{-1} corresponds to the H-O-H bending mode. The band at around 473 cm^{-1} is attributed to Ni-O bending vibration. These results agree with other researches (Wang et al. 2009). The dislocation density, which is a crystallographic defect within a crystal structure affects the properties of materials. The bands at 3368 cm^{-1} are assigned to O-H stretching vibration and 1585 cm^{-1} are due to O-H-O bending vibration mode because the calcined powder tends to absorb water. The bands due to carbonate groups and C-O stretching bonds are observed at 1424 cm^{-1}, 872 cm^{-1}, and 1036 cm^{-1} respectively. The appearance of new bands was observed at 557 cm^{-1}, 405 cm^{-1} which are assigned to Ni-O stretching vibration mode (Rajesh 2010, Shanaj 2016 & Motlagh 2011). The broadness of the band indicates the nanocrystalline nature of the samples.

Scanning Electron Microscopy

The surface morphological features of synthesized nanoparticles were studied by scanning electron microscope. The images were recorded with magnification of 500 and 10000 as shown in Fig. 3. The results indicate that NiO nanoparticles are hexagonal. We can observe that the particles are highly agglomerated. (Mallikarjuna et al. 2019). Further, the particles are aggregated with irregular particle morphology having a diameter of 1 μm and they are essentially a cluster of nanoparticles.

The presence of some larger nanoparticles may be attributed to the fact that NiO nanoparticles tend to agglomerate due to their high surface energy and high surface tension of the ultrafine nanoparticles (Muhammad et al. 2016)

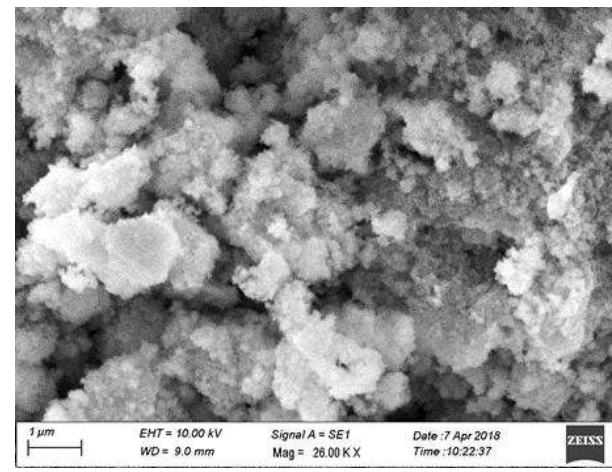

Fig. 3: SEM image of synthesized NiO nanoparticles.

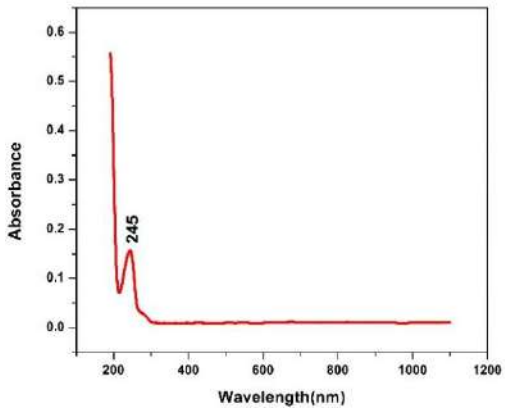

Fig. 4: UV-visible spectroscopy synthesized peak for NiO nanoparticles.

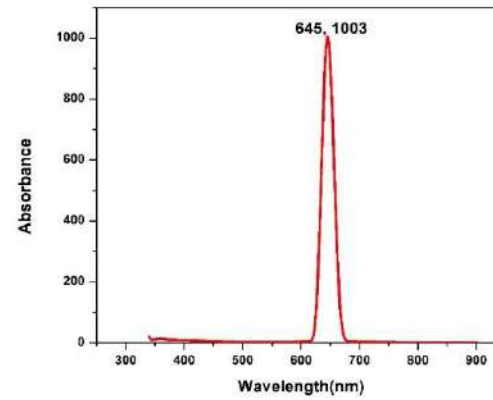

Fig. 5: FL peaks of Nickel oxide nanoparticles.

Ultra Violet Visible Spectroscopy

The UV spectral studies are taken for the NiO nanoparticles in regions ranging between 200 and 1200 nm. The absorption spectra of plant extract mediated synthesis of NiO nanoparticles in terms of wavelength are shown in Fig. 4.

The UV spectra show that the absorption peak wavelength for plant extract mediated synthesis of NiO nanoparticles is around 245 nm. From the absorption spectra, it is confirmed that the peak is due to the Nickel oxide nanoparticle present here. The plots of variation of wavelength versus absorption for the plant extract mediated synthesis NiO nanoparticles are presented (Mallikarjuna et al. 2017 & Haque et al. 2009). The UV-visible absorption spectrum of the NiO particles obtained at plant extract mediated synthesis. A slight shift towards a higher wavenumber is seen for the absorption edges by increasing the processing temperature. This shift indicates a decrease in the bandgap, which can be attributed to an increase in particle size. The increasing trends of the bandgap energy upon the decreasing particle size is likely due to the defects or vacancies present in the intergranular regions generating new energy levels to reduce the bandgap energy.

Fluorescence Spectroscopy

The fluorescence spectra of Nickel oxide nanoparticles, which are essential in comparing the fluorescence properties. Fig. 5 shows the fluorescence spectrum of Nickel oxide nanoparticles where the peaks are observed at 645 nm, where 645 nm luminescence peak is based on the near-and-edge emission of Nickel oxide nanoparticles (Linsebigler et al. 1995).

The fluorescence of the plant-mediated synthesis of Nickel oxide nanoparticle exhibited emission peaks at 645 nm as shown in Fig. 5. The fluorescence spectra were not quenched and showed good fluorescence (Helan et al. 2016 & Dutta et al. 2011). The emission peaks were red-shifted on the change of the excitation from 645 nm and the intensity of fluorescing spectra was reduced by increasing the excitation wavelength (Haque et al. 2009).

Particle Size Analyzer

The Particle Size Distribution (PSA) of plant-mediated synthesized Nickel oxide nanoparticles was analysed by PSA as shown in Fig. 6. PSA result showed the particle size distribution of plant-mediated synthesized by Nickel oxide nanoparticles at 10-50 nm. This size proved that the synthesized Nickel oxide nanoparticle using *Lantana camara* leaf extract was in nanoparticle form. Fig. 6 shows the PSA graph of plant-mediated synthesis of nickel oxide nanoparticles.

The synthesized plant-mediated Nickel oxide nanoparticle exhibits a mean particle size of 21 nm under dynamic light scattering. The crystalline size was calculated from PSA is further counter-verified by Powder X-Ray Diffraction (PXRD).

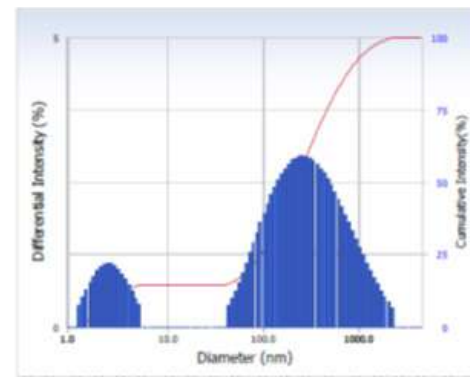

Fig. 6: DLS peaks of Nickel oxide nanoparticles.

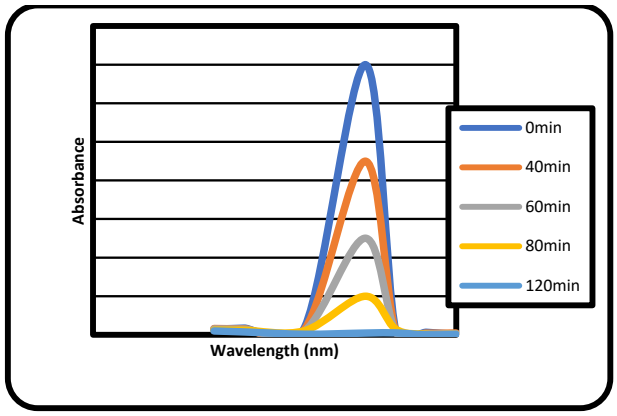

Fig.7: Photocatalytic image of NiO nanoparticles.

Photocatalytic Activity

Fig. 7 shows the photocatalytic degradation of methylene blue dye molecule using plant-mediated synthesis. Nickel oxide nanoparticles are performed at room temperature under UV light at a wavelength of 664 nm. The least peak was noticed at 650 nm indicates the decreased level of methylene blue (MB) dye molecule with increasing UV exposure time that denotes the degradation of dye molecule at UV-irradiation.

This shows 85% of the degradation rate of dye molecule using biologically synthesized nickel oxide nanoparticles within 120 min is due to excitation of semiconductor by UV-light to produce free radicals in the degradation of dye in which the excited electrons move from the valence band to the conduction band and generates high energy electron-hole pairs which transfer to adsorbed species on semiconductor results heterogeneous photocatalysis (Wu et al. 2015 & Linsebigler et al. 1995). The photocatalytic activity was done within 2 hrs and the methylene blue dye (0.2 L) was degraded successfully. Moreover, we have observed NiO NPs as an efficient photocatalytic adaptive nanoparticle.

Antibacterial Studies

The antibacterial activities of plant-mediated synthesis of nickel oxide nanoparticles are generally known to be a function of the surface area which is in contact with the microorganisms. Reactions take place at the surface of a plant-mediated synthesis of nickel oxide nanoparticles (Dola et al. 2017 & Miessya et al. 2019). The antibacterial activity of NiO NPs can generate oxidative stress to damage the structure, protein, and bacterial cells. Further, it prevents the formation of biofilms and assists in wound healing (Srihasam et al. 2020). Hence, the smaller size and the higher surface to volume ratio, i.e. larger surface area, enhanced interaction with the microbes is seen. Fig. 8 shows the antibacterial activity of plant-mediated synthesis of Nickel oxide nanoparticle from the microorganism such as *Escherichia coli, Bacillus subtilis,* and *Enterobacter*.

The activity was found to be highest in the case of Gram-negative bacteria and Gram-positive bacteria. Plant-mediated synthesis of Nickel oxide nanoparticle samples showed activity for Gram-positive and Gram-negative bacteria such as *Escherichia coli, Bacillus subtilis,* and *Enterobacter*. The concentration of Plant-mediated synthesis of Nickel oxide nanoparticles such as 20 µL, 40 µL, 60 µL, 80 µL and then the zone of inhibition of the nickel oxide nanoparticle against Gram-positive and Gram-negative bacteria. The mechanism depends not only on the concentration of NiO NPs; it also depends on the sensitivity of bacterial species. The increased antibacterial effect may be due to reactive radicals Ni^{2+} ions (Rajesh et al. 2010 & Krishnamoorthy et al. 2012), released continuously in the solution (Wang et al. 2007), may be attached to the negatively charged bacterial cell wall due to electrostatic force. The strong adhesion of Ni^{2+} ions to the bacterial cells causes the distraction of cell membranes (Morones et al. 2005. Wang et al. 2007, Makhluf et al. 2005, Sawai et al. 2003 & Jadhav et al. 2011), and hence antimicrobial efficacy at higher NPs concentration (Rajesh et al. 2010 & Fu et al. 2005). The antibacterial results also revealed that Gram-positive bacteria are more susceptible to NiO nanoparticles as compared to Gram-negative bacteria due to the difference in the cell wall structure. The cell wall of Gram-positive bacteria is made of a thick layer of

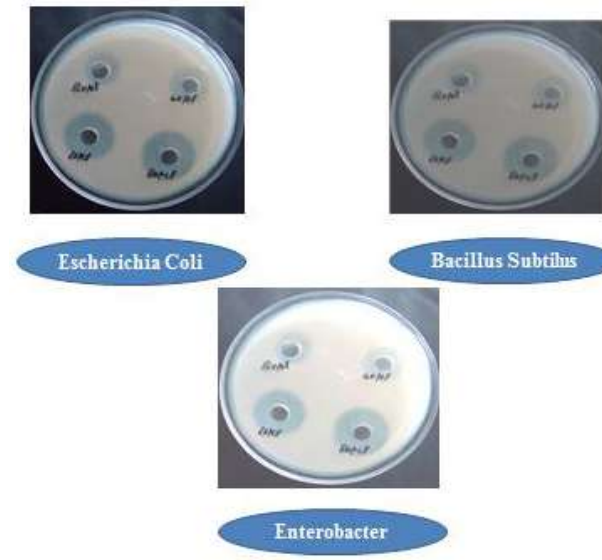

Fig. 8: Antibacterial activity of the plant-mediated synthesis of NiO nanoparticles.

peptidoglycan, which is attached to teichoic acids that are unique to Gram-positive bacteria and can be damaged more easily (Rajesh et al. 2010 & Motlagh et al. 2011). But in Gram-negative bacteria, the cell wall contains a thin peptidoglycan layer and an outer membrane, constructed from tightly packed lipopolysaccharide (LPS) molecules (Rajesh et al. 2010), which is selectively permeable and regulates the transport through the plasma membrane. This renders Gram-negative bacteria less susceptible to NiO NPs (Mani et al. 2013, Tortora et al. 2016).

CONCLUSION

In conclusion, this paper provides an overview of the plant-mediated synthesis of nickel oxide nanoparticles by using plant extract. Although all these green protocols for NiO nanoparticle synthesis have their advantages and limitations use of plant extract as a reductant is more beneficial as compared to microbial extract because of the rapid rate of production of nanoparticles with a former green reductant. Synthesis of NiO nanoparticles was carried out by the green synthesis method using *Lantana camara* leaf extract. XRD and FT-IR confirm the formation of pure and crystalline NiO nanoparticles and various functional groups present in these particles to synthesize with high purity and crystallinity, reduced particle size, and more surface defects, which are the advantageous factors to be used for various environmental and applications. The UV-visible spectra showed that the wavelength is around 245 nm. FTIR studies were carried out for the functional group from the crystalline sample and the vibrational bands are assigned. From SEM images, it is observed that the nanoparticles are arranged as regular beads in shape. The fluorescence spectrum of nickel oxide nanoparticles where the peaks are observed at 645 nm, where 645 nm luminescence peak is based on the near-band-edge emission of nickel oxide nanoparticles. It is also concluded that the antimicrobial property of NiO nanoparticles increased with an increase in surface area to volume ratio due to a decrease in particle size. Hence, smaller-sized NiO nanoparticles can be used as an antimicrobial agent more effectively. Based on the results, it is concluded that particle size and optical properties are controlled by calculations time. Hence, NiO nanoparticles can also be used in optoelectronic devices. The morphology and chemical composition were elucidated by SEM. The photocatalytic degradation of methylene blue dye molecule using the plant-mediated was successfully synthesized. The least peak is noticed at 650 nm indicates the decreased level of MB dye molecule with the increasing UV exposure time denotes the degradation of dye molecule at UV-irradiation.

ACKNOWLEDGEMENT

Myself, T. Arthi Feiona (Register No: 17211232272011) acknowledge the Research Centre Sri Paramakalyani Centre for Excellence in Environmental Science, Manonmaniam Sundaranar University, Alwarkurichi, for providing the support for this research work.

REFERENCES

Abolanle, S., John Oyekunle, A., Oluwatobi, S. and Abiodun J. O. 2011. Comparative catalytic properties of $Ni(OH)_2$ and NiO nanoparticles towards the degradation of nitrite (NO_2^-) and nitric oxide (NO). Int. J. Electrochem. Sci., 9: 3008-3021.

Alamelu, K., Ramasami, M., Reddy, V., Geetha, R. and Balakrishna, R. 2015. Combustion synthesis and characterization of NiO nanoparticles. Materials Science in Semiconductor Processing, 40: 194-202.

Azam, A., Ahmed, A.S., Oves, M., Khan, M.S. and Memic, A. 2012. Size-dependent antimicrobial properties of CuO nanoparticles against Gram-positive and negative bacterial strains. Int. J. Nanomed., 7: 3527-3535.

Dola, S. T., Vijaya Kumar, P.S., Subba Rao, R., Ravikumar, V.S.S.N. and Gopala Krishna, A. 2017. Green synthesis and characterization of Ag nanoparticles from *Mangifera indica* leaves for dental restoration and antibacterial applications. J. Bio and Tribo-Corrosion, 6: 57-66.

Dutta, M., Jana, S. and Basak, D. 2011. Quenching of photoluminescence in ZnO QDs decorating multiwalled carbon nanotubes. Chem. Phys. Chem., 11(8): 1774-1779.

Fu, G. Vary, P.S. and Lin, C.T. 2005. Anatase TiO_2 nanocomposites for antimicrobial coatings. J. Phys Chem, B., 12: 8889-8898.

Ganjewala, D., Sam, S. and Khan, K.H. 2009. Biochemical compositions and antibacterial activities of *Lantana camara* plants with yellow, lavender, red, and white flowers. Eurasian J. Bio. Sci., 3: 69-77.

Ghisalberti, E.L. 2000. *Lantana camara L.* (Verbenaceae). Fitoterapia, Fitoterapia, 71(5): 467-486.

Haque, F.Z., Singh, N., Pandey, P. and Parra, M.R. 2009. Study of zinc oxide nano/micro rods grown on ITO and glass substrates. Optik-Int. J. Light Electron. Opt., 124(20): 4167-4171.

Helan, V., Joseph Prince, J., Al-Dhabi, N.A., Valan Arasu, M., Ayeshamariam, A., Madhumitha, G., Roopan, S.M. and Jayachandran, M. 2016. Neem leaves mediated preparation of NiO nanoparticles and their magnetization, coercively, and antibacterial analysis. Results Phys., 6: 712-718.

Jadhav, S., Gaikwad, S., Nimse, M., Rajbhoj, A. and Clust, J. 2011. Copper oxide nanoparticles: synthesis, characterization, and their antibacterial activity. J. Cluster Sci., 22: 121-129.

Joerger, R., Klaus, T. and Granqvist, C.G. 2011. Biologically produced Ag-C composite for optically functional thin-film coating. Adv. Mate., 12: 407-409.

Krishnamoorthy, K., Moon, J.Y., Hyun, H.B., Cho, S.K. and Kim, S.J. 2012. Mechanistic investigation on the toxicity of MgO nanoparticles toward cancer cells. J. Materials Chemistry, 22: 24610- 24617.

Laokul, P., Amornkitbamrung, V., Seraphin, S. and Maensiri, A. 2009. Growth of p-type ZnO thin film on n-type silicon substrate and its application. Curr. Appl. Phys., 4: 101-111.

Linsebigler, A.L., Lu, G.Q. and J.T. 1995. Photocatalysis on TiO2 surfaces: principles, mechanisms, and selected results. Chem. Rev., 95: 735-758.

Makhluf, S., Dror, R., Nitzan, Y., Abramovich, Y. and Jelinek, R. 2005. Microwave assays synthesis of nanocrystalline MgO and its use as a bacterioside. Adv. Funct. Mater., 15: 1708-1715.

Mallikarjuna, K., Kotesh Kumar, M., Subba Reddy, B.V. and Kim, H. 2019. Hydrogen production from water splitting: Fabrication of ZnO nanorod

decorated Cu NW heterogeneous hybrid structures for photocatalytic applications. J. Clust. Sci., 30: 449-457.

Mallikarjuna, K., Raju, B.D.P. and Kim, H.S. 2017. Sustainable fabrication of palladium nanoparticles using *Stevia rebaudiana* tea and its catalytic activity. J. Nanosci. Nanotechno., 217: 4251-4256.

Mani, R. K., Padmanathanb, N., Reji, P., Balamurugand, S. and Kanakam, C.C. 2013. Size determination of nickel oxide nanoparticles by electrochemical reduction method and its antibacterial activity. Appl. Surface Sci., 282: 656-661.

Mariam, A.A., Kashif, M. and Arokiyaraj, S. 2014. Bio-synthesis of NiO and Ni nanoparticles and their characterization. Dig. J. Nanomater. Bios., 9: 1007-1019.

Miessya, W., Yoki, Y., Iman, A., Dewangga, O. and Bagus, A. 2019. Synthesis of NiO nanoparticles via green route using *Ageratum conyzoides* L. leaf extract and their catalytic activity. IOP Conf. Series: Materials Science and Engineering, 509: 012- 077.

Morones, J.R., Elechiguerra, J.L. and Camacho, A. 2005. The bactericidal effect of silver nanoparticles. Nanotechnology, 16: 2346-2353.

Morton, J.F. 2016. The horseradish tree, *Moringa pterygosperma* (Moringaceae)-a boon to arid lands?. Economic Botany, 45(3): 318-333.

Motlagh, M., Kashani, M., Youzbashi, A. and Sabaghzadeh, L. 2011. Synthesis and characterization of nickel hydroxide/oxide nanoparticles by the complexation-precipitation method. Int. J. Phy. Sci., 6(6): 1471-1476.

Muhammad, A.R., Zakia, K., Anum, R., Anjum, N.S., Saira, R. and Shahzad, N. 2016. Size- and shape-dependent antibacterial studies of silver nanoparticles synthesized by wet chemical routes. Nanomaterials, 6: 74-76.

Rajesh, K., Ashwani, S., Nawal, K. and Narender, B. 2010. Preparation and characterization of NiO nanoparticles by co-precipitation method. Int. J. Eng. Appl. Manag. Sci. Paradig., 6(01): 2320-6608.

Raju, A. 2000. Wild Plants of Indian Sub-Continent and Their Economic Uses. CBS Pub. & Distribution, New Delhi 65.

Sawai, J. and Microbiol, J. 2003. Quantitative evaluation of antibacterial activities of metallic oxide powders (ZnO, MgO and CaO) by conductimetric assay. Journal of Microbiological Methods, 54: 177-182.

Shanaj, B.R. and John, X.R. 2016. Effect of calcination time on structural, optical and antimicrobial properties of nickel oxide nanoparticles. J. Theor. Comput. Sci., 2(2): 1-10.

Srihasam, S., Thyagarajan, K., Korivi, M., Lebaka, V.R., and Mallem, S.P.R. 2020. Phytogenic Generation of NiO Nanoparticles Using Stevia Leaf Extract and Evaluation of Their In-Vitro Antioxidant and Antimicrobial Properties. Journal of Biomolecules, 10(1): 89.

Tortora, G., Funke, R.B. and Case, L.C. 2016. Microbiology: An Introduction. 12th Edition, Addison Wesley. ISBN-13: 978-0321929150- ISBN-10: 0321929152.

Wang, X., Yang, F., Yang, W. and Yang, X. 2007. A study on the antibacterial activity of one-dimensional ZnO nanowire arrays: Effects of the orientation and plane surface. Chem. Commun., 14: 4419-4421.

Wang, Y. 2009. Mutation in Rpa1 results in defective DNA double-strand break repair, chromosomal instability, and cancer in mice. **Nat**. *Genet*., *37*(7): 750-755.

Nature Environment and Pollution Technology
An International Quarterly Scientific Journal

p-ISSN: 0972-6268
(Print copies up to 2016)
e-ISSN: 2395-3454

Vol. 20 | No. 2 | pp. 665-673 | 2021

Original Research Paper

https://doi.org/10.46488/NEPT.2021.v20i02.025

Open Access Journal

Statistical Modelling of 3-Hourly Wind Patterns in Melbourne, Australia

Mayuening Eso*(**), Prashanth Gururaja* and Rhysa McNeil*(**)†

*Department of Mathematics and Computer Science, Faculty of Science and Technology, Prince of Songkla University, Mueang Pattani, 94000, Thailand

**Centre of Excellence in Mathematics, Commission on Higher Education (CHE), Ministry of Education, Ratchathewi, Bangkok, 10400, Thailand

†Corresponding author: Rhysa McNeil; rhysa.m@psu.ac.th

Nat. Env. & Poll. Tech.
Website: www.neptjournal.com

Received: 31-05-2020
Revised: 25-07-2020
Accepted: 31-07-2020

Key Words:
Wind prevalence
Wind gust
Wind speed
Logistic and linear regression

ABSTRACT

Modelling wind speed and trends helps in estimating the energy produced from wind farms. This study uses statistical models to analyze wind patterns in Melbourne, Australia. Three-hourly wind data during 2004-2008 was obtained from the Australian Government, Bureau of Meteorology, for Avalon Airport, Essendon Airport, Point Wilson, and View Bank stations. A logistic regression model was used to investigate the pattern of 3-hourly winds and gust prevalence while a linear regression model was applied to investigate wind speed trends. The 3-hour periods of the day, month, and year were used as the independent variables in the analysis. At four stations, wind speed and wind gust prevalence were mostly high between 9 AM and 6 PM. The monthly wind and wind gust prevalence were high from November to January while the highest annual prevalence occurred in 2007. The wind speed increased from 7 AM to 6 PM within which the maximum occurred. The monthly wind speed increased from November to January where it attained the maximum, decreasing to a minimum in May. The annual mean wind speed was highest in 2007.

INTRODUCTION

Wind is the dominant air current that affects the Earth's climate. The movement of the wind on the Earth's surface has a diverse range of magnitude and is constantly changing direction. This intriguing wind behaviour has a tremendous impact on global climate and weather conditions (Csavina et al. 2014), ecosystems, and human life imbalance (Mitchell 2012). Sudden wind gusts have an enormous influence on climate and weather events (Cheng et al. 2014). Its extreme can cause an enormous amount of damage and destruction to man-made structures and result in devastation to humans and ecosystems (Jamaludin et al. 2016).

Several studies have investigated wind patterns over the Earth's surface. Studies of long-term austral summer wind speed trends over southern Africa have shown that a decline in wind speed was caused by deceleration of mid-latitude westerly winds, and Atlantic south-easterly winds with a poleward shift in the subtropical anticyclone (Nchaba et al. 2016). The average monthly maximum and minimum wind speeds in the United States from 1961 to 1990 reduced in spring and summer. The decreasing wind speeds in western and southeastern United States may be due to variable topography and high atmospheric pressures mostly throughout the year. However, the central and the northeastern regions have a gentle topography and are located near common storm tracks (Klink 1999). In Europe, high wind variability was evident over 140 years in the north-east Atlantic (Bett et al. 2013). In China, the warm and cold Arctic Oscillation and El Niño-Southern Oscillation phases have a significant influence on the probability distribution of wind speeds. Thus, internal climate variability is a major source of both interannual and long-term variability (Chen et al. 2013).

Daytime surface wind speeds were shown to be broadly consistent whereas night-time surface wind speeds are more positively skewed. However, in the mid-latitudes, these strongly positive skewness were shown to be associated with conditions of strong surface stability and weak lower-tropospheric wind shear (Mohanan et al. 2001).

The island continent of Australia features a wide range of climatic zones, from the tropical regions of the north, through to the arid expanses of the interior, to the temperate regions of the south. Australia experiences many of nature's more extreme weather phenomena, including tropical cyclones, severe storms, bushfires, and the occasional tornado. Australia's climate is largely determined by its latitudes, with the mainland lying between 10° South to 39° South, extending to 44° South, and longitudes 112° East and 154° East (Trewin 2005). The average wind speed varies throughout the year with distinctive seasonal patterns. In the southern region, the strongest winds occur during

winter (June-August) and spring (September-November). In terms of daily variation, wind speed increases in the afternoons (Coppin et al. 2003). The city of Melbourne lies on the latitude and longitude of 37.8136°S and 144.9631°E, respectively. It is in the vulnerable zone of a significant increase in intense frontal systems which bring extreme winds and dangerous fire conditions (Hasson et al. 2009). An increase in the frequency of conditions makes the city conducive to thunderstorm development in the southern and eastern areas (Allen et al. 2014). The city is situated on the boundary of the very hot inland areas and the cool Southern Ocean and experiences frequent changes in weather conditions due to its geographical location. The autumn months (March-May) have lighter winds than other months (Bureau of Meteorology 1968). Prevailing winds come in over the poleward areas on the high-pressure area known as the subtropical ridge in the horse latitudes. These prevailing winds mainly blow from the west to the east and bring extra-tropical cyclones. The winds come predominantly from the southwest in the Northern Hemisphere and from the northwest in the Southern Hemisphere. These winds are stronger in the winter due to the lower atmospheric pressure over the poles. In this study, we aim to investigate the wind and wind gust prevalence using logistic regression models, and to analyze wind speed patterns in Melbourne using linear regression model.

MATERIALS AND METHODS

The 3-hourly wind observations of four selected stations, namely Essendon Airport, Avalon Airport, Point Wilson, and View Bank were obtained from the Australian Government, Bureau of Meteorology at (http://reg.bom.gov.au/reguser/) for the years 2004-2008. The measurements recorded for consecutive 3-hourly periods were associated with a well-known primaeval Bronze-Age meteorological system, and ancient time metrics of the Roman system (Graham & Kamm 2014); and noteworthy heuristic weather measurement instruments of Bureau of Meteorology, Australia (BOM 2011). Moreover, eight periods of 3 hours each during the day were classified into the following time intervals: mid-night, dawn, morning, forenoon, afternoon, evening, dusk, and night (Glickman & Zenk 2000). The wind speed magnitude was measured in kilometres per hour (km/h) on the Earth's surface and the prevalence was classified as any occurrence of wind of at least 3 km/h (Wheeler & Wilkinson 2004) while wind speeds of at least 18 km/h (Geer 1996) were classified as gusts as given in Table 1.

Statistical Methods

The wind prevalence and wind gust prevalence are the binary outcomes, therefore logistic regression models were used to investigate the wind pattern. The logistic regression model takes the following form:

Table 1: Wind observations prevalence and wind gust categories.

stations	Sample size	Wind (km/h)		Wind gust (km/h)	
		<3	≥3	< 18	≥18
Avalon Airport	14,493	4,066	10,427	7,579	6,914
Essendon Airport	14,524	4,493	10,031	7,909	6,615
Point Wilson	14,293	2,495	11,798	5,205	9,088
View Bank	14,586	8,052	6,534	11,318	3,268

$$ln\left(\frac{p_{ijk}}{1-p_{ijk}}\right) = \mu + \alpha_i + \beta_j + \gamma_k, \quad \ldots(1)$$

Where p_{ijk} is the probability of wind or wind gusts occurring, μ is a constant, α_i is the coefficient for each period of the day, β_j is the coefficient for each month of the year, and γ_k is the coefficient for each year. The Receiver Operating Characteristic (ROC) curve (Westin 2001) was used as a measure of goodness-of-fit of the model. The ROC curve is popularly known for determining the capability of the prediction of a binary outcome.

The trends of wind speed of at least 3 km/h was also investigated. Since the wind speed was a continuous outcome, a multiple linear regression model was used. The model takes the following form:

$$y_{ijk} = \mu + \alpha_i + \beta_j + \gamma_k \quad \ldots(2)$$

where y_{ijk} represents wind speed at period i, month j and year k, μ is the overall mean, α_i is the coefficient for each period of the day, β_j is the coefficient for each month of the year, and γ_k is the coefficient for each year. The goodness of fit of the model was assessed using the coefficient of determination (R-square) and Quantile-Quantile plots (Q-Q plots). Since the normality assumption was not satisfied, the wind speed values were transformed by taking the natural logarithm.

The sum contrasts (Tongkumchum & McNeil 2009) were applied to obtain 95% confidence intervals (CI) to compare the fitted model means with the overall wind speed means. This contrast gives criteria to classify levels of the factor into three groups, according to whether each relating CI is greater than or equal to, or is less than the overall mean. All analysis was done in R (R Development Core Team 2008)

RESULTS

For each station, a logistic regression model (model 1) was fit to the 3-hourly wind prevalence from 2004 to 2008 with 3 categorical predictors. The first predictor was the 3-hourly period of the day with 8 factors, the second predictor was

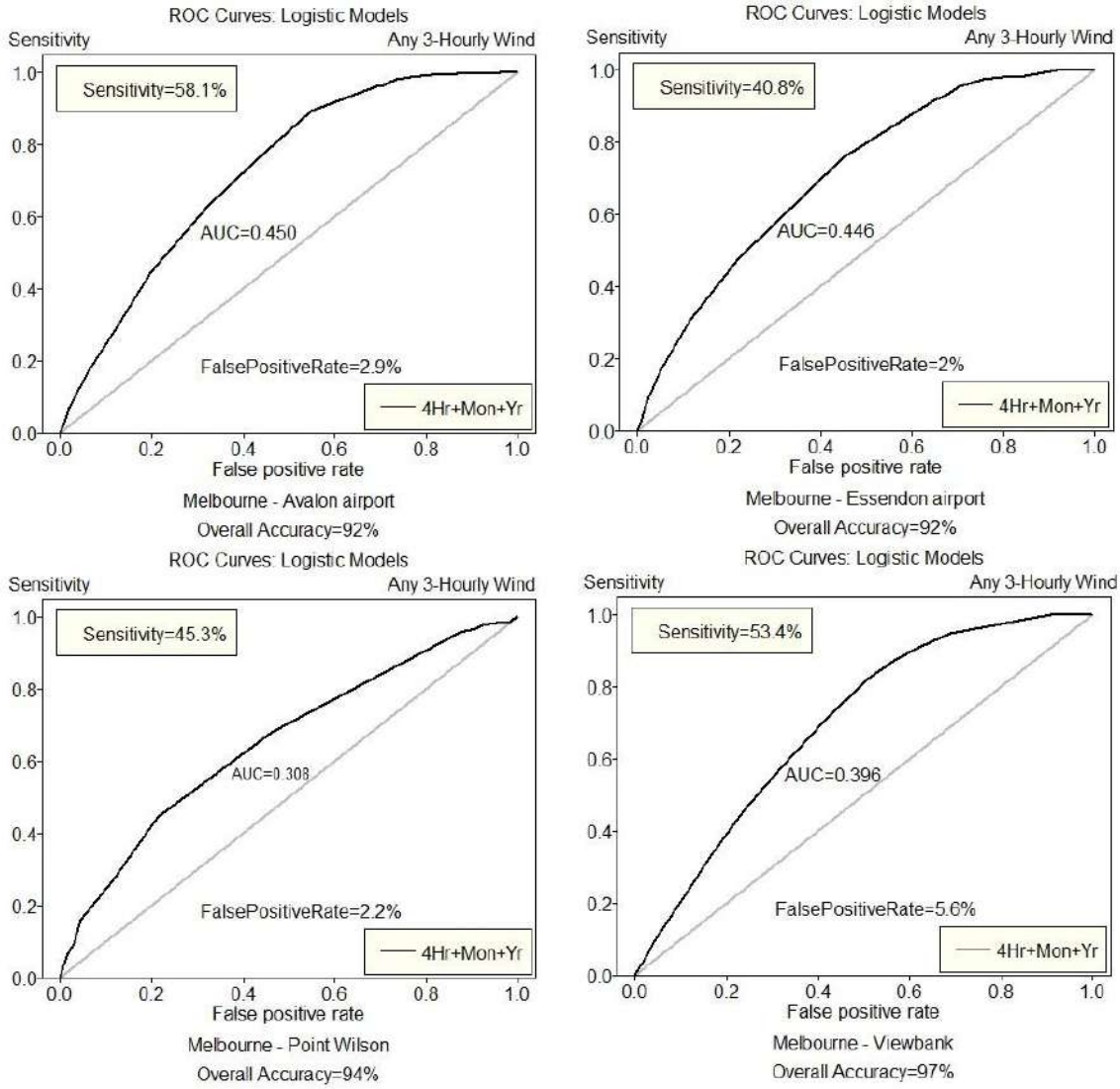

Fig. 1: ROC curves from the logistic regression models for the 3 hours of wind at 4 stations in Melbourne, Australia.

the month of the year (12 factors), and the third predictor was the year (5 factors). There were 26 parameters including the constant term in the model. The parameters were highly significant and influential in the model as displayed in Fig. 2 and Fig. 3. The ROC curve (Fig. 1) revealed area under the curve (AUC) values of 0.450, 0.446, 0.308, and 0.396 for the four stations.

The overall accuracy at each station on correctly classifying the occurrence or non-occurrence of wind were 92%, 92%, 94%, and 97%, the true positive rates were 58.1%, 40.8%, 45.3%, and 53.4%, and the false positive rates were 2.9%, 2%, 2.2%, and 5.6% respectively.

Fig. 2 and Fig. 3 show the patterns of wind prevalence for the day, month and year, and the crude percentage for the four stations. The horizontal red line denotes the overall percentage of wind prevalence at each station. The plot of the wind prevalence revealed that the patterns for the day and month were significantly different from the overall percentage for all stations.

At Avalon Airport and Essendon airport, there were quite similar patterns of wind prevalence with an overall average percentage of approximately 70%. During the day, the highest wind prevalence occurred from 12 PM to 3 PM with around 90%. The monthly wind prevalence was below the average from March to June. The yearly wind prevalence did not differ from the overall percentage.

At the Point Wilson station, the overall percentage of wind prevalence (over 80%) was higher than the other three

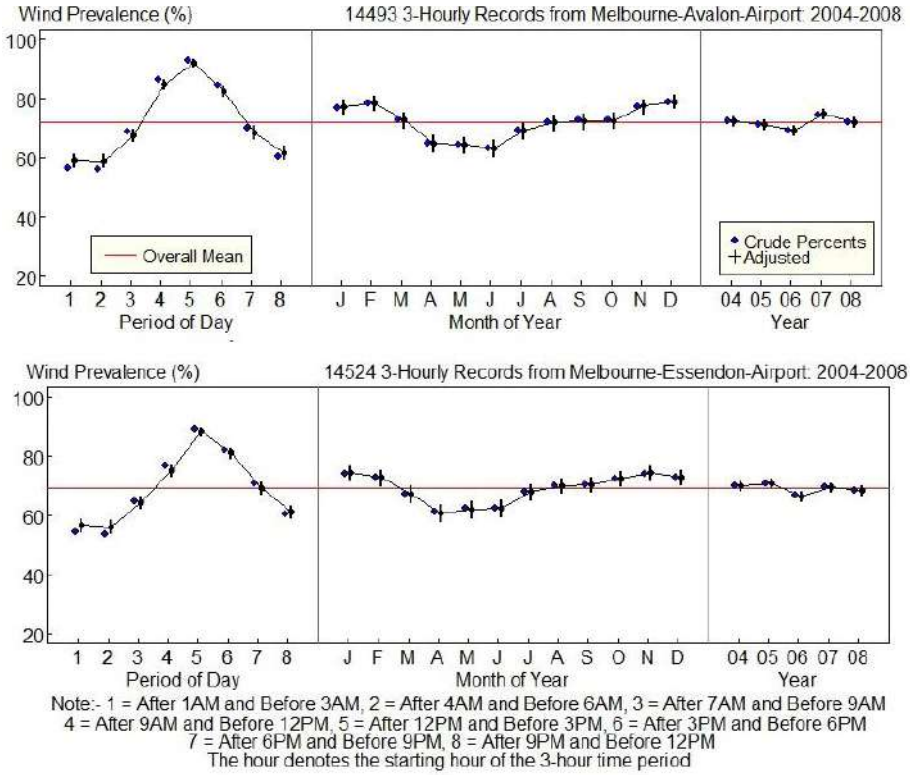

Fig. 2: Patterns of wind prevalence at Avalon Airport and Essendon Airport.

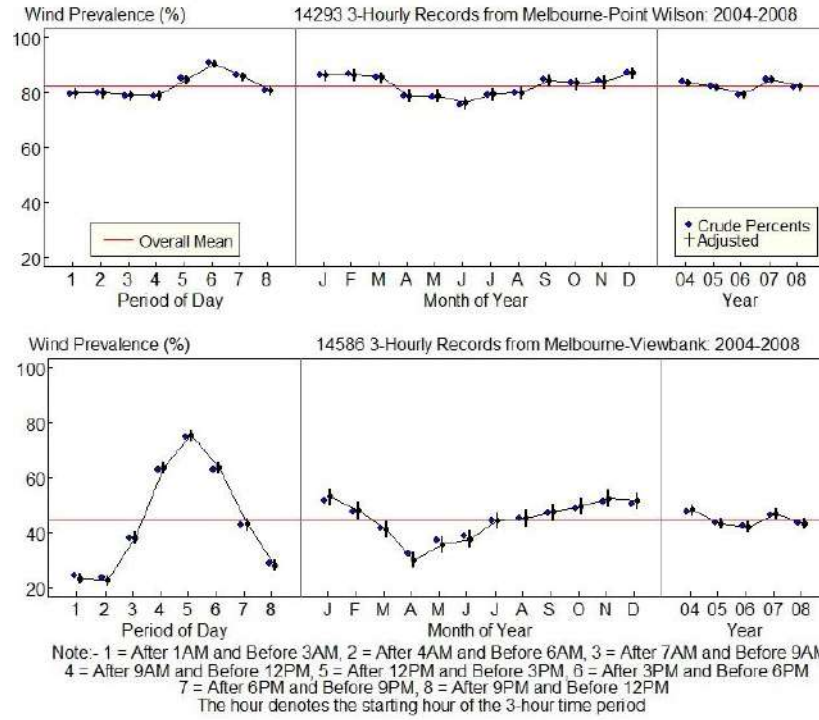

Fig. 3: Patterns of wind prevalence at Point Wilson and Viewbank.

stations. The prevalence of wind was below the average from 1 AM to 12 PM and peaked during 3 PM to 6 PM. Wind prevalence rates were observed to be less than the overall mean from April to August. The prevalence decreased steadily to attain a minimum (75%) in June and increased gradually to attain a maximum (85%) in December. At the Viewbank station, the overall percentage of wind prevalence (40%) was lower than the other three stations. However, the pattern for the day, month and year were similar to Avalon and Essendon airports.

Fig. 4 and Fig. 5 reveal the pattern of gusty wind prevalence for the day, month and year and the crude percentage for the selected stations. The horizontal line denotes the overall percentage of wind gust prevalence. The results at all stations were similar to the wind prevalence.

For the stations at Avalon airport, Essendon airport and Viewbank, there were similar patterns of gusty wind prevalence. The highest prevalence occurred from 12 PM to 3 PM. The monthly gusty wind prevalence was below the average from March to June and the yearly prevalence were not different from the overall percentage.

At the Point Wilson station, the prevalence of gusty wind was below the average from 1 AM to 12 PM and peaked during 3 PM to 6 PM. Wind gust prevalence rates were observed to be less than the overall percentage from April to June and decreased steadily to attain a minimum of 55% in May and increased gradually to attain a maximum of 70% in December. The yearly gusty wind prevalence patterns for the selected stations were not significantly different from the overall mean between 2004 and 2005.

Trends and patterns of 3-hourly wind speeds of at least 3 km/h for all stations were determined using linear regression models (model 2). The model contained the same 3 predictors as the logistic regression models, period of the day, month of the year, and year. The results are displayed using graphical methods as shown in Fig. 7 and Fig. 8.

The quantile-quantile (Q-Q) plot (Fig. 6) illustrates that the residuals from the model are approximately normally distributed. However, there were some deviations from both the lower and upper tails of the model. This deviation may

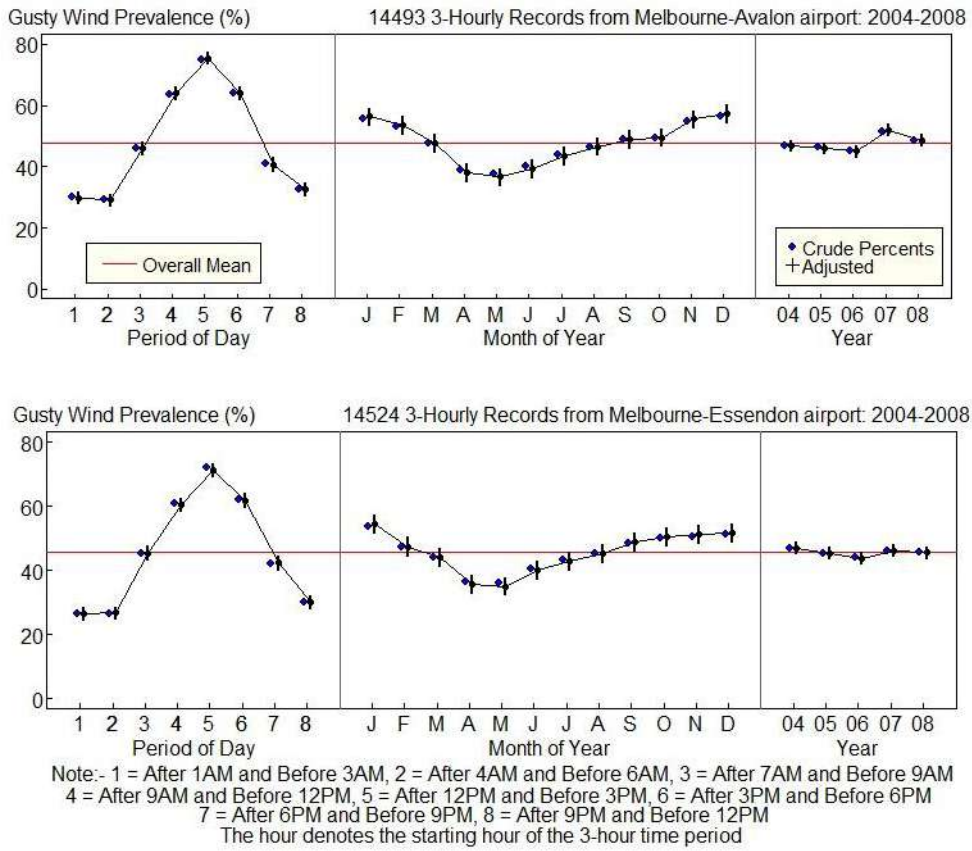

Fig. 4: Patterns of wind gusts at Avalon Airport and Essendon Airport.

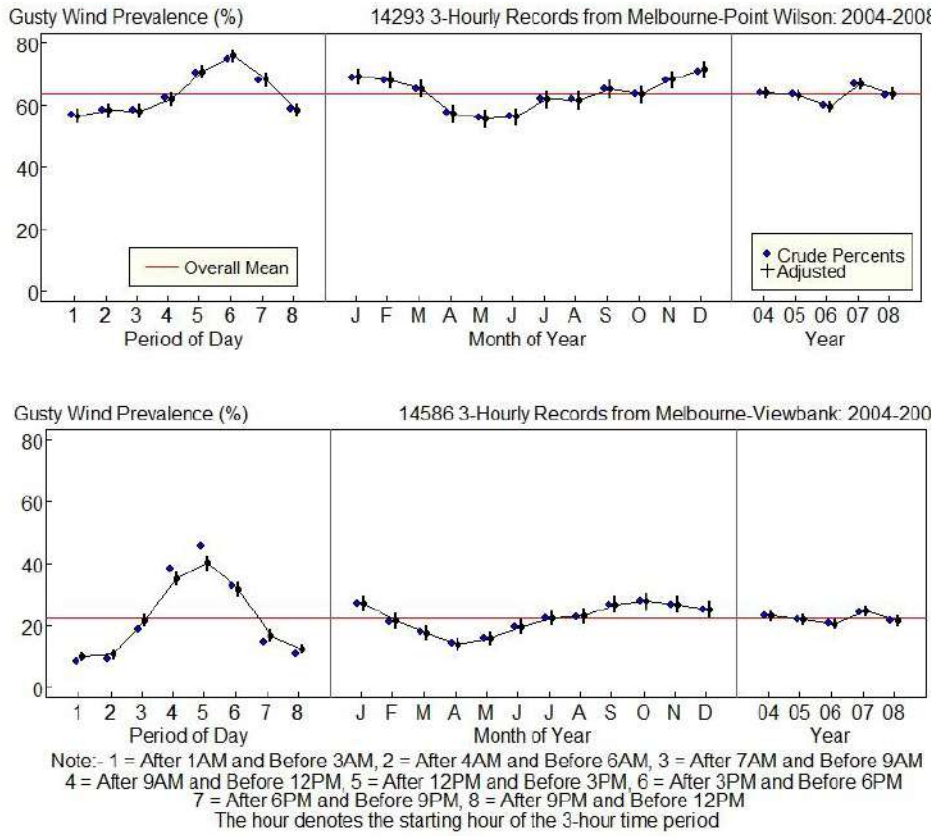

Fig. 5: Patterns of wind gusts at Point Wilson and Viewbank.

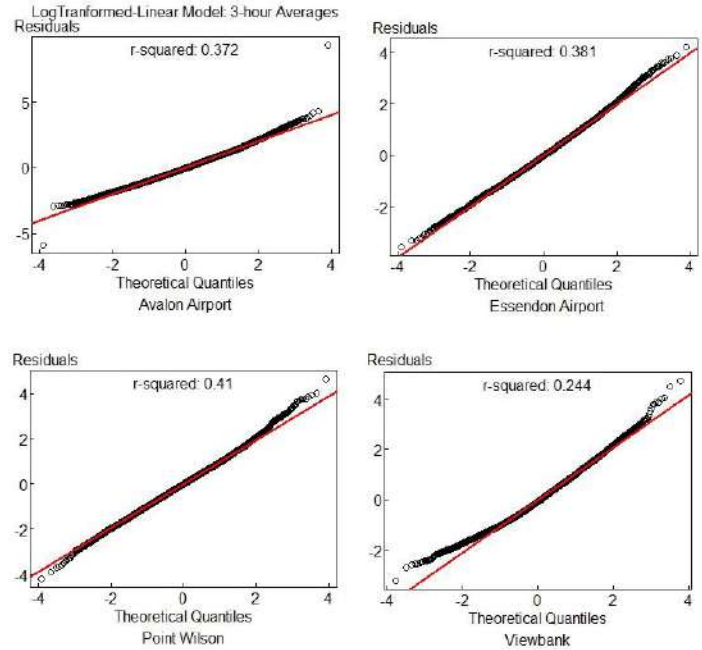

Fig. 6: Q-Q plots for linear models of wind speed at Avalon airport, Essendon airport, Point Wilson, and Viewbank.

be due to extreme values in the data and some variations that could not be explained by the predictors.

Fig. 7 and Fig. 8 show the wind speed trends for the day, the month of the year, and the year and the crude mean for the four stations. The horizontal red line denotes the overall mean wind speed. The wind speed trends for the day were significantly different from the overall mean.

Four distinct trends were observed for the wind speed at the four stations. At Avalon airport, there was a significant increasing trend from 4 AM to 3 PM. A declining trend was apparent from 3 PM to midnight. The wind speed was higher than the overall mean from 7 AM to 6 PM. The wind speed trends were observed to be higher than the overall mean from September to January. The yearly wind speed trend was mostly below the overall mean from 2004 to 2006, but above the overall mean between 2007 and 2008 where the maximum occurred.

At Essendon Airport, the highest wind speed occurred during 9 AM to 12 PM. Declining trends were apparent from noon to midnight. The wind speed trends were observed to be higher than the overall mean from September to January. The wind speed decreased gradually to attain a minimum in May and increased steadily to attain a maximum in September. The yearly wind speed trend was not different from the overall mean.

At Point Wilson, the wind speed was higher than the overall mean from 9 AM to 6 PM. Declining trends were apparent from 3 PM to midnight. The wind speed trends were observed to be higher than the overall mean from July to January. Wind speeds decreased gradually to attain a minimum in May and increased steadily to attain a maximum in December. The yearly wind speed trend was mostly below the overall mean but above the overall mean in 2007 where the maximum occurred.

At Viewbank station there was a significant increasing trend with the highest wind speeds occurring during 9 AM to 3 PM. The maximum wind speed occurred in September and the yearly wind speed was highest in 2007.

DISCUSSION

The 3-hourly wind and wind gust patterns of four stations at Essendon airport, Avalon airport, Point Wilson, and

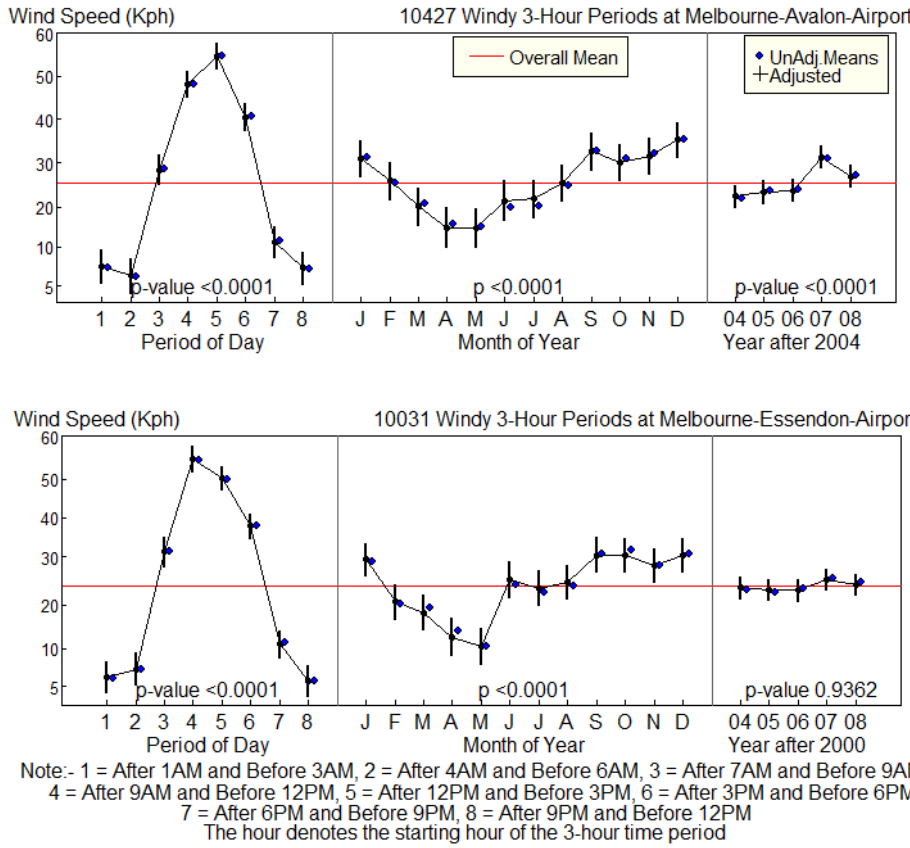

Fig. 7: Wind speed trends at Avalon Airport and Essendon Airport.

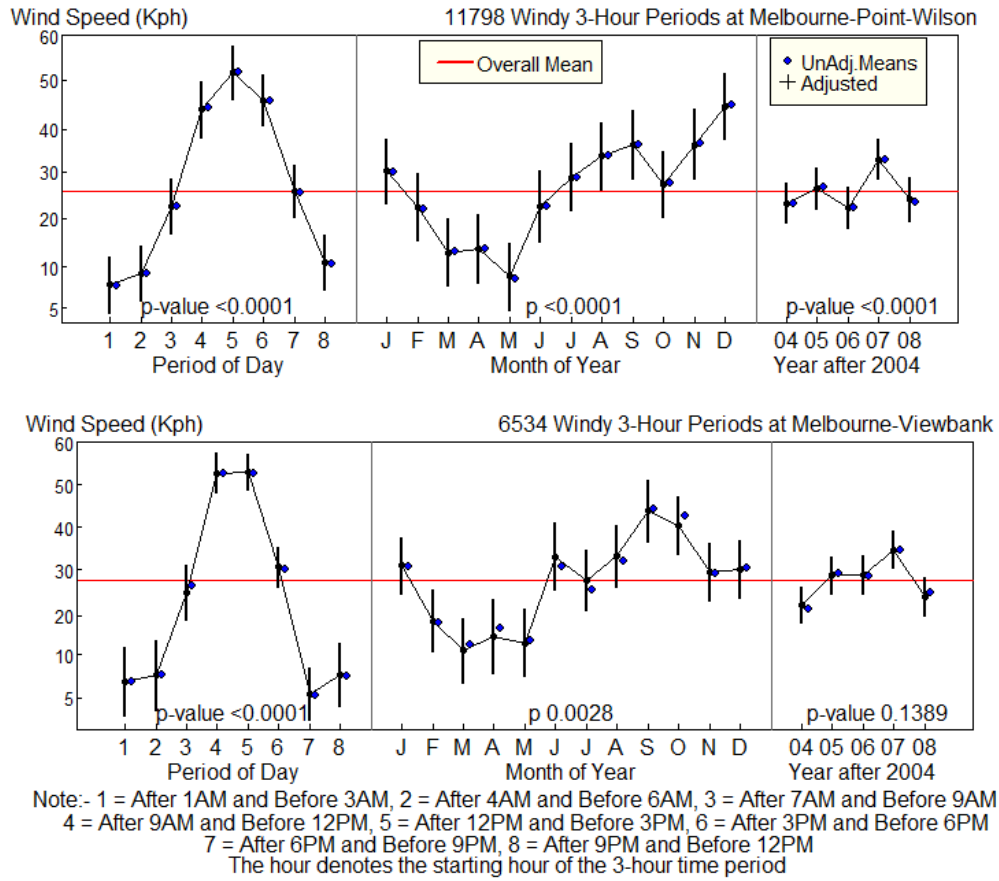

Fig. 8: Wind speed trends at Point Wilson and Viewbank.

Viewbank, Australia during 2004-2008 were similar. The wind prevalence was above the overall average between 9 AM and 6 PM at Essendon airport, Avalon airport, and Viewbank, and from 12 PM to 9 PM at Point Wilson. The wind prevalence was higher than the overall average from September to February and lower than the overall average from March to June at all four stations. This finding confirmed that spring is the windiest time of the year (Carmoday 2016). These observed patterns were due to variability of the surface winds produced by the Asian Monsoon, seasonal variations in the westerly winds in both hemispheres (Hemer et al. 2010), and temporal atmospheric circulation variations (Troccoli et al. 2010) on the north and eastern Australian region.

The linear regression models revealed that the pattern of wind speed among the four stations was not different. The overall mean wind speeds ranged between 25-30 km/h with maximum speeds ranging between 50-60 km/h. The wind speeds were higher than the overall mean during 7 AM to 6 PM at Avalon and Essendon airports and during 9 AM to 6 PM at Point Wilson and Viewbank stations.

Wind speeds were higher than the overall mean from September to January and slowly decreased with a minimum wind speed occurring between March and May at all stations. Wind speeds were highest in 2007. Victoria's climate is heavily influenced by coastal force winds, which occur frequently between June and November. During these months, large pressure gradients between high pressures over the continent and deep depressions to the south produce gale-force and occasionally storm-force westerly winds (BOM 2020). In Melbourne, autumn months have lighter winds than other months (BOM 1968).

This study model of 3-hourly wind data using common climatic predictors which described wind trends and patterns. Further investigation can consider other variables that can affect wind patterns and trends such as air pressure, solar radiation, and humidity.

ACKNOWLEDGEMENT

This work was supported by the Higher Education Research Promotion and Thailand's Education Hub for Southern

Region of ASEAN Countries Project Office of the Higher Education Commission under grant no. THE/033. We thank Emeritus Prof. Dr. Don McNeil for his supervision. Thanks to the Centre of Excellence in Mathematics, Commission on Higher Education, Thailand.

REFERENCES

Bett, P.E., Thornton, H.E. and Clark, R.T. 2013. European wind variability over 140 yr. Advances in Science and Research, 10(1): 51-58.

Bureau of Meteorology (BOM) 1968. Climatic Survey: Region 10 - Port Phillip, Victoria, Melbourne.

Bureau of Meteorology (BOM) 2011. Climate, Available at: http://www.bom.gov.au/jsp/ncc/climate_average wind-velocity/index.jsp [January 25, 2017].

Bureau of Meteorology (BOM) 2020. Climate of Victoria, http://www.weather-climate.com/victoria.html [March 31, 2020].

Carmody, B. 2016. Melbourne weather: Why spring has been so windy. https://www.theage.com.au/national/victoria/melbourne-weather-why-spring-has-been-so-windy-20161102-gsg0h5.html [April 30, 2020].

Chen, L., Li, D. and Pryor, S.C. 2013. Wind speed trends over China: quantifying the magnitude and assessing causality. International Journal of Climatology, 33(11): 2579-2590.

Cheng, C.S., Lopes, E., Fu, C. and Huang, Z. 2014. Possible impacts of climate change on wind gusts under downscaled future climate conditions: Updated for Canada. Journal of Climate, 27(3): 1255-1270.

Coppin, P.A., Ayotte, K.A. and Steggel, N. 2003. Wind energy research unit CSIRO land and weather. Wind Energy Research Unit, Australia.

Csavina, J., Field, J., Félix, O., Corral-Avitia, A.Y., Sáez, A.E. and Betterton, E.A. 2014. Effect of wind speed and relative humidity on atmospheric dust concentrations in semi-arid climates. Science of the Total Environment, 487(1): 82-90.

Hemer, M.A. 2010. Historical trends in Southern Ocean storminess: Long‐term variability of extreme wave heights at Cape Sorell, Tasmania. Geophysical Research Letters, 37(10): 1-5..

Geer, I.W. 1996. Glossary of Weather and Climate : With Related Oceanic and Hydrologic Terms. Collection Atmosphere.

Glickman, T.S. and Zenk, W. 2000. Glossary of Meteorology, American Meteorological Society, Boston, USA.

Graham, A. and Antony K. 2014. The Romans: An Introduction. Routledge.

Jamaludin, A.R., Yusof, F., Kane, I.L. and Norrulasikin, S.M. 2016. A comparative study between conventional ARMA and Fourier ARMA in modeling and forecasting wind speed data. In Advances in Industrial and Applied Mathematics: Proceedings of 23rd Malaysian National Symposium of Mathematical Sciences (SKSM23) (Vol. 1750, p. 60022).

Klink, K. 1999. Trends in mean monthly maximum and minimum surface wind speeds in the coterminous United States, 1961 to 1990. Climate Research, 13(3): 193-205.

Mitchell, S.J. 2012. Wind as a natural disturbance agent in forests: a synthesis. Forestry, 86(2): 147-157. doi:10.1093/forestry/cps058.

Mohanan, A.H., He, Y., Mcfarlane, N. and Dai, A. 2011. The probability distribution of Land surface wind speeds. Journal of Climate, 24(15): 3892-3909.

Nchaba, T., Mpholo, M. and Lennard, C. 2016. Long-term austral summer wind speed trends over southern Africa: Austral summer wind speed trends over Southern Africa. International Journal of Climatology, 37(6): 2850-2862.

R Development Core Team 2008. A Language and environment for Statistical Computing, R Foundation for Statistical Computing, Vienna, Austria.

Schindler, D., Bauhus, J. and Mayer, H. 2012. Wind effects on trees. European Journal of Forest Research, 131(1): 159-163.

Tongkumchum, P. and McNeil, D. 2009. Confidence intervals using contrasts for regression model. Songklanakarin Journal of Science and Technology, 31(2): 151-156.

Troccoli, A., Muller, K., Coppin, P., Davy, R., Russell, C. and Hirsch, A.L. 2012. Long term wind speed trends over Australia. Journal of Climate, 25(1): 170-183.

Westin, L.K. 2001. Receiver operating characteristic (ROC) analysis: Evaluating discriminance effects among decision support systems. UMINF report, Department of Computer Science, Umea University, Sweden: Available from: http://www.cs.umu.se/research/reports/2001/018/part1.pdf [December 08 2017]

Wheeler, D. and Clive W. 2004. From calm to storm: the origins of the Beaufort wind scale. The Mariner's Mirror, 90(2): 187-201.

Nature Environment and Pollution Technology
An International Quarterly Scientific Journal

p-ISSN: 0972-6268
(Print copies up to 2016)
e-ISSN: 2395-3454

Vol. 20 | No. 2 | pp. 675-683 | 2021

Original Research Paper

https://doi.org/10.46488/NEPT.2021.v20i02.026

Open Access Journal

Resource Allocation Strategy and Soil Driving Factors of Vegetation Concrete Restoration System Under Co-Operating Environment

Mingyi Li*(**), Wennian Xu*(**), Zhenyao Xia*(**), Yanyan Shao*, Yueshu Yang* and Hai Xiao*(**)†

*Key Laboratory of Geological Hazards on Three Gorges Reservoir Area (China Three Gorges University), Ministry of Education, Yichang, 443002, People's Republic of China

** Engineering Research Center of Eco-environment in Three Gorges Reservoir Region, Ministry of Education, China Three Gorges University, Yichang, 443002, People's Republic of China

†Corresponding author: Hai Xiao; oceanshawctgu@163.com

Nat. Env. & Poll. Tech.
Website: www.neptjournal.com

Received: 29-05-2020
Revised: 23-07-2020
Accepted: 31-07-2020

Key Words:
Disturbed slope
Vegetation concrete
Ecological restoration
Biomass
Soil factor

ABSTRACT

The ecological function optimization strategy of vegetation directly affects the self-stability and engineering sustainability of the vegetation concrete ecological restoration system, which is the key to the successful restoration of an ecosystem. To clarify the survival strategies of slope protection plants and their response mechanisms to the soil environment in the process of vegetation concrete ecological restoration, the resource allocation strategies and soil driving factors of typical slope protection plants, such as *Cynodon dactylon* (Linn.) Pers. and *Indigofera amblyantha*, in a co-operation environment mode, were investigated by controlled simulation experiments. The results showed that (1) the co-operating environmental model had a significant effect on the biomass (leaf, stem and root) and root shoot ratio of slope protection vegetation; (2) the sensitivity of plant biomass in the co-operating environmental model was leaf biomass ratio > root biomass ratio > stem biomass ratio, and the most sensitive organ was the leaf; (3) a common allometric growth index for the plants of all slopes existed, the root and leaf grew at the same rate, and the plant roots and stems showed allometric growth with the synergistic effect of rainfall and slope; (4) the total nitrogen content of soil had a significant correlation with the vegetation R/S (root shoot ratio) ($p < 0.05$) due to the synergistic effect of vegetation type and slope, while the total phosphorus content of the P3 slope had a significant negative correlation with the vegetation R/S ($p < 0.05$). The co-operating environmental model significantly affected the spatial distribution of vegetation biomass and had the greatest impact on leaf biomass. The contents of soil nitrogen and phosphorus were the key soil driving factors that affected the distribution pattern of plant biomass. The resource allocation characteristics of different vegetation and its response to soil factors had species specificity.

INTRODUCTION

With the increasing attention to the ecological environment, the former extensive slope protection and engineering construction mode cannot meet the requirements of ecological green sustainable development. Vegetation concrete slope treatment method has realized the organic combination of mechanical stability and ecological function, it has become one of the most extensively applied ecological slope protection substrate (Wang et al. 2020, Xu et al. 2012).

The growth of vegetation, and positive and stable succession of its community are key to the success of ecosystem restoration (Norton & Young 2016). However, the stress factors in the slope vegetation restoration system are often unfavourable to plant growth, which hinders ecological restoration (Zhang et al. 2017). The optimal allocation of the resources of plants in adverse conditions is a basic strategy for protecting plants against environmental stress (Fang et al. 2012, Cao & Chen 2015). The allocation strategy of plant biomass is regulated by multiple factors (Daniel et al. 2014). Changes in environmental factors often affect the absorption and transportation of nutrients by changing the physical and chemical properties of soil, which causes a difference in the growth strategies between the root system and the aboveground part of a plant. There are few studies on the influence of a co-operating environmental model on the vegetation resource allocation strategy and soil driving mechanism of vegetation concrete ecological restoration.

In this paper, resource allocation strategy and soil driving factors of vegetation concrete restoration system under the influence of slope, precipitation and vegetation type is investigated. The purpose of this study is to solve three scientific problems: (1) Does specificity exist in the biomass allocation of different functional plants? (2) What is the relationship between the heterogenic growth rate of slope protection plants and co-environmental factors?

(3) What are the strategies of plant biomass allocation and the response mechanism to the soil environment in the process of ecological restoration? The study of the response mechanism of a vegetation resource allocation strategy to soil factors and allometric growth relationship has guiding significance for clarifying the ecological function optimization strategy of vegetation, consolidating and improving the restoring ecological system function, and realizing the stability and sustainability of slope restoration.

MATERIALS AND METHODS

Materials

The experimental site was located in China Three Gorges University (30°43' N; 111°18' E). Typical vegetation, *Cynodon dactylon* (Linn.) pers. and *Indigofera amblyantha*, which are commonly employed in a slope protection project, were chosen as the experimental vegetation. The test soil is the Yellow Soil from the surface of the cultivated land of Nanjinguan slope of Yichang City. According to the local rock content distribution, the test rock was obtained from Xiazhou Avenue in Yichang City, and the material was sandstone.

Experimental Design

Seven experimental models were constructed based on different environmental modes of vegetation type (combination of herbs, shrubs and grass irrigation), slope (45°,60° and 75°) and precipitation (10 mm, 15 mm, and 20 mm). The size of each model was 2 m × 2 m; the thickness of the argillaceous sandstone was 20 cm, and the thickness of vegetation concrete was 10 cm. There is a certain proportion on the mass of each component during the vegetation concrete collocation. When 100 kg of planting soil is used, 6 kg, 8 kg and 3 kg of cement, organic matter and activation additive are used respectively. The vegetation concrete is laid in two layers of base (8 cm) and surface layer (2 cm). There are no plant seeds in the base layer, and the surface layer is planted with single or mixed plant seeds according to 15 g/m^2. Table 1 gives the design of the test group and Fig. 1 shows the structural diagram of the slope system.

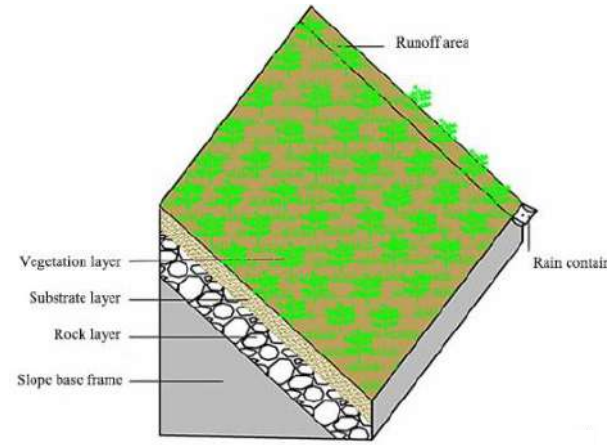

Fig. 1: Structural diagram of the slope system.

Experimental Method

Experimental determination: The experiment started in March 2018, and samples were collected once in the middle of March, June, September and December every year (the first year is represented by "I"; and the second year is represented by "II"). The ring knife method was employed for soil sampling. Soil organic carbon was determined by the $K_2Cr_2O_7$ volumetric method and external heating method. Total nitrogen and total phosphorus were determined by the SKALAR SAN $^{++}$ continuous flow analyser. The aboveground parts of the plant were sampled by the quadrat harvesting method, while the underground parts of the plant roots were sampled by the root drilling method. After sampling, the samples are weighed fresh, dried at 80°C to a constant weight and re-weighed. The root, stem and leaf were treated with 5 replicates each.

Root shoot ratio (R/S), Leaf mass ratio (LMR), Stem biomass (SMR), Root mass ratio (RMR) and Coefficient of

Table 1: Test group design.

Number	Precipitation per week/mm			Vegetation allocation mode			Slope/°		
	10	15	20	Grass	Grass + shrubs	Shrub	45	60	75
P1		•		•				•	
P2		•				•		•	
P3		•			•			•	
P4			•		•			•	
P5	•				•			•	
P6		•			•		•		
P7		•			•				•

Variation (CV) can be estimated by using Equation 1, 2, 3, 4 and 5, respectively.

$$R/S = RB/AB \quad \ldots(1)$$

$$LMR = LB/TB \quad \ldots(2)$$

$$SMR = SB/TB \quad \ldots(3)$$

$$RMR = RB/TB \quad \ldots(4)$$

$$CV = SD/AV \times 100\% \quad \ldots(5)$$

Where, *RB* is Root biomass of Vegetation, *AB* is Aboveground biomass of Vegetation, *LB* is Leaf biomass of Vegetation, *TB* is Total biomass of Vegetation, *SB* is Stem biomass of Vegetation, *SD* denotes Standard deviation, *AV* denotes Average value.

Allometric growth analysis: The allometric growth relationship can be expressed as $Y = \beta \times X^{\alpha}$, where Y is a biological feature or function, β is a standardized constant, X is the individual size, and α is the heterogenic growth index. $\alpha = 1$ is the isokinetic relationship, $\alpha \neq 1$ is the allometric relationship. To determine the parameters of allometric growth, the power function should be transformed into the form $1gY = 1g\beta + \alpha \times 1gX$, and the reduced major axis (RMA, model type II) regression method should be employed to calculate the index, 95% confidence interval (95% CI) and determination coefficient (R^2) of the regression model. The logarithmic α is the slope of the linear regression after the power function logarithm, and 1gβ is the intercept of the linear regression. All these calculations were completed by SMARTR software.

Statistical analysis: The data were analysed by Excel and SPSS 22.0. Duncan analysis was performed to test the average difference and significance level of biomass for different vegetation types, slopes and precipitation models.

RESULTS

Leaf Biomass

A multivariate analysis of variance showed that the slope, vegetation type and precipitation had a significant effect on the leaf biomass of slope protection plants ($p < 0.05$). The leaf biomass of slope protection plants increased significantly with an increase in the vegetation type and reached the maximum for the condition of grass and shrub mixed planting, while the difference was not significant in the vegetation single planting mode, which indicated that the leaf biomass of plants was more sensitive to the vegetation type for the same slope and precipitation. The biomass of plant leaves increased significantly with the decline of the slope, especially for the condition of the high slope. Leaf biomass increased with an increase in precipitation; however, the increase was not obvious compared with the slope and vegetation type. The biomass of plant leaves on each slope increased gradually with time, except in winter, and reached the highest value and increased the most in autumn (Fig. 2).

Stem biomass

The synergism of the slope and precipitation had a significant effect on the stem biomass of slope protection plants ($p < 0.05$) (Fig. 3). The stem biomass of plants increased with an increase in rainfall, reached the maximum value when the rainfall was 20 mm. The stem biomass decreased with an increase in slope and decreased significantly when the slope was higher than 60°. The biomass of plant stem was the largest for the condition of grass and shrub mixed planting.

Root Biomass

Vegetation type and precipitation had a significant effect

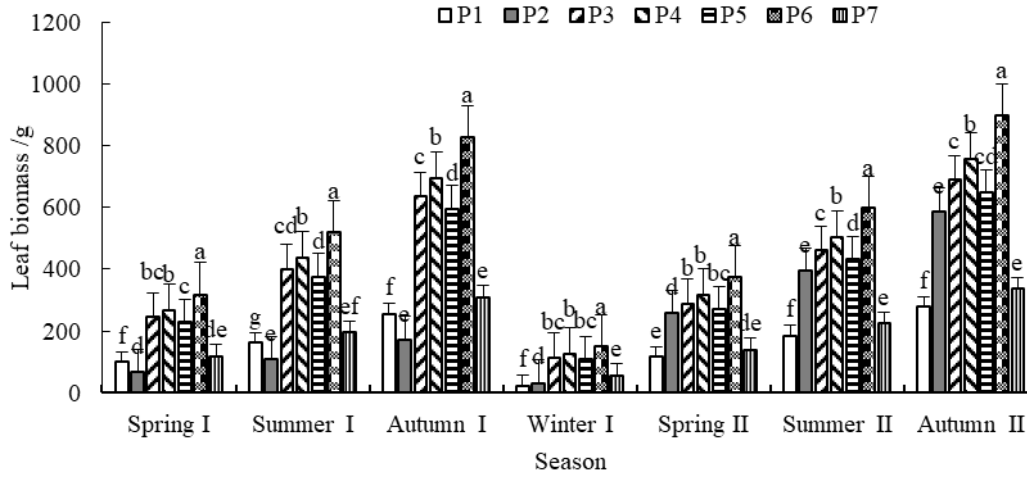

Fig. 2: Interaction of slope, vegetation type and precipitation on leaf biomass of slope protection plants.

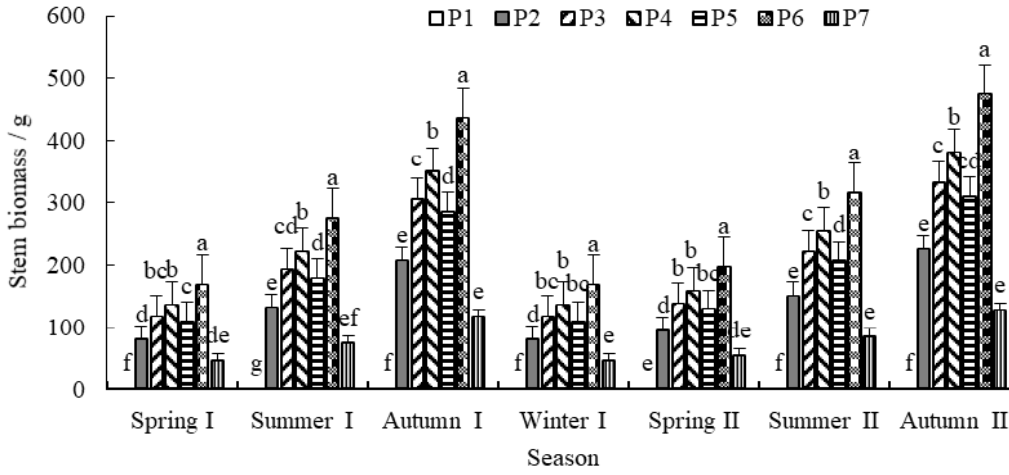

Fig. 3: Interaction of slope, vegetation type and precipitation on stem biomass of slope protection plants.

on root biomass ($p < 0.01$) in Fig. 4. The biomass of each slope root increased significantly with an increase in vegetation type and precipitation but decreased significantly with an increase in slope gradient. The root biomass of slope protection plants increased gradually with time, and the increase in amplitude was the largest in the condition of grass and shrub mixed planting and 10 mm precipitation, and was sensitive to water changes with the same slope and vegetation type model. For the same vegetation type and precipitation mode, the root biomass and increase range were the largest when the slope was 45°.

Root Shoot Ratio (R/S)

The synergistic effect of slope, vegetation type and precipitation had a significant effect on the slope plant R/S ($p < 0.05$). In Fig. 5 R/S was greater than 1 in the shrub single planting mode with a slope of 75° and less than 1 in other modes and reached its maximum value in winter.

With the same slope and precipitation model, the R/S of the grass and shrub mixed slope ranges from 0.55-0.92, the grass single slope is the smallest, and the shrub single slope reaches a maximum. The R/S is the largest at 15-js (slope with 15 mm precipitation), and the root shoot distribution was more sensitive to low water. The R/S decreased and then increased with an increase in slope, and the resource acquisition of the root system is larger at a high slope.

Sensitivity Analysis of Biomass Allocation of Vegetation under Co-operating Environment

According to Table 2, the variation coefficient of leaf biomass

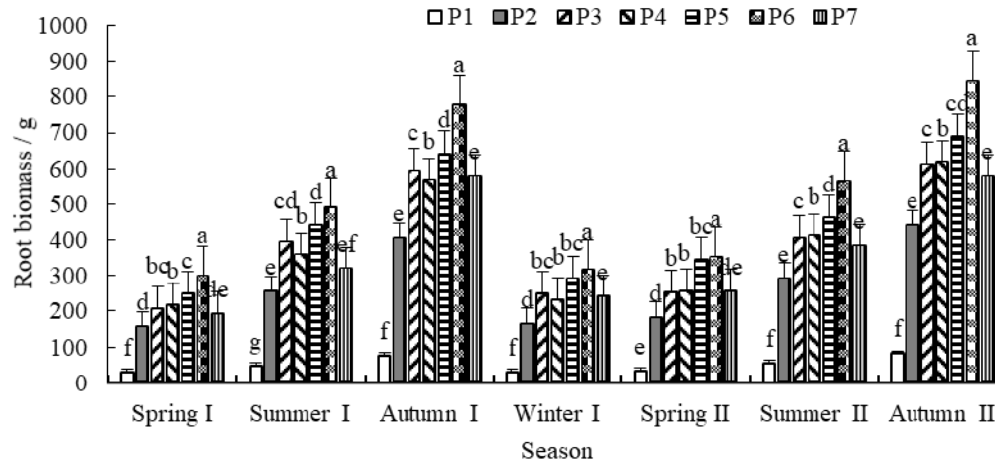

Fig. 4: Interaction of slope, vegetation type and precipitation on root biomass of slope protection plants.

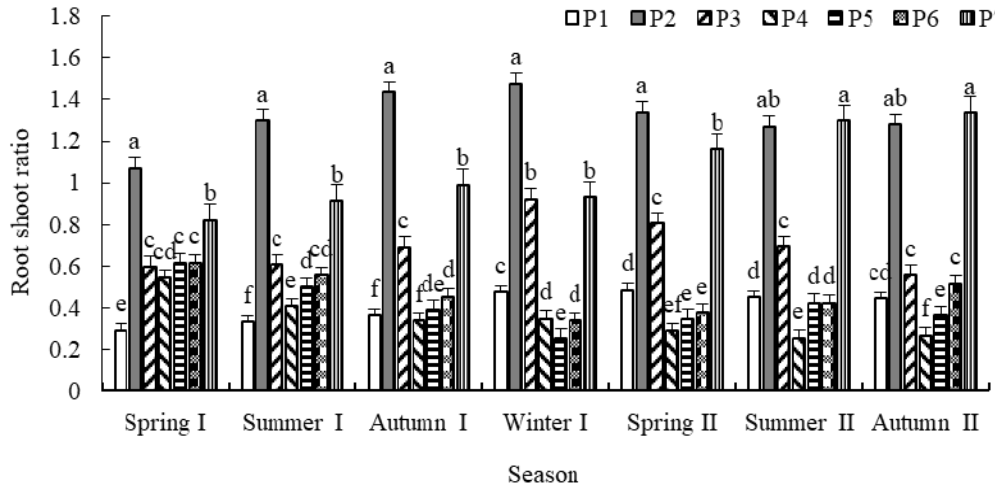

Fig. 5: Interaction of slope, vegetation type and precipitation on R/S of slope protection plants.

ratio (LMR) in the pure grass slope with vegetation type was the largest, that is, the slope plant leaves were the most sensitive to the synergistic effect of slope, vegetation type and precipitation. The variation coefficient of the biomass ratio of each organ with the change in precipitation was LMR > root biomass ratio (RMR)> stem biomass ratio (SMR), that is, the sensitivity of each organ of slope vegetation was leaf > root > stem for the synergistic effect of slope, vegetation type and precipitation. With an increase in slope, the coefficient of variation of the SMR with precipitation and vegetation type was unchanged, which indicates that the SMR was relatively stable for the synergistic effect of slope, vegetation type and precipitation.

Allometric Growth Relationship of Aboveground and Underground Biomass under Co-Operating Environment

Through the biomass analysis of seven slope plant organs, a significant difference between them ($p < 0.05$) was observed (Fig. 6). According to the analysis of the BGB (Below ground biomass)-ALB (Above ground leaf biomass) correlation growth index, the allometric growth indexes of the seven slopes were 1.3567, 2.0096, 1.2518, 1.3283, 1.4993, 1.3589 and 1.4099. According to the analysis of the ASB (Aboveground stem biomass)-BGB correlation growth index, the allometric growth indexes α of six slopes, except P1, were 0.8552, 0.8769, 0.8932, 0.7527, 0.8826 and 0.7077. According to the analysis of the ASB-ALB correlation growth index, the abnormal growth index α of six slopes, except P1, were 1.7781, 1.2069, 1.2188, 1.2040, 1.2318 and 1.1282. The results of the constant growth test showed that the biomass growth rate of underground and aboveground plants and the root and leaf biomass of each slope showed an equal proportion relationship. The root and stem biomass ratio of the P5 and P7 slope was 0.75 in the 95% confidence interval, which revealed α = 3/4 constant growth relationships, that is, the distribution rate of root biomass of the P5 and P7 slope was lower than that of stem biomass, while the biomass of roots and stems of the slopes of P2, P3, P4 and P6 did not conform to the allometric growth relationship with a 3/4 power index. The growth index was close to the theoretical value of 1 at the upper limit of the 95% confidence interval.

Table 2: Sensitivity of biomass allocation of slope vegetation under co-operating environment.

Variables	Treatment						
	P1	P2	P3	P4	P5	P6	P7
RMR	2.26	5.17	3.74	3.52	3.81	3.81	4.51
SMR	0.00	2.64	2.03	2.17	2.00	2.14	1.51
LMR	7.74	2.19	4.23	4.31	4.19	4.05	3.99

Soil Driving Force Analysis of Vegetation Biomass Distribution (R/S) in Slope for Co-Operating Environment

Through the correlation analysis of seven slope vegetation R/S with soil nutrients, including N, P, K and organic matter, the TN content of slope soil had a significant positive correlation with the vegetation R/S of P2 and P3 ($p < 0.05$) but did not have a significant positive correlation with the vegetation R/S of P1. The TN content of slope soil did not have a significant negative correlation with the vegetation R/S of P4, P5 and P6 but had a significant negative correlation with the vegetation R/S of P7 ($p < 0.01$). Except for P3, no

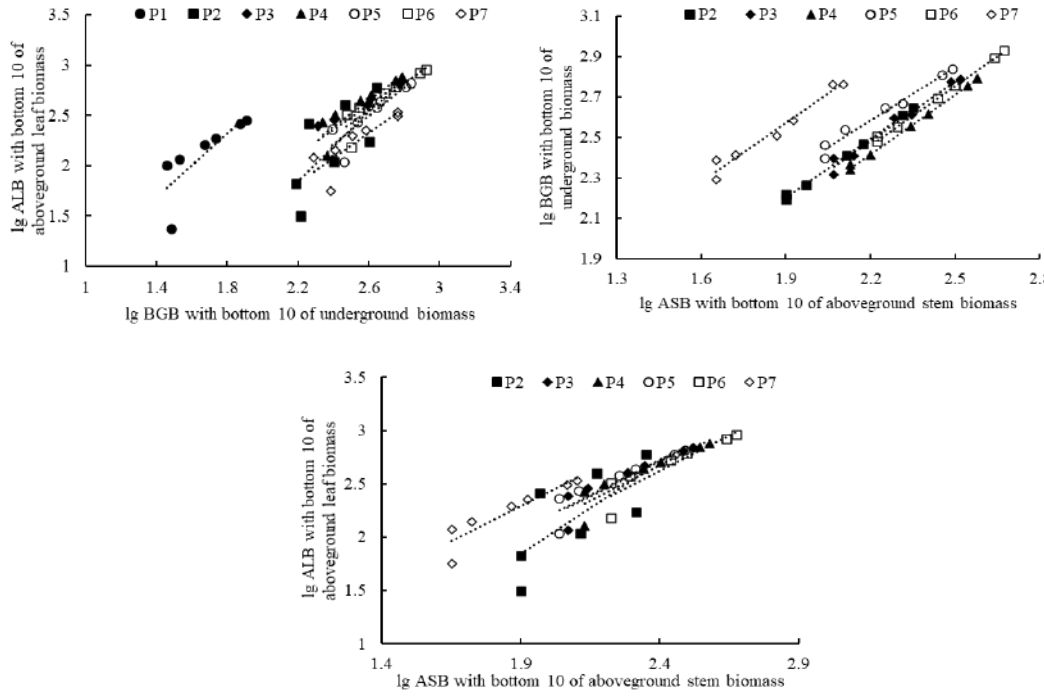

Fig. 6: RMA linear fitting relationship of slope plants ALB-BGB, BGB-ASB and ASB-ALB in double logarithmic coordinates.

significant negative correlation was obtained between the TP content of soil and the R/S of slope vegetation. For the conditions of P3, a significant negative correlation was observed between the total phosphorus content of soil and the R/S of slope vegetation ($p < 0.05$). No significant negative correlation was obtained between the TK content of soil and the R/S of seven types of slope vegetation ($p > 0.05$). A significant negative correlation between the soil organic matter content of the P4 slope and the R/S of vegetation was observed. No significant positive correlation between the content of soil organic matter and the vegetation R/S ($p > 0.05$) was obtained in P2 and P3, and no significant negative correlation between the content of the soil organic matter and the vegetation R/S ($p > 0.05$) was observed in P1, P5, P6 and P7 (Table 3) .

Table 3: Correlation between N, P, K content of slope soil and vegetation R/S.

Resource	TN	TP	TK	Organic matter
P1	0.213	-0.301	-0.288	-0.109
P2	0.049*	-0.269	-0.097	0.304
P3	0.027*	-0.037*	-0.217	0.079
P4	-0.281	-0.204	-0.237	0.024*
P5	-0.245	-0.215	-0.257	-0.149
P6	-0.349	-0.212	-0.223	-0.251
P7	-0.010**	-0.392	-0.209	-0.201

DISCUSSION

Distribution Characteristics and Sensitivity of Vegetation Biomass in Slope Protection Under Co-Operating Environment

Biomass allocation is affected by biological and abiotic factors, and balanced allocation enables plants to reach the optimal state of resource acquisition to improve their survival fitness (Wang et al. 2019). The relationship between plant biomass and species richness exhibits the hump type, and certain interspecies competition is beneficial to the increase in plant biomass (Mason et al. 2017). In this study, the effect of the mixed planting mode of grass and shrub on the community plant biomass was higher than that of a single herb or shrub. Different slopes will significantly affect the distribution of water and nutrients on slopes, which causes a difference in vegetation growth (Vaezi et al. 2017). Plant biomass decreased with an increase in slope for different slope modes, which was consistent with the results of Huang Meifen et al. (2009). The higher gradient precipitation model was more conducive to the accumulation of vegetation biomass, and the moderate increase in precipitation would improve the photosynthetic capacities of plants (Huang et al. 2009, Hsu et al. 2012).

The root shoot ratio is an important index for measuring plant growth, especially the plant response to soil nutrients

and water states (Li et al. 2019). In this study, the root shoot ratio of the plant for the condition of grass-shrub mixed planting was higher than that for the condition of herb single planting but lower than that for the condition of shrub single planting. For the condition of mixed planting, plants tend to allocate more photosynthetic products to the aboveground parts under the competitive pressure on growth space and light resources (Wang et al. 2019). On the other hand, the distribution mode of plant biomass is not only affected by the external environment but also limited by its size (Husáková et al. 2018). The research of Ledig et al. (Ledig & Perry 1966) showed that the root-shoot ratio of herbage decreased with growth, while that of woody plant seedlings yielded the opposite results. Low precipitation and high slope will cause water or nutrient utilization pressure, and plants will weaken the growth of the aboveground part to a certain extent, and strengthen the absorption of water and nutrients by increasing the number of roots, root activity and root shoot ratio (Yang et al. 2018).

Studies have shown that leaf traits are closely related to plants' acquisition and utilization of resources and are highly sensitive to environmental changes on different scales (Picotte et al. 2009). This finding is consistent with the results of this study, the most sensitive organ of biomass allocation in plants to the synergistic effect of slope, vegetation type and precipitation was the leaf. The stable distribution of stem and root biomass ensured the adaptability of slope protection plants to environmental change in the recovery process, which reflected the sensitivity and integrity of each organ of the plant to collaborative change in interactive environmental factors and showed that slope protection plants had a certain self-protection and regulation ability to environmental stress.

Allometric Growth Relationship of Plants Under Co-Operating Environment

This study showed that the underground and aboveground biomass and root and leaf biomass of the plants on slopes had a constant growth rate relationship, which was consistent with previous research results on the same growth rate of the biomass among the components of plants, which reflected the general law of resource allocation strategy for plant acquisition and the allocation strategy of plants (Vasseur et al. 2018). Habitat conditions, phylogenetic history and interspecific relationships drive allometric growth relationships of plant components on different spatial and temporal scales, and the regional habitat gradient formed by water and soil affects the allocation pattern of biomass of plant components (Wills et al. 2016, Jiang & Wang 2017). In this study, the root and stem biomass of slope plants with different rainfall and slope is $\alpha = 3/4$ of heterogenic growth, while the biomass of plant roots and stems of each slope were not consistent in the interactive condition. The same slope was obtained among the roots and leaf organs of all slopes, that is, the allometric growth index was 0.6418. The differences in the growth relationship among the organ components of plants for different environmental models further confirmed that plants could achieve and maintain maximum growth by regulating the biomass distribution in different organs due to the influence of external environmental conditions (Wang et al. 2019).

Response Characteristics of Plant Biomass Allocation (R/S) to Soil Factors Under Co-Operating Environment

As the main environmental factor that restricts the growth of vegetation, the soil factor also indirectly affects the distribution trend of plant biomass (Yuan et al. 2020). TN of soil had a significant positive correlation with the R/S of P2 and P3 vegetation, which may be due to the dense shallow root system of herbage that concentrates on the surface of the soil. In addition, the deposition of organic matter in soil accelerated the absorption, transportation and circulation of nitrogen and other nutrients in the soil, which promotes the increase in aboveground biomass of plants, while perennial shrubs need to store more material and energy in the underground part to ensure that the plants would germinate again next year. Certain inter-species competition would also promote plants to increase the root shoot ratio to occupy the space and resource advantage (Zuo et al. 2018). However, a very significant negative correlation with the R/S of P7 vegetation was observed. Some studies have shown that high slope will cause a large degree of variation in soil water or nutrients, while plants can enhance the absorption and utilization of water and nutrients by adjusting the morphological characteristics, such as the root shoot ratio (Ledig & Perry 1966, Yang et al. 2018). The increase in the soil pH value can improve the utilization rate of phosphorus in the soil, and the extension of the plant root system and the accumulation of biomass can be promoted by the alkalinity of soil pH value in a proper range (Ma et al. 2012). In this study, the proportion of base material mixed with cement was weak alkaline, which promoted the absorption of phosphorus by plants to a certain extent and showed a significant negative correlation with the slope vegetation R/S.

CONCLUSION

1. A significant effect on leaf biomass, stem biomass, root biomass and R/S of slope vegetation ($p < 0.05$) was observed under co-operating environment. The biomass of leaf, stem and root increased significantly with the increase in vegetation type and precipitation but decreased significantly with an increase in slope.

The root shoot ratio was less than 1, except for the mode of shrub unicast and a slope 75°, and reached the maximum value in winter, which indicates that the spatial distribution of the biomass of slope protection plants and their response mechanisms to environmental factors were quite different.

2. The variation coefficient of LMR was the largest under co-operating environment, and the sensitivity of the biomass allocation of each organ was leaf biomass ratio > root biomass ratio > stem biomass ratio, which indicated that leaf biomass was most susceptible to the environmental model, while stem biomass was less affected.
3. Significant differences in the biomass of each organ of plants on different slopes ($p < 0.05$) were obtained. The root and leaf showed an isokinetic growth relationship ($\alpha = 1$), while the plant roots and stems showed an allometric growth relationship ($\alpha = 3/4$) due to the synergistic effect of precipitation and slope (P5 and P7 slopes). The vegetation on each slope had the same slope, and their allometric growth index was 0.4109 (root-leaf), 0.5961 (stem-root) and 0.6418 (stem-leaf).
4. The correlation analysis of the influence of soil factors on the biomass allocation (R/S) revealed that the TN of soil was significantly correlated with the R/S of vegetation ($p < 0.05$) due to the synergistic effect of vegetation type and slope (P2, P3 and P7 slope); the TP of soil and R/S of vegetation of P3 were significantly negatively correlated ($p < 0.05$); while the remaining slope soil nutrient and vegetation R/S had no significant correlation ($p > 0.05$).
5. The content of soil nitrogen and phosphorus were the key soil driving factor affecting the distribution pattern of plant biomass. The resource allocation characteristics of different vegetation and its response to soil factors had specificity.

ACKNOWLEDGEMENTS

This research was supported by the National Key R&D Program of China (2017YFC0504902), National Natural Science Foundation of China (51678348, 51979147) and the Natural Science Foundation of Yichang City (A21-3-007), the Natural Science Foundation of Hubei Province (2020CFB317) and the CRSRI Open Research Program (CKWV2019753/KY).

REFERENCES

Cao, Y. and Chen, Y.M. 2015. Biomass, carbon and nutrient storage in a 30-year-old Chinese cork oak (*Quercus variabilis*) forest on the south slope of the Qinling mountains, China. Forests, 6: 1239-1255.

Daniel, P.B., Jorge, Á.F., Neil, C.H., Jorge, L. and Carlos, C.M. 2014. Winter cereal root growth and aboveground-belowground biomass ratios as affected by site and tillage system in dryland Mediterranean conditions. Plant and Soil, 374: 925-939.

Fang, J.M., Wu, F.Z., Yang, W.Q., Zhang, J. and Cai, H.X. 2012. Effects of drought on the growth and resource use efficiency of two endemic species in an arid ecotone. Acta Ecologica Sinica, 32(4): 195-201.

Hsu, J.S., Powell, J. and Adler, P.B. 2012. Sensitivity of mean annual primary production to precipitation. Global Change Biology, 18(7): 2246-2255.

Huang, M.F., Xu, C., Cao, H.Y., Hang, X.S., Yuan, F.J., Yin, Y.C., Zhong, S., Yin, Z.F., Kui, J.X., Luo, Z.R., Duan, X.H., Wang, H.X., Dai, C.L. and Guan, R.F. 2009. Vegetative growth of *Eupatorium adenophorum* in different habitats. Chinese Journal of Tropical Crops, 30(10): 1429-1436 (in Chinese).

Husáková, I., Weiner, J. and Münzbergová, Z. 2018. Species traits and shoot-root biomass allocation in 20 dry-grassland species. Journal of Plant Ecology, 11(2): 273-285.

Jiang, Y. and Wang, L. 2017. Pattern and control of biomass allocation across global forest ecosystems. Ecology and Evolution, 7(14): 5493-5501.

Ledig, F.T. and Perry, T.O. 1966. Physiological genetics of the shoot-root ratio [C]//Proceedings of the Society of American Foresters Annual Meeting. Washington, USA: Society of American Forester, 39-43.

Li, C.B., Zheng, Z., Peng, Y.F., Nie, X.Q., Yang, L.C., Xiao, Y.M. and Zhou G.Y. 2019. Precipitation and nitrogen addition enhance biomass allocation to aboveground in an alpine steppe. Ecology and Evolution, 9(21): 12193-12201.

Ma, Q., Yue, L.J., Zhang, J.L., Wu, G.Q., Bao, A.K. and Wang, S.M. 2012. Sodium chloride improves photosynthesis and water status in the succulent xerophyte *Zygophyllum xanthoxylum*. Tree Physiology, 32: 4-13.

Mason, C.M., Goolsby, E.W., Davis, K.E., Bullock, D.V. and Donovan, L.A. 2017. Importance of whole-plant biomass allocation and reproductive timing to habitat differentiation across the North American sunflowers. Annals of Botany, 119(7): 1131-1142.

Norton, D.A. and Young, L.M. 2016. Effect of artificial shade and grazing removal on degraded grasslands: Implications of woody restoration for herbaceous vegetation. Ecological Management & Restoration, 17(2): 140-146.

Picotte, J.J., Rhode, J.M. and Cruzan, M.B. 2009. Leaf morphological responses to variation in water availability for plants in the *Piriqueta caroliniana* complex. Plant Ecology, 200: 267-275.

Vaezi, A.R., Zarrinabadi, E. and Auerswald, K. 2017. Interaction of land use, slope gradient and rain sequence on runoff and soil loss from weakly aggregated semi-arid soils. Soil & Tillage Research, 172: 22-31.

Vasseur, F., Exposito-Alonso, M., Ayala-Garay, O. J., Wang, G., Enquist, B.J., Vile, D., Violle, C. and Weigel, D. 2018. Adaptive diversification of growth allometry in the plant *Arabidopsis thaliana*. Proceedings of the National Academy of Sciences of the United States of America, 115(13): 3416-3421.

Wang, D.Y., Zun, Q.J., Wang, J. and Huang, W.Y. 2020. Three-dimensional geonet ecological slope protection technology and its engineering application. IOP Conference Series Materials Science and Engineering, 794: 012055.

Wang, Q.W., Daumal, M., Nagano, S., Yoshida, N., Morinaga, S.I. and Hikosaka, K. 2019. Plasticity of functional traits and optimality of biomass allocation in elevational ecotypes of *Arabidopsis halleri* grown at different soil nutrient availabilities. Journal of Plant Research, 132(2): 237-249.

Willis, A., Harris, P.J.C., Rodrigues, B. and Sparks, T. 2016. Primary sand-dune plant community and soil properties during the west-coast India monsoon. Nephron Clinical Practice, 2(1): 60-71.

Xu, W.N., Xia, Z.Y., Zhou, M.T., Liu, D.X. and Xia, D. 2012. The vegetation concrete eco-restoration technology theory and practice. China Water & Power Press, Beijing (in Chinese).

Yang, Y., Dou, Y.X., An, S.S. and Zhu, Z.L. 2018. Abiotic and biotic factors modulate plant biomass and root/shoot (R/S) ratios in grassland on the Loess Plateau, China. Science of the Total Environment, 636: 621-631.

Yuan, Y., Xiong, D.H., Wu, H., Zhang, S., Zhang, B.J., Dahal, N.M., Liu, L., Li, W.X., Zhang, W.D. and Shi, L.T. 2020. Spatial variation of soil physical properties and its relationship with plant biomass in degraded slopes in dry-hot valley region of Southwest China. Journal of Soils and Sediments, 20: 2354-2366.

Zhang, L.Y., Liu, D.X., Xu, W.N. and Tong, B. 2017. A study on the change of three functional microorganism quantities in habitat substrate under freezing-thawing cycles. Journal of Glaciology and Geocryology, 39(5): 1122-1129 (in Chinese).

Zuo, Y.L., Wang, Z.M., Xi, X.Q., Xiang, S. and Sun, S.C. 2018. Plant biomass allocation strategies of the dominant species in an alpine meadow of northwestern Sichuan, China. Chinese Journal of Applied & Environmental Biology, 24(6): 3-11 (in Chinese).

Nature Environment and Pollution Technology
An International Quarterly Scientific Journal

p-ISSN: 0972-6268
(Print copies up to 2016)
e-ISSN: 2395-3454

Vol. 20 | No. 2 | pp. 685-693 | 2021

Original Research Paper

https://doi.org/10.46488/NEPT.2021.v20i02.027

Open Access Journal

Level Assessment of Ecological Environment of China and Sustainable Development Strategies

Yong Li
School of Marxism, Huanghuai University, Zhumadian 463000, China
†Corresponding author: Yong Li: 178719267@qq.com

Nat. Env. & Poll. Tech.
Website: www.neptjournal.com

Received: 05-03-2021
Revised: 02-04-2021
Accepted: 15-04-2021

Key Words:
Ecological Environment
Level Assessment
Sustainable Development
strategy

ABSTRACT

China's ecological environmental level is not high because of the intensifying resource constraint, heavy environmental pollution, and ecosystem degradation. The highly industrialized process leads to resource exhaustion, energy shortage, environmental deterioration, and ecological imbalance, which threaten sustainable economic growth and social progress. Effective living environmental level assessment in different provinces in China is an important premise to insist on the new development mode of high resource utilization, good environmental protection effect, and evident ecological efficiency in the new stage. In this study, studies on ecological environment level assessment and sustainable development strategies of the ecological environment were summarized. An ecological environment level assessment index system was constructed from the perspectives of water environment, living environment, forest environment, agricultural environment, and sudden environmental event. The ecological environmental level measurements of 31 provinces, municipalities, and autonomous regions in China in 2019 were measured by the entropy weight-technique for order preference by similarity to an ideal solution (TOPSIS) model. Results demonstrate that total water resources, forestry investment, and completed investment in industrial pollution control are the three most important indexes to measure the ecological level of a province, which account for 50% of weights. The relative closeness (C) of TOPSIS estimation results range in the interval of 0.215-0.510. The ecological environmental level of 31 provinces, municipalities and autonomous regions in China in 2019 could be generally divided into three types. To realize China's ecological environment and economic social coordinated development, some sustainable development strategies, including 1) optimizing energy structure and accelerating economic development; 2) strengthening environmental control and relieving industrial waste emissions; 3) strengthening ecological construction planning and increasing law enforcement in ecological environmental pollution; 4) increasing bearing capacity of ecological environment and protecting ecological environment sustainable development, were proposed. Research conclusions have an important role in exploring the current provincial ecological environmental levels, promoting coordinated development of the economy-resource-environment system, and enriching policies concerning China's ecological environment sustainable development.

INTRODUCTION

The ecological environment is the basis of human survival. However, resource exhaustion and environmental pollution caused by the increase in the artificial reconstruction of nature are serious threats to the sustainable social development of human. Therefore, strengthening ecological civilization construction and establishing a resource-saving and environmental-friendly society that takes the bearing capacity of resource environment as the basis, natural laws as the criteria, and sustainable development as the objective are great events that are related with the overall human and social development, which have become two national strategies. With the progress in industrialization and urbanization, demands of the social-economic system for natural resources and pollutant emissions increase significantly. Many factors have influenced the health of the ecological environment. Sustainable development theory is a key to solve resource environmental bottleneck in the process of regional development, and it has become a research hotspot on geoscience and environmental science. The implementation of the sustainable development strategy of ecological environmental governance is an important aspect and an effective tool in realizing the harmonious development of the ecological environment and economic society. Nowadays, this stage is an important phase that Chinese cities are facing with transformation and upgrading. In the past decades, urban construction development in China is an old strategy at the cost of the environment, and it brought many ecological environmental pollution phenomena. For example, the healthy lifestyle of people has been challenged by urban expansion, extensive division

of urban functional regions, traffic jam, and environmental deterioration. Facing the serious situation of decreasing the bearing capacity of the resource environment and deteriorating urban ecosystem in China, the application of the philosophy of sustainable development into ecological environmental protection is suggested.

Negative external environmental issues, such as atmospheric pollution, global warming, soil–water loss and water quality deterioration, become increasingly prominent in China because of industrialization and urbanization and have brought economic prosperity and social progress. Severe environmental pollution and ecological failure not only threaten the physical health and property safety of people but also restrict the improvement of human development and life level and influence the benefits of several generations. Ecological environmental safety is faced with unprecedented challenges. Although China has achieved outstanding successes in economic construction, environmental pollution problems and ecological environmental damages are intensifying continuously. This series of problems attracts growing attention as the consciousness of citizens toward environmental protection rises and living quality and demands for a high-quality ecological environment are increased. Proposing sustainable development strategies by accurate and objective measurement of ecological environmental levels in provinces in China has important theoretical significance and practical values.

EARLIER STUDIES

Ecological environmental level assessment and strategies on sustainable development study have been the research hotspots worldwide. As an effective measurement and management mean of economy-resource environmental coordinated sustainable development, the accurate measurement of ecological environmental level has been widely applied in many countries. With respect to ecological environmental level assessment, De Lange et al. summarized the applications of ecological vulnerability analysis in rick assessment, introduced new progress in ecological vulnerability analytical methodology, and proposed a new ecological vulnerability analysis frame that could be used as a part of ecological risk assessment and used in risk management (De Lange et al. 2010). Liu et al. believed that the balance between China's economic development and ecological protection became a key problem. Given that ecological impact assessment is a component of environmental impact assessment, he summarized the general trend of ecological impact assessment development to show future development tracks (Liu et al. 2015). Munns et al. carried out an ecological risk assessment on ecosystem services in America and found that ecosystem service was used as an assessment end to increase the values of risk assessment to environmental decision-making. He suggested the combination of ecological risk and human welfare and provided a better way to express these risks (Munns et al. 2016). Chu et al. evaluated the current water quality in the Qili Sea wetland in China and recognized the pollution source. Supported by data in 2010-2013, he established a water quality evaluation index system by single-factor assessment and comprehensive evaluation method. According to the evaluation results, the water pollution in the Qili Sea wetland was serious (Chu et al. 2017). Meng et al. believed that the construction of the Olympic Winter Games had some ecological impacts in mountain regions with the sensitive and vulnerable ecosystem and evaluated multi-scale suitability of ecological suitability development in Olympic Winter Games areas based on the ecological suitability evaluation method of GIS spatial analysis (Meng et al. 2018). He et al. constructed a comprehensive ecological vulnerability index that could describe vulnerability conditions in hotspot ecological zones in China and proved the poor ecological vulnerability in China. According to spatial comparison, the spatial difference in the ecological vulnerability in China is observed. Specifically, the ecological vulnerability in provinces in Northwest China was higher than those in Northeast China and Southern China (He et al. 2018). Chen et al. assessed the influences of the improved group AHP-FCE model on the ecological environment in highway construction, which had outstanding applicability and promotion values in ecological environmental assessment (Chen et al. 2020). They believed that the wetland ecosystem had comprehensive ecological functions, and it was sensitive to climate changes. They studied changes in productivity and diversity of plants in the ecosystem in Sanjiang Plain in China. The results showed that wetland protection and management should focus on hydrological configuration and potential ecological risk in the national wetland nature reserve (Chen et al. 2020). With respect to ecological environmental sustainable development strategies, Fu et al. believed that how the local government cope with and promote sustainable development under the environmental decentralization system were important problems. Research results demonstrated that public consciousness, financial imbalance, and market-oriented reform could increase law enforcement efforts of local governments in environmental protection and promote ecological environment sustainable development (Fu et al. 2019). Bu et al. (2019) proposed a game model of social welfare maximization and analyzed the policy of how the government adjusts the total sewage emission control timely according to sewage stock under relevant policies. He suggested that the government should pay more attention to provide capital and technical support

to enterprises with fund shortage and poor technological level. Chandel et al. (2020) believed that dependence on fossil fuel was increasing stupendously, thereby resulting in the resource exhaustion state. A new sustainable biological energy source method was needed. Thus, emission reduction and even the implementation of a zero-emission policy are important pathways to realize the sustainable development of biological energy source. Khim et al. investigated scientific evidence on the association between the sustainable development objectives of Belgium and the United Nations (UN), as well as the correlation and consistency of stakeholders in the relationship between Belgium and sustainable development. He believed that determining a realizable objective and indexes of sustainable development goal played an important role in economic prosperity and social development (Khim et al. 2020). Abdul-Rahaman et al. studied the effects of foreign direct investment (FDI) on China's sustainable development by using a regression model. Results demonstrated that the implementation of stricter environmental policies and strategies can decrease breaches of contract of foreign investors (Abdul-Rahaman et al. 2020). Xuan chang et al. believed that ecological restoration, economic development, and social progress were related to the realization of the national sustainable development objective directly. A sustainable LP sustainable development strategy was proposed based on the 3Cs (classification, coordination and cooperation) system method (Xuanchang et al. 2021). Ahl et al. (2021) believed that biological technology played a key role in changing the existing land use system, and it could increase the productivity of farm or planting gardens, supplement deterioration land, and improve the bearing capacity of the ecological environment. Existing associated studies on the ecological environmental level focus on the ecological design of products, system development, and guidance of enterprise sustainable development. In China, few studies on the ecological effect of enterprises and products are mostly qualitative analysis of ecological environmental level on the regional scale and industrial fields. Chinese enterprises pay insufficient attention to ecological environmental protection, and inadequate statistical data on the ecological environment of Chinese enterprises and products are available. Studies on the sustainable protection mechanism of the regional ecological environment are not thorough yet. Hence, an ecological environmental level assessment system was constructed based on the data of 31 provinces, municipalities, and autonomous regions of China in 2019. The ecological environmental level in different provinces was measured by the entropy weight-TOPSIS model. Finally, sustainable development strategies that can improve different regional ecological environmental levels were proposed.

MODEL INTRODUCTION AND CONSTRUCTION OF INDEXES

Brief Introduction to Entropy Weight-TOPSIS Model

The concept of entropy originated from thermodynamics, and it is a parameter that characterizes the substance state. Entropy is a measurement of the degree of system disordered. An index with the smaller information entropy can provide a bigger information size, plays more role in the comprehensive evaluation, possesses higher weight, and imposes greater impacts on evaluation structures. Entropy has been widely applied in studies on system engineering, economical, and social studies, which have achieved many successes. The calculation of entropy can be performed as follows.

First, the evaluation factor matrix is expressed in Eq. (1) as:

$$A=\begin{bmatrix} a_{11} & \cdots & a_{1n} \\ \vdots & & \vdots \\ a_{m1} & \cdots & a_{mn} \end{bmatrix} \quad \ldots(1)$$

where m is the evaluated object and referred to 31 provinces in this study. n refers to the number of factors that influence the comprehensive index of ecological environmental level. Through the standardization of factor matrix A, the range transformation formula was applied for dimensionless data processing. The positive index was processed by Eq. (2).

$$r_{ij}=\frac{a_{ij}-\min(a_{ij})}{\max(a_{ij})-\min(a_{ij})} \quad \ldots(2)$$

The negative index was processed by Eq. (3).

$$r_{ij}=\frac{\max(a_{ij})-a_{ij}}{\max(a_{ij})-\min(a_{ij})} \quad \ldots(3)$$

In Eqs. (2) and (3), a_{ij} is an element in the evaluation factor matrix.

Entropy is used to characterize information size. The factor that carries the bigger information size has larger entropy. The system entropy can be expressed as:

$$H_i=(P_1,P_2,P_3,...,P_4)=-K\sum_{i=1}^{m}P_iLn(P_i),(i=1,2,...,m) \quad \ldots(4)$$

Where, $k = 1 / \ln(m)$ and m refers to the state that the system might be in. P_i is the probability of occurrence of a state of the system. $0 < P_i < 1$, $\Sigma P_i = 1$. When $P_i = 0$, then:

$$-K\sum_{i=1}^{m}P_iLn(P_i)=0 \quad \ldots(5)$$

By combining the standardized characteristic matrix gained from Eq. (5), the entropy of factor i is:

$$H_i=-K\sum_{i=1}^{m}f_{ij}Ln(f_{ij}),f_{ij}=\frac{a_{ij}}{\sum_{i=1}^{m}a_{ij}} \quad \ldots(6)$$

Finally, the entropy weight of factor *i* is defined as:

$$W_j = \frac{1-H_i}{\sum_{i=1}^{n}(1-H_i)} \quad \ldots(7)$$

Subsequently, a weighted normalization matrix (Eq. (8)) was formulated.

$$R=(V_{ij})_{m\times n}=\begin{bmatrix} W_1r_{11} & W_2r_{12} & \cdots & W_nr_{1n} \\ W_1r_{21} & W_2r_{22} & \cdots & W_nr_{2n} \\ & & \cdots & \\ W_1r_{m1} & W_2r_{m2} & \cdots & W_nr_{mn} \end{bmatrix} \quad \ldots(8)$$

Next, the positive ideal solution (V^+) and negative ideal solution (V^-) of the evaluation scheme were determined and shown in Eq. (9).

$$V^+=\max(V_{i1},V_{i2},\ldots,V_{in}),V^-=\min(V_{i1},V_{i2},\ldots,V_{in}) \quad \ldots(9)$$

The Euclidean distances from various indexes to the optimal and the worst vectors were calculated:

$$D_i^+=\sqrt{\sum_{j=1}^{m}(V_{ij}^+-V_{ij})^2},D_i^-=\sqrt{\sum_{j=1}^{m}(V_{ij}^--V_{ij})^2}, \quad \ldots(10)$$

Finally, the comprehensive evaluation index of ecological environmental level of different provinces was calculated:

$$C_i=\frac{D_i^-}{D_i^++D_i^-},0\le C_i\le 1(i=1,2,\ldots,m) \quad \ldots(11)$$

Construction of Indexes

Currently, no uniform index system is available for ecological environmental level assessment in the academic circle. Based on existing literature, the ecological environmental level is defined as when people attempt to reduce waste emissions during daily production and life activities, prevent environmental pollution effectively, and protect and continuously optimize natural ecological environmental society, that is, the human-environmental harmonious society; people's efforts in protecting, improving, and optimizing the environment; and current support degree of the environment to the sustainable development of society and economy. Based on the review of abundant comprehensive evaluation index system of ecological environmental level, an evaluation index system of the provincial ecological environmental level was constructed by observing five principles of scientificity, objective, comparability, hierarchy, and operability and referred to previous selection of relevant indexes. The system is shown in Table 1.

In this study, the ecological environmental index data in 31 provinces, municipalities, and autonomous regions in China in 2019 were collected from the China National Statistics Library (https://data.stats.gov.cn/).

EMPIRICAL STUDY

The numerical values of specific indexes were determined according to the collected data. First, ecological environmental index data in 31 provinces, municipalities, and autonomous regions in China in 2019 were normalized. The entropy weights of indexes were calculated from Eqs. (1)-(7). The weights of relevant indexes were determined according to the general influences of their relative variations on the system. Therefore, indexes with greater relative variations possess

Table 1: Ecological environmental evaluation index system.

Level-1 indexes	Level-2 indexes	Index No.	Unit	Type of indexes
Water environment	Total water supply	A1	100 million cubic meters	-
	Total water resources	A2	100 million cubic meters	+
	Total ecological water consumption	A3	100 million cubic meters	-
Living environment	Amount of household garbage clean-up	B1	10,000 tons	-
	Harmless disposal of household wastes	B2	%	+
	Number of harmless treatment plants	B3	Plants	+
Forest environment	Total afforestation area	C1	1000 ha.	+
	forestry investment	C2	10,000 yuan	+
	Number of forest fire disasters	C3	Times	-
	Forest area of diseases and pests	C4	10,000 ha.	-
	Forest coverage	C5	%	+
Agricultural environment	Crop failure area	D1	1000 ha.	-
	Affected population of natural disasters	D2	Per 10,000 users	-
	Direct economic loss of natural disasters	D3	100 million yuan	-
Sudden events	Number of sudden environmental events	E1	Times	-
	completed investment to industrial pollution control	E2	10,000 yuan	+

(In Table 1, + indicates that the index is a positive index, and a higher numerical value indicates better ecological environment-indicates that this index is a negative index, and a higher numerical value indicates a poorer ecological environment.)

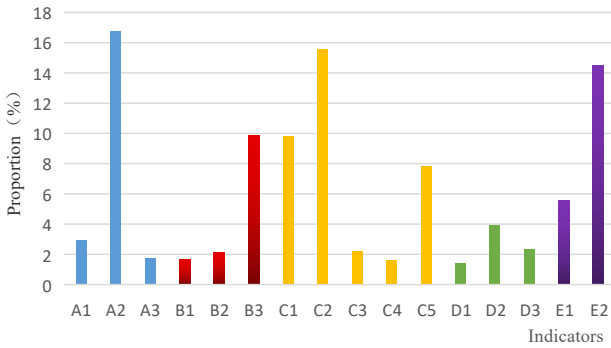

Fig. 1: Weights of the evaluation indexes.

higher weights. In other words, the index with smaller information entropy has a greater utility value.

Fig.1 shows that total water resources (A2), forestry investment (C2), and completed investment in industrial pollution control (E2) are the three most important indexes in measuring the ecological level of a province. The proportion of these indexes reached as high as 50%. Considering that China is a country with a relative per capita water resource shortage, especially in Northwest China, water shortage becomes the most important index in measuring a regional ecological environmental level. Forestry investment increases annually and became the second most important index of ecological environmental level. Increasing completed investment in industrial pollution control can control industrial environmental pollution in different provinces and improve "three industrial waste" pollution brought by the high-speed industrial development in China.

TOPSIS analysis was carried out by the data produced by weighting after entropy weight method to determine the evaluation indexes and assure that all evaluation indexes have a positive trend (the index with the higher value is suitable). According to Eqs. (7)-(10), the results in Table 2 were calculated. In Table 2, D+ and D- referred to the distances from the evaluation objects to the positive and negative ideal solutions. C refers to the closeness between the evaluation objects and the optimal scheme. The higher value of C indicates that the scheme is closer to the optimal scheme.

Table 2 presents that: (1) Shandong Province, Guangdong Province, Guangxi Zhuang Autonomous Region, and Tibet

Table 2: TOPSIS Estimation results.

Provinces Indexes	Positive ideal solution distance D	Negative ideal solution distance D-	Relative closeness C	Rank
Beijing	0.279	0.1	0.263	24
Tianjin	0.302	0.089	0.228	30
Hebei Province	0.241	0.13	0.351	11
Shanxi Province	0.259	0.104	0.287	18
Inner Mongolia Autonomous Region	0.248	0.136	0.354	9
Liaoning Province	0.276	0.093	0.251	29
Jilin Province	0.275	0.100	0.266	23
Heilongjiang Province	0.252	0.114	0.311	15
Shanghai	0.290	0.100	0.256	26
Jiangsu Province	0.254	0.131	0.340	13
Zhejiang Province	0.233	0.134	0.365	7
Anhui Province	0.257	0.096	0.272	22
Fujian Province	0.241	0.127	0.346	12
Shanxi Province	0.231	0.132	0.363	8
Shandong Province	0.222	0.187	0.457	2
Henan Province	0.260	0.100	0.279	19
Hubei Province	0.247	0.109	0.307	16
Hunan Province	0.218	0.144	0.398	6
Guangdong Province	0.216	0.162	0.428	3
Guangxi Zhuang Autonomous Region	0.197	0.204	0.510	1
Hainan Province	0.298	0.111	0.272	21
Chongqing	0.274	0.103	0.274	20
Sichuan Province	0.206	0.147	0.417	5
Guizhou Province	0.239	0.117	0.329	14
Yunnan Province	0.236	0.129	0.353	10
Tibet Autonomous Region	0.258	0.19	0.425	4
Shaanxi Province	0.253	0.104	0.292	17
Gansu Province	0.276	0.098	0.262	25
Qinghai Province	0.283	0.095	0.252	28
Ningxia Hui Autonomous Region	0.303	0.083	0.215	31
Xinjiang Uygur Autonomous Region	0.267	0.091	0.254	27

Autonomous Region show the best ecological environment. C of these four provinces was higher than 0.425, which was far higher than those of the other provinces. Guangxi Zhuang Autonomous Region and Tibet Autonomous Region are mainly located in provinces with the backward economy in the national border in Western China. These regions have good ecological environmental quality and provide important environmental inclusiveness. Guangdong Province and Shandong Province play an important role in investment in environmental protection because they have the maximum total economic development. Abundant capitals to environmental pollution control can assure a remarkable ecological environmental level. In these provinces, citizens became aware of ecological environmental protection earlier, and relevant policies and laws are perfect. Local governments support the construction of ecological cities and the development of ecological industry, respect objective natural laws, and maintain accurate ecological philosophy. They realize collaborative progress in economic development and environmental protection. To realize sustainable development truly, great efforts are made to promote the development and use of clean energy, and production and lifestyle of energy saving and emission reduction are advocated. Citizens generally have strong consciousness toward environmental protection, the implementation of the philosophy of environmental protection in daily life, and the formation of advanced ecological civilization. As such, the conventional conclusion proves indirectly that the ecological environment in the early stage of industrialization was good because of the light industrial pollution and high economic gross in the late stage of industrialization, thereby resulting in the high efficiency of environmental pollution.

(2) Hebei Province, Inner Mongolia Autonomous Region, Zhejiang Province, Hunan Province, and Yunnan Province show the second-best ecological environment. The ecological environment in these provinces belong to the average level in China, and the environment is lightly friendly. These provinces belong to the mild environmental-friendly society, and most of them are in central China, which still has certain differences from developed regions. These provinces belong to resource relative consumption type because local industrial structures and scale effect are not evident enough. Generally, the environmental-friendly comprehensive scores of these provinces are basically in the middle level. Economic development mode in these provinces proposes an urgent demand for the transformation to a modernized intensive economy and high-level industrial structure. The industrial development level of these provinces is relatively high because of advanced technology and high production efficiency, which decreases energy wastes and waste emission pollutions. Influenced by the "deindustrialization" tide, these provinces not only reduce the proportion of heavy industries positively and make great efforts to develop ecological-friendly industries and new energy sources but also strengthen citizens' consciousness of ecological protection and promote the exploration in green sustainable economic development.

(3) The remaining regions, including Tianjin, Beijing, and Shanxi, have a backward ecological environment. Most of these regions have witnessed haze and serious environmental pollution in recent years. The mean environmental-friendly comprehensive score of these provinces is far lower than those of other provinces. These regions have poor ecological environmental quality and low environmental bearing capacity, and shall further strengthen environmental control. People in these regions have poor consciousness toward ecological protection, and they ignore environmental damages in economic development. Economic development emphasizes resource mining and primary processing, and it is characterized by high energy consumption, high environmental pollution, low production efficiency, and low economic benefits. These regions need industrial upgrading urgently and have to pay attention to the relation between ecological environmental protection and economic development. The provincial economic social development level in these regions is generally low, and it cannot consider ecological environmental protection simultaneously. The quality of local citizens has to be improved. Moreover, ecological environmental damages are relatively serious, thereby taking a long time to restore. Among these regions, some provinces mainly depend on husbandry development and they rely highly on the natural environment and climate. Furthermore, the ecological environment might be overused. The use of primary product processing as the major industrial-economic mode not only has low economic benefits but may also have low resource utilization because of the background production technology and immature technological level. Consequently, it might cause energy overuse and waste emission environmental pollution. Finally, to make it easier to understand, the C of 31 Provinces, Municipality and Autonomous Regions in China is shown in Fig. 2 in 2019.

SUSTAINABLE DEVELOPMENT STRATEGIES OF IMPROVING ECOLOGICAL ENVIRONMENTAL LEVEL

Optimizing Energy Structure and Accelerating Economic Development

China must strengthen the consciousness of energy saving in production, transportation, and consumption; increase efforts in cyclic economic development; improve energy use structure, increase industrial structure; reduce energy consumption

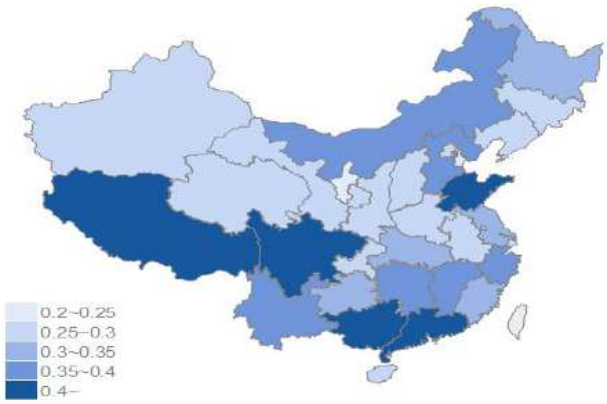

Fig. 2: *C* of 31 Provinces, Municipality and Autonomous Regions in China in 2019.

per GDP through a series of measures; and increase economic development quality. Additionally, China has to: 1) lower energy consumption at the terminal consuming enterprises by using advanced technologies and techniques and developing a cyclic economy. 2) Improve energy structure in industrial and agricultural production around the country and accelerate the development of clean energies, including solar energy, wind energy, and biological energy. 3) Establish a reasonable energy price formation mechanism. The value of energy shall be reflected through the market, and energy price shall be reflected by market supply-demand relations to encourage users to save energy and producers to increase investment to find substitutive energy sources. 4) Accelerate industrial structural updating, pay attention to the adjustment of industrial structure, increase support to new high-tech industries, such as environmental protection and new energy industries, and protect economic sustainable development. 5) Strengthen regional coordinated development, integrate regional resource advantages from the global perspective, form complementation of regional industrial advantages, realize regional resource sharing, environmental coexistence and coordinated development, increase overall economic competitiveness and benign interaction of regions, and drive the development of all economic circles in China.

Strengthening Environmental Control and Relieving Industrial Waste Emissions

The industrial layout shall be designed reasonably. Existing industrial layout and planning industrial layout shall have detailed arrangement and deployment. The planning industrial layout shall not be in urban areas. In particular, heavily polluted industrial enterprises are at the downwind places of the city that are far away from regions with high population density. The following approaches are suggested: 1) strengthen pollution source control and control the pollutant emission at the lowest extent. 2) Strengthen protection of drinking water sources and test water quality in source regions to discover illegal architectural structures and plants which might cause the water environment. These pollutions have to be solved properly, and the safety of drinking water must be protected. 3) Increase monitoring over rivers and efforts in pollution control and monitor and manage the corresponding pollutant discharging unit according to the requirement of water quality function. 4) Make plans on solid waste processing, the perfect system for solid waste collection in all cities, and prevent secondary pollution during the garbage disposal process in refuse landfills and garbage incinerator. 5) Classify solid wastes according to certain standards and process independently, and recycle according to unique properties.

Strengthening Ecological Construction Planning and Increasing Law Enforcement in Ecological Environmental Pollution

Experts in different fields must be organized to make a systematic and scientific ecological environmental construction plan. During the compilation of the system, various social-economic activities in cities have to be planned scientifically by combining the urban ecological status, urban economic social development strategies, and ecological environmental construction goal, thereby enabling to increase resource transformation efficiency of cities, energy-saving efficiency of facilitates, harmless processing rate of wastes, and self-cleaning capacity of urban ecological environment. Urban management shall be strengthened so that each detail in ecological urban construction is subjected to scientific urban management activities. Urban management requires a complete management system to manage economic activities, social construction, and natural environmental construction. Meanwhile, management departments at all levels shall strengthen correlations. It has to accelerate the establishment of laws and regulation system, which adapt to ecological urban development, to enlist ecological urban construction into the legalization orbit. This method is an effective way to protect ecological urban construction. In the process of ecological urban construction, encountering various behaviours that disagree with the ecological development of cities is inevitable. Hence, some laws and administrative means have to be adopted to assure smooth implementation of ecological urban construction. Ecological legislation can provide relevant legal guarantees. Protecting ecological urban construction by-laws is conducive to guide it to the road of legalization, planning, and systematism.

Increasing Bearing Capacity of Ecological Environment and Protecting Ecological Environment Sustainable Development

Ecological civilization construction is based on the bearing capacity of the ecological environment. It has to accelerate the construction of ecological civilization pilot demonstrations and national ecological civilization test site. Under the hard constraint of bearing capacity of ecological environment, the following recommendations are presented: 1) adopt economic-environmental coordinated development and continue to promote ecological civilization construction in provinces in China. 2) Increase financial investment to environmental protection, innovate PPP mode of ecological construction, and expand investment and financial channels for environmental protection. 3) Increase investment in the construction of urban environmental infrastructure, adopt the new urbanization road, and construct ecological-oriented cities. 4) Implement natural resource property right system natural resource use control system, increase the area of natural reserves and inventory of per capita land and forest resources, determine a protection red line, increase the ecological space, and improve bearing capacity of ecological environment continuously. 5) Adapt to new normal status positively, implement structural reform on the supply side, insist on the development philosophy of "innovation, coordination, green, open, and sharing," promote development by new driving forces, transform economic motivations, increase total factor productivity, lower energy consumption and increase resource utilization, and relieve pressure over the ecological environment.

CONCLUSIONS

The rapid progress in industrialization and urbanization have brought a series of problems, including resource exhaustion, energy shortage, environmental deterioration, and ecological imbalance. These problems are against economic sustainable growth and social progress, thereby making ecological crisis appear gradually. Economic-resource environment coordinated sustainable development becomes a topic that is widely concerned in the world. Accordingly, the philosophy of sustainable development is proposed. China's economic growth is achieved at the cost of excessive resource consumption and environmental pollutions. Rapid industrialization further increases the pressure on the resource environment. In this study, an ecological environmental level assessment index system is constructed, and the ecological environmental level in 31 provinces, municipalities, and autonomous regions in China in 2019 is measured by the entropy weight-TOPSIS model. Results demonstrate that total water resources, forestry investment, and completed investment in industrial pollution control become the three most important indexes to measure the ecological level of a province. The relative closeness (C) ranges in the interval of 0.215–0.510. The ecological environmental level of 31 provinces, municipalities and autonomous regions in China in 2019 could be divided into three types. To realize China's ecological environment and economic social coordinated development, some sustainable development strategies, including optimizing energy structure and accelerating economic development, strengthening environmental control and relieving industrial waste emissions, strengthening ecological construction planning and increasing law enforcement in ecological environmental pollution, increasing the bearing capacity of ecological environment, and protecting ecological environment sustainable development, were proposed. In-depth studies from perspectives of regional differences in ecological environmental level, perfect ecological efficiency evaluation index system, and multi-dimensional estimation of factors that influence regional ecological environmental level must be conducted in the future.

REFERENCES

Abdul-Rahaman, A. R., Ayamba, E. C., Haibo, C., Osei-Agyemang, A. and Serwaa, O. E. 2020. The impact of foreign direct investment on sustainable development in China. Environmental science and pollution research international, 27(20): 25625-25637.

Ahl, A., Goh, C. S. and Woo, W. T. 2021. Sustainable Transformation of Land-Based Economic Development in the Era of Digital Revolution. Trends in Biotechnology, 39(1): 1-4.

Bu, Y., Cheng, J., Guo, M. and Jiang, Z. 2019. Supporting Sustainable Development of Water Resources: A Social Welfare Maximization Game Model. International journal of environmental research and public health, 16(16): 2896.

Chen, B., Chen, W., Fu, J., Liu, J., Wang, X. and Zhang, M. 2020. Ecological risk assessment of wetland vegetation under projected climate scenarios in the Sanjiang Plain, China. Journal of environmental management, 273, 111108.

Chandel, A. K., Dhanya, B. S., Mishra, A. and Verma, M. L. 2020. Development of sustainable approaches for converting the organic waste to bioenergy. The Science of the total environment, 723: 138109.

Chu, C., Ju, M., Liu, L., Ruan, X., Xu, S. and Zhang, Y. 2017. Water Environment Assessment as an Ecological Red Line Management Tool for Marine Wetland Protection. International journal of environmental research and public health, 14(8): 870.

Chen, Y., Yang, C., Yang, S., Wang, Z. and Zhang, D. 2020. Assessment of ecological environment impact in highway construction activities with improved group AHP-FCE approach in China. Environmental monitoring and assessment, 192(7): 451.

De Lange, H. J., Faber, J. H., Sala, S. and Vighi, M. 2010. Ecological vulnerability in risk assessment--a review and perspectives. The Science of the total environment, 408(18): 3871-3879.

Fu, S., Tang, P. and Zeng, H. 2019. Local government responses to catalyse sustainable development: Learning from low-carbon pilot programme in China. The Science of the total environment, 689: 1054-1065.

He, L., Shen, J. and Zhang, Y. 2018. Ecological vulnerability assessment for ecological conservation and environmental management. Journal of environmental management, 206: 1115-1125.

Khim, J. S., Lee, K. H. and Noh, J. 2020. The Blue Economy and the United Nations' sustainable development goals: Challenges and opportunities. Environment International, 137: 105528.

Liao, C., Li, D., Liu, X., Li, Y., Li, Z., Tang, Z., Wang, Q. and Zhu, A. 2015. The development of ecological impact assessment in China. Environment International, 85: 46-53.

Munns, W.R., Rea, A.W., Suter, G.W., Martin, L., Blake-Hedges, L., Crk, T., Davis, C., Ferreira, G., Jordan, S., Mahoney, M. and Barron, M.G. 2016. Ecosystem services as assessment endpoints for ecological risk assessment. Integrated environmental assessment and management, 12(3): 522-528.

Meng, J., Song, S., Wang, T., Zhang, H., Zhang, S. and Zhou, Y. 2018. Balancing conservation and development in Winter Olympic construction: evidence from a multi-scale ecological suitability assessment. Scientific reports, 8(1): 14083.

Xuanchang, Z., Yansui, L., Yurui, L., Zhengjia, L., Zhi, C. and Zhi, L. 2021. Towards the progress of ecological restoration and economic development in China's Loess Plateau and strategy for more sustainable development. The Science of the total environment, 756: 143676.

Nature Environment and Pollution Technology
An International Quarterly Scientific Journal

p-ISSN: 0972-6268
(Print copies up to 2016)
e-ISSN: 2395-3454

Vol. 20 | No. 2 | pp. 695-701 | 2021

Original Research Paper

https://doi.org/10.46488/NEPT.2021.v20i02.028

Open Access Journal

Comparative Toxicity Study of Chemical Pesticide and Biopesticide by *Daphnia* Bioassay

Amrita I. Kakka†, Mihir D. Herlekar and Shivani Awale

Department of Environmental Science, The Institute of Science, Dr. Homi Bhabha State University, Mumbai-400032, Maharashtra, India

†Corresponding author: Amrita I. Kakka; amritakakka27@gmail.com

Nat. Env. & Poll. Tech.
Website: www.neptjournal.com

Received: 12-06-2020
Revised: 04-08-2020
Accepted: 27-08-2020

Key Words:
Neemark
Tafgor
LC_{50}
Combination ratio treatment
Two-way ANOVA
Aquatic ecosystem

ABSTRACT

A comparative study was conducted to evaluate the toxicity of a biopesticide and a chemical pesticide using *Daphnia magna* as a model aquatic faunal species. The primary survey revealed that Neemark and Tafgor are being commonly used by the farmers. The acute toxicity tests were conducted on *Daphnia magna* for two series of concentration ranges 100 ppm to 1000 ppm and 1000 ppm to 4000 ppm. The (Lethal Concentration) LC_{50} values for series 1 of Neemark and Tafgor were 522.86 ppm and 439.46 ppm, respectively, whereas it was 1840.48 ppm and 1335.97 ppm, respectively for for Series 2. A significant difference in the mortality rates between Neemark and Tafgor in the concentration range of 1000 ppm to 4000 ppm was observed ($t = 2.483$, $p < 0.05$). A combination treatment of Neemark and Tafgor in different proportions showed that the 2:1 v/v (Neemark: Tafgor) ratio showed the lowest toxicity with a LC_{50} value of 1067.78 ppm, suggesting its preferability in application on the field. Two–way ANOVA shows that the concentration of pesticides plays a significant role in the mortality of *Daphnia* ($F = 19.729$, $p < 0.05$) and so does the combination ratio treatment ($F = 7.166$, $p < 0.05$). These results suggest that these two factors along with the selection of a suitable plant-based pesticide play a critical role in the reduction in mortality rates of aquatic organisms.

INTRODUCTION

India primarily has an agro-based economy with an 18% contribution of agriculture to the total GDP (Bharadwaj & Sharma 2013, Kekane 2013). To sustain such a large economy, the longevity of crops and their resistance to myriad pests becomes a fundamental necessity. Pesticides play a vital role in maintaining world food production. Any substance that intends to prevent, destroy, repel or lessen the damage of any pest is called a pesticide (Eldridge 2008). There have been estimates that crop losses to pests would increase by 10% if no pesticides would be used at all (Pimentel et al. 1992). The most common categories of pesticides are insecticides, herbicides, fungicides, and rodenticides (Yadav et al. 2015). The type of pesticides used depends on the type of target pests.

The Green Revolution in India has resulted in the phenomenal growth in agricultural productivity by the use of high yielding varieties, chemical fertilizers, and pesticides (Kumar 2012). The pesticide consumption in India has risen from 434 metric tonnes to 46,195.16 metric tonnes during the period 1954 to 2000 (Bharadwaj & Sharma 2013). In India, the total as well as per hectare consumption of pesticides increased significantly after 2009-10. The pesticide consumption was 0.29 kg/ha during 2014-15 which is nearly 50% higher than the use during 2009-10 (Subash et al. 2017). Two main types of pesticides viz., chemical and biological, originating from the respective sources are used to fight the menace of pests targeting high economic value crops. Some of the chemical insecticides used are DDT (Dichloro Diphenyl Trichloroethane), BHC (Benzene hexachloride), Malathion, and Carbaryl (Yadav & Devi 2017). Chemical pesticides are known to have several negative impacts on human as well as environmental health. Synthetic chemical pesticides are known to exist as residues in soil, water, food etc., which may, in turn, lead to phytotoxicity, physiological deformities, diseases, mortality, population changes, genetic disorders etc. in many living organisms. They may enter the food chain and coupled with bioaccumulation could cause grave consequences. The increased concerns about the environmental effects associated with the use of these synthetic chemical pesticides have led to the search for chemical extracts from various biological organisms having insecticidal properties (Kumar 2012). A promising alternative is the use of biopesticides. A biopesticide is a formulation derived from naturally occurring substances that control pest populations in an eco-friendly way and through non-toxic mechanisms. The sources of biopesticides could be microorganisms, plants or animals and could include living organisms, their products or

their by-products which could be used for the management of pests. Nearly 700 biopesticide products are available globally with 175 registered biopesticide active ingredients (Kumar 2012). The share of biopesticide in the total crop protection worldwide is small with a value of about 3 billion dollars and accounts for just 5% of the total crop protection market (Marrone 2014). The most commonly produced and used forms of biopesticides in India are neem-based compounds, *Bacillus thuringensis*, nuclear polyhedrosis virus (NPV) and Trichoderms (Khandpal 2014). Biopesticides derived from the entomo-pathogenic bacterium, *Bacillus thuringiensis* (Bt), form 90% of the total microbial biopesticides available (Kumar & Singh 2015). The plant-based biopesticide derived from neem is eco-friendly and very effective against many species of arthropods, nematodes, and fungi (Kandpal 2014). The seeds of the neem tree (*Azadirachta indica*) contain the active ingredient Azadirachtin which is a natural antifeedant, insect growth regulator, and sterilant (Hummel et al. 2015).

Any pesticide used in agriculture can enter the adjoining water body through agricultural runoff and soil erosion, which could lead to adverse impacts not only on the water quality but also on the associated aquatic life. After the entry into the aquatic ecosystems, pesticides can cause fishery losses in many ways such as increased mortality, killing of susceptible fish fry, and elimination of essential fish foods, such as insects and other invertebrates (Pimentel et al. 1992). Chlorpyrifos, an organophosphate pesticide, being very toxic to fish has caused fish mortality in waterways adjacent to treated fields (United States Environmental Protection Agency [US EPA] 2000). Pesticides are known to cause serious problems because they are designed to kill organisms, both target and non-target ones (Hanazato 2000).

The toxicity of pesticides on an aquatic ecosystem can be assessed using different test organisms. The effects of two chemical pesticides viz. Imidacloprid and RH-5849 on earthworm (*Eisenia foetida*) were studied (Luo et al. 1999) in terms of their acute toxicity, effects on sperm morphological deformity, and biochemical toxicity. Some toxicity tests use fish such as *Danio rerio* as the test organism to determine the (lethal concentration) $LC_{50\text{-}96h}$ of neem-based pesticides (Maranho et al. 2014). *Daphnia magna*, a zooplankton, is also often used as the test organism. Since zooplanktons are very sensitive to toxic chemicals and occupy a central position in the lentic food chain, they are frequently used in ecotoxicological tests. The responses of zooplankton to toxicity tests provide information on the relative impacts on the ecosystem as a whole (Hanazato 2000). *Daphnia* has been used to test the effects of anthropogenic chemicals, such as dieldrin on the sex ratio and alteration in the male individuals' production (Dodson et al. 1999). They quantified the swimming behaviour of free-living *Daphnia* that were exposed to the pesticide. Two types of behaviours were seen: (1) 'spinning' (extreme and continuous escape behaviour) in response to acutely toxic levels of 'carbaryl' and (2) 'irritation' (an increase in escape-like behaviour) in response to sublethal levels. *Daphnia magna* has been used in acute toxicity test for neem-based biopesticides to determine the median Effective Concentration ($EC_{50\text{-}48h}$). After these acute toxicity tests, chronic toxicity tests for 21 days were conducted (Maranho 2014). The moulting process of crustaceans has been interfered by azadirachtin, the active component in neem and some other aquatic invertebrates may also be susceptible (Stark 2007).

The objective of the present study was to generate a database on the most frequently used pesticides (chemical and/or biological) amongst a group of farmers of the Palghar district of Maharashtra, India. Subsequently, the toxicity testing of the most preferred biological pesticide and chemical pesticide was performed individually and in combination using *Daphnia* to ascertain the one, which is comparatively less harmful to the aquatic organism. This is the first of such an experimental analysis using the actual field concentrations of pesticides to assess their toxicity in terms of the LC_{50} values. Along with this, the combination ratio treatment experiments can provide a guideline to assess their potential use by farmers which could reduce the toxic effects on the aquatic ecosystem. The toxicity data so obtained were analysed statistically using the PAST software and MS Excel.

MATERIALS AND METHODS

The entire study was divided into two parts, wherein the first part included a questionnaire survey of farmers and the second half consisted of laboratory analysis of the toxicity of the most commonly used pesticides in the study area.

Questionnaire Survey

The questionnaire survey regarding the use of pesticides for agriculture was conducted among a group of 20 farmers in the Palghar district of Maharashtra. It comprised of a set of questions to collect data in terms of the type of crops cultivated, type of pesticide used (biological/ chemical), and the most preferred market-based pesticide product. Based on the questionnaire survey, the most preferred market products of biopesticide and chemical pesticide were found to be Neemark and Tafgor, respectively. These were chosen for the laboratory analysis to ascertain their respective LC_{50} values using the test aquatic organism *Daphnia magna.*

LC_{50} Studies

Stock solutions of Neemark and Tafgor of concentrations 500 ppm and 2500 ppm, respectively were prepared. These

concentrations were based on the volumes of pesticide used in the study sites by the farmers. Two series of diluted stock solutions of varying concentrations viz., 100 to 1000 ppm with an interval of 100 pm and 1000-4000 ppm with an interval of 500 ppm were prepared for both the pesticides. Thus, two concentrations range each for Neemark and Tafgor were prepared. This was done to accommodate both the pesticide concentrations used in the field.

Experiments were conducted to determine the lethal concentration of the pesticide that killed fifty percent of the population (LC_{50}) using probit analysis. The experimental work included two parts. The first part included finding the LC_{50} values for the individual pesticide range. In the second set of experiments, *Daphnia* was subjected to combination treatments of different volume: volume (v: v) ratios viz. 1:1, 1:2 and 2:1 of Neemark and Tafgor, respectively. This was done to determine the most favourable treatment that could be used by the farmers which are the least damaging to the aquatic fauna. In these combination treatment sets, varying concentrations of the two pesticides in the range of 100 ppm to 500 ppm were used to find the LC_{50} value of the particular combination treatment. All the experiments were initiated by transferring 15 live *Daphnia* into clean petri plates where each plate represented a particular concentration. Respective volumes of the pesticide concentrations from the series were inoculated in the plates. The number of dead *Daphnia* individuals was counted after an incubation time of 60 min. All the experiments were carried out in duplicates. The percent mortality was calculated using the following formula presented in Equation 1.

$$\text{Percent Mortality} = (\text{Number of dead } \textit{Daphnia} / \text{Initial Number of live } \textit{Daphnia}) \times 100 \quad \ldots(1)$$

The percent mortality was calculated and transformed into probit values using Finney's probit table (Finney 1971). All the probit values were plotted against the log values of the concentrations. The log concentration value for the probit value 5 (representing fifty percent mortality) was found, the antilog of which yielded the lethal concentration that caused 50 percent mortality. The acute toxicity tests were conducted in a manner similar to the previous studies (Demetrio et al. 2014, Maranho et al. 2014) with a few changes to suit the present study.

Two–way ANOVA was done to estimate whether the different combination treatments and different pesticide concentrations used for the combination treatment affected the percent mortality significantly or not. The significant difference in the percent mortality between the different concentration ranges of Neemark and Tafgor was checked with the help of unpaired t-test. The statistical analysis and graphical representations were done using PAST and MS Excel.

RESULTS AND DISCUSSION

Questionnaire Survey

The questionnaire survey conducted in the Palghar district of Maharashtra to understand the proportion of farmers using biopesticide and chemical pesticide revealed that out of the 20 farmers surveyed, 40% used only biological pest control measures, such as cow urine, Neemark and other neem products; 20% of them used only chemical pesticides such as Tafgor, Karathane, and Rogor, whereas 40% of the surveyed farmers used both chemical and biological pesticide. The different chemical and biological pesticides were used as a common application against all types of pests including aphids. The most common form of biopesticide and chemical pesticide used was Neemark (35%) and Tafgor (55%), respectively.

LC_{50} of Pesticides

Based on the results of the survey, Neemark and Tafgor were selected as the toxicants to carry out further acute toxicity tests. The median lethal concentration for Neemark for Series 1 (100-1000 ppm) and Series 2 (1000-4000 ppm) was found to be 522.86 ppm and 1840.48 ppm, respectively. Various acute toxicity tests have been conducted on *Daphnia* using neem-based compounds, such as Neemix, Bioneem, and Margosan-O. In one of the studies, effective concentration (EC_{50}) (48 h) of Margosan-O on *Daphnia magna* was as high as 125 ppm as against the LC_{50} (48 h) value of 13 ppm (Scott & Kaushik 1998). Another research found the EC_{50} for Margosan-O on *Daphnia magna* at 103 ppm (Saucke & Schmutterer 1992). The LC_{50} (48 h) of Neemix for *Daphnia pulex* was estimated to be 0.68 ppm by Stark (2001). He also found that the LC_{50} of Azatin for *D. pulex* was 0.57 ppm. Another acute toxicity test revealed that LC_{50} (48 h) values for Neemix and Bioneem on *Daphnia pulex* were 0.028 µg/mL and 0.033 µg/mL, respectively (Goktepe & Plhak 2002). Maranho et al. (2014) observed that the neem oil based biopesticide showed an EC_{50} of 0.17ml/L for *D. magna*. Comparison of the LC_{50} values obtained from the previous studies of other neem-based pesticides shows that the LC_{50} value of Neemark from the present study is very high. This could be attributed to the high range selected for the study along with the possible indication of Neemark being less toxic to the invertebrate aquatic fauna as compared to other neem derived products. Other biopesticides have also shown comparatively high toxicity as compared to Neemark. Camphor, a major ingredient of biopesticides, was assessed for its acute toxicity to *D. magna* (Yim et al. 2014). In their study, they observed immobilization of *D. magna* over 98.8µM and the EC_{50} was found to be 395µM after 48 h.

The median lethal concentration for Tafgor for Series 1 (100-1000 ppm) and Series 2 (1000-4000 ppm) was found to be 439.46 ppm and 1335.97 ppm, respectively. The LC_{50} values for other organophosphate pesticides, such as chlorpyrifos and malathion for *Daphnia magna* were found to be 0.001µg/mL and 0.033µg/mL, respectively by Leight & Dolah (1999). Several other studies for the LC_{50} of Chloropyrifos on *D. magna* were conducted which gave the results as follows; 0.19 µg/mL (Kikuchi et al. 2000) and 1.0 µg/mL (Kersting & van Wijngaarden 1992). There are a few acute toxicity studies of Tafgor conducted on *Daphnia*. As per the EPA report (US EPA 1983), the 48 h LC_{50} value for Tafgor in *D. magna* is 2.5µg/mL. Various studies have assessed the toxic effects of other chemical groups of insecticides on *Daphnia*. The LC_{50} values for carbaryl on *Daphnia pulex* were found to be 50.1µg/L, 33.1µg/L, and 26.4µg/L for 24, 48 and 72 h, respectively, and 1.5mg/L and 1.09mg/L for 24 and 48 h, respectively for imidacloprid (Hassoon & Salman 2016). However, the LC_{50} values were higher when *D. magna* were exposed to imidacloprid with concentrations going beyond 102000µg/L for 48 h (Raby et al. 2018). This suggests that variation in the threshold to imidacloprid can occur in different species of *Daphnia*. A study in Turkey showed that the acute toxic lethal concentration values for Abamectin, a chemical insecticide, were 0.02µg/L and 0.0043µg/L for 24 and 48 h, respectively (Azgin & Goksu 2016). A study to examine the effects of fungicides on *D. pulex* in Chile revealed that the LC_{50} of carbendazim was 26.1µg/L (Encina et al. 2017). In the present study, *Daphnia* showed a relatively higher tolerance to Tafgor which could be due to the lower exposure time as opposed to the other reference studies where the exposure time was greater and thus, the subsequent LC_{50} values were comparatively lower than Tafgor. Thiamethoxam is an insecticide belonging to the class of neonicotinoids, which is used in agriculture to control a broad range of insect pests. The acute toxicity of these pesticides was examined for different aquatic organisms. The results showed that the organisms were least sensitive with acute median effective concentrations greater than 80 mg/L. The EC_{50} for *Daphnia magna* for 24 and 48 h exceeded 100 mg/L (Finnegan et al. 2017). The acute toxicity of Thiamethoxam on *D. magna* showed an LC_{50} value to exceed 80000µg/L for 48 h implying higher tolerance to the insecticide (Raby et al. 2018). Neonicotinoids are chemically similar to the natural component nicotine. The literature assessed for the toxicity of thiamethoxam shows that it consequently poses less risk to the aquatic organisms. This could suggest future directives to promote the use of similar types of pesticides imitating natural components or use the biological components completely (Finnegan et al. 2017). The results of the median lethal concentration obtained for Neemark and Tafgor showed that Tafgor is comparatively more lethal to *Daphnia* than Neemark and thus, showing more toxicity. This also indicates that the current dosage of Tafgor of 2500 ppm used on the field by farmers may be highly toxic to the aquatic fauna. The current dose of Neemark that is used on the field i.e. 500 ppm may be comparatively less toxic to the aquatic fauna as compared to Tafgor. The percent mortality for the two pesticides for the respective series was converted into probit values using the probit table and the concentrations were converted into log (concentration) values. The corresponding findings (Figs. 1-4) indicate that there is an increase in the probit value with the increase in the pesticide concentration. The probit values for Series 1 of Neemark and Tafgor show a similar mortality trend (Figs. 1 and 3). In contrast, the percentage mortality for Tafgor Series 2 shows close to 100% mortality at probit values of 8.09 for the last two log (conc.) i.e. for 3500 ppm and 4000 ppm (Fig. 4). This trend was absent in the Neemark Series 2, which shows maximum mortality of 73% at probit 5.61 (Fig. 2).

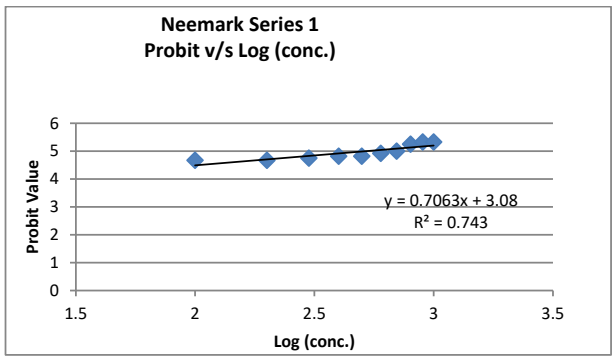

Fig. 1: Effect of varying concentrations of Neemark Series 1 (100-1000 ppm) on the Probit.

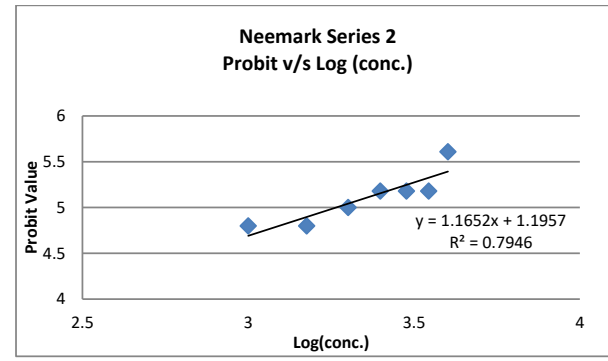

Fig. 2: Effect of varying concentrations of Neemark Series 2 (1000-4000 ppm) on the Probit.

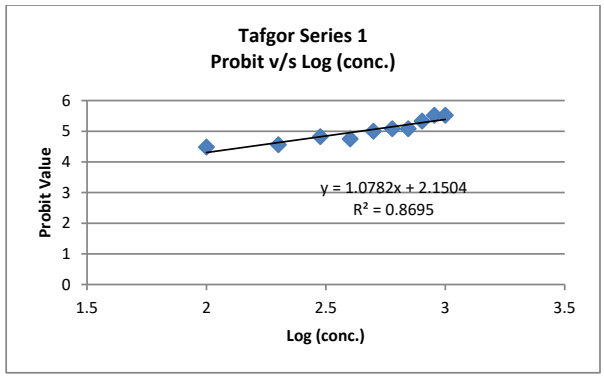

Fig. 3: Effect of varying concentrations of Tafgor Series 1 (100-1000 ppm) on the Probit.

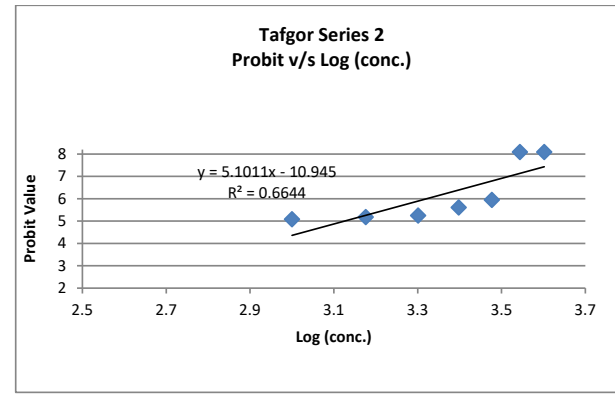

Fig. 4: Effect of varying concentrations of Tafgor Series 2 (1000-4000 ppm) on the Probit.

An overall comparison of the average percentage mortality of the two series of Neemark and Tafgor against different pesticide concentrations showed that the percentage mortality of Tafgor remained, in general, greater than that of Neemark (Figs. 5 and 6).

This highlights the possible subsequent negative implications of Tafgor on aquatic life when used on fields due to its highly toxic chemical composition. The concentrations of Neemark used, which are the same as that of Tafgor however, shows comparatively lower mortality rates compared to those of Tafgor and thus, subsequently pointing to lesser negative effects on the aquatic fauna.

Combination Ratio Treatment

As some of the farmers use a combination of Neemark and Tafgor, the *in vitro* combination ratio treatment of Neemark and Tafgor was done to find a suitable ratio treatment that would cause minimum harm to the aquatic fauna. The highest percentage mortality (50%) and the corresponding lowest LC_{50} value (255.86 ppm) was seen in the 1:1 (Neemark: Tafgor) ratio treatment. However, the median percentage mortality was 40% for both 1:2 (Neemark: Tafgor) and 2:1 (Neemark: Tafgor) ratios and the corresponding LC_{50} values for the 1:2 and 2:1 ratio treatment were 427.43 ppm and 1067.78 ppm, respectively. The median percentage of mortality values have been depicted in Fig. 7. The least lethal treatment was found to be the 2:1 v/v ratio treatment, which suggests that that combination treatment with two volumes of Neemark against one volume of Tafgor is the preferred treatment if a combination of Neemark and Tafgor are to be used on the field as Neemark is a natural ingredient product with low ill effects on non-target fauna. However, the efficiency of this pesticide used in killing the pest organisms needs further assessment.

Two-way ANOVA was carried out to assess whether the different concentrations and the combination ratio treatment of Neemark and Tafgor affected the percentage mortality significantly or not. To the best knowledge of the authors, two-way ANOVA is being used for the first time to study the impact of concentration and combination ratio treatments on *Daphnia*'s mortality. The percent mortality showed a

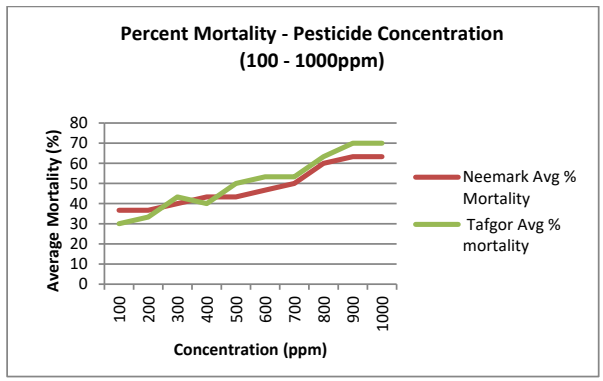

Fig. 5: Comparison of average percentage mortality for series 1 (100-1000 ppm) of Neemark and Tafgor.

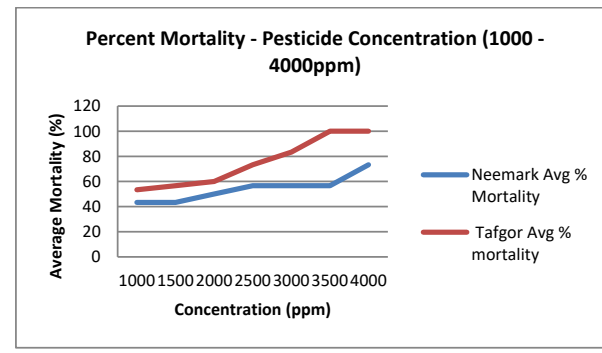

Fig. 6: Comparison of average percentage mortality for series 2 (1000-4000 ppm) of Neemark and Tafgor.

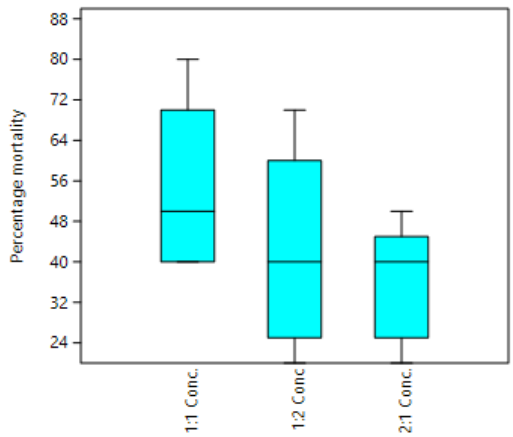

Fig. 7: Boxplot showing the median percent mortality of *Daphnia*.

significant difference for different combination treatments ($F = 7.166$, $p < 0.05$) and the different concentrations ($F = 19.729$, $p < 0.05$) but the combined effect of both the concentration and the combination treatment showed no significant effect on the percentage mortality. The results are shown in Table 1.

The statistical t-test has been used for the first time to compare and check for the significant difference in the mortality rates of *Daphnia magna* between the two pesticides. Unpaired t-test was applied to check whether the percentage mean mortality of Series 2 (1000 ppm-4000 ppm) of Tafgor showed a significant difference from the Series 2 (1000 ppm-4000 ppm) of Neemark and a significant difference was seen ($p < 0.05$, $p = 0.034$, $t = 2.483$). No significant statistical difference was seen between the two series of Tafgor and Neemark of the range 100 ppm to 1000 ppm ($p > 0.05$). Thus, the concentration of Tafgor could be used within the concentration of 1000 ppm on the field by the farmers and still not show much difference in the death of the *Daphnia* when compared to Neemark. However, increasing the concentration of the two pesticides above 1000 ppm would cause a significant effect on the mortality rates with the possibility of Tafgor showing more lethality to the aquatic fauna. This suggests that the current dosage concentration of 2500 ppm may show more toxic effects on the aquatic fauna.

Table 1: Results for Two-way ANOVA analysis.

	F value	P value	F critical
Combination Ratio Treatment	7.1666	0.006538*	3.68232
Pesticide Concentration (ppm)	19.7291	7.74E-06*	3.055568
Interaction between combination ratio treatment and pesticide concentration	1.3854	0.278997	2.640797

*significant at p = 0.05

CONCLUSION

Non-target toxicity of pesticides on the aquatic fauna stands to be an important environmental concern. The LC_{50} values of Neemark and Tafgor pesticides showed that the chemical pesticide, Tafgor, was comparatively more toxic to *Daphnia* than the biological counterpart, Neemark. A greater proportion of farmers used either only biopesticides or a mixture of biopesticide and chemical pesticide. In comparison, a few of the surveyed farmers used only chemical pesticides in their fields. Further reduction in this proportion would be possible with more awareness among the farmers backed up with scientific study.

The initial evaluation of the combination ratio treatments suggests that if both the types of pesticides need to be used for better protection against pests, then the most preferable treatment would be to use a mixture of two volumes of Neemark with one volume of Tafgor. This combination exhibits the lowest toxicity to *Daphnia* as opposed to 1:1 v/v or 1:2 v/v of Neemark and Tafgor. Our study has shown that concentration and the combination ratio treatment critically affect the percent mortality of *Daphnia*. Thus, these can act as governing factors that can be considered, when using a combination of these pesticides on the field which would, in turn, ensure a healthy aquatic environment. The efficiency of these pesticides, with varying concentrations and combination treatments, to eradicate the target pest organisms needs further assessment which would strengthen their application on the field. This would not only promote good crop and soil health but also facilitate a healthy aquatic ecosystem sustainable for other aquatic life forms.

REFERENCES

Azgin, C. and Goksu, M. Z. L. 2016. Acute toxicity of Abamectin (insecticide) on *Daphnia magna* (Straus, 1820). Journal of Biological and Environmental Science, 10(30): 125-128.

Bharadwaj, T. and Sharma, J. P. 2013. Impact of pesticides application in agricultural industry: an Indian scenario. International Journal of Agriculture and Food Science Technology, 4(8): 817-822.

Demetrio, P. M., Bonetto, C. and Ronco, A. E. 2014. The effect of cypermethrin, chlorpyrifos, and glyphosate active ingredients and formulations on Daphnia magna (Straus). Bulletin of Environmental Contamination and Toxicology, 93: 268-273.

Dodson, S. I., Merritt, C. M., Torrentera, L., Winter, K. M., Tornehl, C. K. and Girvin, K. 1999. Dieldrin reduces male production and sex ratio in Daphnia galeata mendotae. Toxicology and Industrial Health, 15: 192-199.

Eldridge, B. F. 2008. Pesticide Application and Safety Training for Applicators of Public Health Pesticides. Sacramento: California Department of Public Health, Vector-Borne Disease Section.

Encina, F., Escalante, P. de L. R. and Salazar, K. 2017. Acute toxicity (LC_{50}) of a pesticide (Carbendazim) on two native crustacean zooplankton species: *Daphnia pulex* Leidig, 1860 and *Tumeodiaptomus diabolicus* (Brehm 1935) from northern Patagonian lakes (Chile). Crustaceana, 90(2): 199-206.

Finnegan, M. S., Baxter, L. R., Maul, J., Hanson, M. L. and Hoekstra, P. F. 2017. Comprehensive characterization of the acute and chronic toxicity of the neonicotinoid insecticide Thiamethoxam to a suite of aquatic primary producers, invertebrates and fish. Environmental Toxicology and Chemistry, 36(10): 2838-2848.

Finney, D. J. 1971. Probit Analysis 3rd ed. Cambridge University Press, London.UK.

Goktepe, I. and Plhak, L. C. 2002. Compartive toxicity of two azadirachtin - based neem pesticides to Daphnia pulex. Environmental Toxicology and Chemistry, 21(1): 31-36.

Hanazato, T. 2000. Pesticide effeccts on freshwater zooplankto: an ecological perspective. Environmental Pollution, 112: 1-10.

Hassoon, H. A. and Salman, S. A. 2016. The acute effect of pesticides Carbaryl and Imidacloprid on *Daphnia pulex* species. Journal of International Environmental Application and Science, 11(1): 18-28.

Hummel, H. E., Hein, D. F. and Schmutterer, H. 2012. The coming of age of azadirachtins and related tetranortriterpenoids. Journal of Biopesticides, 5: 82-87.

Kandpal, V. 2014. Biopesticides. International Journal of Environmental Research and Development, 4: 191-196.

Kekane, A. 2013. Indian agriculture - status, importance and role in Indian economy. International Journal of Agriculture and Food Science Technology, 4(4): 344 - 346.

Kersting, K. and van Wijngaarden, R. 1992. Effect of chloropyrifos on a microecosystem. Environmental Toxicology and Chemistry, 11: 365-372.

Kikuchi, M., Sasaki, Y. and Wakabayashi, M. 2000. Screening of organophosphate insecticide pollution in water by using Daphnia magna. Ecotoxicology and Environmental Safety, 47(3): 239-245.

Kumar, S. 2012. Biopesticides: A need for food and environmental safety. Journal of Biofertilizers and Biopesticides, 3(4): 1-3.

Kumar, S. and Singh, A. 2015. Biopesticides: Present status and the future prospects. Journal of Fertilizers and Pesticides, 6(2): 1-2.

Leight, A. K. and Dolah, R. F. V. 1999. Acute toxicity of the insecticides endosulphan, chloropyrifos and malathion to the epibenthic estuarine amphipod Gammarus palustris(Bousfeild). Environmental Toxicology and Chemistry, 18(5): 958-964.

Luo, Y., Zang, Y., Zhong, Y. and Kong, Z. 1999. Toxicological study of two novel pesticides on earthworm Eisenia foetida. Chemosphere, 39(13): 2347-2356.

Maranho, L. A., Botelho, R. G., Inafuku, M. M., de A.R. Nogueira, L., de Olinda, R. A., de Sousa, B. A. and Tornisielo, V. L. 2014. Testing the neem biopesticide (Azadirachta indica A. Juss) for acute toxicity with Danio rerio and for chronic toxicity with Daphnia magna. Journal of Agricultural Science and Technology, 16: 105-111.

Marrone, P. G. 2014. The market and potential for biopesticides. In: Coates, et al. Biopesticides: State of the Art and Future Opportunities. Proceedings of the American Chemical Society Symposium Series.

Pimentel, D., Acquay, H., Biltonen, M., Rice, P., Silva, M., Nelson, J., Lipner, V., Giordano, S., Horowitz, A. and D' Amore, M. 1992. Environmental and economic costs of pesticide use. BioScience, 42(10): 750-760.

Raby, M., Nowierski, M., Perlov, D., Zhao, X., Hao, C., Poirier, D. G. and Sibley, P. K. 2018. Acute toxicity of six neonicotinoid insecticides to freshwater invertebrates. Environmental Toxicology and Chemistry, 37(5): 1430-1445.

Saucke, H. and Schmutterer, H. 1992. Investigations on side-effects of various neem products on Daphnia magna Straus (Crustacea: Cladocera). Journal of Pest Science, 65: 121-126.

Scott, I. M. and Kaushik, N. K. 1998. The toxicity of Margosan-O, a product of neem seeds, to selected target and nontarget aquatic invertebrates. Archives of Environmental Contamination and Toxicology, 35: 426-431.

Stark, J. D. 2001. Population-level effects of the neem insecticide, Neemix, on Daphnia pulex. Journal of Environmental Science and Health, B36(4): 457-465.

Stark, J. D. 2007. Ecotoxicology of neem. ACS Symposium Series, 947: 275-286.

Subash, P.S., Prem Chand, S., Pavithra, J. B. S. and Pal, S. 2017. Pesticide use in Indian agriculture: trends, market structure and policy. ICAR - National Institute of Agricultural Economics and Policy Research, 1-4.

U.S. Environment Protection Agency (EPA). Fate and environmental risk assessment chapter. 2000. Available online: http://www.epa.gov/pesticides/op/chlorpyrifos/efedrra1.pdf. Accessed on 5th September 2019.

U.S. Environmental Protection Agency. 1983. Dimethoate: Proposed Tolerance. Federal Register 48.

Yadav, I. C. and Devi, N. L. 2017. Pesticides classification and its impact on human and environment. Environmental Science and Engineering, 6: 140-158.

Yadav, I. C., Devi, N. L., Syed, J. H., Cheng, Z., Li, J., Zhang, G. and Jones, K. C. 2015. Current status of persistent organic pesticides residues in air, water, and soil, and their possible effect on neighboring countries: A comprehensive review of India. Science of the Total Environment, 511: 123-127.

Yim, E. C., Kim, H. J. and Kim, S. J. 2014. Acute toxicity assessment of camphor in bio-pesticides by using *Daphnia magna* and *Danio rerio*. Environmental Health and Toxicology, 29: 1-8.

Nature Environment and Pollution Technology
An International Quarterly Scientific Journal

p-ISSN: 0972-6268
(Print copies up to 2016)
e-ISSN: 2395-3454

Vol. 20 | No. 2 | pp. 703-711 | 2021

Original Research Paper

https://doi.org/10.46488/NEPT.2021.v20i02.029

Open Access Journal

Sensitivity Analysis of the Smart City Environmental Sustainability Index (SCESI)

Shruti†, P. K. Singh and A. Ohri
Department of Civil Engineering, Indian Institute of Technology, BHU, Varanasi-221005, Uttar Pradesh, India
†Corresponding author: Shruti; drshrutisingh984@gmail.com

Nat. Env. & Poll. Tech.
Website: www.neptjournal.com

Received: 26-06-2020
Revised: 05-08-2020
Accepted: 27-08-2020

Key Words:
Environmental indicators
Sensitivity analysis
Smart city environmental sustainability index

ABSTRACT

In recent years, the field of Sustainable Smart Cities is rapidly burgeoning, and the related research carried out is unexplored, heterogeneous, and involves a plethora of issues. In this research, the framework for the Smart City Environmental Sustainability Index (SCESI) is defined and evaluated to guide the investments and monitor the progressive environmental development of Indian cities. The index is based on 24 environmental indicators, and their corresponding significance is assessed by the expert panel. SCESI is an integrated tool on a scale of 0 to 100, which depends upon the value of indicators and their relative weights. However, sometimes data for all the 24 environmental indicators may not be available. The present work determines the sensitivity analysis by applying certain interventions. Eight scenarios have been generated by taking various combinations of high and low weight indicators. The analysis of the study indicates that the occurrence of error is marginal in both cases of non-availability of high and low weight indicators. Thus, the sensitivity analyses critically assess the variations in the SCESI when there are uncertainties involved in the input data.

INTRODUCTION

Rapid urbanization worldwide had created sheer pressure on the urban built environment (Turner 1990). According to the United Nations, the urban population worldwide will increase by up to 60% by the year 2050 (United Nations 2014). The bloom in the urban population will give rise to significant challenges regarding unemployment, congestion, environmental pollution and social sustainability (OECD 2012). Urban population in India is expected to reach 814 million by the year 2050, making it the second most populated country in the world (Randhawa & Kumar 2017). Due to the rapid increase in urbanisation rate the five Indian megacities Bangalore, Delhi, Mumbai, Kolkata, and Chennai will increase to 7 by 2030, with the new addition of Ahmadabad and Hyderabad (Randhawa & Kumar 2017). The rapid urbanization and technological advancement urge to recreate and manage the cities to cope with the challenging issue of urban population explosion. Over the last decades, the rise in environmental awareness has resulted in an opportunity to reconstruct the existing cities under a new heading as Environmentally Sustainable Smart Cities (ESSC).

Ministry of Urban Development (MoUD), Government of India (GOI) launched Smart Cities Mission (SCM) in the year 2015 with an idea to model 100 cities (MoUD 2015). The mission aims to cope up with the massive urbanization challenges of the coming decades. The concept of the mission aims towards improving the quality of life by integrating technological solutions through ICT, which can be considered as sustainable development for the cities. But the mission lacks concerns towards environmental dimensions, the most crucial aspect of sustainability. Moreover, none of the programs implemented in India prior to SCM focuses on a sustainable approach (Randhawa & Kumar 2017), thus this mission can be taken as an opportunity to develop ESSC in India.

Topical studies reveal that there is no assessment framework available to inter-relate sustainability and smartness quotient, and the measurement methodologies to measure both strands for a particular city. Thus, a framework for ESSC has been designed using 24 indicators (Singh et al. 2020). The developed Smart City Environmental Sustainability Index (SCESI) combines the design concepts of sustainability with smartness to evaluate their practicality performance. However, city managers and policymakers may face difficulty in collecting data of all 24 indicators included in SCESI. Hence sensitivity analysis is carried out to investigate the variation of SCESI result to the variation of input data. It is carried out to enhance the reliability of the developed index by evaluating the scenarios generated due to the unavailability of data generation.

CONCEPT OF SMART CITY ENVIRONMENTAL SUSTAINABILITY INDEX (SCESI)

Smart City Environmental Sustainability Index (SCESI) has

been developed by selecting 24 environmental indicators divided into four domains Solid Waste Management (SWM), Water Supply Management (WSM), Sewerage, Sanitation and Storm water Management (SSS) and Ambient Environment Condition (AEC). The index developed involves four steps: i. Selection of Indicators for Environmentally Sustainable Smart Cities, ii. Benchmarking of selected indicators, iii. Assigning weights for the indicators, and iv. Calculation of Smart City Environmental Sustainability Index (SCESI). The four steps used in the index formulation are briefly described here.

The first stage is the most crucial as the selection of appropriate indicators will guide the policymakers in performance assessment, monitoring and target-setting (Huovila et al. 2019). For the said purpose, Singh et al. (2020) selected 14 indicators from MoUD guidelines and 24 additional indicators through a literature survey. Further, these two groups of indicators were tested on the sustainability criteria given by World Bank (Segnestam 2002). The indicators qualified were further tested on smartness criteria given by City Key Indicators (Bosch et al. 2017). Finally, 24 indicators were selected under four broad environmental factors: Solid Waste Management (SWM), Water Supply Management (WSM), Sewerage, Sanitation and Storm Water Drainage (SSS) and Ambient Environment Conditions (AEC) which serve the purpose of ESSC (Singh et al. 2020). The second stage is allocating weights according to the relative importance of each indicator. Equal weighting approach is used for the environmental domains and Delphi methodology is carried out for assigning weight to the indicators under the same

Table 1: Selected indicator and their corresponding weights.

Indicators	Weights (W_k)	Indicator Score $IS_k = (w_k . x_k)$ (Indicator Score Code)
A. Solid Waste Management (SWM)		
1. Efficiency in the collection of MSW (EC)	0.155	ECS
2. Degree of Segregation (DS)	0.171	DSS
3. Extent of solid waste recovered (SWR)	0.163	SWRS
4. Degree of scientific disposal of MSW (SD)	0.165	SDS
5. Recycling and reduction of construction and demolition waste (RCD)	0.133	RCDS
6. Extent of cost recovery in Solid Waste Management (CR_{SWM})	0.130	$CR_{SWM}S$
7. Solid Waste Management programs carried in the city during the last 3 years (SWMP)	0.083	SWMPS
Total	**1.000**	**SWMI = Σ (IS)**
B. Water Supply Management (WSM)		
8. Adequacy of Water Supply (AW)	0.151	AWS
9. Smart meters and Management (SMM)	0.145	SMMS
10.Leakage identification (LI)	0.138	LIS
11.Continuity of water supplied in terms of average no of hrs per day(CW)	0.127	CWS
12. Water Quality Monitoring (WQ)	0.167	WQS
13. Exploitation of underground water ($E_{UG}W$)	0.163	$E_{UG}WS$
14. Extent of cost recovery in water supply services (CR_{WS})	0.109	CR_{WS} S
Total	**1.000**	**WSMI = Σ (IS)**
C. Sewerage, Sanitation and Storm water Management (SSS)		
15.Collection efficiency of Sewage Network (CE)	0.156	CES
16. Adequacy of sewage treatment capacity (AS)	0.149	ASS
17.Quality of treated sewage (QTS)	0.152	QTSS
18.Waste water recycling(WWR)	0.148	WWRS
19. Extent of Cost Recovery (CR_{SSS})	0.101	$CR_{SSS}S$
20.Coverage of toilets (CT)	0.160	CTS
21.Coverage of Storm Water Drainage (CSWD)	0.134	CSWDS
Total	1.000	**SSSI = Σ (IS_k)**
D. Ambient Environment Condition (AEC)		
22. Ambient Air Quality (AAQ)	0.376	AAQS
23. Ambient Sound Level (ASL)	0.325	ASLS
24.Ambient Surface Water Quality (ASW)	0.299	ASWS
Total	**1.000**	**AECI = Σ (IS_k)**

domain. A survey among 30 experts comprising of researchers, policymakers, and academicians were conducted who gave the score on the scale of 1 (Least important) to 5 (Most important) to indicators under the same domain. Then Delphi analysis was carried out and weights were allocated to each indicator. For more precision, the number of experts can be increased. The 24 selected weights and their corresponding weights are shown in Table 1.

The third stage involves benchmarking each of the 24 indicators for quality standards on a scale of 0 to 100 (Poor, Average, Good, and Excellent). This will help the policymakers to ascertain gaps and perform the best remedial measures for improvement in the city. The scale range of benchmarking for each indicator is taken from the data-book of Service Level in the urban water and sanitation sector (MoUD 2012). The fourth and final stage is the calculation of the index with the help of selected indicators. This index is unidirectional with increasing value on the scale of 100 (<20 = Critically low; 20-40 = Poor; 40-60 =Fair; 60-80 = Good; >80 = Excellent).

Variable Aggregation

Smart City Environmental Sustainability Index (SCESI) is the summation of the domain indices: Solid Waste Management Index (SWMI), Water Supply Management Index (WSMI), Sewerage, Sanitation and Stormwater Management Index (SSSI) and Ambient Environment Condition Index (AECI). Individual domains are the summation of indicator score eq. (1) which is calculated using weighted sum linear aggregation eq. (2). To bring uniformity, SCESI is divided by the number of environmental domains and computed using eq. (3).

$$DI = \sum_{j=1}^{n} ISj, \quad \ldots(1)$$

Where, DI is the respective Domain Index, j is the serial number of Indicator, n is the number of indicators in the chosen domain and IS_j is the Indicator Score of j^{th} indicator

$$IS_k = (w_k \,.\, x_k), \quad \ldots(2)$$

Where, w is the weight of the indicator, x is the benchmarked indicator Value and k is the identification number of a chosen indicator.

$$SCESI = (SWMI + WSMI + SSSI + AECI)/4 \quad \ldots(3)$$

When the data is not available for all the 24 environmental indicators included in environmental domains, then the domain index is calculated using eq. (4). Summation of normalised domain indices (DI_m) gives the normalised Smart City Environmental Sustainability Index ($SCESI_m$).

$$DI = \frac{\sum_{j=1}^{n} ISj}{\sum_{i=1}^{n} Wi} \quad \ldots(4)$$

Where, W_i is the summation of the weights given by experts to the indicators in each domain; $W_i \leq 1$.

Non-availability of data can cause an error in the calculation of SCESI which can be calculated by using eq. (5).

$$\text{PercentageError} = \frac{\text{SCESIm} - \text{SCESI}}{\text{SCESI}} \quad \ldots(5)$$

AIM OF THE RESEARCH

In the present research, Sensitivity Analysis is carried out for the index developed known as Smart City Environmental Sustainability Index (SCESI). Sensitivity Analysis investigates the variation in output factor when there is a variation in input factors (Pianosi et al. 2016). SCESI developed depends on the weight given by experts and data generated for each indicator. It is justified to assume that data gathered by municipalities or reliable sources is not flawless, and some percentage of error may be expected (Saisana & Saltelli 2008). Moreover, non-availability of data for all the 24 environmental indicators may be possible, which affects the overall index result. Hence, sensitivity analysis is carried out by generating eight scenarios. The result of the analysis can address a wide range of questions like which indicator has the highest dependency, lowest dependency or negligible effect on the SCESI. The methodology adopted for Sensitivity Analysis is discussed in the further section.

MATERIALS AND METHODS

To assess the uncertainties involved due to the non-availability of the data, case study of five Indian cities: Delhi (D), Patna (P), Varanasi (V), Allahabad (A) and Bhubaneswar (B) is taken up. The sources of data for Solid Waste Management, Water Supply Management and Sewerage, Sanitation and Stormwater Management are City Development Plan (CDP) and Swachh Sarvechhan Report (SSR) from the Swachh Bharat Mission program. Ambient Environment condition data is obtained through the Central Pollution Control Board (CPCB) and ENVIS website of respective cities. To avoid discrepancy in the result a factor of 0.25 is taken for indicator having a critically low performance. To estimate the errors involved in calculating the Smart City Environmental Sustainability Index, due to the non-availability of indicator data, an approach of Ignoring indicator data based on weight factor is used (Kumar & Alappat 2005, Ohri & Singh 2011). Further, in this approach, two options are explored. In the first option, the data of the environmental indicator having high weight in each of the four domains are ignored and in the second option, the data of the environmental indicator having low weight in all the four domain data are assumed

to be unavailable. The results obtained in the two options are discussed further.

Removing Indicators with High Weight Factor

1. In the first step, the Domain indices are calculated using 7 indicators (7I) for SWMI, 7 indicators (7I) for WSMI, 7 indicators for SSSI (7I) and 3 indicators for AECI (3I). Respective Domain Indices is calculated using eq. (1) and (2).
2. In the second step, the indicator having the highest weight in each domain is presumed to be unknown. For calculating domain indices, 6 indicators (6I) for SWMI, 6 indicators (6I) for WSMI, 6 indicators for SSSI (6I) and 2 indicators for AECI (2I) is involved. Degree of Segregation (0.171) in SWM, Water Quality Monitoring (0.167) in WSM, Coverage of toilets (0.160) in SSS and Ambient Air Quality (0.376) in AEC is ignored (Table 2). As the data of indicator having the highest weight is presumed to be unknown the domain indices are calculated using eq. (4).
3. In the third step, it is presumed that indicators having the second-highest weight are unavailable along with the indicators involved in step 2. For calculating domain indices, 5 indicators (5I) for SWMI, 5 indicators (5I) for WSMI, 5 indicators for SSSI (5I) and 2 indicators for AECI (2I) is taken up. Degree of scientific disposal of MSW (0.165) in SWM, Exploitation of underground water (0.163) in WSM and Collection efficiency of Sewage Network (0.156) in SSS is ignored (Table 2). Respective domain indices are calculated using eq. (4).
4. The percentage error occurred due to calculating domain index value with respect to the domain index value when data for all the indicators are available is also reported in the last row (Table 2).

Removing Indicators with Low Weight Factor

1. In the first step, the Domain indices are calculated using 7 indicators (7I) for SWMI, 7 indicators (7I) for WSMI, 7 indicators for SSSI (7I) and 3 indicators for AECI (3I). Respective Domain Indices is calculated using eqns. 1 and 2.
2. In the second step, the indicator having the lowest weight in each domain is presumed to be unknown. For calculating domain indices, 6 indicators (6I) for SWMI, 6 indicators (6I) for WSMI, 6 indicators for SSSI (6I) and 2 indicators for AECI (2I) is involved. Solid Waste Management programs carried in the city during the last 3 years (0.083) in SWM, Extent of cost recovery in water supply services (0.109) in WSM, Extent of Cost Recovery (0.101) in SSS and Ambient Surface Water Quality (0.299) in AEC is ignored (Table 3). As the data of indicator having the lowest weight is presumed to be unknown the domain indices are calculated using eq. (4).
3. In the third step, it is presumed that the second-lowest weight indicators are unavailable along with the indicators involved in step 2. For calculating domain indices, 5 indicators (5I) for SWMI, 5 indicators (5I) for WSMI, 5 indicators for SSSI (5I) and 2 indicators for AECI (2I) is taken up. Extent of cost recovery in Solid Waste Management (0.130) in SWM, Continuity of water supplied in terms of average no of hrs per day (0.127) in WSM and Coverage of Storm Water Drainage (0.134) in SSS is ignored (Table 3). Respective domain indices are calculated using eq. (4).
4. The percentage error occurred due to calculating domain index value with respect to the domain index value when data for all the indicators are available is also reported in the last row (Table 3).

RESULTS AND DISCUSSION

The precision of the outcome is determined by sensitivity analysis when certain interventions are applied (Sözer & Takmaz 2020). Each intervention has a different impact on the overall index developed. Eight scenarios have been generated in high and low weight factors respectively. The different combinations involved in eight scenarios are as follows: 7 indicators of SWM, 7 indicators of WSM, 7 indicators of SSS, 3 indicators of AEC (Total=24); 6 indicators of SWM, 7 indicators of WSM, 7 indicators of SSS, 3 indicators of AEC (Total 23); 5 indicators of SWM, 7 indicators of WSM, 7 indicators of SSS, 3 indicators of AEC (Total 22); 5 indicators of SWM, 6 indicators of WSM, 7 indicators of SSS, 3 indicators of AEC (Total 21); 5 indicators of SWM, 5 indicators of WSM, 7 indicators of SSS, 3 indicators of AEC (Total 20); 5 indicators of SWM, 5 indicators of WSM, 6 indicators of SSS, 3 indicators of AEC (Total 19); 5 indicators of SWM, 5 indicators of WSM, 5 indicators of SSS, 3 indicators of AEC (Total 18); 5 indicators of SWM, 5 indicators of WSM, 5 indicators of SSS, 2 indicators of AEC (Total 17).

Normalised SCESI is calculated by summing up the normalised domain indices values. Percentage error is calculated using eqn 5. The result of the analysis is shown in Fig. 1 and Fig. 2. The highest error of 8.8% is introduced when 2 indicators of high weight indicators are ignored in the city Bhubaneswar. A marginal error upto 5% is reported in the other cities. An error of 12.95% is reported in the city Delhi when 7 indicators of low weight factor are ignored. An assessment of the result shows that the error involved in

Table 2: Estimating Errors introduced in calculation of domain indices due to non-availability of High Weight indicators (AMRUT 2015; CBUD 2015 a,b; HoUD 2015; MOEF 2017).

	Wt.	D	7I	6I	5I	P	7I	6I	5I	V	7I	6I	5I	A	7I	6I	5I	B	7I	6I	5I
Solid Waste Management (SWM)																					
DSS	0.171	0.31	5.40	-	-	0.30	5.13	-	-	0.25	4.27	-	-	0.25	4.27	-	-	0.25	4.27	-	-
SDS	0.165	0.25	4.12	4.12	-	0.25	4.12	4.12	-	0.25	4.12	4.12	-	0.25	4.12	4.12	-	0.25	4.12	4.12	-
SWRS	0.163	0.31	5.15	5.15	5.15	0.25	4.07	4.07	4.07	0.25	4.07	4.07	4.07	0.25	4.07	4.07	4.07	0.80	13.04	13.04	13.04
ECS	0.155	0.80	12.52	12.52	12.52	0.80	12.40	12.40	12.40	0.80	12.40	12.40	12.40	0.80	12.40	12.40	12.40	0.90	13.95	13.95	13.95
RCDS	0.133	1.00	13.30	13.30	13.30	0.25	3.32	3.32	3.32	0.25	3.32	3.32	3.32	0.25	3.32	3.32	3.32	0.25	3.32	3.32	3.32
$CR_{SWMS}S$	0.130	0.01	0.15	0.15	0.15	0.25	3.25	3.25	3.25	0.25	3.25	3.25	3.25	0.25	3.25	3.25	3.25	1.00	13.00	13.00	13.00
SWMPS	0.083	1.00	8.30	8.30	8.30	1.00	8.30	8.30	8.30	1.00	8.30	8.30	8.30	1.00	8.30	8.30	8.30	1.00	8.30	8.30	8.30
Summation	1.000		48.95	43.55	39.43		40.60	35.47	31.35		39.75	35.47	31.35		39.75	35.47	31.35		60.01	55.74	51.61
Total Weight			1.000	0.829	0.664		1.000	0.829	0.664		1.000	0.829	0.664		1.000	0.829	0.664		1.000	0.829	0.663
Normalized SWM			48.95	52.54	59.38		40.60	42.79	47.21		39.75	42.79	47.21		39.75	42.79	47.21		60.01	67.23	77.73
Percentage Error			0	7.31	21.29		0.00	5.38	16.27		0.00	7.65	18.77		0.00	7.65	18.77		0.00	12.03	29.52
Water Supply Management (WSM)																					
WQS	0.167	0.99	16.53	-	-	0.80	13.36	-	-	0.96	16.03	-	-	0.80	13.36	-	-	1.00	16.70	-	-
$E_{UG}WIS$	0.163	0.25	4.07	4.07	-	0.25	4.07	4.07	-	0.25	4.07	4.07	-	0.25	4.07	4.07	-	0.25	4.07	4.07	-
AWS	0.151	1.00	15.10	15.10	15.10	0.52	7.92	7.92	7.92	1.00	15.10	15.19	15.10	1.00	15.10	15.10	15.10	1.00	15.10	15.10	15.10
SMMS	0.145	0.55	8.01	8.01	8.01	0.25	3.62	3.62	3.62	0.25	3.62	3.62	3.62	0.01	0.14	0.14	0.14	0.01	0.20	0.20	0.20
LIS	0.138	0.47	6.56	6.56	6.56	0.70	9.66	9.66	9.66	0.42	5.79	5.79	5.79	0.70	9.66	9.66	9.66	0.37	5.17	5.17	5.17
CWS	0.127	0.12	1.52	1.52	1.52	0.33	4.19	4.19	4.19	0.41	5.20	5.20	5.20	0.41	5.20	5.20	5.20	0.08	1.01	1.01	1.01
$CR_{WS}S$	0.109	0.41	4.46	4.46	4.46	0.50	5.45	5.45	5.45	0.61	6.64	6.64	6.64	0.81	8.82	8.82	8.82	0.31	3.38	3.38	3.38
Summation	1.000		56.28	39.75	35.68		48.28	34.92	30.85		56.48	40.45	36.37		56.37	43.01	38.94		45.65	28.95	24.88
Total Weight			1.000	0.833	0.670		1.000	0.833	0.670		1.000	0.833	0.670		1.000	0.833	0.670		1.000	0.833	0.670
Normalized WSM			56.28	47.72	53.25		48.28	41.93	46.05		56.48	48.56	54.29		56.37	51.63	58.12		45.65	34.76	37.14
Percentage Error			0	15.20	5.39		0	13.16	4.63		0	14.02	3.87		0	8.40	3.09		0	23.86	18.65
Sewerage, Sanitation and Storm water Drainage (SSS)																					
CTS	0.160	0.78	12.48	-	-	0.45	7.2	-	-	0.82	13.12	-	-	0.25	4.00	-	-	0.81	12.96	-	-
CES	0.156	0.63	9.82	9.82	-	0.25	3.9	3.9	-	0.5	7.80	7.80	-	0.99	15.44	15.44	-	0.01	0.15	0.15	-
QTSS	0.152	0.94	14.37	14.37	14.37	0.25	3.8	3.8	3.8	1	15.20	15.20	15.20	0.25	3.80	3.80	3.80	0.80	12.16	12.16	12.16
ASS	0.149	0.89	13.26	13.26	13.26	0.63	9.38	9.38	9.38	0.5	7.45	7.45	7.45	0.99	14.75	14.75	14.75	0.01	0.14	0.14	0.14
WWRS	0.148	0.27	4.05	4.05	4.05	0.7	10.36	10.36	10.36	0.25	3.70	3.70	3.70	0.25	3.70	3.70	3.70	0.25	3.70	3.70	3.70
CSWDS	0.134	0.05	0.72	0.72	0.72	0.65	8.71	8.71	8.71	0.1	1.34	1.34	1.34	0.22	2.94	2.94	2.94	0.45	6.07	6.07	6.07

	Wt.	D	7I	6I	5I	P	7I	6I	5I	V	7I	6I	5I	A	7I	6I	5I	B	7I	6I	5I
$CR_{SSS}S$	0.101	0.39	4.02	4.02	4.02	0.25	2.52	2.52	2.52	0.55	5.55	5.55	5.55	0.81	8.18	8.18	8.18	0.34	3.52	3.52	3.52
Summation			58.75	42.24	36.44		45.88	38.68	34.78		54.16	41.04	33.24		52.82	40.64	33.38		38.72	25.76	25.60
Total Weight			1.00	0.840	0.684		1	0.84	0.684		1.000	0.840	0.684		1.000	0.840	0.684		1.00	0.840	0.684
Normalized SSS			58.75	50.29	53.28		45.88	46.05	50.85		54.16	48.86	48.60		52.82	48.38	48.80		38.72	30.66	37.43
Percentage Error			0.00	14.40	9.30		0	0.36	10.82		0.00	9.78	10.26		0.00	8.40	7.61		0.00	20.79	3.32
Ambient Environment Condition (AEC)																					
AAQS	0.376	0.30	11.43	-		0.55	20.83	-		0.33	12.40	-		0.65	24.59	-		0.78	29.55	-	
ASLS	0.325	0.25	8.12	8.12		0.36	11.70	11.7		0.25	8.12	8.12		0.75	24.37	24.37		0.37	12.18	12.18	
ASWS	0.299	0.25	7.47	7.47		0.50	14.95	14.95		0.25	7.47	7.47		0.50	14.95	14.95		0.50	14.95	14.95	
Summation			27.03	15.60			47.48	26.65			28.00	15.60			63.91	39.32			56.69	27.13	
Total Weight			1.000	0.624			1.000	0.624			1.000	0.624			1.000	0.624			1.000	0.624	
Normalized AEC			27.03	25			47.48	42.70			28.00	25.00			63.91	63.02			56.69	43.48	
Percentage Error			0	7.51			0	10.08			0	10.73			0	1.39			0	23.28	

Table 3: Estimating Errors introduced in the calculation of domain indices due to non-availability of Low Weight indicators.

	Wt.	D	7I	6I	5I	P	7I	6I	5I	V	7I	6I	5I	A	7I	6I	5I	B	7I	6I	5I
Solid Waste Management (SWM)																					
DSS	0.171	0.31	5.40	5.40	5.40	0.30	5.13	5.13	5.13	0.25	4.27	4.27	4.27	0.25	4.27	4.27	4.27	0.25	4.27	4.27	4.27
SDS	0.165	0.25	4.12	4.12	4.12	0.25	4.12	4.12	4.12	0.25	4.12	4.12	4.12	0.25	4.12	4.12	4.12	0.25	4.12	4.12	4.12
SWRS	0.163	0.31	5.15	5.15	5.15	0.25	4.07	4.07	4.07	0.25	4.07	4.07	4.07	0.25	4.07	4.07	4.07	0.80	13.04	13.04	13.04
ECS	0.155	0.80	12.52	12.52	12.52	0.80	12.40	12.40	12.40	0.80	12.40	12.40	12.40	0.80	12.40	12.40	12.40	0.90	13.95	13.95	13.95
RCDS	0.133	1.00	13.30	13.30	13.30	0.25	3.32	3.32	3.32	0.25	3.32	3.32	3.32	0.25	3.32	3.32	3.32	0.25	3.32	3.32	3.32
$CR_{SWMS}S$	0.130	0.01	0.15	0.15	-	0.25	3.25	3.25	-	0.25	3.25	3.25	-	0.25	3.25	3.25	-	1.00	13.00	13.00	-
SWMPS	0.083	1.00	8.30	-	-	1.00	8.30	-	-	1.00	8.30	-	-	1.00	8.30	-	-	1.00	8.30	-	-
Summation	1.000		48.95	40.65	40.50		40.60	32.30	29.05		39.75	31.45	28.20		39.75	31.45	28.20		60.01	51.71	38.71
Total Weight			1.000	0.917	0.787		1.000	0.917	0.787		1.000	0.917	0.787		1.000	0.917	0.787		1.000	0.917	0.787
Normalized SWM			48.95	44.33	51.46		40.60	35.22	36.91		39.75	34.29	35.83		39.75	34.29	35.83		60.01	56.39	49.19
Percentage Error			0	9.43	5.11		0	13.23	9.07		0.00	13.71	9.85		0.00	13.71	9.85		0.00	6.03	18.03
Water Supply Management (WSM)																					
WQS	0.167	0.99	16.53	16.53	16.53	0.80	13.36	13.36	13.36	0.96	16.03	16.03	16.03	0.80	13.36	13.36	13.36	1.00	16.70	16.70	16.70
$E_{UG}WIS$	0.163	0.25	4.07	4.07	4.07	0.25	4.07	4.07	4.07	0.25	4.07	4.07	4.07	0.25	4.07	4.07	4.07	0.25	4.07	4.07	4.07

	Wt.	D	7I	6I	5I	P	7I	6I	5I	V	7I	6I	5I	A	7I	6I	5I	B	7I	6I	5I
AWS	0.151	1.00	15.10	15.10	15.10	0.52	7.92	7.92	7.92	1.00	15.10	15.10	15.10	1.00	15.10	15.10	15.10	1.00	15.10	15.10	15.10
SMMS	0.145	0.55	8.01	8.01	8.01	0.25	3.62	3.62	3.62	0.25	3.62	3.62	3.62	0.01	0.14	0.14	0.14	0.01	0.20	0.20	0.20
LIS	0.138	0.47	6.56	6.56	6.56	0.70	9.66	9.66	9.66	0.42	5.79	5.79	5.79	0.70	9.66	9.66	9.66	0.37	5.17	5.17	5.17
CWS	0.127	0.12	1.52	1.52	-	0.33	4.19	4.19	-	0.41	5.20	5.20	-	0.41	5.20	5.20	-	0.08	1.01	1.01	-
$CR_{WS}S$	0.109	0.41	4.46	-	-	0.50	5.45	-	-	0.61	6.64	-	-	0.81	8.82	-	-	0.31	3.38	-	-
Summation	1.000		56.28	51.81	50.29		48.28	42.83	38.64		56.48	49.83	44.62		56.37	47.54	42.34		45.65	42.26	41.25
Total Weight			1.000	0.891	0.764		1.000	0.891	0.764		1.00	0.891	0.764		1.00	0.891	0.764		1.000	0.891	0.764
Normalized WSM			56.28	58.15	65.83		48.28	48.07	50.58		56.48	55.93	58.41		56.37	53.36	55.41		45.65	47.43	53.99
Percentage Error			0.00	3.32	16.95		0.00	0.43	4.75		0.00	0.97	3.41		0.00	5.34	1.69		0.00	3.90	18.25
Sewerage, Sanitation and Storm water Drainage (SSS)																					
CTS	0.160	0.78	12.48	12.48	12.48	0.45	7.20	7.20	7.20	0.82	13.12	13.12	13.12	0.25	4.00	4.00	4.00	0.81	12.96	12.96	12.96
CES	0.156	0.63	9.82	9.82	9.82	0.25	3.90	3.90	3.90	0.50	7.80	7.80	7.80	0.99	15.44	15.44	15.44	0.01	0.15	0.156	0.15
QTSS	0.152	0.94	14.37	14.37	14.37	0.25	3.80	3.80	3.80	1.00	15.20	15.20	15.20	0.25	3.80	3.80	3.80	0.80	12.16	12.16	12.16
ASS	0.149	0.89	13.26	13.26	13.26	0.63	9.38	9.38	9.38	0.50	7.45	7.45	7.45	0.99	14.75	14.75	14.75	0.01	0.14	0.14	0.14
WWRS	0.148	0.27	4.05	4.05	4.05	0.70	10.36	10.36	10.36	0.25	3.70	3.70	3.70	0.25	3.70	3.70	3.70	0.25	3.70	3.70	3.70
CSWDS	0.134	0.05	0.72	0.72	-	0.65	8.71	8.71	-	0.10	1.34	1.34	-	0.22	2.94	2.94	-	0.45	6.07	6.07	-
$CR_{SSS}S$	0.101	0.39	4.02	-	-	0.25	2.52	-	-	0.55	5.55	-	-	0.81	8.18	-	-	0.34	3.52	-	-
Summation			58.75	54.72	54.00		45.88	43.30	34.64		54.16	48.61	47.27		52.82	44.64	41.69		38.72	35.19	29.12
Total Weight			1.000	0.899	0.765		1.000	0.899	0.765		1.000	0.899	0.765		1.000	0.899	0.765		1.000	0.899	0.765
Normalized SSS			58.75	60.87	70.59		45.88	48.22	45.29		54.16	54.07	61.79		52.82	49.65	54.50		38.72	39.14	38.07
Percentage Error			0.00	3.60	20.14		0.00	5.11	1.28		0.00	0.17	14.07		0.00	5.99	3.17		0.00	1.10	1.67
Ambient Environment Condition (AEC)																					
AAQS	0.376	0.30	11.43	11.43		0.55	20.83	20.83		0.33	12.40	12.40		0.65	24.59	24.59		0.78	29.55	29.55	
ASLS	0.325	0.25	8.12	8.12		0.36	11.70	11.70		0.25	8.12	8.12		0.75	24.37	24.37		0.37	12.18	12.18	
ASWS	0.299	0.25	7.47	-		0.50	14.95	-		0.25	7.47	-		0.50	14.95	-		0.50	14.95	-	
Summation			27.03	19.55			47.48	32.53			28.00	20.53			63.91	48.96			56.69	41.74	
Total Weight			1.000	0.701			1.000	0.701			1.000	0.701			1.000	0.701			1.000	0.701	
Normalized AEC			27.03	27.89			47.48	46.40			28.00	29.29			63.91	69.85			56.69	59.54	
Percentage Error			0.00	3.20			0.00	2.26			0.00	4.58			0.00	9.28			0.00	5.03	

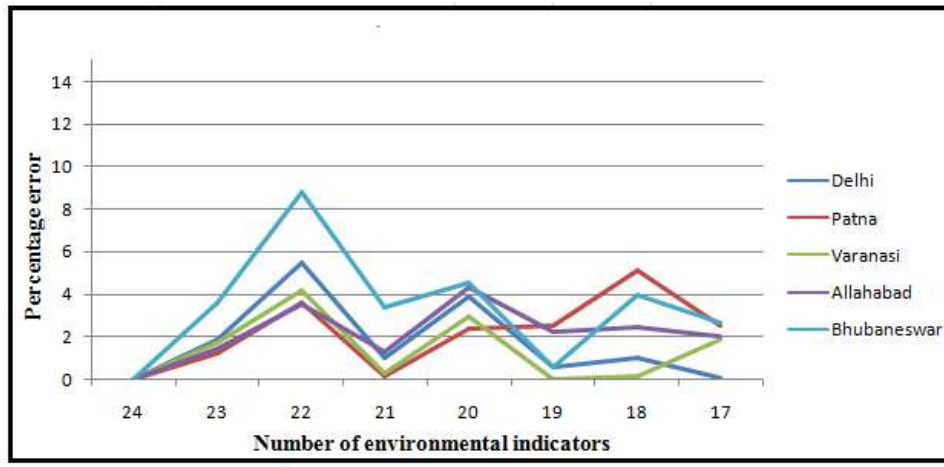

Fig. 1: Variation of percentage error in SCESI with decreasing number of indicators due to non-availability of high weight parameters.

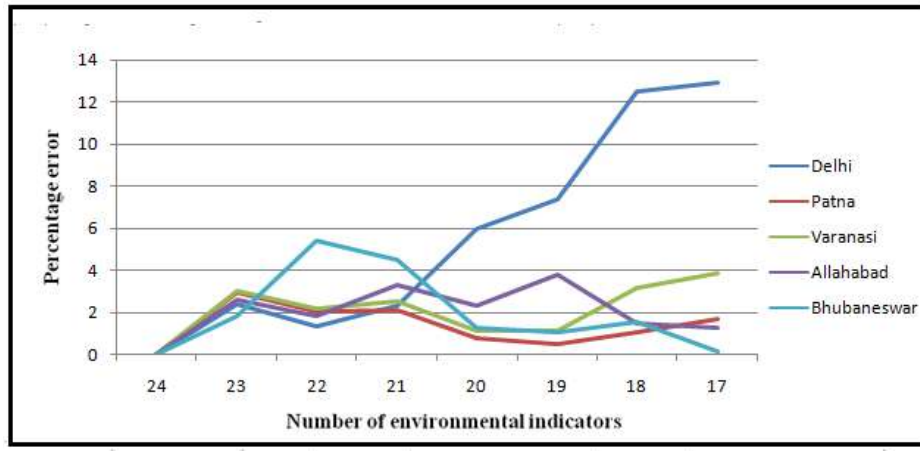

Fig. 2: Variation of percentage error in SCESI with decreasing number of indicators due to non-availability of Low weight parameters.

the different scenarios is not significantly dependent on the number of environmental indicators considered, for which data is unavailable.

CONCLUSIONS

Smart City Environmental Sustainability Index (SCESI) is calculated on the basis of 24 environmental indicators and their corresponding weights. Due to resource and time constraint, unavailability of data is a general phenomenon. For this purpose sensitivity analysis is carried out to explore the possible sets of missing data set. A classification of indicators in high and low weight categories has been done to show its effect on SCESI, in case of non-availability of data. Eight scenarios have been generated, which showed that percentage error is highest when 7 indicators of low weight category are ignored. A marginal error up to 12% is introduced if there is non-availability of high or low weights indicators. Thus, SCESI can be reported with a marginal error but the policymakers should prioritize the efforts for data collection to be non-biased towards the development of Environmentally Sustainable Smart Cities.

REFERENCES

AMRUT, 2015. Bihar State Annual Action Plan for proposed schemes under AMRUT. Available from http://amrut.gov.in/upload/uploadfiles/files/19%20BiharSAAP.pdf.

Bosch, P., Jongeneel, S., Rovers, V., Neumann, H.M., Airaksinen, M. and Huovila, A. 2017. CITYkeys Indicators for smart city projects and smart cities. CITYkeys report.

CBUD 2015a. City Development Plan for Allahabad, 2041 (Final City Development Plan). Available from http://allahabadmc.gov.in/documentslist/City_Development_Plan_Allahabad-2041.pdf.

CBUD 2015b. City Development Plan for Varanasi, 2041 (Final City Development Plan). Available from http://nnvns.org/data/Final%20CDP%20Varanasi.pdf.

HoUD 2015. Declaration of Service Standards. Available from http://www.urbanodisha.gov.in/Admin/Upload_Files/Service%20Level%20Benchmark/SLB%202014-15-%20%202015-16.pdf.

Huovila, A., Bosch, P. and Airaksinen, M. 2019. Comparative analysis of standardized indicators for Smart sustainable cities: What indicators and standards to use and when? Cities, 89: 141-153.

Kumar, D. and Alappat, B.J. 2005. Errors involved in the estimation of leachate pollution index. Pract. Period. Hazard. Toxic Radioact. Waste Manage., 2: 103-111.

MoEF 2017. Air and noise pollution in Delhi and NCR.

MoUD 2012. Service levels in Urban water and sanitation sector Status Report (2010-2011). Ministry of Urban Development, Government of India.

MoUD 2015. Mission statements and Guidelines. Available from http://smartcities.gov.in/upload/uploadfiles/files/SmartCityGuidelines(1).pdf.

OECD 2012. Environmental outlook to 2050. The consequences of inaction [cited 23 February 2016]. Availablefromhttp://www.naturvardsverket.se/upload/miljoarbeteisamhallet/internationelltmiljoarbete/multilateralt/oecd/outolook-2050-oecd.pdf.

Ohri, A. and Singh, P.K. 2011. Error involved in estimation of site sensitivity index (SSI) for landfilling of municipal solid waste. Int. J. Environ. Sci., 1: 767-770.

Pianosi, F., Beven, K., Freer, J., Hall, J.W., Rougier, J., Stephenson, D.B. and Wagener, T. 2016. Sensitivity analysis of environmental models: A systematic review with practical workflow. Environ. Modell. Softw., 79: 214-232.

Randhawa, A. and Kumar, A. 2017. Exploring sustainability of smart development initiatives in India. Int. J. Sustain. Built. Environ., 6: 701-710.

Saisana, M. and Saltelli, A. 2008. Sensitivity Analysis for the 2008 Environmental Performance Index. European Commission: Fermi.

Segnestam, L. 2002. Indicators of Environment and Sustainable Development, (No. P01 234). World Bank, Washington, DC (EUA).

Singh, P.K., Shruti and Ohri, A. 2020. selecting environmental indicators for sustainable smart cities mission in India. Nat. environ. Pollut. Technol., 19: 201-210.

Sözer, H. and Takmaz, D. 2020. Calculation of the sensitivity factors within the defined indexes in a building level. J. Sustain. Dev. Energy Water Environ. Syst., 1: 1-21.

Turner, B.L. 1990. The earth as transformed by human action: global and regional changes in the biosphere over the past 300 years: CUP archive.

United Nations, 2014. World urbanization prospects. The 2014 revision. New York: Department of Economic and Social Affairs [cited 22 May 2016]. Available from http://esa.un.org/unpd/wup/Publications/Files/WUP2014-Report.pdf.

Nature Environment and Pollution Technology
An International Quarterly Scientific Journal

p-ISSN: 0972-6268
(Print copies up to 2016)
e-ISSN: 2395-3454

Vol. 20 | No. 2 | pp. 713-719 | 2021

Original Research Paper

https://doi.org/10.46488/NEPT.2021.v20i02.030

Open Access Journal

The Effect of COVID-19 on the Atmospheric Parameters Over the Indian Subcontinent

C. Ramprasad†
School of Civil Engineering, SASTRA Deemed to be University, Thanjavur, Tamil Nadu, India
†Corresponding author: C. Ramprasad; ramprasad@civil.sastra.edu

Nat. Env. & Poll. Tech.
Website: www.neptjournal.com

Received: 05-07-2020
Revised: 10-09-2020
Accepted: 16-09-2020

Key Words:
Aerosol index
Carbon monoxide
COVID 19
Nitrogen dioxide
Spatio-temporal variation

ABSTRACT

In the present study, the atmospheric concentrations of various pollutants over the Indian subcontinent before the COVID-19 (during 2019) and during COVID-19 phases (2020) were studied. The COVID-19 has created a negative impact on the country's economy but has positivity over the atmospheric resources. The levels of carbon monoxide (CO), nitrogen dioxide (NO_2), and UV aerosol index were assessed using satellite images for the two different phases. The obtained results can be interpreted and can be substantiated with the lockdown effect due to the COVID -19 pandemic. The pollutants are mostly emitted from anthropogenic sources like vehicular emissions, industrial emissions, power plants, construction works, commercial and institutional places. It was evident that the levels of carbon monoxide, nitrous dioxide and aerosols levels have drastically decreased during the lockdown period. Hence, it can be concluded that COVID-19 has cleaned the atmospheric pollution as well as climate change scenario and nature on its own.

INTRODUCTION

The Corona diseases 2019 (COVID-19) has become a global pandemic and was the greatest threat to more than 200 countries and infected more than 3 million people globally (WHO 2020). The United Nations Department of Economic and Social Affairs (UNDESA) has predicted that the COVID-19 pandemic has troubled the global economy and it could shrink by 1% in 2020. Many countries have adopted the control measures like social distancing, wearing personal protective equipment like a mask, hand-wash, regular sanitizing, regional lockdown, closing the mass gathering places like schools, colleges, industries, pilgrim centre, shopping malls, tourist spots and other non-essential business (Zhang et al. 2020). In India, the COVID-19 has affected over 70,000 people and killed 2,200 people, subsequently, the infected persons usually experience mild to moderate respiratory issues. The Ministry of Health and Family Welfare, Government of India has stated that many older people affected with COVID-19 and other multiple health illness like cardiovascular disease, chronic respiration problem, diabetes, and cancer are most likely to build up serious illness and fatality.

The novel COVID -19 inception in late December 2019 has reduced the anthropogenic activities raised by the humans like vehicular transport, industrial emissions, fossil fuel burning and energy consumption. The pollutants such as carbon monoxide, black carbon, ozone, particulate matters, nitrous oxide and aerosols are the most common pollutants that are emitted from anthropogenic activities and which can harm human begins (Badarinath et al. 2007, Kumar et al. 2010, Ding et al. 2013, Zhang et al. 2020). The prediction of the atmospheric and climate changes can be envisaged by quantifying the primary and secondary air pollutants. Carbon monoxide (CO) is a colourless, tasteless, odourless, and non-irritating gas formed due to the incomplete or partial combustion of carbon materials (Badarinath et al. 2007). Nitrous oxide is an excellent tracer of human-induced activities, it is mostly emitted as NO from anthropogenic combustion sources like vehicular emission, power plants and residential combustion (Martin et al. 2003, Zhang et al. 2018). Aerosols are a suspension of small water droplets or solid particles carried over by the air or other gases into the atmosphere. Aerosols significantly affect the radiation and cause an imbalance between the radiation energy scattering and absorbing (Jia et al. 2019). All these pollutants are highly responsible for causing much illness to the human begins like respiratory problems, bronchitis, asthma, skin cancer and many other problems (Ghude et al. 2019). Additionally, the above-mentioned gases are an important commodity in the greenhouse gases, which are responsible for global climate change. Hence, it is necessary to understand the air quality

trends before and after the COVID-19 situation over the Indian Sub-continent. In the present study, the spatial-temporal variation of the gaseous pollutants like carbon monoxide (CO), and Nitrogen dioxide (NO_2), using the satellite data over the Indian subcontinent were simulated and the trend of Ultraviolet Aerosol index (UVAI) was analysed before and after the novel COVID-19 pandemic situation.

MATERIALS AND METHODS

Study Area

Most of the megacities around the world are affected by air pollution and pressing a growing concern on human health. The study focused on the Indian subcontinent as many reports are suggesting the quality of urban air pollution and its related problems. The trends of the air pollution levels over the Indian subcontinent before and after the COVID-19 pandemic are analysed using satellite images. The Indian cities are grouped into six different zones which consist of many mega cities – The northern zone consists of 29 cities; Southern zone consists of 26 cities; Eastern zone consists of 21 cities; Western zone consists of 33 cities; Central zone consists of 8 cities; North-east zone consists of 11 cities. Data criterion was collected from the satellite images (https://giovanni.gsfc.nasa.gov/giovanni/) for the year 2019 and 2020 i.e., one year before the COVID-19 and during the pandemic situation.

Satellite Datasets for Gaseous Air Pollutants

GIOVANNI is an open broad web interface that allows the users to view and analyze NASA's gridded data from various satellites and surface observations. Giovanni provides the users with the data's pertaining to the atmospheric chemistry, atmospheric temperature, water vapour, atmospheric aerosols, hydrology, ocean chlorophyll, and surface temperature and analytical functions were performed by Grid Analysis and Display Systems (GrADS) (Acker & Leptoukh 2007). The Atmospheric Infrared Sounder (AIRS) is a grating spectrometer aboard the second earth observing system (EOS) and the polar orbiting platform. AIRS comprises of an innovative atmospheric sound group with infrared, visible and microwave sound sensors with a combination of Advanced Microwave Sounding Unit (AMSU) and Humidity Sounder for Brazil (HSB). The carbon monoxide (CO) map was prepared by considering the monthly averaged mean mole fraction values in air and measured in ppbv during the ascending day time at 1 × 1 degree grid cells at 925 hPa (Kahn et al. 2014). The Nitrogen dioxide (NO_2) satellite data sets were acquired from the time average OMI-AURA (Ozone Monitoring Instrument-AURA) tropospheric column level 3 daily gridded at 0.25 × 0.25 degree resolution and measured with a unit 1 per sq. cm (Nickolay et al. 2019).

The UV aerosol index (AI) map was obtained from the daily time-weighted average from Ozone Monitoring Instrument (OMI) at 1 × 1 degree resolution. The index detects the particulate maters mostly dust and soot emissions from the anthropogenic activities. It is based on the spectral contrast method in a UV region where the ozone is very minimal. The AI is the difference between the observations and model values of absorbing and non-absorbing spectral radiance ratios and given by the below equation (1),

$$AI=100\,[\log_{10}(I_{360}/I_{331})_{measured}-\log_{10}(I_{360}/I_{331})_{calculated}]\ldots(1)$$

Where, $(I_{360}/I_{331})_{measured}$ are the radiances measured at 360 nm and 331 nm and $(I_{360}/I_{331})_{calculated}$ are the calculated radiances at 360 nm and 331 nm assuming a Rayleigh scattering atmosphere. Positive values of the Aerosol Index generally represent absorbing aerosols (dust and smoke) while small or negative values represent non-absorbing aerosols and clouds (Pawan & Bhartia 2012).

RESULTS AND DISCUSSION

Carbon Monoxide (CO)

Spatial-temporal variation: Carbon monoxide (CO) is produced by the incomplete combustion of various carbon fuels of both biomass and fossil origins as well as from the oxidation of methane and other hydrocarbons. CO is a poisonous, odourless, and colourless gas. CO is not a direct greenhouse gas; however, CO and other pollutants can affect tropospheric ozone, carbon dioxide, and methane. Thus, CO can have an indirect effect on climate. The mixing ratio of CO is widely used as a tracer of polluted air in remote regions mainly due to its specific emission sources and longer atmospheric lifetimes of about 2 months (Sahu et al. 2019, Tang et al. 2019). CO is measured by the total column measurement; it is the number of molecules of CO in an atmospheric column from the Earth's surface to the top of the stratosphere above a square centimetre of the surface, it is the volume mixing ratio in parts per billion (ppbv). In South Asia, the major sources of CO emissions are biomass burning and anthropogenic activities including the usage of fossil fuels (Shindell et al. 2006). Yoon & Pozzer (2014) estimated a rapid increase in CO mixing ratios over South Asia due to the increasing anthropogenic emissions by combining observations with a global climate model. In urban and polluted regions, the oxidation of CO can lead to the formation of ozone (O_3) in the presence of oxides of nitrogen (NOx = NO + NO_2) and sunlight. Additionally, CO is a criterion pollutant as exposure to its elevated levels adversely affects the regional to global air quality and human health (Prockop

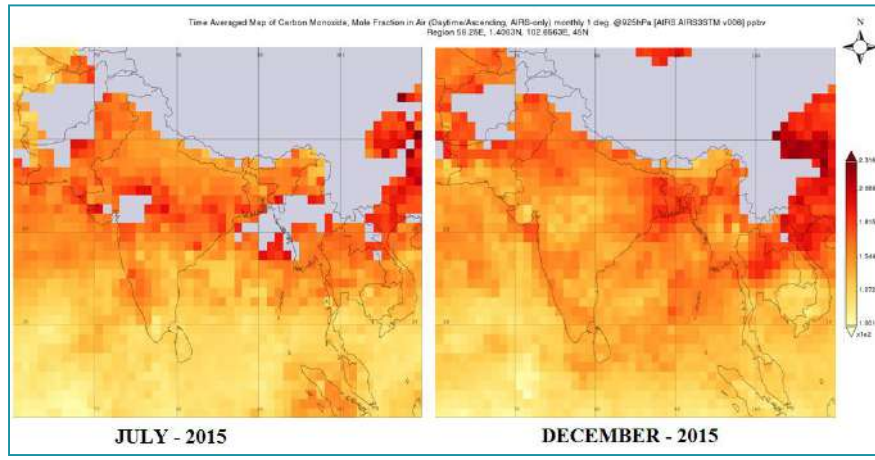

Fig. 1: Spatio-temporal variation of CO during July and December 2015.

& Chichkova 2007). Therefore, it is important to investigate the spatio-temporal variations of CO and the contribution of various emission sources, especially over the South Asia region where anthropogenic activities are increasing rapidly.

During July, the CO concentrations in the Indian peninsular region are much lesser in the range of 7.9 – 14.9 × 10^{-1} ppbv (Fig. 1). Whereas, the concentrations of CO during the December month were over the Indian subcontinent were in the range of 10.6 – 18.1 × 10^{-1} ppbv (Fig.1). The spatio-temporal variability of CO in the troposphere depends on the source locations and the mixing/transport associated with the horizontal and vertical winds (Chandra et al. 2016). In the lower troposphere, the strength of local emission, dilution due to horizontal winds and vertical ventilation due to convection control the seasonal variations of primary pollutants such as CO. In contrast, the seasonality of CO aloft strongly depends on the vertical transport near the ground to the middle and upper troposphere, especially in the tropics favoured by strong convection activities (Sheel et al. 2014). The near-surface wind speeds in July are higher compared to December, leading to dilution effect and hence lower CO concentration in July than in December. The spatial variation of CO is visible from the figure, as it is lesser in the oceans and more in the overland. The above scenario explains to us that as the anthropogenic activities (Burning of fossil fuel) are more in the land surface than in the ocean; hence concentrations of CO are higher in land. It was also evident from the figure that the spatial variation of CO over the Bay of Bengal was much higher compared to the Arabian Sea. The above scenario explains the fact that proximity of land directly affects CO levels. The Bay of Bengal is in between two landmasses and is more vulnerable to the continental wind-driven outflow of pollutants into the oceans.

Effect of COVID-19 on carbon monoxide levels: The lockdown scenario due to COVID-19 has shut many of the industries and transportation paved a negative impact on the

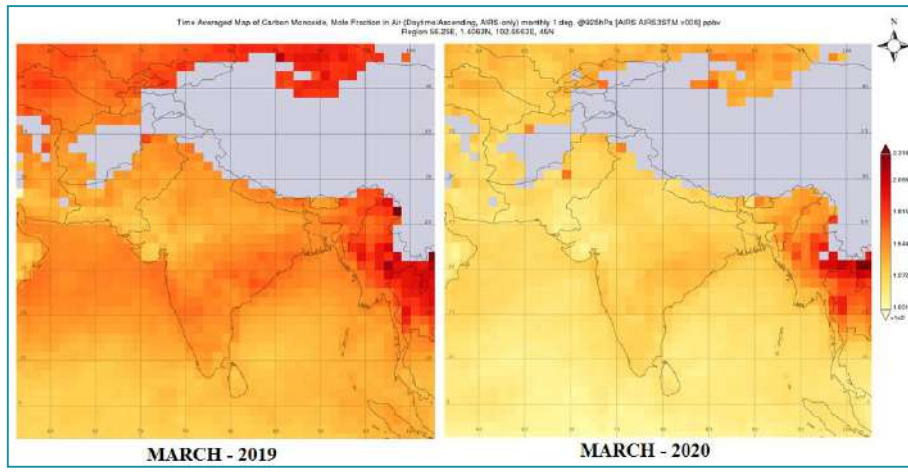

Fig. 2: Spatio-temporal variation of CO over Indian Subcontinent during March.

economy of the country. But, there is positivity from the COVID-19, the atmospheric pollution levels have drastically come down. It was seen from the carbon monoxides levels in the air during the ascending day time at 925 hPa (Fig. 2). During March 2019 the Indian subcontinent has emitted a carbon monoxide value ranging from 15.14 - 18.15 × 10^{-1} ppbv while the levels of carbon monoxide came down to 1 -1.27 × 10^{-1} ppbv during the lockdown period. A similar trend was observed for the carbon dioxide values over the city of Kolkata (Mitra et al. 2020).

Nitrogen dioxide (NO_2)

The emissions of nitrogen dioxide (NO_2) are mainly from mobile and stationary fuel combustion sources. It is an irritant gas, which can cause inflammation of the airways at a higher concentration. As the fuel gets combusted, the nitrogen present in that combine with the oxygen molecules to create nitric oxide (NO), which further reacts with nascent oxygen to form the NO_2. Both these compounds are together considered as oxides of nitrogen (NO_x), where NO are not that harmful like NO_2. The NO_x gases react to form smog and acid rain which can cause adverse health effects like lung diseases, respiratory problems and skin allergies, further higher concentration of nitrous oxides may damage the vegetation, leaf damages and yield (Haris et al. 2011, Deng et al. 2018, Marescaux et al. 2018).

Similar to carbon monoxide values over the Indian subcontinent, the concentrations of nitrogen dioxide have decreased due to the lockdown (Fig. 3 and 4). As it can be visualized from Fig. 4 satellite images that there were many red-orange colour pockets during March 2019, but that was significantly reduced during the 2020 period. In the same way, the May concentrations of NO_2 have reduced due to lesser mobile emissions. Also, it can be visualized that over the 20-25° N and 80-85° E there were many red pouches (highlighted by encircling). The concentrations over that regions were in the range of 1.24-1.65 × 10^{-16} OMI per sq. cm (Fig. 4). The reason may be due to may stationary emissions i.e., power plants are operational over Chhattisgarh and were in good agreement with Patra (2017).

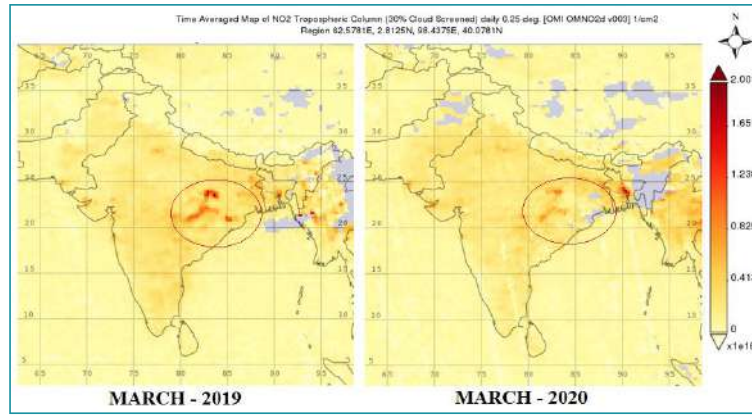

Fig. 3: Spatio-temporal variation of NO_2 over Indian Subcontinent during March.

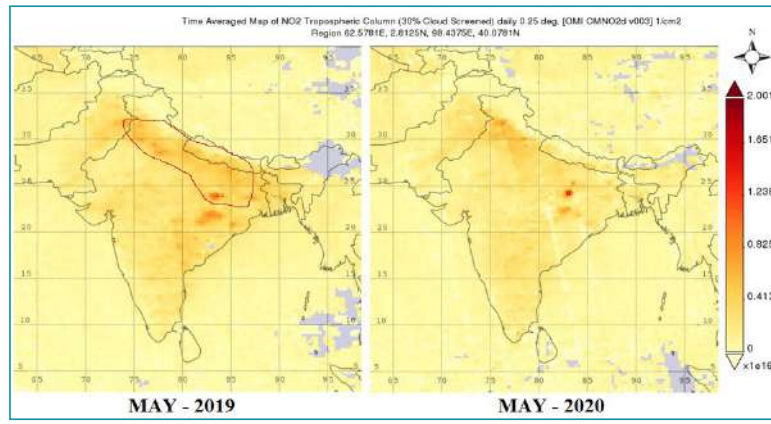

Fig. 4: Spatio-temporal variation of NO_2 over Indian Subcontinent during May.

UV Aerosol Index

The UV aerosol index (UVAI) is the vital method that detects the absorbing aerosol from the satellite near to UV wavelength range. It was explained by researchers that if a positive UVAI value was recorded, it implies that aerosol absorption is happening; a negative value indicates a non-absorbing aerosol. If the AI is close to zero, it indicates the minimal aerosol absorption or non-aerosol related effects such as clouds, ocean colour effects or sun glint (Hammer et al. 2015). The mean OMI UVAI observations for April and May 2019 and 2020 were shown in Fig. 5 and 6. It was visible that clear signals over many Indian cities during April and May 2019.

The UVAI in many of the northern cities like Noida, Delhi, Kanpur and Punjab regions were above 1.5 and 3.0. It resembles that the regions dominant in the mineral dust and biomass burning, and were in good agreement with Kumar & Kumar (2017). After the COVID-19 lockdown situation, the UVAI has significantly reduced in many of the Indian cities as seen in the figure. The places that recorded maximum UVAI during April and May 2019 has shown decline values of UVAI (highlighted with red rounds in figures) during the same month in 2020.

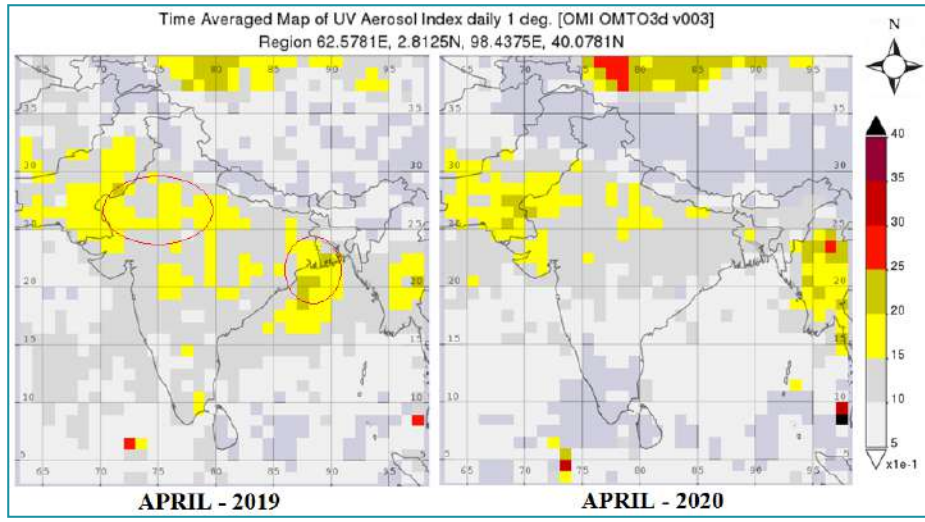

Fig. 5: Spatio-temporal variation of Aerosol Index over Indian Subcontinent during April.

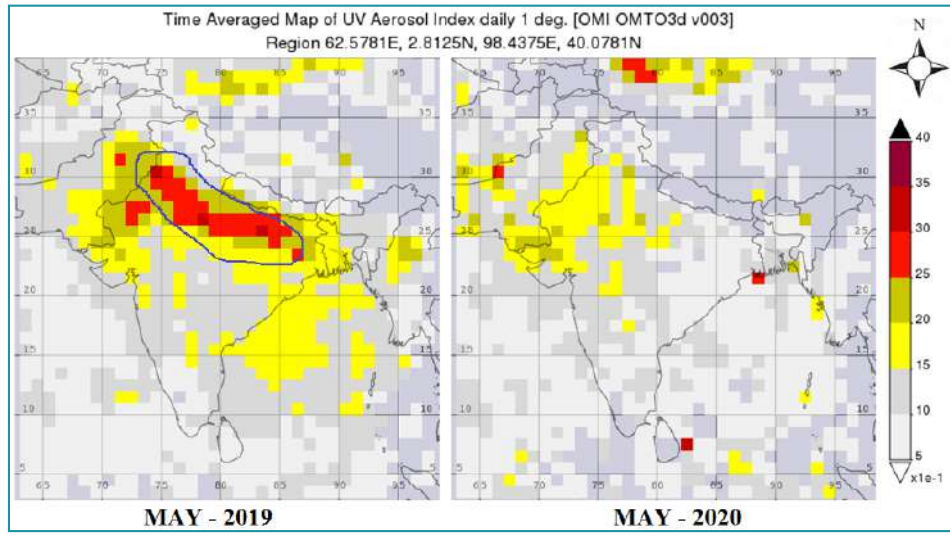

Fig. 6: Spatio-temporal variation of Aerosol Index over Indian Subcontinent during May.

CONCLUSION

The extent of change in the atmospheric parameters like carbon monoxide (CO), nitrogen dioxide (NO_2) and ultraviolet aerosol index (UVAI) are studied over the Indian subcontinent during the unprecedented worldwide COVID-19 pandemic scenario. The global pandemic and subsequent lockdown have flattened the world economy but it reduced the anthropogenic emission sources to a great extent. A significant reduction of primary pollutants, like NO_2 (~65%) and CO (~7%) reveals that the reduced emissions from the vehicular movements and other essential anthropogenic activities, and reveals a better air quality during the lockdown. There was more than a 57% reduction in the UV aerosol index (UVAI) as the value was 1.5-3.5 during the year May 2019 and reduced to 0.5-2.0 during the year May 2020. The above results are evident that apart from the local meteorological and natural emissions like sea spray and pollen grains, the lockdown of various industries, lesser vehicular emissions have decreased the dust as well as smoke emissions thereby the reduced UVAI values. Amongst the three atmospheric pollutants studied, CO was the least impacted by the lockdown. The emissions of CO were predominantly from fossil fuel burning, and the least contribution was seen during the lockdown as well as CO has a longer atmospheric lifetime. Hence, the novel COVID-19 has many negative impacts worldwide but showed few positive effects on the environment by reducing the atmospheric pollutants level and provided a unique opportunity for the researchers to explore sustainable and balanced mitigation strategies.

REFERENCES

Acker, J. G. and Leptoukh, G. 2007. Online analysis enhances use of NASA earth science data. Eos. Trans. AGU., 88(2): 14-17.

Badarinath, K. V. S., Kharol, S. K., Chand, T. K., Parvathi, Y. G., Anasuya, T. and Jyothsna, A. N. 2007. Variations in black carbon aerosol, carbon monoxide and ozone over an urban area of Hyderabad, India, during the forest fire season. Atmos. Res., 85(1): 18-26.

Chandra, N., Venkataramani, S., Lal, S., Sheel, V. and Pozzer, A. 2016. Effects of convection and long-range transport on the distribution of carbon monoxide in the troposphere over India. Atmos. Pollut. Res., 7(5): 775-785.

Deng, J., Guo, L., Salas, W., Ingraham, P., Charrier–Klobas, J. G., Frolking, S. and Li, C. 2018. Changes in irrigation practices likely mitigate nitrous oxide emissions from California cropland. Global Biogeochem. Cycles, 32(10): 1514-1527.

Ding, A., Wang, T. and Fu, C. 2013. Transport characteristics and origins of carbon monoxide and ozone in Hong Kong, South China. J. Geophys. Res. D: Atmos., 118(16): 9475-9488.

Ghude, S. D., Karumuri, R. K., Jena, C., Kulkarni, R., Pfister, G. G., Sajjan, V. and Kulkarni, S. H. 2019. What is driving the diurnal variation in tropospheric NO_2 columns over a cluster of high emission thermal power plants in India? Atmos. Environ., X: 100058.

Hammer, M. S., Martin, R. V., van Donkelaar, A., Buchard, V., Torres, O., Ridley, D. A. and Spurr, R. J. 2015. Interpreting the Ultraviolet Aerosol Index observed with the OMI satellite instrument to understand absorption by organic aerosols: implications for atmospheric oxidation and direct radiative effects. Atmos. Chem. Phys. Discuss., 15(19).

Haris, A. A., Pragyan, K., Vandna, C. and Sandeep, B. 2011. Modeling the impact of anticipated climate change on wheat yields in two different agro-climatic zones of eastern India. J. Agrometeorol., 13(2): 116-118.

Jia, R., Luo, M., Liu, Y., Zhu, Q., Hua, S., Wu, C. and Shao, T. 2019. Anthropogenic aerosol pollution over the eastern slope of the Tibetan Plateau. Adv. Atmos. Sci., 36(8): 847-862.

Kahn, B. H., Irion, F. W., Dang, V. T., Manning, E. M., Nasiri, S. L., Naud, C. M. and Fetzer, E. J. 2014. The atmospheric infrared sounder version 6 cloud products. Atmospheric Chemistry and Physics, 14(1): 399-426.

Kumar, R., Sharma, S. K., Thakur, J. S., Lakshmi, P. V. M., Sharma, M. K. and Singh, T. 2010. Association of air pollution and mortality in the Ludhiana city of India: a time-series study. Indian J. Public Health, 54(2): 98.

Kumar, S. and Kumar, S. 2017. Impact of aerosol on climate and productivity of rice and wheat crop in Bihar. J.Agrometeorol., 19(1): 23.

Marescaux, A., Thieu, V. and Garnier, J. 2018. Carbon dioxide, methane and nitrous oxide emissions from the human-impacted Seine watershed in France. Sci. Total Environ., 643: 247-259.

Martin, R. V., Jacob, D. J., Chance, K., Kurosu, T. P., Palmer, P. I. and Evans, M. J. 2003. Global inventory of nitrogen oxide emissions constrained by space□based observations of NO_2 columns. J. Geophys. Res. D: Atmos., 108(D17).

Mitra, A., Chaudhuri, T. R., Mitra, A., Pramanick, P., Zaman, S., Mitra, A. and Zaman, S. 2020. Impact of COVID-19 related shutdown on atmospheric carbon dioxide level in the city of Kolkata. Sci. Edu., 6(3): 84-92.

Nickolay, A., Krotkov, Lok N. Lamsal, Sergey, V. Marchenko, Edward A. Celarier, Eric J. Bucsela, William, H. Swartz, Joanna Joiner and the OMI core team. 2019. OMI/Aura NO_2 Cloud-Screened Total and Tropospheric Column L3 Global Gridded 0.25 degree x 0.25 degree V3, NASA Goddard Space Flight Center, Goddard Earth Sciences Data and Information Services Center (GES DISC), (Accessed on May 13, 2020), 10.5067/Aura/OMI/DATA3007

Patra, A. K. 2017. Accounting methane and nitrous oxide emissions, and carbon footprints of livestock food products in different states of India. J. Cleaner Prod., 162: 678-686.

Pawan, K. and Bhartia 2012. OMI/Aura TOMS-Like Ozone, Aerosol Index, Cloud Radiance Fraction L3 1 day 1 degree x 1 degree V3, NASA Goddard Space Flight Center, Goddard Earth Sciences Data and Information Services Center (GES DISC), (Accessed on May 13, 2020), 10.5067/Aura/OMI/DATA3001

Prockop, L. D. and Chichkova, R. I. 2007. Carbon monoxide intoxication: an updated review. J. Neurol.Sci., 262(1-2): 122-130.

Sahu, L. K., Tripathi, N., Sheel, V. and Ojha, N. 2019. The influence of local meteorology and convection on carbon monoxide distribution over Chennai. J. Earth Syst. Sci., 128(5): 119.

Sheel, V., Sahu, L. K., Kajino, M., Deushi, M., Stein, O. and Nedelec, P. 2014. Seasonal and interannual variability of carbon monoxide based on MOZAIC observations, MACC reanalysis, and model simulations over an urban site in India. J. Geophys. Res. D: Atmos., 119(14): 9123-9141.

Shindell, D. T., Faluvegi, G., Stevenson, D. S., Krol, M. C., Emmons, L. K., Lamarque, J. F. and Wild, O. 2006. Multimodel simulations of carbon monoxide: Comparison with observations and projected near-future changes. J. Geophys. Res. D: Atmos., 111(D19).

Tang, W., Emmons, L. K., Arellano Jr, A. F., Gaubert, B., Knote, C., Tilmes, S. and Blake, N. J. 2019. Source contributions to carbon monoxide concentrations during KORUS-AQ based on CAM-chem model applications. J. Geophys. Res. D: Atmos., 124(5): 2796-2822.

WHO, World Health Organization. Coronavirus Disease (COVID-19) Pandemic. Available online: https: //www.who.int/emergencies/diseases/novel-coronavirus-2019 (accessed on 5 May 2020).

Yoon, J. and Pozzer, A. 2014. Model-simulated trend of surface carbon monoxide for the 2001-2010 decade. Atmos. Chem. Phys., 10465.

Zhang, R., Wang, Y., Smeltzer, C., Qu, H., Koshak, W. and Boersma, K. F. 2018. Comparing OMI-based and EPA AQS in situ NO2 trends: towards understanding surface NOx emission changes. Atmos. Meas. Tech., 11(7): 3955-3967.

Zhang, R., Zhang, Y., Lin, H., Feng, X., Fu, T. M. and Wang, Y. 2020. NOx emission reduction and recovery during COVID-19 in East China. Atmos., 11(4): 433.

Nature Environment and Pollution Technology
An International Quarterly Scientific Journal

p-ISSN: 0972-6268
(Print copies up to 2016)
e-ISSN: 2395-3454

Vol. 20 | No. 2 | pp. 721-727 | 2021

Original Research Paper

https://doi.org/10.46488/NEPT.2021.v20i02.031

Open Access Journal

Spatial Analysis of the Impact of Flood and Drought on Food Security Index

A. C. T. Rosalia†, Suryanto and L. Hakim
Department of Economics and Business, Sebelas Maret University, Surakarta 57127, Indonesia
†Corresponding author: A. C. T. Rosalia; ameliachoya@gmail.com

Nat. Env. & Poll. Tech.
Website: www.neptjournal.com

Received: 02-06-2020
Revised: 06-07-2020
Accepted: 16-07-2020

Key Words:
Flood
Drought
Food security index

ABSTRACT

This research aims to spatially analyze the impacts of climate change, specifically flood and drought on the level of food security in the Bengawan Solo watershed. Agriculture is one of the sectors that is significantly affected by the phenomenon. Flood and drought disrupt agricultural productivity, resulting in farmers having difficulty accessing their livelihoods. This has the potential to threaten food security. This research was conducted in the Bengawan Solo watershed which flows through three provinces on the island of Java. Widespread watersheds and inadequate infrastructure make it difficult to monitor so that the areas through which rivers flow are vulnerable to flood and drought. The impact of these climate-related problems on food availability makes this research important. This research was started with the calculation of the food security index in each regency/city in the Bengawan Solo watershed regions and mapped it with a Geographic Information System (GIS). The step then proceeded to the impact assessment of flood and drought on food security using the quantitative method of panel data regression in the 2014-2018 period. To sum up, flood and drought contributed in a negative way to the level of food security. Information about food security is useful in planning the allocation of resources by the government. Therefore, efforts to strengthen food security can be more directed according to the needs.

INTRODUCTION

Climate change is happening more rapidly and is bringing an impact in various regions of Indonesia. From weather changes that endanger food production, to rising sea levels (United Nation 2019). Food security affected by climate change through increasing temperatures and extreme events (IPCC 2019). Climate variation will increase the risk of flood and drought. The connection between climate change and agricultural production is vigorous (Suryanto et al. 2020). Agricultural productivity is highly affected if there is any climate variation and it leads to food insecurity. Agricultural failure caused by nature and climatic conditions is quite high (Budhathoki et al. 2019). This has an impact on the quality of agricultural production and results in losses for farmers (Yang et al. 2010). So, it requires the development of calculations for farmers to address climate risks. Indonesia is an agricultural country whose population livelihood structure is dominated by the agricultural sector by 27.33% (Statistical Bureau of Indonesia 2019). Indonesia's Gross Domestic Product of 13.45% is occupied by the agricultural sector which is ranked the second largest after the industrial sector (Statistical Bureau of Indonesia 2019). This means that the survival of society depends on the agricultural sector. If agricultural productivity is disrupted, it will cause losses and increase poverty which also affects food security.

The agricultural product is prone to climate change (Deryugina & Konar 2017). Climate change threatens food production systems that affect livelihoods and food security (Bhagawati et al. 2017). Referring to the data of the Centre for Research on the Epidemiology of Disaster (2018), Indonesia ranks 4th in the world as the country experiencing the most natural disasters in 2018. The frequent occurrence of drought, water scarcity, and unsustainable intensive farming practices affect food security (Hameed et al. 2020). In a previous study in the Waduk Minyun watershed, it was found that watershed management had to be adjusted according to future climate change (Qiu et al. 2020). Community perceptions about floods and their impacts are extremely indispensable for Flood Risk Management exercises because they can increase the level of preparedness, response and recovery (Masud et al. 2018). Hunger and climate risk have a high correlation, particularly for areas most affected by food insecurity (Krishnamurthy et al. 2014). Food security is when everyone has sufficient, safe and nutritious food (Food Agricultural Organization 2006).

Flood and drought have proven agricultural failure, as happened in South Kulon Progo, Yogyakarta Province (Suryanto et al. 2020). The result of mapping areas prone to flood and drought using a Geographic Information System (GIS) was used to identify flood and drought effect on agricultural land (Saptutyningsih 2011). Sianturi et al. (2018)

determined the crop pattern system in West Java Province which was applied in the form of mapping of the areas prone to flood vulnerability. Highly vulnerable areas have low productivity and high financing.

The purpose of this research is to investigate the impact of climate change, especially floods and drought in the Bengawan Solo watershed on the level of food security. The maps areas that are prone to flood, drought, and food insecurity showed by using geographic information systems that facilitate the identification of disaster-prone areas. Information about vulnerability to flood and drought in an area is highly significant in determining the treatment that will be provided by the government to prevent and overcome the risk of food vulnerability.

MATERIALS AND METHODS

The selected area for this research was the Bengawan Solo watershed. Watersheds are land areas that channel rainfall and snowmelt to tributaries, rivers, and streams, and eventually to exit points such as reservoirs, bays, and seas (National Oceanic and Atmospheric Administration 2020). Bengawan Solo is the largest river on Java island and drains water from a watershed of ± 16,100 km^2 (Kementerian PUPR Ditjen Sumber Daya Air BBWS Bengawan Solo 2017). The research process was divided into 3 stages. First, mapping and ranking the scores of the food security index (FSI). Second, processing the data using panel data regression to determine the impact of flood and drought on food security in the Bengawan Solo watershed, and the last, processing the data of flood, drought, and food security using Geographic Information System (GIS).

Flood and drought are among the main challenges in watershed management systems. The frequency rising of rainfall can reduce the efficiency of management practices. River sedimentation also increases during climate change due to high rainfall (Qiu et al. 2020), this increases the potential for future floods and droughts. Flood risk prediction is useful for adaptation (Xu et al. 2019), as well as the risk of drought. Drought monitoring and assessment are important for mitigation and prediction (Okal et al. 2020). Spatial data analysis is needed to obtain information about potential floods, drought, and food security in the form of maps. Afterwards, the analysis of the effect of flood and drought on the level of food security can be performed. This research employed three analytical methods namely Food Security Index (FSI), geographic information systems, and panel data regression. Geographic Information System (GIS) in this study is to simulate food security levels based on food security index scores. Research on developing flood risk zone maps is very important and several research studies have been carried out on this issue worldwide (An et al. 2020)

Strategies to improve food security in each region are still constrained by the identification of the level of food security. Food Security Index (FSI) aims to show how to develop and validate potential indicators by comparing them with other indicators (Ibok et al. 2019). Spatial identification and scores of the food security index can help to both imaging and predicting, thus reducing losses. Meanwhile, panel data regression with Stata is a stated approach to find out the impact of flood and drought on the level of food security in the 5 years of 2014-2018.

There are several determining factors of food security, namely food accessibility, food availability, and food adequacy (Food Security Agency, 2018). The parameters used referred to the standard indicators by The Economist Intelligence Unit (2019) on the Global Food Security Index.

Table 1: Scores of expert judgement indicator.

No	The Indicator Scores of Each Regency/City based on Expert Judgment	Score	
		Regency	City
Food Availability			
1	The ratio of normative consumption to the net availability per capita per day	0.30	-
Food Accessibility			
2	The percentage of population below the poverty line	0.15	0.20
3	The percentage of households with a proportion of expenditure on food is higher than 65% of total expenditure	0.08	0.125
4	Percentage of households without access to electricity	0.08	0.125
Food Utilization			
5	The average years of schooling of women above 15 years	0.05	0.08
6	Percentage of households without access to clean water	0.15	0.18
7	The ratio of total population per health worker to population density	0.05	0.08
8	Prevalence of stunting	0.05	0.08
9	Life expectancy	0.10	0.13

Source: (Food Security Agency, 2018)

The Food Security Index (FSI) is to evaluate achievements and classify food security. The three main steps of FSI calculation are as follows:

Step 1: Determination and ranking of the scores of the factors based on expert judgment: To calculate the index, each group of variables was scored based on the result of expert judgement from the Food Security Agency. The three aspects of food security, namely availability, accessibility, and utilization of food were investigated. Based on these three aspects, the results are provided in Table 1.

Step 2: Calculation of the food security index: Given that aspects of the food security index indicator have different units, it is necessary to do a normalization process in the calculation of the food security index. The normalization process in this research used the approach of Z max-min value and distance to scale (0-100). This was intended to make each data that had different units comparable. So that it could be used to generate conclusions. Following the max-min, normalization was performed using the formula below:

$$Z = \frac{X - Xmin}{Xmax - Xmin}$$

Where:

X = the score of each data

Xmin = the minimum score of X

Xmax = the maximum score of X

FSI score is the result of multiplication of each standardized indicator value with the score of the indicator (Food Security Agency, 2018), using the following formula:

$$Y(j) = \Sigma_{n=1}^{9} a_i X_{ij}$$

Where:

Yj = food security index of the jth regency or city

αi = score of each indicator

Xij = standardized indicator score of the jth regency or city

Step 3: Geographic Information System of a food security index: The Geographic Information System (GIS) application was used to analyze floods, droughts, and food security levels, then the results were displayed on maps.

Losses caused by climate change can reduce agricultural productivity. Farmers crop failure can be caused by flood and drought as happened in Kulon Progo (Saptutyningsih 2011) and the Yangtze River watershed (Liu et al. 2019). The variables used in this research were as follows:

$$FSI = \alpha + \beta X_1 + \beta_2 X_2 + \beta_3 X_3 + \beta_4 X_4 + \beta_5 X_5 + \beta_6 X_6 + \beta_7 X_7 + e$$

Where,

FSI	= Food security index	=	Food security scores
X_1	= Flood index	=	Frequency of flood manifested in dummy variables (0 means no flood, and 1 means it experiences flood)
X_2	= Drought index	=	Frequency of drought manifested in dummy variable (0 means no drought, and 1 means it experiences drought)
X_3	= Human development index	=	The level of human development
X_4	= Inflation	=	Rate of change in price
X_5	= Farm size	=	Farm size
X_6	= Total population	=	Total population
X_7	= Gross Regional Domestic Product (GRDP) per capita	=	Economics output per capita

RESULTS AND DISCUSSION

The Bengawan Solo watershed stretches through three provinces namely Central Java, East Java and Yogyakarta Special Region. Areas in the present research consisted of three cities namely Surakarta, Madiun, Surabaya and 20 regencies which are Klaten, Boyolali, Wonogiri, Sukoharjo, Sragen, Karanganyar, Blora, Pacitan, Ponorogo, Rembang, Ngawi, Madiun, Magetan, Bojonegoro, Lamongan, Tuban, Gresik, Mojokerto, Trenggalek and Gunung Kidul. In this research, we used secondary data from the Central Statistics Agency (BPS), the National Disaster Management Agency (BNPB), and the Bengawan Solo River Region Centre. The Bengawan Solo watershed tends to have flood and drought vulnerability as shown in the maps provided in Fig. 1 and Fig. 2.

The Bengawan Solo watershed is an area that is vulnerable to flood and drought (Kementerian PUPR Ditjen Sumber Daya Air BBWS Bengawan Solo 2017). Therefore, it needs the role of various parties to prevent and minimize losses incurred. In Fig. 1, the GIS results show that almost the whole regencies/cities in the Bengawan Solo watershed

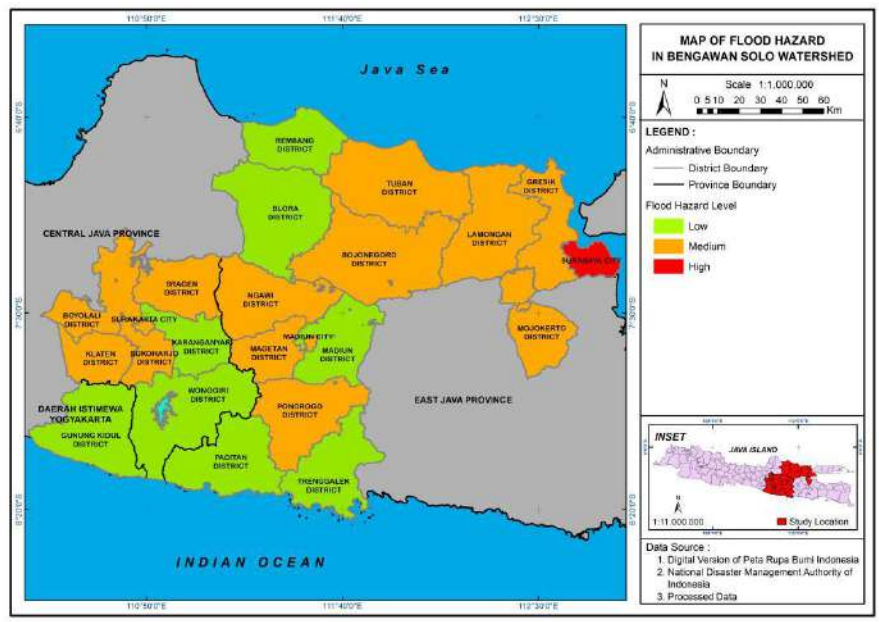

Fig. 1: Map of flood Risk in the Bengawan Solo Watershed.

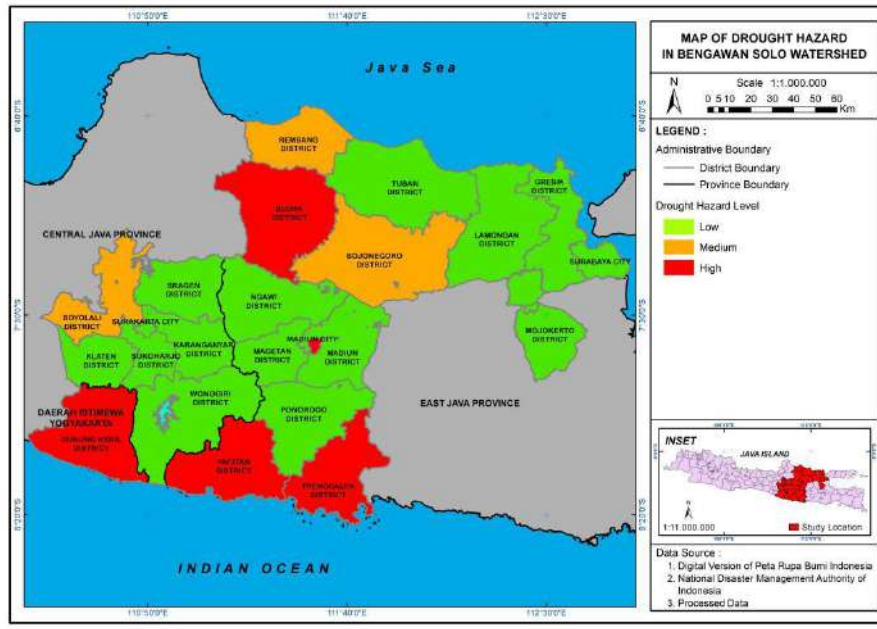

Fig. 2: Map of drought Risk in the Bengawan Solo Watershed.

have the potential to experience flood risk, but Surabaya has the highest risk of all. Some areas situated in Surakarta, Boyolali, Klaten, Sukoharjo, Sragen, Ngawi, Magetan, Ponorogo, Bojonegoro, Tuban, Lamongan, Gresik, and Mojokerto are also prone to flood at a moderate risk. Other areas have a low flood risk.

The drought risk areas are presented in Fig. 2. All the regencies/cities in the Bengawan Solo watershed have the potential to experience drought, but Gunung Kidul, Pacitan, Trenggalek, and Blora are considered as the regions with the highest risk. Some areas with moderate risks located in Boyolali, Rembang, and Bojonegoro. Drought occurs due

Table 2: Food Security Index Score in Bengawan Solo Watershed.

No.	Regency/City	FSI Score 2014-2018
1	Surakarta	67.43
2	Madiun	70.32
3	Surabaya	69.74
4	Boyolali	63.8
5	Klaten	63.4
6	Sukoharjo	68.15
7	Wonogiri	42.25
8	Karanganyar	60.5
9	Sragen	47.3
10	Blora	40.9
11	Rembang	58.75
12	Pacitan	32.4
13	Ponorogo	37.5
14	Madiun	39.55
15	Magetan	46.15
16	Ngawi	23.8
17	Bojonegoro	35.95
18	Tuban	36.4
19	Lamongan	41.05
20	Mojokerto	61.3
21	Trenggalek	39.45
22	Gresik	72.95
23	Gunung Kidul	30.75

Source: Processed data, 2020

to minimal rainfall caused by climate change. While other areas have a low risk of drought.

It is necessary to measure regional food security scores to find out which regions have low food security (Table 2) so that the government can provide more intervention. The attempts to overcome food vulnerability can be well planned when it is visualized on a map. The region that has the highest FSI score is categorized as an area with good food security, on the contrary, the smallest FSI score indicates the regency/city is vulnerable to food security.

Areas with a food security index map are presented in Fig. 3. All regencies/cities in the Bengawan Solo Watershed have the potential to experience food vulnerability risks. Based on the index score, the locations with the highest food security are Surabaya, Gresik, and Sukoharjo. This is due to the high level of GRDP per capita compared to other regions in the Bengawan Solo watershed. On the other hand, areas that have low food security/food insecurity are Gunung Kidul, Pacitan, and Ngawi. This is because these regencies/cities have areas that tend to be vulnerable to floods and drought. Inadequate production of the agricultural sector has resulted in high levels of poverty in these regions. Other regencies/cities are categorized as regions with moderate levels of food security. The level of food security is influenced by several factors as described in the results of panel data regression (Stata) in the period of 2014-2018.

Table 3 presents panel data regression result of the variables that have the potential to affect the level of food security. Regression results show that flood and drought

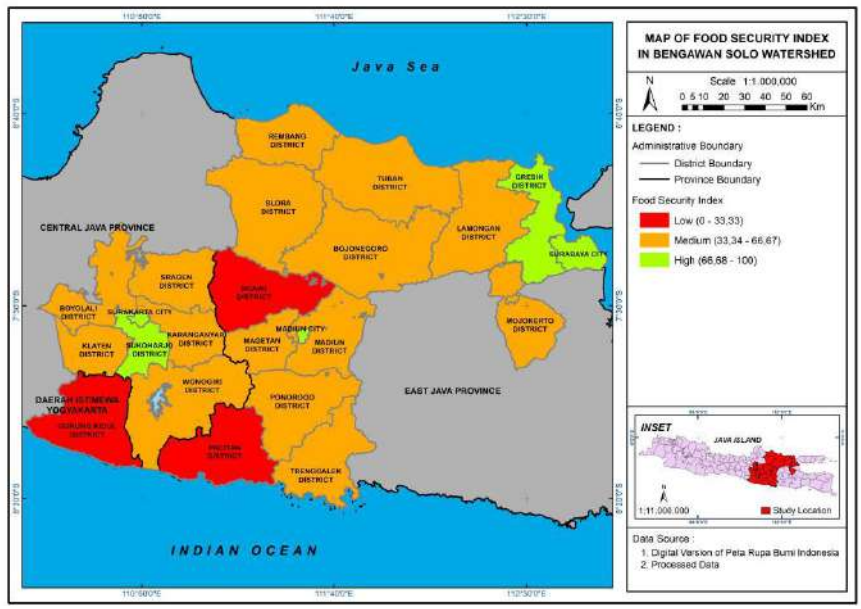

Fig. 3: Map of Food Security Index in the Bengawan Solo Watershed.

Table 3: Variables contributing to the food security index.

Variable	Definition of variables	Coefficient	Probability
IB	Dummy for flood	-4.809	0.034
IK	Dummy for drought	-6.407	0.006
IPM	Human development index	2.902	0.000
INF	Inflation	0.232	0.409
LLP	Farm size	2.748	0.000
JP	Total population	1.317	0.493
GRDP per capita	Gross regional domestic product per capita	5.332	0.009
_cons		0.000	
F (7.107)		31.48	
Prob > F		0.000	
R^2		0.673	
Adjusted R^2		0.651	
Root MSE		9.089	
Classic Assumption	Heteroscedasticity Multicollinearity	- -	

Source: Processed Data, 2020

have a significant negative effect of 5% on the food security index, which means it reduces food security. In addition to flood and drought, other variables that influence the level of food security in the Bengawan Solo watershed are the human development index, farm size, and GRDP per capita which have a significant positive effect of 5%, which means these variables increase food security.

Climate change, which causes flood and drought, is of concern to researchers because it will disrupt the supply of food availability. Areas that are identified as having low levels of food security must anticipate reducing the risk of potential losses. Food security in Indonesia is closely related to the price of rice (Timmer 2011) since it is the staple food of Indonesian. Indonesia is the 4th largest population in the world with a total of 264 million population based on (World Bank 2019). This causes the consumption of food to be relatively high. This research is expected to give support to the government in tackling the risk of food insecurity caused by climate change. By using GIS, areas that are prone to flood, drought, and food insecurity have been incorporated into the map so that it will ease the government in providing special treatment and intervention.

CONCLUSION

The contribution of climate change, especially floods and drought, to the level of food security in the Bengawan Solo watershed is crucial. Scores are grouped into three sectors of vulnerability in the Bengawan Solo watershed from the highest to lowest food security levels. From the results of the research, it can be concluded that flood and drought reduce the level of food security. That is, climate change causes additional burdens for the government to achieve development goals namely food security. Surabaya, Gresik and Sukoharjo are areas with high levels of food security. Whereas Gunung Kidul, Pacitan, and Ngawi are areas that have low food security or food vulnerability. Adaptation options for climate change and food distribution between regions can be alternatives. This research is expected to support the community and also the government so that it is easier to identify areas that need more attention to prevent food vulnerability in the rainy and dry seasons.

ACKNOWLEDGMENT

Thanks to the National Research and Innovation Agency of the Republic of Indonesia for part of the funding provided in this study.

REFERENCES

An, N. G. H. , Nh, H. À. T. ., Thi, H., Huong, L. and Dzung, L. H. 2020. Flash flood risk zone map development for Thanh Hóa. Disaster Advances, 13(4): 40-51. Retrieved from https://worldresearchersassociations.com/disascurrissue/5.pdf

Bhagawati, R., Bhagawati, K., Jini, D., Alone, R. A., Singh, R., Chandra, A. and Shukla, K. K. 2017. Review on climate change and its impact on agriculture of Arunachal Pradesh in the Northeastern Himalayan region of India. Nature Environment and Pollution Technology, 16(2): 535-539.

Budhathoki, N. K., Lassa, J. A., Pun, S. and Zander, K. K. 2019. Farmers' interest and willingness-to-pay for index-based crop insurance in the lowlands of Nepal. Land Use Policy, 85(October 2018): 1-10. https://doi.org/10.1016/j.landusepol.2019.03.029.

Center for Research on the Epidemiology of Disaster 2018. Annual Disaster Statistical Review 2017. Retrieved from https://www.cred.be/

Deryugina, T. and Konar, M. 2017. Impacts of crop insurance on water withdrawals for irrigation. Advances in Water Resources, 110: 437-444. https://doi.org/10.1016/j.advwatres.2017.03.013.

Food Agricultural Organization 2006. Food Security. Retrieved March 8, 2020, from http://www.fao.org/fileadmin/templates/faoitaly/documents/pdf/pdf_Food_Security_Cocept_Note.pdf

Food Security Agency 2018. Indeks Ketahanan Pangan Indonesia 2018. Retrieved from http://bkp.pertanian.go.id

Hameed, M., Ahmadalipour, A. and Moradkhani, H. 2020. Drought and food security in the middle east: An analytical framework. Agricultural and Forest Meteorology, 281(October 2019): 107816. https://doi.org/10.1016/j.agrformet.2019.107816.

Ibok, O. W., Osbahr, H. and Srinivasan, C. 2019. Advancing a new index for measuring household vulnerability to food insecurity. Food Policy, 84(February): 10-20. https://doi.org/10.1016/j.foodpol.2019.01.011

IPCC 2019. Food Security. In Amfiteatru Economic (No. IPCC; Vol. 21). https://doi.org/10.24818/EA/2019/51/281

Kementerian PUPR Ditjen Sumber Daya Air BBWS Bengawan Solo. 2017. Sejarah Singkat. Retrieved March 20, 2020, from http://sda.pu.go.id/bbwsbengawansolo/portal/index.php/sejarah-singkat/

Krishnamurthy, P. K., Lewis, K. and Choularton, R. J. 2014. A methodological framework for rapidly assessing the impacts of climate risk on national-level food security through a vulnerability index. Global Environmental Change, 25(1): 121-132. https://doi.org/10.1016/j.gloenvcha.2013.11.004

Liu, Y., You, M., Zhu, J., Wang, F. and Ran, R. 2019. Integrated risk assessment for agricultural drought and flood disasters based on entropy information diffusion theory in the middle and lower reaches of the Yangtze River, China. International Journal of Disaster Risk Reduction, 38(May): 101194. https://doi.org/10.1016/j.ijdrr.2019.101194.

Masud, M. M., Sackor, A. S., Ferdous Alam, A. S. A., Al-Amin, A. Q. and Abdul Ghani, A. B. 2018. Community responses to flood risk management – An empirical Investigation of the Marine Protected Areas (MPAs) in Malaysia. Marine Policy, 97(September): 119-126. https://doi.org/10.1016/j.marpol.2018.08.027.

National Oceanic and Atmospheric Administration 2020. What is a watershed? Retrieved April 29, 2020, from https://oceanservice.noaa.gov/facts/watershed.html

Okal, H., Ngetich, F. and Okeyo, J. 2020. Spatio-temporal characterisation of droughts using selected indices in Upper Tana River Watershed, Kenya. Scientific African, 7: e00275. https://doi.org/10.1016/j.sciaf.2020.e00275.

Qiu, J., Shen, Z., Hou, X., Xie, H. and Leng, G. 2020. Evaluating the performance of conservation practices under climate change scenarios in the Miyun Reservoir Watershed, China. Ecological Engineering, 143(July 2019), 105700. https://doi.org/10.1016/j.ecoleng.2019.105700.

Saptutyningsih, E. S. S. 2011. Hedonic Price Approach of Flood Effect on Agricultural Land. Economic Journal of Emerging Markets, 3(1): 87-96.

Sianturi, R., Jetten, V. G. and Sartohadi, J. 2018. Mapping cropping patterns in irrigated rice fields in West Java: Towards mapping vulnerability to flooding using time-series MODIS imageries. International Journal of Applied Earth Observation and Geoinformation, 66(November 2017): 1-13. https://doi.org/10.1016/j.jag.2017.10.013.

Statistical Bureau of Indonesia 2019. Indonesia Dalam Angka. Retrieved from https://www.bps.go.id/

Suryanto, N. A., Gravitiani, E., Daerobi, A. and Susilowati, F. 2020. Crop insurance as farmers adaptation for climate change risk on agriculture in Surakarta residency-Indonesia. International Journal of Trade and Global Markets, 13(2): 251. https://doi.org/10.1504/ijtgm.2020.106771.

The Economist Intelligence Unit 2019. Global Food Security Index. Retrieved from https://foodsecurityindex.eiu.com/

United Nation 2019. Climate Change. Retrieved from https://www.un.org/en/sections/issues-depth/climate-change/

Xu, X., Wang, Y. C., Kalcic, M., Muenich, R. L., Yang, Y. C. E. and Scavia, D. 2019. Evaluating the impact of climate change on fluvial flood risk in a mixed-use watershed. Environmental Modelling and Software, 122, 104031. https://doi.org/10.1016/j.envsoft.2017.07.013.

Yang, R., Wang, L. and Xian, Z. 2010. Evaluation on the efficiency of crop insurance in China's Major Grain-Producing Area. Agriculture and Agricultural Science Procedia, 1: 90-99. https://doi.org/10.1016/j.aaspro.2010.09.011.

Nature Environment and Pollution Technology
An International Quarterly Scientific Journal

p-ISSN: 0972-6268
(Print copies up to 2016)
e-ISSN: 2395-3454

Vol. 20 | No. 2 | pp. 729-735 | 2021

Original Research Paper

https://doi.org/10.46488/NEPT.2021.v20i02.032

Open Access Journal

Biosorption of Hexavalent Chromium by *Paenibacillus pabuli* and *Bacillus cereus* Isolated from Alkaline Industrial Contaminated Soil in Puducherry, India

Anandbabu Rangasamy, Subashchandrabose Gandhi and Vignesh Tamilchelvan†
Department of Community Medicine, Aarupadai Veedu Medical College & Hospital, Kirumampakkam, Pondicherry-607403, India
†Corresponding author: Vignesh Tamilchelvan; getanand09@gmail.com

Nat. Env. & Poll. Tech.
Website: www.neptjournal.com

Received: 13-03-2020
Revised: 28-04-2020
Accepted: 27-05-2020

Key Words:
Alkaliphilic bacteria
Hexavalent chromium
Paenibacillus pabuli
Bacillus cereus
Bioremediation

ABSTRACT

In the present study, we intended to remediate Cr(VI) with alkaliphilic bacteria *Paenibacillus pabuli* (JX561107) and *Bacillus cereus* (JX561108) isolated from alkaline industrial contaminated soil in Pondicherry. The isolated bacteria were tested for the removal efficiency of hexavalent chromium at different concentrations (50 mg/L, 200mg/L, 400mg/L). At 50 mg/L of hexavalent chromium concentration, *Paenibacillus pabuli* and *Bacillus cereus* were found to be highly efficient in removing Cr(VI) in 72 hrs at the inoculum rate of 1% of overnight grown bacterial cultures. The isolates could remove 98% and 74% of Cr(VI) within 72 hrs of treatment at 9.5 pH. When the concentration of the Cr(VI) was increased to 400 mg/L, there was a gradual decrease in Cr(VI) removal. SEM images were obtained from the tested bacteria to observe the bacterial cell surface for the changes in the morphology and EDX analysis were also carried out to confirm whether the adhered particles are of chromium.

INTRODUCTION

Alkaliphilic microorganisms attract increased attention during the last decades in the context of their great potential for biotechnological applications and research of ecological diversity (Rossi et al. 2003). Several alkaliphilic bacteria have been isolated from different environments, for example, deserts, soda lakes, and arid soils (Li et al. 2002). Most intense and extensive intervals of organisms have been observed generally in "moderate" environments. It would also have been known to have an "extreme" environment on the Earth are considered to avoid the endurance of existence. Habitats in these ecological environments, for instance, pH, temperature and salinity concentrations are exceedingly elevated or low. The extreme environment is populated by a group of organisms that have been particularly modified to these specific circumstances and these types of intense microbes are frequently referred to as alkaliphiles, halophiles, thermophiles and acidophiles, and reflect an exacting type extreme environment in which they inhabit (Horikoshi 1991).

Hexavalent chromium is a strong oxidizing agent, frequently present as hydrochromate ($HCrO_4$), chromate (CrO_4)) or dichromate (Cr_2O_7) oxyanions, depending on the pH (United States, Environmental Protection Agency, US EPA 1998). The widespread utilization of hexavalent chromium in industries such as stainless steel production and tanning, cause chromium contamination of soil and groundwater in and around the production site (Turick & Carmiol 1996). Microbes that can resist this stress are more likely to survive and influence chromium speculation (Francisco et al. 2002, Branco et al. 2005). The chromium resistant bacterial isolates showed removal efficiency of around 45.5% at 28°C ambient temperature (Sen et al. 2019). The rationale of this study was to examine the ability of alkaliphilic bacteria *Paenibacillus pabuli* and *Bacillus cereus*, isolated from alkaline industrial contaminated soil, to remediate hexavalent chromium at different concentrations.

MATERIALS AND METHODS

Collection of Soil Samples

Soil samples were collected from alkaline industry-contaminated soil from Pondicherry in the area of Thavalakuppam. Triplicate sampling at each station was collected in a plastic container during the post-monsoon months from October-December. Before the collection of the soil, the pH of the soil sample was measured at the collection site and recorded as 9.5 (alkaline). The soil samples were collected from five randomly selected spots from the locations with the help of a scooper from the topmost sediment layer, i.e. 0-15 cm layer of sediment samples (approximately 500 g) and transferred

into a sterile sample container and brought to the laboratory (Das et al. 2011).

Isolation of Alkaliphilic Bacteria

Isolation of alkaliphilic bacteria from the soil samples collected aseptically from contaminated soil using rich alkaline nutrient agar medium containing sodium sesquicarbonate solution (modified method of Horikoshi 1999) and was performed by making serial dilution of the samples. The dilution used for the study was 100µL of the 10^{-7} dilution spread in Alkaline Nutrient Agar. The pH of the soil was adjusted to 9.5. The plates were incubated at 37°C for 48 hrs. The isolated colonies were sub-cultured with alkaline nutrient agar to check the purity of the isolates. Identification of the bacterial isolates was carried out by bacteriological methods based on colony morphology, Gram staining, motility and biochemical tests. Barcoding of bacterial isolates was done by the method described by Marmur (1961).

DNA Bar Coding

Genomic DNA isolation: Alkaline strains were grown in an alkaline nutrient broth of pH 9.5 at 37°C. After 12 hours of incubation, 1.5 mL of the cultured broth was taken and centrifuged at 8,000 rpm for 6 min. The pellets were re-suspended with 330 µL of GTE solution and incubated at 37°C for 30 minutes. The pinch amount of lysozyme was added to the same solution and incubated at 37°C for 1 h. Ten µL of 20% SDS was added and incubated at 37°C for overnight. RNase (0.1 mg/mL) was added to the solution to remove the RNA from the solution and kept at 37°C. After 3 h of incubation, 17 µL of EDTA (0.5M) was mixed and incubated at 50°C for 10 min. Proteinase K (10 µL) was added and incubated at 37°C for 3 h. After incubation, 200 µL of phenol:chloroform (24:1) was mixed slowly and centrifuged at 16,000 rpm for 15 min. After centrifugation, the aqueous phase layer was collected and mixed with an equal volume of isopropanol. It was slowly shaken up and down until to see the pool of DNA, and centrifuged at 16,000 rpm for 15 min. The DNA pellet was washed with 1 mL of 95% ethanol and centrifuged at 16,000 rpm for 15 min. After centrifugation, the pellet was air-dried and dissolved in 40 µL of 1X TE buffer. It was confirmed by running the agarose gel electrophoresis.

Agarose gel electrophoresis: The isolated DNA sample was separated on 0.8% agarose gel. 1X TAE buffer was prepared by an appropriate concentration of 1 mL of 50X TAE buffer and mixed with 49 mL distilled water. Further, 0.4 g of powdered agarose was added and mixed well. They were allowed to boil until agarose dissolved completely. Then 3 µL of ethidium bromide (0.5 µg/mL) was added from the stock solution of 10 mg/mL and mixed well. The warmed agarose solution was poured into the gel casting tray and allowed to set for 30-45 min at room temperature. The gel was mounted in the electrophoresis tank. Electrophoresis buffer was added to cover the gel to a depth of about 1mm. The isolated DNA sample was mixed with a loading buffer and loaded into the well of the submerged gel using a micropipette. A voltage of 50-60V was applied. After 1-2 h, the gel was taken out from the buffer and examined under a UV illuminator (UVI-TEC). The clear band was observed as red, orange fluorescence. The molecular weight was measured by using appropriate marker DNA.

Polymerase Chain Reaction (PCR)

The total genomic DNA from the isolates was done by 16SrDNA PCR assay by using the 16SrDNA universal primers (F- 5'AGA GTT TGA TCC TGG CTC AG-3' and R- 5'-CGG TTA CCT TGT TAC GAC TT-3'). They were amplified using the above mentioned PCR mixture. The PCR was run using Eppendorf Gradient thermocycler, the gradient PCR assay was done by using the various annealing temperatures. The PCR cycle used was initial denaturation at 95ºC; 4 min denaturation at 95ºC; 30 s. Annealing 55ºC; 30 s. Extension 72ºC; 30 s. Final extension 72ºC; 10 min cycles 30 cycles. The PCR products were analysed by 0.8% agarose gel electrophoresis. The PCR-amplified 16SrDNA's were purified using the quick PCR purification kit from Bangalore Genie. The sequencing was performed (Eurofins, Bangalore) and sequencing was deposited in the NCBI Genbank. The study of the arrangement and homology and the construction of a phylogenetic tree for the sequenced nucleotide were carried out by the bioinformatics tools.

Experimental Study

Degradation of Cr(VI): The experimental study involving three different hexavalent chromium concentrations, i.e. 50 mg/L, 200 mg/L and 400 mg/L was carried out in 250 mL conical flasks (100 mL in each) at 9.5 pH. One per cent of sucrose was added to all the conical flasks and 1 % of overnight grown bacterial cultures were seeded in each conical flask. The flasks were kept on a rotary shaker at 180 rpm at 37°C. Hexavalent chromium depletion was estimated at an interval of 24 h till 72 h to depletion by the isolated bacterial strains with different chromium concentrations. After absorption, the mixture was centrifuged at 4000 rpm for 15 min. The remaining metal concentration in the solution was measured. Quantity of metals bound was taken to be the distinction among the initial and final concentrations of metal (Gardea-Torresdey et al. 1998). The concentration of metal in the solution was estimated with an atomic absorption spectrophotometer. The experiment was done thrice and the average value was taken for discussion.

Scanning Electron Microscopic Study and EDX Analysis

Scanning Electron Microscopic (SEM) studies were performed to examine the changes in surface morphology before and after treatment and elemental composition of the biosorbent along with EDX study using a scanning electron microscope. Pellets of bacterial culture obtained through centrifugation were used for these spectral studies. The pellets were washed twofold with 0.1 M phosphate-buffered saline (PBS; 15 mM phosphate buffer, 138 mM NaCl, 2.7 mM KCl, pH 7.4 at 25ºC) and fixed overnight in 2% glutaraldehyde (prepared in 0.1 M PBS). The cells were washed with PBS and distilled water earlier to dehydration throughout an ethanol series (10% in absolute), held at each concentration for 30 minutes. Samples were positioned on a brass stub, sputter-coated with gold and examined by Scanning Electron Microscope (De et al. 2008). SEM and EDX studies were performed with a Hitachi S-3400N Scanning electron microscope, available at Central Instrumentation Facility (CIF) Pondicherry University.

RESULTS

Identification of Isolated Alkaliphilic Bacteria from Alkaline Industry-Contaminated Soil

Alkaliphilic bacteria were isolated from alkaline industrial-contaminated soil. They exhibited most favourable growth at pH 9.5. *Paenibacillus pabuli* and *Bacillus cereus* were isolated from the alkaline industry-contaminated soil, and the molecular characterizations were done. Based on phylogenetic analyses, 16S rDNA gene sequence of alkaliphilic bacteria was compared with sequence existing in the Genbank catalogue by BLAST software and sequence were submitted to NCBI Genbank.

The phylogenetic tree derived from 16S rRNA gene sequence of *Paenibacillus pabuli* and *Bacillus cereus* and sequences of the closest phylogenetic neighbours obtained by NCBI BLAST analysis confirmed the relationships among the selected isolates (Fig. 1 and Fig. 2)

Removal of Hexavalent Chromium from Tannery Effluent by Isolated Alkaliphilic Bacteria

Chromium was removed from the tannery effluent by alkaliphilic bacterial strains isolated from alkaline industrial soil at pH 9.5 (pH of the alkaline industry effluent contaminated soil from which bacterium was isolated). The removal efficiencies of hexavalent chromium in solution were calculated from the differences between the initial and the residual concentration after 72 hrs of treatment at 37°C at pH 9.5. The concentration of total Cr(VI) was reduced to 1.1 mg/L from 50 mg/L in 72 hrs of treatment with *Paenibacillus pabuli* showed 98 % efficiency and *Bacillus cereus* removed Cr(VI) to 12.92 mg/L from 50 mg/L in 72 hrs with 74 % efficiency (Fig. 3). When the concentration of Cr(VI) was increased to 200 mg/L there was a gradual decrease in the Cr(VI) concentration to 57% from 200 mg/L in 72 hrs of treatment with *Paenibacillus pabuli* and *Bacillus cereus* reduced Cr(VI) to 33% from 200 mg/L in 72 hrs of

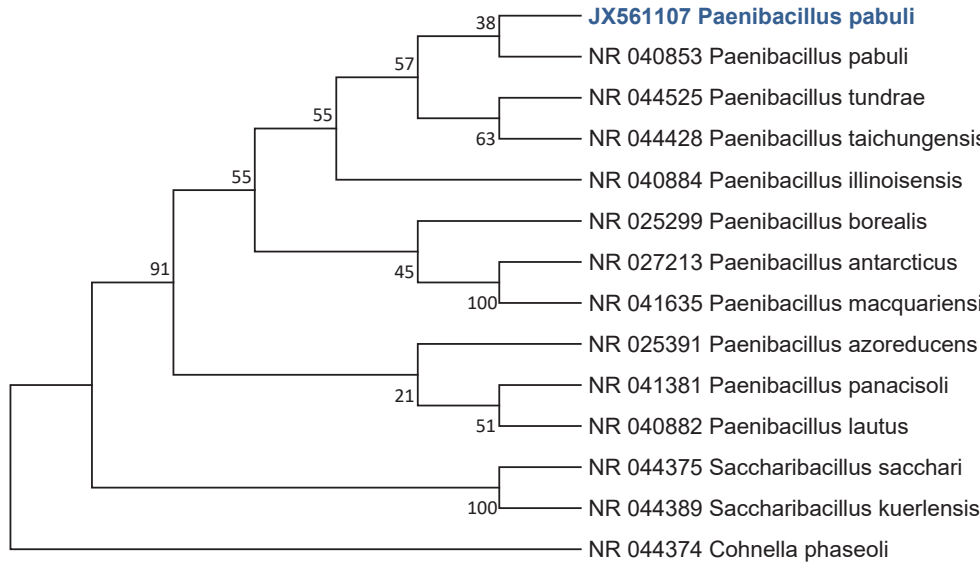

Fig. 1: Phylogenetic tree of *Paenibacillus pabuli* and NCBI accession number - JX561107.

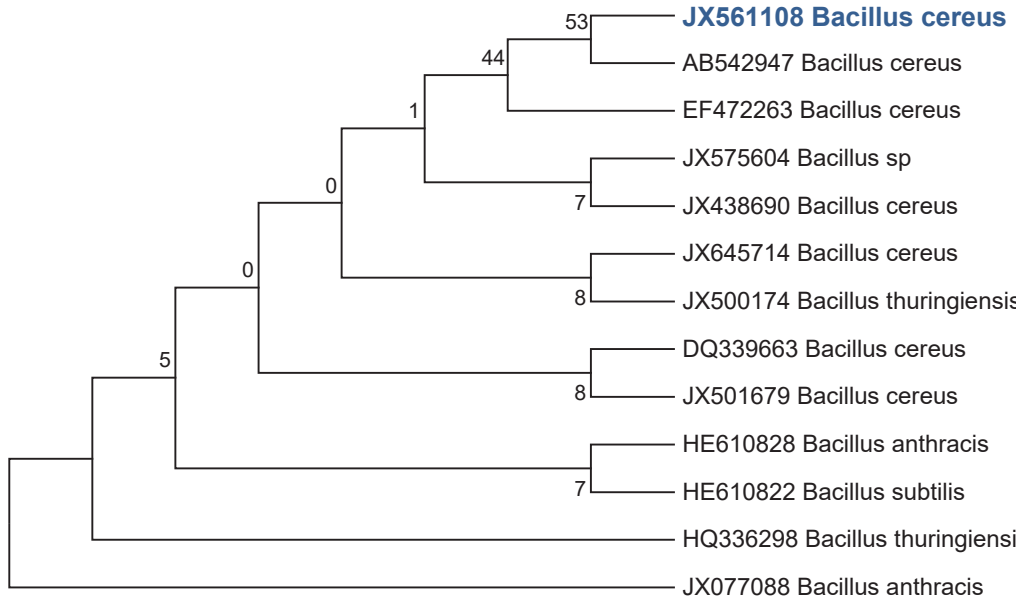

Fig. 2: Phylogenetic tree of *Bacillus cereus* and NCBI accession number - JX561108.

treatment (Fig. 4). Whereas, when the Cr(VI) concentration is increased to 400 mg/L, there was no absorption indicating the intolerance of bacterial biomass in a higher concentration of chromium due to high stress exerted by the higher level of metal ions in the medium.

SEM and EDX Analysis

Bacterial species *paenibacillus pabuli* and *Bacillus cereus* showed high efficiency in the removal of chromium in 72h of treatment. SEM analysis was conducted to differentiate the morphological changes due to adsorption of Cr(VI). Before biosorption, the cell surface was smooth and even. After the biosorption, there was a significant change on the surfaces of the bacterial cell. The figures clearly show that the bacterial cell surfaces before the treatment were smooth without any adhesion of Cr(VI), while after the treatment the cell surface was rough and wrinkled due to the adhesion of metal on the bacterium (Fig. 5 and Fig. 7). The EDX spectrum confirms the existence of Cr(VI) in the pellets of bacteria used in chromium treatment (Fig. 6 and Fig. 8).

DISCUSSION

Current awareness has been drawn to the expansion of the absorption technique as a method of bioremediation. It has been focused on a relatively inexpensive and easier than using a chemical treatment to overcome the contamination of heavy metals (Nies 2000). Moreover, countless researchers have reported the biosorption of heavy metal into pure cultures of bacteria and algae and onto the natural microbial population, which is possible through efficient and environmentally friendly remediation technologies (Gutnick & Bach 2000).

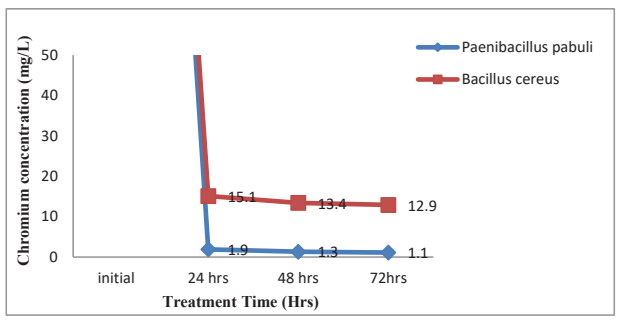

Fig. 3: Chromium sorption by isolated strain at 50 mg/L of chromium concentration in 72 hrs treatment at 9.5 pH.

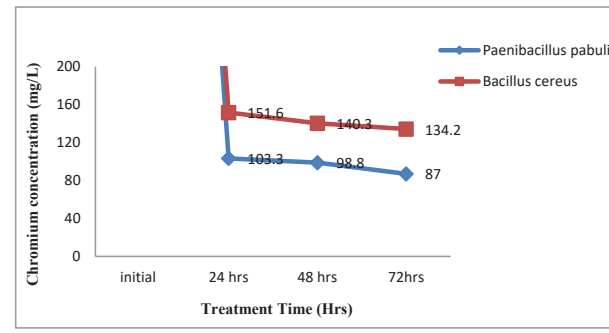

Fig. 4: Chromium sorption by isolated strain at 200 mg/L of chromium concentration in 72 hrs treatment at 9.5 pH.

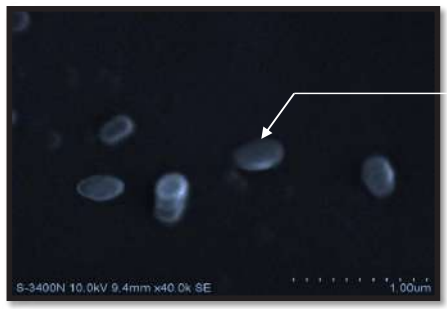

Before treatment with Cr effluent

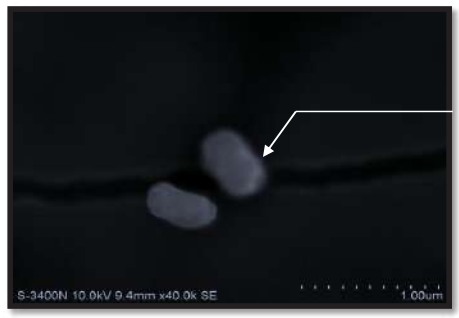

After treatment with Cr effluent

Fig. 5: SEM images of *Paenibacillus pabuli* before and after the treatment.

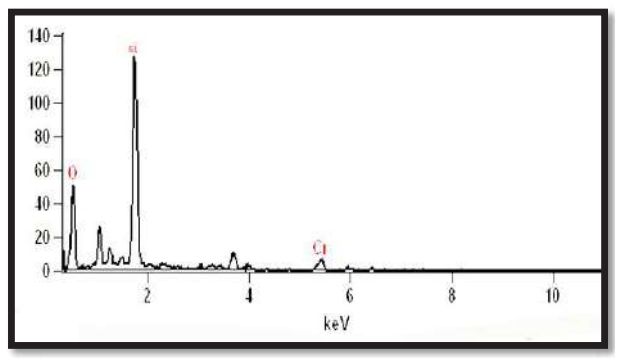

Fig. 6: EDX spectrum of *Paenibacillus pabuli.*

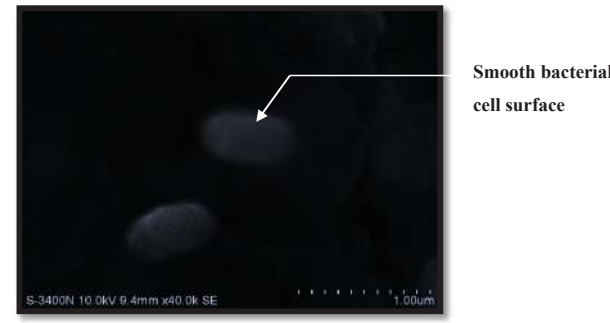

Before treatment with Cr effluent

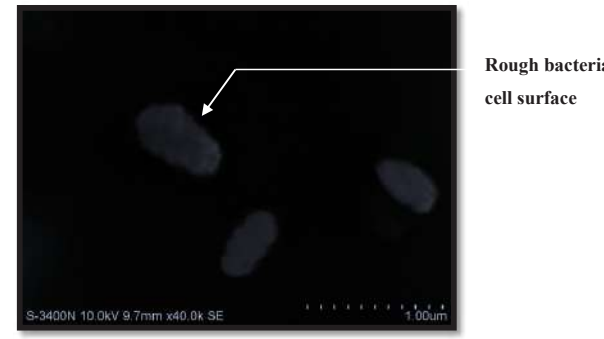

After treatment with Cr effluent

Fig. 7: SEM images of *Bacillus cereus* before and after treatment.

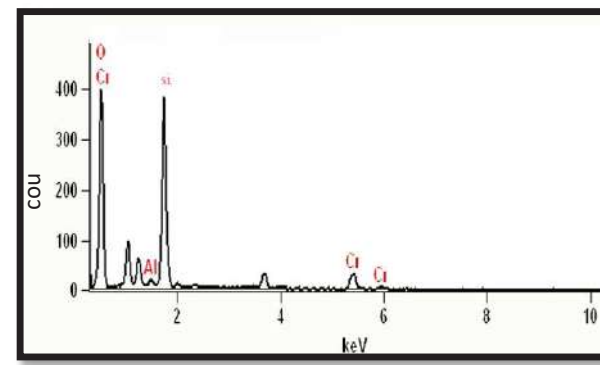

Fig. 8: EDX spectrum of *Bacillus cereus.*

In the present study, *Paenibacillus pabuli* and *Bacillus cereus* from alkaline industry-contaminated soil were evaluated for their chromium removal efficiency at 9.5 pH (pH of alkaline industry contaminated soil from which alkaliphilic bacteria were isolated). The results are quite encouraging, recording higher adsorption capacity at higher pH. The chromium(VI) efficiency of bacteria isolated from alkaline industrial contaminated soil, namely *Paenibacillus pabuli* and *Bacillus cereus* revealed 98% and 74% efficiency.

Further experimental study on evaluation of concentration based efficiency, 200 mg/L of Cr(VI) concentration and the tested bacteria recorded about 57% removal; but at higher concentration of chromium (400 mg/L), there was no removal by isolated bacterial strain tested. Such observation indicates the intolerance of bacterial biomass in a higher concentration of chromium due to high stress exerted by the higher level of metal ions in the medium. Up to 200 mg/L of chromium, the bacteria were able to remove more than 57% of Cr(VI) but when the concentration was doubled (i.e., 400 mg/L), there was no removal. It has been also reported that the high chromium concentration prohibited the development of bacteria (Bopp & Ehrlich 1988).

Such intolerance of a higher concentration of chromium by the bacteria reveals that the capability of a given amount of bacterial biomass could have played a significant role in maintaining its effectiveness. In the present study, a loop full of overnight grown pure culture biomass was inoculated in different Cr(VI) concentrations. The amount of biomass given cannot be tolerated due to the high concentration of metal in the medium and it is assumed that the actual threshold level of each bacterium might be scaled out to maintain the high efficiency of the bacterium for future research. The present findings are in close conformity with the observation made by Wang & Xiao (1995) in *Bacillus* sp. Further, Basu et al. (2014) and Yilmaz (2003) reported that the removal percentage was decreased with increasing chromium concentration. This is because the amount of inoculum was constant, relatively less biomass was available for chromium (VI) removal from the media. It is proving to be reported at low concentrations that all the metal ions in the solution will interact with the binding sites and thus facilitate 100% adsorption. The higher the concentration, the sites available for adsorption are less compared to the molecules of the solute present. Thus, observations made in the experimental studies are in close conformity with previous reports.

On examining the mechanism behind the adsorption of chromium to the bacterial cell surface, it has been reported that to endure under metal-stressed circumstances, bacteria have emerged numerous types of mechanisms to endure and survive through biomechanism of the uptake of heavy metal ions. These mechanisms comprise the discharge of metal ions outer the surface of the cell, aggregation and complexation of the metal ions within the cell (Nies 1999). Further, the adhesion of metal to the bacterial cell surface might be due to the presence of an exopolysaccharide production (Loaëc et al. 1997).

To examine the current findings regarding the adsorption of hexavalent chromium on the surface of bacterial cells, SEM images of the bacterial cell surface of treated and untreated bacteria show the metal adhered on the surface of the bacterial strains, giving a wrinkled and rough surface morphology in *Paenibacillus pabuli* and *Bacillus cereus.* Similar images were also recorded by Jun Guo et al. (2012) in *Pseudomonas plecoglossicida* showing that before the absorption the cells were rod-shaped with a smooth surface, but after the absorption, there were changes on the cell surfaces. Similarly, Dhal et al. (2010) also obtained SEM-EDX images indicating adherence of hexavalent chromium on the surface of bacterial cells. Besides, to substantiate whether the adsorbed material is made of chromium, the EDX spectrum was obtained for *Paenibacillus pabuli* and *Bacillus cereus* used in treatment studies. The EDX spectrum established the occurrence of Cr(VI) in the pellets of bacteria treated in Cr(VI) remediation. Silica (Si) peak in the EDX spectrum may be due to the preparation of smear on glass slides and the peak of Al might have originated from the sample holder.

CONCLUSION

Concludingly, it is reported that for bioremediation, having less than 200 mg/L of chromium, the alkaliphilic bacteria *Paenibacillus pabuli* and *Bacillus cereus* were able to tolerate and adsorb high Cr(VI) concentrations and could be the potential species as bioadsorbents. The suitability of these alkaliphilic isolates, particularly for chromium removal, would open up new lines of application through suitable biotechnological tools and techniques.

ACKNOWLEDGMENTS

We sincerely thank Central Instruments Centre at Pondicherry University for analysing samples under a scanning electron microscope.

REFERENCES

Basu, S., Dasgupta, M. and Chakraborty, B. 2014. Removal of chromium (VI) by *Bacillus subtilis* isolated from east Calcutta Wetlands, West Bengal, India. Int. J. Biosci. Biochem. and Bioinformatics, 4(1): 7-10.

Bopp, L. H. and Ehrlich, H. L. 1988. Chromate resistance and reduction in *Pseudomonas fluorescens* strain LB300. Archives of Microbiology, 150(5): 426-431.

Branco, R., Chung, A. P., Veríssimo, A. and Morais, P. V. 2005. Impact of chromium-contaminated wastewaters on the microbial community of a river. FEMS Microbiology Ecology, 54(1): 35-46.

Das, S., De, M., Ray, R., Ganguly, D., Kumar Jana, T. and De, T. K. 2011. Salt tolerant culturable microbes accessible in the soil of the Sundarban Mangrove forest, India. Open Journal of Ecology, 1(02): 35-40.

De, J., Ramaiah, N. and Vardanyan, L. 2008. Detoxification of toxic heavy metals by marine bacteria highly resistant to mercury. Marine Biotechnology, 10(4): 471-477.

Dhal, B., Thatoi, H., Das, N. and Pandey, B. D. 2010. Reduction of hexavalent chromium by *Bacillus* sp. isolated from chromite mine soils and characterization of reduced product. Journal of Chemical Technology and Biotechnology, 85(11): 1471-1479.

Francisco, C. A., Casciotti, K. L. and Tebo, B. M. 2002. Localization of Mn(II)-oxidizing activity and the putative multicopper oxidase, MnxG, to the exosporium of the marine *Bacillus* sp. strain SG-1. Archives of Microbiology, 178(6): 450-456.

Gardea-Torresdeya, J. L., Arenasb, J. L., Franciscob, N. M. C., Tiemanna, K. J. and Webbb, R. 1998. Ability of immobilized cyanobacteria to remove metal ions from solution and demonstration of the presence of metallothionein genes in various strains. Journal of Hazardous Substance Research, 1(2-1): 2-18.

Gutnick, D. L. and Bach, H. 2000. Engineering bacterial biopolymers for the biosorption of heavy metals; new products and novel formulations. Applied Microbiology and Biotechnology, 54(4): 451-460.

Horikoshi, K. 1991. General view of alkaliphiles and thermophiles. In: Superbugs: Micro-organisms in Extreme Environments, (Eds. K. Horikoshi and W.D. Grant), Springer Verlag, Berlin. 3-13.

Horikoshi, K. 1999. Alkaliphiles. Kodahansa. Harwood Academic Publishers, Australia.

Jun Guo, Zheng, X. D., Chen, Q. B., Zhang, L. and Xu, X. P. 2012. Biosorption of Cd (II) from aqueous solution by *Pseudomonas plecoglossicida*: Kinetics and mechanism. Current Microbiology, 65(4): 350-355.

Li, Z., Kawamura, Y., Shida, O., Yamagata, S., Deguchi, T. and Ezaki, T. 2002. *Bacillus okuhidensis* sp. nov., isolated from the Okuhida spa area of Japan. International Journal of Systematic and Evolutionary Microbiology, 52(4): 1205-1209.

Loaëc, M., Olier, R. and Guezennec, J. 1997. Uptake of lead, cadmium and zinc by a novel bacterial exopolysaccharide. Water Research, 31(5): 1171-1179.

Marmur, J. 1961. A procedure for the isolation of deoxyribonucleic acid from micro-organisms. Journal of Molecular Biology, 3(2): 208-218.

Nies, D. H. 1999. Microbial heavy-metal resistance. Applied Microbiology and Biotechnology, 51(6): 730-750.

Nies, D.H. 2000. Microbial heavy-metal resistance. Appl. Microbiol. Biotechnol., 51: 451- 460.

Rossi, M., Ciaramella, M., Cannio, R., Pisani, F. M., Moracci, M. and Bartolucci, S. 2003. Extremophiles 2002. Journal of Bacteriology, 185(13): 3683-3689.

Sen, P., Pal, D. and Debsarkar, A. 2019. Isolation of chromium resistant bacteria from contaminated soil and its performance evaluation for hexavalent chromium removal. International Journal of Engineering and Advanced Technology (IJEAT), 9(1): 2249-8958.

Turick, C.E., Apel, W.A. and Carmiol, N.S. 1996. Isolation of hexavalent chromium-reducing anaerobes from hexavalent-chromium-contaminated and noncontaminated environments. Applied Microbiol. Biotechnol., 44: 683-688.

Yilmaz, E. I. 2003. Metal tolerance and biosorption capacity of *Bacillus circulans* strain EB1. Research in Microbiology, 154(6): 409-415.

Nature Environment and Pollution Technology
An International Quarterly Scientific Journal

p-ISSN: 0972-6268
(Print copies up to 2016)
e-ISSN: 2395-3454

Vol. 20 | No. 2 | pp. 737-741 | 2021

Original Research Paper

https://doi.org/10.46488/NEPT.2021.v20i02.033

Open Access Journal

Application of Eco-Friendly Natural Dye on Cotton Obtained from the Flower of *Opuntia ficus-indica* Using Combination of Mordants

M. Kumaresan
Department of Chemistry, Arasu Engineering College, Kumbakonam, Tamil Nadu, India
†Corresponding author: M. Kumaresan; mkumsrenu@gmail.com

Nat. Env. & Poll. Tech.
Website: www.neptjournal.com

Received: 26-03-2020
Revised: 00-00-00
Accepted: 27-05-2020

Key Words:
Cotton, Fastness
Mordant
Natural dye
Opuntia ficus-indica

ABSTRACT

The fastness properties of the flower of *Opuntia ficus-indica* dyed cotton fabric have been studied using different combinations (1:3, 1:1 and 3:1) of various mordants, such as myrobolan-nickel sulphate, myrobolan-aluminium sulphate, myrobolan-potassium dichromate, myrobolan-ferrous sulphate and myrobolan-stannous chloride. The wash, rub, light and perspiration fastness of the dyed samples have been evaluated. It is found that the flower of *Opuntia ficus-indica* dye can be successfully used for the dyeing of cotton to obtain a wide range of colours by using various combinations of mordants.

INTRODUCTION

Environmental pollution due to the discharge of dyeing industry effluents is the matter of major concern nowadays. For many years, people have been using all types of natural substances, derived mainly from plants and animals. The use of natural dyes for textile dyeing purposes decreased to a large extent after the discovery of synthetic dyes in 1856. Synthetic dyestuffs produce hazardous by-products (Gulrajani et al. 1992), some of which possess carcinogenic intermediates, and hence a ban has been imposed by Germany and some other European countries on the use of benzidine dyes in textile garments exported into their countries (Anderson 1971 & Kumaresan et al. 2010). Hence, due to the current eco-consciousness, the attention of researchers has been shifted to the use of natural dyes for dyeing textile materials (Kumaresan et al. 2012, Kumaresan et al. 2015). Dyes derived from natural sources have emerged as an important alternative to synthetic dyes.

MATERIALS AND METHODS

In the present work, the flower of *Opuntia ficus-indica* (Fig. 1) growing in all warm and damp parts of India, have been used. *Opuntia ficus-indica* (prickly pear) is a species of cactus that has long been a domesticated crop plant grown in agricultural economies throughout arid and semiarid parts of the world. Opuntia is grown primarily as a fruit crop, and also for the vegetable nopales and other uses. The dye was used to dye cotton at optimized dyeing conditions, using a combination of mordants and to evaluate the resultant colour fastness of the dyed samples to washing, rubbing, perspiration and light.

Bleached plain weave cotton fabric, obtained from Gandhigram Rural University, Dindigal**,** was used for the study. AR grade ferrous sulphate, aluminium sulphate, nickel sulphate, potassium dichromate, stannous chloride, and commercial grade acetic acid, common salt and sodium carbonate were used. A natural mordant myrobolan (*Terminalia chebula*) powder (Kumaresan 2016) was also used for the study. The ethanol extract of the flower of *Opuntia ficus-indica* was used to get pale brown colour for dyeing fabrics. Depending upon the mordant used, the colour obtained on textiles may give different shades.

A known quantity of flowers of *Opuntia Ficus-Indica* was dried, powdered and soaked in warm water overnight. The flower of *Opuntia ficus-indica* extract was obtained by boiling it in the same water. The dye extract was allowed to cool, filtered and used for dyeing. The dyeing was carried out at optimized conditions namely dye extraction time 60 min, material to liquor ratio 1:20, and dyeing time 50 min.

The mordant combinations viz., myrobolan-nickel sulphate, myrobolan-aluminium sulphate, myrobolan-potassium dichromate, myrobolan-ferrous sulphate, and myrobolan-stannous chloride were used in the ratio of 1:3, 1:1 and 3:1. The total amount of two mordants used in each

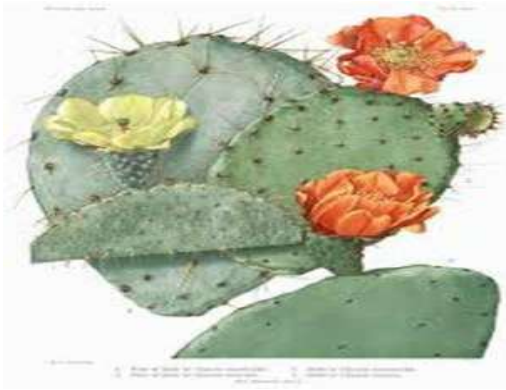

Fig. 1: Floweres of *Opuntia ficus-indica*.

combination was 5% on the weight of the fabric i.e., 5 g of the mordant/100 g of the fabric. Each of the five mordant combinations in three different ratios mentioned above was used with all the three mordanting methods namely pre mordanting, simultaneous mordanting and post mordanting for dyeing (Kumaresan 2019). After dyeing, the solution was allowed to cool, removed from the dye bath, rinsed under running water to remove excess dye and shade dried.

For optimizing the extraction method, the ethanol extraction of dye liquor was carried out under varying conditions, such as time of extraction, temperature of extraction bath and material-to-liquor ratio (Kundal et al. 2016, Sharada Devi et al. 2002). In each case, the optical density or absorbance value at a particular maximum absorbance wavelength (λ420 nm) for the ethanol extract of plant parts were estimated by using Hitachi-U-2000 UVVIS absorbance spectrometer.

Colour fastness to the washing of the dyed fabric samples was determined as per IS: 764-1984 method using a Sasmira launder-O-meter following IS-3 wash fastness method (Samanta et al. 2003, Bains et al. 2003). The wash fastness rating was assessed using greyscale as per ISO-05-A02 (loss of shade depth) and ISO-105-AO3 (extent of staining) and the same was cross-checked by measuring the loss of depth of colour and staining using Macbeth 2020 plus computer-aided colour measurement system attached with relevant software.

Colour fastness to rubbing (dry and wet) was assessed (Senthilkumar et al. 2002) as per IS: 766-1984 method using a manually operated crock meter and greyscale as per ISO-105-AO3 (extent of staining). Colour fastness to exposure to light was determined as per IS: 2454-1984 method. The sample was exposed to UV light in a Shirley MBTF Microsal fade-O-meter (having 500 Watt Philips mercury bulb tungsten filament lamp simulating daylight) along with the eight blue wool standards (BS1006: BOI: 1978).

Colour fastness to perspiration, assessed according to IS: 971-1983 composite specimen, was prepared by placing the test specimen between two adjacent pieces of fabrics of silk and cotton and stitched all among four sides. The sample was soaked in the test solution (acidic/alkaline) separately with MLR 1:50 for 30 minutes at room temperature. The sample was then placed between two glass plates of perspirometer under the load of 4.5 kg. The apparatus was kept in the oven for four hours at 37 ± 2°C. At the end of this period, the specimen was removed and dried in air at a temperature not exceeding 60°C. The test samples were graded for change in colour and staining using grey scales.

Table 1: Fastness grades of the flower of *Opuntia ficus-indica* dye, dyed on cotton at optimum dyeing conditions (wavelength 440 nm, dye extraction time 60min, material to liquor ratio 1:20, dyeing time 50 min) using Mb-NS mordant combination.

Mordanting Method	Mordant Properties	Light Fastness Grade	Wash Fastness		Rub Fastness			Perspiration Fastness			
			Grades		Grades			Acidic		Alkaline	
			CC	CS	Dry		Wet	CS	CC	CS	CC
					CC	CS	CC				
Pre Mordanting	1:3	3-4	4	5	5	5	5	4	5	4	5
	1:1	3-4	4-5	5	5	4-5	5	4	5	4-5	5
	3:1	3-4	4	5	4-5	5	5	5	5	5	5
Simultaneous Mordanting	1:3	3-4	4-5	5	5	5	5	5	5	5	5
	1:1	3-4	4	5	5	5	5	5	5	5	5
	3:1	3-4	4-5	5	5	4-5	5	4	5	5	5
Post Mordanting	1:3	3-4	4	4	5	5	5	4	5	5	4-5
	1:1	3-4	4-5	5	4-5	5	5	4	5	4-5	4-5
	3:1	3-4	4	5	5	5	5	4	5	5	5

Mb-NS = Myrobolan-Nickel sulphate, CC = Colour change, CS = Colour staining

RESULTS AND DISCUSSION

Mordant Combination: Myrobolan-Nickel Sulphate

The evaluation of colour fastness to light, washing, rubbing and perspiration of flower of *Opuntia ficus-indica* dyed cotton samples treated with myrobolan-nickel sulphate combination in the aqueous medium is presented in Table 1. All the treated samples subjected to light showed fairly good (3-4) light fastness for all ratio mordant combinations. The washing fastness grades ranged between 4 and 5-4 for all the treated samples and there was no colour staining. The colour change to dry and wet rubbing for all the treated samples was excellent (5).

Mordant Combination: Myrobolan-Aluminium Sulphate

The evaluation of colour fastness to light, washing, rubbing and perspiration of flower of *Opuntia ficus-indica* dyed cotton samples treated with myrobolan-aluminium sulphate combination in the aqueous medium is presented in Table 2. All the treated samples subjected to light showed fairly good (3-4) light fastness for all ratios of mordant combinations. The treated samples for pre mordanting showed fair (3 to 2-3) washing fastness grades, but they ranged from excellent to good (4-5 to 4) for all the treated samples for simultaneous and post mordanting. There was no colour staining. The colour change to dry and wet rubbing for all the treated samples was excellent (5). There was no colour staining ranged from no staining to negligible staining (5 to 4-5) in dry rubbing.

Mordant Combination: Myrobolan-Potassium Dichromate

The evaluation of colour fastness to light, washing, rubbing and perspiration of flower of *Opuntia ficus-indica* dyed cotton samples treated with Myrobolan-potassium dichromate combination in an aqueous medium is presented in Table 3. The treated samples subjected to light showed fairly good (3-4) light fastness for all ratio mordant combinations. The washing fastness grades showed fairly good (3-4) for all the treated samples. The colour change to dry and wet rubbing for all the treated samples was excellent (5).

Mordant Combination: Myrobolan-Ferrous Sulphate

The evaluation of colour fastness to light, washing, rubbing and perspiration of flower of Opuntia Ficus-Indica dyed cotton samples treated with myrobolan: ferrous sulphate combination in an aqueous medium is presented in Table 4. The treated samples subjected to light showed fairly good (4-3-4) light fastness for all ratios of mordant combinations. The washing fastness grades ranged from excellent to good (5-4) for all the treated samples. The colour change to dry and wet rubbing for all the treated samples was excellent (5).

Mordant Combination: Myrobolan-Stannous Chloride

The evaluation of colour fastness to light, washing, rubbing and perspiration of flower of *Opuntia ficus-indica* dyed cotton samples treated with myrobolan-stannous chloride combination in an aqueous medium is presented in Table 5. The treated samples subjected to light showed fairly good (4 to 3-4) light fastness for all the ratios of mordant

Table 2: Fastness grades of the flower of *Opuntia ficus-indica* dye, dyed on cotton at optimum dyeing conditions (wavelength 440 nm, dye extraction time 60 min, material to liquor ratio 1:20, dyeing time 50 min) using Mb-AS mordant combination.

Mordanting Method	Mordant Properties	Light Fastness Grade	Wash Fastness		Rub Fastness			Perspiration Fastness			
			Grades		Grades			Acidic		Alkaline	
			CC	CS	Dry		Wet	CS	CC	CS	CC
					CC	CS	CC				
Pre Mordanting	1:3	3-4	4	5	4	5	4-5	4	5	4	5
	1:1	3	5	5	4	4-5	4-5	4	5	4-5	5
	3:1	4	4	5	4	5	5	5	5	5	4-5
Simultaneous Mordanting	1:3	4	5	4-5	5	5	5	5	5	4-5	4-5
	1:1	4	5	4-5	5	5	5	5	5	5	5
	3:1	4	4-5	5	5	4-5	5	4	5	5	5
Post Mordanting	1:3	4	4	4	5	5	5	4	4	4-5	4
	1:1	3-4	4	4	4-5	5	4	4	4	4-5	4
	3:1	3-4	4	4	5	5	4	4	4-5	5	5

Mb-AS = Myrobolan-Aluminium sulphate, CC = Colour change, CS = Colour staining

Table 3: Fastness grades of the flower of *Opuntia ficus-indica* dye, dyed on cotton at optimum dyeing conditions (wavelength 440 nm. dye extraction time 60min, material to liquor ratio 1:20, dyeing time 50 min.) using Mb-PD mordant combination.

Mordanting Method	Mordant Properties	Light Fastness Grade	Wash Fastness		Rub Fastness			Perspiration Fastness			
			Grades		Grades			Acidic		Alkaline	
			CC	CS	Dry		Wet	CS	CC	CS	CC
					CC	CS	CC				
Pre Mordanting	1:3	3-4	4	4	3	4	3	4	4	4	4
	1:1	3-4	4-5	4	3	3-4	3	4	4	4	4
	3:1	3-4	4	4	3	4	3	3	3-4	3-4	3
Simultaneous Mordanting	1:3	3-4	3-4	4	3-4	4	4	3	3-4	3-4	3-4
	1:1	3-4	3-4	4	3-4	4	4	3	3-4	3-4	4
	3:1	3-4	3-4	3-4	3-4	4	3-4	3	3	3	4
Post Mordanting	1:3	3-4	4	4	4	4	4	4	4	3	3-4
	1:1	3-4	4-5	3	3	3	3	4	4	3	3
	3:1	3-4	4	3	3	3	3	4	4	3-4	3-4

Mb-PD = Myrobolan-Potassium dichromate, CC = Colour change, CS = Colour staining

Table 4: Fastness grades of the flower of *Opuntia ficus-indica* dye, dyed on cotton at optimum dyeing conditions (wavelength 440 nm. dye extraction time 60min, material to liquor ratio 1:20, dyeing time 50 min.) using Mb:FS mordant combination.

Mordanting Method	Mordant Properties	Light Fastness Grade	Wash Fastness		Rub Fastness			Perspiration Fastness			
			Grades		Grades			Acidic		Alkaline	
			CC	CS	Dry		Wet	CS	CC	CS	CC
					CC	CS	CC				
Pre Mordanting	1:3	3-4	4	4	4-5	5	5	4	4-5	4	4-5
	1:1	3-4	4-5	4	4-5	4-5	5	4	4-5	4-5	4-5
	3:1	3-4	4	4	4-5	4-5	5	4	5	5	4-5
Simultaneous Mordanting	1:3	3-4	3-4	4	5	5	5	5	5	5	5
	1:1	3-4	3-4	4	5	5	5	5	5	5	5
	3:1	3-4	3-4	3-4	5	5	5	5	5	5	5
Post Mordanting	1:3	3-4	4	4	5	4-5	4-5	4	4	5	4-5
	1:1	3-4	4-5	3	4-5	4-5	4-5	4	4-5	4-5	4-5
	3:1	3-4	4	3	4-5	4-5	4-5	4	4	4	5

Mb-FS: Myrobolan-Ferrous sulphate, CC = Colour change, CS = Colour staining

Table 5: Fastness grades of the flower of *Opuntia ficus-indica* dye, dyed on cotton at optimum dyeing conditions (wavelength 440 nm, dye extraction time 60min, material to liquor ratio 1:20, dyeing time 50 min) using Mb-SC mordant combination.

Mordanting Method	Mordant Properties	Light Fastness Grade	Wash Fastness		Rub Fastness			Perspiration Fastness			
			Grades		Grades			Acidic		Alkaline	
			CC	CS	Dry		Wet	CS	CC	CS	CC
					CC	CS	CC				
Pre Mordanting	1:3	3-4	4	4	3-4	4	3-4	4	3-4	3-4	4
	1:1	3-4	4-5	4	3-4	4	4	4	4	4	4
	3:1	3-4	4	4	4	3-4	4	4	3-4	3-4	3
Simultaneous Mordanting	1:3	3-4	4-5	4	4	4	4	4	3-4	3-4	3-4
	1:1	3-4	4-5	4	4	4	4	4	3-4	3-4	4
	3:1	3-4	4	4-5	3-4	3-4	3-4	4	3	4	4
Post Mordanting	1:3	3-4	4-5	4	4	4	4	4	4	4	4
	1:1	3-4	4-5	4	3-4	3-4	3-4	4	4	4	4
	3:1	3-4	4	4	3-4	3-4	3-4	4	4	4	4

Mb-SC = Myrobolan-Stannous chloride, CC = Colour change, CS = Colour staining

combinations. The washing fastness grades ranged be- tween excellent to good (4-5 to 3-4) for all the treated samples and there was no colour staining. The colour change to dry and wet rubbing for all the treated samples was excellent (5). The colour staining ranged from negligible to slight staining (4-5) in both dry and wet rubbing.

CONCLUSION

It was found from the study that flower of *Opuntia ficus-indica* dye can be successfully used for dyeing cotton to obtain a wide range of soft, pastel and light colours by using a combination of mordants. With regards to colour fastness, test samples exhibited excellent fastness to washing (except for pre- mordanting using myrobolan-potassium dichromate combination); excellent fastness to rubbing (except for pre-mordanting using myrobolan-potassium dichromate combination); and good to excellent fastness to perspiration in both acidic and alkaline media and fairly good fastness to light.

ACKNOWLEDGEMENT

The authors are thankful to Dr P. N. Palanisamy, Department of Chemistry, Kongu Engineering College for his support and help for the completion of this work.

REFERENCES

Anderson, B. 1971. Creative spinning, weaving and plant dyeing. Angus and Robinson, Singapore, pp. 24-28.

Bains, S., Singh, O.P., Goraya, G. and Kang, M. 2003. Dyeing of cotton with Goldendrop (*Onosma echioides*) dye. Journal of the Textile Association, pp. 183-186.

Gulrajani, M. L. and Gupta, Deepti 1992. Natural Dye and their Application to Textiles (Department of TextileTechnology, IIT, Delhi), 25.

Kumaresan, M 2015. Comparison of properties of eco-friendly natural dyed cotton fabric. International Journal of Der Pharma Chemica, 7(4): 257-260.

Kumaresan, M. 2016. Application of eco-friendly natural dye obtained from *Spathodea campanulata* on silk using combination of mordants. Management of Environmental Quality, 27(1): 15-21.

Kumaresan, M. 2019. Dyeing of cotton fabric with eco-friendly natural dye obtained from *Opuntia ficus-indica* using single mordants. Journal of Applied Science and Computations, V(XII): 2290-2294.

Kumaresan, M., Palanisamy, P.N. and Kumar, P.E. 2012. Application of eco-friendly natural dye on cotton using combination of mordants. Indian Journal of Fibre & Textile Research, 37: 194-198.

Kumaresan, M., Palanisamy, P.N. and Kumar, P.E. 2010. Application of eco-friendly natural dyes on cotton obtained from the stem of *Achras sapota* using a combination of mordants. Nature Environment and Pollution Technology, 9(3): 547-552.

Kundal, J.S.V.S., Singh, S.V. and Purohit, M.C. 2016. Extraction of natural dye from *Ficus cunia* and dyeing of polyester cotton and wool fabric using different mordants, with evaluation of colour fastness properties. Natural Products Chemistry & Research, 4(3): 1-6.

Samanta, A. K. and Singhee, D. 2003. Application of single and mixture of selected natural dyes on cotton fabric - A scientific approach. Colourage, 50(10): 29-42.

Senthilkumar, P., Umashankar, P. and Sujatha, B. 2002. Ultrasonic dyeing of cotton fabrics with neem leaves. The Indian Textile Journal, 58(3): 15-18.

Sharada Devi, A. Sumanthy, B. S. and Katyayini, V.K.L.T. 2002. *Eclipta prostate*- A weed rich in coloured pigments for silk. Man Made Textiles in India, pp. 181-189.

Nature Environment and Pollution Technology
An International Quarterly Scientific Journal

p-ISSN: 0972-6268
(Print copies up to 2016)
e-ISSN: 2395-3454

Vol. 20 | No. 2 | pp. 743-746 | 2021

Original Research Paper

https://doi.org/10.46488/NEPT.2021.v20i02.034

Open Access Journal

Synchrotron Based TXRF for Assessment of Treated Wastewater

Vijay Kumar Garg*, Arun Lal Srivastav*, M. K. Tiwari, Ajay Sharma*† and Varinder Singh Kanwar***
*Chitkara University School of Engineering and Technology, Chitkara University, Himachal Pradesh-174103, India
**Raja Ramanna Centre for Advanced Technology, Indore, India
†Corresponding author: Ajay Sharma; ajay.sharma@chitkarauniversity.edu.in

Nat. Env. & Poll. Tech.
Website: www.neptjournal.com

Received: 03-05-2020
Revised: 11-06-2020
Accepted: 26-06-2020

Key Words:
Elemental analysis
Synchrotron radiation
Water treatment
X-ray fluorescence

ABSTRACT

The use of wastewater for diverse applications is gaining popularity for protecting scarce freshwater resources. The global supply of freshwater is limited and is threatened by the masses. Communities are competing over the allocation of limited freshwater resources to meet the increasing demand for water for agriculture, industry and cities. Wastewater treatment units are being used to treat wastewater for irrigation, firefighting, and other domestic purposes. The environment and human health can be adversely affected if wastewater is not accurately treated. Treated wastewater if free from toxicity can help in preserving the natural environment. In the present work, the synchrotron-based Total Reflection X-ray Fluorescence (TXRF) has been used to assess the trace elements present in the treated wastewater collected from a sewerage treatment plant in the study area. The results are compared with the World Health Organization (WHO) recommended values and concluded that the concentration of all detected elements (Cr, Mn, Ni, Cu, Zn and Pb) are within permissible limits (except iron). Investigations are further incorporated in calculations of the water quality index (WQI) that is used for the treated water standards. The present WQI 82.70 lies in the good quality range 80-94 by Canadian Council of Ministers of the Environment (CCME 2001) standards and does not pose any hazard to the environment, therefore, recommended for irrigation, toilet flushing, firefighting etc.

INTRODUCTION

Approach to freshwater is crucial for anthropological development, the environment and the economy. More than two billion people have a paucity to clean drinking water and hygiene (World Health Organization 2017) that blocks continual growth attempts worldwide. The increasing burden on existing water resources has resulted in higher water paucity and an expanding need for adequate quality water. An integrated *One Water* concept can facilitate meeting this demand by limiting discharges from wastewater treatment (Mitchell 2006). Three general types of water reuse include agricultural, environmental, and industrial applications. The main objective of wastewater treatment is to abolish as much of the pollutants as possible before the remaining water, called effluent, can be discharged back to the environment. Water reuse produces substantial environmental benefits. It helps in mitigating the adverse effects of sewage or industrial effluent on the environment. The end use of wastewater decides the required water quality and management measures to ensure safety. World health organization and other countries have provided guidelines and standards for the secure use of wastewater in irrigation and other environments (WHO 2006).

Water sample analysis in terms of trace elements and their concentration is a topic of great concern in many fields. It can be done by a number of procedures. Researchers have used various methods like atomic absorption spectroscopy (AAS), inductively coupled plasma atomic emission spectroscopy (ICP-AES) and X-ray fluorescence (XRF) technique to analyse the elemental quantification of water samples. Bamford et al (2004) applied XRF technique for trace elemental analysis of environmental samples e. g. soil, water and plants and recommended XRF for determination of elements in the range Na to U. Melquiades et al. (2004) used XRF technique for simultaneous heavy metal contamination in water. X-ray fluorescence is considered as a non-destructive simultaneous analysis of the sample, but the use is preferred for solid samples only (Margui 2014). TXRF (total reflection X-ray fluorescence) is another version of X-ray fluorescence technique, where the intricacy of the Compton spectral background is eradicated to a large extent. This is due to the high reflectivity of the flat surface and low penetration depth of the primary X-ray beam in the substrate material, on which the incident X-rays can impinge at glancing incidence angles. The above characteristics enhance the detection sensitivities of TXRF technique by two or three times or higher compared to normal X-ray fluorescence: typically, in the range of parts per billion (ppb) (Tiwari 2018). Synchrotron radiation has multiple edges over conventional X-ray sources like monochromacy, high incident flux, high convergence, and linear polarization, which results in increased signal strength and reduced scattered background. Moreover, tun-

ability of the incident photons energy to the characteristic absorption edge of an element identified in the sample leads to higher fluorescence intensities and hence making this technique appropriate for swift elemental analysis. TXRF is thus suitable for quickly studying all considered elements. TXRF spectroscopy has attracted interest in recent years. Examining the extraordinary competencies of synchrotron radiation, TXRF can be efficiently applied to detect trace concentrations of contaminants.

Water quality has been studied extensively in acceptable and standard ways by applying the water quality index (Tyagi et al. 2013). The possibilities of using treated wastewater for diverse applications need to be strengthened with elements of affordability, sustainability and above all public acceptance. In the present work, synchrotron-based TXRF has been used to measure the trace elemental concentration of treated wastewater collected from a sewerage treatment plant in the study area.

MATERIALS AND METHODS

To achieve a thin and homogenous sample layer 100 µL of polyvinyl alcohol was added to 10 mL of the treated water sample. 10 µL of gallium was added as an internal standard in the water sample. After complete homogenization, 10 µL of the liquid sample was placed on a siliconized quartz glass substrate and the sample was vacuum dried for about 10 minutes. The sample reflector carrying the water sample was placed in the experimental set-up as shown in Fig. 1 (a) and 1(b) along with other instrumentations involved in TXRF.

The measurements were performed on a synchrotron beam line 16 (BL-16) specially commissioned for X-ray fluorescence studies at Raja Ramanna Centre for Advanced Technology, Indore-India. The experimental arrangement of beam line (BL-16) consists of a double crystal monochromator with Si(111) symmetric and asymmetric crystals. The set-up also has focusing optics and a combination of slits to reduce the scattered X-ray background and improve the collimation of the X-ray beam. For accurate detection of trace elements present in the sample, the set-up is equipped with a silicon drift detector having an energy resolution of 129 eV at 5. 9 keV. The fluorescent spectra were recorded for 500 seconds. Fig. 1(a) depicts a schematic design of the TXRF set up at BL-16, whereas Fig. 1(b) shows an actual photograph of the TXRF set up at BL-16.

RESULTS AND DISCUSSION

Fig. 2 shows typical TXRF spectra obtained for sewerage treated water mixed with 10 ppm of Ga standard at 18 keV synchronous X-ray energy, whereas the inset shows fitted TXRF spectra of the same sample on a logarithmic scale. Solid black and red lines, respectively, are the experimental and fitted data, whereas the green line represents a good estimation of the spectral background.

Most of the trace elements Cr, Mn, Fe, Ni, Cu, Zn and Pb were identified in the treated water sample with the best detection sensitivity. The measured concentration of trace elements (ppb) in the treated water sample is listed in Table 1 and Fig. 3 along with the permissible WHO limits (2008). The comparison shows that the measured concentration of trace metals is within permissible standards for almost all the elements except iron that is more than 20 times of its permissible limit. The probabilistic reasons for the high content of iron may be geological deposits (regional soils, rocks), acidic nature of wastewater and chemical reactions enhancing iron concentration in the STP (EPA 2001). Many studies have also found that the presence of iron in huge amounts in the water can act as an adsorbent for the pollutants after making complexes in presence of some favourable chemical agents

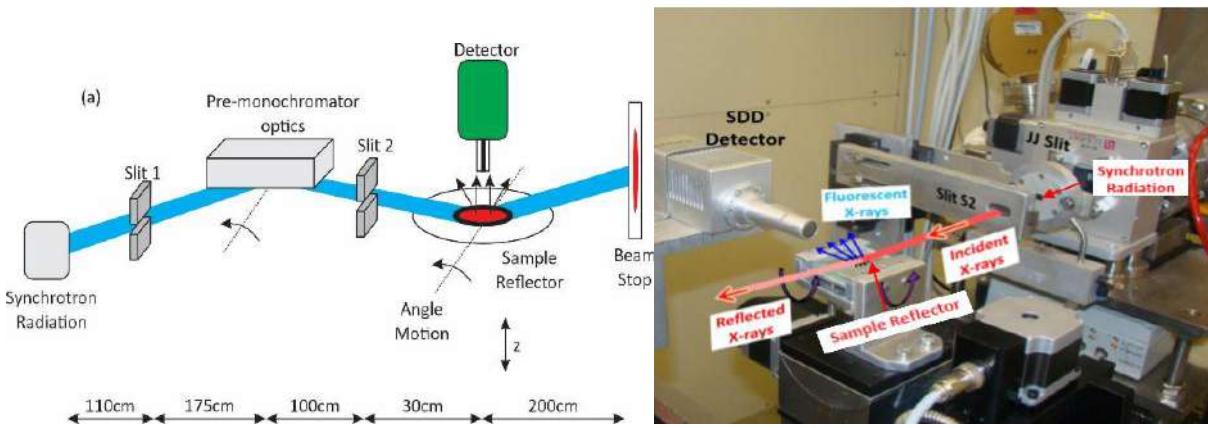

Fig. 1: (a) Schematic diagram of the experimental TXRF set-up developed at RRCAT (b) Actual photograph of the TXRF spectrometer.

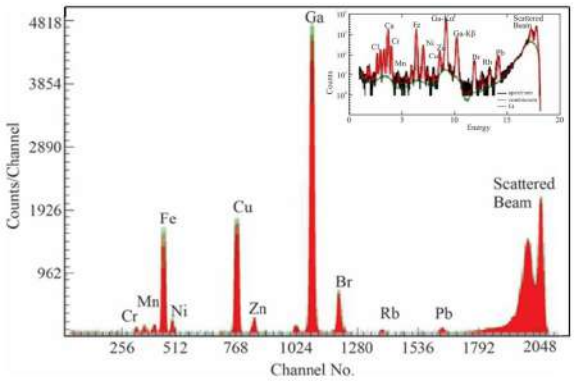

Fig. 2: Typical TXRF spectra obtained for sewerage treated water mixed with 10 ppm Ga standard at 18 keV. The inset shows fitted TXRF spectra of the same sample on a logarithmic scale.

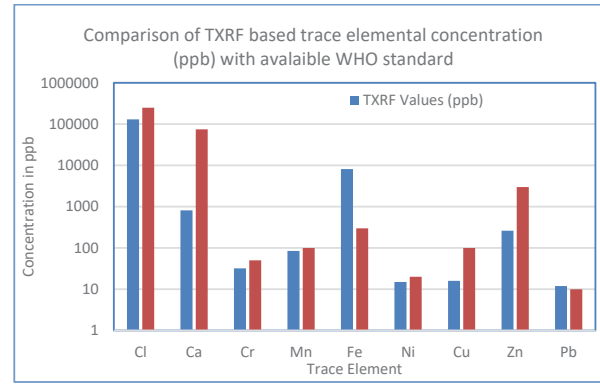

Fig. 3: Graphical representation of trace elemental concentration (ppb) in sewerage treated water mixed with 10 ppm Ga standard.

(Najafpoor et al. 2020). For example, nanoparticles of iron oxide are sufficient to remove (Hu et al. 2005) chromium, selenium, copper, lead, and nickel, from the simulated as well as natural waters (Zhang et al. 2016). It is also possible that the abundant iron present in water may get mixed with sludge and form complexes, which can act as an adsorbent for the removal of heavy metals from the water. Furthermore, both manganese, and nickel in treated water are observed as 85 ppb and 15 ppb, which are within quite safe levels as suggested by WHO (2006). Manganese is one of the most abundant metals in Earth's crust, usually occurring with Iron. Manganese, Iron and Nickel occur naturally in many food sources, leafy vegetables, nuts, grains, and animal products etc. Therefore, anthropological activities can also be responsible for the marginal concentration of Manganese and Nickel as compared to other trace elements in the treated water samples collected from domestic sewerage plant.

Water Quality Index (WQI)

The water quality index (WQI) is an essential mean to ascertain the water quality in urban, rural and industrial areas. WQI is documented by Canadian Council of Ministers of the Environment (CCME 2001). The index enables us to understand how far the physical parameters related to water quality surpass their respective limits. Therefore, WQI demonstrates water quality standards for all settings as determined by the World Health Organisation. WQI calculations are related to various physical, chemical, and bacteriological parameters, but in developing and underdeveloped nations, the primary concern is to provide affordable solutions due to limited funds (Ongley 1998, Ongley & Booty 1999). Therefore, in these type of circumstances, only major parameters can be used to calculate WQI (Kannel et al. 2007). The general WQI equation involves three factors as below (eq. i):

Table 1: The concentration of trace elements (ppb) in sewerage treated water along with WHO standards.

Sr No.	Trace metal (parameters)	TXRF results (7% uncertainty)	Permissible limits (WHO year)
1	Cl	130276(±9119.32)	250000
2	Ca	815(±57.05)	75000
3	Cr	32(±2.24)	50
4	Mn	85(±5.95)	100
5	Fe	8136(±569.52)	300
6	Ni	15(±1.05)	20
7	Cu	16(±1.12)	100
8	Zn	262(±18.34)	3000
9	Pb	12(±0.84)	10

$$WQI = 100 - \left(\frac{\sqrt{F_1^2 + F_2^2 + F_3^2}}{1.732} \right) \quad \ldots(1)$$

F1 represents the percentage of parameters that exceed the guideline, F2 represents the frequency with which the parameters exceed the guideline and F3 represents the magnitude by which the parameters have not met/exceeded. The individual values of parameters F1, F2 and F3 are calculated as follows.

$$F1 = \left(\frac{\text{Number of exceeded/unmet parameters}}{\text{Total number of parameters}} x \right) 100 \quad \ldots(2)$$

$$F2 = \left(\frac{\text{Number of failed tests}}{\text{Total number of tests}} x \right) 100 \quad \ldots(3)$$

$$F3 = \left(\frac{\text{Failed test value}}{\text{guideline Value}} \right) - 1 \quad \ldots(4)$$

The value of the factors F1, F2 and F3 calculated using equations (ii), (iii) and (iv) are 7.69, 12.5 and 26.12 respectively are substituted in equation (i) to produce WQI value (between 0 and 100) that characterizes water quality. WQI ranges and descriptions are:

Excellent (95-100)
Good (80-94)
Fair (65-79)

Table 2: Physical parameters like pH value, turbidity, total hardness and TDS of the water samples of study area along with reference ranges [*].

Sr. No.	Parameter	Jan, 2019	Feb, 2019	March, 2019	April, 2019	May, 2019	June, 2019	July, 2019	August, 2019	Reference range [*]
1	pH value	7.65	7.5	7.6	7.45	7.5	7.46	7.65	7.5	6.5-8.5
2	Turbidity (NTU)	4.5	4.5	4.5	5	4.5	4.5	5	5	1-5
3	Total hardness (mg/L)	180	190	180	184	185	180	184	185	200
4	TDS (mg/L)	85	80	80	85	85	80	90	85	500

*(Bureau of Indian Standards 2012)

Marginal (45-64) Poor (0-44)

In the present analysis, physical parameters like pH value, turbidity, total hardness, and TDS of the same water (Table 2) have also been taken into consideration for WQI calculations.

The water quality index (WQI) for the treated water is calculated by drawing analysis from Table 1 and Table 2 and the approximated value of the same is 82.70, which is considered as good quality as per CCME (2001).

CONCLUSION

The results of wastewater analysis show how synchrotron-based TXRF measurements can successfully be applied for multi-elemental analysis of liquid samples to simultaneously quantify almost all elements after a precise and systematic sample preparation technique. The detection sensitivities of the TXRF technique is far better compared to conventional XRF and other analytical methods. Synchrotron TXRF (SR-TXRF) is advantageous in terms of experimental time, minimum background, high monochromatic radiation flux along with sample preparation and calibration. It is concluded that the measured elemental concentration for almost all trace metals in the treated water is within permissible WHO guidelines (except iron). Furthermore, it is quite evident from the calculated value of the water quality index (WQI) that the treated water has no significant threats and can be recommended as an alternative to freshwater for irrigation, toilet flushing, firefighting etc in the study area.

ACKNOWLEDGEMENT

The authors would like to thank the Department of Environment, Science and Technology, Himachal Pradesh-India for financial support in this work (DEST sanction no. Env. S & T (F)/5-1/2018-8886). The authors also acknowledge the technical assistance and guidance extended by RRCAT Indore-India to carry on this work.

REFERENCES

Bamford, S., Wegrzynek, D., Chinea-Cano, E. and Markowicz, A. 2004. Application of X-ray fluorescence techniques for the determination of hazardous and essential trace elements in environmental and biological materials. Nukleonika, 49(3): 87-95.

BIS, I.S.D.W.S. 2012. Bureau of Indian Standards. New Delhi: 2-3.

Canadian Council of Ministers of the Environment, 2001. Canadian Water Quality Guidelines for the Protection of Aquatic Life: CCME Water Quality Index 1.0, User's Manual. Canadian Environmental Quality Guidelines.

Environmental Protection Agency EPA, 2001. Parameters of water quality: interpretation and standards.

Hu, J., Chen, G. and Lo, I.M. 2005. Removal and recovery of Cr (VI) from wastewater by maghemite nanoparticles. Water Research, 39(1): 4528-4536.

Kannel, P.R., Lee, S., Lee, Y.S., Kanel, S.R. and Khan, S.P. 2007. Application of water quality indices and dissolved oxygen as indicators for river water classification and urban impact assessment. Environmental Monitoring and Assessment, 132(1-3): 93-110.

Marguí, E., Zawisza, B. and Sitko, R. 2014. Trace and ultratrace analysis of liquid samples by X-ray fluorescence spectrometry. TrAC Trends in Analytical Chemistry, 53: 73-83.

Melquiades, F.L. and Appoloni, C.R. 2004. Application of XRF and field portable XRF for environmental analysis. Journal of Radioanalytical and Nuclear Chemistry, 262(2): 533-541.

Mitchell, V.G. 2006. Applying integrated urban water management concepts: a review of Australian experience. Environmental Management, 37(5): 589-605.

Najafpoor, A., Norouzian-Ostad, R., Alidadi, H., Rohani-Bastami, T., Davoudi, M., Barjasteh-Askari, F. and Zanganeh, J. 2020. Effect of magnetic nanoparticles and silver-loaded magnetic nanoparticles on advanced wastewater treatment and disinfection. Journal of Molecular Liquids, 303: 112640.

Ongley, E.D. 1998. Modernisation of water quality programmes in developing countries: issues of relevancy and cost efficiency. Water Quality International, pp. 37-42.

Ongley, E.D. and Booty, W.G. 1999. Pollution remediation planning in developing countries: Conventional modelling versus knowledge-based prediction. Water International, 24(1): 31-38.

Tiwari, M.K. 2018. Recent trends in X-ray fluorescence spectrometry: precise investigation of nanomaterials. Spectroscopy Europe, 30: 15-19.

Tyagi, S., Sharma, B., Singh, P. and Dobhal, R. 2013. Water quality assessment in terms of water quality index. American Journal of Water Resources, 1(3): 34-38.

World Health Organization. 2006. WHO Guidelines for the Safe use of Wastewater Excreta and Greywater (Vol. 1). World Health Organization.

World Health Organization. 2008. WHO Guidelines for Drinking-water Quality, Volume 1. World Health Organization.

World Health Organization. 2017. United Nations Children's Fund (UNICEF). Progress on drinking water, sanitation and hygiene, 110.

Zhang, Y., Wu, B., Xu, H., Liu, H., Wang, M., He, Y. and Pan, B. 2016. Nanomaterials-enabled water and wastewater treatment. NanoImpact, 3: 22-39.

Nature Environment and Pollution Technology
An International Quarterly Scientific Journal

p-ISSN: 0972-6268
(Print copies up to 2016)
e-ISSN: 2395-3454

Vol. 20 | No. 2 | pp. 747-751 | 2021

Original Research Paper

https://doi.org/10.46488/NEPT.2021.v20i02.035

Open Access Journal

Performance of Phosphorus Adsorption by Acid-Activated Iron-Based Waterworks Sludge Adsorbent

J. X. Tie*(**), Y. F. Niu*, H. Xiao*, Y. S. Wang*, C. B. Du****, M. Zhang*, J. M. Zhang* and Z. H. Zheng*****†**

*School of Environmental and Municipal Engineering, North China University of Water Resources and Electric Power, Zhengzhou, 450045, PR China

**Zhong Zhou Water Holding Co. Ltd., Zhengzhou, 450000, PR China

***Bureau of Hydrology and Water Resources in Henan Province, Zhengzhou, 450004, PR China

****College of Chemistry and Chemical Engineering, Xi'an Shiyou University, Xi'an 710065, PR China

*****Henan Vocational College of Water Conservancy and Environment, Zhengzhou 450008, PR China

†Corresponding author: Z. H. Zheng; 15202843@qq.com

Nat. Env. & Poll. Tech.
Website: www.neptjournal.com

Received: 14-05-2020
Revised: 18-07-2020
Accepted: 20-07-2020

Key Words:
Acid-activated iron-based waterworks sludge (AAIBWS)
Phosphorus adsorption
Influencing factors

ABSTRACT

Iron-based waterworks sludge was activated using 0.5-3 mol/L H_2SO_4 acid to obtain the acid-activated iron-based waterworks sludge (AAIBWS). The sludge treated with 1 mol/L H_2SO_4 acid was best for phosphorus adsorption and used to carry out batch phosphorus adsorption experiments. The influencing factors including solution pH, contact time and reaction temperature were investigated. The results indicated that the acid environment was favourable for P adsorption. The phosphorus adsorption increased with the rising reaction time and temperature. The pseudo-second-order equation was best to describe the adsorption process among the three kinetic models. The Langmuir isotherm provided a better fit of the data than the Freundlich model. Thermodynamic parameters showed that the phosphorus adsorption on AAIBWS-1 had a spontaneous and endothermic nature.

INTRODUCTION

Phosphorus (P) discharged from industrial, agricultural sections and household is a limiting nutrient that causes eutrophication. It was reported that more than 60% of the lakes have been eutrophicated in China (Pan et al. 2004). The most stringent discharge standard for 'P' has been set as 0.5 mg/L for the effluent discharged from the municipal sewage treatment plants to reduce the eutrophication in the water bodies accepting the effluent.

Chemical, physical and biological technologies have been developed to remove phosphorus from wastewater (Chang et al. 2017, Liu et al. 2018, Braun et al. 2019). Among the technologies, adsorption has attracted special concern due to its advantages such as low cost, high efficiency and simple operation.

Globally, the coagulation/flocculation process is used to produce drinking water in surface water treatment works. Aluminium and iron salts are two chemical coagulants used widely to remove turbidity from raw water (Faisal et al. 2020). During the coagu-flocculation process, the hydrolysed coagulants react with the suspended solids and colloids to form the flocs which settle down in the sedimentation tank, resulting in the generation of a large quantity of waterworks sludge globally (Fang et al. 2019, Faisal et al. 2020, Shrestha et al. 2020, Wang et al. 2018). The sludge contains coagulant residual, silica, clay minerals, and dissolved organic matters (Kang et al. 2019). Currently, the sludge is mainly dewatered and disposed of in landfills subsequently (Zhao et al. 2011), whereas, more and more landfills refuse to accept the de-watered waterworks sludge due to the scarce land resources and stringent environmental requirements in China. Hence, recycling and reuse of waterworks sludge is a promising way to deal with the massive sludge.

Acid activation could significantly enhance the porosity, surface area and roughness of the particles (Zhu et al. 2018, Lian et al. 2020), and increase the adsorption capacity subsequently. As a result, iron-based waterworks sludge was acid-activated and used as an adsorbent to remove 'P' from its aqueous solution in this study.

MATERIALS AND METHODS

Iron-based waterworks sludge: The iron-based waterworks sludge was collected from a drinking water treatment plant in Liaoning province, China. The collected sludge was dried in the open air and at 105°C in a drier for 2 h in sequence. The sludge was cooled and sieved through an 80 mesh sieve. 40 g sifted sludge powder was mixed with 400 mL of 0.5-3 mol/L H_2SO_4 acid, and the mixture was reacted at 90°C for 2 h. The mixture was then processed using alternate treatment of centrifugation at 4000 rpm for 5 min and washed with deionized water several times until the supernatant became neutral. The activated sludge was re-dried at 105°C for 2 h. Finally, the dried acid-activated iron-based waterworks sludge (AAIBWS) was collected for the experiment.

Characterization of AAIBWSs: A scanning electron microscope (JSM- 6460LV, Japan Electronic Co., Ltd.) was used to record the surface morphologies of AAIBWSs. The surface area was measured using the Brunauer-Emmett-Teller (BET) method of N_2 adsorption and desorption (Autosorb-I, Quantachrome, USA). The chemical compositions of AAIBWSs were analysed using an X-ray fluorescence spectrometer (XRF, Model ARL PERFORM'X, Thermo Fisher Scientific Inc.).

'P' adsorption studies: Batch experiment of 'P' adsorption was conducted in the following way: 10 mL P-containing solution and 0.08 g sludge were added into a glass bottle and reacted in a shaker at different temperatures for various times given explicitly in the following experiments. At the end of the reaction, the mixture was taken out and filtered through a 0.45 μm filter membrane and the residual 'P' in the supernatant was determined using the ascorbic acid method. The 'P' uptake was calculated using the following equation

$$q = \frac{(C_0 - C_e)V}{m} \quad \ldots(1)$$

Where q(mg/g) is the 'P' uptake by per unit mass of the sludge. C_0 and C_e (mg/L) are the initial and final 'P' concentrations, respectively and 'm' (g) is the mass of AAIBWS used in the experiment. Each adsorption test was repeated three times, and the mean value of the three results was used in this article. The experimental errors were calculated and expressed with error bars.

RESULTS AND DISCUSSION

Characterization of the AAIBWS: Fig. 1 shows the SEM images of AAIBWSs treated with H_2SO_4 solutions of different concentrations. It can be seen clearly that the raw sludge had the largest particle size of about 30 nm which decreased to about 20 nm as the H_2SO_4 solution concentration rose to 3 mol/L since more iron compounds dissolved in H_2SO_4 solution of higher concentration which was also the main reason that caused the decrease of the content of iron compounds of acid-activated AAIBWSs (Table 1). The specific surface area of raw sludge was 81.41 m^2/g that increased to 140.32 m^2/g after acid treatment by 1 mol/L H_2SO_4 acid, and then decreased to 51.93 m^2/g as the H_2SO_4 concentration increased to 3 mol/L.

Tab1e 1: The main compositions and specific areas of AAIBWSs.

H_2SO_4 concentration (mol/L)	Oxide content (wt%)				Specific surface area (m^2/g)
	Fe_2O_3	SiO_2	Al_2O_3	MoO_3	
0	83.54	8.66	3.24	1.02	81.41
0.5	82.77	9.63	3.13	1.28	130.59
A-1	80.37	11.54	3.45	1.39	140.32
2	69.84	19.35	5.29	1.7	78.12
3	25.66	55.12	12.07	0.299	51.93

Effect of H_2SO_4 concentrations on AAIBWS adsorption capacity: Fig. 2 shows the effect of H_2SO_4 concentrations on the adsorption capacity of AAIBWSs. 'P' adsorption on raw sludge was 2.36 mg/g that increased to 3.79 mg/g as the H_2SO_4 concentration increased to 1 mol/L, and then decreased to 0.63 mg/g dramatically with the rising H_2SO_4 concentration to 3 mol/L. The 'P' adsorption of AAIBWSs has same trend as their specific areas, indicating that the specific area is very crucial for 'P' adsorption on AAIBWS. AAIBWS treated with 1 mol/L H_2SO_4 (AAIBWS-1) solution was used to carry out the following experiments.

Effect of solution pH on 'P' adsorption: Fig. 3 shows the effect of solution pH on the 'P' adsorption on AAIBWS-1. In the pH range of 3-6, the 'P' adsorption was very stable and changed only from 7.15 mg/L to 7.26 mg/L, and decreased to 6.32 mg/L at pH 7, and further decreased to 6.02 mg/L at pH 10. The results indicated that the acid environment was favourable for 'P' adsorption.

Kinetic study: Fig. 4 shows the effect of reaction time on AAIBWS-1 at two initial '*P*' concentrations. Each curve contains both a fast and a slow adsorption stage. Both of the two fast stages lasted from the beginning of the experiment to the 15th min when AAIBWS-1 had more free active sites to make fast adsorption, whereas, the reaction slowed down due to less active sites and the competition between '*P*' in the solution and '*P*' on the AAIBWS-1 surface in the following slow stage.

Three kinetic models including pseudo-first-order, pseudo-second-order, and Elovich equations are adopted to fit the data as shown in Fig. 4. The models are shown as follows:

$$\log(q_e - q_t) = \log q_e - \frac{k_1}{2.303}t \quad \ldots(2)$$

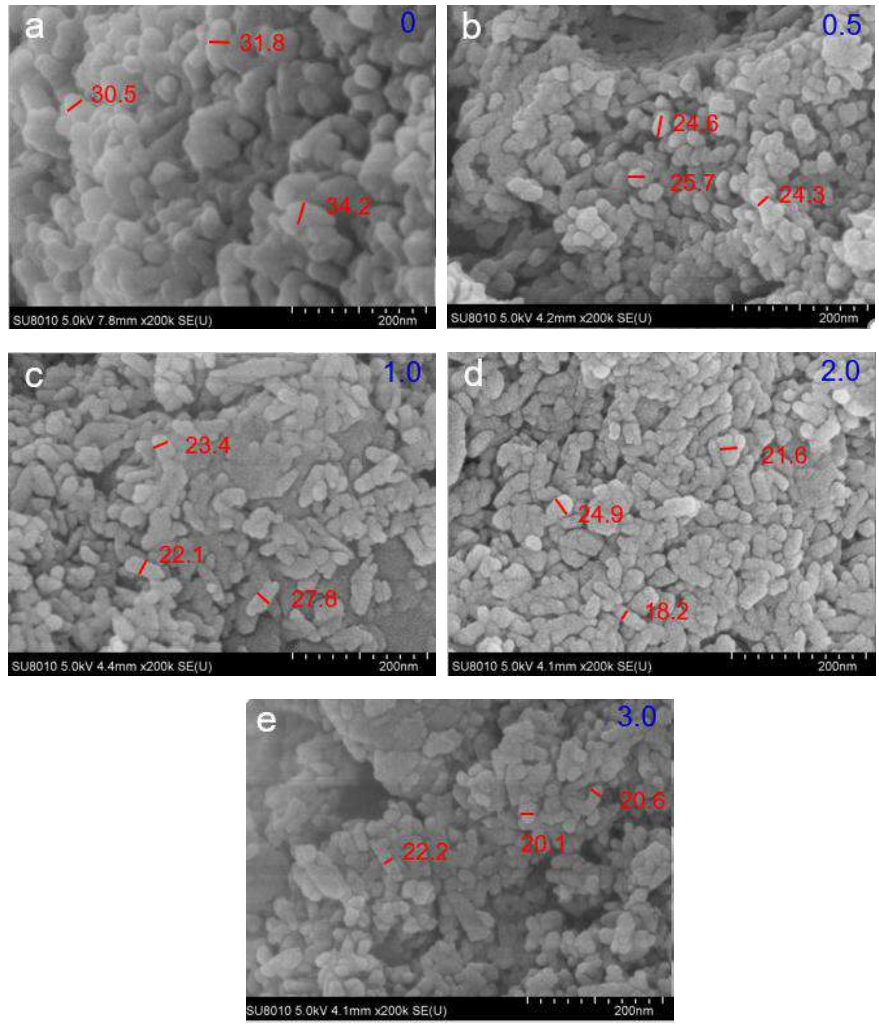

Fig.1: SEM images of AAIBWS treated with H_2SO_4 solution of different concentrations (a-0；b-0.5；c-1；d-2；e-3).

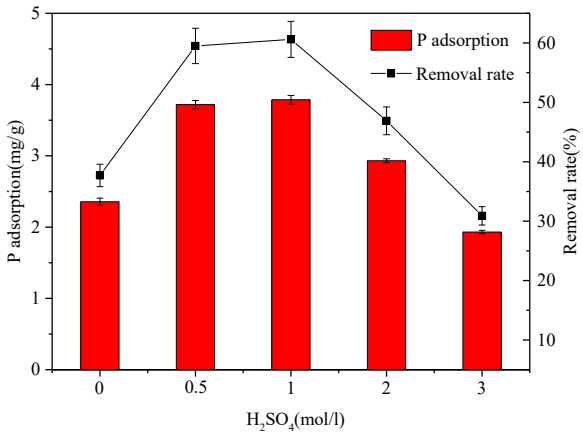

Fig. 2: Effect of H_2SO_4 concentrations on the P adsorption on AAIBWSs
（C_0 = 50mg/l, Time=220min,Temperarture = 30°C）

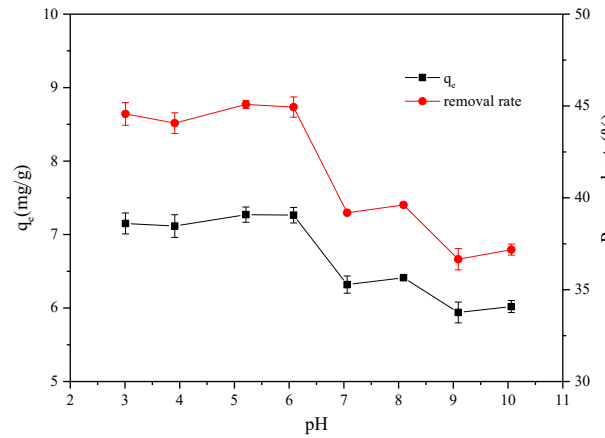

Fig. 3: Effect of solution pH on'*P*' adsorption *on* AAIBWS-1
(C_0 = 130mg/L, Time = 600min,Temperarture = 30°C)

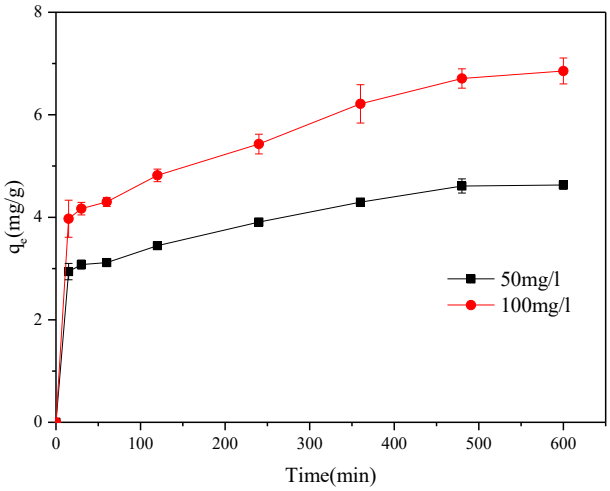

Fig. 4: Effect of reaction time on '*P*' Adsorption *on* AAIBWS-1 (Temperarture = 30°C, pH = 7).

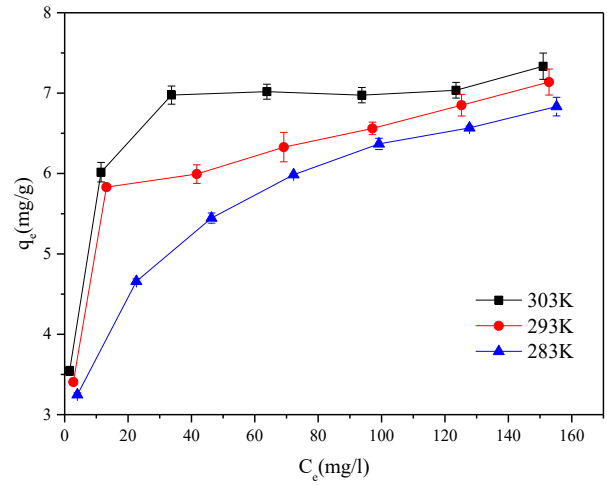

Fig. 5: Relationship between 'P' adsorption capacity and its equilibrium concentration at different temperatures (Time = 1440min, pH = 7).

$$\frac{t}{q_t} = \frac{t}{q_e} + \frac{1}{k_2 q_e^2} \quad \ldots(3)$$

$$q_t = \frac{1}{\beta}\ln(\alpha\beta) + \frac{1}{\beta}\ln t \quad \ldots(4)$$

Where q_t and q_e (mg/g) are the '*P*' adsorption at time *t* and at equilibrium respectively. Both k1 (min^{-1}) and k2 [g/(mg min)] are the equilibrium rate constants for pseudo-first-order and pseudo-second-order kinetic models, respectively. α [(mg/(g min)] is the initial adsorption rate and the constant associated with the fraction of surface coverage, and β (g/mg) is the activation energy for chemisorption, respectively.

As given in Table 2, the correlation coefficients of the pseudo-second-order equation are highest among the three equations, indicating the pseudo-second-order equation was best to describe the adsorption process.

Adsorption isotherms: Adsorption isotherm models are very important to understand the adsorption mechanisms. Hence, Langmuir and Freundlich models were used to fit the data shown in Fig. 5. The linearized forms of the two models are shown as the following equations, respectively:

$$\frac{c_e}{q_e} = \frac{1}{q_m b} + \frac{c_e}{q_m} \quad \ldots(5)$$

$$\log q_e = \log k_f + \frac{1}{n}\log c_e \quad \ldots(6)$$

Where c_e (mg/L) and q_e (mg/g) are the concentration and adsorption capacity at equilibrium, respectively. '*b*' (L/mg) is the Langmuir constant related to binding energy, and q_m (mg/g) is the maximum adsorption capacity. k_f is the Freundlich constant related to adsorption capacity, and '*n*' is adsorption intensity.

As given in Table 3, the correlation coefficients of the Langmuir equation at all three temperatures are higher than those of the Freundlich equation indicating that the Langmuir equation was better to describe the adsorption process and the nature of monolayer adsorption (Khan et al. 2020).

Thermodynamic studies: The obtained experimental data were analysed using the following three equations to calculate the thermodynamic parameters.

$$\Delta G^0 = \Delta H^0 - T\Delta S^0 \quad \ldots(7)$$

$$lnK = \frac{\Delta S^0}{R} - \frac{\Delta H^0}{RT} \quad \ldots(8)$$

$$K = \frac{q_e}{c_e} \quad \ldots(9)$$

Where K is the distribution coefficient (L/kg); $\Delta S°$ is the standard entropy change (kJ/mol·k); $\Delta H°$ is the standard enthalpy change (kJ/mol); *R* is the ideal gas constant

Table 2: The parameters of the three kinetic equations for 'P' adsorption on AAIBWS-1.

C_0 (mg/L)	Pseudo-first-order equation			Pseudo-second-order equation			Elovich equation		
	q_e	k_1	R^2	q_e	k_2	R^2	a	k_3	R^2
50	2.28	0.0058	0.9571	4.78	0.0070	0.9947	1.35	0.4945	0.9165
100	4.28	0.0066	0.9332	7.09	0.0037	0.9909	1.32	0.8204	0.9101

Table 3: The parameters of Langmuir and Freundlich isotherm for P adsorption on AAIBWS-1.

Reaction Temperature	Langmuir			Freundlich		
	q_m	b	R^2	k_f	n	R^2
10°C	7.14	0.09	0.9958	2.46	4.87	0.9985
20°C	7.19	0.17	0.9964	3.22	6.17	0.8815
30°C	7.30	0.42	0.9990	3.70	6.76	0.8735

Table 4: The thermodynamic parameters of 'P' adsorption on AAIBWS-1.

q_e	ΔH^0	ΔS^0	ΔG^0(kJ/mol)		
(mg/kg)	(kJ/mol)	(kJ/mol·k)	283K	293K	03K
2000	54.77	0.24	-14.38	-16.82	-19.27
4000	55.45	0.24	-13.22	-15.64	-18.07
6000	58.37	0.24	-10.83	-13.27	-15.72

(8.314 J mol/k); T is the reaction temperature (K); $\Delta G°$ is the standard Gibbs free energy change (kJ/mol).

As given in Table 4, the negative values of $\Delta G°$ at the three temperatures indicated the spontaneous nature of 'P' adsorption process, and the decreasing $\Delta G°$ values with the rising temperature suggested that higher temperature was favourable for the 'P' adsorption process. The positive $\Delta H°$ revealed the endothermic nature of the 'P' adsorption process, leading to better 'P' adsorption at the higher temperature.

CONCLUSION

Iron-based waterworks sludge was treated with 0.5-3mol/L H_2SO_4 acid solution to improve its 'P' adsorption capacity, and 1mol/L H_2SO_4 acid solution was proved to be best for the activation. Batch adsorption experiments were conducted to investigate the 'P' adsorption of AAIBWS-1. The results indicated that AAIBWS-1 had a larger 'P' adsorption capacity in the acid environment than in the alkaline environment. The pseudo-second-order equation was better than the pseudo-first-order equation and Elovich equation to describe the 'P' adsorption on AAIBWS-1. Langmuir isotherm was better than Freundlich isotherm to fit the experimental data, and the thermodynamic parameters indicated that 'P' adsorption on AAIBWS-1was spontaneous and endothermic.

ACKNOWLEDGEMENT

We gratefully thank the support for this project by the Science and Technology major project of Henan Province [Grant number 161100310700]

REFERENCES

Braun, J.C.A., Borba, C. E., Godinho, M., Perondic, D., Schontaga, J.M. and Wenzel, B.M. 2019. Phosphorus adsorption in Fe-loaded activated carbon: Two-site monolayer equilibrium model and phenomenological kinetic description. Chem. Eng. J., 361: 751-763.

Chang, H.M., Chen, Sh.S., Nguyen, N.C., Chang, W.S. and Ray, S.S. 2017. Osmosis membrane bioreactor-microfiltration with magnesium based draw solute for salinity reduction and phosphorus recovery. Inter. Biodeter. Biodegr., 124: 169-175.

Faisal, A. A.H., Al-Wakel, S. F.A., Assi, H. A., Naji, L. A. and Naushad, Mu. 2020. Waterworks sludge-filter sand permeable reactive barrier for removal of toxic lead ions from contaminated groundwater. J. Water Process Eng., 33: 101-112.

Fang, X.L., Wang, L., Poon, C.S., Baek, K., Daniel, C.W., Tsang, D.C.W. and Kwok, S. K. 2019. Transforming waterworks sludge into controlled low-strength material: Bench-scale optimization and field test validation. J. Environ. Manage., 232: 254-263.

Kang, S., Choi, J.H., Park, J.G. and Baek, K. 2019. Pellet adsorbent derived from molasses and dewatered alum sludge for arsenic removal. Journal of CO2 Utilization, 33: 31-36.

Khan, Z. H., Gao, M.L., Qiu, W.W., Islam, M. S. and Song, Z.G. 2020. Mechanisms for cadmium adsorption by magnetic biochar composites in an aqueous solution. Chemosphere, 246: 1-9.

Lian, J.J., Zhou, F.J., Chen, B., Yang, M., Wang, S.H., Liu, Z.L. and Niu, S.P. 2020. Enhanced adsorption of molybdenum (VI) onto drinking water treatment residues modified by thermal treatment and acid activation. J. Clean Prod., 244: 1-11.

Liu, H., Yang, Y.K., Sun, H.F., Zhao, L. and Liu. Y. 2018. Effect of tetracycline on microbial community structure associated with enhanced biological N&P removal in sequencing batch reactor. Bioresource Technol., 256: 414-420.

Pan, J.R., Huang, C. and Lin, S. 2004. Re-use of freshwater sludge in cement making. Water Sci. Technol., 9: 183-188.

Shrestha, S., Kulandaivelu, J., Sharma, K., Jiang, G.M. and Yuan, Z.G. 2020. Effects of dosing iron- and alum-containing waterworks sludge on sulfide and phosphate removal in a pilot sewer. Chem. Eng. J., 387: 1-13.

Wang, L., Zou, F.L., Fang, X.L., Tsang, D. C.W., Poon, C.S., Leng, Z. and Baek, K. 2018. A novel type of controlled low strength material derived from alum. Constr. Build. Mater., 165: 792-800.

Zhao, Y.Q., Doherty, L.P. and Doyle, D. 2011. Fate of water treatment residual: an entire profile of Ireland regarding beneficial reuse. Int. J. Environ. Stud., 68(2): 161-170.

Zhu, J.X., Zhang, P., Wang, Y.B., Wen, K., Su, X.l., Zhu, R.L., He, H.P. and Xie, Y.F. 2018. Effect of acid activation of palygorskite on their toluene adsorption behaviors. Appl. Clay Sci., 159: 60-67.

Nature Environment and Pollution Technology
An International Quarterly Scientific Journal

p-ISSN: 0972-6268
(Print copies up to 2016)
e-ISSN: 2395-3454

Vol. 20 | No. 2 | pp. 753-757 | 2021

Original Research Paper

https://doi.org/10.46488/NEPT.2021.v20i02.036

Open Access Journal

Research on the Interconnected River System Network of Three Lakes and One River in Guiyang

Zhang Dan*, Guo Zuo-qing, Yang Hui-xia***† and Liang Li******

*Civil Engineering College, Guizhou University, Guiyang 550025, China

**The Yangtze River Water Resources Committee of Yangtze River Project Supervision Consulting Co. Ltd. (Hubei), Wuhan 430014, China

***Civil Engineering College, Guizhou University, Guiyang 550025, China

****Guizhou Provincial Water Conservancy Research Institute, Guiyang, 550025, China

†Corresponding author: Yang Hui-xia; bt-yanghuixia@163.com

Nat. Env. & Poll. Tech.
Website: www.neptjournal.com

Received: 15-05-2020
Revised: 22-06-2020
Accepted: 16-07-2020

Key Words:
River system network
Karst
River
Lakes

ABSTRACT

The main geological landform in southwest China is karst, and hydrological resources in the region are rich. The water resources in this region cannot be efficiently and rationally used due to the complex topography and difficulty in developing water resources, which has led to problems such as desertification and soil erosion. The most typical area of karst landforms is in Guizhou Province. A water management method for an interconnected river system network is proposed, taking Guiyang as an example. This study provides a foundation for China's South-to-North Water Diversion Project and can improve socioeconomic conditions in China.

INTRODUCTION

Currently, human activities are becoming increasingly intense. With the rapid development of science and the economy, our living standards have significantly improved. However, we have encountered problems related to sustainable development. The territory of China covers 9.6 million square kilometres, which has many advantages and encompasses large quantities of land and natural resources. However, these resources are not evenly distributed in space. For example, the water resources in southeast China account for 46% of the national water resources and 84% of the water resources in the entire western part of the country. Hydropower resources could account for 75.6% of the resources in western regions (Zhang et al. 2004), but the utilization rate is 6%. The problems in the southwest region are related to the ruggedness, vulnerability of the ecological system, low environmental capacity and inability to withstand natural disasters, which have led to difficulty in the development of water resources in karst areas.

An interconnected river system network (IRSN) is an important part of the land -water system, and it has been considered in national water resource management. From the perspective of biodiversity, the connected rivers have more species than the disconnected rivers (Jiang et al. 2020), Moreover, it is important for the river with good connectivity in hydrodynamics (Phillips et al. 2011). In hydraulic, storage thresholds at a range of scales have now been recognized as important, connectivity has become an important concept crucial to understanding how water is transferred through a catchment (Spence 2010), IRSNs provide a solution for repairing and adjusting existing water system patterns by connecting the hydraulic relationships among adjacent reservoirs and mitigating the uneven geographical distribution of water (Li et al. 2011a). This can also provide a solution for rivers about increasing the utilization rate and securing sustainable ability (Xu et al. 2011). Wu et al. (2007) proposed IRSNs could be used as the indexes of river health. Therefore, IRSNs are of great significance to the redistribution of water resources in karst areas.

GLOBAL RESEARCH STATUS OF IRSNS

Most of the IRSN projects connect the disconnected water with some new hydraulic works. There are various IRSN projects in some western countries, such as Nile irrigation project in ancient Egypt, Central Valley Project in the United States and Garrison Water Diversion Project in the United States (Cui et al. 2011). Many scholars have researched on connected river network; Vannote et al. (1979) put forward the river continuum concept, and the implications of the con-

cept in the areas of structure, function, and stability of riverine ecosystems are discussed. Amoros et al. (1988) proposed the interactions between water bodies within the floodplains of large rivers. Ward et al. (1989) proposed the four-dimensional framework in natural lotic ecosystems. Pringle (2001, 2003) had further research, which is the understanding of how the river networks are affected by hydrologic alterations that originate outside of their boundaries. He originally proposed that the calculation of river is at a regional scale or a global scale. In China, the research on IRSNs is relatively recent, and IRSN projects in many areas are in the initial stage. IRSN projects can not only improve the uneven distribution of water resources but also improve the ecological environment and promote socioeconomic benefits. Therefore, many scholars have performed studies on this topic. At the beginning of the 21st century, some scholars began to pay attention to assessing river health. Dong (2005) conducted physical-chemical and biological habitat quality assessments. According to the relevant evaluation criteria for river health, Zhang et al. (2010) analysed the influence of water system connectivity on the Yangtze River in 2010 with three criteria and concluded that water system connectivity has an obvious optimization effect on the ecological environment. Li et al. (2011b), who started from conceptual analysis and proposed a corresponding classification system, performed an in-depth study of a connected water system of rivers and lakes. Later, some Chinese scholars discussed and studied IRSNs in specific cities. For example, Zheng (2017) proposed the IRSN for Shenyang, which involved one district, three corridors, five channels and 20 wetlands. Wang (2017) is planning an IRSN in Taiyuan that includes one lake, nine rivers, dual water diversion sources, and four river and lake connectors.

CHINESE IRSN PROJECTS

As a new approach to solving urban water resource problems, IRSN projects in China have been implemented in most cities. Many cities have started to create IRSN projects to address existing water resource problems. The IRSN projects in some cities are summarized in Table 1.

The IRSN project mechanisms are not yet fully understood and must be assessed from practice, so further studies of IRSNs are necessary; moreover, such projects still have many problems to be solved. Still, IRSN projects have relatively great prospects for development.

WATER DISTRIBUTION AND THE PROBLEMS IN GUIYANG

Guiyang's location is in the central part of Guizhou Province and east of the Yunnan-Guizhou Plateau; the terrain in this area is high in the southwest and low in the northeast, and

Table 1: Some domestic IRSN projects.

Project Site	IRSN Project Name	Project Status
Chongqing	Bibei River to Binan River	Plan to use in 2020
Changsha	Dazhongyuan River	Plan to use in 2020
Xining	Xigan Channel, Guosi Channel, and Jiefang Channel	Finished 60% at the beginning of 2019
Huanggang	Changhe River	Started in 2019
Jiujiang	Bali Lake, Saicheng Lake	Started in 2019
Dazhou	Xi Bridge to Mingyue Bridge	Started in 2017
Mudanjiang	Main river in the city	Started in 2016

there is a main mountainous and hilly landscape (Wang et al. 2015). The mountain area totals 4218 square kilometres, level areas encompass only 912 square kilometres, and canyon areas account for 1.2% of Guiyang. The average annual rainfall in the area is 1129.5 mm, and this rainfall feeds the Wujiang River in the Yangtze Basin and the Hongshui River in the Zhujiang Basin, of which the former is larger. The water flow in Guiyang is very complicated, and the water resources are mainly from rain. According to statistics, there are approximately 98 rivers in Guiyang, including 90 rivers in the Yangtze Basin and 8 rivers in the Zhujiang Basin. Additionally, Hongfeng Lake, Baihua Lake, Aha Lake and Huaxi Reservoir are the main surface waters. According to the Water Resources Bulletin in Guiyang, the water resource volume is less than that in other cities, and the frequency of dry years is high, so the water resource reserves require specific attention. Besides, the proportion of surface water resources accounts for one-third of the total, as given in Table 2.

Problems with Water Resources in Guiyang

Guiyang has a large number of water resources, but these resources are difficult to effectively utilize. Therefore, Guiyang has the same water problems as many large and medium-sized cities, and the specific water shortage problems are as follows:

Table 2: Water resources over the years in Guiyang.

Year	Total Water Resources ($10^{12}m^3$)	Groundwater Resources ($10^{12}m^3$)	Proportion (%)	Level of Runoff
2013	33.58	11.97	35.6	Dry stage
2014	58.09	14.4	24.8	Abundant stage
2015	48.28	13.58	28.1	Normal stage
2016	32.55	9.96	30.6	Dry stage
2017	52.65	13.78	26.2	Abundant stage

1. General water shortage - the annual rainfall is limited from November to March in the subsequent year, and there are no major floods even during the flood season in summer.
2. Engineering water shortage - the site is located near the sources of many rivers near, but also the centre of the karst belt. The karst landform is permeable and has a large altitude gradient. As a result, it is difficult to build hydraulic structures in the area, and most precipitation runs off.
3. Ecological water shortage - as in many cities, agriculture and industry are developing rapidly in Guiyang. However, the drainage of industrial water is not properly regulated, which has led to pollution and the destruction of water sources in the city.
4. Geological water shortage - there is the typical karst landform in Guiyang, so the ecological environment is vulnerable. In addition, mountains divide the water system, which makes the hydrological connectivity poor. Moreover, the strong permeability enriches groundwater resources, reduces the amount of surface water and decrease the total volume of usable water resources.

Main Solutions

Resource water shortage: Due to the lack of precipitation and accessible water, water consumption should be controlled to ensure that sufficient water is available. Urban water resources mainly come from rainfall and rivers. However, the precipitation varies based on the geographical location and climatic environment, and water mainly comes from rainfall; thus, urban rainfall is very difficult to collect and use, and water must be reasonably conserved.

1. Urban water: Residents' awareness regarding water saving must be enhanced. Earth's resources are not inexhaustible, and we must rationally use resources to obtain long-term benefit. The public must be informed about the importance of water savings and the effects of water issues on everyday life.
2. Industrial water: We must emphasize using water reasonably and standardizing wastewater treatment. Industrial water is more treatable than urban water, so the potential effect of saving industrial water is greater. Moreover, industrial wastewater can be recycled. We should reuse water as much as possible to alleviate the problem of insufficient resources.

Engineering water shortage: Because the construction of large-scale hydraulic engineering projects generally requires considerable land resources, there are no large hydro-junctions in the city. The large and medium-sized reservoirs in Guiyang are listed as follows (large and medium-sized reservoirs have a capacity of 10 million cubic meters to 1 billion cubic meters): Aha Lake, Hongfeng Lake, Huaxi Reservoir, Baihua Lake. The details are as in Table 3.

Thus, the large and medium-sized reservoirs are mainly concentrated in the west and south of the city, and there are relatively few water-retaining structures in the eastern area, so the water transport is from the west to the middle and eastern parts of the city. According to the water system conditions, an appropriate water-retaining structure should be built in the eastern part of the city to supply water in multiple directions, thus creating a balanced conveyance network.

Ecological water shortage: For this problem, the level of industrial wastewater generation should be standardized. Heavy polluters, such as Guigang industry, moved out of the city in 2013, but the manufacturing processes resulted in inevitable pollution. In addition, the discharge of polluted wastewater was common. In 2017, Zhongtieyueshan Lake was polluted by construction wastewater from Wanda and resulted in fish death on a large scale. Because of vigorous urban development, many industries have ignored the problem of sewage discharge. Therefore, promoting the management of wastewater and the relevant laws and regulations could curb water source pollution by sewage in a timely manner.

Geological water shortage: Guiyang is a typical region with many karst phenomena. In karst areas, the soil permeability is high, and the groundwater volume is large; this volume mainly comes from surface water seepage and atmospheric precipitation. From a geomorphological perspective, the karst geomorphology accounts for 83% of the whole city.

1. We can increase groundwater use to reduce the consumption of surface water.
2. For facilities that need to collect water, such as artificial lakes in urban areas, to supply water for residents and other domestic water uses, artificial impervious membranes can be adopted; such measures can greatly improve the utilization rate of surface water resources and reduce underground seepage in karst areas.

Table 3: Three lakes and one river in Guiyang.

Reservoir name	Capacity (10^4m^3)	Basin area (km^2)	Location (Relative to the Downtown Area)
Aha Lake	8658	190	Southwestern
Huaxi Reservoir	3140	325	South
Hongfeng Lake	60000	1551	Western
Baihua Lake	19100	1831	Northwestern

PROPOSAL OF AN IRSN PROJECT IN GUIYANG

Karst is a special landform that is mainly composed of carbonate rocks; the soil is slightly alkaline, and carbonate minerals are highly soluble, so they are not easily weathered. As a result, the soil layer in karst areas is thin and is characterised by poor water storage. With barren land and severe calcification, only some plants, such as alkaline plants, can survive in karst areas (Yang 1990). A causality diagram of karst ecosystem sensitivity is provided in Fig. 1. Establishing a reasonable and effective IRSN project can improve the soil ecological environment. The aim of governing the current channels and building a new channel is to strengthen the water area connectivity and improve water quality.

Developing the IRSN Project

The thin soil layer: Areas with good soil quality can provide sufficient nutrients for vegetation growth and reduce soil and water loss during torrential rainfall events. According to the soil properties in karst areas, the thickness of the weathered soil layer is inversely proportional to the erosion rate of the weathered rock. For the farmland in Guiyang, high nutrient levels are needed to support the growth of the crops, so fertilizer in the soil, such as green manure, is needed to increase the mineral content. Besides, ecological slope protection measures should be implemented to reduce landslides, which can also promote the restoration of the ecological system, create good river ecosystems, and improve the ecological environment in the city.

Weak resistance to disaster: There are abundant groundwater resources in Guiyang, and the water storage capability of the soil is poor; thus, it is necessary to enhance the connection between surface water and groundwater. Surface pollutants will seep into the groundwater due to the high permeability of the karst, leading to groundwater pollution, low oxygen concentrations, scarce microorganisms and a poor self-purification capacity. Therefore, we can appropriately increase the number of sewage treatment plants and improve urban wastewater discharge management. For example, the regulation project of the Nanming River in Guiyang is a typical water decontamination project. In addition, it is important to improve water quality by testing the upstream water quality in Hongfeng Lake and Baihua Lake; only when we do this can we mitigate the pollution at the source to improve the water quality in the city and create a healthy and liveable ecological environment.

Based on the ArcGIS, Fig. 2 shows the general distribution of the water system and the variations in the terrain elevation in Guiyang (this paper mainly discusses the area circled in red). The main waters are Hongfeng Lake, Baihua Lake, Aha Lake and Huaxi Reservoir. The four lakes supply seven residential areas (Yunyan district, Nanming district, Wudang district, Guanshanhu district, Baiyun district, Huaxi district and Qingzhen). The reason for the high water conveyance pressure is the long distance between the centralized and regional water conveyance channels. With reference to channel in California, United States, we can build a channel that transports water from the northwestern to southeastern parts of the city and provides water to water-deficient areas such as Wudang district and densely populated areas of Nanming and Yunyan districts. Otherwise, the natural landform leads to abundant resources in the west but limited in the east, we could develop an underground water storage location in the west to mitigate water shortage issues in the dry season.

CONCLUSION

In China, Guiyang is a typical city with regional karst landforms; the area is characterised by abundant hydropower resources and low usage rates. The hydrology in karst

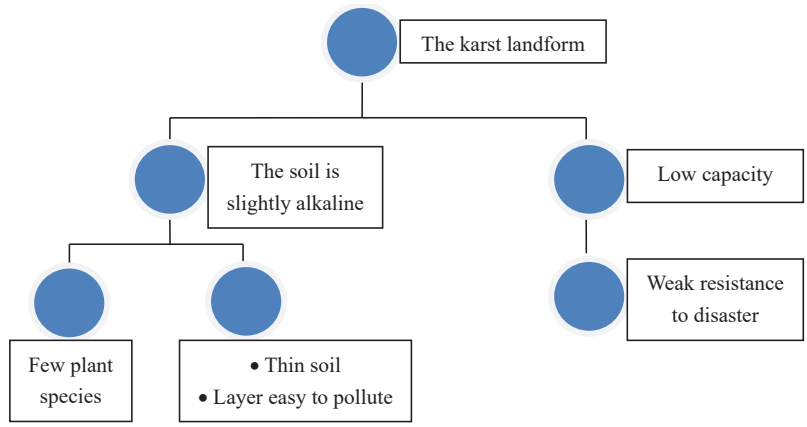

Fig. 1: A causality diagram of karst ecosystem sensitivity.

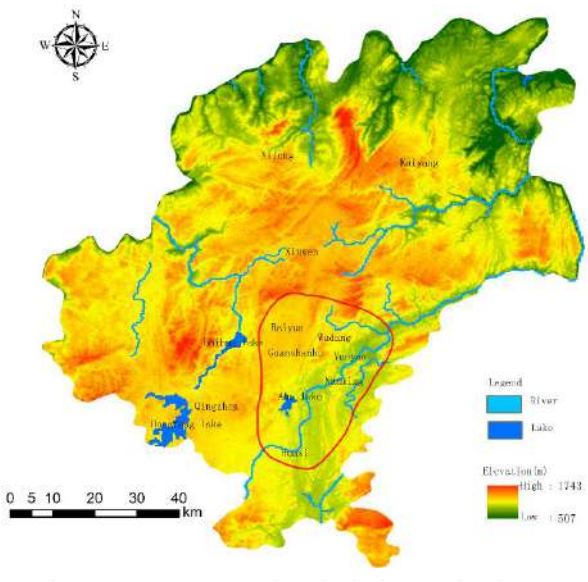

Fig. 2: Water system and geological map of Guiyang.

areas can lead to water conservancy issues. This paper first addresses the basic reasons for the lack of available water resources in the city.

1. Engineering water shortages
2. General water shortages
3. Ecological water shortages
4. Geological water shortage

Based on an IRSN project, this paper proposes a method to solve the water resources issues in Guiyang. If the water resource problem in karst areas can be effectively solved, the utilization rate of water resources in Southwest China can be greatly improved, which can contribute to a national water resource balance and generate great social benefits.

ACKNOWLEDGEMENT

The article is supported by: (1) Young Talents Project of Guizhou Provincial Department of Education [Grant No.KY (2017) 120] and (2) The Special Foundation of the Water Conservancy Bureau of Guizhou Province (Grant No. KT201712)

REFERENCES

Amoros, C. and Roux, A.L. 1988. Interactions between water bodies within floodplains of large rivers: function and development of connectivity. Muensterische eographische Arbeit, Muenster, 1988: 125-130.

Cui, G.T., Zuo, Q.T. and Dou, M. 2011. Development evolution and influences of the interconnected river system network at home and abroad. South-to-North Water Diversion and Water Science & Technology, 9(4): 73-76.

Dong, Z.R. 2005. Principles and methods of river health assessment, China Water Resources, 10: 17-19.

Jiang, X.M., Pan, B.Z., Sun, Z.W., Cao, L. and Lu, Y. 2020. Application of taxonomic distinctness indices of fish assemblages for assessing effects of river-lake disconnection and eutrophication in floodplain lakes. Ecol. Indic., 110: 105955.

Li, Z.L., Li, Y.Y., Wang, Z.G., Hao, X.P. and Liu, X.J. 2011a. Research on interconnected river system network: Conceptual framework. Journal of Natural Resources. 26(03): 513-522.

Li, Z.L., Hao, X.P., Wang, Z.G., Liu, X.J. and Li, H. 2011b. Exploration on classification of interconnected river system network. Journal of Natural Resources, 26(11): 1975-1982.

Phillips, R.W., Spence, C. and Pomeroy, J.W. 2011. Connectivity and run off dynamics in heterogeneous basins. Hydrological Processes, 25: 3061-3075.

Pringle, C.M. 2001. Hydrologic connectivity and the management of biological reserves: A global perspective. Ecological Applications, 11: 981-998.

Pringle, C.M. 2003. What is hydrologic connectivity and why is it ecologically important. Hydrological Progresses, 17(13): 2685-2689.

Spence, C. 2010. A paradigm shift in hydrology: Storage thresholds across scales influence catchment runoff generation. Geography Compass, 4/7: 819-833.

Vannote, R.L., Minshall, G.W., Cummins, K.W., Sedell, J.R. and Cushing, C.E. 1980. The river continuum concept. Canadian Journal of Fisheries and Aquatic Sciences, 1980: 130-136.

Wang, J.J. 2017. Research on urban design for quality improvement in the new era. Shanxi Architecture, 43(36): 18-20.

Wang, S.J., Zhang, X.B. and Bai, X.Y. 2015. An outline of karst geomorphology zoning in the karst areas of southern China, Mountain Research, 33(06): 641-648.

Ward, J.V. 1989. The four-dimensional nature of lotic ecosystems. Society for Freshwater Science Stable, 8(1): 2-8.

Wu, D.X. and Huang, S.P. 2007. Study on the index system of healthy Yangtze River, Express Water Resources & Hydropower Information, 28(12): 1-3.

Xu, Z.X. and Pang, B. 2011. Cognition scientifically of river and lake systems interconnection. China Water Resources, 16: 13-16.

Yang, M.D. 1990. On the fragile of karst environment. Yunnan Geographic Environment Research, 2(01): 21-29.

Zhang, L.Q. and Chen, Y. 2004. The Management of water resources in southwestern region of China. Resource Development & Market, 6: 421-423.

Zhang, O.Y., Pu, H.F., Wang, C.P. and Xiong, M. 2010. Impact of drainage connectivity on river health in Yangtze River Basin. Yangtze River, 41(2): 1-5+17.

Zheng, H. 2017. Planning of river-lake network project in Shenyang City. China Water Resources, 11: 52-53+13.

Nature Environment and Pollution Technology
An International Quarterly Scientific Journal

p-ISSN: 0972-6268
(Print copies up to 2016)
e-ISSN: 2395-3454

Vol. 20 | No. 2 | pp. 759-769 | 2021

Original Research Paper

https://doi.org/10.46488/NEPT.2021.v20i02.037

Open Access Journal

Contagious Progression and Distribution of Arsenic in India: A Key Towards Bioremediation

Ankur Bhardwaj*†, Rakesh Kumar Sharma* and Gajendra Bahadur Singh**

*Department of Biotechnology & Life Sciences, Institute of Biomedical Education & Research, Mangalayatan University, Beswan, Aligarh-202145, Uttar Pradesh, India

**University Institute of Biotechnology, Chandigarh University, National Highway 95, Mohali, Chandigarh-140413 Punjab, India

†Corresponding author: Ankur Bhardwaj; ankurphd995@gmail.com

Nat. Env. & Poll. Tech.
Website: www.neptjournal.com

Received: 20-05-2020
Revised: 18-06-2020
Accepted: 25-07-2020

Key Words:
Bioremediation
Arsenic
ars operon
Arsenate reductase
Arsenite oxidase
Mining

ABSTRACT

Arsenic (As) is a renowned threat to the environment and human well-being. Its concentration is increasing year after year in several countries. The utmost pretentious are mining regions of India, as per government surveys and available research findings. Population residing near mining regions are bounded to consume arsenic tainted water in their routine life and evolve various hazardous health problems. Besides many physicochemical techniques at hand for its purification, none are promising. The microbial mediated arsenic detoxification involving oxidation/reduction and extrusion by a membrane-associated efflux pump may perhaps financially acuity and a promising method for bioremediation. The arsenic richness in mining regions triggered the evolution of bacterial cells to come up with a potential mechanism to survive in As rich environment. Microbial extrusion strategy of As in both As^{3+} and As^{5+} forms may also be involved in increasing As in abandoned mining regions in underground water. So, to understand the involvement of these bacterial cells in the increment of As in these regions the present study was performed by personally visiting these sites and conversation with local residents. We have witnessed many jaw-dropping truths about As exposure risk to humans and domesticated animals, which has been discussed in this article. This review comprehensively summarizes current studies associated with arsenic exposure, environmental dispersal and its bioremediation through arsenic metabolizing bacteria covering recent developments, pathways, action mechanism and understanding arsenic metabolizers with the depiction of future prospects on arsenic bioremediation from contaminated systems.

INTRODUCTION

Life standards have been increased in today's world with the realization of environmental threats and issues. Heavy metals besides PAHs (polycyclic aromatic hydrocarbons) are chronic contaminants broadly distributed in the surroundings, therefore simple remediation methods are privileged over high-priced physicochemical strategies (Singh et al. 2011).

Heavy metals persist in nature for a long time as they cannot be degraded by decomposers rather gets accumulated. Usually, arsenic remains along with minerals, like sulphur and iron. On average, its abundance in earth crust is 1-2 mg/Kg having two forms As^{3+} (arsenite) that is a pretty toxic form than As^{5+} (arsenate) (Meliker et al. 2008). Arsenic (As) tainting in groundwater is a prominent issue among mining regions and utilization of deep tube-wells for water supply, causing arsenic poisoning. Volcanic eruptions, weathering, and anthropogenic sources are accountable for arsenic release in groundwater including smelting, mining, etc. (Bhattacharya et al. 2007). Arsenic discharge from coal ventures likewise represents across the board pollution of soil and groundwater (Dontala et al. 2015).

According to the consolidated hazardous chemicals list of the Environmental Protection Agency (EPA) of 2001, the United States, exposure to arsenic causes acute and adverse health issues. In 2001, EPA declared arsenic limits for drinking water (10 µg/L) which is being employed till today. Arsenic pollution extent and its potential danger to human wellbeing have brought about extensive enthusiasm for concentrate microbial species in-charge of the diminishment of arsenic (Mirza et al. 2017). Drinking water mining from shallow tube-wells is among vital pathways for its entrance into human bodies (Chakraborti et al. 2017b). Human contact to arsenic predominantly occurs by utilizing groundwater (cooking or crop irrigation) which have increased inorganic arsenic levels (WHO) in humans as well as plant body. Various geological and other factors were acknowledged enhancing arsenic mobilization, affecting many regions in India (Philp 2015). Arsenic translocation and bio-magnification have also impacted numerous important crops (Chakraborty et al. 2014).

The As-toxicity relies on its biochemical nature and uses phosphate transporters for entering into a bacterial cell (Nordstrom 2002). Aquaporin mediated As entrance in the cell, blocks the function of many proteins by altering their functional groups. It also affects respiration by binding to PDh (pyruvate dehydrogenase), 2-oxoglutarate dehydrogenase and other enzymes leading to DNA damage by inhibiting its repairing mechanism (Bhattacharjee et al. 2005). Oxidative phosphorylation is caused by As due to hindrance created by it in enzymatic activity (Jomova et al. 2011). Like-wise As^{5+} structural similarity to phosphate is responsible for its access to active cells, interrupting oxidative phosphorylation (Kumari & Jagadevan 2016). The ingestion of large doses of arsenic causes fatal health problems (Fig. 1) and prolonged contact produces lesions in skin (Mazumder 2015). Arsenic carcinogenicity is already well known however, its lung cancer mechanism has not well been understood (Wei et al. 2019). Metals serve vital roles (in small quantities) in living beings, serving essential catalytic roles (Ryan et al. 2005). Microorganisms can metabolize metals through various methods (Silver & Phung 2005). Diverse detoxification strategies were developed by bacteria to encounter arsenic toxicity and among them, one is transforming it to a less lethal form (Turner 2001). Among reduced arsenic species, arsenite is more portable and dangerous while arsenate is less toxic in comparison (Edwards et al. 2000).

National rural drinking water (NRDW) programme has been adapted by State governments for providing clean water to affected habitations (Tomar 2017). An objective of making accessible safe and hygienic drinking water by 2021, is set by the Government of India (GOI) for 28,000 habitations extremely pretentious with arsenic contamination (Dey 2017). Due to increasing health issues, the Ministry of Drinking Water and Sanitation (MDWS) has launched 'National Water Quality Sub-Mission' for the habitants of affected regions (Chakraborti et al. 2017a). The MDWS has also commissioned around 35 developmental projects for water quality improvement in rural and urban areas (Omar et al. 2017).

According to a recent report demonstrated in Rajya-Sabha (Feb. 2017) from MDWS, various schemes have been executed equipping clean water in pretentious areas of the country. Expanding the reliability of numerous nations on groundwater has increased the focus on safe remediation strategies (Kadushkin et al. 2004). Arsenic expulsion technique in influenced regions could be the only option for a healthy water supply. The arsenic alleviation approach has to be implemented according to specific geographical and socio-economic characteristics of the area.

GLOBAL ARSENIC EPIDEMIOLOGY

Arsenic is affecting a major World population with several

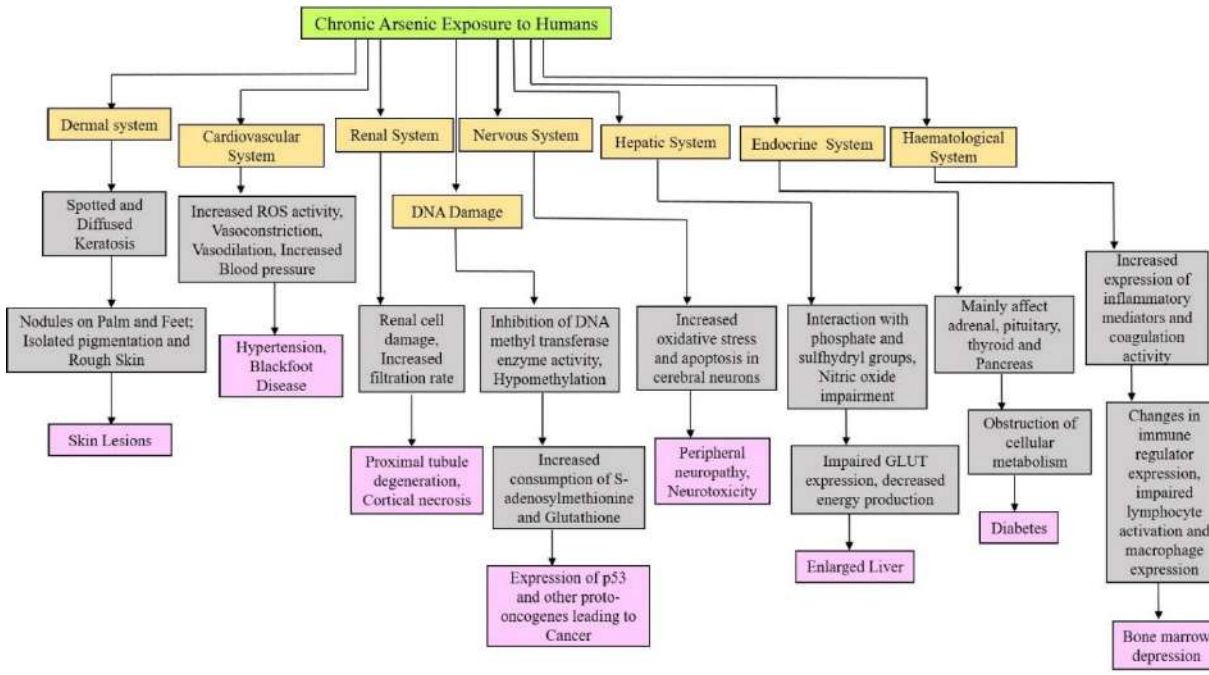

Fig. 1: Arsenic exposure and human health effects.

impacts and has now become a foremost environmental concern (Chikkanna et al. 2019). Detecting arsenic for a normal person is nearly impossible due to the absence of flavour, colour and aroma. People relying on groundwater having eminent arsenic level are vulnerable to its toxicity risk. Abandoned mines cause arsenic arrival in groundwater leading to an increase in its concentration (Hajalilou et al. 2011). Nowadays research on arsenic accumulation is going on to understand its speciation.

The application of arsenic-rich water for irrigation is a key factor responsible for high soil arsenic accumulation. Soil samples were investigated by Sandhi and co-workers during the ripening stage of rice from different paddy fields and arsenic aggregation was observed to be higher (90 to 210 µg/kg) in dehusked grains than in husked grains (Sandhi et al. 2017). Certain ecological advancements contain abnormal arsenic amounts that reach wells and various public water deliveries through leaching (McArthur 2019). Quantitative investigations of groundwater samples of Mongolian regions indicate that arsenic species are vastly associated with Fe species controlled by geographical and redox factors (Jiang et al. 2015). Arsenite was detected in rice samples from Korea with concentrations of 28.51 and 51.91 µg/kg (Kwon et al. 2017).

In Chile, the capital of Santiago, millions of tube wells were found containing arsenic (>50 µg/L) and 7600 people are affected (Quinodóz et al. 2019). Various nations specifically, India, Bangladesh and Vietnam are at great risk, where the one-third population is drinking arsenic-polluted water (WHO 2010). Around 57 million individuals are devouring arsenic-contaminated water above recommended limits in India and many other countries (Table 1) (Jha et al. 2017).

EPIDEMIC ARSENIC CONSEQUENCE IN INDIA

In India, groundwater contamination is severely problematic due to futile purification systems and intermittent floods and monsoon (Kadushkin et al. 2004). Mining, industrialization, ore processing has deleteriously impacted the environment through ecosystem alterations, biodiversity damage and accumulation of toxic pollutants (Singh & Singh 2016). These activities produce enormous hazardous wastes, left without treatment. Abandoned mines contaminate groundwater by redox events and anaerobic conditions,

Table 1: Worldwide distribution of arsenic (Santra et al. 2013, Herath et al. 2016).

S.No.	Country	Region	Groundwater Arsenic level (µg/L)	Permissible limit (µg/L)
1	Afghanistan	Ghazni	10-500	10 (WHO)
2	Australia	Victoria (around the gold-mining regions)	1-12 (Groundwater); 1-73 (Drinking-water); 1-220 (Surface water)	NIL
3	Bangladesh	Noakhali	<1-4730	50 (WHO)
4	Brazil	Minas Gerais (Southeastern Brazil)	0.4-350 (Surface water)	10 (WHO)
5	Cambodia	Prey Veng and Kandal-Mekong delta	Up to 900 1-1610	10 (WHO)
6	Canada	Nova Scotia (Halifax County)	1.5-738.8	10 (WHO)
7	China	-	50-4440	50 (WHO)
8	Finland	Southwest Finland	17-980	10 (WHO)
9	Greece	Fairbanks (mine tailings)	Up to 10,000	10 (WHO)
10	India	West Bengal Uttar Pradesh	10-3200	50 (WHO)
11	Japan	Fukuoka Prefecture (southern region)	1-293	10 (WHO)
12	Mexico	Lagunera	8-620	25
13	Nepal	Rupandehi	Up to 2620	50
14	Pakistan	Muzaffargarh (southwestern Punjab)	Up to 906	50
15	Taiwan	-	10-1820	10 (WHO)
16	Thailand	Ron Phibun	1->5000	10 (WHO)
17	USA	Tulare Lake Red River Delta	Up to 2600	10 (USEPA)
18	Vietnam	(Northern Vietnam) Mekong Delta (Southern Vietnam)	<1-3050	10 (WHO)

accumulating particulates in groundwater sources, hence, contaminated water treatment is considerably essential before consumption (Ayangbenro & Babalola 2017). It has been reported that even after abandoning the mining activity, the concentration of As increases, which may be due to the microbial transforming system (Zhang et al. 2019). It adversely affects the flora and fauna of mining regions.

With the aim of providing safe drinking water, a number of wells were developed earlier (advocated by UNICEF and World Bank) resulted in decreased newborn mortality and diarrheal disease by 50%. But as per investigation, approximately one among five wells are now arsenic tainted above EPA standard (Chakraborti et al. 2008). Nine hundred villages were found to have arsenic above the standard limit, where groundwater is mostly extracted by deep tube-wells having higher 'As' sediments (Shah 2010).

WHO has reported many regions of West-Bengal and other states, consuming high arsenic-contaminated drinking water (Ahamed et al. 2006). Government programs to provide 'safe' drinking-water, controlled arsenicosis, but in a few areas problem is still the same. The districts situated nearby Ganga and Gandaki river were scrutinized and found that the arsenic affected far above WHO defined limit (10 µg/L) (Shah 2010). In 2016, the Mahavir Cancer Institute, Bihar analysed 23,000 new malignancy patients, and these cases were due to arsenic poisonous quality (Chakraborti et al. 2017b). A number of other states like, Jharkhand, Madhya Pradesh, Chhattisgarh and Assam are facing arsenic tainted water issues. Sahibganj district of Jharkhand situated in the middle Ganges plain has arsenic >50 µg/L (Ramanathan et al. 2006). People residing in those areas have no alternative and are continuing with the same exposed risk (Chakraborti et al. 2003). Arsenic disasters are happening today and most outstandingly due to drinking water contamination. More than 40 million individuals in India, are exposed to 50 µg/L or above arsenic. The scenario is equally bad in some districts of Bihar, West Bengal and Uttar Pradesh (Milton et al. 2001). Chhattisgarh state was parted from Madhya Pradesh (year 2000). Border regions of MP and Chattisgarh district are mostly affected by arsenic contamination. In 1999 Rajnandangaon district of Madhya Pradesh was reported to have high groundwater arsenic concentration and above a million of the population of Rajnandangaon is consuming arsenic polluted water (Patel et al. 2017). Some dug-wells, along with hand tube-wells, are contaminated with higher (520 µg/L) arsenic concentration in West Bengal and Rajnandgaon (Saha & Ray 2019).

The As^{3+} concentration in groundwater of Barasat (Gangetic plain), West Bengal was found excessive than As^{5+} (10 to 538 µg/L), showing reducing conditions (Kar et al. 2010). The reduction activity of iron/sulphur oxides was a foremost mechanism for arsenic release into groundwater (Sichone 2019). Several states were also discovered as influenced with maximum arsenic level (3,700 µg/L) (Tchounwou et al. 2019).

Groundwater arsenic release mechanism was investigated in Balia district, U.P and 468 µg/L concentration was found at depths of 30-33 m (Chauhan et al. 2009). Groundwater arsenic concentration of Sahibganj district, Jharkhand was highest in post-monsoon (133 µg/L) compared to monsoon (98 µg/L) and pre-monsoon (115 µg/L) (Alam et al. 2016). The water standard of the Dhanbad area, Jharkhand was not up to the mark (Masto et al. 2011). Hydro-geochemical processes and isotropic rock tracing of aquifers were studied in the East-Singhbhum area of Jharkhand. Temporal and seasonal differences affect groundwater quality significantly (shallow aquifers) due to disparity in flow, recharge, geochemical processes. Groundwater arsenic concentration of Bishnupur locality, Manipur was found highest in post-monsoon and increase is anticipated in nearby future (Chakraborti et al. 2018).

Many people of West-Bengal are affected by arsenic exposure, as per the latest report presented in Lok-Sabha. Although State governments are determined to manage the arsenic peril, still more is left to finish (Gupta & Singh 2019). Since the skill for arsenic elimination from water is novel and expensive, there is a progress lag in setting water management plants (Shan et al. 2019). Comprehensive detail on groundwater, Kolkata Municipal Corporation (KMC) stated a higher arsenic level (>50 µg/L) (Chakraborti et al. 2017a). A proceeding of Lok Sabha, 2017 by MDWS, says that states like Himachal Pradesh, Punjab, Haryana, Assam, Arunachal Pradesh, Karnataka, Kerala and many additional regions are moderately or severely affected with arsenic (soil or water) contamination (Ali et al. 2019).

ARSENIC DETOXIFICATION GENES

The majority of microorganisms have evolved with arsenic detoxification systems (Yan et al. 2019). Various studies elucidating its molecular processes were conducted against many microorganisms. Microbes deliberate arsenic detoxification with the assistance of the ars operon framework (Thul et al. 2019). This operon possesses either three (arsR, B, C) or five (arsR, A, B, C, D) gene components (Table 2). This (ars) operon exists either on plasmids or integrated with genome (Firrincieli et al. 2019). The operon (ars) gene encrypts proteins for repression in absence of arsenic, arsenate reduction, its efflux supporting detoxification system. The ars homologs were studied in diverse biological structures like; fungi, plant and animals (Fernández et al. 2014).

MICROBIAL ARSENITE RESISTANCE

Microbes evolved mechanism for enzymatic oxidation (As^{3+} to As^{5+}) for arsenite or reduction (As^{5+} to As^{3+}) for arsenate. They do carry redox events and are imperative players in the arsenic geocycle (Turner 2001). Bacteria resist their toxic effects by preventing their intake or actively exporting the arsenicals or by modifying them enzymatically or chemically. Therefore paramount search for more oxidizing (arsenite) bacteria concerning bioremediation is greatly significant (Verma & Kuila 2019). Many microorganisms show resistance to arsenic especially arsenate, while there are only a few bacterial isolates known exhibiting arsenite resistance (Tian et al. 2019). Arsenite concentration was proved lethal on or above 200 µg/L for many bacteria. However, arsenite directly can be methylated by *P. alcaligenes* (arsenite S- adenosylmethionine methyltransferase) (Zhang et al. 2015). Arsenite oxidation attenuates toxicity, provided its re-conversion in the cell does not happen. Bacteria harbour transport protein for both arsenic valencies and their transformation catalysing enzymes (Oremland & Stolz 2003). Presently, it is typically assumed that arsenite oxidizing microbes can harbour both oxidase and reductase enzymes. Both enzyme system in arsenic resistant isolate was found, however, the simultaneous occurrence of two enzymatic systems jeopardize the bioremediation process (Dunivin et al. 2019).

SOLUBILIZATION, MOBILIZATION AND UPTAKE OF ARSENIC

Arsenic solubilization depends on its speciation and transformation (Smedley & Kinniburgh 2002, Cullen & Reimer 1989). Arsenic is additionally found in different methylated forms in the mine drainage system and geothermal inputs. Anaerobic condition in the underground region holds the highest arsenic concentration, where it favours the geochemical conditions for its solubilization (Cullen & Reimer 1989). Fe-Mn oxides at the water-sediment interface scavenge arsenic from mine tailings and from contaminated water that causes As concentrations to remain enriched in the upper sediments even after mine tailings have been ceased (Sprague & Vermaire 2018).

Structural similarity of As^{3+} and As^{5+} to phosphate

Table 2: Characterized arsenic resistance gene cluster among microorganisms.

S.No	Name of organism	*ars* genes	References
1	*E. coli* plasmid R773.	arsR, A, B, D, C	Hedges & Baumberg 1973
2	*Staphylococcus xylosus* plasmid pSX267.	arsR, B, C	Rosenstein et al. 1992
3	*Staphylococcus aureus* plasmid pI258	arsR, B, C	Ji & Silver 1992
4	E coli W3110	arsR, B, C	Carlin et al. 1995
5	Yersiniae sp.	arsR, B, C, H	Neyt et al. 1997
6	*Acidiphilium multivorum* AIU 301 plasmid pKW301	arsR, D, A, B, C	Carlin et al. 1995
7	Bacillus subtilis	*arsR*, B, C *ORF2*	Sato & Kobayashi 1998
8	Pseudomonas aeruginosa	arsR, B, C	Cai et al. 1998
9	Acidithiobacillus ferrooxidans	*arsR, C* and *arsB, H*.	Butcher et al. 2000
10	*Pseudomonas fluorescens* strain MSP3	arsR, B, C	Prithivirajsingh et al. 2001
11	*Synechocystis* sp. Strain PCC 6803	arsB, H, C	López-Maury et al. 2003
16	*Shewanella* species ANA-3	arsR, B, C	Saltikov et al. 2003
12	*Halobacterium* sp. Strain NRC-1	arsA, D, R, C, arsR2, M	Wang et al. 2004
13	*Corynebacterium glutamicum* ATCC 13032	arsR, B, C	Ordóñez et al. 2005
14	Sinorhizobium meliloti.	arsR,apqs C	Yang et al. 2005
15	Acidithiobacillus caldus	arsD, A, B	Kotze et al. 2006
17	*Streptomyces* sp. Strain FR-008.	arsR, O, B, T, C	Wang et al. 2006
18	Leptospirillum ferriphilum	arsR, B, C, arsR, C, D, A, B	Fournier et al. 2006
19	Acinetobacter baumannii	arsR, B, H, C	Fournier et al. 2006
20	*Ochrobactrum tritici* SCII24T	arsR, A, B, D and arsR, C, H ,ACR3	Branco et al. 2008

Note: (i) arsR (arsenical resistance operon repressor), arsB (arsenical pump membrane protein), arsC (arsenate reductase), arsH (unknown), arsD (arsenic operon regulator), arsA (ATPase subunit). (ii) arsR, B, C makes the main detoxification system, arsD and arsA are supporting proteins.

typically aid prokaryotic cells for their uptake through various transporters (Fig. 2). More specifically, the Pit-phosphate transporter is in-charge of arsenate uptake in *E.coli* cells (Willsky & Malamy 1980). Pst-phosphate transporter is also found transporting arsenate in some bacterial cells but at a low level than "Pit" (Bertin et al. 2011). Microbial flora which is continually presented to high measures of arsenate express just "Pst" according to lessen arsenate take-up (Meng et al. 2004). In *E.coli*, GIpF (aquaglyceroporins) is stated for foremost As^{3+} uptake (Banerjee et al. 2018). Dissimilatory Arsenate Reducing Bacteria (DARB) phylogenetically belong to a diverse group and respire As^{5+} by reducing it anaerobically. DARB own a conserved arsenate reductase (arrA) gene, essential for reduction system (Burton et al. 2014). It is mostly utilized biomarker estimating variations in arsenic reducing microbes across different environments. Most bacteria utilize a similar process of As detoxification involving its uptake, reduction and extrusion using an efflux pump (Kumari & Jagadevan 2016).

ARSENITE OXIDATION (AS^{3+} TO AS^{5+})

Oxidation of As^{3+} represents a promising detoxification process that allows microorganisms to tolerate their toxic levels in tainted locations (Santini & Hoven 2004). So far, isolated arsenite oxidising prokaryotes can be grouped in two categories: (i) Chemolithoautotrophs (aerobes or anaerobes, using arsenite as electron donor and CO_2/ HCO_3^- as specific carbon source) (ii) Heterotrophs (grow in organic matter) (Oremland et al. 2002). Chemolithoautotrophic bacteria *NT-26* and *MLHE-1* oxidizes As^{3+} to As^{5+} using oxygen and NO_3^- as electron acceptor (Ellis et al. 2001). Several heterotrophic bacteria are persuaded to oxidise As^{3+} provided in growing media using arsenite oxidase. Arsenite oxidase activity was measured biochemically in presence of azurin or cytochrome-C (Pandey et al. 2009). Yet, at the alike period, it looks that most ecological isolates don't have this potential, in spite of the fact that many microorganisms were recognized having arsenite oxidase gene, which proves that arsenite oxidase is the most important factor for counteracting arsenic toxicity. Microorganisms can indirectly disturb arsenic mobility via sulphate reduction, iron-oxide reduction and mineral dissolution by oxidation (McArthur et al. 2004). The As^{3+} oxidation to As^{5+} (a less toxic form of arsenic) occurs due to bacterial arsenite oxidase in the peri-plasm of microorganism (Rosen 2002). A sensor kinase (AoxS) recognizes the presence of As^{3+} and activates a controller protein (AoxR). AoxR is a point control for aox operon clubbed with RpoN (an option of 54 of RNA polymerase) (Satyapal et al. 2016). The RpoN is the requisite factor for

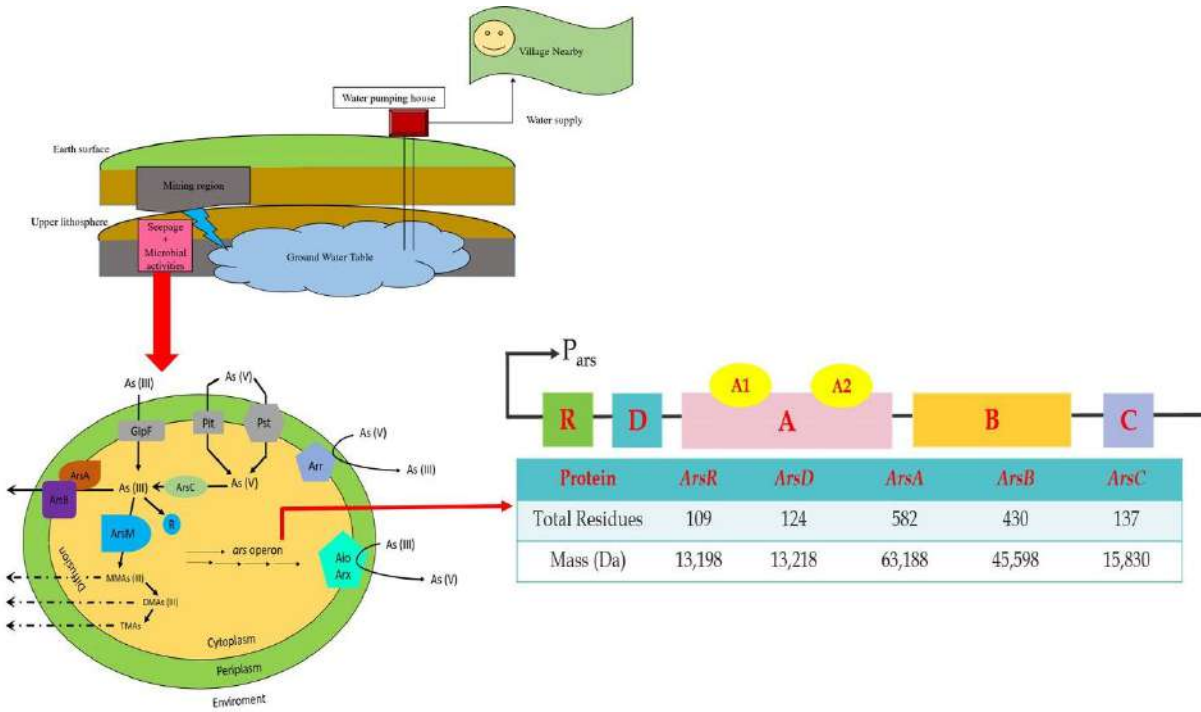

Protein	*ArsR*	*ArsD*	*ArsA*	*ArsB*	*ArsC*
Total Residues	109	124	582	430	137
Mass (Da)	13,198	13,218	63,188	45,598	15,830

Fig. 2: Pandect of arsenic seepage in groundwater and bacterial interaction. The development of wells and human activities quickens this process by providing necessary oxidants.

the transcriptional onset of aox operon, the products of which are transferred to peri-plasm by 'Tat' protein in *A. tumefaciens*. In peri-plasm, 'Tat' is engaged in the oxidation of As^{3+} (Shankar & Shanker 2014).

ARSENATE REDUCTION (AS^{5+} TO AS^{3+})

Arsenate uptake by the bacterial cell is done by dual phosphate transporters Pst (specifically) and Pit (generally). Arsenite expulsion is finished by (i) carrier-mediated arsenite protein and (ii) through ATPase engaged in arsenite translocation (Shankar & Shanker 2014). Bacteria harbour two systems for arsenate reduction; cytoplasmic and periplasmic reduction systems. When As^{5+} is intruded by Pst/Pit transporters (membrane), the arsC (arsenate reductase) reduces it to As^{3+} followed by extrusion using arsAB pump (Biswas et al. 2019). In cytoplasmic reduction arsC uses glutaredoxins providing reducing potential. In the reaction cascade (Fig. 3), arsenate first unites with an anionic site of arsC forming an arsenate thioester transition with the active site and reduced by glutathione, extruding arsenite (Hare et al. 2019).

Various arsenic forms display different toxicity degrees. Among organic acids of arsenic MMAV (monomethylarsonic acid) and DMAV (dimethylarsinic acid) are barely harmful than inorganic arsenic, whereas MMAIII (monomethylarsonous acid) and DMAIII (dimethylarsonous acid) are highly toxic (Santra et al. 2013). Different arsenic metabolizing bacteria are classified into arsenite oxidizing and reducing (arsenate) bacteria which are skilled in coinciding in the environment, demonstrating a fact that they do play an essential part in metabolizing arsenic (Yan et al. 2019).

ARSENIC BIOREMEDIATION

Bioremediation technology for eliminating hazardous metals have gained considerable importance over the years. Microbial biosorbents are eco-friendly, cost-effective and a competent substitute for remediating arsenic (Sylvia et al. 2005). The flexibility of microorganisms to detoxify huge pollutants range makes bioremediation an innovative strategy in this regard (Singh 2014). Bioremediation skill relies on encouraging the growth of specific micro-flora that are indigenous to the specified contaminated sites and are capable to perform desired activities (Dixit et al. 2015).

The arsenic inescapability in nature has constrained the development of resistant mechanism in specific microorganisms utilising As in metabolism. *K. pneumonia*, a gram-negative, non-motile, rod-shaped bacteria possess the ability to oxidize As^{3+} and reduce As^{5+} (Daware & Gade 2015). It is also reported to have high resilience regarding both arsenate/ arsenite. Through the transformation assay redox ability of *K. pneumonia* towards arsenic was determined to clarify the detoxification mechanism (Batool & Rehman 2017). Although arsenic bioremediation has received great consideration, still this technology hasn't been implemented at commercial or field-scale to rectify contaminated sites. For successful bioremediation, the design requires three main factors which are: bacteria should exist in arsenic-contaminated sites, should bear high metabolic capacities and could perform under distinct environmental conditions (Nookongbut et al. 2017). Recent investigation depicted, purple non-sulphur *Rhodopseudomonas* bacteria (*R. palustris* & *R. faecalis*) are attractive organisms for application in arsenic bioremediation as they possess the most versatile growth modes and can flourish under a variety of conditions (Zhao et al. 2015). Bacterial nucleotide sequence having ars operon encodes for various regulatory components like arsA, arsB, arsC, arsD and arsR respectively (Table 3).

Recent advances in various biotechnological tools have prompted the beginning of a few non-conventional bioremediation strategies advancing their components and

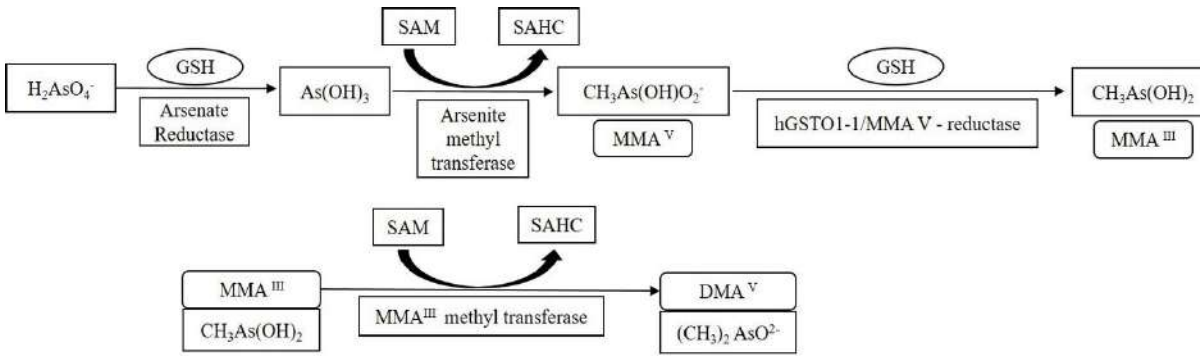

Note: GSH (Glutathione), SAM (S-adenosyl-L-methionine), SAHC (S-adenosyl-L-homocysteine), hGSTO1-1 (human glutathione-S-transferase omega 1-1), MMAIII (monomethylarsonous acid), DMAIII (dimethylarsinous acid).

Fig. 3: Enzymatic method for arsenate reduction.

Table 3: The *ars* operon genes and their putative function (Branco et al. 2008).

ORF	Putative function
arsR	Regulatory Protein
arsD	Regulatory Protein/Chaperone protein
arsA	Oxyanion-translocating ATPase
arsB	Arsenite membrane pump
arsC	Arsenate reductase

performance under diversified natural conditions (Gorny et al. 2018, Palit et al. 2019). Metallothioneins (MTs) are low molecular weight proteins, introduced recently and found in a variety of microorganisms. The cysteine-rich amino acid content of MTs have a greater binding affinity with heavy metals and are efficiently suitable for remediating them at low concentrations (Ma et al. 2011). Recombinant *E.coli* plasmid with a copy of the MT gene was constructed resulting in a three times increase in bioaccumulation of arsenic (Ma et al. 2011). Voluntary As^{3+} oxidation at the anode of microbial fuel cells (MFCs) with bioelectricity production was also studied and evaluated (Li et al. 2016).

CONCLUSION AND DISCUSSION

The bacterial arsenic encounter varies greatly among bacterial species. Various bacterial cells were recognized harbouring genes for metabolizing and transforming arsenic species. The Arsenic oxidizing ability of bacterial isolates are well understood and many microbes were being diagnosed and isolated. Arsenic reducing (As^{5+} to As^{3+} transformation) property of bacterial cells are not very well understood, so emphasis should be given in this area as it is too dangerous for the biotic community as well as humans. It has already been reported that in the abandoned mining regions the concentration of arsenite is increasing year after year minutely. This is because the native bacterial cells take up arsenate, reduce and extrude arsenite in the underground environment. This process increases the arsenite concentration in underground water severely, making it unfit for drinking and irrigation purpose. The arsenite when consumed by humans for a long period, leads to various abnormal deformities, as reported in this review. Crops if grown on As contaminated soil or irrigated with As contaminated water, either sequester it or accumulate it. This process further leads to the development of crops that are not suitable for human or animal consumption.

When we visited some contaminated regions of MP and Jharkhand, we came to know about a fact by talking to the native people, that none individual is survived above 52 years of age. The living population, especially adults have developed skin lesions (grey or black spots) on their palms, foot and front abdominal region. We also came to know that, if they use those crop plants which are being grown of contaminated soil, as fodder for milk yielding animals like cow and buffalo, they gradually become weak and decreases the milk yielding capacity and finally, dies within 10 to 12 months. Likewise, many regions are there in India, facing these types of moderate to severe problems. Government and non-government agencies are also playing their part to improve the vegetation and livelihood of arsenic affected regions, but it is not up to the mark. Every year the problem persists and increases in a dramatic mode. So, biological remediation methods employing bacterial community may prove a valuable and cost-effective method, to achieve arsenic decontamination from affected regions.

Bacterial activity and various factors (biotic or abiotic) including complexation, sorption, precipitation, detoxification, redox events impacts the fate of arsenic. More profound knowledge regarding As^{3+} oxidizers dispersal and metabolic pathways in the natural environment could be a plausible marker for arsenic remediation. However, there are many gaps in the area that needs attention and resolved before exploring in-situ bioremediation as a viable treatment option. Notwithstanding the antiquated origin and wide dispersion of arsenite oxidase in an anoxic environment, a comprehension on its part and effect on regular habitat is yet inadequate. The current improvements in metabolic pathways engaged in arsenic metabolization are yet incomplete and need exhaustive study. This review provides a deeper understanding of the distribution of its metabolizers in the natural environment and depicts future prospects for remediating arsenic. The use of an integrated approach of biomarkers of arsenic exposure and early genotoxic effects will provide a better understanding and mechanistic insight into the health risks of arsenic exposure. The information obtained here highlights the importance of the prevention of arsenic exposure and the need for effective strategies to reduce the risk for the development of diseases associated with such exposure.

FUTURE PROSPECTS

The profligate growing industry and advancement in technology have put heavy metals encumbrance on the environment contaminating water and soil. As the conventional approaches are slow, complex and expensive, microbial remediation strategies help to surmount such situation. Existing technologies still need modification on a pilot-scale and to be implemented effectively to remove these contaminants in a cost-effective and user-friendly mode. So, it is unambiguously suggested that sheltered and

effective advances ought to indorse for arsenic expulsion from drinking water. Microbial assisted bioremediation strategy has some margins but still grants a secured and swift way for remedying contaminated sites. Microorganisms play a crucial role in remediating arsenic from the underground environment through the genes harboured by them. If the mechanisms and functions of these genes can be understood, they can be easily employed in the construction of genetically modified organisms (GMOs). The GMOs could be the best significant turning point that can concurrently endeavour on several heavy metals. Essentially, a more profound investigation is required to boast proficiency of GMOs. Manipulation in the exterior membrane can be discouraging for its uptake and even on expressing precise transforming gene, further boost the bioremediation capability by employing GMOs.

REFERENCES

Ahamed, S., Sengupta, M.K., Mukherjee, A., Hossain, M.A., Das, B., Nayak, B., Pal, A., Mukherjee, S.C., Pati, S. and Dutta, R.N. 2006. Arsenic groundwater contamination and its health effects in the state of Uttar Pradesh (UP) in upper and middle Ganga plain, India: a severe danger. Sci. Tot. Environ., 370: 310-322.

Alam, M.O., Shaikh, W.A., Chakraborty, S., Avishek, K. and Bhattacharya, T. 2016. Groundwater arsenic contamination and potential health risk assessment of Gangetic Plains of Jharkhand, India. Exposure and Health, 8: 125-142.

Ali, S., Fakhri, Y., Golbini, M., Thakur, S.K., Alinejad, A., Parseh, I., Shekhar, S. and Bhattacharya, P. 2019. Concentration of fluoride in groundwater of India: A systematic review, meta-analysis and risk assessment. Groundwater Sustain. Develop. J., 9: 100199-100224.

Ayangbenro, A.S. and Babalola, O.O. 2017. A new strategy for heavy metal polluted environments: a review of microbial biosorbents. Int. J. Environ. Res. Public Health, 14: 94-105.

Banerjee, A., Jhariya, M., Yadav, D. and Raj, A. 2018. Micro-remediation of metals: a new frontier in bioremediation. In: Hussain C. (eds.) Handbook of Environmental Materials Management. Springer, Cham, 1-36.

Batool, K. and Rehman, Y. 2017. Arsenic–redox transformation and plant growth promotion by purple nonsulfur bacteria *Rhodopseudomonas palustris* CS2 and *Rhodopseudomonas faecalis* SS5. BioMed Res. Int., 11: 1-8.

Bertin, P.N., Heinrich–Salmeron, A., Pelletier, E., Goulhen–Chollet, F., Arsène–Ploetze, F., Gallien, S., Lauga, B., Casiot, C., Calteau, A. and Vallenet, D. 2011. Metabolic diversity among main microorganisms inside an arsenic–rich ecosystem revealed by meta–and proteo–genomics. ISME, J., 5: 1735-1747.

Bhattacharjee, S., Chakravarty, S., Maity, S., Dureja, V. and Gupta, K. 2005. Metal contents in the groundwater of Sahebgunj district, Jharkhand, India, with special reference to arsenic. Chemosphere, 58: 1203-1217.

Bhattacharya, P., Welch, A.H., Stollenwerk, K.G., Mclaughlin, M.J., Bundschuh, J. and Panaullah, G. 2007. Arsenic in the environment: biology and chemistry. Sci. Tot. Environ., 379: 109-120.

Biswas, R., Vivekanand, V., Saha, A., Ghosh, A. and Sarkar, A. 2019. Arsenite oxidation by a facultative chemolithotrophic *Delftia* spp. BAs29 for its potential application in groundwater arsenic bioremediation. Int. Biodeterior. Biodegrad., 136: 55-62.

Branco, R., Chung, A.P. and Morais, P.V. 2008. Sequencing and expression of two arsenic resistance operons with different functions in the highly arsenic–resistant strain *Ochrobactrum tritici* SCII24T. BMC, Microbiol., 8: 95-105.

Burton, E.D., Johnston, S.G. and Kocar, B.D. 2014. Arsenic mobility during flooding of contaminated soil: the effect of microbial sulfate reduction. Environ. Sci.Technol., 48: 13660-13667.

Butcher, B.G., Deane, S.M. and Rawlings, D.E. 2000. The chromosomal arsenic resistance genes of *Thiobacillus ferrooxidans* have an unusual arrangement and confer increased arsenic and antimony resistance to *Escherichia coli*. Appl. Environ. Microbiol., 66: 1826-1833.

Cai, J., Salmon, K. and Dubow, M.S. 1998. A chromosomal ars operon homologue of *Pseudomonas aeruginosa* confers increased resistance to arsenic and antimony in *Escherichia coli*. Microbiol., 144: 2705-2729.

Carlin, A., Shi, W., Dey, S. and Rosen, B.P. 1995. The ars operon of *Escherichia coli* confers arsenical and antimonial resistance. J. Bacteriol., 177: 981-986.

Chakraborti, D, Biswas, B., Chowdhury, T.R., Basu, G., Mandal, B., Chowdhury, U., Mukherjee, S., Gupta, J., Chowdhury, S. and Rathore, K. 1999. Arsenic groundwater contamination and sufferings of people in Rajnandgaon district, Madhya Pradesh, India. Curr. Sci., 77: 502–504.

Chakraborti, D., Das, B., Rahman, M.M., Nayak, B., Pal, A., Sengupta, M.K., Ahamed, S., Hossain, M.A., Chowdhury, U.K. and Biswas, B.K. 2017a. Arsenic in groundwater of the Kolkata Municipal Corporation (KMC), India: Critical review and modes of mitigation. Chemosphere, 180: 437–447.

Chakraborti, D., Rahman, M.M., Das, B., Chatterjee, A., Das, D., Nayak, B., Pal, A., Chowdhury, U.K., Ahmed, S. and Biswas, B.K. 2017b. Groundwater arsenic contamination and its health effects in India. Hydrogeol. J., 4: 1165-1181.

Chakraborti, D., Singh, E.J., Das, B., Shah, B.A., Hossain, M.A., Nayak, B., Ahamed, S. and Singh, N.R. 2008. Groundwater arsenic contamination in Manipur, one of the seven North–Eastern Hill states of India: a future danger. Environ. Geol., 56: 381-390.

Chakraborti, D., Singh, S.K., Rahman, M.M., Dutta, R.N., Mukherjee, S.C., Pati, S. and Kar, P.B. 2018. Groundwater arsenic contamination in the Ganga River basin: a future health danger. Int. J. Environ. Res. Public Health, 15: 180-190.

Chakraborty, S., Alam, M.O., Bhattacharya, T. and Singh, Y.N. 2014. Arsenic accumulation in food crops: a potential threat in Bengal Delta Plain. Water Quality, Exposure and Health, 6: 233-246.

Chauhan, V.S., Nickson, R., Chauhan, D., Iyengar, L. and Sankararamakrishnan, N. 2009. Ground water geochemistry of Ballia district, Uttar Pradesh, India and mechanism of arsenic release. Chemosphere, 75: 83-91.

Chikkanna, A., Mehan, L., Sarath, P. and Ghosh, D. 2019. Arsenic exposures, poisoning, and threat to human health: arsenic affecting human health. In: Environmental Exposures and Human Health Challenges, IGI Global, pp. 86-105.

Cullen, W.R. and Reimer, K.J. 1989. Arsenic speciation in the Environment. Chem. Rev., 89: 713-764.

Dey, S. 2017. Mission to make 28,000 habitations arsenic–free by 2021. https://timesofindia.indiatimes.com/india/mission-to-make-28000-habitations-arsenic-free-by-2021/articleshow/57952655.cms

Dixit, R., Malaviya, D., Pandiyan, K., Singh, U.B., Sahu, A., Shukla, R., Singh, B.P., Rai, J.P., Sharma, P.K. and Lade, H. 2015. Bioremediation of heavy metals from soil and aquatic environment: an overview of principles and criteria of fundamental processes. Sustain., 7: 2189-2212.

Dontala, S.P., Reddy, T.B. and Vadde, R. 2015. Environmental aspects and impacts its mitigation measures of corporate coal mining. Procedia Earth and Planetary Sci., 11: 2-7.

Dunivin, T.K., Yeh, S.Y. and Shade, A. 2019. A global survey of arsenic related genes in soil microbiomes. BioRxiv, 44: 55-102.

Edwards, K.J., Bond, P.L., Gihring, T.M. and Banfield, J.F. 2000. An archaeal iron–oxidizing extreme acidophile important in acid mine drainage. Sci., 287: 1796-1799.

Ellis, P.J, Conrads, T., Hille, R. and Kuhn, P. 2001. Crystal structure of the 100 kDa arsenite oxidase from *alcaligenes faecalis* in two crystal forms at 1.64 Å and 2.03 Å. Structure, 9: 125-132.

Fernández, M., Udaondo, Z., Niqui, J.L., Duque, E. and Ramos, J.L. 2014. Synergic role of the two ars operons in arsenic tolerance in *Pseudomonas putida* KT2440. Environ. Microbiol. Rep., 6: 483-489.

Firrincieli, A., Presentato, A., Favoino, G., Marabottini, R., Allevato, E., Stazi, S.R., ScaraSciencea–mugnozza, G., Harfouche, A., Petruccioli, M. and Zannoni, D. 2019. Identification of resistance genes and response to arsenic in *Rhodococcus aetherivorans* BCP1. Front. Microbiol., 10: 888-898.

Fournier, P.E., Vallenet, D., Barbe, V., Audic, S., Ogata, H., Poirel, L., Richet, H., Robert, C., Mangenot, S. and Abergel, C. 2006. Comparative genomics of multidrug resistance in *Acinetobacter baumannii*. PLoS Genetics, 2: e7.

Gorny, J., Billon, G., Noiriel, C., Dumoulin, D., Lesven, L. and Madé, B. 2018. Redox behaviour of arsenic in the surface sediments of the Marque River (Northern France). J. Geochem. Explor., 188: 111-122.

Gupta, A. and Singh, E.J. 2019. Arsenic–iron relationships in aquifers of North East India: implications for public health and the environment. environ. Manage., 63: 437-443.

Hajalilou, B., Mosaferi, M., Khaleghi, F., Jadidi, S., Vosugh, B. and Fatehifar, E. 2011. Effects of abandoned arsenic mine on water resources pollution in north west of Iran. Health Promotion Perspect., 1: 62-72.

Hedges, R. and Baumberg, S. 1973. Resistance to arsenic compounds conferred by a plasmid transmissible between strains of *E.coli*. J. Bacteriol., 115: 459-469.

Herath, I., Vithanage, M., Bundschuh, J., Maity, J.P. and Bhattacharya, P. 2016. Natural arsenic in global groundwaters: distribution and geochemical triggers for mobilization. Curr. Pollut. Rep., 2: 68-89.

Jha, S.K., Mishra, V.K., Damodaran, T., Sharma, D.K. and Kumar, P. 2017. Arsenic in the groundwater–occurrence, toxicological activities, and remedies. J. Environ. Sci. Health, 35: 84-103.

Ji, G. and Silver, S. 1992. Reduction of arsenate to arsenite by the arsC protein of the arsenic resistance operon of *Staphylococcus aureus* plasmid pI258. Proceed. Nat. Acad. Sci., 89: 9474-9478.

Jiang, Y, Guo, H., Jia, Y., Cao, Y. and Hu, C. 2015. Principal component analysis and hierarchical cluster analyses of arsenic groundwater geochemistry in the Hetao basin, Inner Mongolia. Chemie Der Erde–Geochem., 75: 197-205.

Jomova, K., Jenisova, Z., Feszterova, M., Baros, S., Liska, J., Hudecova, D., Rhodes, C. and Valko, M. 2011. Arsenic: toxicity, oxidative stress and human disease. J. Appl. Toxicol., 31: 95-107.

Kadushkin, A., Siddiqui, Z. and Shipin, O. 2004. Groundwater quality assessment and management in selected countries of East and Southeast Asia. 41 st CCOP Annual Session 15–18 November 2004, Tsukuba, Japan, 147-157.

Kar, S., Maity, J.P., Jean, J.S., Liu, C.C., Nath, B., Yang, H.J. and Bundschuh, J. 2010. Arsenic–enriched aquifers: occurrences and mobilization of arsenic in groundwater of Ganges Delta Plain, Barasat, West Bengal, India. Appl. Geochem., 25: 1805-1814.

Kotze, A.A., Tuffin, I.M., Deane, S.M. and Rawlings, D.E. 2006. Cloning and characterization of the chromosomal arsenic resistance genes from *Acidithiobacillus caldus* and enhanced arsenic resistance on conjugal transfer of ars genes located on transposon TnAtcArs. Microbiol., 152: 3551-3560.

Kumari, N. and Jagadevan, S. 2016. Genetic identification of arsenate reductase and arsenite oxidase in redox transformations carried out by arsenic metabolising prokaryotes–A comprehensive review. Chemosphere, 163: 400-412.

Kwon, J.C., Nejad, Z.D. and Jung, M.C. 2017. Arsenic and heavy metals in paddy soil and polished rice contaminated by mining activities in Korea. Catena J., 148: 92-100.

Li, Y., Zhang, B., Cheng, M., Li, Y., Hao, L. and Guo, H. 2016. Spontaneous arsenic (III) oxidation with bioelectricity generation in single–chamber microbial fuel cells. J. Hazard. Mat., 306: 8-12.

López–Maury, L., Florencio, F.J. and Reyes, J.C. 2003. Arsenic sensing and resistance system in the *Cyanobacterium synechocystis* sp. strain PCC 6803. J. Bacterio., 185: 5363-5371.

Ma, Y., Lin, J., Zhang, C., Ren, Y. and Lin, J. 2011. Cd (II) and As (III) bioaccumulation by recombinant *E. coli* expressing oligomeric human metallothioneins. J. Hazard. Mat., 185: 1605-1608.

Masto, R.E., Ram, L.C., George, J., Selvi, V.A., Sinha, A.K., Verma, S.K. and Prabal, P. 2011. Status of some soil trace elements and their potential human health risks around a coal beneficiation plant. Int. J. Coal Prep. Utiliz., 31: 61-77.

Mazumder, D.N.G. 2015. Health Effects Chronic Arsenic Toxicity. Handbook of Arsenic Toxicology, 2015, edn. DNGM Research Foundation, New Alipore, Kolkata, India, pp. 137-177.

McArthur, J., Banerjee, D., Hudson-Edwards, K., Mishra, R., Purohit, R., Ravenscroft, P., Cronin, A., Howarth, R., Chatterjee, A. and Talukder, T. 2004. Natural organic matter in sedimentary basins and its relation to arsenic in anoxic ground water: the example of West Bengal and its worldwide implications. Appl. Geochem., 19: 1255-1293.

McArthur, J.M. 2019. Arsenic in groundwater. Groundwater Development and Management: Issues and Challenges in South Asia. pp. 279–308. doi:10.1007/978-3-319-75115-3_12

Meliker, J.R., Avruskin, G.A., Slotnick, M.J., Goovaerts, P., Schottenfeld, D., Jacquez, G.M. and Nriagu, J.O. 2008. Validity of spatial models of arsenic concentrations in private well water. Environ. Res., 106: 42-50.

Milton, A.H., Hasan, Z., Rahman, A. and Rahman, M. 2001. Chronic arsenic poisoning and respiratory effects in Bangladesh. J. Occupat. Health, 43: 136-140.

Mirza, B.S., Sorensen, D.L., Dupont, R.R. and Mclean, J.E. 2017. New arsenate reductase gene (arrA) PCR primers for diversity assessment and quantification in environmental samples. Appl. Environ. Microbiol., 83: e02725-16.

Neyt, C., Iriarte, M., Thi, V.H. and Cornelis, G.R. 1997. Virulence and arsenic resistance in *Yersiniae*. J. Bacteriol., 179: 612-619.

Nookongbut, P., Kantachote, D., Krishnan, K. and Megharaj, M. 2017. Arsenic resistance genes of As-resistant purple nonsulfur bacteria isolated from As-contaminated sites for bioremediation application. J. Basic Microbiol., 57: 316-324.

Nordstrom, D.K. 2002. Worldwide occurrences of arsenic in ground water. Sci., 296: 2143-2145.

Omar, Y.Y., Parker, A., Smith, J.A. and Pollard, S.J. 2017. Risk management for drinking water safety in low and middle income countries-cultural influences on water safety plan (WSP) implementation in urban water utilities. Sci. Tot. Environ., 576: 895-906.

Ordóñez, E., Letek, M., Valbuena, N., Gil, J.A. and Mateos, L.M. 2005. Analysis of genes involved in arsenic resistance in *Corynebacterium glutamicum* ATCC 13032. Appl. Environ. Microbiol., 71: 6206-6215.

Oremland, R.S. and Stolz, J.F. 2003. The ecology of arsenic. Sci., 300: 939-944.

Oremland, R.S., Hoeft, S.E., Santini, J.M., Bano, N., Hollibaugh, R.A. and Hollibaugh, J.T. 2002. Anaerobic oxidation of arsenite in Mono Lake water and by a facultative, arsenite–oxidizing chemoautotroph, strain MLHE–1. Appl. Environ. Microbiol., 68: 4795-4802.

Palit, S., Misra, K. and Mishra, J. 2019. Arsenic Contamination in South Asian Regions: The Difficulties, Challenges and Vision for the Future. Separation Science and Technology, 11edn. Elsevier, pp. 113-123.

Pandey, P.K., Choubey, S., Verma, Y., Pandey, M. and Chandrashekhar, K. 2009. Biosorptive removal of arsenic from drinking water. Biores. Technol., 100: 634-637.

Patel, K.S., Sahu, B.L., Dahariya, N.S., Bhatia, A., Patel, R.K., Matini,

L., Sracek, O. and Bhattacharya, P. 2017. Groundwater arsenic and fluoride in Rajnandgaon District, Chhattisgarh, northeastern India. Appl. Water Sci., 7: 1817-1826.

Philp, R.B. 2015. Ecosystems and Human Health: Toxicology and Environmental Hazards, Crc Press, London. doi: 10.1093/acrefore/9780199389414.013.86

Prithivirajsingh, S., Mishra, S.K. and Mahadevan, A. 2001. Detection and analysis of chromosomal arsenic resistance in *Pseudomonas fluorescens* strain MSP3. Biochem. Biophys. Res. Commun., 280: 1393-1401.

Quinodóz, F.B., Maldonado, L., Blarasin, M., Matteoda, E., Lutri, V., Cabrera, A., Albo, J.G. and Giacobone, D. 2019. The development of a conceptual model for arsenic mobilization in a fluvio–eolian aquifer using geochemical and statistical methods. Environ. Earth Sci., 78: 206-216.

Ramanathan, A., Bhattacharya, P. and Tripathi, P. 2006. Arsenic in groundwater of the aquifers of central Gangetic plain of Uttar Pradesh, India. In Philadelphia annual meeting, pp. 22-25. https://doi: 10.1201/b11334-26

Rosen, B.P. 2002. Biochemistry of arsenic detoxification. FEBS lett., 529: 86-92.

Rosenstein, R., Peschel, A., Wieland, B. and Götz, F. 1992. Expression and regulation of the antimonite, arsenite, and arsenate resistance operon of *Staphylococcus xylosus* plasmid pSX267. J. Bacteriol., 174: 3676-3683.

Ryan, R., Ryan, D. and Dowling, D. 2005. Multiple metal resistant transferable phenotypes in bacteria as indicators of soil contamination with heavy metals. J. Soils and Sediments, 5: 95-100.

Saha, D. and Ray, R.K. 2019. Groundwater resources of India: potential, challenges and management. Groundwater Development and Management, Springer, South Asia. doi:10.1007/978-3-319-75115-3

Saltikov, C.W., Cifuentes, A., Venkateswaran, K. and Newman, D.K. 2003. The ars detoxification system is advantageous but not required for As (V) respiration by the genetically tractable *Shewanella* species strain ANA-3. Appl. Environ. Microbiol., 69: 2800-2809.

Sandhi, A., Greger, M., Landberg, T., Jacks, G. and Bhattacharya, P. 2017. Arsenic concentrations in local aromatic and high–yielding hybrid rice cultivars and the potential health risk: a study in an arsenic hotspot. Environ. Moniter. Assess., 189: 184-196.

Santini, J.M. and Hoven, R.N.V. 2004. Molybdenum–containing arsenite oxidase of the chemolithoautotrophic arsenite oxidizer NT-26. J. Bacteriol., 186: 1614-1619.

Santra, S.C., Samal, A.C., Bhattacharya, P., Banerjee, S., Biswas, A. and Majumdar, J. 2013. Arsenic in foodchain and community health risk: a study in Gangetic West Bengal. Proced. Environ. Sci., 18: 2-13.

Sato, T. and Kobayashi, Y. 1998. The ars Operon in the skin element of *Bacillus subtilis* confers resistance to Arsenate and Arsenite. J. Bacteriol., 180: 1655-1661.

Satyapal, G., Rani, S. and Kumar, M. 2016. Potential role of arsenic resistant bacteria in bioremediation: current status and future prospects. J. Microbiol. Biochem. Technol., 8: 256-258.

Shah, B. 2010. Arsenic–contaminated groundwater in Holocene sediments from parts of Middle Ganga Plain, Uttar Pradesh, India. Curr. Sci., 98: 10-21.

Shan, Y., Mehta, P., Perera, D. and Varela, Y. 2019. Cost and efficiency of arsenic removal from groundwater: a review. UNU-INWEH Report Series, Issue 05. United Nations University Institute for Water, Environment and Health, Hamilton, Canada. https://inweh.unu.edu/cost-and-efficiency-of-arsenic-removal-from-groundwater-a-review/

Shankar, S. and Shanker, U. 2014. Arsenic contamination of groundwater: a review of sources, prevalence, health risks, and strategies for mitigation. Scientific World J., https://doi: 10.1155/2014/304524

Sichone, K. 2019. Control of leachate contamination from mine wastes through an appropriate operating practice. In: Gaustad G. et al. (eds) Rewas 2019. The Minerals, Metals & Materials Series, Springer, Cham.

Silver, S. and Phung, L.T. 2005. Genes and enzymes involved in bacterial oxidation and reduction of inorganic arsenic. Appl. Environ. Microbiol., 71: 599-608.

Singh, G.B., Gupta, S., Srivastava, S. and Gupta, N. 2011. Biodegradation of carbazole by newly isolated *Acinetobacter* spp. Bullet. Environ. Contam. Toxicol., 87: 522-526.

Singh, P.K. and Singh, R.S. 2016. Environmental and social impacts of mining and their mitigation. In: Kolkata (India): National Seminar ESIMM-2016.

Singh, R. 2014. Microorganism as a tool of bioremediation technology for cleaning Environment: A review. Proceed. Int. Acad. Ecol. Environ. Sci., 4: 1-6.

Smedley, P. and Kinniburgh, D. 2002. A review of the source, behaviour and distribution of arsenic in natural waters. Appl. Geochem., 17: 517-568.

Sprague, D.D. and Vermaire, J.C. 2018. Legacy arsenic pollution of lakes near cobalt, Ontario, Canada: arsenic in Lake water and sediment remains elevated nearly a century after mining activity has ceased. Water, Air, & Soil Pollut., 229: 87-105.

Sylvia, D.M., Fuhrmann, J.J., Hartel, P.G. and Zuberer, D.A. 2005. Principles and Applications of Soil microbiology. Pearson Prentice Hall Upper Saddle River, New Jersy.

Tian, H., Wang, J., Li, J., Wang, Y., Mallavarapu, M. and He, W. 2019. Six New Families of Aerobic Arsenate Reducing Bacteria: *Leclercia, Raoultella, Kosakonia, Lelliottia, Yokenella,* and *Kluyvera*. Geomicrobiol J., 36: 339-347.

Tomar, N.S. 2017. Fluoride and Arsenic in Drinking Water. 09 March 2017. http://www.who.int/water_sanitation_health/en/poster8.pdf

Turner, R.J. 2001. Tellurite toxicity and resistance in Gram–negative bacteria. Rec. Res. Develop. Microbiol., 5: 69-77.

Verma, S. and Kuila, A. 2019. Bioremediation of heavy metals by microbial process. Environ. Technol. Innovat., 14: 100369-100381.

Wang, G., Kennedy, S.P., Fasiludeen, S., Rensing, C. and Dassarma, S. 2004. Arsenic resistance in *Halobacterium* sp. strain NRC–1 examined by using an improved gene knockout system. J. Bacteriol., 186: 3187-3194.

Wang, L., Chen, S., Xiao, X., Huang, X., You, D., Zhou, X. and Deng, Z. 2006. arsRBOCT arsenic resistance system encoded by linear plasmid pHZ227 in *Streptomyces* sp. strain FR–008. Appl. Environ. Microbiol., 72: 3738-3742.

Wei, S., Zhang, H. and Tao., S. 2019. A review of arsenic exposure and lung cancer. Toxicol. Res., 8: 319-327.

WHO 2010. Exposure to arsenic: a major public health concern. Geneva: Public Health Environ., 1: 1-5.

Willsky, G.R. and Malamy, M.H. 1980. Effect of arsenate on inorganic phosphate transport in *E.coli*. J. Bacteriol., 144: 366-374.

Zhang, D., Wang, S., Wang, Y., Gomez, M.A. and Jia, Y. 2019. The long-term stability of calcium arsenates: Implications for phase transformation and arsenic mobilization. J. Environ. Sci., 84: 29-41.

Zhang, J., Cao, T., Tang, Z., Shen, Q., Rosen, B.P. and Zhao, F.J. 2015. Arsenic methylation and volatilization by arsenite S–adenosylmethionine methyltransferase in *Pseudomonas alcaligenes* NBRC14159. Appl. Environ. Microbiol., 81: 2852-2860.

Zhao, C., Zhang, Y., Chan, Z., Chen, S. and Yang, S. 2015. Insights into arsenic multi–operons expression and resistance mechanisms in *Rhodopseudomonas palustris* CGA009. Front. Microbiol., 6: 986–997.

Nature Environment and Pollution Technology
An International Quarterly Scientific Journal

p-ISSN: 0972-6268
(Print copies up to 2016)
e-ISSN: 2395-3454

Vol. 20 | No. 2 | pp. 771-774 | 2021

Original Research Paper

https://doi.org/10.46488/NEPT.2021.v20i02.038

Open Access Journal

Assessing Antibiotic Residue Removal from Milk Using Biochar

M. Suguna Devakumari
Department of Agriculture, School of Agriculture and Biosciences, Karunya Institute of Technology and Sciences, Karunya Nagar, Coimbatore-641 114, T.N., India
†Corresponding author: M. Suguna Devakumari; sugisathish@yahoo.com

Nat. Env. & Poll. Tech.
Website: www.neptjournal.com

Received: 27-04-2020
Revised: 21-05-2020
Accepted: 04-06-2020

Key Words:
Biochar
Antibiotic residue
Prosopis
Rice husk
Coconut shell

ABSTRACT

The aim of this study was to evaluate the antibiotic residue removal from milk using biochar. The milk samples were collected from the local milk distributors of Coimbatore city and screened for antibiotic residues by using 3-1 Dip Stick which can screen the three major antibiotic groups like Beta lactam, tetracycline and sulfonamide**.** The present investigation analyses the methodology for removing antibiotics from milk using *Prosopis* wood biochar, Rice husk biochar and Coconut shell biochar at different temperatures and contact time. The results revealed that *Prosopis* biochar of 0.2 mm sieve size at higher temperatures subjected to 60 minutes contact time performed better and removed the antibiotics from a maximum number of milk samples.

INTRODUCTION

The use of antibiotics therapy to treat and prevent udder infections in cows is a key component of mastitis control in many countries. Due to the widespread use of antibiotics for treatment of mastitis in dairy cows, much effort and concerns have been directed towards the proper management and monitoring of antibiotics usage in treatments in order to prevent contamination of raw milk. As the widespread use of antibiotics has created potential residue problems in milk and milk products that are consumed by the general public (Jones & Seymour 1988, Oliver et al.1990). Because of the public health significance, milk and milk products contaminated with antibiotics beyond a given residue level, are considered unfit for human consumptions.

Antimicrobial resistance is a complex issue and a global threat. Therefore, the responsible use of antibiotics is absolutely necessary and regulation is needed. However, in countries like India, it is common practice to use antibiotics on healthy animals, in order to prevent disease and infection and to promote growth which paves way for the entry of antibiotics into dairy products and milk. Residual antibiotics in milk can seriously affect consumers' health causing allergic reactions and developing resistant strains. Antibiotic contamination in milk can also cause significant economic losses for producers and manufacturers of milk and milk products. Although antimicrobial drugs are useful for the treatment of human infections, their occurrence in milk causes adverse public health effects such as drug resistance and hypersensitivity that could be life-threatening (Khaskheli et al.2008, Nisha 2008)

Biochar is cheaper and chemically inert material causing no harm and also economically feasible method for removing antibiotics from contaminated milk. Adsorption is one of the most efficient means of limiting antibiotic contamination and displays advantages such as low cost, simple design and easy operation. The adsorption capacity of biochar depends on the biomass feedstock and the pyrolysis process because these factors influence biochar characteristics such as surface area, surface functional groups and porosity and can be altered easily to remove specific antibiotics present in milk (Mitchell et al. 2015, Liu et al. 2012).

In this study, antibiotic residues in raw milk samples were screened and the contaminated samples were treated with biochar to remove antibiotics through adsorption.

METHODOLOGY

Biochar produced by pyrolysis of three different plant sources *Prosopis* wood, coconut shell and rice husks are procured from Tamil Nadu Agricultural University. The biochar samples were pulverized using pestle and mortar and sieved with 2 mm sieve and 0.2 mm sieve to get 2 particle sizes of each biochar (Fig. 1).

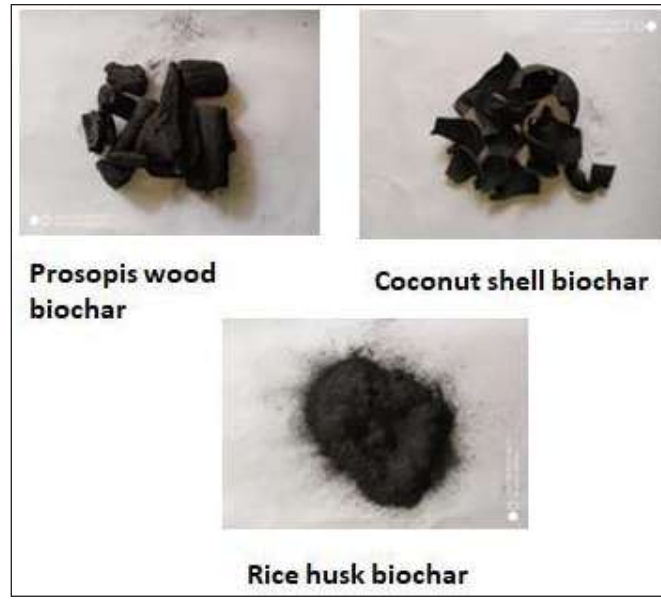

Fig.1: Biochar types used in the study.

Three separate glass columns, having an internal diameter of 1 cm and a length of 40 cm, were packed with known weight (25 cm) of biochar from three different plant origins (*Prosopis* wood, Coconut shell and Rice husk) as shown in Fig. 2.

Initially, milk sample free from antibiotic residue is allowed to pass through the biochar packed column to remove the air spaces in the adsorbent. 20 mL of whole milk samples tested positive for antibiotics was added separately through each column. The columns were maintained at three different temperatures (30°C, 40°C and 60°C) by placing inside the water bath. The milk samples were allowed to be in contact with the biochar in the glass column for two different contact periods (30 minutes and 60 minutes) and then drained out and tested for antibiotic residue presence using the 3-1 Dip Stick which can screen the three major antibiotic groups like Beta lactam, Tetracycline & Sulfonamide. The antibiotic positive samples were noted.

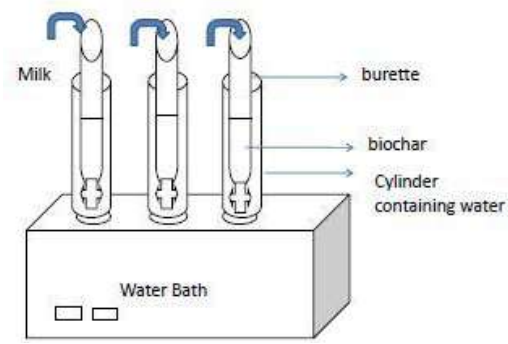

Fig. 2: Laboratory set up of the experiment.

RESULTS AND DISCUSSION

The three types of biochar (*Prosopis* wood, coconut shell and rice husks) were characterised for their physicochemical properties as shown in Table 1.

Among the three types of biochar, *Prosopis* wood biochar of 0.2 mm size performed better in removing the antibiotic residues from milk samples Table 2.

As the contact time with the adsorbent (biochar) increased the removal of antibiotic residue was observed in more number of samples. Similarly when the temperature of the column increased the removal rate of antibiotic residue was found to be in more number of samples (Fig. 3-5).

Table 1: Characteristics of the biochar types used in the study.

Parameters	Rice husk Biochar	Coconut shell biochar	*Prosopis* Biochar
Temperature of pyrolysis ºC	300	300	300
Biochar yield %	32	45	34
pH	7.48	8.66	8.73
EC dSm^{-1}	0.41	0.98	2.20
Bulk density $g.cm^{-3}$	0.86	0.54	0.34
CEC C mol p^{+} kg^{-1}	12.6	19.9	14.3
Ash content %	8.6	7.4	7.2
Total C %	42	34.4	67

Table 2: Number of positive samples (samples containing antibiotics) after the biochar adsorption.

Biochar type and size	Number of positive samples containing antibiotic residues						
	Initial no. of positive samples (Control)	25°C Temperature		40°C Temperature		60°C Temperature	
		Contact time 30 min	Contact time 60 min	Contact time 30 min	Contact time 60 min	Contact time 30 min	Contact time 60 min
Prosopis 0.2 mm	6	3	2	2	0	0	0
Prosopis 2 mm	6	4	3	3	1	1	1
Rice husk 0.2 mm	6	4	3	3	2	2	2
Rice husk 2mm	6	4	4	4	2	2	2
Coconut shell 2 mm	6	4	3	3	1	1	1
Coconut shell 0.2 mm	6	4	4	2	1	1	1

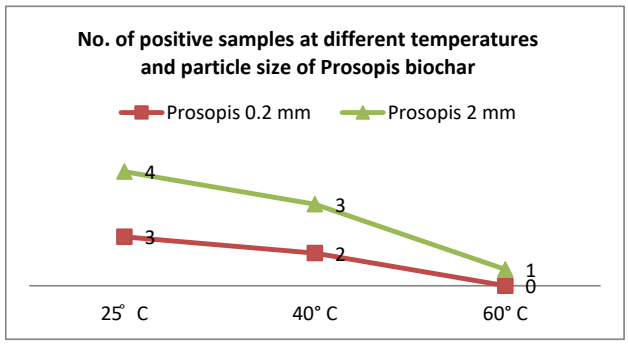

Type & Size	25°C	40°C	60°C
Prosopis 0.2 mm	3	2	0
Prosopis 2 mm	4	3	1

Fig. 3: Number of positive samples at different temperatures and particle size of Prosopis biochar.

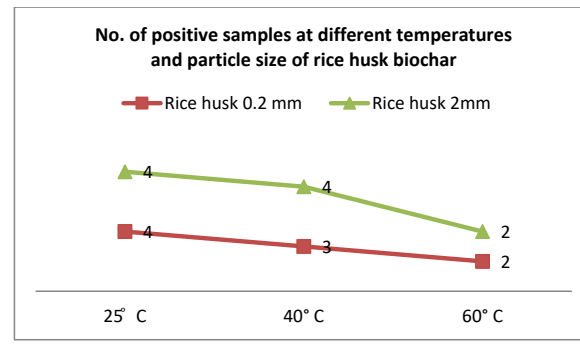

Type & Size	25°C	40°C	60°C
Rice husk 0.2 mm	4	3	2
Rice husk 2mm	4	4	2

Fig. 4: Number of positive samples at different temperatures and particle size of rice husk biochar.

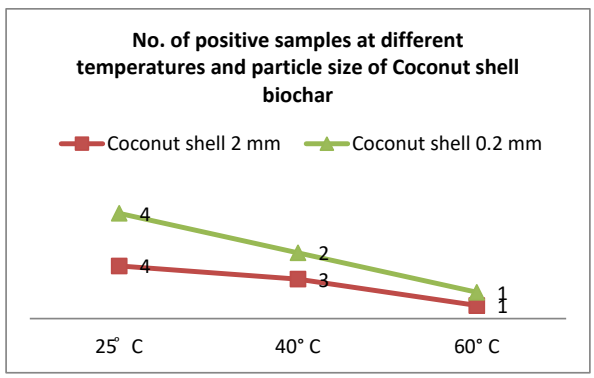

Type & Size	25°C	40°C	60°C
Coconut shell 2 mm	4	3	1
Coconut shell 0.2 mm	4	2	1

Fig. 5: Number of positive samples at different temperatures and particle size of Coconut shell biochar.

The above graphs infer that small particle size and higher temperature of the adsorbent (biochar) favours removal of antibiotic residue from milk samples. Among the type of biochar used *Prosopis* performed better in removing the antibiotic residues. So biochar could be used as an adsorbent for antibiotic residues in milk. This is in accordance with the previous report that the biochar pyrolyzed at 500 and 700°C were relatively high efficient at removing tetracycline from an aqueous solution (Wang et al. 2017).

CONCLUSION

Overall, biochar derived from pyrolyzing *Prosopis* wood offers a promising option for a low-cost method of removing antibiotic residue from milk and the other biochar produced from rice husk and coconut shell also removed the antibiotic from more number of positive samples. Moreover higher temperature and increased contact time with the adsorbent increased the antibiotic removal efficiency.

REFERENCES

Jones, G. M. and Seymour, E.H. 1988. Cowside antibiotic residues testing. Journal of Dairy Science, 71: 1691-1699.

Khaskheli, M., Malik, R. S., Arain, M. A., Soomro, A. H. and Arain, H.H. 2008. Detection of β–lactam antibiotic residues in market milk. Pakistan Journal of Nutrition., 7: 682-685.

Liu, P., Liu, W.J., Jiang, H., Chen, J.J., Li, W.W. and Yu, H.Q. 2012. Modification of biochar derived from fast pyrolysis of biomass and its application in removal of tetracycline from aqueous solution. Bioresour. Technol., 121: 235-40.

Mitchell, S.M., Subbiah, M., Ullman, J. L., Frear, C. and Call, D.R. 2015. Evaluation of 27 different biochars for potential sequestration of antibiotic residues in food animal production environments. J. Environ. Chem. Eng., 3(1): 162-9.

Nisha, A.R. 2008. Antibiotic residues - a global health hazard. Veterinary World, 1: 375-377.

Oliver, S. P., Maki, J. L. and Dowlen, H. H. 1990. Antibiotic residues in milk following antimicrobial therapy during lactation. Journal of Food Protection., 53: 693-696.

Wang, H., Chu, Y., Fang, C., Huang, F., Song, Y. and Xue, X. 2017. Sorption of tetracycline on biochar derived from rice straw under different temperatures. PLoS ONE, 12(8): e0182776.

Nature Environment and Pollution Technology
An International Quarterly Scientific Journal

p-ISSN: 0972-6268
(Print copies up to 2016)
e-ISSN: 2395-3454

Vol. 20 | No. 2 | pp. 775-783 | 2021

Original Research Paper

https://doi.org/10.46488/NEPT.2021.v20i02.039

Open Access Journal

Detection of Chromium(VI) in Water Using an Electrochemical Sensor Based on Ketjen Black-Modified Carbon Cloth

Yuxi Zhang*(**)(***), Xi Chen*†, Jingtao Liu* and Fengchun Yang****

*The Institute of Hydrogeology and Environmental Geology, Chinese Academy of Geological Sciences, Shijiazhuang 050061, China

**China University of Geosciences, Beijing 100083, China

***Key Laboratory of Groundwater Contamination and Remediation, China Geological Survey & Hebei Province, Shijiazhuang 050061, China

****Northwest University, Xi'an 710027, China

†Corresponding author: Xi Chen; mluzy_3335@163.com

Nat. Env. & Poll. Tech.
Website: www.neptjournal.com

Received: 30-04-2020
Revised: 18-06-2020
Accepted: 16-07-2020

Key Words:
Ketjen Black
Carbon cloth
Electrochemical sensor
Cr(VI)

ABSTRACT

A CB/CCE electrochemical sensor for Cr(VI) detection was prepared by ultrasonic dispersion of Ketjen Black and then the coating of modified carbon cloth electrode. Material morphology and composition were characterized based on XPS, TEM, BET, BJH; electrochemical performance of the electrode was studied based on LSV, EIS and CV. The results show that the high conductivity of Ketjen Black accelerates charge transfer on the electrode surface, while the abundant mesoporous structure and large specific surface area enhance Cr(VI) adsorption and reduction by the electrode. Under the optimal experimental conditions, the relationship between the reduction peak current of Cr(VI) and its concentration in the sample was studied by the i-t method. The reduction peak current intensity and its concentration demonstrate a good linear relationship in the range of 0.025-57μM and 57-483μM. The linear equations are: Ip(μA) = -0.2452C(μM)-0.0303 (R = 0.9908), Ip(μA) = -0.0329C(μM)-15.9212 (R = 0.9853), LOD is 9.88nM (S/N = 3). Compared with other methods, the sensor displays outstanding detection performance advantages. Plus the advantages of low cost and environmental protection, it has good application prospects in detecting Cr(VI) in water.

INTRODUCTION

Cr(VI), as one of the highly toxic ions, means strong carcinogenic risk to the human body (Jin et al. 2016). The increasingly serious Cr(VI) pollution in the water environment has greatly jeopardized water safety and the ecological environment. As an effective detection method for various metal ions, electrochemical detection has been greatly developed in the past decade (Zhang et al. 2014). Various electrode materials such as Au NPs, Ag/TiO_2 NPs/GCE, Fe_3O_4/MoS_2, NiFe/C/GCE have been used for detection of Cr(VI) in water (Ravindran et al. 2012, Zhang et al. 2016, Liu et al. 2017). However, metal nanomaterials feature complicated synthesis process, low stability and physiological toxicity, which limits their application in actual commercialization. Developing a non-metallic material with excellent electrocatalytic activity provides an effective way to overcome these problems (Dehghani et al. 2015). Some carbon nanomaterials with sp^2 hybrid structure, such as graphene (G), conductive carbon black (CB) and single-walled nanotubes (SWNTs), are regarded as the main candidates for non-metallic electrocatalysts. Electrode materials generally have abundant pore structure, numerous defect sites and high specific surface area, which facilitates the electrocatalytic process (Punckt et al. 2014). Recent studies have shown that mesopores (2-50 nm) act on the inner surface as ion transport channels, demonstrating high catalysis and low resistance (Kang et al. 2015). Hence, among the many candidates sp^2 hybrid carbon materials, carbon black with abundant mesopores and surface oxygen-containing functional groups undoubtedly displays a greater advantage.

Ketjen Black is carbon black made by a special process. Due to its stronger conductivity than ordinary conductive carbon black, its small addition will greatly improve battery quality and durability (Zhao et al. 2016). Its application is also common in high-end batteries, supercapacitors and many conductive and shielding materials. Carbon cloth (CC) is a conductive textile, which has received special attention as a flexible substrate due to its high specific surface area, electrical conductivity and chemical stability (Shao et al. 2017). CC features low cost, high resistance to damage, natural abundance and good mechanical properties, which

can greatly reduce the device integration difficulty while meeting the economic and high activity requirements of the sensor. Xu et al. (2017) constructed a new flexible non-enzymatic glucose electrochemical sensor using CC loaded with gold nanoparticles and polyaniline. Hai et al. (2015) used CC modified with NiAl layered double hydroxide for the electrochemical detection of glucose. Barsan (2012) reported that the use of CC modified with carbon nanotubes and nitrogen-doped carbon nanotubes resulted in a powerful biosensor. Although development based on CC electrode enjoys many applications in the medical and biological fields, its use is still relatively rare in the field of environmental detection.

In this study, an electrochemical sensor based on Ketjen black-modified carbon cloth electrode (CB/CCE) was prepared for the determination of Cr(VI) in water. The materials were characterized using X-ray photoelectron spectroscopy (XPS), Brunauer-Emmett-Teller (BET), Barrett-Joyner-Halenda (BJH), and transmission electron microscope (TEM). The electrochemical performance of the electrode was studied using linear sweep voltammetry (LSV), electrochemical impedance spectroscopy (EIS) and cyclic voltammetry (CV). The impact of experimental conditions was analysed, and the current concentration curve was obtained by the current-time method (i-t) to find the detection limit in the linear range. Finally, the electrode was checked for stability and anti-interference performance and successfully used in the detection of Cr(VI) in water samples.

MATERIALS AND METHODS

Reagents and Materials

Ketjen Black EC 300J, N, N-dimethylformamide (DMF) and $K_2Cr_2O_7$ (CP, 99%), graphene (900561-500MG) were procured from Sigma-Aldrich, Shanghai, China; carbon cloth was purchased from China Taiwan Carbon Energy Chemical Co. Ltd.; KCl, $K_3[Fe(CN)_6]$, $K_4[Fe(CN)_6]$, acetone, ethanol were purchased from Xi'an Jingbo Biotechnology Co. Ltd. Except for $K_2Cr_2O_7$, all other chemical reagents and electrochemical measuring reagents are of analytical grade without further purification.

The supporting electrolyte solution was 0.1M H_2SO_4-adjusted 0.1M Na_2SO_4 solution (pH=4.0); the analysis of electrochemical impedance chart was carried out in 0.1M KCl solution containing 5mM $[Fe(CN)_6]^{3-/4-}$. The solution was prepared using deionized water (18.3MΩ·cm) produced by the Millipore water purification system.

Electrode Modification

Before the experiment, the bare carbon cloth electrode was ultrasonically cleaned in acetone, ethanol, and secondary water for 15 minutes each, dried in a vacuum oven, and then cut into a small rectangle with a size of 1.0cm × 2.0cm for use. 1mg weighed Ketjen black nanoparticle sample was dispersed in 1 mL DMF solution, first undergoing ultrasonic dispersion in a low-frequency ultrasonic cleaner, and then sonication under a high-frequency ultrasonic instrument until ink-like Ketjen black dispersion liquid was formed, which was then evenly coated on the carbon cloth surface and baked under an infrared lamp to complete the modification.

Electrochemical Research

The composition of Ketjen black was analysed using XPS (ThermoFisher EscaLab 250Xi X-ray photoelectron spectrometer, USA), and its specific surface area and pore width were calculated using BET and BJH (Beishide 3H-2000PS1 static nitrogen adsorption specific area analyser, Beijing, China). Before measurement of N_2 adsorption isotherm, all test materials were degassed at 423 k for 12 hours. Morphology of the material was observed by TEM (transmission electron microscope FEI Tecnai G2 F30, USA).

All electrochemical measurement tools were provided by an electrochemical workstation (Chenhua CHI 660D, Shanghai, China). A conventional three-electrode system was used, including a carbon cloth electrode (1.0cm×2.0cm) as the working electrode, an Ag/AgCl electrode (saturated KCl) as the reference electrode, and a platinum wire as the auxiliary electrode.

Electrochemical impedance spectroscopy EIS was performed in the buffer under the same three-electrode configuration with a frequency range of 0.1~100000Hz and an AC probe amplitude of 50mV. Linear scanning voltammetry was carried out in Na_2SO_4 electrolyte solution at a sweep speed of $50mV \cdot s^{-1}$ and a scanning potential of -0.6~0.6V. The current-time method was performed in an electrolyte solution with a constant voltage of 0.1V and a pH of 4.0. Trace amount of Cr(VI) solution with fixed concentration was dropped into the magnetically stirred electrolyte solution every 50s. Record the i-t curve showing response current change with Cr(VI) concentration. All experiments were conducted at room temperature in the laboratory.

RESULTS AND DISCUSSION

Characterization of Materials

As shown in Fig. 1A, XPS analysis results clearly show that Ketjen Black is mainly composed of C and a small amount of O. Fig. 1B shows the C 1s peak of Ketjen Black, whose characteristic peaks are 284.6eV and 285.4eV, respectively, corresponding to C-C and C-O (Contarini et al. 1991). It

indicates that Ketjen Black almost has no heteroatoms and displays typical non-metallic properties.

Fig. 1 C and D are TEM images of Ketjen Black, which reflect its porous structure and pore size. There are various types of mesopores with different sizes and irregular shapes. The special porosity characteristics carry great significance for rapid charge transfer and accelerated reaction based on efficient use of internal structure.

In this study, Ketjen black was compared with other carbon nanomaterials graphene and single-walled carbon nanotubes in sp^2 hybrid orbital structure. Specific surface area and pore size distribution of the material were characterized by N_2 adsorption/desorption isotherm measurements. Fig. 2A shows different N_2 adsorption/desorption stages with linear single-layer/multi-layer adsorption properties, and hysteresis curves at relatively high pressures. The hysteresis loop has a relation with the capillary condensation process in the mesopore (Carrott et al. 1987). Compared to graphene and single-walled carbon nanotubes, Ketjen Black's Type IV isotherms exhibit a greater hysteresis loop, indicating the presence of more abundant mesopores (Liu et al. 2016). At the same time, under the relative pressure of 0.8~1.0, obvious macroporous absorption is shown on the Ketjen black surface. In addition, the Ketjen black pore size measured by the BJH method has a narrow mesopore

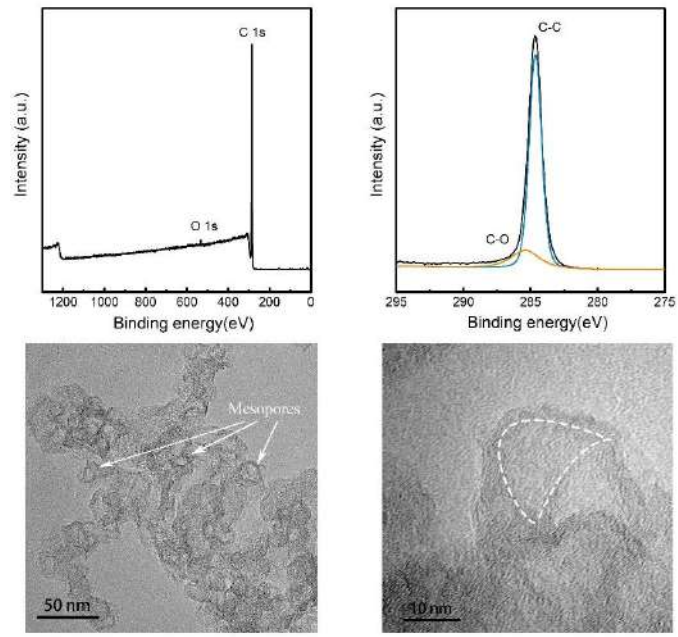

Fig. 1: (A)XPS analysis of CB. (B)High-resolution XPS analysis of the C 1s peak of CB. TEM characterizations of CB porous structure and size. Scale bars: 50nm (C); 10nm (D).

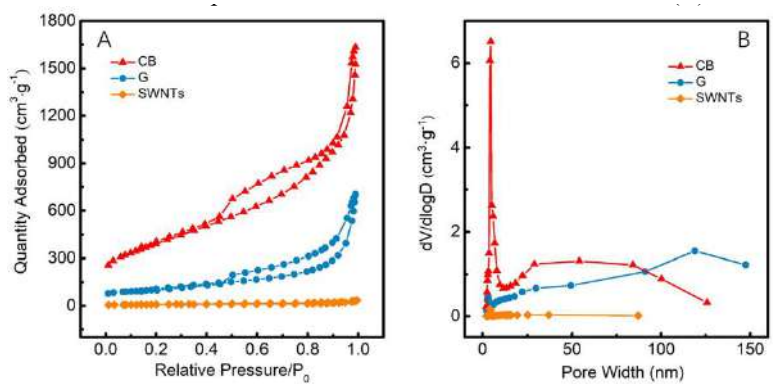

Fig. 2: Nitrogen adsorption-desorption isotherms (A) and pore size distribution by BJH method using the adsorption branch of isotherm (B) of CB, G and SWNTs.

Table 1: The surface area, pore volume and average pore diameter parameters of SWNTs, G and CB measured by the BET and BJH methods

Sample	BET Surface area ($m^2 \cdot g^{-1}$)	Total pore volume ($cm^3 \cdot g^{-1}$)	Average pore diameter (nm)
SWNTs	26.09	0.0403	6.17
G	328.69	0.8060	9.81
CB	1333.52	1.8528	5.56

distribution at around 5.56 nm (Fig. 2B), which facilitates the entry of accessible hydrated Cr(VI) into inner and outer pore surfaces during the rapid charge and discharge process.

Using BET and BJH methods, the relevant parameters of Ketjen Black are derived as given in Table 1. It shows that Ketjen Black has the largest specific surface area of $1333.52 m^2 \cdot g^{-1}$, the largest total pore volume of $1.8528 cm^3 \cdot g^{-1}$, and the smallest average pore size of 5.56nm. Specific surface area, pore size distribution and TEM images jointly prove that Ketjen Black has a rich mesoporous structure to provide an effective charge transfer channel for Cr(VI).

Electrochemical Performance of the Electrode

Fig. 3A shows the EIS diagram of CCE and modified CB/CCE in 5mM $[Fe(CN)_6]^{3-/4-}$ in 0.1M KCl. CB/CCE has a smaller semicircle diameter than CCE, indicating that CB/CCE has fast electron migration and great interface electron transfer between solution and interface material, which facilitates oxidation-reduction of iron ions on the working electrode while reducing the resistance value. CCE with great semicircle can promote oxidation-reduction of electrochemical probe iron, but with slow electron transfer. Ketjen Black with abundant mesoporous structures and the high surface area provides more active sites for the electrode reaction while improving the conductivity of the working electrode, facilitating charge transfer within the material, and accelerating charge transfer on the electrode surface, thus basically guaranteeing high sensitivity in Cr(VI) measurement.

To more directly investigate the increase in Ketjen Black electron migration rate, reduction peaks of CCE and CB/CCE were comparatively analysed by LSV. As shown in Fig. 3B, CCE has no obvious reduction peak in the range of -0.6~0.6V, while CB/CCB has a clear electrochemical reduction peak against Cr(VI) at a voltage of about 0.1V, indicating that CB has obvious electronic transfer.

CB on CCE played a significant catalytic role in the reduction of Cr(VI), demonstrating excellent electron conductivity. This is because CB with strong conductivity and great ion landing area has a strong absorption capacity against Cr(VI). The above results are consistent with EIS analysis conclusions, both indicating that the electrode surface with rich active sites and specific surface area can absorb and reduce Cr(VI) in large amounts. Hence, Ketjen Black displays outstanding performance in catalysing Cr(VI) and can significantly enhance the reduction of current strength against Cr(VI).

LSV was used to record the peak current response of the electrode during Cr(VI) concentration change from 1mM to 5mM. Fig. 4A shows that the reduction peak current increases with the increasing Cr(VI) concentration, exhibiting a good linear relationship. The linear regression equation is $I_p(\mu A) = -0.04826C(\mu M)-14.35$ ($R = 0.9987$) (Fig. 4B). Where, I_p represents the reduction peak current, and C represents Cr(VI) concentration. It also indicates Ketjen Black's excellent ability in reducing Cr(VI). Fig. 4C shows the logarithmic relationship between reduction peak current and peak voltage under different Cr(VI) concentrations. For a concentration as low as 1 mM, the peak current value and the peak voltage value remain almost unchanged at 0.11V. When the concentration varies between 1~5mM, a linear relation is shown between the logarithm of peak current and that of the peak voltage. In the reversible reaction, it is possible to predict the peak voltage value and electrolyte solution concentration in the experiment based on the above linear electrochemical

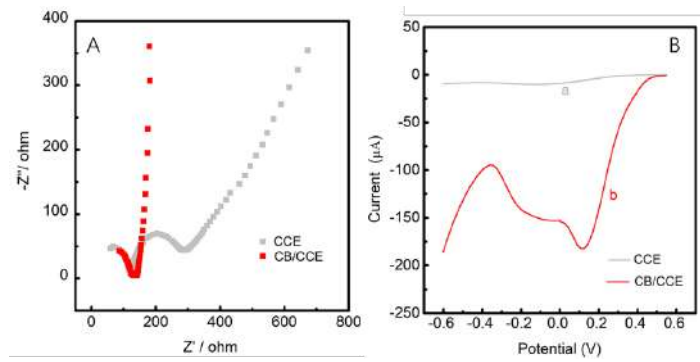

Fig. 3: (A) EIS of CCE and CB/CCE in a solution of 5mM $[Fe(CN)_6]^{3-/4-}$ in 0.1M KCl. (B) CCE(a) and CB/CCE(b) in 0.1M Na_2SO_4 (pH=4.0) of 5mM Cr(VI), Scan rate: $50 mVs^{-1}$.

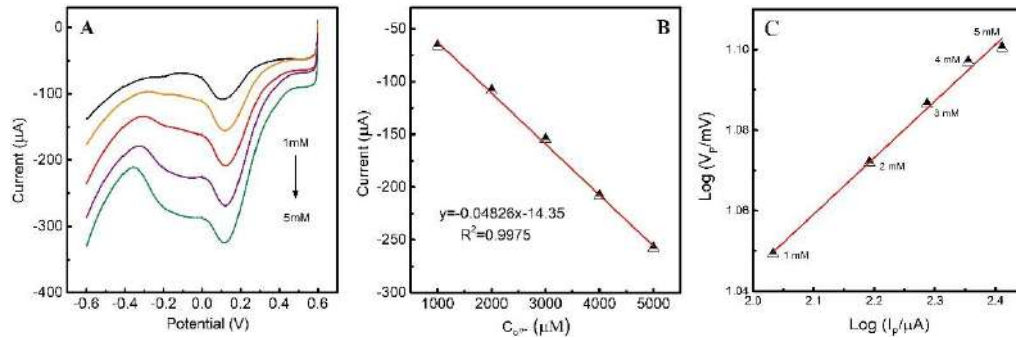

Fig. 4: (A) CV of Cr(VI) at Carbon black modified electrode in 0.1M Na_2SO_4 (pH = 4.0) when Cr(VI) concentrations are from 1mM to 5mM; (B) The plot of Ip versus Cr(VI) concentration; (C) Log(Vp/mV) vs Log(Ip/μA) for different concentration Cr(VI) .

model. If this model is not established, the reaction is an irreversible process. Hence, the electrode reaction here is a reversible process.

Fig. 5A shows that when the potential is set to -0.2~0.8V, changes in redox peak current in the test solution can be studied by changing sweep speeds so that kinetic properties can be analysed. As can be seen, redox has an increased response to current as the sweep speed increases from 10mV·s^{-1} to 130mV·s^{-1}, suggesting that CB/CCE has a good ability to reverse oxidation-reduction of iron ions. The peak current value in Fig. 5B has a good linear relationship with the square root of the sweep speed, and the corresponding peak current is proportional to the square root of the sweep speed. This indicates that an electrochemical process controlled by diffusion occurs on the modified electrode.

In this experiment, LSV was used to investigate the electrochemical behaviour of CB/CCE in the electrolyte solution with pH = 1.0~6.0. Fig. 6A shows the response of modified electrode to the electrochemical reduction current of 5mM Cr(VI) under different pH values. Obviously, in the voltage range of -0.6~0.6V, the electrochemical reduction current peak value of Cr(VI) increases as the pH value

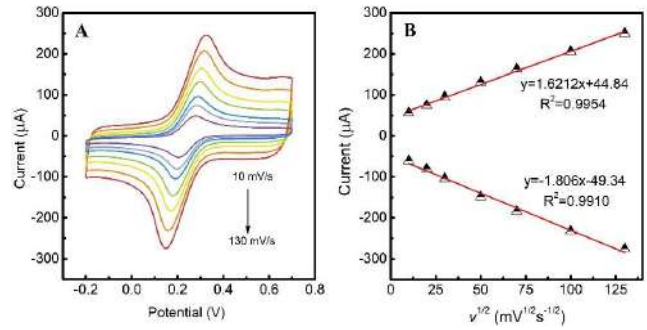

Fig. 5: (A) CVs of carbon black modified electrode in 0.1M Na_2SO_4 (pH = 4.0) with 0.5mM Cr(VI) at different scan rates of 10, 20, 30, 50, 70, 100, 130mVs^{-1}. (B) The plot of peak current versus the square root of scan rate.

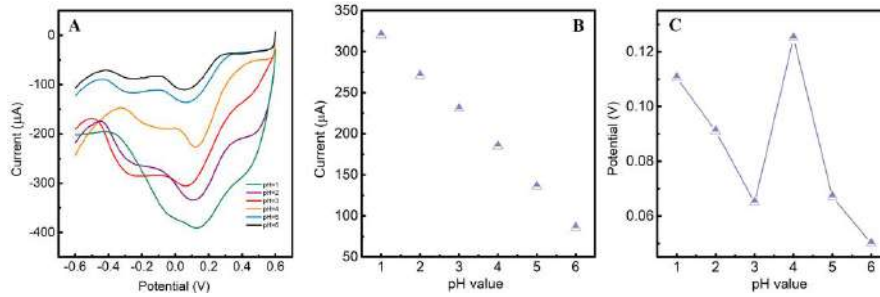

Fig. 6: (A) The current response of 5.0 mM Cr(VI) of different solution pH values; (B) The plot of current response for 5.0 mM Cr(VI) with the influence of solution pH; (C) the effect of potentials and pH value.

decreases. At low pH, Cr(VI) mainly exists in the form of $HCrO_4^-$. The electrostatic interaction between $HCrO_4^-$ and CB surface-functionalized with H^+ will facilitate Cr(VI) ion adsorption by CB in an acidic medium. Fig. 6B shows a significantly increased reduction current of Cr(VI) with increasing acidity. Fig. 6C reflects that in the corresponding relationship between the peak potential and different pH values, electrolyte solution with a pH value of 4.0 has the most positive potential when detecting Cr(VI).

Due to the extremely high H^+ conductivity in transferring electrons through hydrogen bonds, when the H^+ exponent in the solution increases exponentially, electrolyte solution has redoubled electron migration rate, so that Cr(VI) (0~0.2V) and Cr(III) (-0.1~0.3V) peaks continuously expand. At the same time, with the increasing acidity, a large reduction peak also appears at 0.4~0.6V. It is speculated that excessive Cr(VI) adsorbed on the Ketjen black material at the same time results in great changes in material structure and its electron transfer capacity so that saturation peak appears. When the solution has excessive acidity, the two impurity peaks even block the reduction peak of Cr(VI), making trace detection of Cr(VI) impossible. In view of the above reasons, it was finally decided to select pH 4.0 as the most appropriate pH value for Cr(VI) detection.

Linear Range and Detection Limit

The linear range of Cr(VI) detection by electrodes was studied by the i-t method. First, fix the potential at 0.12V, and add a certain amount of Cr(VI) in 40 mL electrolyte solution (pH=4.0) every 50 s, then record the response curve of current over time, as shown in Fig. 7A. The mosaic reveals that the current shows a clear response at the addition of the first drop of 0.025 μM Cr(VI). At the same time, the detection limit (LOD) is calculated to be 9.88 nM, S/N = 3 according to the calculation formula: LOD = $3S_y/m$. Where S_y is the standard deviation and m is the slope of the calibration curve.

Fig. 7B shows the calibration curve about the relationship between the current response of CB/CCE and Cr(VI) concentration. There is a good linear relationship between the two, and the two equations of linear regressions between the peak current value and Cr(VI) concentration are as follows:

$$Ip(\mu A) = -0.2452C(\mu M) - 0.0303 \quad (R=0.9908),\ (0.025\sim57\mu M) \qquad \ldots(1)$$

$$Ip(\mu A) = -0.0329C(\mu M) - 15.9212 \quad (R=0.9853),\ (57\sim483\mu M) \qquad \ldots(2)$$

The linear response range is 0.025~483 μM. Sensitivity calculated based on low concentration range is 0.25 $\mu A \mu M^{-1} \cdot cm^{-2}$. The good linear relationship also reflects the accurate and sensitive ability of CB/CCE in detecting Cr(VI). The two-stage linear phenomenon may be a result of the two electrochemical processes of diffusion and adsorption during the reaction. In the diffusion process, the current increases with the increasing concentration, while in the adsorption process, excessive molecules completely occupy the material, resulting in reduced removal efficiency. At the end of the reaction, the oxide is adsorbed on the electrode, reducing the effective area of the electrode and leading to lower resulting sensitivity.

Table 2 lists the comparison of Cr(VI) detection performance of sensors built herein and by other modified materials. It suggests that the electrode has a lower detection limit and a wider linear range.

Stability and Anti-Interference

First, electrode reproducibility was studied by current measurement. A total of 4 evaluations were performed,

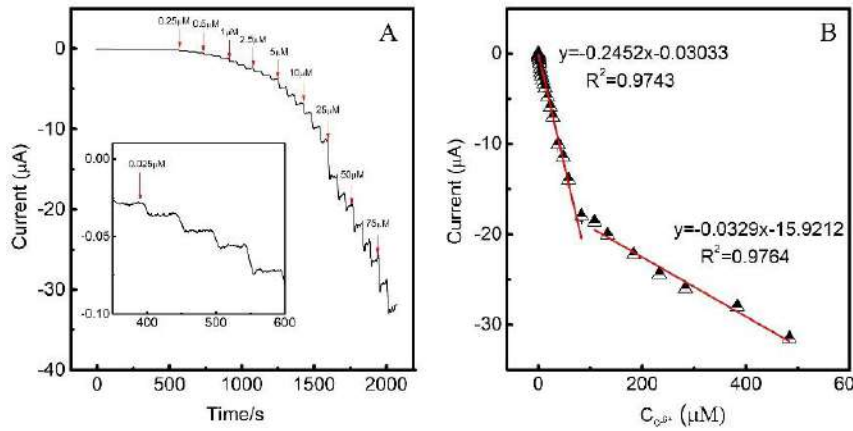

Fig. 7: (A) Various concentrations of Cr(VI) from 0.025 to 483μM in 0.1M Na_2SO_4 (pH = 4.0) at an applied potential of 0.12V. The lower concentrations were showed in the inset.(B) The calibration curve between the current and the concentration of Cr(VI).

Table 2: Comparison of quality parameters between Cr(VI) sensors developed in different literatures.

Electrode/surface	pH	Linear range (μM)	LOD (nM)	Reference
Ag/TiO_2 NPs/GCE	1.0	0.01~3.1	10	(Ravishankar et al. 2015)
Fe_3O_4/MoS_2	1.0	0.5~328	200	(Zhang et al. 2016)
NiFe/C/GCE	4.0	0.025~98.3	10	(Liu et al. 2017)
LMB/MB	2.0	10~500	100	(Sadeghi & Garmroodi 2013)
MWCNTs-SPCE	1.0	1~200	300	(Korshoj et al. 2015)
SPEs	1.0	3~10000	1000	(Miscoria et al. 2014)
PANI/GQDs	1.0	1.92~192	1865	(Punrat et al. 2016)
Ti/TiO_2NT/Au	1.0	0.1~105	30	(Jin et al. 2014)
Activated GCE	6.0	0.4~250	100	(Richtera et al. 2016)
BDD	1.0	0.192~96	57.7	(Fierro et al. 2012)
GCE/NF/Ag nano	2.0	0.38~4.42	12	(Xing et al. 2011)
Gold plated carbon	0.5	0.385~38.462	85	(Kachoosangi & Compton 2013)
PVC/POT/GCE	2.0	0.03~1.3	12	(Izadyar et al. 2016)
CB/CCE	4.0	0.025~483.2	9.88	This work

and the relative RSD was about 4.3% in the 4 test results, showing good test reproducibility. At the same time, before Cr(VI) addition, the current curves were static and balanced, demonstrating high electrode stability. According to the current response of the electrode towards 5 mM Cr(VI) for 7 consecutive days, the current response signal is 88% of the initial after 7 days, indicating good stability of the electrode.

Cr(VI) detection performance of the electrode was studied using the i-t method in the presence of common coexisting ions. First, Cr(VI) with a concentration of 10μM was added to 0.1M Na_2SO_4 (pH 4.0) solution. Afterwards, 1.0mM interfering ions K^+, Zn^{2+}, Mg^{2+}, Cu^{2+}, Ca^{2+}, Ni^{2+}, Fe^{2+}, Mn^{2+}, Pb^{2+}, Cl^- and SO_4^{2-} were added in succession. Finally, 10μM Cr(VI) was added. Fig. 8 indicates that the 10μM Cr(VI) added successively produces a current response of about 2μA, and the measurement current has insignificant changes after the addition of all interfering ions. That is, the fluctuation of interfering ions is extremely weak compared to Cr(VI). It suggests that the electrode still has extraordinary Cr(VI) detection performance in the presence of high-concentration interfering ions.

Sample Testing

To evaluate the performance of the built Cr(VI) electrochemical sensor in practical applications, real water samples were tested. The water sample was taken from a sewage outfall in an industrial park in Xi'an, China. After the sample filtration using a 0.45μm filter membrane, the pH value was adjusted to 4.0 using a buffer solution. Samples were detected by the "standard addition method", and ICP-AES test results were compared, as given in Table 3. It reveals that in real water sample detection, the sensor has a small relative standard deviation (2.3%~3.4%), a high recovery rate (98%~103%), and detection result consistent with ICP-AES, demonstrating the reliability of the sensor in actual detection.

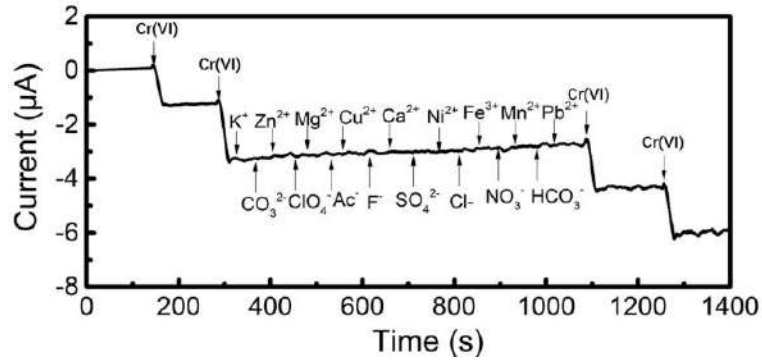

Fig. 8: Interference test of the sensor in 0.1M Na_2SO_4 (pH = 4.0) at 0.12V with 10μM Cr(VI) and 1.0mM other interferents as indicated

Table 3: Determination of Cr(VI) in the water sample using the standard addition method.

Sample	Added (μM)	Found (μM)	Determined (μM)	Recover (%)	RSD (n=3, %)	ICP-AES (μM)
1	10	10.57	0.58	98	3.1	0.57
	20	20.57		99	3.0	
	30	30.57		98	3.4	
2	10	11.08	1.06	102	2.6	1.02
	20	21.07		101	2.7	
	30	31.07		101	2.3	
3	10	12.63	5.47	103	3.0	5.48
	20	22.60		102	3.2	
	30	32.52		101	3.4	

CONCLUSION

A CB/CCE electrochemical sensor for Cr(VI) detection was prepared by ultrasonic dispersion of Ketjen Black and then a coating of modified carbon cloth electrode. The high conductivity of Ketjen Black accelerates the charge transfer on the electrode surface, and the abundant mesoporous structure and large specific surface area enhance Cr(VI) adsorption and reduction by the electrode. Under the optimal conditions, the linear range of Cr(VI) was determined to be 0.025~483μM using the i-t method, with two-step linear regression equations being Ip(μA) = -0.2452C(μM)-0.0303 (R = 0.9908), I_p(μA) = -0.0329C(μM)-15.9212 (R = 0.9853), and LOD is 9.88 nM, S/N = 3. The sensitivity was 0.25 μA $\mu M^{-1} \cdot cm^{-2}$ under the low concentration range. The sensor has been successfully used for testing Cr(VI) in actual water samples. In contrast with previous research reports, Ketjen black modified electrode not only has better ability in detecting Cr(VI) than other metal nanoparticle modified electrodes but also has microscopic advantages like abundant adsorption specific surface area, as well as macroscopic advantages of environmental protection, low cost and easy availability. At the same time, flexible carbon cloth substrate with low cost and high resistance to damage favours use in fieldwork.

ACKNOWLEDGEMENTS

The study was financially supported by projects of the China Geological Survey (No. DD20160308 and No. DD20190331).

REFERENCES

Barsan, M. M., Carvalho, R. C., Zhong, Y., Sun, X. and Brett, C. M. 2012. Carbon nanotube modified carbon cloth electrodes: Characterisation and application as biosensors. Electrochim. Acta, 85: 203-209.

Carrott, P., Roberts, R. A. and Sing, K. 1987. Adsorption of nitrogen by porous and non-porous carbons. Carbon, 25(1): 59-68.

Contarini, S., Howlett, S. P., Rizzo, C. and De Angelis, B. A. 1991. XPS study on the dispersion of carbon additives in silicon carbide powders. Appl. Surf. Sci., 51(3-4): 177-183.

Dehghani, M. H., Taher, M. M., Bajpai, A. K., Heibati, B., Tyagi, I., Asif, M., Agarwal, S. and Gupta, V. K. 2015. Removal of noxious Cr (VI) ions using single-walled carbon nanotubes and multi-walled carbon nanotubes. Chem. Eng. J., 279: 344-352.

Fierro, S., Watanabe, T., Akai, K. and Einaga, Y. 2012. Highly sensitive detection of Cr^{6+} on boron doped diamond electrodes. Electrochim. Acta, 82: 9-11.

Hai, B. and Zou, Y. 2015. Carbon cloth supported NiAl-layered double hydroxides for flexible application and highly sensitive electrochemical sensors. Sensor. Actuat. B-Chem., 208: 143-150.

Izadyar, A., Al-Amoody, F. and Arachchige, D. R. 2016. Ion transfer stripping voltammetry to detect nanomolar concentrations of Cr (VI) in drinking water. J. Electroanal. Chem., 782: 43-49.

Jin, W., Du, H., Zheng, S. and Zhang, Y. 2016. Electrochemical processes for the environmental remediation of toxic Cr (VI): A review. Electrochim. Acta, 191: 1044-1055.

Jin, W., Wu, G. and Chen, A. 2014. Sensitive and selective electrochemical detection of chromium (VI) based on gold nanoparticle-decorated titania nanotube arrays. Analyst, 139(1): 235-241.

Kachoosangi, R. T. and Compton, R. G. 2013. Voltammetric determination of Chromium (VI) using a gold film modified carbon composite electrode. Sensor. Actuat. B-Chem., 178: 555-562.

Kang, D., Liu, Q., Gu, J., Su, Y., Zhang, W. and Zhang, D. 2015. "Egg-Box"-assisted fabrication of porous carbon with small mesopores for high-rate electric double layer capacitors. ACS Nano, 9(11): 11225-11233.

Korshoj, L. E., Zaitouna, A. J. and Lai, R. Y. 2015. Methylene blue-mediated electrocatalytic detection of hexavalent chromium. Anal. Chem., 87(5): 2560-2564.

Liu, J., Ding, Y., Ji, L., Zhang, X., Yang, F., Wang, J. and Kang, W. 2017. Highly sensitive detection of Cr (VI) in groundwater by bimetallic NiFe nanoparticles. Anal. Methods-UK, 9(6): 1031-1037.

Liu, Y., Shi, Z., Gao, Y., An, W., Cao, Z. and Liu, J. 2016. Biomass-swelling assisted synthesis of hierarchical porous carbon fibers for supercapacitor electrodes. ACS Appl. Mater. Inter., 8(42): 28283-28290.

Miscoria, S. A., Jacq, C., Maeder, T. and Negri, R. M. 2014. Screen-printed electrodes for electroanalytical sensing, of chromium VI in strong acid media. Sensor. Actuat. B-Chem., 195: 294-302.

Punckt, C., Pope, M. A. and Aksay, I. A. 2014. High selectivity of porous graphene electrodes solely due to transport and pore depletion effects. J. Phys. Chem. C, 118(39): 22635-22642.

Punrat, E., Maksuk, C., Chuanuwatanakul, S., Wonsawat, W. and Chailapakul, O. 2016. Polyaniline/graphene quantum dot-modified screen-printed carbon electrode for the rapid determination of Cr(VI) using stopped-flow analysis coupled with voltammetric technique. Talanta, 150: 198-205.

Ravindran, A., Elavarasi, M., Prathna, T. C., Raichur, A. M., Chandrasekaran, N. and Mukherjee, A. 2012. Selective colorimetric detection of nanomolar Cr (VI) in aqueous solutions using unmodified silver nanoparticles. Sensor. Actuat. B-Chem., 166: 365-371.

Ravishankar, T. N., Muralikrishna, S., Nagaraju, G. and Ramakrishnappa, T. 2015. Electrochemical detection and photochemical detoxification of hexavalent chromium (Cr (VI)) by Ag doped TiO_2 nanoparticles. Anal. Methods-UK, 7(8): 3493-3499.

Richtera, L., Nguyen, H. V., Hynek, D., Kudr, J. and Adam, V. 2016. Electrochemical speciation analysis for simultaneous determination of Cr(III) and Cr(VI) using an activated glassy carbon electrode. Analyst, 141(19): 5577-5585.

Sadeghi, S. and Garmroodi, A. 2013. A highly sensitive and selective electrochemical sensor for determination of Cr(VI) in the presence of Cr(III) using modified multi-walled carbon nanotubes/quercetin screen-printed electrode. Mat. Sci. Eng. C-Mater, 33(8): 4972-4977.

Shao, X., Zheng, X., Zou, W., Luo, Y., Cen, Q., Ye, Q., Xu, X. and Wang, F. 2017. Alkali conversion of Ni-Co nanoarrays on carbon cloth for a high-capacity supercapacitor electrode. Electrochim. Acta, 248: 322-332.

Xing, S., Xu, H., Chen, J., Shi, G. and Jin, L. 2011. Nafion stabilized silver nanoparticles modified electrode and its application to Cr(VI) detection. J. Electroanal. Chem., 652(1-2): 60-65.

Xu, M., Song, Y., Ye, Y., Gong, C., Shen, Y., Wang, L. and Wang, L. 2017. A novel flexible electrochemical glucose sensor based on gold nanoparticles/polyaniline arrays/carbon cloth electrode. Sensor. Actuat. B-Chem, 252: 1187-1193.

Zhang, X., Yu, S., He, W., Uyama, H., Xie, Q., Zhang, L. and Yang, F. 2014. Electrochemical sensor based on carbon-supported $NiCoO_2$ nanoparticles for selective detection of ascorbic acid. Biosens. Bioelectron., 55: 446-451.

Zhang, Y., Chen, P., Wen, F., Yuan, B. and Wang, H. 2016. Fe_3O_4 nanospheres on MoS_2 nanoflake: Electrocatalysis and detection of Cr(VI) and nitrite. J. Electroanal. Chem., 761: 14-20.

Zhao, D., Qian, X., Jin, L., Yang, X., Wang, S., Shen, X., Yao, S., Rao, D., Zhou, Y. and Xi, X. 2016. Separator modified by Ketjen black for enhanced electrochemical performance of lithium-sulfur batteries. RSC Adv., 6(17): 13680-13685.

Nature Environment and Pollution Technology
An International Quarterly Scientific Journal

p-ISSN: 0972-6268
(Print copies up to 2016)
e-ISSN: 2395-3454

Vol. 20 | No. 2 | pp. 785-791 | 2021

Original Research Paper

https://doi.org/10.46488/NEPT.2021.v20i02.040

Open Access Journal

Vulnerability Measurement of Groundwater Inrush Channel in Mining Areas and Environmental Governance Measures – A Case Study on Taoshan Mine, China

Wei Xiao Gang*(**), Dai Jun Wu*, Li Guang Hui†, Hu Zhi Kai*** and Qin Sai*****

*Key Laboratory of Earthquake Engineering and Engineering Vibration, Institute of Engineering Mechanics, China Earthquake Administration, Harbin 150080, China

**College of Civil Engineering and Architecture, Zhengzhou University of Aeronautics, Zhengzhou 450046, China

***Kexing Construction Engineering Group Co., Ltd., Zhengzhou 450046, Henan, China

†Corresponding author: Li Guang Hui: 15136136550@163.com

Nat. Env. & Poll. Tech.
Website: www.neptjournal.com

Received: 05-03-2021
Revised: 31-03-2021
Accepted: 05-04-2021

Key Words:
Underground coal mines
Water inrush channel
Vulnerability measurement
Environmental governance
Taoshan mine

ABSTRACT

The unrestricted resource behaviour of mines has caused considerable geological environmental problems. Specifically, the increasing water-induced accidents in mines affect safety production and environmental safety in coal mines. To further decrease water inrush disasters to the maximum extent, vulnerability assessment of groundwater inrush channel in coal mines has become a primary problem of chain-cutting disaster mitigation. In this study, first, influencing factors against formation and project of water inrush channel in coals were analyzed comprehensively. Second, 14 indexes, which influence the vulnerability of the water inrush channel, were selected from three perspectives of coal seam features, coal quality features, and hydrogeological features. A case study based on data of 56# coal seam and 68 coal seam of Taoshan Mine, China was carried out. The vulnerability of the groundwater inrush channel in the Taoshan Mine was estimated by analytic hierarchy process (AHP) and fuzzy comprehensive evaluation. Results demonstrate that coal quality features, hydrogeological features, and coal seam features are major factors that influence the vulnerability of the water inrush channel. Among them, coal quality features contribute 48.36% of explanations to the vulnerability of the water inrush channel. According to the vulnerability grade evaluation results of fuzzy mathematics, the membership degree of belonging to "III" was 0.3731, which was the highest. This finding indicates that the vulnerability of the water inrush channel in Taoshan Mine belongs to grade III, which is a moderate state. Research conclusions have important references to perfect the evaluation index system for the vulnerability of water inrush channel in coal mines, provide early warning analysis of water inrush disasters in coal mines, and realize the mining–environmental protection coordinated development.

INTRODUCTION

China has tremendous coal mines. The ecological environment in coal mines is damaged seriously. Geological environmental protection and governance of coal mines are a large system project, which is characterized by a long period, large task, and complicated problems. Thus far, China has not issued a perfect geological environmental governance system of coal mines, divided the geological environmental protection and governance in coal mines clearly, and released relevant technological standards at an appropriate time. The geological environmental protection and governance of coal mines still cannot be balanced. With the long-term development of coal resources, excessive mining phenomena occur, thereby causing a series of environmental and geological problems, such as water and soil pollution, land resource damages, geomorphologic landscape damages, and collapse of water inrush channel. Recently, China has never stopped evaluations on the geological environmental impacts of coal mines. Systematic evaluations of geological environmental problems of coal mines by introducing scientific and reasonable evaluation systems can not only provide technical support to management planning of coal mines and solve environmental problems in coal mines but also are one of the important topics of modern environmental geological studies.

In particular, water inrush accidents in coal mines have been increasing continuously. To realize essential safety and decrease disasters to the maximum extent, studying water diversion structures of the disaster causing ring in the coal disaster chain has become a primary problem to chain-cutting disaster mitigation. With the increase in exploitations in complicated and difficult-to-mine coal bodies, the underground hydrogeological conditions become more complicated. Traditional flooding disaster control technology of coal mines cannot adapt to new exploitation environment and deviate from the engineering practices. New detection technology and method are necessary. The vulnerability of water inrush channel of coal mines refers to the possibility of disaster activation of the geological

physical environment and engineering response features of water diversion structures in strata when the water inrush channel is used as the carrier and mining face approaches the underground water source as well as the difficulties of system recovery after the disaster. An evaluation index system for the vulnerability of water inrush channel in coal mines was established. The higher vulnerability grade indicates that disasters can easily occur in coal mines, and specific defence measures are required.

PAST STUDIES

Studies on the vulnerability of water inrush channel in coal mines are relatively weak. In engineering practices, the concept of vulnerability assessment is introduced for rapid, reliable, and comprehensive detection of water inrush channel. Vulnerability, as an important index to measure risk performance, characterizes the ability of the system to resist disasters and maintain stability, including adaptability, risks, and restorability. Janssen et al. (2006) introduced the relevant concept of environmental vulnerability in the global environment changes for groundwater vulnerability, the vulnerability of water inrush channel in coal mines and comprehensive environmental governance in coal mines. Wu et al. (2008) believed that in Northern China, coal exploitation was often influenced by groundwater inrush from underground karst aquifer, established a geographical information system (GIS) for water inrush vulnerability evaluation, and determined weight coefficients of different influencing factors by using the artificial neural network. Qiang et al. (2009) believed that water inrush was a geological disaster that influenced coal mine safety production in China seriously. Based on powerful spatial data analysis functions of GIS, they established a neural network model of water inrush risk assessment and carried out a case study by using the water inrush vulnerability index histogram. Rupert (2010) corrected the point rating scheme based on practical groundwater quality data to improve the validity of the underground water vulnerability map significantly by using the parameter statistical technology and geological information system. Qiang et al. (2011) pointed out that water inrush from seam floor was a complicated nonlinear phenomenon, and it was controlled by various factors. In addition, a case study based on data of three coal seams in Tashan Mine, China was carried out using the vulnerability index method of GIS. Research results demonstrated that the vulnerability index method of GIS had many potential advantages in evaluating the possibilities of water inrush. Fijani et al. (2013) proposed a model based on artificial intelligence to improve the groundwater vulnerability evaluation method of the aquifer in Maragheh–Bonab Plain, Iran. Qiang et al. (2013) believed that water inrush disasters influenced the safety production of many coal mines in China, explored influencing factors of water inrush by AHP, established a vulnerable index histogram, and proposed control measures to each risk grade. Based on the south region of Perak, Malaysia, Mogaji et al. discussed the groundwater vulnerability prediction model by using the ordered weighted average DRASTIC (The term "DRASTIC" stands for seven parameters in the model which are depth to groundwater table (D), net recharge (R), aquifer media (A), soil media (S), topography (T), impact of vadose zone (I), and hydraulic conductivity (C) method of GIS (Mogaji et al. 2014). Xiao et al. (2014) estimated water inrush evaluation of seam floor in 9# coal seams of Shanxi Liulin Hongsheng Jude Coal Industry Co. Ltd. through the vulnerability index analysis. They compared the evaluation results with the results of the traditional water inrush coefficient evaluation technique. The results demonstrated that the vulnerability index method, which considered various factors, was more advantageous. Liu et al. (2014) proposed an AHP vulnerability index method based on GIS to evaluate the water inrush phenomenon of many aquifers in seam floor under complicated hydrological conditions and used it to evaluate the water inrush vulnerability of aquifers in a coal mine. The results demonstrated that the proposed method solved the water inrush indication problem of seam floor under complicated hydrogeological conditions. Li et al. (2014) established a vulnerability index model of water inrush channel of coal mines according to the coupling theory of GIS and AHP, evaluated the probability of water inrush in major minable seam roof and floors of the well field, and proposed suggestions for safety production and water disaster control. Abdullah et al. (2015) designed the groundwater pollution vulnerability diagram by using the standard DRASTIC method and applied the linear structural density diagram into the standard DRASTIC model to assure the accuracy of effects of potential pollution vulnerability. Wu et al. (2015) evaluated the water inrush vulnerability of aquifer in Mengkeqing Mine, predicted mine inflow under natural conditions and mining conditions, and proposed corresponding control measures. Li et al. (2016) evaluated water inrush risk in mines by hydrochemical method and evaluated water inrush risk by analyzing concentrations of conservation ions through detailed hydrochemical investigation and sampling. Wu, Qiang et al. (2017) believed that hydraulic pressure and water yield of the aquifer, equivalent thickness of the water-resistant layer, and geological structural property are the main factors to control water inrush; they evaluated water inrush risks by vulnerability index (VI) method by combining GIS and AHP. Based on existing studies, the vulnerability of the water inrush channel of coal mines is developed and perfected with the comprehensive environmental governance of coal mines gradually. The

possibility of disaster activation of the geological physical environment and engineering response characteristics of water diversion structure in rock strata as well as difficulties of system recovery after a disaster are influencing factors of vulnerability of water inrush channel in coal mines. Hence, an index system for the vulnerability of water inrush channel in coal mines was set up by combining the development law of water inrush channel, incidence on the underground project after disasters, and difficulties in governance technology. This index system was used to evaluate the vulnerability grade of the water inrush channel, and some specific defence measures were adopted. These concepts have extremely important effects on guaranteeing safe production and realizing environmental protection of coal mines. The vulnerability of the water inrush channel of coal mines was assessed based on existing studies. Evaluation indexes of the vulnerability of water inrush channel in coal mines were determined, and an index system was constructed. The weights of influencing factors were concluded by AHP, and vulnerability grade was judged by combining fuzzy mathematics. Finally, specific comprehensive environmental protection measures of coal mines were proposed.

MODEL AND INDEX SYSTEM

Fuzzy Hierarchy Comprehensive Evaluation Method

Fuzzy hierarchy comprehensive evaluation is used to quantize the fuzzy indexes of the evaluated object by constructing a grade fuzzy subset (this approach determines the degree of membership). Then, various indexes are combined by the fuzzy transformation principle.

First, the domain of discourse of factors of the evaluated object was determined; it refers to the P evaluation index, as follows:

$$u = \{u_1, u_2, \cdots\cdots, u_p\} \quad \ldots(1)$$

Second, the domain of discourse of comment grades was determined, as follows:

$$v = \{v_1, v_2, \cdots\cdots, v_p\} \quad \ldots(2)$$

After constructing the grade fuzzy subset, evaluation factors u_i ($i = 1, 2, \ldots, p$) of the evaluated object are quantized one by one. In other words, the degree of membership ($R|u_i$) of the evaluated object to the grade subset was determined from a single factor to obtain the fuzzy relation matrix, as follows:

$$R = \begin{bmatrix} R|\ u_1 \\ R|\ u_2 \\ \cdots \\ R|\ u_p \end{bmatrix} = \begin{bmatrix} r_{11} & r_{12} & \cdots & r_{1m} \\ r_{21} & r_{22} & \cdots & r_{2m} \\ \cdots & \cdots & \cdots & \cdots \\ r_{p1} & r_{p2} & \cdots & r_{pm} \end{bmatrix} \quad \ldots(3)$$

In the matrix R, the element in the row i and column j (r_{ij}) indicates the degree of membership of the evaluated object to the grade fuzzy subset (v_j) from the factor (u_i). The performances of the evaluated object on u_i is depicted through the fuzzy vector $(R|u_i) = (r_{i1}, r_{i2}, \ldots, r_{im})$ by the actual value of one index in other evaluation methods. Finally, the weight vector of the evaluation factors was determined. In the fuzzy comprehensive evaluation, the weight vector was determined as follows:

$$A = (a_1, a_2, \ldots\ldots, a_p) \quad \ldots(4)$$

In Eq.(3), element a_i in the weight vector A is the degree of membership of factor u_i to the fuzzy subset (important factors to the evaluated object). The relative importance sequence of evaluation indexes was determined by AHP; thus, the weight coefficient can be obtained. All evaluation indexes were normalized before synthesis. $\sum_{i=1}^{p} a_i = 1,\ a_i \geq 0,\ i = 1, 2, \cdots\cdots, n$. A and R of the evaluated objects were synthesized by using an appropriate operation, through which the vector of fuzzy comprehensive evaluation results (B) of the evaluated objects were obtained.

$$A \times R = (a_1, a_2, \cdots\cdots, a_p) \begin{bmatrix} r_{11} & r_{12} & \cdots & r_{1m} \\ r_{21} & r_{22} & \cdots & r_{2m} \\ \cdots & \cdots & \cdots & \cdots \\ r_{p1} & r_{p2} & \cdots & r_{pm} \end{bmatrix} = (b_1, b_2, \cdots\cdots, b_m) = B \quad \ldots(5)$$

where b_i is obtained from operation of A and column j of R. It expresses the degree of membership of the evaluated object to the grade fuzzy subset v_j, in general.

Index System

Influencing factors of the vulnerability of water inrush channel in coal mines were summarized based on academic studies on permeability law of water inrush formation and engineering practice experiences. Meanwhile, an index system of the vulnerability of groundwater inrush channel in Taoshan Mine was proposed, considering the possibility of available index data (Table 1).

Indexes are divided into qualitative indexes and quantitative indexes in studies on the vulnerability of groundwater inrush channel in coal mines. The qualitative indexes in Table 1 contain mine ventilation system, coal seam stability, water-resisting layer, water filling characteristics, number of coal seams, and fault nature. The data of all six indexes were statistical evaluation results through a questionnaire survey of geological experts and research members. The data of the remaining quantitative indexes were collected from the geological survey and research reports in Taoshan Mine.

EMPIRICAL STUDY

Taoshan Mine is located in the eastern regions of the Western

Table 1: Index system of the vulnerability of groundwater inrush channel in coal mines.

Level-1 indexes	Level-2 indexes	Units	Variable No.
Coal seam features	Mine ventilation system	State grade	X1
	Relative gas emission volume	m^3/t	X2
	Coal seam stability	State grade	X3
	Coal seam thickness	m	X4
Coal quality features	Water content	Ma%	X5
	Ash content	Ad%	X6
	Volatile content	V_{daf}%	X7
	Gel layer	Ymm	X8
	S	St,d%	X9
	P	Pd%	X10
Hydrogeological features	Water-resisting layer	State grade	X11
	Water filling characteristics	State grade	X12
	Number of coal seams	State grade	X13
	Fault nature	State grade	X14

Production Zone in Qitaihe Mine, and the administrative region is classified to Taoshan District, Qitaihe City. Taoshan mine is bordered at Taoshan Fault in the east, and it is adjacent to the Xinfu Mine. In the coal mine, the striking length and inclined width were approximately 5 and 5 km, respectively. The inclined area and the area of mining right were approximately 25 and 22.9952 km^2, respectively. On the north edge, railways run through the Qitaihe Station, connect to the National Railway, and extend all regions in China. Highways extend to Yilan, Kiamusze, Jixi, Baoqing, Mishan and Harbin, and Duisu Port. Hence, the traffic conditions are very convenient. The mine exploitation began in 1958. The disk deviation well group was adopted, followed by technological reconstruction and construction. In the coal mine, the total thickness of the coal-bearing seam was approximately 1470 m, which covers 65 coal seams, and the average total thickness of coal seams was 38 m. The coal-bearing coefficient was 2.6%. The 56# coal seam and 68# coal seam were selected as the research object for fuzzy comprehensive evaluation of the vulnerability of water inrush channel.

Determination of the Weight of Evaluation Indexes Based on AHP

AHP transforms the semiqualitative and semiquantitative problems into quantitative computation by constructing a pairwise matrix, calculating weight vectors, consistency test, and weight sequencing, and making a comprehensive judgment on weights of evaluation indexes of water inrush channel. When selecting evaluation indexes, the principle of reflecting the primary and the most comprehensive information by the least indexes should be observed. An index system of the vulnerability of groundwater inrush channel was constructed based on the principle of AHP (Saaty et al. 1985). Calculation results are listed in Table 2.

Table 2 shows that coal quality features, hydrogeological features, and coal seam features can influence the vulnerability of the water inrush channel significantly. The coal quality features contribute 48.36% of the explanation to the vulnerability of the water inrush channel. The upper 40–48 coal seams in Taoshan Mine belong to the semi-bright coals, which are mainly dominated by bright coals. Bright coals have glassy lustre, stripped structure, endogenous fracture development, and high vulnerability. The middle 55–79 coal seams belong to semi-bright coals and semidark coals in stripped and lamellar structures. Massive structures account for a high proportion, and the coal seams have a large amount of internal dirt. Hydrogeological features contribute 34.87% of the explanation to the vulnerability of the water inrush channel. Taoshan mine has many small rivers and valleys, and it belongs to an aged river. After several diversion, the watercourse twists and turns, forming many cutoff lakes. The river width is 20-30 m, the water depth is approximately 4 m, and the maximum flooding water level is 165 m. Large and small gobs below the groove are superficial, and the surface soil is thin; thus, the water filling in the ore bed is affected to some extent, easily causing vulnerability of water inrush channel. Moreover, surface water bodies are a water filling factor in Taoshan Mine; they are mainly catchments during rainy seasons in several valleys. Surface runoffs penetrate underground through surface collapse pits in the gob and can influence water filling in coal mines. Coal seam features contribute 16.77% of the explanation to the vulnerability of the water inrush channel. Recently, Taoshan mine manage-

Table 2: Weights of Indexes of the vulnerability of water inrush channel.

Variable No.	Name of variables	Level-1 weights	Level-2 weights	Total weights
X1	Mine ventilation system	0.1677	0.1113	0.0187
X2	Relative gas emission volume		0.0674	0.0113
X3	Coal seam stability		0.5329	0.0894
X4	Coal seam thickness		0.2884	0.0484
X5	Water content	0.4836	0.1590	0.0769
X6	Ash content		0.1845	0.0892
X7	Volatile content		0.1983	0.0959
X8	Gel layer		0.0494	0.0239
X9	S		0.1554	0.0751
X10	P		0.2535	0.1226
X11	Water-resisting layer	0.3487	0.1399	0.0488
X12	Water filling characteristics		0.4551	0.1587
X13	Number of coal seams		0.0723	0.0252
X14	Fault nature		0.3327	0.1160

ment agency has focused on safety management and adopted centralized inflow and zoned ventilation measures. The gross installed capacity of the major fan is 1615 kW. The total air inflows in the entire coal mine are 13100 m^3/min, and the total ventilation volume is 1435 m^3/min. The effective wind volume in the entire mine is 92%. As a result, the possibility of gas explosion is decreased. The level-2 weight of coal seam stability (X3) is 0.5329, which has occupied more than half of the weights of the level-1 index coal seam features. The reason is that the total coal seam thickness in wells is approximately 1470 m, which covers 65 coal seams. The average total thickness of the coal seam is 38 m, and the coal-bearing coefficient is 2.6%. The coal seam features have four stable coal seams and four relatively stable coal seams, and the remainder includes unstable coal seams.

Vulnerable Grade Evaluation Based on Fuzzy Mathematics

The fuzzy mathematics maximum membership principle was used to evaluate the vulnerability of the water inrush channel and obtain specific and explicit ambiguous problems. A comprehensive fuzzy mathematics model was constructed. In accordance with the index system and quota of the indexes, the standard eigenvalues of five levels of indexes were recognized, thereby obtaining the standard eigenvalue matrix A. Subsequently, fuzzy evaluation was implemented. The fuzzy subset was evaluated by combining the weights of AHP and the membership matrix. The principle of obtaining the larger product was used. After normalization, the maximum was selected as the evaluated grade of the vulnerability of the water inrush channel according to the maximum fuzzy mathematics membership principle. According to Eqs. (1)-(4), the fuzzy evaluation matrix of level-1 indexes was as below.

$$\begin{bmatrix} 0.3970 & 0.4234 & 0.0966 & 0.0257 & 0.0573 \\ 0.1367 & 0.1657 & 0.4775 & 0.2046 & 0.0155 \\ 0.2315 & 0.3243 & 0.3613 & 0.0829 & 0.0000 \end{bmatrix}$$

According to Eq. (5), the comprehensive fuzzy evaluation vector was [0.2134 0.2642 0.3731 0.1322 0.0171]. The results show that the five numbers are memberships of the vulnerability of water inrush channel to "I, II, III, IV and V", and the membership to "III" is 0.3731, which is the highest. Hence, the maximum membership principle indicates that the vulnerability of the water inrush channel in Taoshan mine belongs to Grade III, indicating the moderate state of vulnerability of the water inrush channel in Taoshan mine.

POLICY SUGGESTIONS

Strengthening Geological Environmental Monitoring in Coal Mines

Strengthening geological environmental monitoring and management in coal mines. A responsibility system shall be implemented for geological environmental restoration in coal mines. The principle that the party that explores coal mines is held responsible for the protection and the party that destroys the coal mines is responsible for governance shall be observed. Responsibilities of all links shall be implemented thoroughly, and a management mechanism and system shall be established and perfected to strengthen monitoring and management of all coal mines, especially those that are

destroyed seriously. Thus, regulations on the protection and governance of coal mines are developed. The monitoring of geological environmental restoration and governance in coal mines shall be strengthened. Relevant departments shall increase supervision and verification of mining application, expanding secondary mining scale and changing the mining mode. Mining protection and governance restoration scheme shall be formulated. Mining closing, mining termination, and land reclamation can only be implemented after acceptance by relevant departments.

Improving Environmental Engineering Governance of Coal Mines

Barren rocks at open mining edges are cleaned. Two sides are solidified, and the surface is greened. On one hand, catchwater should be constructed on top of mountains to stop water flow into the stope and further cause groundwater pollutions or trigger geological disasters. On the other hand, the land use scope of mining activities must be restricted. Land resources shall be used reasonably and standardly, and all random stacking phenomena shall be eradicated. Waste residues, which are produced in the mining process, are used scientifically, and resource recycling is realized. When coal mines are closed, waste residues can fill in the stope to prevent pollution from the source. The green vegetation in the mining area that protects some vegetation transplantation shall be adopted in the mining process rather than deforestation. This approach can prevent excessive vegetation damages, thereby causing great disasters. Moreover, trees and grasses shall be planted appropriately, the green area shall be expanded in the coal mine, and the vulnerable ecological problem in the mining area must be eliminated. After coal exploitation, a large-area gob can cause floor cracks, surface collapse, and settling. The collapse and fractures shall be filled up timely, and large-area settlement shall be flattened timely.

Strengthening Technological Content of Environmental Protection in Coal Mines

Details are introduced as follows: (1) increasing efforts in research and development of deep processing of mineral resources, expansion of peripheral industrial chains of mineral resources, and increasing mining products; (2) enriching deep processing technology of mineral resources and extending industrial chain; (3) adjusting mineral exploitation technology and introducing the automatic and scientific mineral mining system; (4) improving management level, decreasing number of operation posts, and attempting to realize unmanned mineral exploitation comprehensively; (5) promoting green clean mineral industrial development positively, shutting down mines with resource wastes and severe pollutions through technological reforms, optimizing management, and improving standards; (6) adopting comprehensive governance, controlling energy and water resources, which are collected from coal mines, performing full-process monitoring on wastes and emissions during mining activities, increasing monitoring strength, and urging enterprises to reform green clean mineral industries; (7) promoting green clean mining technologies positively and applying the philosophy of green cleaning mining industry into mining, transportation, and processing of coal mines.

CONCLUSIONS

Excessive or disordered coal resource exploitation leads to occurrences of geological disasters in coal mines, such as collapse, landslide, debris flow, and surface collapse. The ecological environment in mining areas and surrounding areas are worsened and the ecosystem is degenerated due to vegetation damages. Water inrush in coal mines is a typical natural disaster, which negatively affects normal production and environmental protection of coal mines. Influencing factors of formation and project of water inrush channel in coal mines are analyzed. Then, 14 indexes that influence the vulnerability of the water inrush channel are selected. A case study based on data of 56# and 68# coal seams in Taoshan Mine, China is carried out. The vulnerability of the water inrush channel is estimated by AHP and fuzzy comprehensive evaluation. Results demonstrate that coal quality features influence the vulnerability of water inrush channel mostly, followed by hydrogeological features and coal seam features successively. The vulnerability grade evaluation results of fuzzy mathematics suggest that the membership of "Ⅲ" is 0.3731, indicating that the Taoshan Mine belongs to "III" in terms of vulnerability of the water inrush channel. This reflects that the vulnerability of the water inrush channel of Taoshan mine is in a moderate state. Finally, three governance measures of strengthening geological environmental monitoring, improving environmental governance, and increasing technological content for environmental protection in coal mines are proposed. In-depth studies on enriching influencing factors of vulnerability of water inrush channel, geological environmental comprehensive evaluation, and recovery and governance of geological disasters in coal mines are required in the future.

ACKNOWLEDGMENT

This work was supported by the Foundation of Science and Technology Innovation Leading Talent project of Centaline thousand talents plan (194200510015), Foundation of Henan Science and Technology Project(192102310465, 202102310240), Foundation of Key Scientific Research Project of Universities of Henan Province (19A560023), and

Foundation of Science and Technology Project of Housing and Urban Rural Construction of Henan Province (K-1915, HNJS-2020-K38).

REFERENCES

Abdullah, T. O., Ali, S. S., Al-Ansari, N. A. and Knutsson, S. 2015. Groundwater vulnerability mapping using lineament density on standard drastic model: case study in Halabja Saidsadiq Basin, Kurdistan Region, Iraq. Engineering, 7(10): 644-667.

Janssen, M.A., Schoon, M.L., Ke, W. and Börner, K. 2006. Scholarly networks on resilience, vulnerability and adaptation within the human dimensions of global environmental change. Global Environmental Change, 16(3): 240-252.

Fijani, E., Nadiri, A. A., Moghaddam, A. A., Tsai, T. C. and Dixon, B. 2013. Optimization of drastic method by supervised committee machine artificial intelligence for groundwater vulnerability assessment in Maragheh-Bonab plain aquifer, Iran. Journal of Hydrology, 503(Complete): 89-100.

Li, P. T., Jia, X. and Zeng, Y. F. 2014. Water inrush risk evaluation of seam roof and floor at Mayingbao coal field in Shuozhou city, Shanxi province. Advanced Materials Research, 838-841(838-841): 2158-2161.

Li, G., Meng, Z., Wang, X. and Jian, Y. 2016. Hydrochemical prediction of mine water inrush at the Xinli mine, china. Mine Water and the Environment, 36(1): 1-9.

Liu, S. Q., Wu, Q., Zeng, Y. F., Cao, Y. F. and Zhang, X. J. 2014. Study on a new coal floor water inrush evaluation technique and its application. Advanced Materials Research, 864-867: 2322-2326.

Mogaji, K. A., Lim, H. S. and Abdullah, K. 2014. Modeling groundwater vulnerability prediction using geographic information system (GIS)-based ordered weighted average (OWA) method and DRASTIC model theory hybrid approach. Arabian Journal of Geosciences, 7(12): 5409-5429.

Qiang, W., Fan, S., Zhou, W. and Liu, S. 2013. Application of the analytic hierarchy process to assessment of water inrush: a case study for the no. 17 coal seam in the Sanhejian Coal mine, china. Mine Water & the Environment, 32(3): 229-238.

Qiang, W., Liu, Y. and Liu, Y. 2011. Using the vulnerable index method to assess the likelihood of a water inrush through the floor of a multi-seam coal mine in China. Mine Water & the Environment, 30(1): 54-60.

Qiang, W., Zhou, W., Wang, J. and Xie, S. 2009. Prediction of groundwater inrush into coal mines from aquifers underlying the coal seams in China: application of vulnerability index method to Zhangcun Coal mine, China. Environmental Geology, 57(5): 1187-1195.

Rupert, M. G. 2010. Calibration of the drastic ground water vulnerability mapping method. Groundwater, 39(4): 625-630.

Saaty, T. L. and Vargas, L. G. 1985. Modeling behavior in competition: The analytic hierarchy process. Applied Mathematics and Computation.16(1): 49-92.

Wu, Q., Hua, X. and Wei, P. 2008. GIS and ANN coupling model: an innovative approach to evaluate vulnerability of karst water inrush in coalmines of north China. Environmental Geology, 54(5): 937-943.

Wu, Qiang., Liu, Yuanzhang., Wu, Haixia and Zeng, Yifan 2017. Assessment of floor water inrush with vulnerability index method: application in Malan coal mine of Shanxi province, china. Quarterly Journal of Engineering Geology and Hydrogeology, 50(2): 169-178.

Wu, Q., Liu, Y., Zhou, W., Li, B., Zhao, B., Liu, S., Sun, W. and Zeng, Y. 2015. Evaluation of water inrush vulnerability from aquifers overlying coal seams in the Menkeqing coal mine, China. Mine Water & the Environment, 34(3): 258-269.

Xiao, M. L., Qi, M. Z., Xiao, R. X. and Liu, J. 2014. Application of vulnerability index method in floor water inrush evaluation. Applied Mechanics & Materials, 614: 321-326.

Nature Environment and Pollution Technology
An International Quarterly Scientific Journal

p-ISSN: 0972-6268
(Print copies up to 2016)
e-ISSN: 2395-3454

Vol. 20 | No. 2 | pp. 793-799 | 2021

Original Research Paper

https://doi.org/10.46488/NEPT.2021.v20i02.041

Open Access Journal

Suitability Evaluation of Groundwater Quality for the Intent of Irrigation

G. Shyamala†*, K. Rajesh Kumar, R. Gobinath* and N. Saravanakumar*****

*Department of Civil Engineering, S R Engineering College, Warangal, India

**Centre for Construction Methods and Materials, Department of Civil Engineering, S. R. Engineering College, Warangal, India

***Arba Minch University, Sawla Campus, Ethiopia

†Corresponding author: G. Shyamala; civilshyamala@gmail.com

Nat. Env. & Poll. Tech.
Website: www.neptjournal.com

Received: 28-03-2020
Revised: 23-04-2020
Accepted: 27-05-2020

Key Words:
Groundwater quality
Irrigation
Sodium adsorption ratio
SAR

ABSTRACT

Exploration was conducted in the study area of Coimbatore district by collecting 60 samples from the agricultural belt. The groundwater is neutral to alkaline in character with pH varying from 6.70 to 9.02 among the mean of 7.37. Elevated electrical conductivity (EC) was observed in upstream parts of the study area. Water quality for irrigation is determined by several key components like electrical conductivity (EC), total suspended solids (TDS), residual sodium carbonate (RSC), chloro alkali Indices (CA I & CAII), sodium adsorption ratio (SAR), percent sodium (%Na), Kelley's ratio (KR), magnesium hazard (MH), permeability index (PI) and soluble sodium percent (SSP). In total, six samples were found to be with high salinity hazard. The mean value of SAR was found to be 5.24, maximum sample falls under C2S1 to C4S1 category as per USSL Salinity diagram. As per Piper diagram in the anionic regime, Cl dominates HCO_3^-, CO_3^{2-} and SO_4^{2-}. Higher magnesium hazard in the groundwater is owing to the consequence of dyeing and bleaching industries. Magnesium hazard value indicates that 51 samples out of 60 are unsuitable for irrigation. According to the study, it is revealed that groundwater in the study area is contaminated by both natural factors and anthropogenic activities.

INTRODUCTION

Characteristics of water based quality are gaining extraordinary significance with the ascent in the number of sectors and for agribusiness. Sufficient measure of water is significant for a legitimate yield of plants, yet the quality of water utilized for water system should be well within the standards as far as possible, else it could unfavourably influence the plant yield. Questions have been raised with regards to the social and natural supportability of this escalated method of yield creation, i.e. the source of water for irrigation as groundwater (Shyamala et al. 2008). Groundwater quality is considered of great importance with rapid industrialization. Deterioration in groundwater quality has an adverse impact on plant growth. Soil becomes saline and the permeability of soil decreases if the inferior water is used continuously without proper drainage for irrigation purpose. The quality of crop and yield are affected by irrigation water quality. The water utilized for the water system is a crucial factor for improving the yield and nature of irrigated plants. The agricultural water quality relies basically upon the presence of dissolved salts and their intensity.

Ayuba et al. (2013) carried out a preliminary survey by analysing the topography map of Enugur metropolis before sampling. The test wells are twist drill-bored and hand-burrowed wells with breadth extending from 0.7 to 0.9 m in all the three settlement zones. Groundwater samples of 42 numbers were collected from Erugur metropolis. Piper diagram and scatter plot for the three settlement areas were analysed (Ramesh et al. 2020). The study reasoned that the groundwater extricated from the location of low contamination stacking is probably going to be more secure and increasingly consumable when contrasted with those of the other contamination types.

Basamba et al. (2013) concluded that the worsening of freshwater is a global problem. The demand for clean water is based on the increase in population growth and the living standard of people. Most of the study areas have good potable water, except a few which are contaminated by faecal contamination (Shyamala et al. 2019). Al-ahmadi (2013) studied groundwater table in western Saudi Arabia in which he found the water table at superficial depth ranges from 1.08 to 2.40 m. Samples were procured from the Wadi and tested in the laboratory for major cation and anion composition. Groundwater has been assessed for potability and irrigation purposes based on salinity and sodium hazard and total dissolved solids. Ramkumar et al. (2013) conducted studies to appraise the hydrogeochemical properties of water of Kottur block, Thiruvarur district, Tamil Nadu. Predom-

inance of cations in the range for $Na^+ > Ca^{2+} > K^+ > Mg^{2+}$ and anions $Cl^- > SO_4^{2-} > HCO_3^- > NO_3^-$ was seen in the two seasons. From flautist trilinear outline it is seen that most groundwater tests are Na^+ - Cl^- and Ca^{2+} - Mg^{2+} - SO_4^{2-}. It is obvious from the Wilcox graph that tests that tumble from low to high, saltiness threat is not reasonable for rural areas. Kelly's proportion and magnesium proportion demonstrates that most examples are appropriate for water system reason.

The pH range of groundwater diverse from 7.6 to 8.4, the electrical conductivity was found between 2992 and 2894 mmho/cm at 26°C in the study area. Salifu et al. (2015) conducted groundwater hydrogeochemical analysis based on water quality for irrigation. RSC was used to discover the appropriateness of groundwater for water system use. The USSL graph result uncovers that the examples fall in the classification, which demonstrates high to high saltiness.

All three seasons indicate reverse ion exchange parameters of calcium and magnesium with the majority of rich components in groundwater (Shyamala et al. 2008). Quality of groundwater was analysed for 23 samples with irrigation water quality standards Wilcox, USSL (Sappa et al. 2014). Groundwater quality and its appropriateness for agriculture and domestic activity were inspected by different physico-synthetic parameters, for example, pH, total hardness, electrical conductivity, total dissolved solids, total hardness, calcium, magnesium, potassium, sodium, bicarbonate, sulphate and chloride (Ahamed et al. 2015). Percolation of water in the soil was condensed as the sodium content of the water reacts with the soil chemicals which are naturally present. The arrangement of the soil grains was also destructed and the physical properties get altered (Shyamala et al.2016). Alkali soils are formed when sodium reacts with carbonate and saline soil was formed when sodium reacts with chloride, both of the soils do not favour the growth of plants (Srinivas et al. 2015). HCO_3^- combines with Ca^{2+} and Mg^{2+} and the concentration gets elevated (Krishnasamy et al. 2020).

High SAR in irrigation water transforms the physical construction of the soil particles. Soil particles are attracted towards sodium and adsorbed on the surface, making soil impervious (Mohamed et al. 2018). High EC content in the irrigation water reduces the ion intake capacity of plant roots from the soil, which results in the reduction of crop yield (Srinivasamoorthy et al. 2012). Even if the moisture content of the soil is high, the plant would not be able to absorb the moisture and nutrients required for growth. Salinity condition exists as salts get accumulated in the root zone of the plants if the groundwater with high TDS is used for irrigation continuously. In saline solution, crops are unable to extract water and subsequently, the yield gets reduced. Ion exchange between the water quality parameters is denoted by CAI. Positive CAI indicates that there is no exchange of ions between Na^+ K^+ and Ca^{2+} Mg^{2+}. Shanmugasundharam et al. (2015) used the Wilcox diagram to determine the aptness of groundwater for irrigation purpose. He computed sodium Kelley ratio, adsorption ratio, magnesium hazard, percentage sodium permeability index and residual sodium carbonate (RSC) along with Wilcox diagram and USSL diagram. High salinity was observed in most of the location, hence ample drainage should be provided to improve crop yield (Shyamala et al. 2020, Shyamala & Jeyanthi 2017). Water quality in the area Godavari Upazila was analysed for agricultural application impact due to irrigating with polluted water which may lead to toxicity; salinity and affect water infiltration rate factor analysis was performed using XLSTAT Version 2013.6.03. The objective of the research is to analyse the groundwater quality in the Coimbatore district and determine its suitability for irrigation purpose.

MATERIALS AND METHODS

Study Area

Mettupalayam, the investigation area, is situated on the foot slopes of Nilgiris, India. The Bhavani River situated in the lower regions of Nilgiris, located in the Western Ghats is the perpetual stream in India. Lately, numerous ventures have been set up at the spring limit of Bhavani River, which has the perennial flow of water to the individuals in the taluk. Different sources incorporate borehole and hand-wells, and channel water. The selected study area is a significant exchanging centre and travel community for slope products. This study was attempted by arbitrarily gathering 60 groundwater tests from open wells inside Mettupalayam, India. The investigation zone and the sample areas are introduced in Fig. 1. The samples were gathered in plastic containers, sanitized with distilled water before gathering the groundwater samples.

RESULTS AND DISCUSSION

Irrigation Water Quality Parameters

The groundwater samples were analysed following standard methods recommended by APHA (1998). The colour and odour of the samples were observed physically. The pH, Total Dissolved Solids (TDS), Electrical Conductivity (EC) and temperature were analysed on-site using digital meters. Other parameters such as turbidity, Total Solids (TS), Total Suspended Solids (TSS), Total Hardness (TH), calcium hardness, magnesium hardness, sodium, potassium, sulphate, chlorides, carbonate and bicarbonates, ammonia, iron, chromium, and fluoride were determined in the laboratory by the volumetric and instrumental methods. The quality

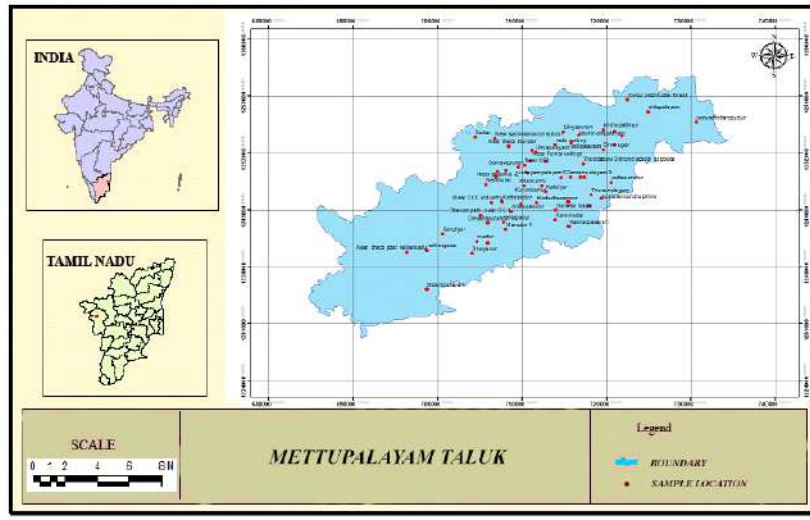

Fig. 1: The study area.

of sampled groundwater was compared with BIS (2009) standards. Quality of water for irrigation is determined by several key factors like Residual Sodium Carbonate (RSC), Chloro Alkali Indices (CA I & CAII), Sodium Adsorption Ratio (SAR), percent sodium (%Na), Kelley's Ratio (KR), Magnesium Hazard (MH), Permeability Index (PI) and Soluble Sodium Percent (SSP) as given in Table 1.

Salinity Hazard

EC is an upright quantity of saltiness danger to crops as it reflects total dissolved solids in groundwater. Elevated EC shows high salt substance water. Overabundance saltiness will decrease the osmotic movement of plants. Ions may be positively or negatively charged, which are produced by breaking compounds that conduct electricity. The mobility of ions dissolved in water increases conductivity.

Total dissolved solids can be indirectly measured from electrical conductivity. The limiting values for electrical conductivity are provided in Table 2. Out of 60 samples tested, none of the samples is in the category of low or medium. High electrical conductivity is observed in 54 samples and 6 samples are of very high electrical conductivity, i.e. in the range greater than 2250 µS/cm as shown in Fig. 2.

Table 1: Minimum and maximum value of irrigation water quality parameters.

S.No.	Variable	Minimum	Maximum	Mean
1	SAR	1.81	9.30	5.24
2	% Na	17.088	52.52	38.76
3	RCS (meq/L)	0.134	1.32	0.425
4	KR	0.123	0.706	0.375
5	MH	36.56	77.44	57.31
6	CA I	-17.64	0.47	-1.054
7	CA II	-0.964	3.643	0.542
8	SSP	10.8564	41.369	25.62
9	PI	21.076	77.939	41.889

Table 2: Categorization of irrigation water quality based on EC.

S.No	Limiting value	category	No. of samples
1.	<250 (µS/cm)	Low	-
2.	250-750 µS/cm)	Medium	-
3.	750-2250 (µS/cm)	High	54
4.	>2250 (µS/cm)	Very high	6

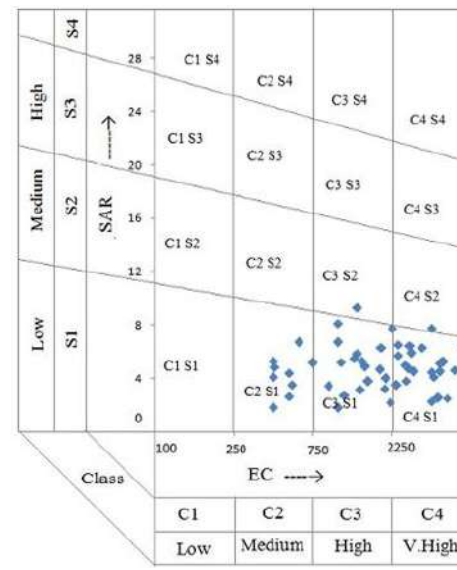

Fig. 2: USSL diagram for Salinity Hazard.

Total Dissolved Solids

Groundwater contains a negligible quantity of suspended solid as these are filtered out by soil strata through mechanical straining action. The amount of dissolved solids in groundwater increases with the input of manmade contamination. Total dissolved solids in the study location are given in Table 3. In 60 samples considered for analysis 58 samples are fit for agricultural usage and 2 samples are unfit for both potable and agricultural usage. The presence of total dissolved solids is owing to the sediments or the contact of water with the atmosphere or soil.

Sodium Adsorption Ratio

The Sodium Adsorption Ratio (SAR) shows the impact of relative cation fixation on sodium build up in the soil; consequently, sodium adsorption proportion (SAR) is another technique for deciding the impact of sodium.

Suitability of groundwater for agricultural use is found by Sodium Adsorption Ratio. Continuous use of water with high SAR may cause a prolonged dent to soil. Due to the formation of stable aggregates, the soil structure is affected. Permeability of soil is reduced and in turn, crop yield is decreased. Sodium adsorption ratio (SAR) is computed by the following formula 1.

$$SAR = \frac{Na^{+}}{\sqrt{(Ca^{2+} + Mg^{2+})/2}} \quad \ldots(1)$$

If the SAR is less than 3.0 the groundwater can be used for all varieties of crops. For sensitive crop, the usage should be minimized if SAR value is in the range of 3-6. Categorization of groundwater based on SAR is given in Table 4.

Percent Sodium

Presence of sodium in groundwater is represented by soluble sodium or percent sodium. Sodium percent is classified into five types: unsuitable, doubtful, permissible, good and excellent. Percent sodium is computed using equation 2.

$$\%Na = \frac{(Na^{+}K^{+})X100}{(Ca^{2+}+Mg^{2+}+Na^{+}K^{+})} \quad \ldots(2)$$

All the samples in the study location are in 60 %, hence it falls in the range of excellent to permissible category (Table 5). As per sodium concentration, the groundwater does not have negative impacts like growth retardation or yield reduction. Table 5 shows the categorization of agricultural water quality based on percent sodium.

All the 60 samples fall in the group of excellent to permissible category. Wilcox diagram (Fig. 3) is used to assess the appropriateness of groundwater for irrigation using percent sodium and electric conductivity.

Residual Sodium Carbonate

Water with a carbonate concentration larger than the calcium and magnesium concentration is recognized by the term "residual sodium carbonate". Residual Sodium Carbonate (RCS) index refers to alkalinity hazard to the soil. If the sodium in clayey soil is higher, it causes swelling and reduces infiltration capacity. The potential of sodium vulnerability is

Table 3: Categorization of irrigation water quality based on TDS.

S.No	Limiting value	Category	No. of samples
1	<500	Fit for drinking	-
2	500-1000	Unfit for drinking	14
3	<3000	Useful for irrigation	44
4	>3000	Unfit for drinking and irrigation	2

Table 4: Categorization of irrigation water quality based on SAR.

S.No	Limiting value	category	No. of samples
1	0-3	No problems	45
2	3-6	Moderate problems	15
3	>6	Severe problems	0

Table 5: Categorization of irrigation water quality based on Percent sodium.

S.No.	Limiting value	category	No. of samples
1	<20	Excellent	1
2	20-40	Good	35
3	40-60	Permissible	24
4	60-80	Doubtful	-
5	>80	Unsuitable	-

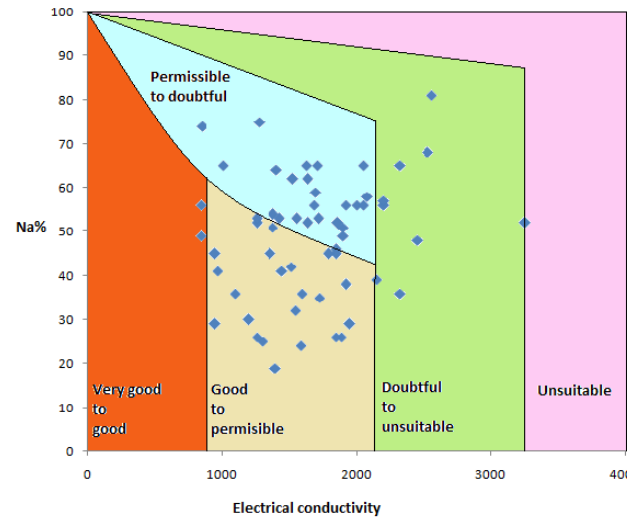

Fig. 3: Wilcox diagram for groundwater in the study area.

Table 6: Classification of irrigation water quality based on RSC.

S.No	Limiting value	category	No. of samples
1	<1.25	Good	58
2	1.25-2.50	Doubtful	2
3	>2.50	Unsuitable	Nil

increased as Residual sodium carbonate (RSC) rises. Residual Sodium Carbonate (RSC) is calculated by the formula 3.

$$RSC = (CO_3^{2-} + HCO_3^-) - (Ca^{2+} + Mg^{2+}) \quad \ldots(3)$$

To identify the aptness of groundwater in clay soil, RCS index is used. If the groundwater with elevated RCS is applied for irrigation it leads to alkali soil formation. As per calculated RCS index for the 60 samples collected in the agricultural belt, 58 samples have low RCS value of less than 1.25 and are apt for irrigation as given in Table 6.

Kelly's Ratio

Sodium tested against calcium and magnesium is used to calculate Kelley's Ratio. Kelley Ratio indicates the highest value of sodium in the groundwater. The formula (4) is applied to calculate the Kelley's ratio.

$$KR = \frac{Na^+}{(Ca^{2+} + Mg^{2+})} \quad \ldots(4)$$

Kelley's Ratio (KR) of more than 1 reveals an abundance level of sodium in waters. Subsequently, waters with Kelley's Ratio of less than one are most appropriate for irrigation, while those with a proportion of more than one are unacceptable for irrigation. Groundwater is classified based on KR and the results are given in Table 7. Sixty samples were analysed in the agricultural area and the Kelley ratio falls less than 1 for all the samples which indicate that the groundwater is good for irrigation in the study area.

Magnesium Hazard

Groundwater with elevated concentration of magnesium, if used for irrigation, damages soil structure and causes high salinity. Calcium and magnesium are present in water in an equilibrium state and they behave independently in the soil system. Magnesium hazard is given by equation 5.

$$MH = \frac{Mg^+ X\ 100}{(Ca^{2+} + Mg^{2+})} \quad \ldots(5)$$

From the analysis, MH value for the samples is in the range of 35.68 to 77.89. MH value should be less than 50. Out of 60 samples, 9 samples were apt for agriculture as per magnesium hazard as revealed in Table 8. If the magnesium hazard value is greater than 50, it affects plant growth and becomes unsuitable for agricultural use. In most of the samples in the study area, i.e. in about 51 samples, the Magnesium Hazard value is above 50, which makes it unsuitable for agricultural use.

Table 7: Classification of irrigation water quality based on KR.

S.No	Limiting value	Category	No. of samples
1	<1	Suitable	59
2	>1	Unsuitable	1

Table 8: Categorization of irrigation water quality based on MH.

S.No	Limiting value	Category	No. of samples
1	<50	Suitable	9
2	>50	Unsuitable	51

Chloro Alkali Indices

Groundwater chemistry is influenced by the ion exchange process. It is an important criterion for the mass transport of pollutants in aquifers and soils. Cation-anion exchange reaction takes place between the particles. Sodium and potassium ions exchange with calcium and magnesium in the presence of water. The CA I and CA II value may be positive or negative based on the reaction taking place. In the current study, 38 groundwater samples are with positive values which represents reverse ion exchange, and 22 samples of negative assessment indicating normal ion exchange.

Total Hardness as $CaCO_3$

Hardness in water is brought about by the occurrence of divalent metallic cations like calcium, magnesium, ferrous iron, strontium, manganese and so on. It is relevant to take note that the greater part of the industrial sector in the zone, pre-treat water to evacuate hardness; else it blocks the working of their boilers. In the examination zone, 56 examples are in the class of hard to very hard (Table 9).

Soluble Sodium Percent (SSP)

Soluble Sodium Percent (SSP) for groundwater was determined using the formula 6. The groupings of Ca^{2+}, Mg^{2+} and Na^+ are articulated in milli equivalents per litre. The Solvent Sodium Percent (SSP) values of 50 or under 50 signify great quality water, and if in excess of 50, it denotes the intolerable water quality for irrigation (Kshetrimayum & Bajpai 2012).

Table 9: Categorization of irrigation water quality based on TH.

S.No	Limiting value	category	No. of samples
1.	<75	Soft	0
2.	75-150	Moderately hard	3
3.	150-300	Hard	36
4.	>300	Very hard	20

$$SSP = \frac{Na\ X\ 100}{Ca^{2+} + Mg^{2+} + Na^{+}} \quad \ldots(6)$$

Permeability Index

Groundwater for irrigation was investigated dependent on the Permeability Index (PI). PI is computed from equation 7.

$$PI = \frac{(Na^{+} + \sqrt{HCO_3})\ X100}{(Ca^{2+} + Mg^{2+} + Na^{+})} \quad \ldots(7)$$

Accordingly, the permeability index is classified under class I, class II and class III as presented in Table 10. Class I and class II water samples are categorised as good. In the study area, 59 samples are in class I and II. Class III waters are non benefiting for agriculture with 25% of maximum permeability.

Piper's Trilinear Diagram

Piper Trilinear Diagram is used for depicting hydro substance attributes of groundwater. It is a standard strategy of anticipating hydro concoction facies, which is appropriate for arranging the water quality. Flautist chart created for the water quality is as shown in Fig. 3, and delineates likenesses and dissimilarities among the groundwater tests. Flautist outline comprises of 2 triangles, left triangle demonstrates cation and right triangle demonstrates anion, all the samples depicted in the triangle are in meq/L and jewel shape in the

Table 10: Categorization of irrigation water quality based on PI.

S.No	Limiting value	Category	No. of samples
1	<25%	Class I	1
2	25-75%	Class II	58
3	>75 %	Class III	1

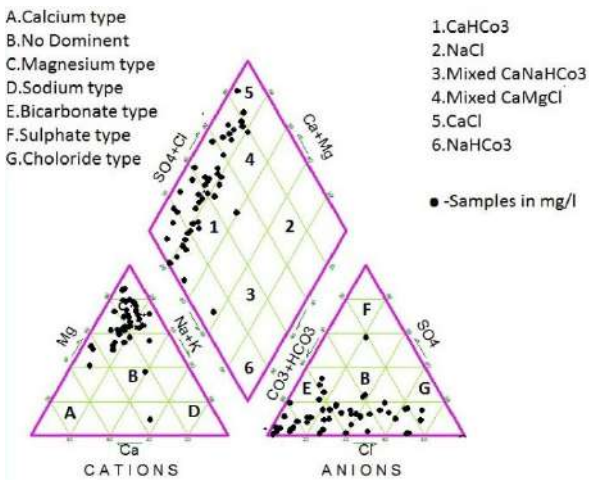

Fig. 4: Piper trilinear diagram.

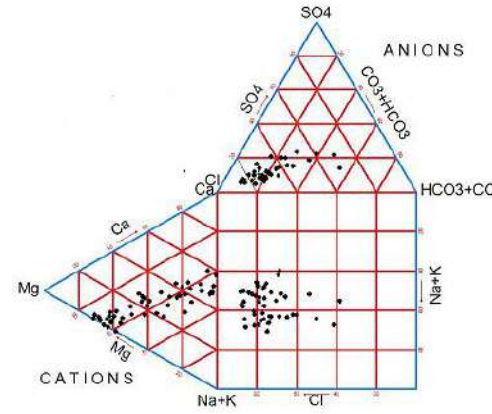

Fig. 5: Durov plot for cations and anions.

Piper Trilinear graph connotes both anion and cation field. All the 60 sampling stations were represented in the diagram. Rockworks16 software was used to create a piper trilinear diagram as shown in Fig. 4.

The input for constructing this diagram is Ca^{2+}, Mg^{2+}, Na^{+}, K^{+}, cations and anions are HCO_3^{-}, CO_3^{2-}, Cl^{-} and SO_4^{2-}. The cation triangle reveals that dominating ion is magnesium as 92% of samples are in the Mg^{2+} portion, very few samples are under the no dominant nature and sodium nature. In the anionic regime, Cl dominates HCO_3^{-}, CO_3^{2-} and SO_4^{2-}, very few samples fall in sulphate type. The yield from the Piper trilinear diagram chart proposes rock water interface and disintegration of rocks. Raised estimation of calcium hardness is expected to groundwater association with rocks and does not have a risky impact.

Durov Diagram

Most important ions like Ca^{2+}, Mg^{2+}, HCO_3^{-}, CO_3^{2-}, Na^{+}, K^{+}, Cl^{-} and SO_4^{2-} are considered for plotting Durov diagram and the trace elements are neglected for classification**.** Durov diagram is capable of classifying the water quality based on ionic concentration in the samples and the chemical composition of the water is given in Fig. 5. It has two base triangles and 1 square. All the cations and anions in the samples are projected as points in the triangular portion of the drawing. The plots in the triangular portion are transferred to the square grid.

The samples of similar ionic composition are clustered together. From the illustration Cl^{-} dominated the HCO_3^{-}, CO_3^{2-}, SO_4^{2-} in the anionic plot. The cationic plot reveals that magnesium ions and calcium ions dominate the other cations. It is concluded from the plot, that the water quality in the study location is dominated by calcium and magnesium. The weathering of metamorphic rock and the hydrogeological framework in the study location might be the grounds for calcium-magnesium dominance. The

dominance of ions in groundwater is of Ca, Mg and Cl as per the Piper diagram.

CONCLUSION

Groundwater quality in the Coimbatore region is evaluated regarding groundwater system based on water quality parameters. The sequence of profusion of chemical deliberation is $Na^+ > Ca^{2+} > Mg^{2+} > K^+ = HCO_3^- > Cl^- > NO_3^-$ and $Ca^{2+} > Mg^{2+} > Na^+ > K^+ = HCO_3^- > Cl^- > NO_3^-$. Strong acids ($SO_4^{2-}$, Cl^-) overwhelm week acids (HCO_3^-, CO_3^{-2}) in the study location. Elevated EC is limited in the length of upstream, and marginal in the downstream demonstrating the predominance of domestic, industrial and irrigational activities. High TH is noted in areas limited to the event of colouring and dying businesses. The larger part of groundwater tests are built up in Ca^{2+}-HCO_3^- and blended Ca^{2+}-Mg^{2+}-Cl^-. Very rarely some examples are found in zone 2, 3, which shows groundwater sort of Na^+-Cl^-, Ca^{2+}-Na^+-HCO_3^- separately. The water category is Ca-Mg-Cl type, as it is analysed by the Piper diagram. According to the Wilcox graph, the greater part of the example falls in the passable range. In the total samples of 60 tested, 11 samples location SAR value is below 6. If the value is 6-9, the soil should be monitored and tested frequently for the increase of sodium. In 22 examples, SAR is more noteworthy and 9 samples are appropriate for irrigation. Magnesium risk is high in the examination territory. Demonstrating filtering and disintegration of salts throughout rainfall infiltrates into the aquifer matrix. The outcome uncovers that water quality falls in the classification of high in saltiness and low in SAR according to the USSL outline.

REFERENCES

Ahamed, A. Jafar, Loganathan, K. and Jayakumar, R. 2015. Hydrochemical characteristics and quality assessment of groundwater in Amaravathi River Basin of Karur District, Tamil Nadu, South India. Sustainable Water Resources Management, 1(3): 273-291.

Al-Ahmadi and Masoud Eid. 2013. Groundwater quality assessment in Wadi Fayd, Western Saudi Arabia. Arabian Journal of Geosciences, 6(1): 247-258.

APHA,1998. Standard Methods for the Examination of Water and Wastewater. 20th Edition, American Public Health Association

Ayuba, R., Omonona, O.V. and Onwuka, O.S. 2013. Assessment of groundwater quality of Lokoja Basement Area, North-Central Nigeria. Journal of the Geological Society of India, 82(4): 413-420.

Basamba, Twaha, Kassim Sekabira, A., Mary Kayombo and Paul, Segawa 2013. Application of factor and cluster analyses in the assessment of sources of contaminants in borehole water in Tanzania. Pol. J. Environ. Stud., 22(2): 337-346.

BIS, 2009. Drinking Water-Specification, Bureau of Indian Standards. New Delhi.

Krishnasamy, R ., Shyamala, G., Johnson, S., Christian, Sabarinathan, K., Sakthivel, S. and Rajesh Kumar, K. 2020. Performance management of transmission line tower foundations against corrosion by non destructive testing. International Journal of Engineering and Advanced Technology, 9(3): 443-447.

Kshetrimayum, K. S. and Bajpai, V. N. 2012. Assessment of groundwater quality for irrigation use and evolution of hydrochemical facies in the Markanda River Basin, Northwestern India. Journal of the Geological Society of India, 79(2): 189-198.

Mohamed, Adam Khalifa, Dan Liu, Mohamed, A., A. Mohamed and Kai Song 2018. Groundwater quality assessment of the quaternary unconsolidated sedimentary basin near the Pi River using fuzzy evaluation technique. Applied Water Science, 8(2): 1-12.

Ramesh, S., Shyamala, G., Ramesh, N., Kalaivani, M., Mageshkumar, P. and Rajesh Kumar, K. 2020. Assessment of irrigation water quality in Orathupalayam Dam, Tamil Nadu, India. International Journal of Scientific & Technology Research, 9(02): 5399-5403.

Ramkumar, Thirunavukkarasu, Senapathi Venkatramanan, Irudhayanathan Anithamary and Sheik Mohamed Syed Ibrahim 2013. Evaluation of hydrogeochemical parameters and quality assessment of the groundwater in Kottur Blocks, Tiruvarur District, Tamilnadu, India. Arabian Journal of Geosciences, 6(1): 101-108.

Salifu, Musah, Felix Aidoo, Michael Saah and Hayford Dickson 2015. Evaluating the suitability of groundwater for irrigational purposes in some selected districts of the upper west region of Ghana. Applied Water Science, 10.1007/s13201-015-0348-1

Sappa, Giuseppe, Sibel Ergul and Flavia Ferranti 2014. Water quality assessment of carbonate aquifers in Southern Latium Region, Central Italy : A case study for irrigation and drinking purposes. Applied Water Science, 4: 115-128.

Shanmugasundharam, A., Kalpana, G., Mahapatra, S. R., Sudharson, E. R. and Jayaprakash, M. 2015. Assessment of groundwater quality in Krishnagiri and Vellore Districts in Tamil Nadu, India. Applied Water Science, 10.1007/s13201-015-0361-4.

Shyamala, G. and Jeyanthi, J. 2017. Integrated weighted overlay model using inverse distance weightage for assessing groundwater quality. Journal of Environmental Science and Management, 20(1): 26-32.

Shyamala, G., Jeyanthi, J. and Gobinath, R. 2016. Nested hydrochemical and principle component analysis in predicting groundwater quality. Eco. Env. & Cons., 22(1): 225-233.

Shyamala, G., Arun Kumar, B., Manvitha, S. and Vinay Raj, T. 2020. Assessment of spatial interpolation techniques on groundwater contamination. Springer International Publishing, http://dx.doi.org/10.1007/978-3-030-24314-2_33.

Shyamala, G., Shivanand, K. P. and Suresh Babu, S. 2008. A preliminary report on the physico-chemical nature of water pollution in and around Erode Town, Tamil Nadu. Nature Environment and Pollution Technology, 7(3): 555-559.

Shyamala, G., Shivanand, K. P. and Suresh Babu, S. 2008. Identification of pollution potential along Cauvery basin b satellite images. Nature Environment and Pollution Technology, 7(1): 93-95.

Srinivas, Y., Aghil, T. B., Hudson Oliver, D., Nithya Nair, C. and Chandrasekar, N. 2015. Hydrochemical characteristics and quality assessment of groundwater along the Manavalakurichi Coast, Tamil Nadu, India. Applied Water Science, 10.1007/s13201-015-0325-8.

Srinivasamoorthy, K., Vasanthavigar, M., Chidambaram, S., Anandhan, P., Manivannan, R. and Rajivgandhi, R. 2012. Hydrochemistry of groundwater from Sarabanga Minor Basin, Tamilnadu. Proceedings of the International Academy of Ecology and Environmental Sciences, 2(3): 193-203.

Nature Environment and Pollution Technology
An International Quarterly Scientific Journal

p-ISSN: 0972-6268
(Print copies up to 2016)
e-ISSN: 2395-3454

Vol. 20 | No. 2 | pp. 801-804 | 2021

Original Research Paper

https://doi.org/10.46488/NEPT.2021.v20i02.042

Open Access Journal

Design and Development of Solar Charging System for Electric Vehicles: An Initiative to Achieve Green Campus

Gnanasekaran Sasikumar*† and A. Sivasangari**

*Department of Mechanical Engineering, GMR Institute of Technology, Srikakulam-532127, Andhra Pradesh, India

**Department of Electronics and Communication Engineering, GMR Institute of Technology, Srikakulam-532127, Andhra Pradesh, India

†Corresponding author: Gnanasekaran Sasikumar; sasikumar.g@gmrit.edu.in

Nat. Env. & Poll. Tech.
Website: www.neptjournal.com

Received: 18-05-2020
Revised: 11-06-2020
Accepted: 13-07-2020

Key Words:
Green energy
Renewable energy
Solar photovoltaic
Solar vehicle

ABSTRACT

Renewable energy is a kind of energy that is obtained through different resources such as sunlight, wind energy, tides, geothermal etc. It provides clean energy that comes from natural sources which can be replenished continuously. The utilization of more amount of renewable energy will lower the prices of and demand for fossil fuels. Solar photovoltaic energy is predominantly used for many applications like heating, cooking and power generation. Recent inventions helped in developing vehicles that are driven by solar energy. In this paper, the design and development of a solar charging system for electric vehicles using a charge controller is discussed. Implementation of the proposed system will reduce the electricity cost and charging and discharging losses. Also, the proposed solar charging system will be one of the initiatives taken to achieve Green campus. This paper will demonstrate the system design and performance analysis of a solar-charged electrical vehicle system.

INTRODUCTION

The demand for energy is increasing due to the increase in population and the economic conditions of many countries. Recent research works reported that fossil fuels have limitations such as global warming, limited resources and economical issues. The energy crisis is expected in the near future and the utilization of renewable energy is to be explored to the maximum possible extent to overcome the problems that arise out from fossil fuels. Many researchers suggested the use of renewable energies considering many environmental aspects. Renewable energy such as solar energy can be an effective alternative in terms of its availability, cost-effectiveness and environmental friendliness.

ELECTRIC VEHICLE CHARGING SYSTEM

The combination of electric vehicles (EVs) and photovoltaic generation (PV) was developed and their performance was studied. In the model, a linear optimization model is used to assess its impact on the energy system (Fattori et al. 2014). The design criteria, setting up, control strategies and experimental tests applicable for a power configuration of DC micro-grid for rapid charging of full electric and plug-in hybrid vehicles. The proposed charging architecture is derived from an analysis comparing the main characteristics of well-known architectures. The study of the proposed power conversion architecture is focused on the evaluation of charging/discharging power, efficiency, energy flux management and its impact on the main grid. In addition, proper control strategies are evaluated and implemented, allowing the proposed architecture to follow the required operations. The operation of electric vehicles using renewable energy systems is an environmentally friendly technology (Capasso et al. 2015). A smart charging station was developed for Plug-in Hybrid Electric Vehicles (PHEVs) based on DC link voltage sensing (Goli et al. 2014).

A specific combination of electric vehicles with photovoltaic systems was reported which are mainly used for home to work or home to education transports operated from a grid connected photovoltaic system. For this application, two strategies for the smart charging of electric scooters are investigated. The study also concluded that this application permits operation of electric scooters against fuel scooters with no higher costs and with less CO_2 emissions (Mesentean et al. 2010). An electric circuit-based battery and a capacity fade model was developed suitable for electric vehicles (EVs) in vehicle-to-grid applications. A control algorithm was developed for the battery to compute the processed energy, charge or discharge rate, and state of charge limits of the battery. The obtained battery characteristics were in close agreement with the measured characteristics (Thirugnanam et al. 2014).

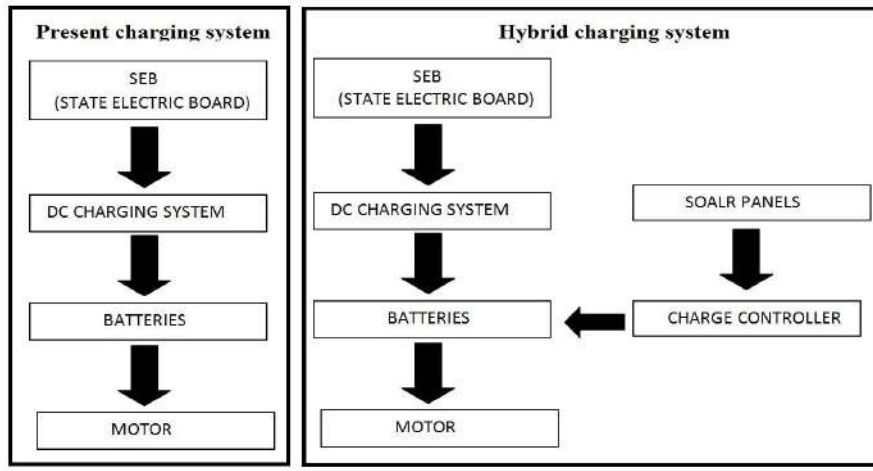

Fig. 1: Vehicle charging system.

A novel bi-directional battery charger for PHEV/EV with a photovoltaic generation system was proposed and the operation algorithm of the battery charger system was studied (Choe et al. 2010). The Charging Stations (CSS) of Electric Vehicles (EVs) and their coordination at the substation level were presented by Fuzzy Logic Controllers (FLCs) at the substation and the CS level (Singh et al. 2013). The design of a power-electronic-assisted On-circuit tap changer (OLTC) was proposed for grid voltage regulation (Chandra Mouli et al. 2015).

Electric vehicles require electricity for charging the batteries. This involves the increment of operational costs hence replacing this system with solar energy would nullify the high operational costs. So in order to convert the normal electric vehicles into hybrid electric vehicles, some solar panels and a specialised charge controller is necessary. Solar panels help in trapping and converting the solar energy into electrical energy while the charge controller regulates and selects the source for charging as shown in Fig. 1.

Solar charging for electrical vehicles is a basic and viable application of using solar energy to achieve sustainable energy development. The solar charging is based on the utilization of solar PV panels for converting solar energy to DC voltage. The DC voltage can be stored in the battery bank by a charge controller. An inverter is employed to convert the DC voltage from the battery bank to 110 volt AC at 60 Hz frequency that is identical to the power from the electric outlet. This paper will address the fundamental concepts of designing and developing solar PV systems for charging electrical vehicles for an educational institute.

COMPONENTS OF VEHICLE CHARGING SYSTEM

For successful implementation of the project, the following are the main components required:

1. Electric vehicle
2. Solar Photo-Voltaic module
3. Charge controllers

Electric Vehicle

The following section explains the requirements of the vehicle which will be charged by solar energy. The Graphical representation of electric vehicle is shown in Fig. 2.

Design calculations: Power (Watts) = Weight of vehicle (kg) × g(m/s^2) × max. speed (m/s) × gradient (%)

$P = 175 \times 9.81 \times 5.5 \times 3\% = 282.9$ Watts

Hence, the Motor specification selected for this electrical vehicle is 300 Watts, 48 V BLDC motor.

Load current = 300 W/ 48V = 6.25 A

The vehicle is used for 2 hours/day and assuming 20% losses,

So, load current per day = $2.0 \times 6.25 \times 1.2 = 18$ AH/ day

Energy required for 300 W motor is $6.25 \times 18 = 864$ W/day

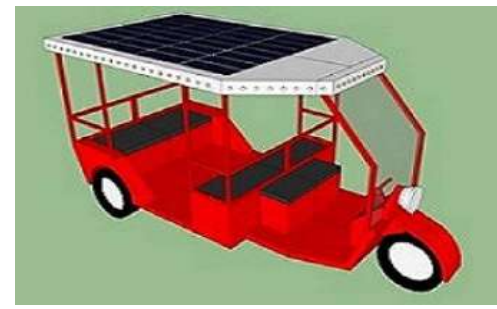

Fig. 2: Graphical representation of the electric vehicle.

Table 1: Specifications of available electric vehicle

Parameter	Rating
No. of batteries	4
Rating of the batteries	12V, 150AH
Charging voltage	48V
Area on top (in ft)	5”3(L) · 3”2(B)
Seating capacity	4+1
Motor specifications	48V, 300W, BLDC motor

Therefore 48V, 18 AH /day is required for the system which can be supplied by four 12V batteries of 150AH. Based on the above calculations, the specifications of the electrical vehicle are listed in Table 1.

Solar PV Module

PV modules consist of many PV cell circuits, normally in series, sealed in an environmentally protective laminate and are the fundamental building block of PV systems. The PV cells convert sunlight into DC current electricity. The specifications of solar PV panel required for the project is depicted in Table 2.

Charge Controller

The charge controller is used to receive and regulate the input voltage from PV power source and stores the energy by charging the battery bank. The charge controller circuit diagram connecting with other components such as solar panels and battery is shown in Fig. 3.

The complete assembly of the solar-powered vehicle system is shown in Fig. 4.

COST ESTIMATION FOR SOLAR CHARGING INSTALLATION

Cost of Solar PV panels	Rs.12000
Charge controller	: Rs.1500
Cables, clamps and other accessories	: Rs.1500

Table 2: Specifications of solar PV module.

Parameter	Rating
Operating Voltage	12 V
Maximum Power (Pmax)	75 W
Open Circuit Voltage (Voc)	22.72 V
Short Circuit Current (Isc)	4.32 A
Maximum Power Voltage (Vmp)	19.04 V
Maximum Power Current (Imp)	3.89 A
Maximum System Voltage	1000 V

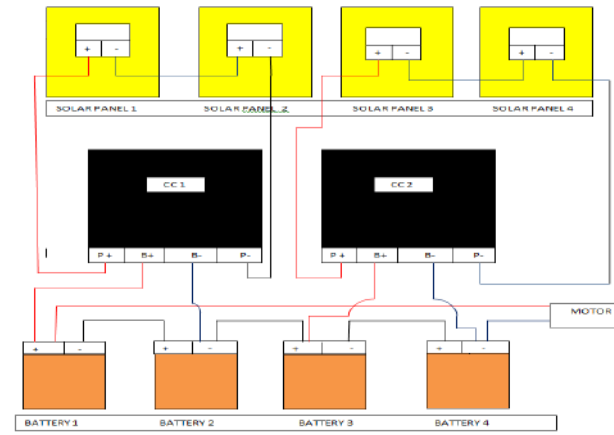

Fig. 3: Charge controller circuit diagram.

Fig. 4: Assembly of solar powered vehicle system.

Generation/day	: 1.5 units/day
Generation/year	: 547.5 units/year
Charge/unit	: Rs.7.8/unit
Revenue /year	: Rs.4270/year
Payback period	: 3.5 years

COMPARISON OF PROPOSED SOLAR AND EXISTING ELECTRICAL CHARGING SYSTEM

The cost and other operating parameters related to the proposed solar and existing electrical charging system are shown in Table 3. From Table 3, it is understood that the proposed solar charging system is superior in terms of functional and economical considerations.

Table 3: Comparison of the proposed solar and existing electrical charging system.

Parameters	Proposed Solar charging system	Existing Electrical charging system
Maximum speed	20 Km per Hour	20 Km per Hour
Initial cost (Rs)	15000	10000
Distance covered after 100% charging	42-45 Km	40 Km
Charging time (Hours)	8	7 to 8
Operating cost (Rs)	Nil	7.5 per unit
System operation guarantee (Years)	25	5

CONCLUSION AND FUTURE SCOPE

The development of the Solar Charging system for electrical vehicles project comprised of various disciplines like electrical, electronics, and mechanical engineering technologies. This paper attempted to provide a framework for the design and development of a solar charging system which would provide an opportunity for the students to learn the theoretical aspects and hands-on experience of utilizing solar energy. The proposed solar charging system will be one of the initiatives taken to achieve a Green campus. The design considerations and calculation for various components are presented in detail. The economic analysis of the proposed system reveals that the payback period of the project is 3.5 years. It is clearly evident from Table 3 that the proposed solar-based vehicle charging system is better than the existing electrical charging system both in terms of operation and economical aspects. Researchers work on this project get a basic idea of the design and building of Solar PV systems for several useful applications such as electrical vehicle system.

Based on the proposed project, many new works will be developed to design an efficient system for further applications. The performance analysis of the solar-charged vehicle system will be carried out to enhance the efficiency of the pilot project. As a measure to reduce the carbon footprint to achieve energy sustainability, this project will be further enhanced. In addition to this solar charging system, an effort will be made to operate all battery-operated vehicles available on the campus to utilize solar energy by establishing more charging stations. This initiative will encourage energy sustainability on campus and inspire the various stakeholders such as students, faculty and staff to use public transportation and electric vehicles that are charged by solar energy.

ACKNOWLEDGEMENT

The authors are grateful to their management for allowing them to do this research and thankful to the anonymous referees for their valuable suggestions to enhance the features of the content.

REFERENCES

Capasso, C. and Veneri O. 2015. Experimental study of a DC charging station for full electric and plug in hybrid vehicles. J. Applied Energy, 152: 131-42.

Chandra Mouli, G.R., Bauer, P. and Zeman, M. 2016. System design for a solar powered electric vehicle charging station for workplaces. J. Applied Energy, 168(15): 434-443. doi.org/10.1016/j.apenergy.2016.01.110.

Choe, G.Y., Kim, J.S. and Lee, B.K. 2010. A Bi-directional battery charger for electric vehicles using photovoltaic PCS systems. In: IEEE Vehicle Power Propuls Conf., IEEE, pp. 1-6.

Fattori, F., Anglani N. and Muliere G. 2014. Combining photovoltaic energy with electric vehicles, smart charging and vehicle-to-grid. J. Solar Energy, 110: 438-51.

Goli, P. and Shireen, W. 2014. PV powered smart charging station for PHEVs. J. Renewable Energy, 66: 280-7.

Mesentean, S., Feucht, W., Mittnacht, A. and Frank, H. 2011. Scheduling methods for smart charging of electric bikes from a grid-connected photovoltaic-system. In: UKSim 5th Eur Symp Computer Modeling Simulation, IEEE; p. 299-304.

Singh, M., Thirugnanam, K., Kumar, P. and Kar, I. 2015. Real-time coordination of electric vehicles to support the grid at the distribution substation level. J. IEEE Syst., 9: 1000-10. doi.org/10.1109/JSYST.2013.2280821.

Thirugnanam, K., Ezhil Reena, JTP., Singh, M. and Kumar, P. 2014. Mathematical modelling of Li-ion battery using genetic algorithm approach for V2G applications. IEEE Trans. Energy Convers., 29: 332-43.

Nature Environment and Pollution Technology
An International Quarterly Scientific Journal

p-ISSN: 0972-6268
(Print copies up to 2016)
e-ISSN: 2395-3454

Vol. 20 | No. 2 | pp. 805-818 | 2021

Original Research Paper

https://doi.org/10.46488/NEPT.2021.v20i02.043

Open Access Journal

Statistical Downscaling of Rainfall Under Climate Change in Krishna River Sub-basin of Andhra Pradesh, India Using Artificial Neural Network (ANN)

K.V.R. Satya Sai*, S. Krishnaiah and A. Manjunath*****

*Jawaharlal Nehru Technological University Anantapur, Anantapuramu, Andhra Pradesh, India

**Department of Civil Engineering, Jawaharlal Nehru Technological University Anantapur, Anantapuramu, Andhra Pradesh, India

***Civil Engineering Department, MVSR Engineering College, Nadergul, Hyderabad, India

†Corresponding author: Dr. A. Manjunath, manjunath.aluru@gmail.com

Nat. Env. & Poll. Tech.
Website: www.neptjournal.com

Received: 22-04-2020
Revised: 03-06-2020
Accepted: 26-06-2020

Key Words:
SDSM
Downscaling
Climate change
Rainfall
Artificial neural network

ABSTRACT

Due to the very coarse spatial resolution of the different global circulation model (GCM), we cannot use them in their natural form to study the various impacts of climate change. For matching this spatial inequality between the GCMs output (predictor) and historical precipitation data (predictands), we need to establish a relation between them which is known as downscaling. In the present study, we tried to examine the efficiency of the Artificial Neural Network (ANN) with Principal Component Analysis (PCA) for downscaling the rainfall for 3 districts of Andhra Pradesh of India. Firstly, for all the regions, the downscaling was performed by using ANN. Then seasonal and annual analysis was performed based on the R^2 and RMSE. The results show that the ANN worked adequately based on the statistical parameters. The study uses the Canadian Earth System Model (CanESM2) of the IPCC Fifth Assessment Report, re-analysis from the National Centre for Environmental Prediction (NCEP) as GCM model, and observed rainfall data as the observed rainfall. The analysis was performed for the three RCPs scenario, RCP 2.6, 4.5 and 8.5. Finally, the ANN model is applied to downscale the precipitation.

INTRODUCTION

Krishna River is one of the important rivers in AP and Telangana. Krishna basin is the second-largest eastward draining interstate river in peninsular India. It starts its journey near Jor village (near Mahabaleswar) in the Western Ghats at an elevation of about 1337 m above MSL and ends its journey into the Bay of Bengal near Hamsala Deevi near Vijayawada. The Krishna basin covers an area of nearly 8% of the total geographical area of the country. The Krishna river basin is located in the south part of Andhra Pradesh and Telangana. The basin spreads over parts of administrative limits of Mahabubnagar, Kurnool, Krishna, Nalgonda, Guntur, and Prakasam districts. It flows for a distance of 305 km in Maharashtra, 483 km in Karnataka and 612 km in Andhra Pradesh and Telangana combined before finally out falling into the Bay of Bengal.

The present study area (Fig. 1) is from Nagarjuna Sagar dam to Hamsala Deevi passing through Krishna, Guntur, and parts of Prakasam districts. The climate of the river basin varies from humid to sub-humid and arid conditions. Most precipitation occurs in the southwest monsoon season (June to September). In other seasons all tributaries and master stream are also ephemeral streams. It is necessary to study climate change impacts on hydrological and water resources of the study area (Krishna River sub-basin containing 3 districts namely Krishna, Guntur and Prakasam Districts).

If we see the historical data, we can visualize that the frequency of heavy rainfall events is increasing year by year. As per the report of the Intergovernmental Panel on Climate Change (IPCC) 2013-AR5, it is predicted that the increase in temperature from the year 1990 to 2100 will be approximately 1.7°C to 4.9°C (Chen et al. 2012; Crawford et al. 2007). The study consists of the following steps: The Intergovernmental Panel on Climate Change (IPCC) in their fifth assessment report AR5, reported that the change in local precipitation and temperature due to climate change may cause the increase of hazards like droughts and floods and their severity (Cardona 2012; Randall et al. 2007) particularly at continental and larger scales. Confidence in these estimates is higher for some climate variables (e.g., temperature. General Circulation Model (GCM) models are capable to predict the expected change in climatic conditions for the future (Chen et al. 2012; Rajan 2014). Since the GCM model events are produced on a very massive grid

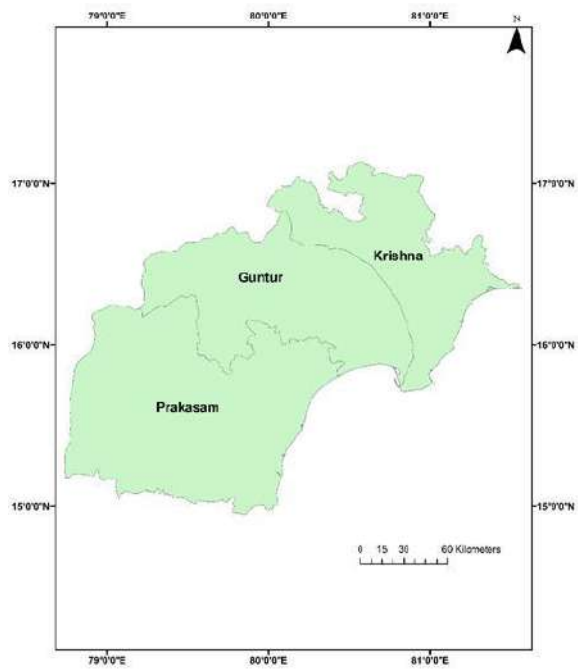

Fig. 1: Study area with longitudes and latitudes.

system (300 to 750 km) (Tan et al. 2017). Due to this large grid which is courser in nature the results obtained are not precise enough to be used directly to study the variation of different hydrological impacts at a local scale (Huang et al. 2011). General Circulation Model (GCM) models are capable to predict the expected change in climatic conditions for the future. Since the GCM model results are created on a very larger grid-scale (200 to 650 km) (Shukla et al. 2016). Due to this large grid which is courser in nature the results obtained are not precisely sufficient to be applied straight to study the change of different hydrological influences at the local scale (Nourani et al. 2019; Xu et al. 2020) little information is available regarding the downscaling using machine learning methods, specifically at hydrological basin scale. To overcome these scale parameters, we used downscaling which is capable to fill the rift among the local scaled climatic inputs and global scaled climatic parameters (Mahmood and Babel 2014, Wilby et al. 2002, Wilby & Dawson 2015). In the 21st century, climate change is considered to be one of the greatest environmental threats to the world, and the changes in climate extremes are estimated to have greater negative impacts on human society and the natural environment than the changes in mean climate. This study presents the projections of future changes in extreme temperature events under A2 and B2 SRES scenarios using the statistical downscaling model (SDSM). So, we can say that projection across different scales which is also known as downscaling is a procedure that relates local and regional-scale climate variables to the larger-scale atmospheric components.

DOWNSCALING USING ANN MODEL

In the present study, the Artificial Neural Networks (ANNs) along with PCA has applied to downscale the precipitation in different three regions of Andhra Pradesh. In the present study, we have applied Feed Forward Back Propagation (FFBP) algorithm to develop a multi-layer perceptron (MLP) ANN model for downscaling of precipitation in the study area. The detailed process of the general downscaling process and the downscaling by ANN are shown in Fig. 2 and Fig. 4 respectively. Available precipitation data is used for predictands and CanESM2 model is used as GCM for predictor (Fig.7). While a random selection of data is used in the ANN model, 70 % of the data is used for the model and the remaining 30 % is used for testing and validation of the model. The performance evaluation of the ANN model is tested by R^2 and RMSE value.

The Multi-Layer Perceptron (MLP)

An artificial neural network (ANN) is a knowledge processing method based on the different data which has a comparable similar function like neurons of the human brain (Hannan et al. 2010; Kumar et al. 2012).

MLPs are the commonly accepted and the simplest type of ANN model (Joshi 2016). The MLPs are used to derive the relationship between different input and outputs (Ghosh and Misra 2010; Pervez and Henebry 2014). Multi-layer perceptron is feed-forward networks that comprise one or more hidden layers as shown in Fig. 3. The MLP used in the present study comprised a three-layer framework consisting of an input layer, a hidden layer, and an output layer. The

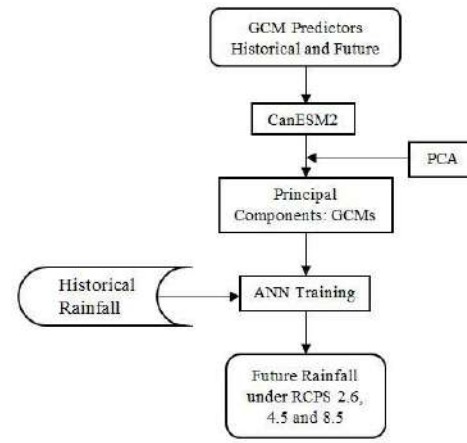

Fig. 2: The flowchart for downscaling using ANN.

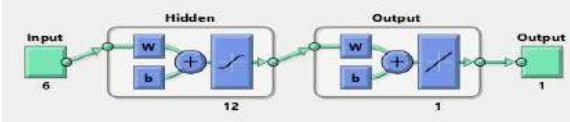

Fig. 3: The basic model of the ANN (Multi-layer Perceptron) used in the study.

Levenberg-Marquardt (LM) algorithm (Luo et al. 2013) is an effective learning strategy for multilayer feed-forward networks (Kusunoki and Arakawa 2015; Onyutha et al. 2016). This method is a revised variant of the classic Newton approach for obtaining an optimum result for any optimization problem. This method uses an approach to the Hessian matrix as presented in Eq. (1).

$$x_{k+1} = x_k - [J^T J + \mu I]\text{^}{-1} J^T e \quad \ldots(1)$$

Where, x is different weights of the neural network, J is the performance criteria Jacobian matrix and μ and e are learning process related parameter and residual error vector, respectively.

Principal Component Analysis (PCA)

Principal component analysis, also recognized as the Karhunen Loeve transform, is one of the commonly accepted techniques for reducing dimensionality (Beaumont 2012; Yang et al. 2017). PCA is used to modify a set of correlated M-dimensional predictors (as shown in Table 1) into another set of N-dimensional uncorrelated vectors called principal components (PCs) by using a linear combination (shown in Table 2). While transformation it is necessarily maintained that maximum information captured by the original data set is saved in the first few dimensions of the new set as presented in Table 3. In the present study, PCA was done to decrease the dimensionality of the predictors from 26 to 7, which contains the 99.98% information of the original data as shown in Table 1. These new datasets are used as input to the ANN downscaling model. So, we can say that to lessen the input dimension to the downscaling method and to pick the best set of predictors that hold all basic climate data we used PCA i.e. in PCA, the main aim is to find a set of N principal components which:

1. Is much less than the original set of M variables,
2. Having descriptions for nearly all of the total specimen variance.

MATERIALS AND METHODS

Study Area and Data Used in the Downscaling Process

The Krishna basin climate is dominated by the southwest monsoon, which provides most of the rainfall or precipitation for the basin. Maximum flow in the river occurs during

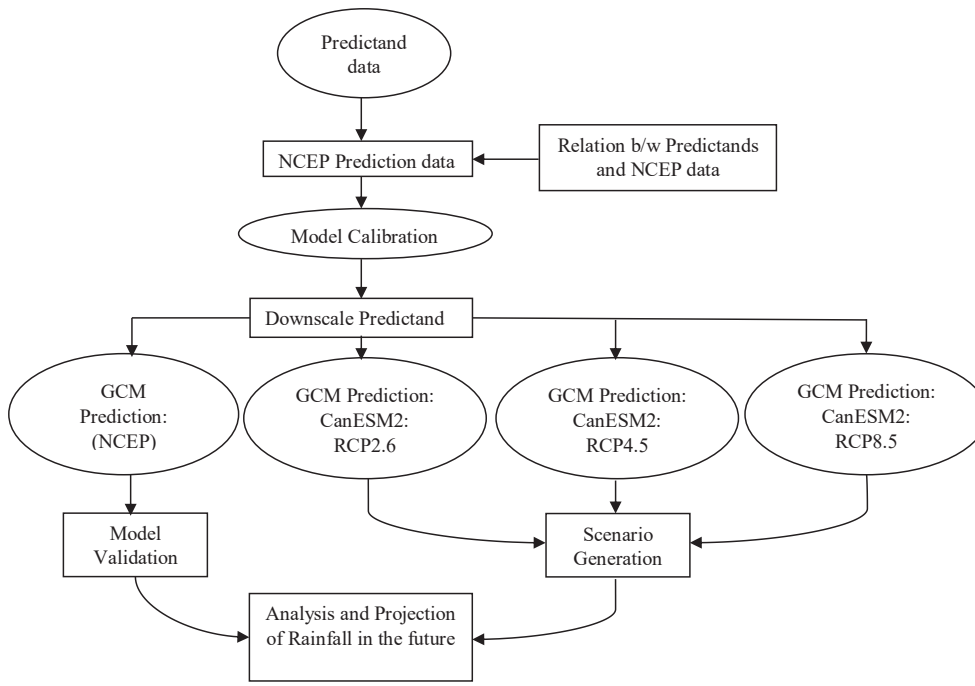

Fig. 4: The flowchart of the downscaling process using GCM Predictor.

the months of August-November and the low flow season is from April to May (at Vijayawada). The South-Central part of the basin is truly arid. On average, annual rainfall in the Krishna basin is 784 mm. The southwest monsoon sets in by the middle of June and withdraws by the middle of October. The annual rainfall received during the monsoon months is about 90%. Except for the monsoon months, the climate of the catchment remains dry. From the climatological observations, it is seen that the mean daily maximum temperature in the basin varies from 27°C to 40°C and the mean daily minimum temperature varies from 20°C to 27°C. The relative humidity in the basin ranges from 17 to 92%. Mean relative humidity is high during the monsoon period and comparatively low during the post-monsoon period. In summer, the weather is dry and the humidity is low. The catchment is influenced by south-west winds during the monsoon season. In the post-monsoon season, they blow from north-west to north. In the winter season, the winds blow from the north-west and south-west directions. In the Krishna basin, wind speed varies from 4.0 to 21.7 kmph.

Table 1: The score of different predictors after PC.

PCs	Score	Total Summation of first 7 PCs
PC1	89.99004	89.99004
PC2	09.56467	99.35471
PC3	0.352653	99.80737
PC4	0.035374	99.74274
PC5	0.022946	99.97569
PC6	0.013162	99.96585
PC7	0.006646	99.98555
PC8	0.003629	99.98913
PC9	0.002732	99.99186
PC10	0.001984	99.99384
PC11	0.001901	99.99574
PC12	0.001244	99.99699
PC13	0.001054	99.99804
PC14	0.000668	99.99871
PC15	0.000487	99.99919
PC16	0.000318	99.99951
PC17	0.000190	99.99971
PC18	0.000137	99.99984
PC19	8.43E-05	99.99992
PC20	6.74E-05	99.99999
PC21	7.79E-06	100.0000
PC22	1.12E-11	100.0000
PC23	2.48E-13	100.0000
PC24	1.56E-13	100.0000
PC25	1.15E-13	100.0000
PC26	5.83E-14	100.0000

We have used shapefiles and rainfall data for our analysis. Fig. 5 shows the area for which shapefiles were digitized from various topo sheets and mosaicked using QGIS3.

The study area comprised of Krishna, Guntur and Prakasam Districts, which lies in the southern part of the Krishna River basin. The rainfall data is procured from Indian Meteorological Department, Hyderabad and http://imdpune.gov.in/ndc_new/ stations.html.

RAINFALL PATTERN

Theissen Polygons method: This method is applied to calculate average precipitation in different villages of the district.

The working principle of the Thiessen Polygon method is explained in Eq. (2) and shown in Fig. 6.

$$P_{avg} := \frac{\sum_{i=1}^{n} (A_i \cdot P_i)}{\sum_{i=1}^{n} A_i} \quad ..(2)$$

Where P_{avg} is the areal average precipitation over the watershed, A_i is the area of polygon i and P_i is the precipitation for polygon i. The integer n is the number of polygons and gauges.

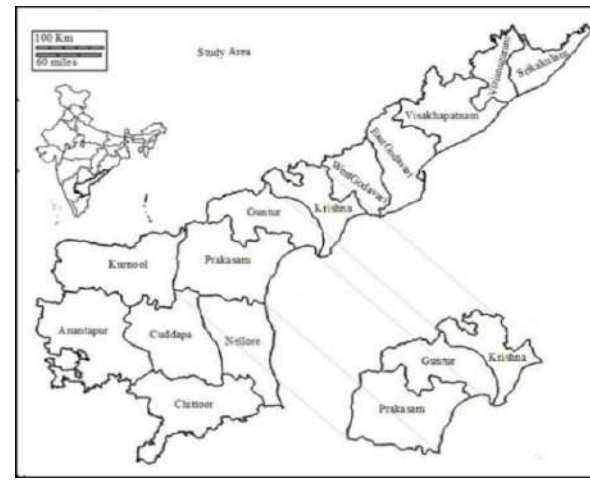

Fig. 5: Study area showing Krishna, Guntur and Prakasam districts.

Table 2: Correlation between 9 predictors before PCA.

	PC1	PC2	PC3	PC4	PC5	PC6	PC7	PC8	PC9
PC1	1	0.527673	0.255703	0.672074	0.685847	0.188658	0.797942	0.665339	0.673378
PC2	0.527673	1	0.696146	0.885125	0.479155	0.014698	0.487015	0.930171	0.850616
PC3	0.255703	0.696146	1	0.665569	0.242076	0.123365	0.217838	0.673246	0.722237
PC4	0.672074	0.885125	0.665569	1	0.552003	0.02717	0.578878	0.907174	0.859587
PC5	0.685847	0.479155	0.242076	0.552003	1	0.137442	0.867429	0.604516	0.640432
PC6	0.188658	0.014698	0.123365	0.02717	0.137442	1	0.182404	0.024236	0.006538
PC7	0.797942	0.487015	0.217838	0.578878	0.867429	0.182404	1	0.640683	0.669715
PC8	0.665339	0.930171	0.673246	0.907174	0.604516	0.024236	0.640683	1	0.960464
PC9	0.673378	0.850616	0.722237	0.859587	0.640432	0.006538	0.669715	0.960464	1

Table 3: Correlation between 9 predictors after PCA.

	PC1	PC2	PC3	PC4	PC5	PC6	PC7	PC8	PC9
PC1	1	8.44E-34	3.73E-31	4.75E-33	3.33E-32	5.10E-34	2.12E-34	6.80E-33	1.38E-33
PC2	8.44E-34	1	8.16E-32	4.96E-35	2.08E-32	1.50E-31	5.75E-32	1.71E-32	4.86E-33
PC3	3.73E-31	8.16E-32	1	1.62E-32	1.33E-31	5.61E-32	1.37E-33	6.20E-33	8.34E-34
PC4	4.75E-33	4.96E-35	1.62E-32	1	1.57E-31	4.26E-33	5.04E-33	1.56E-33	3.21E-32
PC5	3.33E-32	2.08E-32	1.33E-31	1.57E-31	1	4.87E-31	1.31E-31	5.69E-33	3.46E-32
PC6	5.10E-34	1.50E-31	5.61E-32	4.26E-33	4.87E-31	1	7.50E-34	1.78E-32	1.51E-32
PC7	2.12E-34	5.75E-32	1.37E-33	5.04E-33	1.31E-31	7.50E-34	1	2.08E-33	2.79E-32
PC8	6.80E-33	1.71E-32	6.20E-33	1.56E-33	5.69E-33	1.78E-32	2.08E-33	1	5.96E-32
PC9	1.38E-33	4.86E-33	8.34E-34	3.21E-32	3.46E-32	1.51E-32	2.79E-32	5.96E-32	1

Table 4: List of 26 NCEP/GCM predictors.

S.No.	Predictors (Atmospheric Variables)	Origin (i.e. NCEP or GCM)	Time Window
1.	Mean Sea Level Pressure	CanESM2	1961-1990 (baseline climate) 2000-2099
2.	1000hPa Wind Speed		
3.	1000hPa Zonal Velocity		
4.	1000hPa Meridional Velocity		
5.	1000hPa Vorticity		
6.	1000hPa Wind Direction		
7.	1000hPa Divergence		
8.	500hPa Wind Speed		
9.	500hPa Zonal Velocity		
10.	500hPa Meridional Velocity		
11.	500hPa Vorticity		
12.	500hPa Geopotential		
13.	500hPa Wind Direction		
14.	500hPa Divergence		
15.	850hPa Wind Speed		
16.	850hPa Zonal Velocity		
17.	850hPa Meridional Velocity		
18.	850hPa Vorticity		
19.	850hPa Geopotential		
20.	850hPa Wind Direction		
21.	850hPa Divergence		
22.	Specific Humidity at 500hPa		
23.	Specific Humidity at 850hPa		
24.	Specific Near Surface Humidity		
25.	Mean Temperature at 2m		
26.	Total Precipitation		

Climate Change Downscaling

Downscaling, or projection across different scales, is a procedure that links local and regional-scale climate variables to the larger scale atmospheric components (Zhang et al. 2016).

Downscaling joins the gap between large and local scale climatic data. The interpretation across scales is based on the assumption that similar atmospheric models produce similar climatic conditions. Now the basic question is that why we need downscaling?

In a better way, we can answer this question that: GCM (General Circulation Models) outputs are of insufficient spatial and temporal resolution, causing an insufficient representation of orography and land surface characteristics, when interoperated may cause lack of some of the features which may have important impacts on the local climate. To overcome these faults, we have to find a way which fulfils the gap by connecting the information that the climate modeling society can currently provide and that needed by different researchers. To overcome this scale mismatch two approaches have been suggested:

1. Develop finer resolution regional climate models that are driven by boundary conditions simulated by global GCMs at coarser scales i.e. RCMs. But they are computationally costly and time taking (Feyissa et al. 2018; Zhang et al. 2016) which have been shown to benefit water resources management and prediction, especially at the basin scale. In this study, the Soil and Water Assessment Tool (SWAT).
2. Derive statistical models from the observed relationship between the large-scale atmospheric fields and local variables and that is achieved by Statistical Downscaling (Chen et al. 2012).

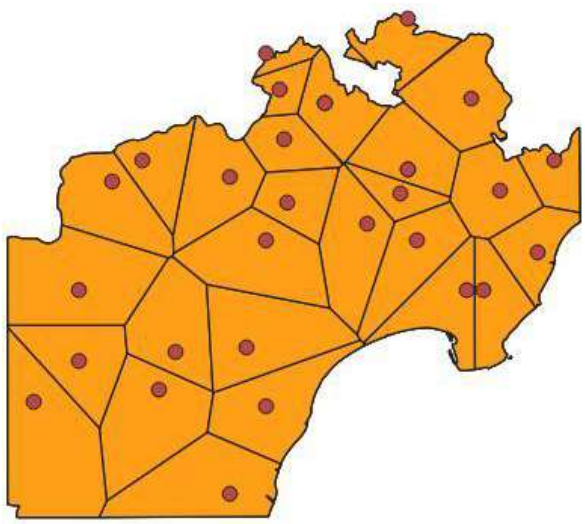

Fig. 6: Theissen Polygons method.

Selection of GCM Model

Global Climate Change Model: CanESM2 Predictors: CMIP5 Experiments: The second generation Canadian Earth System Model (CanESM2):

CanESM2 is the fourth generation coupled global climate model developed by the Canadian Centre for Climate Modelling and Analysis (CCCma) of Environment and Climate Change Canada. CanESM2 represents the Canadian contribution to the IPCC Fifth Assessment Report (AR5). This CanESM2 model is a combination of CanCM4 model and the Canadian Terrestrial Ecosystem Model (CTEM), which based on the terrestrial carbon cycle (Feyissa et al. 2018) which helps us to determine consequences earlier and prepare for necessary adaptation measures. However, it is difficult to apply the raw data of GCMs at a local scale, such as the urban scale, without downscaling due to coarse resolution. This study, therefore, statistically downscaled daily maximum temperature, minimum temperature, and precipitation in 30-year intervals from the second generation of the Earth System Model (CanESM2). The CTEM model explains the land-atmosphere carbon transaction phenomena. CanESM2 consists of three Scenarios: RCP2.6, RCP4.5, and RCP8.5. The Representative Concentration Pathways (RCPs) are four greenhouse gas concentration (not emissions) trajectories selected by the IPCC for its Fifth Assessment Report (AR5) (Kim et al. 2016; Zhang et al. 2016) several downscaling methods have been developed. These methods predominantly focus on a single meteorological series at specific sites. Spatial and temporal correlation of the precipitation and temperature fields is important for hydrologic applications. This research uses a nearest neighbor-genetic algorithm (NN-GA). The four RCPs, RCP2.6, RCP4.5, RCP6.0, and RCP8.5, are described after a reasonable range of radiative forcing values projected in the year 2100. The different RCP Scenarios studied in this study is RCP2.6, RCP4.5, and RCP8.5. RCPs represent a broad area of possible problems related to Climate Change like the effect of greenhouse gases, air pollutants, and their emissions, and different land-use scenario. RCP8.5 considers the highest and RCP2.6 considers the lowest scenarios of greenhouse gases that have been recently reviewed by the study based on climatic research.

Structure of Predictor/Large Scale Dataset Files

A series of the graded daily value of long-term datasets are extracted into a single column text file per grid cell (box). This grid is uniform along the longitude with a horizontal

resolution of 2.8125° and nearly uniform along the latitude of roughly 2.8125°, which is available at the Canadian Climate service centre site. The predictors correlated with each grid cell are designed by the identical folder named *BOX_iiiX_jjY*, where iii represents longitudinal and jj represents the latitudinal index. The predictors organized this way can be used as input in statistical downscaling models.

Selection and Screening of Predictor Variables for Downscaling Process in Case of Precipitation

Choosing a predictor is a major measure in the downscaling method since finally, it reflects the main output i.e. nature of the generated scenarios. In the SDSM, it is a cyclic process that lasts until we get the optimized objective function (Chu et al. 2010; Mahmood and Babel 2014) evaporation, and precipitation in Haihe River basin, China. The data used for evaluation were large-scale atmospheric data encompassing daily NCEP/NCAR reanalysis data and the daily mean climate model results for scenarios A2 and B2 of the HadCM3 model. Selected as climate variables for downscaling were measured daily mean air temperature, pan evaporation, and precipitation data (1961-2000). The selection of large-scale predictors is a two-step process: firstly, we performed a correlation analysis between the NCEP reanalysis historical data with the past precipitation data to screen all the 26 predictor variables (NCEP Re-Analysis) for predictand data. Then the predictors having the highest correlation are selected for further processing. The metrological stations used for downscaling is listed in Table 5.

ANN performs two ways of model calibration based on the characteristics of climate data. They are known as conditional and unconditional methods. A conditional process is established for the precipitation and evaporation data analysis as they are based on the local scale predictors i.e. it is assumed that there is an indirect connection between the data and predictors. In case of an unconditional process, which is used for downscaling of temperature data with considering that there is a direct link to the predictor's i.e. large-scale datasets. During the calibration process, the NCEP-Re-analysis data set is used in accordance with the specified year period for each predictand (as shown in Table 6). The historical data of predictands in this study i.e., precipitation, are divided into two segments: the first segment is used for calibration of the model and the second part of the dataset is used for validation as an independent dataset.

Model Calibration and Validation

In ANN there are two ways to optimize the model output, one is Ordinary Least Square (OLS) method and the other one is Dual Simplex (DS). In the present study, OLS is used because it is faster than DS (Chu et al. 2010; Wilby and Dawson 2015). The Root Mean Square Error (RMSE) and Coefficients of Correlation (R^2) were used to compare the performance of historical and simulated data of the model during the calibration and validation period. The model was calibrated for the period from 1961-1995 is used as the base period and simulate the daily rainfall for the period of 1996-2005 with the help of NCEP and CanESM2 predictors which is used for the validation of the model. The description of R^2 and RMSE of rainfall data are given in Table 7.

WORKING OF ANN MODEL

Data Used in the ANN Model

The rainfall data obtained from IMD are shown in Fig.8 (a-c) for all the three districts of Andhra Pradesh. In case of any missing rainfall data in IMD database, the linear interpolation method is used to find the missing data. As discussed earlier that PCA is applied to select the predictor to train the ANN model. The first seven principal components i.e. predictors are used in the analysis which covers the 99.77% of the predictor data property. In the ANN model the selection of data is random and 70% of data is used for training purpose and the remaining 30% is used for testing and validation. Multi-layer perceptron is feed-forward networks that are based on the Levenberg-Marquardt (LM) algorithm that has been

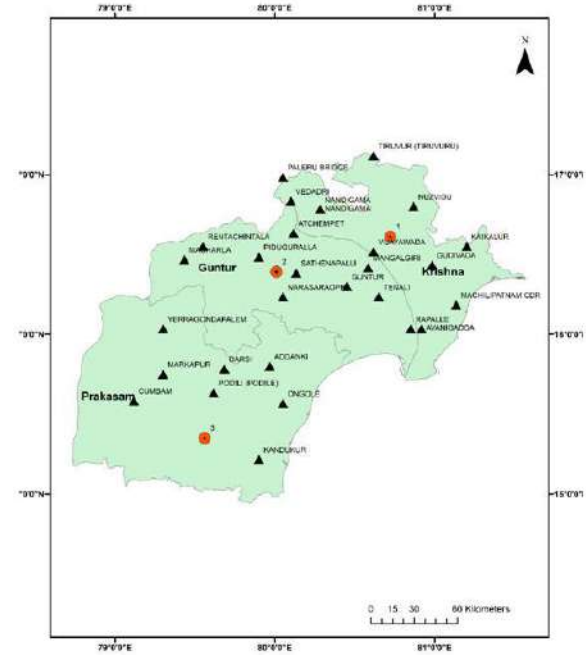

Fig. 7: Rain gauge stations (Black Triangles) and GCM Points (Round Points) in the study area.

used in the ANN model. A total of twelve hidden layers are used in the model along with the six inputs as shown in Fig. 3. The nine hidden layer combination give the best Correlation Coefficient in comparison with the other combination when we are using more or less than nine hidden layers. In this study, three statistical indicators were used to measure the efficiency of the artificial neural network models developed. The assessment indicators include coefficient determination (R^2), Nash Coefficient (E) and Root Mean Square Error (RMSE), as the same is used in the evaluation of the SDSM model.

(a) Root Mean Square Error (RMSE)

The Root Mean Square Deviation (RMSD) or Root Mean Square Error (RMSE) is commonly used to measure the deviations between sample or population values predicted by a model and the observed values (Xiao et al. 2015).

$$RMSE = \sqrt{\frac{\sum_{i=1}^{n}(X_{obs,i} - X_{model,i})^2}{n}} \quad ...(4)$$

Where X_{obs} is observed values and X_{model} is modelled values at time/place *i*.

(b) Coefficient of Determination (R^2)

The coefficient of Determination (R^2): Shows the intensity and control of a linear relationship between two variables (Kazmi et al. 2014). The correlation is +1 in the case of a perfect increasing linear relationship, and -1 in the case of a decreasing linear relationship.

$$R^2 = \frac{[\sum_{i=1}^{n}(O_i - \overline{O_i}) * (P_i - \overline{P_i})]^2}{[\sum_{i=1}^{n}(O_i - \overline{O_i}) * \sum_{i=1}^{n}(P_i - \overline{P_i})]} \quad ...(5)$$

Where, O_i and P_i is observed and simulated value, n is the total number of test data $\overline{P_i}$, $\overline{O_i}$ is the mean value.

(c) Nash-Sutcliffe Coefficient (E)

The Nash-Sutcliffe Model Efficiency Coefficient (E) is commonly used to assess the predictive power of hydrological discharge models (Chen et al. 2012; D. N. Moriasi et al. 2007). It is defined as:

$$E = 1 - \frac{\sum_{i=1}^{n}(X_{obs,i} - X_{model})^2}{\sum_{i=1}^{n}(X_{obs,i} - \overline{X_{obs}})^2} \quad ...(6)$$

Table 5: Metrological stations used for downscaling.

Station Name	Longitude (degrees)	Latitude (degrees)	Period (year)
Krishna	80.7214 E	16.6100 N	1961-2012
Guntur	80.0088 E	16.3906 N	1961-2012
Prakasam	79.5603 E	15.3485 N	1961-2012

Table 6: Data used for calibration and validation of ANN.

Station Name	Longitude (degree)	Latitude (degree)	Data available Period (year)	Calibration Period	Validation Period
Krishna	80.7214 E	16.6100 N	1961-2012	1961-1995	1996-2005
Guntur	80.0088 E	16.3906 N	1961-2012	1961-1995	1996-2005
Prakasam	79.5603 E	15.3485 N	1961-2012	1961-1995	1996-2005

Table 7: R^2 and RMSE value during calibration and validation of the model.

Station Name	Calibration			Validation		
	R^2	RMSE	Nash Coefficient, E	R^2	RMSE	Nash Coefficient, E
Krishna	0.82	3.88	0.80	0.83	3.31	the 0.82
Guntur	0.77	3.29	0.78	0.69	3.34	0.81
Prakasam	0.81	2.91	0.71	0.86	1.99	0.70

Table 8: The parameters selected for the ANN downscaling model.

ANN Network Type	Parameters	Name
MLP (Multi-Layer Perceptron: feed-forward networks)	Number of layers:	03
	Neurons:	
	Inputs:	05
	Hidden:	12
	Output:	01
	Number of iteration:	Sigmoid Losing linear
	Activation function:	Logsig linear
	Activation function in output layer:	Levenberg-Marquardt

Where X_{obs} is observed values and X_{model} is modelled values at time/place *i*. Nash-Sutcliffe efficiencies can range from -∞ to 1. An efficiency of 1 (E = 1) corresponds to a perfect match between model and observations.

Sensitivity Analysis shows that the ANN model combined with PCA for the selection of predictors is more suitable than the SDSM model as shown in Table 4 and Table 8. Now for the Scenario Analysis for the three RCPs 2.6, 4.5 and 8.5, the ANN model is used.

Scenario Analysis

In the present study, for predicting the effect of Climate Change on precipitation trends CanESM2 GCM scenario, i.e. RCP2.6, RCP4.5, and RCP8.5 is used. The period from 1961-2000 is selected as the base period to visualize the changing pattern of rainfall. The selection of the base period is based on the literature review available and these 40 years of data is sufficient to assess the transformation in climate. So, the prediction of future rainfall is based on

Table 9: Projected future changes of mean precipitation in the 3 districts of Andhra Pradesh.

Scenario Variable	RCP2.6				RCP4.5				RCP8.5			
	2020s	2050s	2080s	2100s	2020s	2050s	2080s	2100s	2020s	2050s	2080s	2100s
Guntur (ΔP/P (%))	-1.69	-0.33	4.73	5.25	1.02	-1.78	7.07	8.59	5.82	5.38	9.27	19.51
Krishna (ΔP/P (%))	-0.22	1.25	-1.89	4.66	1.30	4.81	6.13	8.09	8.00	11.39	12.53	18.50
Prakasam (ΔP/P (%))	-1.08	2.70	1.53	5.05	1.05	2.80	5.17	10.7	4.32	9.18	10.85	15.99

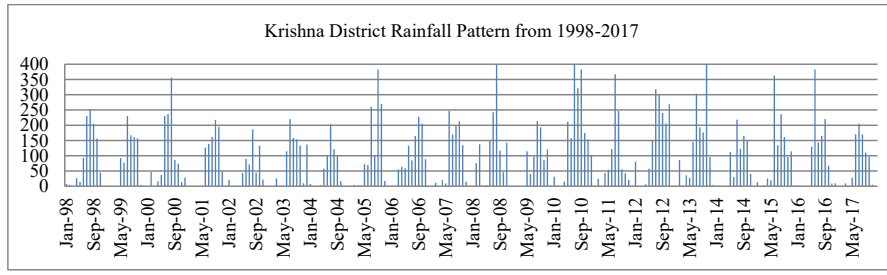

(a) Krishna District Rainfall Pattern

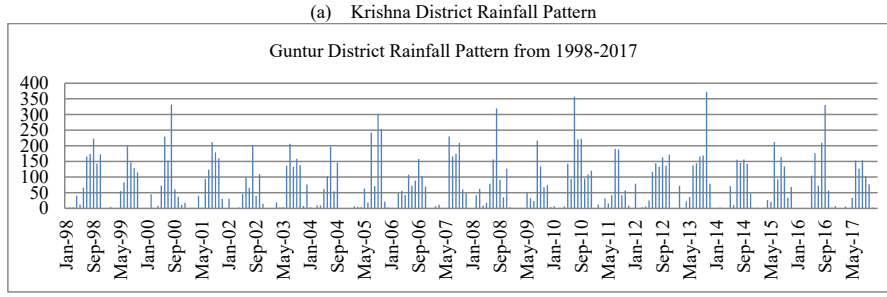

(b) Guntur District Rainfall Pattern

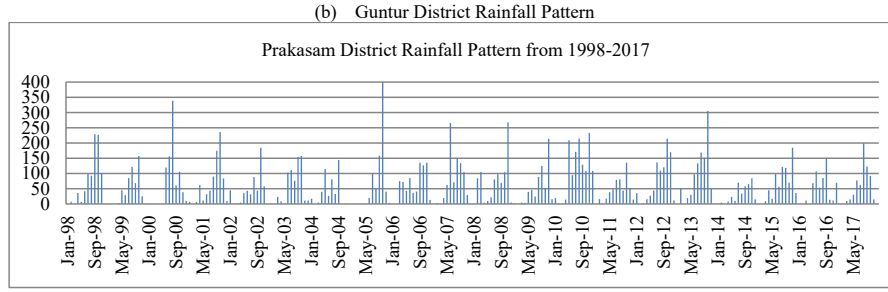

(c) Prakasam District Rainfall Pattern

Fig. 8(a-c): Mean monthly rainfall from three districts of Andhra Pradesh.

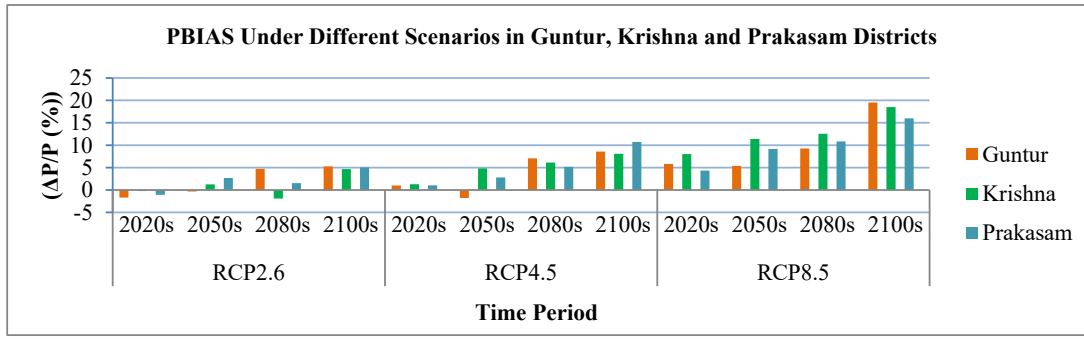

Fig. 9: Showing PBIAS under different scenarios.

the comparison of these two-time extents i.e., 1961-2000 and 2005-2100.

After calibration and validation of the ANN model, the model is used to downscale the large scale predictor variables derived from the RCP2.6, RCP4.5, and RCP8.5 scenarios of CanESM2, with daily precipitation simulated for the following periods: historical (1961-2000), the 2020s (2005-2021), 2050s (2022-2051), 2080s (2052-2080) and 2100s (2081-2100). As mentioned above, the historical simulation (1961-2000) acts as a reference for future projection and changes. Predicted changes in annual mean precipitation during future periods (the 2020s, 2050s, 2080s, and 2100s) in the three districts namely Guntur, Krishna, Prakasam of Andhra Pradesh are shown in Table 9, which shows a mixed pattern of positive or negative changes, with different trends in the 2020s and 2050s, and steady with the increases in the 2080s and 2100s. The trend shows that the overall amount of rainfall will increase significantly in this region of all areas from 2081 to 2100 as compared to the base period due to climate change. While there is a mixed trend in rainfall, under CanESM2 scenarios of RCP2.6 and RCP4.5, the fluctuation in rainfall is slightly different for two scenarios i.e. RCP2.6 and RCP4.5 as compared to the emission scenario of RCP8.5. In RCP2.6, up to 2080s sometimes the rainfall is increasing and in some decades it goes down. In RCP4.5, the trend is slightly higher than the base period for the 2020s and 2050s and in 2080s and 2100 it increases abruptly.

The approximate predicted change up to the 21st century will be 19.51%, 18.50%, and 15.99% for Guntur, Krishna and Prakasam basin respectively under the scenarios of RCP8.5 (Table 9) and PBIAS under different scenarios is as shown in Fig. 9.

The ANN model calibration and validation results are shown in Fig. 10(a-i).

CONCLUSIONS

The present study attempted to forecast the rainfall pattern in three different basins of Andhra Pradesh. The present study tried to investigate the use of the ANN model as a tool for downscaling monthly precipitation for application in Climate Change studies. Firstly, three basins are chosen to perform the downscaling analysis using ANN model. The selection of predictors is based on the PCA was performed for the ANN

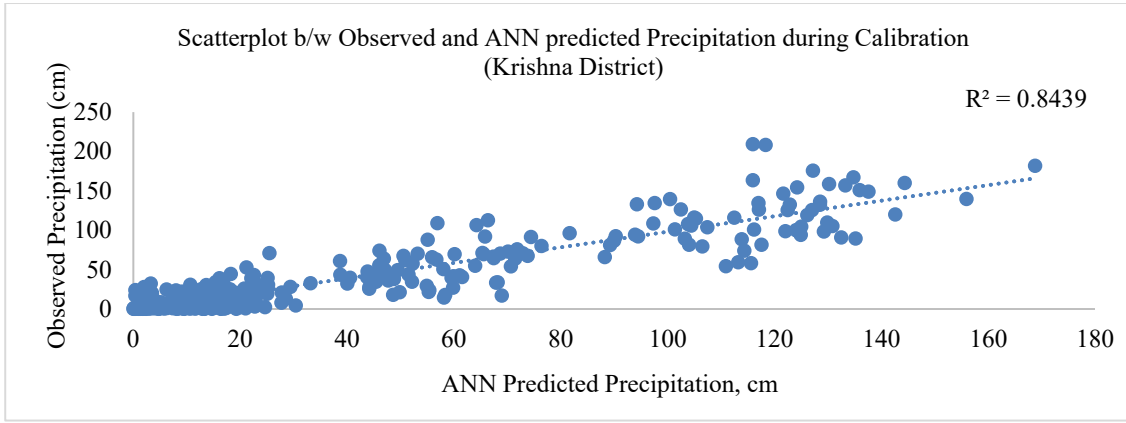

Fig.10(a): Scatterplot b/w observed and ANN predicted precipitation during Validation (Krishna District).

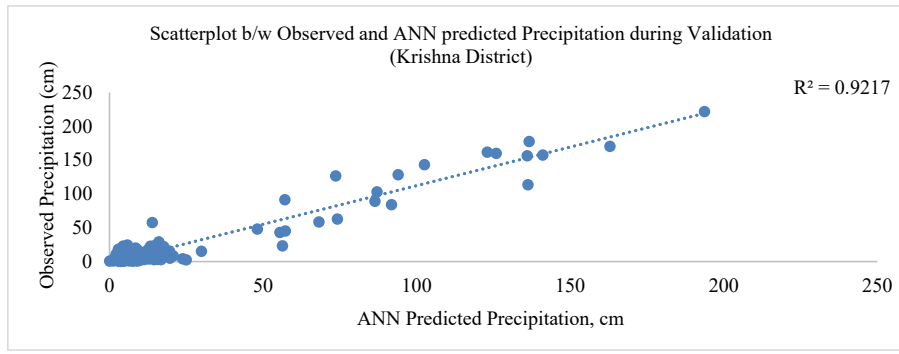

Fig.10(b): Scatterplot b/w observed and ANN predicted precipitation during Validation (Krishna District).

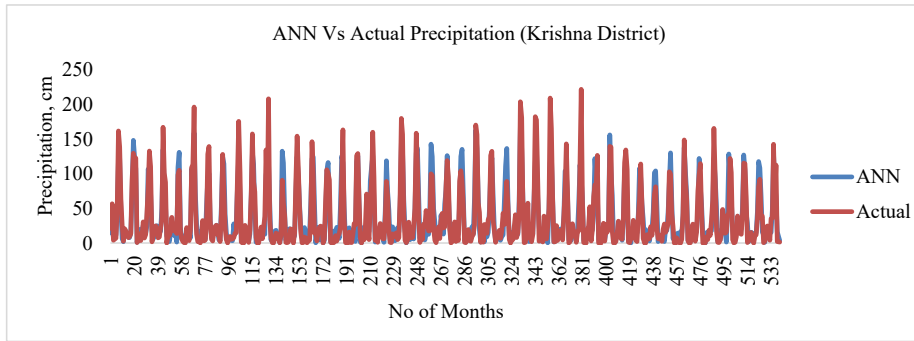

Fig. 10(c): Plot between ANN and actual precipitation (Krishna District).

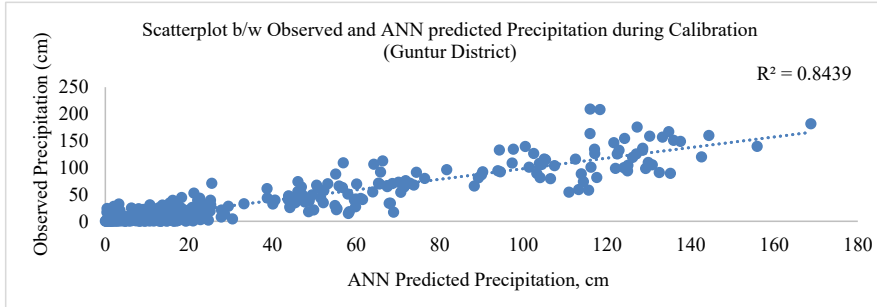

Fig. 10(d): Scatterplot b/w observed and ANN Predicted Precipitation during Calibration (Guntur District).

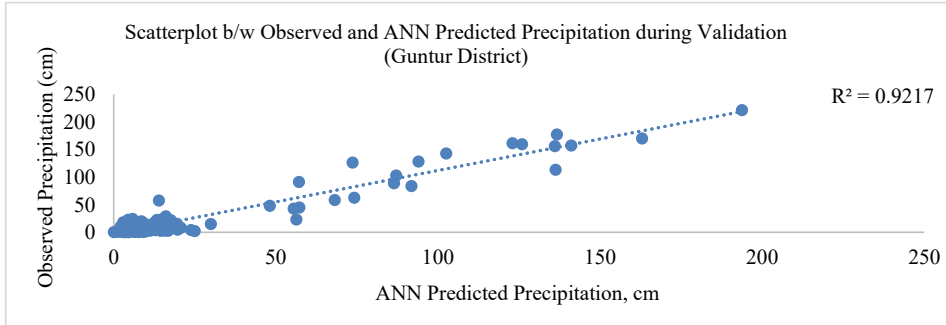

Fig.10(e): Scatterplot b/w Observed and ANN Predicted Precipitation during Validation (Guntur District).

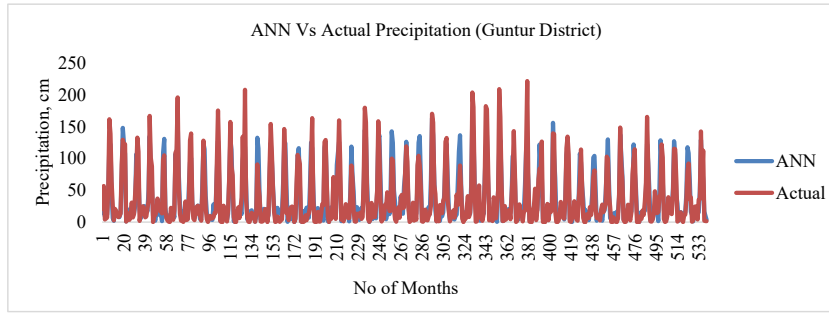

Fig.10(f): Plot between ANN and actual precipitation (Guntur District).

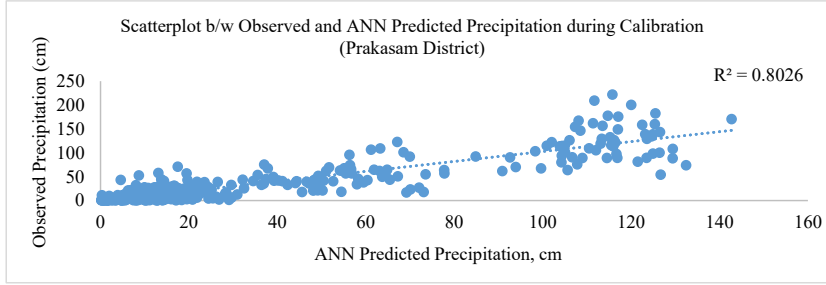

Fig.10(g): Scatterplot b/w observed and ANN predicted precipitation during calibration (Prakasam district).

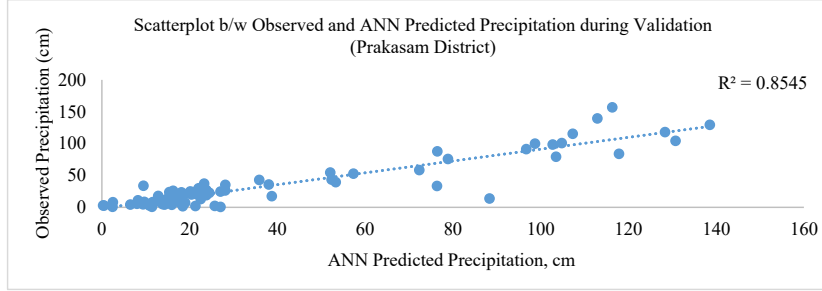

Fig.10(h): Scatterplot b/w Observed and ANN Predicted Precipitation during Validation (Prakasam district).

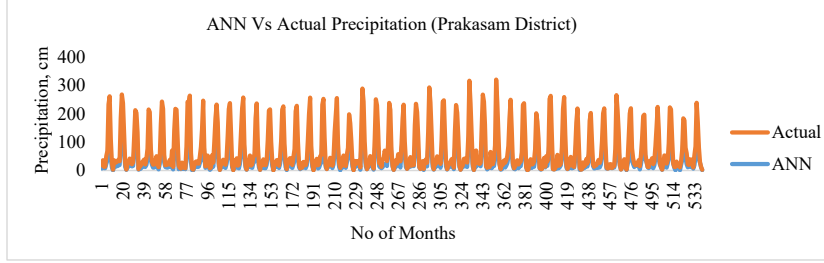

Fig.10(i): Plot b/w ANN and Actual Precipitation (Prakasam district).

model. After the calibration and validation of both the model, the sensitivity analysis was performed using R2, RMSE, and E value and also by plotting the observed versus simulated scatter plots for both. The analysis shows that the ANN is performed well in these three different basins of Andhra Pradesh. The Scenario Analysis was performed for all the regions using the ANN model under three different RCPs 2.6, 4.5 and 8.5 to visualize the impact of Climate Change

in the regions. The purpose behind finding out the projected change in precipitation in different regions of the state is to see the impact of Climate Change on Vulnerability. In this study, the historical data of three stations was used from the period of 1961-2000. The result of ANN model predicted that rainfall will be increased under the entire RCP scenario especially in the case of RCP8.5. In RCP2.6, there is little fall of rainfall in the 2020s and 2050s. The seasonal rainfall varies from one station to another, especially during the monsoon season where there will be very high rain, especially in RCP8.5 scenarios.

In all the scenarios, it can be visualized that the change in the rainfall is considerable after the 2050s. The changes in rainfall up to 2050s are not notable. However, in 2080, and 2100, the predictions are alarming in nature. The Seasonal Analysis of rainfall data also shows the shifting of the monsoon trend up to September especially in the case of RCP8.5, besides, the supposed rise of rainfall due to global climate change. Finally, the conclusions (findings) are summarized as:

1. The approximate predicted change up to the 21st century will be 19.51%, 18.50% and 15.99% for Guntur, Krishna and Prakasam basin respectively under the scenarios of RCP8.5.
2. The approximate predicted change up to the 21st century will be 8.59%, 8.09% and 10.70% for Guntur, Krishna and Prakasam basin respectively under the scenarios of RCP4.5.
3. In RCP2.6 scenario, there is little fall of rainfall in the years 2020s and 2050s and in RCP4.5 Scenario, there will be little rainfall in the year 2020.
4. In RCP8.5 scenario, there will be high rainfall in the years 2080 and 2100, and rainfall is highest in Guntur district, second highest Krishna district.
5. As per RCP8.5, the rainfall in Guntur districts in the year 2100 is nearly double that in the year 2080. The rainfall in Krishna and Prakasam districts in the year 2100 is nearly 1.5 times that in the year 2080.

Hence, based on the conclusions of this research it is suggested that we should develop better mitigation measures to counter such heavy rainfall trends in the future. The policymakers and the local governments should focus on the better planning of water management in the state especially for water storage capacity and harmless drainage system.

REFERENCES

Beaumont, R. 2012. An introduction to principal component analysis & factor analysis using SPSS 19 and R (psych package). Journal of Geophysical Research, (April), P.No.24-32.

Cardona, O.D., Van Aalst, M.K., Birkmann, J., Fordham, M., Mc Gregor, G., Rosa, P., Pulwarty, R.S., Schipper, E.L.F., Sinh, B.T., Décamps, H. and Keim, M., 2012. Determinants of risk: Exposure and vulnerability. In: Managing The Risks of Extreme Events and Disasters to Advance Climate Change Adaptation: Special Report of the Intergovernmental Panel on Climate Change, pp. 65-108, Cambridge University Press.

Chen, H., Xu, C.Y. and Guo, S. 2012. Comparison and evaluation of multiple GCMs, statistical downscaling and hydrological models in the study of climate change impacts on runoff. Journal of Hydrology, 434: 36-45.

Chu, J. T., Xia, J., Xu, C. Y. and Singh, V. P. 2010. Statistical downscaling of daily mean temperature, pan evaporation and precipitation for climate change scenarios in Haihe River, China. Theoretical and Applied Climatology, 99(1-2): 149-161.

Crawford, T., Betts, N. L. and Favis-Mortlock, D. 2007. GCM grid-box choice and predictor selection associated with statistical downscaling of daily precipitation over Northern Ireland. Climate Research, 34(2): 145-160.

Feyissa, G., Zeleke, G., Bewket, W. and Gebremariam, E. 2018. Downscaling of future temperature and precipitation extremes in Addis Ababa under climate change. Climate, 6(3): 58.

Ghosh, S. and Misra, C. 2010. Assessing hydrological impacts of climate change: modeling techniques and challenges. The Open Hydrology Journal, 4: 115-121.

Hannan, S. A., Manza, R. R. and Ramteke, R. J. 2010. Generalized regression neural network and radial basis function for heart disease diagnosis. International Journal of Computer Applications, 7(13): 7-13.

Huang, J., Zhang, J., Zhang, Z., Xu, C., Wang, B. and Yao, J. 2011. Estimation of future precipitation change in the Yangtze River basin by using statistical downscaling method. Stochastic Environmental Research and Risk Assessment, 25(6): 781-792.

Joshi, R. 2016. Artificial neural network (ANN) based empirical interpolation of precipitation. International Journal of Mathematical, Engineering and Management Sciences, 1(3): 93-106.

Kazmi, D. H., Rasul, G., Li, J. and Cheema, S. B. 2014. Comparative study for ECHAM5 and SDSM in downscaling temperature for a geo-climatically diversified region, Pakistan. Applied Mathematics, 2014 (January), 137-143.

Kim, S., Kwak, J., Kim, H. S., Jung, Y. and Kim, G. 2016. Full access nearest neighbor-genetic algorithm for downscaling of climate change data from GCMs. Journal of Applied Meteorology and Climatology, 55(3): 773-789.

Kumar, D., Bhishm, S. K. and Khati, S. 2012. Black box model for flood forecasting. Journal of Civil Engineering (IEB), 40(June 2011): 47-59.

Luo, Y., Ficklin, D. L., Liu, X., and Zhang, M. (2013). "Assessment of climate change impacts on hydrology and water quality with a watershed modeling approach." *Science of the Total Environment*, Elsevier B.V., 450–451, 72–82.

Kusunoki, S. and Arakawa, O. 2015. Are CMIP5 models better than CMIP3 models in simulating precipitation over East Asia? Journal of Climate, 28(14): 5601-5621.

Mahmood, R. and Babel, M. S. 2014. Future changes in extreme temperature events using the statistical downscaling model (SDSM) in the trans-boundary region of the Jhelum river basin. Weather and Climate Extremes, 5(1): 56-66.

Moriasi, D. N., Arnold, J. G., Van Liew, M. W., Bingner, R. L., Harmel, R. D. and Veith, T. L. 2007. Model evaluation guidelines for systematic quantification of accuracy in watershed simulations. Transactions of the ASABE, 50(3): 885-900.

Nourani, V., Razzaghzadeh, Z., Baghanam, A. H. and Molajou, A. 2019). ANN-based statistical downscaling of climatic parameters using decision tree predictor screening method. Theoretical and Applied Climatology, 137(3-4): 1729-1746.

Onyutha, C., Tabari, H., Rutkowska, A., Nyeko-Ogiramoi, P. and Willems, P. 2016. Comparison of different statistical downscaling methods

for climate change rainfall projections over the Lake Victoria basin considering CMIP3 and CMIP5. Journal of Hydro-Environment Research, 12: 31-45.

Pervez, M. S. and Henebry, G. M. 2014. Projections of the Ganges-Brahmaputra precipitation - Downscaled from GCM predictors. Journal of Hydrology, 517: 120-134.

Rajan, S. 2014. Statistical downscaling of gcm output, hydrological simulation and generation of future scenario using variable infiltration capacity (VIC) model for the Ganga basin, India. Uttarakhand: Andhra University, 132.

Randall, D. A., Wood, R. A., Bony, S., Colman, R., Fichefet, T., Fyve, J., Kattsov, V., Pitman, A., Shukla, J., Srinivasan, J., Stouffer, R. J., Sumi, A. and Taylor, K. E. 2007. Climate models and their evaluation. Climate Change 2007: The Physical Science Basis. Contribution of Working Group I to the Fourth Assessment Report of the Intergovernmental Panel on Climate Change, 591-662.

Shukla, R., Khare, D. and Deo, R. 2016. Statistical downscaling of climate change scenarios of rainfall and temperature over Indira Sagar canal command area in Madhya Pradesh, India. Proceedings - 2015 IEEE 14th International Conference on Machine Learning and Applications, ICMLA 2015, 313-317.

Tan, M. L., Ibrahim, A. L., Yusop, Z., Chua, V. P. and Chan, N. W. 2017. Climate change impacts under CMIP5 RCP scenarios on water resources of the Kelantan River Basin, Malaysia. Atmospheric Research, 189: 1-10.

Wilby, R., Dawson, C. and Barrow, E. 2002. SDSM - a decision support tool for the assessment of regional climate change impacts. Environmental Modelling & Software, 17(2): 145-157.

Wilby, R. L. and Dawson, C. W. 2015. Statistical DownScaling Model-Decision Centric (SDSM-DC) Version 5.2 Supplementary Note 6 March 2015, 5.

Xiao, R., He, X., Zhang, Y., Ferreira, V. G. and Chang, L. 2015. Monitoring groundwater variations from satellite gravimetry and hydrological models: A comparison with in-situ measurements in the mid-atlantic region of the United States. Remote Sensing, 7(1): 686-703.

Xu, R., Chen, N., Chen, Y. and Chen, Z. 2020. Downscaling and projection of multi-CMIP5 precipitation using machine learning methods in the upper Han river basin. Advances in Meteorology, Atmospheric Research, 2020.

Yang, P., Xia, J., Zhan, C., Qiao, Y. and Wang, Y. 2017. Monitoring the spatio-temporal changes of terrestrial water storage using GRACE data in the Tarim River basin between 2002 and 2015. Science of the Total Environment, 595: 218-228.

Zhang, Y., You, Q., Chen, C. and Ge, J. 2016. Impacts of climate change on streamflows under RCP scenarios: A case study in Xin River Basin, China. Atmospheric Research, 178-179: 521-534.

Nature Environment and Pollution Technology
An International Quarterly Scientific Journal

p-ISSN: 0972-6268
(Print copies up to 2016)
e-ISSN: 2395-3454

Vol. 20 | No. 2 | pp. 819-824 | 2021

Original Research Paper

https://doi.org/10.46488/NEPT.2021.v20i02.044

Open Access Journal

Environmental Pollution Evaluation of Urban Rail Transit Construction Based on Entropy Weight Method

Yang Yin* and Yu Zhang†**
*School of Management, Wuhan University of Technology, Wuhan 430070, China
**School of Economics & Management, Hubei University of Arts and Science, Xiangyang 441000, China
†Corresponding author: Yu Zhang: hbuaszy@163.com

Nat. Env. & Poll. Tech.
Website: www.neptjournal.com

Received: 12-11-2020
Revised: 24-03-2021
Accepted: 12-05-2021

Key Words:
Urban rail transit
Environmental pollution
Entropy weight method
Evaluation index system

ABSTRACT

With the development of cities, urban rail transit has entered into a stage of rapid construction and development, but the environmental pollution caused by rail transit construction cannot be ignored. To evaluate the environmental pollution of urban rail transit construction, an evaluation system for the environmental pollution induced by urban rail transit construction was established by using the literature survey method and the entropy weight method. The evaluation index system involved three first-level indicators of the physical environment, natural environment and social environment, and 11 second-level indicators. The impact of XA-XDM project construction on urban environmental pollution in Wuhan, China was evaluated by using the evaluation system. Results show that the evaluation score of XA-XDM project is 76.5, which means that the XA-XDM project construction has a strong impact on environmental pollution. It should be paid to the prevention, control and monitoring of various pollution indicators, reducing environmental pollution, and realizing green construction.

INTRODUCTION

Urban rail transit is the main transportation mode currently promoted, and its construction will inevitably pass through transportation hubs such as urban arterial roads, prosperous business districts and densely populated areas. However, the construction of urban rail transit projects needs a long period and is on large scale. Construction in existing transportation hub areas unavoidably faces difficulties such as a harsh construction environment and narrow working space. Meanwhile, the construction process inevitably creates a great deal of pollution to the existing urban environment (Wang 2019). Relevant studies reveal that the environmental pollution caused by urban construction has become more and more serious (Wang et al. 2015, Wang et al. 2015). For example, the frequent urban smog pollution in recent years has mainly occurred in major cities. Contrarily, such pollution in small cities is relatively light. The main pollution source generates from the construction of urban buildings and the continuous expansion of the scale of municipal public construction. These constructions have caused dust, exhaust gas in the air, noise pollution and vegetation destruction, increasing pollution sources and exceeding the city's ecological self-purification ability (Xue et al. 2017). Data show that there were more than 500,000 complaints about environmental pollution in China in 2018, accounting for 35.3% of the total complaints, while the number of noise pollution cases caused by construction reached 46.1%, which is the largest proportion (Ministry of Environmental Protection of the People's Republic of China 2018).

Due to the complex construction environments, the environmental pollution caused by urban rail construction is difficult to be evaluated. Therefore, how to evaluate the pollution degree of construction to the environment is important to control the construction process, and then adopting targeted measures to reduce environmental pollution and improving the urban environment. It is of great significance to realize the green construction of urban rail transit and the sustainable development of urban construction.

EARLIER STUDIES

As the country attaches importance to environmental protection, people's awareness of urban environmental protection has been continuously improved. The pollution of the urban environment caused by construction has attracted widespread attention from all walks of life. Requirements and guidance on environmental aspects of rail transit construction have been made by "*Notice on Doing a Good Job in Environmental Impact Assessment of Urban Rail Transit Projects (2014)*" and "*Technical Specification for Environmental Vibration and Noise Control Engineering of Urban Rail Transit (HJ2055-2018)*" issued by the Ministry

of Environmental Protection and the Ministry of Ecology and Environment, respectively.

Concerning the research on air pollution caused by urban rail transit construction, Huang et al. (2007) compared and analyzed the environmental pollution caused by construction in different construction stages. The results showed that excavation and construction can cause more environmental pollution than other stages. Li et al. (2014) used point monitoring TSP to achieve the monitoring of work areas, construction sheds and roadsides, and found that the earth and stone cause the most serious dust pollution to the environment. Hala et al. (2015) applied the dust concentration prediction model (FDM) to monitor the fugitive dust and particulate matter on the construction site in Doha, Qatar, and the results showed that the FDM simulation can determine the characteristics of fugitive dust pollution.

Regarding the research on noise pollution caused by urban rail transit construction, Bowlby studied the construction noise of high-speed rail construction projects, abstracting the noise source into points, lines, and surfaces, and considering the attenuation and propagation of noise by sound insulation panels (Haron et al. 2009). Based on the above conditions, a noise simulation model was finally established. Wang et al. (2018) analyzed environmental noise monitoring and evaluation methods in China, Japan, the European Union and the United States. Liu (2005) monitored the noise at the boundary of the construction project, and the results showed that the noise pollution to the surrounding environment during the piling stage was serious, which even affects the health of surrounding residents. Zhang (2013) used noise simulation software to analyze the impact of loaders, rammers, and vibration-impact ramming on the noise pollution and pointed out the largest noise source.

Considering the land subsidence caused by urban rail transit construction, Yang et al. (2013) used the finite element software MIDAS to simulate the track excavation project in the Wuhan rail transit project. The influence of track excavation on the ground settlement was studied. Meng et al. (2016) used the finite element software ANSYS to analyze the effect of track excavation on the impact of ground subsidence in the Qingdao rail transit project. Zhang (2021) analyzed the construction of Hefei Rail Transit Line 6 and Line 8 and found that the installation of urban rail transit has a non-negligible impact on ground settlement and surrounding buildings.

Studies on the vibration pollution caused by urban rail transit construction indicate that noise and vibration are mainly caused by the driving process of rail vehicles such as trains, subways, and light rails. They result from the collision between the wheels and the track and the mutual transmission of the power unit of the locomotive. Long-term noise interference can cause headache, dizziness, tinnitus, irritability, irritability, insomnia, neurasthenia, etc. (Yang 2011). Continuous vibrations cause the human brain to reduce the level of arousal, distracted, and have difficulty in spatial orientation, damaging mental function. Hu (2020) took the construction of the Chongqing subway as the main research object and conducted effective investigations on the vibration pollution caused by it with different prevention methods to provide a reference for environmental governance.

The pollution of land subsidence, air pollution, vibration pollution and urban landscape caused by urban rail transit construction has become an urgent problem to be solved in the process of urban civilization construction. This is not only related to the daily life of citizens but also concerned the image of the city. This is the core issue of this study.

MATERIALS AND METHODS

Environmental Pollution Evaluation Index System

With the demand for transportation in urban development, more and more long-term requirements have been put forward for the planning and design of urban rail transit, such as long routes, multiple lines, and large intersections. The development of rails needs to not only meet the transportation requirement of the city centre, but also consider the development of the suburbs, and even take into account the development of surrounding satellite cities. The construction methods for urban rail transit are different in various construction sites. Underground construction is mostly used in urban centres, while ground construction is mainly employed in suburban areas. Different construction methods cause different pollution to the surrounding environment. Xue et al. (2018) analyzed the pollution to the ecological and natural environment caused by rail transit construction. It showed that construction and excavation damage surrounding vegetation, muck transfer generates dust, and foundation pit construction causes soil settlement and other pollution. Zhu (2018) pointed out that the negative environmental pollution caused by rail transit construction involves noise, water, atmosphere, vibration, and residents' health quality. Zhang et al. (2020) constructed environmental pollution indicators of hydropower projects from the natural, social and ecological environment. The weights of 14 pollution indicators were also analyzed based on probabilistic language close to entropy, and scientific suggestions for project selection was provided.

According to Guan (2018), the environmental pollution caused by urban rail transit construction involves water and soil pollution, vegetation destruction, agricultural ecology, land subsidence, water pollution, air pollution, solid waste,

Table 1: Environmental Impact Assessment Index system of urban rail transit construction.

Target layer	First-level index	Second-level index	Meaning
Environmental Pollution Assessment of Urban Rail Transit Construction A	Ecosystem B1	Water and soil pollution C1	Pollution of groundwater caused by cement and chemical grout during construction
		Vegetation destruction C2	Ground excavation and ground track erection damage surrounding vegetation
		Agricultural ecology C3	Damage to farmland caused by rail transit route planning
	Natural environment B2	Ground subsidence C4	Excavation of underground rail transit lines and excavation of station foundation pits cause deformation and settlement of roads and surrounding buildings
		Water pollution C5	Engineering wastewater from construction operations, cleaning wastewater from construction machinery, domestic wastewater from construction workers, etc.
		Air pollution C6	During the construction process, the dust generated by vehicles entering and exiting, earth excavation and backfilling, and the fuel exhaust gas generated by mechanical equipment and vehicles
		Solid Waste C7	Waste soil, waste rock and construction waste generated during construction
	Social environmental pollution B3	Sound pollution C8	The sound produced by the mechanical equipment and construction process during the construction, which has an interference effect on the surrounding residents
		Vibration pollution C9	Vibration generated during the construction of large engineering equipment, shock vibration generated by blasting
		City view C10	The impact of construction on the scale, vision and aesthetics of the original urban space occupation, construction enclosure, and exposed buildings
		Population health C11	The impact of urban rail transit construction on the work, travel, daily life and rest of the surrounding residents

noise pollution, vibration pollution, urban landscape and population health, etc. Moreover, further categorization of the various pollution indicators can result in environmental pollution involving the ecological, natural and social environment. This paper summarizes and sorts out the environmental impact evaluation index system of urban rail transit construction, as given in Table 1.

Evaluation Model

Entropy is originally a thermodynamic concept. In 1948, Shannon introduced information theory based on the principle of entropy, which was used to describe and measure the degree of disorder in a system. The description of the degree of system order is information. So, the increase or decrease of information is inversely proportional to entropy. Richer information means less entropy. The entropy weight method is a method of calculating indicator weights by objectively assigning weights. According to the degree of variation of selected indicators, a matrix is established, and the threshold method is used to non-dimensionalize the matrix to calculate the information entropy, and then obtain the entropy weight through the difference coefficient (Lu & Liu 2021). The detailed steps are as follows:

Firstly, the evaluation index and evaluation object are digitized, and the original matrix X is established. The evaluation target M_i (I = 1, 2, 3, ···, m) is the row of the matrix, the evaluation index N_j (j = 1, 2, 3, ···, n) is the column of the matrix, and X_{ij} is the M_i evaluation The value of the N_j index of the object.

$$X = \begin{bmatrix} x_{11} & x_{12} & \cdots & x_{1n} \\ x_{21} & x_{22} & \cdots & x_{2n} \\ \cdots & \cdots & \cdots & \cdots \\ x_{m1} & x_{m2} & \cdots & x_{mn} \end{bmatrix}$$

Secondly, it should be considered that there are differences in dimensions of different orders of magnitude in the original matrix. When this situation occurs, matrix X should be non-dimensionalized so that the value of X_{ij} is in the range of 0~1.

Positive dimensionless:

$$X_{ij} = \frac{x_{ij} - \min(x_j)}{\max(r_j) - \min(r_j)} \quad \ldots(1)$$

Negative dimensionless:

$$X_{ij} = \frac{\min(x_j) - x_{ij}}{\max(r_j) - \min(r_j)} \quad \ldots(2)$$

Calculate the weight of each index X_{ij}:

$$P_{ij} = X_{ij} / \sum_{i=1}^{m} X_{ij} \quad \ldots(3)$$

Get the entropy value of each index X_{ij}

$$e_{ij} = -1/\ln(m) \sum_{i=1}^{m} P_{ij} \ln P_{ij} \quad \ldots(4)$$

Finally, calculate the entropy weight W_j

$$W_j = (1 - e_{ij}) / \sum_{j=1}^{n} d_j \quad \ldots(5)$$

RESULTS ANALYSIS AND DISCUSSION

Project Background

The XA-XDM project belongs to a bid section of XA Rail Transit Line 10 in Wuhan, China. The XDM station of the project is located at Fortune Plaza in the city centre of Wuhan, surrounded by facilities such as Fortune Plaza, parks, office buildings and residential areas, as shown in Fig. 1.

Taking into account the particularity of the project location, it is necessary to evaluate the environmental pollution during the construction period before the project construction, analyze the weight of each index, and help the project make the best construction plan. To ensure the scientific and fair evaluation, many experts and citizen representatives were invited to make an evaluation team to score 11 evaluation indicators. The evaluation involves the magnitude of the impact on each indicator, and the impact is "Very big", "Larger", "General", "Smaller" and "Very small". By recovering the evaluation data to form the original matrix X and using formulas (1)-(3) to non-dimensionalize and normalize the collected data, we obtain the environmental pollution of each indicator. The evaluation results are shown in Table 2.

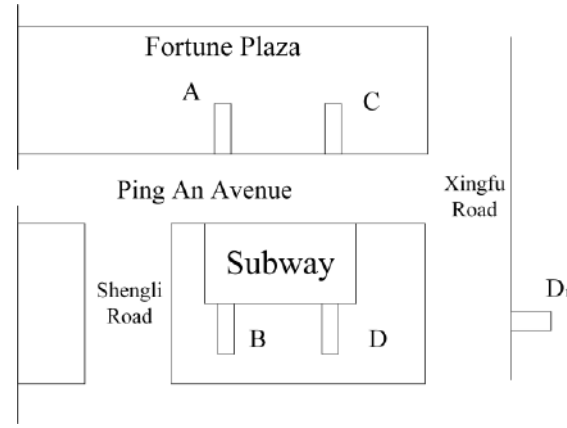

Fig. 1: Schematic diagram of XDM station.

Analysis of the Weight of Environmental Pollution Index

Based on the evaluation results of environmental pollution by various indicators, the entropy weight method is used to calculate the entropy value and entropy weight of the standardized matrix. Formulas (4) and (5) are used to obtain the entropy weight of environmental pollution indicators, as shown in Table 3.

The entropy weight results show that the environmental pollution indicators of the project's XDM station construction are ranked as land subsidence, air pollution, vibration

Table 2: Evaluation results of the project's environmental impact assessment indicators.

Target layer	First-level index	Second-level index	Environmental pollution assessment				
			Very big	Larger	General	Smaller	Very small
Environmental Pollution Assessment of Urban Rail Transit Construction A	Ecosystem B1	Water and soil pollution C1	0.06	0.06	0.19	0.30	0.40
		Vegetation destruction C2	0.15	0.20	0.10	0.30	0.25
		Agricultural ecology C3	0.03	0.20	0.40	0.25	0.12
	Natural environment B2	Ground subsidence C4	0.70	0.20	0.05	0.03	0.02
		Water pollution C5	0.45	0.30	0.15	0.08	0.02
		Air pollution C6	0.45	0.40	0.09	0.05	0.02
		Solid waste C7	0.20	0.40	0.30	0.06	0.04
	Social environmental pollution B3	Sound pollution C8	0.25	0.48	0.10	0.13	0.05
		Vibration pollution C9	0.35	0.45	0.10	0.05	0.05
		City view C10	0.35	0.40	0.15	0.05	0.05
		Population health C11	0.25	0.25	0.40	0.05	0.05

Table 3: Entropy weight of environmental pollution indicators.

Target layer	First-level index	Weights	Second-level index	Weights
Environmental Pollution Assessment of Urban Rail Transit Construction A	Ecosystem B1	0.1533	Water and soil pollution C1	0.0719
			Vegetation destruction C2	0.0189
			Agricultural ecology C3	0.0625
	Natural environment B2	0.5083	Ground subsidence C4	0.2050
			Water pollution C5	0.0943
			Air pollution C6	0.1327
			Solid waste C7	0.0763
	Social environmental pollution B3	0.3385	Sound pollution C8	0.0783
			Vibration pollution C9	0.1026
			City view C10	0.0847
			Population health C11	0.0728

pollution, water pollution, urban landscape pollution, noise pollution, solid waste, population health, and water and soil pollution. It indicates that the most serious environmental pollution caused by rail transit construction in the city centre is ground subsidence (0.2050). The reason is that since the urban centre construction has been completed, the newly constructed rail transit inevitably damages and affects the original urban structure. The project needs to focus on construction to protect the surrounding structure, reduce the impact on ground settlement, and restore the damaged environment after the construction is completed. Among the environmental pollution indicators, the urban landscape (0.0847) is ranked in the top five, indicating that in the current urban development, urban landscapes also attract a lot of attention. The construction of urban rail transit in the city centre should pay full attention to match the original urban landscape. The impact of enclosure and work area on the urban environment during the construction should also take into account. The image of the city should not be ignored during rapid construction. Moreover, air pollution (0.1327), vibration pollution (0.1026), water pollution (0.0943), as well as the results of previous studies on environmental pollution, indicate that the application of the entropy method to evaluation of environmental pollution caused by urban rail transit construction is scientific. The results also show that air pollution causes greater environmental pollution than vibration pollution.

Based on the entropy weight data of the Second-level index, the First-level index weights are obtained. The data shows that the natural environmental pollution caused by the construction of rail transit in the city centre (0.5083) exceeds the sum of other indicators, i.e., the social environment, and the ecological environment. Natural environmental pollution, as a direct pollution object of track construction, has been relatively concerned by all parties. Its higher weight is in line with the actual situation. However, the social environmental pollution is also relatively high, indicating that with social development, people are increasingly paying attention to the urban environment. The requirements for the social environment are getting higher and higher. The construction of rail projects should pay attention to the social environmental pollution, reducing noise and vibration pollution. It also should consider urban landscaping, which effectively avoids unnecessary impacts on the project due to pollution to the social environment. The low weight of the ecological environment means that the construction of rail transit in the city centre relatively weakens the ecological damage, and the energy of the project in this regard may be weak.

Environmental Pollution Assessment of XA-XDM Project by Combining Weight Method

The combination weight method to determine the emergency capability index score is similar to the entropy weight method. The row vector for all indicators of the XA-XDM project is calculated by $W \times R = R_{row}$, and the specific scores of each index are $R_{final} = R_{row} \times [100,80,60,40,20]^{T}$, among which the environmental impact is 100 to 80 points, the stronger is 80 to 60 points, the general is 60 to 40 points, the weaker is 40 to 20 points, and the weak is 20 to 0 points. Combining the right of environmental pollution indicators, the specific score of each indicator is [41.6, 54.0, 55.4, 90.6, 81.6, 84.3, 73.2, 75.0, 80.0, 79.0, 72.0], and further calculations based on the weight of the indicators were made to investigate the environmental pollution impact of the XA-XDM project. The evaluation score is 76.5. The evaluation results show that the XA-XDM project has a strong impact on environmental pollution. During the construction process, attention should be paid to the prevention, control and monitoring of various pollution indicators to reduce environmental pollution and achieve green construction.

CONCLUSION

Aiming at evaluation of the environmental pollution caused by urban rail transit construction, an environmental impact assessment index system for urban rail transit construction was constructed by using the literature research method, and the entropy method was used to evaluate the pollution of the XA-XDM project construction on the urban environmental pollution, and the following conclusions are obtained:

1. An environmental impact assessment index system for urban rail transit construction is established, which fully summarizes the environmental pollution caused by rail construction, and provides a certain reference for subsequent research on environmental pollution caused by urban construction.
2. The entropy weight method is used to evaluate the environmental pollution caused by urban rail transit construction, and the weight of each pollution indicator is determined based on the results of quantitative analysis. The weighted result is in accordance with the law of previous research results, indicating that the entropy weight method is feasible to evaluate the environmental pollution of urban rail transit construction by law.
3. The environmental pollution impact assessment score of the XA-XDM project is 76.5. This result indicates that the XA-XDM project has a strong impact on environmental pollution. The construction of rail transit in the centre of the city should focus on indicators such as land subsidence, air pollution, and vibration pollution. Meanwhile, the protection of the urban landscape should not be neglected during track construction.

REFERENCES

Guan, L. 2018. Environmental Impact Assessment of Urban Rail Transit: Taking Xiaodongmen Station of Wuhan Rail Transit Line 7 as an example. World of Transportation, (21): 178-180.

Hala, A., Vasiliki, K. and Konstantinos, E. 2015. Developing Emission Factors of Fugitive Particulate Matter Emissions for Construction Sites in the Middle East Area. International Journal of Environmental, Chemical, Ecological, Geological and Geophysical Engineering, 9(2): 50-54.

Haron, Z., Yahya, K. and Mohamad, M.I. 2009. Probability approach for prediction of construction site noise. Journal of Asian Architecture and Building Engineering, 8(2): 571-577.

Hu, M.Q., Liu, M., You, D. and Zhang, Y. 2020. Influence of train arrival characteristics on unorganized ventilation in underground subway station with platform screen doors. Journal of Wind Engineering and Industrial Aerodynamics, 198, p.104089.

Huang, Y.H., Tian, G., Qin, J.P., Li, G. and Yan, B.L. 2007. Research on the characteristics of dust pollution in different construction stages. Environmental Science, (12): 2885-2888.

Li, X.D., Su, S., Huang, T.J. and Lin, Y. 2014. Comparative study on dust monitoring during earthwork and main structure construction. China Safety Science Journal, 24 (5): 126-131.

Liu, H.W. 2005. Pollution and control of construction noise. Petrochemical Environmental Protection, 28(4): 43-45.

Lu, L. and Liu, C.Y. 2021. Research on Airport Comprehensive Evaluation Model Based on Entropy Weight Method. Aeronautical Computing Technology, 51 (01): 64-66.

Meng, Y. P. and Xu, L.H. 2016. Numerical simulation study of ground settlement caused by subway tunnel excavation. Journal of Anhui Jianzhu University, 24 (3): 8-11.

Ministry of Environmental Protection of the People's Republic of China. 2018. China Environmental Noise Pollution Prevention and Control Report, available at http://www.mee.gov.cn/hjzl/sthjzk/hjzywr/.

Wang, P., Cao, J., Shen, Z.X., Han, Y.M., Lee, S.C., Huang, Y., Zhu, C.S., Wang, Q.Y., Xu, H.M. and Huang, R.J. 2015. Spatial and seasonal variations of PM2.5 mass and species during 2010 in Xi'an, China. Science of the Total Environment, 508: 477-487.

Wang, R., Zou X., Cheng H., Wu, X., Zhang, C. and Kang, L. 2015. Spatial distribution and source apportionment of atmospheric dust fall at Beijing during spring of 2008-2009. Environmental Science & Pollution Research International, 22 (5):3547-57.

Wang, Y., Wei, J.S., Li, X.T., Bai, Y. and Wen, X.C. 2018. Comparison and enlightenment of environmental noise monitoring methods at home and abroad. China Environmental Monitoring, 34 (4): 150-154.

Wang, Y.Z. 2019. Research on the impact of urban rail transit on urban development and environment. Engineering Construction and Design, (5): 140-141.

Xue, Y. F., Zhou, Z., Huang, Y.H., Wang, K., Nie, T., Nie, L., Qin, J.P. 2017. Characteristics of fugitive dust emissions from building construction in Beijing. Environmental Science, 38 (6): 2231-2237.

Xue, X.F., Liu, H. and Wen M.Y. 2018. The environmental impact of urban rail transit construction. Qinghai Transportation Science and Technology, (5): 18-19.

Yang, F.L., Liu, Y.L. and Hu, B. 2013. Numerical simulation study on ground settlement caused by excavation of Wuhan subway tunnel. Journal of Engineering Geology, 21(1): 85-91.

Yang, X.X. 2011. Urban traffic noise and its hazards. Frontier Science, 5 (2): 21-28.

Zhang, H.Y., Zhang, W.L. and Guan, Y. 2020. Research on environmental impact assessment of hydropower projects based on probability language close to entropy. Mathematics in Practice and Knowledge, 50(17): 271-278.

Zhang, Q. 2013. Research on the noise coupling effect of simultaneous operation of multiple machines on the construction site. Building Construction, 35(9): 859-861.

Zhang, Z. W. 2021. Numerical simulation study on the environmental impact of the construction team of urban rail transit station. Anhui Architecture, 28(1): 161-163.

Zhu, Z.L. 2018. Research on the environmental impact and management status of domestic urban rail transit. Railway Communication and Signal Engineering Technology, 15 (10): 101-104.

Nature Environment and Pollution Technology
An International Quarterly Scientific Journal

p-ISSN: 0972-6268
(Print copies up to 2016)
e-ISSN: 2395-3454

Vol. 20 | No. 2 | pp. 825-831 | 2021

Original Research Paper

https://doi.org/10.46488/NEPT.2021.v20i02.045

Open Access Journal

Analysis and Modelling of Slope Failures in Municipal Solid Waste Dumps and Landfills: A Review

Abdullah Ansari*† and Prashant B. Daigavane**
*Department of Civil Engineering, Indian Institute of Technology, New Delhi-110016, India
**Department of Civil Engineering, Government College of Engineering, Nagpur-441108, India
†Corresponding author: Abdullah Ansari; ansariaa@civil.iitd.ac.in

Nat. Env. & Poll. Tech.
Website: www.neptjournal.com

Received: 15-04-2020
Revised: 26-05-2020
Accepted: 04-06-2020

Key Words:
Landfill
MSW
Modelling
Slope failures
Environment

ABSTRACT

The essential issues solved by geoenvironmental engineers relate to the assurance of uncontaminated regions of the subsurface just as the remediation of locales of the subsurface that have been sullied by releasing waste materials, spilling over the ground and underground stockpiling tanks and penetration of pesticides. In city areas, garbage and waste materials are generally dumped into landfills. A landfill site, which is otherwise called a trash dump, is used for the disposal of waste materials by burial. A safe landfill is a deliberately built sorrow in the ground into which wastes are put. The principal objective is to stay away from any water driven association between the wastes and the surrounding environment especially groundwater. This paper discusses landfill, in terms of its construction, stability and failure. The analysis and modelling of the landfill failure occurred in different countries like Poland, Turkey, Israel, the Philippines, China and Sri Lanka which are discussed.

INTRODUCTION

The primary problems addressed by geoenvironmental engineers pertain to the protection of uncontaminated regions of the subsurface as well as the remediation of regions of the subsurface that have been contaminated by one or more events which involve industrial chemical spills, leaking waste containment facilities, leaking above-ground and underground storage tanks, and infiltration of pesticides.

A landfill site which is also known as a garbage dump or dumping ground is a site for the disposal of waste materials by burial. Some landfills are also used for waste management purposes, such as the temporary storage, consolidation and transfer, or processing of waste material. Processing of waste materials includes sorting, treatment and recycling. Unless they are stabilized, these areas may experience severe shaking or soil liquefaction of the ground in case of a large earthquake. A secure landfill is a carefully engineered depression in the ground into which wastes are put. The main objective is to avoid any hydraulic connection between the wastes and the surrounding environment particularly groundwater.

A landfill is a bathtub in the ground; a double-lined landfill is one bathtub inside another. Bathtubs leak two ways, one out the bottom and another over the top. An important feature in the identification and assessment of potential failure mode is the fact that both covers and liners for modern landfills are typically multilayer composites composed of both soil and geo-synthetic materials. The liner system contains several interfaces whose resistance against interface shear stresses may be low, and thus these act as possible failure surfaces. Additionally, all classical geotechnical failure modes are possible depending on site-specific conditions (usually involving saturated fine-grained soils) and the placement and geometry of the waste mass. Landfill failure can be studied by carrying out the analysis and modelling of failure surfaces. For these computational techniques, computer programs are used. This paper discusses landfill, in terms of its construction, stability and failure. The analysis and modelling of the landfill failure occurred in different countries like Poland, Turkey, Israel, the Philippines, China and Sri Lanka which are given in Table 1.

ANALYSES OF LANDFILL SLOPE FAILURES

Sarihan & Stark (2008) carried out a back analysis of landfill failures and investigated the shear strength of municipal solid waste (MSW) using the techniques of back analyses for different slope failures associated with wastes across the world. Slope failure for landfills may be resulted due to heavy rainfall or the development of tension cracks. Sometimes it may be associated with the harmful effects of leachate. Leachate is a widely used term in the environmental

Table 1: Historical record of slope failures in municipal solid waste dumps and landfills.

Year	Location	Failure Reason	Reference
1965	Warsaw, Poland	Steep slopes, excessive leachate level	Bouzza & Wojnarowicz 2000
1988	California, USA	Sliding along interfaces within the composite liner system	Mitchell et al. 1990
1993	Istanbul, Turkey	Heavy rains, excessive leachate level	Kocasoy & Curi 1995
1996	Cincinnati, Ohio, USA	Softening of underlying native soils	Stark et al. 2000
1996	Mahoning, Ohio, USA	Failure along wet bentonite layer of the unreinforced GCL	Stark et al. 1998
1997	Hiriya, Israel	Steep slopes, lack of drainage controls, high moisture content	Huvaj-Sarihan & Stark 2008
2000	Payatas, Manila, Philippines	Failure along MSW and clay subsoil induced by heavy rains	Huvaj-Sarihan & Stark 2008
2005	Bandung, Indonesia	High water pressure in the soft subsoil	Koelsch et al. 2005
2008	Shenzhen, China	High water level within landfill	Peng et al. 2016

sciences where it has the specific meaning of a liquid that has dissolved or entrained environmentally harmful substances that may then enter the environment. It is most commonly used in the context of land-filling of putrescible or industrial waste. An investigation found that the landfill doesn't have an engineered bottom liner, final cover or leachate and gas control systems. Analysis of failure slopes of Gnojna Grora landfill in Poland, Istanbul Landfill in Turkey, Hiriya Landfill in Israel, and Payatas Landfill in the Philippines are discussed below.

Gnojna Grora Landfill in Poland

Bouzza & Wojnarowicz (2000), described the Gnojna Grora Hill landfill, in Warsaw, Poland. The archaeological work performed for this landfill revealed that the landfill dates to the 14th century which showed that it is an old landfill without any liner or cover system layers. In 1965, cracks were observed in nearby buildings due to the movements in the landfill which showed that fill is composed of large amounts of demolition debris composed of old domestic MSW. The unit weight of the waste material was estimated to be 17 kN/m^3 as the waste is mixed with demolition debris. Groundwater or leachate level was found to be 3 to 5 meters below the ground surface based on piezometer records (Fig. 1a).

To back-calculate, the Municipal Solid Waste (MSW) was assumed to exhibit a cohesion intercept (c') of 0 kPa and the back-calculated friction angle (φ') is 21º. They estimated that the average effective normal stress and corresponding back-calculated shear strength on the observed failure surface through the waste are 106 kPa and 40.7 kPa respectively. The shear strength of MSW decreases with age (Siegel et al. 1990, Brandl 1998, Gabr et al. 2002, Reddy & Bogner 2003). So it is acceptable to assume cohesion intercept is equal to 0 for a 300 years old MSW demolition debris mix and back-calculate the friction angle.

Istanbul Landfill in Turkey

This landfill of Turkey described by Kocasoy & Curi (1995) and Koerner & Soong (2000) which is about 30 km away from the city centre in Istanbul (Turkey), operated since 1976. Their study showed that maximum MSW slope height was about 45 m, with steep front slopes of up to 45 degrees or even more and MSW was placed without any liner system. Waste in this landfill was not compacted and not covered with soil. Landfill failure occurred on April 28, 1993, and resulted in 27 casualties and involved approximately 500,000 m^3 to more than 1,000,000 m^3 of waste. Fires were known to be burning on the surface of the waste at several places during most of the year before the slide which is shown in Fig. 1b reported by Kocasoy & Curi (1995).

In this case, the explosion could not have been the main cause of the movement of the waste. They also confirmed that the heavy rains, and excessive leachate level built up within the old decomposed waste caused by water infiltrating

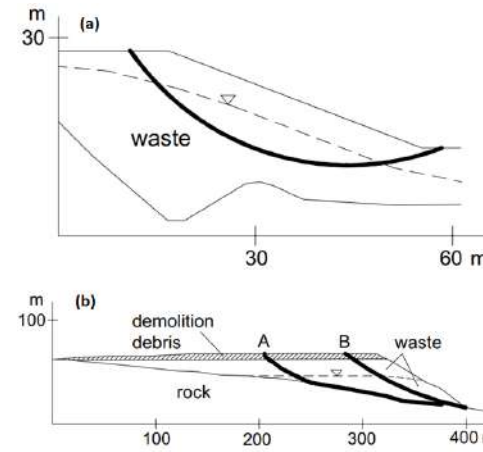

Fig. 1: Approximate slope profile of (a) Gnojna Grora Landfill (Poland) (b) Istanbul Landfill (Turkey).

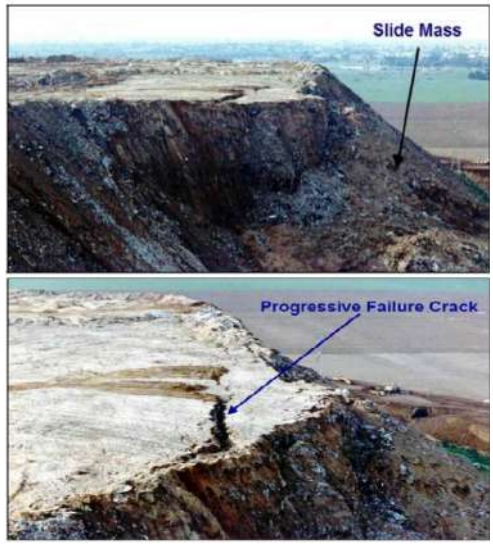

Fig. 2: Failure of Hiriya Landfill (Israel).

from the adjacent surface water ponds were likely the triggering mechanism, together with recently placed demolition debris on top of the waste. As shown in Fig. 1b, the waste mass there is impermeable rock. The authors assumed the unit weight of 11 kN/m^3 because no further information is available. It is assumed that the failure surface is the most reliable because it is based on their observations at the site and data they obtained from the municipality of Istanbul. A and B represent the non-circular and circular failure surface respectively.

Hiriya Landfill in Israel

The Hiriya landfill in Israel failed in 1997 due to steep slopes, lack of drainage controls and high moisture content which is located east of Tel-Aviv which is an open area at the convergence of the Shappirim River and the Ayalon River (Fig. 2). Isenberg et al. (2004) investigated that the dump has been used for the disposal of MSW for the greater Tel-Aviv area for decades. They also confirmed that the landfill does not have an engineered bottom liner, cover and gas control systems.

Prayatas Landfill in Philippines

The Prayatas Landfill is located in the NE part of Manila. It has been in operation since 1973 and about 1500 tonnes of MSW are placed since 1996. The exact mechanism of failure is not known but several factors like heavy rainfall may lead to cause saturation of MSW and water ponding on top of the slopes were reported by Merry et al. (2005).

MODELING OF LANDFILL SLOPE FAILURES

Guangming Landfill at Shenzhen, China

Ouyang et al. (2017) studied catastrophic landslide of the construction waste landfill at Guangming, Shenzhen, China

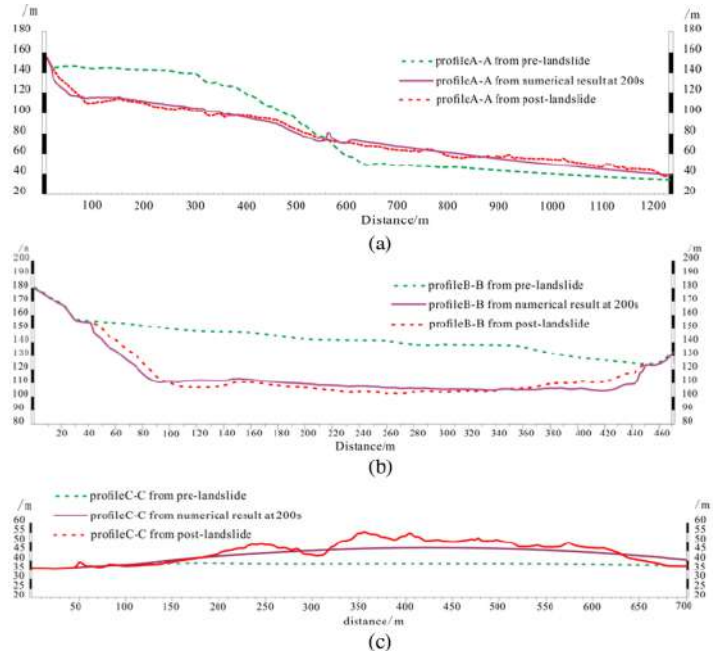

Fig. 3: Comparison of numerical results and field investigation results along (a) the main sliding profile A-A, (b) transverse profile B-B, and (c) transverse profile C-C for Guangming landfill at Shenzhen, China (Ouyang et al. 2017).

occurred in December 2015 which destroyed 33 buildings and caused 69 deaths (Yin et al. 2016). This type of landfill occurred without the involvement of rainfall or heavy rainfall with H=111 m and L=1.2 km. The mesh-free Smooth Particle Hydrodynamics (SPH) method is applied in modelling the landslide over natural terrain.

Investigation for this landslide showed that the soil is almost fully liquefied in the sliding surface due to plenty of water. Thus, it is highly possible that plenty of water was stored in the waste fill. Unmanned Aerial Vehicle (UAV) used to collect the pictures two days before the event and three days after the event. Snapshots of the computed flow height were collected at different time intervals. Graphs were plotted in which the author compared the profile before and after the landslide event (Fig. 3).

Liang et al. (2019) studied the Shenzhen landslide based on dynamic simulation using Smooth Particle Hydrodynamics (SPH) modelling considering dilatancy effects. As shown in the Fig. 4, the most obvious feature of the landslide was that its travelling distance exceeded 1.2 km and the landslide mobility index equal to 0.092 was much lower than that of a general landslide. A landslide mobility index lower than 0.3 denotes high mobility. The Dilatancy model describes the interaction between the fluid and solid phases. The key role of these dilatancy models is the combination of the dilation and contraction behaviours with the equilibrium solid volume fraction, which is related to the solid volume fraction and effective stress. The grid or mesh-based methods have been widely applied in various areas of computational fluid dynamics and computational solid mechanics (Anderson & Wendt 1995, Fung & Tong 2001).

However, the existence of the grid or mesh can cause various difficulties in solving problems related to the free surface, extremely large deformations, a deformable boundary, and a moving interface (Liu & Liu 2010). Mesh-free methods have been developed in the recent past (Liu & Gu 2005), and SPH methods, which were invented to solve astrophysical problems, have been widely applied in many fields (Lucy 1977, Liu & Liu 2003, Violeau 2012). The soil on the sliding surface was liquefied (Ouyang et al. 2016), and the bottom of the deposited body exerted excess pore water pressure.

Udapalatha Municipal Landfill at Udapalatha, Sri Lanka

Prathapan et al. (2015) carried out the modelling of Udapalatha Municipal landfill (Sri Lanka) to discuss the spatial variation of shear strength and consolidation characteristics. Chances of slope failure of a landfill can

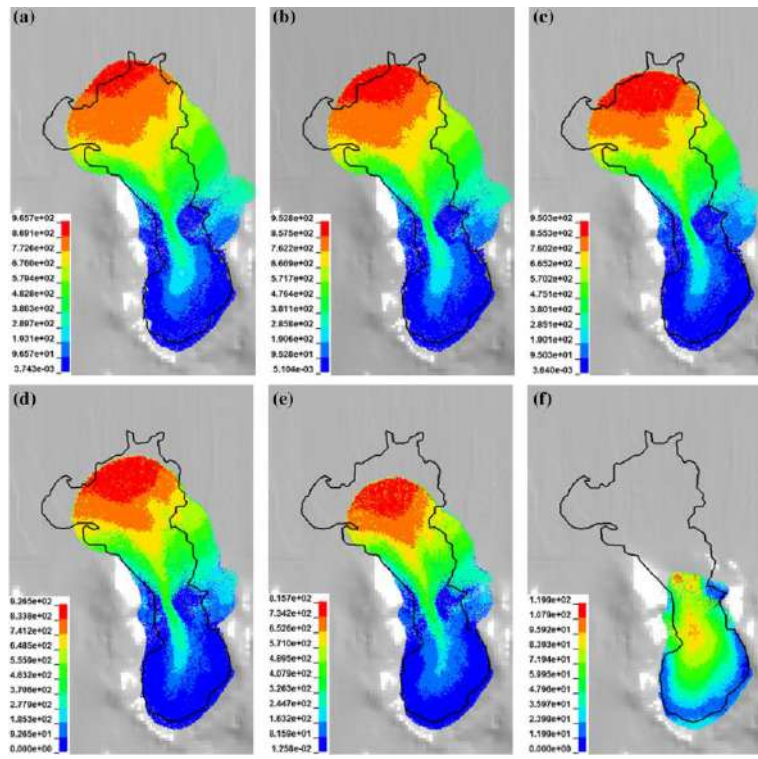

Fig. 4: Modelling output in terms of deposition area and displacements of different solid volume fractions at t = 200s for (a) m_0 = 0.57; (b) m_0 = 0.59; (c) m_0 = 0.61; (d) m_0 = 0. 62; (e) m_0 = 0.63; and (f) m_0 = 0.64 (Liang et al. 2019).

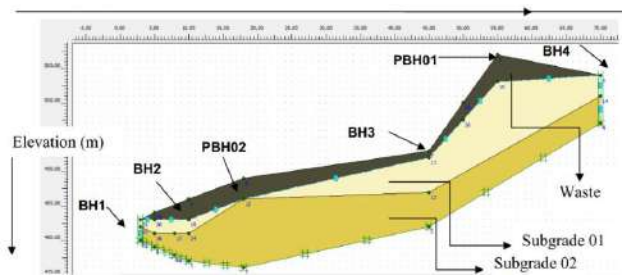

Fig. 5: Modelling of Cross-section of new site and locations of boreholes.

Table 2: Shear strength and consolidation parameters (Prathapan et al. 2015).

Location	Shear strength parameters		Consolidation parameters	
	c′ (kPa)	φ′ (degree)	κ*	λ*
BH 02	46.7	19.8	0.0020	0.0616
PBH 02	50.2	14.0	0.0021	0.0707
PBH 01	15.4	31.8	0.0056	0.0790

occur during the construction of the landfill or after the closure of the landfill.

The shear strength and consolidation were determined using direct shear and Oedometer tests. Stability is measured in terms of the factors of safety, which can be evaluated using SLOPE/W and PLAXIS 2D software considering both homogeneities as well as the heterogeneity of the material properties. The above analysis yielded critical factors of safety ranging between 1.18 and 1.72 in Slope/W and 1.14 and 1.43 in PLAXIS 2D when heterogeneous properties were used in separate analyses assuming homogeneity (Fig. 5). However, by considering spatial variation, the factor of safety was found to be 1.62 and 1.32 in SLOPE/W and PLAXIS 2D analyses respectively, emphasizing the importance of considering the spatial variation of shear strength properties in stability analyses.

The parameters for PLAXIS 2D analysis are effective cohesion (c′), effective friction angle (φ′), modified compression index (λ*), modified swelling index (κ*), modified creep index (μ*) and unit weight (γ). While, on another hand, the input parameters for SLOPE/W software are effective cohesion (c′), effective friction angle (φ′) and unit weight (γ). Results for both the direct shear test and consolidation shear test at three different locations are given in Table 2. Cross-section of the landfill modelled by both PLAXIS 2D and SLOPE/W for calculating the Factor of Safety (FOS) which is shown in the Figs. 6 & 7. The estimated value of FOS using both the methods is also mentioned in Table 3.

Based on the analyses carried out considering uniform as well as spatial variations of properties, the following conclusions are made.

(a) Both shear strength, as well as consolidation parameters, showed considerable variation within the landfill.

(b) The range of values of FOS obtained corresponding to the uniform variation of lowest and highest values of effective cohesion were significant.

Table 3: Summary of the factor of safety values (Prathapan et al. 2015).

Analysis Method		Cohesion (kPa)	Friction Angle (degree)	Factor of Safety	
				SLOPE/W	PALXIS 2D
Spatial Variation	-	-	-	1.618	1.319
Uniform	PBH 01	15.4	31.8	1.184	1.139
	BH 02	46.7	19.8	1.594	1.382
	PBH 02	50.2	14.0	1.722	1.428

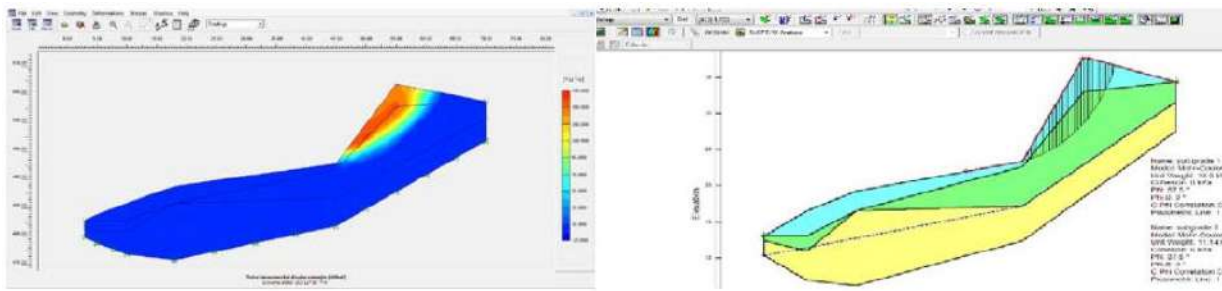

(a) (b)

Fig. 6: Critical failure surfaces obtained from (a) PLAXIS 2D and (b) SLOPE/W analyses using a higher value of cohesion obtained from PBH02.

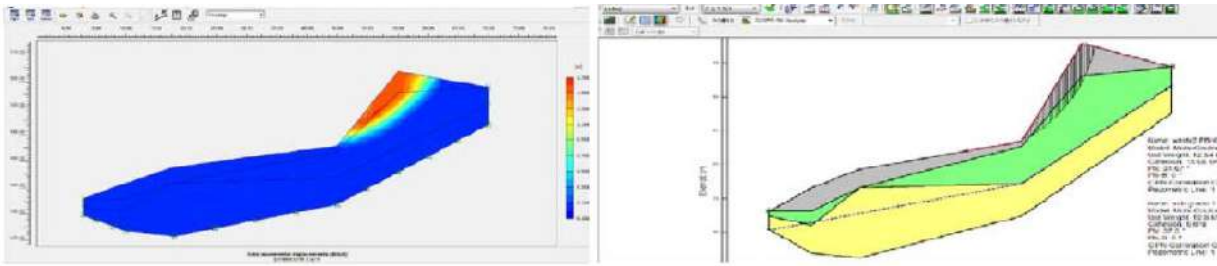

Fig. 7: Critical failure surfaces obtained from (a) PLAXIS 2D and (b) SLOPE/W analyses using a lower value of cohesion obtained from PBH01.

(c) The existing landfill is found to be stable considering the spatial variation of shear strength properties.

CONCLUSION

Expansion of waste generation, economy and rapid population growth in particularly among developing nations increased the landfill demands. Inferable from money related limitations, landfills built as a rule endured with the absence of natural reduction measures, for example, leachate assortment frameworks and coating materials. Subsequently, a lot of contamination is incurred upon the environment. It is likewise accepted that weak layers in the landfill brought about via occasional or different elements, or inadequately compacted soil spread layers may have added to the failures. The most significant conclusion is that proprietors and administrators of landfills, be they dump or built, structured landfills should utilize prepared and skilled enough to work their landfills. The administrative or controlling specialists ought to likewise be prepared and proficient. Measures for controlling and expanding ability ought to be presented, if not present. The disposal of MSW by uncompacted revealed end-tipped dumping ought to be eliminated at the earliest opportunity. Where impractical, steeps, hilly regions and especially sites crossed by streams or other watercourses, or situated in marshes or lakes should be avoided.

REFERENCES

Anderson, J.D. and Wendt J. 1995. Computational Fluid Dynamics. McGraw-Hill, New York, 206.

Bouzza, A. and Wojnarowicz M. 2000. Stability assessment of an old domestic waste slope in Warsaw (Poland). Slope Stability 2000, ASCE GSP No. 101, Proc. of Sessions of GeoDenver, (D.V. Griffiths, G.A. Fenton and T.R. Martin ed.), August 2000, Denver, Colorado, pp. 48-57.

Brandl, H. 1998. Risk analyses, quality assurance, and regulations in landfill engineering and environmental protection. In: (Seco E. Pinto, ed.), Proc. of Environ. Geotech. Balkema Publishers, Rotterdam, pp. 1299-1328.

Fung, Y.C. and Tong, P. 2001. Classical and Computational Solid Mechanics, World Scientific.

Gabr, M.A., Hossain, M.S. and Barlaz, M.A. 2002. Review of shear strength parameters of municipal solid waste with leachate recirculation. Proc. 2nd Intercontinental Landfill Research Symposia, October 2002 in Asheville, North Carolina.

Huvaj-Sarihan, N. and Stark, T.D. 2008. Back analyses of landfill slope failures. In: Proceedings of 6th International Case Histories Conference. Arlington, VA, pp. 11-16.

Isenberg, R.H., Peterson, E. R. and Sternberg, D. 2004. From landfill to leisure: Closure and rehabilitation of Hiriya Landfill. Waste Management World, pp. 45-53.

Kocasoy, G. and Curi, K. 1995. The Umraniye-Hekimbasi open dump accident. Waste Management and Research, 13(4): 305-314.

Koelsch, F., Fricke, K., Mahler, C. and Damanhuri, E. 2005. Stability of landfills-the Bandung dumpsite disaster. In: Sardinia 2005, Tenth International Waste Management and Landfill Symposium. Cagliari, Italy.

Koerner, R.M. and Soong, T.Y. 2000. Stability assessment of ten large landfill failures. Adv. in Transport. and Geoenviron. Systems Using Geosynthetics, ASCE GSP No.103, J. G. Zornberg and B.R. Christopher ed., pp. 1-38.

Liang, H., He, S., Lei, X., Bi, Y., Liu, W. and Ouyang, C. 2019. Dynamic process simulation of construction solid waste (CSW) landfill landslide based on SPH considering dilatancy effects. Bull. Eng. Geol. Environ., 78(2): 763-777.

Liu, G.R. and Gu, Y.T. 2005. An Introduction to Mesh Free Methods and their Programming. Springer, Berlin.

Liu, G.R. and Liu, M.B. 2003. Smoothed Particle Hydrodynamics: A Mesh Free Particle Method. World Scientific.

Liu, M.B. and Liu, G.R. 2010. Smoothed particle hydrodynamics (SPH): An overview and recent developments. Arch. Comput. Methods Engg., 17: 25-76.

Lucy, L.B. 1977. A numerical approach to the testing of the fission hypothesis. Astronom. J., 82: 1013-1024.

Merry, S. M., Kavazanjian Jr, E. and Fritz, W. U. 2005. Reconnaissance of the July 10, 2000, Payatas landfill failure. Journal of Performance of constructed Facilities, 19(2): 100-107.

Mitchell, J.K., Seed, R.B. and Seed, H.B. 1990. Kettleman Hills waste landfill slope failure. I: Liner-system properties. J. Geotech. Eng, 116(4): 647-668.

Ouyang, C., Zhou, K., Xu, Q., Yin, J., Peng, D., Wang, D. and Li, W. 2017. Dynamic analysis and numerical modeling of the 2015 catastrophic landslide of the construction waste landfill at Guangming, Shenzhen, China. Landslides, 14(2): 705-718.

Peng, R., Hou, Y., Zhan, L. and Yao, Y. 2016. Back-analyses of landfill instability induced by high water level: Case study of Shenzhen landfill. Int. J. Env. Res. Pub. He., 13(1): 126.

Prathapan, R., Jeyakaran, T., Thakshajini, L. and Kurukulasuriya, L.C. 2015. Spatial variation of shear strength and consolidation characteristics of a municipal landfill and its implications on the stability of the fill- A Case Study. 3rd International Symposium on Advances in Civil and

Environmental Engineering Practices for Sustainable Development (ACEPS-2015), Hapugala, Galle, Sri Lanka.

Reddy, K.R. and Bogner, J.E. 2003. Bioreactor landfill engineering for accelerated stabilization of municipal solid waste. Intern. e-Conf. on Modern Trends in Foundation Engg.: Geotechnical Challenges and Solutions, Indian Institute of Technology, Madras.

Sarihan, N.J. and Stark, T.D. 2008. Back-analyses of landfill slope failures. International Conference on Case Histories in Geotechnical Engineering, 12.

Siegel, R.A., Robertson, R.J. and Anderson D.G. 1990. Slope stability investigation at a landfill in Southern California. Geotechnics of Waste Fills - Theory and Practice, ASTM STP 1070, A. Landva and D. Knowles, ed, American Society for Testing and Materials, Philadelphia, Pennsylvania, pp. 259-284.

Stark, T.D., Arellano, D., Evans, W.D., Wilson, V.L. and Gonda, J.M. 1998. Unreinforced geosynthetic clay liner case history. Geosynth. Int., 5(5): 521.

Stark, T.D., Eid, H.T., Evans, W.D. and Sherry, P.E. 2000. Municipal solid waste slope failure. II: Stability analyses. J. Geotech. Geoenviron. Eng., 126(5): 408-419.

Violeau, D. 2012. Fluid Mechanics and the SPH Method: Theory and Applications. Oxford University Press, Oxford

Yin, Y., Li, B., Wang, W., Zhan, L., Xue, Q., Gao, Y., Zhang, N., Chen, H., Liu, T. and Li, A. 2016. Mechanism of the December 2015 catastrophic landslide at the Shenzhen landfill and controlling geotechnical risks of urbanization. Engineering, 2(2): 230-249.

Nature Environment and Pollution Technology
An International Quarterly Scientific Journal

p-ISSN: 0972-6268
(Print copies up to 2016)
e-ISSN: 2395-3454

Vol. 20 | No. 2 | pp. 833-842 | 2021

Original Research Paper

https://doi.org/10.46488/NEPT.2021.v20i02.046

Open Access Journal

Potential Ecological and Health Risk Assessment of Dumpsite from Ibadan, Southwestern Nigeria

R. A. Obasi† and H. Y. Maduekwe
Department of Geology, Ekiti State University, Ado Ekiti, Ekiti State, Nigeria
†Corresponding author: R.A Obasi; romanus.obasi@eksu.edu.ng

Nat. Env. & Poll. Tech.
Website: www.neptjournal.com

Received: 05-04-2020
Revised: 19-06-2020
Accepted: 25-06-2020

Key Words:
Dumpsites
Ecological risks
Hazard index
Cancer risks

ABSTRACT

Dumpsites have elevated the contamination and pollution of soils by heavy metals, hence the need to study the potential ecological and health risks impact on the soil and humans. Ten soil samples collected from the soil around the dumpsites at Awotan Ibadan were analysed using the inductively coupled plasma-mass spectrometry (ICP-MS) analytical technique. The data were interpreted using contamination indices such as contamination and enrichment factors, geo-accumulation index and pollution index to determine the ecological and health risks posed by the heavy metals. The results of the spatial distribution of heavy metals across the sampling sites showed the following ranges: Cu (43.71-469.64) with a mean of 113.74 mg/kg, Zn (53.50-615.60) with a mean of 130.52 mg/kg, Rb (83.14-225.35) with a mean value of 145.37 g/kg and Pb (28.38-209.15) with a mean of 68.01 mg/kg in descending order: Zn > Cu >Rb> Pb >V. The enrichment factors indicated very high enrichment of Cu (25.07), significant enrichment of Pb (18.78) and moderate enrichment of Zn (15.14) and minor enrichments of Co, Ni, Rb and Cs. The results of the contamination factor showed that Sc, Co, Zn, Rb, Cs have moderate contamination while Cu and Pb indicated high contamination. The results of geo-accumulation (Igeo) indicated that Cu and Pb are positive in contrast to the other metals suggesting some anthropogenic influences of the duo heavy metals in the study area. Cu and Zn indicated low ecological risks however, Cu and Pb showed considerable risks (Er 80-160) and moderate risk (Er 40- 80) respectively in sample site number one. The results of the modified ecological risk index (MRI) revealed that about 62.53% of this sample site number one showed a considerable ecological risk of the heavy metal Cu and 47.61% of the moderate ecological risk of Pb. The health-risk study indicated that hazard quotient HQ_{ing}, HQ_{derm} and hazard index (HI) values were below the acceptable limit of 1×10^{-6} and 1×10^{-4} and therefore showed no obvious non-carcinogenic risk and negligible cancer risk from the soils and environment.

INTRODUCTION

Nigeria like any other developing country of the world increases in population on daily basis, and this increases infrastructure and waste discharges. Cities such as Ibadan the second largest after Lagos in South-West Nigeria produces large quantities of solid wastes from domestic, industrial and institutional wastes. These wastes exist in semi-solid or solid form except for industrial hazardous wastes (USEPA 2012). In most cities in Nigeria, the wastes are not sorted out unlike in developed countries like the UK where there are separate containers for semi and solid wastes collections and these are disposed of according to the environmental protection guidelines of the country in question. In Nigeria, the wastes are dumped in open places called dumpsites or landfills. The wastes decompose or broken down by microorganisms producing leachates which filtrate into the soils and reposited. The plants absorb the leachates through their roots and some of the leached constituents enter the water regime to make it unusable for a drink. Some major problems faced by the cities concerning wastes are improper disposal methods which have serious negative effects on human beings, animals and the environment. The environment represented by the ecosystem via the soil becomes the repository of the heavy metals. Heavy metals are one of the important pollutants in the environment through natural or anthropogenic activities of man. Living organisms require a trace amount of heavy metals but excess of it could be deleterious to them.

Exposures of heavy metals can lead to accumulation in human body parts such as the brain, liver, bones, and kidneys resulting in serious health hazards (Kamunda et al. 2016). Health risk assessment of heavy metals is usually performed to estimate the total exposure to heavy metals among the residents in a particular area. Risk assessment of contaminants in humans is based on the fact that the leachates from the heavy metals can contain chemicals that may either be carcinogenic or non-carcinogenic (Dorne et al. 2011). In the same way, the accumulation of these metals in the body

system could result in serious life-threatening illnesses and in some cases death.

However, the accumulation of these metals in the body of mammals over time can cause serious illness (Aderinola et al. 2009). Another way heavy metals could be deposited in the body is through agricultural activities. Crop cultivation, happening around dump site could be contaminated since some of the heavy metals gets leached deep into the soil and crops get their nutrient from the soil. When such food is consumed by man, he unintentionally ingests these metals along with the food, poisoning his system and if not checked, over time could result in life-threatening issues. Environmental contamination by heavy metals has become a worldwide problem in recent years since heavy metals unlike some other pollutants are not biodegradable (Bazrafshan et al. 2015). Soil pollution by heavy metals has serious health implication especially with regards to crops/vegetables grown on such soils (Steffan et al. 2017, and Nwaogu et al. 2014). Most of these heavy metals are necessary for both plants and animal growths at uncontaminated levels.

Long-term effect of heavy metal exposure to human and higher animals includes mental lapse, kidney failure, and central nervous system disorder (Nwaogu et al. 2014). Exposure to lead (Pb) may cause anaemia, nephropathy, gastrointestinal colic, and central nervous system symptoms (Hu et al. 2017). As a result of increasing anthropogenic activities, heavy metals pollution of soil, water, and atmosphere represents growing environmental problems affecting food quality and human health. Heavy metals may enter the food chain as a result of their uptake by edible plants (Shaapera et al. 2013). Ibadan, like any other city in South-Western Nigeria, faces problems of environmental sanitation such as improper disposal of refuse near residential areas, along the roads and streets, poor refuse collection and handling. There are four major dumpsites in Ibadan namely; Lapite, Awotan, Ajakanga and Aba Eku and unfortunately farmers use them as fertilizers. This, however, leads to the accumulation of heavy metals in plants grown around the dumpsite soils or on soils fertilized with dumpsite manure thus posing potential health risks.

Dumpsite wastes are commonly burnt and ashes produced are richer in metal contents. These ashes are either dissolved in rainwater and leached into the soil contaminating the underground water, or washed away by runoff into streams and rivers, thereby contaminating the environment. It is based on these facts that this study is aimed at determining the total lethal concentrations or otherwise of Scandium (Sc), Lead (Pb), Copper (Cu), Nickel (Ni), Vanadium (V), Rubidium (Rb), Molybdenum (Mo), Cobalt (Co), Cesium (Sc) and Zinc (Zn) in dumpsite soils in Ibadan area, Nigeria. The topography of the sites is gently undulating with isolated inselbergs at the Awotan area. Migmatite gneisis and quartz schist ridges dominate the terrain. The annual average rainfall in the area is 1300 mm (Ileoje 1987). The vegetation is the tropical rain forest with thick undergrowth. Dendritic drainage pattern characterizes the area with unmodified stream channels flowing in the southward and east-west directions. The Awotan dumpsite is drained by River Alapata

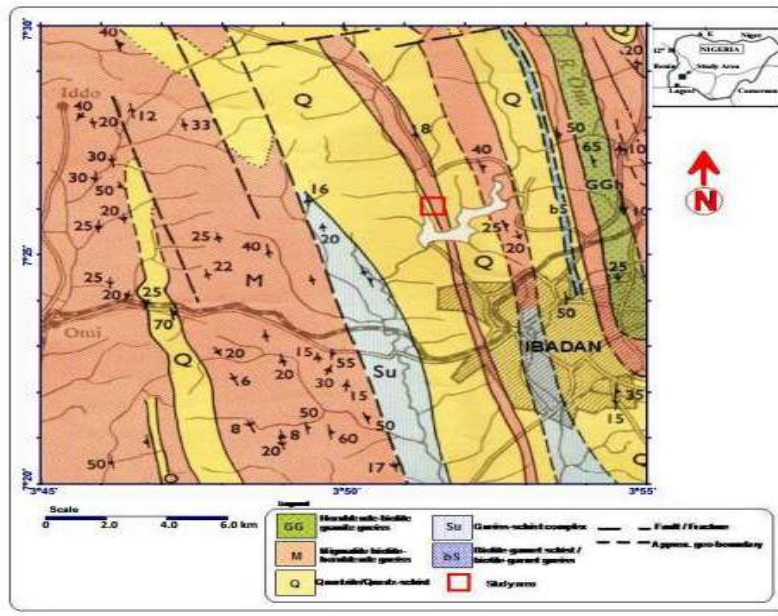

Fig. 1: Geological map of Ibadan showing the study area (Oladunjoye et al. 2013).

a **b**

Fig. 2: Awotan dumpsite areas.

and its tributaries. The area is usually well-drained during the rainy season but the tributaries dry up during the dry season. The main rock types underlying the dumpsite belong to the Migmatite-gneiss-quartzite complex (Rahaman 1976, 1988) consisting of quartz, schist and migmatite gneiss, while pegmatite and quartz occur as veins in the major rocks (Fig. 1). The quartz schist and the biotite gneiss trend North-South direction and are variously jointed. The quartz schist covers more than 60% of the area while migmatite gneiss covers the remaining 40% area. The migmatite gneiss occurs mainly as low-lying outcrops while the quartz schist forms ridges.

MATERIALS AND METHODS

Study Area

The Awotan dumpsite is located between Latitudes 7°27.59'N and 7°27.73'N and Longitudes 3°50.93' E and 3°51.17' E and found along Awotan-Akufo Road, Apete area of Ibadan Metropolis, Southwestern Nigeria (Fig. 2). The Awotan area has a unique environmental setting characterized by a wide range of land-use activities such as small scale arable farming, animal husbandry, residential and commercial settlements. Leachate emanating from the wastes is washed down into the surrounding areas thereby impacting the soils within the area.

Sample Collection

Ten (10) soil samples were collected for this study. Sampling was done at regular intervals with the aid of an auger at a depth of 0-30 cm. The soil samples were stored in plastic bags and labelled according to the location at which they were collected. The sampling points are presented in Fig. 3. Each sample was immediately placed in a plastic bag and tightly sealed to avoid contamination from the environment and transportation.

Sample Analysis

The heavy metals were analysed by the inductively coupled plasma mass spectrometry (ICP-MS) and X-Ray fluorescence spectrometry (XRF) methods. Ten soil samples were analysed by Laser ablation microprobe Inductivity Coupled Plasma-Mass Spectrometry (La ICP-MS) method (Jackson et al. 1992) at the Central laboratory of the Stellenbosch University, South Africa. The ICP-MS instrument is Perkin-Elma Sciex ELAN 5100 coupled with a UV (266 μm)

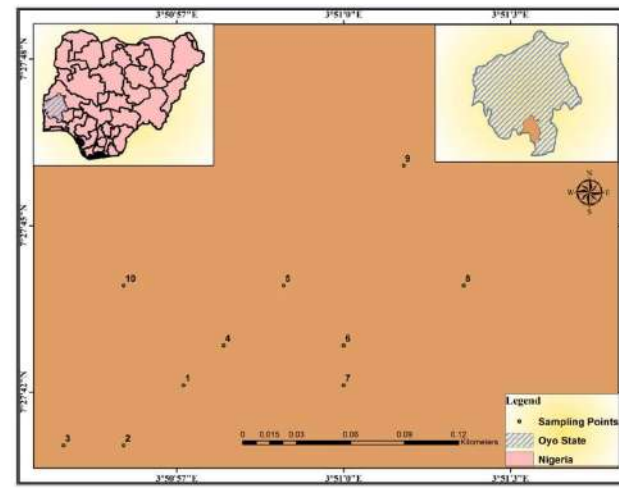

Fig. 3: Map of the study area.

laser. The laser was operated with 1 mJ/Pulse energy and 4 Hz frequency for carbonates and silicate glass. The spot diameter for these analyses is 30-50 m. NIST 610 glass was used as a calibration standard for all the samples with ^{44}Ca as an internal standard. The analytical precision is 5% at the ppm level. Details of ICP-MS and laser operating conditions have been published by Norman et al. (1996) and Norman (1998). The results of the compositions of the heavy metals are presented in Table 1.

RESULTS AND DISCUSSION

The variations in the concentrations of each heavy metal across the sampling points showed the following ranges: Cu (43.71-469.64) with a mean of 113.74 mg/kg, Zn (53.50-615.60) with a mean of 130.52 mg/kg, Rb (83.14-225.35) with a mean value of 145.37 mg/kg and Pb (28.38-209.15) with a mean of 68.01 mg/kg. The concentration of some heavy metals in the soil of the dumpsite is presented in descending order as Zn > Cu >Rb> Pb >V.

Methods of Assessment of Contamination in Dumpsite Soil

Contamination indices used to assess the heavy metal contamination levels in the soil around the dumpsite include the enrichment factor (Ef), contamination factor (Cf), geo-accumulation index (Igeo), pollution load index (PLI), degree of contamination (Cd), and ecological risk index. (Er).

Enrichment Factor

The computation of enrichment factor (EF) has been adopted to evaluate the impact of anthropogenic and naturally occurring sources of heavy metals as well as the metal abundance in soil. Yongming (2006) stated that EF has been used to determine the degree of modification in the composition of heavy metals in the area of atmospheric aerosols, sediments, soil and solid wastes. The EF of metals has been defined using Scandium (Sc) as a natural element of reference.

$$EF = \frac{Cx(sample)/Cref(sample)}{Bn(background)/Bref(background)} \quad \ldots(1)$$

Where, Cx (sample) is the concentration of the element in the examined environment and C_{ref} (sample) is the concentration of the reference element for normalization, Bx(background) is the concentration of the element in the crust, and B_{ref} is the concentration of the reference element used for the normalization in the crust (Ato et al. 2010, Cevik 2009). Five contamination categories have been suggested based on enrichment factor where EF < 2 = minor enrichment; EF = 2–5 = moderate enrichment; EF = 5–20 = significant enrichment; EF = 20–40 = very high enrichment; and EF > 40 extremely high enrichment (Yongming 2006). The maximum enrichment factors shown in Table 2 in decreasing values are 25.07 for Cu, (very high enrichment), 18.78 for Pb and 15.14 for Zn (significant enrichment), 2.05 for Mo (moderate enrichment) and Co, Ni, Rb and Cs have minor enrichment since they are less than two (2) (Birch 2003).

Table 1: Heavy metal concentration (mg/kg) in soil obtained from the dumpsites.

Sampling point	Sc	V	Co	Ni	Cu	Zn	Rb	Mo	Cs	Pb
1	11.35	70.34	16.92	46.55	469.64	615.60	122.65	2.72	4.18	164.39
2	11.10	70.95	15.95	28.85	52.00	81.30	138.35	1.56	4.39	39.02
3	13.02	87.78	21.27	38.95	64.65	77.95	158.95	1.72	4.48	50.69
4	18.47	137.30	28.79	57.50	53.43	72.35	151.65	2.39	6.29	41.75
5	21.86	165.85	26.67	65.95	61.20	91.85	186.81	2.73	7.82	34.76
6	18.19	130.64	17.45	52.95	64.72	101.25	225.35	1.97	7.79	28.38
7	17.70	115.50	16.99	46.60	59.90	88.75	182.65	1.95	7.43	31.84
8	21.25	131.30	16.09	42.00	43.71	53.50	83.14	2.45	4.99	39.09
9	19.94	122.95	17.04	42.35	123.36	60.05	98.04	2.65	4.48	41.03
10	19.82	166.07	47.89	42.75	144.80	62.60	106.08	1.46	4.12	209.15
Min	11.10	70.34	15.95	28.85	43.71	53.50	83.14	1.46	4.12	28.38
Max	21.86	166.07	47.89	65.95	469.64	615.60	225.35	2.73	7.82	209.15
Mean	17.27	119.87	22.50	46.45	113.74	130.52	145.37	2.16	5.59	68.01
SD	4.00	34.49	10.02	10.33	129.34	171.10	44.66	0.49	1.57	63.76

Table 2: Average, min and max values of Enrichment Factor.

	V	Co	Ni	Cu	Zn	Rb	Mo	Cs	Pb
Average	0.65	0.85	0.79	3.63	2.12	0.91	0.76	0.92	3.24
Min	0.57	0.33	0.38	0.49	0.20	0.11	0.50	0.27	0.91
Max	0.82	1.16	1.63	25.07	15.14	1.43	2.05	1.33	18.78
SD	0.07	0.26	0.32	7.59	4.58	0.40	0.47	0.27	5.51

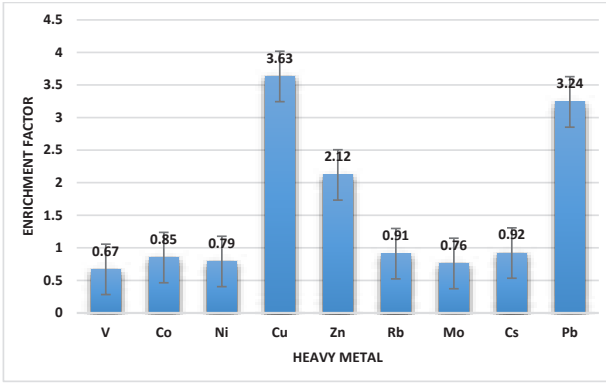

Fig. 4: Average enrichment of Cu, Pb and Zn.

Fig. 4 presents the histogram of the average enrichment of Cu, Pb and Zn along with the other heavy metals in the soil. The very high and significant enrichment of Cu, Pb and Zn is an initial indication of an anthropogenic influence of the metals in the soil.

Contamination Factor (CF)

Contamination factor is a quantification of the degree of contamination relative to either the average crustal composition of a respective metal or to the measured background values from a geologically similar and uncontaminated area (Tijani et al. 2004). It is expressed in equation 2 given by Hakanson (1980) as:

$$C_F = C_x/B_m \quad \ldots(2)$$

Where, Cx and Bm are the concentrations of metal in a soil sample and background environments. The background values of heavy metals were taken from Taylor and McLennan (1995). The CF is classified into four groups ($CF < 1$; indicates low metal contamination), ($1 \leq CF < 3$; indicates moderate contamination), ($3 \leq CF \leq 6$; indicates considerable contamination), and ($CF > 6$ indicates very high contamination) (Hakanson 1980).

The results of the contamination factor (CF) for the heavy metals are presented in Table 3. The results show that Cu ranges from 0.53 to 23.02 mg/kg with a mean value of 3.90 mg/kg, Zn varies from 0.38 to 12.37 mg/kg with a mean of 1.98 while Pb varies between 1.12 and 15.35 mg/kg with a mean value of 363.72 mg/kg with a mean of 3.22. Going by the groupings and using the mean values V, Ni and Mo have values that are less than one showing low contamination ($CF< 1$). Sc, Co, Zn, Rb, Cs have values that are more than 1 and less than three ($1<CF<3$) thus indicating moderate contamination. Cu and Pb have values that are more than 3

Table 3: Contamination factors, (CF), PLI and mCd.

Sample no	Sc	V	Co	Ni	Cu	Zn	Rb	Mo	Cs	Pb	PLI	mCd
1	0.82	0.41	0.93	1.33	23.02	12.37	0.94	0.17	0.69	15.35	1.69	5.60
2	0.91	0.37	0.86	0.52	0.53	0.72	0.82	0.05	0.99	1.12	0.55	0.69
3	0.81	0.42	0.83	0.64	2.12	0.99	1.16	0.08	0.77	2.81	0.77	1.06
4	1.21	0.55	1.40	0.91	1.09	0.64	1.11	0.06	1.03	2.24	0.79	1.02
5	1.64	0.97	1.63	1.37	1.59	0.89	1.04	0.12	1.48	1.93	1.06	1.27
6	1.69	0.87	1.19	1.30	1.47	1.05	1.62	0.09	1.65	1.55	1.03	1.25
7	1.12	0.58	0.65	0.81	1.77	1.07	1.60	0.06	1.46	1.32	0.81	1.04
8	1.59	0.71	1.14	1.05	1.24	0.80	1.00	0.09	1.52	1.85	0.90	1.10
9	1.70	0.75	0.56	0.64	0.94	0.38	0.18	0.11	0.45	2.08	0.56	0.78
10	1.36	0.62	1.23	1.06	5.23	0.90	1.22	0.09	1.34	1.99	1.04	1.50
Mean	1.28	0.62	1.04	0.96	3.90	1.98	1.07	0.09	1.14	3.22	0.92	1.53
Max	1.70	0.97	1.63	1.37	23.02	12.37	1.62	0.17	1.65	15.35	1.69	5.98
Min	0.81	0.37	0.56	0.52	0.53	0.38	0.18	0.05	0.45	1.12	0.55	0.50

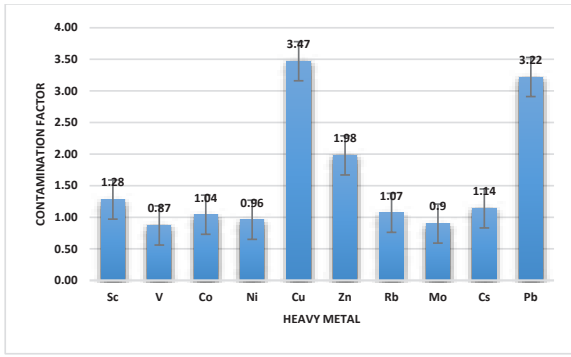

Fig. 5: Histogram of contaminating heavy metals.

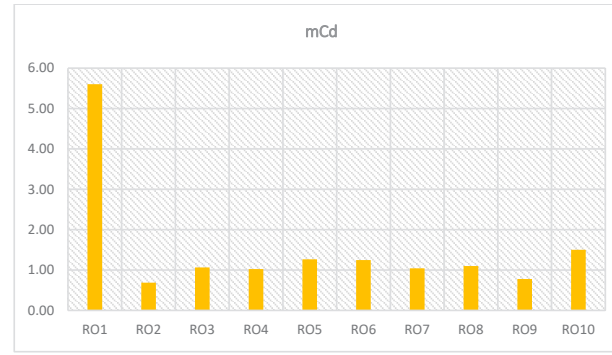

Fig. 6: Histogram of the modified degree of contamination (mCd).

and less than 6 indicating high contamination. Fig. 5 presents a picture of the contaminating heavy metals. It should be noted that sampling site one (1) has high contaminations of Cu (23.02), Zn (12.37) and Pb (15.35) respectively. The modified degree of contamination (mCd) expressed in Fig. 6 agrees with the contamination levels at site one (1) with a value of 5.60 (Table 3).

Geo-accumulation Index (Igeo)

The geo-accumulation index of (Igeo) is widely used to measure the level of pollution caused by heavy metals in the soil. The I_{geo} values were calculated using equation 3 first proposed by Muller (1969) as:

$$I_{geo} = Log_2\left[\frac{Cx}{1.5B_n}\right] \quad \ldots(3)$$

Where, Cx represents the measured concentration of the elements studied and Bn is the geochemical background value of the element or average shale (Taylor & McLennan 1985). The constant 1.5 takes care of changes in the concentration of the heavy metals in the environment (Wei & Yang 2010, Loska 2004) grouped Igeo as Igeo $\leq$ 0 = no pollution; Igeo (0-1), moderate pollution; Igeo (1-2), strong pollution; Igeo (2-3), high pollution; Igeo (3-4), very high pollution; Igeo (4-5) severe pollution and Igeo (> 5) extreme pollution. The results of Igeo indicated that Cu and Pb are positive (Fig.7) in contrast to the other metals suggesting some anthropogenic influences of these heavy metals in the study area. The Cu (3.77), Zn (3.04), and Pb (3.35) at site one (1) have values that are more than 3, Igeo (3-4), indicating very high pollution in the soil and tandem with (Fig.6) mCd. Similarly, Cu alone at site ten (10) has a value of 1.63, Igeo (1-2), thereby showing strong pollution.

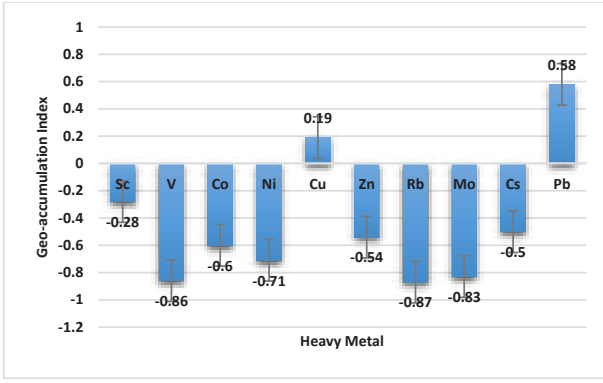

Fig.7: Average geo-accumulation of the heavy metals.

Ecological Risk Assessment (RI).

The ecological risk index (RI) evaluates the potential ecological risk of heavy metals in the sediment /soil as suggested by Hakanson (1980) in Equation 4.

$$RI = CFn \times T_R \quad \ldots(4)$$

Where, C_{Fn} and T_R are CF and the toxicological response factor of individual heavy namely Cu (5), Zn (1) Ni (5) and Pb (5) (Hakanson 1980, Kumar et al. 2018). In a way to know the ecological risks of anthropogenic and lithogenic influences, the CFn in the RI is replaced by computation with EF. The ecological RI worked out from EF is the modified potential ecological index MPI (Kumar et al. (2018) written as in Equation 5.

$$MPI = EFn \times Tr \quad \ldots(5)$$

Where, EFn and Tr are the EF and the toxicological response factor of individual heavy metals respectively. The classes used for risk assessment are as follows:

Er < 40 (low risk); 40- 80 (moderate risk); 80 -160 (considerable risk); 160-320 (high risk) and > 320 (very high risk). In the case of risk index, (equation 5) RI < 95 indicates a low potential ecological risk; 95-190 moderate risk; 190-380 considerable risk while RI > 380 very high risk.

The ecological risks of Ni, Cu, Zn and Pb were assessed using the potential ecological risk index RI (Fig. 8) and the modified potential ecological risk index MRI (Fig. 9).

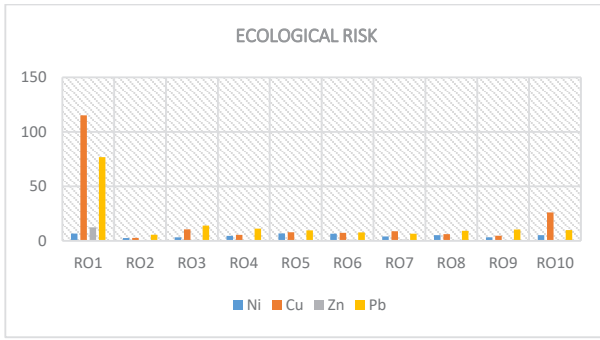

Fig. 8: The ecological risk factor (RI) for Ni, Cu, Zn and Pb in each sample sites.

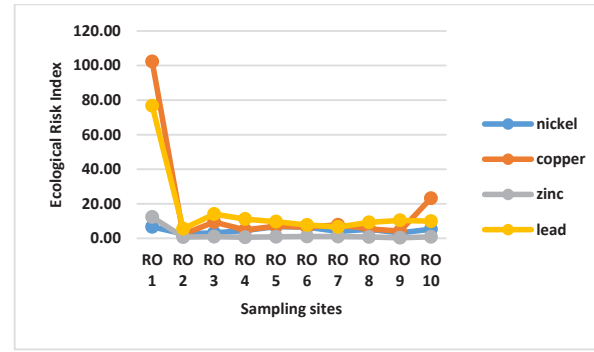

Fig. 9: Modified potential ecological risk index (MRI).

The results in Table 4 revealed that Er values for Cu and Zn are less than 40 (Er <40) respectively indicating low ecological risk of these heavy metals. Cu and Pb have varying values. Sampling sites from 2 to 10 have values that are less than 40 showing low ecological risks by these heavy metals, however, site one (1) has the value of 115.10 for Cu and 76.74 for Pb indicating considerable risks (Er 80-160) and moderate risk (Er 40- 80) respectively. The results of MRI revealed that about 62.53% of sample site one showed a considerable ecological risk of the heavy metal Cu and 47.61% of the moderate ecological risk of Pb respectively

Assessment of Ecological Risks

The variation in the ecological risk index of the heavy metals across the sampling sites is presented in Fig. 9. The relatively considerable ecological risk index recorded for Cu and moderate ecological risk of Pb respectively at sampling sites one (1) suggests an anthropogenic source of Cu and Pb in this part of the study area.

Table 4: Ecological risk factor for nickel, copper, zinc and lead.

Sample no.	Ni	Cu	Zn	Pb
1.	6.65	115.10	12.37	76.74
2.	2.61	2.65	0.72	5.61
3.	3.20	10.61	0.99	14.04
4.	4.56	5.46	0.64	11.18
5.	6.87	7.94	0.89	9.66
6.	6.50	7.35	1.05	7.73
7.	4.04	8.83	1.07	6.62
8	5.23	6.21	0.80	9.26
9.	3.21	4.71	0.38	10.41
10.	5.28	26.13	0.90	9.93
TR	5	5	1	5
Mean	4.815	19.4975	1.980579	16.1175
Ranges	2.61-6.65	2.65-115.10	0.38-12.37	6.67-76.74

HEALTH RISK ASSESSMENT

Health risk assessment in this study is a way to determine the probable level of the harmful health impacts of heavy metals on the soil. The assessment of each metal contaminant is based on the level of risk of using the soil and it is classified as carcinogenic or non-carcinogenic health hazards (Wongsasuluk et al. 2014). Hazard quotients (HQ), Hazard index (HI), are used in the calculation of the potential carcinogenic and non-carcinogenic health risk caused through ingestion and dermal absorption of heavy metals in the soil by adults. HQ (for each heavy metal) is the ratio of an average daily intake (ADI, mg/kg/day) of metal ingested to the reference oral dose (RfD) through oral ingestion and dermal absorption for the adult residents around the environment. ADI (mg/kg-day) for the different pathways were calculated using the exposure equations (6) and (7) (USEPA 2012).

Ingestion of Heavy Metals through Soil

$$\mathrm{ADI}_{\mathrm{ing}} = \frac{c \times Ring \times CF \times ED}{BW \times AT} \quad \ldots(6)$$

Where, $\mathrm{ADI}_{\mathrm{ingestion}}$ is the average daily intake of heavy metals ingested from the soil in mg/kg-day, C = concentration of heavy metal in mg/kg for soil. IR in mg/day is the ingestion rate, EF in days/year is the exposure frequency, ED is the exposure duration in years, BW is the bodyweight of the exposed individual in kg, AT is the time over which the dose is averaged in days. CF is the conversion factor in kg/mg.

Inhalation of Heavy Metals Via Soil Particulates

$$\mathrm{ADI}_{\mathrm{inh}} = \frac{c \times Rinh \times EF \times ED}{PEF \times BW \times AT} \quad \ldots(7)$$

Where $\mathrm{ADI}_{\mathrm{inh}}$ is the average daily intake of heavy metals inhaled from the soil in mg/kg-day, CS is the concentration of heavy metal in the soil in mg/kg, IRair is the inhalation rate in m3/day, PEF, is the particulate emission factor in

m3/kg. EF, ED, BW and AT are as defined earlier in Equation (7) above.

Dermal Contact with Soil

$$ADI_{dems} = \frac{c \times SA \times CF \times SL \times ABS \times ED}{BW \times AT} \quad \ldots(8)$$

Where ADI_{dems} is the exposure dose via dermal contact in mg/kg/day. CS is the concentration of heavy metal in the soil in mg/kg, SA is exposed skin area in cm^2, FE is the fraction of the dermal exposure ratio to the soil, AF is the soil adherence factor in mg/cm^2, ABS is the fraction of the applied dose absorbed on the skin. EF, ED, BW, CF and AT are as defined earlier in Equation (8).

Non-Carcinogenic Risk

The results for ingestion, inhalation and dermal pathways presented in Table 5 indicated that HI values for ingestion pathways and dermal pathways are 9.84636×10^{-5} and 7.85357×10^{-7} respectively implying that the values are less than one (HI < 1) and no obvious risks.

The HI value for ingestion is greater than that of the dermal pathway indicating that the ingestion pathway contributes the greatest non-carcinogenic effect. The inhalation pathway is the least contributor (Fig. 10). Sultana et al. (2019) suggested that when HI > 1 there is the possibility that non-carcinogenic impacts may occur in the adult residents whereas when HI < 1 it is expected that the exposed person may not experience noticeable harmful health impacts.

Carcinogenic Risk

The results of the carcinogenic risk calculated for heavy metals are presented in Table 6. Pb is singled out for carcinogenic health risk assessment because of its toxicity and its known CSF. The cancer slope factor is defined as the risk generated by a lifetime average amount of one mg/kg/day of carcinogen around the sampled area. Table 6 indicated that

Table 5: The Hazard Index (HI) of some selected heavy metals.

	Pb	Ni	Cu	Zn	HI
HQ ingestion (ing)	7.01E-05	9.42E-06	1.65E-05	2.45473E-06	9.84636E-05
HQ inhalation (inh)	-	-	-	-	-
HQ dermal	-	3.83E-07	2.9E-07	1.11936E-07	7.85357E-07
Risk pathway ing	2.14E-09	-	-	-	-
Risk pathway inh	2.81E-10	-	-	-	-
Risk Total	2.43E-09	-	-	-	-

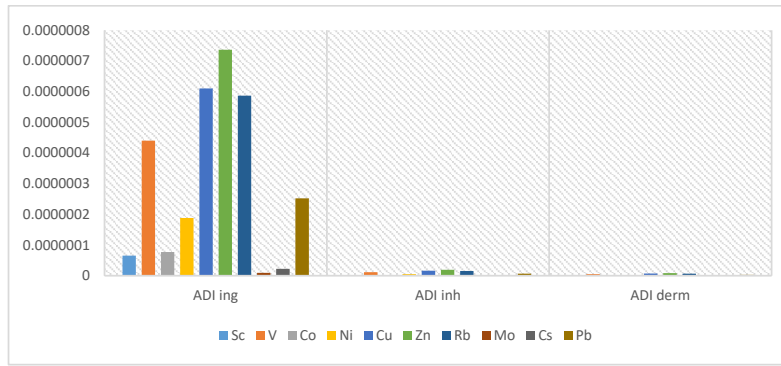

Fig.10: Histogram of heavy metals in different pathways.

Table 6: Average daily intake (ADI) of heavy metals in the sampled soil.

	Sc	V	Co	Ni	Cu	Zn	Rb	Mo	Cs	Pb
ADI ingestion	6.54E˙08	4.4E ˙07	7.74E-08	1.88356E-07	6.10489E-07	7.36419E-07	5.87E-07	9.23E-09	2.23E-08	2.52329E-07
ADI inhalation	1.73E-09	1.17E-08	2.05E-09	4.9859E-09	1.616E-08	1.94934E-08	1.55E-08	2.44E-10	5.9E-10	6.67929E-09
ADI dermal	7.45E-10	5.02E-09	8.83E-10	2.14726E-09	6.95958E-09	8.39517E-09	6.69E-09	1.05E-10	2.54E-10	2.87655E-09

the values of the heavy metals are less than one meaning that it is below the generally acceptable value which Tepanosyan (2017) suggested should be 1×10^{-6} for a single carcinogenic element and 1×10^{-4} [f] for multi-element carcinogens. The value 2.43×10^{-9} is less than the acceptable value implying a negligible cancer risk for the soils of the dumpsites.

CONCLUSIONS

The ecological and health risks of some heavy metals of dumpsites at Wotan, Ibadan were studied. The results of the enrichment factor indicated a very high enrichment of Cu (25.07), and 15.14 significant enrichment of Pb (18.78), moderate enrichment of Zn (15.14) and minor enrichment of Co, Ni, Rb and Cs. The very high, significant and moderate enrichments of Cu, Pb and Zn are an initial indication of an anthropogenic influence of the metals in the soil. V, Ni and Mo have shown low contamination. Sc, Co, Zn, Rb, Cs indicated moderate contamination while Cu and Pb indicated high contamination. It should be noted that sampling site one (1) has high contaminations of Cu (23.02), Zn (12.37) and Pb. Cu and Pb exhibited high contamination levels. The relatively considerable ecological risk index recorded for Cu and moderate ecological risk of Pb respectively at sampling sites one (1) suggests an anthropogenic source of Cu and Pb in this part of the study area. The health-risk study indicated that hazard quotient HQ_{ing}, HQ_{derm} and hazard index (HI) values were below the acceptable limits of $1x10^{-6}$ and $1x10^{-4}$ and therefore showed no obvious non-carcinogenic risk and negligible cancer risk from the soils on health and environment.

REFERENCES

Aderinola, O.J., Clarke, E.O., Olarinmoye, O.M., Kusemiju, V. and Anatekhai, M.A. 2009. Heavy metals in surface water, sediments, fish and perwinkles of Lagos lagoon. American-Eurasian J. Agric. & Environ. Sci., 5 (5): 609-617.

Ato, A.F., Samuel, O., Oscar, Y.D., Alex, P., Moi, N. and Akoto, B. 2010. Mining and heavy metal pollution assessment of aquatic environments in Tarkwa, Ghana using multivariate statistical analysis. Journal of Environmental Statistics, 1(4): 1-13.

Bazrafshan, E., Leli, M., Alireza, A.M. and Amir, H.M. 2015. Heavy metal removal from aqueous environments by electrocoagulation process- a systematic review. Journal of Environmental Health Science and Engineering, 13(1): 1-16.

Birch, G. and Woodroffe, F. 2003. Coastal GIS 2003, Wolloongong University Papers in Center of Maritime Policy, 14, Australia, Edition Edn.

Cevik, F., Goksu, M. Z.L., Derici, O.B. and Findik, O. 2009. An assessment of metal pollution in surface sediments of Seyhan dam by using enrichment factor, geo-accumulation index and statistical analyses. Environmental Monitoring and Assessment, 152(1-4): 309-317.

Dorne, J., Kass, G., Bordajandi, L.R., Amzal, B., Bertelsen, U., Castoldi, A.F., Heppner, C., Eskola, M., Fabiansson, S. and Ferrari, P. 2011. Human risk assessment of heavy metals: Principles and applications. Met. Ions Life Sci., 8: 159-171.

Hakanson, L. 1980. Ecological risk index for aquatic pollution control, a sedimentological approach. Water Research, 14(8): 975-1001.

Hu, Z., Yang, Z., Liang, X., Salakhutdino, V. and Xing, E.P. 2017. On unifying deep generative models arxiv preprint arxiv 1706. 00550 3-10.

Ileoje, N.P. 1987. A New Geography of Nigeria. Longman Nigeria Limited, Ikeja, pp. 201.

Jackson, S.E., Longerich, H.P., Dunning, G.R and Fryer, B.J. 1992. The application of Laser- ablation micro- probe-inductively coupled plasma-mass spectrometry (LAM-ICP-MS) to in situ trace element determination in minerals. Canadian Mineralogist 30, 1049-1064.

Kamunda, C., Mathuthu, M. and Madhuku, M. 2016. Health risk assessment of heavy metals in soils from Witwatersrand gold mining basin, South Africa. Int. J. Environ. Res. Public Health, 13: 663.

Kumar, V., Sharma A., Minakshi, S. 2018. Temporal distribution, source apportionment, and pollution assessment of metals in the sediments of Beas river, India. Hum Ecol Risk Assess 5: 1–20. Doi.org/10.1080 /10807039.2018.144052

Loska, K., Wiechula, D. and Korus, I. 2004. Metal contamination of farming soils affected by industry. Environment International, 30:159 -165.

Muller, G. 1969. Index of geo-accumulation in the sediments of the Rhine River. Geojournal, 2: 108-118.

Nwaogu, L.A., Ujowundu, C.O., Iheme, C.I., Ezejiofor, T.N. and Belonwu, D.C. 2014. Effect of sublethal concentration of heavy metal contamination on soil physicochemical properties, catalase and dehydrogenase activities. International Journal of Biochemistry Research & Review, 4(2): 141-149.

Norman, M. D., Pearson, N. J., Sharma, A. and Griffin, W. L. 1996. Quantitative analysis of trace elements in geological materials by laser by ablation ICPMS: instrumental operating conditions and calibration values of NIST glasses. Geostandards Newsletter, 20: 247-261.

Norman, M.D. 1998. Melting and metasomatism in the continental lithosphere: laser ablation ICPMS analyses of minerals in spinel, herzolites from eastern Australia. Contributions to Mineralogy and Petrology, 130: 240-255.

Oladunjoye, M.A., Sanuade, O.A., and Olaojo, A..A. 2013. "Variability of Soil Thermal Properties of a seasonally cultivated Agricultural Teaching and Research Farm, University of Ibadan, South-western Nigeria," Global Journal of Science Frontier Research Agriculture and Veterinary, vol. 13, no. 8, 40-64

Rahaman, M.A. 1976. Review of the basement geology of southwestern Nigeria, In: Kogbe, C.A. (ed.) Geology of Nigeria. Elizabethan Publishing Company, Lagos, pp. 5-41.

Rahaman, M.A. 1988. Recent advances in the study of the basement complex of Nigeria. In: Geological Survey of Nigeria (ed) Precambrian Geol., Nigeria, pp. 11-43.

Shaapera, U., Nnamonu, L.A. and Eneji, I.S. 2013. Assessment of heavy metals in *Rana esculenta* organs from River Guma, Benue State Nigeria. American Journal of Analytical Chemistry, 4(9): 496-500.

Steffan, J.J., Brevik, E.C., Burgess, L.C. and Cerda, A. 2017. The effect of soil on human health: an overview. European Journal of Soil Science, 159-171.

Sultana, M.S., Rana, S., Yamazaki, S., Aono, T. and Yoshida, S. 2019. Health risk assessment for carcinogenic and non-carcinogenic heavy metal exposures from vegetables and fruits of Bangladesh. Cogent. Environ. Sci., 543-552.

Taylor, S.R. and Mclennan, S.M. 1985. The Continental Crust: Its Composition and Evolution. Blackwell, Oxford, pp.312.

Taylor, S.R. and Mclennan, S.M. 1995. The geochemical evolution of the continental crust. Reviews of Geooysics, 33(2): 241-265.

Tepanosyan, G., Maghakyan, N., Sahakyan, L. and Saghatelyan, A. 2017. Heavy metals pollution levels and children health risk assessment of Yerevan kindergartens soils. Ecotoxicol. Environ. Saf., 142: 257-265.

Tijani, M.N., Jinno, K. and Hiroshiro, Y. 2004. Environmental impact of heavy metal distribution in water and sediments of Ogunpa

River, Ibadan area, southwestern Nigeria. J. Mining Geol., 40(1): 73-83.

USEPA 2012. Integrated Risk Information System of the US Environmental Protection Agency, Office of Emergency and Remedial Response: Washington, DC, USA,

Wei, B. and Yang L. 2010. A review of heavy metal contaminations in urban soils, urban road dusts and agricultural soils from China. Microchemical Journal, 94(2): 99-107.

Wongsasuluk, P., Chotpantarat, S., Siriwong, W. and Robson, M. 2014. Heavy metal contamination and human health risk assessment in drinking water from shallow groundwater wells in an agricultural area in Ubon Ratchathani province, Thailand. Environ. Geochem. Health, 36: 169-182.

Yongming, H., Peixuan, D., Junji, C., & Posmentier, E. 2006. Multivariate analysis of heavy metal contamination in urban dusts of Xi'an, Central China. Science of the Total Environment, 355(1–3), 176–186.

Nature Environment and Pollution Technology
An International Quarterly Scientific Journal

p-ISSN: 0972-6268
(Print copies up to 2016)
e-ISSN: 2395-3454

Vol. 20 | No. 2 | pp. 843-849 | 2021

Original Research Paper

https://doi.org/10.46488/NEPT.2021.v20i02.047

Open Access Journal

Evaluation of Urban Architecture Design and Construction on Environmental Pollution under the Visual Threshold of Green Development

Xin Fu and Shisheng Lyu†
College of Art and Design, Wuhan Textile University, Wuhan 430070, China
†Corresponding author: Shisheng Lyu: lvgege007@163.com

Nat. Env. & Poll. Tech.
Website: www.neptjournal.com

Received: 27-02-2021
Revised: 13-04-2021
Accepted: 25-04-2021

Key Words:
Green development
Urban building construction
Architectural design
Environmental protection
Evaluation model

ABSTRACT

The obvious manifestation of urban development is the integrated development of urban architectural design and construction. The environmental protection of green building design and construction has become an important link that cannot be ignored in the process of urban green development. Green building materials, green design, and other environmentally friendly building programs are the subjective manifestations of the implementation of the green development concept. However, the degree of environmental protection is still a black box that needs to be explored urgently. To explore the environmental pollution caused by urban architectural design and construction in the process of urban development, an evaluation model of urban architectural design and construction on environmental pollution was constructed. The first-level evaluation indicators include ecology, natural, and social environments, of which the corresponding secondary indicators mainly include noise, water, and air pollution and other 12 indicators. The weights of the evaluation indicators at all levels were calculated using the expert evaluation method, and the weighting method was then combined to evaluate the pollution. Results show that the main sources of environmental pollution caused by urban building design and construction are solid waste pollution and traffic congestion rather than traditional noise and air pollution. Noise and air pollution are effectively controlled in the construction process. The evaluation system provides further directions for improvement in the prevention and control of environmental pollution in building construction and provides a reference for effective improvement of environmental governance.

INTRODUCTION

Adhering to green development is a profound revolution in the outlook on development. Extraordinary measures must be taken in terms of transforming the economic development model, comprehensive management of environmental pollution, natural ecological protection and restoration, resource conservation and intensive utilization, and perfecting the ecological civilization system. Ecological environmental protection must also be performed in all directions, all regions, and the whole process (Liu 2020). The green development concept guides the construction of ecological civilization, promotes social progress, and improves the quality of urban life. The obvious manifestation of urban development is the replacement of urban planning and urban buildings. The construction of urban buildings caused by the building replacement process will inevitably cause "non-green" phenomena, such as the occupation of space, noise pollution, road closures, and inhalable particle pollution. Some studies have indicated that urban construction pollution has become a short-term key consideration factor for migrants in choosing a place to live. Solving the problem of environmental pollution caused by urban construction has become an effective way to stimulate population distribution in urban areas.

Urban construction is an urban planning activity that meets the needs of urban development, increases the occupancy rate of urban areas, and improves the appearance of cities. Urban development urgently needs the participation of urban construction (Teng 2020). The construction process requires a large amount of water supply to maintain the normal operation of the construction. At the same time, a large amount of wastewater and sewage is discharged, which causes a certain amount of water pollution to the surrounding environment.

In addition, modern building construction uses mechanical operations instead of traditional labour, which improves the efficiency of construction but causes serious mechanical noise pollution. As a result, it has a great impact on the daily life and health of surrounding residents. Building construction requires granular materials such as cement and sand. When the particle diameter is less than 10 μm, polluting inhalable particles will be formed in the air, posing a threat

to the health of residents. When a large number of inhalable particles accumulate, the increase in concentration will reduce the visibility of the air and cause serious pollution to the atmosphere.

Moreover, building construction is sometimes conducted at night and requires a considerable amount of lighting to maintain normal operations. The resulting light pollution affects the normal rest of the surrounding residents and reduces the quality of life and wellbeing of surrounding residents (Li et al. 2015). Furthermore, if the solid waste generated by the building (e.g., residues from the demolition of old buildings, the abandonment of excess materials during the construction process, and the muck produced by underground excavation during the construction process) is discarded without treatment, it will not only cause a waste of resources but also cause great pollution to the environment (Roberto et al. 2012).

Therefore, urban construction under the background of green development must not only ensure the normalization of its development but also minimize the environmental pollution that it causes. How to evaluate the environmental pollution caused by urban construction is conducive to controlling different sources of pollution during the construction process, taking targeted measures to effectively reduce construction pollution, realizing urban green construction, and promoting urban green development.

PAST WORK CARRIED OUT

With the continuous advancement of the green development process, the concept of green sustainability has penetrated all areas of social life. The most intuitive manifestation of the green development of urban construction is the application of green building materials and the implementation of green building design concepts (Wang et al. 2020). The core purpose of urban green buildings is to reduce environmental pollution caused by the construction process. Based on existing research, urban construction pollution is mainly reflected in water, air, noise, light, and solid waste pollution.

Water Pollution Caused by Urban Building Construction

Water pollution refers to the deterioration of the physical, chemical, and biological characteristics of the water body due to the discharge of pollutants. As a result, it will destroy the original ecosystem and water body functions, exceed the self-purification capacity of the waterbody and prevent the water from being effectively used (Cheng et al. 2021). It even endangers the health of animals and plants. Water pollution in the process of building construction mainly comes from rainwater and sewage (Sandeep et al. 2019).

Sewage is divided into domestic water for on-site staff and construction water. Rainwater and sewage diversion technology is used to realize the recycling of rainwater and sewage. The rainwater flows directly into the municipal rainwater pipeline through the drainage ditch. For the domestic sewage generated by the on-site construction personnel, in addition to the centralized treatment, the site toilet should be equipped with septic tanks or use mobile public toilets to reduce sewage discharge. The main sources of construction water are: (1) mechanical operation and cleaning; (2) sewage discharge from construction operations; (3) drainage and precipitation of foundation pits; and (4) sewage and wastewater generated by exposed building materials and toxic and harmful substances after being washed by rain (Lu et al. 2021).

For this type of construction water, after using the sedimentation tank to settle the debris, most of the wastewater can be recycled and used for sprinkling on construction sites to reduce dust. A small part of the more polluted sewage and wastewater is discharged into the municipal pipeline after being treated by the biological tank (Wang 2020). Construction sewage containing special substances, such as chemicals and oil materials containing toxic and hazardous substances, should be treated by an oil-water separator and discharged reasonably.

Air Pollution Caused by Urban Building Construction

Air pollution is general pollution caused by construction projects. Building dust and exhaust gas seriously affect urban air quality, such as urban smog, which seriously affects the human respiratory system and restricts urban development. At present, the control measures for air pollution mainly focus on preventive measures, supplemented by control measures (Huang et al. 2007).

Air pollution during construction is mainly dust and waste gas. Fugitive dust includes that generated during the transportation and loading and unloading of materials, the dust formed after mud accumulation and drying, and the large amount of fugitive dust generated during the demolition of the original buildings on the site. The exhaust gas mainly comes from the exhaust emissions of machinery and automobiles during the construction phase and the toxic and harmful gases released after the use of volatile materials (Haron et al. 2009). Moreover, during the implementation of construction projects, some paints and other materials used generally contain formaldehyde and other easily volatile harmful components, which cause the air to be polluted by harmful gases.

Noise Pollution Caused by Urban Building Construction

Construction noise refers to the environmental noise generated on construction sites, which is mainly generated by equipment operation, material processing, transportation, loading and unloading, earth and stone construction, piling, and structural construction (Zheng et al. 2015). The noise pollution caused by the construction of a large number of buildings considerably affects the people living nearby. Construction noise must be strictly managed and controlled from the three links of noise sources, noise transmission channels, and noise receivers.

Regarding noise sources, machinery should be upgraded, optimized, and maintained. Moreover, the noise interference caused by night construction should be minimized, noise-prone mechanical equipment should be kept away from the crowd as much as possible, and the construction schedule should be reasonably arranged to minimize noise pollution. The construction should also follow the relevant standards for noise control, following the *Environmental Noise Emission Standards at the Boundary of Construction Sites* formulated by the Ministry of Ecology and Environment. During the construction process of a building project, the specified range of noise caused by construction should be less than 70 dB during daytime construction and less than 55 dB during night construction.

Light Pollution and Waste Pollution Caused by Urban Building Construction

Light pollution is also a part of environmental pollution. To complete the construction schedule or part of the project needs to be completed at night; lighting must be used to ensure the smooth progress of the construction. This pollution will affect the quality of people's rest at night, and in severe cases will affect people's physical and mental health. In this regard, the control of light pollution is also in need of improvement in construction projects (Bagula et al. 2015.).

The solid waste generated at construction sites is mainly domestic waste and industrial solid waste, which refer to construction waste and waste residues, such as broken bricks, mortar, concrete, wood, and steel. At this stage, an increasing amount of construction waste is generated during construction. Related data show that construction waste accounts for 30%-40% of urban waste in our country, and construction waste is prone to secondary pollution, such as dust and wastewater during transportation (Frauke 2016). This phenomenon causes great harm to the ecological environment while endangering human health.

In the initial stage of construction, the relevant construction unit should strictly perform garbage classification management for domestic garbage and clean up in time to avoid secondary pollution caused by random disposal of garbage. For industrial solid waste, classification and reduction treatment should be implemented (Wang et al. 2018). The recycled materials should be recovered and processed in time. Some of the materials that cannot be recycled should enter the social recycling system to achieve sustainable development under the circular economy. The other part should be processed by physical methods (e.g., crushing and landfill after pressure storage) and chemical methods (e.g., high-temperature decomposition and oxidation) to reduce the accumulation of garbage.

MATERIALS AND METHODS

Evaluation Indicators

The pollution caused by urban construction causes considerable damage to the environment. To effectively control the adverse effect of construction on the environment, the multi-party pollution caused by urban construction must be rationalized, and targeted treatment must be performed to minimize the index of environmental pollution. While ensuring people's quality of life, it also allows the green and sustainable development of a country's construction industry.

Aiming at different aspects of environmental pollution, Wang et al. (2020) calculated the improvement effect of green energy-saving building construction on environmental pollution through the weighting index. Then, they constructed an analysis model and realized the improvement effect analysis of green energy-saving building construction. Cheng et al. (2021) proposed environmental protection in terms of policy factors, planning factors, technical applications by using the method of the green construction evaluation of prefabricated building based on the G1-entropy-independence weight method, and probability language close to entropy to analyze the weight of 21 pollution indicators. Finally, they provided scientific advice for the selection of the project plan.

Based on a large number of literature searches, the environmental pollution caused by urban construction involves water, air, solid waste, noise, and light pollution; urban landscape; and population health. Further classification of the pollution indicators can determine the environmental pollution, involving the ecological, natural, and social environments. This study summarizes and sorts out the evaluation indicators of the impact of urban construction on the environment, as shown in Fig. 1.

Evaluation Model

The entropy weight method is an objective weighting method to determine the index weight coefficient according to the

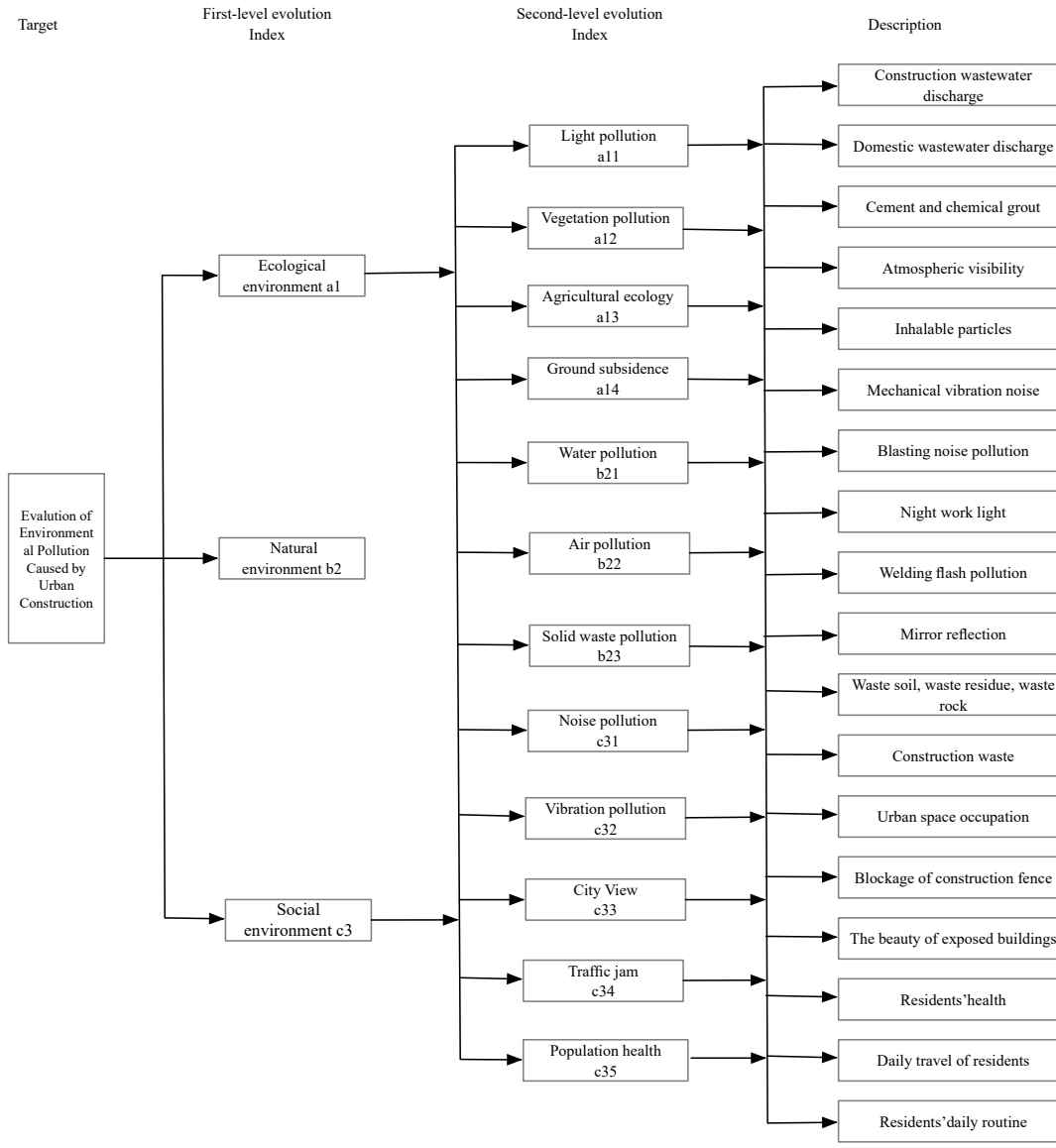

Fig. 1: Evaluation Index System for environmental pollution caused by urban construction.

amount of sample information contained in the evaluation index. Entropy is a measure of the disorder degree of index information. The smaller the entropy value of an index is, the greater the variation degree of its index value is, and the more information it can provide (Smart 2015). Therefore, the greater the role of this index in the comprehensive evaluation, the greater its weight value should be. The weight calculation steps of the entropy weight method are as follows:

1. The original data is standardized, and then the normalized standard matrix is constructed.

$$A = \left(a_{ij}\right)_{m\times n} = \begin{bmatrix} A_{11} & \cdots & A_{n1} \\ \vdots & A_{ij} & \vdots \\ A_{m1} & \cdots & A_{mn} \end{bmatrix} \quad \ldots(1)$$

2. According to the definition of entropy, the entropy value of the *j*-th index is calculated as follows:

$$Y_j = -k\sum_{i=1}^{m} p_{ij} \ln p_{ij} \quad \ldots(2)$$

Among them:

$$\begin{cases} k = (\ln m)^{-1} \\ p_{ij} = \dfrac{r_{ij}}{\sum_{i=1}^{m} r_{ij}} \end{cases} \quad \ldots (3)$$

By selecting the size of the constant k, the entropy value is always controlled within the interval of [0,1].

3. Calculate the difference of the jth index.

$$c_j = 1 - Y_j \quad \ldots(4)$$

Calculate the weight value of the jth index:

$$w_j^{'} = \frac{c_j}{\sum_{j=1}^{n} c_j}, \quad j = 1,2,\cdots,m \quad \ldots (5)$$

Among them, the difference coefficient A represents the importance of this index in the whole evaluation system. The greater the value of A is, the greater the importance of this index in the overall evaluation system, and the greater the weight value of the corresponding index B is.

RESULTS ANALYSIS AND DISCUSSION

Case Description

A residential project of Wanke in Wuhan of China covers an area of 59,917 m^2 and a building area of 386, 968.7 m^2, with a total of 12 buildings. The project has a large construction volume and a long construction period. The index system and evaluation model constructed in this study will be used to perform an environmental pollution assessment on this project.

Six qualified experts from the engineering construction environmental pollution control industry were invited to score the pollution of the project. To ensure the effectiveness and independence of the scoring, high industry requirements were observed for the qualification review of experts. Experts should have been engaged in the industry for a long time with rich field experience and have unique insights into management. Based on construction evaluation standards and environmental pollution, they would quantitatively evaluate the indicators constructed in Fig. 1 and score them on a five-point system. The evaluation results of the various indicators on environmental pollution are shown in Table 1.

Weight Analysis

Based on the evaluation results of environmental pollution by various indicators, the entropy weight method is used to process the entropy value and entropy weight of the standardized matrix. Formulas (4) and (5) are used to obtain the entropy weight of the environmental pollution indicators, as shown in Table 3.

The results of entropy weighting of the environmental pollution indicators for urban building design and construc-

Table 1: Evaluation results of primary indicators.

Index	Expert					
	Expert 1	Expert 2	Expert 3	Expert 4	Expert 5	Expert 6
Ecological environment a1	3	2.5	3.5	2	2.5	3
Natural environment b2	3	3.5	3.5	3	3.5	3.5
Social environment c3	3.5	4	3.5	4	4	4

Table 2: Evaluation results of secondary indicators.

Index	Expert					
	Expert 1	Expert 2	Expert 3	Expert 4	Expert 5	Expert 6
a11	3.5	3.5	4.5	2	2.5	3
a12	3	3.5	2.5	3	3.5	3.5
a13	3.5	3	2.5	3	3	3
a14	3	2.5	2.5	3.5	3	2.5
b21	3	3	2.5	3	2.5	3
b22	2	2.5	2.5	3	2.5	3
b23	2.5	1.5	2.5	3.5	3	3
c31	3	3	3.5	3	3	2.5
c32	3	3.5	3	2.5	2.5	3
c33	3.5	3	3	3	3.5	2.5
c34	3	3	3.5	3	3	2.5
c35	3	3	3	3.5	3	3

Table 3: Entropy weight of environmental pollution indicators.

Target layer	First-level index	Weight	Second-level index	Weight
Evaluation of Environmental Pollution Caused by Urban Construction	Ecological environment a1	0.222	a11	0.243
			a12	0.098
			a13	0.3 91
			a14	0.068
	Natural environment b2	0.172	b21	0.222
			b22	0.229
			b23	0.460
	Social environment c3	0.101	c31	0.089
			c32	0.203
			c33	0.371
			c34	0.426
			c35	0.127

tion show that the environmental pollution indicators of this Wanke residential project in Wuhan are ranked as solid waste pollution, traffic congestion, agricultural ecological pollution, urban landscape pollution, light pollution, air pollution, water pollution, and vibration, as well as pollution, population health, vegetation pollution, noise pollution, land subsidence. The result shows that the most significant environmental pollution caused by the design and construction of buildings in the city centre is solid waste pollution (0.460).

The above finding is due to the replacement of urban buildings requiring the re-planning and demolition of the building design. The demolition of old buildings is prone to generate a large amount of solid waste pollution. The treatment of solid waste pollution cannot be treated like a landfill in a large rural area. Solid waste will be transported after crushing, which leads to the accumulation of solid waste pollution.

Before the project starts, preparations for solid waste treatment should be made, and solid waste must be eliminated to the maximum extent. In the pollution in architectural design and construction, the widely criticized weight indicators of air, vibration, and noise pollution rank sixth, eighth, and eleventh, respectively. This result shows that in today's urban architectural design and construction, air, vibration, and noise pollution are all well prevented and controlled. Land subsidence causes the least pollution, with a weight of only 0.068. Thus, urban construction is the most serious problem for people's daily travel. Given the strict control of underground space in urban planning and design, the ground subsidence caused by construction has the smallest impact.

The results indicate that noise and air pollution have been effectively controlled during the construction of urban buildings. Urban construction is also responding to green development, and rational architectural design is a limited way to effectively reduce traditional pollution. The entropy method is used to evaluate the environmental pollution of urban buildings and constructions, which can be a positive test of the existing prevention and control work when it can effectively detect pollution indicators.

The weight of the primary indicator is obtained based on the data of the entropy weight of the secondary index. The data show that the pollution of the primary indicator of environmental pollution caused by urban building design and construction is the ecological environment pollution (0.222), which exceeds the other two indicators, followed by natural environmental pollution and finally social-environmental pollution. As the direct pollution object of urban architectural design and construction, ecological environmental pollution is relatively a concern. The reason is that with the development of the city, the green environment inside the city is destroyed, and the ecological pollution inside the city is aggravated[15]. The continuous expansion of the city has also caused great damage to the suburban environment around the city, and the external ecological pollution of the city has also increased. How to solve the problems of urban expansion and ecological environment protection has become an important issue that the government needs to consider. Second is the pollution of the natural environment. With the destruction of the ecological environment, the pollution of the natural environment also increases. The lower weight of the social environment indicates that social environmental damage caused by urban architectural design and construction is relatively small, and the project can improve pollution prevention and control for this matter.

Assessment of Environmental Pollution

The combination weight method to determine the emergency capability index score is similar to the entropy weight method. All indicators of the community project in Wanke are calculated by $W \times R = R_{line}$, and the final specific scores of each indicator are obtained from $R_{score} = R_{line} \times [100, 80, 60, 40, 20]^T$. The strongest, stronger, general, weaker, and weak environmental impact is 100-80, 80-60, 60-40, 40-20, and 20-0 points, respectively. The entropy weight of the environmental pollution indicators is combined. The specific scores of each indicator are [78.5, 52.1, 86.2, 43.2, 75.8, 76.2, 93.1, 48.6, 71.6, 83.7, 91.0, 68.5]. Further calculation of the project based on the indicator weight shows that the score of the environmental pollution impact assessment is 72.38 points, indicating that the project has a strong impact on environmental pollution. The evaluation results indicate that during the construction of the community project in Wanke, attention should be paid to the prevention, control, and monitoring of various pollution indicators to reduce environmental pollution and achieve green design and construction.

CONCLUSION

Aiming at the environmental pollution caused by urban construction, an environmental evaluation index system was constructed and the entropy method was used to evaluate t the urban environmental pollution caused by the construction of a residential project in Wanke in Wuhan of China. The conclusions are drawn as follows.

1. The evaluation of environmental pollution in urban architectural design and construction includes three aspects: ecological environment, natural environment and social environment.
2. Taking a residential project in Wanke as an example, the evaluation results show that the environmental pollution caused by the construction of the project is mainly reflected in solid waste pollution, and the treatment of solid waste can be controlled to a certain extent through effective recycling. Conclusions indicate the feasibility of using the entropy weight method to evaluate the environmental pollution of urban construction design and construction.

This study solves the main aspects of pollution caused by the construction of this residential area in Wuhan. It can also be compared to other areas to uncover the black box of environmental pollution caused by urban construction, which will help promote the green and harmonious development of society.

REFERENCES

Bagula, A., Castelli, L. and Zennaro, M. 2015. On the design of smart parking networks in the smart cities: An optimal sensor placement model. Sensors, 15(7): 168-173.

Cheng, H., Lu, Y. H. and Liu, S. F. 2021. Green construction evaluation of prefabricated building based on g1-entropy-independence weight method. Mathematical Practice and Theory, 4(51): 75-87.

Frauke, B. 2016. Why cycling matters for smart cities, internet of bicycles for intelligent transport. Journal of Transport Geography, 56(3): 125-136.

Haron, Z., Yahya, K. and Mohamad, M.I. 2009. Probability approach for prediction of construction site noise. Journal of Asian Architecture and Building Engineering, 8(2): 571-577.

Huang, Y.H., Tian, G., Qin, J.P., Li, G. and Yan, B.L. 2007. Research on the characteristics of dust pollution in different construction stages. Environmental Science, (12): 2885-2888.

Li, M., Wei, Y. W. and Wang, Y. Q. 2015. Analysis of solid waste treatment and reuse technology on construction site. Earth, 12(7): 296-296.

Liu, X. 2020. Application of building construction emission reduction technology in environmental pollution control. Technical Analysis. 4(12): 45-46.

Lu, L. and Liu, C. Y. 2021. Research on airport comprehensive evaluation model based on entropy weight method. Aviation Computing Technology, 51(1): 64-66.

Roberto, P. and Esther, R. 2012. Development of environmental quality indexes based on fuzzy logic. A case study. Ecological Indicators, 23(3): 32-41.

Sandeep, B. and Geetha, G. 2019. Advanced evaluation methodology for water quality assessment using artificial neural network approach. Water Resources Management, 33(9): 129-141.

Smart, C. 2015. A conjuncture of four forces. Cities, 47(8): 95-106.

Teng, F.X. 2020. Research on green construction management of engineering buildings. Green Environmental Protection Building Materials, 7(26): 56-58.

Wang, Y., Wei, J.S., Li, X.T., Bai, Y. and Wen, X.C.Wang, Z. M. 2020. Application of ecological environment protection concept in residential building design. Low Carbon World, 209(11): 107-108.

Wang, W. and Sun, X. B. 2020. Analysis and research on the improvement effect of green energy-saving building construction on environmental pollution. Environmental Science and Management, 5(45): 164-168.

Zheng, R., Yao, C. W., Jin, H., Zhu, L., Zhang, Q. and Deng, W. 2015. Parallel key frame extraction for surveillance video service in a smart city. PloS One, 10(8): 13-18.

Nature Environment and Pollution Technology
An International Quarterly Scientific Journal

p-ISSN: 0972-6268
(Print copies up to 2016)
e-ISSN: 2395-3454

Vol. 20 | No. 2 | pp. 851-863 | 2021

Original Research Paper

https://doi.org/10.46488/NEPT.2021.v20i02.048

Open Access Journal

Unsegregated Municipal Solid Waste in India - Current Scenario, Challenges and Way Forward

Prashant Shukla*†, Pankaj Kumar Sharma*, Shyam Pandey* and V. Chintala**

*Department of Mechanical Engineering, University of Petroleum & Energy Studies, Dehradun, Uttarakhand, India

**School of Engineering and Applied Sciences, National Railway Transportation Institute (Deemed to be University), Vadodara, Gujrat, India

†Corresponding author: Prashant Shukla; prashantshukla1617@gmail.com

Nat. Env. & Poll. Tech.
Website: www.neptjournal.com

Received: 09-06-2020
Revised: 17-07-2020
Accepted: 27-08-2020

Key Words:
Source segregation
Mixed municipal solid waste
Biodegradable waste
Non-biodegradable waste
Recyclable waste

ABSTRACT

Solid waste management (SWM) is one of the most neglected aspects and becoming a challenge for India as well as other developing nations' environment. India is one of the world's large and fastest-growing economy. Based on the trends in different nations like the US, China and European countries, it is clear that a developing economy of the nation and population of the country is also playing a vital role in the increasing rate of solid waste generation. Unsegregated waste is the root cause of the inefficient municipal solid waste management (MSWM) systems in India. The existing approach to managing the MSW such as collection, transportation and treatment results in poor utilization of resources. This review paper addresses the current status of MSWM in India. In this paper, various issues and challenges to obtain 100 % source segregated municipal solid waste are also discussed through different cases of urban areas. A way forward through an overview of the municipal waste management policies and practices adopted is being presented in the paper.

INTRODUCTION

Unsegregated municipal solid waste has become a challenging issue not only for India, but even for other developing countries. MSWM (municipal solid waste management) system suffers various problems related to the waste treatment options, i.e. composting or recycling or energy generation (Annepu 2012, Rajkumar & Sirajuddin 2016). If the existing MSWM system does not offer the solution to these problems, the entire municipal mixed waste will be ended up at dumpsites and therefore causing the MSWM system to be dependent upon landfill sites. A huge amount of dumped MSW (municipal solid waste) is becoming the main reason for groundwater pollution, soil contamination, and environmental pollution. The MSW typically includes domestic and commercial wastes generated in municipalities or notified areas either in solid or semi-solid form (Table 1). It does not include industrial hazardous wastes but includes treated bio-medical wastes. According to data (Table 2), Metro cities are the major contributor in the process of waste generation and due to continuous infrastructure development the production of inert waste is also higher than other regions. Southern region produces larger quantity of compostable waste due to relying on coconut and banana leaves for wide range of applications (Karelia 2019, Priya 2019). Fig. 1 reveals that about 80% of the total generated waste is being collected by various means while the rest 20% is again mixed up and lost in the urban environment (Ministry of Housing and Urban Affairs 2019). Out of total waste generated, about 50% waste is found segregated at the source which is suitable to process further. Hence, out of total generated waste, around 40% of waste is being processed in the existing MSWM system and the rest of the unsegregated waste is being dumped into landfill sites. Most of the time sorting of waste is done by unorganized sector and from time to time rehearsed by waste producers. Segregation and sorting process takes place in exceptionally dangerous and unsafe conditions and the viability of segregation is sensibly low as unorganized sector segregates just important disposed of constituents from the waste stream which can promise them similarly higher monetary return in the reusing market.

Due to lack of space for inventory many waste processing industries are utilizing the waste from the dumpsite and essentially handle mixed waste which usually gets contaminated. It does not only increase the cost of waste processing but also produces poor quality products such as recyclable contents, compost etc. (Pandey & Malik 2015, Rawat et al. 2013).

In India, recent solid waste management guidelines 2016 (Lavasa et al. 2016) have made it compulsory to the concerned authority of an area to undertake responsibility

Table 1: Contents of waste materials in MSW (Sujauddin 2008).

MSW Components	Materials
Compostable	Food waste, landscape, and tree trimmings
Recyclable	Papers, cardboard, plastics, glass, metals
Inert	Stones and slit, bones and other inorganic materials

for all activities related to SWM (Solid Waste Management). These guidelines are applicable beyond the municipal areas also, such as urban cluster, census towns, notified industrial townships, areas under the mastery of Indian railroad tracks, airports, airbase and seaport, defence establishments, special economic zones, state and central government organizations, places of the pilgrimage, religious and historical importance etc. Despite all the positive moves put up by the Government of India, the current status of the Indian MSWM system is not satisfactory.

Existing Solid Waste Management Strategies

As per the SWM guidelines 2016 (Lavasa et al. 2016) waste generator has to identify the category of waste and keep it separately i.e. source segregation. This is the key function at the root level of MSWM process, which redirects the right type of waste to its right place. Therefore to get 100 % source segregated waste, Govt. has started various awareness programs through social media, television, newspaper etc. Few megacities like Bengaluru, Indore and many others have implemented a fine system for observing no source segregation of solid waste (Akshatha 2018). Once the MSWM system receives all the 3 categories of segregated waste, it is processed for its treatment and the only inert is dumped into landfill sites. Common treatment techniques are recycling of plastics, composting and waste to energy.

Fig. 1: MSWM practices in Indian cities.

The combination of waste treatment methods with MSWM makes an IMSWM (integrated municipal solid waste management) system (Fig. 2). It is being followed by most of the developed countries because its advantageous principle maintains the correct flow of segregated waste and does not allow it to be on the dumpsite (Planning Commission 2014).

Even if there is no source segregation a sustainable waste management system is supposed to handle the mixed waste. Therefore many countries have already moved a step ahead by introducing advanced waste to energy plants such as plasma arc recycling. It involves heating waste to super-high temperatures to produce gas that can be burned for energy and rocky solid waste that can be used for building (Woodford 2019). This process does not involve combustion like a conventional incineration process. Instead of only burning the waste (at a few hundred degrees), the waste is heated at higher temperatures (thousands of degrees) so it gets melt and then vaporizes. This process is performed by the plasma arc method, which is a kind of super-hot "torch" made by passing gas through an electrical spark.

Current Scenario of Unsegregated Waste and Failures in MSWM System in India

With an increasing population, MSW management in the country has come into view like a serious problem not only due to environmental and esthetic issues but also due to the sheer quantities produced every day.

Table 2: Composition of MSW in India and its regional variation (Annepu 2012).

Region/city	MSW (TPD)	Compositions of MSW			
		Compostable (%)	Recyclables(%)	Inert(%)	Moisture (%)
Metros	51402	50.89	16.28	32.82	46
Other cities	2723	51.91	19.23	28.86	49
East India	380	50.41	21.44	28.15	46
North India	6835	52.38	16.78	30.85	49
South India	2343	53.41	17.02	29.57	51
West India	380	50.41	21.44	28.15	46
Overall Urban India	130000	51.3	17.48	31.21	47

Hence the government of India is driving various awareness campaigns with the help of NGOs and some agencies like Shuddhi, Vatvaran, Ruchi, etc. for the efficient performance of the MSWM system. These campaigns are promoting various positive activities like zero or minimum waste generation, segregation of waste at source, lesser use of the non-recyclable and non-degradable substances through social media, print media and TV channels, etc. These efforts have shown remarkable improvements in a few cities like Indore, Ambikapur, Mysuru and Tirunelveli. In these cities, residents have started showing their interest towards source segregation, because either local urban body fines for non-segregation of waste at source or on the positive side new startups of recycling and composting (such as Saahas

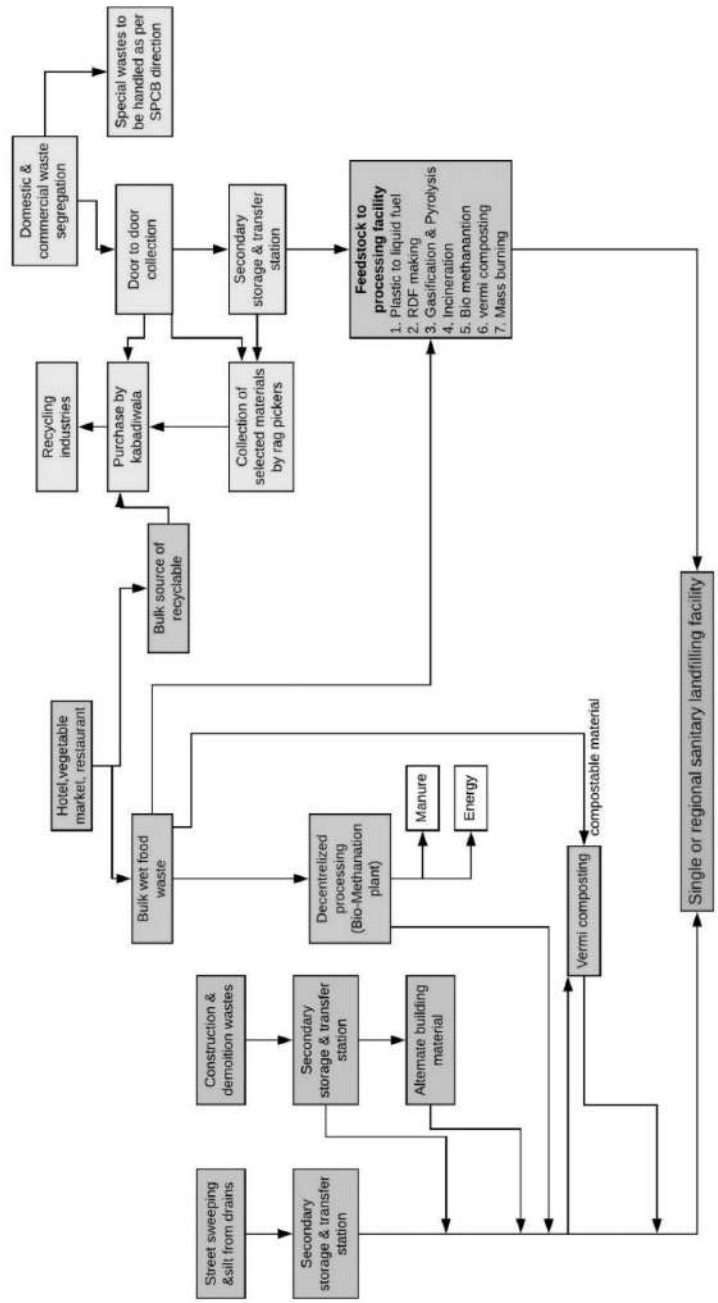

Fig. 2: Integrated MSW Management.

Fig. 3: Trucks dumping garbage at Ghazipur Landfill site in New Delhi, India

Zero Waste, Hasiru Dala, Namo E-waste, GEM Enviro Management, Citizengage, Paperman, Vital Waste, Extra Carbon, etc.) are rewarding for segregating the recyclable and non-recyclable waste at a source point and depositing the garbage at a predefined location. These ideas are helping to minimize the open dumping of MSW (Dash 2017, Manohar 2019, Rai 2017, Subramanian 2017).

Despite all these positive moves and promotions, the major portion of India is still facing many problems related to solid waste such as lack of land space for dumping MSW, spilt out waste on roads, poor quality of compost due to the presence of plastic and metals. Segregation at source, collection, transportation, processing and scientific disposal of waste is not sufficient and leading to the degradation of the environment and poor quality of life. Some key issues are affecting proper management of MSW such as limited primary collection at the doorstep, reluctance in public to take ownership, unavailability of adequate funds, lack of access to technical exposer and unscientific disposal of MSW at dumpsites (CPCB 2018, Lahiry 2017, Lavasa et al. 2016, Press Trust of India Ltd. 2019).

Ghazipur landfill can be a relatable example of such a scenario (France-Presse & Agence 2019), this site has already taken about 40 football pitches of land on the eastern edge of New Delhi (Fig. 3), which is widely recognized to be the world's most polluted capital. The vast dump of waste rises by 10m every year. It is already 65m high and will be taller than the 73m Taj Mahal next year.

Fig. 4 represents the current practice of MSWM in India (Ministry of Housing and Urban Affairs, 2019), where around 82% of waste is collected by the door to door pick up or by community bin, and around 48% of waste is found in segregated manner i.e. source segregated. Therefore only 37% of waste can be processed for further treatment like composting, WTE or recycling. The remaining amount of un-segregated waste is directly dumped into landfill areas.

Failure of Solid Waste Management Projects in India

In Shrinagar, India, J&K Municipal Corporation (SMC) has failed to segregate waste at source in the summer capital (Yaqoob 2018). It has also not received individual garbage dustbins at sources as Solid Waste Management Rules

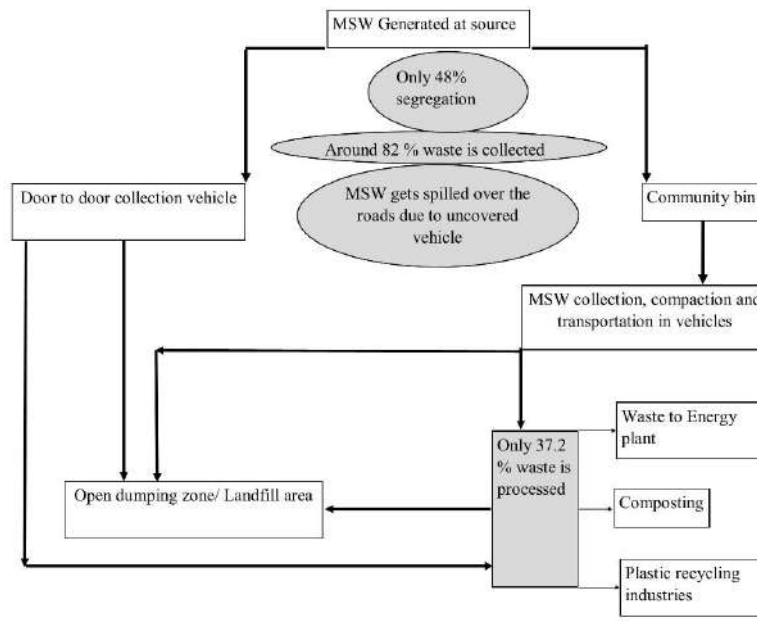

Fig. 4: Process flow of MSWM n India.

(SWMR) are yet to be enforced. The SMC began waste separation as a pilot project last year in many districts, such as Sanat Nagar. After segregating garbage collected from households, the SMC used to again mix the waste. Therefore, the segregation at the source served no purpose.

The aspiring source segregation program organized by the civic bodies in Delhi (Vibha et al. 2017) has failed to achieve desired results. After the 4 months of this initiative, very few changes in the situation have been observed on the ground. Residents complained that in the absence of adequate supervision and control by authorities, the initiative was running out of steam. The north and east Delhi civic bodies had started the source segregation program at 10 selected neighbourhoods on the occasion of World Environment Day. The motive behind this project was to motivate the people to sort out their domestic trash. The initiative was designed to set up model colonies to demonstrate the introduction of the 2016 Centre's Solid Waste Management Rules. The agencies were expected to disseminate bins, run awareness drives, and engage vehicles with partitioned cabins for collecting bio-degradable and non-biodegradable waste.

However, after four months, residents in the areas continued to dump waste without segregating them. Similarly, after the launch of the source segregation campaign in the north and east Delhi (Vibha et al. 2017) local urban bodies have also been unable to acquire enough vehicles for disposing of source segregated waste. The project initiated with a series of introductory workshops educating the public about the value of source segregation of waste. However, after two interactions, the north municipal officials became unreachable. Vehicles assigned to collect dry and wet waste disappeared too. It was also observed that the sanitation workers coming to collect garbage rarely help the residents in emptying the contents of the garbage bins into the vehicles (tippers). It is also reported that the height of the tipper is too much for any individual man or women to reach. A major proportion of the garbage litters on the road, while one try emptying the contents on to the tippers. Once it is dumped into the tippers, the dry and wet waste gets mixed, then there is no meaning of segregating waste at the source.

In Bengaluru (Harshtha & Nisar 2019), door-to-door garbage pickup from small apartments and unorganized residential areas across the city has been tangled. Reason: collectors come for a very small time, while residents have no systematic plan to keep the solid waste segregated and ready to be picked up. Many residents complained that their entire effort towards segregation and collection turns nothing when the garbage collection system does not meet the schedules. Even though residents keep the waste segregated, the garbage collectors dump them altogether. This results in a lack of interest among residents to segregate. The BAF (Bengaluru apartment federation) provides a solution that fits well over thousands of flats: segregate the garbage, place them at a central point from where the sanitation workers pick it at the time of their choice. In the same city, a new and innovative step has been taken to tackle the MSW. A not for a profit think tank in Bangalore named PAC (Public Affairs Center) (Nagendra et al. 2019), launched a mobile app "PAC Waste Tracker" which works on citizen science and visual mapping to find out the various issues affecting the waste collection mechanism in the city. This pilot project implemented in the four wards, which has recorded the issues coming at each collection point. Such challenges have been reported for a total of 9 months including non-segregation of waste, inconsistent waste collection, collection annoyance and non-compliance.

Agra, classified as one of India's most polluted cities (Lavania 2018), transports tons of waste in open lorries daily on city roads to the Kuberpur sites. As the trucks ply, loads of garbage spill over the sides. Some of these even get dropped on commuters and cars alike. These trucks have only added to Agra's pollution levels. the civic authority has not been able to ensure modern vehicles for the storage and disposal of the Civic Solides (MSW) even after strict directions have been given by the NGT (National Green Tribunal) to Agra Municipal Corporation. According to officials, the civic body trucks collect around 500 metric tonnes of garbage from various parts of the city every day and transfer it to the Kuberpur site. According to norms, these vehicles must be covered both from the rear and topsides. But around 40% of these vehicles run without covers. The back of many of these trucks is damaged, causing more spillage.

Similar issues have been identified in two major cities of Uttarakhand, i.e. Dehradun and Haridwar (Sharma 2018), where uncovered vehicles were used for transporting waste. Out of the total available vehicles, only 58% and 64% of vehicles were operational in Dehradun and Haridwar, respectively. Further, only 7% and 46% of vehicles were covered in Dehradun and Haridwar. Authors reported that inefficient transportation has become another reason for floating garbage in Kolkata city (Hazra & Goel 2009). Poor route planning, lack of information about collection schedules, poor roads and numbers of vehicles for waste collection drastically affects the process of MSWM.

Quantitative Analysis of Performance of Indian MSWM Systems

As per the latest report of the CPCB (Central Pollution Control Board), published in February 2018, the total quantity of waste generated in the country is estimated at

around 43298.385 tons per day. Out of which, 45082.15 tons is being collected and the remaining 18% is littered. Out of the total collected waste, only 15386.81 ton is being treated and remaining 22904.70 tons is being disposed of (Sambyal & Agarwal 2018). A standard MSWM system has two basic functions i.e. collection and segregation. The following data highlights the current scenario of collection & segregation under the Indian MSWM system.

In India, every state has around 84000 wards and 3/4th of these wards have successfully adopted door to door waste collection system. But without a proper waste disposal system, such an effort is not meaningful (Jadhav 2018). Municipal bodies in Maharashtra generate maximum garbage, i.e. 22,570 MT daily, then Tamil Nadu (15,437 MT), Uttar Pradesh (15,288 MT), Delhi (10,500 MT), Gujarat (10,145 MT) and Karnataka (10,000 MT) (Jadhav 2018). These data reflect that the municipal bodies of the above-mentioned states are dumping such a big amount of waste on to their landfill sites, which are actually beyond their capacity to handle, hence it is polluting the surrounding land, groundwater and air. According to the Delhi-based Centre for Science and Environment (CSE), cities are now lacking for land space where they can dump their waste. This scenario is leading them to throw it in the 'backyards' of smaller towns, suburbs, and villages.

It is found that only 8 out of 35 states have the practice of processing more than half the daily garbage generated in their cities, hence not one has achieved 100% processing (Jadhav 2018). Jharkhand, Bihar, Odisha, Andhra Pradesh, Tamil Nadu, Haryana, West Bengal, Jammu & Kashmir do not process even 10% of their MSW, while Arunachal Pradesh and Dadra & Nagar Haveli do not have the practice of processing their waste (Jadhav 2018). There are only four states that process more than 60% of municipal waste. In this list, Chhattisgarh comes first, where almost 74% of waste is processed. Then this legacy is followed by Telangana (67%), Sikkim (66%) and Goa (62%). Delhi processes 55% of its daily garbage (Jadhav 2018).

Fig. 5 (The World Bank 2018) shows the comparative data between MSW collection and its treatment in major Indian cities. According to these data, the Indian MSWM system is collecting a major proportion of waste (i.e. around 82%) from door to door collection service, then half of the collected waste is being treated because the collected waste is not completely segregated at source. Among all the major cities in India, Hyderabad, Kochi, Pimpri, Kanpur, Ahmedabad, Coimbatore and Mumbai can treat their entire collected waste. It has become possible, these cities have started maintaining all the possible ways of treatment of waste. Such as in Kanpur, there is a plant to process 1500 tonnes per day capacity of solid waste was set up with a tipping platform, a pre-segregation unit, a composting unit, an RDF (Refuse Derived Fuel) unit, a plastic segregating unit, a briquette manufacturing unit, and a secured landfill in place (Goel 2017).

Similarly in Hyderabad, The GHMC (Greater Hyderabad Municipal Corporation) has done some good work in the solid management system, i.e., segregation of dry and wet waste at the source itself by involving residential welfare associations, NGOs, self-help groups and citizens. Through this, the collection of garbage has increased from 3,000 tonnes to 4,800 tonnes daily basis. Whereas Rudrapur, Cuttack, Kota, Amritsar, Leh, Vishakhapatnam, Bhubaneshwar are failed to treat their waste. Table 3 shows the MSWM and related facilities available in major Indian states. Among all the mentioned states Tamil Nadu has a higher number of waste treatment facilities whereas Orissa and Uttarakhand do not have any facility to treat their solid waste. All these data reflect that only 36% of states in India are having treatment plant, and due to the unavailability of the desired form of waste (segregated waste) some of them like in Maharashtra, Delhi, Gujrat, Tamil Nadu are not able to perform at its maximum capacity. Hence, the mixed waste is being dumped in open land areas and getting stockpiled (Kumar et al. 2017, Ministry of New and Renewable Energy 2016).

Problems Associated with Unsegregated Waste

As is discussed in the previous section that the unsegregated waste is not easily acceptable by the waste processing industry therefore it gets dumped into the landfill sites. Subsequently, this practice is promoting the improvement of new sanitary landfills or extension of an existing landfill in different urban areas in India (Moghadam et al. 2009). Landfill practice caused many accidents in history (Doshi 2016, Manohar 2017, TNN 2018) like landfill fire in Delhi and West Bengal, landfill sliding in Addis Ababa (Ethiopia) & Shenzhen (China), etc. Hence, when mixed waste is ended to landfill sites it brings out many other issues such as landfill fires (Lee et al. 2018), landfill sliding (Pulat et al. 2017), environmental impact due to food waste (Tonini et al. 2018).

Apart from environmental issues, mixed waste has become the main cause of the poor performance of waste processing industries like WTE, composting or plastic recycling industries. Many WTE plants in the country are either combustion-based or gasification based. Combustion based plant requires a dry form of waste and wet for gasifier based plants. But due to the unavailability of the required form of segregated waste, most of the WTE plants are in the "Not Working" condition (Sharholy et al. 2008).

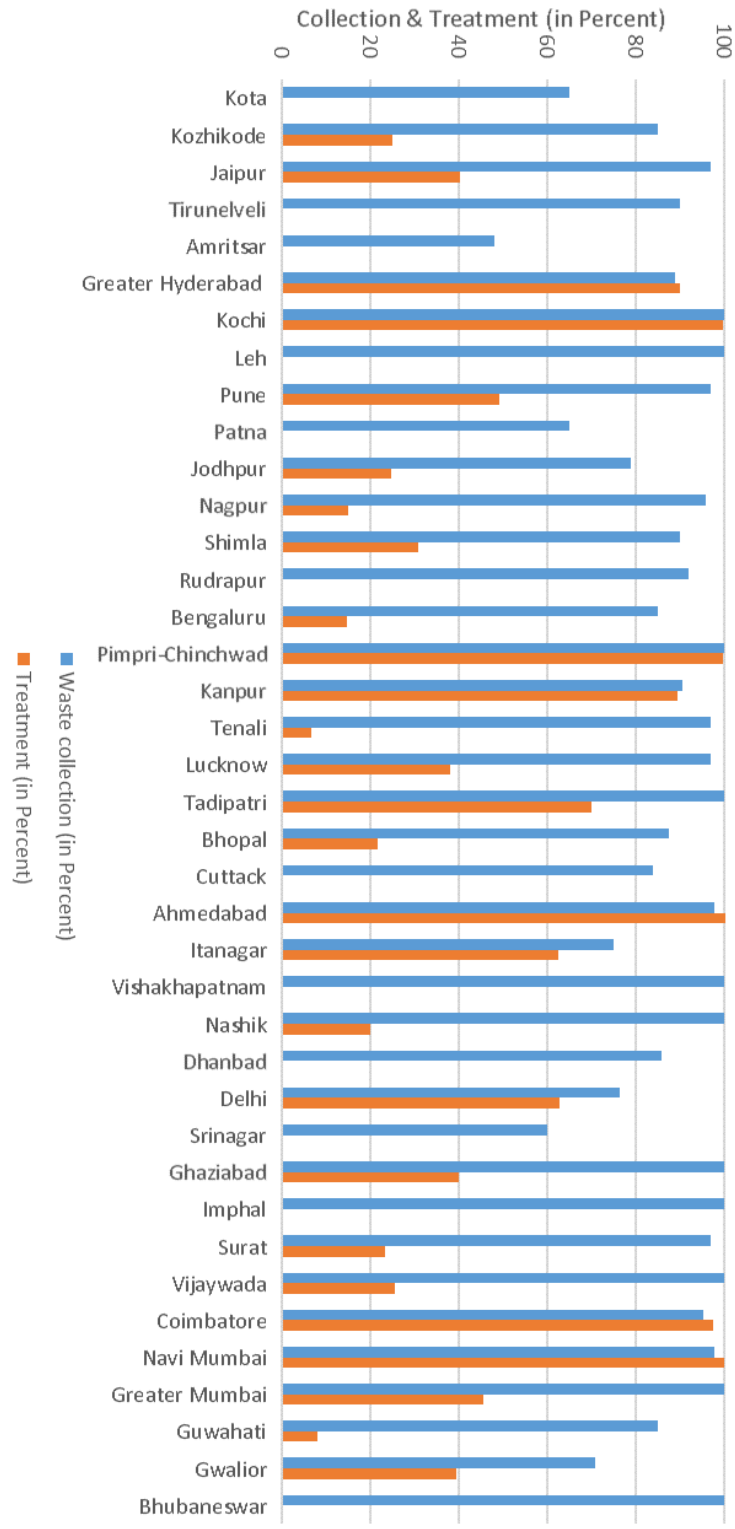

Fig. 5: Collection Vs. Treatment in major Indian cities.

Table 3: Facilities for MSWM in major Indian states (Ministry of New and Renewable Energy, 2016).

S. No.	States	No. of Units for treatment				
		Composting	Vermicomposting	Biomethenation	Pelletization	Waste to Energy
1	Andhra Pradesh & Telangana	24	0	0	11	2
2	Andaman& Nicobar	1	0	0	0	0
3	Chandigarh	0	0	0	1	0
4	Delhi	3	0	0	0	3
5	Goa	14	0	0	0	0
6	Gujrat	3	93	0	6	0
7	Himachal Pradesh	10	0	0	0	0
8	Karnataka	0	0	0	0	0
9	Kerala	21	7	10	1	1
10	Madhya Pradesh	7	0	0	2	0
11	Maharashtra	6	2	5	5	2
12	Orissa	1	0	0	0	0
13	Punjab	1	3	0	0	0
14	Rajasthan	0	0	0	0	0
15	Tamilnadu	102	24	0	3	0
16	Uttarakhand	0	0	0	0	0
17	Uttar Pradesh	0	0	0	0	0
18	West Bengal	13	7	0	0	0

Similarly, the majority of MSW compost produced in Delhi is not able to meet quality control guidelines of fertilizer control order standard (Mandal et al. 2014). Fertilizing index values of MSW compost was satisfactory, whereas clean index values were much below the desired value due to the presence of plastics & excess heavy metals in the compost which may come through many sources like electronic and electrical waste. The chances of availability of plastic and heavy metals in compost are increased when mixed waste/partially segregated waste is processed in the compost plants. Even if there is a practice of source separation, bio-degradable waste still contains some contaminants which may affect the treatment process and impact the quality of the compost (Jank et al. 2015). Contaminants can be present in the separated bio-degradable waste, it is because segregation of bio-waste is not always done in a correct way, such as the collection of segregated waste in plastic bags causes contamination of biowaste. Such products cannot be sold in the market at a competitive price hence affect the financial viability of the project. Whereas mixed waste causes wear and tear in the waste handling equipment and when it is combusted it becomes a source of emission of toxic pollutants (Rawat et al. 2013, Malcolm Richard et al. 2011, Mandal et al. 2014). It is also observed that in India, sorting of waste is done by rag pickers, who manually pick up waste from the roads and dumping zones which can be recycled and re-used. Hence, they are exposed to health damage and infection while manually sorting the waste without any protection. Furthermore, it has to be segregated either manually or mechanically in addition to the manual segregation. It is a time-consuming process to segregate the useful waste out of total random mixed waste. Apart from rag pickers, the segregation of waste is largely fulfilled by the unorganized sector and infrequently practised by waste producers (Pandey & Malik 2015).

It is also reported that (Hindu 2012) the plastic waste on either on dumpsite or streets, roads and community bin chokes the stormwater drainage system. As per the report, the dumping of garbage in water bodies has been increasing the decay of lakes and ponds in the southern suburbs of Chennai. Because residents are releasing sewage and dumping plastic and other waste in channels linking water bodies and stormwater drains. Therefore every single stormwater drain and channel in the city, which connects one lake with the other has been nearly ruined. People find it easiest approach to throw waste outside their homes through windows directly into these drains and water channels. A huge amount of floating garbage is observed in such drains all over the southern suburbs of Chennai.

Hence, proper segregation of waste leads to scientific disposal of waste and on the other hand recyclables could be directly sent to recycling units (Sharholy et al. 2008,

Shwetmala et al. 2011). It can lead to various benefits such as enabling technology up-gradation, better quality products, saving of valuable raw material resources of the country, reducing the need for landfill space. Therefore various methods have been intervented into the MSWM system to get segregated waste and its further treatment.

Significant Challenges for the Process of Source Segregation

In many developing countries including India, residents response towards the segregation of waste is affected by the partial involvement of residential community, real estate developers, other residents, and charges involved in MSWM (Agbefe et al. 2019, Speier et al. 2019, Basnayake et al. 2019). It is reported (Planning Commission 2014, Rawat et al. 2013) that the waste that is generated in the country is a mixed waste comprising a large amount of inert material and a very high moisture level unlike in other countries. A high level of moisture and inertness in the waste creates problems to derive power from it. The Govt. of India took the initiative to increase awareness amongst the public through SBM (Swachh Bharat Mission) (Agarwal 2018), and the all India segregation campaign was launched on June 5, 2017. The main objective of this campaign is to ensure, cities must design a mechanism through which 100 per cent source segregation can be done within one year, which is a challenge and yet has been a game-changer wherever implemented properly. According to the CPCB report, 2018 there is no proper public system of primary collection from the source of waste generation and municipal sanitation workers collect waste primarily through street sweeping, etc. Also, there is no practice of sorting waste at source in a scientific way except few places like Indore, Tirunelveli, Goa, Chandigarh, where source segregation is under regular practice (CPCB 2018). As per SBM August 2018 data (Agarwal 2018), 43% of the total wards in the country are segregating their waste at source. In 2017, door-to-door collection coverage increased from 53% to 80%.

As per the SWM rules 2016, waste must be segregated into different disposal bins with different colour codes for biodegradable. However, most of the source location like slum areas, which belongs to lower socio-economic condition, does not have enough space to occupy different disposal bins. Hence, the waste collected at the source point is in the mixed form and it moves from source to primary location, primary to secondary location then landfill sites as it is (Padilla & Trujillo 2017). Therefore, the author has concluded through a survey that source segregation is affected by SEC (socio-economic conditions). As per the survey higher SEC gives a higher rate of source segregation whereas lower sections are the major representative of the population of any developing country. SEC has also affected the collection coverage of MSW, according to reports of CPHEEO (Central Public Health and Environmental Engineering Organisation) and CPCB (Central Pollution Control Board) (Mandal 2019), collection coverage in the peri-urban or slum areas is low compared to commercial or high-income group or middle-income group areas.

Many of the cities in India have a limited practice of segregation (Agarwal 2018) through the distribution of blue and green dustbins. At present, the majority of urban and metro housing societies/communities are facilitated with three different bins of different colours for collecting waste like biodegradable, non-biodegradable and domestic hazardous waste, thus it requires time and effort for segregations of waste. Whereas there are inadequate treatment techniques and facilities for the transportation and disposal of segregated MSW. These factors affect the willingness of residents towards source segregations.

In addition, the efficiency of a solid waste collection system depends on the type of vehicles, its capacities and the number of staffs. The collection system is classified into two categories, i.e., door-to-door collection and communal collection. Door to door collection system generally exists in societies those who are willing to pay whereas in slums and low-income areas are covered under the communal collection system. In many cities (Agarwal 2018), the collection of source segregated waste has started but to lack of facilities, mixed waste ends up in the dumpsite. Such as, in Tirunelveli, a city in Tamil Nadu awarded by the government for achieving 100 per cent source segregation, residents segregate only recyclable plastic and handover it to the collector on predefined days. Whereas mixed waste is collected daily, however SWM Rules, 2016 mandate that waste must be segregated into wet, dry and domestic hazardous at the source itself.

Way forward by the Government of India

To make the existing MSWM system more efficient and for the optimum utilization of the resources Govt. of India has given the following recommendations (CPCB 2018):

(i) At the central level, a technical cell must be formed to help the state urban development department and local bodies to enable them for the execution of SWM Rules, 2016.

(ii) For proper implementation of SWMR, 2016, every State should display strategy & time-targeted action plan, which should be displayed on their website. Every state should have a cell to assist local bodies in terms of evolving plans and policies to provide technical and financial assistance.

(iii) Every State/UT should follow the guidelines for designating the landfill site and setting-up of a shielding zone around the landfill and waste processing sites.

(iv) State Pollution Control Boards to take-up with the local urban bodies and suggest setting up of waste treatment facilities either by themselves or by private entrepreneurs.

(v) Ministry of Environment & Forest should have a closer look at the matter of execution of SWMR, 2016 with Chief Secretaries/ Chief Ministries of the States/UTs.

(vi) Segregation of waste at source is to be made compulsory for having safe disposal of MSW. The wet/biodegradable waste should be converted into compost and dry waste should be recycled/recovered

(vii) If recycling is not done, then the dry waste must be transported to cement kilns for co-processing.

(viii) Every local body is supposed to submit a time-targeted work plan for the implementation of the SWM Rules, 2016, in cities/ towns.

(ix) The status of the implementation of solid waste management rule, 2016, must be reviewed regularly by the secretary to get satisfactory results.

Success Story of Indore Municipal Corporation (IMC), India- A Case Study

Indore city is situated in Indian state Madhya Pradesh over the area of 275 km^2 with a population density of 10000 P/km^2. There are around 6.20 Lac household and commercial places, which are the main sources of MSW generation. Being an urban area, the quantity of MSW is also being increased every year along with its population. As per the observation quantity of MSW since 2001, has been increased from 617 MT/Day to 1115 MT/Day till now. Such a rapid increase in the quantity of MSW has become a challenging task for local urban bodies. Hence a survey was conducted in September 2015. Presentations were made to the commissioner and mayor-in-council. which reported the following observations ("A2Z to restore garbage" n.d.; Bhargava n.d.; "Indore: Converting solid waste into electricity still a distant dream | Free Press Journal," n.d.; "The Curious Case of a Clean Clean Indore- Business News," n.d.):

(i) There were around 1380 garbage containers, which were old and dilapidated. Even in posh residential and more upmarket areas, there would usually be open garbage spots either in empty plots. Likewise around 480 open spots were identified where waste was being dumped and burnt.

(ii) It was observed that cleaning staffs were a bit reluctant towards supervision and management of allotted tasks, which causes littered waste on sites, road, and streets.

(iii) It was found the number of machinery used for waste management operation was not sufficient and it was not properly maintained.

(iv) Using landfill sites was not under the practice to dump the MSW.

(v) There was no door to door waste collection facility, which brings a neutral response in public towards waste management.

On the basis of the above observations, some revolutionary steps have been decided to initiate such as ("A2Z to restore garbage" n.d.; "How Indore Became Garbage-Free" n.d.; "Indore: converting solid waste" n.d.; "Smart City Indore" n.d.; "The Curious Case" n.d.):

An integrated MSWM has been introduced which has a predefined solution of MSW from collection to its treatment & disposal. It starts from door to door collection of solid waste through vehicles, equipped with different chambers for segregated waste.

(i) A mechanized road and street sweeping have been initiated, which helps to prevent littering of waste. Whereas manual picking of littered waste has also become the routine task under MSWM.

(ii) Construction and demolition debris is being collected separately.

(iii) Small composting units have been deployed.

(iv) Special units have been established for the treatment of plastic waste.

(v) A system was formed to penalized if anyone is found littering.

(vi) Treatment facility for biomedical waste like Incinerator (capacity of 300 Kg/Hr) has been installed.

(vii) Twin litter bins have been installed in all commercial areas.

(viii) Two dustbins became compulsory in the household for ensuring source segregation.

(ix) Stray cattle/pigs have been removed from the city.

(x) Established 9 modern transfer stations facilitated with the following advancement:

- The cylindrical design of the storage to prevent the surface from corrosion.
- Hydraulic compactor with a capacity of 15 MT.

(xi) Two scientific landfill sites of 6.25 acre each have been brought into operation.

(xii) Bioremediation of 2 Lakh MT old waste is being done in the area of 5 acres.

(xiii)A concrete road with the drainage facility has been brought into service.

Indore through its commendable collaborative efforts has achieved 100% segregation of waste at source and door-to-door garbage collection. The cleanliness scenario of Indore was changed by the improved habits of its people. Within one year the Municipal Corporation successfully sensitized citizens for segregation at source and not dumping garbage in open areas. The cleanliness story of Indore is a true transformation through community participation. Therefore according to Swachh Survekshan 2018 Results ("Swachh Survekshan" n.d.) Indore has been declared the cleanest city in India. Madhya Pradesh's capital Bhopal ranked as India's second cleanest city for two years in a row. Chandigarh is the third cleanest city.

RECOMMENDATIONS AND CONCLUSIONS

Various reports, research papers and news articles show that the un-segregated waste has affected the environment at its extreme and it is continuously causing many problems in the field of MSWM in India. Hence, there is an urgent need for proper segregation of waste that would lead to scientific disposal of waste. It can lead to various benefits such as enabling technology up-gradation, better quality products, saving of valuable raw material resources of the country, reducing the need for landfill space. Every citizen in India should be encouraged to keep segregated bins for wet, dry and hazardous waste and stop littering on the streets and segregation of waste should be made mandatory. Apart from adopting these habits, improving waste collection efficiency and developing suitable technologies for waste segregation, transportation, treatment, and disposal could be a step towards the solution of this problem. Besides, there should be an efficient mechanism for the segregation of waste at the source as it has become a herculean task all over the country. Also, there is a need to have a proper policy and cost-effective technological support for WTE Sector as existing technologies do not seem to be compatible with local requirements. Whereas a mechanized segregation system can also be introduced at primary or secondary storage, in which mixed MSW will be dumped and segregated in different categories such as compostable, non-compostable and recyclable waste. This system can be an effective intervention for the existing MSWM system and will be helpful to increase the segregation rate especially at high MSW producer location like institutions and commercial areas.

ACKNOWLEDGMENT

This paper is an outcome of a SEED funded project, Project Id: UPES/R&D/07022019/01, supported by the University of Petroleum and Energy Studies (UPES) Dehradun, Uttarakhand, India.

REFERENCES

A2Z to restore garbage processing plant in Indore in 15 days. (n.d.). Hindustan Times. Retrieved October 8, 2018, from https://www.hindustantimes.com/indore/a2z-to-restore-garbage-processing-plant-in-indore-in-15-days/story-B1IeevhPMLNQkci1pwDrNP.html

Agarwal, S. S. S. 2018. Is Swachh Bharat Mission ensuring waste segregation systems? Retrieved June 15, 2019, from Down to Earth website: https://www.downtoearth.org.in/blog/waste/is-swachh-bharat-mission-ensuring-waste-segregation-systems--61885

Agbefe, L. E., Lawson, E. T. and Yirenya-Tawiah, D. 2019. Awareness on waste segregation at source and willingness to pay for collection service in selected markets in Ga West Municipality, Accra, Ghana. Journal of Material Cycles and Waste Management, 0(4): 905-914. https://doi.org/10.1007/s10163-019-00849-x

Akshatha, 2018. Not segregating waste? BBMP mulls hefty fine - The Economic Times. Retrieved January 21, 2020, from Economic Times website: https://economictimes.indiatimes.com/news/politics-and-nation/not-segregating-waste-bbmp-mulls-hefty-fine/articleshow/65588209.cms?from=mdr

Annepu, R. K. 2012. Sustainable Solid Waste Management in India. Columbia University, New York, 2(01).

Basnayake, B. F. A., Popuri, S., Visvanathan, C., Jayatilake, A., Weerasoori, I. and Ariyawansha, R. T. K. 2019. Concerted initiative for planned management of municipal solid waste in target provinces in Sri Lanka. Journal of Material Cycles and Waste Management, 21(3): 691-704. https://doi.org/10.1007/s10163-018-0815-5

Bhargava, Anjuli (n.d.). How Indore Became Garbage-Free and Beat Every Other City to It. Retrieved June 24, 2019, from https://www.thebetterindia.com/114040/indore-madhya-pradesh-clean-garbage-free-india/

CPCB, 2018. CPCB Annual Report as per MSW Rules, 2016.

Dash, D. K. 2017. Solid waste management: Tirunelveli first to have 100% waste segregation | India News - Times of India. Retrieved May 21, 2019, from Times of India website: https://timesofindia.indiatimes.com/india/tirunelveli-first-to-have-100-waste-segregation/articleshow/57485885.cms

Doshi, V. 2016. The Kolkata dump that's permanently on fire: "Most people die by 50" | Cities | The Guardian. Retrieved September 27, 2018, from The Guardian website: https://www.theguardian.com/cities/2016/oct/24/difficult-breathe-inside-kolkata-india-rubbish-dump-permanently-fire

France-Presse & Agence 2019. Garbage mountain at Delhi's Ghazipur landfill to rise higher than Taj Mahal by 2020 - India news - Hindustan Times. Retrieved January 8, 2020, from Hindustan Times website: https://www.hindustantimes.com/india-news/garbage-mountain-at-delhi-s-ghazipur-landfill-to-rise-higher-than-taj-mahal-by-2020/story-RC0kwZdUmdHHfDs3rJGngI.html

Goel, S. 2017. Solid and hazardous waste management : an introduction. In: Advances in Solid and Hazardous Waste Management, pp. 1-27. https://doi.org/10.1007/978-3-319-57076-1

Harshitha, V. and Nisar, M. 2019. Door-to-door collection of garbage in a mess | Deccan Herald. Retrieved June 19, 2019, from Deccan Herald website: https://www.deccanherald.com/city/bengaluru-infrastructure/door-to-door-collection-of-garbage-in-a-mess-739969.html

Hazra, T. and Goel, S. 2009. Solid waste management in Kolkata, India: Practices and challenges. Waste Management, 29(1): 470-478. https://doi.org/10.1016/j.wasman.2008.01.023

Hindu, T. 2012 July 7. Plastic waste chokes storm water drains. The Hindu. Retrieved from https://www.thehindu.com/news/plastic-waste-chokes-storm-water-drains/article3613373.ece

Indore: Converting solid waste into electricity still a distant dream (n.d.). Free Press Journal. Retrieved October 8, 2018, from http://www.freepressjournal.in/indore/indore-converting-solid-waste-into-electricity-still-a-distant-dream/1185419

Jadhav, R. 2018. 75% of municipal garbage in India dumped without processing | India News - Times of India. Retrieved June 20, 2019, from Times of India website: https://timesofindia.indiatimes.com/india/75-of-municipal-garbage-in-india-dumped-without-processing/articleshow/65190477.cms

Jank, A., Müller, W., Schneider, I., Gerke, F. and Bockreis, A. 2015. Waste separation press (WSP): A mechanical pretreatment option for organic waste from source separation. Waste Management, 39: 71-77. https://doi.org/10.1016/j.wasman.2015.02.024

Karelia, G. 2019. Chennai store uses banana leaves to package veggies. Retrieved January 3, 2020, from The Better India website: https://www.thebetterindia.com/179800/chennai-eco-friendly-shop-banana-leaf-packaging-india/

Kumar, S., Smith, S. R., Fowler, G., Velis, C., Kumar, S. J., Arya, S., Cheeseman 2017. Challenges and opportunities associated with waste management in India. Royal Society Open Science, 4(3). https://doi.org/10.1098/rsos.160764

Lahiry, S. 2017. India's challenges in waste management. Retrieved from http://www.downtoearth.org.in/blog/india-s-challenges-in-waste-management-56753

Lavania, D. 2018. Open garbage trucks litter Agra roads every day. Agra News - Times of India. Times of India. Retrieved from https://timesofindia.indiatimes.com/city/agra/open-garbage-trucks-litter-city-roads-every-day/articleshow/62449605.cms

Lavasa, S. A., General, A., Secretary, M., Tiger, N., Authority, C. and Bonal, S. B. S. 2016. Press Information Bureau, Government of India, Ministry of Environment and Forests.

Lee, Y. Y., Jung, H., Ryu, H. W., Oh, K. C., Jeon, J. M. and Cho, K. S. 2018. Seasonal characteristics of odor and methane mitigation and the bacterial community dynamics in an on-site biocover at a sanitary landfill. Waste Management, 71: 277-286. https://doi.org/10.1016/j.wasman.2017.10.037

Malcolm Richard, G., Mario, M., Javier, T. and Susana, T. 2011. Optimization of the recovery of plastics for recycling by density media separation cyclones. Resources, Conservation and Recycling, 55(4): 472-482. https://doi.org/10.1016/j.resconrec.2010.12.010

Mandal, P. K. 2019. Review on evolution of municipal solid waste management in India : Practices , challenges and policy implications. Journal of Material Cycles and Waste Management, (0123456789). https://doi.org/10.1007/s10163-019-00880-y

Mandal, P., Chaturvedi, M. K., Bassin, J. K., Vaidya, A. N. and Gupta, R. K. 2014. Qualitative assessment of municipal solid waste compost by indexing method. International Journal of Recycling of Organic Waste in Agriculture, 3(4): 133-139. https://doi.org/10.1007/s40093-014-0075-x

Manohar, M. 2017. Bhalswa landfill: Bhalswa landfill fire rages on as city chokes | Delhi News - Times of India. Retrieved September 27, 2018, from Times of India website: https://timesofindia.indiatimes.com/city/delhi/delhi-pollution-bhalswa-landfill-fire-rages-on-as-city-chokes/articleshow/61656243.cms

Manohar, M. 2019. Segregate waste at source or face Delhi corporation fines of up to Rs 1L. Times of India. Retrieved from https://timesofindia.indiatimes.com/city/delhi/segregate-waste-at-source-or-face-delhi-corporation-fines-of-up-to-rs-1-lakh/articleshow/66278957.cms

Ministry of Housing and Urban Affairs. 2019. Solid waste management including hazardous waste, medical waste and e-waste twenty, 25th Report. Retrieved from http://164.100.47.193/lsscommittee/Urban Development/16_Urban_Development_25.pdf

Ministry of new and renewable energy, 2016. Standing committee on energy (2015-16) (Vol. 20).

Moghadam, M. R. A., Mokhtarani, N. and Mokhtarani, B. 2009. Municipal solid waste management in Rasht City, Iran. Waste Management, 29(1): 485-489. https://doi.org/10.1016/j.wasman.2008.02.029

Nagendra, B., Lakshmisha, A. and Agarwal, P. 2019. Mobile application in municipal waste tracking: a pilot study of "PAC waste tracker" in Bangalore city, India. Journal of Material Cycles and Waste Management, 21(3): 705-712. https://doi.org/10.1007/s10163-018-00819-9.

Padilla, J.A. and Trujillo, J. C. 2017. Waste disposal and households' Heterogeneity. Identifying factors shaping attitudes towards source-separated recycling in Bogotá, Colombia. Waste Management, 74: 16-33. https://doi.org/10.1016/j.wasman.2017.11.052.

Pandey, S. and Malik, J. K. 2015. Industrial and Urban Waste Management in India. The Energy and Resources Institute.

Planning Commission, 2014. Report of the Task Force on Waste to Energy (Volume I): In the context of Integrated Municipal Solid Waste Management. In Task Force on Waste to Energy. Retrieved from http://planningcommission.nic.in/reports/genrep/rep_wte1205.pdf

Press Trust of India Ltd. 2019. Lack of waste management in Bihar can lead to emergency-like situation: NGT | Delhi News - Times of India. Times of India. Retrieved from https://timesofindia.indiatimes.com/city/delhi/lack-of-waste-management-in-bihar-can-lead-to-emergency-like-situation-ngt/articleshow/68524020.cms

Priya, L. 2019. Going green: Kerala moots banana leaves as plastic-free food wrappings - the better India. Retrieved January 3, 2020, from The Better India website: https://www.thebetterindia.com/169650/kerala-green-packing-banana-leaves-food-parcel/

Pulat, H. F. and Yukselen-Aksoy, Y. 2017. Factors affecting the shear strength behavior of municipal solid wastes. Waste Management. https://doi.org/10.1016/j.wasman.2017.08.030

Rai, S. 2017. Making the best out of waste: These 8 startups are helping Indian cities manage trash. Retrieved July 16, 2019, from Your Story website: https://yourstory.com/2017/11/waste-management-startups

Rajkumar, J. and Sirajuddin, A. 2016. Status and challenges of municipal solid waste management in India : A review. Cogent Environmental Science, 2(1): 1-18. https://doi.org/10.1080/23311843.2016.1139434

Rawat, M., Ramanathan, a L. and Kuriakose, T. 2013. Characterisation of municipal solid waste compost (MSWC) from selected Indian cities-a case study for its sustainable utilisation. Journal of Environmental Protection, 4: 163-171. https://doi.org/10.4236/jep.2013.42019

Sambyal, S. S. and Agarwal, R. 2018. Forum of cities that segregate. In: Assessment Report 2017-18. Retrieved from https://www.cseindia.org/model-framework-for-segregation-8603

Sharholy, M., Ahmad, K., Mahmood, G. and Trivedi, R. C. 2008. Municipal solid waste management in Indian cities - A review. Waste Management, 28(2): 459-467. https://doi.org/10.1016/j.wasman.2007.02.008

Sharma, N. 2018. Dehradun, Haridwar ULBs flout waste disposal rules, says CAG | Dehradun | Hindustan Times. Retrieved June 18, 2019, from Hindustan Times website: https://www.hindustantimes.com/dehradun/dehradun-haridwar-ulbs-flout-waste-disposal-rules-says-cag/story-Dqfbt0GkL42Ogpjg7HG46J.html

Shwetmala, Chanakya, H. and Ramachandra, T. 2011. ICON SWM 2011 2nd International conference on solid waste management and exhibition Assessment of solid wastes choking open sewers and vulnerability to urban flooding. Retrieved from http://wgbis.ces.iisc.ernet.in/energy/paper/iconswm_urban_flooding/ufsw.pdf

Smart City Indore (n.d.). Solid Waste Management. Retrieved June 24, 2019, from https://www.smartcityindore.org/solid-waste/

Speier, C. J., Nair, R. R., Mondal, M. M. and Weichgrebe, D. 2019. Multi-sector evaluation of generation, composition and sustainable treatment systems for commercial waste streams in India. Journal of Material Cycles and Waste Management, (0123456789). https://doi.org/10.1007/s10163-019-00869-7

Subramanian, A. 2017. At this ATM, deposit garbage to withdraw rewards - the better India. Retrieved May 21, 2019, from The better India website: https://www.thebetterindia.com/95751/garbage-waste-segregation-atm/

Sujauddin, M. 2008. Household solid waste characteristics and management in Chittagong, Bangladesh. Waste Management, 28: 1688-1695. https://doi.org/10.1016/j.wasman.2007.06.013

Swachh Survekshan 2018 Results: Top 10 Highlights (n.d.). Retrieved August 23, 2019, from https://swachhindia.ndtv.com/swachh-survekshan-2018-top-10-highlights-19749/

The Curious Case of a Clean Clean Indore- Business News (n.d.). Retrieved June 24, 2019, from https://www.businesstoday.in/magazine/columns/the-curious-case-of-a-clean-clean-indore/story/254144.html

The World Bank, 2018. Data Catalog. Retrieved June 27, 2019, from The World Bank website: https://datacatalog.worldbank.org/dataset/what-waste-global-database

TNN, 2018. Ghazipur: Fire at Ghazipur landfill, more expected as mercury rises | Delhi News - Times of India. Retrieved September 27, 2018, from Times of India website: https://timesofindia.indiatimes.com/city/delhi/fire-at-ghazipur-landfill-more-expected-as-mercury-rises/articleshow/63372938.cms

Tonini, D., Albizzati, P. F. and Astrup, T. F. 2018. Environmental impacts of food waste: Learnings and challenges from a case study on UK. Waste Management, 76: 744-766. https://doi.org/10.1016/j.wasman.2018.03.032

Vibha Sharma and Snehal Tripathi, 2017. Four months on, garbage segregation at source still not doable for Delhi residents | delhi news | Hindustan Times. Retrieved June 15, 2019, from Hindustan Times website: https://www.hindustantimes.com/delhi-news/four-months-on-garbage-segregation-at-source-still-not-doable-for-delhi-residents/story-NxOX2lQqAfDmiR3OZmE0RJ.html

Woodford, C. 2019. Plasma arc waste recycling - A simple introduction. Retrieved January 21, 2020, from Expalinthatstuff.com website: https://www.explainthatstuff.com/plasma-arc-recycling.html

Yaqoob, M. 2018. Much-hyped waste segregation at source non-starter, Greater Kashmir. Retrieved June 15, 2019, from Greaterkasmir.com website: https://www.greaterkashmir.com/news/srinagar/much-hyped-waste-segregation-at-source-non-starter/

Nature Environment and Pollution Technology
An International Quarterly Scientific Journal

p-ISSN: 0972-6268
(Print copies up to 2016)
e-ISSN: 2395-3454

Vol. 20 | No. 2 | pp. 865-874 | 2021

Original Research Paper

https://doi.org/10.46488/NEPT.2021.v20i02.049

Open Access Journal

A Comparative Study of Machine Learning Techniques in Prediction of Exhaust Emissions and Performance of a Diesel Engine Fuelled with Biodiesel Blends

Quang Hung Do*†, Shih-Kuei Lo and Jeng-Fung Chen****

*Faculty of Information Technology, University of Transport Technology, Hanoi 100000, Vietnam

**Department of Industrial Engineering and Systems Management, Feng Chia University, Taichung 40724, Taiwan

†Corresponding author: Quang Hung Do; hungdq@utt.edu.vn

Nat. Env. & Poll. Tech.
Website: www.neptjournal.com

Received: 20-04-2020
Revised: 18-07-2020
Accepted: 20-07-2020

Key Words:
Exhaust emissions
Diesel engine performance
Biodiesel engine
Machine learning

ABSTRACT

Biodiesel has been receiving increasing attention because of its fuel properties and compatibility with petroleum-based diesel fuel. Therefore, it is necessary to measure the engine performance and exhaust emissions of engines using petroleum-based diesel fuel and biodiesel blends. The main goal of this study is to investigate the capability of several machine learning (ML) techniques including artificial neural network (ANN), adaptive neuro-fuzzy inference system (ANFIS), general regression neural network (GRNN), radial basis function (RBFN), and support vector regression (SVR) for predicting performance and exhaust emissions of the diesel engine fuelled with biodiesel blends. The case application is a Hyundai D4CB 2.5 engine together with B0, B10 and B20 biodiesel blends which are popularly used in Vietnam. The engine process parameters are used as inputs and the outputs include predicted torque and NOx emission. Different predicting models based on ML techniques are developed and validated. The performance of each model is evaluated and compared using root mean squared error (RMSE), mean absolute percentage error (MAPE), mean absolute error (MAE), and correlation coefficient (R). The obtained results indicate that SVR can be used to develop the model for the prediction of performance and exhaust emissions. The study also provides a better understanding of the effects of engine process parameters on performance and exhaust emissions.

INTRODUCTION

The diesel engines have been proved to be cost-effective and an ideal replacement for steam engines. The increasing use of diesel engines in on-road, off-road vehicles and other fields such as industry and agriculture sector results in the climbing threat of air pollutions. Biodiesel is an alternative, renewable, clean diesel fuel similar to conventional or 'fossil' diesel. The process to produce biodiesel is the conversion from the triglyceride fats to esters which is called transesterification with methanol/ethanol. Biodiesel can be made from natural sources such as vegetable oil, animal oil/fats, tallow and waste cooking oil (Meher et al. 2006, Ramadhas et al. 2005, Van 2005). Biodiesel in blends or neat form is a good successor for petroleum diesel and could be used directly in any diesel engine (Agarwal et al. 2008). However, it is more practical that biodiesel should substitute for a fraction of petroleum diesel in use when the alternative fuel is gradually introduced as blends with diesel (Mamilla & Rao 2016, Shailaja & Raju 2017). Blending biodiesel with diesel in an adequate percentage can achieve a better result than that of diesel or pure diesel. Therefore, it is necessary to evaluate the blends of biodiesels for their performances and exhaust emissions.

The computational intelligence approach can explore the nonlinear relationship and discover hidden knowledge from the dataset. As a result, the approach has been applied to several practical problems in various scientific disciplines. In recent years, computational intelligence approaches in general, and machine learning (ML) techniques, in particular, have been used to predict engine performance and exhaust emissions (Canakci et al. 2009, Do et al. 2020, Liu et al. 2018). Ghanbari et al. (Ghanbari et al. 2015) used a support vector machine (SVM) to predict the performance parameters and exhaust emissions of a diesel engine operating on nano diesel blended fuels. The results showed that SVM is capable of predicting diesel engine performance and emissions. The use of machine learning methods may be highly recommended to predict engine performance and exhaust emissions instead of having to carry out complex and time-consuming experiments. Other than that, in the field of automotive engineering, ML techniques provided a more accurate and simple method than in the analysis of engine

performance and exhaust emissions. In modelling biodiesel processes, artificial intelligence has been a good replacement for conventional computing based on polynomial and linear regressions in resolving the nonlinear prediction problems (Noor 2014).

In general, the above-mentioned studies have shown that the ML-based models are efficient in predicting water quality. In developing ML-based models, since each dataset has its characteristics and features, no model can be efficiently applied to all types of data. In this study, the main objective is to develop different ML models including ANN, ANFIS, GRNN, RBFN, SVR for predicting performance and exhaust emissions of the diesel engine fuelled with biodiesel blends. In the study, an experimental setup was firstly designed to collect the dataset. The experimenter was conducted in Motors Research Laboratory at the University of Transport Technology. Biodiesel blends including B0, B10 and B20 were used as fuel in a Hyundai engine. The performance and exhaust emissions were then recorded in real-time. This study examined the validity of developed models. The obtained dataset was applied to the developed models to perform the prediction of performance and emissions of the engine. Several performance criteria were utilized to identify which model is the best one that can provide superior predictions of exhaust emissions and performance of a diesel engine fuelled with biodiesel blends.

PRELIMINARIES

Artificial Neural Network (ANN)

A neural network in which activations spread only in a forward direction from the input layer through one or more hidden layers to the output layer is known as a multilayer feed-forward network. For a given set of data, a multi-layer feed-forward network can give a good non-linear relationship. It is affirmed that a feed-forward network even with only one hidden layer can approximate any continuous function (Hornik et al. 1989, Ken-Ichi 1989). In Fig. 1, *R*, *N*, and *S* are the numbers of input, hidden neurons, and output, respectively; *iw* and *hw* are the input and hidden weights matrices, respectively; *hb* and *ob* are the bias vectors of the hidden and output layers, respectively; *x* is the input vector of the network; *ho* is the output vector of the hidden layer, and *y* is the output vector of the network. A network with a structure that is more complicated than necessary over fits the training data (Caruana et al. 2001).

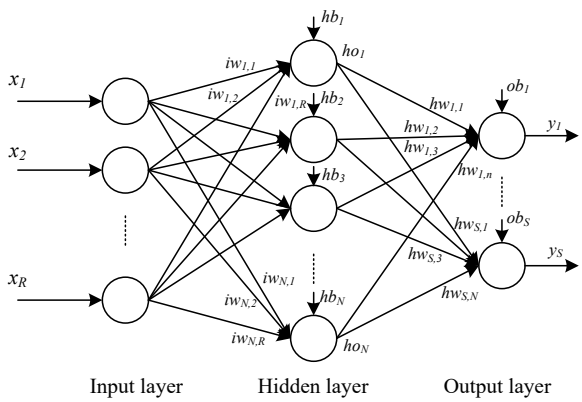

Fig. 1: A feed-forward network with three layers.

Adaptive Neuro-Fuzzy Inference System (ANFIS)

A fuzzy inference system (FIS) employs fuzzy if-then rules when acquiring knowledge from human experts to deal with imprecise and uncertain problems (Yusof et al. 2012). FISs have been widely used to solve different classification problems (Fakhrahmad et al. 2012). However, fuzzy systems cannot learn from or adjust themselves (Ata & Kocyigit 2010). The system can overcome some limitations of neural networks, as well as the limits of fuzzy systems (Nauck et al. 1997, Singh et al. 2005) when it can represent knowledge in an interpretable manner and the ability to learn. The details of the neuron-fuzzy system were proposed by Takagi and Hayashi (Takagi & Hayashi 1991). Among the neuron-fuzzy systems, ANFIS, introduced by Jang (Jang 1993), has been one of the most common tools.

To present the ANFIS architecture and simplify the explanations, assume that the FIS has two inputs, x_1 and x_2, two rules, and one output, y as shown in Fig. 2. A FIS has two inputs and two fuzzy if-then rules that can be expressed as in Equation 1.

Where x_1 and x_2 are the inputs; A_1, A_2, B_1, B_2 are the linguistic labels; p_i, q_i and r_i (i = 1 or 2) are the consequent parameters (Jang 1993) that are identified in the training process; and y1 and y2 are the outputs within the fuzzy region. Eq. (1) represents the first type of fuzzy if-then rules, in which the output part is linear. The output part can also be constants (Sugeno 1985) and represented as:

Rule 1: If x_1 is A_1 and x_2 is B_1 then $y_1 = C_1$

Rule 2: If x_1 is A_2 and x_2 is B_2 then $y_2 = C_2$ …(1)

Where (i = 1 or 2) are constant values.

For complicated problems, the first type of if-then rules is widely used to model the relationships of inputs and outputs (Wei et al. 2007). In this research, we also used a linear function for the output.

It can be seen that the ANFIS architecture has two adaptive layers: layer 1 and layer 4. Layer 1 has parameters related to the fuzzy membership functions and layer 4 has parameters {pi, qi, ri} related to the polynomial. Adjusting

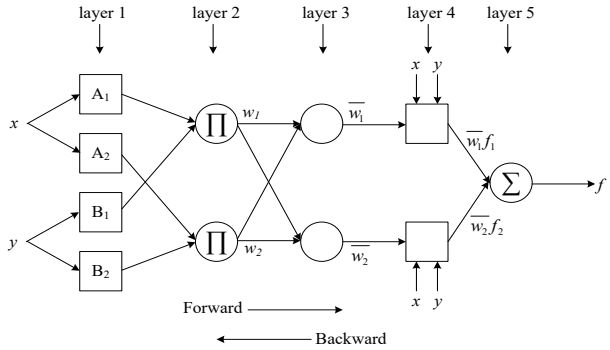

Fig. 2: An ANFIS architecture of two inputs and two rules.

the parameters includes two steps. In the forward pass of the learning algorithm, the premise parameters are fixed, functional signals go forward until layer 4, and the consequent parameters are identified by the least squares method to minimize the measured error. In the backward pass, the consequent parameters are fixed, the error signals go backward, and the premise parameters are updated by the gradient descent method (Jang et al. 1997). This hybrid learning algorithm can decrease the complexity of the algorithm and increase learning efficiency (Singh et al. 2005).

Radial Basis Function (RBFN)

The architecture of RBF network includes three layers: the input layer, the hidden layer, and the output layer, as shown in Fig. 3. Although the structure of Radial Basis Function (RBF) neural network is rather simple, the network has a strong generalization ability (Jiang et al. 2016). The RBF neural network has shown a good classification and approximation performance in various applications (Batool et al. 2013, Guan et al. 2016).

As shown in Fig. 3, the estimated output is a weighted summation using the following equation:

$$y_s = \sum_{j=1}^{J} w_{js} R_j(x), s = 1,2,\ldots,S \quad \ldots(2)$$

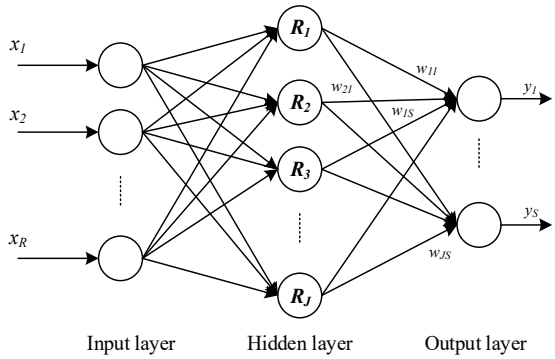

Fig. 3: A RBF network.

Where S denotes the number of outputs, J is the number of nodes in the hidden layer and w_{js} is the connection weight between j-th node of the hidden layer and s-th node of the output layer. There are several radial basis functions, the most commonly used one is as follows:

$$R_j(x) = exp\left(-\frac{\|x-c_j\|}{2\sigma_j^2}\right), \text{j=1,2,..., J} \quad \ldots(3)$$

Where x is the input pattern vector, each input is represented by the N-dimensional vector; c_j and σ_i are the centre and the width of RBF, respectively; $\|x - c_j\|$ is the norm of the vectors x and c_j, which can be considered as the distance between the vectors x and c_j.

General Regression Neural Network (GRNN)

GRNN, a modified version of radial basis function (RBF) networks, is designed for function regression and approximation (Yaseen et al. 2016). GRNN can be successfully applied to deal with various linear and non-linear problems and can accurately perform predictions without requiring large samples (Alilou & Yaghmaee 2015).

GRNN represents a structure that contains along with a hidden radial layer both probabilistic hidden and output layers. These networks are based on the method for approximation of probability density with the help of Gaussian kernel functions.

$$\psi(x) = \frac{1}{\sqrt{2\pi}} e^{-\frac{x^2}{2}} \quad \ldots(4)$$

GRNN has several outstanding characteristics including the ability to approximate any smooth function and generating consistent forecasts when the training data set size becomes big and the estimation error closes to zero, with only mild restrictions on the function (Cigizoglu & Alp 2006, Kim & Kim 2008). There are four layers in GRNN, including the input, pattern, summation, and output layers. The number of neurons in the input and output layers represent the independent and dependent variables, respectively. The number of neurons in the pattern layer is the number of data patterns in training. The summation layer has the number of neurons that is equivalent to the number of output nodes plus one (Ji et al. 2017).

Support Vector Regression

Support Vector Machine (SVM) method is a supervised learning method influenced by advances in statistical learning theory (Abe 2010, Meyer et al. 2003). SVM has been successfully applied in solving classification, prediction and recognition problems (Do & Chen 2013). If a training dataset has feature-label pairs (x_i, y_i) with $i = 1,\ldots, n$. The optimum separating hyperplane will be represented as follows:

$$g(x) = sign\left(\sum_{i=1}^{n} y_i\, \alpha_i K\left(x_i, x_j\right) + b\right) \quad \ldots(5)$$

Where $K(x_i, x_j)$ denotes kernel function; α_i is a Lagrange multiplier; and b is the offset of the hyperplane from the origin. The constraints are $0 \le \alpha_i \le C$ and $\sum \alpha_i y_i = 0$, where α_i is a Lagrange multiplier for each training point and C is the penalty. Only the training points being close to the support vectors have nonzero α_i. However, in real-world applications, data are noisy and no linear separation exists in the feature space. Thus, the optimum hyperplane is written as:

$$y_i(w, x_i + b) \ge 1 - \vartheta_i, \vartheta_i \ge 0 \quad \ldots(6)$$

Where w denotes the weight vector that determines the orientation of the hyperplane in the feature space; ϑ_i is the ith positive slack variable that estimates the amount of violation according to the constraints.

RESEARCH DESIGN

Experimental Setup

As shown in Fig. 4, the assembled model includes Alpha 160 which is a brake testing device. Moreover, AVL-553S-200 is a temperature controller for cooling water; AVL PLU 160 estimates fuel consumption. BOBCAT is a system for automation of measurement and testbed. I/O Cube is designed to get signals from sensors; FEM is for converting the signal. K57 is a control board; ECU is an engine control unit; throttle pedal is used for the brake and clutch pedal assembly; FTIR (Fourier-transform infrared spectroscopy) is used to obtain an infrared spectrum of absorption or emission; AVL415SE is a smoke meter. Testo 350 is an emission gas analyser and a picoscope is used to test the control signal.

The study was conducted in Motors Research Laboratory at the University of Transport Technology. The connection of the modules is shown in Fig. 4. The operating parameters and the number of emissions were updated in real-time; a picoscope module connected to a computer was used to record the control signal from the EGR valve.

Motor moment was measured by an eddy current dynamometer (Alpha 160) which has a max power of 160 kW, a max torque of 400 Nm and a max speed of 10000 RPM. With a throttle actuator, testing brake can adjust the driving resistance load and the speed of an automobile.

Fuel flow was measured and analysed by AVL PLU 160 - a high precision fuel consumption measurement system in which a gear meter driven by a servo motor with encoder defines a geometric volume to pulse frequency ratio when gear rotation is adjusted to media flow. The system is a 0-160 litre/hour volumetric flow meter with a maximum error of 2%.

The FT-IR (Fourier transformation infrared spectroscopy) was applied to a continuous measurement of main pollutant emissions from biodiesel engines (i.e., carbon monoxide-CO, hydrocarbons-HC, nitrogen oxides-NOx, carbon dioxide-CO_2).

Particulate matter-PM was measured and analysed by an AVL Smoke Meter (AVL 415SE) which uses the filter paper method to determine the Filter Smoke Number (FSN defined according to ISO 10054) and the soot concentration in mg/m³. The measurement precision is 0.0001 FSN.

AVL 553S200 is used to bring the engine coolant and excellent temperature stability. This model is designed for the

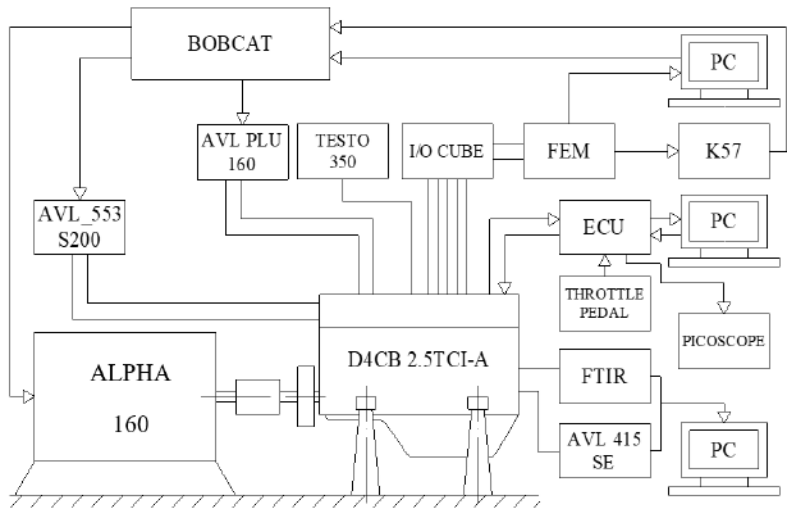

Fig. 4: The experimental setup.

Table 1: Fuel properties of B0, B10 and B20.

Property	B0	B10	B20
Density at 15°C (kg/m^3)	0.830	0.8355	0.841
Calorific value (MJ/kg)	42.5	41.84	41.18
Kinematic viscosity at 40°C (mm2/s)	0.830	0.8355	0.841
Cetane number	48	48.35	48.68

Table 2: Input variables used for predicting exhaust emissions and performance.

No.	Input variables	Abbreviation	Source
1.	Throttle position (%)	Alpha	Sensor
2.	Air intake pressure (bar)	P_INTAKE	Sensor
3.	The speed engine (rpm)	SPEED	Sensor
4.	Cooling water temperature (°C)	T_WATER	Sensor
5.	Intake air temperature (°C)	T_INTAKE	Sensor
6.	Exhausted emissions temperature (°C)	T_EXHAUST	Sensor
7.	EGR temperature (°C)	T_EGR	Sensor
8.	EGR rate (%)	%EGR	Sensor
9.	Lambda	Lambda	Calculated

maximum engine power of 250 kW. Intake air temperature and pressure, exhaust emission, exhaust gas recirculation (EGR) are measured by K-sensor and residual pressure meter.

The control of the test-bed and engine was done by Bobcat 2.0 in which all signals from the test-bed and other modules in the laboratory were recorded. In this study, the engine performance and emissions of biodiesel blends (B10, B20) and diesel fuel (B0) were studied. Fuel properties of B0, B10 and B20 are presented in Table 1.

Data Description

Descriptive statistics of observed variables including the maximum (Max), minimum (Min), mean and standard deviation (Std) are summarized in Table 3.

The experiment can collect and measure 26 kinds of exhaust emissions including NO, H_20, CH_4, CO, NO_2, N_2O, NH_3, SO_2, HCHO, C_2H_2, C_2H_4, NC_8, C_3H_6, C_4H_6, NOx, HC, etc. As suggested in the standards developed by national and international bodies, this study focuses on investigating two kinds of emissions including NOx (ppm) and HC (ppm). The performance parameter predicted in this study is Torque (Nm) that is a measure of rotational effort applied on engine crankshaft by the piston. Torque in an engine is the amount of rotational force that the engine produces. Descriptive statistics of dependent variables are represented in Table 4. Fig. 5 includes correlation matrixes showing correlation coefficients between sets of variables. Each cell indicates the correlation between two variables.

Table 3: Descriptive statistics of observed variables.

No.	Input	Min	Max	Mean	Std.
		B0			
1.	Alpha	9.94	44.87	26.3	9.246
2.	P_INTAKE	0	1.49	0.331	0.349
3.	P_EGR	0	1.46	0.334	0.34
4.	SPEED	1244.64	2753.25	1684.993	482.888
5.	T_WATER	65.55	96.18	82.438	6.21
6.	T_INTAKE	42.37	170.6	80.428	33.272
7.	T_EXHAUST	148.05	786.74	429.945	164.312
8.	T_EGR	44.9	348.8	139.243	64.642
9.	%EGR	0	56.592	31.349	21.363
10.	Lambda	0.529	5.758	1.951	1.135
		B10			
1.	Alpha	14.91	39.82	27.55	6.652
2.	P_INTAKE	0.04	1.09	0.315	0.239
3.	P_EGR	0.05	1.07	0.313	0.234
4.	SPEED	1211.31	2501.56	1823.697	411.672
5.	T_WATER	75.11	111.81	91.879	8.148
6.	T_INTAKE	52.79	150.64	88.741	22.784
7.	T_EXHAUST	280.11	712.43	471.083	116.475
8.	T_EGR	50.9	330.2	143.235	60.123
9.	%EGR	0	44.084	21.784	16.639
10.	Lambda	0.658	3.845	1.605	0.629
		B20			
1.	Alpha	9.94	44.86	26.479	9.94
2.	P_INTAKE	0	1.48	0.35	0
3.	P_EGR	0	1.45	0.347	0
4.	SPEED	1209.11	2753.11	1896.502	1209.11
5.	T_WATER	57.79	95.91	82.211	57.79
6.	T_INTAKE	38.75	170.93	84.775	38.75
7.	T_EXHAUST	143.4	775.15	423.069	143.4
8.	T_EGR	42.9	334.3	146.845	42.9
9.	%EGR	0	54.733	27.909	0
10.	Lambda	0.626	6.365	2.056	0.626

Table 4: Descriptive statistics of dependent variables.

Input	Min	Max	Mean	Std.
	B0			
NOx	22.573	733.963	176.584	160.813
Torque	3.54	211.91	81.826	56.706
	B10			
NOx	14.487	704.4	199.178	175.057
Torque	27.87	202.16	94.328	46.407
	B20			
NOx	16.362	616.581	154.334	140.244
Torque	4.97	204.67	74.32	55.348

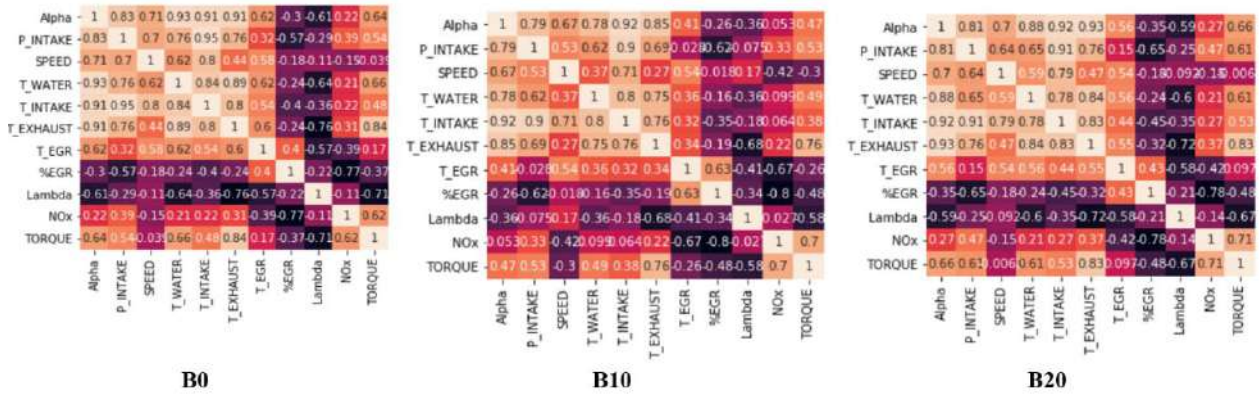

Fig. 5: Correlation matrix.

Model Development

The first step of the development of ML-based models is the preparation of the dataset. In this step, the collected dataset is divided into two groups - training and testing datasets. The training and testing dataset are used for the construction and validation of the models, respectively. In this study, 70% and 30% of the dataset is for training and testing, respectively. The next stage is designing the structure of the model and adjusting the parameters. For example, in developing an ANN-based model, the number of hidden layers, the number of neurons per layer, and the type of transfer function need to be adjusted.

Performance Evaluation Criteria

To evaluate the performance of the developed models, several criteria are used. These criteria are applied to the

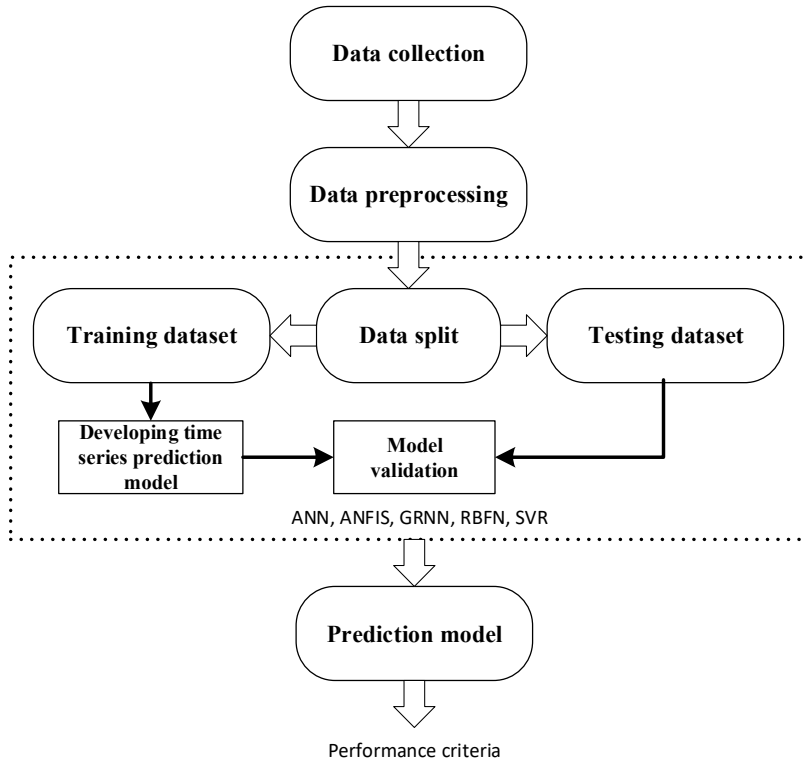

Fig 6: The model development.

model to know how well it worked. The criteria are used to compare predicted values and actual values. They are: Root mean squared error (RMSE), Mean absolute percentage error (MAPE), Mean absolute error (MAE) and Correlation coefficient ().

RESULTS AND DISCUSSION

All models were coded in Matlab 2015a environment. To avoid the over-fitting problem, the 10-fold cross-validation was utilized. For each technique, various sets of parameters were tried to obtain the best architecture of each classifying model. To evaluate the performance of the classifying model, several performance criteria were used. These criteria were applied to know how well the developed models worked. Several main parameters are set for each model as follows: the architecture of the ANN model is with two hidden layers (the number of hidden nodes are 12 and 6, respectively). The parameters were set as follows: the training algorithm is Levenberg-Marquardt; the number of epochs is set to 100. For the ANFIS model, the number of fuzzy rules was 2. For the SVR model, the kernel function was Gaussian. For GRNN and RBFN models, the spread constants were 0.12 and 0.2, respectively.

Tables 5-7 show the performance statistics of all models. It is clearly seen that the SVR model has the smallest RMSE, MAPE, and MAE values as well as the biggest *R*-value. This means that the SVR has a better performance in all criteria.

The comparison between actual values and corresponding forecasting values obtained by the SVR model are shown in Figs. 7-9. The figures present prediction values and actual values. In all scenarios, the forecasting values tend to be close to the actual values. This indicates a good agreement between the prediction values obtained by the developed models and the actual values. This finding also indicates that SVR provides accurate forecasting results.

Based on the results, it can be inferred that the SVR model can be used as a suitable tool in the prediction of exhaust emissions and performance of a diesel engine fuelled

Table 5: Performance criteria on the testing set obtained by different techniques for B0.

Predicted parameter	Model	RMSE	MAPE	MAE	R
NOx	ANFIS	129.8523	0.3673	70.5089	0.7738
	ANN	95.6113	0.3857	51.7597	0.7756
	GRNN	164.2776	0.5149	92.1703	0.5135
	RBFN	212.6085	0.6062	120.7113	-2.5466e-16
	SVR	**71.6624**	**0.4577**	**47.9384**	**0.8572**
Torque	ANFIS	12.0361	0.1876	7.3354	0.9846
	ANN	10.8662	0.1268	6.0425	0.9840
	GRNN	20.3166	0.1147	11.0365	0.9332
	RBFN	72.2844	1.5029	58.4099	-3.7701e-16
	SVR	**8.3087**	**0.1887**	**6.5485**	**0.9875**

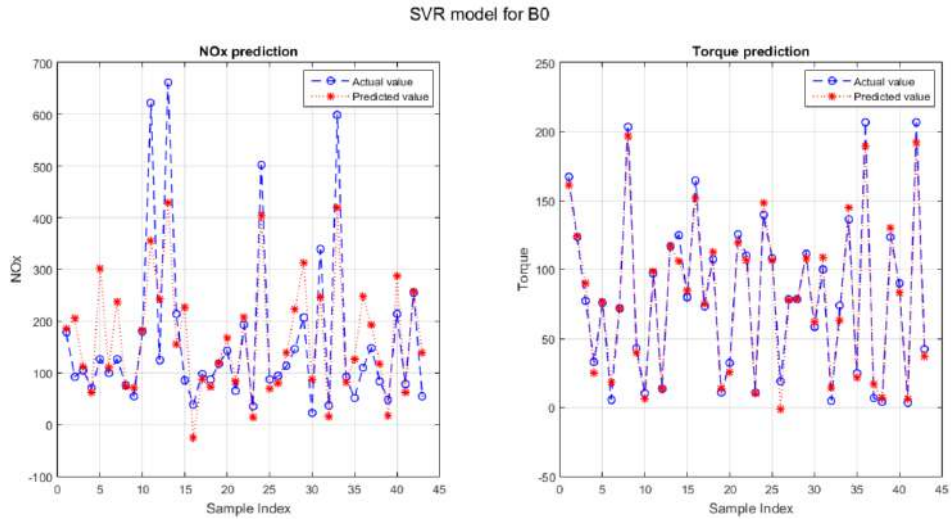

Fig. 7: Performance of SVR model for B0.

Table 6: Performance criteria on the testing set obtained by different techniques for B10.

Predicted parameter	Model	RMSE	MAPE	MAE	R
NOx	ANFIS	95.2373	0.4499	55.6865	0.8160
	ANN	87.6310	0.2139	47.9662	0.9139
	GRNN	153.8600	0.7406	102.2467	0.7405
	RBFN	241.2296	0.6787	162.5765	-1.9499e-16
	SVR	60.5215	0.7055	49.9064	0.9359
Torque	ANFIS	7.1567	0.3762	4.7942	0.9920
	ANN	9.1031	0.0883	5.3696	0.9889
	GRNN	11.6969	0.0881	6.0004	0.9803
	RBFN	74.7863	0.9549	57.7388	1.0034e-16
	SVR	6.5670	0.2766	5.6123	0.9944

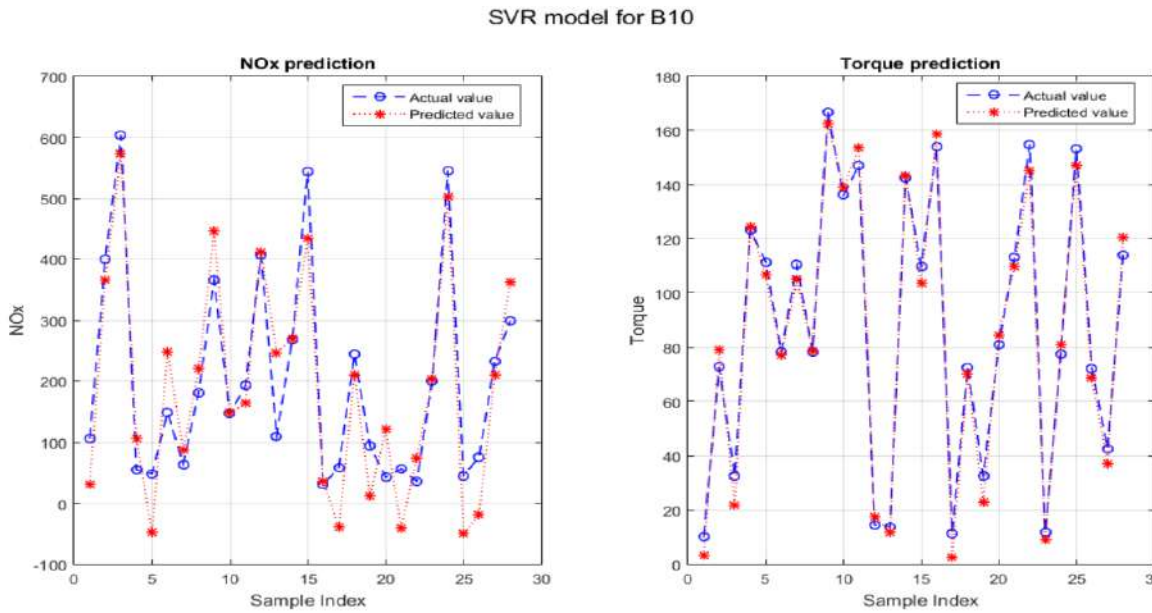

Fig. 8: Performance of SVR model for B10.

Table 7: Performance criteria on the testing set obtained by different techniques for B20.

Predicted parameter	Model	RMSE	MAPE	MAE	R
NOx	ANFIS	108.4337	0.8895	67.7203	0.7059
	ANN	83.5869	0.5381	49.9563	0.7040
	GRNN	99.4999	0.4343	53.3029	0.7706
	RBFN	150.7342	0.6662	85.4440	0.5930
	SVR	**60.8779**	**0.6113**	**49.1192**	**0.8910**
Torque	ANFIS	12.2276	0.1232	7.2107	0.9806
	ANN	3.8390	0.0813	2.6034	0.9973
	GRNN	12.5482	0.0682	5.2313	0.9840
	RBFN	79.5727	1.2715	62.7723	-1.7801e-16
	SVR	**7.9331**	**0.2259**	**6.1559**	**0.9917**

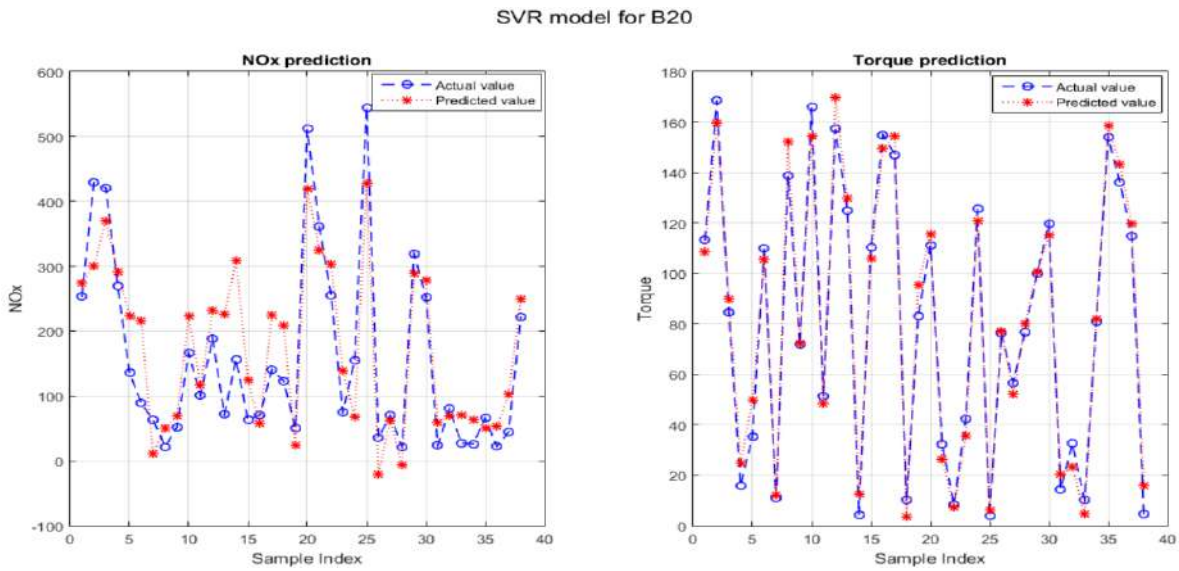

Fig. 9: Performance of SVR model for B20.

with biodiesel blends. Moreover, all the obtained results of developed models are highly correlated and precise. It can be concluded that the SVR-based model can be acceptable in serving as a forecasting method for operational parameters of the diesel engine.

CONCLUSIONS

In the study, the forecasting models based on ANFIS, ANN, GRNN, RBFN and SVR techniques were proposed for forecasting exhaust emissions and performance of a diesel engine fuelled with biodiesel blends. In the case application, The B0, B10 and B20 biodiesel blends were used in the Hyundai D4CB 2.5 engine. The engine operational parameters were used as inputs and the outputs include forecasting values of the torque and NOx emission. The obtained results showed that the SVR outperformed in all scenarios. These findings also demonstrated the remarkable advantage of ML-based techniques in forecasting for particular applications. The results of the present study also show that a comparative analysis of different techniques is always supportive in enhancing the performance of a forecasting model. This work can thus contribute to the development of selecting the best forecasting model for other purposes. For future research, we will develop and incorporate our forecasting model in a user-friendly software tool to make this forecasting task easier.

REFERENCES

Abe, S. 2005. Support Vector Machines for Pattern Classification. Springer, London, pp. 44.

Agarwal, D., Kumar, L. and Agarwal, A.K. 2008. Performance evaluation of a vegetable oil fuelled compression ignition engine. Renewable energy, 33(6): 1147-1156.

Alilou, V. K. and Yaghmaee, F. 2015. Application of GRNN neural network in non-texture image inpainting and restoration. Pattern Recognition Letters, 62: 24-31

Ata, R. and Koçyigit, Y. 2010. An adaptive neuro-fuzzy inference system approach for prediction of tip speed ratio in wind turbines. Expert Systems with Applications, 37(7): 5454-5460.

Batool, F., Adeel, S., Azeem, M., Khan, A. A., Bhatti, I.A., Ghaffar, A. and Iqbal, N. 2013. Gamma radiations induced improvement in dyeing properties and color fastness of cotton fabrics dyed with chicken gizzard leaves extracts. Radiation Physics and Chemistry, 89: 33-37.

Canakci, M., Ozsezen, A.N., Arcaklioglu, E. and Erdil, A. 2009. Prediction of performance and exhaust emissions of a diesel engine fueled with biodiesel produced from waste frying palm oil. Expert systems with Applications, 36(5): 9268-9280.

Caruana, R., Lawrence, S. and Giles, C.L. 2001. Overfitting in neural nets: Backpropagation, conjugate gradient, and early stopping. In: Advances in Neural Information Processing Systems, pp. 402-408.

Cigizoglu, H.K. and Alp, M. 2006. Generalized regression neural network in modelling river sediment yield. Advances in Engineering Software, 37(2): 63-68.

Do, Q.H. and Chen, J.F. 2013. A neuro-fuzzy approach in the classification of students' academic performance. Computational Intelligence and Neuroscience, 2013.

Do, Q.H., Tuan, T.T., Ha, L.T.T., Doan, T.T.H. and Nguyen, T.V.A. 2020. Development of artificial neural networks trained by heuristic algorithms for prediction of exhaust emissions and performance of a diesel engine fuelled with biodiesel blends. In: Applied Nature-Inspired Computing: Algorithms and Case Studies (pp. 275-253). Springer, Singapore.

Fakhrahmad, S.M., Rezapour, A.R., Jahromi, M.Z. and Sadreddini, M.H. 2012. A new fuzzy rule-based classification system for word sense disambiguation. Intelligent Data Analysis, 16(4): 633-648.

Ghanbari, M., Najafi, G., Ghobadian, B., Mamat, R., Noor, M.M. and Moosavian, A. 2015. Support vector machine to predict diesel engine performance and emission parameters fueled with nano-particles additive to diesel fuel. In IOP Conference Series: Materials Science and Engineering. IOP Publishing.

Guan, X., Zhu, Y. and Song, W. 2016. Application of RBF neural network improved by peak density function in intelligent color matching of wood dyeing. Chaos, Solitons & Fractals, 89: 485-490.

Hornik, K., Stinchcombe, M. and White, H. 1989. Multilayer feedforward networks are universal approximators. Neural Networks, 2(5): 359-366.

Jang, J.S.R., Sun, C.T. and Mizutani, E. 1997. Neuro-fuzzy and soft computing - A computational approach to learning and machine intelligence [Book Review]. IEEE Transactions on automatic control, 42(10): 1482-1484.

Jang, J.S. 1993. ANFIS: adaptive-network-based fuzzy inference system. IEEE Transactions on Systems, Man, and Cybernetics, 23(3): 665-685.

Ji, X., Shang, X., Dahlgren, R.A. and Zhang, M. 2017. Prediction of dissolved oxygen concentration in hypoxic river systems using support vector machine: a case study of Wen-Rui Tang River, China. Environmental Science and Pollution Research, 24(19): 16062-16076.

Jiang, J., Cao, D. and Chen, H. 2016. Boundary value problems for fractional differential equation with causal operators. Applied Mathematics and Nonlinear Sciences, 1(1): 11-22.

Funahashi, K.I. 1989. On the approximate realization of continuous mappings by neural networks. Neural networks, 2(3): 183-192.

Kim, S. and Kim, H.S. 2008. Neural networks and genetic algorithm approach for nonlinear evaporation and evapotranspiration modeling. Journal of hydrology, 351(3-4): 299-317.

Liu, Z., Zuo, Q., Wu, G. and Li, Y. 2018. An artificial neural network developed for predicting of performance and emissions of a spark ignition engine fueled with butanol–gasoline blends. Advances in Mechanical Engineering, 10(1).

Mamilla, V.R. and Rao, G.L.N. 2016. Optimal performance and emission analysis of diesel engine fuelled with palm oil methyl ester with an artificial neural network. American Journal of Modern Energy, 2(4): 17-21.

Meher, L.C., Sagar, D.V. and Naik, S.N. 2006. Technical aspects of biodiesel production by transesterification - A review. Renewable and Sustainable Energy Reviews, 10(3): 248-268.

Meyer, D., Leisch, F. and Hornik, K. 2003. The support vector machine under test. Neurocomputing, 55(1-2): 169-186.

Nauck, D., Klawonn, F. and Kruse, R. 1997. Foundations of Neuro-Fuzzy Systems. John Wiley & Sons, Inc.

Noor, R.M. 2014. Recent developments of neural networks in biodiesel applications. In: International Conference on Swarm, Evolutionary and Memetic Computing, pp. 339-350, Springer, Cham.

Ramadhas, A. S., Jayaraj, S. and Muraleedharan, C. 2005. Biodiesel production from high FFA rubber seed oil. Fuel, 84(4): 335-340.

Shailaja, M. and Raju, A.S.R. 2017. Neural network - Based diesel engine emissions prediction for variable injection timing, injection pressure, compression ratio and load conditions. In: Emerging Trends in Electrical, Communications and Information Technologies. Springer, Singapore, pp. 109.

Singh, T.N., Kanchan, R., Verma, A.K. and Saigal, K. 2005. A comparative study of ANN and neuro-fuzzy for the prediction of dynamic constant of rockmass. Journal of Earth System Science, 114(1): 75-86.

Sugeno, M. 1985. An introductory survey of fuzzy control. Information sciences, 36(1-2): 59-83.

Takagi, H. and Hayashi, I. 1991. NN-driven fuzzy reasoning. International Journal of Approximate Reasoning, 5(3): 191-212.

Van Gerpen, J. 2005. Biodiesel processing and production. Fuel Processing Technology, 86(10): 1097-1107.

Wei, M., Bai, B., Sung, A. H., Liu, Q., Wang, J. and Cather, M.E. 2007. Predicting injection profiles using ANFIS. Information Sciences, 177(20): 4445-4461.

Yaseen, Z. M., Jaafar, O., Deo, R. C., Kisi, O., Adamowski, J., Quilty, J. and El-Shafie, A. 2016. Stream-flow forecasting using extreme learning machines: a case study in a semi-arid region in Iraq. Journal of Hydrology, 542: 603-614.

Yusof, N., Ahmad, N.B., Othman, M.S. and Mohammad, F.A. 2012. A concise fuzzy rule base to reason student performance based on rough-fuzzy approach. In Fuzzy inference system–theory and applications. INTECH Open Access Publisher, pp. 63.

Nature Environment and Pollution Technology
An International Quarterly Scientific Journal

p-ISSN: 0972-6268
(Print copies up to 2016)
e-ISSN: 2395-3454

Vol. 20 | No. 2 | pp. 875-880 | 2021

Original Research Paper

https://doi.org/10.46488/NEPT.2021.v20i02.050

Open Access Journal

A New Approach for Environmental Modelling of LULC Changes in Semi-arid Regions of Anantapur District, Andhra Pradesh, India Using Geospatial Techniques

B. Pradeep Kumar*, K. Raghu Babu*†, P. Padma Sree, M. Rajasekhar* and M. Ramachandra***
*Department of Geology, Yogi Vemana University, Kadapa, Andhra Pradesh, India
**Department of Geology, Government College (A), Anantapur, Andhra Pradesh, India
†Corresponding author: K. Raghu Babu; dr.kraghu@gmail.com

Nat. Env. & Poll. Tech.
Website: www.neptjournal.com

Received: 04-05-2020
Revised: 23-07-2020
Accepted: 27-08-2020

Key Words:
LULC
Satellite data
NDVI
Ecosystem degradation
Remote Sensing and GIS

ABSTRACT

This study aims to define the changing pattern of land use and its geo-environmental impacts on the semi-arid region of Anantapur district of AP state, India. Satellite imageries were analysed to perceive the variations in land use and land cover in the past 9 years from 2010 to 2019. RS and GIS modelling has helped in the mapping of land use and land cover changes. The study has assumed five characteristic features, they are (i) Waterbodies, (ii) Vegetation, (iii) Fallow land, (iv) Cultivation lands, and (v) Degraded lands. The results reveal that, from 2010 to 2019, there is a decrease in water bodies, vegetation and fallow lands of 6.75 km^2, 42.96 km^2 and 105.45 km^2 respectively. While cultivation lands and degraded lands increased to 4.7 km^2 and 105.45 km^2 respectively. The environmental ecosystem is disturbed due to the increase in degraded lands, thus making the study area turn into a desert. Normalized Differential Vegetation Index (NDVI) and Soil Adjusted Vegetation Index (SAVI) are very useful for the accuracy assessment of vegetation, cultivation land and waterbodies in this LULC change detection studies.

INTRODUCTION

Geo-environment, not only from the environmental point of view but also in relative social pecuniary aspect has a specific perception in the human life. The role of the geo-environment in the aforesaid aspects has been undervalued and we are still far from exploiting it to its full extent. An empathetic of the possessions of the Earth's resources and their undercurrents is vital for unravelling difficulties in fluctuating fields, such as soil, air, water contamination, soil destruction, waste disposal and construction provisions and foundations (Senthil 2013, Badapalli et al. 2019). Empathetic geological and geomorphological processes are also important to other parts of the study including the progression and alleviation of natural and man persuaded threats and jeopardizes, land protection and renovation, landscape and urban planning, ecosystem inventories and natural heritage assessments (Chao et al. 2004, Rawat et al. 2013).

Land Use and Land Cover (LULC) are often blended. This is somewhat logical for the reason that both terms are scarcely related and to more or less scope even overlap. In this normal state, land cover systematizes a flawless arrival of the environmental equilibrium among parent rock, climatic ailment, soil, and vegetation. Landcover eminent in various categories i.e., area of vegetation, bare soil, rock outcrops, wet and water bodies etc. in simple terms land cover is the result of observation. Land use denotes land cover but differs in relations to its socio-economic persistence and global use (Harshika & Sopan 2012). This is in pure contrast with land cover as stated above which is most expressive and deals with physical observations. Land use may differ in nature and intensity, with the purpose it dealt with during the physical observations (Dewan et al. 2009, Anees et al. 2014, Kumar et al. 2020). Land use varies from land cover for the reason intentional on and role of people to familiarize the natural land cover to their assistances.

Geographical Information System (GIS) epitomizes a commanding set of tools for gathering, filament, recovering and presenting spatial data from the real world. Remote Sensing (RS) from airborne and spaceborne platforms delivers appreciated data for mapping, geo-environmental monitoring (Babu et al. 2012). The incorporation of RS and GIS modelling technologies in the field of environmental protection is inevitable and assists in decision making.

STUDY AREA

The present study region falls under semi-arid provinces of Anantapur district (13°40' and 15°15' Northern latitude and 76°50' and 78°30' Eastern longitude) which falls within

the rain shadow range of Western Ghats, in the interior of Deccan Plateau (Fig. 1). The district is circumscribed by Kurnool District in the north Kadapa District in the north-east, Chittoor District in the south-east, and Karnataka State in the West. Two main rivers flows over the study region, one is Hagari/Vedavathi and another one is Penna River. There are two seasons in the study region, they are South-west monsoon (June-September), and the North-east monsoon (October to December). Hot weather from March to May and the cold period from January to February.

DATA AND METHODOLOGY

Data Acquired

1. SOI (Survey of India) topo sheet no. 57F/1, 57F/2, 57F/5, 57F/6, 57B/13 and 57B/14.
2. Landsat imageries of three dissimilar periods i.e.,2010 and 2019 have taken freely from USGS earth explorer site (http://earthexplorer.usgs.gov/) and from NRSC site (http://bhuvan.nrsc.gov.in). with the resolution of 30m and 15m, datum WGS 1984 and UTM zone 44N.

Software Used

1. ERDAS imagine 2014
2. ArcGIS

Methodology

The data sets were improved in ERDAS Imagine 2014, satellite image processing software to create a false colour composite (FCC). The layer stack option in the image interpreter toolbox was used to generate FCCs for the study regions. The sub-setting of satellite images were performed for extracting study region from both images by taking geo-referenced outline boundary for better classification of LULC through Unsupervised option, NDVI and SAVI were also adopted to assess the vegetation and water bodies in the classification.

RESULTS AND DISCUSSION

LULC Change Detection and Analysis

For the execution of LULC change detection, a supervised classification method was engaged. A pixel-based evaluation was cast-off to collect the transformation info on pixel base and hence, infer the variations more precisely. Classified image pairs of the two-fold dissimilar period (2010 to 2019) information are linked by means of cross-tabulation in order to determine qualitative and quantifiable variation features. A change matrix (Babu et al. 2012, Kumar et al. 2018 & 2019, Rajasekhar et al. 2019) was shaped with the help of ERDAS imagine 2014 software. Measurable extent data of the complete LULC variations as well as increases and upset in apiece category between 2010 and 2019 were compiled.

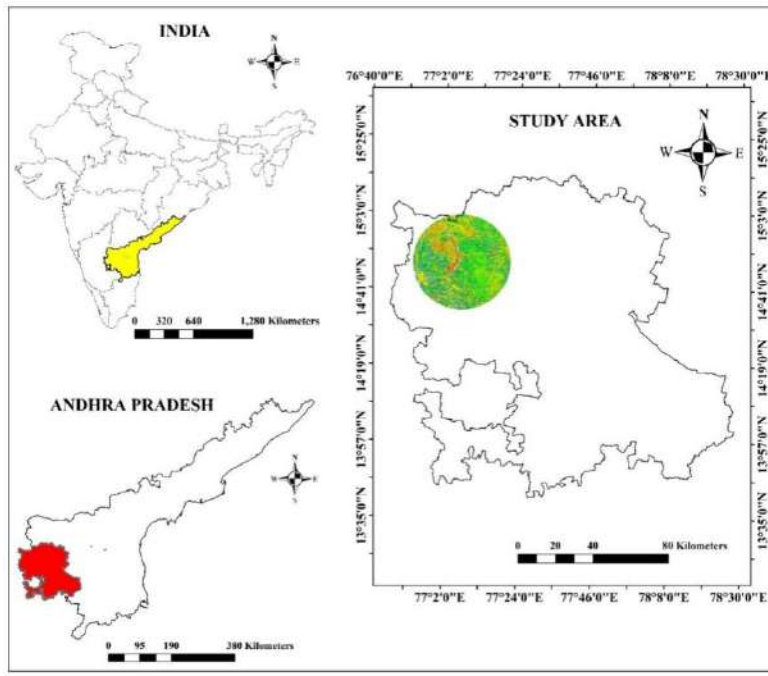

Fig. 1: Location map.

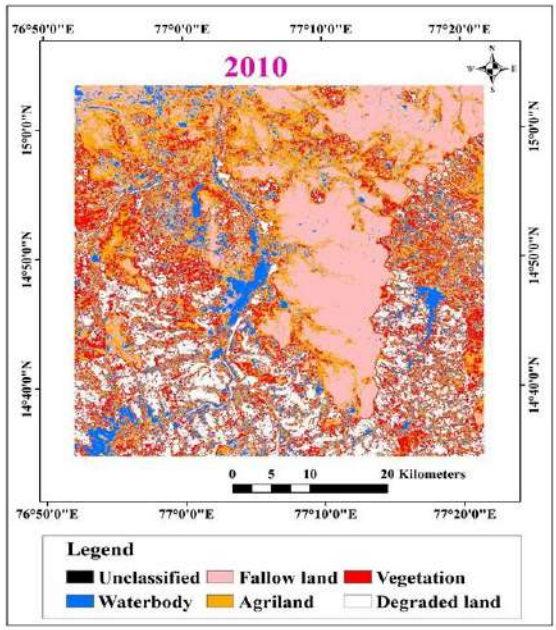

Fig. 2: 2010 LULC

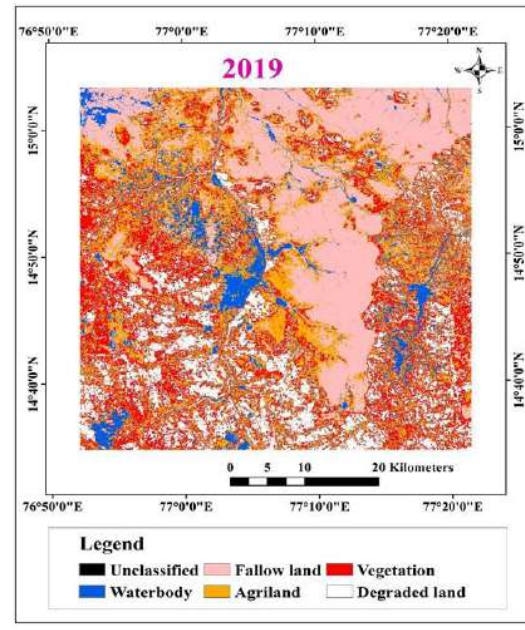

Fig. 3: 2019 LULC

Accuracy Assessment of LULC Using NDVI and SAVI

NDVI and SAVI techniques have been adopted for the accuracy assessment of vegetation, cultivation land, and waterbodies existing in the study region examination for the LULC change detection. NDVI is involved in the examination of vegetation and cultivation land, and SAVI for water bodies assessment. Both the techniques were used to assess, whether vegetation, cultivation land and waterbodies extended in the unsupervised classification are identical to the NDVI and SAVI categorized areas or not. Fig. 4 and Fig. 5 depict the NDVI and SAVI respectively. The results revealed that both the unsupervised and NDVI, SAVI are almost the same.

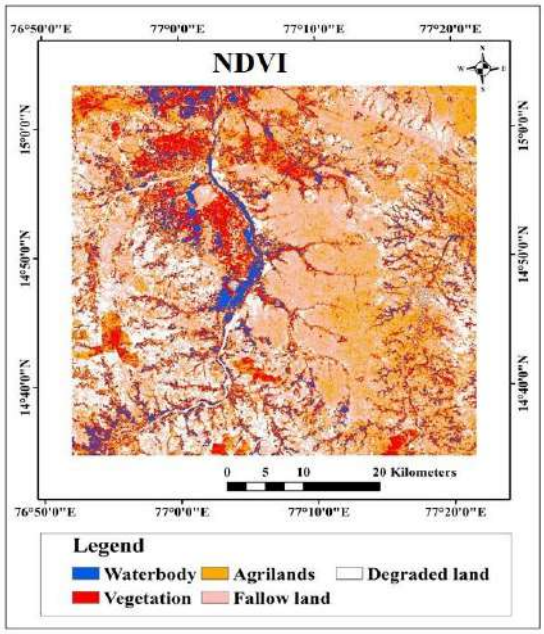

Fig. 4: NDVI

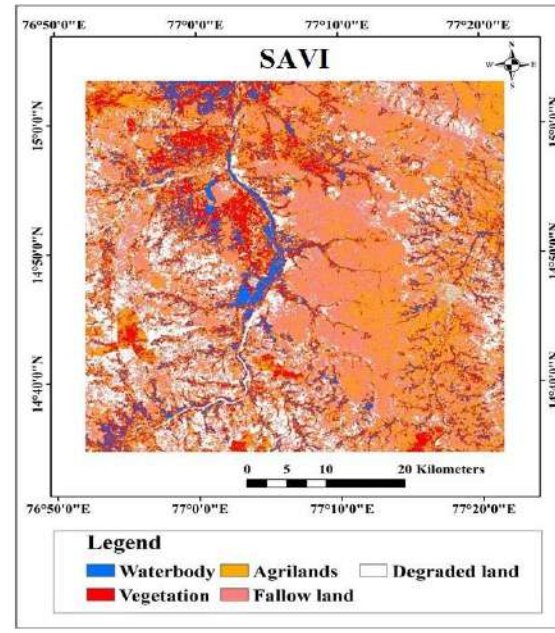

Fig. 5: SAVI

NDVI

Established on the values of NDVI and in relation to the Google Earth imageries to classify and enumerate the vegetation change during the period of 2010 and 2019 (Fig. 2 and Fig. 3), have been applied to five classes i.e., Waterbody, Vegetation, Cultivation land, Fallow land, and Degraded lands. This was carried out in ERDAS imagine 2014, with the formula or combination of bands given below.

NDVI = (near-infrared (NIR) band – RED band) /(near-infrared (NIR) band + RED band) ...(1)

near-infrared (NIR) band and the RED band are the reflectance radiated in the NIR band 7 and the visible red 5 (0.8-1.1 µm and 0.6-0.7 µm) waveband of the Land sat 8. The procedure of the NDVI in the ERDAS imagine software is shown in Fig. 6.

SAVI

In the present study, the computed SAVI is used to evaluate the variations in surface porousness between 2010 and 2019. Usually, SAVI specifies waterbody, vegetation, and cultivation exposure and health with respect to saturation, soil colour, and moisture therefore accounts for the high inconsistency areas. SAVI correspondingly controls the influence of soil brightness in NDVI and thus, minimizes soil brightness related noise in vegetation coverage estimation. Since coverage, brightness, and health of vegetation are strappingly related to surface permeability, SAVI delivers a significant proxy for the identification of impermeable surfaces. Calculations of SAVI could be done through the formula.

SAVI = ((NIR – RED)/(NIR+RED+L)) * (1+L) …(2)

Where RED is the reflectance of band 3 and NIR is the reflectance value of the near-infrared band (Band 4). L is the soil brightness correction factor. For dense vegetation and highly permeable surface areas, L = 0 and for vegetation scarce and impermeable surface areas, L = 1. The procedure of the SAVI in the ERDAS imagine software is shown in Fig. 7.

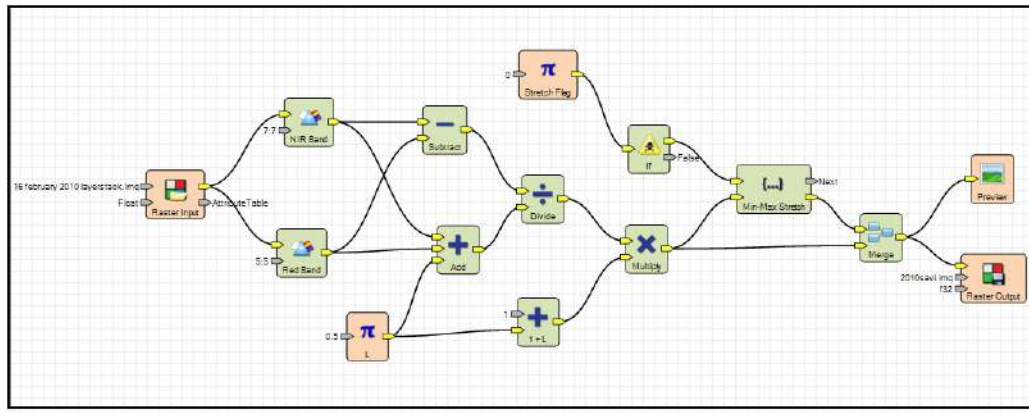

Fig. 6: NDVI bands in ERDAS imagine software.

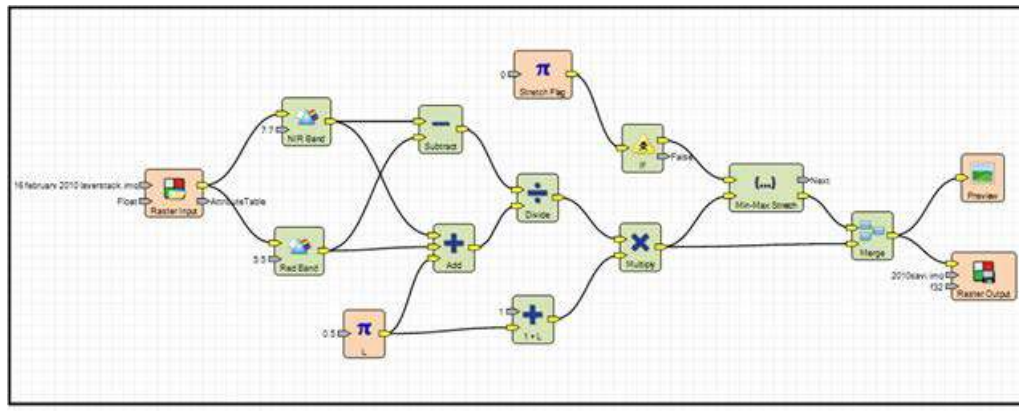

Fig. 7: SAVI bands in ERDAS imagine software.

Table 1: statistical calculation.

LULC categories	2010		2019		Changes from 2000-2019	
	km^2	Percentage%	km^2	Percentage	km^2	Percentage
waterbody	207.06	7.43	200.31	7.18	- 6.75	- 0.25
Vegetation	793.92	28.49	750.96	26.95	- 42.96	- 1.54
Agri land	671.07	24.08	675.77	24.25	4.70	0.17
Fallow land	589.24	21.14	483.79	17.36	-105.45	- 3.78
Degraded land	524.94	18.84	675.40	24.24	150.46	5.40
	2,786.23	100	2,786.23	100		

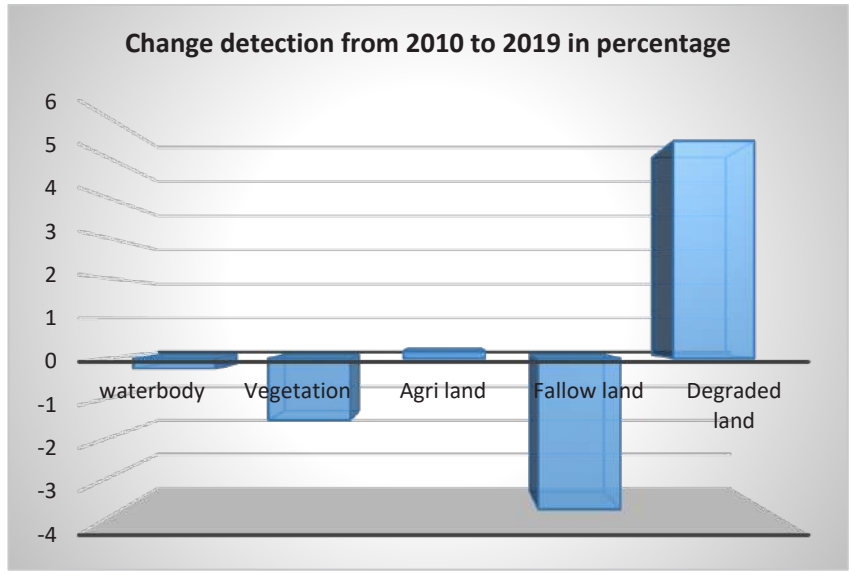

Fig. 8: Change detection from 2010 to 2019.

LULC Status

LULC classification results obtained from 2010 to 2019 were shown in Table 1. Waterbody has calculated as 207.06 km^2 in the year 2010 and it is decreased to 200.31 km^2 in the year 2019. Vegetation is calculated as 793.92 km^2 in the year 2010 and it is decreased to 750.96 km^2 in the year 2019. There is little increase in Cultivation land, i.e., 671.07 km^2 in the year 2010 and in the year 2019 it is increased to 675.77 km^2. Fallow land and is calculated as 589.24 km^2 in the year 2010 and it is decreased to 483.79 km^2 in the year 2019. Degraded land is increased at alarming rates and it is calculated as 524.94 km^2 in the year 2010 and it is increased to 675.40 km^2 in the year 2019. Fig. 8 shows the graphical representation of LULC and its impact on geo-environmental changes in the percentage during the decade, i.e. 2000 to 2019.

CONCLUSION

This study evaluated land use patterns, major improvement activities and environmental influences of land-use change in the study region over the past 9 years using an integrated method of Remote Sensing and GIS modelling. Fallouts evidently reveal that LULC variations were significant throughout the period from 2010 to 2019. There is a negative sign in certain factors like the decrease in waterbodies is noticed (0.25 %) there also a prominent decrease in vegetation, fallow land (1.54 % and 3.78 % respectively). Positive sign observed in Cultivation land with an increase of 0.17%. Degraded land is increased at an alarming rate (5.4%) and it is a negative sign for the environmental ecosystem immanence. Most of the people living in these villages are getting migrated to other villages or towns for their livelihood. This may lead to an environmental ecosystem imbalance. Our results clearly reveal this severe condition through the NDVI and SAVI in relation to that of the unsupervised classification studies. Geospatial techniques like RS and GIS provide pointers on tools to monitor, approximation, appraise and achieve supervisory factors on the environmental imperils to save the life and the society.

ACKNOWLEDGEMENT

B. Pradeep Kumar, greatly thankful to the Department of Science and Technology (DST), Government of India, for financial support through Inspire programme (Sanction order No. DST/INSPIRE Fellowship/2017/IF170114). Also thankful to USGS for remote sensing data utilization, Department of Geology, Yogi Vemana University, for necessary facilities for carrying out the research work.

REFERENCES

Anees, M. T., Javed, A. and Khanday, M. Y. 2014. Spatio-temporal land cover analysis in Makhawan Watershed (MP), India through remote sensing and GIS techniques. Journal of Geographic Information System, 6(4): 298-306.

Babu, K. R. and Raju, G. S. 2012. Application of remote sensing for delineation of uranium bearing Vempalli dolomites in and around Tummalapalli area, Cuddapah Basin, India. International Journal of Geomatics and Geosciences, 2(3): 842-852.

Badapalli, P. K., Raghu Babu, K., Rajasekhar, M. and Ramachandra, M. 2019. Assessment of aeolian desertification near Vedavathi river channel in Central part of Andhra Pradesh: Remote Sensing Approach, Remote Sensing of Land, 3(1): 39-49.

Chao, H.A.N. 2004. Some research advances and methods on detecting land cover change by remote sensing. Journal of Arid Meteorology, 22(2): 76-81.

Dewan, M. Ashraf, Yamaguchi Yasushi, 2009. Land use and land cover change in Greater Dhaka, Bangladesh using remote sensing to promote sustainable urbanization. Applied Geography Journal, 29: 390-401.

Harshika and Sopan I. 2012. Land use land cover classification and change detection using high resolution temporal satellite data. Journal of Environment, 1(4): 146-15.

Kumar, B. P., Babu, K. R., Rajasekhar, M. and Ramachandra, M. 2019. Assessment of land degradation and desertification due to migration of sand and sand dunes in Beluguppa Mandal of Anantapur district (AP, India), using remote sensing and GIS techniques. J. Ind. Geophys. Union, 23(2): 173-180.

Kumar, B. P., Raghu Babu, K., Rajasekhar, M., Narayana Swamy, B. and Ramachandra, M. 2019. Landuse/landcover changes and geo-environmental impacts on Beluguppa Mandal of Anantapur District of Andhra Pradesh, India, using remote sensing and GIS modelling. Research & Reviews: Journal of Space Science & Technology, 8(2): 6-15.

Kumar, B.P., Babu, K.R., Rajasekhar, M. et al. 2020. Identification of land degradation hotspots in semiarid region of Anantapur district, Southern India, using geospatial modelling approaches. Model. Earth Syst. Environ. 6: 1841-1852. https://doi.org/10.1007/s40808-020-00794-x.

Rajasekhar, M., Raju, G.S. and Raju, R.S. 2019. Data on artificial recharge sites identified by geospatial tools in semi-arid region of Anantapur District, Andhra Pradesh, India. Data Brief, 19: 462-474.

Rawat, J. S., Biswas, V. and Kumar, M. 2013. Changes in land use/cover using geospatial techniques: A case study of Ramnagar town area, district Nainital, Uttarakhand, India. The Egyptian Journal of Remote Sensing and Space Science, 16(1): 111-117.

Senthil, S., Arivazhagan, S. and Rangarajan, N. 2013. Remote sensing and GIS applications in environmental science. J. Environ. Nanotechnol, 2: 292-101. doi:10.13074/jent.2013.06.132025.

Nature Environment and Pollution Technology
An International Quarterly Scientific Journal

p-ISSN: 0972-6268
(Print copies up to 2016)
e-ISSN: 2395-3454

Vol. 20 | No. 2 | pp. 881-889 | 2021

Original Research Paper

https://doi.org/10.46488/NEPT.2021.v20i02.051

Open Access Journal

Coordination Relationship Between Green Innovation Efficiency and Environmental Protection: Evidence From the Yangtze River Economic Belt

Na Hou, Zhi Zeng, Qianying Zhu, Dahong Zhang and Wenwen Liu†
School of Economics and Management, Beijing Forestry University, Beijing 100083, China
†Corresponding author: Wenwen Liu: wenwensummer@163.com

Nat. Env. & Poll. Tech.
Website: www.neptjournal.com

Received: 27-02-2021
Revised: 13-04-2021
Accepted: 25-04-2021

Key Words:
Green innovation efficiency
Environmental protection
Yangtze river economic belt
Ecological environment

ABSTRACT

Green innovation plays an important role in coordinating the relationship between ecological environment and economic development and has become a new driving force for the development of a resource-saving and environment-friendly economy. To explore the effects and logic of innovation efficiency and environmental protection, using the inter-provincial (city) panel data of the Yangtze River Economic Belt from 2007 to 2017 in China, the green innovation efficiency and environmental protection level of the upper, middle, and lower reaches of the Yangtze River Economic Belt were analyzed. Results show that the overall environmental protection level of the Yangtze River Economic Belt is on the rise. From a regional perspective, the environmental protection level in the upper reaches is the highest, which is greater than the overall level of the Yangtze River Economic Belt, followed by the lower and middle reaches, which are less than the overall level of the Yangtze River Economic Belt. The efficiency of green innovation has promoted the overall environmental protection level of the Yangtze River Economic Belt, inhibited the environmental protection level in the downstream areas, promoted the environmental protection level in the upstream areas, and has no obvious impact on the environmental protection level in the middle reaches. Further mechanism analysis shows that the possible transmission path of green innovation efficiency to environmental protection is as follows: green innovation efficiency promotes the environmental protection level by improving the ecological environmental efficiency. The robustness of the above conclusion is tested, and it has good robustness. The research conclusions of this study provide reliable empirical evidence and policy enlightenment for the development and optimization of green innovation efficiency and the realization of green innovation efficiency driving environmental protection.

INTRODUCTION

Green innovation efficiency is the key factor to maintain economic growth. After the economic development of developing countries has gone through the barbaric stage of economic growth in exchange for resources and the environment, ecological problems have become increasingly exposed and have severely limited the quality of economic growth and the quality of life of people. The importance of dynamic reconciliation of contradictions among economy, society, and ecology has gradually become prominent. The manner by which to rationally and objectively measure the relationship among economic growth, social development, and the protection of the ecological environment and explore the dynamic balance between the three to promote the harmony of the whole society must be explored. Development has become an urgent question in the academic and practical fields at this stage and has further reached the national strategic level, thereby becoming an important strategic issue for countries to transform, develop, and adapt to a new environment. In the exploration of many developing countries, China's experience is remarkable, and it has provided other countries with a model for reference. In recent years, China's green innovation efficiency level has moved to the forefront of the former world. Many remarkable achievements have been made; however, many deficiencies exist in the level of environmental protection compared with developed countries, such as Japan, Canada, and the United States. On the one hand, China's green innovation efficiency activities have always been characterized by large quantity, low quality, and policy catering, resulting in the dilemma of low-end locking of green innovation efficiency technologies in the global agricultural modernization level and product industrial chain. On the other hand, the level of environmental protection in most areas of China is not high, and large regional differences are observed, with the south, central, and northeast being in a long-term imbalance and the southeast coast and northeast having a gradual deterioration in environmental protection. At present, these deficiencies in China's environmental protection have a major contribution to the unbalanced and insufficient development of the green innovation efficiency system, which has the functions

of amplification and acceleration, and its effects also have two sides, namely, improved efficiency and induced risks. Previous studies have also shown that green innovation efficiency has an important impact on the development of the ecological economy (Feng et al. 2018) and is the main way to effectively relieve environmental pressure. In the examination of green innovation efficiency, the role of the ecological environment is critical and even directly affects the trend of environmental protection. The efficiency and green orientations must be followed to avoid the impact of scientific and technological pollution on the environment, and the agricultural economy must be transformed to a green development state with green innovation efficiency (Li 2017). Therefore, the role of green innovation efficiency on environmental protection must be explored in the context of the actual situation of each region in the Yangtze River Economic Zone, and the possible paths of green innovation efficiency on environmental protection must be determined. The vitality of green innovation efficiency must be stimulated and green development of social economy in various regions of the Yangtze River Economic Belt must be promoted to provide theoretical completeness and practical operability for improving ecology.

PAST STUDIES

Environmental protection can not only promote long-term economic growth but also effectively drive the transformation of regional economic industrial structure to achieve high-quality economic development. Many studies on the mechanism by which to drive environmental protection have been conducted, and the core perspectives of the research are mainly divided into three categories: governmental perspective, environmental perspective, and environmental protection measurement. From the perspective of the government, this concept mainly includes agricultural supply-side structure (Li et al. 2020), agricultural support policy (Ma et al. 2020), industrial structure (Shi et al. 2019), industrial agglomeration (Xue et al. 2019), and land use (Lu et al. 2017). From the environmental perspective, this concept mainly focuses on environmental constraints (Wang et al. 2020), ecological compensation (He 2020), ecological cycle (Peng et al. 2019), and institutional environment. In the measurement of environmental protection, the environmental protection level of Tibet (Zhou 2019), the northeast of central and southern China, Zhejiang (Wei et al. 2018), and other regions is mainly measured. These studies illustrate that this concept must be supported from the aspects of the agricultural supply side, industrial structure, and institutional environment to promote a systematic project of environmental protection and the advancement of environmental protection.

Green innovation efficiency will directly cooperate with environmental regulation to promote the environmental protection level, and the clear water and green mountains are equal to mountains of gold and silver (Duan et al. 2020). A large number of studies have shown that green innovation efficiency has an important impact on the development of the ecological economy and is the main way to effectively relieve environmental pressure. In the examination of green innovation efficiency, the role of the ecological environment is critical and directly affects the trend of environmental protection. The efficiency and green orientations are followed to avoid the impact of scientific and technological pollution on the environment, and the agricultural economy is transformed into a green development state with green innovation efficiency. At present, China's green innovation efficiency level lags behind the comprehensive development level of the ecological environment, especially in the northeast, central, and western regions of China, which are all regions with lagging green innovation efficiency level; This notion shows that the coordinated development level of green innovation efficiency and ecological environment is generally low with large differences between provinces, demonstrating a pattern of high in the east and low in the central and western regions. The efficiency of green innovation is the main driving force to promote the growth of the regional green economy (Wang 2013). The environmental protection level of the Yangtze River Economic Belt, a major developmental strategic region of the country, is related to the overall situation of the national ecological environment health. However, the overall green innovation efficiency level of the Yangtze River Economic Belt is low and relatively stable. This level is high in the east, low in the west and unchanged in the central region because of the limitation in scientific and technological investment and market environment factors. The positive impact of green innovation efficiency in the Yangtze River Economic Belt on ecological environmental efficiency has an obvious threshold effect, showing an inverted U-shaped change trend; however, it has not yet formed a long-term mechanism effect of positive interaction (Yan et al. 2019). The green innovation efficiency and green development index of the Yangtze River Economic Belt are generally rising, but the level is relatively low. The coordination degree of green innovation efficiency and green development in the Yangtze River Delta is higher than those in other regions (Wang et al. 2016).

This paper attempts to explore the impact of green innovation efficiency on environmental protection and clarify what role the ecological environment plays in green innovation efficiency and environmental protection and its internal mechanism, which helps promote the realization of green innovation technology, the improvement of the ecological

environment, and the development of green agriculture. The marginal contributions of this paper are as follows: First, the environmental protection level of the Yangtze River Economic Belt is measured, and the reasons for the differences are analyzed. Second, the environmental protection level verifies the relationship between green innovation efficiency and environmental protection. Third, the identification test is carried out based on the path of ecological environment mechanism by using the intermediary effect model to clarify the mechanism of green innovation efficiency on environmental protection.

MATERIALS AND METHODS

Model Design

Benchmark model construction: A basic regression model is constructed to analyze the impact of green innovation efficiency on environmental protection in the Yangtze River Economic Belt as a whole and in the upper, middle, and lower reaches of the region:

$$AGD_{it} = \beta_0 + \beta_1 \text{Technology}_{it} + \sum Control + \varepsilon_{it} \quad \ldots(1)$$

Where i means province, t means year, AGD_{it} is an explanatory variable that indicates environmental protection. $Technology_{it}$ is the core explanatory variable and represents the efficiency of green innovation. β_0 is a constant term. $\Sigma Control$ is a control variable and mainly includes the main factors affecting environmental protection: economic development level, government intervention, openness, urbanization rate, industrial modernization, higher educational level, governmental scale, marketization level, and openness. ε_{it} is the interference item.

Construction of the mediation model: This study first separately includes green innovation efficiency into the regression equation to test the mechanism of green innovation efficiency on environmental protection [Formula (2)]. Subsequently, the separate effect of green innovation efficiency on environmental protection is analyzed. Then, the effect of green innovation efficiency on the ecological environment is examined (Formula (3)). Finally, the ecological environment is incorporated into Formula (3), see Formula (4), to judge whether the efficiency of green innovation affects the level of environmental protection through the ecological environment. The specific model is as follows:

$$AGD_{it} = \beta_0 + \beta_1 \text{Technology}_{it} + \sum Control + \varepsilon_{it} \quad \ldots(2)$$

$$AEE_{it} = \alpha_0 + \alpha_1 \text{Technology}_{it} + \sum Control + \varepsilon_{it} \quad \ldots(3)$$

$$AGD_{it} = \pi_0 + \pi_1 \text{Technology}_{it} + \pi_2 \text{AEE}_{it} + \sum Control + \varepsilon_{it} \quad \ldots(4)$$

Where AEE_{it} represents the ecological environment. AGD_{it} and $\Sigma Control$ represent the explained and controlled variables, respectively, and their meanings are the same as those in Formula (1). β_1 reflects the total effect of green innovation efficiency on environmental protection. π_1 reflects the direct effect of green innovation efficiency on environmental protection. $\alpha_1\pi_2$ reflects the size of the mediation effect. The ratio of the mediation effect to the total effect is used to reflect the relative size of the mediation effect. Sobel statistics can be used to test the significance of the mediation effect.

Variable Setting

Explained variables: Environmental protection level. This variable involves society, economy, population, resources, ecological environment, and other aspects, and is a comprehensive concept, which mainly describes the response of various factors to the environmental protection level of each province. The DPSIR conceptual model is an evaluation model for measuring the sustainable development of the social environment, which can comprehensively summarize the above-mentioned aspects and accurately describe the relationship between human activities and the ecological environment. This model has the advantages of comprehensiveness, scientific, and systematic and is widely used in ecological resource and environmental impact analysis, water resource security evaluation, regional ecological environment security, and other fields. The DPSIR conceptual model is applied to the index system of environmental protection. The logic can be expressed as follows: The changes of potential factors, such as society, economy, population, resources, and ecological environment, are taken as the driving forces D; pressure is exerted on the ecological environment P; and the ecological environment is changed, causing the state S of the ecological environment to change and affecting the ecological environment I. These influences encourage human beings to respond to the ecological environment R and take certain measures. These responses R will affect the pressure P, driving force D, state S, and influence I. Therefore, this study draws lessons from the practices of Liu (2020) to apply the environmental protection evaluation model and entropy method to calculate the weight of each index. Moreover, the comprehensive evaluation method is adopted to weigh and sum the environmental protection indexes of each index to obtain the environmental protection values of each province in the Yangtze River Economic Belt from 2007 to 2017. The environmental protection index system is shown in Table 1.

Core Explanatory Variables

Green innovation efficiency. In this study, green innovation efficiency is expressed by comprehensive efficiency, which better reflects the relationship between the input and the

Table 1: Evaluation index system of environmental protection in provinces of Yangtze River Economic Belt.

Target Layer	Criteria layer	Indicator layer	
Environmental protection	Driving force (D)	Added value of primary industry	Per capita output value of agriculture, forestry, animal husbandry and fishery
		Per capita income of rural residents	Consumption level of rural residents
		Land output rate	
	Pressure (P)	Use amount of chemical fertilizer, pesticide and agricultural film per unit area	
		Proportion of disaster area to disaster area	
		Proportion of effective irrigation area	
	Status (S)	Agricultural water consumption	Output value of agricultural GDP per unit area
		Grain output per unit area	Water-saving irrigation area
		Road mileage per capita in rural areas	
	Impact (I)	Output of green agricultural products	Forest coverage
		Coverage rate of sanitary toilets	Qualified rate
		Wastewater discharge	
	Response (R)	Government Investment in Rural Water and Toilet Improvement	Industrial structure adjustment index
		Proportion of budget expenditure for energy conservation and protection	
		Research and experimental development personnel	Proportion of investment in environmental pollution control

output of green innovation efficiency. Innovation investment includes capital and manpower investment. This study selects the main investment of scientific and technological research and development, the number of scientific research personnel invested in scientific and technological research and development, and the total financial expenditure on science and technology as input variables. The output includes scientific, technological, economic, and social benefit outputs. This study selects patent level, new variety level, the annual growth rate of added value, the full-time equivalent of R&D personnel, the total number of published articles, patent authorization amount, invention patent authorization amount, the transaction amount of various technology contracts, profit of high-tech products, and non-governmental expenditure in scientific and technological activity expenditure. This study calculates the comprehensive efficiency value of green innovation efficiency of each province in the Yangtze River Economic Belt from 2007 to 2017.

Ecological environment. In this study, references are made to the ecological efficiency of German environmental and economic accounting account according to the requirements and realistic path of ecological environment development. The input indicators include resource consumption and environmental cost. This study selects human, financial, and material resources engaged in production to express, and environmental cost is expressed by material consumption (mainly including fertilizer, pesticide, agricultural film, and fuel input) that will cause pollution in production input. The

Table 2: Index system of ecological environmental efficiency.

Index system	System layer	Indicator layer	
	Unexpected output	Carbon emissions (kg)	
	Expected output	Total agricultural output value (100 million yuan)	
	Input	Manpower input	Number of Agriculture, Forestry, Animal Husbandry and Fishery (10,000)
		Material consumption	Total sown area of crops (thousands of hectares), total rural electricity consumption (KW.H), effective irrigation area (thousands of hectares), and total power of agricultural machinery (10,000 kilowatts)
		Consumption of financial resources	Agricultural investment (yuan)
		Environmental cost	Fertilizer usage (10,000 tons), agricultural film usage (10,000 tons), pesticide usage (10,000 tons) and agricultural diesel usage (10,000 tons).

output indicators are expressed by gross output value and carbon emissions. An input-output index system for evaluating ecological environmental efficiency is constructed to measure ecological environmental efficiency by using the non-radial super-efficiency EBM model proposed by Tone (2010) as a reference (Table 2).

Control variables: Based on previous research results, this study takes economic development level, government intervention degree, openness degree, urbanization rate, industrial modernization degree, higher education level, government scale, marketization degree, and opening level as control variables. The level of economic development is expressed by the actual GDP per capita. The degree of government intervention is expressed by general budget expenditure/GDP. The degree of industrial modernization is expressed by tertiary GDP/primary GDP. The level of higher education is expressed by the number of graduates from junior college or above. The scale of government is expressed by governmental consumption expenditure/GDP. The level of opening to the outside world is expressed by FDI/GDP. The degree of opening to the outside world is expressed by import and export/GDP.

Data Sources

According to the availability and integrity of data, this study selects 11 provinces (cities) belonging to the Yangtze River Economic Belt from 2007 to 2017 as the research objects. According to the national administrative division standard, the Yangtze River Economic Belt as a whole and the upper, middle, and lower reaches are divided. The upper reaches include Chongqing, Sichuan, Yunnan, and Guizhou, the middle reaches consist of Jiangxi, Hunan, and Hubei, and the lower reaches comprised Jiangsu, Shanghai, Zhejiang, and Anhui. All the data come from the provincial statistical yearbooks, science and technology statistical yearbooks, and the official website of the National Bureau of Statistics.

RESULTS ANALYSIS

Differences in Environmental Protection Levels in the Yangtze River Economic Belt and Their Causes

The following trend analysis is conducted to reveal the differences and causes of environmental protection levels in the three regions of the Yangtze River Economic Belt. Fig. 1 reflects the differences and evolution trends of environmental protection levels in the overall, upper, middle, and lower regions of the Yangtze River Economic Belt.

From the regional level, the environmental protection level in the upper reaches is the highest, followed by the lower and middle reaches. The environmental protection level in the upper reaches is greater than the overall level of the Yangtze River Economic Belt. Meanwhile, the environmental protection level in the lower and middle reaches is lower than the overall level of the Yangtze River Economic Belt. The possible reason is that the upstream areas are located in the western region of China. Although the economic level is low, the region has natural ecological advantages. The clear water and green are equal to mountains of gold and silver because the region is the ecological barrier area in China, highlighting the remarkable green ecological economy; thus, the environmental protection level is the highest. The lower reaches of the Yangtze River are located in the eastern region of China, with coastal location advantages and rapid economic development, attracting international advanced technology and first-class talents and taking the lead in realizing the transformation of economic development mode to green, ecological, and high-quality development through rapid human capital and material capital. Hence, the level of environmental protection takes second place. The middle reaches region is located in the central part of China. With the policy of the rise of the central region and its proximity to the lower reaches region, the area became the first choice for the transfer of pollution-intensive industries in the lower reaches region, virtually prompting the middle reaches region to exchange economic growth at the expense of the environment. This situation resulted in a rough industrial structural dependence path. Accordingly, the environmental protection level is the lowest.

Impact of Green Innovation Efficiency in the Yangtze River Economic Belt on Environmental Protection

The previous part reveals the regional differences and causes of environmental protection levels in the Yangtze River Economic Belt and various regions. This study aims to further explore the influencing factors of environmental

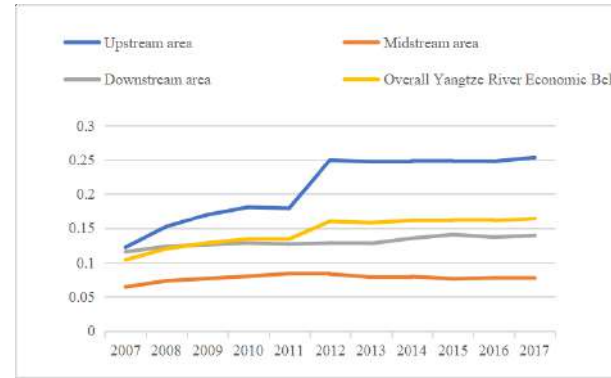

Fig. 1: Changes in the environmental protection level in the Yangtze River Economic Belt.

Table 3: Regression results of the impact of green innovation efficiency on environmental protection in the Yangtze River Economic Belt and the upper, middle, and lower reaches.

	Yangtze River Economic Belt	Downstream area	Midstream region	Upstream region
	(1)	(2)	(3)	(4)
	Environmental protection	Environmental protection	Environmental protection	Environmental protection
Green innovation efficiency	0.00103**	−0. 0138**	0.00188	0.131***
	(0.07)	(−2.28)	(0.38)	(4.33)
Economic development level	0.187***	0.0963***	0.00437	−0.133
	(2.90)	(4.38)	(0.25)	(−1.14)
Degree of government intervention	0.000990	0.000636	−0.000906*	−0.00730***
	(0.57)	(0.67)	(−1.72)	(−3.56)
Openness	0.00278***	0.0000803	0.000525	0.00570***
	(6.95)	(0.51)	(1.35)	(3.80)
Urbanization rate	−0.0124***	0.000434	−0.0000591	−0. 0103**
	(−4.06)	(0.58)	(−0.07)	(−1.97)
Degree of industrial modernization	−0.0000679	0.000201**	0.00751**	0.0265
	(−0.17)	(2.01)	(2.40)	(1.50)
Higher education level	0.00246**	0.00223***	−0.000285	0.00436
	(1.26)	(−7.72)	(−1.00)	(0.89)
Government size	−0.00442	0.000418	−0.000394	−0.0343***
	(−1.35)	(0.29)	(−0.64)	(−8.72)
Marketization degree	0.000877	0.00112**	−0.0000308	−0.00304
	(0.66)	(2.10)	(−0.06)	(−0.84)
Level of opening to the outside world	−0.0293***	−0.00382*	−0.0138***	−0.0346***
	(−6.08)	(−1.84)	(−4.42)	(−2.67)
Constant term	−1.306**	−0.827***	0.0834	1.847**
	(−2.54)	(−4.46)	(0.58)	(2.25)
N	121	44	33	44

Note: *, ** and *** represent $P < 0.1$, $P < 0.05$ and $P < 0.01$, respectively

protection levels in the Yangtze River Economic Belt and various regions. A reasonable explanation for the regional differences affecting the environmental protection level of the Yangtze River Economic Belt can be obtained by analyzing the changes of the coefficients of various influencing factors in different regions of the Yangtze River Economic Belt from 2007 to 2017. Accordingly, the coordinated improvement of the environmental protection level in the development process of the Yangtze River Economic Belt is advanced. Table 3 lists the regression results of the impact of green innovation efficiency on the environmental protection level in the Yangtze River Economic Belt as a whole and various regions.

Column (1) in Table 3 reports the regression results of the impact of green innovation efficiency on the overall environmental protection of the Yangtze River Economic Belt. The results show that the coefficient of green innovation efficiency is considerably positive at the 5% level. This result indicates that the green innovation efficiency of the Yangtze River Economic Belt has promoted environmental protection. The possible reason is that the green innovation efficiency can promote the economic growth of the Yangtze River Economic Belt in the face of environmental constraints and improve the environmental quality and environmental protection level. The coefficient of economic development level is significantly positive at the 1% level. This notion shows that the economic development level of the Yangtze River Economic Belt has promoted environmental protection. The possible reason is that the economic development level is better, which can gather more high-level human capital and attract more high-green innovation efficiency enterprises, and the government's environmental protection supervision will

be stronger, thereby effectively improving the environmental protection level. The openness coefficient is considerably positive at the 5% level. This result shows that the improvement of the openness of the Yangtze River Economic Belt has promoted the environmental protection level. The possible reason is that the improvement of openness can attract more high-tech enterprises, eliminate local backward production enterprises, introduce environment-friendly scientific and technological equipment and advanced technology level, save energy, and reduce emissions. This situation is conducive to the improvement of environmental protection level. The coefficient of higher educational level is drastically positive at the 5% level, which indicates that the improvement of educational level in the Yangtze River Economic Belt can promote the environmental protection level. The possible reason is that the improvement of educational level can increase people's awareness and behavior of environmental protection and promote the environmental protection level.

Analysis of the Differences Among the Lower, Middle and Upper Reaches

Columns (2), (3) and (4) in Table 3 are the comparison of the impact of green innovation efficiency on environmental protection in the lower, middle, and upper reaches of the Yangtze River. Column (2) results show that the coefficient of green innovation efficiency is negative at the 5% level. This result shows that the efficiency of green innovation has a meaningful inhibitory effect on the environmental protection level in the downstream areas. The possible reason is that the proportion of secondary industry in the downstream areas continues to rise. Industrial pollution is one of the main sources of ecological environment pollution. Excessive industrial pollution aggravates the pollution of the ecological environment, resulting in a lower level of environmental protection in the downstream areas. Column (3) results show that the coefficient of green innovation efficiency is not significantly positive. This notion shows that the efficiency of green innovation has no obvious promotion effect on the environmental protection level in the middle reaches. The logic behind this may be that the middle reaches are close to the lower reaches and are the first choice for the transfer of pollution-intensive industries in the eastern region, such as paper industry, chemical industry, building materials industry, and other industries, which have degraded the ecological environment in the middle reaches. Column (4) results show that the coefficient of green innovation efficiency is clear positive at the 1% level. This notion shows that the efficiency of green innovation can promote the environmental protection level in upstream areas. The upstream area is typical mountain agriculture with inconvenient transportation, less industrial transfer in the east, and a relatively high proportion of primary industry. In addition, this area is China's ecological barrier and functional area, and the environmental protection level is better. Therefore, the environmental protection level is promoted.

Mechanism of Green Innovation Efficiency on Environmental Protection

The coefficient of green innovation efficiency in column (1) of Table 4 is positively at the 1% level, thus indicating that green innovation efficiency has greatly enhanced the improvement of ecological environmental efficiency. Green innovation efficiency promotes technological progress, brings advanced technological level to economic development, and realizes modernization level, thus promoting the improvement of ecological environmental efficiency. The coefficient of green innovation efficiency in column (2) is significantly positive at the 1% level, which indicates that green innovation efficiency is very effective in accelerating the improvement of environmental protection level. Green innovation efficiency promotes environmental protection by improving production methods, increasing land output efficiency, reducing rural environmental pollution, promoting green, organic, and high-quality agricultural products, completing the rural toilet revolution, and increasing forest and grass coverage. Column (3) shows that the ecological environmental coefficient is considerably positive at the 1% level, which indicates that the improvement of ecological environmental efficiency significantly promotes the level of environmental protection. The coefficient of green innovation efficiency is appreciably positive at the 10% level. The comparison of the green innovation efficiency coefficients in column (2) indicated that the variable coefficient of green innovation efficiency is smaller (from 0.127 to 0.0758) after ecological environmental efficiency variables are added to column (3). The significance also decreased by a noticeable percentage (from 1% to 10%), that is, the promotion of green innovation efficiency to environmental protection weakened with the addition of ecological environmental efficiency variables. This notion indicates that ecological environmental efficiency plays an important intermediary effect between green innovation efficiency and environmental protection. Accordingly, a positive transmission path of "green innovation efficiency (improving) ecological environmental efficiency (promoting) environmental protection level" has been formed.

CONCLUSION

Based on the panel data of provinces and cities in the Yangtze River Economic Belt from 2007 to 2017, this study analyzes the change trend and causes of environmental protection

Table 4: Transmission mechanism of green innovation efficiency to environmental protection in Yangtze River Economic Belt

	Yangtze River Economic Belt			Upstream region		
	(1)	(2)	(3)	(4)	(5)	(6)
	Ecological efficiency	Environmental protection	Environmental protection	Ecological efficiency	Environmental protection	Environmental protection
Ecological environment efficiency			0.324***			0.198**
			(2.90)			(2.49)
Green innovation efficiency	0.159***	0.127***	0.0758*	0.210***	0.196***	0.154***
	(5.11)	(3.36)	(1.87)	(3.06)	(5.09)	(3.90)
Economic development level	0.189*	-0.660***	-0.736***	-0.0571	-0.151*	-0.140*
	(1.70)	(-4.67)	(-5.19)	(-0.36)	(-1.71)	(-1.69)
Degree of government intervention	-0.00771*	-0.00597	-0.00334	0.0178***	0.00315	-0.000365
	(-1.85)	(-1.35)	(-0.72)	(2.85)	(0.90)	(-0.10)
Openness	-0.00344***	-0.00448***	-0.00343***	-0.00556	-0.00129	-0.000195
	(-4.59)	(-4.74)	(-3.46)	(-1.47)	(-0.61)	(-0.10)
Urbanization rate	0.0151**	0.0508***	0.0463***	-0.00751	0.000844	0.00233
	(2.26)	(6.46)	(5.88)	(-0.77)	(0.15)	(0.45)
Degree of industrial modernization	-0. 00210**	0.000175	0.000834	-0.148***	-0.131***	-0.102***
	(-2.53)	(0.19)	(0.86)	(-2.78)	(-4.36)	(-3.34)
Higher education level	0.00574	0.00482	0.00335	0.0313**	0.0179**	0.0117
	(1.51)	(0.98)	(0.70)	(2.31)	(2.35)	(1.55)
Government size	-0.0119*	-0.0241***	-0.0207***	-0.0271***	-0.0270***	-0.0216***
	(-1.95)	(-3.10)	(-2.75)	(-2.89)	(-5.13)	(-4.03)
Marketization degree	0.0000800	-0.0109***	-0.0110***	0.0261**	0.00714	0.00198
	(0.03)	(-3.35)	(-3.54)	(2.55)	(1.24)	(0.34)
Level of opening to the outside world	-0.0100	-0.0309***	-0. 0271**	0.00678	0.00181	0.000467
	(-1.07)	(-2.61)	(-2.38)	(0.19)	(0.09)	(0.02)
Constant term	-2.041**	5.890***	6.682***	-0.247	1.610**	1.658**
	(-2.28)	(5.10)	(5.73)	(-0.19)	(2.24)	(2.46)
N	121	121	121	44	44	44

Note: *, **, *** represent $P < 0.1$, $P < 0.05$, $P < 0.01$ respectively

level and empirically tests the impact and mechanism of green innovation efficiency on environmental protection. Moreover, this study conducts robustness tests and proposes relevant policy implications.

The main conclusions are as follows. The overall environmental protection level of the Yangtze River Economic Belt is on the rise, with the highest level of environmental protection in the upper reaches, the second in the lower reaches, and the lowest in the middle reaches. Green innovation efficiency promotes the overall environmental protection level of the Yangtze River Economic Belt, inhibits the environmental protection level of the downstream areas, promotes the environmental protection level of the upstream areas, and has no obvious impact on the environmental protection level of the middle reaches. The analysis of the impact mechanism shows that green innovation efficiency can improve the level of environmental protection through ecological environmental efficiency.

This study has the following policy implications. From the perspective of green innovation efficiency level, green innovation efficiency is not conducive to the improvement of environmental protection level in downstream areas, which shows that the input-output performance of green innovation efficiency in downstream areas is low, and

the growth rate of green innovation efficiency is less than that of the environmental protection level. Therefore, the government should improve the efficiency level of green innovation in downstream areas and focus on improving the output rate of science and technology to ensure that the growth rate of green innovation efficiency exceeds the level of environmental protection. Although China's environmental protection level is on the rise, the overall level is still not high. The economic benefits of green development in agriculture and rural areas are low, the farmers' ideology is not in place, and subsidies for green development are not matched. Therefore, a cooperative promotion mechanism must be established between townships and counties, agricultural superior resources must be integrated and ecological environment, product innovation, and economic benefits must be considered. Moreover, financial support in promoting environmental protection with green innovation efficiency, and green innovation efficiency and environmental protection must be jointly promoted.

ACKNOWLEDGEMENT

This study was supported by State Forestry Administration Research on major forestry issues (ecological safety) in 2014 (ZDWT201415); The Joint Fund Project of Guizhou University of Finance and Economics and the Research Institute of International Trade and Economic Cooperation of the Ministry of Commerce "Study on the Influencing Factors of Carbon Emission and Total Factor Energy Efficiency in Ecological Fragile Areas" (2017SWBZD13) and The Mining Growth Opportunities from Customer Experience: A Deep Case Study (2020HXZXJGXY003).

REFERENCES

Duan, X., Dai, S.L. and Liao, K.C. 2020. Research on the coupling and coordination and influencing factors of industrial enterprise eco-efficiency and green innovation efficiency. Science and Technology Management Research, 1: 89-100.

Feng, Y.J., Qi, Q. and Han, J.B. 2018. Spatiotemporal evolution and driving factors of China's agricultural ecological efficiency. Bulletin of Soil and Water Conservation, 12: 254-262.

He, S.K. 2019. Research on the dynamic mechanism and policy of collaborative promotion of rural ecological environment compensation and green development. Modern Economic Research, 6: 106-113.

Li, S. 2017. Green innovation efficiency drives the transformation of agricultural economic development mode. Agricultural Economics. 4: 20-21.

Li, X.W. and Xu, S.B. 2020. The measurement and spatial characteristics of the imbalance of China's agricultural supply structure. Journal of Guangxi University of Finance and Economics, 4: 87-102.

Liu, Z. 2020. Correlation analysis of China's provincial environmental protection index. Statistics and Decision, 7: 91-95

Lu, W.M., Zhang, T.F. and Jiang, Q.J. 2017. Promoting urban green development through the transformation of land use mode: exploration and practice in Shanghai. Environmental Protection, 4: 59-64.

Ma, H.K. and Mao, S.P. 2020. Research on the green ecological transformation of agricultural support policies-based on the comparative analysis of China, Japan and Korea. Economic System Reform, 2: 157-165.

Peng, S. and Wang, Y.H. 2019. Boosting green development with ecological recycling agriculture: Taking Hunan as an example. Journal of Hunan University (Social Science Edition), 3: 1-7.

Shi, Z.H., Mu, H.J. and Sun, Y. 2019. Research on the impact of agricultural subsidies on farmers' participation in environmental protection. Economic Review, 3: 144-154.

Tone, K. and Tsutsui, M. 2010. Dynamic DEA: A Slacks-Based Measure Approach. Omega, 38(3): 145-156.

Wang, B.Y. and Zhang, W.M. 2018. Inter-provincial differences and influencing factors of agricultural ecological efficiency in China: based on panel data analysis of 31 provinces from 1996 to 2015. Rural China Economics, 1: 46-62.

Wang, Q. 2013. Research on the contribution of agricultural green innovation efficiency to agricultural economic growth based on Solow residual value-taking Hubei province as an example. Agricultural Economics, 6: 6-9.

Wang, Y.Q. and Wan, W.T. 2020. Regional environmental regulation decision-making model guided by green development. System Engineering, 1: 14-15.

Wei, Q., Zhang, B. and Jin, S.Q. 2018. China environmental protection index construction and regional comparative research. Issues of Agricultural Economy, 11: 11-20.

Xue, L., Xu, C.H. and Shen, Y. 2019. Agglomeration of agricultural industry and environmental protection: coupling degree and synergistic effect. Economic Statistics and Decision, 17: 125-129.

Yan, X. and Chang, C. 2019. Research on the dynamic response between green innovation efficiency and ecological environment in the Yangtze River Economic Belt. Journal of Nantong University (Social Science Edition), 5: 22-25.

Zhou, L. 2019. Research on Tibet's environmental protection under the background of rural revitalization. Northwestern Ethnic Studies, 3: 116-127.

Nature Environment and Pollution Technology
An International Quarterly Scientific Journal

p-ISSN: 0972-6268
(Print copies up to 2016)
e-ISSN: 2395-3454

Vol. 20 | No. 2 | pp. 891-898 | 2021

Original Research Paper

https://doi.org/10.46488/NEPT.2021.v20i02.052

Open Access Journal

Synergy Effect of Environmental Factors on the Growth and Toxins Production by *Microcystis aeruginosa*

Hou Wei, Song Yundi, Lu Nan, Zhang Runjie, Bu Naishun, Miao Bin, He Zhe and Fu Baorong†
College of Environmental Science, Liaoning University, Shenyang 110036, P.R. China
†Corresponding author: Fu Baorong; 826923232@163.com

Nat. Env. & Poll. Tech.
Website: www.neptjournal.com

Received: 14-03-2020
Revised: 19-04-2020
Accepted: 13-06-2020

Key Words:
Microcystis aeruginosa
Microcystins
Illumination intensity
Orthogonal analysis

ABSTRACT

Microcystis is one of the most common algal genera that causes water eutrophication. The effect of water quality on the growth and toxins production of *Microcystis* has been attracting high research attentions. The relationship of different combinations of temperature, illumination intensity, nitrogen and phosphorus with the growth and toxin production of *Microcystis aeruginosa* was explored through an orthogonal test. Results showed that illumination intensity influences the growth of *Microcystis aeruginosa* mostly, followed by temperature, total nitrogen (TN) and total phosphorus (TP). Illumination intensity affects the toxin production of *Microcystis aeruginosa* most significantly, followed by TP, TN and temperature successively. 200Lx illumination intensity, 22°C temperature, 20 mg.L^{-1} TN and 0.6 mg.L^{-1} are the optimum toxin production conditions for *Microcystis aeruginosa*.

INTRODUCTION

Harmful cyanobacterial blooms are one of the most severe problems in freshwater ecosystems. A Survey of the United Nations Environment Programme (UNEP) reported that 30-40% of lakes and reservoirs in the world are suffering from eutrophication (Ingrid & Jamie 1999). *Microcystis aeruginosa* is the most successful bloom-forming organisms in many freshwater ecosystems (Lin et al. 2019). *Microcystis* is not only the dominant algae in eutrophic water but also toxin-producing algae that can produce Microcystins (MCs) (Puschner et al. 1999, Azevedo et al. 2002). These toxins are harmful to a wide range of organisms (Gilbert 1996, Liu et al. 2006, Tilimanns et al. 2008). Microcystins are a kind of heptad peptide monocyclic compound. Its ring structure is D-Ala-L-X-red-β-methyl-D-isoaspartate-L-Z-Adda-D-isoglutamic acid-N-methyl dehydroalanine. Currently, 75 isomers of MC have been discovered (Van Apeldoorn et al. 2006). MCs are water-soluble and have strong heat resistance, but are difficult to be deposited or adsorbed. In 1998, the World Health Organization (WHO) has determined the base value of MCs in water at 1 μg/L (WHO 1998).

Both existing Chinese and foreign researches on toxin production mechanism of *Microcystis* mainly focus on genetic and environmental factors (Joung et al. 2011, Jähnichen et al. 2011, Reichwaldt & Ghadouani 2012). Environmental factors mainly include water temperature, illumination intensity and nutritive salts like nitrogen and phosphorus (Watanabe & Oishi 1985, Rapala 1988, Oh et al. 2000, Kameyama et al. 2002). However, no agreement on the influence of the environment on toxin production mechanism has been reached yet. Utkilen & Gjølme (1992) pointed out that illumination may be the only influencing factor of toxin production of *Microcystis*. Wiedner et al. (2003) cultured *Microcystis* PCC7806 continuously, finding that the MC content per unit cell has a significant positive correlation with illumination intensity under limited illumination, but turns into a negative one under adequate illumination. Kameyama et al. (2003) conducted batch cultivation of *Microcystis viridis* NIES102 under different concentrations of nitrogen and phosphorus but didn't find a significant relationship between intracellular MC and nitrogen concentration within the logarithmic growth period. Downing et al. (2005) studied *Microcystis* PCC7806 and *Microcystis* UV027, and found that MC concentration per unit cell is related to N/P. Although some studies have involved the effect of illumination, nitrogen and phosphorus content on toxin production mechanism of *Microcystis*, growth and toxin production of algae have abundant influencing factors and no research has explored the effect degrees of different factors on toxin production mechanism of *Microcystis* and their combined effect. Hence, it is necessary to study the combined effect of different factors on the growth and toxin production characteristics of algae.

Based on the effect of a single factor on the growth and toxin production of *Microcystis*, this paper further explored the combined effect of nitrogen, phosphorus, temperature and illumination by using the L9(3^4) orthogonal test.

MATERIALS AND METHODS

Experimental Chemicals

Methanol: chromatographically pure (≥99.9%), Sinopharm Chemical Reagent Co., Ltd. Trifluoroacetic acid (TFA): chromatographically pure (≥99.5%), Sinopharm Chemical Reagent Co., Ltd. Algal toxin-LR standards: 50 μg, Biobase Co., Ltd.

Experimental Methods

1. **Algae culture:** Testing *Microcystis (Microcystis aeruginosa FACHB-315)* was bought from Freshwater Algae Culture Collection at the Institute of Hydrobiology (FACHB-collection) and then cultured in an HP 1000GS incubator under artificial climate. The culture medium was improved BG-11. Culture conditions are: 30°C, 1000-1500 Lux illumination intensity and 14:10 illumination/dark. The position of the triangular flask was adjusted randomly and shook 2-3 times regularly every day during the culture.
2. **Solution preparation:** Monopotassium phosphate solution: 6.8 g monopotassium phosphate was dissolved in 1,000 mL ultrapure water.

   Phosphate buffered solution: pH of the monopotassium phosphate solution was adjusted to 3.0 by 20% phosphoric acid solutions.

   Leaching solutions: 10 mL ultrapure water and 10 mL 20% methanol aqueous solutions.

   Elution solution: 0.1 mL TFA (chromatographically pure) was dissolved into 100 mL methanol (chromatographically pure).
3. **Test conditions setting:** After the *Microcystis* had been starved for 3 days, concentrations of nitrogen and phosphorus in the culture medium were adjusted by $Ca(NO_3)_2$ and K_2HPO_4. Culture temperature, illumination intensity and illumination/dark of *Microcystis* were set by the illumination incubator. The experiments were designed based on the orthogonal test (Table 1).
4. **Algae cell density measurement:** Blood counting chamber method: water sample was stirred evenly. Three test samples were collected from the upper, middle and bottom layer of the triangular flask respectively to measure the number of algae cells. The mean of three measurements was taken as the final results.

Table 1: Orthogonal experimental scheme.

Number	Temperature (°C)	Light intensity (Lx)	TN (mg/L)	TP (mg/L)
1#	22	200	20	0.4
2#	22	500	60	0.6
3#	22	800	100	1.0
4#	25	200	60	1.0
5#	25	500	100	0.4
6#	25	800	20	0.6
7#	28	200	100	0.6
8#	28	500	20	1.0
9#	28	800	60	0.4

The specific growth rate of *Microcystis* during the logarithmic phase was analyzed according to its growth curves under different culture conditions (Margarita et al. 2002).

$$K = \frac{\ln N_t - \ln N_0}{t - t_0} \quad \ldots(1)$$

Where K is the relative growth rate of cells, t0 means the initial time of the logarithmic phase, N_0 is the initial concentration of the logarithmic phase, and N_t is the algae concentration at time t.

5. **Absorbance value of *Microcystis:*** Before the test, some *Microcystis* solution at stable phase was taken and scanned by ultraviolet spectrophotometer under 200-800 nm wavelength, determining that 600-700 nm is the optimum absorption wavelength. The absorbance value of *Microcystis* solution under 600-700 nm was tested every other day.
6. **Determination of MCs:** 80 mL *Microcystis* solution was taken and extracted by microwave digestion/extraction instrument (Italy MILESTONE) for 10 min under 100°C. The extract was then filtered by 0.45μm fibre filter membrane to collect *Microcystis* solution.

Activation of C18 solid-phase extraction column (Bona SPE500mg/3cc): 10mL methanol was injected into the extraction column activated by 10mL water when the methyl alcohol level reached the upper screen of the extraction column.

The collected *Microcystis* solution was injected into the activated solid-phase column for enrichment. The effluent was reinjected into the column again for secondary enrichment.

After sample enrichment, the C18 solid-phase extraction column was rinsed by the leaching solution (10 mL pure water and 10 mL 20% methanol solution).

MCs in the column was eluted with 10 mL elution solution. The effluent was collected.

The effluent was decompressed and steamed to dry by a rotary evaporator (Shanghai HongjiRe-52cs). Add 0.5 mL 50% methanol solution until the effluent was completely dissolved. The 2 mL effluent was used to test.

Detection conditions of HPLC (Varian LC-210): mobile phase: methanol (V): phosphate buffered solution (V)= 57:43; flow rate: 1 mL/min; detection wavelength: 238 nm. 20 uL sample was injected. Three parallel tests were conducted.

After finishing the test, the HPLC was rinsed by 10% methanol aqueous solution firstly to eliminate salts and then washed with pure methanol. The experimental design, data acquisition and data processing process shall comply with QA/QC requirements.

RESULTS AND DISCUSSION

Growth Curve of *Microcystis*

Growth curves of *Microcystis* under different culture conditions in the orthogonal test are shown in Fig. 1. *Microcystis* in 1#, 2#, 3#, 4# and 7# begin the logarithmic growth on the 9th day and the growth enters into the stable phase on the 27th day. The growth of *Microcystis* in 5# and 6# enters into the logarithmic phase on the 5th day. *Microcystis* in 5# and 6# grows quickly and the number of algae cells reaches the peak on the 23rd day. *Microcystis* in 8# and 9# begin to grow logarithmically on the 7th day and then the stable phase on the 25th day. Meanwhile, *Microcystis* in 1#, 4# and 7# under 200Lx illumination intensity grow slowly with the low algae biomass. This indicates that low illumination intensity can inhibit the growth of *Microcystis* significantly.

The specific growth rate and the maximum biomass of *Microcystis* at the logarithmic phase were further analyzed

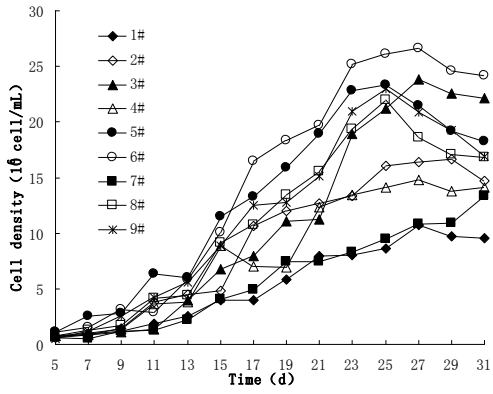

(1-9 # are corresponding to those in Table 2)

Fig. 1: Variation curves of *Microcystis* density under different culture conditions.

Table 2: Comparison of growth rate and the maximum biomass of *Microcystis* under different culture conditions.

Number	Compared growth rates during logarithmic growth /d	Maximum biomass (10^6a/mL)
1#	0.123	10.75
2#	0.137	16.65
3#	0.170	23.8
4#	0.133	14.8
5#	0.167	23.35
6#	0.176	26.6
7#	0.124	13.375
8#	0.158	21.975
9#	0.164	22.95

according to the growth curves under different culture conditions (Table 2). There is the largest biomass (26.6×10^6/mL) in 6#, which is followed by 3# (23.8×10^6/mL). The growth rates of *Microcystis* in 6# and 3# are 0.176 and 0.170, respectively. The best growth of *Microcystis* was in 6# in these treatments which might be from the compensation of different factors because it is supplied with lower nitrogen content and the longest illumination. The lowest maximum biomass (10.75) and growth rate(0.123) were in 1# due to the lowest temperature, nutrient salt content and short illumination. Moreover, there is a positive correlation between the maximum biomass and the growth rate in these treatments.

Variation of MCs

Effect of mutual orthogonality of temperature, illumination intensity, TN and TP on MCs is presented in Table 3. The contents of MCs increase continuously during the culture in all treatments. The MCs contents on the 23rd day are highest for all treatments. Treatment group 4 achieves the highest MCs content on the 15th day. The content of MCs increases quickly during the first 15 days and becomes stable subsequently. This might be caused by the short logarithmic phase of *Microcystis* in 4#. The content of MCs on the 23rd day is the highest among all treatments. The MCs content in 6# was the highest, and the reason might be that there are the most algae cells in it. However, although the maximum biomass in 3# is next to that in 6#, the content of MCs is only half of that in 6#. This means that the content of MCs is not only related to biomass, but also other factors.

Synergy Effect of Temperature, Illumination Intensity, Nitrogen and Phosphorus on Biomass of *Microcystis*

To study the effect of degrees of temperature, illumination intensity, nitrogen and phosphorus on *Microcystis* growth, a statistical analysis on the biomass of *Microcystis* was con-

Table 3: Content of MCs (μg.L^{-1}) during 23-day culture.

Number	The 7th day	The 11th day	The 15th day	The 19th day	The 23rd day
1#	0.5240	1.7556	4.3031	18.0597	20.8622
2#	0.1937	3.2324	5.8781	12.9239	21.9742
3#	0.1588	2.7712	5.6402	10.0309	15.1562
4#	0.1674	2.3533	27.4981	30.5777	31.5704
5#	0.4844	2.8458	5.8047	10.9054	18.9009
6#	0.2952	3.7680	14.0460	32.1244	46.3429
7#	0.5303	2.0560	6.5060	10.3597	20.8562
8#	0.2407	2.2880	10.8364	17.4097	18.2394
9#	0.5552	2.2081	10.6787	13.5437	15.3474

ducted. The orthogonal test was implemented according to Table 2. The absorbance value of algae solution was tested every other day since 7d, getting variation curves (Fig. 2). All treatment groups enter into the logarithmic phase since 9d and have a long logarithmic phase. The maximum absorbance value of treatment group 6 is significantly higher than those of other treatment groups. The absorbance value of treatment group 1 changes slightly, but absorbance values of treatment group 2, 3, 4 and 7 vary similarly.

The relationship between the final optical density and specific growth rate during the growth of *Microcystis* is presented in Fig. 3. According to regression analysis, the correlation of specific growth rates of different treatment groups and their absorbance values is y = 7.3662x - 0.6187 (R^2 = 0.9763. Therefore, the growth of *Microcystis* can be represented by the orthogonal analysis based on the final absorbance value.

Statistics were calculated according to the final absorbance values of *Microcystis.* The intuitive analysis results are listed in Table 4. The mean value in Table 4 represents the average absorbance values of each level of different

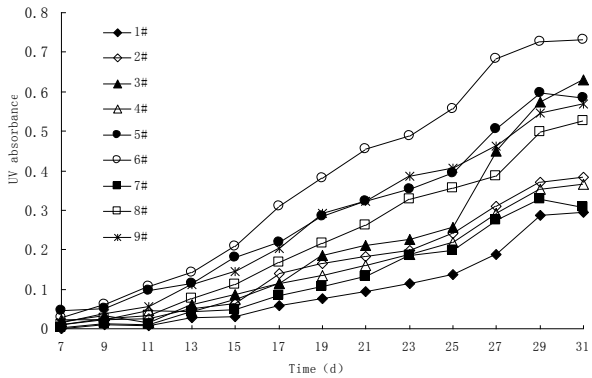

Fig. 2: Absorbance value of *Microcystis* under different culture conditions.

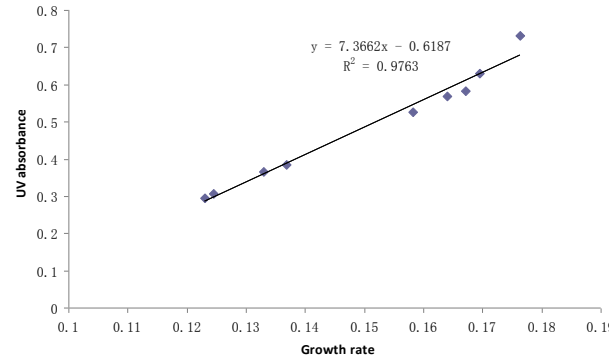

Fig. 3: Correlation between *Microcystis* absorbance and specific growth rate.

factors. For example, T_{11}, T_{21} and T_{31} represent the final absorbance values at 22°C, 25°C and 28°C, respectively. It can be observed that *Microcystis* growth increases with the temperature rise, but the algal density begins to decrease after the temperature increases to a certain level. The content of *Microcystis* increases with the increase of illumination intensity. *Microcystis* growth changes similarly as TN and TP increases, decreasing first and then increasing. The range in Table 4 means the different effect of the factors on algae growth. The higher the range is, the stronger the effect was. As a result, illumination intensity influences the algal growth strongly, followed by temperature, TN and TP.

Illumination provides energies for the cellular metabolism of algae and affects algal growth and reproduction. *Microcystis aeruginosa* is known to respond to light availability with photoacclimation (Wyman et al. 1983). Huisman et al. (1999) reported that algal growth has specific "critical illumination intensity". For example, in the water column inoculated with *Microcystis* and *Chlorella*, *Microcystis* will be replaced by *Chlorella* gradually below 3,000Lx illumination intensity. However, in natural lakes and reservoirs, *Microcystis* could beat others in the light fight due to its strong buoyancy. When the controlled illumination intensity is lower than the "critical illumination intensity", algal biomass will decrease significantly. Our experiment also confirmed that very low illumination intensity will inhibit *Microcystis* growth. *Microcystis aeruginosa* is known for its resistance to photoinhibition and high light due to protective pigmentation (Paerl et al. 1983). The temperature has been shown to have a positive effect on the growth of *M. aeruginosa* (Rainer et al. 2016). Temperature affects algal growth directly or indirectly mainly by controlling physicochemical progress, such as the enzymatic reaction of photosynthesis, respiration intensity and decomposition of nutrient substances in water. In this study, it is discovered that algal content increases with the temperature rise, but algal density begins to decrease when

Table 4: Visual analysis table about absorbance values of *Microcystis.*

Number	Environmental factors				Absorbance values
	Temperature (°C)	Light intensity (Lx)	TN ($mg.L^{-1}$)	TP ($mg.L^{-1}$)	
1	22	200	20	0.4	0.294
2	22	500	60	0.6	0.384
3	22	800	100	1.0	0.631
4	25	200	60	1.0	0.366
5	25	500	100	0.4	0.584
6	25	800	20	0.6	0.7325
7	28	200	100	0.6	0.3075
8	28	500	20	1.0	0.5265
9	28	800	60	0.4	0.568
Mean value T_1	0.436	0.322	0.518	0.482	
Mean value T_2	0.561	0.498	0.439	0.475	
Mean value T_3	0.467	0.644	0.507	0.508	
Range	0.125	0.322	0.079	0.033	

the temperature increased to a certain level. Within the appropriate temperature range, cell activity enhances with the temperature rise. However, after the temperature reaches a certain level, algal metabolism accelerates, which requires more nutrients. Due to the decreasing nutrients in the water, algal cell death rate under high temperature is higher than the reproduction rate and algal growth is inhibited. Zhao et al. (2007) found that water temperature was an important factor in the shift of *Microcystis* and *Oscillatoria* dominance in a simulated, shallow, eutrophic lake. Algal reproduction is closely related to nitrogen and phosphorus concentrations in water (Stockner & Shortreed 1988, Borchardt 1994). Tsukada et al. (2006) found that P limitation did not occur during the study period. The effect of N was stronger than that of P for blooms of *Microcystis*. The ratio of N/P plays an important role in *Microcystis* growth, and the low N/P ratio could be a consequence of the capacities and rates of uptake of nitrogen and phosphorus by cyanobacteria (Marinho & Sandra 2007).

Synergy Effect of Temperature, Illumination Intensity, Nitrogen and Phosphorus on Toxin Production by *Microcystis*

In the experiment, a statistical analysis of MCs per unit cell was conducted on the 23rd day. Intuitive analysis results are

Table 5: Visual analysis table about single-cell toxin production by *Microcystis.*

Number	Environmental factors				Toxin production of single cell ($fg.a^{-1}$)
	Temperature (°C)	Light intensity (Lx)	TN ($mg.L^{-1}$)	TP ($mg.L^{-1}$)	
1	22	200	20	0.4	2.5996
2	22	500	60	0.6	1.6429
3	22	800	100	1.0	0.8009
4	25	200	60	1.0	2.3560
5	25	500	100	0.4	0.8290
6	25	800	20	0.6	1.8390
7	28	200	100	0.6	2.5280
8	28	500	20	1.0	0.9426
9	28	800	60	0.4	0.7326
Mean value T_1	1.681	2.495	1.794	1.387	
Mean value T_2	1.675	1.138	1.577	2.003	
Mean value T_3	1.401	1.124	1.386	1.367	
Range	0.280	1.371	0.408	0.636	

listed in Table 5. The high MCs content per unit cell is in 1, 4 and 7 #, which indicated that low illumination intensity is beneficial for toxin production of *Microcystis*. Toxin production per unit cell of treatment group 9 is only next to that of treatment group 3, indicating that other factors could compensate for inadequate phosphorus to a certain extent. This reflects that there's mutual compensation among factors. Furthermore, illumination intensity affects the toxin production of *Microcystis* mostly, followed by TP, TN and water temperature.

In the experiment, levels of four factors are shown in the horizontal coordinate and their meaning is presented by the toxin production per unit cell at the vertical coordinate (Fig. 4). Four curves in Fig. 4 show the effect of temperature, illumination intensity, TN and TP on MCs content per unit cell of *Microcystis*. Effect of TP on toxin production per unit cell of *Microcystis* increases firstly and then decreases, indicating that there's an optimum P concentration within the selected range for *Microcystis* to produce MCs. In this experiment, it was concluded that 0.6 $mg.L^{-1}$ is the optimum P concentration for the production of MCs. MCs content per unit cell of *Microcystis* increases with the decrease of illumination intensity. The effect of temperature and TN is similar to that of illumination intensity. In this study, the optimum illumination intensity, temperature and TN for *Microcystis* to produce toxin are 200Lx, 22°C and 20 $mg.L^{-1}$, respectively.

According to the orthogonal test results, low illumination intensity could facilitate toxin production of *Microcystis*. This agrees with the research results of Rapala et al. (1997). Meanwhile, the effect of illumination intensity on toxin production is affected by temperature. With the increase of TP, MCs show an inverse "V-shaped" variation. Low TP could accelerate MCs production. This echoes with many results (Vonshak et al. 1994, Christina & Pedro 1994, Kameyama et al. 2002). The results of this study showed that there was a slight increase in MCs production at low temperature and a slight decrease in toxicity at high temperature, similar to the results from the studies of Watanabe & Oishi (1985), Sivonen (1990) and Gilbert (1996). With limited phosphorus, both isomers of MCs and MCs increase. Nitrogen is an essential element for MCs synthesis. The proportion of nitrogen in MCs molecular structure was up to 14% (Botes et al. 1985). However, based on our orthogonal test results, N influences MCs slightly. Orr & Jones (1998) found a linear relationship between cell division rate and total MCs production rate in *Microcystis* solution. MCs content per unit cell keeps constant during the cell cycle even though both total MCs content in algal solution and cell concentration increase with the increase of TN in culture medium. Therefore, it is speculated that the effect of TN on total MC may be insignificant because nitrogen changes total MCs content in *Microcystis* solution by influencing the algae cell growth, but there is no direct impact on MCs content per unit cell. Meanwhile, the orthogonal test results reveal that the optimum growth condition and the optimum toxin production condition of *Microcystis* are different from each other. Abundances of toxic strains of *Microcystis* have been specifically enhanced by additions of inorganic N (Davis et al. 2010).

CONCLUSIONS

Variation trends of *Microcystis* biomass and extracellular MCs are analyzed through a 29-day orthogonal test of tem-

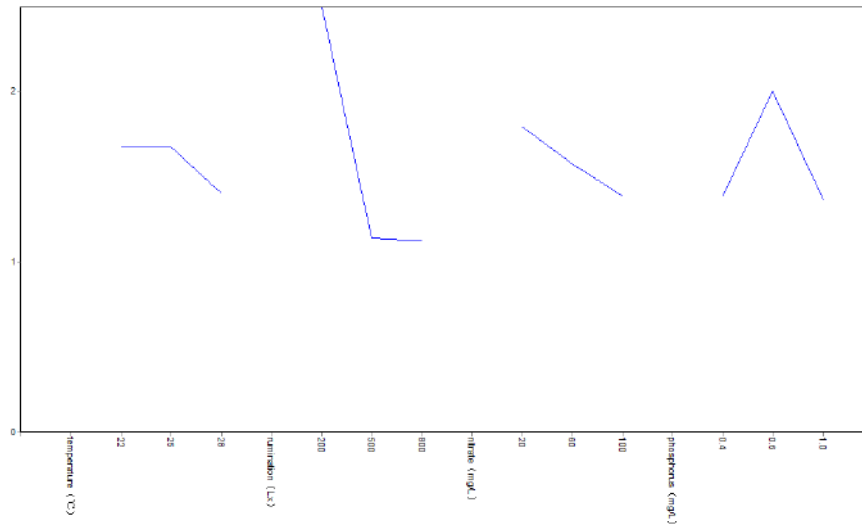

Fig. 4: Orthogonal test of temperature, illumination intensity, nitrogen and phosphorus.

perature, illumination intensity, nitrogen and phosphorus. The conclusions are as following:

1. According to the intuitive analysis on optical density of *Microcystis* solution, illumination intensity influences *Microcystis* growth mostly, followed by temperature, TN and TP.
2. The MCs content in 6# was the highest, and the reason might be that there are the most algal cells in it. However, although the maximum biomass in 3# is next to that in 6#, the content of MCs is only half of that in 6#. This means that the content of MCs is not only related to biomass, but also other factors
3. Illumination intensity influences toxin production of *Microcystis* strongly, followed by TP, TN and water temperature successively. With the increase of TP, MCs content per unit cell increases firstly and then decreases. In this study, the optimum TP for toxin production of *Microcystis* is 0.6 $mg.L^{-1}$. Toxin production per unit cell is inversely proportional to illumination intensity, temperature and TN. The optimum illumination intensity, temperature and TN for toxin production of *Microcystis* are 200Lx, 22°C and 20 $mg.L^{-1}$, respectively.

ACKNOWLEDGEMENTS

This research has been financed by the National Natural Science Foundation of China (31600311) and (31972522), the National Key Research and Development Project of China (2018YFC1801200), Major Science and Technology Project of Liaoning Province (2019JH1/10300001).

REFERENCES

Azevedo, S.M., Carmichael, W.W., Jochimsen, E.M., Rinehart, K.L., Lau, S., Shaw, G.R. and Eagleshan, G.K. 2002. Human intoxication by microcystins during renal dialysis treatment in Caruaru-Brazil. Toxicology, 181(24): 441-446.

Borchardt, M.A. 1994. Effects of flowing water on nitrogen-nitrogen and phosphorus limited photosynthesis and optimum N:P ratios by *Spirogyra fluviatilis* (Charophyceae). Journal of Phycology, 30(3): 418-430.

Botes, D.P., Wessels, P.L. and Kruger, H. 1985. Structural studies on cyanoginosins-LR, -YR, -YA and- YM, peptide toxins from *Microcystis aeruginosa*. Journal of the Chemical Society-Perkin Transactions, 1: 2747-2748

Christina, W.C. and Pedro, A.C. 1994. Factors influencing the development of *Cylindrospermosis raciborskii* and *Microcystis aeruginosa* in the Paranoa Reservoir, Brasilia, Brazil. Archive Fur Hydrobiologie Supplementband, 105: 85-96.

Davis, T.W., Harke, M.J., Marcoval, M.A., Goleski, J., Orano-Dawson, C., Berry, D. L. and Gobler, C.J. 2010. Effects of nitrogenous compounds and phosphorus on the growth of toxic and non-toxic strains of *Microcystis* during cyanobacterial blooms. Aquatic Microbial Ecology, 61(2): 149-162.

Downing, T.G., Sember, C.S., Gehringer, M.M. and Leukes, W. 2005. Medium N:P ratios and specific growth rate comodulate microcystin and protein content in *Microcystis aeruginosa* PCC7806 and *M. aeruginosa* UV027. Microbial Ecology, 49(3): 468-473.

Gilbert, J.J. 1996. Effect of temperature on the response of planktonic rotifers to a toxic cyanobacterium. Ecology, 77(4): 1174-1180.

Huisman, J., Jonker, R.R., Zonneveld, C. and Weissing, F.J. 1999. Competition for light between phytoplankton species: Experimental tests of mechanistic theory. Ecology, 80(1): 211-222.

Ingrid, C. and Jamie, B. 1999. Oxic Cyanobacteria in Water. London and New York. E&FN Spon Publisher, 416-419.

Jähnichen, S., Long, B.M. and Petzoldt, T. 2011. Microcystin production by *Microcystis aeruginosa*: Direct regulation by multiple environmental factors. Harmful Algae, 12(4): 95-104.

Joung, S.H., Oh, H.M., Ko, S.R. and Ahn, C.Y. 2011. Correlations between environmental factors and toxic and non-toxic *Microcystis* dynamics during bloom in Daechung Reservoir, Korea. Harmful Algae, 10(2): 188-193.

Kameyama, K., Sugiura, N., Isoda, H., Inamori, Y. and Maekawa, T. 2002. Effect of nitrate and phosphate concentration on production of microcystins by *Microcystis viridis* NIES 102. Aquatic Ecosystem Health & Management, 5(4): 443-449.

Lin, Y.Q., Chen, A.W., Luo, S., Kuang, X.L., Li, R.H., Lepo, J.E., Gu, J.D., Zeng, Q.R. and Shao, J.H. 2019. Cyanobacterial bloom mitigation by sanguinarine and its effects on aquatic microbial community structure. Environmental Pollution, 253: 497-506.

Liu, Y., Xie, P. and Wu, X.P. 2006. Effects of toxic and non-toxic *Microcystis aeruginosa* on survival, population-increase, and feeding of two small cladocerans. Bulletin of Environmental Contamination and Toxicology, 77: 566-573.

Margarita, M., Jorge, H. and Comin, F.A. 2002. Effect of nitrogen and phosphorus supply on growth, chlorophyll content and tissue composition of the macroalga *Chaetomorpha linum* (O. F. M üll.) Kütz in a Mediterranean coastal lagoon. Journal of Marine Science and Technology, 66: 355-364.

Marinho, M.M. and Sandra, M.F. 2007. Influence of N/P ratio on competitive abilities for nitrogen and phosphorus by *Microcystis aeruginosa* and *Aulacoseira distans*. Aquatic Ecology, 41(4): 525-533.

Oh, H.M., Lee, S.J., Jang, M.H. and Yoon, B.D. 2000. Microcystin production by *Microcystis aeruginosa* in a phosphorus-limited chemostat. Applied Environmental Microbiology, 66(1): 176-179.

Orr, P.T. and Jones G.J. 1998. Relationship between microcystin production and cell division rates in nitrogen-limited *Microcystis aeruginosa* cultures. Limnology & Oceanography, 43(7): 1604-1614.

Paerl, H.W., Tucker, J. and Bland, P.T. 1983. Carotenoid enhancement and its role in maintaining blue-green algal (*Microcystis aeruginosa*) surface blooms. Limnology & Oceanography, 28(5): 847-857.

Puschner, B., Galey, F.D., Johnson, B., Dickie, C.W. and Holstege, D.M. 1999. Blue-green algae toxicosis in cattle. Journal of the American Veterinary Medical Association, 213(11): 1605.

Rainer, K., Li, D. and Elisabeth, E. 2016. Role of toxic and bioactive secondary metabolites in colonization and bloom formation by filamentous cyanobacteria *Planktothrix*. Harmful Algae, 54: 69-86.

Rapala, J. 1998. Toxins production by freshwater cyanobacteria: Effects of environmental factors [Dissertation]. University of Helsinki.

Rapala, J., Sivonen, K., Lyra, C. and Niemelä, S.I. 1997. Variation of microcystins, cyanobacterial hepatotoxins, in *Anabaena* spp. as a function of growth stimuli. Appl. Environ. Microbiol., 63(6): 2206-2212.

Reichwaldt, E.S. and Ghadouani, A. 2012. Effects of rainfall patterns on toxic cyanobacterial blooms in a changing climate: Between simplistic scenarios and complex dynamics. Water Research, 46(5): 1372-1393.

Sivonen, K. 1990. Effects of light, temperature, nitrate, orthophosphate, and bacteria on growth of and hepatotoxic production by *Oscillatoria agardhii* strains. Applied & Environmental Microbiology, 56(9): 2658-2666.

Stockner, J.G. and Shortreed, K.S. 1988. Response of *Anabaena* and *Synechococcus* to manipulation of nitrogen: Phosphorus ratios in a lake fertilization experiment. Limnology & Oceanography, 33(6): 1348-1361.

Tilimanns, A., Wilson, A., Frances, R. and Sarnelle, O. 2008. Meta-analysis of cyanobacterial effects on zooplankton population growth rate: Species-specific responses. Fundamental & Applied Limnology, 171(4): 285-295.

Tsukada, H., Tsujimura, S. and Nakahara, H. 2006. Effect of nutrient availability on the C, N, and P elemental ratios in the cyanobacterium *Microcystis aeruginosa*. Limnology, 7(3): 185-192.

Utkilen, H. and Gjølme, N. 1992. Toxin production by *Microcystis aeruginosa* as a function of light in continuous cultures and its ecological significance. Applied Environmental Microbiology, 58(4): 1321-5.

Van Apeldoorn, M.E., Van Egmond, H.P., Speijers, G.J. and Bakker, G.J. 2006. Toxins of cyanobacteria. Molecular Nutrition & Food Research, 51(1): 7-60.

Vonshak, A., Torzillo, G. and Tomaseli, L. 1994. Use of chlorophyll fluorescence to estimate the effect of photoinhibition in outdoor cultures of *Spirulina platensis*. Journal of Applied Phycology, 6(1): 31-34.

WHO 1998. WHO Guidelines for Drinking Water Quality. Health criteria and other supporting information, 2: 95-110.

Watanabe, M.F. and Oishi, S. 1985. Effects of environmental factors on toxicity of a cyanobacterium (*Microcystis aeruginosa*) under culture conditions. Applied Environmental Microbiology, 49(5): 1342-1344.

Wiedner, C., Visser, P.M., Fastner, J., Metcalf, J.S., Codd, G.A. and Mur, L.R. 2003. Effects of light on the microcystin content of *Microcystis* strain PCC 7806. Applied Environmental Microbiology, 69(3): 1475.

Wyman, K., Siegelman, H.W. and Falkowski, P.G. 1983. Adaptation of the cyanobacterium *Microcystis aeruginosa* to light intensity. Plant Physiology, 72(3): 829-832.

Zhaosheng, C., Xiangcan, J., Norio, I. and Yuhei, I. 2007. The effect of temperature on growth characteristics and competitions of *Microcystis aeruginosa* and *Oscillatoria mougeotii* in a shallow, eutrophic lake simulator system. Hydrobiologia, 581: 217-223.

Nature Environment and Pollution Technology
An International Quarterly Scientific Journal

p-ISSN: 0972-6268
(Print copies up to 2016)
e-ISSN: 2395-3454

Vol. 20 | No. 2 | pp. 899-907 | 2021

Original Research Paper

https://doi.org/10.46488/NEPT.2021.v20i02.053

Open Access Journal

Fish Stocks Around the Gezhouba and Their Response During Fishing Moratorium in the Yangtze River, China

Congfeng Wang*†, Ping Zhao*(**), Defu Liu*, Jianguo Wang****, Xiaohui Qin*****, Lvbo Liu**** and Zhengjian Yang***

* Hubei Field Observation and Scientific Research Stations for Water Ecosystem in Three Gorges Reservoir, Three Gorges University, Yichang 443002, P. R. China

**College of Civil Engineering, Guizhou University, Guiyang 550025, P. R. China

*** College of Resources and Environment, Hubei University of Technology, Wuhan 430068, P. R. China

****The Pearl River Hydraulic Research Institute, Guangzhou 510611, P. R. China

***** Department of Civil and Geomatics Engineering, Lyles College of Engineering, California State University, Fresno 559-278-5634, USA

†Corresponding author: Congfeng Wang; wangcf274407@163.com

Nat. Env. & Poll. Tech.
Website: www.neptjournal.com

Received: 03-05-2020
Revised: 13-06-2020
Accepted: 16-07-2020

Key Words:
Gezhouba Dam
Fish stocks
Fishing moratorium
Hydro-acoustics

ABSTRACT

To explore the impact of the fishing moratorium on fish stocks, some parameters and environmental factors were monitored downstream of Gezhouba Dam in April, June and August of 2013. Fish density and target length were get using hydro-acoustics (DIDSON). The results indicated that the fish density distributions in April, June and August were significantly different. The fish density decreased with time but kept a level that was close and steady in April and June. The average fish density of April was significantly greater than that in August ($P<0.05$). The percentage of fish target length distribution was consistent in time and space. In the study, the hydraulic and environmental factors were not the main reasons for the decrease of fish density and target body length in the spatial and temporal scale. Overfishing was the main cause and the fishing moratorium was substantially effective for keeping the sustainability of the fish resources in the adjacent areas of Gezhouba Dam.

INTRODUCTION

Building dams in a river causes habitat fragmentation by obstructing the migration pathway for fish and interrupting their reproduction (García et al. 2011, Morita & Yamamoto 2002, Macdougall et al. 2007, Santos et al. 2006). It negatively affects fish community structure and declines the fish stocks (Yi et al. 2010, Draštík et al. 2008, Yang et al. 2012). The Gezhouba Dam and the Three Gorges Dam are the largest two hydraulic structures in the middle reach of the Yangtze River. They exert much pressure on the downstream fish resources. The Gezhouba Dam is located at the end of the Three Gorges and is the only pathway for fish migration. It is dense for the local fish and partly for the migration fish (Yi et al. 2010, Zhou et al. 2014). The local fish species mainly include the four major Chinese carps. The migration fish species include *Chinese sturgeon, Coreius heterodon,* and *Coreius guichenoti*. The migration fish mainly inhabits and spawns in the Dajiang area, while the four major Chinese carps inhabit the Sanjiang area. Because the investigation area is the gathering place of different fish species which come from upstream and downstream of the Yangtze River, it is the favourite fishing area for fishers (Liu et al. 1990, Tao et al. 2010). The main fish species in the middle reaches of the Yangtze River reduce because of overfishing and the varying ecological environment (Yi et al. 2010, Liu et al. 2004, Yi et al. 2010). To restore the fish resources and protect fish biodiversity of the Yangtze River, the Ministry of Agriculture of China has promulgated the regulation of closing fishing in spring since 2003 (Duan et al. 2008).

The impact of fishing moratorium or the prohibited fishing areas on rejuvenating fish stocks has been widely investigated (Moustakas et al. 2006, Bavinck et al. 2008, Barnes & Sidhu 2013). For example, how fishing moratorium affects fishery production using the Cymbula Granatina model has been studied for more than ten years. And the target parameters of the modelling research include body length, wet flesh mass of individual, growth rate and mortality rate (Arendse et al. 2007). Although reasonable and sophisticated modelling results can be obtained, the

model development is unsatisfied on time-consuming. And the model application was constrained by many real-world conditions and calculation capacity. Some researchers studied how fishery production was affected by closures of fishing areas under four distinct management strategies (Barnes & Sidhu 2013). This method provided an indirect assessment of the impact of marine fishery management on fishing fishery resources. The fishing closure measures are evaluated by analysing the evolution of fish community structure and catches biodiversity on time sequence (Duan et al. 2008, 2013). The fish catches of direct acquisition on time sequence provide relatively accurate information, but it may damage the limited fish resources. According to these previous studies, fishing closure has been widely used as an effective measure to ensure the reliability of fishery production (Barnes & Sidhu 2013). Among various technologies for fishing closure investigation, fisheries hydro-acoustic technology, especially the Dual-frequency Identification Sonar (DIDSON), has been extensively applied in fish resources detection (Tao et al. 2012, Petreman et al. 2014, Han et al. 2009, Boswell et al. 2008, Maxwell & Smith 2007, Maxwell & Gove 2004). The goal of this study was to evaluate the impact of the fishing moratorium on the fish stocks near the Gezhouba Dam area using water fisheries acoustics technology, which had the advantages of zero damage to fish resources, easy operation and high precision. The acoustic information was collected using DIDSON with an acoustic camera in the near-dam area. Flow velocity and some water quality data including water temperature, pH and DO were monitored at the same time. Fish density and fish body length were used as the target parameters to quantify the fish and were statistically analysed to correlate with flow velocity and the environmental factors. Finally, the conclusion of the relationship between the fishing moratorium and fish resources was reached.

MATERIALS AND METHODS

Study Area

According to the regulation enacted by the Ministry of Agriculture of China (Misund 1997), the closed fishing period in the middle and lower reaches of the Yangtze River is from April 1 to June 29. The study time was on 3-5 April, 22-24 June, 4-5 August, and the acoustic data and water quality data (Water temperature, pH, DO, and Flow velocity) were collected meanwhile. The investigation area covers four kilometres long of the Gezhouba Dam mainstream. Based on the riverbed topography, flow characteristics, and water quality properties, the investigation area was divided into three regions including the Dajiang region (DJ), the confluence region (CF), and the Sanjiang region (SJ). The three regions were further divided into eight sub-regions. Eight sub-regions are as follows 1# Ship-lock (I), First station (II), Second station (III), Ship-yard (IV), Miao-zui (V), Junction (VI) Third bridge (VII), 2# and 3# Ship-lock (VIII). DJ included sub-regions I-V, CF included sub-region VI, and SJ included sub-regions VII-VIII (Fig. 1). The "Z" shaped lines in Fig.1 were the regional monitoring roadmap.

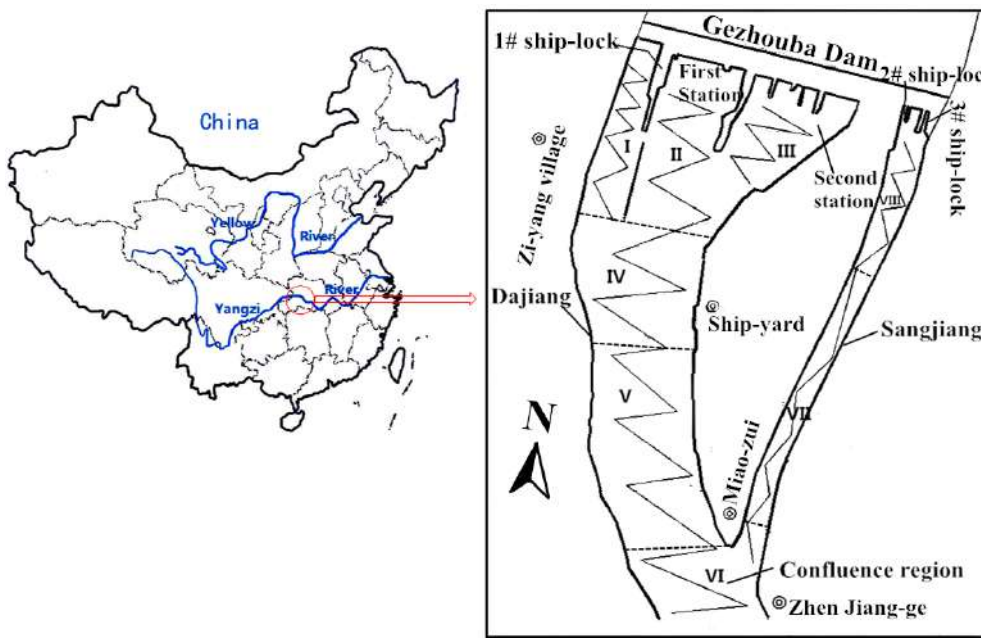

Fig.1: Location of the study area in the Gezhouba Dam.

Methods

The fish were real-time identified and monitored using dual-frequency identification sonar (DIDSON) SMC-300produced by the Sound Metrics Company of the USA. The monitoring route was positioned using a GPS apparatus (Mobile Mapper 10). The hydro-acoustic data were processed with the auxiliary software DIDSON V5.25 for the fish count. Some water quality parameters including water temperature, pH, DO and water depth were obtained using the multi-parameter water quality analyser Hydrolab-DS5 made by Hach Company and the data were exported to Excel processed; flow-velocity using the VectrinoPlus produced by Norway Nortek Company. The DIDSON mounted on the starboard side of the boat was used to monitor the fish distribution downstream of the Gezhouba Dam. Fig. 1 shows the distribution of the monitoring and sampling locations. The mean cruise speed of the sampling boat was maintained as 7km/h. The submerged depth of the boat was 0.5m and the angle between the axis of the DIDSON and the horizontal direction was maintained 30°. The monitoring route was z-shaped as showed in Fig. 1. The operating frequency of the sonar was adjusted corresponding to the varying bottom elevation of the river during the cruise. The water quality data and flow velocity were monitored at each flexion point on the route.

Data Analysis

Fish density (ρ): Fish density (ρ) can be defined as the ratio of the count of fish to the bulk volume when fish is sparsely distributed in spatial as individuals (Misund 1997). The count of fish can be obtained from the DIDSON detecting fish within a pyramid range (Fig. 2) and ρ can be calculated as follows:

$$b = 2h * \tan 7° \quad \ldots(1)$$

$$S_b = 0.5\ h\ b \quad \ldots(2)$$

$$V = S_b * L_s \quad \ldots(3)$$

$$\rho = 1000n / V \quad \ldots(4)$$

Where h is the length of water body detected by DIDSON (m), b is the width of the end section of the pyramid (m), S_b is the vertically projected area of the pyramid side (m^2), L_s is the cruise distance of the ship (m), V is the pyramid bulk volume of the detected water (m^3), ρ is the fish density in the study (ind./1000 m^3), n is the count of the detected fish in the area.

Fish body length: The Fish Target Strength was defined by referring to the general Sonar Target Strength (TS) formula as follows:

$$TS = 10 \log (I_r / I_i) \quad \ldots(5)$$

Where I_i is the incident acoustic intensity, I_r is the acoustic intensity of the reflection at the location 1 m from the target acoustic centre. *TS* is the key parameter for both quantitatively evaluating fish resources and fish size inversion. The literature has shown that fish TS depends not only on the body characteristics but also on the wavelength of the acoustic emission (Rakowitz et al. 2008, Knudsen et al. 2004, Godlewska et al. 2012). Richard (1969) believed that since the condition of $1 \leq L/\lambda \leq 100$, is suitable for most fish in

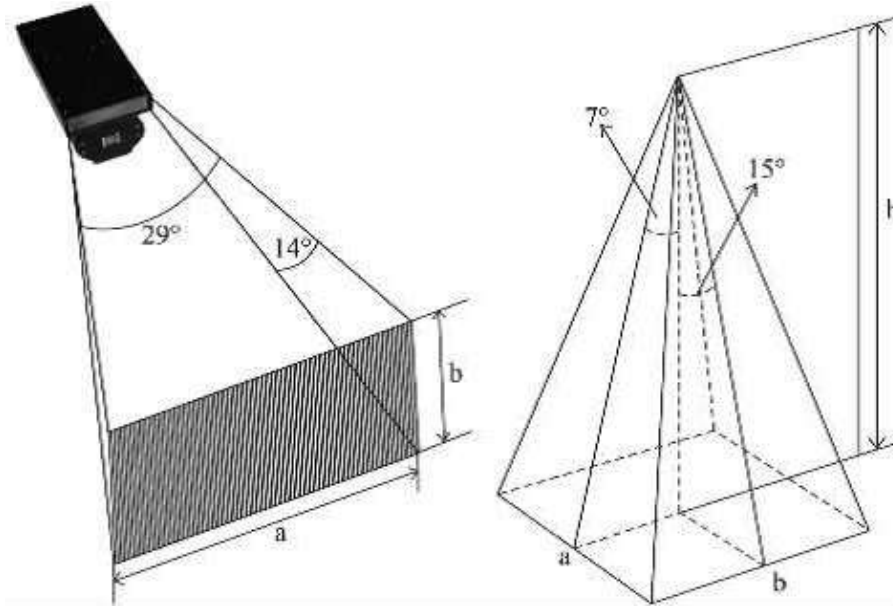

Fig. 2: Sketch of the fish detection range of DIDSON for fish density calculation.

freshwater, the TS for an individual body can be calculated with the following formula,

$$TS = 24.1\log L - 4.1\log \lambda - 33.2 \quad \ldots(6)$$

Where L is the target length; lambda λ is the acoustic wavelength. Based on the above principle, the information of fish body length and the corresponding distribution can be automatically collected with the DidsonV5.25 software.

The literature of the fish study in the Gezhouba area shows that the body length ranges of the four major Chinese carps are 140 to 1100 mm during 1994 to 1999, 53 to 750 mm with the acoustic strength of -58-35 dB in the reach from Gezhouba Dam to Gulaobei during 2004 to 2006 (Liu et al. 2004, Zhang et al. 2007). The target body length in 2008 was 753 mm with the maximum acoustic strength of -35.07 dB. In summary, the fish body length remained in the range of 0-1000mm except that some general Pro long fish occasionally appear during the Chinese sturgeon spawning period (between October and November) near Gezhouba Dam area. When a high-density fish group was detected with the DIDSON, the group was identified as one single fish body (Liang et al. 2012) with an exceptionally large size, which needs to be screened from the data series. Therefore, to study the relationship between fish density the distribution of the target body length, the fish only with the length between 0 and 100 cm were counted. The collected data were statistically analysed according to SPSS19.0 with Kolmogorov-Smirnov (K-S) method to investigate fish density distribution and to test the normality of fish density and distribution and the target body length. To distinguish the difference caused by different periods during the closed season, the t-test was conducted for fish density distribution and target body respectively between any two independent samples collected during April, June, and August. The result ($P<0.05$) shows the difference is statistically significant (Shen et al. 2007).

Water quality and velocity: Water quality data were collected for each meter below surface water at five different locations in each sub-region. The monitoring data were used to calculate the average velocity and water quality parameters. The t-test result ($p < 0.05$) for water quality and flow velocity of any two independent samples from the three periods showed the difference is statistically significant. Finally, to identify the decisive factors affecting fish density distribution, some sensitivity analysis was conducted using ANOVA analysis by SPSS19. Several environmental parameters, including water quality, flow velocity, and time, were set as independent variables varied with an interval within a typical range, and fish density was used as a dependent variable (Gao et al. 2008).

RESULTS

Fish Density (ρ)Distribution

Table 1 shows fish density in all stages of closure. The fish density of I-VIII were 22.86, 67.74, 34.12, 14.54, 14.25, 2.45, 2.69, 7.03 ind./1000 m^3 in April, III was the maximum while VI was minimum. The fish density of I-VIII was 15.24, 2.3, 13.34, 6.40, 6.33, 0.3, 4.77, 10.56 ind./1000m^3 in August, and the fish density of I was the maximum while VI was minimum. The fish density of DJ was significantly higher than that of the Confluence region and SJ. Especially, the fish density of II-III in April and June was larger than other sub-regions. In II and III, the average fish density in April was 50.93 ind./1000 m^3, and 40.21 ind./1000 m^3 in June. It was steady in April and June while dropped to 7.82 ind./1000 m^3 in August. The fish density in IV and V decreased in June and August.

The complexity in underwater topography and flow pattern of the DJ provided the habitat, bait and spawning grounds for various fish with different ecological habits, especially for jet-flow and slow-flow fish. The intrusion of wastewater from upstream Zi-yang village caused an increase in water temperature and sunlight exposure. Then zooplankton and phytoplankton bloomed in sub-region I. The blooms lead to oxygen depletion and negatively impacted the distribution of fish resources. Therefore, fish density in June and August was lower than that in April. Fish mainly gathered to II in August and III in April and June. II and III had wide cross-sections but few shipping vessels, which provided ideal habitat for fish and a preferable fishing area for fishers. The fish density in IV and V decreased in June and August. There may exist a link between the density drop and some external factors such as the pharmaceutical industry, fishing activities, pollution by vessel manufacture. In the confluence of DJ and SJ, the narrow channel and the high flow rate were not suitable for fish to habitat. Therefore, the fish density in the three stages was low (0.3-4.12 ind./

Table 1: Fish density within a survey region (ind./1000m^3).

Region	Sub-region	April	June	August
DJ	I	22.86	13.45	15.24
	II	67.74	29.36	2.3
	III	34.12	51.06	13.34
	IV	14.54	14.48	6.40
	V	14.25	6.18	6.33
CF	VI	2.45	4.12	0.3
SJ	VII	2.69	3.32	4.77
	VIII	7.03	5.21	10.56

1000 m^3). The SJ is an artificial channel. The flow field in this reach was uniform and the mean velocity (less than 0.5 m/s) was significantly lower than that in the DJ area. In SJ, the operations of 2# and 3# ship-lock and scouring sluice caused abundant bait and versatile flow patterns, the fish preferred together in VIII neighbouring ship-locks.

Fish Target Length (*L*) Distribution

Fig. 3 and Fig. 4 show percentile distribution of target fish body length in April, June and August in the eight sub-regions I-VIII. The P_L curves in sub-region VIII (Fig. 3d and 4c) had a high similarity. The channel in region VIII remains naturally growth conditions with less external interference exerted. The high likeness was also observed in regions II, VI and VII from April to June. However in August when the season was over, the overall body length increase in regions II and VI and decrease in VII. The body length of the fish in the channels was highly-screened using a gill net with a certain hole size in the fishing season (Liang et al. 2012). In all stages of the season (April-August), P_L values varied with L values within 0-50cm significantly and irregularly in regions I, III, IV, and V. This shows that fish growth in these areas was either randomly affected by the municipal and industrial pollution or disturbed by overfishing.

Distribution of Temperature, DO, pH and Flow-Velocity

The results of the t-test for any two independent samples indicate that there is no significant difference in velocity at different stages of the season (P>0.05). The spatial distribution of velocity was determined by the underwater topography, operations of the power station and the sluice. The cooperative operations of the Three Gorges reservoir and Gezhouba reservoir resulted in fewer variations of flow rate and flow speed in different seasons. The flow speed in all regions except VI and IV was steady during the three surveying periods. And the change of the original hydrological conditions and the disappearance of scouring and silting under seasonal flooding impact impacted the downstream fish. Water temperature is another important parameter that affects the living, metabolism, reproductive behaviour and population of aquatic organisms, and eventually affect mass circulation, energy redistribution, and function of the aquatic ecosystem. The survey results (Table 2) showed the temperature changed significantly in different stages of the season ($P < 0.05$ in two independent sample t-test:) and the changing range was 16.15 + 0.62°C 27.19 + 0.08°C. Comparing with temperature, the change of pH (8.12 ± 0.05 - 9.35 ± 0.1) and flow-velocity (0.93 ± 0.23 m/s- 1.07 ± 0.2m/s) was not obvious.

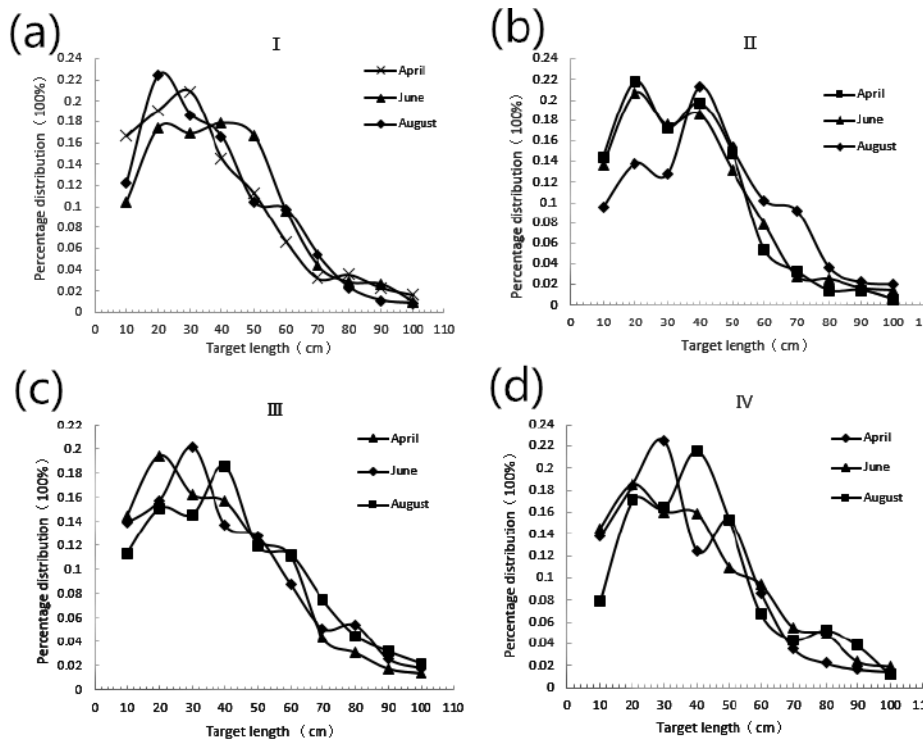

Fig. 3: Percentile target length (P_L) distribution in regions I-IV.

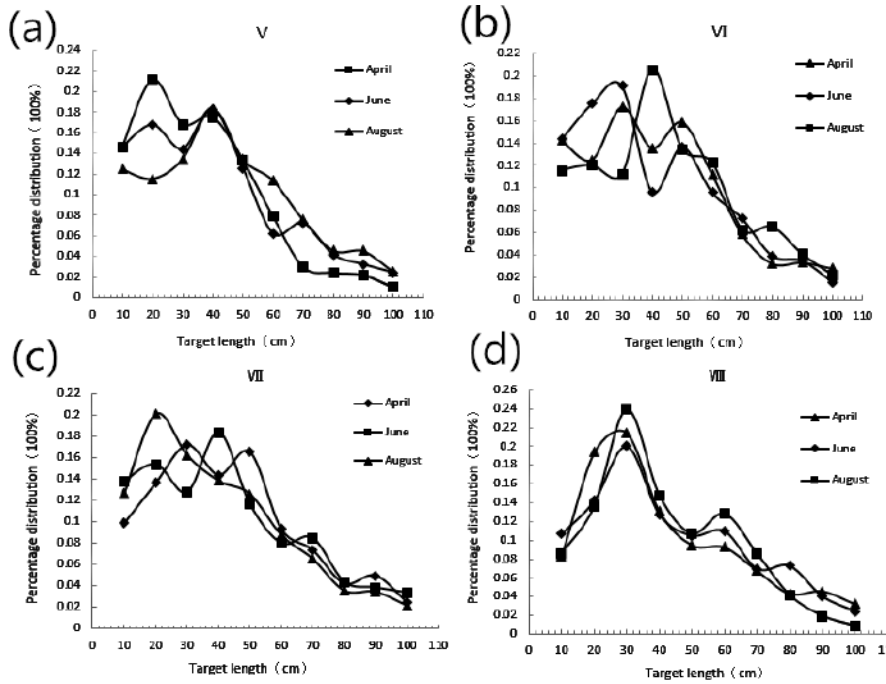

Fig. 4: Percentile target length (P_L) distribution in regions V-VIII.

Relationship between Flow rate, Temperature, DO and pH

The temperature range was divided into three zones, 14.38-18.34°C, 23.34-24.21°C and 26.92-27.56°C, to study the impact of the temperature. Previous studies show that the lowest spawning temperature for *Coreius heterodon* and *Coreius guichenoti* is 17°C and the temperature during the peak spawning period is 19-22°C (Liu et al. 1990). The lowest breeding temperature for the four major Chinese carps is 18°C and the temperature during the peak spawning is 21-24°C. All these species concentrated to spawn only in the fishing moratorium. The Kolmogorov-Smirnov analyses showed that the fish density was not normally distributed within the range of 23.34-24.21°C. However, it appeared normal distribution with a Sig of 0.254 (which was greater than 0.05) after conducting logarithmic conversion. The F of 2.478 and P of 0.024 (which was less than 0.05) in the Anova results showed significant differences in the fish distribution density at different temperature levels.

To analyze the impact of flow-velocity on fish density distribution, the monitoring data of the flow velocity was divided into three ranges, 0-0.7m/s, 0.7-1.2m/s and 1.2-2.1m/s. The Kolmogorov-Smirnov test showed that the fish density was normally distributed in three ranges. In the ANOVA

Table 2: Temperature, DO, pH of regions I-VIII in April, June and August.

zone	Temperature (°C)			pH			DO (mg/L)		
	April	June	August	April	June	August	April	June	August
I	18.34	23.56	27.13	8.09	8.63	9.12	9.78	7.86	7.45
II	17.99	23.35	26.96	8.21	8.40	9.15	9.48	7.49	7.11
III	18.32	23.34	26.92	7.91	8.50	9.32	7.91	7.46	7.10
IV	14.38	23.37	27.01	8.13	8.53	8.96	8.31	7.62	7.13
V	14.41	24.09	27.36	7.87	8.48	9.58	8.43	7.68	6.74
VI	15.09	24.21	27.56	8.15	8.09	9.82	8.18	8.89	6.45
VII	15.32	24.15	27.37	8.27	8.54	9.25	8.55	8.08	6.48
VIII	15.37	23.98	27.21	8.31	8.68	9.56	8.09	7.50	6.56

results, the F was 28.56 and P was 0.007 (<0.05) indicating that the fish distribution density at different flow-velocity levels was different. It showed that in the near-dam area of downstream Gezhouba, the fish had selectivity to the velocity of three ranges. The flow velocity could affect fish density distribution.

The average values of DO and pH showed no significant differences (p>0.05), and the survey would not be discussed in this paper (Table 2).

DISCUSSION

Influence of Environmental Factors on the Fish Distribution in Spatial and Temporal

Many studies have investigated the influence of ecological factors including water temperature, DO, velocity, pH, the availability of food on the spatial and temporal distribution of fish (Yi et al. 2010, Yuan et al. 2012, Liu et al. 2009, Xiong et al. 2014). In particular, the water temperature has a close relationship with survival, metabolism, reproductive behaviour and the population distribution of aquatic organisms (Wang et al. 2008). The monitoring data showed the fish density in the area adjacent to the Gezhouba Dam was spatially and temporally affected by water temperature and flow velocity. The average water temperature significantly increased from 16.15°C in April to 23.75°C in June and to 27.19°C in August. The water temperature in April was too low for the majority of the local fish to spawn. Some studies have reported that *Coreius heterodon*, *Coreius guichenoti* and *Pelteobagrus fulvidraco* mainly eat fish eggs as the primary food and their percentage often change (Luo et al. 20013). The spawning water temperature of *Pelteobagrus fulvidraco* is from 24 to 28°C. The broodstock largely consumes food when the water temperature is higher than 15°C and its peak breeding season is from May to July. *Cyprinus carpio* and *Siniperca chuatsi* mainly distribute in SJ. The most suitable temperature for *Siniperca chuatsi* to actively prey, swim, is from 23 to 25°C. The four major Chinese carps are the primary fishes near the Gezhouba Dam in upstream of the Yangtze River to support the local economy. The rich fish stocks in June and August was probably associated with a large quantity of breeding occurring meanwhile. The earliest and the latest beginning date for the four major Chinese carps to spawn is April 28 and May 10, and the lasts tending date is June 15 and July 5. The optimum temperature range for growth and reproduction is from 22°C to 28°C (Guo et al. 2011). Therefore, if only considering the effect of temperature on fish density, the fish density in the near dam area should increase with the increase of temperature to a certain extent However, the monitoring data did not reflect the analysis. On the contrary, the fish density showed a decreasing trend from April to June and August. Therefore, the temperature was not the key factor for fish density change in this research scale.

Fish density distribution is closely related to hydrologic conditions including water depth, flow velocity, flow rate and flow direction (Guo et al. 2011, Kynard 1995). Among these factors, fish determines its swimming route, even migratory route, based on its sense to the flow velocity (Yuan et al. 2011). The results in this study have confirmed the influence of the flow speed on the fish density distribution in the near-dam region, which is consistent with Zhang Huijie (2007). While the mainstream in II and III kept average flow-velocity greater than 1.4 m/s, it provided a steady habitat for fish and led to high fish densities. The majority of the species in II and III are slow-current loving type fish, such as *Pelteobagrus fulvidraco* and *Coreius heterodon* (Liu et al. 2012). All three monitoring results indicated the greater fish density occurs in the area close to the dam (Table 1), and the flow velocity in this region was distributed in the range of fish's favourite and the extreme velocities. Therefore, the flow field was suitable for most fish to live in. Fish habitat is also affected by the underwater topography (Ban & Li 2007), so the diversion dike may diversify the flow patterns in the river reach to maintain biological diversity.

Influence of the Fishing Moratorium on Downstream Fish Stocks of the Gezhouba

The body length of catches or acoustic body length is directly or indirectly used to analyze the community structure and growth trends of fish, to evaluate the temporal change of fish stocks and the effect of the fishing moratorium (Liu et al. 2004, Duan et al. 2008, Zhang et al. 2006, Li et al. 2014). In this study, comparing with the observation of August when the fishing moratorium was over, the echo signals of target length within 10-40 cm were stronger in most areas in the closed season both in April and June. Although the echo signals of some body lengths were increased in a few regions, there was no significant difference (P > 0.05) for the overall target length. The fish density substantially varied with different monitoring areas and it decreased significantly from April to August. The water quality analysis showed little impact of the DO, pH and water temperature on the fish density. Although the fish density was much sensitive to the flow velocity in the three monitoring, there was no significant difference between the periods of the fishing moratorium and after the fishing moratorium. So the flow-velocity was not a key factor for fish stocks in the research scales.

The fish stocks kept a stable level during the fishing moratorium. Once the fishing moratorium was over on June 31, many fishing activities were conducted in the near-dam area. Monitoring results of August showed the overall fish

density dropped and it plummeted in some areas where fish densely distributed in April and June. This was mainly caused by fishing activities with high frequency in the near-dam during the fishing season. Therefore, the fishing moratorium played a key role in maintaining the sustainability of fish and overfishing was one major factor related to the decline of fish stocks during the investigation period. This conclusion was consistent with Arendse et al. (2007).

CONCLUSIONS

As one of the most important measures of management, the fishing moratorium plays an important role to protect the fish resources in the Yangtze River. The results of this study demonstrated that there existed a significant difference in fish density distributions in April, June and August. The distribution in DJ was much higher than that in SJ. The fish density generally decreased with time but maintained a close and steady level in April and June. The average density of April was significantly greater than that in August ($P<0.05$). The percentage of fish body length distribution was fairly uniform in time and space. In this study, the change of temperature and flow velocity were not the main reasons for the decrease in fish density and target body length. The fishing moratorium had an obvious effect on maintaining the stability of fish resources near Gezhouba. Overfishing was one of the important reasons for the decline of fish resources.

ACKNOWLEDGEMENTS

This study was financially supported by the National Natural Science Foundation of China (Grant No. 52079074, 91647207, 51879099, 51709096 and 51779128), Non-profit Industry Program for special scientific of Ministry of Water Resources of China (No. 201201030), and Young talents project of Guizhou Provincial Department of Education KY(2017)120.

REFERENCES

Arendse, C.J., Govender, A. and Branch, G.M. 2007. Are closed fishing seasons an effective means of increasing reproductive output? : A per-recruit simulation using the limpet *Cymbula granatina* as a case history. Fisheries Research, 85: 93-100.

Ban, X. and Li, D.M. 2007. Ecological hydrological influence of large water conservancy projects on Acipenser Sinensis in Yangtze River. Engineering Journal of Wuhan University, 40: 10-13.

Barnes, B. and Sidhu, H. 2013. The impact of marine closed areas on fishing yield under a variety of management strategies and stock depletion levels. Ecological Modelling, 269: 113-125.

Bavinck, M., De Klerk, L., Van Dijk, D., Rothuizen, J.V., Blok, A.N., Bokhorst, J.R., Van Haastrecht, E.K., van de Loo, T., Quaedvlieg, J. and Scholtens, J. 2008. Time-zoning for the safe-guarding of capture fisheries: A closed season in Tamil Nadu, India. Marine Policy, 32: 369-378.

Boswell, K.M., Wilson, M.P. and Cowan Jr, J.H. 2008. A semiautomated approach to estimating fish size, abundance, and behavior from dual-frequency identification sonar (DIDSON) data. North American Journal of Fisheries Management, 28: 799-807.

Draštík, V., Kubečka, J., Tušer, M., Čech, M., Frouzová, J., Jarolím, O. and Prchalová, M. 2008. The effect of hydropower on fish stocks: Comparison between cascade and non-cascade reservoirs. Hydrobiologia, 609: 25-36.

Duan, X.B., Liu, S.P., Xiong, F., Chen, D.Q., Yang, R.H., Chi, C.G. and Mu, T.R. 2008. Analysis of fishing structure and biodiversity in the upper mainstream of the Yangtze River before and after three years' spring fishing off. Resources and Environment in the Yangtze Basin, 17: 878-885.

Gao, Z. J., Shi, S. L. and Li, Y. 2008. Application of SPSS in ANOVA of biological statistics. Progress in Modern Biomedicine, 2116-2120.

García, A., Jorde, K., Habit, E., Caamaño, D. and Parra, O. 2011. Downstream environmental effects of dam operations: changes in habitat quality for native fish species. River Research and Applications, 27: 312-327.

Godlewska, M., Frouzova, J., Kubecka, J., Wiśniewolski, W. and Szlakowski, J. 2012. Comparison of hydroacoustic estimates with fish census in shallow Malta Reservoir - which TS/L regression to use in horizontal beam applications? Fisheries Research, 123-124, 90-97.

Guo, W. X., Wang, H. X., Xu, J. X. and Xia, Z. Q. 2011. Effects of Three Gorges reservoir on the downstream eco-hydrological regimes during the spawning of important fishes. Journal of Hydroelectric Engineering, 30: 22-26.

Han, J., Honda, N., Asada, A. and Shibata, K. 2009. Automated acoustic method for counting and sizing farmed fish during transfer using DIDSON. Fisheries Science, 75: 1359-1367.

Knudsen, F.R., Fosseidengen, J.E., Oppedal, F., Karlsen, Ø and Ona, E. 2004. Hydroacoustic monitoring of fish in sea cages: target strength (TS) measurements on Atlantic salmon (*Salmo salar*). Fisheries Research, 69: 205-209.

Kynard, B., Wei, Q.W. and Ke, F.N. 1995. Use of ultrasonic telemetry to locate the spawning area of Chinese sturgeons. Chinese Science Bulletin, 40: 668-671.

Liu, L.H., Wang, G.X. and Wang, Z.L. 1990. Reproduction ecology of *Coreius heterodon* and *Coreius guichenoti* in the mainstream of the Yangtze River after the construction of Gezhouba Dam. Acta Hydrobiologica Sinica, 14: 205-215.

Li, Y.F., Li, X.H., Yang, J.P., Lek, S., Shuai, F.M. and Li, J. 2014. Effect of Pearl River closed fishing on *Megalobrama hoffmanni* recruitment stock. Journal of fisheries of China, 38: 502-508.

Liang, Z.L., Yan, W., Sun, P., Huang, L.Y. and Tang, Y.L. 2012. A study on the impact of Gill Net on the phenotypic traits of fish population. Oceanologia Et Limnologia Sinica, 43: 329-334.

Liu, C.C., Gao, X., Lin, P.C., Yang, S.R., Liu, H.Z. and Cao, W.X. 2012. Fish community structure in Gezhouba reservoir. Resources and Environment in the Yangtze Basin, 21: 843-849.

Liu, S.P., Chen, D.Q., Duan, X.B., Qiu, S.L. and Huang, M.J. 2004. Monitoring of the four famous Chinese carps resources in the middle upper reaches of the Yangze River. Resources and Environment in the Yangtze Basin, 13: 183-186.

Liu, W., ZhuGe, Y.S., Ou, Y.L., Yu, W. and Liu, D.F. 2009. Experimental study of the effect of hydrodynamic conditions on fish growth. Advances In Water Science, 20: 812-817.

Luo, J., Jiang, W., Chen, Q.W., Liu, D.F., Tang, X.L., Tu, Z.Y. and Shi, X.T. 2013. Estimation on abundance of egg-predatory fishes in the spawning ground of Chinese sturgeon below the Gezhouba Dam. Freshwater Fisheries, 43: 27-30.

MacDougall, T.M., Wilson, C.C., Richardson, L.M., Lavender, M. and Ryan, P.A. 2007. Walleye in the Grand River, Ontario: an overview of

rehabilitation efforts, their effectiveness, and implications for eastern Lake Erie fisheries. Journal of Great Lakes Research, 33: 103-117.

Maxwell, S.L. and Gove, N.E. 2004. The Feasibility of estimating migrating salmon passage rates in turbid rivers using a dual frequency identification sonar (DIDSON). Alaska Department of Fish and Game Regional Information Report.

Maxwell, S.L. and Smith, A.V. 2007. Generating river bottom profiles with a dual-frequency identification sonar (DIDSON). North American Journal of Fisheries Management, 27: 1294-1309.

Misund, O.A. 1997. Underwater acoustics in marine fisheries and fisheries research. Reviews in Fish Biology and Fisheries, 7: 1-34.

Morita, K. and Yamamoto, S. 2002. Effects of habitat fragmentation by damming on the persistence of stream-dwelling charr populations. Conservation Biology, 16: 1318-1323.

Moustakas, A., Silvert, W. and Dimitromanolakis, A. 2006. A spatially explicit learning model of migratory fish and fishers for evaluating closed areas. Ecological Modelling, 192: 245-258.

Petreman, I.C., Jones, N.E. and Milne S.W. 2014. Observer bias and subsampling efficiencies for estimating the number of migrating fish in rivers using Dual-frequency Identification Sonar (DIDSON). Fisheries Research, 155: 160-167.

Rakowitz, G., Herold, W., Fesl, C., Keckeis, H., Kubečka, J. and Balk, H. 2008. Two methods to improve the accuracy of target-strength estimates for horizontal beaming. Fisheries Research, 93: 324-331.

Santos, J.M., Ferreira, M.T., Pinheiro, A.N. and Bochechas, J.H. 2006. Effects of small hydropower plants on fish assemblages in medium-sized streams in central and northern Portugal. Aquatic Conservation. Marine and Freshwater Ecosystems, 16: 373-388.

Shen, X.P., Ding, J.S., Li, J.S., Liu, X.N., Li, J.H. and Mi, A.J. 2007. 2-Independent-Samples t-test undertaking by the means of mean and standing deviation in SPSS. Modern Preventive Medicine, 4066-4067.

Tao, J., Gong, Y., Tan, X., Yang, Z. and Chang, J. 2012. Spatiotemporal patterns of the fish assemblages downstream of the Gezhouba Dam on the Yangtze River. Science China Life Sciences, 55: 626-636.

Wang, W., Li, W.C., Ma, X.Z., He, L. and Ye, F.F. 2008. Effects of water temperature and light intensity on the behaviors of *Pelteobagrus vachelli* fingerlings. Chinese Journal of Ecology, 27: 791-796.

Xiong, F., Wang, C.F., Liu, D.F., Wang, L.L., Qin, X.H. and Shi, X.T. 2014. Fish assemblages under different running status of the 1# ship-lock of the Gezhou Dam. Journal of Hydroecology, 35: 8-14.

Yang, S., Gao, X., Li, M., Ma, B. and Liu, H. 2012. Interannual variations of the fish assemblage in the transitional zone of the Three Gorges Reservoir: persistence and stability. Environmental Biology of Fishes, 93: 295-304.

Yi, Y., Wang, Z. and Yang, Z. 2010. Impact of the Gezhouba and Three Gorges Dams on habitat suitability of carps in the Yangtze River. Journal of hydrology, 387: 283-291.

Yi, Y., Yang, Z. and Zhang, S. 2010. Ecological influence of dam construction and river-lake connectivity on migration fish habitat in the Yangtze River basin, China. Procedia Environmental Sciences, 2: 1942-1954.

Yuan, X., Li, L.P., Tu, Z.Y., Shi, X.T., Liu, G.Y., Liu, D.F. and Huang, Y.P. 2012. A review of fish physiological and ecological behavior responding to river ecological factors. Resources and Environment in the Yangtze Basin, 21: 24-29.

Yuan, X., Tu, Z.Y., Han, J.C., Shi, X.T., Liu, G.Y. and Huang, Y.P. 2011. Effects of flow rate on swimming behavior and energy consumption of *Carassius auratus*. Journal of Hydroecology, 32: 103-109.

Zhang, H.J., Yang, D.G., Wei, Q.W., Du, H., Zhang, H. and Chen, X.H. 2007. Hydro-acoustic survey on fishes in the reach from Gezhouba Dam to GuLaoBei of the Yangze River. Resources and Environment in the Yangtze Basin, 16: 86-91.

Zhang, M.Y., Liu, K., Xu, D.P. and Shi, W.G. 2006. Primary study on effect of Spring-Fishing-Ban season on fishery community structure and biodiversity in ChangShu section of the Yangze River. Resources and Environment in the Yangtze Basin, 15: 442-446.

Zhou, J., Zhao, Y., Song, L., Bi, S. and Zhang, H. 2014. Assessing the effect of the Three Gorges reservoir impoundment on spawning habitat suitability of Chinese sturgeon (<i> *Acipenser sinensis*) in Yangtze River, China. Ecological Informatics, 20: 33-46.

... Continued from inner front cover

- The text of the manuscript should run into **Abstract, Introduction, Materials & Methods, Results, Discussion, Acknowledgement** (if any) and **References** or other suitable headings in case of reviews and theoretically oriented papers. However, short communication can be submitted in running with **Abstract and References.** The references should be in full with the title of the paper.
- The figures should preferably be made on a computer with high resolution and should be capable of withstanding a reasonable reduction with the legends provided separately outside the figures. Photographs may be black and white or colour.
- Tables should be typed separately bearing a short title, preferably in vertical form. They should be of a size, which could easily be accommodated in the page of the Journal.
- References in the text should be cited by the authors' surname and year. In case of more than one reference of the same author in the same year, add suffix a,b,c,.... to the year. For example: (Thomas 1969, Mass 1973a, 1973b, Madony et al. 1990, Abasi & Soni 1991).

List of References

The references cited in the text should be arranged alphabetically by authors' surname in the following manner: (Note: The titles of the papers should be in running 'sentence case', while the titles of the books, reports, theses, journals, etc. should be in 'title case' with all words starting with CAPITAL letter.)

Dutta, A. and Chaudhury, M. 1991. Removal of arsenic from groundwater by lime softening with powdered coal additive. J. Water Supply Res. Techno. Aqua., 40(1) : 25-29.

Hammer, D.A. (ed.) 1989. Constructed Wetlands for Wastewater Treatment-Municipal, Industrial and Agricultural. Lewis Publishers Inc., pp. 831.

Haynes, R. J. 1986. Surface mining and wetland reclamation. In: Harper, J. and Plass, B. (eds.) New Horizons for Mined Land Reclamation. Proceedings of a National Meeting of the American Society for Surface Reclamation, Princeton, W.V.

Submission of Papers

- The paper can be submitted by e-mail as an attachment in a single WORD file at **contact@neptjournal.com**
- The paper can also be submitted online in a single WORD file through the **online submission portal** of journal's website: **www.neptjournal.com**

Attention

1. Any change in the authors' affiliation may please be notified at the earliest.
2. Please make all the correspondence by e-mail, and authors should always quote the manuscript number.

Note: In order to speed up the publication, authors are requested to send the publication charges as soon as they get the 'initial acceptance' letter, and also correct the galley proof immediately after receipt. The galley proof must be checked with utmost care, as publishers owe no responsibility for mistakes. The papers will be put on priority for publication only after receiving the processing and publication charges.

Nature Environment and Pollution Technology

(Abbreviation: Nat. Env. Poll. Tech.)

(An International Quarterly Scientific Journal)

Published by

Technoscience Publications

A-504, Bliss Avenue, Opp. SKP Campus

Balewadi, Pune-411 045, Maharashtra, India

In association with

Technoscience Knowledge Communications

Mira Road, Mumbai, India

For further details of the Journal, please visit the website. All the papers published on a particular subject/topic or by any particular author in the journal can be searched and accessed by typing a keyword or name of the author in the 'Search' option on the Home page of the website. All the papers containing that keyword or author will be shown on the home page from where they can be directly downloaded.

www.neptjournal.com

Published for Proprietor, Printer and Publisher: Mrs. T. P. Goel, B-34, Dev Nagar, Tonk Road, Jaipur, Rajasthan, India; Editors: Dr. P. K. Goel (Chief Editor) and Prof. K. P. Sharma